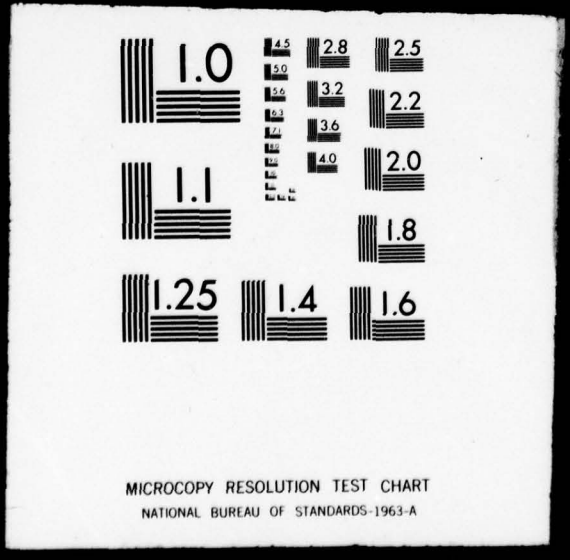
AD-A065 304 NEW YORK ACADEMY OF SCIENCES N Y F/G 7/2
SYNTHESIS AND PROPERTIES OF LOW-DIMENSIONAL MATERIALS,(U)
1978 J S MILLER, A J EPSTEIN N00014-77-C-0374
UNCLASSIFIED NL

1 OF 9
AD A065304



1 OF 9

AD
A065304



AD A065304

ANNALS OF
THE NEW YORK ACADEMY
OF SCIENCES

VOLUME 313

LEVEL II

(1)

SYNTHESIS AND PROPERTIES OF LOW-DIMENSIONAL MATERIALS

DDC FILE COPY



RECEIVED
MAR 6 1979
A

Editors
Joel S Miller
Arthur J Epstein

PUBLISHED BY THE NEW YORK ACADEMY OF SCIENCES
ANYAA9 313 1 828 (1978)

ANNALS OF THE NEW YORK ACADEMY OF SCIENCES

Volume 313

N003r36

EDITORIAL STAFF

Executive Editor
BILL BOLAND

Associate Editors
BEATRICE H. RADIN
RICHARD MALLOY

The New York Academy of Sciences
2 East 63rd Street
New York, New York 10021

THE NEW YORK ACADEMY OF SCIENCES
(Founded in 1817)

BOARD OF GOVERNORS, 1978

CHARLOTTE FRIEND, *President*
JOEL L. LEBOWITZ, *President-Elect*

Honorary Chairman of the Board of Governors
I. B. LASKOWITZ

Honorary Life Governors
SERGE A. KORFF
I. B. LASKOWITZ
MARGARET MEAD
H. CHRISTINE REILLY
IRVING J. SELIKOFF

Vice-Presidents
CRAIG D. BURRELL
DOROTHY CUNNINGHAM
JOHN HAPPEL
HEINZ PAGELS
LUCIE WOOD SAUNDERS

Recording Secretary
MORRIS H. SHAMOS

Treasurer
ALAN J. PATRICOF

Corresponding Secretary
ALLAN GEWIRTZ

Elected Governors-at-Large

1976-1978
WILLIAM T. GOLDEN
EVELYN A. MAUSS
WILLIAM NICHOLSON
BENJAMIN S. P. SHEN

1977-1979
FLORENCE DENMARK
WILLARD J. JACOBSON
KURT SALZINGER
PARITHYCHERY SRINIVASAN

1978-1980
BENJAMIN BEDERSON
MARY J. MYCEK
WALTER N. SCOTT
BABETTE B. WEKSLER

Past Presidents (Governors)
HERBERT J. KAYDEN
PHILIP SIEKEVITZ
PHILIP FEIGELSON
E. CUYLER HAMMOND

SIDNEY BOROWITZ, *Executive Director*

SYNTHESIS AND PROPERTIES OF LOW-DIMENSIONAL MATERIALS

M77640

79 03 01 183

LEVEL II

ANNALS OF THE NEW YORK ACADEMY OF SCIENCES
Volume 313

(1)

(6)

SYNTHESIS AND PROPERTIES OF LOW-DIMENSIONAL MATERIALS,

(10)

Edited by Joel S. Miller and Arthur J. Epstein

(11) 1978

(12) 838 p.

DDC
RECEIVED
MAR 6 1979
A

(15) N00014-77-C-0374

ACCESSION for
NTIS White Section
DDC Buff Section
UNANNOUNCED
JUSTIFICATION
$ 80.00
BY Marrotte for DDC
DISTRIBUTION/AVAILABILITY CODES
Dist. AVAIL. and/or SPECIAL
A 24

The New York Academy of Sciences, N.Y.
New York, New York
1978

256 290
79 03 01 183

Copyright © 1978 by The New York Academy of Sciences. All rights reserved. Under the provisions of the United States Copyright Act of 1976, individual readers of the Annals *are permitted to make fair use of the material in them for teaching or research. Permission is granted to quote from the* Annals *provided that the customary acknowledgment is made of the source. Material in the* Annals *may be republished only by permission of The Academy. Address inquiries to the Executive Editor at The New York Academy of Sciences.*

Copying fees: *The code at the bottom of the first page of each article in this* Annal *states the fee for each copy of the article made beyond the free copying permitted under Section 107 or 108 of the 1976 Copyright Act. (If no code appears, there is no fee.) This fee should be paid through the Copyright Clearance Center Inc., Box 765, Schenectady, New York 12301. For articles published prior to 1978, the copying fee is $1.75 per article.*

This work relates to Department of the Navy Contract N00014-77-C-0374 issued by the Office of Naval Research. The United States Government has a royalty-free license throughout the world in all copyrightable material contained herein.

Library of Congress Cataloging in Publication Data
Main entry under title:

Synthesis and properties of low-dimensional materials.

(Annals of the New York Academy of Sciences; v. 313)
"This series of papers is the result of a conference entitled Synthesis and properties of low-dimensional materials, held by the New York Academy of Sciences on June 13, 14, 15, and 16, 1977."
Bibliography: p. 5.
1. One-dimensional conductors—Congresses. 2. Crystals—Defects—Congresses. I. Miller, Joel S. II. Epstein, Arthur J. III. New York Academy of Sciences. IV. Series: New York Academy of Sciences. Annals; v. 313.

Q11.N5 vol. 313 [QC176.8.E4] 508'.1s [530.4'1]
ISBN 0-89072-069-X 78-10149

SP
Printed in the United States of America
ISBN 0-89072-069-X

ANNALS OF THE NEW YORK ACADEMY OF SCIENCES

VOLUME 313

September 29, 1978

SYNTHESIS AND PROPERTIES OF LOW-DIMENSIONAL MATERIALS*

Conference Chairperson

Joel S. Miller

Editors

Joel S. Miller and Arthur J. Epstein

Conference Organizers

Arthur J. Epstein, Alan G. MacDiarmid, and Henry Taube

CONTENTS

Introduction. *By* JOEL S. MILLER 1

Part I. General Papers

Chemical Classification of Structures and Properties of Low-Dimensional Inorganic Compounds. *By* P. DAY 9

Design and Synthesis of Highly Conducting One-Dimensional Materials. *By* JOEL S. MILLER 25

Chemistry of the Mixed-Valent Charge-Transport Process: The Design of Organic Molecules for Organic Metals. *By* J. H. PERLSTEIN, J. A. VANALLEN, L. C. ISETT AND G. A. REYNOLDS 61

The Future of Organic Metals Composed of Carbon, Hydrogen, Nitrogen, and Sulfur. *By* F. WUDL, A. A. KRUGER, AND G. A. THOMAS 79

The Layered Dichalcogenides: Some Chemistry and Physics, *By* F. R. GAMBLE 86

Synthesis and Characterization of New One- and Two-Dimensional Magnetic Materials. *By* ROGER D. WILLETT 111

Review of the Physics of Low-Dimensional Systems. *By* PAUL M. CHAIKIN 128

Anisotropic Semiconductors and Metals: What Holds Them Together? *By* ROBERT MELVILLE METZGER 145

Electron Interactions with Molecular Vibrations: Their Nature and Consequences. *By* C. B. DUKE 166

The Role of Librons in Quasi-One-D Organic Conductors. *By* H. MORAWITZ . 179

Charge Transport in Molecular Conductors: Role of Mobility. *By* ARTHUR J. EPSTEIN, ESTHER M. CONWELL, AND JOEL S. MILLER 183

*This series of papers is the result of a conference entitled Synthesis and Properties of Low-Dimensional Materials, held by The New York Academy of Sciences on June 13, 14, 15, and 16, 1977.

Framework for Classifying and Interpreting the Physical Properties of Charge-Transfer Salts of TCNQ: The Unifying Feature of Organic Metals. *By* J. B. TORRANCE 210
X-Ray Scattering Studies from One-D Conductors. *By* S. MEGTERT, J. P. POUGET, AND R. COMES 234
X-Ray Diffraction Measurement of Net Atomic and Molecular Charges. *By* P. COPPENS AND T. N. GURU ROW 244
Reflection Spectra and Electronic Structures of Metallic TCNQ Complexes. *By* JIRO TANAKA, MASASHI TANAKA, CHIZUKO TANAKA, TERUAKI OHNO, TERUHIRO TAKABE, AND HIROYUKI ANZAI 256
Solid-State Reactions in Organic Conductors and their Technological Applications. *By* SUSUMU YOSHIMURA AND MUTSUAKI MURAKAMI 269

Part II. Organic Materials

Organic Metals: Basic Crystal-Growth Techniques. *By* JAN R. ANDERSEN, EDWARD M. ENGLER, AND KLAUS BECHGAARD 293
Instrumental Analysis for Purity Determination of TTF-TCNQ Crystals. *By* A. R. MCGHIE, P. J. NIGREY, F. G. YAMAGISHI, AND A. F. GARITO ... 301
Crystal Perfection and the Physical Properties of TTF-TCNQ. *By* LAWRENCE B. COLEMAN 316
Structural Relationships in the Heterofulvalene-TCNQ Family of Organic Conductors. *By* THOMAS J. KISTENMACHER 333
Synthetic Approaches to the Study of Organic Metals. *By* EDWARD M. ENGLER, VISHNU V. PATEL, JAN R. ANDERSEN, YAFFA TOMKIEWICZ, ROBERT A. CRAVEN, BRUCE A. SCOTT, AND SHAHAB ETEMAD 343
Unsymmetrical Tetrathiafulvalenes. *By* M. P. CAVA AND M. V. LAKSHMIKANTHAM 355
New Synthetic Procedure for the Preparation of Monosubstituted Tetrathiafulvalenes. *By* DENNIS C. GREEN 361
A New π-Donor for the Study of Organic Metals. *By* WILLIAM P. KRUG, AARON N. BLOCH, THEODORE O. POEHLER, AND DWAINE O. COWAN 366
Crystal Chemistry of Mixed-Valence TTF Salts. *By* B. A. SCOTT, S. J. LAPLACA, J. B. TORRANCE, B. D. SILVERMAN, AND B. WELBER 369
Metallotetrathiaethylenes. *By* A. R. SIEDLE, G. A. CANDELA, T. F. FINNEGAN, R. P. VAN DUYNE, T. CAPE, G. F. KOKOSZKA, P. M. WOYCIESJES, J. A. HASHMALL, M. GLICK, AND W. ILSLEY 377
Synthesis and Properties of Chalcogen-Bridged Napthalenes: A New Series of Electron Donors. *By* D. DAUPLAISE, J. MEINWALD, J. C. SCOTT, H. TEMKIN, AND J. CLARDY 382
Ion-Radical Salts of Tetrathiotetracene. *By* L. C. ISETT AND E. A. PEREZ-ALBUERNE 395
Molecular Design of Solid-State Systems. Organic-Metal Complex π-Donor-Acceptor Compounds. *By* L. V. INTERRANTE, J. W. BRAY, H. R. HART, JR., J. S. KASPER, P. A. PIACENTE, AND G. D. WATKINS 407
Electronic and Structural Properties of Some Bipyridylium^{2+} $(TCNQ)_4^{2-}$ and Related Complexes. *By* D. D. ELEY, G. J. ASHWELL, S. C. WALLWORK, M. R. WILLIS, AND J. WOODWARD 417
Phenazine Cation Radical Salts: Charge-Transfer Complexes with TCNQ. *By* Z. G. SOOS, H. J. KELLER, W. MORONI, AND D. NÖTHE 442

The Chemical and Physical Properties of the Reaction Product Between Trimethylammonium Iodide and TCNQ. A Ternary 1-D Semiconductor with "Metal-Like" Conductivity. *By* M. A. ABKOWITZ, J. W. BRILL, P. M. CHAIKIN, A. J. EPSTEIN, M. F. FROIX, C. H. GRIFFITHS, W. GUNNING, A. J. HEEGER, W. A. LITTLE, J. S. MILLER, M. NOVATNY, D. B. TANNER, AND M. L. SLADE 459
Chemical Preparation and Physical Properties of a Metallic Organic Charge-Transfer Complex: HMTTF-TCNQ. *By* P. DELHAES, S. FLANDROIS, J. AMIELL, G. KERYER, E. TOREILLES, J. M. FABRE, L. GIRAL, C. S. JACOBSEN, AND K. BECHGAARD 467

Part III. Inorganic Materials

Electronic Coupling Mechanisms in Mixed-Valence Molecules. *By* HENRY TAUBE 481
Design and Synthesis of Mixed-Valence Complexes. *By* THOMAS J. MEYER 496
Synthesis, Structure, and Conductivity of New One-Dimensional Tetracyanoplatinates Containing Fluorine. *By* JACK M. WILLIAMS AND ARTHUR J. SCHULTZ 509
Preparation, Structure, and Electrical Conduction Properties of KCP-Type Compounds. *By* A. E. UNDERHILL AND D. J. WOOD 516
Physical and Structural Properties of Two Conducting One-Dimensional Materials: Guanidinium (GCP) Tetracyanoplatinate Bromide Hydrate and Barium Vanadium Trisulfide. *By* GALEN STUCKY, C. PUTNIK, J. KELBER, M. J. SCHAFFMAN, M. B. SALAMON, G. PASQUALI, A. J. SCHULTZ, J. WILLIAMS, T. F. CORNISH, D. M. WASHECHECK, AND P. L. JOHNSON 525
Spectroscopic Studies of $M_x[Pt(CN)_4] \cdot yH_2O$. *By* HARTMUT YERSIN AND GÜNTER GLIEMANN 539
Structure and Oxidation States of Ir and Pt One-Dimensional Inorganic Complexes. *By* ARTHUR H. REIS, JR. AND SELMER W. PETERSON 560
The Synthesis and Characterization of Some Linear Chain Complexes Containing Isocyanide Ligands. *By* J. G. GORDON II, R. WILLIAMS, C.-H. HSU, E. CUELLAR, S. SAMSON, K. MANN, H. B. GRAY, V. HADEK, AND R. SOMOANO 580
The Solution Photochemical Properties of Oligomeric Iridium Isocyanide Complexes. *By* GREGORY L. GEOFFROY, MARK G. BRADLEY, AND MARK E. KEENEY 588
Rational Synthesis of New Unidimensional Solids: Chemical and Physical Studies of Mixed-Valence Polyiodides. *By* TOBIN J. MARKS 594
Bis (α, β-Dionedioximato) Metal Complexes: Solid-State Design by Molecular Engineering. *By* H. ENDRES, H. J. KELLER, R. LEHMANN, H. VAN DE SAND, DONG VU, AND ARNULFO POVEDA 617
1,2-Benzoquinonedioxime (bqdH) as a Versatile Ligand System for the Synthesis of New One-Dimensional Compounds. *By* MICHEL MÉGNAMISI-BÉLOMBÉ 633
The Construction of Metal-Metal Bonds by Redox Processes. *By* ALAN L. BALCH 651
New Linear Chain Mixed-Valence Platinum Complexes with and without Halide Bridges. *By* HELMUT ENDRES, MOHAMMED EL SHARIF, HEIMO J. KELLER, REINHOLD MARTIN, AND ULRICH TRÄGER 663

Spectroscopic and Structural Studies of Mixed-Valence Linear-Chain Transition-Metal Compounds. *By* R. J. H. CLARK 672
A Crystalline Platinum Blue: Its Molecular Structure, Chemical Reactivity, and Possible Relevance to the Mode of Action of Antitumor Platinum Drug. *By* JACQUELINE K. BARTON AND STEPHEN J. LIPPARD 686
Pseudo-One-Dimensional Niobium Chalcogenides $NbSe_3$, and $I_{0.33}NbSe_4$. *By* J. ROUXEL, A. MEERSCHAUT, P. HAEN, AND P. MONCEAU 701

Part IV. Covalent Materials

Fully Conjugated Polymer Crystals: Solid-State Synthesis and Properties of the Polydiacetylenes. *By* R. H. BAUGHMAN AND R. R. CHANCE 705
Synthesis and Properties of Halogen Derivatives of $(SN)_x$ and $(CH)_x$. *By* M. AKHTAR, C. K. CHIANG, M. J. COHEN, J. KLEPPINGER, A. J. HEEGER, E. J. LOUIS, A. G. MACDIARMID, J. MILLIKEN, M. J. MORAN, D. L. PEEBLES, AND H. SHIRAKAWA 726
Polythiazyl Halides: Bromine Derivatives of $(SN)_x$ and S_4N_4. *By* G. B. STREET, S. ETEMAD, R. H. GEISS, W. D. GILL, R. L. GREENE, J. KUYPER, AND R. D. SMITH 737
$(SN)_x$ Grown under Unusual Conditions. *By* P. LOVE, G. MYER, H. I. KAO, M. M. LABES, W. R. JUNKER, AND C. ELBAUM 747
Mass Spectral Studies of $(SN)_x$ Vapors. *By* F. E. SAALFELD, J. J. DECORPO, J. R. WYATT, P. T. MAH, AND W. N. ALLEN 759
Characterization of Polymeric Sulfur Nitride $(SN)_x$, as an Electrode Material. *By* ROBERT NOWAK, WŁODZIMIERS KUTNER, HARRY B. MARK, JR., AND ALAN G. MACDIARMID 767
Light Scattering in Brominated $(SN)_x$. *By* H. TEMKIN, D. B. FITCHEN, G. B. STREET, AND W. D. GILL 771
Structure of Brominated $(SN)_x$; Raman Scattering and X-Ray Diffraction Studies. *By* Z. IQBAL, R. H. BAUGHMAN, J. KLEPPINGER AND A. G. MACDIARMID 775
The Linear Chain Mercury Compounds: $Hg_{2.86}AsF_6$ and $Hg_{2.91}SbF_6$. Electrical Conductivity, Optical Reflectance, and Thermoelectric Studies. *By* RONALD J. GILLESPIE, DUANE CHARTIER, BRENT D. CUTFORTH, W. ROSS DATARS, AND ANDRÉ VAN SCHYNDEL 788
$Hg_{3-\delta}AsF_6$: A Novel Anisotropic Synthetic Metal. *By* A. J. HEEGER AND A. G. MACDIARMID 800

Appendices

Common Abbreviations 823
Constants 825
Author Index 826

Financial assistance was received from:

- HOOKER CHEMICAL & PLASTICS CORP. RESEARCH CENTER
- INTERNATIONAL BUSINESS MACHINES CORPORATION
- MOLECULAR STRUCTURE CORPORATION
- MONSANTO COMPANY
- NATIONAL SCIENCE FOUNDATION
- OFFICE OF NAVAL RESEARCH
- STREM CHEMICALS, INCORPORATED
- U.S. ARMY RESEARCH OFFICE
- VENTRON CORPORATION (ALFA DIVISION)
- XEROX WEBSTER RESEARCH CENTER

The New York Academy of Sciences believes it has a responsibility to provide an open forum for discussion of scientific questions. The positions taken by the participants in the reported conference are their own and not those of The Academy. The Academy has no intent to influence legislation by providing such forums.

INTRODUCTION*

Joel S. Miller

Xerox Webster Research Center
Xerox Square-114
Rochester, New York 14644

Low-dimensionality is ascribed to materials that exhibit large anisotropic ratios in some intensive physical properties. For example, pseudo-one-dimensional materials typically have significantly greater optical, magnetic, electrical, and/or mechanical properties in one dimension with respect to the orthogonal directions. Similarly, pseudo-two-dimensional complexes exhibit pronounced physical properties in two dimensions with respect to the remaining dimension. These enhanced properties arise from cooperative interactions manifested by linear chain (1-D) or layer (2-D) structures, which principally occur in the solid. For years, advancement in this area of science was dominated by synthetic chemistry; however, in the last decade physicists have characterized the unique properties exhibited by these materials.

Progress in understanding the unique chemistry and physics associated with low-dimensional materials clearly involves the symbiotic collaboration between synthetic and physical inorganic and organic chemists, physicists, materials scientists, and electrical engineers. The requirement for collaboration and communication was serendipitously alluded to by Dr. A. Scott on the occasion of the March 30, 1916 Presidential Address[1] before the Chemical Society, where he drolly displayed "Graphic Formula" for Magnus' Green Salt (FIGURE 1). Magnus' Green Salt has the distinction of being the premiere pseudo-one-dimensional material prepared[2] studied by x-ray diffraction,[3] and found to exhibit unusual optical,[1,4] electrical,[5] and mechanical[6,6a] properties that arise from the linear chain structure.

The implication of this clairvoyant prognostication was not appreciated by the scientific community until 1932, when the structure revealed that the linear chain was comprised of *cooperating* cations and anions. Similarly, in the last decade both chemists and physicists joined hands (FIGURE 1) through strong and fruitful synergistic collaborative efforts which have significantly impacted the understanding of the chemistry and physics of pseudo-one-dimensional substances. Thus, on the occasion of this multidisciplinary international conference on the *Synthesis and Properties of Low-Dimensional Materials*, it is apropos to relate to the "Graphic Formula" of Magnus' Green Salt through the realization that the frontiers of science in this area of low-dimensional materials can be advanced only by communication and collaboration between the "green men."

The intent of this conference is to provide a forum for the participants to accumulate, review, and examine the aspects of low-dimensional materials and, in particular, pseudo-one-dimensional materials of primary but not exclusive interest to chemists, so that the frontiers of science in this interdisciplinary area can be reflected upon and advanced. It is also the aim of our conference to open up

*Manuscript received June 11, 1977.

0077-8923/78/0313-0001 $1.75/1© 1978, NYAS

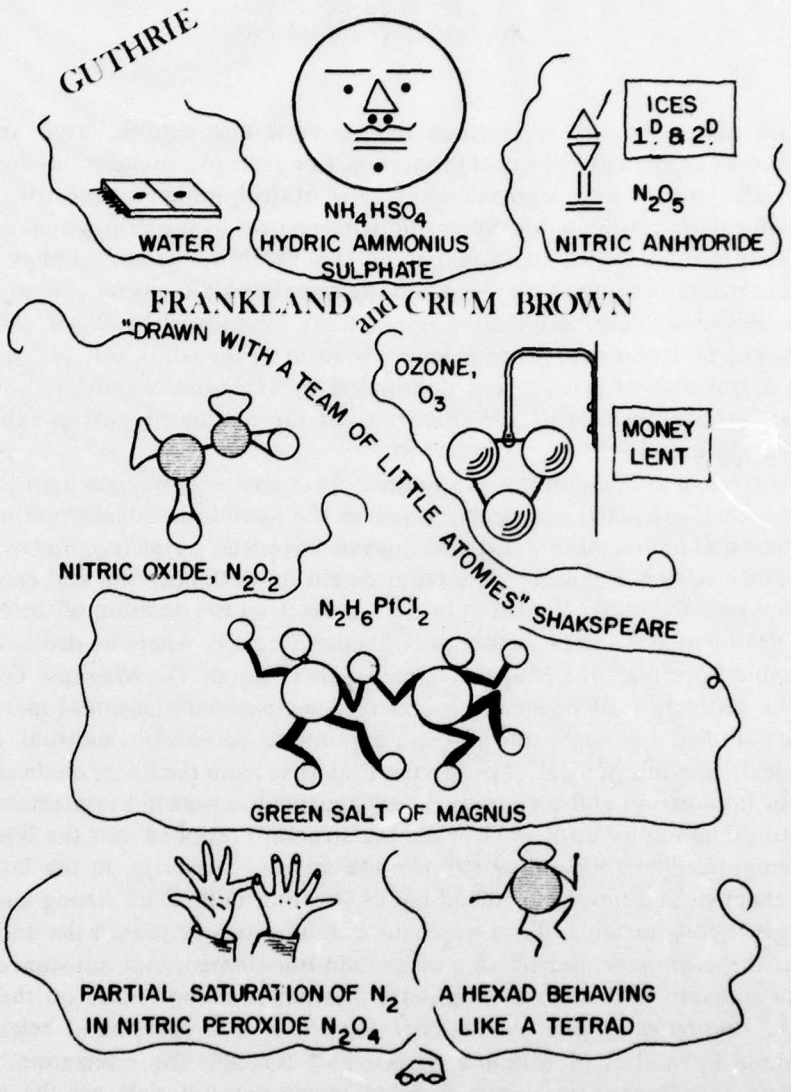


FIGURE 1. "Graphic Formula" presented by Dr. A. Scott in his presidential address to the Chemical Society in 1916.[1] (By permission of the Chemical Society.)

lines of communication between traditionally segregated areas of the sciences, allowing the salient ramifications of new and future scientific discoveries and breakthroughs to be appreciated by the scientific community as a whole. Thus, the conference combines contributions from academic, governmental, and industrial inorganic, organic, polymer, physical chemical, as well as solid-state, laboratories.

Some of the key aspects that are focused upon include a review of the solid-state

physics of reduced dimensional systems as well as the prototype inorganic or organic systems. The philosophies of the design of new inorganic and organic materials and up-to-date descriptions of existing systems are given and discussed. Experimental problems associated with the synthesis and characterization of new materials are also emphasized. Additionally, potential technological applications of such reduced dimensional systems are pointed out, so that better designed materials can be made.

To better acquaint the reader of this *Annal* with the subject matter, it is appropriate to tabulate the chronology of selected landmark papers that have been important in the evolution of the field (TABLE 1). The history of the field can be qualitatively described as maturation through merging of known materials and concepts by collaboration between scientists of historically divergent disciplines. Since the measurement of the conductivity of the first highly conducting organic ($TCNQ^{-}$),[8,8a] polymeric [$(SN)_x$],[9] and inorganic ($K_2Pt(CN)_4Br_{0.30} \cdot 3H_2O$),[10] substances revealing that high conductivity could be achieved by molecular solids,

TABLE 1

CHRONOLOGY OF SELECTED PAPERS IN THE FIELD OF LOW-DIMENSIONAL MATERIALS

Year	Event	Reference
1822	$K_2Pt(CN)_4$ characterized	11
1828	Magnus' Green Salt prepared	2
1842	$K_2Pt(CN)_4Cl_{0.3} \cdot xH_2O$ (KCP) synthesized	12
1878	$Pt(NH_3)_2Cl_3$ prepared	13
1888	$K_{1.75}Pt(CN)_4 \cdot 1.5H_2O$ synthesized	14
1894	$K_{1.64}Pt(ox)_2 \cdot H_2O$ prepared	15
1900	Wolffram's Red Salt prepared	16
1905	$Ni(HDMG)_2$ prepared	17
1910	$(SN)_x$ synthesized	18
1926	Alkali intercalation of graphite reported	19
1940	'$Ir(CO)_3Cl$' synthesized	20
1953	Conductivity of $(SN)_x$ reported	21
1954	Fröhlich model (charge density wave) for superconductivity introduced	22
1954	Conductivity of $Pd(NH_3)_2Cl_3$ reported	23
1960	$TCNQ^{z-}$ synthesized and high conductivity reported	8
1961	$K_{\sim 1/2}Ir(CO)_2Cl_2$ synthesized	24
1963	Molecular Metal postulated	25
1964	Little's Excitonic Superconductor Theory reported	26
1965	$(NMP^{+})(TCNQ^{-})$ synthesized and characterized	27
1966	Anisotropic conductivity of $Ir(CO)_2(acac)$ reported	28
1968	X-ray structural determination and conductivity of $K_2Pt(CN)_4X_{0.3} \cdot xH_2O$	10
1969	Molecular intercalation complexes of TiS_2 with amines reported	29
1970	Superconducting intercalation of NbS_2 and TaS_2 reported	30
1970	TTF cation radical salts synthesized and characterized	31
1971	"One-dimensional" esr lineshape reported for $(Me_4N)MnCl_3$	32
1973	CDW and superlattice distortions reported for KCP	33
1973	(TTF)(TCNQ) synthesized and characterized	34
1974	$Hg_{2.85}AsF_6$ reported	35
1974	CDW and superlattice distortions in 2-D metals reported	36
1975	Superconductivity in $(SN)_x$ reported	37
1975	Spin-Peierls transition for $(TTF)M(S_2C_2(CF_3)_2)_2$	38

hundreds of papers dealing with synthetic and theoretical chemistry and experimental and theoretical physics as well as electrical engineering and materials science have appeared. Thus, to further aid the reader, a bibliography of pertinent review articles is given.

The success of the conference on which this volume is based was assured by the attendance of numerous chemists and physicists from diverse areas of interest. The degree of success of the meeting will be measured by the newly opened lines of communication between traditionally segregated areas of the sciences. It is hoped that such permanent professional relationships will flourish and the ramifications of future scientific discoveries will be appreciated by the scientific community as a whole. In particular, it is the goal that the conference and this volume will be the springboard for the synthesis of new materials and a better chemical understanding which will aid in a fuller appreciation of the solid state.

This Conference Organizing Committee was delighted to have 81 scientists presenting their work, ten session chairmen, and Dr. N. Bruce Hannay delivering a talk entitled "Chemistry and Solids" as our Conference Dinner Keynote Speaker. Consequently, the conference attracted a total of 235 participants. They are from three continents, including eleven countries, 29 states, the District of Columbia, and three Canadian provinces.

Acknowledgments

I am sincerely grateful to those organizations, listed in the front of this volume, which extended financial support to the Conference on *Synthesis and Properties of Low-Dimensional Materials*. Their generous support guaranteed the success of the conference and was deeply appreciated by the conference participants. It is also a pleasure to thank Dr. Arthur J. Epstein, Dr. Alan G. MacDiarmid, and Dr. Henry Taube of the Organizing Committee, and Dr. Edwin H. Abbott, Heidi Abrams, Ann Collins, Ellen Marks, and Renée Wilkerson of The New York Academy of Sciences for their invaluable assistance in bringing the program to fruition. Their hard work and constructive criticism proved to be instrumental in the consummation of the conference. Also, the help of the conference participants and particularly those who gave the Organizing Committee important criticism and valuable suggestions that aided in ensuring the success of the conference is gratefully acknowledged. Special thanks are given to four outstanding physicists, Dr. Paul M. Chaikin, Dr. Anthony F. Garito, Dr. Alan J. Heeger, and Dr. William A. Little, for consenting to deliver review lectures on the fundamentals of solid-state physics, so that the program was particularly enriching for chemists. In addition, the development of the program immensely benefited from the valuable cooperative planning with Dr. Charles B. Duke, chairman of the contiguous Gordon Research Conference on Molecular Solids. Lastly, but by no means last, deep thanks are given to Nancy Kaiser, Linda Kennedy, and Nancy Rickey for their patience and superb secretarial assistance.

References

1. Scott, A. 1916. J. Chem. Soc. 338.
2. Magnus, G. 1828, 1957. Pogg. Ann., **14**: 239. Cited in Gmelin Handbuch **52**.
3. Cox, E. G., F. W. Pinkard, W. Wardlaw & G. H. Preston. 1932. J. Chem. Soc. 2527.

4. YAMADA, S. 1951. J. Am. Chem. Soc. **73:** 1579.
5. ATKINSON, L., P. DAY & R. J. P. WILLIAMS. 1968. Nature **218:** 668.
6. BALLARD, L. F. & J. J. WORTMAN. 1970. J. Appl. Physics. **41:** 4232.
6a. KANTAK, J. F. 1969. O.A.R. Research Rev. **8:** 23.
7. MILLER, J. R. 1961. J. Chem. Soc. 4452.
8. ACKER, D. S., R. J. HARDER, W. R. HERTLER, W. MAHLER, L. R. MELBY, R. E. BENSON & W. E. MOCHEL. 1960. J. Am. Chem. Soc. **82:**6408.
8a. KEPLER, R. G., P. E. BIERSTEDT & R. E. MERRIFIELD. 1960. Phys. Rev. Lett. **5:**503.
9. KRONICK, P. L., H. KAYE, E. F. CHAPMAN, S. B. MAINTHIA & M. M. LABES. 1962. J. Chem. Phys. **36:** 2235.
10. KROGMANN, K. & H. D. HAUSEN. 1968. Z. Anorg. Allg. Chem. **358:** 67.
11. GMELIN, L. 1822, 1940. SCHW, S. **36:** 231. Cited in Gmelin Handbuch. **68C:** 201.
12. KNOP, W. 1842. Just. Liebig Ann Chem. **43:** 111.
13. ST. CLAIRE-DEVILLE, H. & H. DEBRAY. 1878. Compt. Rend. **87:** 926.
14. WILM, T. 1888. Ber. **21:** 1453.
15. SÖDERBAUM, H. G. 1894. Z. Anorg. Chem. **6:** 47.
16. WOLFFRAM, H. 1900, 1957. Ph. D. thesis. Univ. Konigsberg. Konigsberg, Germany. Cited in Gmelin Handbuch. **68D:** 616.
17. TSCHUGAEFF, L. 1905. Z. Anorg. Allg. Chem. **46:** 144.
18. BURT, J. 1910. J. Chem. Soc. 1171.
19. FREDENHAGEN, K. & G. CADENBACK. 1926. Z. Anorg. Allg. Chem. **158:** 249.
20. HIEBER, W. & H. LAGALLY. 1940. Z. Anorg. Allg. Chem. **245:** 321.
21. GOEHRING, M. & D. VOIGT. 1953. Naturwissenschaften. **18:** 482.
22. FRÖHLICH, H. 1954. Proc. Roy. Soc. London, Ser. A. **223:** 296.
23. FIELDING, P. E. & D. P. MELLOR. 1954. J. Chem. Phys. **22:** 1155.
24. MALATESTA, L. & F. CANZIANI. 1961. J. Inorg. Nucl. Chem. **19:** 81.
25. SIEMONS, W. J., P. E. BIERSTEDT & R. G. KEPLER. 1963. J. Chem. Phys. **39:** 3523.
25a. KEPLER, R. G. 1963. J. Chem. Phys. **39:** 3528.
26. LITTLE, W. A. 1964. Phys. Rev. **134:** 1416.
27. MELBY, L. R. 1965. Can. J. Chem. **43:** 1448.
28. PITT, C. G., L. K. MONTEITH, L. F. BALLARD, J. P. COLLMAN, J. C. MORROW, W. R. ROPER & D. ULKÜ. 1966. J. Amer. Chem. Soc. **88:** 4286.
29. WEISS, A. & R. RUTHARDT. 1969. Z. Naturforsch. **24b:** 256.
30. GAMBLE, F. R., F. J. DISALVO, R. A. KLEMM & T. H. GEBALLE. 1970. Science. **168:** 568.
31. WUDL, F., G. M. SMITH & E. J. HUFNAGLE. 1970. Chem. Commun. 1453.
32. DIETZ, R. E., F. R. MERRITT, R. DINGLE, S. L. HOLT, B. G. SILBERNAGEL & P. M. RICHARDS. 1971. Phys. Rev. Lett. **26:** 1186.
33. COMES, R., M. LAMBERT, H. LAUNOIS & H. R. ZELLER. 1973. Phys. Rev. **B8:** 571.
33a. COMES, R., M. LAMBERT & H. R. ZELLER. 1973. Phys. Stat. Solidi. **58B:** 587.
34. FERRARIS, J., D. O. COWAN, V. WALATKA & J. H. PERLSTEIN. 1973. J. Am. Chem. Soc. **95:** 948.
34a. COLEMAN, L. B., M. J. COHEN, D. J. SANDMAN, F. G. YAMAGISHI, A. F. GARITOL & A. J. HEEGER. 1973. Solid State Commun. **12:** 1125.
35. BROWN, T. O., B. D. CUTFORTH, C. G. DAVIES, R. J. GILLESPIE, P. R. IRELAND & J. E. VEKRIS. 1974. Can. J. Chem. **52:** 791.
36. WILSON, J. A., F. J. DISALVO & S. MAHAJAN. 1974. Phys. Rev. Lett. **32:** 882.
37. GREENE, R. L., G. B. STREET & L. J. SUTER. 1975. Phys. Rev. Lett. **34:** 577.
38. BRAY, J. W., H. R. HART, JR., L. V. INTERRANTE, I. S. JACOBS, J. S. KASPER, G. D. WATKINS, S. H. WEE & J. C. BONNER. 1975. Phys. Rev. Lett. **35:** 744.

BIBLIOGRAPHY

Monographs Devoted to 1-D Symposia

INTERRANTE, L. V., ED. 1974. Extended Interactions Between Metal Ions in Transition Metal Complexes. A. C. S. Symp. Ser. **5.** American Chemical Society. Washington, D. C.

KELLER, H. J., Ed. 1975. Low-Dimensional Cooperative Phenomena. NATO Adv. Study Inst. Ser. **7B.** Plenum Press. New York, N. Y.

KELLER, H. J., Ed. 1977. Chemistry and Physics of One-Dimensional Metals. NATO Adv. Study Inst. **25B.** Plenum Press. New York, N. Y.

PÄL, L., G. GRUNER, A. JÁNOSSY, and J. SÓLYOM, Eds. 1977. Organic Conductors and Semiconductors. Lecture Notes in Physics. **65.** Springer-Verlag. New York, N. Y.

SCHUSTER, H. G., Ed. 1975. One-dimensional conductors. Lecture Notes in Physics. **34.** Springer-Verlag. New York, N. Y.

Structural Aspects

DAHM, D. J., P. HORN, G. R. JOHNSON, M. G. MILES & J. D. WILSON. 1975. Classification of electrically conducting "electron-transfer" compounds by crystal structure. J. Cryst. Mol. Struct. **5:** 27–34.

HERBSTEIN, F. H. 1971. Crystalline π-Molecular Compounds: Chemistry, Spectroscopy, and Crystallography. *In* Perspectives in Structural Chemistry. J. D. Dunitz and J. A. Ibers, Eds. **4:** 166–395. John Wiley & Sons. New York, N. Y.

SHIBAEVA, R. P. & L. O. ATOVMYAN. 1972. The structure of conducting 7,7,8,8-tetracyanoquinodimethane complexes. J. Struct. Chem. **13:** 514–531.

STUCKY, G., A. SCHULTZ & J. WILLIAMS. 1977. Structural Aspects of One-Dimensional Conductors. Ann. Rev. of Mat. Sci. **7:** 301–331.

Physical Aspects

ANDRÉ, J.-J., A. BIEBER & F. GAULTIER. 1976. Physical properties of highly anisotropic systems: radical-ion salts and charge transfer complexes. Ann. Physique. **1:** 145–256.

BERLINSKY, A. J. 1976. Organic metals. Contemp. Phys. **17:** 331–354.

BLOCH, A. N., D. O. COWAN & T. O. POEHLER. 1974. Design and study of 1-dimensional organic conductors II: TTF-TCNQ and other organic semimetals. *In* Energy and Charge Transfer in Organic Semiconductors. K. Masuda and M. Silver, Eds. 167–176. Plenum Press. New York, N. Y.

DIETERICH, W. 1976. Ginzburg-Landau theory of phase transitions in pseudo-one-dimensional systems. Adv. Phys. **25:** 615–655.

GLÄSER, W. 1974. Experimental studies of the electron-phonon interaction of one-dimensional conducting systems. Festkörperprobleme. **14:** 205–228.

INTERRANTE, L. V. 1976. Electrical property studies of planar metal complex systems. Adv. Chem. Ser. **150:** 1–17.

LITTLE, W. A. 1965. Superconductivity at room temperature. Scientif. Amer. **212:** (2) 21–27.

MILLER, J. S. & A. J. EPSTEIN. 1976. One-dimensional inorganic complexes. Prog. Inorg. Chem. **20:** 1–151.

RICE, M. J. 1975. One-dimensional metals. 1975. Phys. Bull. **26:** 493–495.

SHCHEGOLEV, I. F. 1972. Electric and magnetic properties of linear conducting chains. Phys. Stat. Sol. **12A:** 9–45.

SOOS, Z. G. 1974. Theory of π-molecular charge-transfer crystals. Ann. Rev. Prog. Phys. Chem. **25:** 121–154.

SOOS, Z. G. & D. J. KLEIN. 1975. Charge-transfer in solid state complexes. Molec. Associations. **1:** 1–109.

YOFFE, A. D. 1976. Electronic properties of some chain and layer compounds. Chem. Soc. Rev. **5:** 51–78.

ZELLER, H. R. 1973. Electronic properties of one-dimensional solid state systems. Festkörperprobleme. **13:** 31–58.

Inorganic Materials

GOMM, P. S. 1973. Electrical conduction studies in transition metal complexes. Pentacol. 22–26.

KROGMANN, K. 1969. Planar complexes containing metal-metal bonds. Angew. Chem. (Internat. Edit.) **8:** 35–42; Angew. Chem. **81:** 10–17.
MILLER, J. S. 1976. Unusual properties associated with one-dimensional inorganic complexes. Adv. Chem. Ser. **150:** 18–30.
MILLER, J. S. & A. J. EPSTEIN. 1976. One-dimensional inorganic complexes. Prog. Inorg. Chem. **20:** 1–151.
THOMAS, T. W. & A. E. UNDERHILL. 1972. Metal-metal interactions in transition-metal complexes containing infinite chains of metal atoms. Chem. Soc. Rev. **1:** 99–120.
UNDERHILL, A. E. 1974. One-dimensional metallic conductors. Plat. Met. Rev. **18:** 21–26.

Organic Materials

BESPALOV, B. P. & V. V. TITOV. 1975. 7,7,8,8-Tetracyanoquinodimethane in addition, substitution, and complex formation reactions. Russ. Chem. Rev. **44:** 1091–1108.
ENGLER, E. M. 1976. Organic Metals. Chemtech. **6:** 274–277.
GARITO, A. F. & A. J. HEEGER. 1974. The design and synthesis of organic metals. Acct. Chem. Res. **7:** 232–240.
NARITA, M. & C. U. PITTMAN, Jr. 1976. Preparation of tetrathiafulvalenes (TTF) and selenium analogs-tetraselenafulvalenes (TSeF). Synthesis. **8:** 489–514.
PERLSTEIN, J. H. 1977. Organic metals-intermolecular migration of aromaticity. Angew. Chem. (Internat. Edit.) **16:** 519–534.
YAGUBSKII, E. B. & M. L. KHIDEKEL'. 1972. High-temperature exciton superconductivity: synthetic aspects. Russ. Chem. Rev. **41:** 1011–1026.

Polymeric Materials

GESERICH, H. P. & L. PINTSCHOVIUS. 1974. Polymeric Sulfur Nitride, $(SN)_x$—a new type of one-dimensional metal. Festkörperprobleme. **14:** 205–228.
GOODINGS, E. P. 1976. Conductivity and Superconductivity in Polymers. Chem. Soc. Rev. **5:** 95–123.
GOODINGS, E. P. 1975. Polymeric conductors and superconductors. Endeavor. **34:** 123–130.
MILLER, J. S. & A. J. EPSTEIN. 1976. One-dimensional inorganic complexes. Prog. Inorg. Chem. **20:** 1–151.
STREET, G. B. & R. L. GREENE. 1977. Preparation and properties of $(SN)_x$. IBM J. Res. Dev. **21:** 99–110.

Magnetic Materials

ACKERMAN, J. F., G. M. COLE & S. L. HOLT. 1974. The physical properties of some transition metal compounds of the ABX_3 Types. Inorg. Chim. Acta. **8:** 323–343.
ACKERMAN, J. F., E. M. HOLT & S. L. HOLT. 1974. The physical properties of linear chain systems I. The optical spectra of $[(CH_3)_4N]NiCl_3$, $Co(Mg, Ni)Cl_3$, $CsNiCl_3$, $RbNiCl_3$, and $CsNiBr_3$. J Solid State Chem. **9:** 279–296.
CARLIN, R. L. 1976. Magnetism and magnetic transitions of transition metal compounds at low temperatures. Accts. Chem. Res. **9:** 67–74.
DE JONGH, L. L. & A. R. MIEDEMA. 1974. Experiments on simple magnetic systems. Adv. Phys. **23:** 1–160.
HONE, D. W. & P. M. RICHARDS. 1974. One and two-dimensional magnetic systems. Ann. Rev. Mat. Sci. **4:** 337–363.
MILLER, J. S. & A. J. EPSTEIN. 1976. One-dimensional inorganic complexes. Prog. Inorg. Chem. **20:** 1–151.
NORDIO, P., Z. G. SOOS & H. M. MCCONNELL. 1966. Spin excitations in ionic molecular crystals. Ann. Rev. Phys. Chem. **17:** 237–260.
STEINER, M., J. VILLAIN & C. G. WINDSOR. 1976. Theoretical and experimental studies in one-dimensional magnetic systems. Adv. Phys. **25:** 87–209.

Mixed Valent Materials

ALLEN, G. C. & N. S. HUSH. 1967. Intervalence-transfer absorption. Part 1. Qualitative Evidence for Intervalence-Transfer Absorption in Inorganic Systems in Solutions and in the Solid State. Prog. Inorg. Chem. **8:** 357–389; N. S. Hush. 1967. Intervalence-transfer absorption. Part 2. Theoretical considerations and spectroscopic data. Prog. Inorg. Chem., **8:** 391–444.

COWAN, D. O., C. LEVANDA, J. PARK & F. KAUFMAN. 1973. Mixed-valence ferrocene chemistry. Acct. Chem. Res. **6:** 1–7.

ROBIN, M. B. & P. DAY. 1967. Mixed valence chemistry—a survey and classification. Adv. Inorg. Radiochem. **10:** 247–422.

Layered (2-D) and Inclusion Materials

BROWN, J. F., JR. 1962. Inclusion Compounds. Scientif. Amer. **207** (2): 82–92.

BULAEVSKII, L. N. 1976. Superconductivity and electronic properties of layered compounds. Sov. Phys. Ups. **18:** 514–532.

CRAMER, F. D. 1955. Inclusion compounds. Rev. Pure Appl Chem. **5:** 143–164.

GAMBLE, F. R., J. H. OSIECKI, M. CAIS, R. PISHARODY, F. J. DISALVO & T. H. GEBALLE. 1971. Intercalation complex of Lewis bases and layered sulfides: a large class of new superconductors. Science 493–497,

GAMBLE, F. R. & T. H. GEBALLE. 1976. Inclusion Compounds. *In* Treatise on Solid State Chemistry. N. B. Hannay, Ed. **3:** 89–156.

GEBALLE, T. H. 1971. New superconductors. Scientif. Amer. **255** (5): 22–38.

MOOSER, E. ED. 1976. Physics and chemistry of materials with layered structures. D. Reidel. Dordrecht, The Netherlands.

TOSATTI, E. 1975. Electronic superstructure of semiconductor surfaces and of layered transition-metal compounds. Festkörperprobleme **15:** 113–14.

WILSON, J. A., F. J. DISALVO & S. MAHAJAN. 1975. Charge density waves and superlattices in the metallic layered transition metal dichalcogenides. Adv. Phys. **24:**117–201.

WILSON, J. A. & A. D. YOFFE. 1969. The transition metal dichalcogenides. Adv. Phys. **18:** 193–335.

YOFFE, A. D. 1976. Electronic properties of some chain and layer compounds. Chem. Soc. Rev. **5:** 51–78.

YOFFE, A. D. 1973. Layered Compounds. Ann. Rev. Mat. Sci. **3:** 147–170.

ZALLEN, R. 1974. Phonons in two-dimensional-network crystals. *In* Proc. 12th Internat. Conf. Physics Semiconductors. M. H. Pilkuhn, Ed.: 621–625. Teubner, Stuttgart. Germany.

CHEMICAL CLASSIFICATION OF STRUCTURES AND PROPERTIES OF LOW-DIMENSIONAL INORGANIC COMPOUNDS*

P. Day

Oxford University
Inorganic Chemistry Laboratory
Oxford OX1 3QR, England

Efforts to find relationships between the crystal and electronic structures of compounds and their physical properties form the lifeblood of physical inorganic chemistry and much of solid-state physics. Ground rules for describing the electronic structures of simple molecules and solids have been available for just about fifty years now, in the form of the Heitler-London (or valence bond) model and the molecular orbital (or band) model. However, the immense variety of structures and compound types available to the chemist, as well as increasingly ingenious efforts in the field of synthesis, constantly challenge our understanding and force us to renew and refine criteria for physical behavior that previously seemed adequate to describe the paradigm cases known to the physicist. The materials whose properties form the subject matter of the conference on which this annal is based present us with many illustrations of this proposition. It may be appropriate to begin by mentioning just one of them.

In 1949 Mott[1] pointed out that quite different physical properties would be expected from compounds whose ground states were best described by a Heitler-London wavefunction from those which one would expect of a compound whose ground state was described by a molecular orbital or band wavefunction. The simplest example is that of a chain of atoms, each carrying a single valence electron. The Heitler-London wavefunction describes a ground state that is insulating, with exactly one electron localized on each atom, and with a considerable activation energy needed to create the charge fluctuations required for conductivity. The molecular orbital model, by contrast, would give us an exactly half-filled band, which permits charge fluctuations, or in other words, ionic states, and hence describes a conductor. Clearly there has to be some crossover from the realm of validity of one model to the other as a function, for example, of orbital overlap, interatomic spacing, electronic density, or some other comparable variable. Much effort over the last twenty years has gone into a search for inorganic compounds lying sufficiently close to this boundary on either side that applying some external variable such as pressure or temperature would transform the ground state from insulating to conducting. Much interesting structural chemistry and solid-state physics, mainly of oxides,[2] has come out of this activity, but the point I wish to make here is that it now appears that there exists at least one whole class of substance to which Mott's idea, at any rate in its simplest form, does not apply. According to the Mott-Hubbard model, if there is an integral number of electrons per

*Manuscript received August 31, 1977.

0077-8923/78/0313-0009 $1.75/1 © 1978, NYAS

site we either have a metal or else an insulator in which each site carries the same number of localized valence electrons. Consider, however, the many metal atom chain compounds of which Wolfram's Red Salt, $[Pt(EtNH_2)_4][Pt(EtNH_2)_4Cl_2]Cl_4 \cdot 4H_2O$, could be thought of as a prototype. These compounds are insulators (at least at ambient pressure,[3] and when not deliberately doped with impurities), and the average Pt oxidation state is +3. Yet there are many reasons[4] for believing that in fact the oxidation states of the Pt atoms alternate between +2 and +4. Instead of having one electron in each $5d_{z^2}$ orbital on every Pt atom we have alternately two and none. Why?

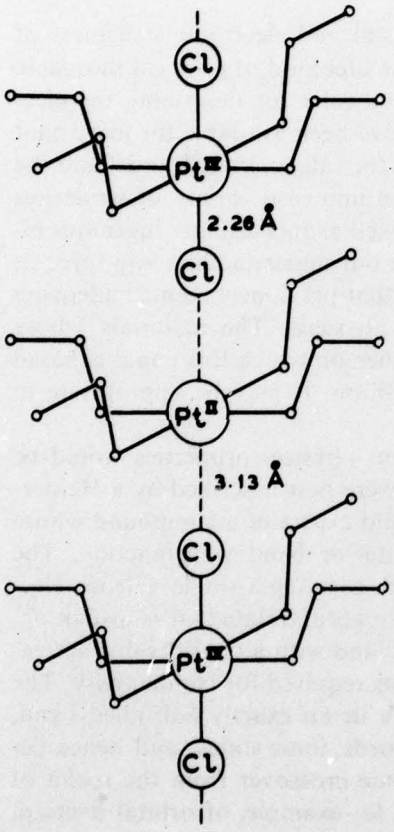


FIGURE 1. The chain structure of Wolfram's Red Salt.

The answer is that if we introduce into our chain of atoms, each carrying one valence electron, a closed-shell atom or molecule bridging every pair of adjacent atoms, then in addition to the intrasite electron correlation U and the intersite transfer integral t (which a chemist would call the electron repulsion parameter and resonance integral), we have a third variable, namely, an electron-phonon coupling constant. Inclusion of the latter can apparently make it energetically favorable for the valence electrons to pair up on alternate centers, displacements of the bridging groups providing the extra variable in the structure that leads to the new kind of ground state.

I mention this example at the outset because it illustrates how even one of the simplest structures one could envisage, the diatomic chain ... ABABA ..., contains features that require us to reappraise some of the most fundamental hypotheses of solid-state theory. Yet although we can write the "operative" part of the chain in a straightforward way, the formula of Wolfram's Red Salt given above and shown in FIGURE 1 exemplifies how relatively complicated molecular architecture is often needed before the requirements for physical behavior approximating to one- or two-dimensional can be realized. There can be no doubt, however, that the incursion into solid-state physics of a whole new range of chemical substances containing layers or chains of interacting atoms has been a strongly revitalizing intellectual influence in the last few years, bringing in its wake both new physical phenomena such as Peierls distortions and charge-density waves, and also a new kind of partnership between chemists and physicists. The object of this paper is to introduce, from a chemist's point of view, some of the compounds whose physical properties are going to be dealt with in detail by later authors, but at the same time to attempt at the broadest level some kind of synthesis between structure and properties in the low-dimensional field. Mere categorization in itself is of little value unless based on a proper appreciation of the magnitudes of the electronic factors that bring about the observed patterns of behavior.

Let us return for a moment to the Hamiltonian describing a chain of atoms, using the form introduced by Hubbard.[5] For hydrogen-like atoms it would be written in its simplest form as

$$\mathcal{H} = \sum_{\sigma} \sum_{ij} C_{i\sigma}{}^{+} C_{j\sigma} t_{ij} + U \sum_{i} n_{i\sigma} n_{i-\sigma}$$

where the summation is taken over all nearest neighbor ions i, j, on which the electron may have a spin of $\pm\sigma$. The spin direction, of course, is conserved when the electron hops from site to site, but two electrons with opposed spins on the same site repel one another to an extent determined by U. Confining our attention to compounds between metallic elements and ones with rather higher electronegativity, such as C, N, and O (though possibly also P and S), the electrons whose behavior determines the collective properties of the solid are the valence-shell electrons on the metal atoms. The transfer integral t_{ij} is therefore going to be a strong function of the metal-metal separation, which, in turn, is going to depend on the size and nature of any bridging groups or anions. If the only pathway between the metal ions lies through such bridges, transfer between the metal ion orbitals could only take place to the extent that there is a set of orbitals on the bridging group nonorthogonal to both sets of metal orbitals, and in proportion to the resulting metal-ligand covalency. Mixing between metal and ligand orbitals is of course governed by the usual symmetry considerations, which also underlie the simple rules relating the dominant sign of the magnetic exchange between localized electrons in partly filled subshells, and interacting through intervening anions, as set out originally by Kanamori[7] and Goodenough.[8] These rules have their basis in a perturbation approach[9] to electron delocalization between metal and ligand orbitals which attempts to estimate metal-ligand electron transfer by supposing mixing between two Heitler-London configurations containing different

numbers of electrons on the two centers, for example $M^{2+}A^{-}$ and $M^{+}A^{0}$. Electronic transitions between configurations of this kind are, quite simply, charge-transfer transitions. In favorable cases it may even be possible to locate the excited state in question in the optical spectrum and hence, by estimating metal-ligand resonance integrals by appropriate overlap integrals, to calculate how much electrons occupying (for example) d-orbitals are delocalized from one metal ion to another through an intervening ligand. In the context of some of the metal-organic substances to be discussed in this volume it is important to realize that, although

TABLE 1

SOME SINGLE-VALENCE LOW-DIMENSIONAL INORGANIC COMPOUNDS

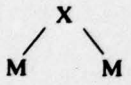
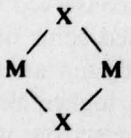
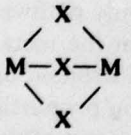
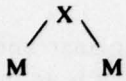
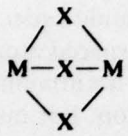
Geometry of Bridging Groups	Chains	Layers
M—X—M	Silicates (pyroxenes, amphiboles) $Sr(PbF_5)F$ $NbOCl_3$ $FeF_3 \cdot 3H_2O$	Silicates (micas and clays, e.g. montmorillonite) K_2NiF_4 and related compounds (Rb_2MnF_4, Cs_2CrCl_4, etc.) Organic intercalated structures related to $K_2NiF_4((RNH_3)_2MX_4)$) High-oxidation state ternary oxides (e.g. Ca_2MnO_4)
	Nonmetal oxides (SeO_2, Sb_2O_3) Polymers of non-metals (e.g. SN_x) CrO_3	
	4-coordinate (a) tetrahedral ($BeCl_2$, SiS_2, $KFeS_2$) (b) planar ($PdCl_2$, PtS) 6-coordinate with terminal groups $MX_2 \cdot 2Y$ (X = halogen, Y = H_2O, pyridine, ½ phenanthroline etc.)	MX_2 (a) halides of 3d elements ($FeCl_2$ etc.) (b) chalcogenides of 4d and 5d elements (TaS etc.) Oxyhalides (FeOCl)
	Hexagonal perovskites (a) halides AMX_3 (A = group IA or organic cation; M = V,Cr,Mn,Fe, Co,Ni,Ca) (b) oxides (e.g. $BaNiO_3$)	—
	Planar d^8 complexes (a) anions: $A_2[Pt(CN)_4]$ (b) neutral molecules: $Nidmg_2$, $Ptbipy_2Cl_2$ (c) salts: $[Pt(NH_3)_4][PtCl_4]$	metal-rich phases: GdCl

TABLE 2

SOME MIXED-VALENCE LOW-DIMENSIONAL INORGANIC COMPOUNDS

Geometry of Bridging Groups	Chains (1D)	Layers (2D)
M—X—M	$Pt(NH_3)_2Cl_3$, Wolfram's Red Salt, etc. Magnetic phases Mo_nO_{3n-1}	$Ca_{2-x}Y_xMnO_4$
	B-subgroup oxides: Pb_3O_4, Sb_2O_4 TlS	KCu_4S_3
	—	—
	$K_2Pt(CN)_4Br_{0.30} \cdot 3H_2O$(KCP) $K_{0.60}Ir(CO)_2Cl_2 \cdot O \cdot 5H_2O$ Gd_2Cl_3	GaS metal-rich phases: Ag_2F, Hf_2S

the kind of strategy we have just described has been applied conventionally to monoatomic bridging anions like oxide[10] or halides, there is no reason at all why we should not use it to calculate electron delocalization through polyatomic ligands that bind simultaneously to two metal ions. The formalism can be applied in a particularly neat fashion when the ligands have conjugated systems of π-orbitals, since one can then use a simple Hückel calculation as a guide to the molecular orbital coefficients in the frontier orbitals (organic chemist's nomenclature for the highest occupied and lowest unoccupied) and even to their energies. We ourselves demonstrated this point a few years ago by calculating "valence delocalization coefficients" for mixed valency Fe(II,III) and Ru(II,III) dimers and polymers in which the metal ions are bridged either by the monoatomic oxide ion, diatomic cyanide,[11] or the aromatic molecule pyrazine.[12]

In TABLES 1 and 2 are set out a series of representative examples of metal atom layer and chain compounds, categorized according to the number, and hence the geometrical arrangement, of the groups bridging the metal atoms. Clearly we cannot include every one of the enormous number of layer and chain compounds now known, but an attempt has been made to include at least one member of each of the major types. Several generalizations can be made immediately on inspecting these lists. First, there is a straightforward distinction between continuous and molecular lattices; that is, between solids in which the strongest low-dimensional interactions are carried between the metallic centers through bonds and those made up from discrete molecular units having an independent chemical existence—for example, in solution or in the gas phase. The latter comprise only chain examples because they appear to be formed exclusively by flat molecules. In that connection it is worth noticing in passing that even the most electronically innocuous aromatic hydrocarbon molecules from distinctly chain-like stacks in

crystals for this very simple reason, although the details of the structures themselves are determined by repulsions between nonbonded hydrogens on neighboring molecules. A second point is that although a few examples of compounds containing only nonmetallic elements have been included, the overwhelming proportion of the examples in TABLES 1 and 2 are compounds of metals. Polymers of nonmetals exist in large numbers, of course (e.g. silicones, phosphonitrilics, and even hydrocarbons!), but few have electronic properties that would make them interesting to a meeting of this kind.

Apart from those molecular solids consisting of essentially planar units, for which packing efficiency alone might justify columnar structures, it is an interesting and not very easy question why three-dimensional lattices should order themselves in such a way as to produce columns or layers of closely spaced atoms. In nonmetallic elements simple operation of the (8-N)-rule based on the attainment of a closed-shell valence-bond configuration is a sufficient explanation. For instance, sulphur atoms in Group VI bind two neighbors and so give chains, whereas the three near neighbors bond in pyramidal configuration around phosphorus define the infinite puckered sheets found in black phosphorus. Among some classes of compound, too, empirical regularities become clear. In the perovskites, ABX_3, there exists a very large body of lore[13] about the conditions needed to produce the hexagonal arrangement, in which chains of octahedral BX_6 groups share opposite faces, rather than the cubic type, with BX_6 groups sharing only apices. According to Stucky and his colleagues,[14] the hexagonal arrangement is favored by increasing ligand field stabilization energy, larger X groups and, up to a point, larger A groups, though beyond a certain point large organic cations may favor the formation of discrete molecular anions such as $NiCl_4^{2-}$.

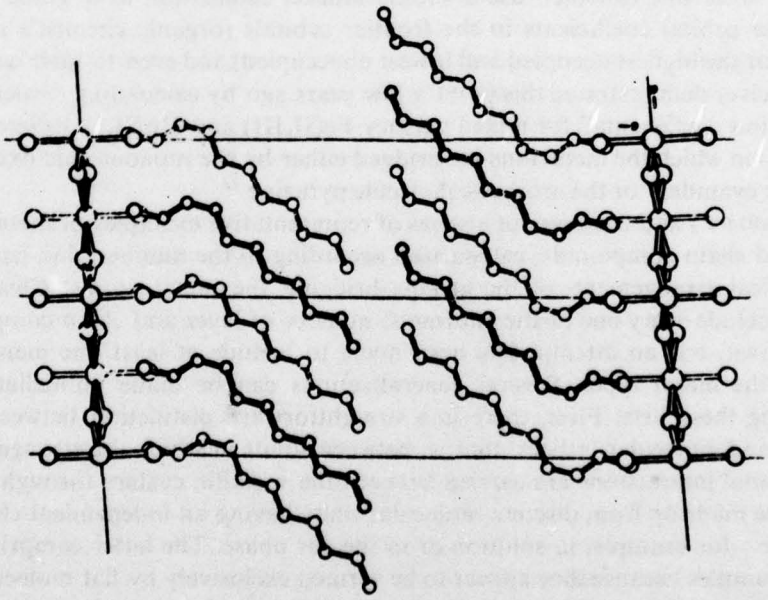


FIGURE 2. The alternating layers of organic and inorganic material in $(C_{10}H_{21}NH)_3)_2MnCl_4$.[15]

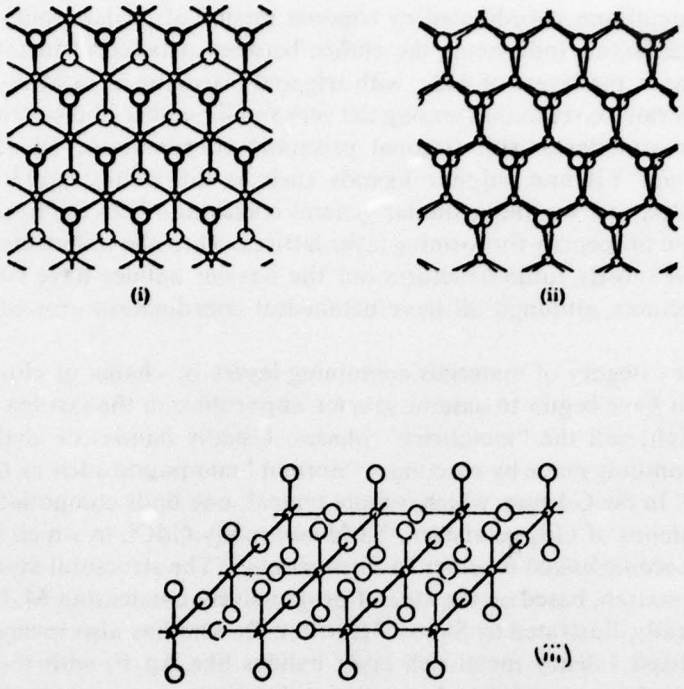


FIGURE 3. MX_2 layers. (i) $CdCl_2$ and CdI_2, (ii) MoS_2, (iii) K_2NiF_4.

Similar correlations with ionic sizes, and consequently preferred coordination numbers, can be found among the compounds with a stoichiometry A_2BX_4, where X is a halogen and A a unipositive cation. Larger X favor smaller coordination numbers around B and so produce lattices containing discrete tetrahedral molecular anions like NiI_4^{2-}. Similarly, bulky A ions lead to discrete molecular anions. On the other hand, small A, such as the lighter Group IA cations, combined with small X (F^-), form compounds with 6-coordination around B, and hence infinite layer anions of the type found in the K_2NiF_4 structure. Shape, as well as total volume, of an organic A-group is also an important influence on the type of lattice formed by the B and X groups with which it is combined. For example, tetra-alkylammonium cations, being bulky but also roughly spherical (or at any rate crab-shaped), yield compounds containing tetrahedral BX_4 anions packed in a three-dimensional array, but monoalkylammonium cations, being roughly cylindrical with the positive charge located at one end, give A_2BX_4 compounds in which the organic and inorganic constituents are segregated from one another, as in FIGURE 2.[15] Willett discusses the magnetic properties of some of these unusual sheet compounds in this volume.

In simple binary compounds MX_2 electronic considerations are as important as mere size in determining whether a three-dimensionally infinite lattice or a layer lattice is formed. For example, many transition metal oxides with the stoichiometry MO_2 have lattices based on the rutile structure, i.e., essentially three-dimensional, while the corresponding sulphides, selenides, and tellurides have layer structures, either of the CdX_2 type, as shown in FIGURE 3(i), or like MoS_2 (FIGURE 3(ii)),

containing metal ions coordinated by trigonal prisms of chalcogenide atoms. In describing the factors influencing the choice between octahedral metal atom coordination, as in the layers of TiS_2, with trigonal prismatic as in MoS_2 and WS_2, it may be relevant to recall that among the very small number of discrete molecular coordination complexes with trigonal prismatic coordination, 5d elements in Groups VI and VII and sulphur ligands such as dithiolates figure strongly.[16] Among halides, too, we find a similar general correlation between ligand electronegativity and propensity for forming layer lattices. Thus the difluorides of the 3d elements have mostly rutile structures but the heavier halides have either $CdCl_2$ or CdI_2 structures, although all have octahedral coordination around the metal atoms.[17]

A further category of materials containing layers or chains of closely spaced atoms, which have begun to assume greater importance in the last few years, are what one might call the "metal-rich" phases. Usually halides or chalcogenides, these are commonly made by reacting a "normal" compound such as $GdCl_3$ with excess metal. In the Gd case, which is quite typical, one finds compounds Gd_2Cl_3, containing chains of Gd_6 octahedra,[18] and eventually GdCl, in which these octahedra have become linked together to form sheets.[19] The structural systematics of this transformation, based on the idea of progressively condensing M_6Cl_8 groups, have been neatly illustrated by Simon[20] (FIGURE 4), who has also reviewed the entire field. Mixed valency metal-rich layer halides like Ag_2F, with the anti-CdI_2 structure, have been known for many years,[21] but have more recently been joined by the chalcogenides Hf_2S,[22] Nb_2Se,[23] and so on. In all examples of this type the concentration of metal atoms is sufficiently high for one to be able to talk of metallic lattices, in one or two dimensions, separated by nonmetal atoms.

Contrasting with the kind of metallic chains in metal-rich compounds, in

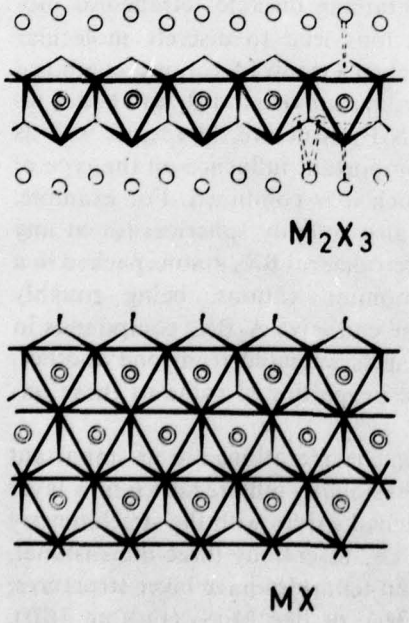


FIGURE 4. Derivation of metal-rich chain and layer structures by condensing M_6X_8 units.[20]

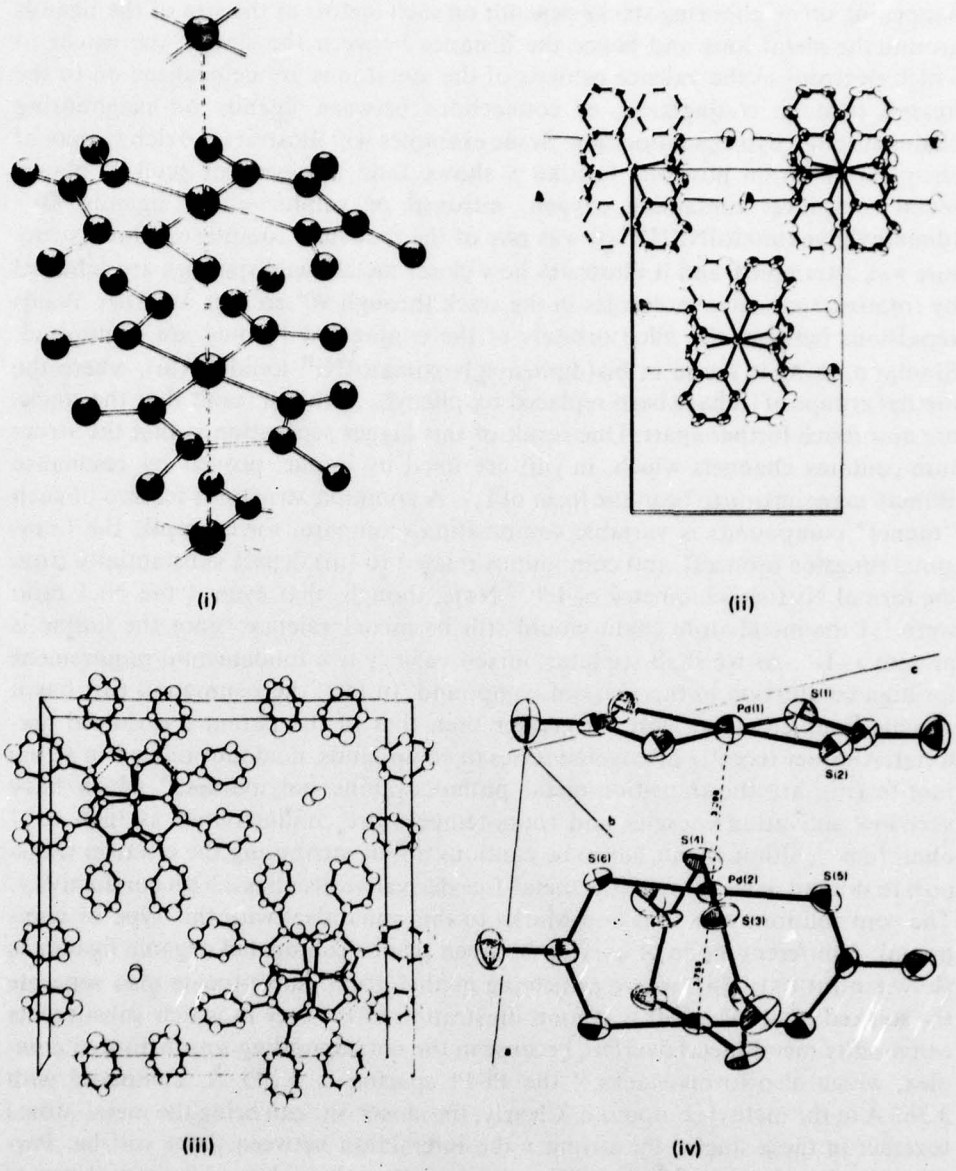


FIGURE 5. Examples of metal chain compounds. (i) Bis(dimethylglyoximato)Ni(II),[24] (ii) Bis(N-ethylpyridinecarboxaldiminato)Pt(II),[29] (iii) Bis(diphenylglyoximato)Ni(II) iodide,[25] (iv) Bis(dithioacetato)Pd(II).[31]

which the repeat unit is itself a metal cluster, metal atom chain compounds formed by square planar complexes containing more elaborate ligands and chelating agents are characterized by strings of singly connected metal atoms. Whether the average oxidation state of the metal atoms is integral or not, simple strings of metal atoms then form the dominant structural feature. How much electrons, excitons, magnons, or phonons propagating on one stack are influenced by what is

happening on neighboring stacks depends on such factors as the size of the ligands around the metal ions and hence the distance between the stacks, the extent to which electrons in the valence orbitals of the metal ions are delocalized on to the ligands through conjugation, or connections between ligands on neighboring chains through hydrogen-bonding. Some examples will illustrate the rich variety of chemical variation possible. FIGURE 5 shows four instances of stacked planar metal complexes containing oxygen, nitrogen or sulphur-donor ligands. Bis-(dimethylglyoximato)Ni(II)[24] (i) was one of the first such complexes whose structure was determined, and it illustrates how closer metal-metal spacings are achieved by rotating successive molecules in the stack through 90° so that Van der Waals repulsions between the filled orbitals of the conjugated ligands are minimized. Similar packing is found in bis(diphenylglyoximato)Ni^{II} iodide[25] (iii), where the methyl groups of (i) have been replaced by phenyls, with the result that the stacks are now much further apart. One result of this bigger separation is that the structure contains channels which, in (iii) are filled by iodine, proved by resonance Raman experiments to be in the form of I_3^-. A common structural feature of such "tunnel" compounds is variable composition (compare, for example, the hexagonal tungsten bronzes), and compounds related to (iii) depart substantially from the formal Ni:I stoichiometry of 1:1.[26] Note, though, that even if the Ni:I ratio were 1:1 the metal atom chain would still be mixed valency, since the iodine is present as I_3^-. As we shall see later, mixed valency is a fundamental requirement for high conduction in this class of compound. In fact, the compound (iii) has a specific conductivity at least 10^5 greater than that of the parent unoxidized material. Another recently discovered series of compounds, no doubt related in structure to (iii), are the transition-metal phthalocyanine polyiodides,[27] which have very low activation energies and room-temperature conductivities as high as 1 $ohm^{-1}cm^{-1}$, although one has to be cautious about attributing the electron transport to d-band overlap, since the metal-free derivative also has a high conductivity. The contributions of Keller and Marks to this annal deal with this type of compound. A different mode of overlap between planar conjugated organic ligands is shown in FIGURE 5(ii), where projecting methyl group substituents also separate the stacked molecules.[28] It is a good illustration of the way in which substituents can modify metal-metal overlap, because in the corresponding unsubstituted complex, which also forms stacks,[29] the Pt-Pt spacing is 3.245 Å, compared with 3.363 Å in the methyl compound. Clearly, the closer one can bring the metal atoms together in these stacks, the stronger the interaction between them will be. Particularly close intermetallic spacings can sometimes be achieved in complexes of sulphur-donor ligands such as the dithiolates, though in bis(ethylenedithiolate) Pd(II) and –Pt(II) this results in formation of discrete dimers, which are not themselves stacked together.[30] Another fascinating possibility (FIGURE 5(iv)) is to join the planar units together by means of bridging ligands, in this case simply dithioacetate, but while the really close contact (2.755 Å) takes place within a discrete dimer, one crystal modification of bis(dithioacetate)Pd(II) contains stacks of dimers, and another contains stacks consisting of alternating dimers and monomers.[31]

It seems to be a reasonable generalization that for really substantial intermetallic interactions in stacked planar Group VIII metal complexes, sufficient, for

example, to yield a high conductivity, the metal-metal spacing should be less than about 3.1 Å. Thus the Schiff base complex of FIGURE 5 (ii) is rather a good insulator. This requirement creates a fundamental difficulty when the ligands bound to the metal ions contain π-electrons, because the metal ions are required to be closer together than the normal Van der Waals approach distance between conjugated organic molecules. In cases where the four groups bound in a square plane around the metal ion have a rod-like shape, for instance, cyanides, the steric problem can be solved by rotating alternate metal complex molecules in the stack so that the ligands avoid one another. Williams and his colleagues[32] have pointed out that in a series of tetracyanoplatinite salts, with both single and mixed valency, there appears to be a rough correlation between Pt-Pt spacing and the torsion angle between adjacent $Pt(CN)_4$ units, varying from a completely eclipsed arrangement

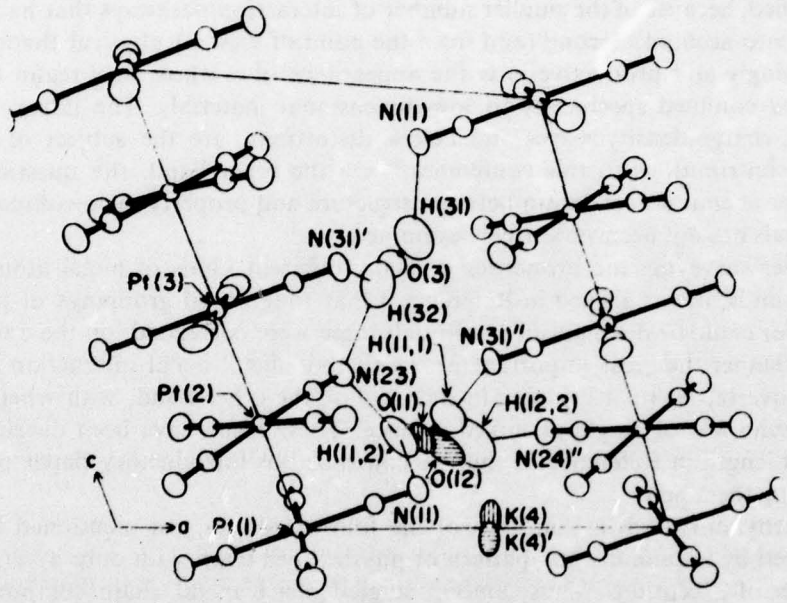


FIGURE 6. Interchain hydrogen bonding in $K_{1.75}Pt(CN)_4 \cdot 1.5H_2O$.[32,34]

in $Na_2Pt(CN)_4 \cdot 3H_2O$ (Pt-Pt spacings 3.65 and 3.75 Å) to completely staggered in $K_2Pt(CN)_4Br_{0.30}3H_2O$ (Pt-Pt spacing 2.89 Å). The point is developed further in Williams' contribution to this volume. On the other hand, Van der Waals repulsion between the cyanides cannot be the only factor determining the torsion angle because in $Rb_2Pt(CN)_4 \cdot 1.5H_2O$, with a Pt-Pt spacing of 3.48 Å the torsion angles vary from 29.2 to 35.2°, but in $Rb_2Pd(CN)_4 \cdot H_2O$ (Pd-Pd spacing 3.72 Å) the torsion angles are only 15.7–16.8°.[33] Since this class of compound invariably contains water molecules separating the stacks along with the alkali metal cations, the other important influence on the arrangement of the cyanide groups is hydrogen-bonding to the nitrogen atoms. A particularly clear illustration of this phenomenon is $K_{1.75}Pt(CN)_4 \cdot 1.5H_2O$[32,34] (FIGURE 6).

Among the low-dimensional compounds we have been describing are examples of metals, insulators, semiconductors, superconductors, ferromagnets, antiferromagnets, and so on; i.e., just about every kind of solid-state physical behavior that could possibly be found. One might perhaps just be tempted to say, therefore, that the electronic factors that determine this behavior are only a trivial extension of the well-known principles at work in simple three-dimensional lattices, like the transition metal oxides. In general terms this is, of course, true. The symmetry requirements of orbitals involved in direct or indirect magnetic exchange pathways and the balance of on-site or intersite electron repulsion and transfer integrals, for example, are all "local" factors dependent on near-neighbor pairwise interactions and thus independent of dimensionality as such. Nevertheless, restricting the dominant intermetallic interactions to one or two dimensions by the kind of structural constraints we have been describing has two important consequences. First of all, the correlation of structure and properties is greatly simplified, because of the smaller number of interaction pathways that have to be taken into account. Second (and from the point of view of physical theory, very intriguingly and productively) is the appearance of a whole new realm of phenomena confined specifically to low-dimensional materials. The latter, for example, charge-density waves and Peierls distortions, are the subject of several other contributions to this conference.[35] On the other hand, the question of a broader chemical correlation between structure and property in low-dimensional materials has not been very widely examined.

After surveying the properties of many different kinds of metal atom chain compounds, it was argued in Reference 4 that four broad groupings of physical behavior could be distinguished, and that these were correlated, on the one hand, with whether the most important near neighbor metal-metal interaction was by direct overlap or *via* a bridging ligand, and on the other hand, with whether the compound was of single or mixed valence. These ideas have been developed at greater length in Reference 36, but we conclude this introductory paper by summarizing them here.

Briefly, our thesis is that each of the four categories just mentioned is characterized by a quite distinct pattern of physical behavior, with only a very small number of exceptions. Thus, among single-valence metal chain compounds in which the intermetallic interaction is carried by bridging anions, for example the hexagonal perovskites, there are no metallic conductors, and the overwhelming proportion are magnetic insulators. Single-valence metal chains having direct metal-metal contact are likewise insulating, unless doped with mixed-valence impurities, but in the best-known examples, such as the tetracyanoplatinites or Magnus' Green Salt, the intermetallic interaction is strong enough to have quite a marked effect on their optical properties, as described by Yersin (this volume). Nevertheless, because they are not photoconductors,[37] one has to conclude that even in the excited state electrons and holes do not become uncoupled. Indeed, in the tetracyanoplatinites the way in which the energies of the excited states vary with intermetallic distance strongly supports the view that they should be described to a first approximation as neutral Frenkel excitons propagating along the stacks of molecules.[38,39]

Mixed valency, defined either as fluctuating or nonintegral electron occu-

pancy of each metal atom site, is a potent factor leading to higher conduction in chain compounds because much less energy is needed to move a charge fluctuation already built into the chain than to create an electron-hole pair in a chain in which each metal atom carries the same integral charge. It is interesting to note that an explanation along these lines has also been put forward[40] for the high conductivity of the organic charge-transfer salts such as TTF-TCNQ which contain segregated stacks of donor and acceptor molecules. Nevertheless, not all mixed valence metal chain compounds conduct; the example we began with—Wolfram's Red Salt—is a good insulator. This is because chains containing anions or molecules bridging between the metal atoms have, as we showed above in the case of Wolfram's Red Salt, a very simple mechanism of electron-phonon interaction that pins the phase of the charge fluctuation along the chain. The result is a simple superlattice of metal oxidation states (... II, IV, II, IV ... in Wolfram's Red Salt) which places the system in class II of our old classification of mixed-valence compounds[41] and consequently leads to an insulating ground state. Still, in mixed-valence anion-bridged metal chains the lowest optically accessible excited state is no longer a neutral Frenkel exciton but an ionic exciton arising from an intervalence charge-transfer transition. The Franck-Condon transition energy of this kind of state is usually of the order of 1–2 eV[36] (the origin of the red color of Wolfram's Salt), but the relaxed excited state must be much lower. How far is the bridging anion displaced when an electron is transferred from Pt(II) to Pt(IV) in Wolfram's Salt? An elegant means of answering this question is resonance Raman spectroscopy, as shown in this volume by Clark. It is precisely the axial stretching mode between the metal and the bridging anion that is selectively enhanced in intensity when one excites the Raman spectrum of this type of compound by irradiating within the Franck-Condon envelope of the intervalence absorption band. The relative intensities of successive overtones of this fundamental enable one to estimate how far along the vibrational coordinate the oscillator is displaced in the relaxed electronic excited state. A calculation[42] based on Mingardi and Siebrand's[43] theory of the resonance Raman effect suggests that at the minimum in the potential energy surface of the Pt(II) → Pt(IV) charge-transfer excited state, the bridging halide ion indeed is nearly equidistant from the two Pt ions, as expected if the Heitler-London configuration of the state is close to Pt(III), Pt(III).

All this implies very strongly that mixed-valence metal chain compounds with bridging groups are unlikely to be good conductors. Removing the bridging groups and bringing the metal atoms into direct contact has two consequences which are expected to increase the chances of finding high conductivity. First, the transfer integral is enhanced but equally important, if charge-compensating anions, necessarily present in simple stoichiometric ratios, are removed from the metal chain itself and placed in sidegroups or channels between the metal chains; one then has an opportunity of varying the average oxidation state, or electron occupancy of the metal atoms' valence shells, away from simple ratios 1:1, 1:2, and so on. This is important if one is to stabilize a conducting ground state, partly because electron-phonon interactions that may trap the desired charge mobility are thereby weakened, but also because the active phonons might have wave-vectors incommensurate with the underlying lattice. Should that be the case the resulting charge-density wave might still be able to carry a current. By contrast, in Wolf-

TABLE 3

PROPERTIES OF METAL-CHAIN COMPOUNDS WITH EXAMPLES FROM THIS VOLUME

	Properties			Examples
	Optical	Magnetic	Electron Transport	(This Volume)
Single Valence				
Bridged	discrete weak ligand field transitions	weak ferro- or antiferromagnetic superexchange	insulators	Willett
Direct	ligand field bands strongly perturbed. Allowed bands strongly shifted by dipolar coupling.	diamagnetic	insulators conducting under pressure	Williams, Yersin Gordon *et al.*, Geoffroy, *et al.*
Mixed Valence				
Bridged (Robin-Day class II)	lowest transition is ionic exciton ($M \rightarrow M$ charge transfer)	diamagnetic	semiconductors metallic under high pressure	El Sharif *et al.*, Meyer Taube
Direct (Robin-Day class III)	plasma edge in visible reflectivity		metals at 300°K become semiconducting at low temperature (Peierls distortion)	Williams, Underhill, Reis, Chartier *et al.*, Metgert *et al.*, Stucky *et al.*, Balch, Keller, Marks, Endres

ram's Red Salt one might regard the superlattice of trapped oxidation states as a consequence of a strong Peierls distortion, producing a static charge-density wave with a wave-vector of 0.5 in the Brillouin zone of the original undistorted diatomic chain. It is in fact among the mixed-valence directly interacting metal chains that the one-dimensional metallic conductors are found, for instance KCP ($K_2Pt(CN)_4Br_{0.30} \cdot 3H_2O$) and its cation-deficient analog in FIGURE 6. Much more is written about them later in this volume. In TABLE 3 we simply summarize the behavior of the four categories of metal chain. Although much of the recent excitement about low-dimensional compounds has resulted from the fact that one could even synthesize such things as "molecular metals" (a conjunction of adjective and noun that would have sounded totally paradoxical five years ago), I believe that as chemists and physicists we should not lose sight of the sheer variety of other types of physical behavior accessible to us through this very broad class of substances. Potentially most exciting of all, though, is the opportunity it presents for chemists to devise quite new kinds of material showing phenomena unpredictable by the physical theories designed in earlier days to rationalize the behavior of much simpler substances. It is to be hoped that the introductory survey presented here has succeeded both in showing some of this variety and setting out some chemical guidelines by which crystal and electronic structure may be related to properties in this fascinating group of substances.

NOTES AND REFERENCES

1. MOTT, N. F. 1949. Proc. Phys. Soc. (London) **A62:** 416.
2. ADLER, D., for example. 1968. Rev. Mod. Phys. **40:** 729.
3. INTERRANTE, L. V. & F. BUNDY. 1974. Inorg. Chem. **13:** 1158.
4. DAY, P. 1974. *In* Extended Interactions between Transition Metal Ions. L. Interrante, Ed.: 234. Amer. Chem. Soc. Washington, D.C.
5. HUBBARD, J. 1963. Proc. Roy. Soc. **A276:** 238.
6. GRAY, H. B. & C. J. BALLHAUSEN. 1962. Molecular Orbital Theory. Benjamin. New York, N.Y.
7. KANAMORI, J. 1959. J. Phys. Chem. Solids **10:** 87.
8. GOODENOUGH, J. B. 1960. Phys. Rev. **117:** 1442.
9. ANDERSON, P. W. 1950. Phys. Rev. **79:** 350.
10. NESBET, R. K. 1960. Phys. Rev. **119:** 658.
11. MAYOH, B. & P. DAY. 1973. J. Chem. Soc., Dalton Trans.: 846.
12. MAYOH, B. & P. DAY. 1974. Inorg. Chem. **13:** 2223.
13. GOODENOUGH, J. B. & J. M. LONGO. 1970. *In* Landolt-Bornstein Tabellen. New Series, Group III. Vol. **4.**
14. SEKUTOWSKI, D., R. JUNGST & G. D. STUCKY. 1974. *In* Extended Interactions between Transition Metal Ions. L. Interrante, Ed.: 142. Amer. Chem. Soc. Washington, D.C.
15. CIAJOLO, R. M., P. CORRADINI & V. PAVONE. 1976. Gazz. Chim. Ital. **106:** 807.
16. EISENBERG, R. & J. A. IBERS. 1965. J. Amer. Chem. Soc. **87:** 3776.
17. WELLS, A. F. 1962. Structural Inorganic Chemistry. 3rd edit.: 334. Clarendon Press. Oxford, England.
18. LOKKEN, D. A. & J. D. CORBETT. 1973. Inorg. Chem. **12:** 556.
19. SIMON, A., H. MATTAUSCH & N. HOLZER. 1977. In press.
20. SIMON, A. 1976. Chem. Unserer Zeit. **10:** 1.
21. OTT, H. & H. SEYFARTH. 1928. Z. Krist. **67:** 430.
22. FRANZEN, H. F. & J. GRAHAM. 1966. Z. Krist. **123:** 133.
23. COWARD, B. R., L. R. NORRBY & H. F. FRANZEN. 1969. Acta Cryst. **B25:** 1729.
24. FRASSON, E., C. PANATTONI & R. ZANNETTI. 1959. Acta Cryst. **12:** 1027.

25. GLEIZES, A., T. J. MARKS & J. A. IBERS. 1975. J. Amer. Chem. Soc. **97:** 3545.
26. MILLER, J. S. & C. H. GRIFFITHS. 1977. J. Amer. Chem. Soc. **99:** 749.
27. PETERSEN, J. L., C. R. SCHRAMM, D. R. STOJAKOVIC, B. M. HOFFMAN & T. J. MARKS. 1977. J. Amer. Chem. Soc. **99:** 287.
28. PHELPS, D. W., W. F. LITTLE & D. J. HODGSON. 1976. Inorg. Chem. **15:** 2263.
29. NORDQUIST, K. W., D. W. PHELPS, W. F. LITTLE & D. J. HODGSON. 1976. J. Amer. Chem. Soc. **98:** 1104.
30. BROWALL, K. W., T. BURSH, L. V. INTERRANTE & J. S. KASPER. 1972. Inorg. Chem. **11:** 1800.
31. PIOVESANA, O., L. SESTILI, C. BELLITTO, A. FLAMINI, M. TOMASSINI, P. F. ZANAZZI & A. R. ZANZARI. 1977. J. Amer. Chem. Soc. In press.
32. WILLIAMS, J. M., K. D. KEEFER, D. M. WASHECHECK & W. P. ENRIGHT. 1976. Inorg. Chem. **15:** 2446.
33. KOCH, T. R., P. L. JOHNSON & J. M. WILLIAMS. 1977. Inorg. Chem. **16:** 640.
34. REIS, A. H., S. W. PETERSON, D. M. WASHECHECK & J. S. MILLER. 1976. Inorg. Chem. **15:** 2455.
35. See, for example, CHAIKIN, P., A. J. HEEGER & W. A. LITTLE. This Annal.
36. DAY, P. 1977. *In* Chemistry and Physics of One-dimensional Metals. H. J. Keller, Ed.: 197. Plenum Publishing Corp. New York, N.Y.
37. PAINE, J. & P. DAY. 1976. Unpublished work.
38. DAY, P. 1969. Inorg. Chem. Acta Rev. **3:** 81.
39. DAY, P. 1975. J. Amer. Chem. Soc. **97:** 1588.
40. TORRANCE, J. B. *In* Chemistry and Physics of One-dimensional Metals. H. J. Keller, Ed. Plenum Publishing Corp. New York, N.Y., and this volume.
41. ROBIN, M. B. & P. DAY. 1967. Adv. Inorg. Chem. Radiochem. **10:** 247.
42. DAY, P. 1977. Unpublished work.
43. MINGARDI, M. & W. SIEBRAND. 1975. J. Chem. Phys. **62:** 1074.

DISCUSSION

J. TORRANCE: There are many effects in organic materials that are strongly analogous to the effects you have described for inorganic materials. In particular, mixed valence is important in both the TTF halides and (TTF)(TCNQ). In addition, the difference you pointed out between integral and subintegral number of electrons per molecule is the difference between insulators and metals in the case of the organic systems.

DAY: The significant feature in all the highly conducting organic and inorganic systems is indeed a nonintegral average number of valence electrons per molecule. On the other hand, at least in the inorganic systems, one has to be aware that the reverse of the preceding statement is *not* always true: a nonintegral number of electrons per molecule is necessary, but not a sufficient condition because charge fluctuations may become very deeply pinned as a result of the different geometrical coordination preferences of different metal-oxidation states.

DESIGN AND SYNTHESIS OF HIGHLY CONDUCTING ONE-DIMENSIONAL MATERIALS*

Joel S. Miller

Xerox Webster Research Center
Rochester, New York 14644

Pseudo-one-dimensionality, 1-D, has been ascribed to inorganic and organic materials that possess an extended columnar structure and anisotropic intensive physical properties in the solid state. Such materials which possess interplanar spacings less than the sum of the van der Waals spacings, nominally < 3.0 Å for inorganic,[1] and <3.3 Å for organic[2,3] based colinear chains, exhibit a variety of significantly anisotropic and unusual optical, magnetic, electrical, and mechanical properties.[4] Some examples of novel chemical and physical properties associated with 1-D materials are listed in TABLE 1. A property that has been a barometer for the interest in 1-D materials is the electrical conductivity. Several 1-D materials exhibit high room-temperature conductivity ($\sim 10^{12}$ times larger than typical inorganic and organic insulators[5,6]), a metallic state at room temperature, and metal-semiconductor, which is commonly denoted as a metal-insulator transition at lower temperature.[7] Thus, due to novel chemical and physical properties associated with one-dimensional materials, which potentially lend themselves to future technologies, and to the historical scientific and technological interest in finding a high temperature superconductor,[9] there has been an avalanche of industrial, governmental, and academic interest in this area.[4] In order to fully understand and extend the salient features and ramifications of the chemical and physical properties of such pseudo-one-dimensional systems, however, new 1-D inorganic, organic, and polymeric materials are required. Furthermore, the chemistry of established materials have to be better understood.

The highly conducting materials thoroughly characterized to date are few in number and are represented by exemplary inorganic. $KCP[K_2Pt(CN)_4Br_{0.30} \cdot 3H_2)]$[10] (FIGURE 1a), organic, (TTF)(TCNQ),[11] [tetrathiofulvalenium-7,7,8,8-tetracyano-*p*-quinodimethanide] (FIGURE 1b), and polymeric, poly(sulfurnitride), $(SN)_x$,[12] (FIGURE 1c) materials. Some specific examples of novel anisotropic physical properties that have been reported for these materials are tabulated in TABLE 2.

Herein we describe the synthetic features of the transition metal and organic charge transfer salts that are amenable to manipulation so that new and modified materials exhibiting some of the properties listed in TABLES 1 and 2 can be prepared. No attempts are made to rigorously discuss the synthetic features of $(SN)_x$.[13] Poly(sulfurnitride) is anomalous among the materials considered herein in the sense that its electronic properties are those of an anisotropic polymer exhibiting superconductivity.[14]

The salient features of a metallic state are now presented. Then the following section discusses the design considerations currently considered for the design and

*Manuscript received July 11, 1977.

0077-8923/78/0313-0025 $1.75/1 © 1978, NYAS

TABLE 1

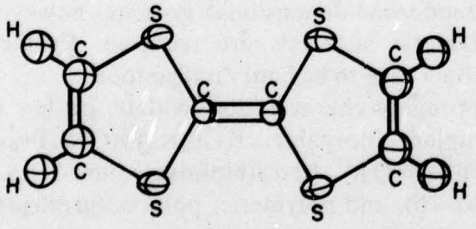
NOVEL CHEMICAL AND PHYSICAL PROPERTIES ASSOCIATED WITH 1-D SUBSTANCES

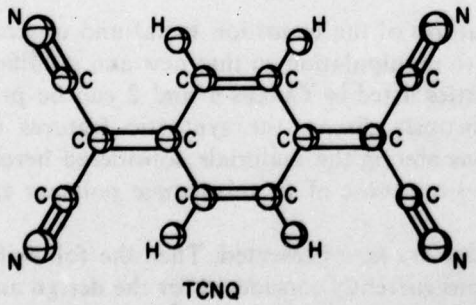
High Conductivity
Metallic State
Metal-Insulator Transition
Charge Density Wave
Superconductivity
Homogeneous Nonstoichiometry
Mixed-Valency (Homo- and Heterogeneous)
Cooperative Magnetic Interactions
Large Anisotropic Ratios for Intensive Properties

synthesis of organic and inorganic materials. Finally, the synthetic efforts throughout the world as well as general preparative techniques are briefly summarized.

THE METALLIC STATE

Since metal-like materials are the principal synthetic goal in this paper, it is apropos to describe briefly the attributes of a metallic state that are useful in its characterization. A metallic state implies several characteristics associated with, but are not exclusive to, elemental metals.[1,15] Fundamentally, metals possess a partially filled electron energy band[16] from which its distinguishing features are derived. A partially occupied band implies the existence of extended unoccupied electronic energy levels infinitesimally separated in energy (i.e., $\ll kT$) from the





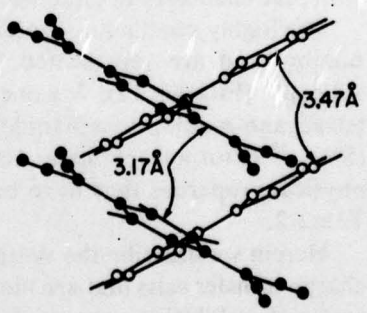


FIGURE 1a. Structure of the prototype 1-D inorganic($K_2Pt(CN)_4Br_{0.30} \cdot 3H_2O$; KCP)[10] system.

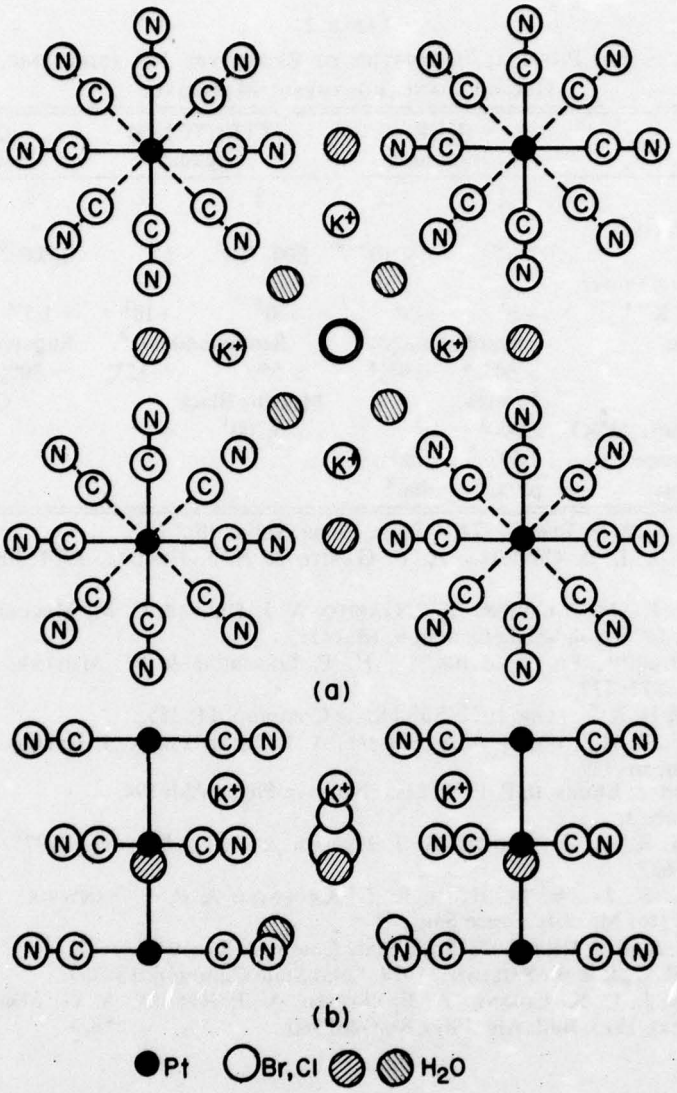


FIGURE 1b. Structure of the prototype 1-D organic $[(TTF)(TCNQ)]$[11] system. Dark circles refer to TCNQ.

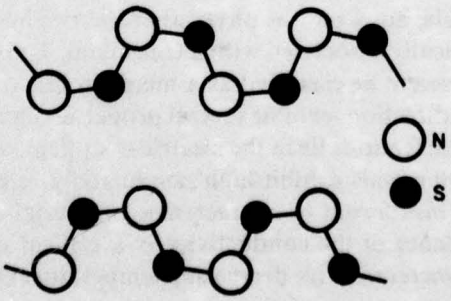


FIGURE 1c. Structure of the prototype 1-D polymeric $[(SN)_x]$[12] system.

TABLE 2

SELECTED PHYSICAL PROPERTIES OF PROTOTYPE 1-D INORGANIC, ORGANIC, AND POLYMERIC MATERIALS

	KCP Inorganic		(TTF)(TCNQ) Organic		$(SN)_x$ Polymeric	
	∥	⊥	∥	⊥	∥	⊥
Conductivity, R_1 T, $\Omega^{-1}cm^{-1}$	300[a]	1×10^{-3}[a]	500–700[5]	5[b]	3,700[14,d]	370[14]
Thermoelectric Power, 300°K, $\mu V\ K^{-1}$	−3[c]	−8[c]	−30[f]	+18[f]	−1.5[m]	−3.5[m]
Ground State	Semiconductor[a]		Semiconductor[b]		Superconductor[14]	
Reflectivity	> 80%[g]	< 9%[g]	> 55%[h]	~ 12%	~ 90%[d]	~ 9%[d]
Appearance	Bronze		Metallic Black		Gold	
Dielectric Const. (4°K)	3,000[l]	4[l]	> 3,200[i]	6[i]		
Refractive Index[j]	2.32	1.80				
Magnetic State	para.[k]	dia.[k]				

[a]ZELLER, H. R. & H. BECK. 1974. J. Phys. Chem. Solids **35:** 77.

[b]COHEN, M. J., L. B. COLEMAN, A. F. GARITO & A. J. HEEGER. 1974. Phys. Rev. B. **10:** 1298.

[c]CHIANG, C. K., M. J. COHEN, A. F. GARITO, A. J. HEEGER, C. M. MIKULSKI & A. G. MACDIARMID. 1976. Solid State Commun. **18:** 1451.

[d] ~ <18,000 cm^{-1}, PINTSCHOVIUS, L., H. P. GESERICH & W. MOLLER. 1975. Solid State Commun. **17:** 477.

[e]KUSE, D. & H. R. ZELLER. 1972. Solid State Commun. **11:** 355.

[f]KWAK, J. F., P. M. CHAIKIN, A. A. RUSSEL, A. F. GARITO & A. J. HEEGER. 1975. Solid State Commun. **16:** 729.

[g]< 15,000 cm^{-1}; BRÜESCH, P. 1975. Lect. Notes in Physics **34:** 194.

[h]See Reference 3.

[i]KHANNA, S. K., A. F. GARITO, A. J. HEEGER & R. C. JAKLEVIC. 1975. Solid State Commun. **16:** 667.

[j]MARTIN, D. S., JR., R. M. RUSH, R. F. KROENING & P. F. FANWICK. 1973. Inorg. Chem. **12:** 301 (for Magnus' Green Salt).

[k]MENTH, A. & M. J. RICE. 1972. Solid State Commun. **11:** 1025.

[l]JAKLEVIC, R. C. & R. B. SAILLANT. 1974. Solid State Commun. **15:** 307.

[m]COHEN, M. J., C. K. CHIANG, A. F. GARITO, A. J. HEEGER, A. G. MACDIARMID & C. M. MIKULSKI. 1975. Bull. Am. Phys. Soc. **20:** 360.

extended occupied states. This allows for a net change in electron momentum when an electric field is applied. Consequently, metals are good conductors and exhibit a variety of other distinguishing properties.[15]

A molecular solid may not possess all of the above criteria as applied to elemental metals; however, the physical properties in some situations simulate several that are typically associated with a true metal. Thus, the metal label is a misnomer. However, even to be classified as a metal by relaxed criteria, a substance must, in at least one direction, exhibit several properties characteristic of a metal. The most characteristic features lie in the electrical, optical, and magnetic properties.

Although metals exhibit high conductivity, e.g. $\sigma > 10\ \Omega^{-1}\ cm^{-1}$, high conductivity is insufficient to characterize a material as being metallic. The temperature dependence of the conductivity is a critical measurement. The conductivity for a metal *increases* with decreasing temperature (FIGURE 2(a)), whereas for semi-

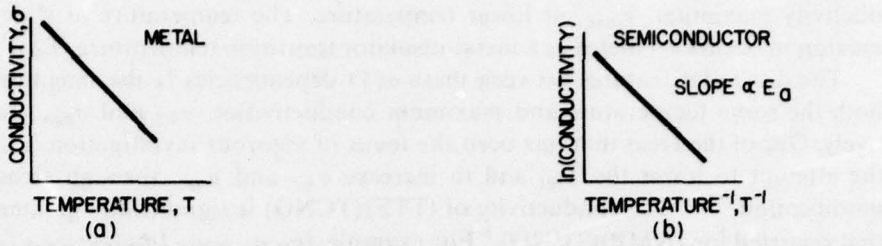


FIGURE 2. Illustrations of the idealized temperature dependence of the conductivity for a metal (a) and a semiconductor (b).

conductors (even semiconductors with a large room-temperature conductivity, $\gtrsim 10\ \Omega^{-1}\ cm^{-1}$) the conductivity *decreases* with decreasing temperature. FIGURE 2 depicts these idealized temperature dependences of conductivity.

It is important to point out that the typical metal-like 1-D inorganic or organic complex exhibits either the temperature-dependent conductivity illustrated[5] by (TTF)(TCNQ) or (NMP)(TCNQ)[17] in FIGURE 3. These two complexes exemplify the two observed types of temperature dependencies of the conductivity for 1-D metals. The common features are that both prototype materials exhibit a metal-like state; i.e., $d\sigma/dT < 0$, at higher temperature and both materials reach a con-

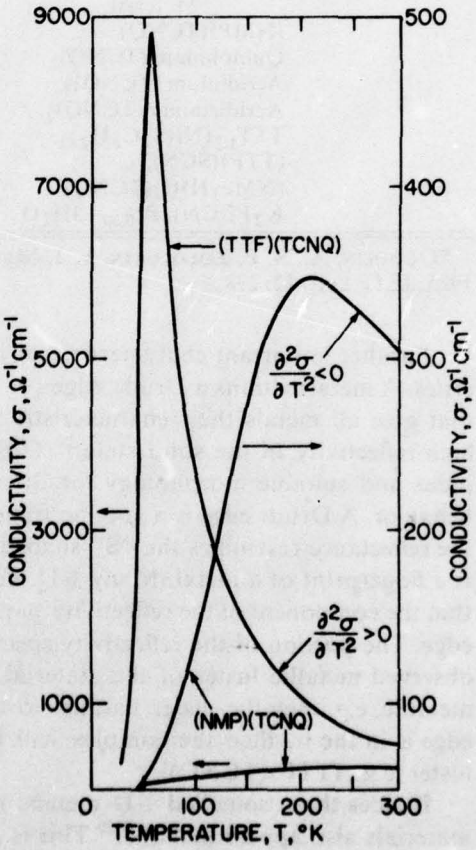


FIGURE 3. The temperature dependence of dc conductivity[5] of (TTF)(TCNQ) and (NMP)(TCNQ).[17] The former charge transfer complex exhibits positive curvature, i.e., $d^2\sigma/\partial T^2 > 0$, whereas the latter complex exhibits negative curvature, i.e., $d^2\sigma/dT^2 < 0$.

ductivity maximum, σ_{max}, at lower temperature. The temperature at which the maximum occurs is labeled as a metal-insulator transition temperature, T_{MI}.[5,7]

The dissimilar features between these $\sigma(T)$ dependencies is the magnitude of both the room temperature and maximum conductivities, σ_{RT} and σ_{max}, respectively. One of the areas that has been the focus of vigorous investigation has been the attempt to lower the T_{MI} and to increase σ_{RT} and σ_{max} through structural modification.[5,18,19] The conductivity of (TTF)(TCNQ) is significantly greater than that reported for (NMP)(TCNQ).[5] For example, $[\sigma_{(TTF)(TCNQ)}/\sigma_{(NMP)(TCNQ)}]_{RT} \gtrsim 2$ and $(\sigma_{max}/\sigma_{RT})_{(TTF)(TCNQ)} \gtrsim 10 \gg (\sigma_{max}/\sigma_{RT})_{(NMP)(TCNQ)} \sim 1.15$. Furthermore, and most significantly, the $\sigma(T)$ for temperatures above T_{MI} exhibit a negative curvature (i.e., $\partial^2\sigma/\partial T^2 < 0$) for (NMP)(TCNQ) and a positive curvature for (TTF)(TCNQ). Only a few organic materials, based on redox active donors and acceptors (e.g. semimetallic (TTF)(TCNQ) and anisotropic 3-D $(SN)_x$) exhibit a positive curvature. The large class of materials that exhibit the negative curvature, e.g., those listed in TABLE 3 appear to be not metallic but to fit a semiconductor with a strongly temperature-dependent mobility description.[17]

TABLE 3

SELECTED HIGHLY CONDUCTING 1-D MATERIALS THAT EXHIBIT NEGATIVE CURVATURE IN THE TEMPERATURE DEPENDENCE OF THE CONDUCTIVITY

Material	References
(NMP)(TCNQ)	16
Quinolinium $(TCNQ)_2$	3
Acridinium $(TCNQ)_2$	3
Acridizinium $(TCNQ)_2$	*
$TTT_{1.2}(Ni(S_2C_2H_2)_2$	80
$(TTF)(SCN)_{0.54}$	98f,k
$(NMe_3H)(I)(TCNQ)$	59
$K_2Pt(CN)_4Br_{0.30} \cdot 3H_2O$	8c

*GOGOLIN, A., S. P. ZOLOTUKIN, V. I. MELŃIKOV, E. I. RASHBA & I. F. SHCHEGOLEV. 1975. JETP Lett. **22**: 278.

Another important characteristic of a metallic state lies in the optical properties. A metal exhibits a Drude edge ($\sim$ 100% reflectivity) and plasma frequency that give all metals their characteristic metallic luster. Many materials exhibit high reflectivity in the solid state.[20] This is a manifestation of a high refractive index and suitable morphology for the solid[20b] and is independent of metallic behavior. A Drude edge is a specific frequency dependence of reflectivity whereby the reflectance resembles the "S"-shaped curve illustrated in FIGURE 4(a), which is a fingerprint of a metal. Many 1-D metals exhibit anisotropic reflectivity such that the component of the reflectivity parallel to the chain axis exhibits the Drude edge. The portion of the reflectivity spectra in the visible region accounts for the observed metallic luster of the material. Consequently, many 1-D metals look metallic, e.g. metallic luster parallel to the chain axis.[21] If, however, the Drude edge is in the ir, then the complex will be black and will not exhibit a metallic luster [e.g., (TTF)(TCNQ)].

Besides these so-called 1-D metals, many inorganic, organic, and polymeric materials also appear metallic.[20] This is a manifestation of the frequency dependence of the reflectivity in the visible portion of the spectra that the human eye

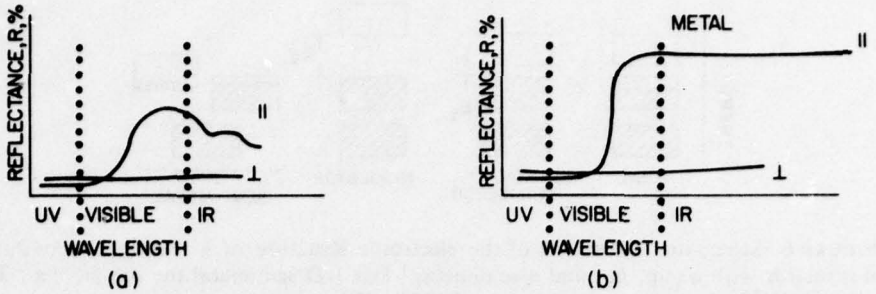


FIGURE 4. Schematic illustration of the frequency dependence of the reflectivity for a metal (a) and a highly reflecting nonmetal (b).

perceives the material to appear metallic. Thus, "... often you have heard that told," that "All that glitters is not gold...."[22] This phenomenon is best illustrated in FIGURE 4. In FIGURE 4(a) an idealized Drude edge and plasma frequency for a metal is presented. Similarly, in FIGURE 4(b) a reflectivity curve for an idealized highly reflecting nonmetal (e.g. semiconductor) is illustrated. Note that the portion of each spectra that is detected by the human eye looks equivalent. Thus, the eye cannot ascertain whether or not a substance is a metal. "Fool's gold" (iron pyrite) is another example where the eye has historically been deceived.

The magnetic properties of a metal may also be used to characterize a molecular solid as being metallic.[15] One-dimensional materials may exhibit a variety of cooperative and localized magnetic properties. Poorly conducting substances that are comprised of paramagnetic building blocks typically exhibit antiferromagnetic (and sometimes ferromagnetic) behavior.[1] Metals, however, exhibit nearly temperature-independent paramagnetism, TIP, which is useful and important in the characterization of a metal. FIGURE 5 schematically illustrates the various types of temperature dependence of the magnetic susceptibility found in interacting magnetic systems.

DESIGN OF HIGHLY CONDUCTING 1-D MATERIALS

A variety of features appear mandatory for the formation of a highly conducting 1-D material. The most important is simply the necessity for the resultant material to possess a partially occupied conduction band.[15] This may be achieved

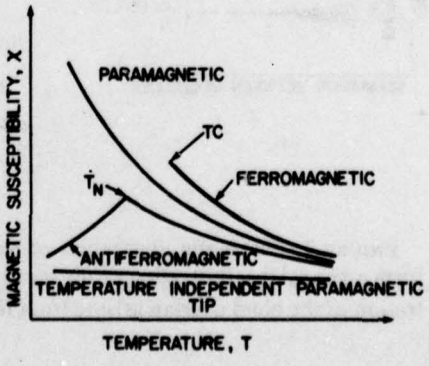


FIGURE 5. Schematic illustration of the temperature dependences of the susceptibility for a paramagnetic, ferromagnetic, antiferromagnetic, and temperature-independent paramagnetic substances.

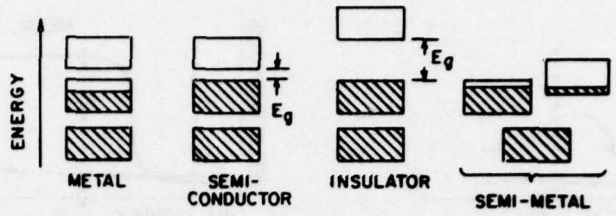


FIGURE 6. Schematic illustration of the electronic structure of a metal, semiconductor, and insulator with a gap, E_g, and a semimetal.[1] For 1-D semimetal the donor, e.g., TTF, gives some electrons to the acceptors, e.g., TCNQ. This gives rise to two partially occupied conduction bands.

through 1) nonstoichiometry of an ion such that the band to conserve charge is not completely occupied; 2) the formation of a semimetal from redox active donors and acceptors such that a fraction of the electrons are transferred from the highest occupied band to a low-lying unoccupied band (this situation does not alter stoichiometric number of electrons in the system); and 3) a chain comprised of radical ions and nonredox active diamagnetic counterions or possibly π-radicals. FIGURE 6 conceptually illustrates the band structures for these cases as well as the semiconductor case. From empirical observation of known materials it turns out that in general the 1-D transition metal complexes achieve a conduction band situation through nonstoichiometry of a charged species, whereas both $(SN)_x$[1] and (TTF)(TCNQ) (and derivatives thereof[2,3,5]) achieve a conduction band through semimetal formation. Closed-shell TCNQ complexes, e.g. (*N*-methylphenazinium) (TCNQ and (quinolinium) $(TCNQ)_2$ are examples of the third type of situation.[2,3] Thus, because of this important distinction the criteria for the design of transition metal complexes differs in some ways with the design of highly conducting organic and polymeric materials.

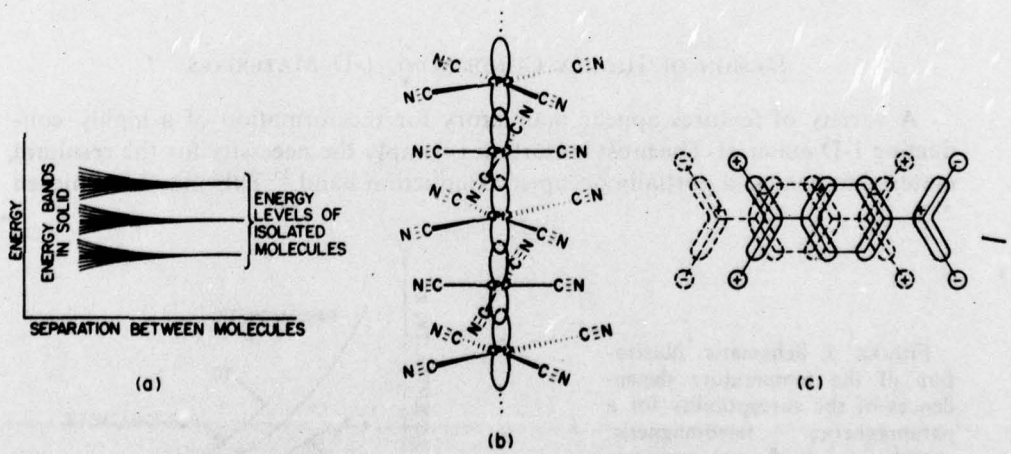


FIGURE 7. Schematic illustration of band formation. (a)-Molecules brought together to form a band;[1] (b)-illustration of the a_g (d_{z^2}) band in the tetracyanoplatinates;[1] and (c)-illustration of the band overlap arising from the overlap of a pair of b_{2g} TCNQ orbitals.

Herein, the chemical requirements for band formation are addressed. It should be clearly stated that design criteria for highly conducting 1-D substances reflect a large component of the author's personal opinions as well as pragmatic results. Besides this article, articles that principally focus on this issue have been written by several other groups.[18,19,33b] Their work has proved invaluable in the preparation of this paper, especially since the topic is evolutionary in nature. It is the principal attempt in this article to avoid in-depth physical arguments, and qualitatively describe briefly in chemical terms the important criteria for the design of highly conducting 1-D substances. The demonstration of the importance of the criteria will emerge only when the results are evaluated.

Hence, in order to achieve high conductivity it is necessary to have band formation arising from the uniform overlap of molecular orbitals between adjacent molecules in the chain (FIGURE 7). Thus, to maximize the probability of strong band formation, a variety of considerations are important which include: 1) steric, 2) electronic, 3) charge, 4) orbital symmetry, 5) Coulombic repulsion, 6) counterion, 7) molecular vibration, 8) disorder, 9) solubility, and 10) hydrogen bonding considerations. These points are described below.

STERIC CONSIDERATIONS

Clearly, in order to facilitate high conductivity, strong band formation (i.e., large bandwidth) must be achieved. Thus, a molecular repeat unit must be able to overlap with each other in such a way that close approach is permitted. This is best accomplished through the judicious use of planar building blocks which possess small nonbulky ligands such as halide, CO, or CN^-, or substituent groups such as CN and H. Rigorously planar inorganic and organic molecules have the greatest probability of permitting the close approach necessary for the achievement of strong band formation. FIGURE 8 illustrates hypothetical molecular geometries for inorganic complexes. Only square planar complexes have as yet been incorporated in a 1-D inorganic complex and planar aromatic organic moieties have been used in the formation of "organic metals."

Since the van der Waals spacing for π-aromatic species ($\gtrsim$ 3.45 Å,[23]) is significantly greater than the metal-metal interactions that have been reported for highly conducting third-row inorganic complexes (< 3.0 Å,[1,21]), it is important to use small nonsterically encumbering ligands and substituent groups to ensure that ligand-ligand repulsions do not prevent the transition metal complex from the necessary close approach needed for band formation. This is an important consideration, especially in Little's prescription for design of an excitonic superconductor.[8] This consideration can be relaxed, however, through the judicious use of ligands with the appropriate MO symmetry to stabilize the 1-D system through intermolecular back-bonding[24,25] (*vide infra*). Furthermore, this size argument is relaxed in the design of highly conducting transition metal-containing complexes based on band formation derived from ligand-ligand overlap (p_z AO's), instead of direct metal-metal interactions (d_{z^2} AO's). An example of this arises from the iodine of oxidation of various phthalocyanine complexes.[26]

Attempts have been made to prepare binuclear complexes with ladder-type 1-D chains.[27,28] This may be accomplished by the use of M_2L_6 or possibly M_2L_4

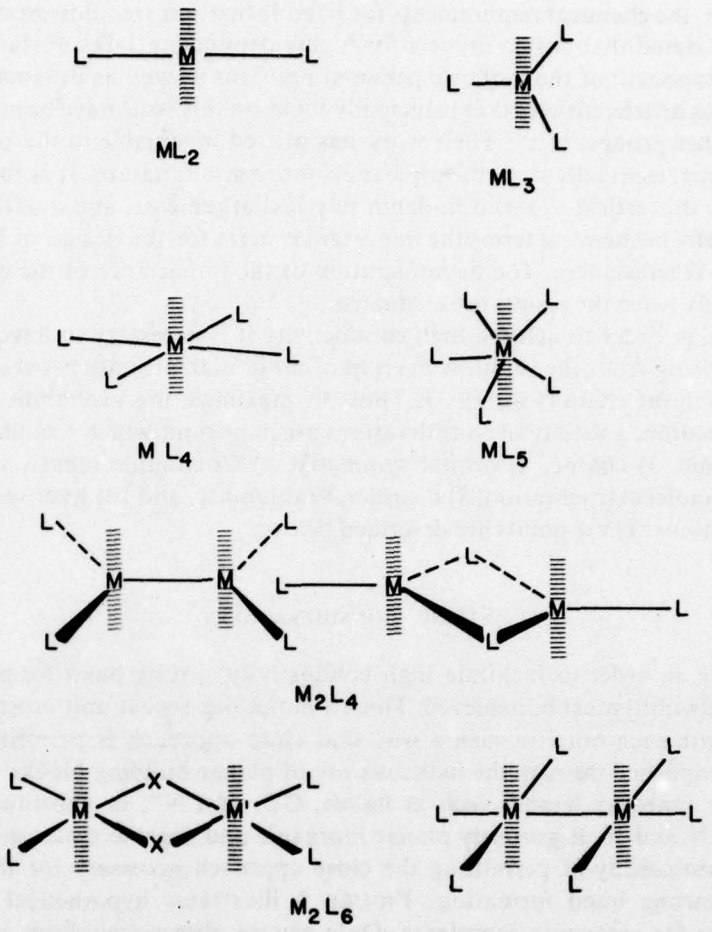


FIGURE 8. Idealized inorganic complexes that could accommodate a 1-D chain. Only the ML_4 situation has been realized for a segregated chain.

materials (FIGURE 8). In either situation, in order to accommodate intramolecular metal-metal overlap, the ligands, L, must be eclipsed. Thus, significant steric repulsions must be overcome. The attempts to prepare 1-D chains comprised of M_2L_6, while involving exciting new chemistry,[28] have not been successful. Another example worth considering is the dicarbonylplatinate trimers which stack as $\{[Pt(\mu\text{-}CO)CO]_3\}$ planes.[29] It is conceivable that an infinite chain of $Pt_3(\mu CO)_3(CO)_3^{z-}$ planes would exhibit extremely interesting anisotropic properties. Synthetic attempts, however, have not yet yielded materials with *n* planes.[29]

In contrast to the rigorously planar building blocks discussed above, some molecules possess nonplanar ligands or substituent groups that are amenable to crystallization of a molecular solid with an interlocking structure and cannot be discounted as possible candidates for achieving high conductivity. For example, the nonplanar bulky ethyl group appears *a priori* to be an undesirable substituent group. This is borne out in the case of going from the 1-D Magnus' Green Salt,

$Pt(NH_3)_4(PtCl_4)$, to the non-1-D $Pt(NEtH_2)_4PtCl_4$ complex.[30] However, the 1-D Wolfframs Red[31a] (FIGURE 9) and Reilers Green salts[31b] both contain ethyl groups. This is not surprising, due to the large Pt-Pt spacings;[21] however, the highly conducting (TTF)(2,5-diethyl-7,7,8,8-tetracyano-*p*-quinodimethanide) contains an appropriate interlocking structure with short Et_2TCNQ-Et_2TCNQ spacings[32] (FIGURE 9(b)) and exhibits a metallic state. Wheland and Gillson further point out that 2,5-TCNQ substitution with five or six side-chain oxygen or carbon atoms does not significantly affect the electrical properties.[33]

The conclusion from the above steric arguments is that although planar building blocks have the greatest probability of forming a highly conducting 1-D segregated chain complex, judicious use of space-filling models can be useful in determining conformations of species with bulky substituents that can form a solid with an interlocking structure, permitting short interplanar spacings. It appears that methyl, ethyl, and fused five-membered rings containing methylene groups may support the type of structure desirable for a 1-D chain.

ELECTRONIC CONSIDERATION

Besides steric considerations, electronic factors are extremely important in the design of a highly conducting 1-D complex. To ensure band formation, the energy, spatial extension, and symmetry of the molecular orbitals that overlap to form the band are important considerations. To ensure band formation, the energy of the band-forming MO's must be as close in energy as possible.[15] The actual energy of band-forming MO's is typically unknown, and, in general, difficult to ascertain. This problem is eliminated, however, when the equivalent MO's overlap. This is accomplished by having the identical inorganic or organic species form a segre-

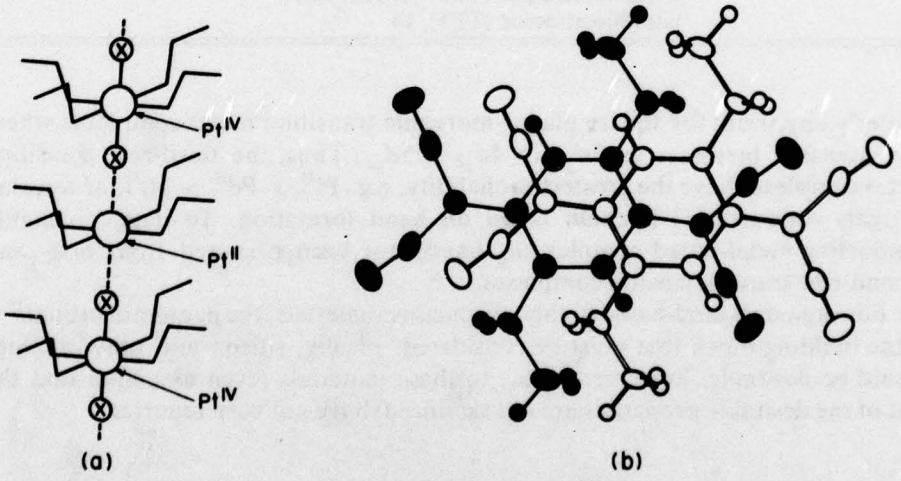


FIGURE 9. 1-D chain structures containing bulky ethyl, C_2H_5, groups. (a)-The structure of Wolfframs Red Salt (X=Cl) and Reilers Green Salt (X=Br); $[Pt^{II}(EtNH_2)_4]$-$[Pt^{IV}(EtNH_2)_2X]X_4$.[31] (b)-The structure of 2,5-diethyl-7,7,8,8-tetracyano-*p*-quinodimethane as the TTF salt.[32]

gated 1-D chain. Many examples of this are listed in TABLE 4. It is important, however, to note that a uniform segregated 1-D chain is insufficient to ensure a metallic-like state or even high conductivity, e.g. $Ir(CO)_2(C_5H_7O)$,[34] bis(glyoximato) complexes,[25,35,36] and N,N,N′,N′-tetramethyl-*p*-phenylenediamine.[37] One-dimensional chains that form alternating [···ADADADAD···] (A ≡ acceptor; D ≡ donor) chains have a low probability of forming a conduction band and consequently probably will not form the structural and electronic basis of a highly conducting 1-D chain. Some examples of this are inorganic complexes with alternating cations and anions, e.g. Magnus' Green Salt, $[Pt^{II}(NH_3)_4][Pt^{II}Cl_4]$,[38] or alternating complexes in different oxidation states[1] e.g. Pt^{II}/Pt^{IV}: Wolfframs Red Salt, $[Pt^{II}(EtNH_2)_4][Pt^{IV}(EtNH_2)_4Cl_2]Cl_4$[31b] (FIGURE 9(a)). Organic examples[39] include various donor-acceptor complexes such as (phenazine) TCNQ.[40]

Given that the molecular building block fits the above steric and electronic criteria, it is important to maximize band formation by maximizing the appropriate d_{z^2} or p_z overlap. Thus, it is desirable to increase the spatial extension of the band-forming MO's. In general, the spatial extension is proportional to the principal quantum number of the elements from which the MO arises. This is particularly important for square planar inorganic transition metal complexes where the extension increases as $3d_{z^2} \ll 4d_{z^2} < 5d_{z^2}$. Thus, the third-row transition metal complexes have the greatest probability, e.g. $Pt^{II} > Pd^{II} > Ni^{II}$, of forming a highly conducting 1-D chain based on band formation. To date, no highly conducting metal-based complex (a_g band) has been prepared from first- and second-row transition metal complexes.

TABLE 4

EXAMPLES OF MOLECULAR SPECIES THAT FORM HIGHLY CONDUCTING SEGREGATED 1-D CHAINS

tetracyanoplatinate (TCP) see FIGURE 1a
bis(oxalato)platinate
dicarbonyldichloroiridate
chlorotricarbonyliridate
7,7,8,8-tetracyano-*p*-quinodimethane (TCNQ) see FIGURE 1b
11,11,12,12-tetracyano-2,6-quinodimethane (TNAP), **19**
tetrathiofulvalene (TTF) see FIGURE 1b,
tetrathiotetracene (TTT), **14**

For organic ligand-based highly conducting materials, the p_z atomic orbital[19,26] is the building block that must be considered. Ideally, silicon and other analogs would be desirable; however, routes to these materials (even assuming that the rest of the desirable properties are not sacrificed) have not been reported.

CHARGE CONSIDERATIONS

For inorganic and organic complexes the spatial extension can also be increased through the introduction of an additional electron (less attractive positive charges to contract the spatial extension of the orbitals in the system). This, of

course, will be counterproductive in the sense that although the additional Coulomb repulsion will increase the spatial extension of the band-forming MO's, the incremental Coulomb repulsion will also prohibit adjacent molecular planes from the necessary close approach. Thus, the Coulomb repulsion must be independently modulated (*vide infra*). For inorganic complexes this can be accomplished by use of a transition metal (third row, *vide supra*) with a smaller nuclear charge. Thus, it is anticipated that the greatest spatial extension would increase for square planar complexes as $Os^0 > Ir^I > Pt^{II} > Au^{III}$. Highly conducting 1-D chains of Ir^I and Pt^{II} have been reported, but none have been reported for Os^0 and Au^{III}.[1,21] Osmium(0), however, prefers to form clusters and does not form square planar complexes.[41] Gold(III), by contrast, forms numerous square planar complexes; however, further oxidation to a higher oxidation state, unlike Pt^{II} and Ir^I, is unrealistic under ordinary conditions.[42]

This alludes to another facet of the electronic criteria, that it is important to utilize a conducting chain building block that has two stable oxidation states,[18,19] for example, Ir^I/Ir^{III}, Pt^{II}/Pt^{IV}, $Hg^{(0)}/Hg^I$; TTF^0/TTF^+; and $TCNQ^0/TCNQ^{1-}$. Such a condition is capable of supporting charge fluctuations along the chain and enhances the probability that the substance can stabilize a highly conducting state. Thus, bivalent materials should be used for the repeat unit.

An additional synthetic variable that can be considered is the use of anionic moieties in the segregated 1-D chain. Clearly, in contrast to a net positive charge that will contract the spatial extension of band-forming MO, a negative charge will increase the spatial extension of the MO. It is thus seen that most of the highly conducting and metallic 1-D complexes reported to date are based on anions such as tetracyanoplatinates and $TCNQ^{1-}$. An example where the differences in the charge on a species can strongly affect the redox ability of a material is illustrated with the comparison between $Pt^{II}(CN)_4^{2-}$ [43] and $Pt^{II}(CNCH_3)_4^{2+}$,[44] which exhibit virtually identical electronic absorption spectra and electronic states in solution. The former anion can easily be oxidized and partially oxidized, whereas the latter cation is unstable with respect to oxidation.[44]

Because of the delicate balance between orbital extension in space (giving a greater bandwidth) and the increase in Coulomb repulsion, it is not known how important the anion criteria is in the formation of a 1-D chain. Clearly, several examples of highly conducting species arising from the segregated cation stacks exist (TABLE 5). High conductivity and even a metallic conductivity has been reported for various substances listed in TABLE 5.

ORBITAL SYMMETRY CONSIDERATIONS

Another aspect of the electronic structure that must be carefully considered is the symmetry of the band-forming MO's. Since highly conducting 1-D materials have uniform interplanar spacings significantly less than the sum of the van der Waal radii, the overlap of the band-forming MO's must be appropriate to support band formation and a net bonding situation where partial oxidation or semimetal formation is achieved. Consequently, the symmetry of the orbitals must be compatible with overlap of the identical wave-function on an adjacent molecule. Were this not the situation, a nonband-forming situation would be operative and close

approach of the molecular planes would be prohibited. For organic 1-D complexes based on TCNQ, the overlap of the b_{2g} POMO orbital on each moiety defines the resultant overlap seen in the highly conducting TCNQ chains (FIGURE 7(b)).[19,45] Similarly, the overlap of the $a_{1g}(d_{z^2})$ platinum orbitals in KCP define the colinear chain (FIGURE 7(c)). Other crystal forces, however, may be important enough for the resultant structure to deviate from linearity.[24,25,45,46] An example of this is seen in the structure of $K_{1.75}Pt(CN)_4 \cdot 1.5H_2O$, which possesses a zig-zag Pt chain. The zig-zag chain has been explained as resulting from dissymmetric electrostatic forces on the tetracyanoplatinate moiety.[47-50]

The considerations of MO symmetry can be extended in inorganic systems containing chelating ligands to include the necessity of inter molecular backbonding so that sterically encumbering ligands can, in fact, support the formation of a highly conducting chain. Intermolecular backbonding between a higher occupied MO on one plane with a lower unoccupied MO on the adjacent plane contributes to the stabilization of the 1-D chain and to the conformation of the chain. This is seen for both the highly conducting bis(oxalato)platinates[24] and a variety of bis(glyoximato) complexes.[25]

For example, *a priori*, the steric interactions anticipated for the bidentate oxalato (ox^{2-}) ligand separated by a short ~ 2.85 Å in the partially oxidized bis(oxalato)platinates can be rationalized via an intermolecular backbonding model.[24] The results of application of the model are in good agreement with the observed 60° and 75° relative rotations for $Mg_{0.86}Pt(ox)_2 \cdot 5.3H_2O$[51] and $K_{1.6}Pt(ox)_2 \cdot 1.2H_2O$,[52] respectively, as HOMO-LUMO ligand-centered backbonding is maximized, at ~ 60° relative rotation (FIGURE 10). Intermolecular backbonding contributes to the stabilization of the partially oxidized 1-D chain by

TABLE 5

SEGREGATED HIGHLY CONDUCTING 1-D CHAINS COMPRISED OF CATIONS

Complex	1-D Chain	σ_{RT}	References
$(TTF)(Cl)_{0.92}$	TTF	3.7	98e
$(TTF)(Br)_{0.7}$	TTF	300	98c,i
$(TTF)(I)_{0.7}$	TTF	360	98f, 98g, 98c, 98h
$(TTF)(SCN)_{0.54}$	TTF	550	98i, 98k
$(TTF)(SeCN)_{0.58}$	TTF	~ 650	98f, 98i, 98k
$TSeT(Cl)_{0.5}$	TSeT	2000	‡
$TTTI_{1.5}$	TTT	900	82, 84
TTTI	TTT	50	84
$Hg_{2.86}AsF_6$	Hg	$> 10^3$	*
Ni(phthalocyanine)I	Ni(phth)	$> 10^2$	26
$Rh(CNCH{=}CH_2)_4{}^+Cl^-$	$Rh(CNCH{=}CH_2)_4$	> 1	†
$M(glyoxime)_2X_y$	$M(glyoxime)_2$	$\sim 10^{-5}$	35, 36

*BROWN, I. D., B. D. CUTFORTH, C. G. DAVIES, R. J. GILLESPIE, P. R. IRELAND & J. E. VEKRIS. 1974. Can. J. Chem. **52**: 791; CUTFORTH, B. D., W. R. DATARS, R. J. GILLESPIE & A. VAN SCHYNDEL. 1976. Adv. Chem. Ser. **150**: 56.

†GORDON, J., II. This volume.

‡ZOLOTUKHIN, S. P., V. F. KAMINSKII, A. I. KOTOV, R. B. LUBOVSKII, M. L. KHIDEKEL, R. P. SHIBAEVA, I. F. SCHEGOLEV & E. B. YAGUBSKII. 1977. Zh. Eksp. Teur. Fiz. Pizma. **25**: 480.

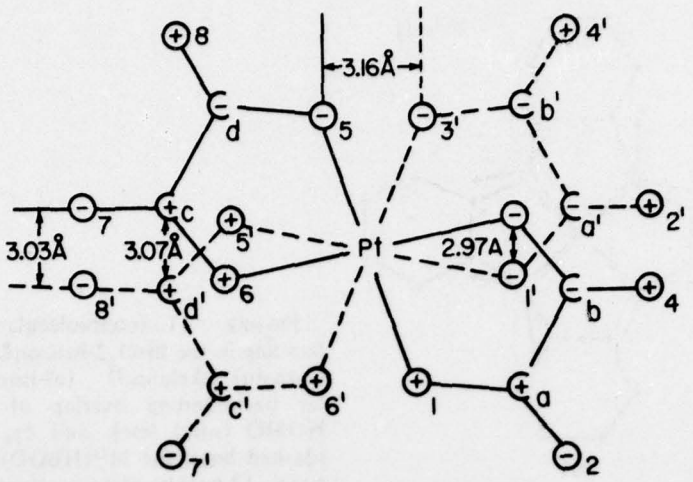
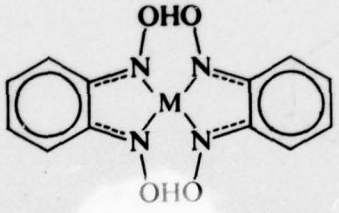


FIGURE 10. Intermolecular backbonding in the bis(oxalato)platinates.[24] Eight intermolecular backbonding overlaps between the HOMO and LUMO of b_{2g} and b_{3g} symmetries, respectively, for the bis(oxalato)platinates. The primed atoms represent the HOMO.

providing an additional, albeit weak, bonding mechanism as well as providing for another mode of backbonding that contributes to the reduction of the Coulomb repulsion in the band (*vide infra*).



I

This concept has also been extended to the poorly conducting square planar bis(glyoximato) complexes. The divalent bis(1,2-benzoquinoneglyoximato) complexes of the nickel triad, **1**, (M = Ni, Pd, Pt) forms a 1-D chain with uniform short interplanar spacings.[32d-h] The unoxidized complexes have a 90° relative rotation between adjacent molecular planes.[36f] This is reconciled by the HOMO-LUMO intermolecular ligand backbonding model (FIGURE 11(a)).[25] Upon oxidation, however, the relative conformation is altered to be ~ 60°.[36d,e] This change in conformation is explained in terms of a change in ligand-ligand interactions (FIGURE 11(b)).[25] Thus, unlike the situation with the bis(diphenylglyoximato) nickel triad complexes,[36a,i] whereby oxidation depletes electrons from the a_g band and consequently the ligand-ligand intermolecular interactions are not altered upon oxidation,[25] the electrons are removed from a ligand-centered MO. Therefore, unlike the former situation where the relative rotation between adjacent planes is unaltered upon oxidation, the latter situation is in accord with the observed change in conformation (FIGURE 11(b)).[25]

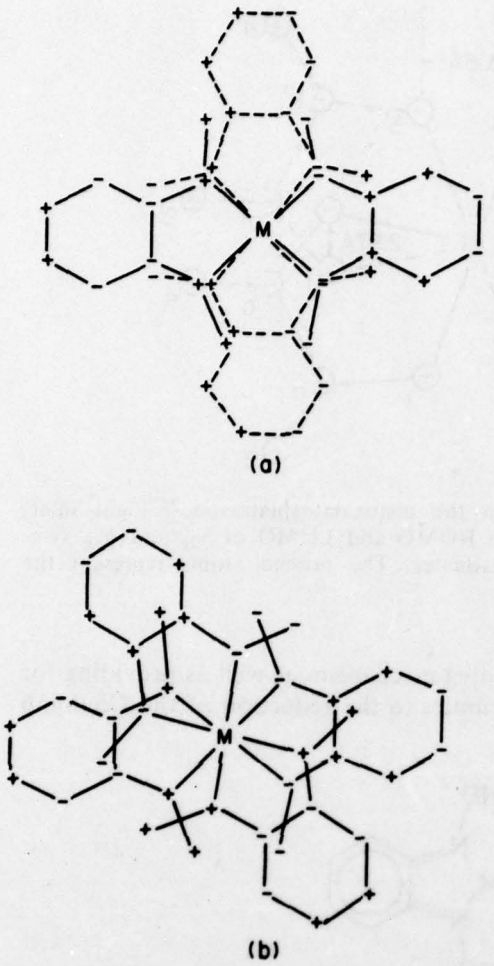


FIGURE 11. Intermolecular backbonding in the bis(1,2-benzoquinoneglyoximato)nickelates.[25] (a)-Intermolecular backbonding overlap of the b_{2g} HOMO (solid line), and b_{3g} LUMO (dashed line), for $M^{II}(HBQD)_2$, giving rise to 12 backbonding overlaps at a 90° relative rotation; (b)-intermolecular back-bonding overlap of the partially filled b_{2g} POMO, with the b_{2g} POMO on an adjacent molecule giving rise to six backbonding overlaps at a 60° relative rotation.

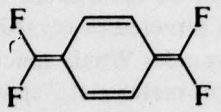
Thus, ligand-ligand intermolecular backbonding enhances the probability of the achievement of a highly conducting material by permitting close approach of molecular planes.

ELECTRON-ELECTRON COULOMB-REPULSION CONSIDERATIONS

The electron-electron Coulombic repulsion in inorganic and organic materials forces the electrons and molecular planes to stay away from each other. This is counterproductive in the sense that it is the goal to have a chain of equivalent molecules with strong M( ) overlap and consequently short equivalent intermolecular spacings. Thus, the design of a highly conducting 1-D must incorporate features that contribute to the reduction of the Coulomb repulsion. This simply requires the removal of electron density away from the conduction band (a_g for inorganic complexes and for organic complexes based on TCNQ). This may be accomplished through introduction of electronegative ligands and substituent groups that are capable of removing electron density away from the band through σ or π induc-

tion. In the case of transition metal complexes, an additional d → π* intermolecular and HOMO → LUMO intermolecular backbonding (*vide supra*) provide additional mechanisms for moving electron density away from the a_g band.

Examples are also seen in the case of TCNQ-based 1-D chains where the electronegative cyano groups provide an induction mechanism for the reduction of Coulomb repulsion. The nitro, $-NO_2$, group is also a strong π electronegative group that, in principle, could be used to form a 1-D chain. Similarly, fluorine is a very electronegative σ group that may, through induction, reduce the Coulomb repulsion and stabilize a 1-D chain. It thus seems appropriate to consider **2** as a potential candidate for the formation of a highly conducting 1-D chain. Furthermore, **2** would be



2

interesting to study in regard to molecular vibration considerations (*vide infra*). Unfortunately, **2** is unstable toward polymerization.[53]

For inorganic complexes electronegative and π-backbonding (strong field)[41] ligands are best for stabilizing a 1-D metallic state. Besides the anionic ligands, which, in the context of organic chemistry, are substituent groups (e.g., NO_2^-, CN^-, and F^-), a variety of small neutral ligands are good d → π* backbonding ligands (e.g. CO and CNR) and can be used to reduce the Coulombic repulsion in a band. For example, $K_{\sim 1/2}Ir(CO)_2Cl_2$ possesses the d → π backbonding CO ligand.[1] Another example is the oxalato, $ox^{2-} \equiv {}^-O_2C_2O_2{}^-$, ligand, which, although sterically encumbering, is able to both inter- and intramolecularly backbond[25] (*vide supra*) and form a highly conducting 1-D substance.[1]

It also seems feasible to prepare PtF_4^{2-} and $Pt(NO_2)_4^{2-}$ and partially oxidize these species to form a highly conducting material. The former complex, which, in principle, may reduce the Coulomb repulsion via induction, is unstable toward disproportionation in aqueous solution.[54] The latter complex, which can (through inspection of space-filled models) accommodate four nitro ligands in a plane, has not been partially oxidized.[55] This is probably due to the nitro ligands being out of the PtN_4 plane in solution, so that oxidation of the Pt^{II} is prohibited. This has also been observed in the oxidation of the sterically crowded $Pt[C(NHMe)_2]_4^{2+}$.[56]

Another facet of the reduction of the Coulomb repulsion lies within the choice of counterions (*vide infra*). Counterions with large polarizabilities per unit volume and in close proximity to the conduction band result in an attractive force that reduces the Coulombic repulsion of electrons in the conduction band. Since polarizability, P, is proportional to the sum of oscillator strength, ε, frequency, ν, ratio,[15]

$$P \propto \int \frac{\epsilon d\tilde{\nu}}{d\nu}, \qquad \text{(A1)}$$

small counterions with large oscillator strengths at greater wavelengths are the counterions of choice. Thus, unsaturated cation (or, in principle, anion) radicals are the type of counterion to be utilized.

Polarizability arguments are also given by Little for the design of an excitonic superconductor.[8] Thus, Little proposes a highly polarizable dye-like ligand that would, by coordinating to the transition metal, be in very close proximity to the conduction band and stabilize the superconducting state. Consequently, the polarizability would help stabilize the excitonic superconductor. Much thought has gone into the design,[7,8,57] but such a material has not been reported to date. Care must be taken to design an appropriately polarizable ligand that retains its polarizability upon coordination. Cyanine dyes with a single plus charge delocalized over a symmetrical species with two equivalent tricoordinate N atoms do not do so, because coordination alters the symmetry of the system. Furthermore, the ligands must possess symmetry-compatible MO's so that intermolecular backbonding and band formation will be facilitated. This is particularly true since large aromatic ligands have been targeted in regard to realization of the excitonic superconductor,[57] and the large van der Waals spacings of the ligands (> 3.3 Å)[23] will prohibit the formation of short metal-metal spacings (< 3.0 Å).[1] Additionally, because of the extended conjugation of the ligand, it is very possible that were high conductivity achieved, the conduction band might be derived from ligand-ligand overlaps. This is particularly true for *bis* glyoximato ligands, which, at least in the case of **1**, have a HOMO of ligand character. This is not to assert that high conductivity achieved via ligand-ligand overlap is not interesting and important. However, the basic precept of Little's model[8,57] is the requirement of use of a conducting chain that has a small (~ 2 Å) cross section.

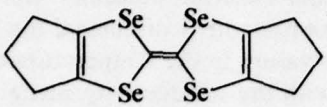
Counterion Considerations

All of the highly conducting inorganic and organic 1-D materials [except for $(SN)_x$ and the poorly characterized "$Ir(CO)_3Cl$"][1] possess counterions. The effect of the counterion on the resultant physical properties can be significant. This can easily be appreciated by reviewing the TCNQ[2,3,5] and tetracyanoplatinate literature.[1] Several important features should be focused upon in choosing a counterion. The shape and size are discussed in this section; other important features (such as polarizability and solubility) are discussed elsewhere.

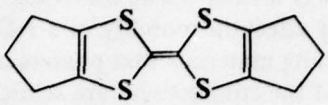
For all highly conducting materials where a "metal-like" state has been reported, the counterions all exhibit high symmetry and are not excessively large. It thus appears that to ensure the required crystal packing to permit close approach of the conducting species, such as tetracyanoplatinate or TCNQ, nonbulky counterions such as small planar or point ions are the materials of choice to stabilize a highly conducting 1-D species. The most asymmetric material that has been reported to exhibit a metal-like state is $N(CH_3)_3H^+(I_3^-)_{1/3}(TCNQ)^{2/3-}$; however, this material is anomalous for a variety of reasons which principally arise from the tertiary nature of the substance.[58-60]

It is generally agreed that the counterion should be of minimal size and maximal polarizability in order to maximize the polarization energy.[18,19] Garito and Heeger stated[19] in this regard: "Molecular design should be dominated by attempts to obtain maximum polarizability with minimum size." While minimization of size within the constraints of planarity is an admirable goal, caution must

be exercised. Consider the TCNQ complexes of hexamethylenetetraselenafulvalene, **3a**, HMTSeF, and the sulfur analogue, HMTTF, **3b**.



HMTSeF
3a



HMTTF
3b

Clearly the pair of trimethylene groups make the latter counterions much larger, and neither contributes to the basic TSeF and TTF chromophore nor enhances disorder (*vide infra*). Thus, the polarizability per unit volume is less for HMTSeF than for TSeF (FIGURE 1b (S = Se)). The TCNQ charge transfer salts, however, clearly show that (HMTSeF)(TCNQ) has higher room-temperature conductivity, which is extended to lower temperatures than that reported for (TSeF)(TCNQ).[5,61]

Therefore, although small planar counterions are desirable, bulkier and, to some extent, even nonplanar molecules should not be neglected, since controlled modification of the properties can be achieved with judicious use of substituent groups.

MOLECULAR VIBRATION CONSIDERATIONS

The conduction electron-vibration (molecular and lattice) interactions (electron-phonon coupling) play an important role in limiting the conductivity of a highly conducting 1-D molecular substance. In particular for conductivity arising from single-particle electron scattering, the a_{1g} vibration frequencies less than the bandwidth will scatter the electrons and consequently lower the mobility and conductivity.[62,63] Thus, by reducing the magnitude of the coupling (the electron-phonon coupling constant (g)), and/or raising the frequency of the mode that couples to the conduction electrons, the mobility will be enhanced. Two synthetic methods involving changes in mass are available to achieve the latter goal. They include modulation of the vibrational frequencies through isotopic and substituent group substitutions raising the a_{1g} molecular vibration in frequency. This requires the isotopic substitution of atoms with elements of lighter isotopes. This is clearly an unrealistic goal. For both inorganic and organic species containing the first-row elements where isotopic substitution would be most pronounced in a shift of the vibrational frequencies, the lightest isotopes are already used.

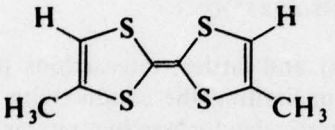
On the other hand, in principle, molecular vibrations can be reduced or possibly deleted. Since the number of vibrations is 3N-6 (N = number of atoms), this may be accomplished through removal of atoms from the molecule. This suffers from a significant redesign problem. Structure **2**, with electronegative F replacing CN, will reduce the number of molecular vibrations from 54 to 42 and, it is hoped, will remove the a_{1g} vibrations with significant electron phonon coupling constants above the bandwidth.[64] Also, since F has a lower mass than CN, the CR_2 scissoring and bending vibrations would increase in frequency as for R=F with respect to R=CN. This idea, however, has limitations in the assumption that **2** will even form a highly conducting 1-D chain. Compound **2**, in fact, is

unstable toward polymerization.[53] In principle, however, molecular vibration considerations are important in the design of a highly conducting 1-D substance.

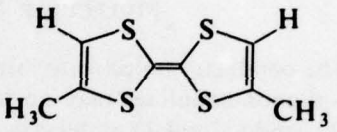
This is further borne out when it is noted that electron-molecular vibrations strongly affect the mobility of a 1-D material. As previously discussed, the highly conducting materials that possess a negative curvature in the temperature dependence of the conductivity are semiconductors, with the conductivity being dominated by the mobility, which is strongly temperature dependent.[17,65]

Disorder Considerations

There exists a school of thought holding that a small amount of disorder is an important attribute to consider in the design of a highly conducting 1-D chain.[18] In the limiting case, too much (unquantifiable) disorder leads to the formation of a band gap and a typical semiconductor behavior (Figure 6). The absence of disorder, however, as observed in bulk (TTF)(TCNQ), does not seem to detract from the intrinsic high conductivity.[5] Introduction of disorder through the use of *cis*- and *trans*-dimethyltetrathiofulvalene, **4**, and **5**, respectively, introduces a small amount of disorder. The result of this disorder is reflected in the shift of the temperature at which the metal insulator transition occurs, T_{MI}, to lower temperature, 58°K[5] and 50°K.[66]

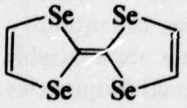


4



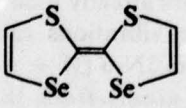
5

This disorder issue is, however, complicated by the introduction of selenium for sulfur. Tetraselenafulvalene, TSeF, **6**, like TTF (Figure 1b),

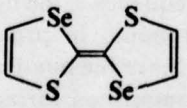


6

has effectively no disorder. However, replacement of two sulfurs with selenium, i.e., a mixture of **7** and **8**, introduces some disorder. However, the



7



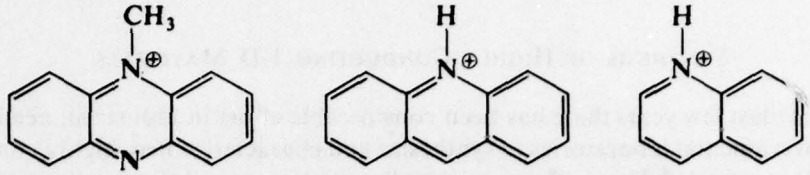
8

disordered charge transfer complex exhibits the highest T_{MI} of 64°K, whereas (TTF)(TCNQ) and (TSeF)(TCNQ) exhibit T_{MI} at 58°K[5] and 40°K,[66,67] respectively.

From this data it is unclear whether the designed introduction of disorder will enhance the electrical properties of the material. It appears, however, that disorder

may do so; thus, the introduction of disorder should not be overlooked in the design of highly conducting 1-D materials.

It is also important to note that for closed shell cations, e.g. N-methylphenazinium, **9**, acridinium, **10**, and quinolinium, **11**, which form



9 **10** **11**

highly conducting salts with TCNQ,[2] have a permanent dipole greater than a Debye unit.[18] Consequently, disorder is anticipated and observed in the molecular solid. That such disorder, as, for example, the methyl groups or adjacent NMP^+ ions in (NMP)(TCNQ) may or may not be eclipsed,[68] has been invoked as a contributing force in the stabilization of a highly conducting 1-D species.[18] Recent work in our laboratory has shown that because of replacement with the symmetrical and neutral phenazine for the NMP^+ cation, disorder has been decreased while T_{MI} has shifted to lower temperature and σ_{max}/σ_{RT} has been enhanced (*vide infra*).[69,70]

Solubility Considerations

Another important consideration, albeit difficult to control *a priori*, is the solubility of a 1-D complex. Typically, 1-D complexes are less soluble than the component used in their preparation. The 1-D substances are consequently moderately easy to prepare (assuming the availability of starting materials). In contradistinction to the typical situation described above, when the counterions are such that the desired product is more soluble than its components, the desired 1-D complex cannot be easily isolated. Examples[55] of this lie in the synthesis of $(H_3C)_4N^+TCNQ^+$ and the $Na_2Pt(CN)_4X_{0.3}\cdot xH_2O$. In principle, these materials should easily be prepared by routes that effect the isolation of the Me_3NH^+ [58-60,71] and K^+ [1] analogs, respectively. However, to date these substances that are seemingly simple to prepare have not been characterized. Possibly, use of different solvents would facilitate their preparation.

Hydrogen-Bonding Considerations

For inorganic complexes that are isolated from aqueous media, the additional feature of ability to hydrogen bond appears to be important. Hydrogen bonding in the structures of $K_2Pt(CN)_4X_{0.3}\cdot 3H_2O$[10] (X=Cl, Br), $K_{1.75}Pt(CN)_4\cdot 1.5H_2O$,[47-50] bis(oxalato)platinates,[52] and presumably the dicarbonydichloroiridate complexes[1,2] knit the structure together and contribute to the stabilization of the 1-D chain. This is emphasized as the loss of water from $K_2Pt(CN)_4X_{0.3}\cdot 3H_2O$ (X=Cl, Br) significantly alters the physical properties as the chain lengths are

severed.[75] Introduction of water to partially rehydrate crystals permits the partial recovery of the physical properties. Hydrogen bonding does not seem important in the design of highly conducting organic materials. A possible exception may arise from the interaction between NMe_3H^+ and TCNQ in $(NMe_3H)(I)(TCNQ)$.[58,60]

Synthesis of Highly Conducting 1-D Materials

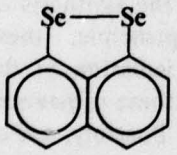
In the last few years there has been considerable effort in industrial, academic, and governmental laboratories to synthesize and characterize new highly conducting 1-D materials.[4] These efforts principally revolve around the synthesis of new organic donors and acceptors, inorganic square planar complexes, and covalent polymeric materials.

Organic Synthesis

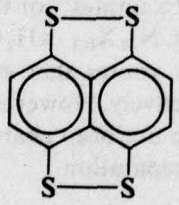
The initial du Pont report[71] and characterization[4] of the high conductivity in samples of (NMP)(TCNQ) and (TTF)(TCNQ) lead to intense efforts in design[18,19] and synthesis of new open-and-closed shell donors and acceptors.

For organic systems the primary effort throughout the world has focused upon expanding the chemistry of the prototype (TTF)(TCNQ) through synthesis of low ionization potential donors,[5,19,76] e.g. TTF derivatives, and acceptors[19] with a large electron affinity, e.g. TCNQ. Most work has been in donor modification. The types of modifications that have been reported include chalcogen substitution (replacement of Se for S in TTF), organosubstitution (introduction of CH_3, etc., groups for the hydrogen in TTF), and combinations of the above. A variety of these TTF based donors are listed in Table 6.

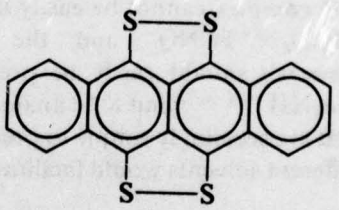
Recently, new types of chalcogen-containing donors (**12**,[77] **13**,[78] **14**,[33,79-84] and **15**[85] as well as closed-shell nitrogen donors (**16**,[86]), have been emphasized. The detailed physical properties of the former chalcogen containing 1:1 and 1:2



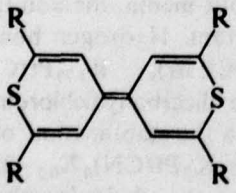
12



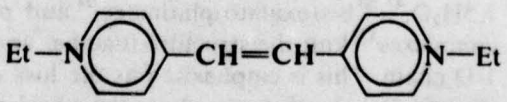
13



14

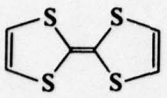
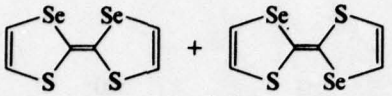
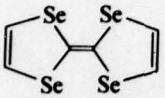
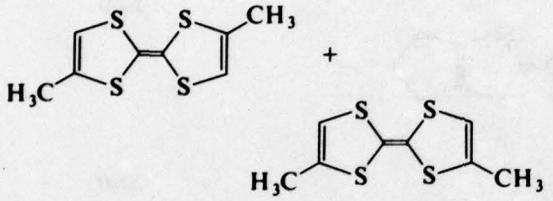
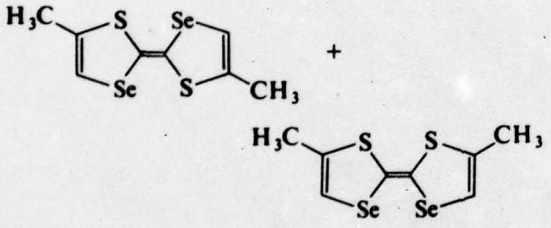
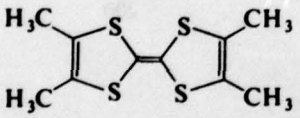
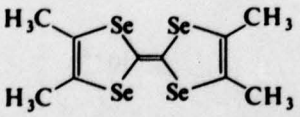
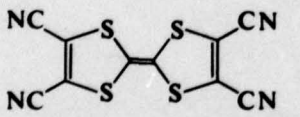
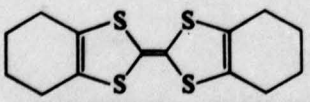


15



16

TABLE 6
SELECTED MODIFICATION OF TETRATHIOFULVALENE*†[5,76]

	Conductivity of TCNQ Salt, RT, Ω^{-1} cm^{-1}
	500
	700
	800
	50
	10
	$\approx 10^3$
	800
	—
	—

*Tetrathiofulvalene (TTF) is the parent compound.
†Tetracyanoquinodimethane (TCNQ) is the parent compound.

TABLE 6 (*continued*)

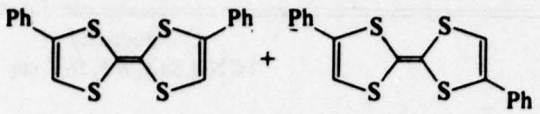
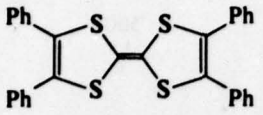
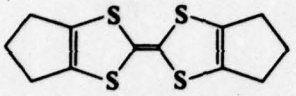
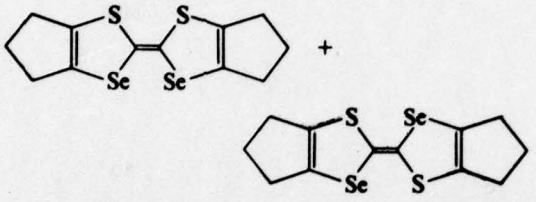
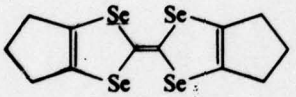
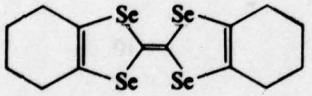
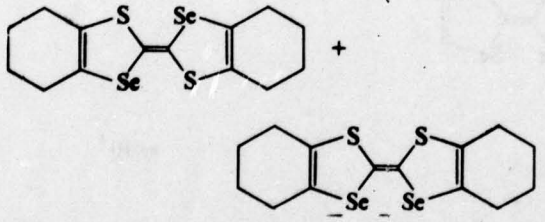
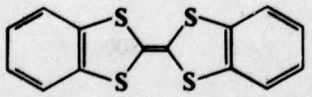
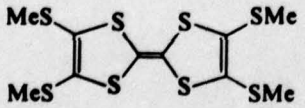
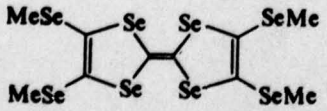
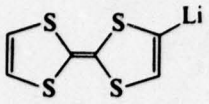
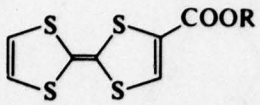
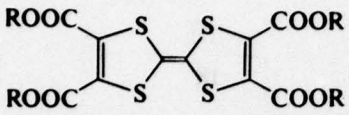
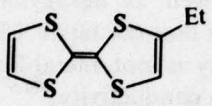
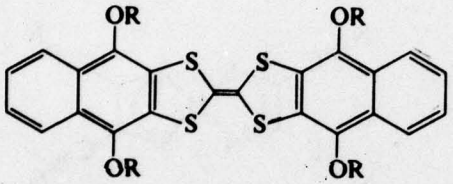
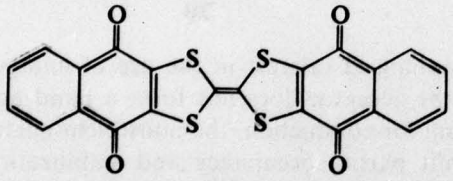
	
	
	500
	2000
	2000
	
	200
	10^{-4}
	—
	—

TABLE 6 (*continued*)

	—
	—
	—
	—
	—
	—

*GREEN, D. C. 1977. J. Chem. Soc. Chem. Commun.: 161.

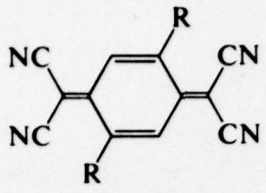
†DEMETRIDIS, N. G., S. J. HUANG & E. T. SAMULSKI. 1978. Tetrahedron Lett. 2233.

‡BERG, C. K. BECHGAARD, J. R. ANDERSEN & C. S. JACOBSEN. 1976. Tetrahedron Lett. 20: 1719.

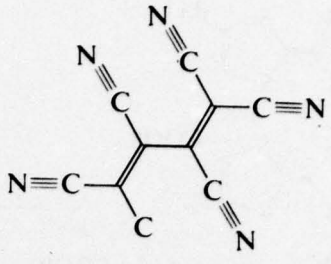
complexes with TCNQ have not been reported. However, preliminary evidence for **12** (TCNQ),[77] **13** (TCNQ),[78] and **15** $(TCNQ)_n$[85] (n = 1, 2) suggests that these materials are not metal-like. The initial report of $(TTT)(TCNQ)_2$,[81] (TTT = tetrathiotetracene, **14**) by contrast, suggests that this complex is metal-like and possibly exhibits a positive curvature, e.g. FIGURE 3. Further work is needed for the full understanding of the structure-function relationship. The **16**$(TCNQ)_4$ complex has been reported to be highly conducting down to 0.03°K,[86] but verification of this result has not been reported.

In the case of conducting TCNQ anion acceptors, less work in the area of structural modification has been reported. Principally, the predominant work has

been revolved around making alkyl and alkoxy derivatives of TCNQ at the 2,5 ring positions, **17**.[32,33]

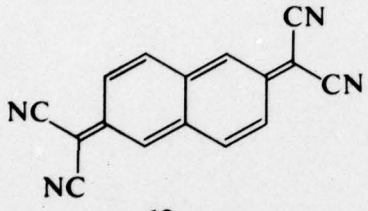


17

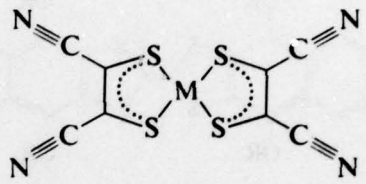


18

Additionally, other acceptors such as TNAP, **18**,[33,87] as well as hexacyanobutadiene, **19**,[88] have been tried. Preliminary evidence suggests that the latter TTF complexes form segregated stacks; however, the conductivity is not metal-like. TNAP complexes with TTF have been reported to exhibit high conductivity,[87a,b]



19



20

In the past few years there has been enhanced interest in the use of halogen and pseudohalogen acceptors. Although the acceptor does not form a band and consequently does not provide a mechanism for conduction, the nonstoichiometry and polarizability of the acceptors permit partial occupancy and stabilization of the donor conduction band. TABLE 5 lists, besides the anomalous $Hg_{2.86}AsF_6$, various cation conductors with halide and pseudohalide acceptors.

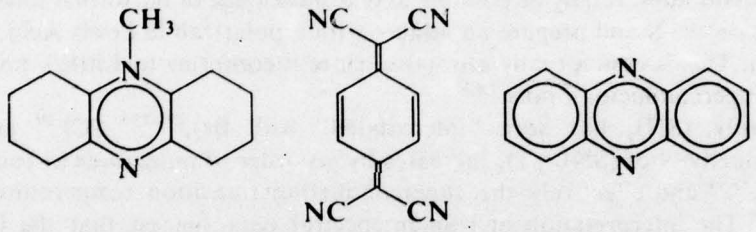
The halogen in these acceptors varies from Br_2 (as well as possibly Br_3^-) in $(SNBr_{0.4})_x$,[89] to I^- in TTF $I_{0.7}$[98j] to I_3^- in $(NMe_3H)(I)(TCNQ)$[59,60] to X_5^- in $M(HDPG)_2X_y$ ($y \leq 1.15$); X = Br, I; M = Ni, Pd; H_2DPG = diphenylglyoxime).[91] The latter complex is further novel in that ~ 80% of the halogen can be removed from the structure without modification of the unit cell.[35]

Another type of open-shell acceptor that has been used is bisditholate metal complexes,[1,33,80] e.g. **20**. For example, **20** (M = Pt) seems to satisfy several important criteria, namely, bivalent, small, planar, electronegative substituent groups and ligands, highly polarizable, good solubility characteristics, and backbonding ligands for the stabilization of a highly conducting 1-D complex. However, the only highly conducting species that have been prepared have the advantage of being salts of radical cations that provide the conduction band.[1,80]

Thus, $M(S_2C_2R_2)_2^{z-}$ apparently does not form a highly conducting 1-D complex. This is easily reconciled by looking at the electronic structure of **20** (M = Pt). The highest occupied MO is not the $a_{1g}(d_{z^2})$.[12] Thus a_g band formation is

prohibited. Furthermore, unlike the bis(oxalato)platinates, the ligand-centered MO's of **20** are not of the desirable symmetry to accommodate intermolecular backbonding and, consequently, colinear chain formation with short interplanar spacings.[70]

Recently in our laboratory[69,70] we have been involved in designing a system in which a comparison of the physical properties as a function of band filling (Fermi Energy) could be easily made for an isomorphous series of complexes so that the traditional comparison between unlike materials could be minimized. With the above criteria in mind we set out to modify $(NMP^+)(TCNQ)^+$, **21**. With the assumption that the TCNQ is the driving force for the parallel 1-D chain, we argued that removal of a NMP^+ cation should deplete electrons from the conduction band, but the voids created in the solid would force the structure to collapse. By judiciously replacing the NMP^+ cation with a neutral molecule of similar size, shape, and polarizability, it seemed feasible that the structure would remain intact, and that since fewer cations were present, fewer electrons would necessarily be present in the conduction band. The molecule we chose was phenazine, **22.** Suffice it to say

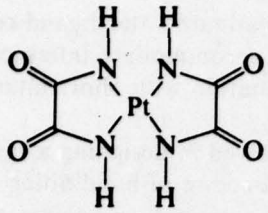


21 **22**

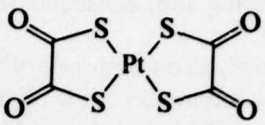
that we have been able to prepare an isomorphous series of complexes with up to a 50% replacement of phenazine for NMP^+ $((NMP^+)_x(\text{Phenazine})_{1-x}(TCNQ^+)_x(TCNQ^0)_{1-x} \equiv (NMP^+)_x(\text{Phenazine})_{1-x}TCNQ(1 \geq x \gtrsim 0.5))$. The physical properties of this novel series of complexes will be reported later.[69,70,93]

Inorganic Syntheses

For inorganic systems it seems appropriate to consider third-row transition metal complexes (Figure 12). By analogy, to the known species the only transformations that have been effected have been achieved through changing of the cations and anions. For example, K^+ was replaced by $C(NH_2)_3^+$[72] and X^- was replaced by F_2H^-,[73] and F^-[74a] and a mixture of Cl^- and Br^-[55] in KCP. The KCP structure (Figure 1a) is somewhat modified, but the short intermolecular spacings were retained. Further information is needed to fully understand the synthetic transformation on the physical properties. Attempts in replacing the alkali counterion with an alkaline ion have failed.[74b] Ligand substitution has not been reported, although attempts in our laboratories and others to prepare partially oxidized derivatives of the bis(oxalato)platines, **23** and **24,** have been attempted; however, the results were not fruitful.[55]



23



24

Polymeric Syntheses

Modifications of poly(sulfurnitride), $(SN)_x$, have been largely ignored in preceeding sections. This is due to the covalent character and the anisotropic three-dimensionality of the system which makes synthetic modifications more difficult to predict and achieve. To a first approximation only elemental substitution can be effected, such as $(SeN)_x$ or $(SeP)_x$.[13]

Electronegativity and chemical stability arguments pragmatically rule out all simple possibilities. It may be possible to take advantage of the formal lone pair of electrons on the S and prepare an adduct with a polarizabile Lewis Acid and the SN chain. This is conceptually attractive, since it conforms to Little's postulated exciton superconductor model.[7,8,57]

Recently, $(SN)_x$ has been "intercalated" with Br_2,[89,94,95] ICl,[89] and I_2.[89] The conductivity of $(SNBr_{0.4})_x$ increases by an order of magnitude at room temperature,[89,94] and effectively the superconducting transition temperature is not altered.[94] The interpretation of Raman spectral data suggest that the bromine exists in $(SNBr_{0.4})_x$ as both bromine and possibly tribromide.[90] Thus, the halogen adducts suggest the possibility of new exciting derivatives of $(SN)_x$ being prepared in the future.

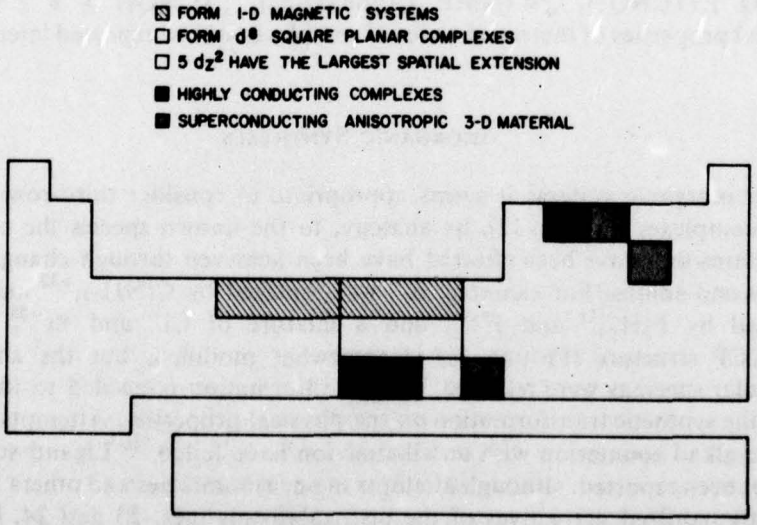


FIGURE 12. Periodic distribution of elements that form anisotropic quasi-1-D chains.

Synthetic Methods

In order to actually prepare new highly conducting 1-D materials, the above Gedanken experiments must be converted into laboratory syntheses. A variety of techniques is available in the synthetic chemist's repertoire for use in the preparation of new highly conducting species. For inorganic complexes the various techniques can be amply illustrated by review of the synthetic procedures for $K_2Pt(CN)_4X_{0.3} \cdot 3H_2O$ (X = Cl, Br) and the iridium chlorocarbonyl complexes.[1] The procedures can be broken down into (1) chemical and electrochemical oxidation, (1) and (2), respectively; and (2) addition of mixed valent species, (3)–(4). Electrochemical oxidation exhibits the desirable feature of incorporating the crystal as an extension of the electrode so that the property to be monitored is used in the synthesis.[96]

Halogen oxidation frequency results in the preparation of various types of materials that may exhibit a variety of structures including highly conducting materials. It must be emphasized, however, that many types of products can be prepared. For example, $Pt^{II}(CN)_4^{2-}$ and bromine or chlorine results in the formation of a highly conducting 1-D chain which has a nonstoichiometric amount of ionic halide in the structure,[1] (1), FIGURE 1a. By contrast, reaction of chlorine or bromine with $Pt^{II}(EtNH_2)_4^{2+}$ (X = Cl, Br) leads to the isolation of the insulating Wolfframs Red or Reilers Green Salt (FIGURE 6), which is characterized by having alternating $Pt^{II}(EtNH_2)_4^{2+}$ and *trans*-$Pt^{IV}(NEtNH_2)_4X_2^{2+}$ ions,[31] (4).

$$2K^+ + Pt(CN)_4^{2-} + X_2 \xrightarrow{H_2O} K_2Pt(CN)_4X_{0.30} \cdot 3H_2O \quad (1)$$

$$2K^+ + Pt(CN)_4^{2-} + 0.3X^- \xrightarrow{H_2O} 0.3e^- + K_2Pt(CN)_4X_{0.30} \cdot 3H_2O \quad (2)$$

$$40\,K^+ + 17\,Pt^{II}(CN)_4^{2-} + 3\,\textit{trans}\text{-}Pt^{IV}(CN)_4X_2^{2-} \xrightarrow{H_2O} 20\,K_2Pt(CN)_4X_{0.3} \cdot 3H_2O. \quad (3)$$

$$4X^- + 2Pt^{II}(A)_4^{2+} + X_2 \xrightarrow{H_2O} [Pt^{II}A_4][\textit{trans}\text{-}Pt^{IV}A_4X_2]X_4 \quad (4)$$

$$A = EtNH_2.$$

The reaction of bromine (or IBr or I_2) with $M(HDPG)_2$ (M = Ni, Pd; H_2DPG = diphenylglyoxime) leads to the formation of a 1-D complex with uniform short metal-metal spacings and a 1-D halogen column filled with a nonstoichiometric amount of polyhalide,[35,36a,91] (5).

$$M(HDPG)_2 + X_2 \rightarrow M(HDPG)_2X_y \qquad y < 1.15 \quad (5)$$

$$X = Br, I; M = Ni; Pd.$$

In contrast to these 1-D chain-forming reactions, the halogen oxidation of $Pt^{II}(HDPG)_2$ (H_2PDG = diphenylglyoxime) leads to only the Pt^{IV} complex, (6).[36i] If less than a stoichiometric amount of halogen is

$$Pt^{II}(HDPG)_2 + X_2 \rightarrow \textit{trans}\text{-}Pt^{IV}(HDPG)_2X_2 \quad (6)$$

used, two phases corresponding to the Pt^{II} and Pt^{IV} complexes can be isolated.[36i] Similarly, the halogenation of $Rh^{I}(CNR)_4^+$ ($R = C_6H_{11}$) leads to dimeric Rh^{II} complexes with an isolated linear $X - Rh^{II} - Rh^{II} - X$ unit,[97] (7).

$$Rh^{I}(CNR)_4^+ + X_2 \rightarrow [XRh^{II}(CNR)_4]_2. \quad (7)$$

In a similar fashion, highly conducting organocation 1-D chains can be prepared. For example, TTF and TTT react with iodine to form $(TTF)(I)_{0.7}$[98] and $(TTT)I_{1.5}$,[82,84] (8) and (9).

$$TTF + X_2 \rightarrow (TTF)X_{0.7} \quad (8)$$

$$(X = Br, I)$$

$$TTT + X_2 \rightarrow TTT_2I_3 + (TTT)I. \quad (9)$$

Not all substances can be prepared by all of these techniques. The electrochemical growth method provides a convenient method for the synthesis of large, high-quality inorganic[96] and organic materials.[33a,80] Williams *et al.*[73] cleverly used this technique to prepare $M_2Pt(CN)_4(F_2H)_{0.39} \cdot xH_2O$ (M = Cs, Rb), (whereas chemical techniques failed).

The $Hg_{2.86}AsF_6$ and iridium complexes have been prepared by less rational techniques; controlled oxidation has not been reported.[1] These latter complexes are simply the result of specific chemical reaction. For example, $K_{\sim 1/2}Ir(CO)_2Cl_2$ and $Hg_{2.86}AsF_6$ are prepared via (10) and (11).

$$K_2Ir^{IV}Cl_6 + HCOOH + HCl \rightarrow K_{\sim 1/2}Ir(CO)_2Cl_2 \quad (10)$$

$$Hg^0 + AsF_5 + SO_2 \rightarrow Hg_{2.86}AsF_6. \quad (11)$$

For organic 1-D complexes, similar synthetic techniques are available, but, due to the redox behavior of some of the planar organic materials utilized, charge transfer can be effected *in situ*, (12) and (13). This, of course, can lead to band overlap and semimetal formation, 13b.

$$Donor^+ + Acceptor^- = (Donor^+)(Acceptor^-) \quad (12)$$

$$Donor + Acceptor = (Donor^+)(Acceptor^-). \quad (13a)$$

$$Donor + Acceptor = (Donor)^{\delta+}(Acceptor)^{\delta-} \quad (13b)$$

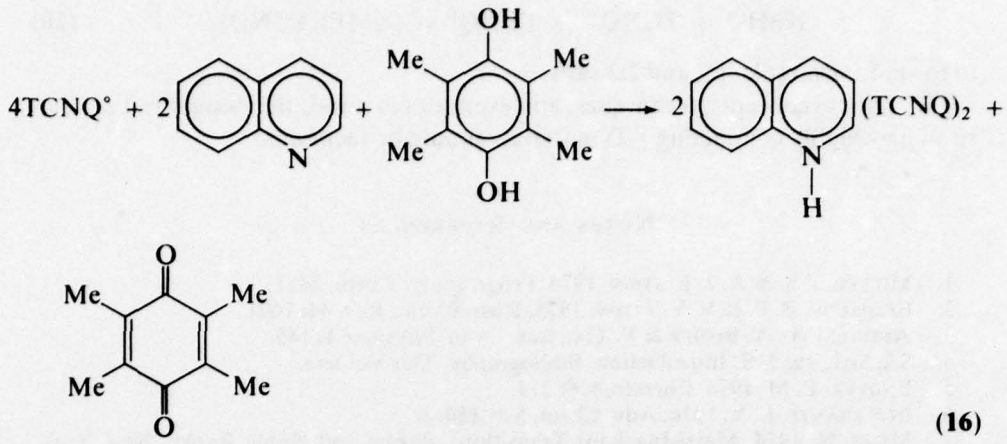
Besides direct oxidation of a donor, TCNQ or, in fact, any good acceptor will oxidize an innocent substance to effect the formation of a desirable charge transfer complex. For example, ionic iodides will be oxidized by TCNQ,[2,71] for example, (14), to

$$3\,Li^+I^- + 2TCNQ^0 = 2\,Li^+TCNQ^{\cdot} + Li^+I_3^- \quad (14)$$

form triiodide and $TCNQ^-$. This technique inadvertently[58] led to the formation of a novel tricomponent "metal-like"[59] complex of $(NMe_3H^+)(I_3^-)_{1/3}(TCNQ^{2/3-})$ stoichiometry, (15),[59,60]

$$NMe_3H^+I^- + TCNQ^0 = (NMe_3H^+)(I_3^-)_{1/3}(TCNQ^{2/3-}). \quad (15)$$

Similarly, durohydroquinone can be oxidized by TCNQ to generate $TCNQ^{\cdot}$, as reported for the preparation of (quinolinium)$(TCNQ)_2$, (16).[71]



(16)

Many complexes are not oxidized by TCNQ in solution, but charge transfer is achieved in the solid. In order to ascertain the extent of the redox in solution it is important to know the $E_{1/2}$ for the donor and acceptor. For TCNQ the half-cell reactions are given in (**17**) and (**18**) for

$$TCNQ^0 + e^- = TCNQ^- \qquad E_{1/2} \sim +0.19v \qquad (17)$$

$$TCNQ^+ + e^- = TCNQ^{2-} \qquad E_{1/2} \sim -0.28v. \qquad (18)$$

$\sim 10^{-4}$ *M* solutions in acetonitrile vs. the SCE.[19,71,100] Thus, donors with $E < -0.19$v are necessary for electron transfer to occur in solution. Even though a solution redox does not occur, however, it is feasible that if a donor acceptor complex crystallizes, the substances may have electron transfer in the solid state.

This is best illustrated by reviewing the reaction of TCNQ with $Nb_3(Cl)_6(C_6Me_6)_3^+$, which results in the isolation of $Nb_3Cl_6(C_6Me_6)_3^{2+}(TCNQ^-)_2$.[101] Were the oxidation affected in solution then the $Nb_3Cl_6(C_6Me_6)_3^{2+}$ paramagnetic ion would dimerize to the diamagnetic $Nb_6Cl_{12}(C_6Me_6)_6^{4+}$ ion.[101] Other examples of this have been reported for the formation of highly conducting ferrocenium TCNQ complexes solution[71] as well as (TTF)(TCNQ).[33] Ferrocene exhibits a $E_{1/2}$ at +0.40 v under the identical conditions (vs. SCE and 0.1 *M* $Et_4N^+ClO_4^-$ supporting electrolyte) that TCNQ's $E_{1/2}$ = 0.19v. Thus, redox does not occur in solution, but a 2 : 1 :: TCNQ : ferrocene can be isolated under the right conditions.[71] Substituting ferrocene with electron-donating groups (e.g. methyl) decreases the $E_{1/2}$ and facilitates the formation of various ferrocene TCNQ complexes of 1 : 1 and 1 : 2 stoichiometries.[55] Recently, the covalent bonded $TCNQ^-$ dimer has been prepared via the reaction of Li^+TCNQ^- and *trans*-$Pt(bipy)_2Cl_2$ (bipy = 2,2′-bipyridyl).[99] This complex, of course, does not form a 1-D chain. In addition to these oxidative reactions, substitution reactions, methasis reactions, where the product is less soluble than the starting material, may be employed,[2,71] e.g. (**19**).

$$Cation^+TCNQ^- + (Cation^+)Anion^- \rightarrow (Cation^+)(TCNQ^-) \qquad (19a)$$

$$Cation^+(TCNQ)_2^- + Cation^+Anion \rightarrow Cation^+)(TCNQ)_2^-. \qquad (19b)$$

Complex TCNQ salts such as 1:2 and 2:3 can be prepared by the addition of excess TCNQ or stoichiometric addition of TCNQ to a simple 1 : 1 salt e.g. (**20**),[102]

$$NMP^{+} + TCNQ^{\cdot} + TCNQ^{0} = (NMP)(TCNQ)_2 \qquad (20)$$

to form, for example, 1:2 and 2:3 salts.

With these concepts, techniques, and examples in mind, the design and synthesis of new highly conducting 1-D materials should be facilitated.

Notes and References

1. Miller, J. S. & A. J. Epstein. 1976. Progr. Inorg. Chem. **20:** 1.
2. Bespalov, B. P. & V. V. Titov. 1975. Russ. Chem. Rev. **44:** 1091.
3. André, J.-J., A. Bieber & F. Gautier. Ann. Physique **1:** 145.
4. See Miller, J. S. Introduction. Bibliography. This Volume.
5. Engler, E. M. 1976. Chemtech. **6:** 274.
6. Interrante, L. V. 1976. Adv. Chem. Ser. **150:** 1.
7. Mott, N. 1974. Metal-Insulator Transitions. Barnes and Noble Books. New York, N. Y.
8. a: Little, W. A. 1964. Phys. Rev. **134:** 1416; b: Little, W. A. 1965. Scientific American **212**(2): 21; c: Yagubskii, E. B. & M. L. Khidekel. 1972. Russ. Chem. Rev. **41:** 1011; d: Little W. A. 1974. *In* Energy and Charge Transfer in Organic Semiconductors. K. Masuda and M. Silver, Eds.: 145. Plenum Press. New York, N. Y. e: Little, W. A. 1975. *In* Low-Dimensional Cooperative Phenomena. NATO ASI, **7B:** 35; f: Little, W. A. & R. Lorentz. 1976. Inorg. Chim. Acta **18:** 273.
9. Komarek, P. 1976. Contemp. Physics **17:** 355; Snowden, D. P. 1973. Sci. Amer. **220**(3): 84.
10. Williams, J. M., J. L. Petersen, H. M. Gerdes & S. W. Peterson. 1974. Phys. Rev. Lett. **33:** 1079; Peters, C. & C. F. Eagen. 1975. Phys. Rev. Lett. **34:** 1132; Deiseroth, H. J. & H. Schulz. 1974. Phys. Rev. Lett. **33:** 963.
11. Phillips, T. E., R. J. Kistenmacher, J. P. Ferraris & D. O. Cowan. 1973. Chem. Commun. 471; Kistenmacher, T. J., T. J. Phillips & D. O. Cowan. 1974. Acta Cryst. **B30:** 763.
12. Boudeulle, M. 1975. Cryst. Structure Comm., **4:** 9, Ph.D. Thesis, University of Lyon, 1974, translation courtesty of IBM Research Lab, San Jose, Calif.; MacDiarmid, A. G., C. M. Mikulski, P. J. Russo, M. S. Saran, A. F. Garito & A. J. Heeger. 1975. J. Am. Chem. Soc. **97:** 6358.
13. Street, G. B. & R. L. Greene. 1977. IBM J. Res. Dev. **21:** 99.
14. Greene, R. L., G. B. Street & L. J. Suter. 1975. Phys. Rev. Lett. **34:** 577.
15. Kittel, C. 1958. Introduction to Solid State Physics. John Wiley & Sons. New York, N.Y.; Mott, N. F. & H. Jones. 1958. The Theory of the Properties of Metals and Alloys. Dover Publications, Inc. New York, N.Y.
16. Gerstein, B. C. 1973. J. Chem. Ed. **50:** 316.
17. Epstein, A. J., E. M. Conwell, D. J. Sandman & J. S. Miller. 1977. Solid State Commun. **24:** 627.
18. Bloch, A. N., D. O. Cowan & T. O. Poehler. 1974. *In* Energy and Charge Transfer in Organic Semiconductors K. Masuda and M. Silver, Eds.: 167–176. Plenum Press. New York, N. Y.
19. Garito, A. F. & A. J. Heeger. 1974. Acct. Chem. Rev. **7:** 232.
20. a: e.g. Selzer, J. O. & B. W. Matthews. 1976. J. Phys. Chem. **80:** 631, and Dessent, T. A., R. A. Palmer & S. M. Horner. 1974. A. C. S., Symp. Ser. **5:** 301. b: Anex, B. G. & W. T. Simpson. 1960. Rev. Mod. Phys. **32:** 466. Fanconi, B. M., G. A. Gerhold & W. T. Simpson. 1969. Mol. Cryst. Liq. Cryst. **6:** 41.
21. Miller, J. S. 1976. Adv. Chem. Ser. **150:** 18.
22. Shakespeare, W. Merchant of Venice. Act II, Sc. 7, l. 65.
23. Bondi, A. 1964. J. Phys. Chem. **68:** 441; Glidewell, C. 1975. Inorg. Chim. Acta **12:** 219; Glidewell, C. 1976. Inorg. Chim. Acta **20:** 113; Pauling, L. 1976. Proc. Nat'l Acad. Sci. **73:** 4290, 1975, **72:** 3799; Pauling, L. 1948. J. Am. Chem. Soc. **69:** 542; 1976. Handbook of Chemistry and Physics, 57th edit.: D-178.

24. MILLER, J. S. 1976. Inorg. Chem. **15:**2357, and references therein.
25. MILLER, J. S. 1977. Inorg. Chem. **16:** 957, and references therein.
26. PETERSEN, J. L., C. J. SCHRAMM, D. R. STOJAKOVIC, B. M. HOFFMAN & T. J. MARKS. 1977. J. Am. Chem. Soc. **99:** 286.
27. MUELLER-WESTERHOFF, U. T. & F. HEINRICH. 1974. A. C. S., Symp. Ser. **5:** 392; MUELLER-WESTERHOFF, U. T. 1976. Adv. Chem. Ser. **150:** 31.
28. KAISER, S. W., R. B. SAILLANT, W. M. BUTLER & P. G. RASMUSSEN. 1976. Inorg. Chem. **15:** 2681, 2688; KAISER, S. W., R. B. SAILLANT & P. G. RASMUSSEN. 1975. J. Am. Chem. Soc. **97:** 425.
29. LONGONI, G. & P. CHINI. 1976. J. Am. Chem. Soc. **98:** 7225.
30. MILLER, J. R. 1961. J. Chem. Soc. 4452; 1965, 713.
31. a: CRAVEN, B. M. & D. HALL. 1961. Acta Cryst. **14:** 475. b: 1966. **21:** 177.
32. SCHULTZ, A. J. & G. D. STUCKY. 1977. J. Phys. Chem. Solids **38:** 269; 1976. SCHULTZ, A. J., G. D. STUCKY, R. CRAVEN, M. J. SCHAFFMAN & M. B. SALAMON. J. Am. Chem. Soc. **98:** 5191.
33. a: WHELAND, R. C. & J. L. GILLSON. 1976. J. Am. Chem. Soc. **98:** 3916; b: WHELAND, R.C. 1976. J. Am. Chem. Soc. **98:** 3926.
34. BAILEY, N. A., E. COATES, G. B. ROBERTSON, F. BONATI & R. UGO. 1967. Chem. Commun. 1041; OLDHAM, G. C. 1969. Ph.D. Dissertation. Univ. North Carolina, Chapel Hill, N.C.; 1969. Disc. abst. **B29:** 4619.
35. See MILLER, J. S. & C. H. GRIFFITHS. 1977. J. Am. Chem. Soc. **99:** 749, and references therein.
36. a: GLEIZES, A., T. J. MARKS & J. A. IBERS. 1975. J. Am. Chem. Soc. **97:** 3545. b: ENDRES, H., H. J. KELLER & R. LEHMANN. 1975. Inorg. Nucl. Chem. Lett. **11:** 769. c: ENDRES, H., H. J. KELLER, R. LEHMANN & J. WEISS. 1975. Acta Cryst. **32B:** 627. d: ENDRES, H., H. J. KELLER, M. MEGNAMISI-BELOMBÉ, W. MORONI & D. NÖTHE. 1974 Inorg. Nucl. Chem. Lett. **10:** 467. e: KELLER, H. J. 1975. NATO Adv. Study Inst. **7B:** 315; f: LEICHERT, F. & J. WEISS. 1975. Acta Cryst. **31B:** 2709; ENDRES, H., H. J. KELLER, M. MEGNAMISI-BELOMBÉ & D. NÖTHE. 1975. Z. Naturforsch. **B30:** 535; g: UNDERHILL, A. E., D. M. WATKINS & R. PETHIG. 1973. Inorg. Nucl. Chem. Lett. **9:** 1269; h: BÉLOMBÉ, M. M. J. Solid State Chem. 1977. **22:** 151; i: MILLER, J. S. & S. Z. GOLDBERG. 1975. Inorg. Chem. **14:** 2294.
37. KAUFMAN, F. B. 1976. J. Am. Chem. Soc. **98:** 5339.
38. COX, E. G., F. W. PINKARD, W. WARDLAW & G. H. PRESTON. 1932. J. Chem. Soc. 2527.
39. a: SOOS, Z. G. & D. J. KLEIN. 1975. Molecular Associations **1:** 1. b: SOOS, Z. G. 1974. Ann. Rev. Prog. Phys. Chem. **25:** 121. c: HERBSTEIN, F. H. 1971. *In* Structural Chemistry. J. D. Dunitz and J. A. Ibers, Eds. Vol. **IV:** 166. John Wiley & Sons. New York, N. Y.
40. GOLDBERG, I. & U. SHMUEL. 1971. Nature **234:** 36.
41. COTTON, F. A. & G. WILKINSON. 1972. Advanced Inorganic Chemistry. 3rd edit. Wiley-Interscience. New York, N. Y.
42. Au(V) has been reported. BARTLETT, N. & K. LEARY. 1976. Rev. Chim. Min. **13:** 82.
43. MARSH, D. G. & J. S. MILLER. 1976. Inorg. Chem. **15:** 720.
44. MILLER, J. S. & D. G. MARSH. 1976. Inorg. Chem. **15:** 2293, and references therein.
45. EPSTEIN, A. J., N. O. LIPARI, D. J. SANDMAN & P. NIELSEN. 1976. Phys. Rev. B **13:** 1569.
46. KRIVOSHEI, I. V. 1976. Zh. Struct. Chem. **17:** 89.
47. REIS, A. H., JR., S. W. PETERSON, D. M. WASHECHECK & J. S. MILLER. 1976. J. Am. Chem. Soc. **98:** 234.
48. REIS, A. H., JR., S. W. PETERSON, D. M. WASHECHECK & J. S. MILLER. 1976. Inorg. Chem. **15:** 2455.
49. KEEFER, K. D., D. M. WASHECHECK, N. P. ENRIGHT & J. M. WILLIAMS. 1976. J. Am. Chem. Soc. **98:** 233.
50. WILLIAMS, J. M., K. D. KEEFER, D. M. WASHECHECK & N. P. ENRIGHT. 1976. Inorg. Chem. **15:** 2446.
51. KROGMAN, K. 1968. Z. Anorg. Allgem. Chem. **358:** 97.
52. a: REIS, A. H., JR., S. W. PETERSON & S. C. LIN. 1976. J. Am. Chem. Soc. **98:** 7839;

b: KOBAYASHI, H., I. SHIROTANI, A. KOBAYASHI & Y. SASAKI. 1977. Solid State Commun. **23:** 409.
53. FUZUA, S. A., R. M. PARKHURST & R. M. SILVERSTEIN. 1964. Tetrahedron **20:** 1625; CHOW, S. W., W. E. LOEB & C. E. WHITE. 1969. J. Appl. Poly. Sci. **13:** 2325.
54. PERROS, T. P., W. F. SAGER & D. E. ICENHOWER. 1957. J. Am. Chem. Soc. **79:** 1301.
55. MILLER, J. S. Unpublished results.
56. BALCH, A. L. 1972. J. Organomet. Chem. **37:** C19.
57. DAVIS, B., H. GUTFREUND & W. A. LITTLE. 1976. Phys. Rev. B **13:** 4766.
58. COUGRAND, A., S. FLANDROIS, P. DELHAES, P. DUPUIS, D. CHASSEAU, J. GAULTIER & J. L. MIANE. 1976. Mol. Cryst. Liq. Cryst. **32:** 165.
59. ABKOWITZ, M. A., A. J. EPSTEIN, C. H. GRIFFITHS, J. S. MILLER & M. L. SLADE. 1977. J. Am. Chem. Soc. **99:** 5304.
60. DELHAES, P., A. COUGRAND, S. FLANDROIS, D. CHASSEAU, J. GAULTIER, C. HAUW & P. DUPUIS. 1976. Abstr. D4. Conf. Organic Conductors and Semiconductors. Biofok, Hungary. September.
61. BLOCH, A. N., D. O. COWAN, K. BECHGAARD & T. O. POEHLER. 1975. Phys. Rev. Lett. **34:** 1561.
62. RICE, M. J., C. B. DUKE & N. O. LIPARI. 1975. Solid State Commun. **17:** 1089; LIPARI, N. O., C. B. DUKE, R. BOZIO, A. GIRLANDO, C. PECILE & A. PADVA. 1976. Chem. Phys. Lett. **44:** 236.
63. Also, bandwidth can be weakened; however, it is desirable to have strong overlap and consequently a large bandwidth to achieve a metallic state.
64. An inspection of the contributing a_g vibrational modes below the band gap[62] show that such a substitution would in fact remove some of the vibrations; however, the important ones (those with large coupling constants) are not deleted.
65. The conductivity is proportional to the mobility which is strongly dependent upon the electron-phonon coupling constants.
66. BLOCH, A. N., J. P. FERRARIS, D. O. COWAN & T. O. POEHLER. 1973. Solid State Commun. **13:** 753.
67. ENGLER, E. M. & V. V. PATEL. 1976. J. Org. Chem. **40:** 387; ENGLER, E. M. & V. V. PATEL. 1974. J. Am. Chem. Soc. **96:** 7376; ETEMAD, S., T. PENNEY, E. M. ENGLER, B. A. SCOTT & P. E. SEIDEN. 1975. Phys. Rev. Lett. **34:** 741.
68. MOROSIN, B. 1975. Phys. Lett. **53A:** 455; KOBAYASHI, H. 1975. Bull. Chem. Soc. Jap. **48:** 1373; EHRENFREUND, E., S. ETEMAD, L. B. COLEMAN, E. F. RYBACZEWSKI, A. F. GARITO & A. J. HEEGER. 1972. Phys. Rev. Lett. **29:** 1269; FRITCHIE, C. H., JR. 1966. Acta Cryst. **20:** 892.
69. MILLER, J. S. & A. J. EPSTEIN. Submitted for publication.
70 EPSTEIN, A. J. & J. S. MILLER. Submitted for publication.
71. MELBY, L. R., R. J. HARDER, W. R. HERTLER, W. MAHLER, R. E. BENSON & W. E. MOCHEL. 1962. J. Am. Chem. Soc. **84:** 3374; ACKER, D. S. & D. C. BLOMSTROM. U.S. Patent 3,162,641.
72. STUCKY, G. D. Private communication. See Ref. 1.
73. WILLIAMS, J. M., D. P. GERRITY & A. J. SCHULTZ. 1977. J. Am. Chem. Soc. **99:** 1668.
74. a: WILLIAMS, J. M. Private communication; b: KOCH, T. R., E. GEBERT & J. M. WILLIAMS. 1976. J. Am. Chem. Soc. **98:** 4017.
75. CZYCHOLL, G., N. GREWE, H. J. LEDER & S. DROSDZIOK. 1977. Solid State Commun. **22:** 67; CAHEN, D. 1973. Solid State Commun. **12:** 1091; WÜRFEL, P., H. D. HAUSEN, K. KROGMANN & P. STAMPEL. 1972. Phys. Stat. Sol. **10A:** 537.
76. NARITA, M. & C. U. PITTMAN, JR. 1976. Synthesis **8:** 489.
77. DAUPLAISE, D. & J. MEINWALD. 1976. J. Am. Chem. Soc. **98:** 6643.
78. WUDL, F., G. A. THOMAS, D. E. SCHAFER & M. W. WALSH, JR. 1976. Mol. Cryst. Liq. Cryst. **32:** 147; WUDL, F., D. E. SCHAFER & B. MILLER. 1976. J. Am. Chem. Soc. **98:** 252.
79. KHIDEKEL, M. L. & E. B. YAGUBSKII. 1975. Izv. Akad. Nauk SSR, Ser. Khim. 1123.
80. INTERRANTE, L. V., J. W. BRAY, H. R. HART, JR. & G. D. WATKINS. 1977. J. Am. Chem. Soc. **99:** 3523.
81. BURAVOV, L. I., O. N. EREMENKO, R. B. LYUBOVSKII, L. P. ROSENBERG, M. L.

KHIDEKEL', R. P. SHIBAEVA, I. F. SHCHEGOLEV & E. B. YAGUBSKII. 1974. JETP Lett. **20:** 208.

82. BURAVOV, L. I., G. I. ZVEREVA, V. F. KAMINSKII, L. P. ROSENBERG, M. L. KHIDEKEL', R. P. SHIBAEVA, I. F. SHCHEGOLEV & E. B. YAGUBSKII. 1976. J. Chem. Soc. Chem. Commun. 720.
83. PERLSTEIN, J. H., J. P. FERRARIS, V. V. WALATKA, JR., D. O. COWAN & G. A. CANDELA. 1973. AIP Conf. Magnetism and Magnetic Materials Proc. 1494.
84. ISETT, L. C. & E. A. PEREZ-ALBURNE. 1977. Solid State Commun. **21:** 433.
85. SANDMAN, D. J., A. J. EPSTEIN, T. J. HOLMES & A. P. FISHER III. 1977. J. Chem. Soc. Chem. Commun. 177; SYPER, L. & A. SUCHARDA-SOBCZYK. 1975. Bull. Acad. Polon., Sci. Ser. Sci. Chim. **23:** 563.
86. ASHWELL, G. J., D. D. ELEY & M. R. WILLIS. 1976. Nature **259:** 201.
87. a: JOHNSON, G. R., M. G. MILES & J. D. WILSON. 1976. Mol. Cryst. Liq. Cryst. **33:** 67; b: BERGER, P. A., D. J. DAHM, G. R. JOHNSON, M. G. MILES & J. D. WILSON. 1975. Phys. Rev. B **12:** 4085; c: SANDMAN, D. J. & A. F. GARITO. 1974. J. Org. Chem. **39:** 1165; d: DIEKMANN, J., W. R. HERTLER & R. E. BENSON. 1963. J. Org. Chem. **28:** 2719.
88. WUDL, F. & E. W. SOUTHWICK. 1974. J. Chem. Soc., Chem. Commun. 254.
89. STREET, G. B., W. D. GILL, R. H. GEISS, R. L. GREENE & J. J. MAYERLE. 1977. J. Chem. Soc., Chem. Commun. 407; GILL, W. D., W. BLUDAU, R. H. GEISS, P. M. GRANT, R. L. GREENE, J. J. MEYERLE & G. B. STREET. 1977. Phys. Rev. Lett. **38:** 1305.
90. TEMKIN, H. D. B. FITCHEN & G. B. STREET. This volume; IQBAL, Z., R. H. BAUGHMAN & A. G. MACDIARMID. This volume.
91. MARKS, T. J. Private communication.
92. EPSTEIN, A. J. & J. S. MILLER. Submitted for publication, and references therein.
93. EPSTEIN, A. J. & J. S. MILLER. This volume.
94. AKHTAR, M., J. KLEPPINGER, A. G. MACDIARMID, J. MILLIKEN, M. J. MORAN, C. K. CHIANG, M. J. COHEN, A. J. HEEGER & D. L. PEEBLES. 1977. J. Chem. Soc. Chem. Commun. 473; CHIANG, C. K., M. J. COHEN, D. L. PEEBLES, A. J. HEEGER, M. AKHTAR, J. KLEPPINGER & A. G. MACDIARMID. 1977. Solid State Commun. **23:** 607.
95. BERNARD, C., A. HEROLD, M. LELAURAIN & G. ROBERT. 1976. C. R. Acad. Sci. (Paris) **283:** 625.
96. MILLER, J. S. 1976. Science **194:** 189.
97. BALCH, A. & M. M. OLMSTEAD. 1976. J. Am. Chem. Soc. **98:** 2354.
98. a: WUDL, F., G. A. THOMAS, D. E. SCHAFER & W. M. WALSH, JR. 1976. Mol. Cryst. Liq. Cryst. **32:** 147; b: KAUFMAN, F. B., E. M. ENGLER, D. C. GREEN & J. Q. CHAMBERS. 1976. J. Amer. Chem. Soc. **98:** 1596. c: WARMACK, R. J., T. A. CALLCOTT & C. R. WATSON. 1975. Phys. Rev. B. **12:** 3336; d: WUDL, F. J. 1975. Amer. Chem. Soc. **97:** 1962; e: SCOTT, B. A., F. B. KAUFMAN & E. M. ENGLER. 1976. J. Am. Chem. Soc. **98:** 4342; f: WUDL, F., D. E. SCHAFER, M. W. WALSH, JR., L. W. RUPP, F. J. DISALVO, J. V. WASZCZAK, M. L. KAPLAN & G. A. THOMAS. 1977. J. Chem. Phys. **66:** 377; g: SOMOANO, R. B., A. GUPTA, V. HADEK, T. DATTA, M. JONES, R. DECK & A. M. HERMANN. 1975. J. Chem. Phys. **63:** 4970; h: DALY, J. J. & F. SANZ. 1975. Acta Cryst **B31:** 620; i: LAPLACA, S. J., P. W. R. CORFIELD, R. THOMAS & B. A. SCOTT. 1975. Solid State Commun. **17:** 635; j: JOHNSON, C. K. & C. R. WATSON, JR. 1976. J. Chem. Phys. **64:** 2271; k: SOMOANO, R. B., A. GUPTA, V. HADEK, M. NOVOTNY, M. JONES, T. DATTA, R. DECK & A. M. HERMAN. 1977. Phys. Rev. B **15:** 595; l: WUDL, F., D. WOBSCHALL & E. J. HUFNAGEL. 1972. J. Am. Chem. Soc. **94:** 670.
99. DONG, V., H. ENDRES, H. J. KELLER, W. MORONI & D. NÖTHE. Submitted for publication.
100. FROIX, M. F. Unpublished results.
101. GOLDBERG, S. Z., B. SPIVACK, G. STANLEY, R. EISENBERG, D. M. BRAITSCH, J. S. MILLER & M. ABKOWITZ. 1977. J. Am. Chem. Soc. **99:** 110.
102. MELBY, L. R. 1965. Can. J. Chem. **43:** 1448.

Discussion

EDWARD ENGLER (*IBM, Yorktown Heights, N.Y.*): In the phenazine work, how do you know which chain the phenazine is going into and what the structure of (phenazine)(TCNQ) is?

MILLER: (Phenazine)(TCNQ) forms an insulating DADA alternating 1-D chain. However, the product we isolated does not resemble this red material. For example, the optical, magnetic, DSC, and x-ray powder pattern show the mixed material to be very similar but not equivalent to (NMP)(TCNQ). In particular, $\sigma_{RT} \gg 10\ \text{ohm}^{-1}\text{cm}^{-1}$ which implies a conducting 1-D charge-transfer complex. Were phenazine in the anion chain, we would anticipate a lower value for σ_{RT} and a different temperature dependence of the conductivity.

PHILLIP COPPENS (*SUNY-Buffalo, N.Y.*): Why does not the HOMO-HOMO interaction lead to an eclipsed structure, i.e., 0° of relative rotation?

MILLER: That is a possibility. Eclipsed configurations have more steric interactions (core repulsions) than other orientations. Clearly, intermolecular backbonding must be evaluated with regard to van der Waals, dipole-dipole, electrostatic forces, and so on, all of which will contribute to the stabilization of the structure.

CHEMISTRY OF THE MIXED-VALENT CHARGE-TRANSPORT PROCESS: THE DESIGN OF ORGANIC MOLECULES FOR ORGANIC METALS*

J. H. Perlstein, J. A. VanAllan, L. C. Isett, and G. A. Reynolds

Research Laboratories
Eastman Kodak Company
Rochester, New York 14650

INTRODUCTION

There are a number of factors in the molecular structure of most organic radicals and radical ions that tend to limit the electron transport process in ordered arrays of such molecules. It is generally believed, based on early ideas expressed by Mott,[1] that a uniform ordered array of radicals will be insulating because of the large coulomb correlation between electrons on neighboring sites which keeps them localized on those sites as in FIGURE 1.

With the discovery of TCNQ by duPont workers[2] it was realized immediately that the presence of mixed oxidation or mixed-valence states, viz. uniform ordered arrays of TCNQ in which there were formally present $TCNQ^0$ as well as $TCNQ^-$, yielded solids whose electrical conductivity was many orders of magnitude larger than that of the nonmixed-valence analogs, presumably due to a reduction in the influence of coulomb correlation as in FIGURE 2 ($\sim$ 1 eV for most TCNQ salts).

Based on this observation, it would have seemed reasonable that *any* stable radical ion that was insulating could be converted into a conductor simply by being made mixed-valent. It has become quite clear, however, that most organic ions cannot coexist with their neutral species in a structurally uniform mixed-valent state, and consequently most radical-ion solids are insulators.

It is the purpose of this paper to point to those organic concepts which empirically seem to be necessary for the formation of the mixed-valent state, to demonstrate the utility of those concepts by numerous examples, and to present some new examples.

INTRAMOLECULAR VS. INTERMOLECULAR ELECTRON TRANSFER

Recently, Rice *et al.*,[3] Lipari *et al.*,[4] and Rice and Lipari[5] have determined the coupling constants for the interaction between the unpaired electron and molecular vibrations for $TCNQ^-$ and TTF^+ radical ions. They have shown that the extra binding energy E_b associated with the distortion of a TCNQ molecule when an electron is added to it (also called the small polaron-binding energy) is about 0.15 eV (3.5 kcal). A similar result is obtained when an electron is removed from TTF (about 0.21 eV). This distortional energy is of the same order as the

*Manuscript received Oct. 3, 1977.

0077-8923/78/0313-0061 $1.75/1 © 1978, NYAS

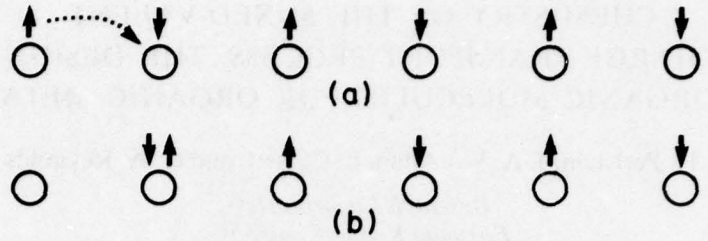


FIGURE 1. (a): Uniform ordered array of radicals with one unpaired electron on each site. (b): Charge transport requires double occupancy of a single site. If the coulomb repulsion on this site is much larger than the intermolecular resonance energy, no transport will occur.

*inter*molecular resonance energy E_r, which is ≤ 0.12 eV. We believe that this important result will determine whether a mixed-valent state will form or not form in the solid state. For if $E_b \gg E_r$, local distortions will favor *intramolecular* localization of charge over *inter*molecular bonding, and thus no one-electron mixed-valent bond will form. Conversely, if $E_r \geq E_b$ a mixed-valent state should form.

One can view this interpretation in the following manner. Suppose we have a neutral molecule A-B (where A and B are two submolecules joined by conjugation) and we arrange a group of such molecules in a slipped stack array as in FIGURE 3(a). If we place an electron on one molecule forming $(A\text{-}B)^{\cdot-}$, the unpaired spin can either 1) delocalize in a molecular orbital over A-B or 2) localize in some part of A-B, on A say, as in FIGURE 3(c). The localization can occur as in FIGURE 3(c) because of some local distortion (such as double-bond fixation) in A which is of lower energy than the delocalized state of FIGURE 3(a). The electrical conductivity (FIGURE 3(a) to 3(b)) will be governed by the size of the intermolecular resonance integral (viz. the transfer integral), which is a measure of the interaction between neighbors. In FIGURE 3(c), however, the electron must first hop by a series of intramolecular distortions (FIGURE 3(d)) (by a series of bond-breaking and bond-forming steps) from A to B before intermolecular transfer can take place (FIGURE 3(e)). Only if the activation energy for the bond-breaking and bond-reforming steps is $< E_r$ will intermolecular bonding and hence efficient charge transport occur.

In designing molecules, then, for electrical conductivity, one must decide

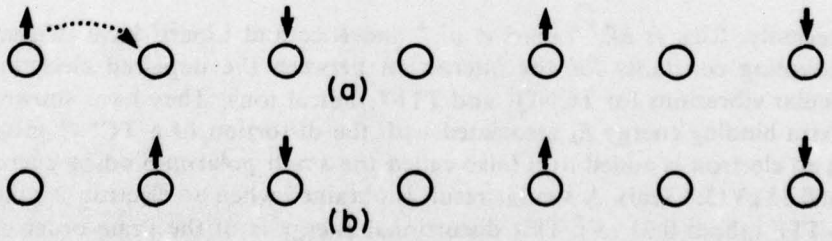


FIGURE 2. (a): Mixed-valence state. Only every other molecule is a radical; (b): Charge transport does not require double-site occupancy. Effect of coulomb repulsion between charge carriers is reduced from that in FIGURE 1(b).

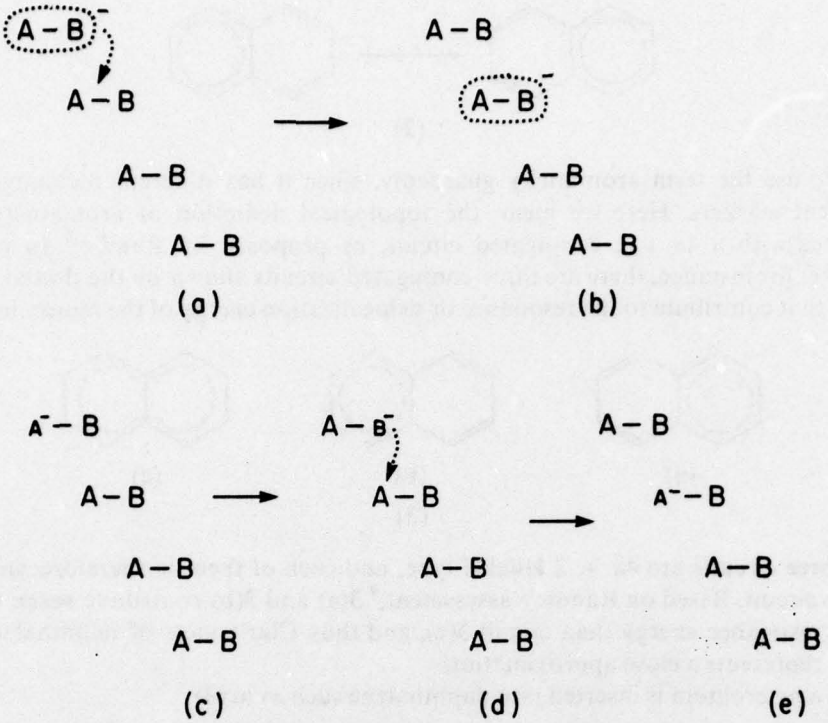
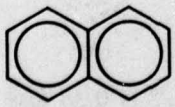


FIGURE 3. (a): Ordered array of A-B molecules with one electron delocalized over a single site (dotted line). In this configuration, nuclear symmetry of $(A\text{-}B)^-$ will be the same as for $(A\text{-}B)^*$. (b): Charge transport occurs. Delocalized state has readily moved to second site. (c): Charge localized on A with large symmetry change in A-B (indicated by small letter A). (d): Charge must overcome distortional energy barrier to get to B. (e): Charge must overcome large distortional energy barrier to get to A on another molecule.

a priori whether the radical ion formed from these molecules will contain a delocalized state, as in FIGURE 3(a). Below, we show how to decide this based on the concept of local $4n + 2$ aromaticity first introduced by Clar[6] and expanded by Herndon and Ellzey,[7] and more recently by Randic.[8]

THE LOCAL AROMATICITY CONCEPT

Clar[6] has pointed out by numerous examples that in describing a structure such as naphthalene, one should not consider the molecule as containing two aromatic rings as in (1)



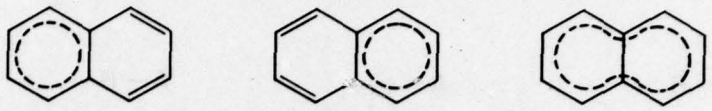
(1)

but only one aromatic ring which can diffuse, as in (2).



(2)

We use the term aromaticity guardedly, since it has different meanings for different workers. Here we mean the topological definition of aromaticity associated with a $4n + 2$ conjugated circuit, as proposed by Randic.[8] In naphthalene, for instance, there are three conjugated circuits shown by the dotted lines in (3) that contribute to the resonance or delocalization energy of the molecule.

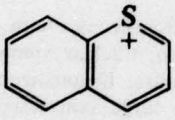


(a) (b) (c)

(3)

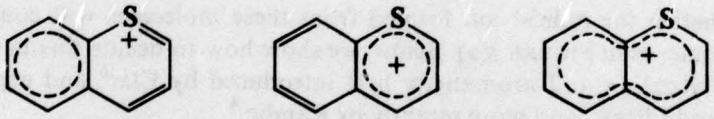
All three circuits are $4n + 2$ Hückel type, and each of them is therefore an aromatic circuit. Based on Randic's assessment,[9] 3(a) and 3(b) contribute seven times more resonance energy than circuit 3(c), and thus Clar's view of naphthalene as in (2) represents a close approximation.

If a heteroatom is inserted into naphthalene such as in (4)



(4)

then the $4n + 2$ conjugated circuits are represented by (5).



(a) (b) (c)

(5)

However, the HMO delocalization energy for thiapyrylium (6),



(6)

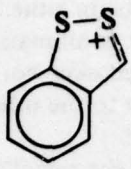
neglecting d-orbital participation,[10] is 0.3β less than benzene, or about 0.23 eV (5.4 kcal) $\gg$ kT. Circuits 5(b) and 5(c) therefore should not contribute very much to the delocalization of charge compared to 5(a). Viewed in this way, a lone

thiapyrylium ring (**6**) contains an aromatic sextet of electrons, whereas an annellated thiapyrylium ring (**4**) contains an aromatic sextet only in the benzene ring with two "fixed" double bonds in the thiapyrylium ring.

The same arguments apply to 1,2-dithiolium (**7**), 1,3-dithiolium (**9**), and their annellated structures ((**8**), (**10**)).



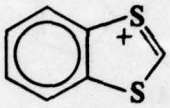
(**7**)



(**8**)



(**9**)

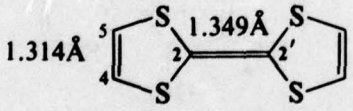


(**10**)

In both cases, the single-ring structures ((**7**), (**9**)) will contain a delocalized sextet, whereas the annellated structures ((**8**), (**10**)) will contain a delocalized sextet only in the benzene ring. We apply this local aromaticity concept in the next section to determine which radical ions will have delocalized charge and favor the formation of mixed-valence states.

Local Aromaticity of Radical Ions

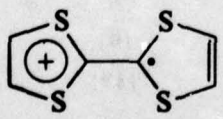
TTF (**11**) contains no $4n + 2$ aromatic circuits.



(**11**)

The C_4—C_5 and C_2—$C_{2'}$ bond lengths[11] are both characteristic of localized double bonds.

If the radical cation is formed as in (**12**)



(**12**)

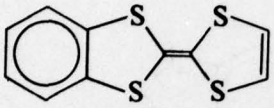
a new 6π aromatic circuit is produced, namely (**9**). This aromatic circuit can be in either ring with the same energy as shown in (**13**).



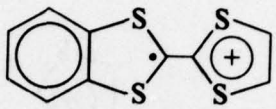
(13)

The unpaired spin can be in either ring and is best described by a molecular orbital involving a linear combination of atomic orbitals on both rings. The unpaired spin is delocalized over both rings, with no activation energy required to transfer it from one ring to the other. TTF, of course, readily forms mixed-valent high-conductivity solids.

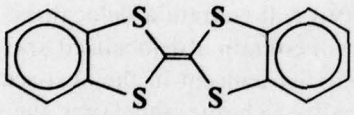
Consider, however, the annellated structures ((14), (16)) of TTF and their radical cations ((15), (17)).



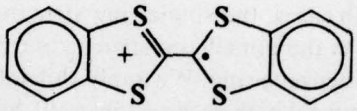
(14)



(15)

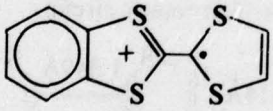


(16)



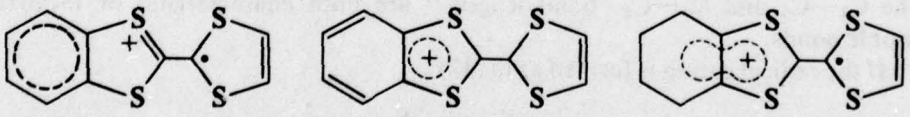
(17)

Although (14) forms a new aromatic sextet upon oxidation to give (15), the unpaired spin is effectively localized in one ring. The structure with the electron in the other ring (18) will be of higher energy, since it destroys a dithiolium aromatic circuit in (15) without creating an equivalently energetic aromatic circuit.



(18)

The circuits of (18) will look like (19).



(a) (b) (c)

(19)

Only 19(b) is comparable energetically to (15), but to form 19(b) from (15) requires the destruction of the benzene aromatic circuit in (15). From HMO calculations,[10] this will require about 0.8 eV (18 kcal). Structure (15) is then not expected to form high-conductivity solids, and it does not.[12]

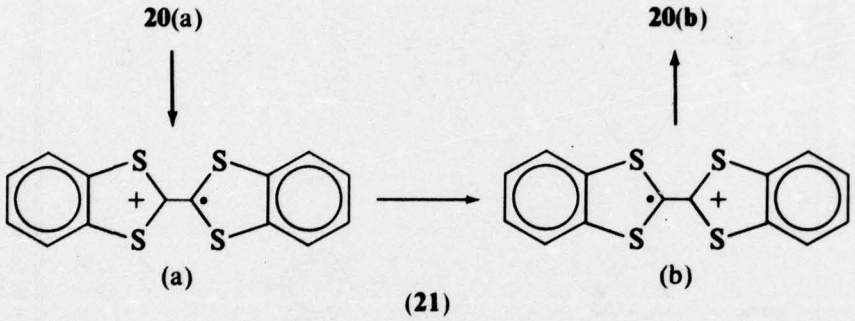
The situation is still worse for the dibenzo TTF (**16**). No new aromatic circuit can be produced in the radical cation (**17**), which will be equienergetic with the two benzene circuits in the neutral structure (**16**). The unpaired spin is effectively "trapped" in one ring. One may ask, why not write resonance structures such as (**20**), which moves the electron from one ring to the other?



(a) (b)

(**20**)

Although (**20**(a)) and (**20**(b)) are equienergetic, there is a barrier for the migration of charge associated with the intermediate structures in (**21**).



(a) (b)

(**21**)

None of the transformations from (**20**(a)) through (**21**) to (**20**(b)) are associated with a $4n + 2$ circuit, and thus each of the transformations will require an activation energy associated with bond—length changes. Based on the discussion in INTRAMOLECULAR VS. INTERMOLECULAR ELECTRON TRANSFER, (**16**) should not effectively form a high-conductivity state (see TABLES 1 and 2).

With these observations and interpretations in mind, we suggest that the following conditions are necessary to form mixed-valent conductors.

Class A Molecules (Good Conductors)

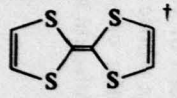
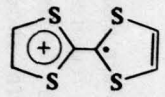
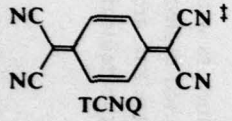
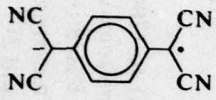
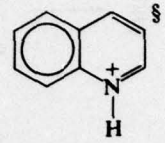
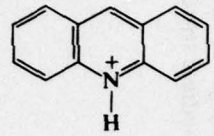
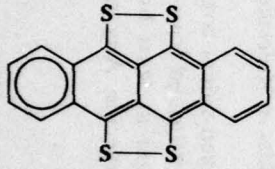
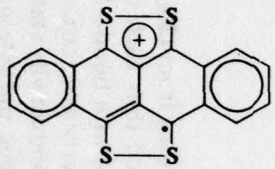
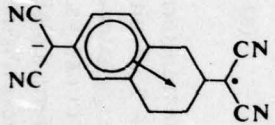
The most efficient mixed-valent conductors (conductors with zero or very low activation energy) will be formed from those conjugated molecules whose radical cations or anions contain at least one new independent aromatic circuit not present in the neutral molecule. Any aromaticity in the neutral molecule must be conserved.

Class B Molecules (Intermediate to Poor Conductors)

Intermediate- to low-conductivity solids will be formed by those molecules whose radical cations or anions contain a new aromatic circuit but whose de-

TABLE 1

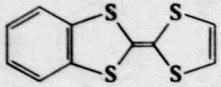
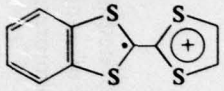
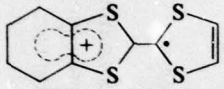
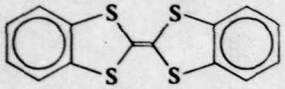
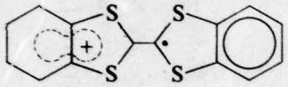
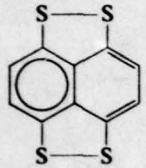
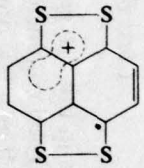
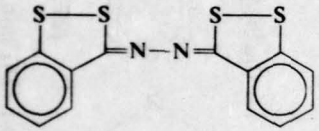
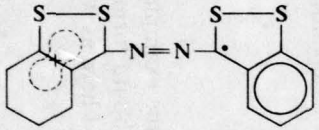
EXAMPLES OF CLASS A MOLECULES THAT FORM MIXED-VALENT SALTS WITH HIGH CONDUCTIVITY

	Neutral Structure	No. of Aromatic Circuits	Radical Ion	No. of New Aromatic Circuits	Gegenion	Stoichiometry	σ^* ($\Omega^{-1}\,cm^{-1}$)	References
(11)	 (TTF)†	0		1	Br^-	1:0.71	100–450	14
					I^-	1:0.71	300–550	14, 15
					$TCNQ^-$	1:1	200–700	16
(22)	 TCNQ‡	0		1	 § 	2:1	100	17–19
						2:1	100	19
(23)	 TTT	1		2	$TCNQ^-$	1:1	1	20, 21
						1:2	1¶	21
					I^-	1:1	1¶	22
					I_3^-	~2:1	700–1500	23, 24
(24)	 TNAP	0		1	TTT^+	1:1	2.5¶	25
					TTF^+	1:1	40	26

†At least 16 derivatives of TTF are now known, a table of which can be found in Ref. 13.
‡At least 22 derivatives of TCNQ are now known, a table of which can be found in Ref. 33.
§A very large number of TCNQ salts with closed-shell cations are known and reported in Ref. 2.
*All data are for single crystals unless indicated otherwise.
¶Data are for compressed powders.

TABLE 2

EXAMPLE OF CLASS B MOLECULES WITH INTERMEDIATE CONDUCTIVITY

	Neutral Structure	No. of Aromatic Circuits	Radical Ion	No. of New $4n + 2$ Circuits	Gegenion	Stoichiometry	σ (Ω^{-1} cm^{-1})	Reference
(14)		1		1	$TCNQ^{-}$	1:1	3×10^{-6}	27
				1				
(16)		2		1	$TCNQ^{-}$ Br^{-}	1:1 1:1.2	10^{-7}* 3.4×10^{-1}†	28 29
(25)		1		1	$TCNQ^{-}$	1:1	40*	30
(26)		2		1	BF_4^{-}	3:2	3×10^{-1}†	29

*Single-crystal data.

†Compressed-powder measurements.

localization energy is less than that of any aromatic circuits present in the unoxidized or unreduced state.

Class C Molecules (Poor Conductors)

Poor conductors (insulators with large activation energy) will be formed by those molecules the radical cations or anions of which contain no new aromatic circuits not already present in the unoxidized or unreduced state.

We believe these conditions to be necessary but obviously not sufficient to categorize all radical-ion conductors. Large bulky substituents, for example, which decrease the intermolecular resonance energy can readily give a Class A molecule, Class C properties. In the next sections we present some examples from each class plus some new examples for Class A.

EXAMPLES

Class A Molecules

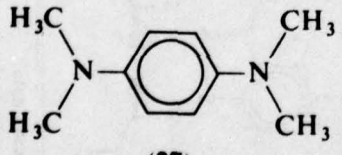
Only a limited number of these are presently known. TABLE 1 presents a few examples; a more complete list has been presented elsewhere.[13] In all cases at least one new independent aromatic circuit is formed.

Class B Molecules

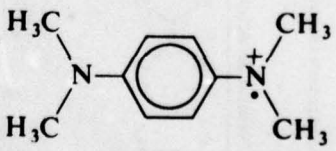
Most of the examples in this category are benzoannellated derivatives of materials that should form good conductors in the absence of annellation. (**14**) and (**16**) are listed here as well as a few others in TABLE 2. A more complete list is in Reference 13.

Class C Molecules

This is by far the largest class known. The best example is TMPD (**27**).



(**27**)

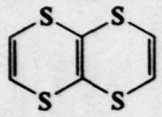
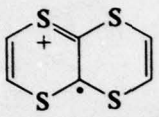
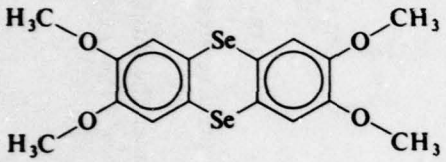
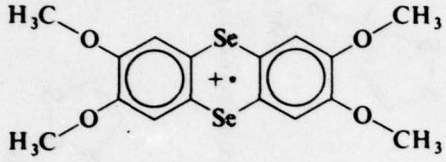
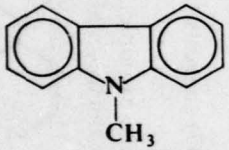
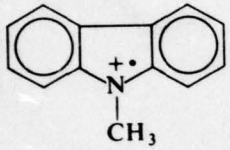


(**28**)

Its radical ion (**28**) contains no new $4n + 2$ circuit not already present in the neutral molecule. Consequently, no conductive mixed-valent states of this molecule should form and none are known. Other examples are presented in TABLE 3 and elsewhere.[13]

TABLE 3

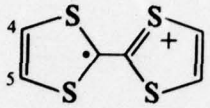
EXAMPLES OF CLASS C MOLECULES WITH POOR CONDUCTIVITY

	Neutral Structure	No. of Aromatic Circuits	Radical Ion	No. of New $4n + 2$ Circuits	Gegenion	Stoichiometry	σ $(\Omega^{-1} cm^{-1})$*	References
(29)		0		0	no complexes	—	—	31
(30)		1		0	ClO_4^- $TCNQ^-$	1:1 1:1 1:2	— 10^{-3}† 5×10^{-2}†	32
(31)		2		0	$TCNQ^-$	1:1	5×10^{-10}	33,34
(32)		2		0	$TCNQ^-$	1:1	10^{-12}	33

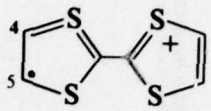
*Compressed-powder data.
†Single-crystal data.

Design of Class A Molecules

Design of Class A molecules requires careful attention to the kinds of substituents placed on the Class A molecular skeleton, their position, and their number. Using TTF^{+} as an example, SCF calculations[35] indicate that little of the unpaired electron density is in positions 4 or 5, indicative of the fact that of resonance structures (**33**) and (**34**), type (**33**) makes the major contribution to the wave function. Protective groups at sites 4 and 5 to prevent further chemical reactivity of the cation are not necessary, since there is little spin density at these sites.

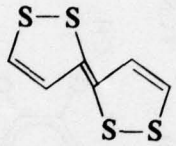


(**33**)



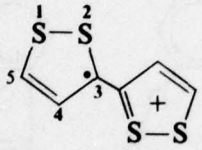
(**34**)

On the other hand, consider the 1,2-dithiolium analogue[36] of TTF (**35**).

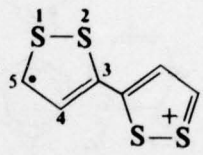


(**35**)

Its radical cation has resonance structure type (**36**) and (**37**).

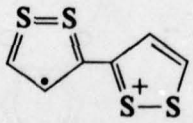


(**36**)



(**37**)

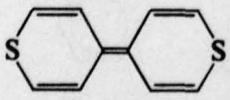
As with TTF^{+}, structure of the type (**38**) should contribute much less to the delocalization energy.



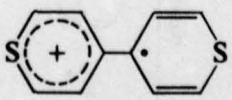
(**38**)

Structure (**37**) suggests that protective groups will be needed at sites 5 and 5′ but not at 4 or 4′.

As a third example, consider the dithiapyranylidene[37,38] (**39**) and its radical cation (**40**), which contains a new $4n + 2$ circuit as shown.

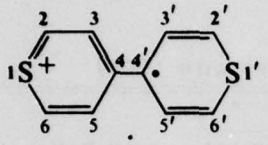


(**39**)

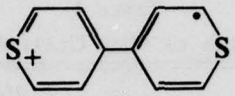


(**40**)

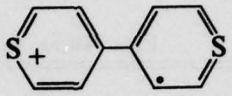
The resonance structure types of (**40**) are (**41–43**).



(**41**)



(**42**)



(**43**)

Structure (**43**), as in (**38**) and (**34**), is not expected to make a major contribution to the delocalization energy. Structure (**42**) then suggests that sites 2, 2′, 6, and 6′ should have protective groups to prevent further chemical reactivity of the radical cation at these sites. Consistent with this interpretation is the fact that from the ESR proton coupling constants,[39] the estimated spin density at site 2 is three times higher than at site 3. ($P_{C_2} = 0.104$, $P_{C_3} = 0.031$, $P_S = 0.059$)

The choice of protective group has been dictated by effects of chemical and electrochemical experience. Methyl groups do not seem to be sufficient, but phenyl rings do. TABLE 4 presents some of our electrical data on powder samples of phenyl-substituted (**39**) and (**35**) TCNQ salts along with some recent data from other laboratories. For the phenyl-substituted compounds, the data are comparable to those from powdered TTF-TCNQ.

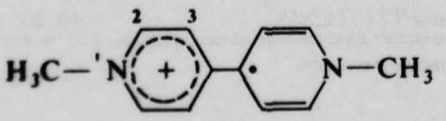
Some additional data suggest the rather unusual nature of these complexes. For instance, (**47**) can be grown as fine filamentary structures within an insulating polymer matrix. A one-micron-thick polymer film containing 5% by weight of filamentary (**47**) has a conductivity of 1 $\Omega^{-1}cm^{-1}$ compared to the pure polymer, which has $< 10^{-14}\,\Omega^{-1}cm^{-1}$.

FIGURE 4 shows the temperature dependence of σ for this film from room temperature down to 50°K. σ is virtually flat near 300°K and then drops off with an activation energy of only 0.07 eV. Near 70°K there seems to be an anomaly. Preliminary magnetic susceptibility data shown in FIGURE 5 for the powdered salt are similar to what one finds in TTF-TCNQ. There also may be an anomaly in χ around 70°K.

It is possible that if the charge-transport processes in these salts are governed by Peierls-Frohlich charge-density-wave (CDW) migration, separating conducting chains by growing them in polymer matrices may have dramatic effects on the pinning temperature of the CDW. Further exploratory studies along these lines are in progress and will be reported elsewhere.

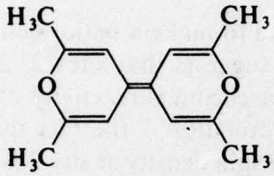
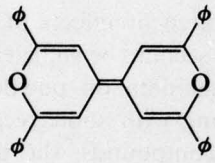
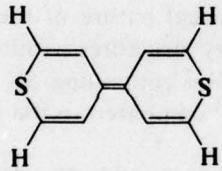
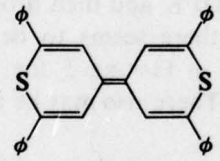
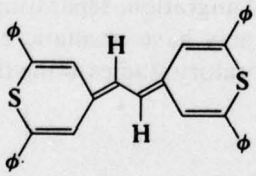
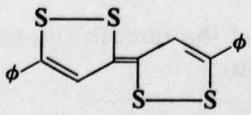
ARE ALL FORMALLY $4n + 2$ CIRCUITS AROMATIC?

It is instructive to compare the properties of the radical cations of (**45**) and (**46**) with their nitrogen analog,[42] the paraquat (**50**).



(**50**)

TABLE 4
ELECTRICAL CONDUCTIVITY OF NEW CLASS A DONORS WITH TCNQ

	Donor	$\sigma(\Omega^{-1}\,cm^{-1})$* (1:1 TCNQ Salt)	Reference
(44)		10^{-6}	40
(45)		1.7	40
(46)		1	41
(47)		10–30	this work
(48)		27	this work
(49)		3–5	this work
	For comparison TTF-TCNQ.	~10–20	

*Compressed-powder measurements.

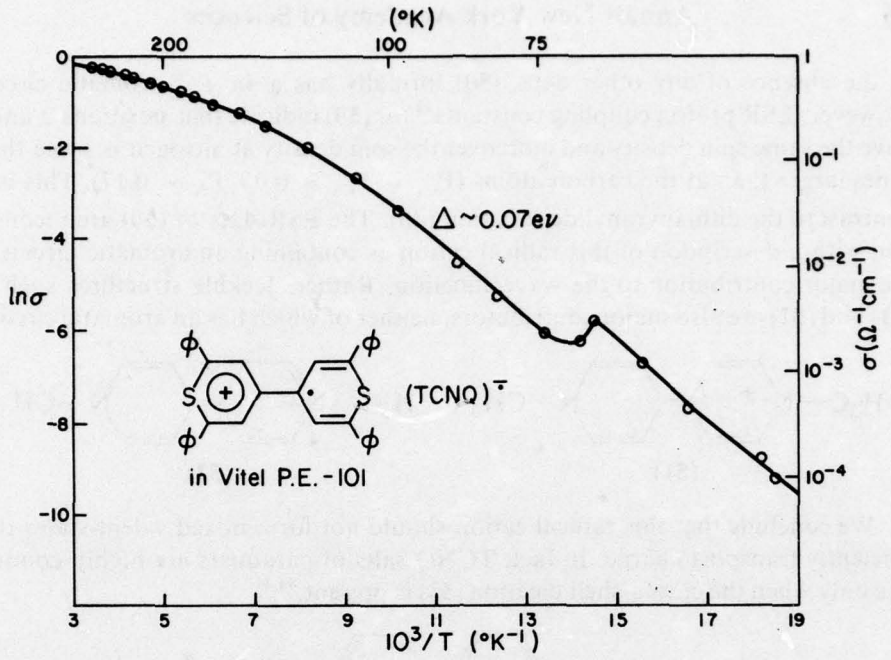


FIGURE 4. Natural logarithm of σ vs. 1/T for 5% by weight of (47) doped into Vitel Polyester 101 (Goodyear Tire and Rubber Company trademark).

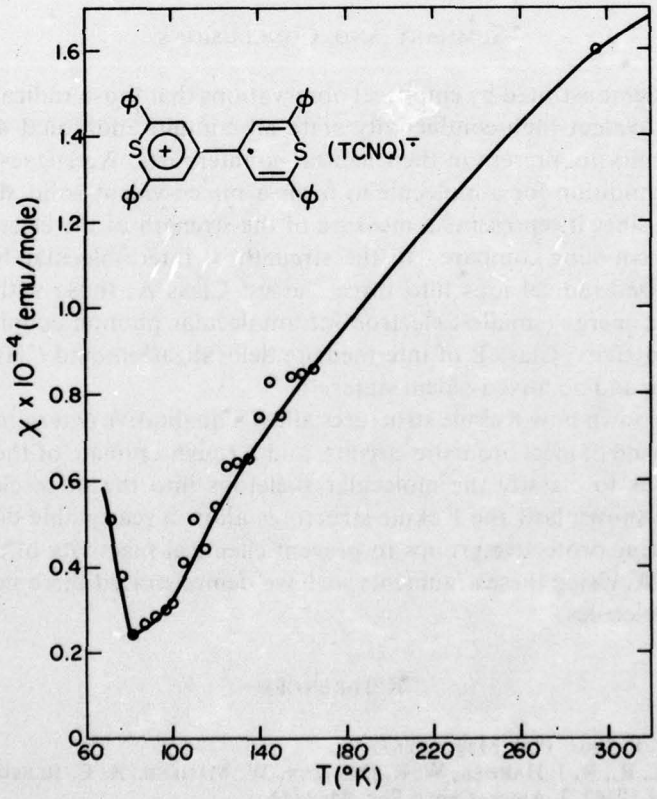
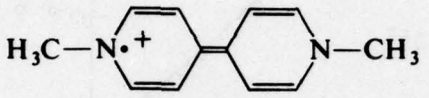
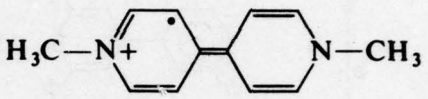


FIGURE 5. Magnetic susceptibility of powdered sample of (47) vs. temperature corrected for core diamagnetism.

In the absence of any other data, (**50**) formally has a $4n + 2$ aromatic circuit. However, ESR proton coupling constants[43] for (**50**) indicate that positions 2 and 3 have the same spin density and moreover the spin density at nitrogen is some three times larger than at the carbon atoms ($P_{C_1} = P_{C_2} = 0.05$, $P_N = 0.17$). This is in contrast to the dithiapyranylidene cation (**40**). The ESR data of (**50**) are inconsistent with a description of this radical cation as containing an aromatic circuit as the major contribution to the wave function. Rather, Kekule structures such as (**51**) and (**52**) are also major contributors, neither of which has an aromatic circuit.

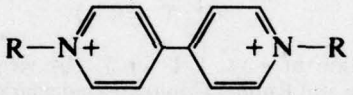


(**51**)



(**52**)

We conclude that this radical cation should not form mixed valent-states that efficiently transport charge. In fact, TCNQ salts of paraquats are highly conductive only when the closed-shell dication (**53**) is present.[44,45]



(**53**)

Summary and Conclusions

We have demonstrated by empirical observations that those radical ions which form a mixed-valent high-conductivity state all contain additional $4n + 2$ local aromatic circuits not present in their neutral counterparts. We suggest that this is a necessary condition for a molecule to form a mixed-valent solid showing high conductivity, since it represents a measure of the strength of the electron-molecular vibration coupling compared to the strength of intermolecular bonding. We have categorized radical ions into three classes: Class A, those with the largest delocalization energy (smallest electron-intramolecular phonon coupling) and the highest conductivity; Class B of intermediate delocalization; and Class C with no delocalization and no mixed-valent states.

We have shown how Kekule structures allow a qualitative determination of the number and kind of local aromatic circuits, and a rough estimate of their energetics has allowed us to classify the molecular skeletons into the three classes above. We have also shown how the Kekule structures allow a reasonable determination of sites requiring protective groups to prevent chemical reactivity of those radical ions in Class A. Using these arguments we have demonstrated three new examples of Class A molecules.

References

1. Mott, N. F. 1961. Phil. Mag. **6**: 287.
2. Melby, L. R., R. J. Harder, W. R. Hertler, W. Mahler, R. E. Benson & W. E. Mochel. 1962. J. Amer. Chem. Soc. **84**: 3374.

3. Rice, M. J., C. B. Duke & N. O. Lipari. 1975. Solid State Commun. **17:** 1089.
4. Lipari, N. O., C. B. Duke, R. Bozio, A. Girlando, C. Pecile & A. Padva. 1976. Chem. Phys. Lett. **44:** 236.
5. Rice, M. J. & N. O. Lipari. 1977. Phys. Rev. Lett. **38:** 437.
6. Clar, E. 1972. The Aromatic Sextet. John Wiley and Sons. New York, N.Y.
7. Herndon, W. C. & M. L. Ellzey, Jr. 1974. J. Amer. Chem. Soc. **96:** 6631.
8. Randic, M. 1977. J. Amer. Chem. Soc. **99:** 444.
9. Randic, M. 1976. Chem. Phys. Lett. **38:** 68.
10. Zahradnik, R. & J. Koutecky. 1963. Coll. Czechoslov. Chem. Commun. **28:** 1117.
11. Cooper, W. F., N. C. Kenny, J. W. Edmonds, A. Nagel, F. Wudl & P. Coppens. 1971. Chem. Commun. 889.
12. Spencer, H. K., M. P. Cava & A. F. Garito. 1976. Chem. Commun. 966.
13. Perlstein, J. H. 1977. Angewandte Chemie Int. edit. **16:** 519.
14. Warmack, R. J., T. A. Callcott & C. R. Watson. 1975. Phys. Rev. **B12:** 3336.
15. Somoano, R. B., A. Gupta & V. Hadek. 1975. J. Chem. Phys. **63:** 4970.
16. Ferraris, J., D. O. Cowan, V. Walatka, Jr. & J. H. Perlstein. 1973. J. Amer. Chem. Soc. **95:** 948.
17. Perlstein, J. H., M. J. Minot & V. Walatka. 1972. Mat. Res. Bull. **7:** 309.
18. Holczer, K., G. Mihaly, A. Janossy & G. Gruner. 1976. Mol. Cryst. Liq. Cryst. **32:** 199.
19. Buravov, L. I., D. N. Fedutin & I. F. Shchegolev. 1971. Sov. Phys. JETP **32:** 612.
20. Perlstein, J. H., J. P. Ferraris, V. V. Walatka, D. O. Cowan & G. A. Candela. 1972. A.I.P. Conf. Proc. Magnetism and Magnetic Materials **10:** 1494.
21. Delhaes, P., S. Flandrois & G. Keryer. 1975. Mater. Res. Bull. **10:** 825.
22. Perez-Albuerne, E. A., H. Johnson, Jr. & D. J. Trevoy. 1971. J. Chem. Phys. **55:** 1547.
23. Isett, L. C. & E. A. Perez-Albuerne. 1977. Solid State Commun. **21:** 433.
24. Mihaly, G., A. Janossy & G. Gruner. 1977. Solid State Commun. **22:** 771.
25. Johnson, G. R., M. G. Miles & J. D. Wilson. 1976. Mol. Cryst. Liq. Cryst. **33:** 67.
26. Berger, P. A., D. J. Dahm, G. R. Johnson, M. G. Miles & J. D. Wilson. 1975. Phys. Rev. **B12:** 4085.
27. Spencer, H. K., M. P. Cava & A. F. Garito. 1976. Chem. Commun. 966.
28. Lyubovskaya, R. N., M. Z. Aldoshina, V. Ya. Rodionov, T. A. Chibisova & M. L. Khidekel. 1974. Bull. Acad. Sci. USSR-Chem. Sci. 168.
29. Barlow, W. A., G. R. Davies, E. P. Goodings, R. L. Hand, G. Owen & M. Rhodes. 1976. Mol. Cryst. Liq. Cryst. **33:** 123.
30. Wudl, F., D. E. Schaeffer & B. Miller. 1972. J. Amer. Chem. Soc. **98:** 252.
31. Mizuno, M., M. P. Cava, A. F. Garito. 1976. J. Org. Chem. **41:** 1484.
32. Somoano, R., V. Hadek, S. Yen, A. Rembaum & R. Deck. 1975. J. Chem. Phys. **62:** 1061.
33. Wheland, R. C. & J. L. Gillison. 1976. J. Amer. Chem. Soc. **98:** 3916.
34. Addison, A. W., T. H. Li & L. Weiler. 1977. Can. J. Chem. **55:** 766.
35. Ratner, M. A., J. R. Sabin & E. E. Ball. 1974. Chem. Phys. Lett. **28:** 393.
36. Behringer, H. & E. Meinetsberger. 1975. Tetrahedron Lett.: 3473.
37. Hunig, S., B. J. Garner, G. Ruider & W. Schenk. 1973. Liebigs Ann. Chem.: 1036.
38. Yoshida, Z., S. Yoneda, T. Sugimoto & O. Kikukawa. 1971. Tetrahedron Lett.: 3999.
39. Yoshida, Z., T. Sugimoto & S. Yoneda. 1972. Chem. Commun. 60.
40. Alizon, J., J. Gallice, H. Robert, G. Delphanque, C. Weyl, C. Fabre & H. Strzelecka. 1976. Mol. Cryst. Liq. Cryst. **33:** 91.
41. Sandman, D. J., A. J. Epstein, T. J. Holmes & A. P. Fisher III. 1977. Chem. Commun.: 177.
42. Rembaum, A., V. Hadek, & S. P. S. Yen, 1971. J. Amer. Chem. Soc. **93:** 2532.
43. Johnson, C. S., Jr. & H. S. Gutowsky. 1963. J. Chem. Phys. **39:** 58.
44. Ashwell, G. J., D. D. Eley & M. R. Willis. 1976. Nature (London) **259:** 201.
45. Ashwell, G. J., D. D. Eley, M. R. Willis & J. Woodward. 1977. Phys. Stat. Sol. (b) **79:** 629.

Discussion

EDWARD ENGLER (*IBM, Yorktown Heights, N.Y.*): I would expect, from your analysis, to see larger differences in the molecular properties of TTF compared to the benzyl and dibenzyl TTF, especially since it is implied that the extent of delocalization is considerably less. I would also then expect the ionization potential to be much higher. That does not appear to be the case. The MO calculations from the literature apparently indicate that the TTF systems are good donors and need only be delocalized over the internal portions of the molecule, and that the external double bonds are not that well coupled into the aromatic character of these systems. Thus, I do not think that we can apply your construct to some of these systems.

PERLSTEIN: Concerning the dibenzyl and benzyl TTF, the oxidation potentials increase with the addition of the benzyl substituents. You can make mixed-valence solids of dibenzyl TTF with bromine, yet the conductivity is only about $10^{-1}\Omega^{-1}cm^{-1}$. I am suggesting that the activation energies will, in general, be larger than those which are not annellated. This may be associated with stronger intramolecular coupling of the electron to the molecular vibrations.

C. H. CHEN (*Eastman Kodak, Rochester, N.Y.*): What are the substituent effects?

PERLSTEIN: Given a system that has this aromatic character, one also has to worry about the location of the spin density in the molecule, and what kinds of substituents be put there to prevent any other chemical reactivity from occurring. We found that phenyl rings are the best in that sense.

THE FUTURE OF ORGANIC METALS COMPOSED OF CARBON, HYDROGEN, NITROGEN, AND SULFUR*

F. Wudl, A. A. Kruger, and G. A. Thomas

Bell Laboratories
Murray Hill, New Jersey 07974

Although we are aware that it is truly pretentious and dangerous to talk about the future of a relatively young research field, we believe that enough information has been gathered so far to warrant a glimpse into the directions it will take. We will restrict ourselves to the treatment of organic materials and will discuss their future only from the infinitely narrow (yet glamorous) point of view of electrical conductivity.

There are two approaches one can take, of which the first and most obvious is chronological; i.e., we can examine the past and present, extract common denominators, and then lunge (extrapolate) into the future. A very difficult task, indeed, to be accomplished within twenty minutes. Particularly at the last session of the last section of this conference! In order to obviate this problem, we have prepared a (grossly oversimplified) table of important events (TABLE 1), starting with the advent of TCNQ and ending sometime in 1977.

From this table we were able to extract the following obvious common denominators:

1. Prior to 1974 (TSeF), all pseudo-one-dimensional organic conductors were discovered more or less accidentally, and not invented or designed.
2. At present, all excellent conductors consist of mixed-valence stacks (formally neutral and formally charged molecules within the same stack).
3. Pseudo-one-dimensional metals cannot become Fröhlich superconductors *on a macroscopic scale.*
4. Increased dimensionality leads to higher conductivities, both at room temperature and at low temperatures.

A second approach is to examine series of compounds and attempt to obtain common features of all members of the group. We have done this with the temperature dependence of the conductivity of a series of compounds and the temperature dependence of the magnetic susceptibility transition[1] of another series of conductors.

In FIGURE 1, we have replotted *on the same scale* (from various published articles),[2] the resistivities of (TTF)(TCNQ), (TTF)(TCNQ) under pressure, (TSeF)-(TCNQ), and (HMTSF)(TCNQ) as a function of inverse temperature. From this plot one can observe the following:

1. All compounds of this series reach the same value of minimum resistivity (maximum conductivity) of *ca.* 1.6×10^{-4} to 10^{-5} Ωcm (6.2×10^{3} to $1.4 \times 10^{4}\,\Omega^{-1}\,cm^{-1}$).

*Manuscript received June 14, 1977.

0077-8923/78/0313-0079 $1.75/1 © 1978, NYAS

TABLE I

DEVELOPMENT OF ORGANIC AND SOME ORGANIC CONDUCTORS OVER A SIXTEEN-YEAR PERIOD

		Knowledge Gained	
Year	Event	Theoretical	Practical
1960	TCNQ	nothing	organic compounds conduct electricity
1964		Little, W. A.	need stacks and complex salts
1965	(NMP)(TCNQ)		No need for complex salts?
1970–1971	(NMP)(TCNQ) revisited TTF	Mott-Hubbard	nothing
1972–1973	(TTF)(TCNQ)(KCP) revisited	Peierls-Fröhlich	first organic "metal"
1974	(TSeF)(TCNQ)	Mixed valence F.R.V.-Fröhlich revisited[5]	No macroscopic Fröhlich superconductors
1975–1976	(HMTSF)(TCNQ) $(SN)_x$ TTT revisited	—	2-D important

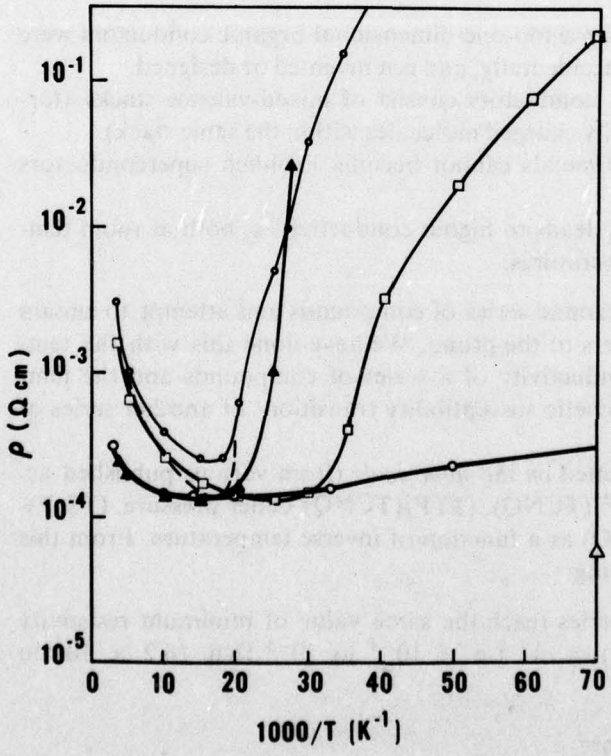


FIGURE 1. Single crystal resistivity as a function of reciprocal temperature. (TTF)(TCNQ) at atmospheric pressure, ●; (TTF)-(TCNQ) at 16.4 kbar, ▲; (TSeF)-(TCNQ) at atmospheric pressure, □; (HMTSF)(TCNQ) at atmospheric pressure, ○; (HMTSF)(TCNQ) at 14 kbar pressure △.

2. (TTF)(TCNQ) under pressure has a behavior remarkably similar to that of (HMTSF)(TCNQ) at atmospheric pressure.
3. (HMTSF)(TCNQ) exhibits the highest conductivity of all, but only under high pressure.

Discussion

The observations based on the table are self-evident and need no further comment.

The reasons for the maximum conductivity value of (1–10) $\times$ $10^4\Omega^{-1}$ cm^{-1} are:

1. That probably "impurities" (chemical impurities and crystal defects) are the overwhelming factor governing the conductivity of all systems studied to date, including the highly conducting TSeT chloride and bromide.[3] This observation also implies that "impurities" in all of these compounds are (not surprisingly) of the same nature, since these are all *organic crystals* grown under very similar conditions and subject to the same types of "impurities."
2. The value (1–10) $\times$ $10^4\Omega^{-1}$ cm^{-1} probably represents the maximum[6] conductivity attainable via supermolecular orbitals based on $\pi - \pi$ overlap of C, N, and S molecular orbitals.

Since, however, the measurement of conductivity is such a gross determination, it could just be fortuitous that all the pseudo-one-dimensional compounds measured to date exhibit a maximum conductivity that centers around the mentioned number.

The fact that (TTF)(TCNQ) under pressure and (HMTSF)(TCNQ) at atmospheric pressure show the same behavior may imply that at high pressure, the band-width and intra- as well as interstack interactions increase; i.e., the sulfur atoms in (TTF)(TCNQ) under these conditions are equivalent to selenium atoms in (HMTSF)(TCNQ) at atmospheric pressure.

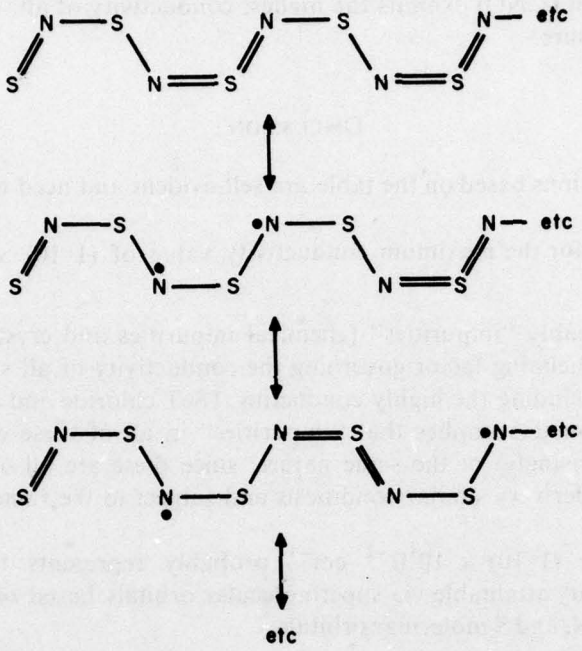
From the foregoing discussion and other information on many materials, one can conclude (in a highly speculative fashion at best) that:

1. All single-crystal organic molecular solids based on pseudo-one-dimensional $\pi - \pi$ interactions (i.e., donor-acceptor solids) will exhibit maximum specific conductivities of (1–10) $\times$ $10^4\Omega^{-1}$ cm^{-1} at atmospheric pressure.
2. All single-crystal *one-dimensional* organic molecular solids based on C,H,N, and S, regardless of degree of charge transfer, will be ground-state insulators.

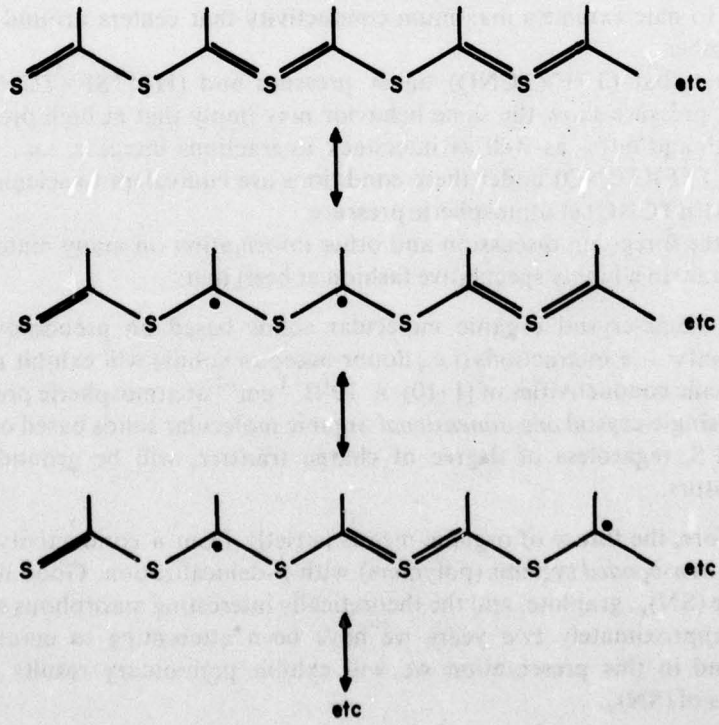
Therefore, the future of organic metals (strictly from a conductivity point of view!) lies in *σ-bonded* systems (polymers) with π-delocalization. Good models, of course, are $(SN)_x$, graphite, and the theoretically interesting amorphous state.

Over approximately two years we have been attempting to emulate these models, and in this presentation we will exhibit preliminary results based on emulations of $(SN)_x$.

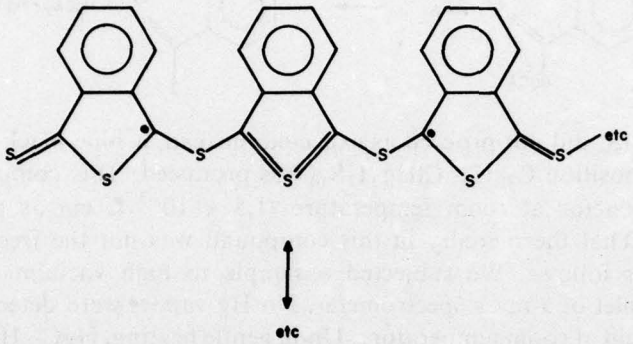
Polythiazyl can be envisioned (strictly for heuristic reasons) as a polymer consisting of mixed-valence sulfur and nitrogen:



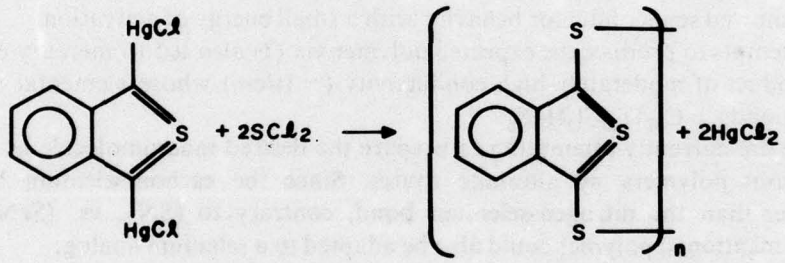
If nitrogen were to be substituted by carbon:



Clearly, a substituent capable of stabilizing a carbon atom bearing an unpaired spin and/or tetravalent sulfur atom must be incorporated. A suitable choice could be —CN, $-N(R)_2$, and so on, but *ortho*-phenylene may be better from an electronic and synthetic point of view:

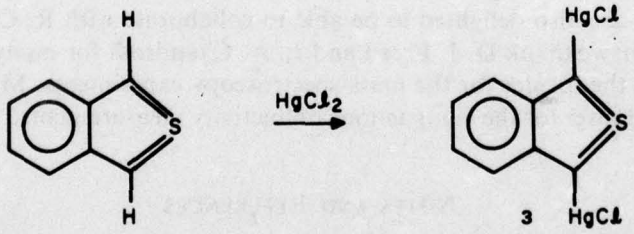


There are several synthetic avenues to such a polymer. One of these, based on the following scheme, will be described here:



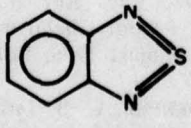
(1)

Isobenzothiophene (**I**), a molecule which was described in the literature sometime ago but most recently by Cava and Lakshmikantham, *et al.*,[4] can be chloromercurated in essentially quantitative yield:



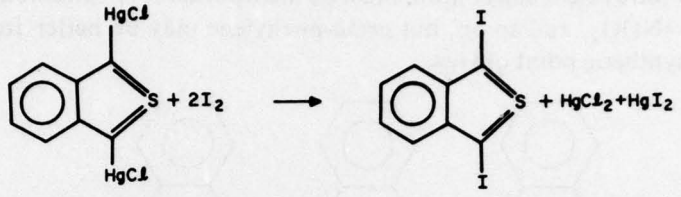
(2)

The mercurial (**2**) is a white solid, insoluble in most solvents, slightly soluble in DMF and DMSO; a solution in the latter exhibited an nmr spectrum practically identical to that of III, below:



III

In order to further characterize this mercurial, we treated it with iodine:



(3)

However, (3) did not proceed as expected; instead, a blue-black lustrous material of composition $C_{80}H_{53}ClHg_3I_7S_{10}$ was produced. This compound was an excellent conductor at room temperature (1.5×10^{-3} Ω cm as a compressed micropellet). That the mercury in this compound was not the free element was established as follows. We subjected a sample to high vacuum ($\sim 10^{-6}$ torr) through the inlet of a mass spectrometer. No Hg vapors were detected when the sample was held at room temperature. Upon gentle heating, HgCl, $HgCl_2$, HgI, I_2, and so on, were the detectable species. An x-ray powder pattern of this unusual solid proved it to be amorphous!

The temperature dependence of the conductivity determined on a compressed pellet showed semiconductor behavior with a small energy of activation.

Attempts to produce the expected polymer via (1) also led to mercury containing product of moderately high conductivity ($\sim 1\Omega$cm) whose elemental analysis corresponds to $C_{42}H_{26}Cl_2HgS_8$.

We are currently attempting to prepare the desired macromolecule as well as analogous polymers by alternate routes. Since the carbon-selenium bond is stronger than the nitrogen-selenium bond, contrary to $(SN)_x$ vs. $(SeN)_x$, the above-mentioned polymer could also be adapted to a selenium analog.

Acknowledgments

I thank the organizing committee of this conference. We are deeply indebted to J. Mock. We are also delighted to be able to collaborate with R. C. Haddon and M. L. Kaplan; we thank D. J. Freed and E. A. Chandross for many hours of discussions and the former for the mass spectroscopy experiments. Many thanks go also to J. J. Hauser for the compaction conductivity measurements.

Notes and References

1. Thomas, G. A., F. Wudl, F. Di Salvo, W. M. Walsh, Jr., L. W. Rupp & D. E. Schafer. 1976. Solid State Commun. **20:** 1009.
2. Bloch, A. N., D. O. Cowan, K. Bechgaard, R. E. Pyle, R. H. Banks & T. O. Poehler. 1975. Phys. Rev. Letters **34:** 1561; Etemad, S. 1976. Phys. Rev. B. **13:** 2254; Thomas, G. A. *et al.* 1976. Phys. Rev. B. **13:** 5105; Jerome, D. & M. Weger. 1977. Proc. NATO Summer School Chemistry and Physics of One-Dimensional Metals. H. G. Keller, Ed. August 1976, Bolzano, Italy. H. G. Keller Editor. Plenum Press. New York, N.Y.
3. Schegolev, I. F., M. L. Khidekhel, E. B. Jagubskii, R. Schibaeva. 1976. Conf. Organic Conduct. Semiconduct. Siofok, Hungary. August. 1963.

4. MAYER, R., H. KLEINERT, S. RICHTER, K. GEWALD. J. Prakt. Chem. **4:** 244. CAVA, M. P., & M. V. LAKSHMIKANTHAM. 1975. Accounts Chem. Res., **8:** 139, and references therein.
5. H. FUKUYAMA, T. M. RICE & C. VARMA. 1974. Phys. Rev. Lett. **36:** 305; LEE, P. A., T. M. RICE & P. W. ANDERSON. 1974. Solid State Commun. **14:** 703.
6. J. TANAKA, M. TANAKA, T. KAWAI, T. TAKABE, O. MAKI. 1976. Bull. Chem. Soc. Jap. **49:** 2358 have arrived at a similar conclusion based on spectroscopic studies.

THE LAYERED DICHALCOGENIDES: SOME CHEMISTRY AND PHYSICS*

F. R. Gamble

Corporate Research Laboratories
Exxon Research & Engineering Co.
Linden, New Jersey 07036

In the last ten or fifteen years, research on the layered dichalcogenides of the transition metals has grown rapidly and has become the focus of an international effort of great magnitude. Discoveries have been made that are largely responsible for the high level of interest. Superconductivity was discovered in the dichalcogenides of tantalum and niobium. Molecular intercalation complexes of the group IVb and Vb dichalcogenides were prepared, with those involving Ta and Nb being highly anisotropic superconductors.[1] Charge-density waves, predicted by Overhauser in 1968,[2] were discovered[3,4] in several of the IVb and Vb dichalcogenides. The discovery of charge density waves has alone provided enormous impetus to the field. The electrochemical insertion of lithium between the layers of the compounds was discovered to be very energetic and now forms the basis of a new, high-energy density battery.[5a–5d] Also during this period, it became clear that two of the work-horse catalysts of the petroleum industry are based on promoted layered group VIb disulfides.[6,7] Finally, also on the technological side, the use of layered compound antiwear, antifriction ingredients in oils and greases, has received attention.

These discoveries and developments have come at a time when there is high interest in the scientific community in materials with limited dimensionality where the effects of dimensionality on the occurrences and nature of phase transitions and other physical phenomena can be examined experimentally. On the technological side, the electrochemical, catalytic, and frictional studies come at a time when science is being asked what it can do for the energy problems we face. Keeping this in mind, one can see why these materials have received the attention they have, and one can predict with some confidence that they will yet continue for some time to be the subject of many investigations.

A comprehensive review of all interesting aspects of this field will not be attempted here. This article touches briefly those areas I have been close to. The reader is referred to previous reviews for more information.[8]

The first crystal structure of a layered dichalcogenide was published by Dickinson and Pauling in the twenties.[9a] They studied the mineral molybdenite, MoS_2, and found it to be composed of layers of MoS_2 stacked upon one another. A schematic representation of these layers is shown in FIGURE 1 for a similar compound, TaS_2. Each layer is a sandwich of a plane of metal atoms in sites of trigonal prismatic symmetry between planes of chalcogen atoms. The bonds within the layer are strong, primarily covalent. Those between the layers are weak, primarily

*Manuscript received October 3, 1977.

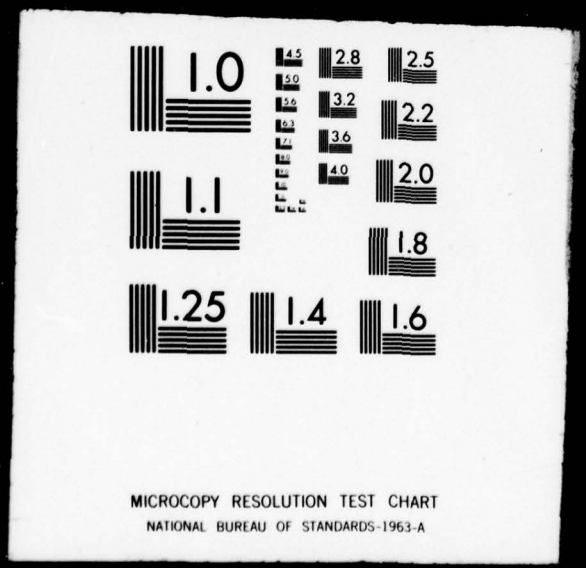
0077-8923/78/0313-0086 $1.75/1 © 1978, NYAS

AD-A065 304 NEW YORK ACADEMY OF SCIENCES N Y F/G 7/2
SYNTHESIS AND PROPERTIES OF LOW-DIMENSIONAL MATERIALS,(U)
1978 J S MILLER, A J EPSTEIN N00014-77-C-0374
UNCLASSIFIED NL

2 OF 9
AD
A065304



2 OF 9
AD
A065304



van der Waals. This structure confers upon these crystals a high degree of anisotropy and some very interesting chemical and physical properties.

A scanning electron micrograph of small crystals of another layered dichalcogenide, titanium disulfide, grown on a titanium wire is shown in FIGURE 2. The crystallites are only a few microns thick, but very nicely formed. The platelike morphology is typical and most likely the result of difficulty in nucleating a new layer on top of an old one. If we take a closer look with the transmission electron microscope, we can see the individual layers, in FIGURE 10a, to be discussed later. Crystals of appreciable thickness, in which the thickness perpendicular to the layers is the greater crystal dimension, are unusual and are often found to contain a screw dislocation that has provided an easy path for growth in the *c* direction. Such dislocations provide a helical path for electron transport so that the *c* axis electron transport properties are sometimes simply proportional to those of the *a*-axis,[20] especially in the molecular intercalation complexes discussed later. Specimens of this type are shown in FIGURE 3.

Many elements form layered dichalcogenides. The periodic table in FIGURE 4

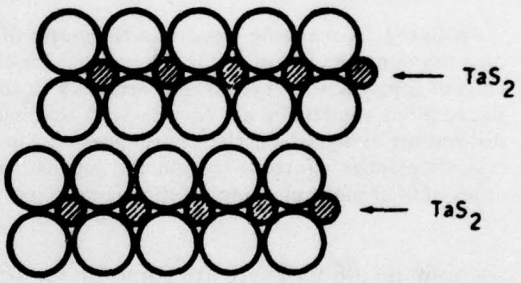


FIGURE 1. Schematic representation of the crystal structure of 2H-TaS_2. The large, open circles represent chalcogen atoms; the small, filled circles, metal atoms. In this structure, peculiar to the sulfides and selenides of Nb, Ta, Mo, and W, the metal atoms are surrounded by six chalcogens in a trigonal prism. Different polytypes are obtained by subtle changes in the manner in which the layers are stacked. Different polymorphs result from changes in the coordination symmetry about the metal atom.

is shaded to indicate those that do. Different symmetries of the sixfold coordination are indicated by different shading. Although the octahedral coordination is most prevalent, four elements—Ta,Nb,Mo, and W—crystallize with the chalcogen atoms in a trigonal prism about them. Tantalum is somewhat ambivalent in this regard and can crystalize with both coordination symmetries.[9b] The group Vb dichalcogenides are metallic and superconducting and possess probably the most remarkable properties of all. The group IVb compounds are either semiconducting (Zr, Hf) or semimetallic (Ti). Group VIb compounds are semiconducting, as are the rest. Most interest has been directed to Groups IVb, Vb, and VIb dichalcogenides.

As you might expect, the similar structures of all these compounds afford a large number of mixed crystal possibilities—and an ability to adjust and fine-tune the crystal properties. In FIGURE 5 are plotted the electrical resistivities of mixed crystals of TiS_2 and TaS_2.[10] The lowest curve is TiS_2 and the uppermost is 1T-TaS_2, the octahedral polytype. You will note that by adjusting the ratio of the mixture a gradual evolution of properties is effected. The letter *x* stands for the fraction of

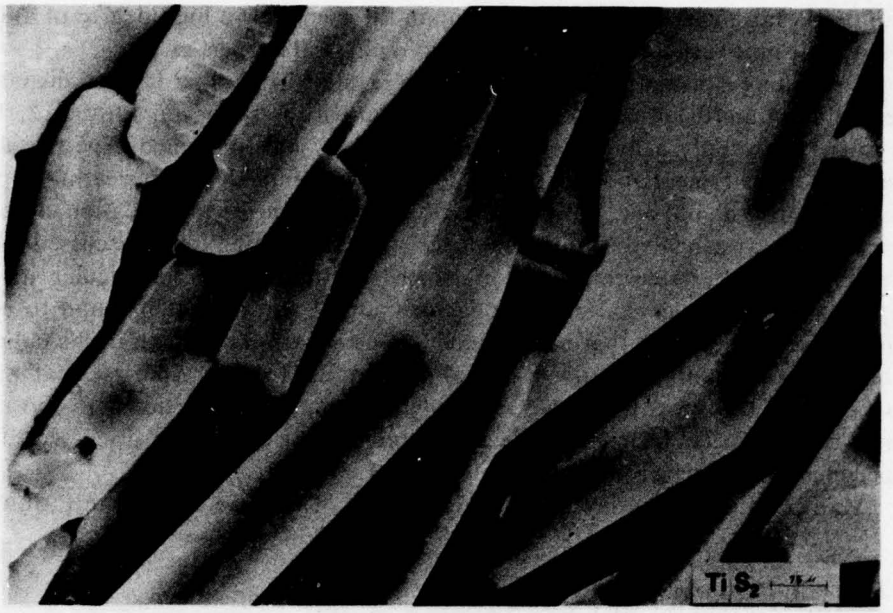


FIGURE 2. A scanning electron micrograph of small crystals of titanium disulfide grown on a titanium wire in hot sulfur. The platelike morphology of these crystals is typical of this class of compounds. Crystals that are thick in the direction perpendicular to the layers are unusual but sometimes are found. Such specimens frequently display a prominent screw dislocation along which they have grown. The presence of screw dislocations in these crystals plagues efforts to obtain the intrinsic anisotropy in the electron-transport properties of their molecular intercalation complexes.

titanium disulfide. There are some rather striking features of these data that were initially very puzzling. One is that in TiS_2 the conductivity is nonactivated, metallic-like, while in the octahedral form of TaS_2 it is activated. This is the reverse of what one might have expected, since TiS_2 has no electrons beyond those required in bonding and TaS_2 has one extra. Another feature is the anomaly in temperature dependence observed for tantalum-rich mixtures. We now know that the "semiconducting" nature of the octahedral TaS_2 and the anomalous electrical resistivities are the result of charge density waves[11] and that the compound TiS_2 probably has a very slight overlap of the valence and conduction bands[10,12a,12b] or a very small gap, rather than the 1 ev gap originally thought.

Charge-density waves strongly affect the properties of the metallic dichalcogenides (i.e., especially group Vb). Reference to them will be frequent here, but the reader is referred to other literature for a thorough treatment of them.[11,13,14] Here it must suffice to say that they result from a Fermi surface instability peculiar to materials of low dimensionality that leads to oscillations in the electron gas density as the temperature decreases.[14] A most striking feature is that in certain regimes they do not possess the periodicity of the lattice. Onset of the CDW destroys Fermi surface and strongly affects the electron-transport properties. As the temperature is lowered still further, a transition from this incommensurate state to a commensurate state occurs, at which point the crystal lattice distorts.

Thompson has shown that this distortion temperature can be predicted from a consideration of the local chemical bond between the chalcogen and the metal.[15] In his picture, a structural instability inherent in the chemical bond is envisioned that is required to account for first-order incommensurate-commensurate transitions. Huisman *et al*[16] had previously suggested that departures from ideal close packing of chalcogen atoms (reflected in c/a) in these hexagonal crystals are the result of covalent mixing of orbitals in the metal chalcogen bond.

TABLE 1 is a listing of known distortion temperatures defined from transport measurements. Thompson[15] shows that it is possible to construct from the lattice parameters a quantity that is linear in the ionicity as revealed by the *d-p* energy gap. This is shown in FIGURE 6. He then applies this to the distortion temperatures

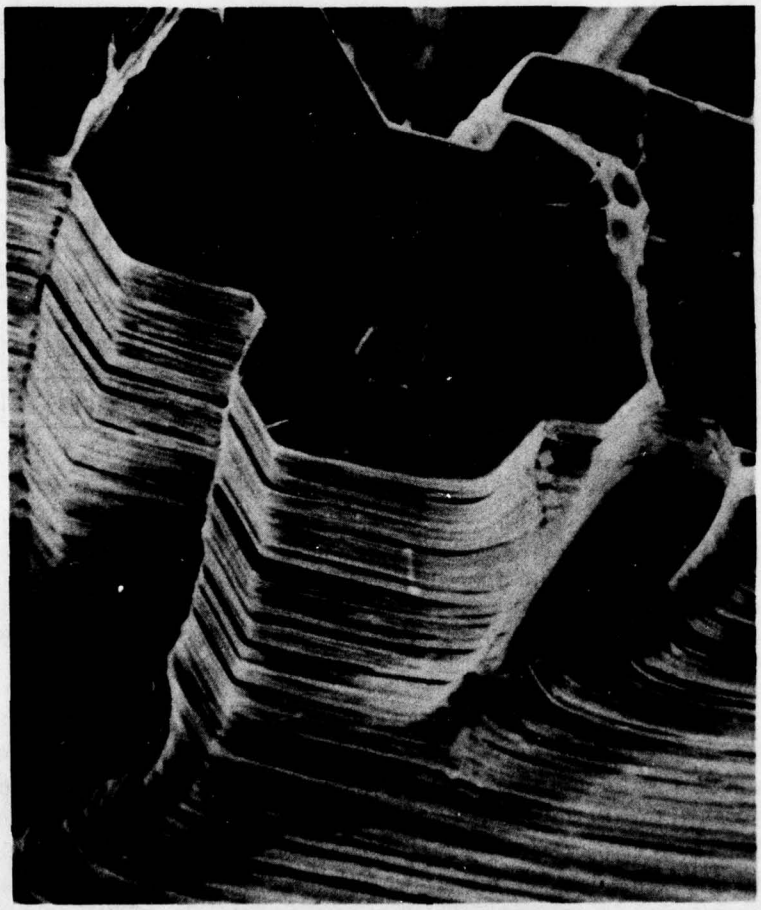


FIGURE 3. *Scanning electron micrograph of a crystal of* NbS_2 that has been intercalated with tributylphosphine to form NbS_2 (tributylphosphine)$_{1/8}$. The crystal is thick along the *c*-axis because it has grown along a screw dislocation. The hexagonal hole is the center of the screw. It is about 1 micron across. The leading edge of the helix is to the left of the dislocation center. Apparently, during the NbS_2 growth process (by chemical vapor transport) material was transported away from the dislocation to relieve strain.

(FIGURE 7). Much remains unanswered here before the observation is placed on a sound theoretical footing, but the notion that local as well as nonlocal considerations need to be invoked appears quite reasonable.

Not only do CDW's produce grossly altered electronic properties when they occur, but incipient CDW's may also, in a more subtle way, be responsible for certain behavior in crystals where the CDW state has not yet been clearly identified. The Thompson correlation would predict a CDW distortion in TiS_2 around 150 K, but no distortion has been seen. TiS_2 has very few charge carriers and so may be distinguished somewhat from its more metallic neighbors. In very pure TiS_2, Thompson[12] showed the temperature-dependent resistivity was proportional

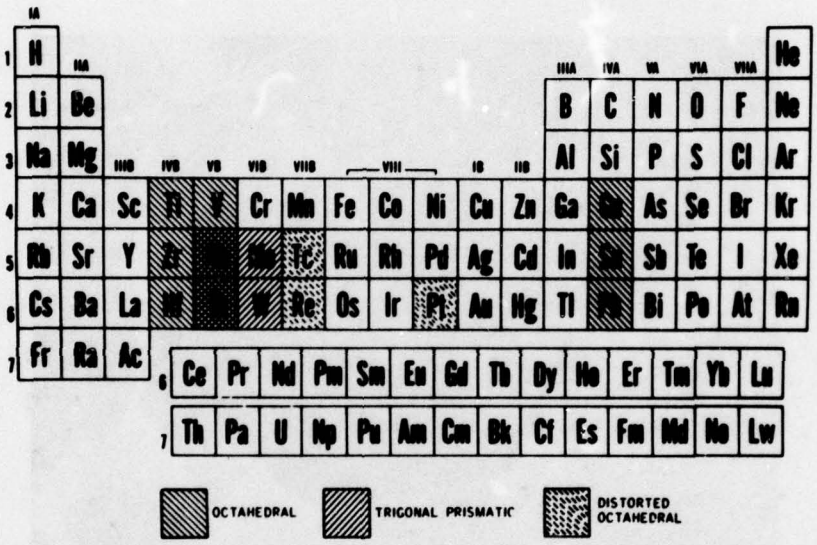


FIGURE 4. Periodic table of the elements indicating those known to form layered dichalcogenides. Trigonal prismatic and octahedral coordination of the metal atom are indicated by different shading. The sulfides and selenides of tantalum and niobium form a large number of layered structures with subtle differences in stacking combined with two allowed coordination symmetries.

to T^2 from 400°K to the lowest temperature measured, about 10°K (FIGURE 8). Thompson has postulated that this truly unique phenomenon is the result of an electron-electron scattering, as first described theoretically by Baber.[17] An exact mechanism for electron-electron scattering in TiS_2 has not been clearly defined, but one possibility is that TiS_2 is a material with an incipient CDW and that electron-electron scattering is enhanced by fluctuations into the CDW state ("paraphasons"). In any case, at present T^2 terms have been identified in a number of limited dimensional materials, including other layered compounds, so that CDW must be suspect.

In 2H-TaS_2 the coordination about the tantalum atom is trigonal prismatic, as

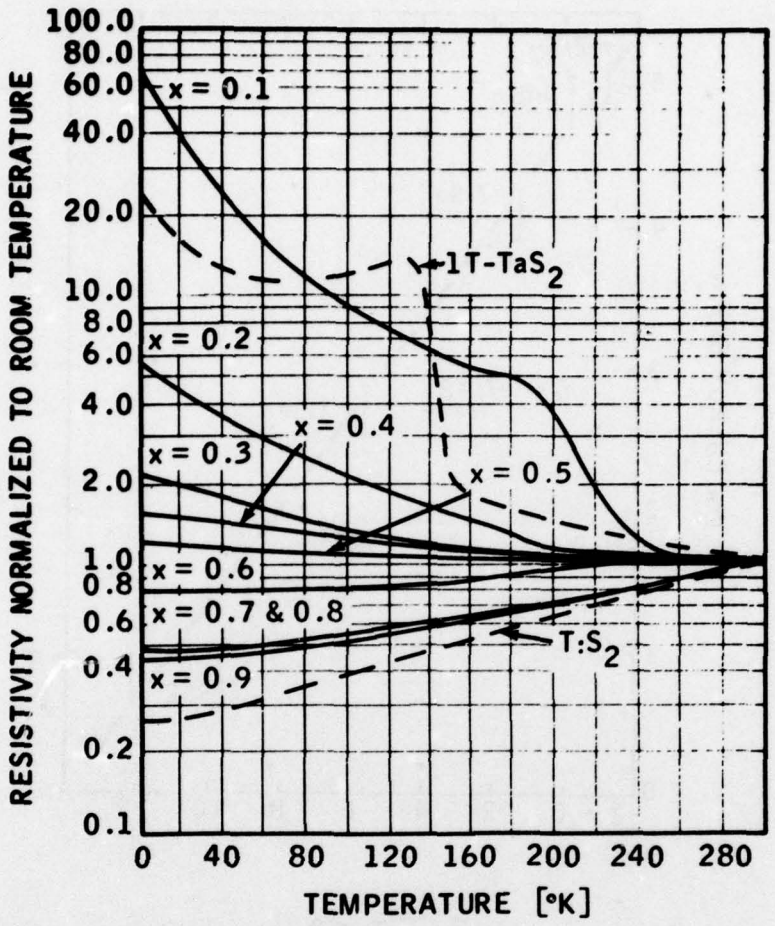


FIGURE 5. The temperature dependence of the electrical resistivity of the mixed crystals $Ta_{1-x}Ti_xS_2$ normalized to 300 K. The tantalum-rich members display an anomaly associated with the charge density wave states of those compounds. The temperature dependence of the electrical resistance of titanium disulfide shown here is somewhat affected by impurities. See FIGURE 8 for the intrinsic behavior of TiS_2(Data from Ref. 10.)

TABLE 1

KNOWN DISTORTION TEMPERATURES DEFINED FROM TRANSPORT MEASUREMENTS

Continuous Distortions			Discontinuous Distortions		
Material	*c/a*	T_c (°K)	Material	c/a	T_c (°K)
2H-$TaSe_2$	1.850 ± 0.002	90	1T-$TaSe_2$	1.805 ± 0.002	473
2H-TaS_2	1.822 ± 0.002	56	1T-TaS_2	1.755 ± 0.003	350
2H-$NbSe_2$	1.8209 ± 0.0004	26	1T-$TiSe_2$	1.697 ± 0.001	200 ± 10
1T-VSe_2	1.817 ± 0.002	55 ± 5	4Hb-TaS_2	1.752 (est)	320
6R-TaS_2	1.805 (est)	15	4Hb-$TaSe_2$	1.806 (est)	410
4Hb-TaS_2	1.793 (est)	15 ± 3	6R-TaS_2	1.763 (est)	311

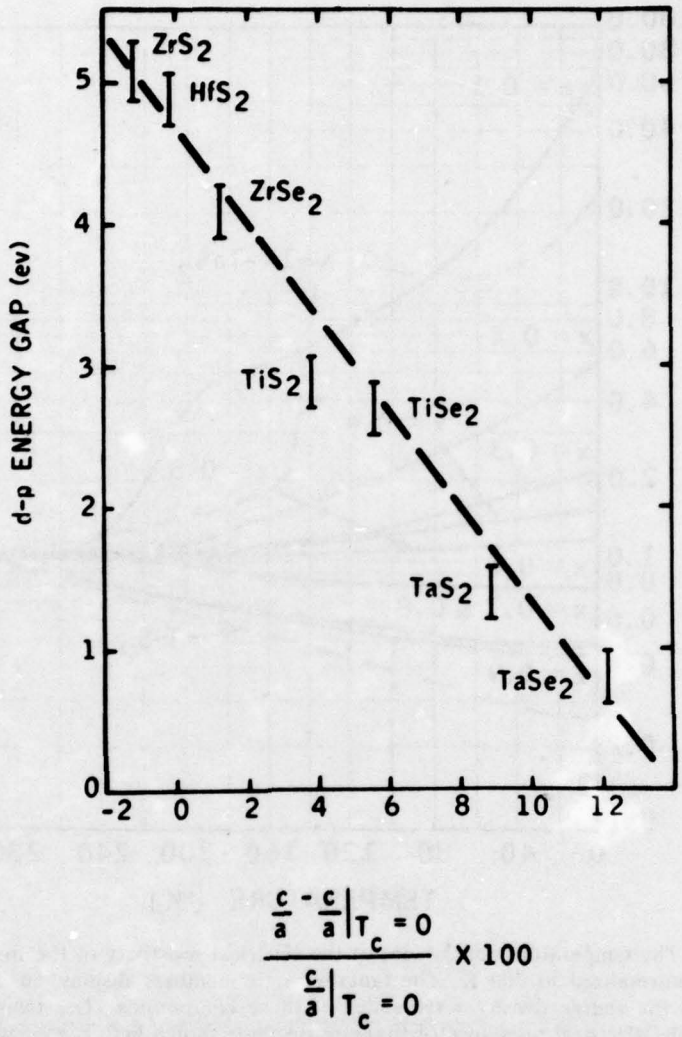


FIGURE 6. The *d-p* energy gap of layered compounds with octahedral coordination vs. a quantity constructed from the lattice parameters c and a. This quantity is the deviation of the ratio c/a from that ratio which corresponds to a distortion temperature of zero. The c/a ratio for $T = 0$ is obtained by plotting the distortion temperatures versus c/a and extrapolation to zero temperature. The *d-p* energy gap is obtained from photoelectron spectroscopy of these materials. It corresponds to the separation between the maxima in the apparent density of states. (Data from Ref. 15.)

shown in FIGURE 9. This phase is metallic at all temperatures and superconducting below 0.8. In 1970 DiSalvo, Geballe, Klemm, and I discovered that certain organic molecules could be inserted between the layers of this crystal by simply exposing the tantalum sulfide to the molecules.[1] A dramatic swelling of the crystals was obvious and their properties were altered. If 2H-TaS_2 is reacted with pyridine, one-half mole of the compound is absorbed per formula unit of TaS_2, the layers

spread apart by 6 Å, and T_c is increased to 3.5°K. One can follow this process in the transmission electron microscope, as shown in FIGURE 10.[18a] A large class of fairly crystalline, stoichiometric complexes are produced with the general formula TaS_2(molecule) $1/\eta$ where η is an integer.[19] If simple substituents such as small alkyl groups are placed on the pyridine ring, η can be varied from two to six. The increase in layer spacing usually remains about 6 Å, but in some cases collapses to about 3 Å, indicative of a molecular monolayer. All of the intercalated compounds are superconducting despite the fact that the electrons are constrained to highly anisotropic motion. I shall return to this point later.

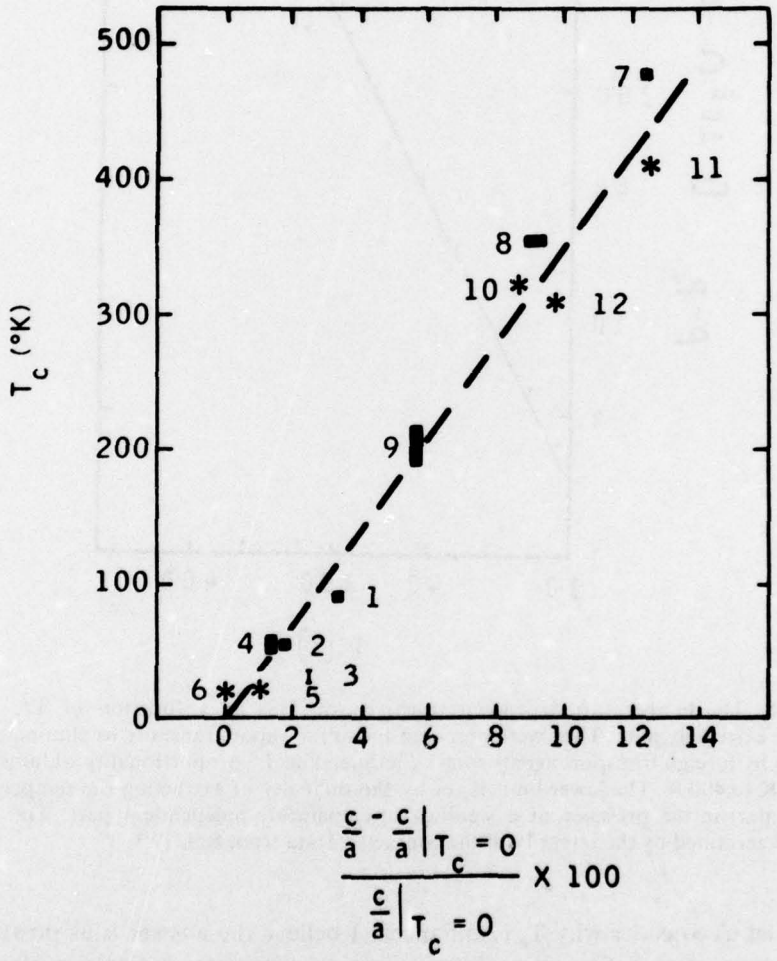


FIGURE 7. The distortion temperature associated with the incommensurate-commensurate transition vs. the ionicity parameter described in FIGURE 6. Asterisks describe points obtained from estimated c/a ratios when the crystals contain alternating octahedral and trigonal prismatic layers. Such crystals have separate transitions associated with the two kinds of layers. (Data from Ref. 15.)

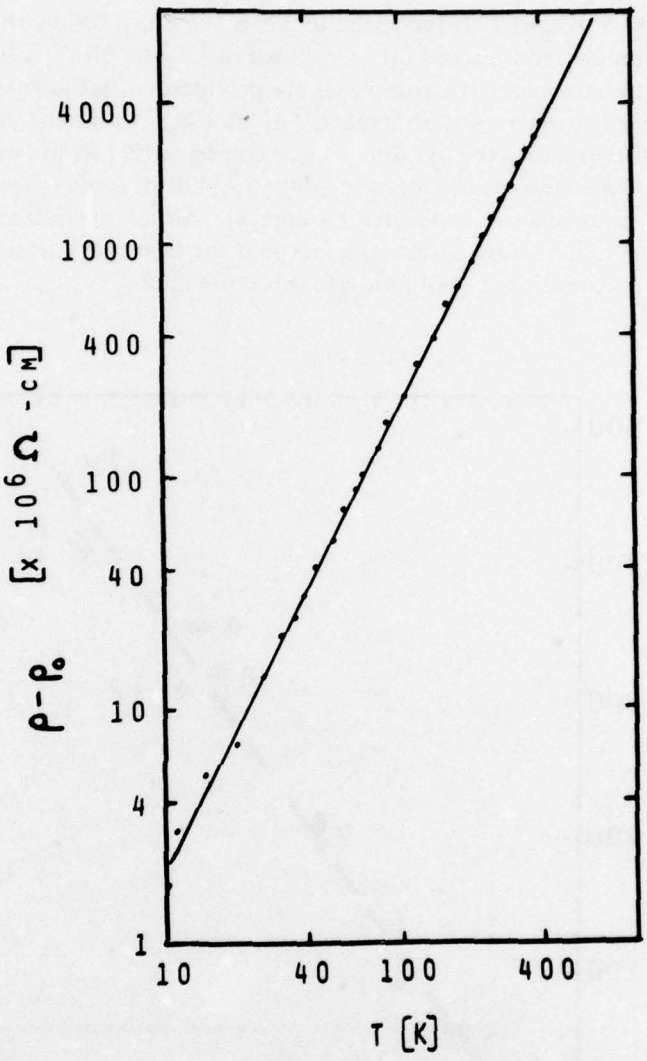


FIGURE 8. The temperature-dependent resistivity of TiS_2 as a function of T^2. These crystals are extremely pure. They were prepared by sulfur-vapor transport to eliminate contamination by foreign transport agents such as iodine. The T^2 proportionality obtains from at least 10 K to 400 K. The lower limit is set by the difficulty of extracting the temperature-dependent part in the presence of a significant temperature-independent part. The upper limit was determined by the integrity of the contacts. (Data from Ref. 12.)

First, let us consider why T_c is enhanced. I believe the answer is as postulated by Thompson *et al.*[20] The intercalation reaction eliminates a Fermi surface instability we now know to result in CDWs. In TaS_2 the onset of charge density waves produces a cusp in the susceptibility that is reduced as the integer η is decreased—i.e., as the number of molecule layer interactions is increased. This can be seen in the data of DiSalvo (FIGURE 11).[21] In FIGURE 11 the value of η goes

from six to two, and as it does so the instability is removed and T_c increases. It is still not clear how the intercalated molecules achieve this, but let us consider what happens if the integer η is held constant and the molecule is altered by substituents that give the same stoichiometry.

The effects of substituents on T_c are shown in FIGURE 12.[22] Here the stoichiometric integer η is a parameter. The critical temperatures for three values of η are plotted vs. an NQR parameter that is linear in the density of electrons in the lone pair orbital of the nitrogen. These results suggest that the molecule interacts with the layer via this lone pair orbital. If $\ell - \sigma_{NC}$ is substantially reduced, the complexes do not form, which suggests that the same interaction responsible for the enhancement of T_c is responsible for complexation.

We have considered effects of changing the molecule from pyridine to substituted pyridines and have found that the lone pair orbital was somehow implicated. What happens when we change the transition metal? A large number of experiments indicate that molecular intercalation complexes can be formed only by di-

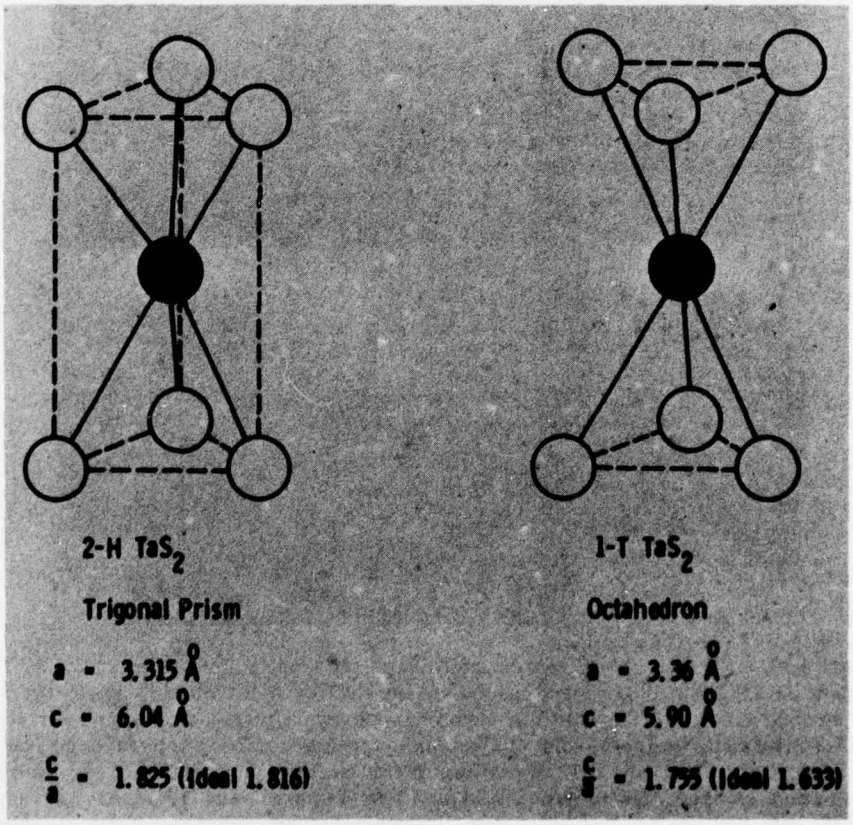


FIGURE 9. The two coordination symmetries observed in TaS_2. Crystals with octahedral, trigonal prismatic, or (in alternating layers) both coordination symmetries can be prepared. The trigonal prismatic 2H-TaS_2 is the phase stable at room temperature and the one that lends itself best to intercalation chemistry.

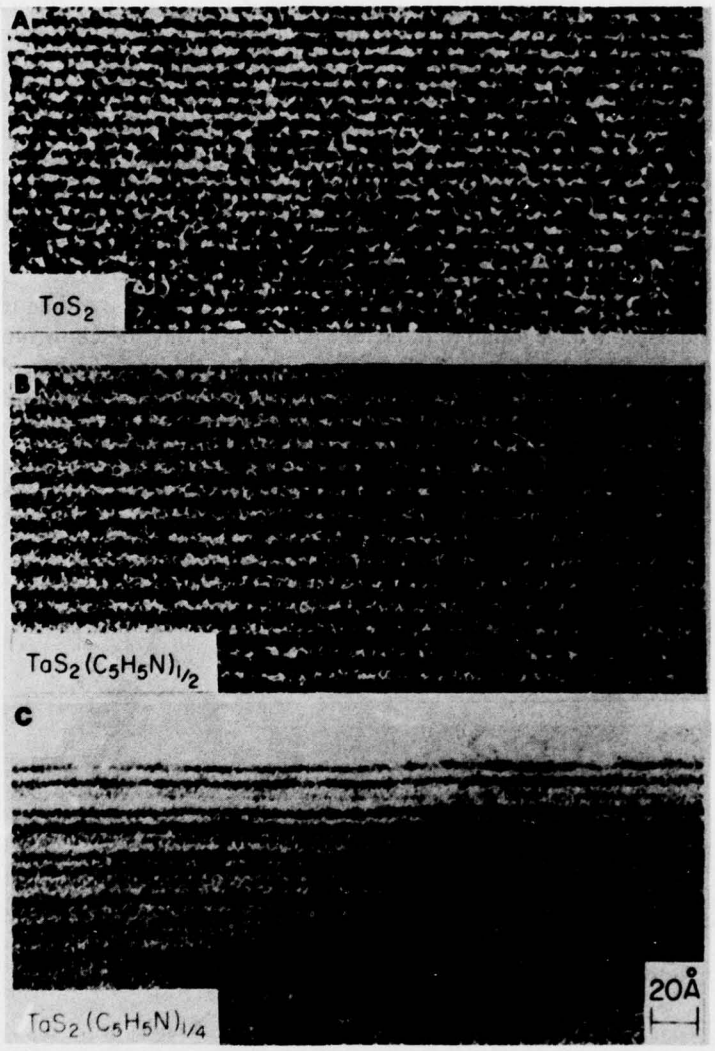


FIGURE 10. a: Transmission electron micrograph showing individual layers in 2H-TaS_2. The dark lines in the photograph correspond to the electron-rich tantalum layers. The interlayer spacing is 6 Å. b: Transmission electron micrograph of the molecular intercalation complex 2H-TaS_2(pyridine)$_{1/2}$. In this complex pyridine has been intercalated. The tantalum layers are 12 Å apart. c: The transmission electron micrograph of the molecular intercalation complex 2H-TaS_2(pyridine)$_{1/4}$. This material was prepared by reacting 2H-TaS_2 with half the amount of pyridine known to fill the interlayer space completely. Complexes of this kind are termed second stage. No higher stage compounds have been observed. Second-stage compounds can be reacted further with different molecules such that the nature of the molecular intercalate alternates 18b. (By permission of the publishers of Science. [18a])

chalcogenides of IVb and Vb metals. Since Nb and Ta dichalcogenides have structures nearly identical to the corresponding Mo and W compounds, it is instructive to ask why the former readily form complexes whereas the latter do not.

I believe the answer can be found in the band structures computed by Mattheiss[23] for representative Vb and VIb compounds. The important feature in these is a low-lying two-electron band that is half full in group Vb dichalcogenides and full in group VIb. The conduction band is empty or nearly so in group IVb dichalcogenides. An empirical rule that serves is that in the host crystal a low-

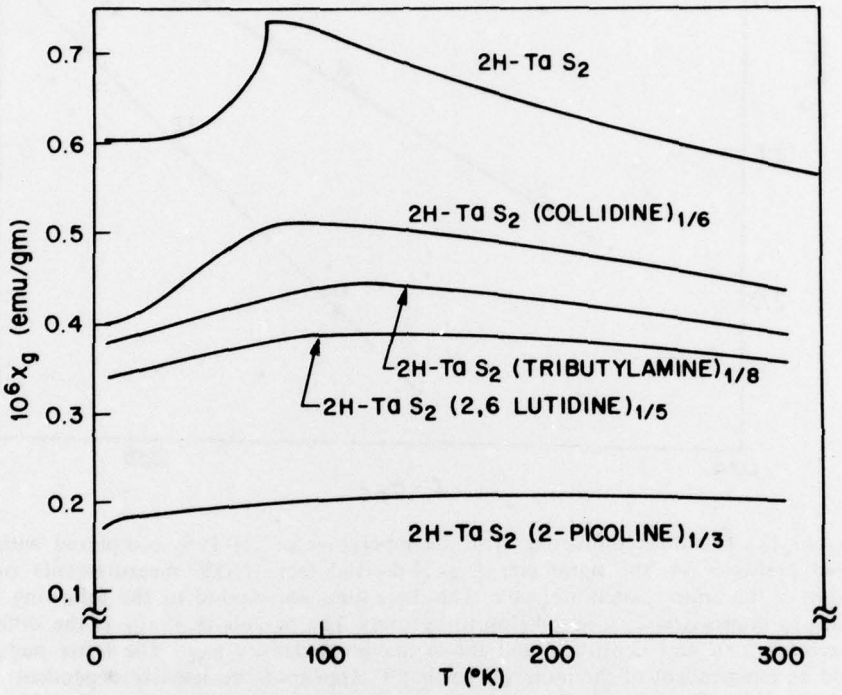


FIGURE 11. The magnetic susceptibility vs. temperature for various intercalation complexes of 2H-TaS_2. Notice that the cusp, associated with the CDW state, is progressively reduced in magnitude as the number of intercalated molecules per formula unit increases. The temperature at which the cusp occurs does not shift. As the cusp disappears, the superconducting critical temperature is increased. (The data for the tributylamine complex should not be compared with those of the substituted pyridine complexes.)

lying band with empty states is required for molecular intercalation to proceed. We have also found that the lone pair state of the molecule is implicated. In fact, with but one exception, that I will treat later, all molecules that form intercalation complexes possess this lone pair state. We therefore postulate that an interaction, perhaps indirect, between this doubly occupied lone pair state of the molecule and the low-lying unoccupied electronic states of the host is responsible for complex formation and is implicated in the chemical modifications of the physical properties of the host.

One interaction of this kind is the ordinary dative chemical bond in which

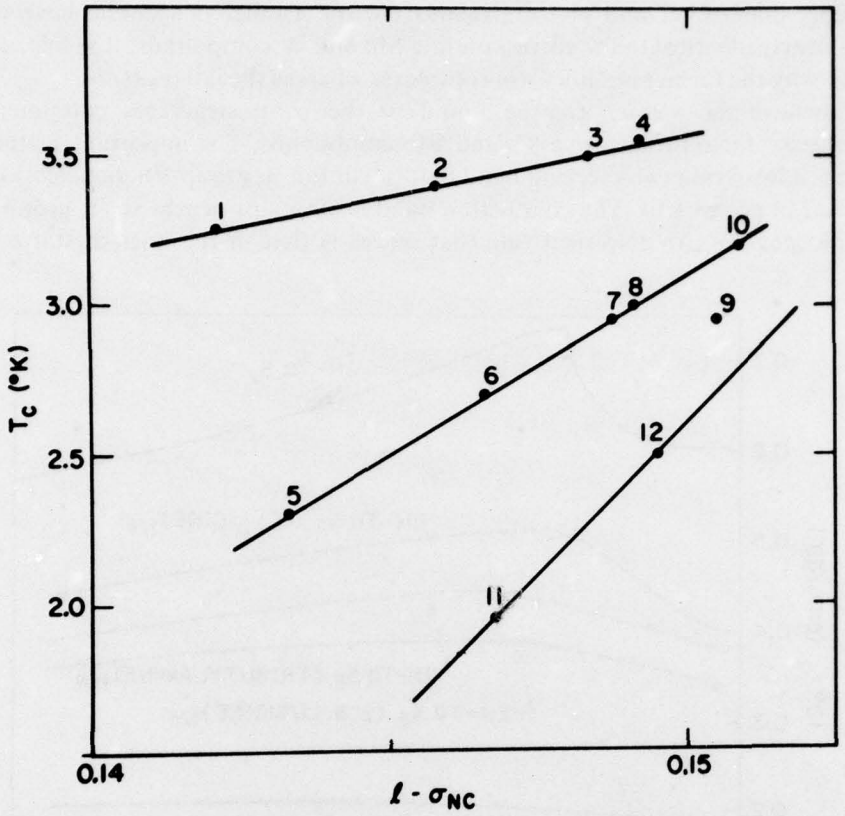


FIGURE 12. The superconducting critical temperature of 2H-TaS_2 complexed with substituted pyridines vs. the parameter ℓ-σ_{NC} derived from NQR measurements on the nitrogen of the unitercalated molecule. The three lines correspond to the following ratios of TaS_2 to intercalate: 2, 3, and 4 (top to bottom). The parameter ℓ-σ_{NC} is the difference between the lone pair density ℓ and the sigma bond density σ_{NC}. The latter parameter should be independent of the molecule so that T_c appears to be linearly dependent on ℓ. Complexes do not form when ℓ-σ_{NC} is much smaller than shown. (Data from Ref. 22.).

there is slight mixing of the lone pair state with the empty layer states. The empty layer states referred to are principally of transition metal character but they possess a substantial admixture of chalcogen orbitals, and this would permit interaction of the sort postulated. This interaction would ordinarily lead one to expect the axis of the lone pair orbital to be perpendicular to the layers. This is clearly not the case in several substituted pyridine cases where the interlayer dilation is only sufficient to accommodate a molecular monolayer with the aromatic ring parallel to the layers.[19]

In an effort to obtain a clearer picture of the bonding interaction in these systems we have studied in detail the complexes formed by ammonia, particularly those with TaS_2 and TiS_2.[24-28] A major effort was directed toward nmr studies, since one has a good selection of resonant nucleii in $^{14}NH_3$, $^{15}NH_3$, and $^{14}ND_3$. One of the first things we learned about this complex is that the molecules are quite

free to diffuse, to reorient, and to spin.[24,27] As an example of this we can consider FIGURE 13, where the proton NMR linewidth is plotted vs. T.[27] The line broadens only around 140°K as molecular hopping and reorientation begin to stop. They are still spinning, however, about their C_3 axis.

The most remarkable results came from a single crystal study of $TaS_2(NH_3)$, where we observed a significant anisotropy in the proton spinlattice relaxation time as the angle between the field and the layers is changed,[24] as shown in FIGURE 14. We have interpreted this as a rapid reorientation of the C_3 axis of the molecule that is possible only if the C_3 axis is parallel—not perpendicular—to the layers, as indicated in FIGURE 15. The implications of this are that the nitrogen is midway between the planes, an implication confirmed by x-ray[26a] and neutron diffraction.[29] This is not the structure that leads to maximum overlap, but it is still

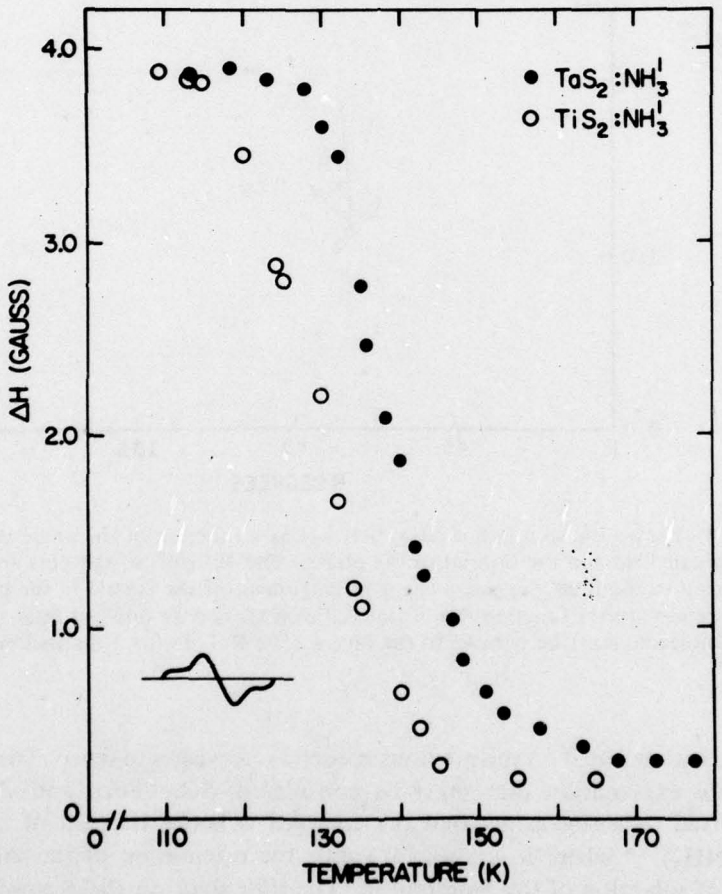


FIGURE 13. The proton NMR line-width vs. temperature in the complexes $TaS_2(NH_3)$ and $TiS_2(NH_3)$. NMR measurements show that the intercalate is quite mobile at room temperature. It can diffuse, tumble, and spin about its C_3 axis. Only the latter degree of freedom is available at 4 K. Unless the samples are contaminated with moisture, the protons undergo intermolecular exchange quite slowly. (Data from Ref. 27.)

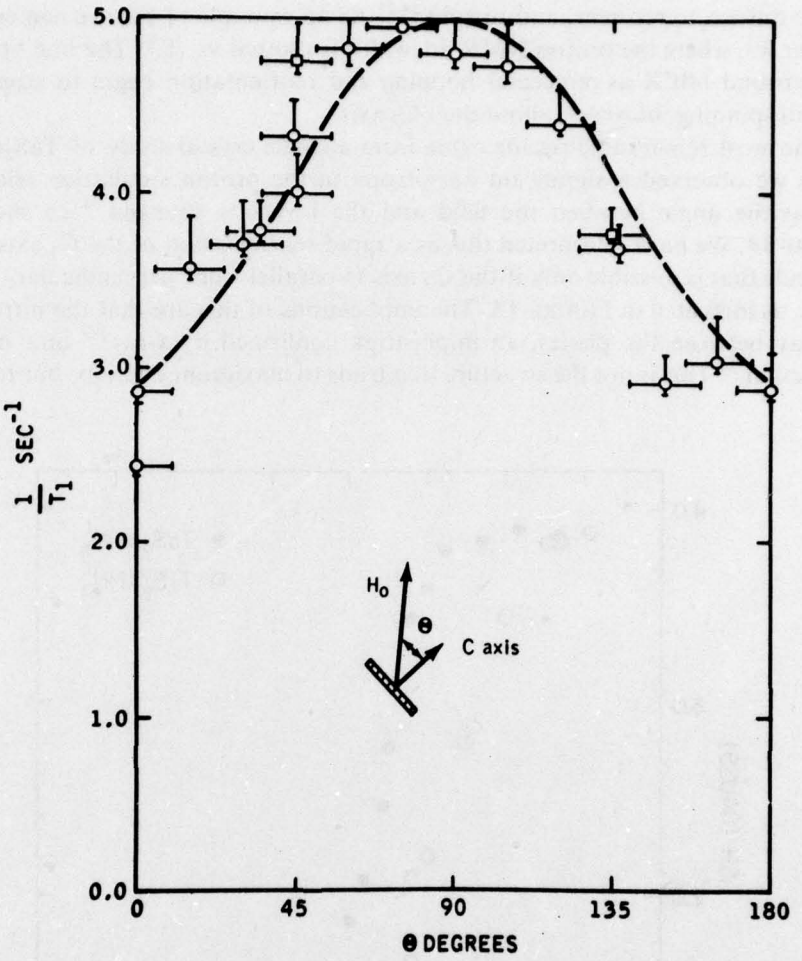


FIGURE 14. The proton spin-lattice relaxation rate as a function of the angle between the applied magnetic field and the normal to the planes. The 10° shift of the data from a symmetric disposition about 90° suggest a slight misalignment of the crystal in the holder. The dashed line represents the function $A + B \sin^2 \Theta$. From these data one can infer that the C_3 axis of the molecule must be parallel to the layers. (See Ref. 25 for a discussion of the experiment.)

possible to rationalize it on the previous model if one wishes to do so. There is now an alternate explanation that must be considered. Schollhorn and Zagefka[26b] have reported data suggesting that the complex is better thought of as $TaS_2^{\alpha-}(NH_4^+)_\alpha(NH_3)^{1-\alpha}$ where α is about 0.1 and the orientation of the lone pair is the result of solvation of the ammonium. The nmr data on these complexes[24–28] show no indication of rapid proton exchange, however, so at present I feel the bonding interaction is still an unresolved issue. Structural information is accumulating, however, and a resolution is foreseeable.

When we first prepared molecular intercalation complexes, one question before us concerned the dimensionality of the superconductivity. In $TaS_2(NH_3)$, where

the layers are only 3 Å apart, or in TaS_2 (pyridine)$_{1/2}$, where they are 6 Å apart, it is reasonable to assume that tunneling of Cooper pairs couples the superconductivity in adjacent layers. What happens if we put larger molecules between the layers? This we can do by attaching n-alkylamines to the nitrogen of ammonia in place of one of the protons.[30] We examined intercalation complexes of TaS_2 with primary normal alkylamines from methylamine to octadecylamine. What happens to the critical temperature as we make the molecule longer? It drops, as we see in FIGURE 16, until we have added 8 or 9 carbon atoms and then it jumps up, and as the molecule is further lengthened by adding additional methylenes, it holds constant. The drop in critical temperature is not associated with spreading the layers further apart, for x-ray diffraction shows the layers are not moving apart. The chains are parallel to the surface. The layers move apart dramatically, however, when the carbon number exceeds ten. A molecular bilayer has been formed (FIGURE 17). The amine TaS_2 ratio is decreasing as carbon number is increased at first, and then the ratio increases to 2/3 when the molecules stand up, and holds constant at that value thereafter. Obviously, the critical temperature is a function of stoichiometry but not interlayer distance.

When the layers are 50 Å (FIGURE 17) apart we might assume that Josephson coupling between them is insignificant. There are those, however, who disagree.

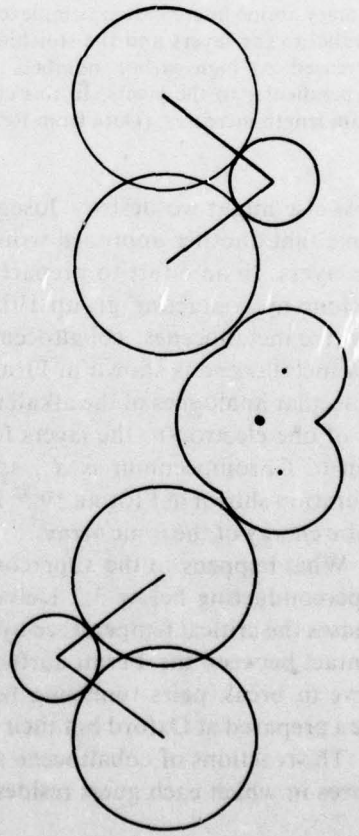


FIGURE 15. The orientation of the ammonia molecule in 2H-$TaS_2(NH_3)$ inferred from the anisotropy of the proton spin lattice relaxation rate. X-ray diffraction of the similar complex $TiS_2(NH_3)$ places the nitrogen midway between the layers in accord with the proposed orientation.

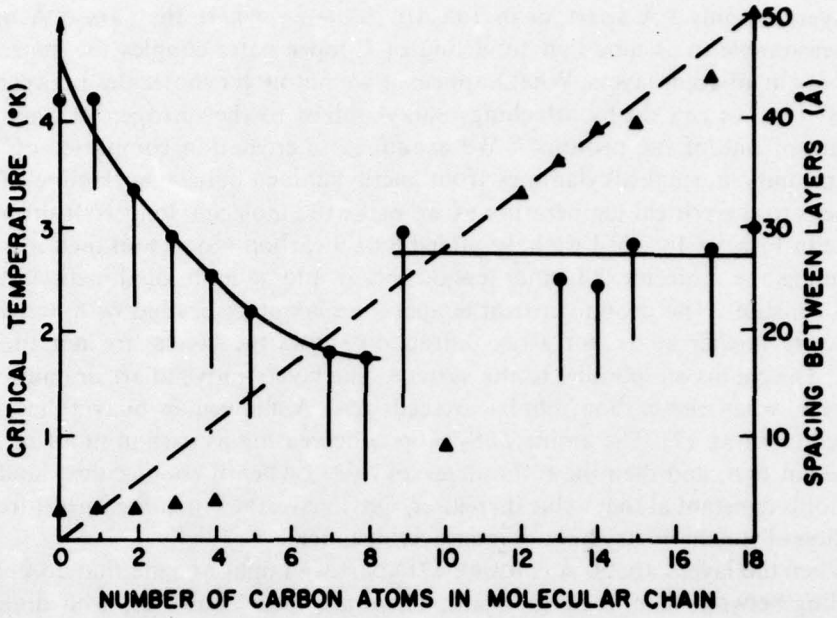


FIGURE 16. The superconducting critical temperature (circles) and the interlayer dilatation (triangles) as a function of the number of carbon atoms in the chain of the normal primary amine intercalation complexes of 2H-TaS_2. For low carbon number the chains are parallel to the layers and the stoichiometry of the complex changes as the chain length is increased. At high carbon numbers the stoichiometry is constant because the chains are perpendicular to the layers. In this configuration the interlayer dilatation increases as the chain length increases. (Data from Ref. 30.)

How else might we destroy Josephson coupling between the layers? It occurred to me that another approach would be to insert paramagnetic molecules between the layers. In an effort to prepare such complexes, Dines[31] discovered this could be done by contacting group IVb or Vb dichalcogenides with the most electropositive metallocenes: cobaltocene and chromocene. A schematic representative of a metallocene is shown in FIGURE 18. We can think of the two in question as molecular analogues of the alkali metals. They form complexes by complete transfer of one electron to the layers forming molecular cations. Cobaltocenium is d^6, spin 0. Chromocenium is d^3, spin 3/2. On intercalation they adopt the configuration shown in FIGURE 19.[32] This is probably adopted to minimize the electrostatic energy of the ionic array.

What happens to the superconductivity? The diamagnetic $TaS_2(CoCp_2)_{1/4}$ is superconducting below 3.2 Kelvin.[33] Substituting the paramagnetic species decreases the critical temperature by about 10%. This is probably the result of some contact between the Fermi surface electrons and the spins. This contact should serve to break pairs tunneling between layers. Similar complexes have recently been prepared at Oxford but their magnetic properties have not been measured.[34a]

The reactions of cobaltocene and chromocene result in the formation of complexes in which each guest resides as a cation between negatively charged layers.

This kind of compound was first discovered by Rudorff, and Sick,[35] who found that alkali metals dissolved in ammonia would react with the layered dichalcogenides to form intercalation compounds. These were, in fact, the first intercalation compounds of the layered dichalcogenides. Now, several years ago, in examining the technical obstacles preventing the construction of long-lived, high-energy density electric storage batteries, we realized that research in this area should be directed at cathode materials that would react reversibly at ambient temperatures with light electropositive metals. Now, lithium reacts to form intercalation compounds with most of the layered dichalcogenides.[34b,34c] Whittingham discovered[5] that the intercalation of alkali metals, in particular, lithium, could be achieved electrochemically with the release of substantial electrical energy. He further established that this reaction could be reversed electrochemically. A single-

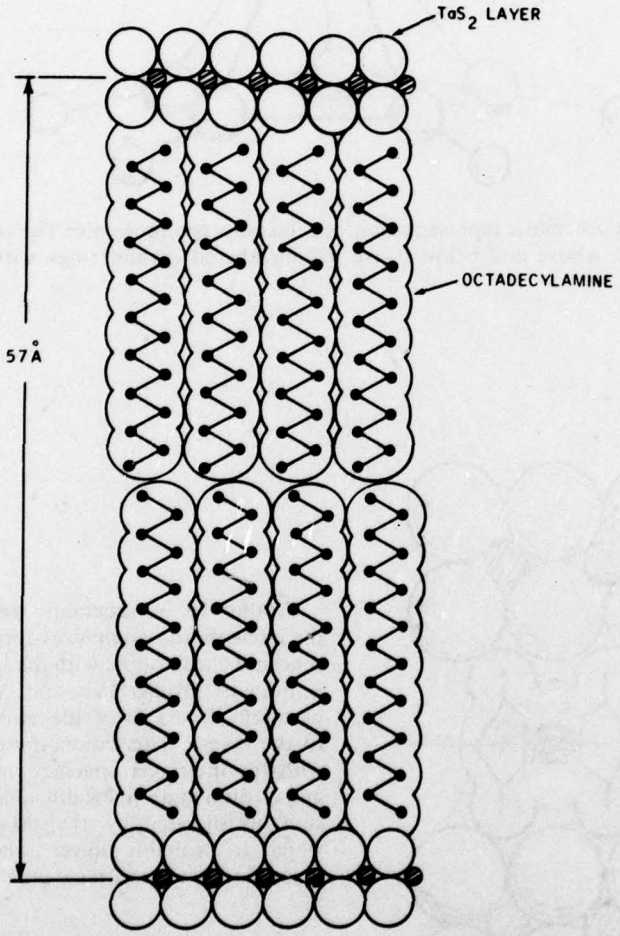


FIGURE 17. Schematic representation of the intercalation complex 2H-TaS_2(octadecylamine)$_{2/3}$. The amine function (not shown) is adjacent to the layers. The complex is superconducting below 3°K. Josephson coupling between the layers should be exceedingly weak.

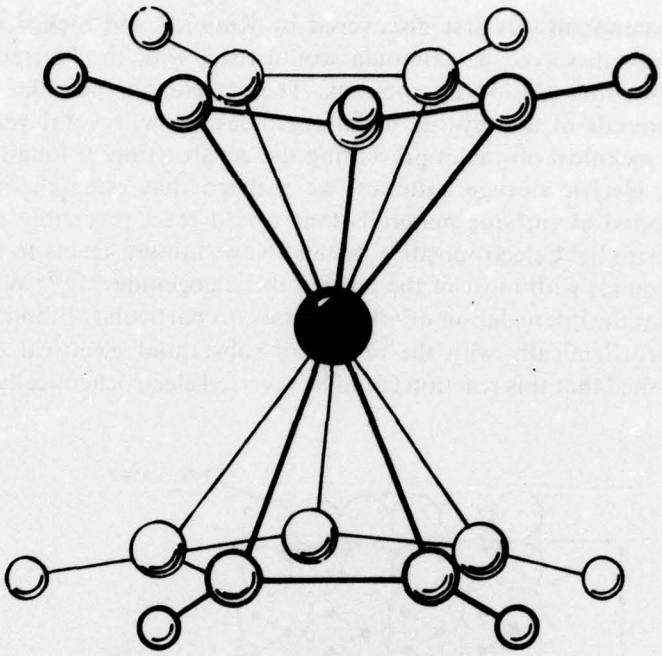


FIGURE 18. A schematic representation of a metallocene molecule. The central atom is a transition metal. Above and below it are five-membered carbon rings with hydrogens attached.

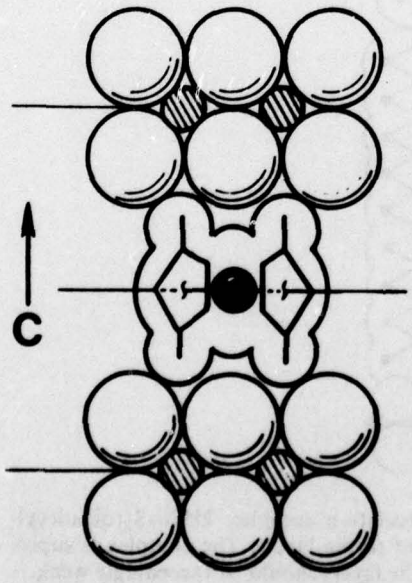


FIGURE 19. A schematic representation of the intercalation complexes formed by cobaltocene and chromocene with the layered dichalcogenides of groups IVb and Vb metals. The pseudofivefold axis of the molecule is parallel to the layers. This configuration is consistent with the interlayer spacing, the stoichiometry, and proton nmr linewidth analysis. It is presumably dictated by the Madelung energy, which is probably lower when the smaller dimension of the molecule separates the layers.

cell battery based on this concept is shown schematically in FIGURE 20. The anode of the couple is metallic lithium; the cathode is a compacted powder of titanium disulfide on an electrically conducting metallic grid. The electrolyte is an organic ether with a lithium salt dissolved in it. When the external circuit is completed, electrons flow from the anode through the circuit to the titanium sulfide cathode. Concomitantly, lithium ions are ejected from the lithium anode into solution, while lithium ions are intercalated in the titanium disulfide.

The reaction between lithium and titanium disulfide under these conditions yields a continuum of products $Li_x TiS_2$ where $0 \leq x \leq 1$. These appear to be of a

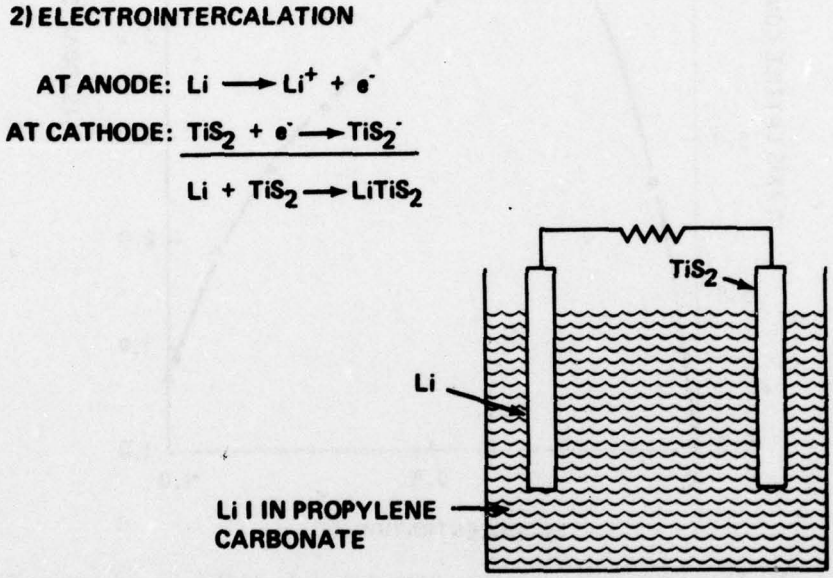


FIGURE 20. A schematic representation of an electrochemical cell based on the intercalation of lithium in titanium disulfide. On discharge, electrons flow in the external circuits from lithium to titanium disulfide. A current imposed in the opposite direction causes the lithium to deintercalate and redeposit on the lithium anode. The intercalation reaction proceeds without altering the structural integrity of the layers. The high energy density of the cell is the result in part of the fact that no bonds in TiS_2 have to be ruptured on discharge.

single phase, such that all properties of the system vary smoothly with x. This can be seen by reference to FIGURES 21–23, where the cell voltage, interlayer spacing, ^{7}Li Knight shift, and ^{7}Li NQR parameters are given as a function of discharge.[36] The picture that evolves is one in which at low intercalate concentrations the lithium resides in the octahedral holes present between the TiS_2 layers.[37] It is almost completely ionized. As the lithium concentration is increased, the layers move farther apart, the ion site is distorted from octahedral symmetry, the size of the ion increases, its Knight shift moves slightly toward that of metallic lithium, and the cell voltage drops. These observations are perfectly consistent internally.

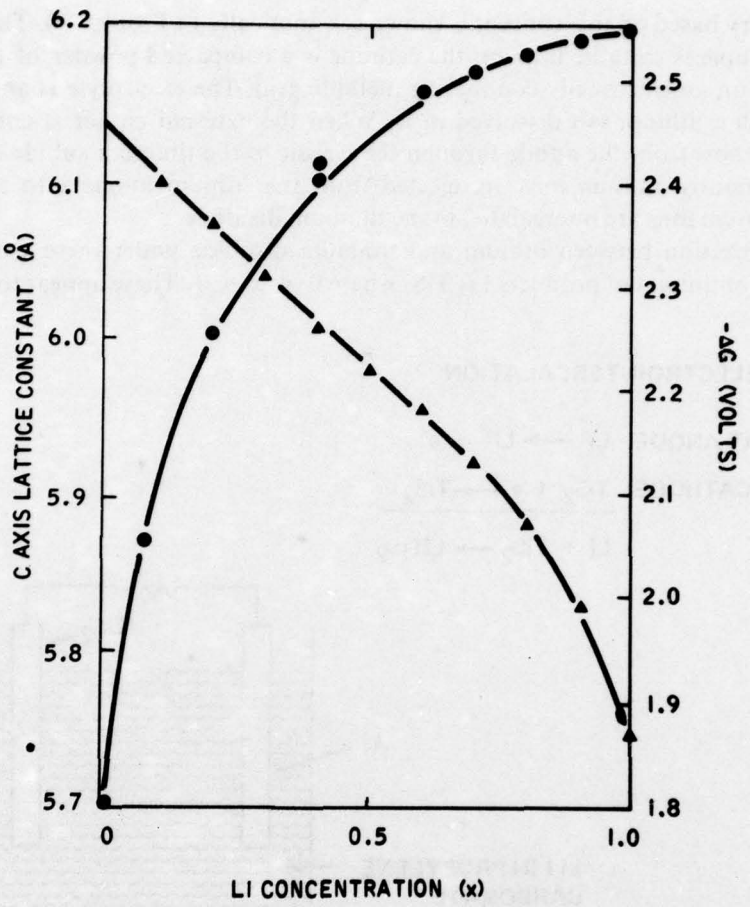


FIGURE 21. The open circuit cell voltage (triangles) of the Li/TiS_2 as a function of state of discharge. The product of the reaction is a continuum of compounds Li_xTiS_2 ($0 \leq x \leq 1$) such that no phase boundary exists between TiS_2 and $LiTiS_2$. From these data one can compute a theoretical upper limit to the energy density of a battery based on this reaction, 480 watt hours per kg. (Although the voltage curve is essentially featureless, its first derivative contains information that suggest incipient ordering of the lithium ion array at certain rational stoichiometries. Thompson, A. H. To be published.) (Data from Refs. 5a, 5c.)

The interlayer spacing (circles) of the titanium disulfide host as a function of the state of discharge. The crystals swell on total discharge by approximately 10%. The apparent size of the lithium guest increases as the reaction proceeds in such a manner that the lithium initially appears to be quite ionic but is somewhat less so when the host is full. The size of a lithium is such that the original octahedral holes between the layer can just accommodate it. (Data from Ref. 36.)

Of course, the available energy would be of no use if it could not be withdrawn at an appreciable rate. The nuclear magnetic resonance measurements also give us a handle on the diffusion of lithium within the layers. If we plot (FIGURE 24) the spin-lattice relaxation rate $1/T_1$ vs. the applied magnetic field in lithium titanium disulfide,[38] the slope yields the jump time of approximately 0.25 microseconds for

the lithium. From this, one can derive a diffusion constant that is in accord with the observed high rate of the cell.

The theoretical energy density of the Li/TiS_2 couple is 480 watt hours per kg. Engineering studies suggest that a battery with a practical energy density of 120 watt hours per kg (about four times that of lead/acid) and 100 watts per kg could be constructed.

In summary, we have seen that the unusual anisotropic bonding in the layered dichalcogenides confers upon them unusual chemical as well as physical properties, that the properties of the host can be manipulated via the intercalated guest, that guests can be selected to examine certain questions in solid-state physics, and that this area of science is able to provide timely technological options.

In conclusion, I want to thank the organizers of this conference for the oppor-

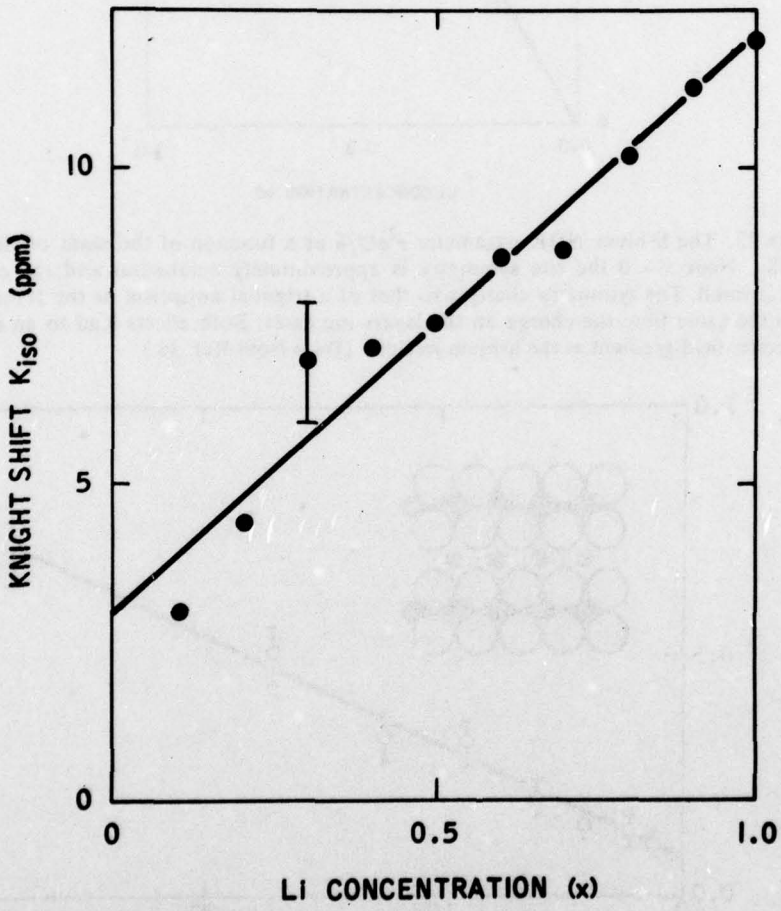


FIGURE 22. The lithium nmr Knight shift as a function of state of discharge in the Li/TiS_2 cell. Initially the Knight shift is only 3 ppm greater than that of LiI standard. As the host is filled the Knight shift increases very slightly toward that associated with metallic lithium (240 ppm). (Data from Ref. 36.)

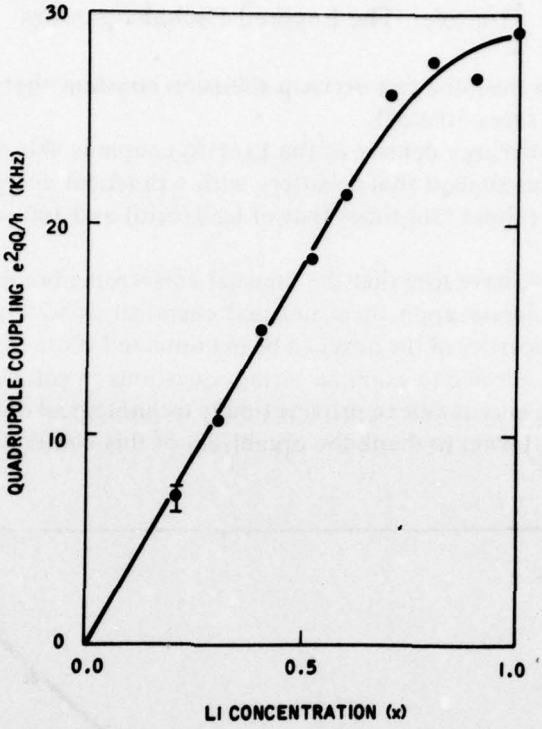


FIGURE 23. The lithium NQR parameter e^2qQ/h as a function of the state of discharge of Li/TiS_2. Near $x = 0$ the site symmetry is approximately octahedral and the coupling constant is small. The symmetry changes to that of a trigonal antiprism as the layers move apart. At the same time the charge on the layers increases. Both effects lead to an increase in the electric field gradient at the lithium nucleus. (Data from Ref. 36.)

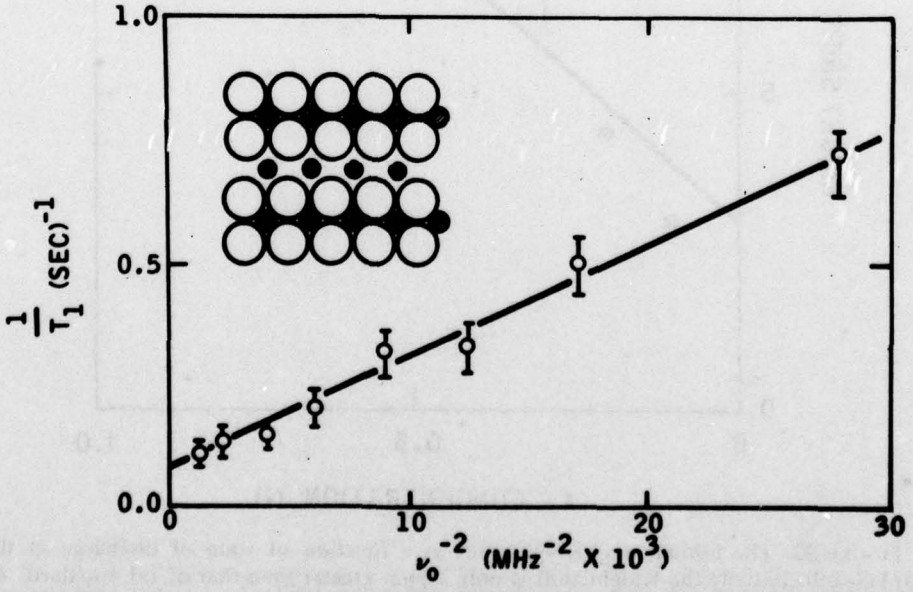


FIGURE 24. Variation of the spin-lattice relaxation rate in $LiTiS_2$ with resonance frequency showing that $1/T_1 = A + B\nu_0^{-2}$. The frequency-dependent component is associated with the motion of the lithium and implies a hop time of 0.25 μ/sec, from which one can compute a diffusion constant consistent with cell performance. The frequency-independent component is associated with guest-host interactions. (Data from Ref. 38.)

tunity to present this review. I regret that mine is the only paper of the conference that treats the layered dichalcogenides, especially because I have not treated several important aspects of the subject and have restricted myself primarily to work performed in our own laboratories.

Notes and References

1. Gamble, F. R., F. J. DiSalvo, R. A. Klemm & T. H. Geballe. 1970. Science **168:** 568.
2. Overhauser, A. W. 1968. Phys. Rev. **167:** 691.
3. Wilson, J. A., F. J. DiSalvo & S. Mahajan. 1974. Phys. Rev. Lett. **32:** 882.
4. Williams, P. M., G. S. Parry & C. B. Scruby. 1974. Phil. Mag. **29:** 695.
5a. Whittingham, M. S. 1976. Science **192:** 1126.
5b. Whittingham, M. S. 1974. J. C. S. Chem. Commun.: 328.
5c. Whittingham, M. S. 1976. J. Electrochem. Soc. **123:** 315.
5d. Whittingham, M. S. & R. R. Chianelli. 1977. Reactivity in Solids. J Wood *et al*, Eds. Plenum Press. New York, N.Y.
6. Hagenback, G., P. Courty & B. Delman. 1971. J. Catalysis **23:** 295.
7. Hagenback, G., P. Courty & B. Delman. 1973. J. Catalysis **31:** 264.
8. Wilson, J. A. & A. D. Yoffee. 1969. Adv. Phys. **18:** 193.
8a. Hulliger, F. 1968. Structure and Bonding **4:** 83.
8b. Gamble, F. R. & T. H. Geballe. 1976. Treatise on Solid State Chemistry **3:** 89.
9a. Dickinson, R. C. & L. Pauling. 1923. J. Am. Chem. Soc. **45:** 1466.
9b. See for example Thompson, A. H. 1975. Sol. State Commun. **17:** 1115.
10. Thompson, A. H., K. R. Pisharody & R. F. Koehler. Phys. Rev. Lett. **29:** 163.
11. Thompson, A. H. 1976. Comments Solid State Phys. **7:** 125.
12a. Thompson, A. H. 1975. Phys. Rev. Lett. **35:** 1786.
12b. Thompson, A. H., F. R. Gamble & C. R. Symon. 1975. Mat. Res. Bull. **10:** 915.
13. Wilson, J. A., F. J. DiSalvo & S. Mahajan. 1975. Adv. Phys. **24:** 117.
14a. Williams, P. M. 1976. Crystallography and Crystal Chemistry of Materials with Layered Structures. F. Levy Ed.: 51-92. D. Reidel Pub. Co. Amsterdam, The Netherlands.
14b. See Ehrenfreund, E., A. C. Gossard, F. R. Gamble & T. H. Geballe. 1971. J. Appl. Phys. **42:** 1491. The first observation of charge redistribution in these materials is reported in this paper.
15. Thompson, A. H. 1975. Phys. Rev. Lett. **34:** 520.
16. Huisman, R., R. DeJonge, C. Haas & F. Jellinek. 1971. J. Solid State Chem. **3:** 56.
17. Baber, W. G. 1937. Proc. Roy. Soc. London, Ser. A **158:** 383.
18a. Fernandez-Moran, H., M. Ohstuki, A. Hibino & C. Hough. Science **174:** 493.
18b. Dines, M. B. 1975. Chem. Commun. 220.
19. Gamble, F. R., J. H. Osiecki & F. J. DiSalvo. 1971. J. Chem. Phys. **55:** 3525.
20. Thompson, A. H., F. R. Gamble & R. F. Koehler. 1972. Phys. Rev. **B5:** 2811.
21. DiSalvo, F. J. 1973. Low Temp. Phys. LT13. K. D. Timmerhaus, Ed. Vol. **3:** 417. Plenum Pub. Corp. New York, N.Y.
22. Bray, P. J. & E. G. Sauer. 1972. Solid State Commun. **11:** 1239.
23. Mattheiss, L. F. 1973. Phys. Rev. **B8:** 3719.
24. Silbernagel, B. G. & F. R. Gamble. 1974. Phys. Rev. Lett. **32:** 1436.
25. Gamble, F. R. & B. G. Silbernagel. 1975. J. Chem. Phys. **63:** 2544.
26a. Chianelli, R. R., J. C. Scanlon, M. S. Whittingham & F. R. Gamble. 1975. J. Inorg. Chem. **14:** 1691.
26b. Schollhorn, R. & H. D. Zagefka. 1977. Angew. Chem. **89:** 193.
27. Silbernagel, B. G., M. B. Dines, F. R. Gamble, L. A. Gebhard & M. S. Whittingham. 1976 (1906). J. Chem. Phys. 65.
28. Silbernagel, B. G. & F. R. Gamble. 1976. J. Chem. Phys. **65:** 1914.

29. REIKEL, C. & R. SCHOLLHORN. 1976. Mat. Res. Bull. **11:** 369.
30. GAMBLE, F. R., J. H. OSIECKI, M. CAIS, R. PISHARODY, F. J. DISALVO & T. H. GEBALLE. 1971. Science **174:** 493.
31. DINES, M. B. 1975. Science **188:** 1210.
32. SILBERNAGEL, B. G. 1975. Chem. Phys. Lett. **34:** 298.
33. GAMBLE, F. R. & A. H. THOMPSON. Phys. Rev. Lett. In press.
34a. DAVIES, W. B., M. L. H. GREEN & A. J. JACOBSON. 1976. Chem. Comman. **19:** 781.
34b. WHITTINGHAM, M. S. & F. R. GAMBLE. 1975. Mat. Res. Bull. **10:** 363.
34c. DINES, M. B. Mat. Res. Bull. 1975. **10:** 287.
35. RUDORFF, W. & H. H. SICK. 1959. Angew. Chem. **71:** 128.
36. SILBERNAGEL, B. G. & M. S. WHITTINGHAM. 1976. J. Chem. Phys. **64:** 3670.
37. CHIANELLI, R. R. J. C. SCANLON & A. H. THOMPSON. 1975. Mat. Res. Bull. **10:** 1379.
38. SILBERNAGEL, B. G. 1975. Solid State Commun. **17:** 361.

DISCUSSION

JEAN ROUXEL (*Univ. of Nantes, Nantes, France*): I would like to emphasize another point about charge-density waves, namely, the effect of pressure. When a charge-density wave forms there is a competition between two terms of the free energy of the system, the strain energy, which increases with increased lattice distortioned, and an electronic energy that is related to the opening of gaps in the Fermi surface. By applying a pressure there is a stiffening of the lattice and a resulting increase in the strain energy; to offset this increase one must lower the temperature in order to have a larger gain in electronic energy. So when applying pressure, one will see the critical temperature decrease, and the effect of charge-density waves would become smaller.

ARTHUR REIS (*Argonne National Laboratory, Argonne, Ill.*): For the pyridine-deficient TaS_2 complex, why do you get one layer being filled up, with two layers of TaS_2 between, and not a random distribution?

GAMBLE: It costs energy to open up a layer, so you are going to open up as few as possible to get these complexes formed. Second, after you have complexed one side of the layer, it probably makes the other side somewhat less attractive for the same kind of interaction; therefore, the molecules will skip over and they will take on a virgin layer.

PETER DAY: In the chromocene compound that you referred to as paramagnetic, is there a transition to a ferromagnetic or antiferromagnetic order at any accessible temperature?

GAMBLE: There is an antiferromagnetic Weiss constant of 7.5°K. We have not seen any indication of ordering down to 0.5°K. One of the things that we did was look for reentrant superconductivity, which would possibly happen if there were ferromagnetic ordering. We did not see that.

ROBERT SOMOANO (*Jet Propulsion Laboratory*): Besides the intercalation of the metallic and superconducting Group V layered dichalcogenides (e.g., $NbSe_2$ and TaS_2) with Lewis bases yielding superconducting compounds with transition temperatures either higher or lower than the starting compounds, one may also intercalate the semiconducting Group VI layered dichalcogenides (e.g. MoS_2) not with Lewis bases, but with alkali and alkaline earth metals. The resulting intercalation compounds are metallic and superconducting with relatively high transition temperatures (e.g. $T_c \sim 7°K$).

SYNTHESIS AND CHARACTERIZATION OF NEW ONE- AND TWO-DIMENSIONAL MAGNETIC MATERIALS*

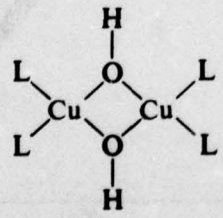
Roger D. Willett

Department of Chemistry
Washington State University
Pullman, Washington 99164

INTRODUCTION

The 1970s have seen a profound interest develop on the part of chemists and physicists in the area of magnetic interactions in low-dimensional systems. For the physicist, this interest developed from a desire to study the validity of models for magnetic interaction, which were easier to apply to one- or two-dimensional systems than to those which contained interactions in three dimensions. The chemist viewed this as an opportunity to extend his interest in structural-magnetic correlations beyond small cluster systems by using structural knowledge to design materials with restricted superexchange pathways. Thus a period of intense activity has transpired in which strong collaboration between chemists and physicists has produced some new insights into magnetic interactions in solids. Although continuing interaction will occur between these two groups, I believe we are starting to see a divergence of interests: The physicists are becoming increasingly more interested in details of ideal systems, while the chemist seeks to extend the studies to more complex chemical systems. In this paper, which will be neither exhaustive nor comprehensive, I will try to outline a few of the developments that have occured in the last several years. Several excellent reviews have come out in recent years which should be consulted for more extensive information.[1]

Historically, the chemist first became interested in magnetic interactions between metal ions in the study of dimeric salts, copper acetate being the classic example.[2] The evidence for spin-spin coupling observed from magnetic susceptibility measurements sparked controversy over direct metal-metal interaction versus superexchange interactions, which is probably not answered to everyone's satisfaction even today. The direct correlation between structure and spin-spin interactions has been clearly demonstrated in recent years by the work of Crawford *et al.*[3] on planar bibridged copper binuclear complexes of the type



*Manuscript received June 27, 1977.

0077-8923/78/0313-0111 $1.75/1 © 1978, NYAS

in which the exchange coupling $2J$ (the energy separation between the singlet and triplet states), varies linearly with the Cu—O—Cu angle, changing from ferromagnet (< 102°) to antiferromagnetic (> 102°) as the angle is increased. De Jongh and Block[4] have recently shown theoretically and experimentally a linear relationship between log J and log r in a series of salts containing linear M—F—M bridges (r = M—M distance). However, the situation gets more complicated rapidly if the symmetry is lowered or higher spins are encountered. Thus, if the dimer in (I) is not planar, the linear correlation no longer holds. Countryman *et al.*[5] have suggested a linear dependence between J and ϕ, the dihedral angle between the O—Cu—O and L—Cu—L planes. We have observed similar effects in $Cu_2Cl_6^{2-}$ binuclear species (see FIGURE 1) although the correlation is not good because the Cu—Cl—Cu angle is also varying.[6] In Cr^{3+} binuclear species, no correlation between J and structural parameters is readily apparent.[7]

Recently Hay *et al.*[8] have carried out extended Hückle MO calculations of the exchange coupling, $2J$, for a number of binuclear species, and we have performed MO calculations on the $Cu_2Cl_6^{2-}$ dimer.[9] For the case of bibridged copper(II) dimers, the orbitals of interest are the symmetric and antisymmetric combinations of the antibonding $d_{x^2-x^2}$ orbitals on the two copper ions. Hay *et al.* showed that, to a first approximation, the exchange energy was related to the energy separation between those two MOs, i.e.,

$$\Delta E = -2K_{ab} + \frac{(\epsilon_1 - \epsilon_2)^2}{J_{aa} - J_{ab}} \qquad (1)$$

This provides a link between the coupling and the single electron energies, and

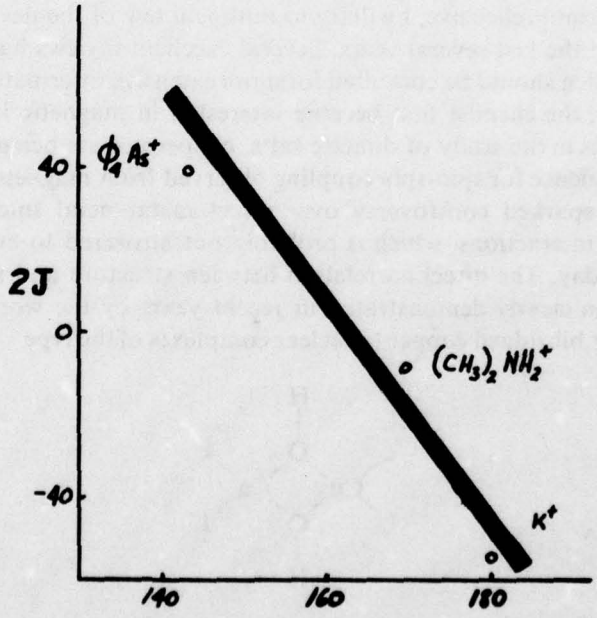


FIGURE 1. Trans Cl—Cu—Cl angle in $ACuCl_3$ salts.

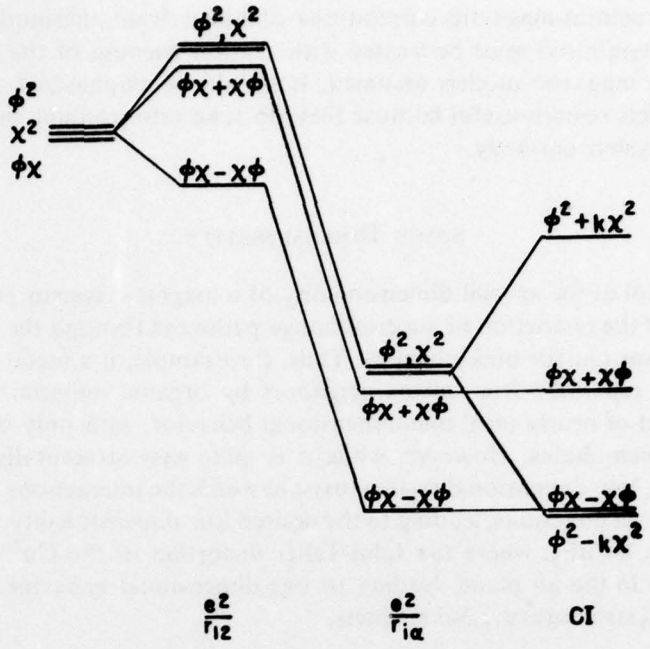


FIGURE 2. Contributions to the energy of various configurations in copper(II) dimers.

although this qualitatively agrees with Crawford *et al.*'s experimental results,[3] it does not appear obvious that $(\Delta\epsilon)^2$ should be proportional to the bridging angle.

It is instructive to examine the source of the singlet-triplet splitting in this system in somewhat more detail. Labeling the two orbitals as ϕ and χ, three configurations are possible: ϕ^2, χ^2, and $\phi\chi$. The orbital portion of the triplet state is, of course, the antisymmetric combination of the $\phi\chi$ configuration, $\frac{1}{2}[\phi\chi - \chi\phi]$. Three singlet states exist, ϕ^2, χ^2, and $\frac{1}{2}[\phi\chi + \chi\phi]$. FIGURE 2 qualitatively traces the various contributions to the energy of these states. The singlet states all lie far above the triplet states until configuration interaction (CI) between the ϕ^2 and χ^2 states is taken into account. CI lowers the level of one linear combination of $\phi^2 + \lambda\chi^2$ down to an energy comparable to that of the triplet (at the expense of the other combination). It is readily apparent that the extent of CI, and thus of the singlet-triplet energy separation, is not a property of the spin state of the system, but depends on the spatial portion of the wave functions. When this is generalized to a many-electron system, it is clear that the energy level spectrum will be very complex and, in general, will not be adequately represented by the usual Heisenberg-Van Vleck spin Hamiltonian

$$\mathcal{H} = -2J \sum_{i<j} \mathbf{S}_i \cdot \mathbf{S}_j \qquad (2)$$

nor by simple modifications to it. Indeed, recent spectroscopic experiments on Cr^{3+} binuclear species[10] show that inclusion of the so-called "biquadratic" interaction, $2J(\mathbf{S}_a \cdot \mathbf{S}_b)^2$, does not reproduce the observed energy level spectrum even though it does produce an adequate fit to the magnetic suceptibility data. Thus,

results of structural-magnetic correlations obtained from thermodynamic data (such as susceptibility) must be treated with caution because of the approximate nature of the magnetic models assumed. It should be emphasized, nevertheless, that the models remain useful because they do take into account the spin properties of the system correctly.

Space Dimensionality

The control of the spacial dimensionality of a magnetic system generally rests on concept of the restriction of superexchange pathways through the introduction of large cations and/or bulky ligands. Thus, for example, if a metal-ligand chain is effectively separated from all its neighbors by organic material, one can be safely assured of nearly ideal one-dimensional behavior, with only dipolar interactions between chains. However, while it is quite easy structurally to identify such systems, low-dimensional systems exist in which the interactions fortutitously cancel in certain directions, leading to the desired low dimensionality. An example of the later is $KCuF_3$, where the Jahn-Teller distortion of the Cu^{2+} ions occurs preferentially in the *ab* plane, leading to one-dimensional behavior, while other cubic $M'MX_3$ structures are 3-d magnets.

One-Dimensional Systems

The classic example of a one-dimensional magnetic system is the hexagonal salt, $[(CH_3)_4]MnCl_3$ (TMMC). As illustrated in FIGURE 3, this contains $(MnCl_3)_n$ linear chains separated by the tetramethylammonium ions. Thus, well-defined superexchange pathways exist along the chains, but the cations block all but dipolar interactions between the chains. As a consequence, the antiferromagnetic intrachain interactions (J) yields a maximum the susceptibility near

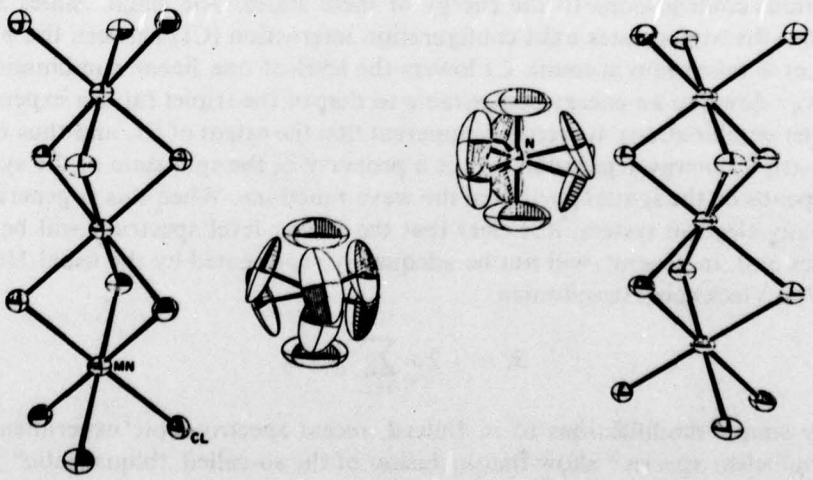


FIGURE 3. A view of $[(CH_3)_4N]MnCl_3$ along the $\bar{2}10$ direction.

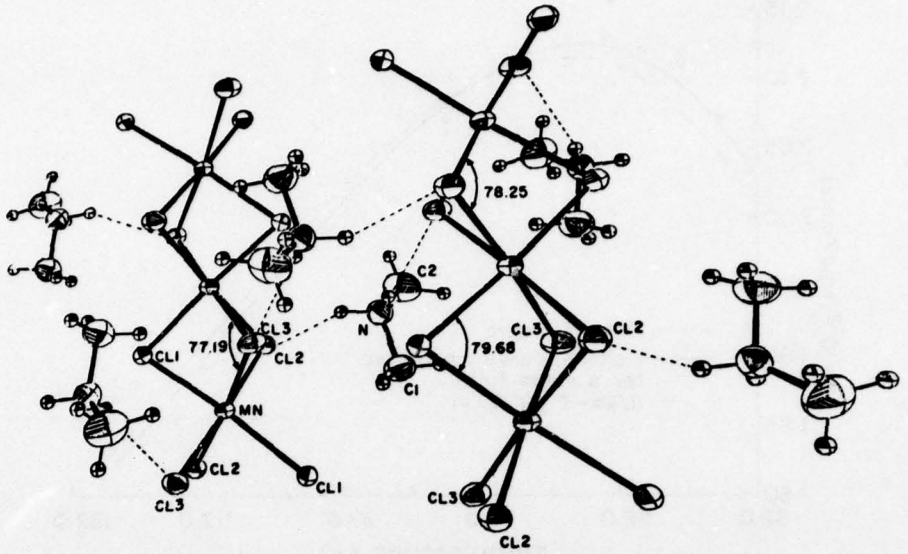


FIGURE 4. A view of $[(CH_3)_2NH_2]MnCl_3$. Chains that run in the *c*-direction are loosely connected by hydrogen bonding into corrugated sheets along the *a*-direction.

70°K, but three-dimensional magnetic ordering does not set in until 0.8°K.[11] Because of the extensive spin correlations above T_N, there is very little contribution from the magnetic entropy to the specific heat at T_N.

TMMC Analogs

The ability to fine-tune the magnetic interactions through manipulation of the cation, as observed in the $Cu_2Cl_6^{2-}$ cluster systems, leads us to seek to prepare analogs of TMMC. We successively synthesized $(CH_3)_2NH_2MnCl_3$ (DMMC), whose crystal structure is shown in FIGURE 4.[12] This low-symmetry (monoclinic) analog of TMMC again has $(MnCl_3)_n$ chains separated from each other by organic cations. However, in this case the cations hydrogen bond adjacent chains together into a 2-d network. The magnetic susceptibility (FIGURE 5) is characteristic of an antiferromagnetic linear chain. Detailed analysis, however, indicated that χ could not be reproduced by a simple 1-d model, but that it was necessary to include an interchain coupling term, $2J/k = -0.05°$ in addition to the intrachain coupling ($2J/k = -6.9°$). No evidence of long-range order was observed down to the limit of the temperature range available (1.5°K).

When the trimethylammonium cation was used, a most intriguing compound was obtained. This hexagonal material, with stoichiometry $[(CH_3)_3NH]_3Mn_2Cl_7$, contains two types of linear chains: TMMC-like $(MnCl_3)_n$ chains of face-shared octahedra and chains of discrete $MnCl_4^{2-}$ tetrahedra.[13] As illustrated in FIGURE 6, these chains are again separated by the organic cations, so that the only interactions between chains are dipolar. The magnetic susceptibility was interpreted in terms of independent linear chain systems with exchange parameters of $-8.0\ cm^{-1}$ and $0.2\ cm^{-1}$, respectively.

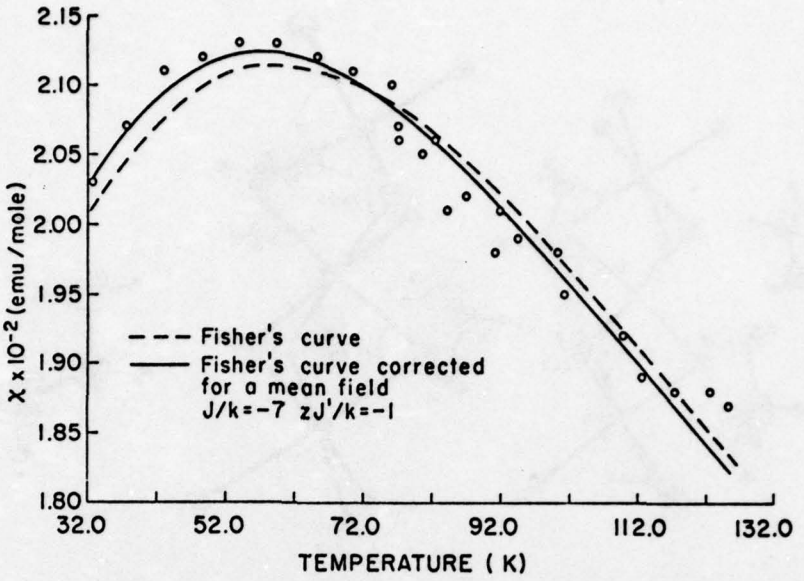


FIGURE 5. Magnetic susceptibility of $[(CH_3)_2NH_2]MnCl_3$ from 30°K to 130°K with curves for the Fisher model and the mean field corrected Fisher model.

In spite of the earlier caveat on the perils of correlations of exchange parameters with geometry, it is interesting to plot $2J$ versus the bridging Mn—Cl—Mn angle in the three salts described above. As seen in FIGURE 7, there is a near linearity, with the expected trend; that is, the coupling becomes more antiferromagnetic as the angular deviation from 90° increases.

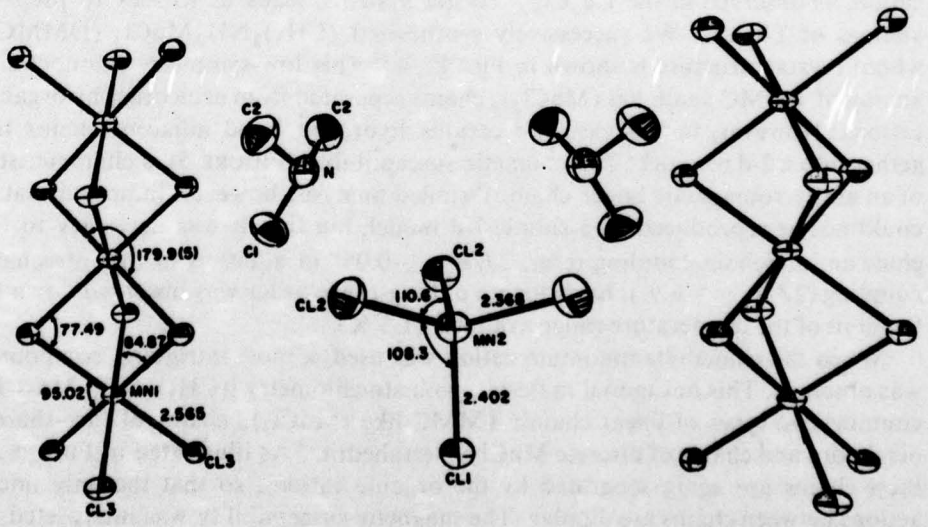


FIGURE 6. A view of $[(CH_3)_3NH]_3Mn_2Cl_7$ along the 110 direction. Linear chains of face-sharing $MnCl_6$ octahedra are separated by $MnCl_4$—and $(CH_3)_3NH^+$ ions.

Linear Chains of Dimers

In the study of a series of dimer copper(II) halides undertaken for a variety of reasons, we have consistently encountered the existence of magnetic coupling between adjacent dimers. A mathematical model developed earlier,[14] consisting of Heisenberg coupling within the dimer and Ising coupling between dimers, has proved capable of accounting for the observed susceptibility behavior very accurately. In this model, the singlet and triplet states of the dimers are assumed to be separated by an energy ΔE ($\Delta E > 0 \rightarrow$ triplet ground state) with adjacent triplet states interacting by an Ising exchange coupling $2J$. This model has the advantage that it reproduces the susceptibility of a dimer system in the limit

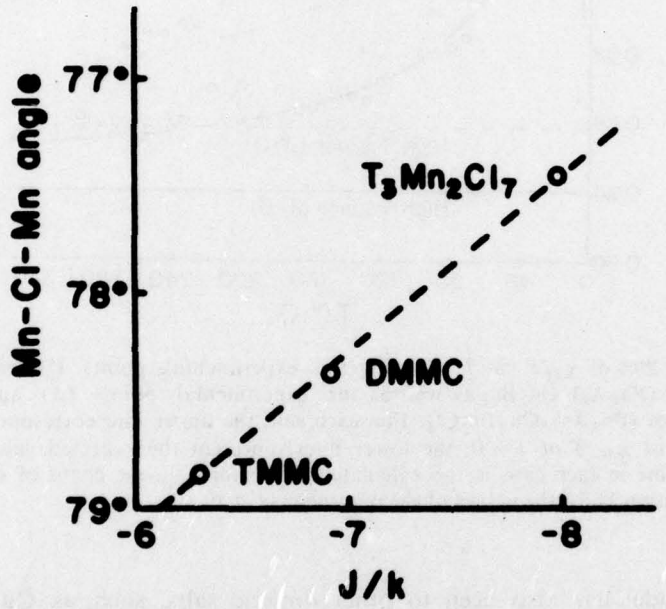


FIGURE 7. Plot of exchange-coupling parameter vs. average Mn—Cl—Mn bond angle for TMMC-like salts.

$2J \rightarrow 0$ while still giving an accurate analytical description of the susceptibility in the intermediate coupling regime.

The salt, $\phi_4AsCuCl_3$, has been shown to contain isolated $Cu_2Cl_6^{2-}$ dimers with a triplet ground state.[6] In the course of the EPR investigation of excited states in the magnetically isolated $Cu_2Cl_6^{2-}$ dimers in $\phi_4AsCuCl_3$, the susceptibility of $\phi_4AsCuCl_2Br$ and $\phi_4AsCuBr_3$ were investigated.[15] Evidently as a result of the size of the large Br^- ions, some antiferromagnetic coupling between the ferromagnetically coupled dimers was found to exist in the latter salts. The results, shown in FIGURE 8, clearly indicated the effects both of the stronger ferromagnetic coupling, ΔE, (high T behavior) and the weaker antiferromagnetic coupling, $2J$ (low T behavior). The excellent agreement between theory and experiment is also observed.

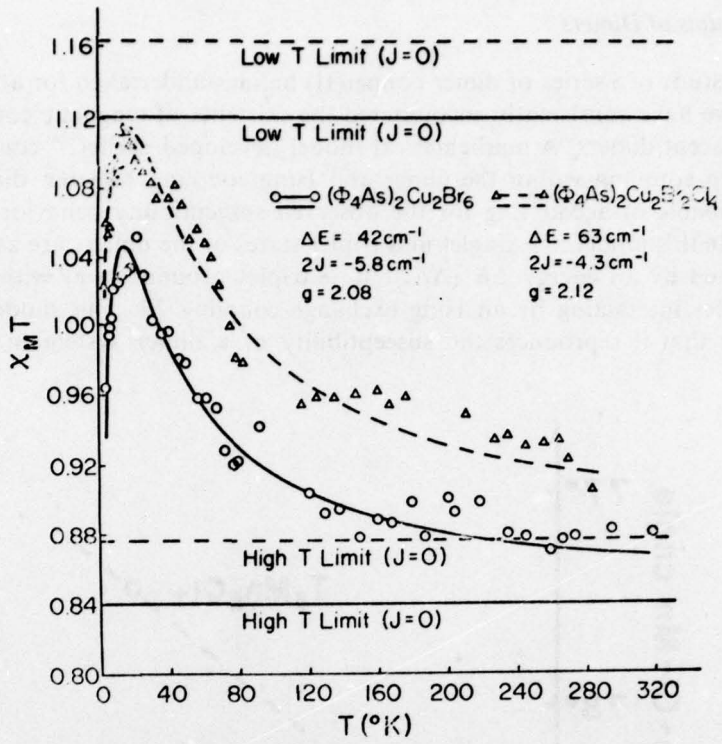


FIGURE 8. Plot of $\chi_M T$ vs. T, showing the experimental points (°) and theoretical curves (-) for $(Ph_4As)_2Cu_2Br_4$ as well as the experimental points (Δ) and theoretical curves (---) for $(Ph_4As)_2Cu_2Br_2Cl_4$. For each salt, the upper line corresponds to the expected value of $\chi_M T$ at $T = 0$; the lower lines represent the expected values at $T = \infty$. The middle line in each case is the calculated curve for a linear chain of dimers (as defined in Equation 1) for the values of the parameters listed.

This model has also been to other dimeric salts, such as $CuBr_2 \cdot py$ and $CuCl(OCH_3)py$ whose crystal structure and magnetic susceptibility have been determined recently in our laboratory. The former, carrier out by Professor Duane D. Swank of Pacific Lutheran University, Tacoma, Washington, was initiated as part of our study of geometries of copper (II) bromide complexes. The latter was part of our work on catalytical systems. Both contain nearly planar dimers that pack to form infinite chains. In the bromide, both intra- and interdimer couplings are antiferromagnetic with $\Delta E \sim 2J \sim 15\ cm^{-1}$. In the methoxy salt it is probable that ΔE and $2J$ are of opposite sign, but because of the interaction of the two parameters in the least-squares process, accurate estimation of the coupling is not possible.

Search for the Elusive 1-d Spin ½ Ferromagnet

One obvious omission in the current zoo of magnetic systems is the 1-d spin ½ ferromagnet. Hence we have undertaken, without success, the study of a number

of compounds where superexchange arguments indicated ferromagnetic interactions might exist.

The structure of the salt, $[(CH_3)_2CHNH_3]_2CuCl_4$, is illustrated in FIGURE 9,[16] may be visualized as a ribbon cut out from the 2-d $(RNH_3)_2CuCl_4$ lattice. In the latter, the exchange interaction is ferromagnetic. Unfortunately, χ measurements showed predominate antiferromagentic behavior. Examination of FIGURE 9 shows that two exchange pathways exist: $2J$ and $2J'$. The first is similar to that in the $(RNH_3)_2CuCl_4$ salts (i.e., interaction is via a Cu-Cl bridge to a square planar $CuCl_4^{2-}$ ion). The latter is different; the interaction is via a Cu-Cl bridge to a tetrahedrally distorted $CuCl_4^{2-}$ ion. The Ising model was solved for this lattice. The fit of the derived equation to the observed data gives $2J/k = 2.5°$

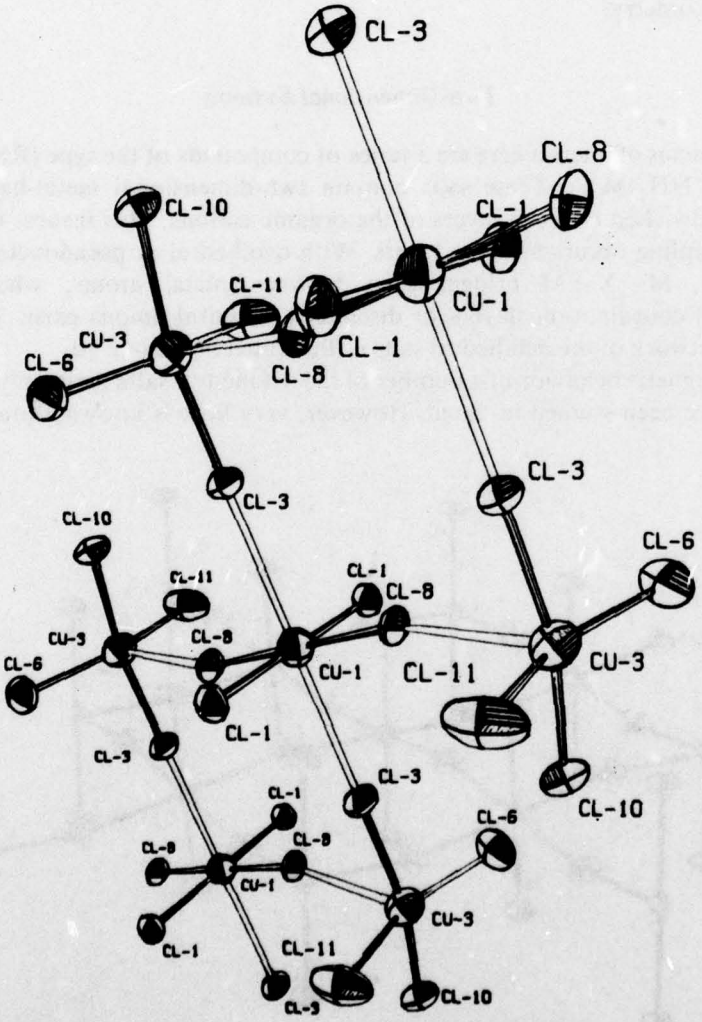


FIGURE 9. The structure of Cu(1) ribbon in $[(CH_3)_2CHNH_3]_2CuCl_4$ (green-low temperature phase). Copper(I) from three-unit cells in the <100> direction are shown.

(ferromagnetic) and $2J'/k = -4.8°$ (antiferromagnetic). Taking cognizance of the relative strength of the two interactions, we may describe the system as ferromagentically coupled antiferromagnetic trimers, yielding to a total antiferromagnetic behavior.

The susceptibility of the salt $[Cu(terpy)CN]X \cdot H_2O$ (where $X = NO_3^-$ and terpy ≡ terpyridine) has also been studied.[17] Because of the near linearity of Cu-C≡N.....Cu interaction, it was reasonable to assume the exchange interaction could possibly be ferromagnetic, as in the $(RNH_3)_2CuCl_4$ salts. The susceptibility data indicated 1-d behavior, with the exchange coupling clearly antiferromagnetic but small ($\approx -4°$). Since the bridging angle, and thus the coupling, is likely to be sensitive to steric forces, Professor Mark Wickolas of Western Washington State College has replaced the NO_3^- ion with other anions. Unfortunately, at this point, all such substitutions have resulted in the destruction of the bridging geometry.

Two-Dimensional Systems

The systems of interest here are a series of compounds of the type $(RNH_3)_2MX_4$ or $(NH_3R'NH_3)MX_4$. These salts contain two-dimensional metal-halogen networks sandwiched between layers of the organic cations. This insures that no exchange coupling occurs between layers. With octahedral or pseudooctahedral coordination, M—X—M bridges exist between metal atoms, whereas with tetrahedral coordination, layers of discrete tetrahedral anions exist. The metal-halogen network of the octahedral salts is illustrated in FIGURE 10.

The magnetic behavior of a number of the octahedral salts (principly Cu^{2+} and Mn^{2+}) have been studied in detail. However, very little is known about the mag-

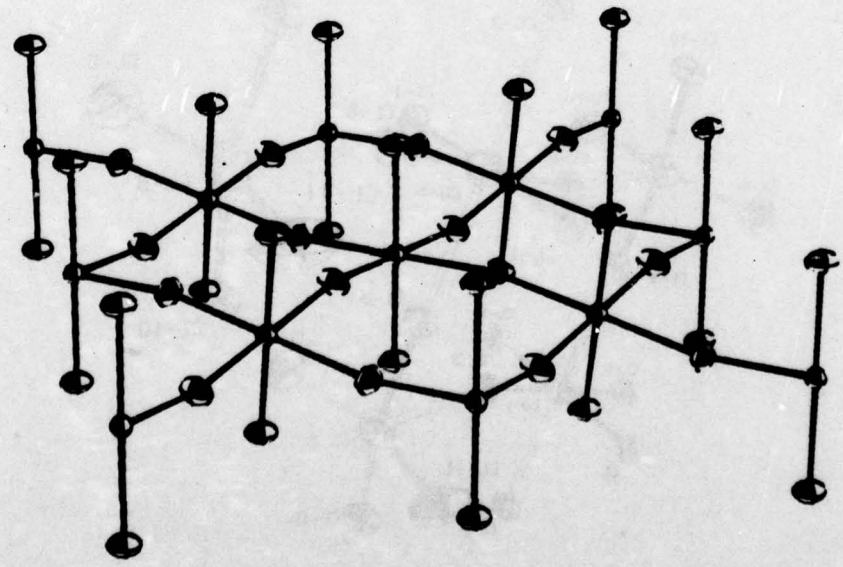


FIGURE 10. Metal-halogen framework in $(RNH_3)_2MX_4$ salts.

TABLE 1

SYNTHESIS OF $(RNH_3)_2MX_4$ SALTS*

	Cr	Mn	Fe	Co	Ni	Cu	Zn	Cd	Pd
Cl	O	O	O	*T*	O	O	*T*	O	O
Br	O	O	D	*T*	—	O	—	O	—
I	—	—	—	—	—	D	—	—	—

*O indicates octahedral or distorted octahedral coordination geometry; — indicates no attempt made yet; D indicates decomposition; and T indicates tetrahedral coordination geometry.

netic coupling in the tetrahedral salts. Since the exchange coupling will proceed via interionic Cl. . .Cl contacts, these may behave as 1-d rather than 2-d systems, as, indeed, some of our preliminary EPR work on the Co^{2+} salts indicate. We expect, in general, however, these compounds to be accurate model systems with which to study the nature of magnetic interactions in two-dimensions.

Synthesis and Crystal Structure Analysis

The metal-halogen systems that have been investigated are tabulated in TABLE 1. The technique for preparing the Ni^{2+} salts has been worked out by Dr. Ferraro of Argonne National Laboratory;[18] Professor Peter Day has developed the synthesis of the Cr^{2+} salts.[19] The structure of $(C_3H_7NH_3)_2ZnCl_4$ has been determined by Professor Kenneth Emerson (as well as that of the $CH_3NH_3^+$ salt).[20]

The crystal structure of a number of new salts has been determined in this laboratory in the last year or two. These have included two diamagnetic salts that are potential host lattices for single-ion EPR studies. The structure of $(C_3H_6N_2H_6)CdCl_4$ is isostructural with the corresponding Mn^{2+} and Fe^{2+} salts, except that the cation is not disordered. The structure of $(C_3H_7NH_3)_2PdCl_4$ is closely related to the analogous Cu^{2+} salts. Each square planar $PdCl_4^{2-}$ ion has Cl^- from neighboring $PdCl_4^{2-}$ ions occupying the axial sites at approximately 3.2A. The propylammonium ion is severely disordered, as is also frequently the case in the Cu^{2+} salts.

Mutual Inductance Susceptibility Studies

A series of magnetic susceptibility studies has been carried out on a wide variety of $(RNH_3)_2MnCl_4$ salts by the mutal-inductance technique. This has the advantage over typical high-field techniques (such as the Gouy and Faraday methods) in that the measurement occurs at essentially zero field. This means that any spin canting (weak ferromagnetism) present in the system is not destroyed by the measurement process. The significance of this is dramatically illustrated in FIGURE 11, which shows the high-field susceptibility of a single crystal of MA_2MnCl_4[21] and FIGURE 12, which shows the low-field susceptibility of a powder speciman of the same salt.[22] In the high field study, the onset of three-dimensional ordering is poorly defined, but with the mutual-inductance technique,

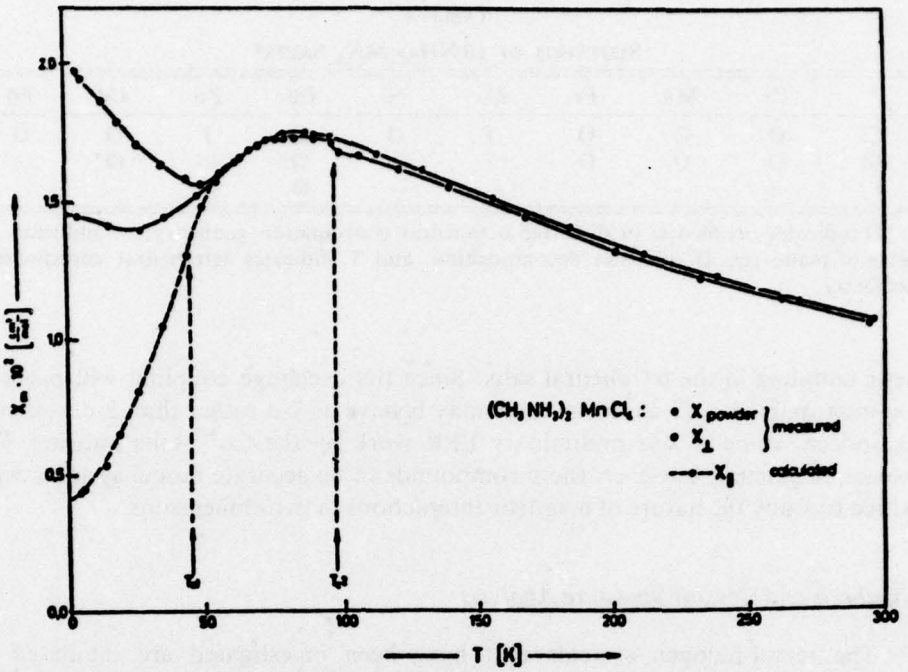


FIGURE 11. High-field susceptibility of MA_2MnCl_4.

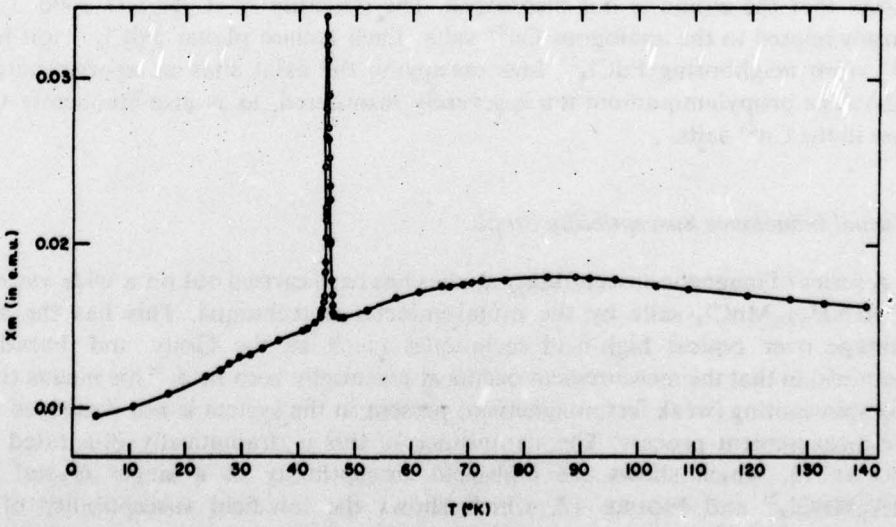


FIGURE 12. Zero-field susceptibility of MA_2MnCl_4.

the Néel temperature is clearly defined. In addition to this advantage, analysis of the data in the region of the transition temperature yields important information about the critical behavior of the system not attainable from the high-field measurements.

Role of Interplanar Spacing. In order to assess the role of interplanar interactions on the Néel temperature, measurements were made of a series of $(RNH_3)_2MnCl_4$ salts, including R = CH_3, C_3H_7, and $C_{15}H_{31}$,[23] as well as $(NH_3R'NH_3)MnCl_4$ with R' = C_3H_6 and $C_2H_4NH_2C_2H_4$. This demonstrated that T_N was essentially independent of the interplanar spacing. Thus, the aniso-

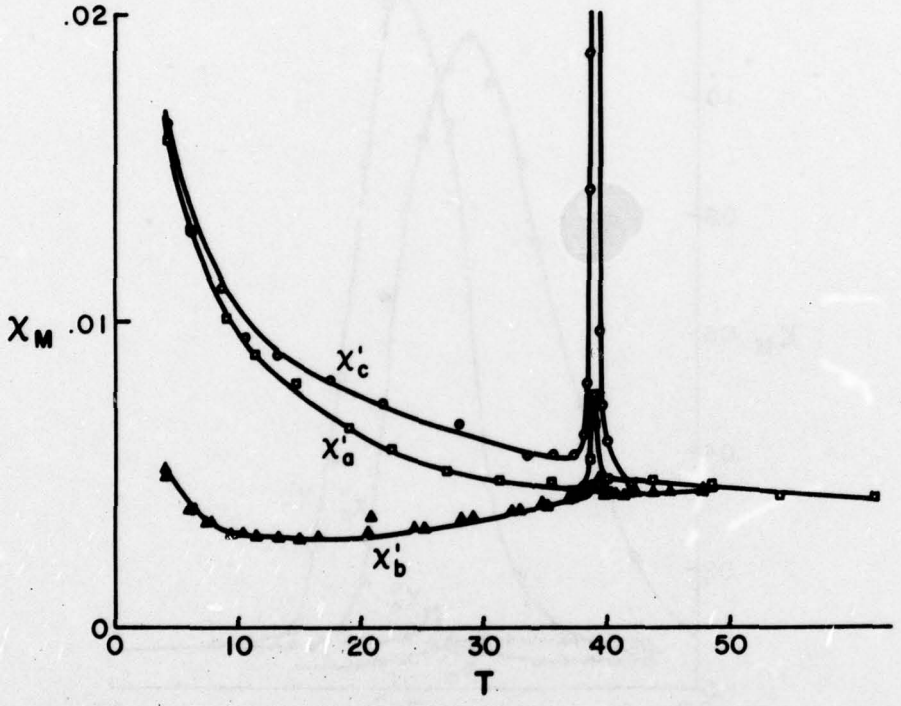


FIGURE 13. Single-crystal magnetic susceptibility of $(C_3H_7NH_3)_2MnCl_4$. X'_b is susceptibility perpendicular to the layer; X'_c is susceptibility parallel to direction of tilt of the octahedra.

tropy that drives the 2-d system into the ordered state must be a characteristic of the layer structure itself.

Single-Crystal Study of Spin-Canting. The magnetic susceptibility of single crystals of $(C_3H_7NH_3)_2MnCl_4$ was measured.[24] The results are shown in FIGURES 13 and 14. The spike in χ'_c and χ''_c confirms the presence of spin canting in that direction. The maximum in the dispersive component (χ') gives T_N, the temperature of the onset of spontaneous magnetization. The maximum in the absorptive component (χ'') gives the temperature at which the width of the hysteresis loop becomes comparable to the applied ac field (~20 gauss). From the data, it is

seen that the direction of spin canting is the same as the direction of the tilt of the octahedra. Thus, the spin orientation is tied to the lattice via spin orbit coupling. The cause of the continued rise of χ and T is lowered is not known.

Attempts to measure the bulk moments of the canted antiferromagnetic phase have not been successful. This may be due to a net cancellation between adjacent layers or to domain formation. It should be noted that a bulk moment was observed for $(NH_3C_3H_6NH_3)MnCl_4$.[25] Both from our mutual inductance studies and from the bulk moment reported by Losee *et al.*, the canting angle can be

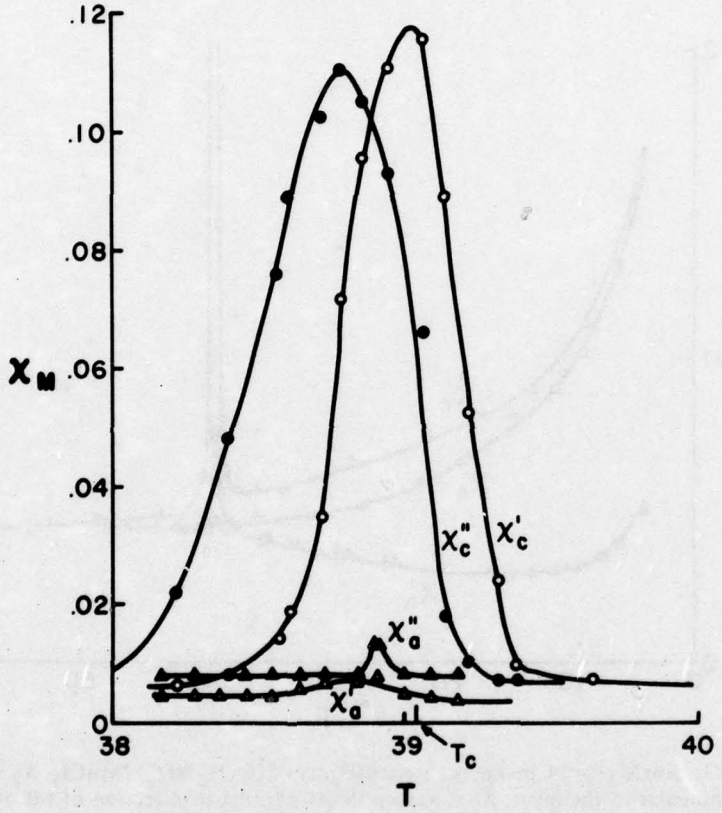


FIGURE 14. X' and X'' near T_c for $(C_3H_7NH_3)_2MnCl_4$. Note X'' peaks about 0.2° below T_c.

estimated to be only 0.05°! Thus, the extent of canting is miniscule, as is not unreasonable for Mn^{2+} salts.

Role of Bulk of Organic Cation. Since the tilt of the $MnCl_6$ octahedra is caused by hydrogen bonding of the cation to the chloride ions, it was reasonably felt that the nature of the magnetic interaction could be influenced by changing the strength of the hydrogen bonding. One way of accomplishing this would be through steric effects by changing the bulk of the cations. This assumption was substantiated by results on the Fe^{2+} system, where the R = CH_3 salt ordered at 96°K, while the R = ϕCH_2 group ordered at 70°K.[26]

Consequently, χ measurements were initiated on Mn^{2+} salt with R = ϕCH_2 obtained from crystallization from aqueous solution, which were subsequently shown to be crystals of $(\phi CH_2NH_3)_2MnCl_4 \cdot H_2O$. This salt contains tetrahedral $MnCl_4^{2-}$ ions packed together in a two-dimensional array. The salt shows antiferromagnetic Curi-Weiss behavior at high temperature ($\theta \sim 90°$) with positive deviation from Curie-Weiss behavior at low T. Significantly, no spike in the susceptibility characteristic of spin canting was observed, as expected with the compound isostructural with $(C_3H_7NH_3)_2ZnCl_4$. In that structure, adjacent metal ions are related by centers of inversion. We see that significant exchange interaction occurs in the tetrahedral salts as well as in the octahedral salts.

Finally, it should be noted that this series can be extended to other anions other than halides. Thus, we have just synthesized and characterized the two-dimensional magnetic system, $(\phi CH_2NH_3)_2Cu(ox)_2$. This salt contains planar $Cu(ox)_2^{2-}$ ions, with one of the noncoordinating oxygen atoms on each oxalate bridging to adjacent copper ions.

Spin Dimensionality

One of the major developments in magnetochemistry recently has been the recognition that the spin-dimensionality can be structurally controlled as well as the space-dimensionality. Thus, if we write the symmetric part of the magnetic spin Hamiltonian as

$$\mathcal{H} = -\sum_{i<j} (2J_x S_x^i S_x^j + 2J_y S_y^i S_y^j + 2J_z S_z^i S_z^j) \tag{3}$$

three limiting cases are generally recognized:

$$\text{a) Heisenberg } \mathcal{H} = -2J \sum_{i<j} \mathbf{S}_i \cdot \mathbf{S}_j \tag{3a}$$

$$\text{b) } XY \ \mathcal{H} = -2J \sum_{i<j} (S_x^i S_x^j + S_y^i S_y^j) \tag{3b}$$

$$\text{c) Ising } \mathcal{H} = -2J \sum_{i<j} (S_z^i S_z^j) \tag{3c}$$

with spin dimensionalities 3, 2, and 1, respectively. Since different magnetic behavior is predicted for each of these three models, it is of interest to be able to systematically synthesize salts which approximate each of these limiting cases. The question is how to relate $\mathbf{J} = (J_x, J_y, J_z)$ to structural properties of the systems of interest. In particular, it is of interest to synthesize systems which behave as XY magnets, since very few have been characterized in the past.

We recognize that the spin Hamiltonian is only an artificial representation of the physically real interactions, introduced for computational convenience. Thus, the interaction of interest is not the spin-spin interaction, but the interaction between the magnetic moments. This is given by

$$\Delta E = \sum_{i<j} -2 \ \mu_i \cdot \mu_j. \tag{4}$$

But we can write, in the usual manner, that $\boldsymbol{\mu}_i = \mu_\beta \mathbf{g}_i \mathbf{S}_i$. If the principal axes of the $\mathbf{g}_i$ tensors are all parallel, we see that for the x component

$$-2\mathcal{J}\mu_x^i\mu_x^j = -2\mathcal{J}\mu_\beta^2 g_x^i g_x^j S_x^i S_x^j$$

or

$$2J_x = 2\mathcal{J}\mu_\beta^2 g_x^2. \tag{5a}$$

and similarly

$$2J_y = 2\mathcal{J}\mu_\beta^2 g_y^2 \tag{5b}$$

$$2J_z = 2\mathcal{J}\mu_\beta^2 g_z^2. \tag{5c}$$

Thus, it is possible to predict the relative magnetude of the components of J if the single ion g tensor is known. For Mn^{2+}, with its isotropic g tensor, a Heisenberg model is clearly predicted to be applicable. On the other hand, the Cu^{2+} ion in its usual Jahn-Teller distorted configuration has $g_\parallel > g_\perp$, and an Ising type anisotropy is expected in the spin Hamiltonian, i.e., $J_z > J_x, J_y$.

This argument has recently been used successfully by Carlin to predict the spin dimensionality of the 1-d antiferromagnet, Cs_2CoCl_4.[27] For this salt, $g_\perp/g_\parallel \sim 2$, so it should be an XY magnet with $J_x/J_z \sim 4$. In a beautiful series of heat-capacity studies on $Cs_2(Co, Zn)Cl_4$ samples in the range 0.1–1.0°K, they showed that the magnetic heat capacity agreed quite accurately with that predicted for an XY magnet with that degree of anisotropy. We have used the same arguments to predict the behavior of the system $[(CH_3)_3NH]_3(Cd, Co)_2Cl_7$. This is isomorphous with the corresponding Mn salt, and the Co^{2+} ions preferentially occupying the tetrahedral sites. Again, the ratio of $g_\perp/g_\parallel \sim 2$, and XY behavior is predicted. This has been confirmed by recent heat-capacity measurements.

For $(RNH_3)_2CuCl_4$ salts, the situation is somewhat different. The fourfold axes of the $CuCl_4^{2-}$ lie alternately in the crystallographic [110] and [$\bar{1}$10] directions (i.e., at 90° to each other in the two-dimensional layer). Thus, $J_x = J_y = \mathcal{J}\mu_\beta^2 g_\parallel g_\perp$ while $J_z = \mathcal{J}\mu_\beta^2 g_\perp^2$. Since $g_\parallel/g_\perp \sim 1.1$, a small (10%) XY anisotropy is anticipated. This has been observed in recent experimental studies.[28]

If the g-tensors are not parallel, cross products occur when (**4**) is expressed in terms of the spin operators. This leads to antisymmetric exchange terms in the spin Hamiltonian,

$$\mathcal{H}_{\text{antisym}} = \sum_{i<j} \mathbf{D} \cdot \mathbf{S}_i \times \mathbf{S}_j.$$

This is one of several possible mechanisms leading to the phenomena of spin canting and weak ferromagnetism.

References

1a. DE JONGH, L. J. & A. R. MIEDEMA. 1974. Adv. in Physics **23**: 1.

1b. STEINER, M., J. VILLAIN & C. G. WINDSOR. 1976. Adv. in Physics **25**: 87.

1c. KELLER, K. J., ed. 1975. Low-Dimensional Cooperative Phenomena. Plenum Press. New York, N.Y.

1d. INTERRANTE, L. V. 1974. Extended Interactions Between Metal Ions in Transition Metal Complexes. Amer. Chem. Soc.

1e. CARLIN, R. L. 1976. Accts. Chem. Res. **9:** 67.
2. BLEANEY, B. & K. D. BOWERS. 1952. Proc. Roy. Soc. **A214:** 451.
3. CRAWFORD, V. H., H. W. RICHARDSON, J. R. WASSON, D. J. HODGSON & W. E. HATFIELD. 1976. Inorg. Chem. **15:** 2107.
4. DE JONGH, L. J. & R. BLOCK. 1975. Physica. **79B:** 568.
5. COUNTRYMAN, R. M., W. T. ROBINSON & E. SINN. 1974. Inorg. Chem. **13:** 2013.
6. CHOW, C., R. CAPUTO, R. D. WILLETT & B. C. GERSTEIN. 1974. J. Chem. Phys. **61:** 271.
7. HODGSON, D. J. 1974. ACS Symp. Ser. 5: Chpt. 9.
8. HAY, P. J., J. C. THIEBEAULT & R. HOFFMAN, 1975. J. Am Chem. Soc. **97:** 4884.
9. CHOW, C. 1974. Ph.D. Thesis. Washington State Univ. Pullman, Wash.
10. MCCANDLISH, L. & G. A. CROSBY. 1977. New Orleans ACS Meeting. March 1977. New Orleans, La.
11. KILBOURN, B. T. & J. D. DUNITZ. 1967. Inorg. Chim. Acta **1:** 209.
12. CAPUTO, R. E., R. D. WILLETT & B. C. GERSTEIN. 1976. Phys. Rev. B **13:** 3956.
13. CAPUTO, R. E., S. ROBERTS & R. D. WILLETT. 1976. Inorg. Chem. **15:** 820.
14. GERSTEIN, B. C., F. D. GEHRING & R. D. WILLETT. 1972. J. Appl. Phys. **43:** 1932.
15. CHOW, C., R. D. WILLETT & B. C. GERSTEIN. 1975. Inorg. Chem. **14:** 205.
16. ANDERSON, D. N. & R. D. WILLETT. 1974. Inorg. Chim. Acta **8:** 167.
17. ANDERSON, O. P., A. B. PACKARD & M. WICHOLAS. 1976. Inorg. Chem. **15:** 1613.
18. FERRARO, J. R. Private Communication. Argonne National Laboratory, Argonne, Ill.
19. BELLITTO, C. & P. DAY. 1976. J.C.S. Chem. Commun.: 870.
20a. EMERSON, K. Private Communication. Montana State Univ. Bozeman, Mont.
21. VANAMSTEL, W. D. & L. J. DE JONGH. 1972. Solid State Commun. **11:** 1423.
22. CHANG, K., B. C. GERSTEIN & R. D. WILLETT. 1974. J. CHEM. Phys. **60:** 3454.
23. GERSTEIN, B. C., C. CHOW, R. CAPUTO & R. D. WILLETT. 1974. AIP Conf. Proc. **24:** 361.
24. WILLETT, R. D. & B. C. GERSTEIN. 1976. Inorganic Gordon Conf.
25. LOSEE, D., D. T. MCGREGOR, W. E. ESTES & W. E. HATFIELD. Phys. Rev. B **14:** 4100.
26. MOUSTAFA, M. F. & R. D. WILLETT. 1971. Phys. Rev. **4B:** 2213.
27a. ALGRA, H. A., L. J. DE JONGH, H. W. J. BLÖTE, W. J. HUISKAMP & R. L. CARLIN. 1976. Physica **82B;** 239.
27b. METSELAAR, J. W., L. J. DE JONGH & D. DE KLERK. 1975. PHYSICA **79B:** 52.
28. DUPAS, A., K. LE DANG, J. P. RENARD, P. VEILLET, A. DAOUD & R. PERRET. 1976. J. Chem. Phys. **65:** 4099.

DISCUSSION

ZOLTAN SOOS: In your suggestion that we should take these anisotropic exchange parameters as proportional to $(\Delta g)^2$, do you feel that there must be many cases where this does not work and where the exchange parameters are much larger?

WILLETT: I will not guarantee that it will work in every case, but in the two-dimensional copper salts you have a small xy anisotrophy and can use this argument. Also, you can use this argument to predict the sign of the zero field splitting in copper dimers and the right prediction is obtained. So it works in a variety of cases.

SOOS: That formulation is a very useful one and I think people have been using it quite generally, but I think the justification of it is only for rather restricted cases involving $S = \frac{1}{2}$ and other nice spin-orbit coupling systems.

REVIEW OF THE PHYSICS OF LOW-DIMENSIONAL SYSTEMS*

Paul M. Chaikin

Department of Physics
University of California
Los Angeles, California 90024

INTRODUCTION

Over the past decade there has been considerable interest in the physics and chemistry of materials that exhibit highly anisotropic properties.[1] The crystals themselves are, of course, three-dimensional, but in some cases the atomic or molecular arrangement is such that the electrons are constrained to move preferentially in only one or two directions, and it is in this sense that the systems may be described as having reduced dimensionality. As we shall see in the following pages, this reduced dimensionality has some unusual consequences which are responsible for the present excitement in this field.

One-dimensional metals are, for example, intrinsically unstable against the formation at low temperatures of a variety of distorted states. They may become magnetic or nonmagnetic insulators, or possibly even superconductors. The instabilities arise from the response of the system to weak perturbations. As the temperature is lowered, we will find that the response "blows up." On the other hand, we shall see that truly one-dimensional systems cannot undergo phase transitions at any temperature above absolute zero. It is this apparent contradiction, that the system is unstable against a distortion but cannot distort, that makes these studies fascinating. The resolution of the problem finally lies in the actual three-dimensional nature of the crystals.

In addition, one-dimensional systems are interesting because some calculations that can be done only approximately in three dimensions can be done exactly in one dimension. Probably most important, there is a general feeling that it is potentially easier to use the apparatus of organic chemistry to synthesize properties that we want in one-dimensional compounds than in three-dimensional compounds.

INSTABILITIES

When we talk about a system being unstable we mean that a small perturbation will evoke a large response. If we consider a system that contains many electrons in equilibrium and we then slightly change the potential they experience, the result will be a change in the electron wave functions and hence a change in the electron density. We will characterize the density change by a response function X_q^2 which gives the proportionality between the amplitude of a periodic poten-

*Research supported by the National Science Foundation under grant DMR 76-83421 and ONR under grant N00014-76-C-1078. Manuscript received June 13, 1977.

0077-8923/78/0313-0128 $1.75/1 © 1978, NYAS

tial $V(r)$ and the amplitude of the density change

$$\delta\rho(r) = X_q V(r). \tag{1}$$

X_q is called a linear response function, and it depends on how rapidly the potential is varying in space through the wave vector q (which is just $2\pi/\lambda$, λ being the wavelength or period). In FIGURE 1 we have illustrated the effect of an attractive interaction of the form $V(r) = V_0 \cos \mathbf{q}\cdot\mathbf{r}$. In the absence of this potential, the initial electron density is uniform. The potential is applied and the electrons move to regions where the attraction is large and away from regions where it is small or repulsive. The difference between the initial and final electron density is the response to the potential and has the same spatial dependence as the applied potential.

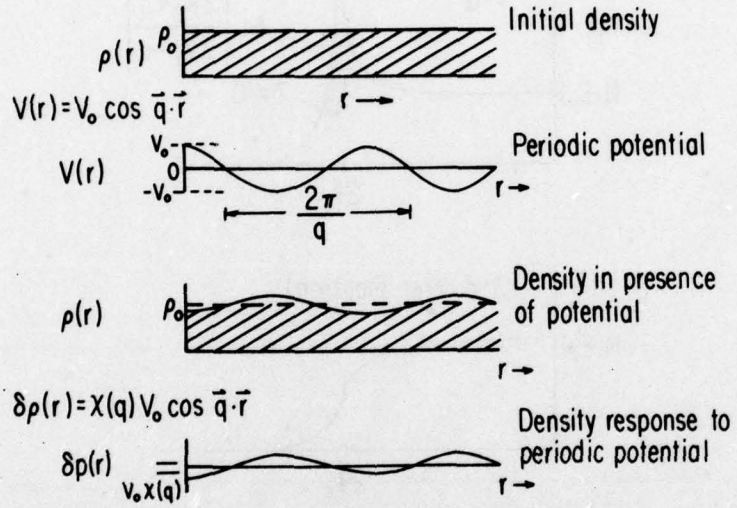


FIGURE 1. Density response of a uniformly dense electron gas in the presence of a periodic potential of wave vector q and amplitude V_0.

To place these abstract ideas on more realistic grounds, we note that the energy of an electron with spin up in a magnetic field H is $-\mu_0 H$, whereas that of an electron with spin down is $+\mu_0 H$, where μ_0 is the magnetic moment of the electron. The total magnetic moment of a collection of electrons is the number with up spins times μ_0 plus the number of down spins times $-\mu_0$ or

$$M = \mu_0(\rho\uparrow - \rho\downarrow). \tag{2}$$

Without a magnetic field, the number up and down are equal so that $M = 0$. If we put on a magnetic field that varies with position we have

$$\delta\rho\downarrow = X_q(-\mu_0 H) \quad \text{and} \quad \delta\rho\uparrow = X_q(\mu_0 H)$$

$$M = \mu_0(\delta\rho\uparrow - \delta\rho\downarrow) = 2\mu_0^2 X_q H. \tag{3}$$

The ratio of M to H is the magnetic susceptibility, and we find it equal to

$2\mu_0{}^2X_q$. If X_q diverges (goes to infinity) for some value of q, then we have some problem in understanding Equation 3. It does *not* mean that a small magnetic field will give us an infinite total magnetic moment. Rather, it implies that with no magnetic field we have a finite total moment. For instance, if $X_q \to \infty$ for $q \to 0$ (which corresponds to very long wavelength or a uniform magnetic field), then we have a uniform magnetic moment with no applied field, and this is the familiar case of a ferromagnet. If $X_q \to \infty$ for some other q, then the magnetic moment varies with position and we have an antiferromagnet.

If we look, instead, at an electric field, the energy of an electron is just its charge e times the potential ϕ. The total charge distribution Q in a metal is e times the electron density ρ plus the positive charge of the ions in the background. With no electric field $Q = 0$.

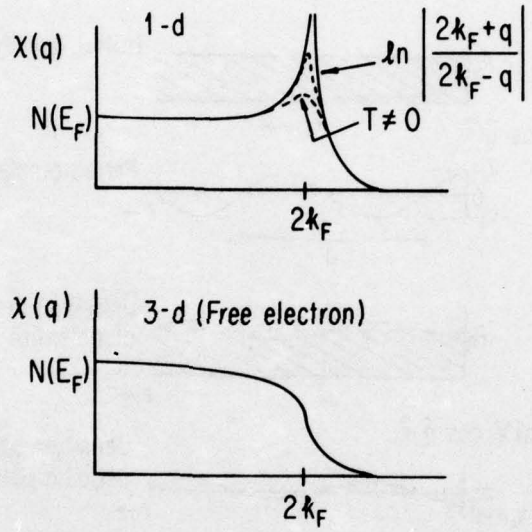


FIGURE 2. The response function or Lindhard function for a one-dimensional and three-dimensional electron gas. The solid lines are for zero temperature; the dashed lines represent nonzero temperature.

Putting on a spatially varying electric field we have

$$\delta Q = e\delta\rho = eX_q e\phi = e^2X_q\phi. \tag{4}$$

If for some value of q, $X_q \to \infty$ the system is unstable against the formation of a periodic charge density. To make further connection with electromagnetic theory, we note that a charge density itself produces a potential according to Maxwell's Equations, so that

$$\nabla^2(\phi_1) = -4\pi e\delta\rho \tag{5}$$

and using this expression we can relate the dielectric constant $\epsilon(q)$ to our response function

$$\epsilon(q) = 1 + \frac{4\pi e^2}{q^2} X_q. \tag{6}$$

Naturally, the reason we are going through all of this is that X_q does diverge for the one-dimensional systems in which we are interested. The actual form of X_q for electrons in a metal is known as the Lindhard function and is given by:[3]

$$X_q = \sum_k \frac{f(k) - f(k+q)}{\epsilon_{k+q} - \epsilon_k}. \tag{7}$$

Here we are summing over the different values of wave vectors k (or momentum $\hbar k$) for the electron. $f(k)$ is the Fermi-Dirac distribution function (and contains the interesting temperature dependence), and ϵ_k is the energy of the electron with momentum $\hbar k$.

The Lindhard function is sketched as a function of q for one- and three-dimensional cases in FIGURE 2. For one dimension there is a peak at a value of q equal to twice the Fermi wave vector. This peak increases as temperature is lowered, diverging logarithmically as $T \to 0$. For three dimensions there is no such peak. Understanding the origin of this peak is then essential to our study.

In order to proceed, we must remember a few simple results of quantum mechanics and what we have learned about electrons in metals. In the simplest case we can view the electrons in a metal as being "free," so that their only energy is kinetic. The wave functions are then

$$\phi_k = e^{i\mathbf{k}\cdot\mathbf{r}} \tag{8}$$

and the energies are

$$\epsilon_k = \frac{p^2}{2m} = \frac{\hbar^2 k^2}{2m}. \tag{9}$$

We now apply a periodic potential of the form $V(r) = V_0 \cos \mathbf{q}\cdot\mathbf{r}$. This perturbation will couple electrons whose wave vectors differ by $\mathbf{q}$. The wave functions for the electrons ψ_k will then be a combination of the original plane waves ϕ_k plus a little bit of the plane wave which is mixed in by the perturbation[4]

$$\psi_k \approx \phi_k + \frac{\langle \phi_{k+q} | V(r) | \phi_k \rangle \phi_{k+q}}{\epsilon_{k+q} - \epsilon_k}. \tag{10}$$

This is very similar to what happens when musical notes are mixed. We obtain additional tones at the sum and difference of the original tones. In our case only one of the additional frequencies is important. The amount of the mixing depends on how strongly the two wave functions are coupled, divided by the original energy difference between the wave functions. This is known as Perturbation Theory in physics and as "configuration interaction" in chemistry. The density change this brings about is just the density with the perturbation minus the original density

$$\rho = |\psi^2| - |\phi|^2 \approx \frac{V_0}{\epsilon_{k+q} - \epsilon_k} \cos \mathbf{q}\cdot\mathbf{r}. \tag{11}$$

As expected, we find that the density change is proportional to the applied periodic potential. If we want to know how the energies of the electron change, the general result is that the energies are pushed apart by the interaction that couples them. The additional splitting is equal to the coupling squared divided again by the energy difference.

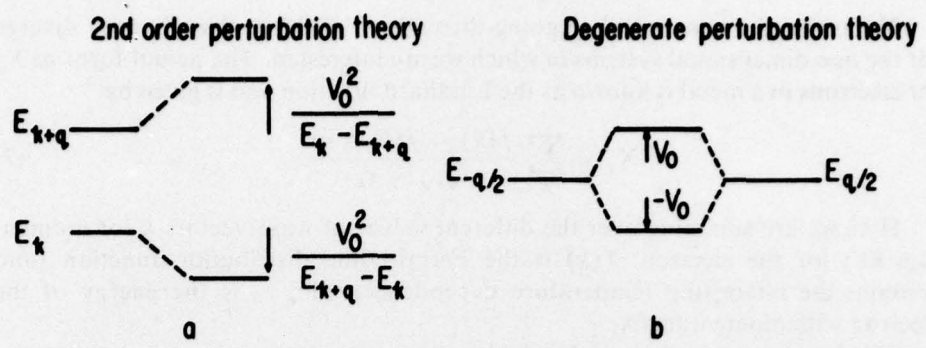


FIGURE 3. The results of quantum mechanical perturbation theory. a: In second-order perturbation theory, energy levels that are coupled by the perturbation repel. b: If states with the same energy are coupled, they are split by the coupling energy.

$$\delta\epsilon_k \approx \frac{V_0^2}{\epsilon_k - \epsilon_{k+q}}$$

$$\delta\epsilon_{k+q} \approx \frac{V_0^2}{\epsilon_{k+q} - \epsilon_k} = -\delta\epsilon_k. \tag{12}$$

This is illustrated in FIGURE 3a. Now if the states that are coupled have the same energy, the energy denominator goes to zero and the expressions in (10)–(13) diverge. This seems to give us the result we are looking for, but unfortunately it is not correct. Equations 10–13 are valid only if the denominator is much larger than the numerator. In fact, the largest the ratio $V_0/(\epsilon_{k+q} - \epsilon_k)$ can legitimately get is unity. This, in fact, is the result of the degenerate perturbation theory we must use. When we couple states with the same energy, they are split by the coupling as illustrated in FIGURE 3b. This, of course, is the origin of the "bonding and antibonding orbitals" which occur throughout organic chemistry.[4]

The electrons that have the same energy and are coupled by $V(r)$ are those with $k = -q/2$ and $k + q = q/2$. The wave function for the lower energy state is then

$$\psi_k = \frac{e^{i\mathbf{q}\cdot\mathbf{r}/2} + e^{-i\mathbf{q}\cdot\mathbf{r}/2}}{\sqrt{2}} = \sqrt{2}\cos\frac{\mathbf{q}\cdot\mathbf{r}}{2}$$

$$\delta\rho = \cos\mathbf{q}\cdot\mathbf{r}. \tag{13}$$

Note that the density change has the same spatial dependence as $V(r)$, but there is not any dependence on how big the perturbation is (i.e., V_0 does not appear in (13)). Thus, for an infinitesimal perturbation we get a finite response. As advertised, this is the true meaning of a divergent response function. If the states $q/2$ and $-q/2$ were both filled (with two electrons each), we would have no effect, because both bonding and antibonding orbits would be filled after the perturbation is applied. Similarly, if both are empty we have no effect. The cases of interest are states that are partially but not completely filled with electrons. Let us see how the states are occupied in a metal.

In FIGURE 4a we see the situation for a three-dimensional metal at low tem-

peratures. The states with low kinetic energy are filled until we have accounted for all of the electrons in the metal. The momentum of the last electron added is called the Fermi momentum k_F, and its energy, the Fermi energy ϵ_F. States with $|k| < k_F$ are filled, and those above are empty.[5] For a particular value of q there are just two states that are connected by q which have the same energy and are partially filled (i.e., lie on the surface of constant ϵ_f, called the Fermi surface). Slightly different values of q will couple other states and give a density change with a different periodicity. Adding random periodicities results in no net contribution to the charge density.

By constrast, we look at the situation for a one-dimensional metal (FIGURE 4b). In one dimension the energy is determined solely by the momentum in one direction; call it $p_x = \hbar k_x$. All k states are occupied up to $|k_x| = k_f$. For any particular value of q, the states connected do not lie on the Fermi surface. However, for $q = 2k_F$ there are many states that are connected by q and lie on the Fermi surface, which in this case is just two parallel planes at $k_x = -k_F$ and $k_x = k_F$. The difference between one and three dimensions merely lies in the shape of the Fermi surface.

From these illustrations it is clear that the divergence we are looking for comes from having a plane of degeneracy, i.e., a vector $\mathbf{q}$, which will bring part of the Fermi surface into coincidence with another part. If one part of the Fermi surface fits into another part in this way, we say the Fermi surface "nests." We will *always* have Fermi surface "nesting" in one dimension, since the Fermi surface is a set of parallel planes. Sometimes we can have a similar occurrence in two or three dimensions. As we have seen, the free electron approximation is not always applicable. For example, if we have a three-dimensional metal described by tight binding bands the electron energies are given by:

$$\epsilon_k = 2\tau_x \cos k_x a + 2\tau_y \cos k_y b + 2\tau_z \cos k_z c \qquad (14)$$

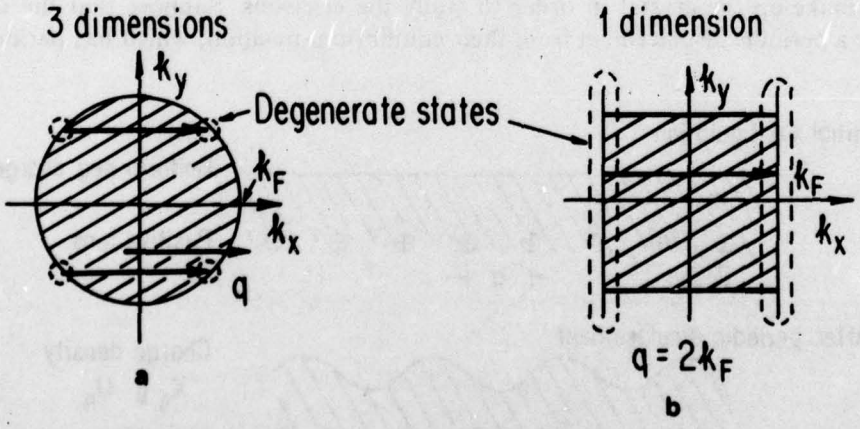


FIGURE 4. The Fermi surfaces of a free electron gas. a: For three dimensions all states with $|\mathbf{k}| < k_F$ are occupied. For a given perturbation of wave vector q only two equal energy states on the Fermi surface are coupled. b: For one dimension all states with $|k_x| < k_F$ are occupied. A perturbation of wave vector $q = 2k_F$ couples a set of planes of degenerate states on the Fermi surface.

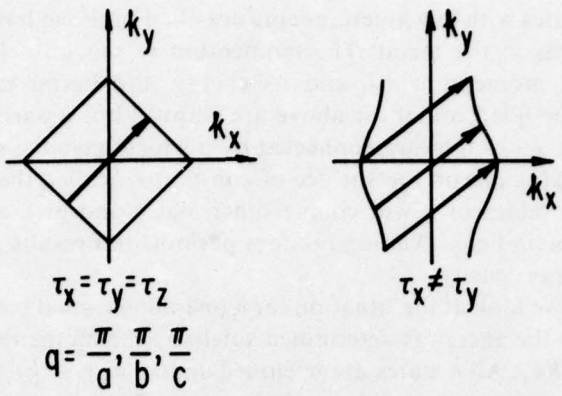


FIGURE 5. For a three-dimensional Fermi surface regions may "nest." For tight binding bands with one electron per unit cell the wavevector $q = (\pi/a_1, \pi/b_1, \pi/c)$ always brings one part of the Fermi surface into juxtaposition with another part.

where the τ's are overlap integrals in each direction and a, b, and c are the unit cell parameters. The Fermi surfaces are shown in FIGURE 5 for a situation with one electron per unit cell. In this circumstance a wave vector $q = (\pi/a, \pi/b, \pi/c)$ will bring one part of the Fermi surface into coincidence with another part, and the response function will diverge for this value of q[6,6a] We will see how these considerations affect the properties of transition metal sulfides, in the following paper.

KOHN ANOMALY

We would now like to investigate the kind of instabilities that result from the divergence of the response function. Up to this point we have neglected the ions that make up the crystal in order to study the electrons. Suppose that the ions have a periodic displacement from their equilibrium position, which has periodic-

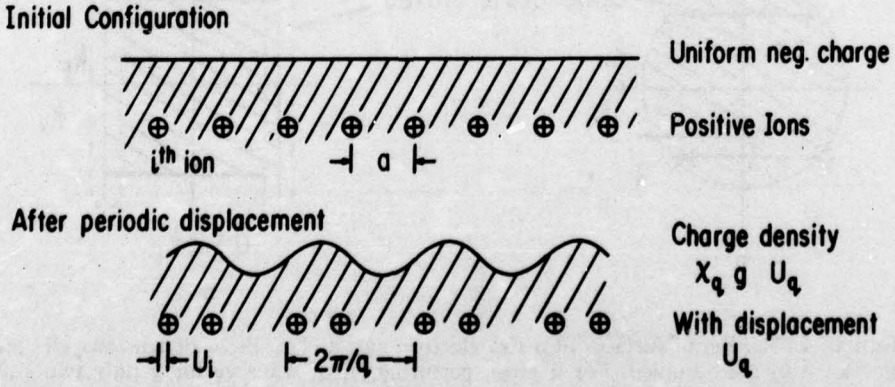


FIGURE 6. If the ions in a crystal are periodically displaced, the electrons respond by setting up a charge density wave.

ity q and amplitude U_q. This is illustrated in FIGURE 6.

$$U_i = U_q \cos \mathbf{q} \cdot \mathbf{r}_i. \tag{15}$$

Here U_i is the displacement of the ion at position r_i from its equilibrium position. Since the ions are charged, the displacement creates a periodic electrostatic potential on the electrons, which we write as:

$$V(r) = gU_q \cos \mathbf{q} \cdot \mathbf{r}. \tag{16}$$

g is a constant that relates the ion displacement to the electron potential and depends on the charge distribution on the ion.

The electrons will respond to this potential according to the X_q we have just developed

$$\delta\rho = X_q V(\mathbf{r}) = X_q g U_q \cos \mathbf{q} \cdot \mathbf{r}. \tag{17}$$

The electron charge density builds up in the region of positive charge created by the ions. The negative electrons in turn produce a force on the ions which tends

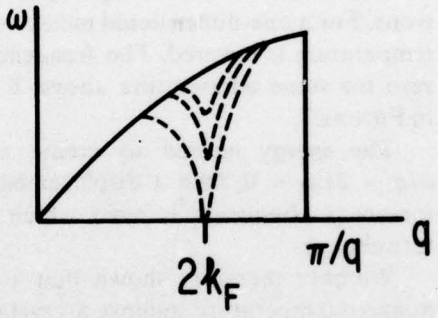


FIGURE 7. The solid line represents the natural frequencies of the lattice vibrations of a crystal. The dashed lines represent the lowering of the frequency of the lattice vibration at $q = 2k_F$ caused by the response of the electrons, known as the Kohn anomaly. As temperature is lowered the frequency is lowered.

to displace them further. The force in the direction of the original displacement uses the same proportionality constant g as for the force of the ions on the electrons.

$$F = g\delta\rho. \tag{18}$$

The magnitude of the force is then:

$$F = g^2 X_q U_q. \tag{19}$$

The periodic displacement of the ions is opposed by the elastic forces that hold the ions in place. The equation of motion for the displacements is usually written as

$$M \frac{d^2 U_q}{d\tau^2} = -K_q U_q \tag{20}$$

where M is the ion mass and K_q is the restoring force. This is just a complicated way of writing $ma = F$ for a simple harmonic oscillator. If we assume that the displacements will vary sinusoidally with time, the frequency of oscillation

$\omega_0(q)$ is given by

$$-M\omega_0^2(q)\,U_q = -K_q U_q$$

$$\omega_0(q) = \sqrt{K_q}/M. \tag{21}$$

This equation gives the frequency as a function of wave vector for the lattice vibrations of a solid.[7] It is shown schematically as the solid line in FIGURE 7. The dependence on q comes from the fact that if the crystal as a whole is displaced there is no restoring force ($q = 0$), while if nearest neighbors ions ($q = \pi/a$) are moved in opposite directions, the restoring force is a maximum.

We now add in the force due to the electronic response.

$$-M\omega^2(q)U_q = (-K(q) + g^2 X_q)U_q$$

$$\omega^2(q) = \frac{K(q)}{M} - g^2\frac{X_q}{M}$$

$$\omega^2(q) = \omega_0^2(q) - g^2\frac{X_q}{M}. \tag{22}$$

The lattice vibration frequencies are lowered by the interaction with the electrons. For a one-dimensional metal we have seen that X_q for $q = 2k_F$ diverges as temperature is lowered. The frequency of this mode then decreases and goes to zero for some temperature above $T = 0$. This is illustrated by the dotted lines in FIGURE 7.

The energy needed to create a periodic lattice displacement is $\hbar\omega$. If $\omega(q = 2k_F) = 0$, then a displacement at this period costs no energy and lasts forever (its frequency is zero), which implies a lattice distortion or crystal structure change.

We have therefore shown that a one-dimensional metal is unstable at some nonzero temperature against a crystal structure change with new periodicity of $q = 2k_F$.

Experimentally, this "softening" of the lattice vibration frequency at $2k_F$ has

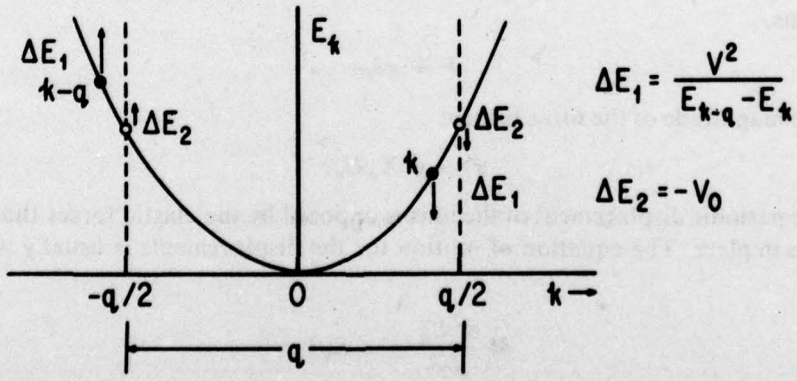


FIGURE 8. The solid line is the energy vs. wave vector (or momentum) of electrons in a metal. The arrows indicate the energy shifts when a periodic potential of wave vector q is applied.

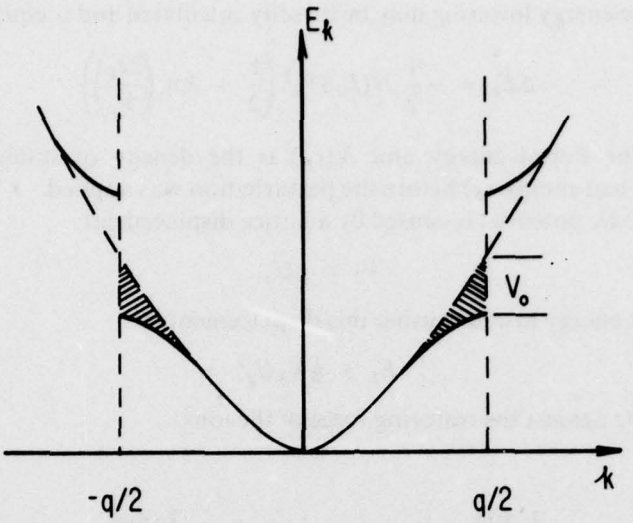


FIGURE 9. The solid lines are the energy vs. wavevector of electrons in a metal after a potential of the form $V_0 \cos \mathbf{q} \cdot \mathbf{r}$ has been applied. Note the energy gap at $k = q/2$. The shaded area is the lowering of the energy experienced by the electrons with $|k| < q/2$.

been seen in several systems, which you will read about in this volume. The effect was first predicted by Kohn and is known as a Kohn anomaly.[8]

Unfortunately, our treatment so far does not tell us what happens after the distortion occurs. To see that, we return to look at the electrons, using a description first presented by Peierls.[9]

PEIERL'S TRANSITION

In FIGURE 8 we have sketched the energy versus wave-vector relationship for electrons in a metal. In the presence of a periodic potential $V_0 \cos \mathbf{q} \cdot \mathbf{r}$, the states k and $k \pm q$ are mixed. As we have seen in FIGURE 3, the energy levels repel one another and the shifts are given by (12). Of course, the shift can never exceed the result that we found in the degenerate limit. If we look at a level with momentum k as shown in FIGURE 8, it mixes with $k-q$. The energy corresponding to k is lowered below its unperturbed value, while the energy of $k-q$ is increased. As k increases toward $q/2$ the energy is lowered even more as the energy difference between k and $k-q$ is getting smaller. The maximum energy lowering occurs when $k = q/2$ and the shift is V_0. Correspondingly, $k-q$ is shifted up by V_0.

The energy vs. k after the potential has been added is shown in FIGURE 9. There is now a region in which no allowed energies are to be found, i.e., an energy gap. Note that all states with $|k| < q/2$ have lower energy than previously. If $k_F = q/2$, then the states filled with electrons have lower energy, whereas the states that have higher energy are empty and thus do not contribute anything. The amount of electronic energy gained is represented by the shaded area in FIGURE 9.

This electronic energy lowering may be directly calculated and is equal to

$$\Delta E_e = -\frac{1}{2} N(E_F) V_0^2 \left(\frac{1}{2} + \ln\left(\frac{2\epsilon_F}{V_0}\right)\right) \tag{23}$$

where ϵ_F is the Fermi energy and $N(\epsilon_F)$ is the density of states (number of electrons that had energy ϵ_F) before the perturbation was applied.

If the periodic potential is caused by a lattice displacement

$$V_0 = gU_q. \tag{24}$$

The elastic energy lost in causing this displacement is

$$E_L = \tfrac{1}{2} K_q U_g^2 \tag{25}$$

as work is done against the restoring force of the ions.

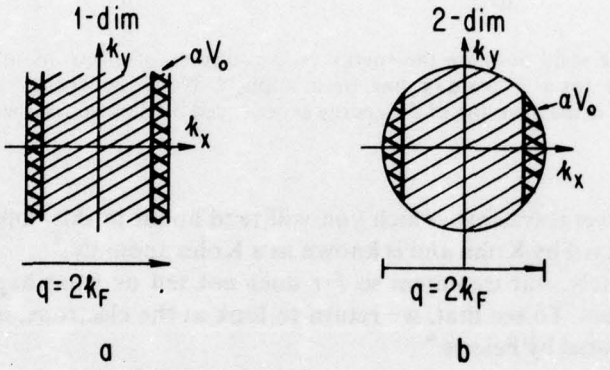


FIGURE 10. The electrons effected by the periodic potential $V_0 \cos \mathbf{q} \cdot \mathbf{r}$ are represented by the shaded area in a and b. The fraction of electrons effected is larger in one dimension (a), than in two dimensions (b).

The total energy change in distorting the lattice and opening the energy gap is:

$$E = E_L + E_e = \frac{1}{2} K_q U_q^2 - \frac{1}{2} N(\epsilon_F) g^2 U_q^2 \left(\frac{1}{2} + \ln\left(\frac{2\epsilon_F}{gU_q}\right)\right). \tag{26}$$

For small distortions the logarithmic term dominates as when $U_q \to 0$ $\ln(2\epsilon_F/gU_q) \to \infty$. The total system always has lower energy with a small distortion. The total energy is at a minimum when

$$gU_q = V_0 = 2\epsilon_F \exp\left[\frac{-K_q}{g^2 N(\epsilon_F)}\right]. \tag{27}$$

So we have calculated the amplitude of the displacements and the size of the energy gap.

We might expect this energy lowering and distortion from any metal. Why is it a one-dimensional effect? The only electrons affected by the distortion are those

connected by the wave vector q and within an energy range V_0 of the Fermi energy. (This last statement is clear when we look at the energies in FIGURE 9). For one dimension the electrons affected lie in the shaded area in FIGURE 10a. This fraction of electrons is V_0/ϵ_F. Each electron in this region has its energy lowered. Those which were at ϵ_F are lowered by V_0, those which were at $\epsilon_F - V_0$ are lowered only slightly. The average energy lowering is then $V_0/2$. For one-dimension the total lowering is the number of electrons affected times their average energy gain or:

$$\text{1 dim} \qquad \Delta E_e \approx \frac{V_0^2}{2\epsilon_F}. \tag{28}$$

In two dimensions the fraction of electrons affected by the opening of the gap is just the shaded slice in FIGURE 10b. The fraction of electrons affected is then approximately (V_0^2/ϵ_F) and the average energy gain is $V_0/2$. For two dimensions the total lowering is then

$$\text{2 dim} \qquad \Delta E_e \approx \frac{V_0^3}{2\epsilon_F^2}. \tag{29}$$

If we performed the calculation more correctly we would have a logarithmic factor, as in (16). The elastic energy is the same for one or two dimensions. The total energy change upon undergoing a distortion is then

$$\begin{aligned} \text{1 dim} \qquad & \Delta E = AV_0^2 - BV_0^2 \ln\left(\frac{E_f}{V_0}\right) \\ \text{2 dim} \qquad & \Delta E = AV_0^2 - BV_0^3 \ln\left(\frac{E_f}{V_0}\right). \end{aligned} \tag{30}$$

For small values of V_0 the second term in the two-dimensional case is smaller than the first, since $V_0 \ln (E_f/V_0)$ goes to zero as V_0 goes to zero.

We must remember, however, that if the Fermi surface "nests" in two or three dimensions, the situation looks very much like the one-dimensional cases. In fact, when Peierls did his original calculation of this effect it was largely to explain why all metals were not in close packed structure. The point is that a distortion is *always* favorable in one dimension and is sometimes favorable in two or three dimensions.

It is also noteworthy that the development of a gap at the Fermi surface of a one-dimensional metal will impede its conductivity (with some exceptions), and we therefore expect a metal insulator transition.

PHASE TRANSITIONS

We have found that a metallic one-dimensional chain that would have a uniform charge density at high temperatures (FIGURE 11a) is unstable against the formation of a distorted lattice and associated charge-density wave at low temperature (FIGURE 11b). This process may be regarded in simple chemical terms. When the ions distort from a uniform arrangement the charge density accumulates

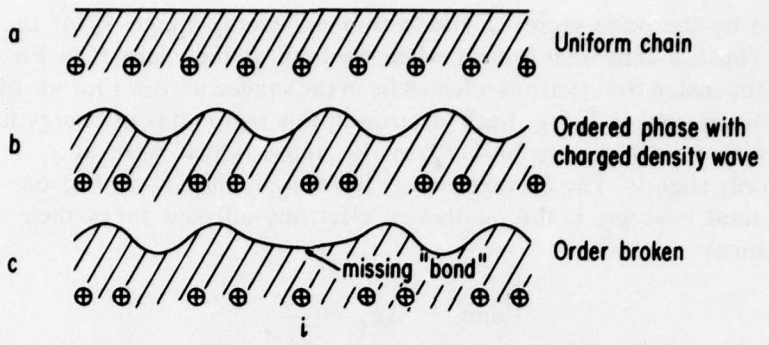


FIGURE 11. In a we illustrate the undistorted lattice with a uniform charge density. In b a lattice distortion and charge density wave are illustrated in a fully ordered phase, corresponding to the lowest energy configuration. In c the order has been broken by skipping a bond at site *i*. The next ion has moved away from *i* and formed a separate bond instead of bonding with the ion at *i*.

in the region where the ions are closest together, essentially creating a chemical bond. The energy of the bond is the energy gap that has been opened, V_0.

Starting from low temperatures we would expect the bonds to be stable. As temperature is increased, more of the bonds are broken or more electrons are excited across the energy gap. This lowers the energy of the distorted state relative to the uniform state. We would then expect the distortion to decrease until, at a temperature where the thermal energy is about equal to V_0, we would return to the undistorted state. If the excitations or broken bonds are treated on the average (in "Mean Field Theory") we find the mean-field transition temperature is related to V_0 by[10]

$$kT_{MF} = \frac{V_0}{1.76}. \tag{31}$$

At this temperature we expect a distortion and gap to form and increase to a maximum value as temperature is lowered toward $T = 0$. This temperature dependence is sketched as the outer line in FIGURE 12. We would assume that for $T < T_{MF}$ the system is completely ordered and the distortion just increases in amplitude. This is not the case.

Let us see what happens if we skip a lattice site when the distortion occurs. In FIGURE 11b we saw the fully ordered phase. In FIGURE 11c we see the order broken by a missed bond. What has happened in this picture is that the ions have paired together up to site *i*. At this site the next atom moved in the opposite direction, rather than toward *i*. After this mistake the ions are again paired. We have two fully ordered regions that meet at point *i*. But the two regions are not ordered with respect to one another.

The energy difference between the phase with complete order and broken order is simply the energy lost by the two electrons in the missing bond $2V_0$. The break can be at any of N places along the chain to give us broken order, where N is the number of sites along the chain. Since there are N ways the break can occur, the associated entropy is $k_B \ell n\ N$. For finite temperatures we should really be using

the Helmholtz free energy, which is internal energy minus the temperature times the entropy. The free energy difference between the ordered and broken phases is:[11]

$$\Delta F = 2V_0 - k_B T \ln N. \tag{32}$$

For a large system ($N \to \infty$) the broken state is always favorable for any temperature above absolute zero. This merely reflects the large number of possible sites for a break.

The result we have found indicates that for temperatures above zero we will have ordered regions separated by breaks. As temperature is raised from zero, there will be more breaks and the average size of the ordered regions will decrease. If a chain has a small number of sites N it may still remain ordered, according to (32) up to a certain temperature. The average number of sites that will remain ordered at a temperature T is then obtained by setting $\Delta F = 0$[12]

$$N_{av.} = \exp\left(\frac{2V_0}{k_B T}\right). \tag{33}$$

Since the average distance between sites is the interatomic spacing a, the length of this chain segment will be $(N_{av.})a$. The average size of the ordered regions is known as the correlation length and is written:

$$\xi(T) = a \exp\left(\frac{2V_0}{k_B T}\right). \tag{34}$$

We again must ask why the situation is different for one dimension than for two or three. In FIGURE 13a we have drawn several chains and assumed that they interact with a two-dimensional electrostatic coupling. The charge density on each chain has large negative charge on a bond and less negative charge between bonds. Each bond would therefore like to see an antibond at the appropriate position on each chain surrounding it. This will occur if nearest neighbor chains have their charge-density waves slipped by one bond, as in the illustration. We can represent

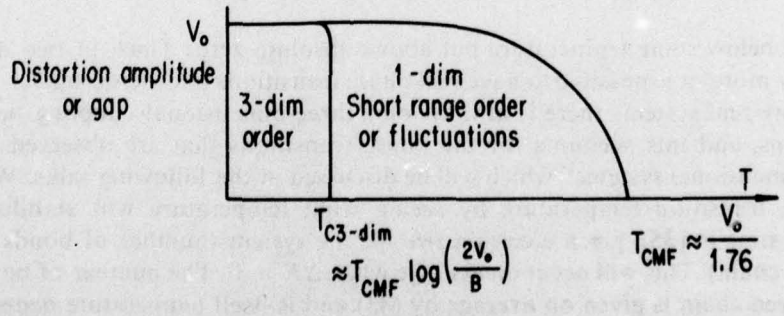


FIGURE 12. The amplitude of the distortion or energy gap is shown as a function of temperature. The outer curve is the result of "mean field theory." The actual phase transition to an ordered phase, however, occurs at T_c "three-dimensions", where the interaction energy between chains is larger than the thermal energy.

the interchain interactions by a (negative) term B, which is added if a bond is adjacent to antibond and subtracted if two bonds or two antibonds are adjacent.

In FIGURE 13b we have shown the situation with a broken bond in one of the chains. In this case we not only lose the bond energy $2V_0$ as in one dimension, but we have a repulsive interaction between the chains out to the end of the crystal (which is about $N/2$ sites away if the break is toward the center of the crystal). Thus we lose an addition $2BN/2$ in energy. The difference in free energy between the ordered and broken states in FIGURE 13 is then

$$\Delta F = 2V_0 + \frac{2BN}{2} - k_B T \ln (N). \tag{35}$$

For a large system ($N \to \infty$) the second term dominates and the ordered phase

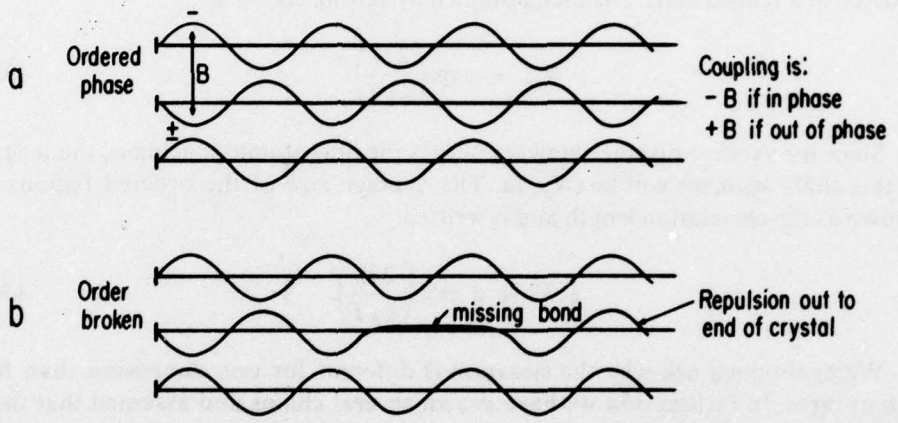


FIGURE 13. When interactions between chains are important the charge density waves arrange themselves so that positive and negative regions are adjacent in nearest neighbor chains. a: We represent this Coulomb interaction energy by $-B$ when a bond is adjacent to an antibond and $+B$ when bond is adjacent to bond or antibond to antibond. b: If one chain has a broken order, with a bond missing, the rest of the chain (to the right of the break) experiences repulsive interactions for the remainder of its length.

is stable below some temperature but above absolute zero. Thus, in two dimensions (or more) it is possible to have real phase transitions to ordered states.

In any real systems there is always some three-dimensional coupling between the chains, and this accounts for the phase transitions that are observed in the "one-dimensional systems" which will be discussed in the following talks. We can find the transition temperature by seeing what temperature will stabilize the ordered state in (35), given a certain size for the system (number of bonds in an ordered chain). This will occur on average when $\Delta F = 0$. The number of bonds in an ordered chain is given on average by (33) and is itself temperature dependent. We find:

$$0 = BN(T_c) - k_B T_c \ln (N(t_c)) \tag{36}$$

or

$$k_B T_c = \frac{2V_0}{\ell n \frac{2V_0}{(B)}}.$$

This expression uses the model depicted in FIGURE 13, where each chain has two nearest neighbors. If there are z nearest neighbor chains, B should be replaced by $ZB/2$. What is physically happening is the correlation length on each chain is increasing as temperature is lowered until the average number of bonds in each ordered region times the interaction energy per bond with neighboring chains is larger than the thermal energy.[13] For temperatures below this, the chains are locked together too strongly to be broken by thermal fluctuations.

It is interesting to note that the three-dimensional ordering temperature T_c is usually below the one-dimensional mean field transition T_{MF} (by a factor of about $\ell n\ (2V_0/B)$). We expect the transitons to have the general behavior shown in FIGURE 12. As temperature is lowered through T_{MF} we form some bonds, the crystal distorts, and charge-density waves appear in isolated regions. The amplitude of the displacements and charge-density waves increases as we get cooler, but the prevalent effect is the growth of the size of the ordered regions or correlation length. Finally, the chains order three dimensionally at T_c, at which temperature the gap, charge density, and distortions are essentially fully developed.

CONCLUSION

We have seen that one-dimensional metals are quite generally unstable against the formation of an insulating distorted state at low temperatures, and that the problem associated with one-dimensional phase transitions is overcome by the three-dimensional nature of most physically realizable crystals.

How these ideas apply to the crystals under discussion at the conference on which this volume is based depends strongly on the values of the different parameters and may vary widely. If coupling between chains is large, the region between T_{MF} and T_c may be too small to be physically significant. If the electron-lattice coupling is small, then T_{MF} may be reduced to a low enough temperature that other interactions predominate. Nontheless, there is ample experimental evidence that these effects have been seen in several compounds[14,15] and we will doubtlessly find even more fascinating properties as new compounds continue to be synthesized. There are, in addition, many other related instabilities that are possible in one-dimensional metals, including a Mott-Hubbard or magnetic insulator transition[16] and superconductivity.[17]

ACKNOWLEDGMENTS

I should like to acknowledge several informative conversations with Professors P. Pincus, T. Holstein, and R. Orbach, and with Dr. R. L. Greene.

Notes and References

1. For several review papers in this field see: KELLER, H. J., ED. 1974. Low Dimensional Cooperative Phenomena. Plenum Press. New York, N.Y.
2. NOZIÈRES, P. 1964. Theory of Interacting Fermi Systems. Chap. 2. W.A. Benjamin, Inc. New York, N.Y.
3. For a relatively simple derivation, see ZIMAN, J. M. 1972. Theory of Solids, 2nd edit. Chap. 5. Cambridge Univ. Press. London, England.
4. PAULING, L. 1960. The Nature of the Chemical Bond. Appendix V. Cornell Univ. Press. Ithaca, N.Y.
5. Kittel, C. 1976. Introduction to Solid State Physics. 5th edit. Chap. 6. John Wiley & Sons. New York, N.Y.
6. CHAIKIN, P. M., P. PINCUS & G. BENI. 1975. J. Phys. **C8, L65.**

6a. HOROVITZ, B., H. GUTFREUND & M. WEGER. 1975. Phys. Rev. **B12:** 3174.

7. See Reference 5, Chap. 4.
8. KOHN, W. 1959. Phys. Rev. Lett. **2:** 393.
9. PEIERLS, R. E. 1955. Quantum Theory of Solids: Clarendon Press. Oxford, England.
10. See for example: BERLINSKY, A. J. 1976. Contemp. Phys. **17:** 331, which also contains a nice description of instabilities and phase transitions. Equation 31 uses the analogy with the BCS treatment of superconductivity; BARDEEN, J., L. N. COOPER & J. R. SCHRIEFFER. 1957. Phys. Rev. **108:** 1175.
11. LANDAU, L. D. & E. M. LIFSHITZ. 1969. Statistical Physics: 479. Addison-Wesley. Reading, Mass.
12. PINCUS, P. 1974. *In* Low Dimensional Cooperative Phenomena. H. J. Keller, Ed. Plenum Press. New York, N.Y.
13. SCALAPINO, D. J., Y. IMRY & P. PINCUS. 1975. Phys. Rev. Bull: 2042.
14. HEEGER, A. J. 1977. *In* Proc. NATO Advanced Study Inst. Chemistry and Physics on One-Dimensional Metals. Bolzano, Italy, Aug. 1976. H. J. Keller, Ed. Plenum Press. New York, N.Y.
15. ZELLER, H. R. 1973. Adv. Solid State Phys. **13:** 31.
16. HUBBARD, J. 1963. Proc. Roy. Soc. (London) **A276:** 238; 1973. **A277:** 237. 1963. **A281:** 401.
17. LITTLE, W. A. 1964. Phys. Rev. **A134:** 1416.

Discussion

RICHARD A. KLEMM (*Iowa State Univ., Ames, Iowa*): Due to the appearance of the $4k_F$ scattering in the x-ray experiments on (TTF)(TCNQ) by Pouget and coworkers, a proper treatment of the interacting electron gas must take into account the possibility of strong or intermediate strength coupling. In addition to explaining such phenomena as the $2k_F$ charge-density wave and $4k_F$ scattering, we would like to be able to determine if any new type of phenomena might be observable in some system. Thus, I have studied a model of two chains with an "inverted" band structure (an electron-like chain and a hole-like chain) appropriate for the charge-transfer salts and have considered the effect of forward (g_2) and backward (g_1) scattering between electrons on each chain, and forward (w_2) and backward (w_1) scattering between electrons on different chains. With this model, the crossover in temperature from $4k_F$ scattering at high temperatures to $2k_F$ phase transition in (TTF)(TCNQ) can be understood. In addition, there are several new types of ground-state behavior for various possible interaction strengths. Of these, the formation of an excitonic molecule (by the excitation of two particles from the molecule to the hole band) is the most intriguing possibility. However, there are also possibilities of $8k_F$ scattering, interchain Cooper pairing, and superconductivity based upon quartets (or four electrons instead of two).

ANISOTROPIC SEMICONDUCTORS AND METALS: WHAT HOLDS THEM TOGETHER?*

Robert Melville Metzger

Department of Chemistry
The University of Mississippi
University, Mississippi 38677

INTRODUCTION

For the past several years considerable effort has gone into understanding the cohesive forces that must explain the stability of organic ionic and partially ionic crystals. These studies have acquired particular relevance in that some of these crystals are quasi-one-dimensional metals (QODM) over an extended temperature range.[1-6] One of the important long-range goals is the development of predictive criteria for the stability of organic conductors, and even, it is hoped, inorganic conductors such as the polymer $(SN)_x$ and the Krogmann salts. That is, if we can learn from calculations which molecules, which crystallographic space groups, which modes of stacking, molecular orientation, and overlap will yield a QODM, then this rapidly developing discipline will acquire some needed maturity and respectability.

We are still somewhat far from that goal. On the one hand, simple-minded Madelung energy calculations do yield decent values for organic insulators and semiconductors,[7-10] such as TMPD TCNQ (where TMPD is *N*,*N*,*N'*,*N'*-tetramethyl-*para*-phenylenediamine, and TCNQ is 7,7,8,8-tetracyanoquinodimethan); on the other hand, grossly inadequate values have been obtained for the QODM NMP TCNQ[11] (where NMP^+ is the diamagnetic *N*-methylphenazinium cation) and TTF TCNQ[12-14] (where TTF is tetrathiofulvalene). Somewhat more elaborate Madelung energy calculations have been performed, with mixed success.[12,14-17] Careful crystal polarization energy calculations are in progress.[17] Attempts to include the cohesive energy contribution due to the conduction electrons are still at an early stage.[15,18] The process of acquiring precise thermochemical data (enthalpies of combustion and sublimation) for these systems has barely been started.[19-21]

The next section will describe the experimental and theoretical components of the cohesive energy and discuss in detail the Born-Haber cycle, as applied to the organic ionic crystals, and the various criteria for ionicity and partial ionicity in these lattices. The section after that reviews the results obtained so far from Madelung energy calculations, from thermochemical measurements, and from the various attempts to overcome the "Madelung energy defect"[12] in QODM. The last section of this paper presents the current status of polarization energy calculations, and introduces a few thoughts about how future calculations should proceed.

*Manuscript received June 14, 1977.

0077-8923/78/0313-0145 $1.75/1 © 1978, NYAS

The Cohesive Energy, and Criteria for Ionicity

The Born-Haber cycle for a binary ionic (D^+A^-) crystal (where D is the electron donor molecule, and A is the electron acceptor molecule) is shown in FIGURE 1. Starting with the neutral donor molecule, D, and the neutral acceptor molecule, A, in the gas phase, one wonders whether the transfer of one electron from the highest occupied donor molecular orbital to the lowest unoccupied acceptor molecular orbital (costing $I_D - A_A$, where I_D is the first adiabatic gas-phase ionization potential of D, and A_A is the first adiabatic gas-phase electron affinity of A) costs less energy than $|U|$, the energy released by forming the D^+A^- crystal lattice; if so, the ionic lattice can form, and U is the cohesive energy (by convention, negative if the ionic crystal is thermodynamically stable). If not,

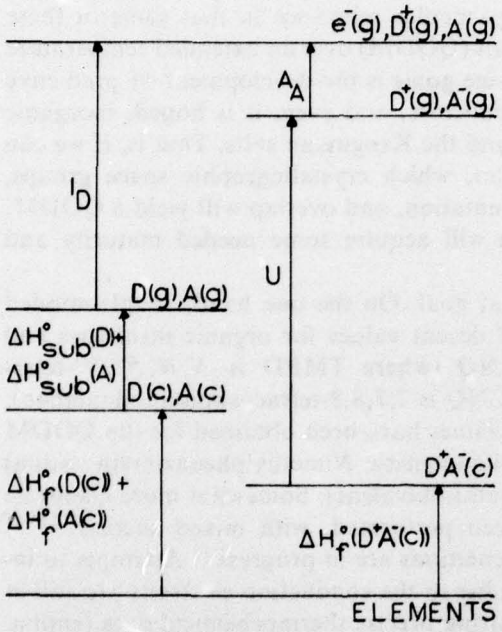


FIGURE 1. Born-Haber cycle for a binary ionic (D^+A^-) crystal (where D is the electron donor molecule, and A is the electron acceptor molecule).

then a neutral lattice will form, with a relatively small cohesive energy U^n. Typically, for "good" organic electron donors such as TMPD and TTF, I_D is between 6 and 7 eV; for good organic electron acceptors such as TCNQ and *para*-chloranil, A_A is between 2 and 3 eV.

Experimentally, then, for an ionic lattice the cohesive energy is:

$$U_{exp} = -\{\Delta H_f^\circ(D,c) + \Delta H_f^\circ(A,c) + \Delta H_{sub}^\circ(D) + \Delta H_{sub}^\circ(A) + I_D - A_A - \Delta H_f^\circ(D^+A^-,c)\}, \quad (1)$$

where the ΔH_f° are standard enthalpies of formation at 298.15°K, and the ΔH_{sub}° are standard enthalpies of sublimation at 298.15°K for the neutral molecules D and A. In some cases, e.g., Cl_2 in the Born-Haber cycle for NaCl, the enthalpy of atomization replaces the enthalpy of sublimation.

For a neutral lattice the cohesive energy is:

$$U_{exp}^{n} = -\{\Delta H_f^\circ(D,c) + \Delta H_f^\circ(A,c) + \Delta H_{sub}^\circ(D) + \Delta H_{sub}^\circ(A) - \Delta H_f^\circ(DA,c)\} \quad (2)$$

and, in general,

$$|U_{exp}^{n}| \ll |U_{exp}|.$$

One may obtain U_{exp} or U_{exp}^{n} if all other quantities in (1) and (2) are measurable. The ionization energy is readily available from mass spectrometry and ion cyclotron resonance spectroscopy appearance potentials, and from optical spectroscopy or gas-phase photoelectron spectra; the usual problem is whether one can really obtain a truly adiabatic I_D. The enthalpies of formation can be obtained from combustion calorimetry.[19] The enthalpies of sublimation can be derived from careful studies of the temperature dependence of the vapor pressure, via the Clapeyron-Clausius Equation.[20,21] The most frustrating and difficult quantity to measure experimentally is the electron affinity:[9] for very small molecules (NO, NO_2) ion cyclotron resonance provides nice absolute values;[22] for large molecules (TCNQ, *para*-chloranil) Briegleb's indirect estimates[23] from the presumed linearity of the optical charge-transfer band ($h\nu_{CT}$) with ($I_D - A_A$) gave values that appeared about 1 eV too low;[8,9] the best method at present seems to be the Cs beam collisional ionization technique.[24]

The temperature dependence of all the quantities in (1) and (2) is sufficiently small, at least in comparison with the usual uncertainty in, say, A_A, that, to first order, almost any reasonable reference temperature can be used interchangeably with 298.15°K.

A complication can arise in the use of (1): many ionic TCNQ salts (e.g., NMP TCNQ, quinolinium $(TCNQ)_2$, triethylammonium $(TCNQ)_2$) have diamagnetic, S = O cations (D^+) which are one-electron oxidation products of unstable $S = \frac{1}{2}$ free radicals ($D\cdot$). Then the enthalpy of formation of $D\cdot$ (*N*-methylphenazyl, quinolinyl, $Et_3NH\cdot$) may be experimentally inaccessible. (In the Born-Haber cycle for NaCl, $\Delta H_f^\circ(Cl\cdot, g)$ is fortunately accessible spectroscopically from the atomization of the dimer, Cl_2). Also, if $\Delta H_f^\circ(D\cdot, g)$ cannot be measured, then the ionization potential I_D for the reaction $D\cdot \rightarrow D^+ + e^-$ (e.g., $NH_4\cdot \rightarrow NH_4^+ + e^-$) may be difficult to determine, and would have value only in trying to compare calculated binding energies (see below) with the cost of ionizing D and A. The thermodynamically correct thing to do is to replace $\{\Delta H_f^\circ(D,c) + \Delta H_{sub}^\circ(D) + I_D\}$ in (1) by the single quantity $\Delta H_f^\circ(D^+, g)$; however, this enthalpy of formation cannot be measured directly by combustion calorimetry, but may be obtained indirectly[25] from bracketed mass spectral reactions, or from a separate Born-Haber cycle for a "simple" salt, such as NMP^+Cl^-, or $Et_3NH^+I^-$, assuming that for this "simple" salt, the binding energy U can be calculated completely and exactly.

The theoretical crystal binding energy for an ionic crystal is:

$$U_{th} = E_{DC} + E_{ex} + E_{pol} + E_{vdW} + E_{conf} + E_{rep} + E_{cond}, \quad (3)$$

where E_{DC} is the quantum-mechanical interionic direct Coulomb binding energy, which consists of terms like:

$$\int d\tau_1\, d\tau_2\, \psi_A^*(1)\, \psi_B^*(2)\, \frac{e^2}{r_{12}}\, \psi_A(1)\, \psi_B(2),$$

where ψ_A is a molecular orbital on ion A, and ψ_B is a molecular orbital on ion B; E_{ex} is the quantum-mechanical interionic exchange Coulomb binding energy, which consists of terms like:

$$\int d\tau_1\, d\tau_2\, \psi_A^*(1)\, \psi_B^*(2)\, \frac{e^2}{r_{12}}\, \psi_B(1)\, \psi_A(2);$$

E_{pol} is the polarization energy, due to the interaction between the Coulomb field and the polarizabilities of the molecular ions; E_{vdW} is the van der Waals, or induced dipole-induced dipole energy, E_{conf} is the configuration interaction term, that corrects for back-charge transfer effects if any; E_{cond} is the term that includes any extra binding energy due to conduction electrons (extra kinetic energy due to finite bandwidth); the internuclear repulsions and the electron-nucleus attraction terms are included in E_{DC} or E_{ex}, but if they cannot be, then E_{rep} is a hard-core repulsion term that should prevent the complete collapse of the ionic lattice onto a single point.

The theoretical cohesive energy for a neutral crystal is:

$$U_{th}^{n} = E_{vdW}^{n} + E_{conf}^{n} + E_{rep}^{n}, \tag{4}$$

where E_{conf}^{n} now is the second-order correction due to the (small) direct charge transfer, and E_{vdW}^{n} is the van der Waals term that now uses the neutral molecule polarizabilities, which (see below) should be sensibly different from the molecular ion polarizabilities.

For a partially ionic crystal (such as a QODM), with degree of formal charge transfer ρ (where $0 < \rho < 1$), the experimental cohesive energy is, trivially:

$$U_{exp}^{\rho} = \rho\, U_{exp} + (1 - \rho)\, U_{exp}^{n}. \tag{5}$$

The theoretical counterpart of (5) is discussed later.

Ideally, a reasonable cohesive energy calculation for an ionic crystal should yield a significant portion of U_{th}. The Madelung energy:

$$E_M = \sum_{i>j}\sum z_i z_j \,|\, \mathbf{r}_i - \mathbf{r}_j \,|^{-1} \tag{6}$$

is a double-lattice sum (immediately reducible by symmetry to a single lattice sum) of the classical Coulomb interactions between all atoms with charge z_i at crystallographic positions $\mathbf{r}_i$ and all other atoms with charge z_j at $\mathbf{r}_j$. It has been a long-standing article of faith that for inorganic ionic crystals E_M is close enough to U_{exp}. In fact, for NaCl, $U_{exp} = -7.918$ eV molecule^{-1}, and $E_M = -8.932$ eV molecule^{-1}, and E_M plus a reasonable guess for E_{rep} can be made to fit U_{exp} quite well.[26]

One might therefore conceive of a *Gedankenexperiment*, where one starts with a neutral crystal (with binding energy U_{th}^{n}), and ionizes the lattice to form an ionic crystal (with binding energy U_{th}). The cost of ionizing the lattice is *grosso modo* $(I_D - A_A)$ per DA pair. The net increase in binding energy is $U_{th} - U_{th}^{n}$. If, by luck:

$$U_{th} - U_{th}^{n} \simeq E_M, \tag{7}$$

that is, if E_M includes reasonably well all the E_{DC} and E_{ex} contributions, then a very simple criterion for ionicity emerges: if

$$E_M + I_D - A_A < 0, \tag{8}$$

then the crystal is ionic; if:

$$E_M + I_D - A_A > 0, \tag{9}$$

then the crystal is neutral; i.e., it remains a van der Waals solid.[27]

Naturally, the cost of ionizing D to D^+ and A to A^- inside a crystal lattice is less than the gas-phase value $I_D - A_A$ by a very appreciable screening effect (a polarizability effect), which, however, is nonlinear with the progressive charging of the crystal lattice, since the polarizabilities of the neutral molecules are sensibly different from the polarizabilities of the ions (this same effect makes E_{vdW} somewhat different from E_{vdW}^{n}). But, in a thermochemical sense, one may just as well construct the lattice from the gaseous ions at infinity, and use the $I_D - A_A$ values as they are, and then require that the correct calculation of U_{th} include all polarization energy corrections. This seems to be the more reasonable approach.

If the simple, "rule-of-thumb" (8) were to fail, then one may try to include into a new energy, E_{Coul}, *all* effects due to formally charging the lattice, i.e., by defining:

$$E_{Coul} \equiv E_{DC} + E_{ex} + E_{pol} + E_{vdW} - E_{vdW}^{n}, \tag{10}$$

a new, more valid criterion of ionicity emerges:

$$E_{Coul} + I_D - A_A < 0. \tag{11}$$

Unfortunately, explicit calculations of E_{Coul} have not yet been reported.

If one wishes to construct a partially ionic lattice, or if one wants to discuss (10) more closely, then one may define a molecular-field energy:

$$E_\rho = \rho^2 E_{Coul} + \rho(I_D - A_A), \tag{12}$$

which can represent the lattice ionization process. In the preliminary approximation $E_{Coul} = E_M$ (where E_M is for the fully ionic lattice), this molecular-field energy has been discussed before,[27] and has been shown to lead to two stable solutions only, at $\rho = 0$ (the fully neutral lattice), and at $\rho = 1$ (the fully ionic lattice). Therefore the partially ionic lattice presents a particular challenge, in that, despite (12), an intermediate value of ρ must somehow be stabilized by calculating E_{Coul}, or at least E_M, for the partially ionic lattice, and obtaining some extra binding energy because of some crucial details in the charge distribution. As we shall see, this is in fact the problem with cohesive energy calculations for organic metals. If the partial ionicity of a crystal lattice can be approximated classically by a relatively simple static representation, where some sites in the lattice are occupied by ions, and the others by neutral molecules, and this distribution is periodic with a short period, then the Madelung energy for this lattice, E_M^{ρ} can be calculated for rational ρ: this is a 0°K "frozen lattice" or Wigner lattice model of the partial ionicity.[12,14,15] The naive hope is that

$$U_{th}^{\rho} \simeq E_M^{\rho} \tag{13}$$

would be a valid approximation. The cohesive energy calculation for a dynamic partially charge-transferred lattice appears very difficult: if the dynamics involve charge-density waves (CDW) propagating through the lattice with some statistical distribution of mutual phases, then one must superimpose onto a periodic lattice of atom positions an aperiodic charge distribution; this makes the Madelung energy calculation well-nigh impossible.

In the next section the known theoretical and experimental cohesive energy contributions for neutral, ionic, and partially ionic organic crystals (and $(SN)_x$) will be discussed. TABLE 1 summarizes Soos's very convenient classification[1] for these crystals. For more details about the chemistry and physics of organic semiconductors and QODM, the reader is referred to the other articles in this volume and to several recent reviews.[1-6]

A practical question, of vital interest to this conference, is: what makes a QODM possible? By now, there must be more than 100 known TCNQ salt crystal structures, and several TTF halide structures. Two necessary crystallographic conditions for QODM conduction seem to emerge:

1) Regular lattice: there must be only one crystallographically unique TCNQ species (or TTF species), arranged in a linear stack with intermolecular distances sensibly less than the typical van der Waals distance of 3.5 Å quoted for weak pi-pi overlap; there must be no intermolecular distance

TABLE 1

TYPES OF CRYSTAL LATTICES, ACCORDING TO SOOS'S CLASSIFICATION[1]

Soos Lattice Type	Formal Charge ρ	Type of Linear Stacks	Alternation of Intermol. Distances?	Examples
MSRN (mixed simple regular neutral)	0.0	D A D A	no	Hexamethylbenzene: *para*-chloranil, Naphthalene:TCNE
MSRI (mixed simple regular ionic)	1.0	$D^+A^-D^+A^-$	no	$TMPD^+TCNQ^-$, $TMPD^+$*para*-chloranil$^-$
SSR (segregated simple regular)	1.0	$D^+D^+D^+D^+$	no	$TMPD^+I^-$ $TMPD^+ClO_4^-$ ($T > 186°K$)
		$A^-A^-A^-A^-$	no	Rb^+TCNQ^- (II, $T = 300°K$)
SSA (segregated simple alternating)	1.0	$D^+D^+D^+D^+$	yes	$TMPD^+ClO_4^-$ ($T < 186°K$)
		$A^-A^-A^-A^-$	yes	Na^+TCNQ^- ($T = 300°K$) Rb^+TCNQ^- (I, $T = 110°K$)
SCA (segregated complex alternating)	<1.0	$A^-A\ A^-A^-$	yes	Cs_2TCNQ_3, TEA $TCNQ_2$
SCR (segregated complex regular)	$\gamma \neq 1.0$	$A.^{-\gamma}A.^{-\gamma}A.^{-\gamma}$ and/or $D.^{-\gamma}D.^{-\gamma}D.^{-\gamma}$	no	TMPD $TCNQ_2$ NMP TCNQ TTF TCNQ

TABLE 2
MADELUNG ENERGIES E_M FOR TWO MSRI AND TWO MSRN CRYSTALS*

Crystal	Soos Lattice Type	Formal Charge ρ_{exp}	E_M (eV/molecule)	$I_D - A_A$ (eV)
(1:1)-(TMPD$^+$TCNQ$^-$)	MSRI	1.0	-3.94 ± 0.05†	3.45‡
(1:1)-(TMPD$^+$*para*-chloranil$^-$)	MSRI	1.0	-4.43 ± 0.03†	3.85§
(1:1)-(Hexamethyl-benzene:*para*-chloranil)	MSRN	0.0	-4.41 ± 0.08†	5.6§
(1:1)-(Naphthalene:TCNE)	MSRN	0.0	−4.31†	5.5¶

*Their experimental classification by Equation 8 is confirmed for each case.
†From Reference 8.
‡Using $A_A = 2.8$ eV (Reference 24) instead of the older, discredited value $A_A = 1.7$ eV (Reference 23).
§Using $A_A = 2.37$ eV, 1.0 eV higher than the older, discredited value $A_A = 1.37$ eV (Reference 23).
¶Using $A_A = 2.6$ eV, 1.0 eV higher than the older, discredited value $A_A = 1.6$ eV (Reference 23).

alternation[1]; the overlap must be regular, with no "zig-zag"; there may be some disorder[28] among the counterions.

2) The lattice must be partially ionic.[1]

Thus, NMP TCNQ, TTF TCNQ, TTF $Br_{0.78}$, quinolinium $TCNQ_2$, and acridinium $TCNQ_2$ satisfy both conditions, and are QODM; TEA $TCNQ_2$ (TEA, triethylammonium) satifies only condition (2), and TMPD $TCNQ_2$ has a zig-zag overlap among the TCNQ sites, and thus, these two salts are semiconductors.

Hence, finally, the two QODM requirements of a regular linear lattice and of partial ionicity must somehow be explained by cohesive energy calculations.

COHESIVE ENERGIES: CALCULATIONS AND EXPERIMENTS

Most cohesive energy calculations reviewed in this section have restricted themselves to the presumed largest contributor to U_{th}, namely the Madelung energy E_M. The lattice sum in (6) is conditionally convergent, and most calculations have used the Ewald method[29] to accelerate its convergence, but one group[13,30,31] has used the modified Evjen method.[32]

MSR Lattices

The first systems studied[8] were the organic mixed simple regular (MSR)[1] lattices, where, experimentally, some are fully ionic semiconductors (e.g., TMPD$^+$TCNQ$^-$, TMPD$^+$ *para*-chloranil$^-$), whereas others are fully neutral insulators (Hexamethylbenzene:*para*-chloranil, Naphthalene:tetracyanoethylene). The results[8] are presented in TABLE 2. For the E_M calculation, it was essential that the formal charge on the ion be distributed over the atoms of the ion; the

fractional atomic charges were obtained from various theoretical calculations, ranging from simple Hückel theory to Pariser-Parr-Pople pi theory; these different charge-distribution models yielded total (interionic plus intraionic) electrostatic Coulomb energies that depended very much on the details of the charge model, but once the intraionic contributions were subtracted, the remaining interionic Madelung energy E_M was very independent of the charge model[8] (see the small standard deviations quoted in TABLE 2). Thus, the calculated E_M were valid crystal energies. Unfortunately, experimental values (U_{exp} and U_{exp}'') for the cohesive energies were not available for comparison with the E_M results. However, a comparison of E_M with $I_D - A_A$, in the sense of (**8**) and (**9**) was quite favorable, provided that an updated set of A_A values[9,24] is used. That is, the MSRI crystals satisfy (**8**), and the MSRN crystals satisfy (**9**). When the earlier A_A values[23] were used, this classification failed,[8] and a Hubbard Hamiltonian calculation was applied, yielding an estimate of E_{ex} of about 0.5 eV[33] for the MSRI crystals. Finally, one should note that whereas for NaCl the cost of ionizing the lattice, $I_D - A_A = 1.53$ eV,[26] is much less than the Madelung energy, $|E_M| = 8.932$ eV, in the MSRI lattices (**8**) is satisfied by a much narrower margin, partly because the charge density per crystallographic unit cell is lower.

SSR and SSA Lattices

These Madelung energy studies were extended to the segregated simple regular (SSR)[1] and segregated simple alternating (SSA)[1] crystals, in part to verify whether these crystals were stabilized by classical Coulomb forces (calculable in E_M), or whether exchange Coulomb forces were needed to supply the necessary cohesion along the linear stacks of radical anions (for the TCNQ salts) or radical cations (for the TMPD salts).[7,9,10] The results are summarized in TABLE 3. For both $TMPD^+I^-$ (Wurster's Blue Iodide) and $TMPD^+ClO_4^-$ (Wurster's Blue Perchlorate) the calculated E_M values are large, independent of charge model, and (for $TMPD^+I^-$) satisfy (**8**). It was, moreover, possible to verify that the Madelung energy difference between the high-temperature phase (SSR) of $TMPD^+ClO_4^-$ and its low-temperature phase (SSA) was of the order of magnitude of the (small) enthalpy of transition at the 186°K phase transition, and that Madelung forces did *not* in fact drive the phase transition.[10] Similarly, for the TCNQ salts in TABLE 3, the E_M values were independent of charge model, and compared favorably with $I_D - A_A$ (Equation 8). Again, no exchange forces were necessary to confirm compliance with Equation 8. However, the TCNQ salts were studied also to attempt to "close" the Born-Haber cycle for $NH_4^+TCNQ^-$, since for this salt, and for neutral TCNQ, the enthalpies of formation had been determined.[20] Unfortunately, the crystal structure of $NH_4^+TCNQ^-$ is very badly disordered, and so its E_M value is open to serious question[9]; nevertheless, if one assumes that, because of the similarities in the crystal structure, the experimental cohesive energies of Na^+TCNQ^- and Rb^+TCNQ^- [from $Na^+(g)$ or $Rb^+(g)$ and $TCNQ^-(g)$] are approximately equal to the cohesive energy of $NH_4^+TCNQ^-$ [from $NH_4^+(g)$ and $TCNQ^-(g)$], then the calculated E_M values for Na^+TCNQ^- and Rb^+TCNQ^- are 1.8 to 2.5 eV short of the presumed U_{exp}. Therefore, the question arises, even for semiconducting TCNQ salts: Is E_M not the preponderant

part of E_{Coul}? If not, what is missing? By using a modification of the Ewald procedure for E_M, we evaluated the electric fields at each atom in the Rb^+TCNQ^- structure (due to the formal charge); and using neutral-atom scalar polarizabilities, we obtained a value $E_{pol} = -0.408$ eV/molecule. It is hoped (see below) that when better polarizabilities are used, this number will become more appreciable. However, it appears, after all, even in semiconducting TCNQ salts, that a proper formalism for calculating E_{DC} and E_{ex} has to be put into practice. Such an Ewald-tight-binding Hartree-Fock formalism has been developed in principle,[35] but a practical program is still in the planning stages. It is possible that a Hubbard Hamiltonian approach may yield a credible estimate of E_{ex} with far less labor.[33]

TABLE 3

MADELUNG ENERGIES E_M FOR SEVERAL SSR AND SSA CRYSTALS*

Crystal	Soos Lattice Type	E_M (eV/molecule)	E_{pol} (eV)	$I_D - A_A$ (eV)	Is (8) OK?	U_{exp} (eV)
$TMPD^+I^-$	SSR	-4.26 ± 0.04†		2.97	yes	
$TMPD^+ClO_4^-$ ($T = 300°K$)	SSR	-4.11 ± 0.02‡				
$TMPD^+ClO_4^-$ ($T = 110°K$)	SSA	-4.13 ± 0.02‡				
Na^+TCNQ^- ($T = 300°K$)	SSA	-5.29 ± 0.02§		2.35	yes	
Rb^+TCNQ^- (I, $T = 110°K$)	SSA	−4.71§ −4.74¶	−0.41§	1.38	yes	
Rb^+TCNQ^- (II, $T = 300°K$)	SSR	−4.64§		1.38	yes	
$NH_4^+TCNQ^-$	disord.	−4.82(?)§				−7.13**

*Their experimental classification by Equation 8 is confirmed. The formal charge ρ_{exp} is presumed to be 1.0 for all these lattices.

†From Reference 7.

‡From Reference 10.

§From Reference 9.

¶From Reference 16. For the Wigner crystal case, with $\rho = 0.5$, $E_M = -1.98$ eV/(RbTCNQ species).

**From Reference 20.

Also, there is a crying need for definitive thermochemical values of U_{exp} for the SSR and SSA salts of TABLE 3.

The SCA Lattices

The segregated complex alternating (SCA)^1 TCNQ salts (semiconductors) were also studied; heretofore unpublished results[17,36] are presented in TABLE 4. For Cs_2TCNQ_3 the crystallographic refinement[37] found that there was one $TCNQ^0$ and two $TCNQ^-$ species per $(TCNQ)_3^{2-}$ trimer, whereas for TEA $TCNQ_2$ the

TABLE 4

MADELUNG ENERGY CALCULATIONS FOR TWO SCA CRYSTALS*

Crystal	Soos Lattice Type	TCNQ Charge from Crystal Structure $TCNQ_A$	TCNQ Charge from Crystal Structure $TCNQ_B$	TCNQ Charge Used‡ $TCNQ_A$	TCNQ Charge Used‡ $TCNQ_B$	Normal Ions§ E_M (eV)	Supermol. Ions§ E'_M (eV)¶	$I_D - A_A$ (eV)	Equation 8 is OK?
Cs_2TCNQ_3**	SCA	0	−1	0	−1	*−9.19*	−10.57	2.21	Yes
				−2/3	−2/3	−8.04	*−10.76†*	2.21	Yes
$TEA^+TCNQ_2^-$**	SCA	−1/2	−1/2	−1/2	−1/2	−2.57	*−2.94*		
				0	−1	*−2.70†*	−2.70		
				−1	0	−2.57	−2.58		

*Where applicable, Equation 8 is obeyed.

†The charge distribution for which the Madelung energy is *minimum* does in two instances disagree with the charge distribution determined in the crystallographic structure refinement. (From Reference 36.)

‡INDO charges, using the crystallographic atom positions, were used throughout.

§E_M is corrected for the intraionic Coulomb repulsions within each TCNQ species, as usual; E'_M is corrected for all the Coulomb interactions within each $(TCNQ)_3^{2-}$ supermolecular ion (in Cs_2TCNQ_3), and within each $(TCNQ)_2^-$ supermolecular ion (in TEA $TCNQ_2$).

¶For Cs_2TCNQ_3, 1 molecule = 1 $Cs_1TCNQ_{1.5}$ unit; for TEA $TCNQ_2$, 1 molecule = 1 TEA_1TCNQ_2 unit.

**For the crystal structure of Cs_2TCNQ_3, see Reference 37; the crystal structure of TEA $TCNQ_2$ (Reference 38) is incorrect, in that it attempts to consider $TCNQ_A$ as being an anion, and $TCNQ_B$ as being neutral; the correct crystallographic refinement (Reference 39) cannot but assign a statistical charge of −0.5 to both $TCNQ_A$ and $TCNQ_B$.

more recent and better structure determination[39] found that the two TCNQ species that were crystallographically distinct were in fact both statistically a $TCNQ^{-0.5}$ species, as had been suspected before,[1] but contrary to a previous, less precise structural determination.[38] A Madelung energy study was therefore done to see whether the E_M values would predict, by themselves, which formal charge would yield the more stable lattice. As had been done before,[9,10,12] INDO charges for the ions and molecules as determined by the crystal structure, were used.[40] For Cs_2TCNQ_3, (**8**) is again amply satisfied, and E_M is more negative for the crystallographically correct assignment of formal charges within the TCNQ stack; for TEA $TCNQ_2$, however, E_M predicts the wrong formal charge assignment. In other words, the Wigner lattice is always energetically favored. E'_M was then calculated: the intraionic correction, which is applied to the total (gross) classical Coulomb energy to yield E'_M, now includes all classical Coulomb interactions between all atoms in the $(TCNQ)_3^{2-}$ "supermolecular ion" in Cs_2 $TCNQ_3$, and between all atoms in the $(TCNQ)_2^-$ supermolecular ion in TEA $TCNQ_2$. This E'_M improves matters in TEA $TCNQ_2$ by predicting the correct formal charge allocation, but spoils a good thing for Cs_2TCNQ_3. Clearly, E_{pol} or other effects must be included in such a *Gedankenexperiment*.

SCR Lattices, Organic Metals, and $(SN)_x$

Finally, TABLE 5 summarizes the cohesive energy data for the compounds of greatest interest to this conference: the QODM: NMP TCNQ, TTF TCNQ, TTF $Br_{0.79}$, and polymeric $(SN)_x$. Also included in TABLE 5 is a compound that is a semiconductor, but probably barely misses being an organic metal: TMPD $TCNQ_2$. Some interest was generated fairly early in the history of Madelung energy calculations by the result that the QODM NMP TCNQ, although a very stable crystal, had essentially a zero Madelung energy, i.e., should not exist as an ionic solid.[11] The severe dependence of the calculated E_M on the charge model was another good clue that something other than just the classical E_M had to bind the NMP TCNQ lattice. In data presented here for the first time, an attempt was made to see whether better E_M values could be obtained[17] if the disorder model of QODM conduction[28] was applied to the NMP TCNQ lattice, by alternating the orientation of the NMP^+ ion in the lattice: as is seen in TABLE 5 (footnote ¶), very little extra binding energy was secured in this attempt.[17] More recently, the Coulomb field in the NMP TCNQ crystal was allowed to modify the pi electron charge distribution of the NMP^+ ion[16]; as can be seen in TABLE 6, (columns C and D), the charge distribution does alter significantly (in fact, possibly even too much), so that we no longer have a true NMP^+ ion, but more Madelung binding energy is secured by this expedient.[16] It is not clear whether the "improved" E_M value does include all other polarization effects that the usual E_M calculation must neglect. Moreover, a Wigner lattice calculation[16] for NMP TCNQ, giving E_M as a function of rational values of ρ between 0 and 1 yields a minimum when $\rho = \frac{1}{2}$, whereas a recent NMR determination of the degree of formal charge transfer in NMP TCNQ yields $\rho_{exp} = 0.94$.[41] Again, a careful look at E_{ex} and E_{pol} and E_{cond} in NMP TCNQ seems to be in order.

Several groups have calculated the Madelung energy of TTF TCNQ, almost

TABLE 5

BINDING ENERGIES FOR SCR CRYSTALS, AS A FUNCTION OF FORMAL CHARGE, ρ*

Crystal	Soos Lattice Type	ρ_{exp}	Binding Energy Calculations: Charge Used ρ	Madelung $E(\rho)$ (eV/molecule)	Polar. E_{pol} (eV)	Cond. E_t (eV)	Cost of Ioniz. $\rho(I_D - A_A)$ (eV)	Eq. 8 OK?	Thermoch. U_{exp}^{ρ} (eV)‡‡
NMP TCNQ	SCR	0.94 [41]	1.00	0.0 to 0.3 [11]			3.7(?)‡		
			1.00	0.35§, 0.86¶			3.7(?)‡		
			1.00	−2.1 to −2.7**			3.7(?)‡		
			0.50†	−1.8††			1.8(?)‡		
TTF TCNQ	SCR	0.59 [42, 43]	1.00	−1.94 to −2.33 [12]	−0.63 [12]		4.15	no	−6.58
			1.00	−1.53 to −2.48 [13]	−0.09 [12]	−0.25 [12]	4.15	no	−6.58
			1.00	−1.8 to −2.2 [14]			4.15	no	6.58
			0.59	−0.68 to −0.81 [12]			2.45	no	−4.88
			0.50	−0.53 to −0.69 [12]			2.08	no	−4.51
			0.50†	−1.57 [12], −1.60 [12]			2.08	no	−4.51
			0.50	−1.55§§			2.08	no	−4.51
			0.295	−0.17 to −0.20 [12]			1.22	no	−3.66
TTF $Br_{0.79}$	SCR	0.74 to 0.79 [45]	1.00	−3.9 [15]			3.22	yes	
			0.74	−3.24 [15]		−0.11 [15]	2.43	yes	
$(SN)_x$	—	0.59¶¶	0.50	−0.03 [30]					
TMPD $TCNQ_2$**	SCR	0.5†††	0.50	−2.81‡‡‡			3.45	no	

*Equation 8 is not obeyed (except for TTF bromide), and the Madelung energy E_M is strongly dependent on charge model. For TTF TCNQ, all binding energy contributions fall well short of the experimental (thermochemical) binding energy U_{exp}^{ρ}. All crystals (except TMPD $TCNQ_2$) are quasi-one-dimensional metals. References are indicated in brackets.

†Use of the Wigner lattice does increase the binding energy, but not enough.

‡Questionable. Reference 15 guesses $I_D = 6.5$, but Reference 16 guesses $I_D = 6.4$ eV for the reaction $NMP\cdot \rightarrow NMP^+ + e^-$, but in reality (see text) one should discuss and measure only $\Delta H_f^{\cdot}(NMP^+, g)$.

§From Reference 17. For $TCNQ^-$, charge model Qa of Reference 8 was used; for NMP^+, the charge model of column A of TABLE 6 below was used. Exact value (good to 1 part in 10^{11}): $E_M = 0.347535842$ eV/molecule.

¶From Reference 17. For $TCNQ^-$, charge model Qa of Reference 8 was used. For NMP^+, the charge model of column B of TABLE 6 below was used. The latter is definitely not of the symmetry required by the apparent crystallographic space group of NMP TCNQ ($P\bar{1}$); the molecular symmetry of NMP^+ could be indicated by the arrow ↑, which denotes the vector from the methylated N atom to the unmethylated N atom. Then the crystallographic site symmetry (at 50% occupancy of either orientation) is indicated by the double-headed arrow ↕. The exact value is E_M = 0.862 470 488 eV/molecule.

If now one averages the ↑ charge model of column B of TABLE 6 to yield the ↕ charge model, then one obtains (for the same $TCNQ^-$ charge model) E_M = 0.845 387 338 eV/molecule.

If, further, one attempts to test the disordered lattice model of NMP TCNQ conductivity proposed by Reference 28, by accosting four NMP^+ ions along the stacking direction as ↑ ↑ ↓ ↓, then E_M = 0.736 751 148 eV/molecule; if one accosts then as ↑ ↓ ↑ ↓, then E_M = 0.623 236 373 eV/molecule. Thus, disorder helps bind NMP TCNQ, but only slightly.

**From Reference 16. The NMP^+ charges used are repeated in TABLE 6 column D.

††From Reference 16. The case ρ = 0.50 represents the Wigner crystal minimum. The other data are: (1 molecule = 1 NMP TCNQ species)

ρ =	3/4	2/3	1/2	1/3	1/4	1/5	0
E_M =	−2.5	−2.8	−3.6	−3.1	−2.9	−2.5	0.1 eV/(NMP^+TCNQ^-)
E_M =	−1.9	−1.9	−1.8	−1.0	−0.7	−0.5	0.0 eV/molecule.

‡‡From Reference 19. Experimental uncertainty (due mainly to A_A and ΔH_{subl}): ±0.17 eV.

§§From Ref. 14. Other Wigner lattice calculations (1 molecule = 1 TTF TCNQ species) are:

ρ =	1	3/4	2/3	1/2	1/3	1/4	
E_M =	−2.0	−2.5	−2.7	−3.1	−3.2	−3.1	eV/(TTF^+TCNQ^-)
E_M =	−2.0	−1.9	−1.8	−1.6	−1.1	−0.8	eV/molecule.

¶¶From Reference 46; note, however, that Reference 47 obtains ρ_{exp} = 0.32 to 0.42.

***Reference 48 indicates that TMPD $TCNQ_2$ is *not* a QODM. It has a SCR lattice, with a 3.24 Å distance between TCNQ planes, but the overlap is "zig-zag."

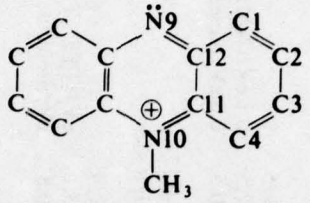
†††Presumed from crystal stoichiometry.

‡‡‡From Reference 17, 36. The $TCNQ^0$, $TCNQ^-$, and $TMPD^+$ fractional atomic charges were obtained from an INDO-level calculation on each of these species, with geometries as given by the crystal structure of TMPD $TCNQ_2$. If, however, a Wigner lattice geometry is formed on the crystal (one TCNQ neutral, the other with −1 charge), then E_M = −2.914 eV/molecule is obtained: as usual, the Wigner lattice helps make the binding energy more negative. However, Equation 8 is still not satisfied.

simultaneously.[12–15,31] For all values of the formal charge transfer, ρ, the calculated E_M falls short of the requirement of (8), i.e., of $\rho\,(I_D - A_A)$. Also, the E_M values depend very strongly on the charge distribution model assumed, indicating again that the crystal is minimizing an energy other than just E_M. A calculation of the polarization energy, E_{pol}, similar to the calculation reported above for Rb^+TCNQ^-, yielded only $E_{pol} = -0.63$ eV/molecule, for $\rho = 1$. The key to understanding the QODM conduction and properties of TTF TCNQ was the experimental discovery of the incommensurate Peierls-type phase transition at

TABLE 6

FRACTIONAL ATOM CHARGES FOR THE DIAMAGNETIC NMP^+ CATION, IN UNITS OF THE ELECTRONIC CHARGE, $|\epsilon|$*



Atom	A	B	C	D
C1	0.044	0.0096	0.08	0.07
C2	0.052	0.0203	0.04	0.13†
C3	0.052	0.0406	0.14	0.24†
C4	0.044	−0.0135	0.0	0.0
N9	0.189	0.6749	0.2	0.17
N10	0.189	−0.1298	0.0	−0.05
C11	0.060	0.1023	0.08	0.0
C12	0.060	0.0624	0.06	0.0

*Charge densities:

A Very approximate charge distribution, used in Reference 11.

B Simple Hückel pi electron charge densities, obtained from a program kindly made available by J. I. Brauman, using the hetero atom parameters suggested in Reference 49: $\alpha_{N9} = 0.6\,\alpha_C$ and $\alpha_{N10} = 0.9\,\alpha_C$.

C Pi electron charge densities, from Reference 16.

†D Pi electron charge densities, from Reference 16, corrected (modified) to include local Madelung field in NMP TCNQ. As a result, the charge distribution is grossly distorted (see in particular the atoms marked).

57°K, which determined that the charge transfer in TTF TCNQ (if it is due to $2k_F$) is $\rho_{exp} = 0.59 \pm 0.02$.[42,43] This finding gives great importance to the Wigner crystal calculations, which in fact yield considerable extra binding energy for $\rho = \frac{1}{2}$.[12,14,15] These Wigner crystal calculations are indicated by a dagger (†) in TABLE 5. Note should also be made that the degree of formal charge transfer, a quantity that is in general very difficult to measure, has been determined by careful integration of the x-ray intensities for the 100°K crystal structure of TTF TCNQ, yielding $\rho_{exp} = (0.48–0.60) \pm 0.15$.[49] The structural and Madelung energy implications of the Wigner crystal model have been analyzed very carefully in a further recent study,[15] which showed that in all SSR, SSA, and SCR structures,

the repulsions within the linear stack must somehow be overcome by attractive Coulomb interactions normal to the stack, if the crystal is to be at all ionic, and that whereas for SSA crystal like Rb^+TCNQ^-, the counterion coordination is sufficient to stabilize the $\rho = 1.0$ lattice; on the other hand, the coordination in TTF $Br_{0.79}$ is poorer, and a Madelung energy minimum is observed away from $\rho = 1$, and in fact, is obtained within the experimental range of composition for this QODM ($\rho = 0.74$). A Hubbard model estimate of the conduction electron contribution to the binding (for TTF bromide, which is a narrow-band metal) yields $E_t = E_{cond} = -0.11$ eV. It should be noted, however, that for TTF $Br_{0.79}$, for all values of ρ, (**8**) is satisfied. Also, no valid Wigner crystal energy minimum is obtained for TTF TCNQ (unless one were to accept the data of footnote ‡‡ to TABLE 5, and believe that for TTF TCNQ $\rho = 0.295$). (As a side issue to the problem of what binds TTF TCNQ, controversy arose about whether an early x-ray photoelectron spectrum of TTF TCNQ had indeed detected bulk TCNQ species in the crystal[51] and by the presence of two N 1s core electron peaks had seen,[52] within the time span of the photoelectron experiment, one $TCNQ^0$ and one $TCNQ^-$ species in the molar ratio of 1:2 (thus proving $\rho = 2/3$),[51] or whether surface layers had been detected,[53] or whether the two crystallographically inequivalent nitrogen atoms in TTF TCNQ were shifted from each other because of a large Madelung site potential inequivalence.[12,31] It was shown that if the Madelung site potential inequivalence was introduced into the CNDO/2† molecular calculation for $TCNQ^-$ and the "new" $TCNQ^-$ charges were used to generate a new Madelung energy and new Madelung site potentials, and the process was repeated to self-consistency, then the site potential inequivalence would vanish.[54] The charge modification on $TCNQ^-$ was, in this case, much less severe[54] than those obtained in the NMP TCNQ E_M minimization.[16] Unfortunately, no mention was made of what happened to E_M in the computation.§[54] Presumably, some of the polarization energy E_{pol}, was absorbed into the self-consistency routine, and the remaining part of E_{pol}, baptized "dipolar polarization binding energy" was found to be only -0.09 eV.[44] Another small headache was encountered when careful molecular polarizability studies were initiated: it is possible that the charge distribution models used for TCNQ and $TCNQ^-$ by several workers may be affected by incomplete convergence of the self-consistent field molecular energy minimization process.[17] As noted by one study,[55] cyano groups in valence-electron calculations cause convergence problems and oscillations in the density matrix values. By averaging the density matrix elements between each two successive cycles, the oscillations are damped down, and good SCF solutions are obtained. In TABLE 7, INDO‡ results[17] for $TCNQ^0$ (with the atom coordinates from the TCNQ and the TTF TCNQ crystal structures) and for $TCNQ^-$ are given, with incomplete ("canned program") convergence and with much improved convergence (better than 1 part in 10^{10} for the density matrix, and 10^{-12} atomic units in the electronic energy). The atomic charges of $TCNQ^0$ for the two crystal structures (TCNQ and TTF TCNQ) approach each other, and some of the differences between chemically

†CNDO/2 is the computer program Complete Neglect of Differential Overlap, version 2.[40]

‡INDO is the computer program Intermediate Neglect of Differential Overlap.[40]

§**NOTE ADDED IN PROOF:** B. D. Silverman (private communication) informs me that the shift in E_M was -0.2 eV.

equivalent atoms smooth out. Therefore, once E_{pol} calculations are well under control, the Madelung site inequivalence, with better charges, may in fact be less than was originally stated,[12,31] and this parenthetical controversy can be settled.) An effort has also been made to explain incomplete charge transfer in TTF TCNQ by using nearest-neighbor on-stack electron overlap and correlation within the confines of the extended Hubbard model;[18] it was shown that large contributions to U_{th}^{ρ} cannot be expected from such a calculation, but if E_M is of the order of $I_D - A_A$, then, without using the Wigner model, the band effects do in fact stabilize the $\rho \neq 1$ state.[18] Parenthetically, much use has been made of the Hubbard hamiltonian (in various forms), and the importance of Coulomb and CDW effects in explaining the properties of TTF TCNQ has been studied,[56-60] but quanti-

TABLE 7

EFFECT OF CAREFUL SELF-CONSISTENT FIELD (SCF) ENERGY CONVERGENCE ON THE INDO NET ATOMIC CHARGES FOR TCNQ AND $TCNQ^-$

Species	TCNQ	TCNQ	TCNQ	TCNQ	$TCNQ^-$	$TCNQ^-$
Crystal	TCNQ	TCNQ	TTF TCNQ (300°K)	TTF TCNQ (300°K)	TTF TCNQ (300°K)	TTF TCNQ (300°K)
Struct. SCF Conv. (a.u.)	10^{-4}	10^{-12}	10^{-4}	10^{-12}	10^{-4}	10^{-12}
Atom label*						
C4	0.1371	0.1331	0.1450	0.1343	0.1569	0.1500
C5	0.1378	0.1331	0.1457	0.1344	0.1573	0.1500
C6	0.0158	0.0112	0.0261	0.0136	−0.1303	−0.1386
C7	0.0702	0.0694	0.0702	0.0694	0.0541	0.0521
C8	0.0080	0.0087	0.0105	0.0128	−0.0281	−0.0263
C9	0.0037	0.0046	0.0120	0.0142	−0.0253	−0.0236
N1	−0.1949	−0.1898	−0.2042	−0.1894	−0.3152	−0.3051
N2	−0.1951	−0.1894	−0.2068	−0.1913	−0.3201	−0.3095
H8	0.0062	0.0063	0.0018	0.0020	−0.0235	−0.0233
H9	0.0113	0.0114	−0.0003	−0.0002	−0.0258	−0.0257

*From Reference 12.

tative contributions to U_{th}^{ρ} have not been reported. Thus, the overall import of the E_M, E_{pol}, and E_t studies for TTF TCNQ is that, to this date, their sum seems to approach $\rho(I_D - A_A)$, but that a bound state, in the sense of Equation 8, is not achieved. The real surprise came when the experimental crystal binding energy was determined for TTF TCNQ by calorimetric methods.[19] The result depends on the formal charge transfer, and for $\rho = 0.59$, $U_{exp}^{\rho} = -4.88$ eV/molecule.[19] Other values, for $\rho = 1.00$ and $\rho = 0.295$, are also listed in the last column of TABLE 5. Even the best Wigner crystal result, for $\rho = \frac{1}{2}$, and an estimate of E_{pol} and of E_t for the $\rho = 0.5$ case, do not yield more than about −2.0 eV. That is, the experimental crystal binding energy is missed *by almost 3 eV*. It is quite possible (see the following section) that a correct calculation of E_{pol} will

yield a surprisingly large result, once that realistic atom-in-molecule polarizability tensors are used. But it is equally possible that the exchange interactions along the linear stacks are unexpectedly large, and that whereas for SSA, SSR, and MSR lattices the E_M values, by their independence of charge model, masked the importance of E_{ex} in those lattices, the very sensitivity of E_M in SCR lattices is a strong indication that E_{ex}, maybe alongside E_{pol}, play a heretofore unsuspectedly crucial role in the binding of organic quasi-one-dimensional metals.

As shown in TABLE 5, a Madelung energy calculation of the binding energy of $(SN)_x$ yielded a very small, almost negligible binding energy, but an experimental binding energy for $(SN)_x$ has not yet been reported.

Finally, the SCR crystal TMPD $TCNQ_2$ has been studied experimentally and has been found to be a semiconductor.[48] A Madelung energy calculation[17,36] of this salt, both with the TCNQ species as $\rho = \frac{1}{2}$ species and in the Wigner crystal limit, shows that a (small) Madelung energy defect does exist in TMPD $TCNQ_2$. Since this salt is not a QODM, we must argue that the existence of a (small) Madelung energy defect does *not* predict QODM behavior (in fact, for TTF $Br_{0.79}$, there is no Madelung energy defect, and the salt is still a QODM). Since the dependence of E_M on charge model was not tried for TMPD $TCNQ_2$, we cannot be 100% sure that a large dependence of E_M on charge model is indicative of QODM behavior in these organic salts.

STATUS REPORT ON MOLECULAR POLARIZABILITIES AND FUTURE DIRECTIONS

As soon as the shortcomings of our E_M results for the SCR and SCA crystals became apparent and the possible large discrepancy between U_{exp}^- and E_M even for the simple SSR and SSA TCNQ salts was suspected, a program was initiated to calculate correct molecular polarizabilities for molecules like TCNQ and TTF and for their radical ions, using INDO and MINDO/3¶ finite perturbation (FP) techniques.[61,62] These techniques have been applied successfully to small molecules.[63–67] Our approach is then to decompose the molecular polarizability into atom-in-molecule polarizabilities (whose sum yields the molecular polarizability), so that the local Coulomb field in the crystal could interact correctly with the effective polarizability of each atom. Extreme demands had to be placed on the quality of the INDO or MINDO/3 calculation, but molecular polarizability tensors whose terms were symmetric and independent of the applied field to 1 part in 10^5, have been calculated. Some initial results are given in TABLE 8. The orientation of the polarizability tensor is such that α_1 is along the long axis of the TCNQ molecule, α_2 is perpendicular to the long axis but is in the molecular plane, and α_3 is perpendicular to the TCNQ molecular plane. It is well known that INDO-FP studies underestimate severely the polarization perpendicular to a chemical bond, and so it is not surprising that α_3 is much smaller than the value obtained by a traditional (classical) polarizability calculation that used established

¶MINDO/3 is the computer program Modified Intermediate Neglect of Differential Overlap Version 3.

compilations.[68] The magnitude of α_2 is not much affected by molecular geometry or by the formal charge, and agrees nicely with the classical estimate (and this was the value used in the note added in proof in Reference 12). However, the long-axis polarizability α_1 is quite sensitive to molecular geometry, and to the formal charge. One can safely say, then, that $TCNQ^-$ is considerably more polarizable than $TCNQ^0$. The decomposition of the molecular polarizability has, however, presented some unexpected mathematical complications: although nothing in the FP formalism seems to require it, the atom-in-molecule polarizability tensor is not symmetrical (the sum over all atoms of the atom tensors *is* symmetrical). The origin of this asymmetry seems to be in the manner in which the polarizability tensor is extracted from the dipole moment calculation: the INDO-CNDO/2-MINDO/3 algorithm for the dipole moment neglects several contributions to it, because similar contributions have also been ignored in the molecular Hamiltonian. At present, an effort is in progress to compute the dipole moment exactly (to *over* compute it), and to see whether such a procedure will explain the asymmetric atom-in-molecule polarizabilities. Even so, by keeping only the symmetric

TABLE 8

MOLECULAR POLARIZABILITIES (A^3) FOR TCNQ AND $TCNQ^-$ FROM CLASSICAL CALCULATIONS AND FROM INDO FINITE PERTURBATION CALCULATIONS

Species	TCNQ	TCNQ	$TCNQ^-$	$TCNQ^-$
Cryst. Struct.	TCNQ	TTF TCNQ	TTF TCNQ	
Method	INDO	INDO	INDO	Class.
Reference	17	17	17	68
Principal polarizability tensor components				
α_1	79.33	91.49	126.48	39.16
α_2	19.90	21.60	25.06	25.69
α_3	5.83	5.86	5.91	15.28
α_{ave}	35.02	39.65	52.49	26.71

part of the atom-in-molecule polarizability tensor, the atom polarizabilities obtained do appear quite reasonable.

Once decent polarizabilities are secured, the polarization energy will be recomputed for the SSR, SSA, SCA, and SCR TCNQ salts, and some of the shortfalls described above in the previous section may go away. However, there is ample room for some extended Hubbard model estimates of E_{ex} for any and all of these salts.

There is also a crying need for good old-fashioned thermochemical measurements of the heat of formation of all these TCNQ salts. The requirement of large samples that must undergo utter destructive testing can be cut down by designing sensitive microcombustion calorimeters, which can burn 50 mg instead of 500 mg per run.

Finally, it is conceivable that a proper marriage of the traditional cohesive energy algorithms with techniques derived from second quantization will yield rapid advances in explaining what keeps quasi-one-dimensional organic metals bound, and perhaps, what structural and electronic parameters confer on some of

them the unusual properties that have made them such exciting new materials for all of us.

Notes and References

1. Soos, Z. G. 1974. Ann. Rev. Phys. Chem. **25:** 121.
2. Herbstein, F. H. 1972. Crystalline pi-molecular compounds. *In* Perspectives in Structural Chemistry. J. D. Dunitz and J. A. Ibers, Eds. Vol. **4:** 166. John Wiley & Sons. New York, N.Y.; Dahm, D. J., P. Horn, G. R. Johnson, M. G. Miles, & J. D. Wilson. 1975. J. Cryst. Molec. Struct. **5:** 27.
3. Shibaeva, R. P. & L. O. Atomvyan. 1972. J. Struct. Chem. **13:** 514.
4. Shchegolev, I. F. 1972. Phys. Status Solidi **A12:** 9.
5. Garito, A. F. & A. J. Heeger. 1974. Acc. Chem. Res. **7:** 232.
6. Keller, H. J., Ed. 1977. Chemistry and Physics of One-Dimensional Metals. Proc. NATO Advanced Study Inst. Bolzano, Italy. Aug., 1976. Plenum Press. New York, N.Y.
7. Metzger, R. M. 1972. J. Chem. Phys. **57:** 1870.
8. Metzger, R. M. 1972. J. Chem. Phys. **57:** 1876.
9. Metzger, R. M. 1975. J. Chem. Phys. **63:** 5090.
10. Metzger, R. M. 1976. J. Chem. Phys. **64:** 2069.
11. Metzger, R. M. 1972. J. Chem. Phys. **57:** 2218.
12. Metzger, R. M. & A. N. Bloch. 1975. J. Chem. Phys. **63:** 5098; Bull. Am. Phys. Soc. **20:** 415.
13. Epstein, A. J., N. O. Lipari, D. J. Sandman & P. Nielsen. 1976. Phys. Rev. **B13:** 1569; 1975. Bull. Am. Phys. Soc. **20:** 465.
14. Klymenko, V. E., V. Ya. Krivnov, A. A. Ovchinnikov, I. I. Ukrainsky & A. Shvets. 1975. Sov. Phys.-JETP **42:** 123.
15. Torrance, J. B. & B. D. Silverman. 1977. Phys. Rev. **B15:** 788; 1975. Bull. Am. Phys. Soc. **20:** 498.
16. Ukrainsky, I. I., V. E. Klymenko & A. A. Ovchinnikov. 1975. Electrostatic energy and electronic structure of donor-acceptor molecular crystals based on tetracyanoquinodimethan. Preprint ITP-75-89E. Inst. Theoretical Physics. Ukrainian Acad. Sci. Kiev, USSR.
17. Metzger, R. M. Unpublished results.
18. Silverman, B. D. 1977. Incomplete charge transfer and segregated stack stability of organic donor acceptor compounds. To be published; 1977. Bull. Am. Phys. Soc. **22:** 396.
19. Metzger, R. M. 1977. J. Chem. Phys. **66:** 2525.
20. Boyd, R. H. 1963. J. Chem. Phys. **38:** 2529.
21. Sandman, D. J., A. J. Epstein & J. S. Chickos. 1976. Abst. Phys. 088, 172nd Amer. Chem. Soc. Nat. Mtg. San Francisco, Calif. Aug. 30–Sept. 3.
22. Cf. e.g. Smith, K. C., R. T. McIver, Jr., J. I. Brauman & R. W. Wallace. 1971. J. Chem. Phys. **54:** 2758.
23. Briegleb, G. 1964. Angew. Chem. (Intern. Ed.) **3:** 617.
24. Klotz, C. E., R. N. Compton & V. F. Raaen. 1974. J. Chem. Phys. **60:** 1177.
25. Haney, M. A. & J. L. Franklin. 1969. J. Chem. Phys. **50:** 2028.
26. Cf. e.g. Kittel, C. 1971. Introduction to Solid State Physics. 1971. 4th edit. John Wiley & Sons. New York, N.Y.
27. McConnell, H. M., B. M. Hoffman & R. M. Metzger. 1965. Proc. Natl. Acad. Sci. USA. **53:** 46.
28. Bloch, A. N., R. B. Weisman & C. M. Varma. 1972. Phys. Rev. Lett. **28:** 753.
29. Ewald, P. P. 1921. Ann. Phys. (Leipzig) **64:** 253.
30. Epstein, A. J. & N. O. Lipari. 1976. Phys. Lett. **56A:** 235.
31. Epstein, A. J., N. O. Lipari, P. Nielsen & D. J. Sandman. 1975. Phys. Rev. Lett. **34:** 914.
32. Evjen, E. 1932. Phys. Rev. **39:** 675.

33. SOOS, Z. G. & A. J. SILVERSTEIN. 1972. Mol. Phys. **23:** 755.
34. KOBAYASHI, H. One-dimensional disorder and the anti-phase domain structure of NH_4^+ $TCNQ^-$. Unpublished.
35. METZGER, R. M. 1972. J. Chem. Phys. **57:** 4748.
36. METZGER, R. M. 1975. Puzzles in the Madelung energy of complex TCNQ salts. Abstr. 486. Amer. Chem. Soc. SE-SW Mtg. Memphis, Tenn. October.
37. FRITCHIE, C. J. JR., & P. ARTHUR, JR. 1966. Acta. Cryst. **21:** 139.
38. KOBAYASHI, H., Y. OHASHI, F. MARUMO & Y. SAITO. 1970. Acta. Cryst. **B26:** 459.
39. POTWOROWSKI, J. A. 1974. Ph.D. Thesis, Univ. Toronto. Toronto, Canada; NYBURG, S. C. & J. A. POTWOROWSKI. To be published.
40. DOBOSH, P. A. CNINDO, CNDO and INDO Molecular Orbital Program. Quantum Chemistry Program Exchange 141, Dept. of Chemistry, Indiana University, Bloomington, Ind. 47401; POPLE, J. A. & D. L. BEVERIDGE. 1970. Approximate Molecular Orbital Theory. McGraw-Hill. New York, N.Y.
41. BUTLER, M. A., F. WUDL & Z. G. SOOS. 1975. Phys. Rev. **B12:** 4708.
42. DENOYER, F., R. COMÈS, A. F. GARITO & A. J. HEEGER. 1975. Phys. Rev. Lett. **35:** 495.
43. KAGOSHIMA, S., H. ANZAI, K. KAJIMURA & T. ISHIGORO. 1975. J. Phys. Soc. Japan. **39:** 1143.
44. SILVERMAN, B. D., W. D. GROBMAN & J. B. TORRANCE. 1977. Chem. Phys. Lett. **50:** 152.
45. LAPLACA, S. J., P. W. R. CORFIELD, R. THOMAS & B. A. SCOTT. 1975. Solid State Commun. **17:** 635.
46. SALANECK, W. R., J. W.-P. LIN & A. J. EPSTEIN. 1976. Phys. Rev. **B13:** 5574.
47. MENGEL, P., P. M. GRANT, W. E. RUDGE, B. H. SCHECHTMANN & D. E. RICE. 1975. Phys. Rev. Lett. **35:** 1803.
48. SOMOANO, R., S. P. S. YEN, A. REMBAUM & R. DECK. 1975. J. Chem. Phys. **62:** 1061; **63:** 1324.
49. ISHIZU, K., H. H. DEARMAN, M. T. HUANG & J. R. WHITE. 1969. Biochemistry. **8:** 1238.
50. COPPENS, P. 1975. Phys. Rev. Lett. **35:** 98.
51. GROBMAN, W. D., R. A. POLLAK, D. E. EASTMAN, E. T. MAAS, JR. & B. A. SCOTT. 1974. Phys. Rev. Lett. **32:** 534.
52. RITSKO, J. J., N. O. LIPARI, P. C. GIBBONS & S. E. SCHNATTERLY. 1970. Phys. Rev. Lett. **37:** 1068.
53. SWINGLE, R. S., R. P. GROFF & B. M. MONROE. 1975. Phys. Rev. Lett. **35:** 452.
54. GROBMAN, W. D. & B. D. SILVERMAN. 1976. Solid State Commun. **19:** 319.
55. LADIK, J., A. KARPFEN, G. STOLLHOFF & P. FULDE. 1975. Chem. Physics. **7:** 267.
56. CHANG, J.-J., S. JAFAREY & D. J. SCALAPINO. 1976. J. Chem. Phys. **65:** 505.
57. CHANG, J.-J., S. JAFAREY & D. J. SCALAPINO. 1975. Phys. Rev. **B12:** 5560.
58. BERGMAN, D. J., T. M. RICE & P. A. LEE. 1977. Phys. Rev. **B15:** 1706.
59. LEE, P. A., T. M. RICE & R. A. KLEMM. 1977. Phys. Rev. **B15:** 2984.
60. TORRANCE, J. B. 1977. The role of Coulomb interactions in TTF TCNQ. *In* Chemistry and Physics of One-Dimensional Metals. H. J. Keller, Ed. Proc. NATO Advanced Study Inst. Bolzano, Italy. Aug., 1976. Plenum Press. New York, N.Y.
61. POPLE, J. A., J. W. MCIVER, JR. & N. S. OSTLUND. 1968. J. Chem. Phys. **49:** 2960.
62. POPLE, J. A., J. W. MCIVER, JR. & N. S. OSTLUND. 1968. J. Chem. Phys. **49:** 2965.
63. HUSH, N. S. & M. L. WILLIAMS. 1970. Chem. Phys. Lett. **6:** 163.
64. HUSH, N. S. & M. L. WILLIAMS. 1970. Chem. Phys. Lett. **5:** 507.
65. DAVIES, D. W. 1969. Mol. Phys. **17:** 473.
66. TEIXEIRA-DIAS, J. J. C. & P. J. SARRE. 1975. J. Chem. Soc. Faraday Trans. **II:** 906.
67. MEYER, H. & A. SCHWEIG. 1973. Theor. Chim. Acta. **29:** 375.
68. BUSH, R. L. Dielectric function for a disordered one-dimensional conductor. Phys. Rev. To be published.

Discussion of the Paper

Aaron Bloch *(Johns Hopkins Univ., Baltimore, Md.):* In the Born-Haber cycle there is a subtle problem when one is dealing with a fractional charge transfer. You are comparing the energy of a crystal with the energy of some kind of partially ionized gas, and the gas you have chosen is a mixed gas of neutrals and ions corresponding to the correct degree of charge transfer. In comparing that with a Madelung energy, you are assuming that the cost of ionizing the lattice for charge transfer 0.6, say, is six-tenths of the ionization potential of the individual molecule. It is not clear that the internal energy of a molecule with six tenths of a charge on it is six tenths of the energy of a fully charged ion. These differences can be very substantial.

Metzger: I agree. They may be of the order 2–3 eV.

B. David Silverman *(IBM, Yorktown Heights, N.Y.):* For the few incompletely charge-transferred 1:1 segregated stack compounds, the calculated Madelung energy at full charge transfer is apparently less than the cost of ionizing the individual molecules. Perhaps one could use this as a simple criterion for incomplete charge transfer in the 1:1 salts. We have recently shown such a rule to work for HMTTF TCNQ.

Epstein *(Xerox Webster Research Center, Rochester, N.Y.):* There is equally as good evidence from inelastic electron scattering (which is a bulk measurement) of the nitrogen 1s level in TTF TCNQ to indicate that there is only a single kind of nitrogen in the material, and hence you do not have a Wigner crystal. Also, with regard to which class of these organic salts do not contribute sufficient Madelung energy to the binding, I suggest it is those where both the donor and acceptor are large planar molecules, rather than the organic metals. In this case, you cannot get a close enough approach to get a sufficient Madelung energy to overcome the $I_D - E_A$.

Metzger: It is true that if you have segregated stacks comprised of large molecules, the coordination around an ion can be very poor in terms of Madelung forces.

ELECTRON INTERACTIONS WITH MOLECULAR VIBRATIONS: THEIR NATURE AND CONSEQUENCES*

C.B. Duke

Xerox Webster Research Center
Xerox Square-114
Rochester, New York 14644

INTRODUCTION

Although a decade ago electron interactions with intramolecular vibrations were widely regarded as the main limitation on the (room temperature) mobility of insulating (e.g., van der Waals) molecular solids,[1,2] it recently has become evident[3,4] that lower energy acoustical and/or librational modes, $\hbar\omega \leq \kappa T$, are responsible for this phenomenon. Simultaneously, models of the static[5,6] and dynamic[7,8] conductivity, as well as the charge-density-wave ground state[9-11] of quasi-one-dimensional organic charge-transfer complexes and radical ion salts, have been proposed in which the electronic interactions with intramolecular vibrations dominate the observed phenomena. In this paper we present a brief synopsis of several recent studies[2,12-17] of electron interactions with molecular vibrations in larger planar organic molecules. In particular, we emphasize the consequences of these studies for the interpretation both of gas-phase photoemission and UV absorption spectra and of the transport and "optical" (including infrared) properties of organic solids embodying such molecules. The electron-intramolecular-vibration interactions constitute one of the major features of organic "metals" and semiconductors which are characteristic of the organic solid state, are absent in conventional covalent and metallic solids, and are a dominant influence on the transport, optical, and charge-density-wave ground-state properties of segregated-stack linear chain organic solids. Consequently, a detailed analysis of these interactions is a necessary prerequisite for constructing a quantitative theoretical description of the electronic structure of organic materials, including polymers.[4,18,19]

We proceed by first reviewing in the next section the basic features of the linear-coupling model. The sections EMPIRICAL ANALYSES and MICROSCOPIC ANALYSES are devoted to brief surveys of its empirical and microscopic applications, respectively. In SOLID-STATE CONSEQUENCES we indicate the consequences of the model results for analyses of the electronic properties of organic solids.

LINEAR COUPLING MODEL

In principle, an analysis of photoemission spectra and the properties of charge-transfer and radical ion salts requires the explicit evaluation of the electronic

*Manuscript received Sept. 16, 1977.

0077-8923/78/0313-0166 $1.75/1 © 1978, NYAS

structure of molecular ion states. In the case of rigid planar molecules like the polyacenes, however, a simpler one-electron molecular orbital model suffices because the neutral molecule and molecular ion exhibit the same symmetry.[2,12,13] In this model, sometimes referred to as the "Principal Model" in the Soviet literature,[20] the ion state is described in a one-electron approximation so that the linear electron-vibration coupling of an anion (cation) is that characteristic of the extra occupied (empty) orbital of the neutral molecule. Whereas changes in the normal mode frequencies rigorously must be neglected[20] in the Principal Model, it is a simple matter to include them in model calculations, and this inclusion has been made in most of the analyses considered below.

Two types of linear coupling between the electronic and intramolecular vibrational degrees of freedom occur: diagonal and off diagonal. The off-diagonal terms are those which mix different molecular orbitals, most importantly those of different symmetries. Consequently, the terms of interest are associated with nontotally-symmetric (n.t.s.) modes of the molecule and cause the Herzberg-Teller effect (the rendering of forbidden transitions allowed by virtue of the coupling of the transition state to one or more n.t.s. modes[21]). Recent calculations reveal that after years of controversy, a consideration of these off-diagonal linear coupling terms yields a quantitative description of the $\pi \rightarrow \pi^*$ transitions in gaseous benzene[22,23] *provided* adequate models of the molecular vibration normal modes and of the molecular orbitals of benzene are utilized. Since the off-diagonal terms rarely play a major role in solid-state charge or exciton transport, however, we do not consider them further here.

Our interest resides in the diagonal linear electron interactions with intramolecular vibrations. These interactions result from the modulation of the molecular orbital eigenvalues (or transition state energies) by intramolecular vibrational normal modes. The terms linear in the normal mode coordinates must be associated with totally symmetric (t.s.) vibrations for nondegenerate electronic states,[2] although more complex linear couplings involving certain n.t.s. vibrations occur for degenerate electronic states.[13] This result emerges naturally from group theoretic symmetry arguments.[2,13] It is obvious physically for the Principal Model, because the linear coupling of an electronic state to a n.t.s. mode leads to a change in the symmetry of the molecule in that state: an effect which the Principal Model neglects by construction.[20]

Stated mathematically, the linear electron-intramolecular-vibration coupling constants, $\{g_{\gamma,i}\}$, for a molecular orbital labeled by γ are defined by expanding the orbital eigenvalues, E_γ, in terms of dimensionless vibrational normal mode coordinates, i.e.:

$$E_\gamma(\{Q_i\}) = E_\gamma(\{0\}) + \sum_i \left(\frac{\delta E_\gamma}{\partial Q_i}\right)_0 Q_i + \sum_{i,j} \left(\frac{\delta^2 E_\gamma}{\delta Q_i \delta Q_j}\right)_0 \frac{Q_i Q_j}{2} + \cdots \qquad (1)$$

The normal coordinates Q_i are related to the lattice displacement vectors $\mathbf{u}_n = \mathbf{r}_n - \mathbf{r}_n^{(0)}$ by well-known relationships.[24] The linear terms in Q_i in (1) correspond to the linear electron-intramolecular-vibration interactions. The corresponding coupling constants are defined by writing (1) in second-quantized form[2,13]

$$H = \sum_{\gamma} E_{\gamma}(0) C_{\gamma}^{+} C_{\gamma} + \sum_{i} \hbar\omega_i \left(b_i^{\dagger} b_i + \frac{1}{2} \right) + \sum_{i,\gamma} g_{\gamma i} \hbar\omega_i C_{\gamma}^{\dagger} C_{\gamma} (b_i^{\dagger} + b_i) \tag{2}$$

in which i denotes the vibrational quantum modes, $C_{\gamma}^{\dagger}$ and $b_i^{\dagger}$ are the creation operators associated with the electronic orbital and vibration quanta of energies E_{γ} and $\hbar\omega_i$, respectively. The $\{g_{\gamma i}\}$ are the desired dimensionless linear electron-intramolecular-vibration coupling constants given by

$$g_{\gamma i} = \frac{1}{\sqrt{2}\hbar\omega_i} \left(\frac{\delta E_{\gamma}}{\delta Q_i} \right)_0 . \tag{3}$$

An important property of Hamiltonian (2) is that it can be solved exactly,[2] thereby providing a simple analytical form for the intensity distribution in the vibrational structure associated with transitions between eigenstates of the Hamiltonian (2). In addition, the lowering in energy of a given orbital γ due to its interaction with the molecular vibrations, often referred to as "polaron binding energy," is given by[2,13]

$$\Delta E_{\gamma} = \sum_{i} g_{\gamma i}^{2} (\hbar\omega_i). \tag{4}$$

Two qualitatively different approaches may be taken to evaluate the coupling constants $\{g_{\gamma i}\}$. In the empirical approach[2,8,12–14,20,25,26] they are obtained by fitting observed photoemission, absorption, and fluorescence spectra, using the $\{g_{\gamma i}\}$ as adjustable parameters. In the microscopic approach[2,12,13,15–17,25–31] they are evaluated by a molecular orbital model for the $E_{\gamma}(\{Q_i\})$ and a force-field model for the $\{Q_i\}$. We consider each of these in turn in the following two sections.

Empirical Analyses

If a perturbation V (e.g. a light wave) induces a transition between two electronic states, each of which is described by (2), then neglecting thermally stimulated vibrations that transition probability between these states is given in closed form by[2]

$$P_{\gamma'\gamma}(E) = \frac{2\pi}{h} \left| <\gamma' \mid V \mid \gamma> \right|^2 \exp\left(-\sum_{i} S_{\gamma'\gamma}(i) \right) \rho_{\gamma'\gamma}(E), \tag{5a}$$

$$S_{\gamma'\gamma}(i) = (g_{\gamma' i} - g_{\gamma i})^2, \tag{5b}$$

$$\rho_{\gamma'\gamma}(E) = \sum_{k_1,\ldots k_n=0}^{\infty} \frac{\Gamma}{\sqrt{\pi}} \exp\left(\frac{\left(E - E_{\gamma} + E_{\gamma'} - \sum_{i} k_i \hbar\omega_i \right)^2}{\Gamma^2} \right) \times \prod_{i} \frac{[S_{\gamma'\gamma}(i)]^2}{k_i!}, \tag{5c}$$

$$E_\gamma = \epsilon_\gamma - \sum_i g_{\gamma i}{}^2 \hbar\omega_i, \tag{5d}$$

in which we have taken the zero-vibration spectral density to be a Gaussian of width Γ (associated, e.g., with instrumental resolution). By treating the $\{g_{\gamma i}\}$ and $\{\omega_i\}$ as adjustable parameters, these quantities may be determined from measured photoemission,[2,12-14,25] UV absorption,[2,13,20,26] or fluorescence[20] spectra. In the case of radical ion salts, the $\{g_{\gamma i}\}$ also can be obtained by an analogous analysis of IR spectra for either charge-density-wave[8] or dimer[32] ground-state geometries of segregated-stack organic linear chain solids.

Detailed analyses of the intensities of photoemission spectra, using (5), have been given for benzene,[2,12,13] deuterobenzene,[12,13] and the fluorobenzenes.[14] Equivalent analyses of UV absorption spectra have been given through the years for benzene,[2,13,20,33] naphthalene,[33] anthracene,[33] diphenylhexatriene,[20] N_2,[26] CO,[26] and a variety of organic dyes.[20] In some of these studies the UV spectra of molecules in solution or embedded in solid state matrices were examined, so that the quoted values of $\{g_{\gamma i}\}$ may not coincide exactly with those extracted from gas-phase studies. Tables of empirical values of $\{g_{\gamma i}\}$ are given by Lipari *et al.*,[13] Sheka,[26] Frank-Kamenetskii and Lukashin,[20] and by Cederbaum and Domcke.[26]

Microscopic Analyses

While it may appear simple and attractive to extract the $\{g_{\gamma i}\}$ directly from experimental spectra, microscopic evaluations of these quantities are desirable for several reasons. First, they afford considerable insight into the physical origin of the electron-vibration coupling constants in terms of molecular wave functions and vibrational normal-mode coordinates. From such insight one can usefully estimate the $\{g_{\gamma i}\}$ for complex molecules in the absence of detailed (and expensive) computations. Second, the successful description of vibronic fine structure is an important confirmation of the validity of microscopic models of molecular electronic structure. Third, the $\{g_{\gamma i}\}$ required for solid-state applications are not always accessible to direct empirical determination. For example, the coupling constants for $TCNQ^-$ in TCNQ charge-transfer salts cannot be inferred directly from the gas-phase photoemission or optical spectra of TCNQ. They either must be calculated via the intermediary of molecular orbital and normal-mode force-field models[15,16] or must be obtained from IR spectra of segregated-stack linear chain TCNQ salts via the intermediary of further microscopic models of these spectra.[7,32] Finally, the resolution of experimental UV or photoemission spectra may well be inadequate to extract a unique set of $\{g_{\gamma i}\}$ from the deconvolution of the spectra using (5). This situation occurs, for example, for photoemission from both TTF[16] and TCNQ,[15,16] and renders a microscopic model necessary *a priori* to interpret vibronic phenomenon even for gas-phase spectra.

Two microscopic procedures have been developed in recent years to evaluate the $\{g_{\gamma i}\}$. Historically the first is the Green's function *ab initio* method of Cederbaum and coworkers,[27,31] which uses Hartree Fock molecular orbitals as the input electronic structure information in a calculation of the one electron spectral

density that can be improved by well-known[34] many-body diagrammatic summations as the need arises. This method has been applied with considerable success to water,[25] formaldehyde,[26,28] dideuteroformaldehyde,[26] N_2,[26,27] CO,[26,27] cyanogen,[29] and benzene.[30] The second procedure[2,13] is the utilization of a spectroscopically parameterized CNDO molecular orbital model in concert with spectroscopically tested molecular-vibration force-field models to evaluate directly the $(\delta E_\gamma/\delta Q_i)_0$ in (1) and (3). This method is less expensive to apply than the Green's Function method and hence is better suited for the study of complex molecules. It has been applied successfully to benzene,[2,12,13] deuterobenzene,[12,13] TCNQ,[15,16] and TTF.[16] Both methods give comparable descriptions of the electron-vibration coupling in the $e_{1g}(\pi)$ and $a_{2u}(\pi)$ states of $C_6H_6^+$: the only cases in which they both have been applied.[2,12,13,30]

In order to illustrate the nature of the insight afforded by the microscopic models into the physical origin of the $\{g_{\gamma i}\}$, we consider briefly the cases of TTF and TCNQ, since we shall utilize these results in the following section. The molecular orbital model employed is the CNDO/S3 model[35–37] and the vibrational

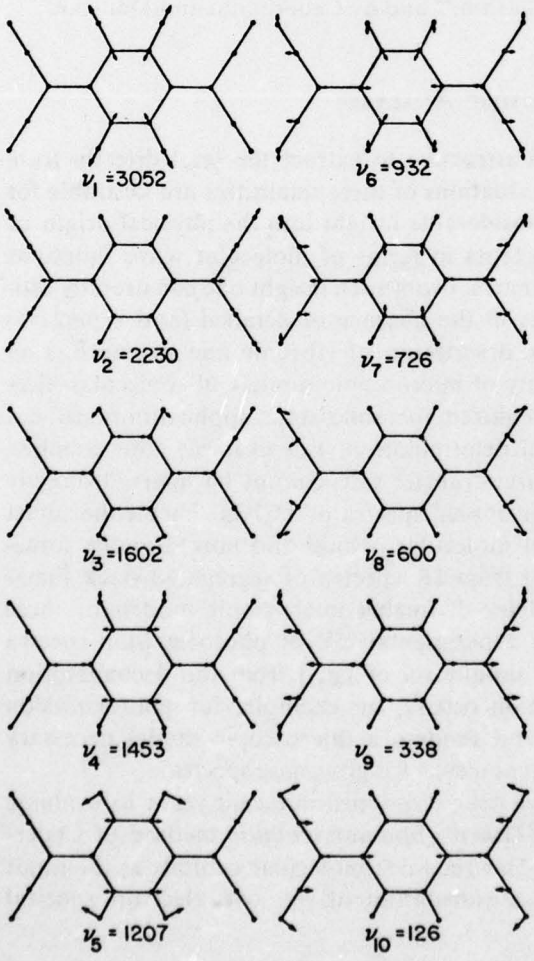


FIGURE 1. Schematic diagram of the normal mode amplitudes for the ten a_g symmetry vibrations of TCNQ.

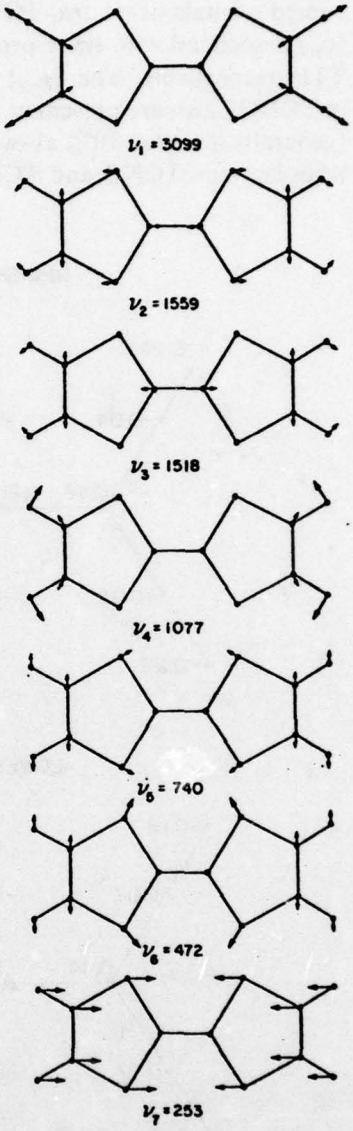


FIGURE 2. Schematic diagram of the normal mode amplitudes for the seven a_g symmetry vibrations of TTF.

normal modes are described using a modified valence force field model.[38] The detailed description of the calculations and results is given elsewhere.[15,16]

The points of interpretation we wish to emphasize are that the electron-intramolecular-vibration coupling constants depend sensitively on the wave function of the molecular orbital (or exciton state) being considered (i.e., *not* on the total charge density), and that this sensitivity can be understood easily by inspection of these wave functions and the normal mode coordinates of the intramolecular vibrations. To illustrate these concepts we indicate the normal mode coordinates for the a_g (i.e., t.s.) modes in TCNQ and TTF in FIGURES 1 and 2, respectively. In FIGURES 3 and 4 we show the highest energy occupied and lowest energy unoc-

cupied orbitals of neutral TCNQ and TTF, respectively. Finally, the calculated[16] $\{g_{\gamma i}\}$ associated with these orbitals are given in TABLES 1 and 2 for TCNQ and TTF, respectively. The $\{g_{\gamma i}\}$ associated with the extra occupied $[b_{2g}(\pi)]$ orbital in $TCNQ^-$ also are presented in TABLE I in order to display the generally modest (generally less than 10%, always less than 45%) shifts in the values of these quantities between TCNQ and $TCNQ^-$. The former is, of course, appropriate for our

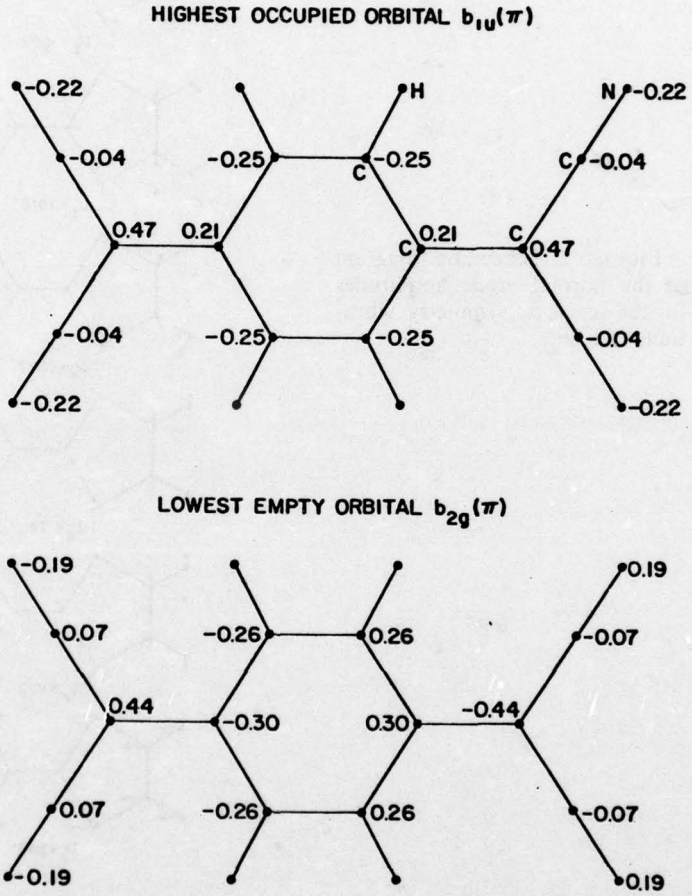


FIGURE 3. The highest occupied molecular orbital, $b_{1u}(\pi)$, and the lowest empty orbital, $b_{2g}(\pi)$, of TCNQ. The coefficients in the expansion of the molecular orbitals in terms of the atomic p_z Slater-type orbitals are indicated.

considerations herein, because the other orbitals relax[13] when the $b_{2g}(\pi)$ orbital is occupied to form $TCNQ^-$. Stated in physical terms, it is the *change* in charge density between the neutral and ionic state that determines the electron-intramolecular-vibration coupling associated with the transition between these two states. In the CNDO/S3 semiempirical formalism, this change happens to be described (by construction) by the orbital which is empited or filled during the

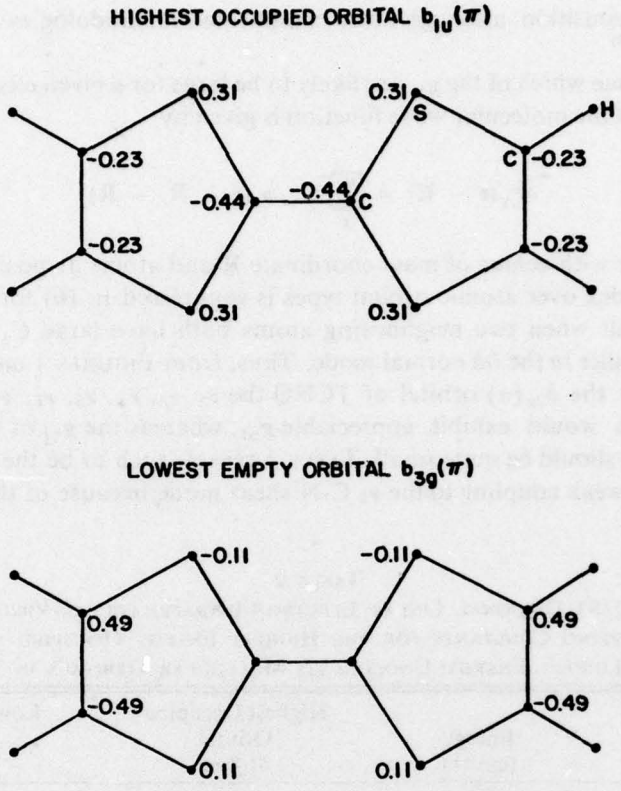


FIGURE 4. The highest occupied molecular orbital, $b_{1u}(\pi)$, and the lowest empty orbital, $b_{3g}(\pi)$, of TTF. The coefficients in the expansion of the molecular orbitals in terms of the atomic p_z Slater-type orbitals are indicated.

TABLE 1

CNDO/S3 DIAGONAL LINEAR ELECTRON-INTRAMOLECULAR VIBRATION COUPLING CONSTANTS FOR THE HIGHEST ENERGY OCCUPIED AND LOWEST ENERGY UNOCCUPIED ORBITAL IN TCNQ*

Vibration	Energy (cm^{-1})	Highest Occupied Orbital $b_{1u}(\pi)$	Lowest Empty Orbital $b_{2g}(\pi)$	$b_{2g}(\pi)$ Orbital of $TCNQ^-$
ν_1	3048	0.0	0.01	0.01
ν_2	2229	0.05	0.19	0.20
ν_3	1602	0.03	0.66	0.71
ν_4	1454	0.23	0.27	0.21
ν_5	1207	0.16	0.19	0.18
ν_6	948	0.12	0.25	0.17
ν_7	711	0.27	0.37	0.21
ν_8	602	0.09	0.03	0.03
ν_9	334	0.19	0.58	0.70
ν_{10}	144	0.01	0.49	0.90

*For comparison, those associated with the highest occupied (i.e., $b_{2g}(\pi)$) orbital in $TCNQ^-$ are also given.

course of the transition, although more complicated methodologies for its estimation exist.[17,27,31]

To determine which of the $g_{\gamma i}$ are likely to be large for a given electronic orbital γ, we note that the molecular wave function is given by

$$\Psi_\gamma(\mathbf{r} - \mathbf{R}) = \sum_t C_{\gamma t}\phi_t(\mathbf{r} - \mathbf{R}_t - \mathbf{R}) \qquad (6)$$

for a molecule with center of mass coordinate **R** and atoms at positions $\mathbf{R}_t$. The summation index over atomic orbital types is suppressed in (6) for convenience. Large $g_{\gamma i}$ result when two neighboring atoms both have large $C_{\gamma t}$ and vibrate against each other in the *ith* normal mode. Thus, from FIGURES 1 and 3 we would expect that for the $b_{2g}(\pi)$ orbital of TCNQ the ν_2, ν_3, ν_4, ν_5, ν_6, ν_7, ν_9, and ν_{10} normal modes would exhibit appreciable $g_{\gamma i}$, whereas the $g_{\gamma i}$ of the ν_1 and ν_8 normal modes should be quite small. TABLE 1 reveals such to be the case. Note in particular the weak coupling to the ν_9 C-N shear mode because of the small value

TABLE 2
CNDO/S3 DIAGONAL LINEAR ELECTRON-INTRAMOLECULAR-VIBRATION COUPLING CONSTANTS FOR THE HIGHEST ENERGY OCCUPIED AND THE LOWEST ENERGY UNOCCUPIED MOLECULAR ORBITALS IN TTF

Vibration	Energy (cm^{-1})	Highest Occupied Orbital $b_{1u}(\pi)$	Lowest Empty Orbital $b_{3g}(\pi)$
ν_1	3083	0.03	0.04
ν_2	1555	0.23	0.37
ν_3	1518	0.62	0.38
ν_4	1094	0.16	0.36
ν_5	736	0.49	0.29
ν_6	475	1.33	0.23
ν_7	245	0.16	0.03

of $C_{\gamma t}$ on the cyanocarbon species for the $b_{2g}(\pi)$ orbital. The small values of these $C_{\gamma t}$ render the coupling to the ν_2 C-N stretch modes appreciable only because of the out-of-phase vibration between the neighboring carbon atoms, as well. Therefore, simple arguments in the literature[10,17,39] involing C-N stretch modes as a major source of electron-vibration coupling for the extra electron on $TCNQ^-$ are seriously in error.

Analogous considerations may be constructed from FIGURES 2 and 4 for the $b_{1u}(\pi)$ orbital characteristic of holes on $TTF.^+$ The large $C_{\gamma t}$ for the central two carbons suggests that ν_3 is strongly coupled to the $b_{1u}(\pi)$ orbital. The large values of the $C_{\gamma t}$ for the other eight carbon species as well indicate that ν_5 and ν_6 also should exhibit strong coupling. These expectations are indeed borne out by TABLE 2. Conversely, the nodes on the central carbons in the $b_{3g}(\pi)$ orbital reveal that the coupling of ν_3 and ν_7 should be greatly diminished for this orbital relative to the $b_{1u}(\pi)$ orbital. Again, this result is documented handsomely by TABLE 2. Similarily, the larger values of the $C_{\gamma t}$ for the four end carbons in the $b_{3g}(\pi)$

relative to the $b_{1u}(\pi)$ orbital lead to its greater coupling to the ν_2 and ν_4 vibrations.

These two examples of TCNQ and TTF valence electron orbitals do, therefore, display clearly our major conclusions from this section. First, the $\{g_{\gamma i}\}$ are indeed sensitive functions of orbital (or exciton) wave functions rather than total charge densities. Second, if the $\Psi\gamma(\mathbf{r})$ and normal mode coordinates are known even qualitatively, physical estimates of the $\{g_{\gamma i}\}$ can be obtained almost by inspection. Third, the numerous low-frequency a_g molecular vibrations in TTF and TCNQ lead to broad, relatively featureless vibrational progressions, which, however, are in satisfactory accord with the CNDO/S3 model predictions.[15] Therefore for these molecules, a microscopic analysis is a necessity, not a luxury, in analyzing vibronic fine structure in gas-phase photoemission and absorption spectra. Fourth and finally, a quantitative microscopic analysis is required to estimate the $\{g_{\gamma i}\}$ on such cases, since simple arguments based on chemical bonding concepts[10,17,39] failed to provide even a semiquantitative estimate of these quantities in the case of TCNQ.[15,16]

Solid-State Consequences

The Hamiltonian describing diagonal linear electron-intramolecular-vibrations in the solid state is obtained by summing the linear coupling term in (2) over all the molecular sites, **R**, in the solid. Furthermore, for nonoverlapping tight binding bands the Bloch states are given by

$$\Psi_{\mathbf{k}\gamma}(\mathbf{r}) = \sum_{\mathbf{R}} \frac{\exp(i\mathbf{k}\cdot\mathbf{R})}{\sqrt{N}} \Psi_\gamma(\mathbf{r} - \mathbf{R}) \tag{7}$$

in which $\Psi_\gamma(\mathbf{r} - \mathbf{R})$ is specified by (6). A similar expansion relates the crystal phonons built from intramolecular normal modes to the molecular normal mode coordinates $\{Q_i\}$. Allowing for some purely electronic mixing of the $E_\gamma(0)$ eigenvalues and lattice dynamic mixing of the ω_i eigenvalues leads to the solid-state Hamiltonian[9]

$$H = \sum_{\mathbf{k},\gamma} \epsilon_\gamma(\mathbf{k}) C_{\mathbf{k}\gamma}^\dagger C_{\mathbf{k}\gamma} + \sum_{\mathbf{k},i} \hbar\omega_i(\mathbf{k}) \left[b_{ki}^\dagger b_{\mathbf{k}i} + \frac{1}{2} \right]$$
$$+ N^{-1/2} \sum_{\gamma,i} g_{\gamma i} \hbar\omega_i \sum_{\mathbf{k},\mathbf{q}} C_{\mathbf{k}-\mathbf{q}\gamma}^\dagger C_{\mathbf{k}\gamma} (b_{qi}^\dagger + b_{-qi}). \tag{8}$$

Equation 8 reveals that the $\{g_{\gamma i}\}$ obtained from molecular spectroscopy are precisely those which occur in a tight-binding model of the solid state energy bands. Consequently, our considerations of the preceeding three sections are directly applicable to the description of solid-state properties. A similar Hamiltonian continues to describe the solid even when the occurrence of strong intramolecular Coulomb repulsions for doubly occupied orbitals is incorporated into the model.[40]

A complete treatment of solid-state properties incorporating the consequences

both of coupling to intramolecular vibrations and of intramolecular Coulomb interactions has not yet been reported. One-electron band model analyses, based on (8) and the $\{g_{\gamma i}\}$ for TCNQ, of the dc transport properties of segregated-stack linear-chain salts of *N*-methylphenazinium,[5] quinolinium,[6] acridinium,[6] acridizinium,[6] and TTF[41] have been given, however, in which the strong temperature dependence of the mobility caused by electron scattering from the low-frequency molecular vibrations suffices to describe quite adequately dc conductivity (and thermopower) data. The "anomolous" ac conductivity in the infrared of a charge-density-wave TCNQ salt, (triethyl ammonium) $(TCNQ)_2$, has been interpreted successfully utilizing (8).[8] Moreover, an elegant analysis of the anomolous IR activity of K(TCNQ) has been based on a generalization of (8) to include explicitly the consequences of both intra- and intermolecular Coulomb interactions for the electronic states of the TCNQ dimers characteristic of this material.[32] The output of this analysis is a set of $\{g_{\gamma i}\}$ and $\{\omega_i\}$ that are extracted from a model fit to the IR reflectivity. These agree with the calculated values[15,16] to within the uncertainties inherent in the two analysis.

We conclude from these examinations of the ac and dc conductivity of segregated stack linear chain materials that for these materials electron interactions with intramolecular vibrations play a dominant role in determining the electronic transport properties. These interactions also may play a dominant role in determining vibration-assisted tunneling through adsorbed TCNQ complexes,[42] an important phenomenon for developing a quantitative understanding of the resonant tunneling mechanism[43] of this process.

Turning finally to the issue of molecular engineering to achieve higher conductivity quasi-one-dimensional organic metals, we note at the outset that different criteria apply in the cases of one-electron band models[5,6,41] and charge-density-wave (CDW) models.[7-9,39] In the former case, mobility enhancements may arise either from reducing the $\{g_{\gamma i}\}$ for the low-frequency intramolecular modes, i.e., those for which

$$\hbar\omega_i < W \tag{9}$$

in which W designates the one-electron bandwidth, or from adjusting both the $\hbar\omega_i$ and the bandwidth so that fewer vibrations satisfy inequality (9). In the CDW case, however, it is a measure of electronic coupling to *all* the intramolecular modes; i.e.,[9]

$$\lambda = N(E_F) \sum_i g_{\gamma i}^2/\hbar\omega_i, \tag{10}$$

which should be minimized to reduce the tendency toward CDW instability. The quantity $N(E_F)$ is the density of one-electron states at the one-electron Fermi energy that would have existed in the absence of the CDW instability.

The central question for molecular engineering, however, is the extent to which the respectably complicated microscopic models described above are able to provide useful insight into the *a priori* identification of new materials exhibiting some desirable property like metallic conductivity. Given the fact that quantitative molecular orbital and valence force field models are required for adequate microscopic analyses, it seems unlikely that such analyses will prove broadly useful for

new materials identification. Moreover, there remains considerable uncertainty concerning the details of the interplay between the one-electron hopping integrals (i.e., bandwidths), the electron-vibration interactions, and the Coulomb interactions in determining the physical properties of organic solids. These considerations do not lead to optimism about the near-term success of efforts at the quantitative molecular engineering of new materials properties, although empirical materials screening criteria are both available and helpful. Such criteria dealing with the electron-molecular-vibration interaction have been proposed by Perlstein *et al.*[44] It is evident both from their work and from the foregoing microscopic considerations that in the segregated-stack systems, high conductivity is enhanced by low electron-molecular-vibration coupling, which, in turn, is achieved by using relatively rigid molecules. The empirical criteria of Perlstein *et al.*, are guidelines for the selection of suitably rigid molecules (specifically, molecules for which the neutral molecule and the radical ions exhibit the same symmetry). They do not, however, address the important issue of trade-offs between the electron-vibration interactions and the other physical phenomena involved in obtaining high mobility and high conductivity in organic solids.

We conclude, therefore, that electron interactions with molecular vibrations play a central role in limiting the mobility of segregated-stack linear-chain organic solids. They also probably are involved in the structural changes thought to be associated with charge-density waves in some of these materials. The microscopic understanding of the nature and origin of electron-molecular-vibration interactions is highly developed for certain molecules, most notably benzene, TTF, and TCNQ. Some of this understanding has been applied rather successfully in analyses of transport in segregated-stack linear-chain materials based on TCNQ. It seems improbable, however, that the empirical or microscopic models considered above of electron-molecular-vibration interactions will prove broadly useful in the near future for the quantitative *a priori* molecular engineering of organic metals with prescribed transport properties.

Acknowledgments

The author is indebted to E.M. Conwell, A.J. Epstein, J.S. Miller, J. Perlstein, and M.J. Rice for numerous informative discussions, to W.H.H. Gunther, M.J. Rice, and R. Bigelow for helpful comments on this manuscript, and to L.J. Kennedy for assistance.

References

1. Munn, R. W. & W. Siebrand. 1970. J. Chem. Phys. **52:** 71; **52:** 6391.
2. Duke, C. B., N. O. Lipari & L. Pietronero. 1975. Chem. Phys. Lett. **30:** 415.
3. Schein, L. B. 1977. Chem. Phys. Lett. **48:** 571.
4. Duke, C. B. 1977. Surface Science **70:** 674.
5. Epstein, A. J., E. M. Conwell, D. J. Sandman & J. S. Miller. 1977. Solid State Commun. **23:** 355.
6. Epstein, A. J. & E. M. Conwell. 1977. Solid State Commun. **24:** 627.
tion.

7. RICE, M. J. 1976. Phys. Rev. Lett. **37:** 36.
8. RICE, M. J., L. PIETRONERO & P. BRÜESCH. 1977. Solid State Commun. **21:** 757.
9. RICE, M. J., C. B. DUKE & N. O. LIPARI. 1975. Solid State Commun. **17:** 1089.
10. CARNEIRO, K. 1976. Phys. Rev. Lett. **37:** 1227.
11. RICE, M. J. & N. O. LIPARI. 1977. Phys. Rev. Lett. **38:** 437.
12. DUKE, C. B. & N. O. LIPARI. 1975. Chem. Phys. Lett. **36:** 51.
13. LIPARI, N. O., C. B. DUKE & L. PIETRONERO. 1976. J. Chem. Phys. **65:** 1165.
14. DUKE, C. B., K. L. YIP, G. P. CEASAR, A. W. POTTS & D. G. STREETS. 1977. J. Chem. Phys. **66:** 256.
15. LIPARI, N. O., C. B. DUKE, R. BOZIO, A. GIRLANDO, C. PECILE & A. PADVA. 1976. Chem. Phys. Lett. **44:** 236.
16. LIPARI, N. O., M. J. RICE, C. B. DUKE, R. BOZIO, A. GIRLANDO & C. PECILE. 1977. Int. J. Quant. Chem. **11:** 583.
17. KROGH-JESPERSEN, K. & M. A. RATNER. 1976. Chem. Phys. Lett. **39:** 123.
18. DUKE, C. B. & T. J. FABISH. 1976. Phys. Rev. Lett. **37:** 1075.
19. DUKE, C. B., T. J. FABISH & A. PATON. 1977. Chem. Phys. Lett. **49:** 133.
20. FRANK-KAMENETSKII, M. D. & A. V. LUKASHIN. 1975. Usp. Fiz. Nauk. **116:** 193 (Eng. Trans. Sov. Phys. Usp. **18:** 391).
21. HERZBERG, C. & E. TELLER. 1933. Zeit. Phys. Chem. Abt. **B21:** 410.
22. ROCHE, M. & H. H. JAFFÉ. 1974. J. Chem. Phys. **60:** 1193.
23. ZIEGLER, L. & A. C. ALBRECHT. 1974. J. Chem. Phys. **60:** 3558.
24. VARSÁNYI, G. 1969. Vibrational Spectra of Benzene Derivatives. Academic Press. New York, N.Y.
25. CEDERBRAM, L. S. & W. DOMCKE. 1974. Chem. Phys. Lett. **25:** 357.
26. CEDERBAUM, L. S. & W. DOMCKE. 1976. J. Chem. Phys. **64:** 612.
27. CEDERBAUM, L. S. & W. DOMCKE. 1974. J. Chem. Phys. **60:** 2878.
28. CEDERBAUM, L. S., W. DOMCKE & W. VON NIESSEN. 1975. Chem. Phys. Lett. **34:** 60.
29. CEDERBAUM, L. S., W. DOMCKE & W. VON NIESSEN. 1975. Chem. Phys. **10:** 459.
30. VON NIESSEN, W., L. S. CEDERBAUM & W. P. KRAEMER. 1976. J. Chem. Phys. **65:** 1378.
31. CEDERBAUM, L. S. & W. DOMCKE. 1976. J. Chem. Phys. **64:** 603.
32. RICE, M. J., N. O. LIPARI & S. STRÄSSLER. 1977. Phys. Rev. Lett. **39:** 1359.
33. SHEKA, E. F. 1971. Usp. Fiz. Nauk. **104:** 593 (Eng. Trans. Sov. Phys. Usp. **14:** 484).
34. ABRIKOSOV, A. A., L. P. GORKOV & I. E. DZYALOSHINSHI. 1963. Methods of Quantum Field Theory in Statistical Physics. Prentice Hall Inc. Englewood Cliffs, N.J.
35. LIPARI, N. O. & C. B. DUKE. 1975. J. Chem. Phys. **63:** 1748, **63:** 1768.
36. DUKE, C. B., N. O. LIPARI, W. R. SALANECK & L. B. SCHEIN. 1975. J. Chem. Phys. **63:** 1758.
37. YIP, K. L., C. B. DUKE, W. R. SALANECK, E. W. PLUMMER & G. LOUBRIEL. 1977. Chem. Phys. Lett. **49:** 530.
38. BOZIO, R. A. GIRLANDO & C. PECILE. 1975. J. Chem. Soc. Farad. Trans. II: 1237.
39. GUTFREUND, H., B. HOROVITZ & M. WEGER. 1974. J. Phys. C: Solid State Phys. **7:** 383.
40. RICE, M. J. 1977. Phys. Rev. Submitted for publication.
41. CONWELL, E. M. 1977. Phys. Rev. Lett. Submitted for publication.
42. KORMAN, C. S. & R. V. COLEMAN. 1977. Phys. Rev. B **15:** 1877.
43. DUKE, C. B. & M. E. ALFERIEFF. 1967. J. Chem. Phys. **46:** 923.
44. PERLSTEIN, J. H., J. A., VAN ALLAN, L. C. ISETT & G. A. REYNOLDS. This volume.

THE ROLE OF LIBRONS IN QUASI-ONE-D ORGANIC CONDUCTORS*

H. Morawitz

IBM Research Laboratory
San Jose, California 95193

INTRODUCTION

The organic charge-transfer salts, which form segregated stacks such as TTF-TCNQ and its various chemical modifications,[1] have been intensively investigated in the past few years as a consequence of their highly anisotropic transport properties.

Of particular interest is the occurrence and origin of the metal-insulator transition at 54°K and the additional phase transitions in the temperature regime immediately below. Although the metal-insulator transition shows the predicted signatures of a Peierls transition such as a Kohn anomaly at temperatures above the ordering temperature as well as diffuse x-ray scattering, it has become apparent in the most recent x-ray and neutron-scattering experiments[2,3] that the transition is not driven by a softening longitudinal acoustic phonon.

We emphasize in this paper the consequences of the additional orientational degrees of freedom, which arise from the internal structure of the molecules. It is highly likely that these modes referred to as librons in molecular crystals couple strongly to the conduction band, since considerable charge density is found at the extremities of the radical ion species where the spatial displacement is largest. In addition, strong mixing occurs at low-symmetry points of the Brillouin zone between translational and rotational motion, where degeneracies in the various acoustic phonon and libron branches appear.

HYBRIDIZED PHONON-LIBRON BRANCHES AND NEUTRON AND X-RAY SCATTERING EXPERIMENTS

The possibility of an orientational Peierls transition based on the coupling of the electron conduction band to torsional modes of a single stack was proposed some time ago.[4,5] It was shown there in a simple model that the Peierls mechanism could affect the orientation of the molecules in the stack, instead of their center of mass positions. The reduction of the translational symmetry along the stack axis due to small changes in tilt of the order of a degree would be sufficient to produce a gap in the electronic spectrum to drive the metal-insulator transition observed. Some indication of such effects have recently been reported, in TTF_7-Br_5[6] and TSeF-TCNQ,[7] although the situation is not completely resolved for the latter system inasmuch as intramolecular modes of the appropriate symmetry may also be responsible for the observed diffuse x-ray scattering. The

*Manuscript received June 2, 1977.

0077-8923/78/0313-0179 $1.75/1 © 1978, NYAS

definitive test for the composition of the local molecular motion in terms of its translational and rotational components is the calculation of the behavior of the structure factor in reciprocal space for scattering from the actual phonon and libron branches of the system. Unfortunately, a detailed calculation of the lattice dynamics of organic charge-transfer crystals with 4 molecules per unit cell is a prohibitively complex task and has not been completed to date. The method of using atom-atom potentials summed over the constituent atoms of the stack molecules to some third or fourth nearest neighbor shell to derive the intermolecular potential functions[8,9] is awkward because of the large number of atoms involved.

In addition, the presence of charges and the resulting complications due to screening further complicate the problem, since static and dynamic Coulomb contributions have to be included in a first-principles calculation of the phonon and libron frequencies in the first Brillouin zone. Nevertheless, the experience acquired with simpler molecular crystals such as naphthalene[10] gives some insight into the interplay of translational and rotational motion at degeneracy and other points of the Brillouin zone. Furthermore, although attempts to detect the low-lying libronic branches in TTF-TCNQ by Raman scattering experiments have not been successful to date, recent Raman measurements[11] on the molecular crystals TTF° and TCNQ° indicate several low-lying libronic branches.

We therefore simply calculate the appropriate structure factors for x-ray and neutron scattering in reciprocal space for various modepatterns consisting of linear superpositions of translational and rotational displacements of the stack molecules. In particular, we investigate rotational motion about the molecular plane, since in many cases the inertial axes found are close to the molecular symmetry axes. Large thermal amplitudes are also common to these motions, as seen in room-temperature x-ray studies.

Libron-Induced Effects on Electronic and Elastic Properties

The low excitation energies ($\hbar\omega_L < 50\ \mathrm{cm}^{-1}$) of the librational branches in organic solids and their flat dispersion (Einstein modes) suggest that their existence can markedly affect the temperature dependence of electronic and lattice properties in the regime $T \geq \hbar\omega_L/k_B$ i.e., between 30°K and room temperature. We present an estimate of the contribution of electron-libron scattering to the resistivity by making a golden-rule calculation for the cross-section of electron-2 libron processes. At temperatures larger than 100°K the libron population factor $n_L = (\exp(\hbar\omega_L/k_B T) - 1)^{-1}$ can be expanded in $(\hbar\omega_L/k_B T)$ and directly leads to a simple quadratic temperature dependence of the conductivity as observed.[12]

The electron-scattering time deduced from such a model also gives reasonable agreement with the experimental values derived from a Drude analysis of the optical data.[13]

The elastic properties of TTF-TCNQ have recently been determined by several workers[14,15] and reflect the anisotropic properties of these materials. We point out that direct analogies to polymer phonon properties[16] are present, since the intrastack forces in segregated stack organic solids are considerably larger than the interstack interactions, suggesting treatment of the individual stacks in terms

of their translational and torsional modes, followed by a perturbative inclusion of interstack forces.

The attempt to fit a single Debye temperature to the observed expansivity data[17] at different temperatures fails, because half the 4 × 6N external degrees of freedom are orientational and lead to sets of flat librons (Einstein-like oscillators), which intersect the acoustic branches in the Brillouin zone. These dispersionless libron branches before their hybridization with the various acoustic branches at degenerate energy eigenvalues also give a distinctive contribution to the lattice specific heat as opposed to the T^3 dependence due to acoustic phonons. Recent experiments on the elastic properties by a measurement of the sound velocities along different crystal axes as a function of temperature[18] suggest such behavior around the metal-insulator transition T_p = 54°K, indicating that some of the libron branches have energies below that value.

Summary and Conclusion

We have shown that the existence of the additional orientational degrees of freedom, which give rise to low-lying lattice excitations (librons) has profound consequences on the nature of the Peierls instability in these quasi-one-dimensional systems. In particular, it seems quite possible that at the observed value of $q_p = 2k_F = 0.29b^*$ the rotational and translational modes are strongly hybridized. The intriguing possibility of explaining the $4k_F$ instability as a harmonic arising from dipolar modulation of the charge-density wave structure at $2k_F$ was recently proposed.[19,20] The consequences of the mixed-mode character for the reciprocal space dependence of the structure factor observed in x-ray and neutron-scattering experiments are calculated in a simple model for the rotational and translational displacements of the mode. The rotational motion of the stack molecules can also strongly modulate the electronic transfer integral and cause strong electron-libron coupling. A straightforward explanation for the observed T^2 behavior of the conductivity arises from quadratic electron-2 libron processes, and reasonable values for the electron scattering times are obtained within the same model. The physical origin of the strong π-electron-libron interaction is the nodal pattern of the π-electron wave-function, which leads to maximal overlap for a dimer geometry slipped by $\frac{1}{4}$ of the molecular size along the long axis of the molecule, and can be strongly affected by relative rotational changes of the molecular planes.

The consequence of the existence of many low-lying libronic branches for the elastic properties of organic conductors is the inadequacy of a single Debye temperature to describe the elastic behavior and expansivities. In addition the heat capacity will deviate from a T^3 behavior and should show several Einstein-like contributions due to librons between 20 and 200 cm^{-1}.

References

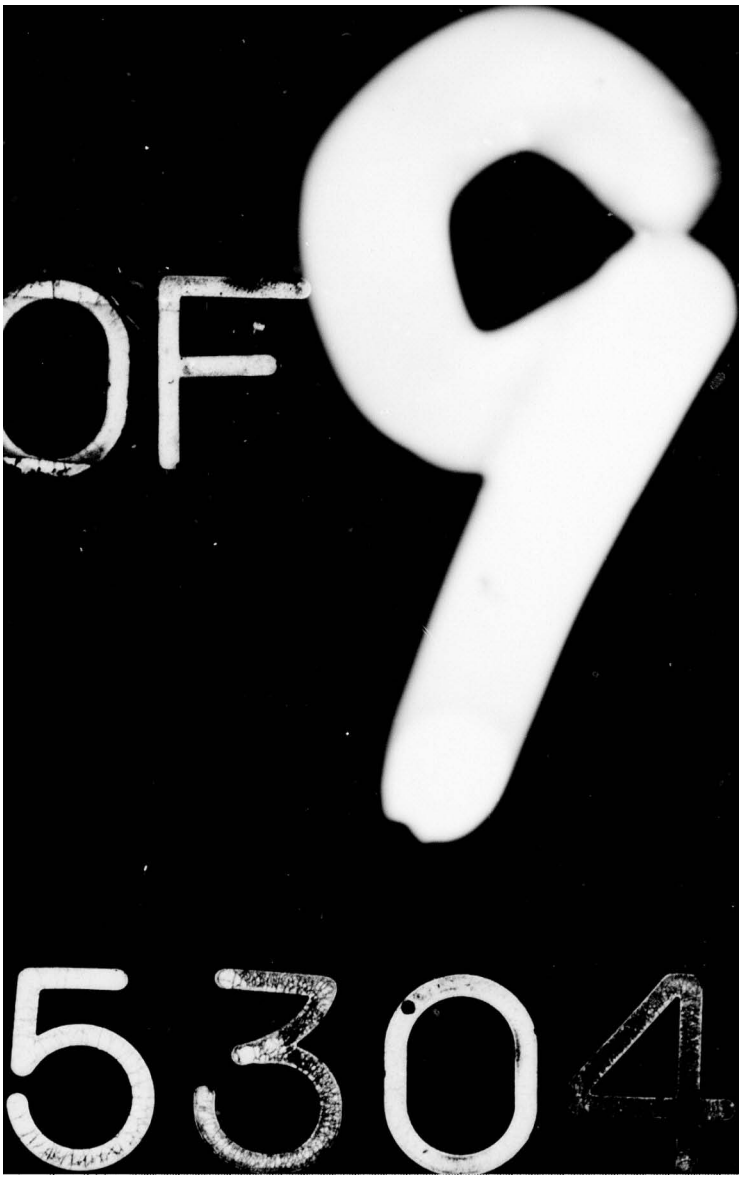
1a. Keller, H. G., ed. Proc. NATO Summer School on Chemistry and Physics of One-Dimensional Metals. 1976. Bolzano, Italy. Plenum Press. New York, N.Y.

1b. LECTURE NOTES IN PHYSICS. Organic Conductors and Semiconductors. Proc. Conf. Siofok, Hungary. Sept., 1976. Springer Verlag. Berlin, Germany.
2. DENOYER, F., R. COMES, A. F. GARITO & A. J. HEEGER. 1975. Phys. Rev. Lett. **35:** 455; KAGOSHIMA, S., H. ANZAI, K. KAJIMURA & T. ISHIGORO. 1975. J. Phys. Soc. Japan **39:** 1143.
3. COMES, R., S. M. SHAPIRO, G. SHIRANE, A. F. GARITO & A. J. HEEGER. 1976. Phys. Rev. Lett. **35:** 1518; Phys. Rev. **B14:** 2376.
4. MORAWITZ, H. 1973. Bull. Am. Phys. Soc. **18:** 1577; 1975. Proc. NATO Summer School on Low Dimensional Cooperative Phenomena H. J. Keller, Ed. Plenum Press. New York, N.Y.
5. MORAWITZ, H. 1975. Phys. Rev. Lett. **34:** 1096.
6. JOHNSON, C. R. & C. WATSON. 1976. J. Chem. Phys. **64:** 2271.
7. WEYL, C., E. H. ENGLER, K. BECHGARD, G. JEHANNO & E. ETEMAD. 1976. Sol. State Commun. **19:** 925.
8. PAWLEY, G. S. 1967. Phys. Stat. Sol. **20:** 347.
9. KITAIGORODSKY, A. I. 1973. Molecular Crystals and Molecules. Academic Press. New York and London.
10. OSTERTAG, R. H. 1973. Doctoral thesis. Univ. Stuttgart. Unpublished.
11. TEMKIN, H. Private communication and to be published.
12. GUTFREUND, H. & M. WEGER. 1977. Phys. Rev. B16: 1753.
13. GRANT, P., R. L. GREENE, G. C. WRIGHTON & G. CASTRO. 1975. Phys. Rev. Lett. **31:** 1311.
14. BARMATZ, M., L. R. TESTARDI, A. F. GARITO & A. J. HEEGER. 1974. Sol. State Commun. **15:** 1299.
15. SCHAFER, D. E., G. A. THOMAS & F. WUDL. 1975. Phys. Rev. **B12:** 5532.
16. WUNDERLICH, B. & H. BAUR. 1970. Adv. Polymer Sci. **7:** 151.
17. DEBRAY, D., R. MILLET, D. JEROME, S. BARISIC, J. M. FABRE & L. GIRAL. 1977. Preprint.
18. *JERICHO, M. Private communication and to be published.*
19. MORAWITZ, H. in Ref. 1b.
20. An alternative explanation was recently provided by WEGER, M. & J. FRIEDEL. 1977. J. Phys. (Paris) **38:** 241.

AD-A065 304 NEW YORK ACADEMY OF SCIENCES N Y F/G 7/2
SYNTHESIS AND PROPERTIES OF LOW-DIMENSIONAL MATERIALS.(U)
1978 J S MILLER, A J EPSTEIN N00014-77-C-0374
UNCLASSIFIED NL

3 OF 9
AD A065304




OF
9
5304

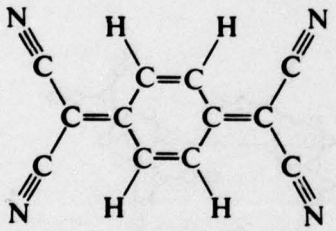
CHARGE TRANSPORT IN MOLECULAR CONDUCTORS: ROLE OF MOBILITY*

Arthur J. Epstein, Esther M. Conwell, and Joel S. Miller†

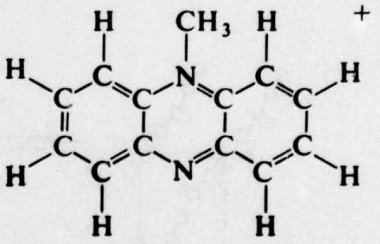
Xerox Webster Research Center
Rochester, New York 14644

INTRODUCTION

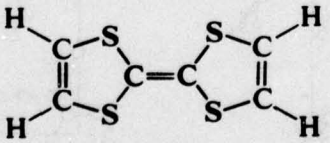
Numerous molecular conductors have been studied in recent years because of many novel physical and chemical properties atypical of molecular solids. Particular emphasis has been placed upon understanding the magnitude and the temperature dependence of the dc conductivity of quasi-one-dimensional, 1-D, materials.[1,2] There are many similarities among the more highly conducting segregated stack molecular conductors. These materials typically contain parallel segregated chains of large planar open-shell molecules. The counterion may or may not be either open shell or planar. For example, the highly conducting compounds based on the acceptor 7,7,8,8-tetracyano-*p*-quinodimethane (TCNQ), **1**, consist of parallel stacks of TCNQ and parallel stacks of either closed shell (e.g., *N*-methylphenazinium,[3,4] NMP^+, **2**), or open shell (e.g., tetrathiafulvalenium,[55] TTF, **3**) counterions. Similarly, the highly conducting compounds based on the donor TTF, for example, consist of parallel stacks of TTF and parallel stacks of either closed shell (e.g., thiocyanate[6]) or open-shell (e.g., TCNQ[5]) molecules.



TCNQ
1



NMP^+
2



TTF
3

*Manuscript received Nov. 14, 1977.

†Current address: Science Center, Rockwell International, 1049 Camino Dos Rios, Thousand Oaks, Calif. 91360.

0077-8923/78/0313-0183 $1.75/1 © 1978, NYAS

Many of these compounds have molecules uniformly spaced along the stacks. In a one-electron picture these materials have a partially filled conduction band, suggesting that they are metallic, examples being (NMP)(TCNQ)[3,7,8] and (Qn)-$(TCNQ)_2$ where Qn is quinolinium. In addition, the closed-shell cations in systems such as (NMP) (TCNQ) and $(Qn)(TCNQ)_2$ have only C_{2v} and C_1 symmetry, respectively. Their orientation in the crystal structure is usually random,[3,9] although crystals of (NMP) (TCNQ) with ordered cations have been reported.[4] FIGURE 1 illustrates the crystal structure of these systems with that of (NMP)(TCNQ).[3]

The temperature dependence of the dc conductivity of molecular conductors falls into three general classes:

I. Those systems with a strongly temperature-activated conductivity, such as $(alkali^+)_n(TCNQ^-)_m$.[8] These materials show a single linear behavior on log σ versus T^{-1} plots as illustrated, for example, by the *b*-axis conductivity of $Cs_2(TCNQ)_3$,[11] FIGURE 2. Generally, the dc conductivity at room temperature for these materials is in the range of $10^{-6} - 10^{0}\ \Omega^{-1}cm^{-1}$. They are usually characterized as "semiconductors."

II. Those systems with a broad weak maximum, σ_m, in the temperature dependence of their dc conductivity at a temperature T_m. For these systems usually $\sigma_m/\sigma(295°K) \lesssim 2$ and $\sigma(295°K) \sim 100\ \Omega^{-1}cm^{-1}$. The σ versus T curves for these systems generally show negative curvature ($d^2\sigma/dT^2 < 0$) over a large temperature range around T_m. This class is typified by the σ versus T behavior of (NMP)(TCNQ)[12,13] (FIGURE 3A). Numerous models have been used to characterize $\sigma(T)$ for this class of materials.

III. Those systems with a sharp maximum in their temperature-dependent dc

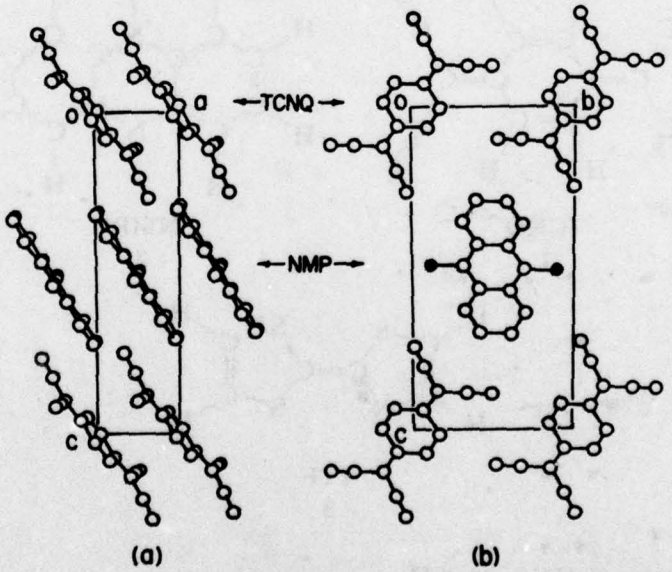


FIGURE 1. Crystal structure of (NMP)(TCNQ) (Ref. 3). (a): View down the *b*-axis; (b): view down the highly conducting *a*-axis. Note that two methyl groups are shown for each NMP^+ indicating random nature of the methyl group location. (From Ref. 3.)

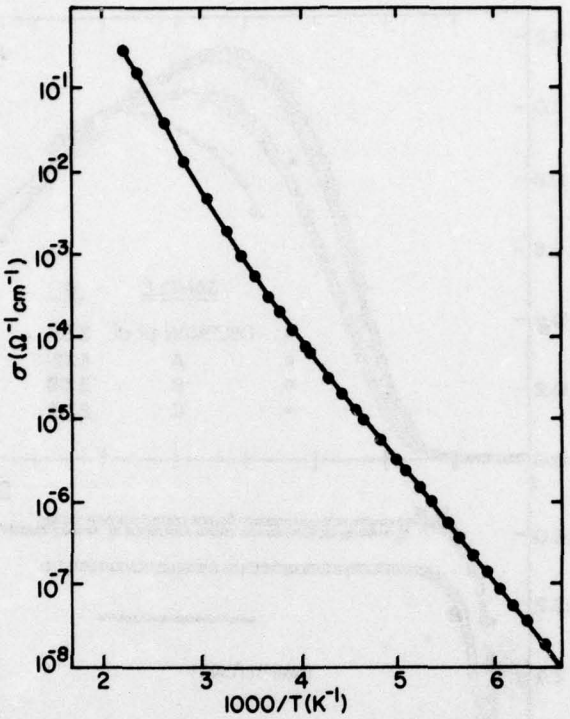


FIGURE 2. Dc conductivity versus (temperature)$^{-1}$ along *b*-axis of a single crystal of $Cs_2(TCNQ)_3$ (after Ref. 11). The curve shown exhibits two activation energies, $\Delta = 0.45$ eV ($T > 300°K$), intrinsic, and $\Delta = 0.3$ eV ($T < 300°K$), extrinsic. See Ref. 11 for more details.

conductivity. This class is typified by the σ versus T behavior of (TTF)(TCNQ)[14,15] (FIGURE 4). Generally, for these systems $\sigma(T_m)/\sigma(295K) \gg 2$ and σ versus T has positive curvature ($d^2\sigma/dT^2 > 0$) for $T > T_m$. The room-temperature conductivity is generally ~ 500–$1000\,\Omega^{-1}cm^{-1}$.

Numerous models have been applied to explain the dc conductivity of these materials, especially classes II and III. We have developed a new model for conductivity that is applicable to molecular conductors in all three classes in the temperature range of $\sim 70°K$ to $400°K$.[13,16,17] We parametrically fit and also quantitatively calculate $\sigma(T)$ for materials in each of these classes as the product of charge-carrier concentration (activated in Classes I and II) and a strongly temperature-dependent mobility determined by known electron-phonon coupling to the molecular vibrations of the conducting chains.

In the following section we review some of the previously reported segrated stack conductor materials in each class. The models used to explain the dc conductivity of these materials are indicated. In PARAMETRIZATION OF CONDUCTIVITY DATA AND INTRODUCTION OF MOBILITY MODEL we show our new parametrization of the dc conductivity data of Class II materials and how this leads to a model of an activated carrier concentration and a large strongly temperature-dependent mobility for $70°K < T < 400°K$. Its relationship to previous parametrizations

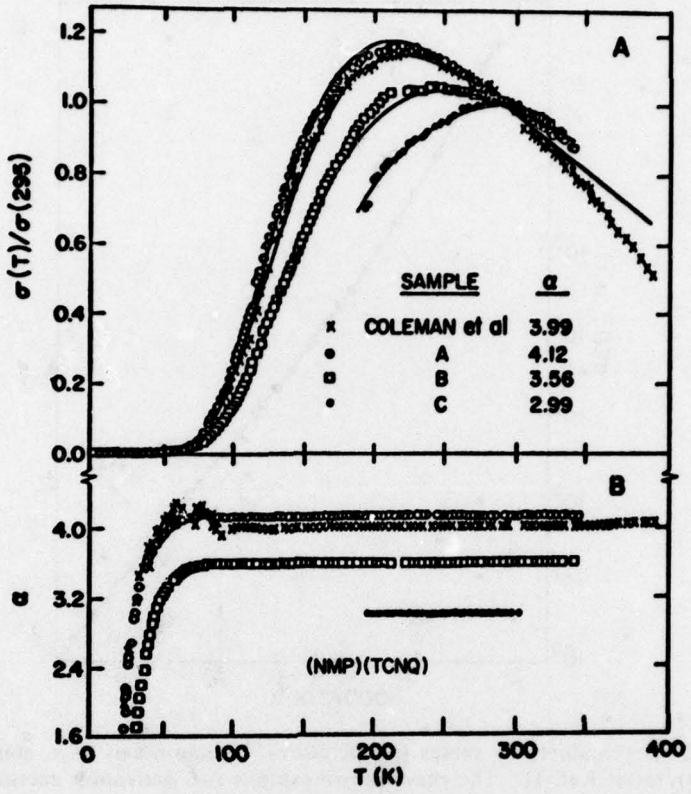


FIGURE 3. A: Normalized four-probe α-axis conductivity, $\sigma(T)/\sigma(295°K)$, versus temperature for some representative (NMP)(TCNQ) samples. The "×" data is from Ref. 12. The solid lines are computer fits to Equation 4 with α indicated. B: Calculated α from Equation 4 with experimental $\sigma(T)$ and $\Delta = 900°K$.

of $\sigma(T)$ data for Class I and Class III materials will be shown. In the section MICROSCOPIC MODEL OF MOBILITY the microscopic basis of the temperature-dependent mobility is examined. COMPARISON WITH EXPERIMENT compares quantitative calculations with $\sigma(T)$ data. In the section after that we discuss results on the new system (N-methylphenazinium)$_x$ (Phenazine)$_{1-x}$(TCNQ), which allows control of band filling and disorder. Finally, we summarize our results and some of their implications.

REVIEW OF PRIOR DATA AND MODELS

Class I

The materials in Class I have generally been termed semiconductors with an activated conductivity. The source of the relatively large activation energies in these materials is as yet uncertain. Perhaps the largest number of conducting molecular salts lie in this class.[1,2]

Class II

There are many materials in Class II besides (NMP)(TCNQ). These include the single-stack conductors $(Qn)(TCNQ)_2$,[9,10,18,19] $(Adn)(TCNQ)_2$,[19,20] and $(Adz)(TCNQ)_2$[21] where Qn is quinolinium, Adn is acridinium, and Adz is acridizinium. These four systems have a random orientation of their closed-shell cations leading to some disorder in the electrostatic potential at each TCNQ site. None of these four systems has a phase transition in the temperature range of interest ($70°K < T < 400°K$). Also in Class II are systems that have an apparent phase transition at a temperature T_c within $70°K < T_c < 400°K$ *in addition* to the weak maximum in $\sigma(T)$ at T_m. Often $T_c < T_m$. This occurs, for example, in $(NMe_3H)(I)(TCNQ)$,[22,23] as well as in some of the TTF halides.[6,24,25] The Class II behavior is also seen in some two-chain conductors, for example, tetrathiafulvalenium methyltetracyanoquinodimethanide (TTF)(MeTCNQ).[26]

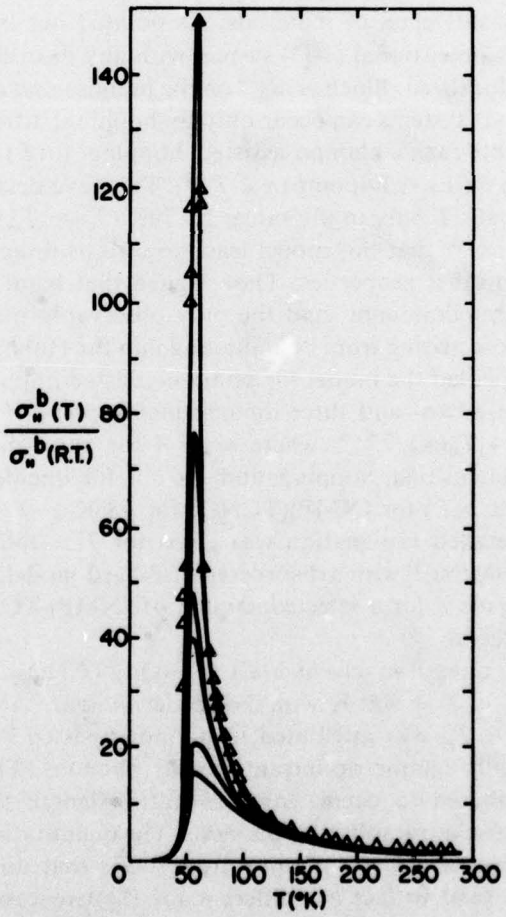


FIGURE 4. Normalized four-probe *b*-axis dc conductivity versus temperature for a number of (TTF)(TCNQ) samples. (After Ref. 15.)

Many models have been proposed for this behavior. These include the presence of a transition at T_m from a metallic state for $T > T_m$ to a semiconducting state for $T < T_m$. The state for $T < T_m$ was proposed to be a Mott-Hubbard semiconductor for (NMP)(TCNQ) and a Peierls semiconductor for (TTF)(MeTCNQ). Epstein *et al.*,[7,8] on the basis of conductivity, magnetic susceptibility, χ, specific heat, and so on, described the low-temperature state of (NMP)(TCNQ) as a Mott-Hubbard semiconductor. Fitting the conductivity data in the 20–70°K range by $\sigma = \sigma_{01} \exp(-\Delta_{01}/T)$, $2\Delta_{01}$ was identified as the low-temperature Hubbard gap. The gap was assumed to be renormalized to zero at T_m. For $T > T_m$, the system was considered to be a correlated metal. Detailed calculations for the conductivity for $T > T_m$ were lacking, although Coleman *et al.*[12] noted that the resistivity on the region 300°K to 400°K could be fit with $\rho(T) = A + BT^4$. Jacobsen *et al.*[26] suggested a broadened Peierls metal-insulator transition for (TTF)(MeTCNQ). A detailed fit of (TTF)(MeTCNQ) in the region $20°K < T < 60°K$ to $\sigma \propto \exp(-\Delta/T)$ gave $\Delta = 360°K$ (0.031 eV = 0.73 Kcal/mole).

Several groups have focused upon the random potentials that exist for a number of members of this class of materials. As pointed out in 1961 by Mott and Twose,[27] in a one-dimensional (1-D) system with any disorder the eigenfunctions are exponentially localized. Bloch *et al.*,[28] on the premise that electronic conductivity in disordered 1-D systems can occur only by hopping, attributed σ at low temperature to variable-range phonon-assisted hopping ($\sigma(T) \propto \exp(-(T_0/T)^{1/2})$, and for $T > T_m$ to diffusive hopping ($\sigma \propto T^{-1}$). This gave detailed agreement with experimental σ versus T only in the range 20–70K ($T \ll T_m$). It was pointed out by Ehrenfreund *et al.*[29] that this model leads to serious disagreement with room-temperature σ and other properties. They argued that band and coulomb interaction effects are predominant, and the only observable manifestations of disorder would be those arising from "bandtailing into the Hubbard gap."

Shante has extended the model for phonon-assisted hopping among localized states to anisotropic two- and three-dimensional hopping.[30] His results are that $\ell n\,[\sigma(T)/\sigma_0] = -[T_0(m)/T]^{1/m}$ where $m \sim 4$ for three-dimensional hopping, $m \sim 3$ for two-dimensional hopping, and $m \sim 1$ for one-dimensional hopping. He is able to fit the $\sigma(T)$ for (NMP)(TCNQ) for $18°K < T < 140°K$, using this expression. No detailed explanation was given for $T > 140°K$. Theodorou and Cohen[31] and Theodorou,[32] with a disordered Hubbard model, were able to obtain a good fit to χ versus T for a selected sample of (NMP)(TCNQ) with high χ at very low temperatures.

Gogolin *et al.* quantitatively fit $\sigma(T)$ for $(Qn)(TCNQ)_2$ and $(Adz)(TCNQ)_2$ in the range $20°K < T < 300°K$ with a disorder model.[21] The rise in σ with increasing T for $T < T_m$ was attributed to phonon-assisted hopping with use of low-frequency totally symmetric intramolecular phonons. The decrease in σ for $T > T_m$ was attributed to decreasing localization length through coupling to nontotally symmetric intramolecular phonons. The quantitative fit to both TCNQ salts requires, however, TCNQ phonon frequencies that do not match the experimental values (and in fact are different for the two cases) and phonon frequency shifts that the authors admit[21] are unreasonably large.

An early model for $\sigma(T)$ proposed for some of these systems was the interrupted strand model.[33–35] This model assumes the crystal to be composed of

parallel linear strands, with each strand being interrupted within itself by perfectly insulating defects. The electrons are assumed to be delocalized over and confined to each strand segment. This "particle in a box" arrangement leads to a discrete splitting of allowed energy values for electrons, with a splitting of the order of 10^{-2} eV for electrons localized in a chain 300 Å long. The dc electrical conductivity for the crystal is then thermally activated, with the activation energy related to the energy required to add another electron to a strand. The conductivity is given[35] by $\ell n\ \sigma \propto T^{-\mu}$ (with $\frac{1}{3} > \mu > \frac{1}{2}$). However, the detailed features of $\sigma(T)$ were not fit, especially for $T > T_m$.

Class III

There has been a similar plethora of models used in an attempt to understand the high-temperature ($T > 70°K$) conductivity for Class III systems, especially (TTF)(TCNQ) (FIGURE 4). One theory is that collective many-body effects are involved.[36,37] Specifically, contributions to σ are supposed to arise from charge-density wave fluctuations that slide via time-dependent phases. The evidence cited for a collective mode contribution to σ[38,39] includes the strong dip observed in $\sigma(\omega)$ at low frequencies.[38-40] This has been interpreted as representing a gap or pseudogap of 1100 cm^{-1} (0.14 eV) in the density of states, although its temperature independence is not easily explained within the model.[38,39] Also cited for evidence of collective behavior in (TTF)(TCNQ) are the nonlinear current-voltage curves observed below 4°K.[41,42]

Another mechanism proposed to account for the variation of σ with T above 58°K in (TTF)(TCNQ) is electron-electron (e-e) scattering between electrons on TCNQ and between holes on TTF.[43,44] The basis of this was the finding of Etemad *et al.* that their data, and some from other laboratories, could be fit by a power law $\sigma^{-1} \equiv \rho = \rho_0 + \rho_2 T^2$ in the range 60 to 250°K.[43] The ratios $\sigma_m/\sigma(295°K)$ for the samples in their study were $\lesssim 20{:}1$. In another study, including higher quality samples as judged by values of $\sigma_m/\sigma(295°K)$ as high as 35:1, Groff *et al.*[45] found a somewhat similar law for σ^{-1} in the range 60 to 300°K. However, the exponent of T was significantly greater than 2, ranging from 2.23 to 2.40 for different samples. All samples were well represented by the exponent of 2.33. Thus, e-e scattering does not in detail account for the observed variation in T-dependence of $\sigma(T)$. In fact, for the 1-D case considered,[44] e-e scattering leads[46] to $\sigma^{-1} \propto T$. Apart from this, estimates of its possible importance[44] were too large because the e-e collisions considered[47] were momentum-conserving ones. To affect σ the collisions must transfer momentum to either the lattice, through umklapp-processes, or to high-mass or low-μ carriers that contribute little to σ, as in the transition metals. As regards the first possibility, umklapp processes are expected to be much less frequent than momentum-conserving ones. This is particularly so for the present case, where the maximum momentum change in an e-e collision is ~4 times the wave vector at ϵ_F, which for (TTF)(TCNQ) is distinctly less than a reciprocal lattice vector. Under the second mechanism one might argue that the holes on TTF chains act like high-mass carriers to drain momentum from the electrons on TCNQ. However, as will be shown subsequently, the hole mobility is comparable to that of the electrons.

A third mechanism proposed to account for $\sigma(T)$ of (TTF)(TCNQ) is the interaction of electrons with the librational modes of TCNQ.[48] The basic point of this model is that the interaction of the electrons with these modes must be a second-order process. This gives a predicted T^2 behavior of the resistivity, not $T^{2.33}$.

In summary, numerous models have been proposed for the temperature dependence of the dc conductivity of molecular conductors in Classes I, II, and III. However, few of these models give a detailed fit to $\sigma(T)$ over a large temperature range nor are any of these models based upon the microscopic parameters of these materials. In addition, these models were claimed to be applicable only to subgroups of these classes.

Parametrization of Conductivity Data and Introduction of Mobility Model

The parametrization of dc conductivity data of Classes I and III has been straightforward, even if the interpretation of the resulting parameters is not unequivocal. Class I materials are usually described[2] by

$$\sigma = \sigma_0 \exp(-\Delta/T) \tag{1}$$

where σ_0 is a constant prefactor and Δ is an apparent activation energy (units of degrees Kelvin). Class III materials are usually described[43] by

$$\sigma^{-1} \equiv \rho = \rho_0 + \rho_1 T^{\alpha} \tag{2}$$

where ρ_1 and α are sample-independent constants and ρ_0 is a sample-dependent constant. Equations 1 and 2 are generally valid for $T > 70°K$, providing that there are no phase transitions in this temperature range.

Parametrization of $\sigma(T)$ for Class II has been more problematic. Only Gogolin *et al.*[21] have been successful at a quantitative fit of $\sigma(T)$ for a wide temperature range on either side of T_m. The shortcomings of this approach have, however, already been pointed out. In order to address this point we have reexamined, in detail, the temperature behavior of the conductivity of (NMP)(TCNQ).[13]

We have made careful measurements of the dc σ of approximately 30 (NMP)-(TCNQ) single-crystal samples at intervals of $\sim 1°K$, using a four-probe technique. Twice-gradient-sublimed TCNQ and glove-box techniques were used in sample preparation to assure high-quality samples. The room-temperature conductivity parallel to the stacking axis ranged from 120 to 300 $ohm^{-1}cm^{-1}$. The results on several crystals, including that of Coleman *et al.*,[12] are shown in FIGURE 3. A range of behavior is observed with $300°K > T_m > 225°K$ and $1.20 > \sigma_n(T_m) > 1.0$, where $\sigma_n(T) = \sigma(T)/\sigma(295°K)$.

In order to examine in more detail the $\sigma(T)$ behavior, we have studied the logarithmic derivative of the resistance, $R(T)$, $F(T) \equiv d(\ln(R(T)/R(295°K))/d(T^{-1})$. $F(T)$ is zero at T_m. The results for one sample are shown in FIGURE 5. The similar simple behavior of $F(T)$ for $T > T_m$ and $T < T_m$ is striking. In fact, a single straight line well approximates the $F(T)$ versus T data for temperatures above and below T_m. That is,

$$F(T) = \frac{d\,\ell n\,(R(T)/R(295°K)}{d(T^{-1})} = \Delta - \alpha T \qquad (3)$$

for 100°K < T < 300°K, where Δ and α are constants. The similar behavior above and below T_m = 225°K strongly implies that the charge-transport mechanism is unchanged at T_m.

Equation 3 can be solved for $\sigma_n(T) \equiv \sigma(T)/\sigma(295°K)$. Doing so we find

$$\sigma_n(T) = AT^{-\alpha} \exp(-\Delta/T). \qquad (4)$$

By computer analysis of the conductivity data of (NMP)(TCNQ) we found that for 65°K < T < 400°K, $\sigma(T)$ is very well fit by Equation 4, with Δ = 900°K for all samples measured and α a sample-dependent constant in the range 3 to 4. The constant A is fixed by $\sigma_n(295°K) \equiv 1$. The solid lines in FIGURES 3 and 6 show the fits obtained with these parameters in Equation 4. The agreement is particularly impressive in view of the large variations in $\sigma(T)$ among samples. The value of α is correlated with sample quality, the highest value being obtained for the sample

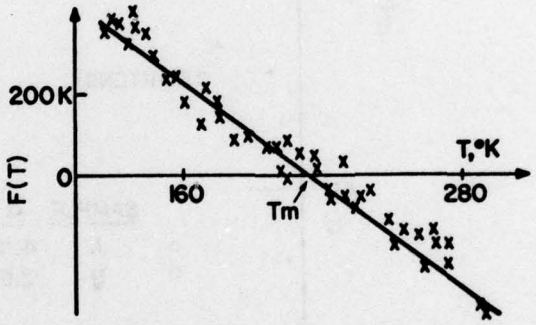


FIGURE 5. $F(T)$ = d(ln($R(T)$/R(295K)))/d(T^{-1}) versus T on (NMP)(TCNQ) sample. The straight line is $F(T) = \Delta - \alpha T$ (Δ and α are constants).

with lowest T_m (best), the lowest value for the sample with highest T_m (poorest). Samples with higher α featured a better fit to Equation 4 to lower temperatures. To show even more convincingly that there is no change in charge-transport mechanism at T_m, or elsewhere in the range 65°K < T < 400°K, we show in FIGURE 3B a plot of α as a function of T calculated from Equation 4 by using for σ the experimental values and for Δ 900°K. The deviations from Equation 4 at the high- and low-temperature ends seen in FIGURES 3A and 6 are typical of all samples.

It is natural to interpret these results and Equation 4 as showing that an energy gap persists throughout the temperature range, leading to an activated carrier concentration, $n \propto \exp(-\Delta/T)$, and a large strongly temperature-dependent mobility, $\mu \propto T^{-\alpha}$. As seen schematically in FIGURE 7, $n(T)$ is a monotonically increasing function of increasing temperature, whereas $\mu(T)$ is monotonically decreasing with increasing temperature. The product of $n(T)$ and $\mu(T)$ to give $\sigma(T) = n(T)e\,\mu(T)$ has a maximum at $T_m = \Delta/\alpha$. Thus, in fitting $\sigma(T)$ to Equation 4, A is fixed by σ_n (259°K) = 1.0, Δ/α is fixed by T_m, so that there is

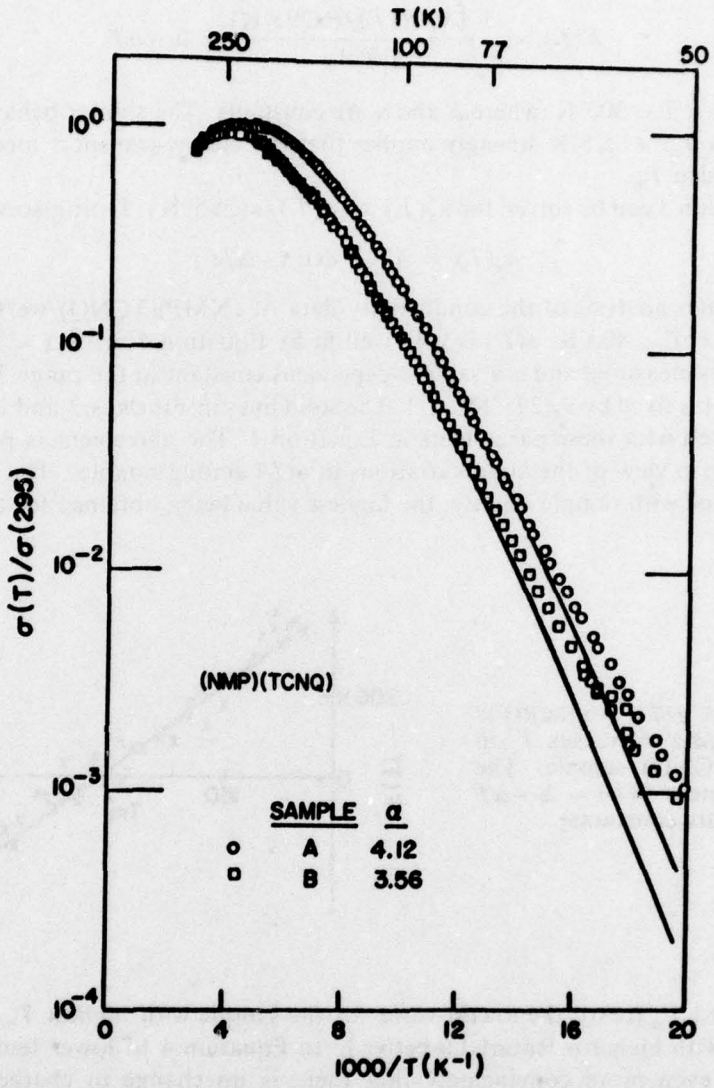


FIGURE 6. Experimental log σ versus $1/T$ for samples A and B of Figure 3A, and computer fits from Equation 4.

only one adjustable parameter to fit the $\sigma(T)$ curve from 65°K to 400°K. Since the gap for (NMP)(TCNQ) is sizeable, it leads to the carrier concentration being fairly small and, as will be detailed later, a mobility, $\mu = \sigma/ne \sim 10$ cm^2/volt-sec at 295°K and larger at lower temperatures.

At low enough temperatures (depending on the property being measured), electrons in localized states may dominate the behavior. This could account, as previously suggested,[7,8,28,29] for the microwave σ[49] being higher than dc σ for $T < 50$°K, and perhaps for the deviation seen in FIGURE 6 at $T < 65$°K between σ from Equation 4 and the experimental data. It also could account for the poorer

fit at low temperatures of $\sigma(T)$ for samples with lower α (poor quality). That is, poor-quality samples may have more localized states so that excess conductivity above that predicted by the model is observed at higher temperatures.

The gap deduced from Equation 4 represents, for electrons (holes), the energy difference between occupied (empty) states in the upper and lower (Hubbard-type) bands. To treat dc σ at $T > 65°K$, we therefore neglect the localized states and use as a model two 1-D tight binding bands separated by a gap 2Δ. Each band is assumed to have N states (N being the number of molecules in a chain), and coulomb correlations are neglected. Note that fitting σ versus T does not make it possible to distinguish between $\Delta = \Delta_0$, independent of T, and $\Delta = \Delta_0 - \beta T$, where β is a constant. (In the latter case σ_0 would represent a constant times e^{β}).

Using the Δ found in fitting the experimental data to Equation 4, η, the concentration of carriers per unit length $L(\eta = nA$ where A is the cross-sectional area of a unit cell), was calculated[17] for a single 1-D tight binding band with $2N$ states and width ϵ_0:

$$\eta = \frac{1}{L}\int_0^{\epsilon_0} [1 + \exp\{(\epsilon - \epsilon_F)/k_B T\}]^{-1}\rho(\epsilon)\,d\epsilon. \tag{5}$$

Here $\rho(\epsilon)$, the number of states per unit energy range, is

$$\rho(\epsilon) = (2L/\pi a)[\epsilon(\epsilon_0 - \epsilon)]^{-1/2} \tag{6}$$

with a being the spacing between adjacent molecules in a segregated stack. To find the exponential dependence of η on T over a wide T range that we deduce from (4), it is necessary that $\exp[(\epsilon - \epsilon_F)/k_B T] \gg 1$. This leads to

$$\eta \simeq (2/a)(k_B T/\pi\epsilon_0)^{1/2} \exp[(\epsilon_F - \epsilon_b)/k_B T], \tag{7}$$

where we have inserted ϵ_b in the exponential as a reminder that the Fermi energy is to be measured from the band edge ϵ_b. Since $\sigma = ne\mu$, we conclude that the mobility $\mu \propto T^{-(\alpha+.5)}$. We identify the quantity $-\Delta = -(\Delta_0 - \beta T)$ as $(\epsilon_F - \epsilon_b)/k_B$. For a Mott-Hubbard band of N states ρ and η are divided by 2.

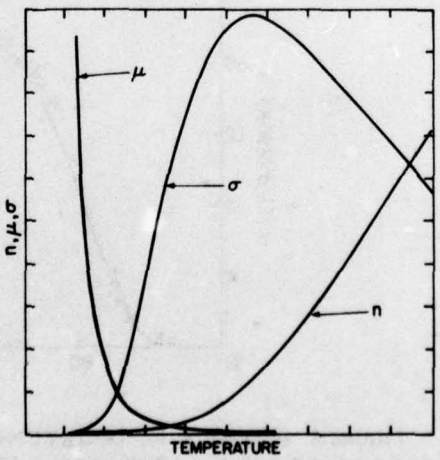


FIGURE 7. Schematic temperature dependence of charge-carrier concentration, $n \propto \exp(-\Delta/T)$, mobility, $\mu \propto T^{-\alpha}$, and conductivity, $\sigma = ne\mu$.

Utilizing $\sigma = ne\mu$, with $\sigma(295°K) = 300\ ohm^{-1}cm^{-1}$, for (NMP)(TCNQ) and the above $\eta(T)$ with $\Delta_0 = 900°K$, $(\epsilon_0/k_B) = 1000°K$ (in accord with other measurements and N states per tight-binding band) we obtain $\mu = 30\ e^{-\beta}(295/T)^{\alpha+0.5}$ cm^2/volt-sec. Using $\beta \sim 1$ obtained from a crude model[13] of the susceptibility of (NMP)(TCNQ), we obtain a mobility $\mu(295°K) \sim 10\ cm^2$/volt-sec.

The mobility obtained by this approach is large enough (>1 cm^2/volt-sec) so that the band approach is self-consistently valid. However, the very strong temperature dependence ($\mu \propto T^{-\alpha}$ with $\alpha \sim 4$ for (NMP)(TCNQ)) is unusual. Acoustic-mode scattering typically yields[50] $\mu \propto T^{-1.5}$, insufficiently steep to account for our results; consequently, a more temperature-dependent scattering mechanism is necessary. The optical modes of crystals are higher in energy, providing a strongly temperature-dependent scattering mechanism. For molecular conductors such as (NMP)(TCNQ) the crystal optical modes are essentially the molecular vibrations. Since the vibrational frequencies[51] and coupling constants[52-56] are well known for TCNQ and several other molecules, a direct calculation of μ is possible. This is detailed in the following section.

The approach taken to understand $\sigma(T)$ for (NMP)(TCNQ) is very general. It involves only activation of a sufficient carrier population to a band of extended states, and the presence of a strongly temperature-dependent mobility determined by charge-carrier interaction with molecular vibrations. It is easy to extend this parametrization to other members of Class II, for example, $(Adz)(TCNQ)_2$ where Adz is acradizinium. As seen in FIGURE 8, an excellent fit of $\sigma(T)$ is obtained by Equation 4 with $\Delta = 450°K$ and $\alpha = 3.04$. Additional examples and details are given in the following sections. TABLE 1 summarizes some of our results in fitting Equation 4 to Class II materials.

Extensions of these ideas for Class II systems to Classes I and III is now apparent. For those molecular conductors with high activation energies ($\Delta \gtrsim 2000°K$), the maximum in $\sigma(T)$ will occur at temperatures greater than 500°K, provided α is 4 or less. For such systems there will be no maximum in σ observed, and Equation 1 will give a good fit since the exponential will dominate the

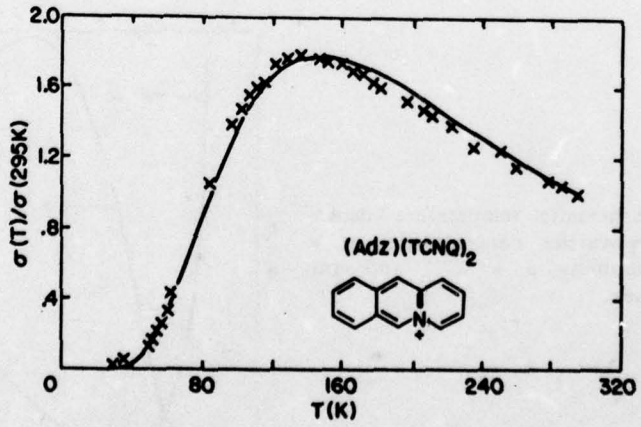


FIGURE 8. σ versus T for $(Adz)(TCNQ)_2$ (from Ref. 21) (X). *The solid line is our fit to Equation 4 with* $\Delta = 450°K$ *and* $\alpha = 3.04$.

TABLE I

PARAMETERS IN FIT OF MEASURED $\sigma(T)$ TO $\sigma_n(T) = A\, e^{-\Delta/T} T^{-\alpha}$

Material	Measured σ(295°K) $ohm^{-1}cm^{-1}$	$\frac{\Delta_0}{°K}$	α
(NMP)(TCNQ)[13]	300	900	3 to 4
$(Qn)(TCNQ)_2$[21]	70	600	2.54
$(Adn)(TCNQ)_2$[19]	100	350	2.34
$(Adz)(TCNQ)_2$[21]	130	450	3.04

T-dependence. As Δ is decreased, T_m shifts to lower temperatures as seen, for example, in (triethylammonium)$(TCNQ)_2$,[57] which exhibits a deviation from (**1**) for $T > 300°K$.

Class III materials may be viewed as the other extreme. In this class $\Delta = 0$ and (**4**) reduces to Equation 2 if one separates out two scattering mechanisms, one T-dependent due to phonons and one T-independent, presumably due to defects or impurities. Considerations for Class III are often more complex because of the presence of two conducting chains, yet simpler because the crystal structures usually show no evidence of disorder.

It is thus seen that a single parametrization of temperature-dependent conductivity data allows one to approach the high temperature ($T > 70°K$) σ of all three classes of molecular conductors in a unified manner. The microscopic understanding of $\mu(T)$ in terms of scattering with molecular vibrations is discussed in the next section.

This model of a large, strongly temperature-dependent mobility is in contrast with a T-independent value of 0.4 cm^2/Volt-sec for TCNQ° crystals for $204°K < T < 306°K$.[58] Because, however, the molecular spacings are much larger for TCNQ°[59] than for TCNQ in (NMP)(TCNQ)[3], the band approach used above would not be valid for TCNQ°. In addition, as has been previously noted[60] for anthracene in this temperature range, a T-independent μ of ~ 0.1–1.0 cm^2/volt-sec is difficult to model quantitatively. Recently, direct evidence has been reported[61] for the onset of band-type motion in naphthalene below 120°K.

MICROSCOPIC MODEL OF MOBILITY

The values of mobility determined from analysis of conductivity data are large enough so that we may use a perturbation calculation. For this we need the matrix element for scattering of a carrier in the tight binding bands arising from the molecular level of energy E_γ by an optical phonon derived from the i'th normal mode of molecular vibration. Using a deformation potential approach, we obtained this matrix element in terms of $g_i = (\sqrt{2}\hbar\omega_i)^{-1}(\delta E\gamma/\delta Q_i)_0$, where $\hbar\omega_i$ is the phonon energy of the i'th normal mode and Q_i its dimensionless normal coordinate.

Although Boltzmann statistics are adequate for wide-gap systems like (NMP)-(TCNQ), we generalize to Fermi-Dirac statistics for use with small- and zero-gap materials. The energies $\hbar\omega_i$ and the coupling constants g_i for the optical phonons

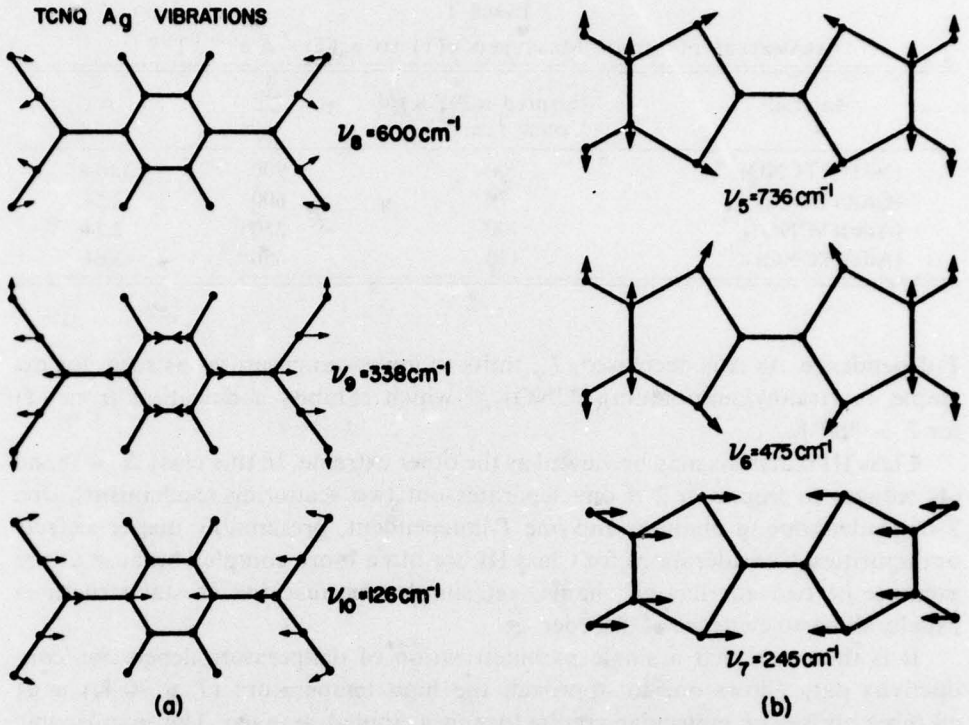


FIGURE 9. (a): The three lowest energy A_g modes of TCNQ. Only A_g modes couple in first order to an electron in the TCNQ b_{2g} orbital from which the TCNQ conduction band is derived. (b): The three lowest energy A_g modes of TTF. Only A_g modes couple in first order to a hole in the TTF b_{1u} orbital from which the TTF conduction band is derived. (After Ref. 53.)

that interact significantly with the carriers have been calculated for the highest occupied orbitals of TCNQ, $TCNQ^-$ and TTF,[52-54] and also deduced experimentally for TCNQ.[56] FIGURE 9 illustrates the lowest energy vibrational modes for TCNQ and TTF that couple in first order to the electrons (TCNQ) and holes (TTF).[53] Since the matrix element for scattering depends on the initial and final electron state only through the energy difference between them, $\hbar\omega_i$, a relaxation time τ exists even for the distribution function f_0 degenerate; i.e.,[16]

$$\frac{1}{\tau} = \frac{2}{h}\sum_i (g_i\hbar\omega_i)^2 \left[(n_i + 1)\frac{1 - f_0(\epsilon - \hbar\omega_i)}{1 - f_0(\epsilon)}\frac{H(\epsilon - \hbar\omega_i)}{(\epsilon - \hbar\omega_i)^{1/2}(\epsilon_0 - (\epsilon - \hbar\omega_i))^{1/2}}\right.$$
$$\left. + n_i\frac{1 - f_0(\epsilon + \hbar\omega_i)}{1 - f_0(\epsilon)}\frac{H(\epsilon_0 - (\epsilon + \hbar\omega_i))}{(\epsilon + \hbar\omega_i)^{1/2}(\epsilon_0 - (\epsilon + \hbar\omega_i))^{1/2}}\right]^{-1} \quad (8)$$

where n_i is the number of phonons in the mode with $\hbar\omega_i$, ϵ is the energy of the carrier measured from the band edge, ϵ_0 the bandwidth and $H(A - B) = 1$ for $A > B$, 0 for $A \leq B$. With this, the Boltzmann Equation is readily solved, leading

to integrals for μ and the thermoelectric power, Q, that must be evaluated numerically, with the appropriate parameters for each case.

The actual values of bandwidths used varied among the systems studied (see TABLE 2). Values were chosen to be of the same order as values generally accepted for ϵ_0. Only those vibrational modes for which $\hbar\omega_0 < \epsilon_0$ can scatter the electrons (holes).

COMPARISON WITH EXPERIMENT

We have quantitatively applied our microscopic model to a number of molecular conductors. TABLE 2 lists the parameters used to calculate $\mu(T)$ due to optical phonons and fit the $\mu(T)$ obtained in parametrization of the data.

FIGURE 10 shows the $\mu(T)$ calculated for (NMP)(TCNQ) for electrons moving in a conduction band on the TCNQ stack. The values of g_i chosen are within the range of uncertainty of the literature values (including $g_8 = 0.20$ and $\hbar\omega_8 = 882.4°K$). The calculated μ has the correct order of magnitude at room temperature and varies, on the average, as T^{-4} over the entire temperature range of interest. The small deviations at both ends of the range may be due to small changes in ϵ_0 or to the onset of additional scattering mechanisms. Variations in α are presumably due to the defect scattering, which we do not discuss here.

FIGURE 11 shows our parametric fits to the measured $\sigma(T)$ and our calculated $\sigma(T)$ for $(Qn)(TCNQ)_2$ and $(Adn)(TCNQ)_2$. Here Qn is quinolinium and Adn is acridinium. Using μ taken from the solution of the Boltzmann Equation, we obtain $\sigma(T)$ as the product of $ne\mu$ indicated by the dashed line in FIGURE 11 with the parameters shown in TABLE 2. Since we varied both ϵ_0 and g_i in obtaining these fits, we do not feel that these individual parameters are precisely pinned down. Further, if crystal quality is not good, it will affect the values of parameters for good fit. (Note, however, that although only limited published σ versus T data are available for these materials, we obtained the same α and Δ_0 for fits of Equation 4 to $(Qn)(TCNQ)_2$ data of two groups.[19,21])

The above considerations are expected to be independent of the origin of the

TABLE 2

PARAMETERS IN FIT OF $\mu(T)$ DUE TO OPTICAL PHONONS TO MEASURED $\mu(T)$

Material	$\hbar\omega_1/k_B$ °K	g_1	$\hbar\omega_2/k_B$ °K	g_2	ϵ_0/k_B °K	Calculated $\sigma(295°K)$ $(ohm\text{-}cm)^{-1}$
(NMP)(TCNQ)[13]	214	.22	485	.70	1000	300
$(Qn)(TCNQ)_2$[21]	214	.45	485	.80	1000	85
$(Adn)(TCNQ)_2$[19]	214	.90	485	.80	500	50
(TTF)(TCNQ)[16]	214	1.54	485	.80	3000	660*
(TTF)(TCNQ)[16]	354	.16	684	1.33	1500	130†

*For TCNQ Band.
†For TTF Band.

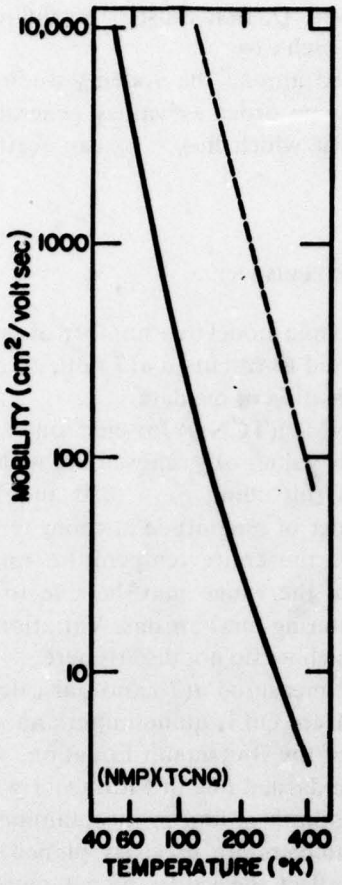


FIGURE 10. Mobility versus temperature calculated for molecular phonon scattering in (NMP)(TCNQ) with parameters indicated in text (solid line). The dashed lines show a T^{-4} dependence.

gap.[13] There is no crystallographic evidence for a superlattice or periodic distortion in $(Adn)(TCNQ)_2$[20] or $(Qn)(TCNQ)_2$;[9] therefore, other sources of the gap must be considered. For (NMP)(TCNQ) we have suggested[7,8,13] that the gap occurs because on-site coulomb repulsion prevents more than one electron settling at a TCNQ site. The gap is then a Mott-Hubbard gap at midband. For the other salts it has already been suggested by Holczer *et al.*[62] that nearest-neighbor coulomb interactions, treated in the extended Hubbard model, are responsible for a gap at the 1/4 band level. (However, they identify this gap as corresponding to the low-temperature slope of log σ versus T^{-1}.) Such a gap has also been invoked by Kwak *et al.*[63] to explain the thermopower of these compounds. A consequence of the extended Hubbard model is that $\rho(\epsilon)$ is decreased by a factor of 4. This decreases n by a factor of 4 and increases μ by this factor, leaving the calculated σ unchanged. In this model our calculated μ for 300°K is 7.6 cm^2/volt-sec for $(Qn)(TCNQ)_2$ and 1.6 cm^2/volt-sec for $(Adn)(TCNQ)_2$.

Woynarovich *et al.*[64] have proposed a model in which coulomb coupling between charge-density waves (CDW's) on the neighboring TCNQ chains is the source of the semiconducting gap. Though this model is attractive in that it leads to a gap at the Fermi energy regardless of the degree of band filling, there is, as

yet, no evidence for the existence of the CDW's on each TCNQ chain which are necessary for the occurrence of this gap. We point out that part (or even all) of Δ may be a mobility gap associated with localization of states at the band edges due to disorder. It has also been suggested[65] that long-range intrachain coulomb interactions may lead to a gap at ϵ_F. Additional studies are necessary in order to identify unambiguously the source of the Δ's obtained in our analysis.

The calculation of $\sigma(T)$ for (TTF)(TCNQ) requires the calculation of $\mu(T)$ for electrons on TCNQ chains and holes on TTF chains. Using the value[66] of $\sigma(295°K) = 660 \pm 130$ ohm^{-1}cm^{-1} and a charge transfer of 0.59 electrons from

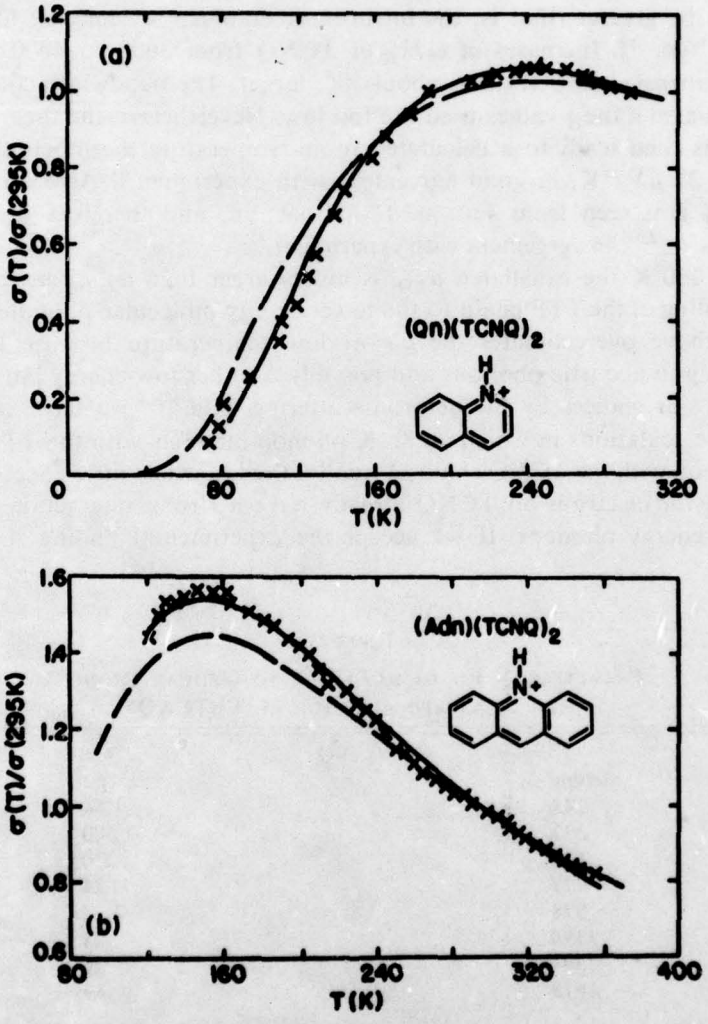


FIGURE 11. (a): Conductivity versus temperature for $(Qn)(TCNQ)_2$ (from Ref. 21) (X). The solid line is our fit in Equation 4 with $\Delta_0 = 650°K$ and $\alpha = 2.54$. The dashed line is our calculated $\sigma(T)$. (b): Conductivity versus temperature for $(Adn)(TCNQ)_2$ (from Ref. 19 (X). The solid line is our fit to Equation 4 with $\Delta_0 = 350°K$ and $\alpha = 2.34$. The dashed line is our calculated $\sigma(T)$.

TTF to TCNQ,[67,68] we deduce from $\sigma = ne\mu$ (where μ is the sum of electron and hole mobilities) that $\mu = 3 \pm 1$ cm^2/volt-sec at room temperature and 300–450 at T_m for the best samples. These values of μ and their temperature dependence are similar to those obtained above for the Class II systems. Assuming that the upper limit[66] of $\sigma(295°K) = 790$ ohm^{-1}cm^{-1} represents a sample without defects, we obtain agreement of theory with experiment for bandwidths[69,70] $\epsilon_0/k_B = 3000°K$ (0.25 eV) for TCNQ, 1500°K for TTF, and values of $\hbar\omega_i$ and g_i given in TABLE 3. For these bandwidths, as seen in FIGURE 12(a) the calculated mobility at room temperature for TCNQ is 3.5, for TTF 1 cm^2/volt-sec, giving a sum, $\Sigma\mu$, of 4.5 in good agreement with the upper limit cited earlier. These bandwidths, particularly those for TCNQ, must be considered lower limits, since the intrinsic $\mu(295°K)$ could well be greater (that is, the intrinsic dc conductivity may be higher than 790 ohm^{-1} cm^{-1}). Increases of ϵ_0/k_B of TCNQ from 3000 to 4000 would require the intrinsic $\mu(295°K)$ to be about 50% larger. The bandwidth could also be underestimated if the g values used are too low. Nevertheless, the theory with the bandwidths cited leads to a calculated room-temperature thermoelectric power, Q_{RT}, of -27 μV/°K, in good agreement with experiment.[71] Also, in the range 140–300°K it is seen from FIGURE 12(a) that $\Sigma\mu$, and therefore σ, varies essentially as $T^{-2.33}$, in agreement with experiment.[45]

Below 150°K the calculated μ_{TTF} is much larger than μ_{TCNQ} because of the weak coupling of the TTF chain to the lower energy molecular phonons. The calculation above overestimates the μ's at low temperature because it neglects the coupling to acoustic phonons and possibly to other low-energy lattice modes. Guided in our choices by the neutron-scattering data,[67,68] we have carried out numerical calculations in which an 85°K phonon interacts with the TTF chain, a 52°K phonon with the TCNQ chain. Actually, the latter has little effect on the results, since the electrons on TCNQ already have a strong interaction with relatively low-energy phonons. If we accept the experimental finding that $\sigma(T_m)$/

TABLE 3

PARMETERS IN FIT OF $\mu(T)$ DUE TO OPTICAL PHONONS TO MEASURED $\sigma(T)$ FOR (TTF)(TCNQ)

$h\omega$(cm^{-1})	g
TCNQ	
148	1.54
337	.80
613	.20
725	.24
978	.20
1196	.22
1391	.20
1615	.49
TTF	
245	.16
475	1.33
736	.49
1094	.16

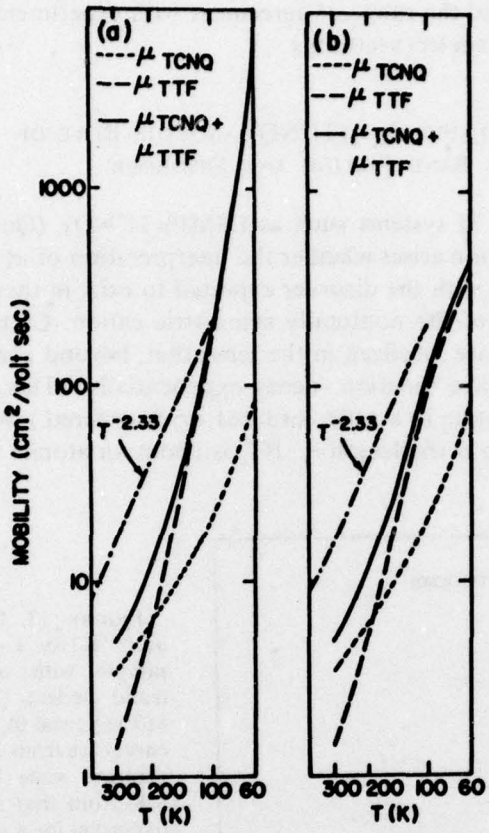


FIGURE 12. (a): Calculated μ versus T to optical phonon scattering for (TTF)-(TCNQ). (b): Calculated μ versus T due to topical phonon scattering plus acoustic phonons of 52°K for TCNQ, 85°K for TTF, both with coupling constant $g = 0.35$. (From Ref. 16)

$\sigma(295°K) = 100$, we must choose the coupling constant g no larger than 0.35 for the 85°K phonon. The results for $g = 0.35$ for both phonons are shown in FIGURE 12(b). Comparison with FIGURE 12(a) confirms that acoustic phonon scattering has little effect above 150°K.

From the large variation observed in σ_m/σ_{RT}[14,15,43,45,66] it appears that some sort of defect scattering is present in actual samples. One possibility is breaks in the chains. To incorporate this, we assume an additional relaxation time $\tau_{def} = \nu a/v$, where νa represents the average chain length, a being the intermolecular spacing, and v the velocity. This differs from the interrupted strand model calculation[35] in that the chain is not assumed to be a perfectly reflecting barrier. The relaxation time was then taken as the reciprocal of the sum of reciprocals of τ_{def} and (8), including the acoustic phonons. Numerical calculations led to the normalized σ versus T shown in FIGURE 13 for $\nu = 50$, which is in good agreement with the sample having $(\sigma_m/\sigma_{RT}) = 35$.[45]

In sum, we have been able to account for $\mu(T)$ and $\sigma(T)$ for materials in Class II and Class III over a wide temperature range through molecular vibration mode

scattering. We can extend the range of agreement with experiment by incorporating acoustic phonon and defect scattering.

$(NMP)_x(PHEN)_{1-x}(TCNQ)$ AND THE ROLE OF BAND FILLING AND DISORDER

Especially for Class II systems such as (NMP)(TCNQ), $(Qn)(TCNQ)_2$, and $(Adn)(TCNQ)_2$, a question arises whether the interpretation of $\sigma(T)$ that we have presented is compatible with the disorder expected to exist in these materials due to random orientation of the nontotally symmetric cation. Certainly we expect that the electron states are localized in the sense that, beyond some extended region of length l_a, the wave functions decay exponentially. (This, incidentally, is true for every electron state in a solid, ordered or disordered.) What determines the nature of conduction is the length l_a. If l_a is about an atomic site, conduction

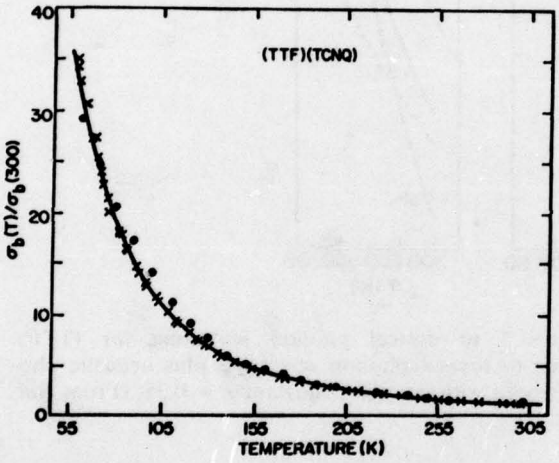
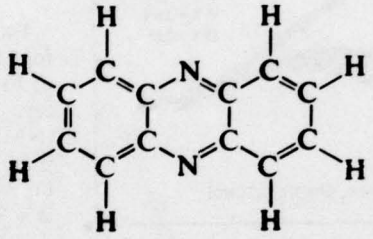


FIGURE 13. Calculated $\sigma(T)/\sigma(300°K)$ for $\nu = 50$ versus T for sample with $\sigma_m/\sigma(300°K) = 35$ (solid circles). The experimental $\sigma(T)$ (X) and fit to the data (solid curve) are from Ref. 45. The temperature scale has been shifted 5°K from that shown in Ref. 45 to correct for a constant deviation in the temperature readings for that sample, communicated to us by Dr. Groff. (From Ref. 16.)

is by hopping. At the other extreme, if l_a is much greater than the mean free path one would calculate for nonlocalized electrons the localization should have little effect on the conduction process. Numerical calculations for finite 1-D chains show that, with small disorder, states at the band edges become localized, while those near the center of the band may have l_a of the order of hundreds of lattice sites.[72] At temperatures high enough for these states to be significantly occupied, which we take to be $T > 65°K$ in our samples, they will dominate the dc σ. It is our view, then, that the major effects of disorder are to give rise to strongly localized states at the band edges (bandtailing). For the (weakly localized) states in the center of the band, a band model is applicable with the disorder providing a scattering mechanism in additional to thermal scattering.

In order to understand the roles of band filling and disorder, we have recently synthesized a new series of materials, $(NMP)_{1-x}(Phen)_x(TCNQ)$, which enable

us to directly test the roles of disorder and band filling.[73] In brief, up to 50% of the NMP^+ molecules, **2**, in (NMP)(TCNQ) are replaced with phenazine Phen° molecules, **4**, which are of similar size, shape, and polarizability to NMP^+, but are neutral, closed-shell, and symmetric. This substitution of Phen° for NMP^+ has two major effects: (1) The number of electrons in the conduction band on the TCNQ stack is reduced as the Phen° content is increased; i.e., for every NMP^+ replaced by a Phen°, the charge on the TCNQ stack is reduced by one. Thus, we can vary the band-filling of $(NMP)_x(Phen)_{1-x}(TCNQ)$ $(1.0 \geq x \gtrsim 0.5)$ from that of a half-filled band in a one-electron picture ($x = 1.0$), i.e., (NMP)(TCNQ), to that of a quarter-filled band in a one-electron picture ($x = 0.50$), similar to $(Qn)(TCNQ)_2$. (2) The randomness of the electrostatic potential at each TCNQ site increases. Before addition of Phen° the random potential at each TCNQ site arises from the random location of the NMP^+ methyl group leading to a random positive-charge distribution on the cation chain. The varying distance of this positive charge to the TCNQ sites leads to a fluctuating electrostatic potential. If a Phen° replaces an NMP^+, this is equivalent to moving the NMP^+ plus charge to infinity, thereby increasing the randomness in the potential at TCNQ sites.



Phen
4

Under most circumstances, if the charge transport in (NMP)(TCNQ) were dominated by hopping among disorder-induced localized states, then one might expect the activation energy for hopping between localized sites to increase as the root-mean-square random potential increases (more Phen°), thus increasing T_m. FIGURE 14(A) compares $\sigma_n(T)$ for samples: (NMP)(TCNQ), $(NMP)_{0.94}(Phen)_{0.06}$-(TCNQ), and $(NMP)_{0.81}(Phen)_{0.19}(TCNQ)$. The results are opposite to the simplistic disorder model prediction, as T_m decreases for the samples with increasing phenazine content. In addition, $\sigma_n(T_m)$ increases with increasing phenazine content, whereas $\sigma(295°K)$ remains at approximately 100 $ohm^{-1}cm^{-1}$.

The $\sigma(T)$ curves[74] in FIGURE 14(A) have the familiar Class II shape. Attempts at fitting the observed $\sigma(T)$ with Equation 4 have been very successful, as seen in FIGURE 4, with the $\Delta = 800°K$ and $\alpha = 3.9$ for the $x = 0.94$ sample and $\Delta = 550°K$ and $\alpha = 3.5$ for $x = 0.81$ sample. FIGURE 14(B) is a plot of α as a function of temperature calculated from Equation 4, using for σ the experimental values and for Δ the values given above. As seen by these flat curves, there is no change of transport mechanism at T_m.

FIGURE 15 shows log σ versus T^{-1} for the same three samples together with the fits to Equation 4. In all cases the model fits the data in the regime of $T >$

60°K. Below this temperature, the dc conductivity is higher than predicted by the model, implying that hopping transport through localized states dominates $\sigma(T)$ for $T < 60$°K. We note that $\sigma(T)$ is much higher in this hopping region for crystals with more phenazine. This implies that it is not three-dimensional hopping at low temperatures but rather hopping along the chain through localized states caused by the disorder.

The source of the energy gap in samples with $x \leq 1.0$ is important in understanding the microscopic aspects of 1-D materials. Several models may be appropriate; however, one model based upon the earlier work of Woynarovich *et al.*[64] appears particularly attractive. In this model interchain interaction between charge-density waves stabilizes the charge density waves and leads to a semiconducting behavior by producing a periodic electrostatic potential on neighboring chains, causing an energy gap at the Fermi energy. The magnitude of this gap depends upon crystal geometry, parallel and perpendicular dielectric

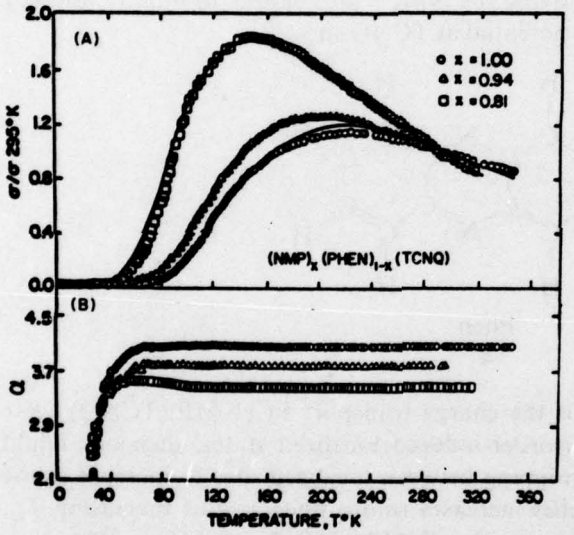


FIGURE 14. (a) Normalized four-probe *a*-axis conductivity, $\sigma(T)/\sigma(295°K)$ versus temperature for some representative $(NMP)x(Phen)_{1-x}(TCNQ)$ samples. The solid lines are computer fits to Equation 4; ○, $x = 1.00$, $\Delta = 900°K$, $\alpha = 4.12$; Δ, $x = 0.94$, $\Delta = 800$, $\alpha = 3.9$; □, $x = 0.81$, $\Delta = 550°K$, $\alpha = 3.5$. (b): $\alpha(T)$ calculated from Equation 4 with experimental $\sigma(T)$ and $\Delta = 900°K$ for $x = 1.00$, $\Delta = 800°K$ for $x = 0.94$, and $\Delta = 550°K$ for $x = 0.81$.

constants, and roughly, the square of the charge density (degree of charge transfer). As formulated[64] the ground state is nonmagnetic, although addition of on-site or intrachain coulomb repulsion would probably make the ground state magnetic. Inasmuch as the crystal structure does not appear to change appreciably with increased phenazine content,[73] the apparent energy gap should vary roughly as the square of the NMP content, x^2, in agreement with available experimental data.[74] These results have broad implications in the interpretation of the source of the observed activation energies in (NMP)(TCNQ), $(Qn)(TCNQ)_2$ and related systems,[74] as well as the source of coulomb correlations in (TTF)(TCNQ).[75]

Additional detailed experimental and theoretical studies are in progress on $(NMP)_x(Phen)_{1-x}TCNQ$ in an effort to quantify the effects of disorder and band filling.

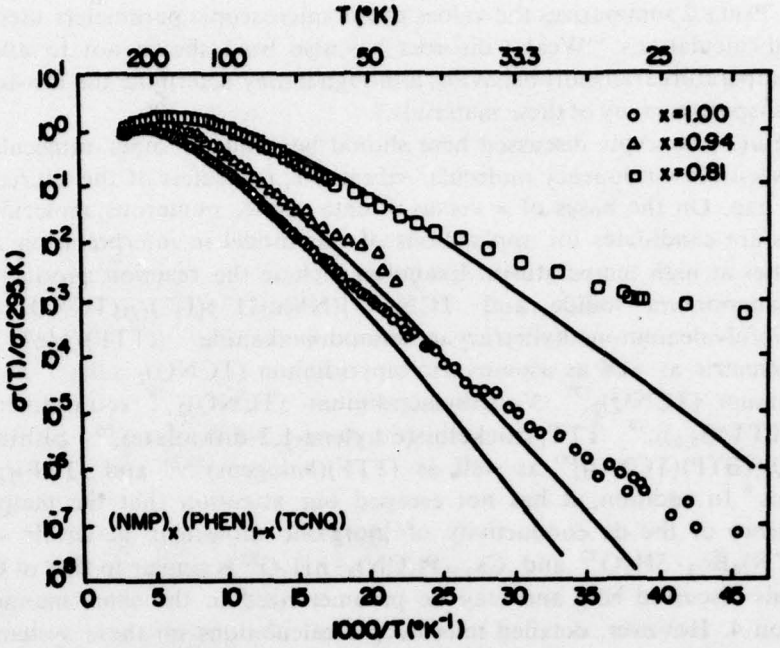


FIGURE 15. Experimental log $[\sigma(T)/\sigma(295°K)]$ versus T^{-1} for $(NMP)_x(Phen)_{1-x}(TCNQ)$ samples of FIGURE 14, and computer fits from Equation 4.

CONCLUSIONS AND SUMMARY

We have shown that the high temperature ($T > 60°K$) charge transport in many molecular conductors is dominated by those charge carriers in (activated to) extended states with a large, strongly temperature-dependent mobility determined mainly by interaction with molecular vibrations. TABLE 4 summarizes some of our parametric fits to $\sigma(T)$ data from a broad range of Class II and Class III ma-

TABLE 4

PARAMETERIZATION OF CLASS II AND CLASS III CONDUCTORS

$$\sigma(T) = \sigma_0 T^{-\alpha} \exp\left(-\frac{\Delta}{T}\right) = n(T)e\mu(T)$$

	α	Δ, °K
(NMP)(TCNQ)	3–4	900
$(NMP)_{.94}(Phen)_{.06}(TCNQ)$	3.9	800
$(NMP)_{.81}(Phen)_{.19}(TCNQ)$	3.5	550
$Qn(TCNQ)_2$	2.7	650
$Adz(TCNQ)_2$	3.0	450
$Adn(TCNQ)_2$	2.3	350
(TTF)(TCNQ)	2.3	0

terials. TABLE 2 summarizes the values of the microscopic parameters used in our detailed calculations. "Weak" disorder has also been shown not to affect this high-temperature transport behavior, although it may determine the low-temperature transport in many of these materials.

The $\mu(T)$ concepts discussed here should be valid for other molecular conductors with low-frequency molecular vibrations, regardless of the source of the energy gap. On the bases of σ versus T data alone, numerous molecular conductors are candidates for applications of this model in interpretation of their properties at high temperatures. Examples include the reaction product of trimethylammonium iodide and TCNQ $[(NMe_3H^+)(I_3^-)_{1/3}(TCNQ)^{2/3-})]$,[22,23] tetrathiofulvalenium-methyltetracyanoquinodimethanide [(TTF)(MeTCNQ)],[26] the symmetric as well as asymmetric bipyridinium $(TCNQ)_2$ salts,[76] *N*-methylquinolinium $(TCNQ)_2$,[77] *N*-methylacridinium $(TCNQ)_2$,[78] tetrathiotetracene-$(I_{1.6})$[(TTT)$(I_{1.6})$],[79] $TTT_{1.2}$nickelbis(ethylene-1,2-dithiolate),[80] bithiopyran-(TCNQ)[(BTP)(TCNQ)][81] as well as (TTF)(halogens)[24,25] and (TTF)(pseudohalogens.[6] In addition, it has not escaped our attention that the temperature dependence of the dc conductivity of inorganic molecular materials such as $K_2Pt(CN)_4Br_{.3}\cdot 3H_2O$[82] and $Cs_{1.75}Pt(CN)_4\cdot nH_2O$[83] is similar to that of Class II materials discussed here and may be parameterized in the same manner with Equation 4. However, detailed microscopic calculations on these systems have been hampered by a lack of information on acoustic and molecular electron-phonon coupling constants in the systems.

ACKNOWLEDGMENTS

It is a pleasure to acknowledge useful discussions with C. B. Duke, J. Mort, M. J. Rice, and D. J. Sandman.

REFERENCES

1. PÁL, L., G. GRÜNER, A. JÁNOSSY & J. SÓLYOM, EDS. 1977. Lecture Notes in Physics **65:**. Proc. Int. Conf. Organic Conductors Semiconductors. Siófok, Hungary, 1976. Springer-Verlag. Berlin, Germany; KELLER, H. J., ED. NATO Advanced Study Institute Series **B25:**. Lectures presented NATO Adv. Study Inst. Chemistry and Physics of One-Dimensional Metals. Bolzono, Italy. August 1976. Plenum Press. New York, N.Y.
2. MILLER, J. S. Introductory Remarks. This volume; ANDRÉ, J. J., A. BIEBER & F. GAULTIER. 1976. Ann. Phys. **1:** 145; MILLER, J. S. & A. J. EPSTEIN. 1976. Prog. Inorg. Chem. **20:** 1; GARITO, A. F. & A. J. HEEGER. 1974. Accts. Chem. Res. **7:** 232; SHCHEGOLEV, I. F. 1972. Phys. Stat. Sol. (a). **12:** 9.
3. FRITCHIE, C. J., JR. 1966. Acta Cryst. **20:** 892.
4. KOBAYASHI, H. 1975. Bull. Chem. Soc. Japn **48:** 1373.
5. KISTENMACHER, T. J., T. E. PHILLIPS & D. O. COWAN. 1974. Acta Cryst. **B30:** 763.
6. WUDL, F., D. E. SCHAFER, W. M. WALSH, JR., L. W. RUPP, JR., F. J. DISALVO, J. V. WASZCZAK, M. L. KAPLAN & G. A. THOMAS. 1977. J. Chem. Phys. **66:** 377.
7. EPSTEIN, A. J., S. ETEMAD, A. F. GARITO & A. J. HEEGER. 1971. Solid State Commun. **9:** 1803.

8. EPSTEIN, A. J., S. ETEMAD, A. F. GARITO & A. J. HEEGER. 1972. Phys. Rev. B. **5:** 952.
9. KOBAYASHI, H., F. MARUMO & Y. SAITO. 1971. Acta Cryst. B. **27:** 373.
10. KEPLER, R. G., P. E. BIERSTEDT & R. E. MERRIFIELD. 1960. Phys. Rev. Lett. **5:** 503.
11. BLAKEMORE, J. S., U. BERNSTEIN, J. E. LANE & D. A. WOODBURY. 1977. Proc. 13th Int. Conf. Physics of Semiconductors. FUMI, F. G., ED.: 345. Rome, Italy. Aug. 30–Sept. 3, 1976.
12. COLEMAN, L. B., J. A. COHEN, A. F. GARITO & A. J. HEEGER. 1973. Phys. Rev. B. **7:** 2122.
13. EPSTEIN, A. J., E. M. CONWELL, D. J. SANDMAN & J. S. MILLER. 1977. Solid State Commun. **23:** 355.
14. COLEMAN, L. B., M. J. COHEN, D. J. SANDMAN, F. G. YAMAGISHI, A. F. GARITO & A. J. HEEGER. 1973. Solid State Commun. **12:** 1125.
15. COHEN, M. J., L. B. COLEMAN, A. F. GARITO & A. J. HEEGER. 1974. Phys. Rev. **B 10:** 1298.
16. CONWELL, E. M. 1977. Phys. Rev. Lett. **39:** 777.
17. EPSTEIN, A. J. & E. M. CONWELL. 1977. Solid State Commun. **24:** 627.
18. WALATKA, V., JR & J. H. PERLSTEIN. 1971. Mol. Cryst. Liq. Cryst. **15:** 269.
19. MIHÁLY, G., K. RITVAY-EMANDITY & G. GRUNER. 1975. J. Phys. C. **8:** L361.
20. KOBAYASHI, H. 1974. Bull. Chem. Soc. Japn. **47:** 1346.
21. GOGOLIN, A. A., S. P. ZOLOTUKHIN, V. I. MELNIKOV, E. I. RASHBA & I. F. SHCHEGOLEV. 1975. JETP Lett. **22:** 278.
22. ABKOWITZ, M. A., A. J. EPSTEIN, C. H. GRIFFITHS, J. S. MILLER & M. L. SLADE. 1977. J. Am. Chem. Soc. **99:** 5304.
23. EPSTEIN, A. J. and J. S. MILLER. To be published.
24. WARMACK, R. J., T. A. CALLCOTT & C. R. WATSON. 1975. Phys. Rev. B. **12:** 3336.
25. SOMOANO, R. B., A. GUPTA, V. HADEK, T. DATTA, M. JONES, R. DECK & A. M. HERMANN. 1975. J Chem. Phys. **63:** 4970.
26. JACOBSEN, C. S., J. R. ANDERSEN, K. BECHGAARD & C. BERG. 1976. Solid State Commun. **19:** 1209.
27. MOTT, N. F. & W. D. TWOSE. 1961. Adv. Phys. **10:** 107.
28. BLOCH, A. N., R. B. WEISMAN & C. M. VARMA. 1972. Phys. Rev. Lett. **28:** 753.
29. EHRENFREUND, E., S. ETEMAD, L. B. COLEMAN, E. F. RYBACZEWSKI, A. F. GARITO & A. J. HEEGER. 1972. Phys. Rev. Lett. **29:** 269.
30. SHANTE, V. K. S. 1977. Phys. Rev. B. **16:** 2597.
31. THEODOROU, G. & M. H. COHEN. 1976. Phys. Rev. Lett. **37:** 1014.
32. THEODOROU, G. 1977. Phys. Rev. B. **16:** 2254, 2264, 2273.
33. KUSE, D. and H. R. ZELLER. 1971. Phys. Rev. Lett. **27:** 1060.
34. RICE, M. J. & J. BERNASCONI. 1972. Phys. Lett. **38A:** 277.
35. RICE, M. J. & J. BERNASCONI. 1973. J. Phys. F. **3:** 55.
36. HEEGER, A. J. & A. F. GARITO. 1975. NATO Advanced Study Inst. Ser. **B7:** 89.
37. HEEGER, A. J. 1977. NATO Advanced Study Inst. Ser. **B25:** 87.
38. TANNER, D. B., C. S. JACOBSEN, A. F. GARITO & A. J. HEEGER. 1974. Phys. Rev. Lett. **32:** 1301, **33:** 1559.
39. TANNER, D. B., C. S. JACOBSEN, A. F. GARITO & A. J. HEEGER. 1976. Phys. Rev. B. **13:** 3381.
40. ELDRIDGE, J. E. 1977. Solid State Commun. **21:** 737.
41. COHEN, M. J., P. R. NEWMAN & A. J. HEEGER. 1976. Phys. Rev. Lett. **37:** 1500.
42. COHEN, M. J. & A. J. HEEGER. 1977. Phys. Rev. B. **16:** 688.
43. ETEMAD, S., T. PENNEY, E. M. ENGLER, B. A. SCOTT & P. E. SEIDEN. 1975. Phys. Rev. Lett. **34:** 741.
44. SEIDEN, P. E. & D. CABIB. 1976. Phys. Rev. B. **13:** 1846.
45. GROFF, R. P., A. SUNA & R. E. MERRIFIELD. 1974. Phys. Rev. Lett. **33:** 418.
46. SODA, G., D. JEROME, M. WEGER, J. M. FABRE, and L. GIRAL. 1976. Solid State Commun. **18:** 1417.
47. ABRAHAMS, E. 1954. Phys. Rev. **95:** 839.

48. a: JEROME, D. & M. WEGER. 1977. NATO Advances Study Inst. Ser. **B25:** 341; b: GUTFREUND, H. & M. WEGER. 1977. Phys. Rev. B. **16:** 1753.
49. BURAVOV, L. I., M. L. KHIDEKEL', I. F. SHCHEGOLEV & E. G. YAGUBSKII. 1970. JETP Lett. **12:** 99.
50. ZIMAN, J. M. 1964. Principles of the Theory of Solids: 194. Cambridge Univ. Press. New York, N.Y.
51. BOZIO, R., A. GIRLANDO & C. PECILE. 1975. J. Chem. Soc. Faraday Trans. II: 1237.
52. LIPARI, N. O., C. B. DUKE, R. BOZIO, A. GIRLANDO, C. PECILE & A. PADVA. 1976. Chem. Phys. Lett. **44:** 236.
53. LIPARI, N. O., C. B. DUKE, R. BOZIO, A. GIRLANDO, C. PECILE & A. PADVA. 1977. Int. J. Quant. Chem. In press.
54. DUKE, C. B., N. O. LIPARI & L. PIETRONERO. 1975. Chem. Phys. Lett. **30:** 415; RICE, M. J. & N. O. LIPARI. 1977. Phys. Rev. Lett. **38:** 437.
55. RICE, M. J., C. B. DUKE & N. O. LIPARI. 1975. Solid State Commun. **17:** 1089.
56. RICE, M. J., L. PIETRONERO & P. BRUESCH. 1977. Solid State Commun. **21:** 757.
57. BRAU, A. & J. P. FARGES. 1972. Physics Lett. **41A:** 179.
58. BRIGHT, A. A., P. M. CHAIKIN & A. R. MCGHIE. 1974. Phys. Rev. B. **10:** 3560.
59. LONG, R. E., R. A. SPARKS & K. N. TRUEBLOOD. 1965. Acta Cryst. **18:** 932.
60. SCHEIN, L. B. 1977. Chem. Phys. Lett. **48:** 571; SCHEIN, L. B. 1977. Phys. Rev. B **15:** 1024.
61. SCHEIN, L. B., C. B. DUKE & A. R. MCGHIE. 1977. Phys. Rev. Lett. In press.
62. HOLCZER, K., G. MIHALY, A. JANOSSY & G. GRUNER. 1976. Mol. Cryst. Liq. Cryst. **32:** 199.
63. KWAK, J. F. & G. BENI. 1976. Phys. Rev. B. **13:** 652.
64. WOYNAROVICH, F., L. MIHALY & G. GRUNER. 1976. Solid State Commun. **19:** 1189.
65. GRANT, P. & J. HUBBARD. Private communication.
66. COHEN, M. J., L. B. COLEMAN, A. F. GARITO & A. J. HEEGER. 1976. Phys. Rev. B. **13:** 5111.
67. COMES, R., S. M. SHAPIRO, G. SHIRANE, A. F. GARITO & A. J. HEEGER. 1975. Phys. Rev. Lett. **35:** 1518.
68. SHIRANE, G., S. M. SHAPIRO, R. COMES, A. F. GARITO & A. J. HEEGER. 1976. Phys. Rev. B. **14:** 2325.
69. RITSKO, J. J., D. J. SANDMAN, A. J. EPSTEIN, P. C. GIBBONS, S. E. SCHNATTERLY & J. FIELDS. 1975. Phys. Rev. Lett. **34:** 1330. (An upper limit on (TTF)(TCNQ) bandwidths of 0.55 eV is given.)
70. RYBACZEWSKI, E. F., L. S. SMITH, A. F. GARITO & A. J. HEEGER. 1975. Phys. Rev. Lett. **34:** 741.
71. CHAIKIN, P. M., J. F. KWAK, T. E. JONES, A. F. GARITO & A. J. HEEGER. 1973. Phys. Rev. Lett. **31:** 601.
72. MOORE, E. J. 1973. J. Phys. C. **6:** 1551.
73. MILLER, J. S. & A. J. EPSTEIN. 1978. J. Am. Chem. Soc. 100:1639; MILLER, J. S. This volume.
74. EPSTEIN, A. J. & J. S. MILLER. To be published.
75. TORRANCE, J. B., Y. TOMKIEWICZ & B. D. SILVERMAN. 1977. Phys. Rev. B **15:** 4738.
76. MIHALY, G., K. RITVAY-EMANDITY, A. JANOSSY, K. HOLCZER & G. GRUNER. 1977. Solid State Commun. **21:** 721.
77. MIHALY, G., K. HOLCZER, G. GRUNER & L. D. KUNSTELJ. 1976. Solid State Commun. **19:** 1091.
78. MIHALY, G., K. RITVAY-EMANDITY & G. GRUNER. 1977. Lecture Notes in Physics. **65:** 535.
79. MIHALY, G., A. JANOSSY & G. GRUNER. 1977. Solid State Commun. **22:** 771.
80. BRAY, J. W., H. R. HART, JR., L. V. INTERRANTE, I. S. JACOBS, J. S. KASPER, P. A. PIACENTE & G. D. WATKINS. 1977. Phys. Rev. B. **16:** 1359.
81. EPSTEIN, A. J. & D. J. SANDMAN. To be published.
82. ZELLER, H. R. & A. BECK. 1974. J. Chem. Phys. Solids. **35:** 77.
83. EPSTEIN, A. J. & J. S. MILLER. To be published.

Discussion

Jerome Perlstein (*Eastman Kodak, Rochester, N.Y.*): Your interpretation of the mobility suggests that the mobility ought to be of the order of $10^3 cm^2/(V \cdot sec)$ at low temperatures. Do you support that?

Epstein: Direct measurement of mobility in (NMP)(TCNQ) and similar materials via time of flight and other standard techniques is difficult because of the high dark conductivity. Also, Hall effect measurements are hampered by anisotropy and small crystal size. We have been able, however, to directly detect the band gap of a system [$(NMe_3H)(I)(TCNQ)$] which exhibits a similar temperature-dependent conductivity at high temperatures via polarized reflectivity and thermoelectric power. These results directly verify the semiconducting nature of $(NMe_3H)(I)$-(TCNQ) despite its "metal-like" conductivity.

Aaron Bloch (*Johns Hopkins Univ., Baltimore, Md.*): We found in collecting (NMP)(TCNQ) samples from many laboratories that the degree of order varies tremendously from batch to batch and even within batches. For example, diffuse x-ray scattering experiments show everything from almost complete order with an alternation of the dipoles which gives semiconducting behavior, to the very disordered material that Epstein described.

Epstein: We are discussing only disordered systems here.

Bloch: As far as the phenazine work is concerned, it is by no means clear to me that one is increasing the RMS random potential experienced for an electron moving along the TCNQ chain. If you are decreasing it, all the conductivity data is consistent with the disorder model.

Epstein: The NMP^+ provides positive sites that act as attractive potentials for electrons moving in a TCNQ chain. If you disorder the attractive potentials you have varying degrees of barrier heights. If you now add a neutral molecule to the NMP^+ chain it acts as a barrier compared to the attraction of NMP^+ of either orientation. Hence, it appears that in this system we are increasing the disorder considerably.

FRAMEWORK FOR CLASSIFYING AND INTERPRETING THE PHYSICAL PROPERTIES OF CHARGE-TRANSFER SALTS OF TCNQ: THE UNIFYING FEATURE OF ORGANIC METALS*

J. B. Torrance†

IBM Thomas J. Watson Research Center
Yorktown Heights, New York 10598

INTRODUCTION

Interest in highly conducting organic solids has concentrated on the charge-transfer salts of the strong organic acceptor TCNQ (tetracyano-p-quinodimethane).[1-8] With use of a wide variety of inorganic and organic donors, approximately 400 salts have been made that have segregated stacks, but only a very small number have room-temperature conductivities greater than 50 $\Omega^{-1}cm^{-1}$. In fact, this large class of materials shows a wide range of magnetic and structural, as well as electrical, properties. For example, the room-temperature conductivities range from 10^{-9} to $10^{+3}\Omega^{-1}cm^{-1}$. At lower temperatures, some TCNQ salts have activation energies larger than 0.35 eV, in contrast to HMTSF-TCNQ,[9,10] which is still highly conducting below 1°K. The magnetic susceptibility in some cases is activated, sometimes roughly constant; in some materials it rises sharply at low temperatures, and sometimes exhibits unusual magnetic field dependence. The stoichiometry of donor to TCNQ is 1:1 in the *simple salts*, but is often found as 2:3, 1:2, or even 1:4 in *complex salts*. The TCNQ molecules in the acceptor stacks are sometimes uniformly spaced, but more often are grouped into units of two, three, or four at room temperature. In some of the salts with uniform stacks at 300°K, a phase transition is observed at lower temperature, at which the stacks become distorted.

Similarly, there are a large number of effects and interactions which are believed to have an important influence on these properties: U_0 (the Coulomb repulsion energy between two electrons on the *same* molecule), V_1 (the Coulomb repulsion between electrons on *neighboring* molecules), $4t$ (the bandwidth arising from the strong π-molecular overlap between molecules along the stack), J (the exchange interaction between neighboring spins), ρ (the number of unpaired electrons per TCNQ), the stoichiometry (whether simple or complex), the polarizability and size of the cations, the interaction between stacks (both overlap and Coulomb), whether the cations are symmetric or asymmetric (and the disorder that may result from random orientation of the donors in the crystals), steric interactions between stacks, impurities, the temperature dependence of the mobility, effects of stacking faults, whether the stacks are uniform or distorted, the coupling of electrons to intermolecular and intramolecular vibrations, as well as

*Manuscript received Aug. 5, 1977.
†Present address: IBM Research Laboratory, San Jose, California 95193

0077-8923/78/0313-0210 $1.75/1 © 1978, NYAS

librational modes, metallic screening, Peierls and other instabilities possible in quasi-one-dimensional systems, structural details, whether cations are radicals or not, and so on. Furthermore, there is no general agreement regarding which of these interactions are most important and which play only a minor role.

Clearly, the situation is extremely complex, with a wide variety of properties and an even wider variety of possible explanations and effects to be considered. Thus, we have no right or reason to expect that any one simple picture or model will be helpful to our understanding of the unusual behavior of these complicated systems. Nevertheless, it is tempting for optimists to at least try to explain the large variations in the properties of the TCNQ salts as due to differences in one variable, assumed to be the most important, key parameter. There have been three attempts to understand the large differences in the *conductivity* between materials: (1) LeBlanc[11] and later Garito and Heeger[12] proposed that differences in the excitonic polarizability of the cations gave rise to differences in the screening (or reduction) of the Coulomb interactions (U_0 and V_1). The variation in the observed conductivity was then attributed to variations in the strength of the Coulomb interactions; i.e., the weaker the Coulomb repulsion, the higher the conductivity. (2) Bloch,[13,14] and subsequently the Hungarian group,[15–18] have emphasized the difference in conductivity between salts with symmetric donor molecules and those with asymmetric donors. The idea here is that the asymmetric donors stack with random orientation, giving rise to a random potential, which can counteract the insulating effects of other interactions and hence increase the conductivity. (3) A number of workers[3,6,19–21] have proposed that certain salts have a high conductivity because they have uniform TCNQ stacks, whereas poorer conductors usually have distorted stacks. Although this is a helpful (but not surprising) observation, it does not add to our understanding until it is explained *why* some stacks are uniform and why some are distorted.

In this paper, we propose another, equally oversimplified (but, it is hoped, better) description of the TCNQ charge-transfer salts, in which it is assumed that polarization and disorder play only a minor role. It is suggested[8,22–26] that *the Coulomb interactions are the dominant interactions and that key variable is ρ, the number of electrons per TCNQ molecule.* We will attempt to explain the variations in the gross features of the conductivity, magnetic susceptibility, optical absorption, and stack distortions as directly determined by variations in ρ. These variations in ρ can occur because of different ratios of donors to TCNQ and/or because the charge transfer from the donor to TCNQ can be either complete or incomplete. It is concluded, for example, that the unifying common feature of the known organic metals is an incommensurate (or nonsimple fractional) value of ρ, due to incomplete charge transfer.[25] It is further proposed[23,24] that ρ is determined by the ionization potential of the donor molecule and the strength of the ionic bonding in these materials.

In an earlier paper,[8] we have concentrated on the properties of the simple (1:1) TCNQ salts, where the differences are larger and more dramatic. In many ways, the present paper is a somewhat more speculative extension of that work to include the complex salts, where the differences are more subtle. It must be emphasized that these are extremely complicated systems and that we are describing a highly oversimplified attempt to identify the most important interactions and param-

eters and to achieve a broad, general understanding of the basic features of these materials. This should provide a framework and a starting point for further work, which must eventually include the many other interactions that play a role. The emphasis of this paper will thus focus on proposing this general framework, and space limitations will not permit extensive discussions of alternative models, explanations, or interpretations of the data. Neither will we be able to reference adequately all of the detailed work or discuss more detailed experiments.

The effects of Coulomb interactions[6,26,27] in these materials have been described in terms of an effective Coulomb repulsion energy, U. The energy U is given by $U = U_0 - V_1$, i.e., the difference between the Coulomb repulsion (U_0) of two electrons on the same molecule and that (V_1) on neighboring molecules. This energy is most readily determined[8] by measuring the energy of the charge transfer band of $(TCNQ^-)_2$ dimers in solution. This band occurs[28] at 1.4 eV (11,500 cm^{-1}) and appears[22,29,30] to be very similar in a variety of different simple and complex TCNQ salts. In addition, the dimer charge transfer bands of many donors and acceptors are not very different, lying in the 1–2 eV range. The point is, presumably, that U_0 and V_1 may vary for different molecules and in different environments, but the *difference* $U = U_0 - V_1$ appears to vary only slightly. This view is supported by recent calculations of Hubbard,[31] which show that high conductivity and large polarizability do decrease both U_0 and V_1 somewhat in TCNQ salts, but the difference U is only weakly affected. Thus, we take $U = 1$ eV as a repre-

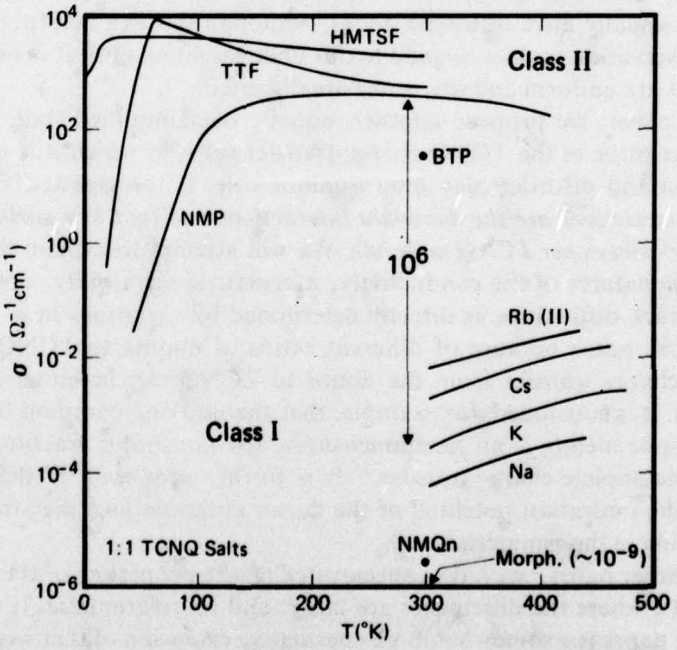


FIGURE 1. The temperature-dependent conductivity for a number of simple (1:1) TCNQ salts, illustrating how they fall into two distinct classes. (For meaning of abbreviations, see TABLE 1.)

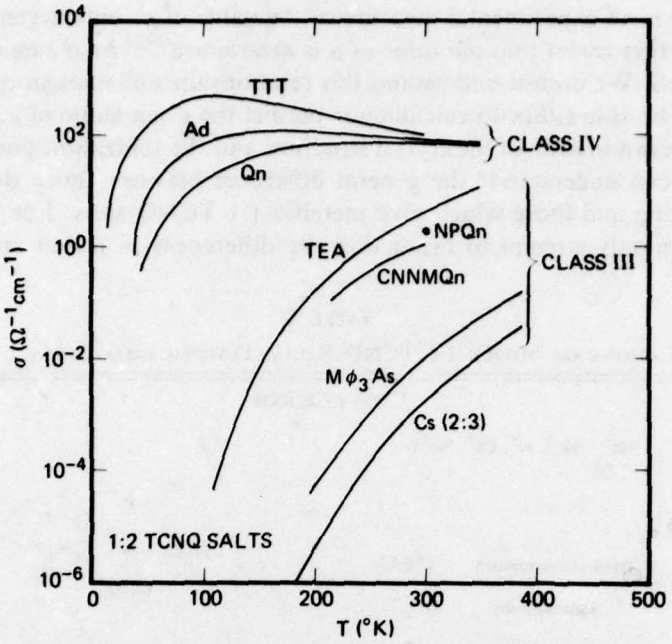


FIGURE 2. The temperature dependence of the conductivity of a number of complex TCNQ salts, illustrating how they can be divided into two classes (III and IV). (For meaning of abbreviations, see TABLE 2.)

sentative value and assume (for simplicity) that it is the same for all TCNQ and donor stacks.

Another important parameter is $4t$, the bandwidth associated with π-molecular overlap down the stack. This quantity can be determined from calculations or from measurements of the plasma frequency. Calculations for the TTF and TCNQ stacks in TTF-TCNQ give[32] $4t \sim \frac{1}{2}$ eV, in agreement with the value inferred from plasma frequency measurements.[33] The observed stack spacings in other salts are not very different,[4,5,34] and the plasma frequencies (for NMP-TCNQ and TEA-$TCNQ_2$) do not appear to differ strongly.[33] For these reasons, it is reasonable to assume (for simplicity) that $4t \sim \frac{1}{2}$ eV for all the donor and TCNQ stacks. (In cases of eclipsed overlap, e.g. K-TCNQ and TTF-Br_ρ, the actual values are appreciably larger than this estimate.)

In our model, the key parameter that differs from one TCNQ salt to another is not U or $4t$, but is ρ, the number of unpaired electrons per molecule (on average). It is variations in this parameter which are responsible for the variation in physical properties observed. For a compound D-$TCNQ_n$ with complete charge transfer from the donor, D, to TCNQ, ρ on the TCNQ stack would be determined by the stoichiometry: $\rho = 1/n$. If the charge transfer is incomplete, ρ will be somewhat less than this value on the TCNQ stack. Similarly, we must consider the number of unpaired electrons on the donor stack. While we can get an estimate of ρ from the stoichiometry, we will be free to postulate incomplete charge transfer in some cases in order to explain the observed properties. In a few of these

cases, there is an experimental measure of the value of ρ, but in general there is not. We further assert that *the value of ρ is determined*[23,24] *by the ionic bonding in these crystals.* We do not understand this relationship well enough quantitatively in order to be able either to calculate or predict the exact value of ρ, but from a qualitative examination of the crystal structure and the ionization potential of the donor, we can understand[8] the general difference between those donors which give insulating and those which give metallic 1:1 TCNQ salts. For the complex salts, we can only attempt to rationalize the differences in ρ that are postulated

TABLE 1.

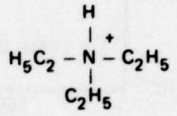
THE CATIONS OF SIMPLE 1:1 TCNQ SALTS, DIVIDED INTO CLASS I AND II

Class I Cations

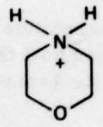
Na^+ (Li^+, K^+, Cs^+, Rb^+)

triethylammonium [TEA]

(ammonium NH_4^+)



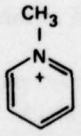
morpholinium [Morph]



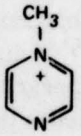
N–methylpyridinium [NMPy]

(pyridinium)

(4-cyano-NMPy)



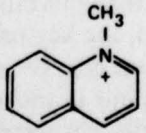
N–methylpyrazinium



N–methylquinolinium [NMQn]

(4-cyano-NMQn ,

(8-hydroxy-NMQn ,



N–methylacridinium [NMAd]

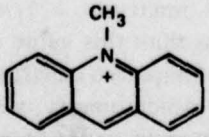
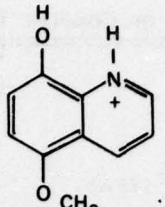


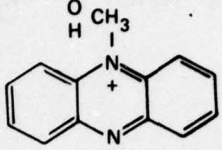
TABLE 1 (*Continued*)

Class II Cations

5, 8 dihydroxyquinolinium

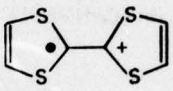


N–methylphenazinium [NMP]

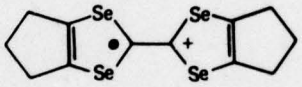


tetrathiafulvalinium [TTF]

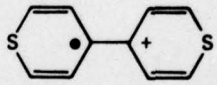
(tetraselenafulvalinium [TSeF])



hexamethylene – TSeF [HMTSF]



Δ 4, 4′ bithiopyranium [BTP]



for these materials on the basis of differences in their crystal structure (see DETERMINATION OF ρ AND CHARGE TRANSFER).

Another possible description of this paper would be: *Assuming only that $U \sim 1$ eV and $4t \sim \frac{1}{2}$ eV for all stacks in all compounds, how much of the variations in the gross properties (conductivity, susceptibility, optics, and stack distortions) can be understood by considering only variations in the parameter ρ?* And how reasonable are these values of ρ which are postulated (from the point of view of the donor ionization potential and the ionic binding energy of the crystal)?

CLASSIFICATION AND CONDUCTIVITY

In this section, charge-transfer salts of TCNQ that have segregated stacks will be classified in a simple, empirical way, based on both their stoichiometry and their conductivity. Thus, the single-crystal conductivity data for a number of representative TCNQ salts are shown separately in FIGURE 1 for simple (1:1) salts[8,9,35] and in FIGURE 2 for complex salts.[1,2,9,36–39] On the basis of their con-

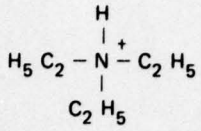
TABLE 2

THE CATIONS OF COMPLEX TCNQ SALTS, DIVIDED INTO CLASS III AND IV

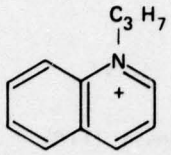
Class III Cations
(1:2 salts unless noted)

Cs^{+}[2,39,63] (2:3)

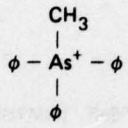
triethylammonium[2,66] [TEA]



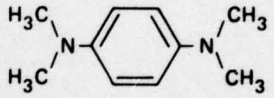
N-propylquinolinium[2,64] [NPQn]
(4-cyano-N-methyl Qn [CNNMQn])



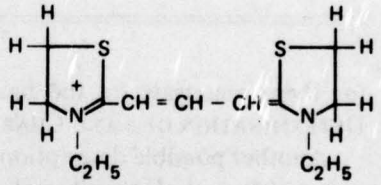
methyl-triphenylarsonium[38,65] [M ϕ_3 As]
(Me ϕ_3 P)[65]



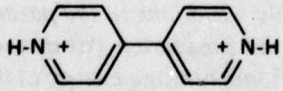
N,N,N′,N′ -tetramethyl-p-phenylenediamine[74] [TMPD]



3,3-diethylthiazolinocarbocyaninium[3] [Et_2 Tz CC]
(intermediate conductivity form)



4-4′ Bipyridinium[16,17]



1,2-di (N-ethyl-4-pyridinium) ethylene[87] [DEPE] (1:4)
(form II)

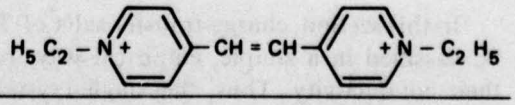
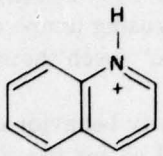


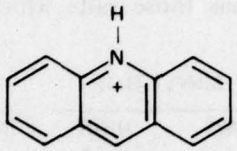
TABLE 2 (*Continued*)

Class IV Cations
(1:2 salts unless noted)

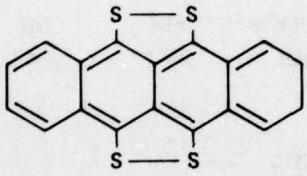
quinolinium[3,37,69] [Qn]
(N-methyl Qn, phase A)



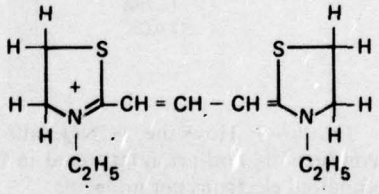
acridinium[3,37,70] [Ad]
(N-methyl Ad)



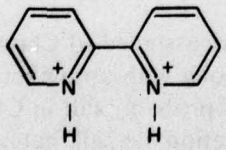
tetrathiotetracene[36,71] [TTT]



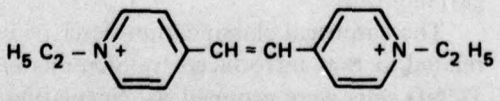
3,3-diethylthiazolinocarbocyaninium[3] [Et_2 Tz CC]
(high conductivity form)



2-2′ Bipyridinium[16,17]



1,2-di (N-ethyl-4-pyridinium) ethylene[87] [DEPE] (1:4)
(form I)



ductivity behavior (FIGURE 1), the simple salts clearly divide themselves[8] into two very distinct groups, called Class I and Class II, whose conductivities at 300°K differ by ~6 orders of magnitude. For example, K-TCNQ, NMQn-TCNQ, and other Class I salts (see TABLE 1) are practically insulating, with large activation energies and $\sigma(300°K) < 10^{-3}\Omega^{-1}cm^{-1}$. On the other hand, salts in Class II (see TABLE 1) such as NMP- and TTF-TCNQ, have a very high conductivity, which initially increases with decreasing temperature below 300°K. For this reason, these salts are called "metallic" (even though they are generally not metallic at low temperatures).

The difference in the conductivity behavior of the complex salts (FIGURE 2) is not as large or as sharply defined as for the simple salts. Nevertheless, we can group those salts with $\sigma(300°K) < 10\Omega^{-1}cm^{-1}$ and with activation energies >0.1 eV into Class III, whereas those salts which are "metallic" near 300°K

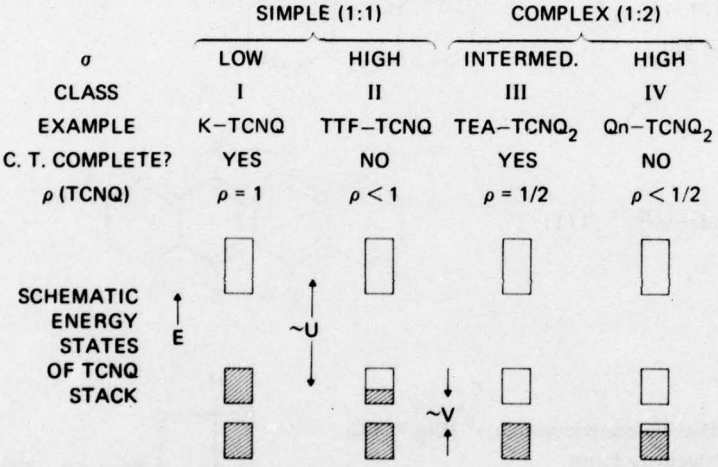


FIGURE 3. How the TCNQ salts are classified on the basis of the magnitude of their conductivity and are interpreted in terms of different values of ρ, the average number of unpaired electrons per molecule.

with $\sigma(300°K) > 50\Omega^{-1}cm^{-1}$ are assigned to Class IV. All of the cations of Class IV salts are listed in TABLE 2, along with a number of those from Class III. Many other complex salts that would probably fall in Class III cannot be classified because of inadequate characterization; i.e., all that is known is the conductivity of a compacted powder at 300°K. Considerable improvement in our understanding of the complex salts of TCNQ can be expected from the recent work of the Hungarian group.[15-17]

The empirical classification described above and summarized in FIGURE 3 is related to that introduced by Siemons *et al.*[2] and by Shchegolev,[3] in which the TCNQ salts were grouped as "insulating," "intermediate," or "highly conducting." For reasons that will be apparent subsequently, we have subdivided their "highly conducting" salts into Classes II and IV, depending on whether they are simple or complex. In addition, we have recognized that the "insulating" salts are

(almost) all simple salts (Class I) and the "intermediate" conductors are almost entirely complex salts (Class III). (Note that we are considering only TCNQ salts with segregated stacks.)

Furthermore, we propose an interpretation for the differences between the properties of salts in different classes, as summarized in FIGURE 3. According to this interpretation, Class I salts have complete transfer of one charge from the donor to TCNQ, so that there is $\rho = 1$ electron per TCNQ molecule. Such salts are insulators, called Mott insulators, because of the large Coulomb repulsion energy, $U \sim 1$ eV; i.e., in order for an electron to move down the stack (and contribute to the conductivity), it must be excited from one molecule to a neighboring one. For $\rho = 1$, the neighboring molecule already has an unpaired electron and the energy to activate conduction involves[40,41] the electron-repulsion energy U. As is discussed extensively in Reference 8, salts in Class II are asserted to have incomplete transfer of electrons from donor to TCNQ, so that there are $\rho < 1$ electrons per TCNQ molecule (on average). Now an unpaired electron may have a neutral TCNQ molecule neighboring and the electron can move down the stack, without having to overcome the large Coulomb interactions (which are still present). Thus, as discussed in Reference 8, the difference between the insulators of Class I and the metals of Class II is the difference between complete and incomplete charge transfer, i.e., the difference between complete and partial reduction of $TCNQ^{\circ}$ to $TCNQ^{-}$, or the difference between monovalence and mixed valence.

Somewhat analogous differences are proposed[25] for the difference between Classes III and IV, with complete and incomplete charge transfer in III and IV, respectively. Since the charge transfer for Class III salts is postulated to be complete, the value of ρ for D-$TCNQ_n$ is determined by the stoichiometry: $\rho = 1/n$. For $n = 2$ (or the less common value of $n = \frac{3}{2}$, as in Cs_2TCNQ_3), $\rho = \frac{1}{2}$ (or $\frac{2}{3}$). Such values, which are simple fractions, are called *commensurate*, as opposed to an *incommensurate* value of ρ, which could not be represented by such a simple ratio of two, relatively small integers. For such commensurate values, such as $\rho = \frac{1}{2}$, there are a number of different mechanisms[15,30,42-44] proposed which would cause the conductivity to be activated with a large activation energy, V. As an example, the repulsion, V_1, between electrons on neighboring molecules (if strong enough) gives rise[45] to a gap of magnitude $V = V_1 - 2t$, for $\rho = \frac{1}{2}$. We will not discuss this or the other mechanisms here, but will simply point out that they apply *only* for commensurate values of ρ ($= \frac{1}{2}, \frac{2}{3}$, etc.).

In Class IV salts, on the other hand, we assert that the charge transfer is incomplete, so that ρ is no longer simply related to the stoichiometry and has some incommensurate values, i.e., a value which is not a simple fraction. Just as a deviation of ρ from $\rho = 1$ enables the conductivity of Class II salts to avoid being limited by U, a deviation from $\rho = \frac{1}{2}$ in Class IV salts enables their conductivity to avoid being limited by the energies V in the mechanisms which have been proposed[15,30,42-44] for Class III salts.

The above discussion can also be made from a band point of view, with the aid of FIGURE 3. Here we give a very schematic representation of the energy states (or bands) of a TCNQ stack, for example. There is an energy gap in the band of magnitude $\sim U$ if $\rho = 1$ and a gap $\sim V$ for $\rho = \frac{1}{2}$. Different values of ρ for the

different classes cause the states to be filled up to different levels, as is self-explanatory from the figure.

The interpretation of the differences in the conductivity between classes may be summarized as follows: if $\rho = 1$ (as in Class I) conduction can occur down the stack at a cost of the large Coulomb energy U, which makes these salts insulating. If $\rho = \frac{1}{2}$ (or $\frac{2}{3}$), the energy cost of conduction is the weaker interaction V and the conductivity is intermediate. If, on the other hand, the charge transfer is incomplete, then ρ will not be commensurate and the conductivity will not be limited by these relatively large Coulomb energies. Thus, the organic metals i.e., those in Class II and IV, have as a common and unifying feature incomplete charge transfer and consequently an incommensurate value of ρ, and this is why they are metallic.[25]

The evidence for $\rho < 1$ in Class II salts is summarized in Reference 8. It comes most convincingly from diffuse x-ray- and neutron-scattering measurements,[46,47] although early indication came from susceptibility,[6] optical,[22] NMR,[48] and thermopower[49] measurements. The incomplete charge transfer postulated here for Class IV salts is evidenced in *our interpretation* of the magnetic susceptibility,[3,50] specific heat,[3,50,51] NMR,[52] and structural measurements, and was also proposed on the basis of thermopower measurements.[53] In particular, we propose that the low-temperature specific heat and tail in the magnetic susceptibility are caused by unpaired electrons on the donor stacks, which were not transferred to the TCNQ stack (see MAGNETIC SUSCEPTIBILITY). Further evidence is contained in recent NMR measurements reported by Shchegolev.[52]

RELATION BETWEEN CONDUCTIVITY, DISTORTIONS, AND ρ

It is clear that the conductivity of a TCNQ stack is related to whether the TCNQ molecules are uniformly spaced down the stack, or whether there is some sort of periodic distortion that makes the stack spacing nonuniform. Indeed, it has been proposed[3,6,19-21] that the difference between the poor conductivities of Classes I and III, compared with the higher conductivities of Classes II and IV (FIGURES 1 and 2), is *caused by* the difference between the distorted stacks observed in the former and the uniform stacks found in the latter salts. Others have suggested[12,14] that in order to design an organic metal, it is necessary to have uniform stacks. There are two problems with this approach of relating the conductivity directly to the distortions: first, the stack uniformity is not the whole effect. It is true that many of the Class I salts are observed to be dimerized (distorted), but it is also true that Na-, K-, and Rb(phase II)-TCNQ each have uniform stacks at high temperatures[54-56] *and they are still insulating*.[57] (The point is that they are insulating because of Coulomb interactions,[22,58] i.e. U, and not because of the distortions.) Similarly, Class III salts would be poor conductors due to V, even if they had uniform stacks. The second problem with this approach is that it is only a correlation and not an explanation: i.e., it gives no understanding of *why* some stacks are uniform and *why* some are distorted and gives no hint of *how* to design a material with uniform stacks. This situation is inadequate, because the types of distortions or lack of them need not be viewed as a feature of the crystal structure

which is beyond our understanding. An important contribution of solid-state physicists to this field is to recognize that, in many cases, the distortions of these quasi-one-dimensional stacks are driven by electronic and magnetic properties and are thus understandable and even predictable. In fact, the distortions can provide valuable experimental information that helps determine the very nature of the electronic and magnetic interactions. Thus, we should not regard distortions as the origin from which all properties are determined; rather, the distortions and the electronic and magnetic properties are all related. In our view, these are all related via ρ, as we shall see. (Just as the above approach is inadequate without an explanation of *why* the stacks in some cases are uniform, our approach is not complete until the Section DETERMINATION OF ρ AND CHARGE TRANSFER, where we show *how* the ρ is determined by donor ionization potential and the ionic bonding.)

The electronic and magnetic properties of quasi-one-dimensional systems cause the stacks to be unstable to a number of possible distortions. For the purpose of this paper, the important point is that the periodicity (λ) of these distortions is related to the Fermi wavevector, which is in turn related to the average number ρ of unpaired electrons per molecule:

$$\frac{\lambda}{d} = \frac{2}{\ell\rho} \tag{1}$$

where d is the intermolecular spacing along the stack and ℓ = 1 or 2, depending on the nature of the instability.[26,59] For example, in the case of the Spin-Peierls transition[60,61] discussed in the next section, ℓ = 1, so that if ρ = 1, (1) gives λ/d = 2; i.e., the stack will dimerize. If ρ is another commensurate value (e.g. $\frac{1}{2}$ or $\frac{2}{3}$), a commensurate distortion is expected (λ/d = 4 or 3). If, on the other hand, ρ is incommensurate (e.g. ρ = 0.59 as in TTF-TCNQ[46]), an incommensurate distortion is expected (and found[46] in TTF-TCNQ at λ/d = 3.38 and 1.69 for ℓ = 1 and 2). This distinction is important because commensurate distortions are expected[62] to be much stronger and to occur at higher temperature than incommensurate ones; it is much easier and more effective if the distortion has to double the stacking period rather than make the period 1.69 times as long. Hence, systems with incommensurate values of ρ will tend to distort weakly and at low temperatures, whereas commensurate systems may well be already strongly distorted at 300°K.

We now discuss the proposed explanation for the distortions (or lack of them) in these salts. For Class I salts, ρ = 1 and, as discussed in the next section, these salts are expected to have and are observed to have phase transitions which we identify as Spin-Peierls transitions,[60,61] below which the stacks are dimerized. For Class III, $\rho = \frac{1}{2}$ (and sometimes $\frac{2}{3}$), a number of distortions and mechanisms are possible.[30,42-44] The most common distortion observed[63-66] at room temperature is a tetramerization for $\rho = \frac{1}{2}$ which could indicate a delicate balance of long-range interactions,[30] even a Spin-Peierls transition, or one of the other mechanisms. Class II and IV salts, on the other hand, are approximately uniform[67-71] at room temperature. More careful examination by diffuse x-ray scattering, however, reveals a distortion in both TTF- and NMP-TCNQ at room temperature,[46,47] with a period of ~1.69 lattice constants for TTF-TCNQ. The important point is

that the magnitude of the distortions in Class II and IV salts are very weak compared to the easily observable distortions in Classes I and III. This difference is because the distortions are much stronger if the period of the distortion, and hence ρ, is commensurate.[62]

Thus, for a commensurate value of ρ, Coulomb interactions and large distortions can combine to severely limit the conductivity, whereas for incommensurate ρ both effects are much weaker, allowing high conductivity in Classes II and IV. These are the reasons *why* an incommensurate value of ρ is the common and unifying feature of organic metals. (The effects of three-dimensional phase transitions are discussed in PHASE TRANSITIONS.)

Although the tetramerized 1:2 TCNQ salts may well be understood with use some of the mechanisms proposed previously, a number of other salts appear to require a different mechanism. Specifically, the combination of (1) low conductivity, (2) $\rho = \frac{1}{2}$; and (3) large magnetic susceptibility of TMPD-$TCNQ_2$,[72-74] Et_4N-$TCNQ_2$,[72] and MEM-$TCNQ_2$[72,75] suggest that in the TCNQ stacks of these materials the long-range Coulomb interactions have caused the electrons to be *ordered on alternate molecules* down the stack, forming a so-called Wigner crystal.[24] As in the other mechanisms, if $\rho < \frac{1}{2}$ (and incommensurate), this system would be much more conducting.

SPIN-PEIERLS TRANSITION IN CLASS I SALTS

The magnetic properties of Class I salts have been extensively studied in the pioneering work of Vegter and coworkers.[19,20] They discovered that NH_4-TCNQ and all of the simple alkali-TCNQ salts[76] (with the exception of Li-TCNQ) show an

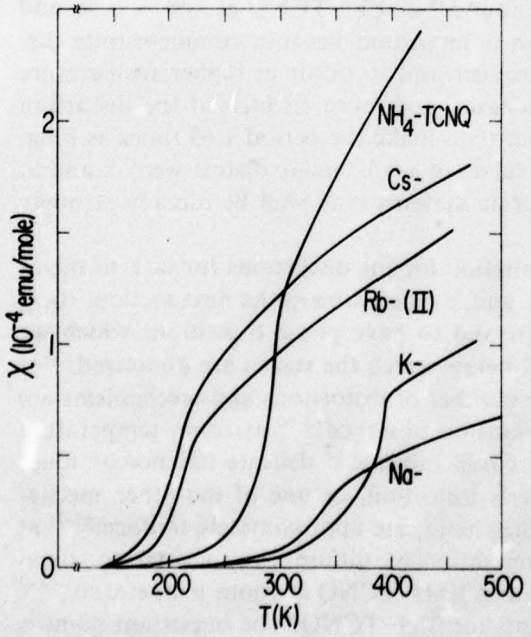


FIGURE 4. The magnetic susceptibility of NH_4^- and a number of alkali-TCNQ salts as measured by Vegter *et al.*[19] The phase transitions indicated by the inflection points in $\chi(T)$ are interpreted here as Spin-Peierls transitions.

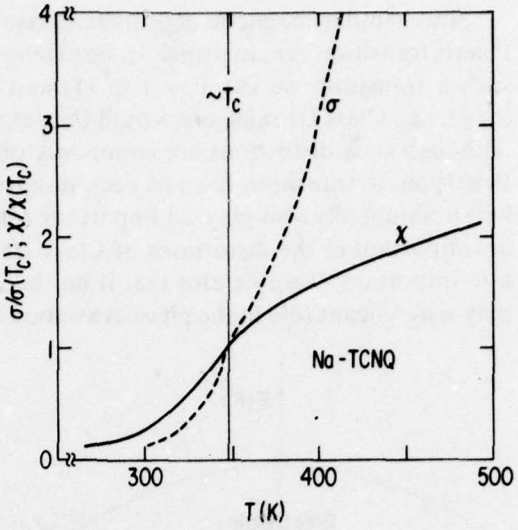


FIGURE 5. A comparison of the conductivity (after Ref. 57) and magnetic susceptibility (after Ref. 19) of Na-TCNQ, showing that σ is still strongly activated (insulating) above the phase transition near 350°K.

anomaly in the magnetic susceptibility as shown in FIGURE 4, indicative of a phase transition. The x-ray structures[54,55] of K- and Na-TCNQ as well as Guinier patterns[19,20] on other salts indicate that the TCNQ stacks are dimerized below the phase transition and uniform above (although there are undoubtedly some strong fluctuations[77]). In some salts the phase transition is second order; in others it is first order. It is important to note that these materials are still insulating above the phase transition,[57] where the stacks are uniform.[19,54-56] As seen in FIGURE 5 for Na-TCNQ, the conductivity[57] is only weakly affected by the onset of the distortion, but there is a strong influence on the magnetic susceptibility.[19] Furthermore, the nature and origin of these phase transitions has not previously been identified.

We identify these phase transitions as Spin-Peierls transitions,[60,61] where the energy gained by the distortion is magnetic rather than electronic as in the usual Peierls transition. Assuming that the Coulomb interactions (U) are strong in these materials, the excitation spectrum[41] can be schematically shown, as in FIGURE 6. As discussed earlier, for $\rho = 1$ (as in the Class I salts being considered here) there is a cost in energy $\sim U$ to excite an electron down the stack. Hence, these materials are insulating with a large activation energy ($\sim U$) and there is no *electronic* degeneracy that could be removed by a Jahn-Teller-like distortion. (One could say that this degeneracy has already been removed by the large intramolecular Coulomb interaction, U.) Although the electronic excitations have no degeneracies, the magnetic or spin excitations for a uniform stack have degeneracies at $k = -\pi/a$, 0 and $+\pi/a$ (FIGURE 6). It is known[60,61] that a dimerization of such a stack removes these degeneracies (actually the degeneracies in the *two-spin wave* states) and thus gain more than enough magnetic energy to compensate for the deformation energy. Such a Jahn-Teller-like distortion has been called a Spin-Peierls distortion by Pytte,[60] who first worked out the dynamics of the Spin-Peierls phase transition. We identify the phase transitions discovered by Vegter and Kommandeur in Class I salts as Spin-Peierls transitions, which we would also expect in other Class I salts.

Since similar magnetic degeneracies remain[78] for cases with $\rho < 1$, the Spin-Peierls transition can, in principle, be extended and generalized to these cases. For such a transition we use $\ell = 1$ in (1) and obtain $\lambda/d = 2/\rho$. Thus for $\rho = \frac{1}{2}$ (or $\frac{2}{3}$), i.e., Class III salts, one would thus expect a tetramerization (trimerization). Although such distortions are commonly observed in this Class, a distinct Spin-Peierls phase transition has not been discovered, and other effects (discussed earlier) undoubtedly also play an important role. Thus, Spin-Peierls effects probably are important in the distortions of Class III salts, but at this stage we cannot say how important. We note also that it has been suggested[79] that Spin-Peierls effects play a significant role in the phase transition in TTF-TCNQ.

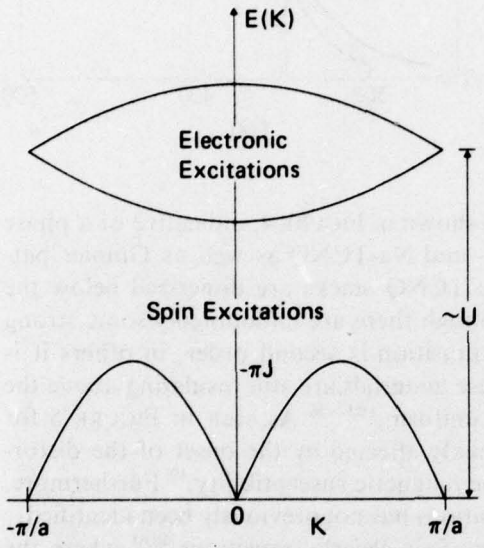


FIGURE 6. The excitation spectrum (schematic) for a $\rho = 1$ uniform stack, showing the degeneracy in the spin excitations (spin waves) and the gap in the electronic (electron-hole) excitations (after Ref. 41).

MAGNETIC SUSCEPTIBILITY

In the case of strong Coulomb interactions (U), it has been shown by Shiba[80] and by Klein and Seitz[81] that the magnetic susceptibility of a uniform stack of molecules with an average number, ρ, of spins (unpaired electrons) can be related[82] to the susceptibility χ_1 of a stack of spins with $\rho = 1$ by

$$\chi(T) = \rho\chi_1(T, J) \tag{2}$$

where the effective exchange interaction[78,81] between spins is given by

$$J = J_0\rho\left(1 - \frac{\sin 2\pi\rho}{2\pi\rho}\right) \tag{3}$$

with $J_0 = 2t^2/U$. Thus, χ is strongly dependent on the value of ρ, through the factor in (2), but more importantly through the dependence of J on ρ in (3). This dependence is plotted in FIGURE 7, using $U \sim 1$ eV and $4t \sim \frac{1}{2}$ eV, which gives $J_0 \sim 350°$K. Using the same value for J_0 for all stacks in all TCNQ salts, the predicted magnetic susceptibility is obtained by use of (2) and (3) with the numerical solution[83,84] for χ_1, *the only variable being the value of* ρ.

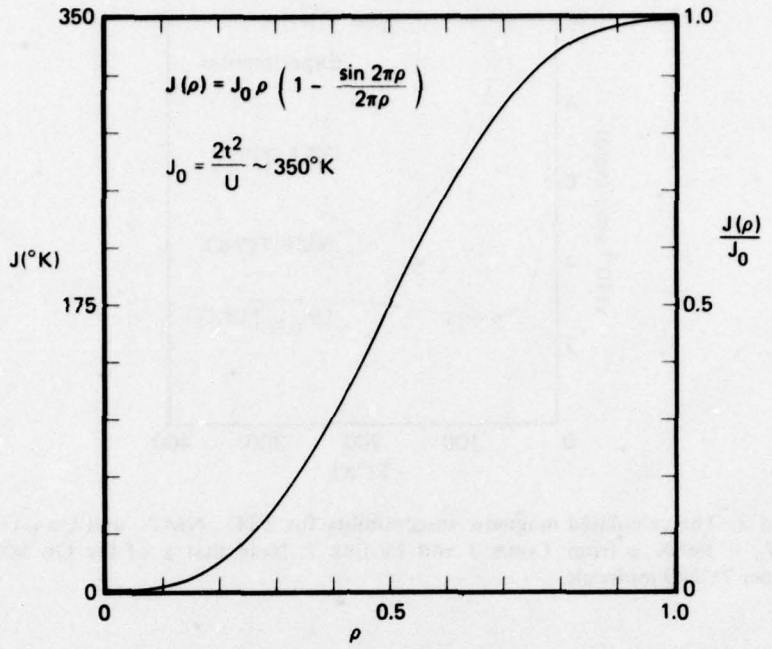


FIGURE 7. The magnitude of the effective exchange interaction, J, as a function of ρ, assuming $U \sim 1$ eV, $4t \sim \frac{1}{2}$ eV, so that $J_0 = 2t^2/U \sim 350°K$.

Using the values of ρ in TABLE 3 for the donor and TCNQ stacks in TTF-TCNQ, NMP-TCNQ, and Qn-$TCNQ_2$, we obtain the calculated $\chi(T)$ shown in FIGURE 8, compared to the observed $\chi(T)$ of FIGURE 9. The major feature to note is how well the differences in general behavior between the different salts are accounted for by including only variations in ρ. The agreement could be improved considerably if $4t$ and U were allowed to vary on different stacks in different materials and if further (weak) interactions were included. Note that $\chi(T)$ contains contribution from *both* the donor and TCNQ stacks. The rise calculated at low temperatures in both NMP-TCNQ[86] and Qn-$TCNQ_2$ is caused by the small value of ρ on the donor stack (TABLE 3). This small number ρ of spins means a small value of the exchange (FIGURE 7) (since they are far apart) and hence a large contribution to χ near $T \sim J \sim 1 - 10°K$.

TABLE 3

VALUES OF THE KEY PARAMETER ρ ASSUMED FOR THE DONOR AND ACCEPTOR STACKS OF THE THREE SALTS LISTED AND THE VALUES OF J OBTAINED FROM (3) OR FIGURE 7

		ρ	$J(\rho)$
TTF-		0.59	235°K
	TCNQ	0.59	235
NMP-		0.10	2
	TCNQ	0.90	348
$Qn_{0.5}$-		$(0.02)\frac{1}{2}x$	0
	TCNQ	0.49	168

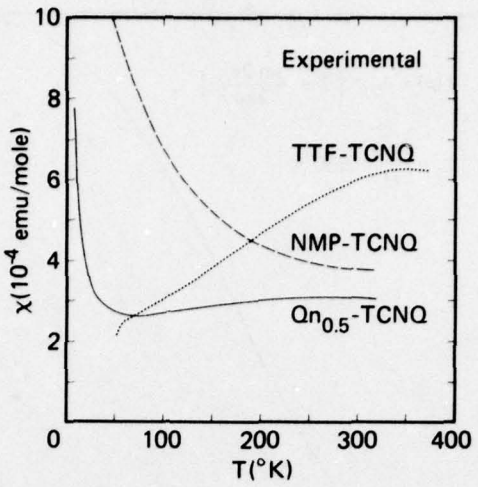


FIGURE 8. The calculated magnetic susceptibility for TTF-, NMP-, and $Qn_{.5}$-TCNQ assuming $J_0 = 350°K$, ρ from TABLE 3 and FIGURE 7. Note that χ of the Qn salt is normalized per TCNQ molecule.

Such a susceptibility tail is found in all Class IV salts[3,15–17,50,87,88] (except TTT-$TCNQ_2$). Shchegolev pointed out that from the same solution of donor and TCNQ, either a Class III or IV salt could be formed, depending on the solution conditions, and that the Class IV salt had the tail in χ. Thus, the χ tail and high conductivity appear to be somehow related. We suggest that both are consequences of incomplete charge transfer, which leaves a small number of spins on the donor chain (to give the tail in χ) and leaves ρ on the TCNQ stack incommensurate (to give high σ)

It is clear from the theoretical analysis[3,88,89] and the elegant experiments[3,51,88] on these χ tails that they are caused by a small number of spins ($\sim 1\%$) which have a distribution of *very weak values of* J ($\sim$0–5°K). In a stack with a high density of spins ($\rho = \frac{1}{2}$) the exchange interactions would be strong ($J \sim 200°K$), and it is necessary to postulate unrealistically strong disorder in order to have a probability of a very weak J. On the other hand, the small number of electrons proposed here to be on the donor stack due to incomplete charge transfer would have a small exchange (FIGURE 7) (since they are far apart on average) and would be strongly affected by even weak disorder or thermal effects. We suggest that this latter approach is a more reasonable *starting point* to examine and interpret the tails observed in the χ of many Class IV salts. It also accounts for their high conductivity.

There are a number of other important features of the susceptibility data in FIGURE 9. The magnitude of χ near 100–300°K in Qn-$TCNQ_2$ is as large as that per TCNQ molecule TTF-TCNQ. Such a large magnitude of χ has been shown[85] to demonstrate the importance of strong Coulomb interactions, which must be present in Qn-$TCNQ_2$ as well. This conclusion is in agreement with that obtained from thermopower measurements,[49] but the conclusion obtained from NMR experiments[90,91] is still unclear. Note also that at low temperatures this large value of χ persists even though the conductivity is decreasing, as is possible in a system with strong Coulomb interactions.

Phase Transitions

As we have seen, many of the *differences* in the general features of the conductivity, optical properties, susceptibility, and stack distortions can be understood in terms of *differences* in ρ, using a model with constant $U(\sim 1$ eV) and constant $4t(\sim \frac{1}{2}$ eV). For some features, it is also necessary to include intermolecular Coulomb interactions as well. For Class I and III salts, we are able to see why the stack distortions are so strong and why the conductivity and susceptibility are activated. In Classes II and IV, we can see why the distortions are much weaker, and why both the conductivity and susceptibility are high. It must be recognized that other interactions must be added to this simple model in order to explain several major features. For example, the amplitude of the distortions would be zero if we did not include a coupling of the intermolecular vibrations with the electronic and/or magnetic interactions. Similarly, the conductivity would be infinite without including some scattering mechanism for the electrons and would remain high to zero temperature unless we added enough interactions to give a phase transition. The essential interaction to achieve a phase transition is interstack coupling.

Thus, differences in interstack coupling are expected to give rise to differences in the phase-transition temperature, for example, between 29°K for TSeF- and 53°K for TTF-TCNQ.[92] It is our view that differences in interstack coupling may play an important role in the determination of observed differences in the phase-transition temperatures of materials within Class II, for example, but that the larger differences between classes are determined by the *stronger* difference between incommensurate and commensurate values of ρ. This is a somewhat complex issue, since the interstack coupling varies with ρ: (1) for commensurate ρ, the phase transition is much less strongly dependent on interstack coupling;[62] and (2) for Coulomb interstack interactions, the magnitude of the interaction de-

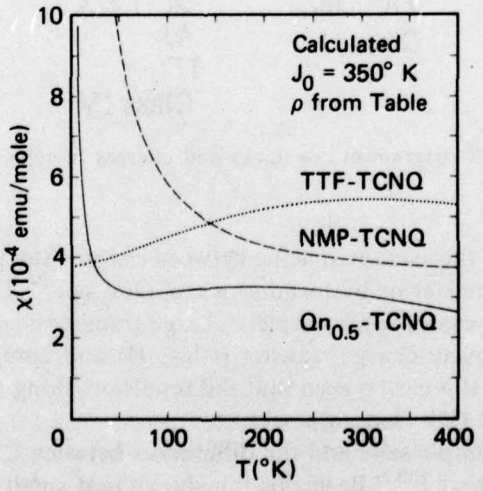


Figure 9. The experimental magnetic susceptibility of TTF-, NMP-, and $Qn_{.5}$-TCNQ from, respectively, Scott *et al.* 1974. Phys. Rev. B10: 3131; Ref. 27; and Mihaly *et al.* 1975. Solid State Commun. 17: 1007.

pends[93] exponentially on ρ. Thus interstack coupling may depend strongly on ρ, and again we conclude that an appropriate and important independent variable is ρ.

Determination of ρ and Charge Transfer

We propose that the value of ρ and the degree of charge transfer in TCNQ salts are determined primarily by two factors: (1) the ionization potential of the donor; and (2) the electrostatic binding energy of the ionic structure formed. In salts with segregated stacks, the important feature is the repulsion between like charges along the stacks. If this repulsion is not compensated, it is energetically

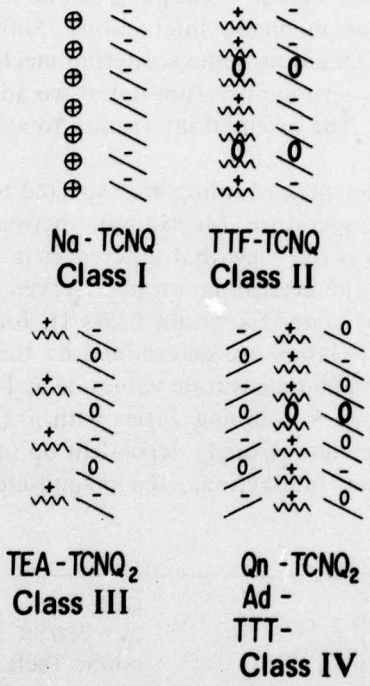


FIGURE 10. Schematic diagram of the stacks and charges in representative examples of each of the four classes.

favorable to increase the average spacing between *charges* along the stack by either incomplete charge transfer or by forming a complex salt.[24] This is illustrated in FIGURE 10, where an example of complete charge transfer is given (Class I) along with cases of incomplete charge transfer (Class II) and complex salt formation (Classes III and IV). It is clearly seen that the repulsion along the stack is reduced in Classes II, III, and IV by having $\rho < 1$.

The case of the simple salts and the differences between Classes I and II have been discussed elsewhere.[8,23,24] Basically, it is shown that small donors (such as *K*) with low ionization potentials form *strongly ionic* salts with TCNQ, hence have $\rho = 1$, and fall into Class I. On the other hand, more bulky donors (such as TTF) with higher ionization potentials form weakly or *partly ionic* salts with TCNQ,

hence have $\rho < 1$, and fall into Class II. These effects are extensively discussed elsewhere.[8,24]

The case of the complex salts is more complicated, since both Class III and IV salts have reduced the intrastack repulsion by forming a complex salt; hence, more subtle reasons must generally be responsible for why they would or would not have incomplete charge transfer. While we readily admit that we do not fully understand the difference between Classes III and IV, we have found one important difference in their structure: There are two generally different ways to form a stacked salt with twice as many TCNQ molecules as donors (for a 1:2 salt): there can be an equal number of TCNQ and donor stacks, with the donor-donor spacing being twice that between TCNQ molecules, as in TEA-$TCNQ_2$ (FIGURE 10); or, there can be twice as many TCNQ stacks as donor stacks, as in Qn-$TCNQ_2$ (FIGURE 10). Although only a few crystal structures are known, those[63-66,74,75] of Class III are of the former type, whereas all those[69-71] known in Class IV have twice as many TCNQ stacks as donors, as shown schematically in FIGURE 10. In the case of complete charge transfer in the Class III-like structures, both the charges along both the donor and TCNQ stacks are separated by a large (~8 Å) distance. Although this would also be true of the charges along the TCNQ stacks in the Class IV-like structures, the charges along the *donor* stack would be only ~4 Å apart. We suggest that the repulsion between these positive charges on the donor stack is alleviated by incomplete charge transfer in these materials (Class IV). It is not clear why this mechanism would favor such a small departure as 4% from complete charge transfer, which is the amount suggested from our interpretation of the tail in the magnetic susceptibility. It is important to determine the crystal structure of other members of Classes III and IV in order to determine how closely these two types of structures are associated with these two classes. There might be other structural reasons in other Class IV salts for why they have incomplete charge transfer.

We should emphasize to what extent we can and cannot predict into which class the TCNQ salt of a given donor will fall. First, it might form alternating stacks or be nonstacking, something we admittedly cannot predict, and hence would not fall into any of the above classes. Secondly, we cannot predict whether a given donor will form complex or simple salts (or both, as some are found to form). But, if a given donor does form a simple salt with segregated stacks, a comparison of its size (for example) and its ionization potential with those donors in TABLE 1 will allow us to predict relatively uniquely whether it will fall into Class I or II. If a given donor forms a complex salt, however, we cannot predict whether it will fall into Class III or IV, since this difference presumably depends largely on the crystal structure formed. Nevertheless, there may be a tendency for nonplanar donors, which do not like to stack, to form Class III salts. Clearly, we have much more to learn if we are ever going to be able to predict the properties of a TCNQ salt with a new donor.

CONCLUSION

It might at first seem somewhat surprising that there are any quasi-one-dimensional organic metals at all. The strong Coulomb interactions would be expected to severely limit the conductivity, and at least one of the number of insta-

bilities possible in such systems should certainly be expected to make them insulating. In fact, the vast majority of TCNQ salts are either insulating (Class I) or intermediate conductors (Class III), with only a handful of organic metals (Classes II and IV) (FIGURES 1 and 2). The large conductivity of these materials has been achieved, not by decreasing the Coulomb and other strong interactions, but by avoiding them by having ρ incommensurate. At the same time, the strong instabilities characteristic of commensurate systems are exchanged for weaker, more subtle instabilities found which occur at lower temperatures when ρ is incommensurate. These features are consistent not only with all the known organic metals with TCNQ as the acceptor, but with the halide salts of TTF as well, where these points are all more clearly evident.[24,94]

NOTES AND REFERENCES

1. MELBY, L. R., R. J. HARDER, W. R. HERTLER, W. MAHLER, R. E. BENSON & W. E. MOCHEL. 1962. J. Am. Chem. Soc. **84:** 3374.
2. SIEMONS, W. J., P. E. BIERSTEDT & R. G. KEPLER. 1963. J. Chem. Phys. **39:** 3523.
3. SHCHEGOLEV, I. F. 1972. Phys. Status Solidi (a)**12:** 9.
4. HERBSTEIN, F. H. 1971. *In* Perspectives in Structural Chemistry. Vol. IV, J. D. Dunitz and J. A. Ibers, Eds.: 166. John Wiley & Sons. New York, N.Y.
5. SHIBAEVA, R. P. & L. O. ATOMYAN. 1972. J. Structural Chem. **13:** 514.
6. SOOS, Z. G. 1974. Ann. Rev. Phys. Chem. **25:** 121.
7. KELLER, H. J., Ed. 1977. Chemistry and Physics of One-Dimensional Metals, Vol. 25. NATO Advanced Study Institutes Series (B—Physics) Plenum Press. New York, N.Y.
8. TORRANCE, J. B. Accts. of Chem. Res. In press. (Compares Classes I and II.)
9. TORRANCE, J. B. This volume. See Tables 1 and 2 for translation of abbreviations used in the text.
10. BLOCH, A. N., D. O. COWAN, K. BECHGAARD, R. E. PYLE, R. H. BANKS & T. O. POEHLER. 1975. Phys. Rev. Lett. **34:** 1561.
11. LEBLANC, O. H. 1965. J. Chem. Phys. **42:** 4307.
12. GARITO, A. F. & A. J. HEEGER. 1974. Accts. of Chem. Res. **7:** 232.
13. BLOCH, A. N., R. B. WEISMAN & C. M. VARMA. 1972. Phys. Rev. Lett. **28:** 753.
14. BLOCH, A. N. 1974. *In* Energy and Charge Transfer in Organic Semiconductors. K. Masuda and M. Silver, Eds.: 159. Plenum Press. New York, N.Y.
15. MIHALY, G., K. RITVAY-EMANDITY & G. GRÜNER. 1977. *In* Organic Conductors and Semiconductors. L. Pal. G. Grüner, A. Janossy, and J. Solyom, Eds.: 65. Lecture Notes in Physics. Series No. 65:535. Springer-Verlag. Berlin, Germany.
16. MIHALY, G., K. RITVAY-EMANDITY, A. JANOSSY, K. HOLCZER & G. GRÜNER. 1977. Solid State Commun. **21:** 721.
17. MIHALY, G., K. HOLCZER, A. JANOSSY, G. GRÜNER & M. MILJAK. 1977. *In* Organic Conductors and Semiconductors. L. Pal, G. Grüner, A. Janossy, and J. Solyom, Eds.: 65. Lecture Notes in Physics. Series No. 65:553. Springer-Verlag. Berlin, Germany.
18. See also LOMBARDO, A., T. R. FICO, J. E. LANE & J. S. BLAKEMORE. Unpublished.
19. VEGTER, J. G., J. KOMMANDEUR & P. A. FEDDERS. 1973. Phys. Rev. **B7:** 2929; Vegter, J. G., Ph.D. Thesis. 1972. Univ. of Groningen. Groningen, The Netherlands.
20. VEGTER, J. G., T. HIBMA & J. KOMMANDEUR. 1969. Chem. Phys. Lett. **3:** 427.
21. DAHM, D. J., P. HORN, G. R. JOHNSON, M. G. MILES & J. D. WILSON. 1975. J. Cryst. Mol. Struct. **5:** 27.
22. TORRANCE, J. B., B. A. SCOTT & F. B. KAUFMAN. 1975. Solid State Commun. **17:** 1369.
23. TORRANCE, J. B. & B. D. SILVERMAN. 1975. Bull. Am. Phys. Soc. **20:** 498.
24. TORRANCE, J. B. & B. D. SILVERMAN. 1977. Phys. Rev. **B15:** 788.
25. Some of these ideas were first presented in TORRANCE, J. B. & Y. TOMKIEWICZ. 1976. Bull. Am. Phys. Soc. **21:** 313.

26. TORRANCE, J. B. 1977. *In* Chemistry and Physics of One-Dimensional Metals. H. J. Keller, Ed. **25:** 137. NATO Advanced Study Institutes Series. Plenum Press. New York, N.Y.
27. EPSTEIN, A. J., S. ETEMAD, A. F. GARITO & A. J. HEEGER. 1972. Phys. Rev. **B5:** 952.
28. BOYD, R. H. & W. D. PHILLIPS. 1965. J. Chem. Phys. **43:** 2927.
29. IIDA, Y. 1969. Bull. Chem. Soc. Japan **42:** 71, 637.
30. TANAKA, J., M. TANAKA, T. KAWAI, T. TAKABE & O. MAKI. 1976. Bull. Chem. Soc. Japan **49:** 2358.
31. HUBBARD, J. 1978. Phys. Rev. **B17:** 494; see also Bush, R. L. 1975. Phys. Rev. **B12:** 5698.
32. HERMAN, F., D. R. SALAHUB & R. P. MESSMER. 1977. Phys. Rev. B. **16:** 2453.
33. GRANT, P. M., R. L. GREENE, G. C. WRIGHTON & G. CASTRO. 1973. Phys. Rev. Letters **31:** 311; WRIGHTON, G. C., Ph.D. Thesis, 1974. Stanford Univ. Stanford, Calif. Unpublished.
34. FLANDROIS, S. & D. CHASSEAU. 1977. Acta Crystallogr. **B33:** 2744.
35. For more complete references on Classes I and II, see Ref. 8.
36. BURAVOV, L. I., O. N. EREMENKO, R. B. LYUBOVSKII, L. P. ROZENBERG, M. L. KHIDEKEL, R. P. SHIBAEVA, I. F. SHCHEGOLEV & E. B. YAGUBSKII. 1974. JETP Lett. **20:** 208.
37. BURAVOV, L. I., D. N. FEDUTIN & I. F. SHCHEGOLEV. 1971. Sov. Phys. JETP. **32:** 612.
38. MÜLLER, E., H. RITSCHEL & H. HÄNSEL. 1969. Phys. Stat. Sol. **33:** K55.
39. BLAKEMORE, J. S., U. BERNSTEIN, J. E. LANE & D. A. WOODBURY. 1976. *In* Proc. XIII Internat. Conf. Physics Semicond. Rome, Italy. To be published.
40. Actually, the activation energy for conduction is $\sim(U_0 - 4t)$, which is in general larger than $U = U_0 - V_1$, since in order to conduct, the electron must escape the attraction V_1 also.
41. OVCHINNIKOV, A. A. 1970. Sov. Phys. JETP **30:** 1160.
42. ZAWADOWSKI A. & M. H. COHEN. 1977. Phys. Rev. B. **16:** 1730.
43. WOYNAROVICH, F., L. MIHALY & G. GRÜNER. 1976. Solid State Commun. **19:** 1189.
44. SUMI, H. 1977. Solid State Commun. **21:** 17.
45. OVCHINNIKOV, A. A. 1973. Sov. Phys. JETP **37:** 176.
46. COMÉS in Ref. 7.
47. UKEI, K. & I. SHIROTANI. 1977. Commun. Physics **2:** 159.
48. BUTLER, M. A., F. WUDL & Z. G. SOOS. 1975. Phys. Rev. **B12:** 4708.
49. KWAK, J. F., G. BENI & P. M. CHAIKIN. 1976. Phys. Rev. **B13:** 641.
50. DELHAES, P., F. ALY & P. DUPUIS. 1973. Solid State Commun. **12:** 1099.
51. AZEVEDO, L. J. & W. G. CLARK. 1977. Phys. Rev. B. **16:** 3252.
52. SHCHEGOLEV, I. F. *et al.* 1978. Sov. Phys. JETP **72:** 1140.
53. KWAK, J. F. & G. BENI. 1976. Phys. Rev. **B13:** 652.
54. KONNO, M. & Y. SAITO. 1977. Acta Crystallogr. **B30:** 1294; 1975, **B31:** 2007.
55. KONNO, M., T. ISHI & Y. SAITO. 1977. Acta Crystallogr. **B33:** 763.
56. SHIROTANI, I. & H. KOBAYASHI. 1973. Bull. Chem. Soc. Japan **46:** 2595.
57. SAKAI, N., I. SHIROTANI & S. MINOMURA. 1972. Bull. Chem. Soc. Japan **45:** 3314, 3321.
58. KHANNA, S. K., A. A. BRIGHT, A. F. GARITO & A. J. HEEGER. 1974. Phys. Rev. **B10:** 2139.
59. EMERY, V. J., in Ref. 7.
60. See for example, PYTTE, E. 1974. Phys. Rev. **B10:** 4637.
61. JACOBS, I. S., J. W. BRAY, H. R. HART, JR., L. N. INTERRANTE, J. S. KASPER, G. D. WATKINS, D. E. PROBER & J. C. BONNER. 1976. Phys. Rev. **B14:** 3036, and references therein.
62. See for example, SCHRIEFFER, J. R. 1974. *In* Collective Properties of Physical Systems. B. Lundqvist and S. Lundqvist, Eds.: 142. Academic Press, New York, N.Y.; LEE, P. A., T. M. RICE & P. W. ANDERSON. 1973. Phys. Rev. Lett. **31:** 462; KOTANI, A. 1977. J. Phys. Soc. Japan **42:** 408, 416.
63. FRITCHIE, C. J., JR. & P. ARTHUR, JR. 1966. Acta Crystallogr. **21:** 139.
64. SUNDARESAN, T. & S. C. WALLWORK. 1972. Acta Crystallogr. **B28:** 1163.
65. MCPHAIL, A. T., G. M. SEMENIUK & D. B. CHESNUT. 1971. J. Chem. Soc. A2174.
66. KOBAYASHI, H., Y. OHASHI, F. MARUMO & Y. SAITO. 1970. **B26:** 459.

67. FRITCHIE, C. J., JR. 1966. Acta Crystallogr. **20:** 892.
68. KISTENMACHER, T. J., T. E. PHILLIPS & D. O. COWAN. 1974. Acta Crystallogr. **B30:** 763.
69. KOBAYASHI, H., F. MARUMO & Y. SAITO. 1971. Acta Crystallogr. **B27:** 373.
70. KOBAYASHI, H. 1974. Bull. Chem. Soc. Japan **47:** 1346.
71. SHIBAEVA, R. P. & L. P. ROZENBERG. 1976. Sov. Phys. Crystallog. **20:** 581.
72. TMPD = tetramethyl-p-phenylenediamine (Wüster's blue); Et_4N = tetraethylammonium; MEM = *N*,*N*'-methyl-ethyl morpholinium.
73. SOMOANO, R., V. HADEK, S. P. S. YEN, A. REMBAUM & R. DECK. 1975. J. Chem. Phys. **62:** 1061.
74. HANSON, A. W. 1968. Acta Crystallogr. **B24:** 768.
75. KUINDERSMA, P. I., G. A. SAWATSKY, J. KOMMANDEUR & C. J. SCHINKEL. 1975. J. Phys. Chem. **8:** 3016; BOSCH, A. & B. van Bodegom. 1977. Acta Crystallogr. **33:** 3013.
76. It is not clear whether the phase transition discovered in morpholinium-TCNQ is or is not a Spin-Peierls transition. BAILEY, J. C. & D. B. CHESNUT. 1969. J. Chem. Phys. **51:** 5718.
77. TERAUCHI, H., N. SAKAMOTO & I. SHIROTANI. 1976. J. Chem. Phys. **64:** 437.
78. COLL, C. F. 1974. Phys. Rev. **B9:** 2150.
79. TORRANCE, J. B. 1978. Phys. Rev. B March 15.
80. SHIBA, H. 1972. Phys. Rev. **B6:** 930.
81. KLEIN, D. J. & W. A. SEITZ. 1974. Phys. Rev. **B10:** 3217.
82. The calculations referred to are strictly valid only in the limit $V_1 = 0$. The results for finite V_1 are not known.
83. BONNER, J. C. & M. E. FISHER. 1964. Phys. Rev. **135:** A640.
84. As an excellent fit to the Bonner-Fisher result, we used:
$$\chi = 1.4892x(0.05031 + 0.013014\,(T/J) + 0.046846\,(T/J)^2 - 0.062319\,(T/J)^3 + 0.030834\,(T/J)^4 - 0.0076763\,(T/J)^5 + 0.00096332\,(T/J)^6 - 0.00004853\,(T/J)^7)/J$$
for χ in emu/mole and J in °K. (From Ref. 85).
85. TORRANCE, J. B., Y. TOMKIEWICZ & B. D. SILVERMAN. 1977. Phys. Rev. **B15:** 4738.
86. SOOS, Z. G. Unpublished.
87. ASHWELL, G. J., D. D. ELEY, M. R. WILLIS & J. WOODWARD. 1977. Phys. Stat. Sol. (b) **79:** 629; SOMOANO, R. B., V. HADEK, S. P. S. YEN, A. REMBAUM, C. H. HSU, R. J. DECK, T. DATTA & A. M. HERMANN. 1977. Phys. Stat. Solidii (b) **81:** 281.
88. BULAEVSKII, L. N., A. V. ZVARYKINA, YU. S. KARIMOV, L. B. LYUBOVSKII & I. F. SHCHEGOLEV. 1972. Sov. Phys. JETP **35:** 384.
89. THEODOROU, G. & M. H. COHEN. 1976. Phys. Rev. Lett. **37:** 1014; Theodorou, G. 1977. Phys. Rev. B **16:** 2273.
90. EHRENFREUND, E., S. ETEMAD, L. B. COLEMAN, E. F. RYBACZEWSKI, A. F. GARITO & A. J. HEEGER. 1972. Phys. Rev. Lett. **29:** 269.
91. DEVREUX, F. 1976. Mol. Cryst. Liq. Cryst. **32:** 241.
92. See, for example, TOMKIEWICZ, Y., E. M. ENGLER, & T. D. SCHULTZ. 1975. Phys. Rev. Lett. **35:** 456.
93. SAUB, K., S. BARISIC & J. FRIEDEL. 1976. Phys. Lett. **56A:** 302.
94. SCOTT, B. A., S. J. LAPLACA, J. B. TORRANCE, B. D. SILVERMAN & B. WELBER. 1977. J. Am. Chem. Soc. **99:** 6631.

DISCUSSION

A. R. SIEDLE (*National Bureau of Standards, Washington, D.C.*): Why are there no partially oxidized TTF's with less than 0.6 bromines?

TORRANCE: The point is that there is an optimum bromine concentration that is determined by a competition between the Madelung energy and the molecular energy ($I_D - E_A$) of charge transfer. The way to get a composition of less aniom, e.g., $\rho \approx 0.33$, is to make another system, one with a poorer acceptor (e.g., I or SCN), a poorer and bulkier donor, or both. Perhaps the phthalocyanine iodides are such systems.

ARTHUR J. EPSTEIN: (1) The scheme you propose relies upon using a Wigner lattice, which is inappropriate for many of the partially charged transfer systems; (2) $I_D^- E_A^+ E_M$ is a very attractive formula. If I follow that logic and replace TCNQ with tetrafluoro TCNQ and replace TTF with something with just a slightly higher ionization energy, you would expect it to be as metallic as (TTF)(TCNQ). But this is not what is observed. Hence I think intramolecular correlation is also important.

TORRANCE: (1) The Wigner lattice is appropriate in the extreme limit of strong electron correlations and was used in the Madelung calculations of Silverman and myself as an approximation in order to make the calculations tractable. I believe that similar results would be obtained if the correlations could be treated more exactly. In addition, we believe that in (TTF)(TCNQ) and (NMP)(TCNQ) these correlations are sufficiently strong that there does exist a charge-density wave (like the Wigner crystal) in the electron density along the stack. We interpret the observed x-ray diffuse scattering at $4k_F$ in these materials as caused by (and hence evidence for) these charge-density waves. (2) Conclusions regarding tetrafluoro TCNQ salts cannot be made until the Madelung energies of these salts are calculated (but the structures have not yet been determined). I would suggest that many of the tetrafluoro TCNQ salts are insulating because the large electron affinity makes $\rho = 1$. I strongly disagree with your belief that intramolecular correlations are an important *difference* between TCNQ and tetrafluoro TCNQ; in fact, experimentally these correlations are almost identical in these two molecules.

X-RAY SCATTERING STUDIES FROM ONE-D CONDUCTORS*

S. Megtert,† J. P. Pouget,‡ and R. Comes†

†*Laboratoire de Physique des Solides*
Université Paris-Sud
91405 Orsay, France
‡*Brookhaven National Laboratory*
Upton, New York 11973

INTRODUCTION

Phonon anomalies leading to structural phase transitions have been investigated extensively in the last ten years, following the soft mode approach initially suggested by Anderson[1] and Cochran[2] for ferroelectric instabilities.

Until recently, all known cases dealt with anomalies taking place at the Brillouin zone center, somewhere on the zone boundary, or more generally at wave vectors, which can be written as simple fractions of the reciprocal lattice vectors. As a consequence, the unit cell of the low-temperature stabilized phase was an integer multiple of the high temperature one.

Paradoxically, the prediction by theory of phonon anomalies occurring in low-dimensional metals at the wave vector $2k_F$ (which is not restricted to a simple fraction of the reciprocal lattice vectors and therefore constitute a more general case) is older.[3] In this case, the low-temperature stabilized structure is not necessarily periodic: the condensed phonon can produce a modulation that is incommensurate with respect to the main lattice periodicity. Such features directly include the $2k_F$ wave vector, and experiments that are able to detect phonon anomalies will therefore provide unique methods for the measurement of the conduction-band filling.

As in the case of the well-known soft modes of the usual phase transitions, the incommensurate Kohn anomalies of the low-dimensional metals can be studied most directly by neutron and x-ray scattering techniques. Inelastic neutron scattering, which allows a detailed determination of the dispersion curves, is clearly the most powerful technique, but it requires relatively large crystals and a sufficiently high flux neutron beam reactor. In many cases, the simpler use of x-ray scattering is sufficient, particularly if the measurements aim mainly at the determination of the precise value of the $2k_F$ wave vector. We shall use this as a simple example of modulation.

DIFFUSE SCATTERING FROM A ONE-D MODULATED LATTICE

For low-frequency phonons the amplitude is proportional to $1/\omega^2$, a phonon anomaly at the wave vector q_0 (FIGURE 1), and therefore corresponds to modes of enhanced amplitude compared to all other thermal vibrations. In the first approxi-

*Manuscript received June 1, 1977.

0077-8923/78/0313-0234 $1.75/1 © 1978, NYAS

mation, one can therefore neglect all but one mode of wave vector q_0. Because x-ray frequencies are much higher than characteristic phonon frequencies, they will measure only a superposition of the instantaneous configurations, and a further simplification is to replace the time dependence of our single mode by its mean squared amplitude Δ. Besides the temperature dependence of the amplitude, which varies as the Boltzman population factor, our phonon anomaly is thus reduced to the elementary case of a static modulation.

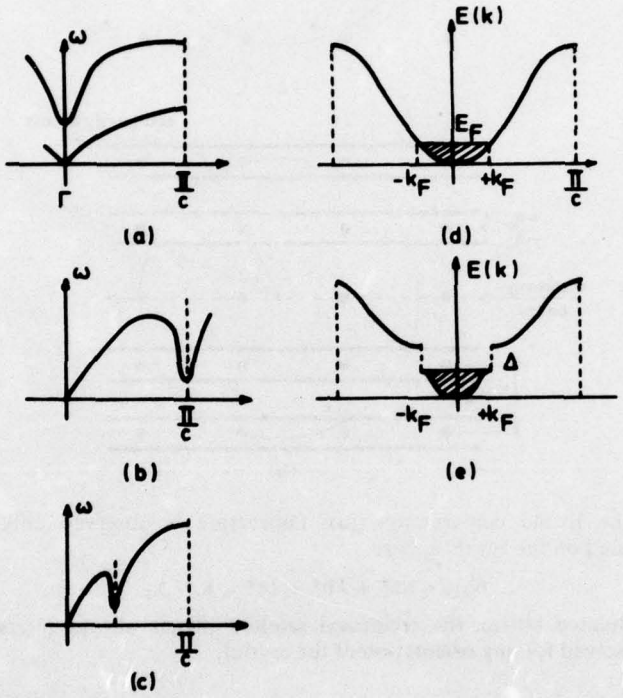


FIGURE 1. Schematic phonon anomalies. (a): ferrodistortive precursors. Zone center soft mode; (b): antiferrodistortive precursors. Zone boundary soft mode; (c): modulated lattices. Arbitrary wave vector soft mode. Schematic modification of the electronic bands in a Peierls transition. (d): the conduction band of the high-temperature metal; (e): the opening of a gap at the wave vector k_F lowers the energy of the occupied states and raises the energy of empty states; k_F becomes a zone boundary of a distorted lattice with a modulation period of $2\pi/2k_F$.

Let us now consider a crystal with one atom per unit cell, lattice constants a, b, and c, and dimensions $N_1a \times N_2b \times N_3c$. Along the c direction, the atoms are displaced sinusoidaly from their average positions n_3c with an amplitude Δ and a wave vector q_0. The phase between the different chains parallel to c is arbitrary. The atoms of the distorted crystal are then located at vectors $\mathbf{r}_l$ given by:

$$\mathbf{r}_l = n_1\mathbf{a} + n_2\mathbf{b} + n_3\mathbf{c} + \Delta \exp i(\pm\, \mathbf{q}_0 \cdot n_3\mathbf{c} + \phi(n_1n_2)) \qquad (1)$$

where $\phi(n_1n_2)$ is the arbitrary phase on the different chains.

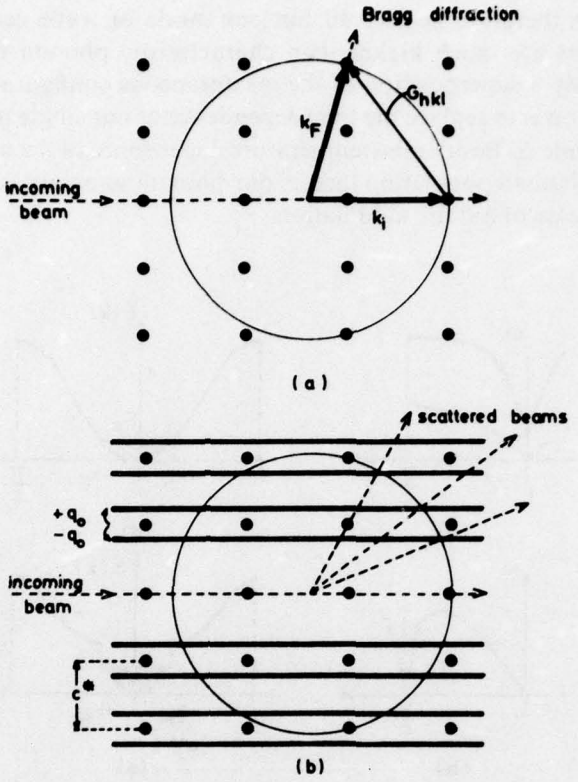


FIGURE 2. The Ewald construction. (a): Diffraction is observed only for reciprocal lattice nods located on the Ewald sphere.

$$\mathbf{G}_{hkl} = h\mathbf{a}^* + k\mathbf{b}^* + l\mathbf{c}^* = \mathbf{k}_i - \mathbf{k}_F.$$

(b): For a modulated lattice, the reciprocal satellite planes always intersect the sphere. Scattering is observed for any orientation of the crystal.

If Ki and K_F are, respectively, the wave vectors of the incoming and scattered beam, the momentum transfer Q *is given by*

$$\mathbf{Q} = \mathbf{K}_i - \mathbf{K}_F \tag{2}$$

and the difference of phase between beams scattered by two atoms distant of r_l is simply $\Delta\phi = \mathbf{Q} \cdot \mathbf{r}_l$. The resulting x-ray amplitude from our modulated crystal is then:

$$A = \sum_{n_1,n_2,n_3} f \exp i\,\mathbf{Q} \cdot (\Delta \exp i[\pm \mathbf{q}_0 n_3 \mathbf{c} + \phi(n_1 n_2)] \exp i\,\mathbf{Q}(n_1\mathbf{a} + n_2\mathbf{b} + n_3\mathbf{c}). \tag{3}$$

For small-amplitude modulations, the first exponential factor can be expanded. To first order, this yields the following terms:

(i) $$A_B = f \sum_{n_1 n_2 n_3} \exp i\mathbf{Q} \cdot (n_1\mathbf{a} + n_2\mathbf{b} + n_3\mathbf{c}).$$

This is just the Bragg diffraction of the average unmodulated lattice. Using

the reciprocal lattice constants a^*, b^*, and c^* of this average lattice:

$$A_B \simeq N_1 N_2 N_3 \delta(\mathbf{q} - \mathbf{G}_{hk1}) \tag{4}$$

with

$$\mathbf{G}_{hk1} = h\mathbf{a}^* + k\mathbf{b}^* + 1\mathbf{c}^*.$$

Equations 4 and 2 justify the well-known Ewald construction shown in FIGURE 2(a).

(ii) $$A_D = f\left(\sum_{n_3} i\,\mathbf{Q}\cdot\Delta \exp i(\mathbf{Q} \pm q_0)\cdot n_3\mathbf{c}\right)$$

$$\left(\sum_{n_1 n_2} \exp i[\mathbf{Q}\cdot(n_1\mathbf{a} + n_2\mathbf{b}) + \phi(n_1 n_2)]\right) \tag{5}$$

which gives rise to an additional diffuse scattering.

Because of the arbitrary phase $\phi(n_1, n_2)$ of the modulation on different chains, the summation on the amplitudes can be performed only on n_3 and the total diffuse scattering I_D is just the sum of the intensities (squared moduli) scattered by independent chains.

$$I_D = |A_D|^2 = f^2(\mathbf{Q}\cdot\Delta)N_1N_2 \left[\frac{\sin^2\left(N_3\frac{(\mathbf{Q}\pm\mathbf{q}_0)}{2}\cdot\mathbf{c}\right)}{\sin^2\left(\frac{(\mathbf{Q}\pm\mathbf{q}_0)}{2}\cdot\mathbf{c}\right)}\right] \tag{6}$$
$$F_d^2$$

This expression contains two main factors:

1) The diffraction term D^2, which localizes the diffuse scattering with maximum intensity for momentum transfers $\mathbf{Q}_s$ given by:

$$(\mathbf{Q}_S \pm \mathbf{q}_0)\cdot\mathbf{c} = 2\pi\ell. \quad \text{or} \quad \mathbf{Q}_S = \ell\mathbf{c}^* \pm \mathbf{q}_0 \,(\ell \text{ integer}). \tag{7}$$

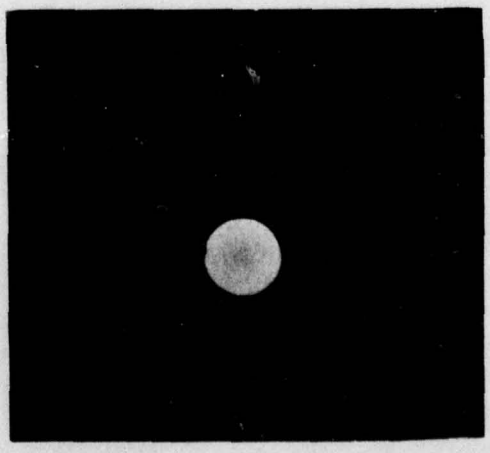


FIGURE 3. X-ray diffuse scattering pattern from $K_2Pt(CN)_4Cl_{0.32}-H_2O$ obtained with MoKα radiation and a planar camera.

This relation shows that Q_S is independent of the coordinates in a^* and b^* directions, thus defining sheets in reciprocal space perpendicular to the c direction of the 1-D modulation, and located at $\pm q_0$ from the reciprocal lattice perpendicular to c. FIGURE 2 (b) shows the corresponding Ewald construction.

2) The factor $F_d^2 = f^2(\Delta \cdot \mathbf{Q})^2$, which determines the relative intensity of each such sheet: the diffuse structure factor. Compared to the intensity of Bragg diffraction, which is proportional to f^2, the diffuse scattering is much weaker. Because phonon amplitudes are usually smaller than 1% of the lattice spacing ($|\Delta| < 0.01 |\mathbf{c}|$), the diffuse intensity is less than 10^{-4} of the usually measured Bragg peaks. This implies the use of x-ray monochromators and very relaxed resolutions for the experimental setup.

This simple example is very close to the case of the platinum-chain Krogman salts,[4] since in these compounds the scattering from platinum is predominant and shadows the contributions of the other lighter atoms. It can therefore account precisely for x-ray pattern as shown in FIGURE 3, which can be relatively easily obtained with the so called "Monochromatic Laue" or "fixed film fixed crystal" technique.[4]

STUDIES OF 1-D KROGMAN SALTS

The oldest known real crystals dispalying such 1-D instabilities and modulated structures are indeed the platinum-chain Krogman salts.[5] These compounds, for which the $2k_F$ value is unambiguously known from the chemical composition, have provided the ideal material for a qualitative experimental check of the earlier theoretical predictions. In KCP ($K_2Pt(CN)_4Br_{0.30} - xH_2O$), which has been investigated in greatest detail by x-ray and neutron scattering, a sharp 1-D $2k_F$ phonon anomaly, observed at room temperature,[4,6,7] gives rise at low temperature to 3-D correlation of $2a \times 2a \times 3.33c$ periodicity.[8,10] Such correlations correspond to the simplest coupling of the 1-D charge density waves; waves on neighboring chains are in opposition of phase.[11,12]

FIGURE 3 shows a pattern from the chlorine analog of KCP ($K_2Pt(CN)_4Cl_{0.32} - xH_2O$) which displays 1-D scattering at room temperature for the wave vector

TABLE 1

COMPOUNDS STUDIED BY X-RAY AND NEUTRON SCATTERING

Cyanides	References
$K_2Pt(CN)_4Br_{0.30} - xH_2O$	4
$K_2Pt(CN)_4Cl_{0.32} - xH_2O$	4
$Na_2Pt(CN)_4Br_{0.23} - xH_2O$	4
$K_{1.75}Pt(CN)_4 - 1.5\ H_2O$	13, 14
$Rb_{1.75}Pt(CN)_4 - xH_2O$	14
$Cs_{1.75}Pt(CN)_4 - xH_2O$	14
$[C(NH_2)_3]_2Pt(CN)_4Br_{0.30} - xH_2O$	14
Oxalates	
$K_{1.62}[Pt(C_2O_4)_2] - xH_2O$	15
$Mg_{0.82}[Pt(C_2O_4)_2] - xH_2O$	16

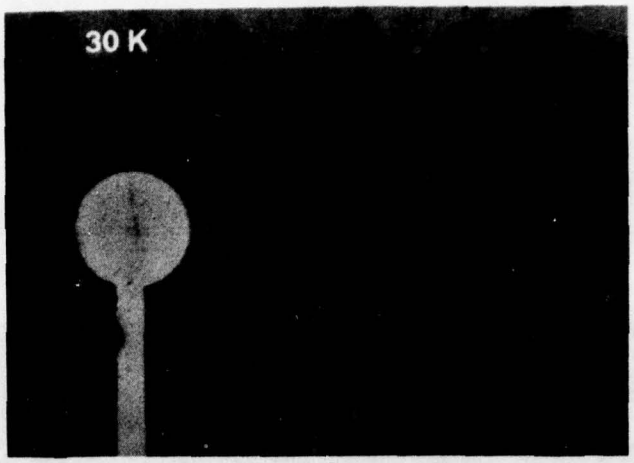


FIGURE 4. X-ray diffuse scattering pattern from TseF-TCNQ at 30°K, showing well-defined $2k_F$ 1-D satellite sheet scattering at the wave vector 0.315 b*. (From Ref. 26.)

$\mathbf{q}_c = (0.32 \pm 0.01)\mathbf{c}^* = 2k_F$ and a development at low temperature of 3-D correlations (periodicity $2a \times 2a \times 3.12c$) closely similar to the observations on KCP.

In spite of the appealing advantage of such compounds, which have only one kind of conducting chains, a detailed understanding of their properties is complicated by the intrinsic disorder due to their nonstochiometry. The incomplete 3-D ordering of the charge-density waves, clearly observed in KCP,[8-10] is usually attributed to this disorder.

TABLE 1 gives a list of such compounds studied so far by x-ray and neutron scattering. In all cases, the 1-D diffuse scattering wave vector is in close agreement with the $2k_F$ value calculated from the chemical composition.

$2K_F$ INSTABILITIES IN ORGANIC 1-D CONDUCTORS

Since the occurrence of $2k_F$ instabilities is well established from the study of the Krogman salts, further 1-D conductors, for which the conduction band filling was not precisely known, could be investigated, namely, the organic charge-transfer salts.[17] All studied compounds showed the expected 1-D scattering, and the wave vector at which it was observed can be assigned to $2k_F$, which allows a direct determination of the charge transfer.

FIGURE 4 shows a pattern of TSeF-TCNQ where such 1-D scattering is particularly well contrasted, again due to the predominant scattering from the heavier selenium atoms. The 1-D scattering differs here from the continuous diffuse satellite lines observed in FIGURE 3 because of the form factor of the four selenium atoms contained in each TSeF molecule.

TABLE 2 gives a list of the organic 1-D conductors of this type which have been studied up to date by x-ray and neutron scattering with the resulting charge transfers.

TABLE 2
ORGANIC 1-D CONDUCTORS STUDIED BY X-RAY AND NEUTRON SCATTERING

Compound	Measured $2k_F$	Charge Transfer	References
TTF-TCNQ	$2k_F = 0.295$	0.59	18–24
TSeF-TCNQ	0.315	0.63	25,26
HMTSeF-TCNQ	0.37	0.74	25
HMTTF-TCNQ	0.36 ± 0.07	0.72	27

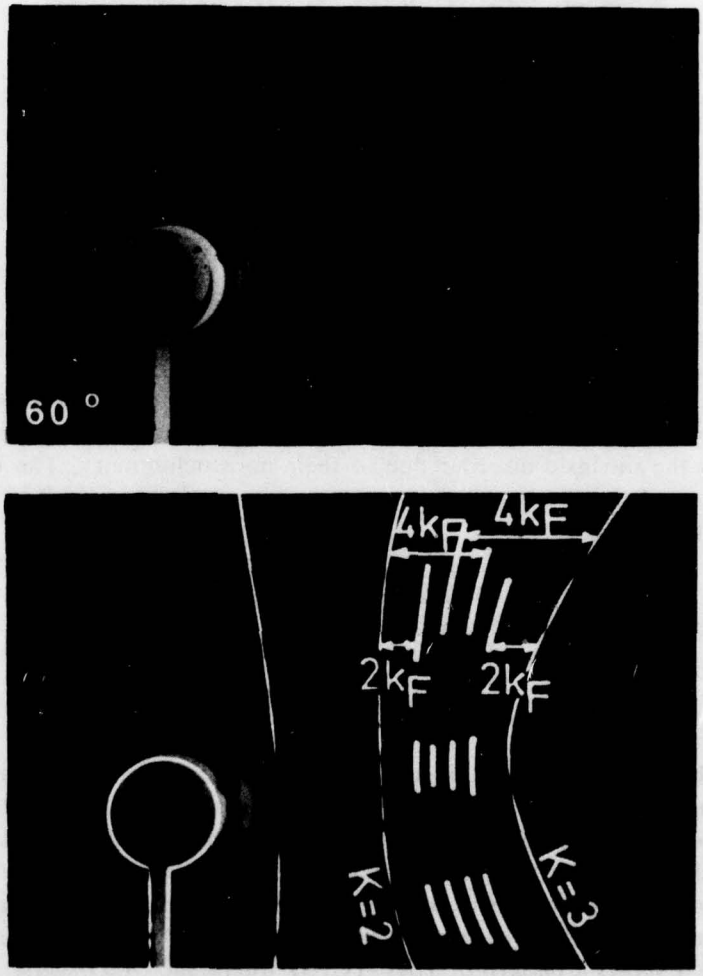


FIGURE 5. Diffuse x-ray pattern of TTF-TCNQ in the undistorted high temperature phase ($T > 54$°K). The sample is oriented with b^* and c^* directions in the equatorial plane; the angle between the incident x-ray beam and b^* is 124°. The rings observed around the incident beam are powder parasites from the sample holder. Bragg spots with $0.5\,b^*$ components are due to the $\lambda/2$ contamination from the continuous spectrum of the x-ray source, which is also reflected by the monochromator. At 60°K, the satellite-diffuse sheets are clearly visible at the wave vectors 0.295 b^* identified as $2k_F$, and 0.59 b^* identified as $4k_F$. (After Ref. 19.)

Most extensively studied is the prototype crystal TTF-TCNQ. Difficult x-ray and neutron-scattering studies have revealed the existence of both $2k_F$ and $4k_F$ precursors, as shown in FIGURE 5,[18-22] and have characterized at low temperature a sequence of long-range ordered modulated structures with phase transitions at 54, 49, and 38°K.[21-24]

FIGURE 6 summarizes schematically the positions of the well-defined, low-

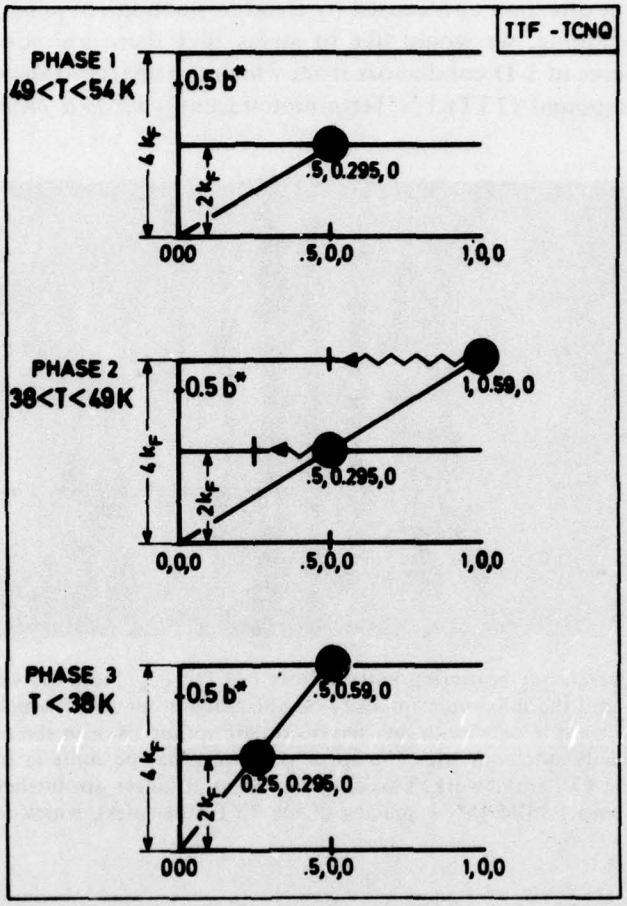


FIGURE 6. Schematic representation of the position in reciprocal space of the satellite spots in the three low-temperature modulated phases of TTF-TCNQ. (a): 49°K < T < 54°K (Phase I); modulation $2a \times 3{,}4b \times c$; (b): 38°K < T < 49°K (Phase II), modulation $x(\tau)a \times 3{,}4b \times c$; (c): T < 38°K (Phase III), modulation $4a \times 3{,}4b \times c$.

temperature satellite reflections obtained from the different investigations.[21-24] The respective assignment of $2k_F$ and $4k_F$ to the 1-D precursors has been made here on the basis of the low-temperature, 3-D ordering of the charge-density waves which is driven by the smallest wave vector anomaly. The greater complexity of the features observed in TTF-TCNQ is believed to have its origin in the existence of two types of conducting stacks,[28-31] the respective contributions of

which have not yet been clearly determined from the structural data, and require further study.

CONCLUSION

We have so far considered cases of 1-D conductors in which satellite sheet 1-D scattering arising from dynamical or static modulations of the intermolecular spacing in chain direction and caused by electron phonon coupling is clearly observed. In concluding, we would like to stress that there are sometimes other particular features in 1-D conductors from which the charge transfer can be deduced. The compound $(TTT)_2I_3$ ([Tetrathiotetracene]$_2$ I_3) is *a priori* believed to

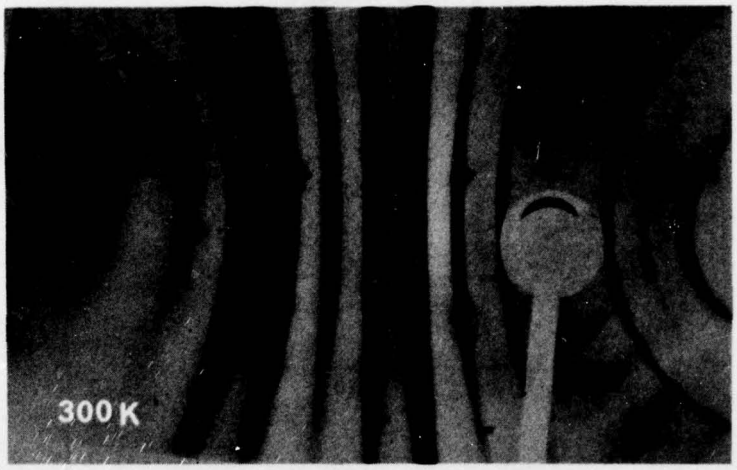


FIGURE 7. Diffuse x-ray scattering pattern from $(TTT)_2I_{3-\delta}$. Note the very intense 1-D sheet scattering, and the maximum intensity on the third-order sheet which demonstrates the existence of I_3 units. Contrary to the simplified description given in the text, the studied sample is not exactly stochiometric. The spacing between iodine units is incommensurate with respect to the TTT framework. Two different repeat distances are further found for the I_3 units: 1.92 b^* and 1.96 b^* (b^* = spacing of the TTT molecules), which is presently not well understood.

correspond to a charge transfer of 1.5 electrons per TTT molecule. This crystal, in fact, reveals a new type of composite lattice. Although confined to channels of the TTT frame-work, the iodine chains behave as independent entities with a spacing (not a modulation period) in chain direction which is incommensurate with respect to the TTT stacking. The iodine chains further reveal the formation of I_3 molecules, very likely implying I_3^- ions, as can be shown from the pattern of FIGURE 7. From such results the charge transfer is inferred to be only 0.5 electrons. This, however, is a particular case.

We are grateful to H.R. Zeller, who long ago provided $K_2Pt(CN)_4Cl_{0.32} - xH_2O$) single crystals, to I. F. Schegolev, who provided the $(TTT)_2I_3$ crystals, and to A. F. Garito, who provided the TSeF-TCNQ samples and participated in their investigations. Detailed reports of the two latter studies will be published separately.

References

1. Anderson, P. W. 1960. Fizika Dielectricov. Skanavi, G. I. Ed. Acad. Nauk. SSSR.
2. Cohran, W. 1969. Phys. Rev. Lett., **3:** 412; 1960. Adv. Phys., **9:** 387; 1961. Adv. Phys., **10:** 401.
3. Frölich, H. 1954. Proc. Roy. Soc. **A223:** 296; Afanasev, A. M., & Y. Kagan. 1963. Sov. Phys. JETP **16:** 1030; Peierls, R. E. 1964. Quantum theory of solids. Clarendon Press. New York, N.Y.
4. Comes, R., M. Lambert, H. Launois & H. R. Zeller. 1973. Phys. Rev. **B8:** 571.
5. Krogmann, K. 1969. Ang. Chem. Int. Ed. Engl. **8:** 35.
6. Renker, B., H. Rietschel, L. Pintchovius, W. Gläser, P. Bruesch, D. Kuse & M. J. Rice. 1973. Phys. Rev. Lett. **30:** 1144.
7. Carneiro, K., G. Shirane, S. A. Werner & S. Kaiser. 1976. Phys. Rev. **B13:** 4258.
8. Comes, R., M. Lambert & M. R. Zeller. 1973. Phys. St. Sol. **58:** 587.
9. Renker, B., L. Pintschovius, W. Gläser, H. Rietschel, R. Comes, L. Liebert & W. Drexel. 1974. Phys. Rev. Lett. **32:** 836.
10. Lynn, J. W., M. Izumi, G. Shirane, S. A. Werner, R. B. Saillant. 1975. Phys. Rev., **B12:** 1154.
11. Barisic, S. 1972. Phys. Rev. **B5:** 941.
12. Horowitz, B., H. Gutfreund & M. Weger. 1974. Phys. Rev., **B9:** 1246.
13. Carneiro, K., J. Eckert & G. Shirane. 1976. Solid State Commun. **20:** 333.
14. Schultz, A. J., G. D. Stucky, J. M. Williams, T. R. Koch & R. L. Mafly. 1977. Sol. St. Comm. **21:** 197.
15. Bertinoti, A., C. Bertinoti & G. Jehanno. 1974. C. R. Acad. Sci. (Paris) **278B:**45.
16. Dubois, J. Y. 1975. Thèse 3ème Cycle. Orsay, France.
17. Garito, A. F. & A. J. Heeger. 1974. Acc. Chem. Res. **7:** 232.
18. Shirane, G., S. M. Shapiro, R. Comes, A. F. Garito & A. J. Heeger. 1976. Phys. Rev. **B14:** 2325.
19. Pouget, J. P., S. K. Khanna, F. Denoyer, R. Comes, A. F. Garito & A. J. Heeger. 1976. Phys. Rev. Lett. **37:** 437.
20. Shapiro, S. M., G. Shirane, A. F. Garito & A. J. Heeger. 1977. Phys. Rev. **B15:** 2413.
21. Khanna, S. K., J. P. Pouget, R. Comes, A. F. Garito & A. J. Heeger, 1977. Phys. Rev. **B16:** 1468.
22. Kagoshima, S., T. Ishiguro & H. Anzai. 1976. J. Phys. Soc. Jap. **41:** 2061.
23. Comes, R., S. M. Shapiro, G. Shirane, A. F. Garito & A. J. Heeger 1975. Phys. Rev. Lett. **35:** 1518; 1976. Phys. Rev. **B14:** 2376.
24. Ellenson, W. D., R. Comes, S. M. Shapiro, G. Shirane, A. F. Garito & A. J. Heeger. 1976. Sol. St. Comm. **20:** 53; Ellenson, W. D., S. M. Shapiro, G. Shirane & A. F. Garito. 1977. Phys. Rev. **B16:** 3244.
25. Weyl, C., E. H. Engler, K. Bechgard, G. Jehanno & S. Etemad. 1976. Sol. St. Comm. **19:** 925.
26. Megtert, S., A. F. Garito & R. Comes. To be published.
27. Megtert, S., J. P. Pouget, R. Comes, A. F. Garito, K. Bechgard, J. M. Fabre & L. Giral. 1978. J. de Phys. (France). To be published.
28. Tomkiewicz, Y., A. R. Taranko & J. B. Torrance. 1976. Phys. Rev. Lett. **36:** 751.
29. Bak, P. & V. J. Emery, 1976. Phys. Rev. Lett. **36:** 978.
30. Schultz, T. D. & S. Etemad. 1976. Phys. Rev. **B13:** 4928.
31. Rybaczewski, E., S. Smith, A. F. Garito, A. J. Heeger & B. Silbernagel. 1976. Phys. Rev. **B14:** 2746.

X-RAY DIFFRACTION MEASUREMENT OF NET ATOMIC AND MOLECULAR CHARGES*

P. Coppens and T. N. Guru Row

Chemistry Department
State University of New York at Buffalo
Buffalo, New York 14214

INTRODUCTION

A variety of physical methods lead to information directly or indirectly related to the net charge on a molecule or molecular fragment. But there is often a conceptual difficulty in interrelating such measurements to each other, or indeed in deducing a net charge from a property that is charge-dependent. For example, experimental bond lengths depend on the relative population of bonding and antibonding orbitals and are insensitive to the occupancy of orbitals that are nonbonding in the regions examined. Similarly, ESCA inner electron ionization potentials depend on the electrostatic interaction between electrons and are therefore not a direct measurement of total charge. Measurements of electron spin resonance or of the field dependence of the second moment of NMR lines give the spin density which can be related to total charge only under certain assumptions regarding spin pairing.

The electronic charge will here be defined as the total number of electrons in the volume associated with a molecule or molecular fragment. Once this volume has been defined, this charge may be derived from experimental time-averaged electron densities, which can be obtained from accurate diffraction data. We will review some aspects of this technique and compare pertinent results with those from other methods.

METHODS OF SPACE PARTITIONING

We are faced with the task of subdividing a continuous crystal-charge density into distinct fragments over which integration can be performed. Such volumes of integration may be defined as having sharp boundaries or, like electron orbitals, may be allowed to interpenetrate. In the latter case the density in the overlapping regions must be subdivided among adjacent fragments. A most rigorous method of the first type for partitioning a total molecular density is the *virial partitioning* of theoretical densities developed by Bader,[1] in which the boundaries between the fragments are surfaces of zero flux of the electron density. The resulting fragments individually satisfy the virial theorem. However, application of this partitioning to experimental densities is not straightforward because of experimental noise and because of uncertainties introduced by thermal smearing. But when the components are well separated (when there is little density in the intermediate region),

*Supported by the National Science Foundation (CHE 7613342A01). Manuscript received June 13, 1977.

0077-8923/78/0313-0244 $1.75/1 © 1978, NYAS

the exact position of the boundary is less important. This is the case in molecular crystals. Thus, if a net molecular charge in a mixed crystal is to be evaluated, the definition of molecular volume may be based on the relative size of the radii of adjacent atoms in neighboring molecules.

If a point is at $\mathbf{r}_A$ and $\mathbf{r}_B$ respectively to atoms A and B, its assignment may be made according to the algorithm:

$$\left|\frac{\mathbf{r}_A \cdot \mathbf{u}_{AB}}{R_A}\right| \overset{?}{\lesssim} \left|\frac{\mathbf{r}_B \cdot \mathbf{u}_{AB}}{R_B}\right| \tag{1}$$

where R_A and R_B are radii assigned to atoms A and B and u_{AB} is a unit vector pointing from A to B (FIGURE 1). The boundaries of a molecule defined in this

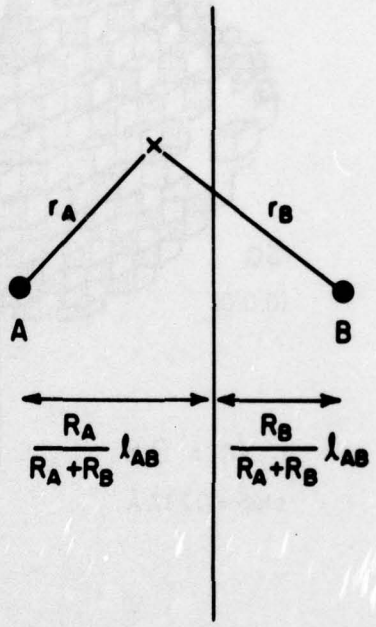


FIGURE 1. Partitioning of space between adjacent atoms. For details see Equation 1.

way are planes, so that the subdivision is into *polyhedral volumes.* For convenience of computation (1) may be replaced by the closely similar expression:

$$\frac{r_A}{R_A} \overset{?}{\lesssim} \frac{r_B}{R_B} \tag{1a}$$

It should be emphasized that in this definition the position of the boundary planes depends only on the relative size of the radii assigned to A and B and not on their absolute value. Nevertheless, calculations with alternative sets of radii are needed to ascertain that the results are not strongly dependent on the position of the boundary surfaces. In the case of a binary system (such as CaF_2 or V_3Si) the integrated charge may be plotted against the radius ratio and the point of the

lowest slope selected as the ratio of best separation (see below). An example of this polyhedral partitioning for CaF_2 is given in FIGURE 2.

In the second type of volume partitioning, the choice of a boundary surface is replaced by selection of each of the fragments' density functions. The Mulliken population analysis of theoretical densities may be considered an example, but its results are dependent on the size of the theoretical basis set and not always representative of the density distribution. Thus, Bats[2] has shown that LiCN and LiNC, for which the three-dimensional density distributions are similar, appear very different according to a Mulliken population analysis.

A more successful method of the second type has recently been proposed by

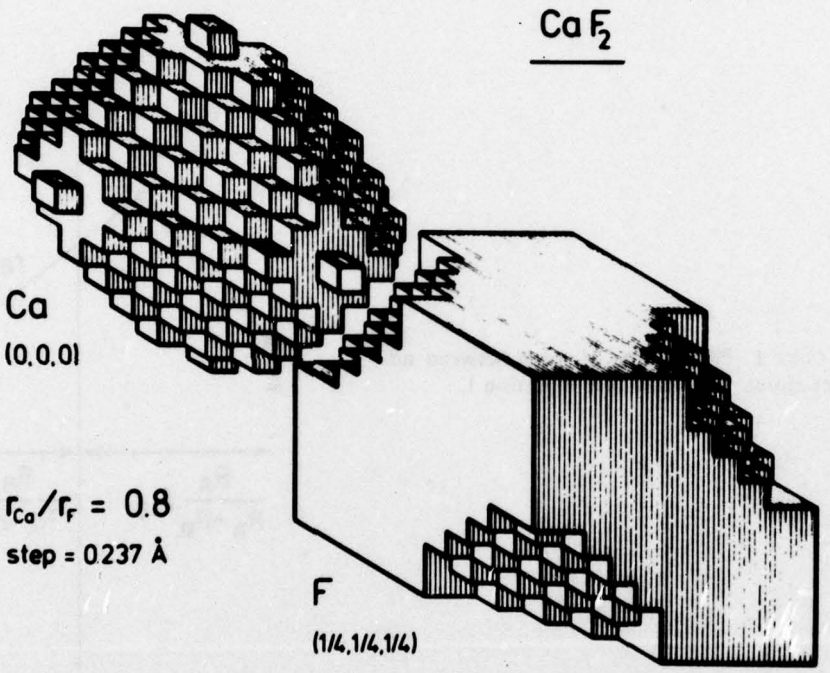


FIGURE 2. Volume partitioning for CaF_2. Radius ratio $R_{Ca}/R_F = 0.8$.

Hirshfeld,[3] in which the electron-partitioning in the intermediate region is relative to the value of the free atom density functions at each point in the region. This partitioning is unique for a rest density and leads to reasonable and consistent net atomic charges, dipole and quadrupole moments. Although this method has been used for atomic partitioning, it has not been applied to subdivide intermolecular space.

The partitioning of the second type, which we will discuss here, is based on the assignment of flexible valence-density functions to each of the atoms, the shape of which is varied to obtain the best fit with the total electronic charge density.[4] As the atomic cores are unaltered by molecule formation within the resolution of

the x-ray diffraction experiment,[5] the atomic density is subdivided into a core and a valence shell density, of which only the latter is varied. Its expansion and contraction is described by a parameter κ which relates the perturbed valence density $\rho'_{\text{valence}}(r)$ to the free atom ground state density $\rho_{\text{valence}}(r)$:

$$\rho'_{\text{valence}}(r) = P_{\text{valence}}\kappa^3 \rho_{\text{valence}}(\kappa r) \tag{2}$$

P_{valence} represents the valence shell population, while the factor κ^3 is required for normalization of the density function. Thus, the total electron density is given by:

$$\rho'_{\text{atom}} = P_{\text{core}}\rho_{\text{core}}(r) + P_{\text{valence}}\kappa^3\rho_{\text{valence}}(\kappa r). \tag{3}$$

The corresponding expression in reciprocal space is in terms of the atomic scattering factors ρ, which are a function of the reciprocal space radial vector $\mathbf{S}$ of length $2 \sin \Theta/\lambda$:

$$f'_{\text{atom}}(S) = P_{\text{core}} f_{\text{core}}(S) + P_{\text{valence}} f_{\text{valence}}(S/\kappa). \tag{4}$$

There is extensive recent work in which (4) is generalized to incorporate angular as well as radial deformation functions.[6-8] Such a formalism has the flexibility to account for details of the electron distribution but is less suited for an analysis of atomic population, because the angular deformation functions must be quite diffuse to fit the observed density. Atoms are therefore less well defined, and the requirement of locality formulated by Kurki-Suonio,[9] which states that only electrons close to the nucleus can be assigned to that nucleus, is no longer obeyed. Hence, we prefer the spherical expression (4) for the derivation of net atomic charges. This expression can be applied conveniently in a least-squares analysis in which P_{valence} and κ are varied in addition to the conventional structural parameters. A neutrality constraint may be included in this procedure to keep the total number of electrons equal to the sum of the nuclear charges. Some alternative methods of constraint have been discussed elsewhere.[10]

Expressions for Charge Integration

If the volume T has been defined and the density function $\rho(\mathbf{r})$ is known, a derived property may be calculated according to the expression:

$$Q = \int_T \gamma(\mathbf{r})\rho(\mathbf{r})\, d\mathbf{r}. \tag{5}$$

This expression is quite general and may be used to evaluate expectation values based on the one-electron density distribution such as dipole and higher moments, or inner moments such as the electrostatic potential at $\mathbf{r} = 0$. When Q represents the charge, $\gamma(\mathbf{r}) = 1$ within the volume of integration.

In the case $\rho(\mathbf{r})$ is an experimental density it may be replaced by the Fourier summation expression

$$\rho(\mathbf{r}) = \frac{1}{V} \sum_{\mathbf{H}} F(\mathbf{H}) \exp(-2\pi i \mathbf{H} \cdot \mathbf{r}) \tag{6}$$

where V is the volume of the crystallographic unit cell, and $F(\mathbf{H})$ the structure factor at $\mathbf{S} = \mathbf{H} = (h\,k)$. For a volume T centered at $\mathbf{r}_0$ we obtain:

$$Q = \frac{1}{V} \int_T \sum_{\mathbf{H}} F(\mathbf{H}) \exp\,[-2\pi i \mathbf{H}\cdot(\mathbf{r} - \mathbf{r}_0)] \exp\,(2\pi i \mathbf{H}\cdot\mathbf{r}_0\,d\mathbf{r})$$

$$= \frac{1}{V} \sum_{\mathbf{H}} F(\mathbf{H}) \int_T \exp\,[-2\pi i \mathbf{H}\cdot(\mathbf{r} - \mathbf{r}_0)]\,d\mathbf{r} \exp\,(2\pi i \mathbf{H}\cdot\mathbf{r}_0). \quad (7)$$

Thus, to calculate the total charge, every structure factor must be multiplied by the shape transform of the volume of integration. In many cases, and especially for a molecule's volume, the integral cannot be evaluated analytically. It is then opportune to subdivide the volume into units of regular shape, and sum after integration over these subunits:

$$Q = \frac{1}{V} \sum_{\mathbf{H}} F(\mathbf{H}) \sum_i \left\{ \int_i \exp\,[-2i\pi\mathbf{H}(\mathbf{r} - \mathbf{r}_i)]\,d\mathbf{r} \exp\,(2\pi i \mathbf{H}\cdot\mathbf{r}_i) \right\}$$

$$\equiv \frac{1}{V} \sum_{H} F(\mathbf{H}) \sum_i [q_i(\mathbf{H}) \exp\,(2\pi i \mathbf{H}\cdot\mathbf{r}_i)], \quad (8)$$

which may be rewritten as

$$Q \equiv \frac{1}{V} \sum_{\mathbf{H}} F(\mathbf{H}) S(\mathbf{H}) \quad (8a)$$

where $S(\mathbf{H})$ is the shape transform of the volume of integration relative to the origin of the unit cell.

The associated expression for the standard deviation in Q is

$$\sigma^2(Q) = \frac{1}{V^2} \left[\sum_H S^2(H)\,\sigma^2\{F(\mathbf{H})\} + \sum_{\substack{\mathbf{H} \\ \mathbf{H}\neq\mathbf{H}'}} \sum^{\mathbf{H}} S(\mathbf{H}) S(\mathbf{H}')\,\mathrm{cov}\,\{F(\mathbf{H})F(\mathbf{H}')\} \right]. \quad (9)$$

The covariance between measured structure amplitudes is generally small, except between symmetry-related reflections generated from the same measurement, for which it is either $+1$ or -1.

The effect of the subunit size on the total volume of integration can be noticed in FIGURE 2. The boundary planes are replaced by stepped surfaces which are smoother, the smaller the subunits.

DISCUSSION OF SELECTED RESULTS

Radial Parameter (κ) Refinements

The Kappa refinement has been applied to several molecular crystals containing first-row atoms. Generally, oxygen atoms are found to be negative in molecules containing C, N, O, and H, whereas hydrogen atoms are positively charged. Nitrogen and carbon atoms are positive or negative, depending on their

immediate environment. Thus, the nitrogen atom in the nitro and nitroxo groups of *p*-nitropyridine *N*-oxide which are bonded to oxygens are positive, while those in cyanuric acid and glycylglycine which are linked to carbon and hydrogen atoms are negatively charged. Similar observations result for carbon atoms which are negative in an aliphatic environment but positive when bonded to nitrogen or oxygen.

Not surprisingly, these observations are in agreement with electronegativity rules. The next question to be addressed concerns the possible relation between the values of the radial parameter κ and the net atomic charge q. To what extent does additional charge lead to increased screening of the nucleus and therefore to an expansion (lower values of κ) of the atomic valence shell? The results for a num-

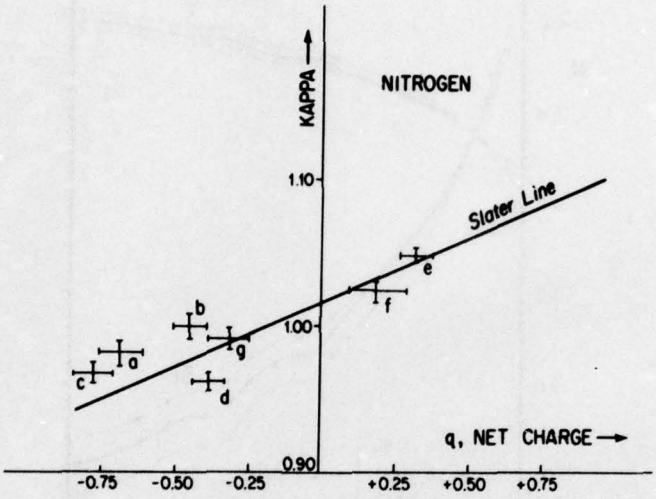


FIGURE 3. Net charge against expansion-contraction parameter κ for nitrogen atoms in a number of structures: a,b) glycylglycine, c) formamide, d) cyanuric acid, e) *p*-nitropyridine *N*-oxide, f) sulfamic acid, g) tetrasulfurtetranitride. All structures were measured at liquid nitrogen temperature except *p*-nitropyridine *N*-oxide, which was analyzed at 30°K. The values for *d*, *e*, and *g* are common to two or more nitrogen atoms; two nitrogen-atoms in glycylglycine were treated separately. The sloping line is the function implied in Slater's empirical rules for atomic orbitals.

ber of nitrogen atoms reproduced in FIGURE 3, show a clear correlation between the two parameters. The sloping line represents the screening as implied in Slater's rules for analytical atomic orbitals.[11] For nitrogen, the Slater orbital exponent in the expression

$$\Phi(2s, 2p) = N_{2s,2p} \exp(-\zeta r)$$

(where N is a normalization factor) is 1.95 au^{-1} and is decreased by 0.175 au^{-1} for each additional electron placed in the valence shell. The intersect of the line at $q = 0$, is derived from the ratio of the Slater exponent for the bonded atom and the orbital exponent for the free atom as given by Clementi and Raimondi,[12] which is 1.919 au^{-1} when averaged over the $2s$ and $2p$ electrons. The "Slater-line"

appears to represent the slope quite well. The agreement is somewhat worse for carbon, for which the Slater line has a larger slope while the experimental results (not reproduced here) are similar to those for nitrogen atoms.

Charge Integration of V_3 Si

V_3Si is a superconductor of the A15 type for which accurate x-ray diffraction data have been collected by Staudenmann[13] and Staudenmann *et al.*[20] Its structure consists of perpendicular (and nonintersecting) chains of vanadium atoms which

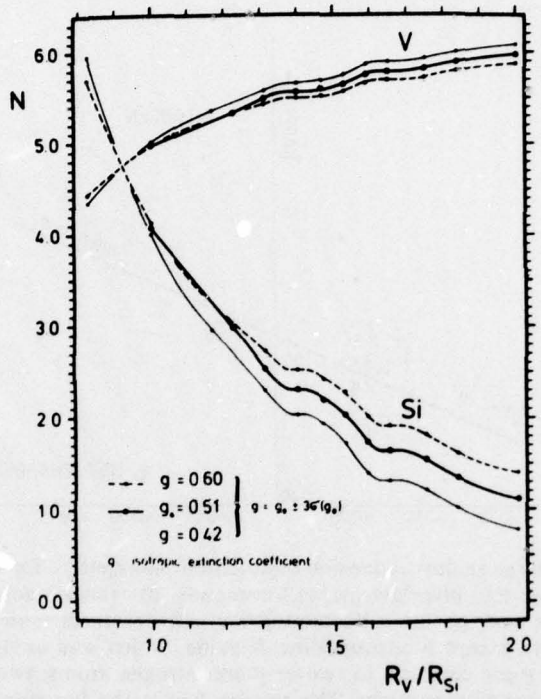


FIGURE 4. Valence electron population as a function of radius ratio for V_3Si. The broken and full lighter curves are calculated with extinction parameters three standard deviations from the least-squares values. (From Reference 20.)

surround each of the silicon atoms. Charge integration by use of expression (8) was performed for a series of values of the radius ratio R_V/R_{Si}. Results are plotted in FIGURE 4. At electron neutrality where the silicon would have four and the vanadium five-valence electrons the curve has a steep slope, but horizontal sections occur at a radius ratio of about 1.5. This indicates that at the corresponding position of the boundary surfaces there is little density near the surface. The horizontal parts in the curve may therefore be described as occurring at the *radius ratio of best separation* of the components. The charge transfer in this part of the curve is about two electrons from each silicon to three vanadium atoms.

TABLE 1

RESULTS OF CHARGE INTEGRATION OF TTF-TCNQ

Van der Waals radii used (Å)				Electron population (electrons)	
S	N	C	H	P_{TCNQ}	P_{TTF}
1.85	1.50	1.75	1.1	72.45	51.56
1.85	1.55	1.65	1.2	72.50	51.51

TTF-TCNQ

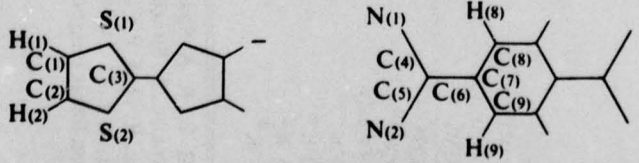
The charge integration of TTF/TCNQ at 100°K was performed with two sets of atomic radii.[14] The results summarized in TABLE 1 indicate a charge transfer averaging 0.48 electrons per molecule, with an estimated standard deviation of 0.15 electrons. We will discard an earlier discussion on the effect of scale-factor bias, since no clear evidence exists for such bias in the TTF-TCNQ data set. The earlier estimate of the standard deviations is approximate, but a similar result is obtained with the aid of expression (**9**).

The kappa refinement was subjected to a constraint that required chemically

TABLE 2

RADIAL PARAMETER REFINEMENT ON TTF-TCNQ

TTF	100°K	45°K			
C(1), C(2)*	−0.03(8)	−0.12(7)			
C(3)	+0.15(9)	+0.10(9)			
S(1), S(2)	−0.05(8)	+0.05(8)			
H(1), H(2)*	+0.12(6)	+0.13(5)			
Sum over Molecule	+0.47(15)	+0.43(16)			
TCNQ			Theoretical† $TCNQ^-$	TCNQ	Theoretical‡ $TCNQ^-$
C(4), C(5)	+0.23(9)	+0.22(9)	−0.15	−0.16	+0.14, +0.16
C(6)	+0.03(14)	−0.02(13)	−0.06	+0.07	
C(7)	+0.04(16)	+0.02(15)	+0.07	+0.10	−0.10
C(8), C(9)	+0.08(9)	+0.15(9)	−0.06	−0.04	
N(1), N(2)	−0.52(8)	−0.64(7)	−0.15	−0.03	−0.35, −0.29
H(8), H(9)	+0.05(6)	+0.08(6)	+0.10	+0.14	
Cyanogroup	−0.29(8)	−0.42(8)	−0.30	−0.19	−0.15
Sum over Molecule	−0.47(15)	−0.43(16)			



*Int. Tables Vol IV, scattering factor curves; hydrogen *f* curves from Stewart, R. F., E. R. Davidson & W. T. Simpson. 1965. J. Chem. Phys. **42**: 3175.

†Johansen, H. 1975. Int. J. Quantum Chem. **9**: 459.

‡Grobman W. D. & B. D. Silverman. 1976. Solid State Commun. **19**: 319.

TABLE 3

BOND LENGTHS AND CHARGE TRANSFER IN TTF-TCNQ

bond	a C(8)-C(8′)	b C(8)-C(9)	c C(6)-C(7)	d C(4)-C(6)	$(a + c)/(b + d)$	Charge Transfer*
$TCNQ^{0}$[a]	1.346 Å	1.448 Å	1.374 Å	1.440 Å	0.942	
$TCNQ^{-1}$[b]	1.373	1.423	1.420	1.416	0.984	
TTF-TCNQ						
100°K[c]	1.352	1.435	1.395	1.434	0.957	→ 0.36 electrons
60°K[d]	1.345	1.437	1.383	1.431	0.951	→ 0.21
53°K[d]	1.353	1.431	1.396	1.429	0.961	→ 0.45
45°K[d]	1.343	1.444	1.393	1.430	0.952	→ 0.31
						average 0.32

[a]Long, R. E., R. A. Sparks & K. N. Trueblood. 1965. Acta Cryst. **18:** 932.
[b]Hoekstra, A., T. Spoelder, C. A. Vos. 1972. Acta Cryst. **B28:** 14.
[c]Blessing, R. H. & P. Coppens. 1974. Solid State Commun. **15:** 215.
[d]Schultz, A. J., G. D. Stucky, R. H. Blessing & P. Coppens. 1976. J. Amer. Chem. Soc. **98:** 3194.
*Based on linear interpolation of the ratio $(a + c)/(b + d)$.

equivalent atoms to have the same charge parameters, even though their crystallographic environments differ.

Because it is a least squares rather than a Fourier method, the kappa refinement does not require a full data set and it can therefore also be applied to the 45°K x-ray data set in which a number of reflections are absent because of equipment failure at data-collection time.

Resulting charges at both temperatures are summarized in TABLE 2. The total charge in each of the molecules and its standard deviation are obtained by summation over the atomic charges taking into account, in the case of the standard deviation, the covariances between atomic charges. The results are the same at both temperatures, the values of 0.47 ± 0.15 (100°K) and 0.43 ± 0.16 (45°K) being equal, and also in good agreement with the charge transfer obtained with the direct integration method.

Net atomic charges are small and not significantly different from zero except on the cyanogroup, which shows a strong polarity in the expected direction and a net charge of −0.29(8) and −0.42(8) at 100° and 45°K, respectively. For comparison, gross Mulliken populations as derived by Johansen[15] from *ab initio* SCF calculations on the isolated TCNQ and $TCNQ^-$ ions are also listed. The agreement for the cyanogroup atoms is rather poor, although total cyanogroup charges are similar in theory and experiment. It may be noted that more approximate CNDO/2 calculations by Grobman and Silverman[16] (last column of TABLE 2) fit the experimental results better, especially with regard to the polarity of the cyanogroup.

ANALYSIS OF BOND LENGTHS

Even before the current interest in "segregated-stack" organic mixed crystals, a number of structure analyses had shown a variation of the bond lengths with increasing negative charge on the TCNQ molecule.[17] The general trend corresponds to a lengthening of the shorter quinoid bonds and a shortening of the remaining bond lengths, which is in agreement with theoretical predictions. There are five chemically different bonds in TCNQ, of which C≡N is least well determined because of the larger thermal motion of the extremes of the molecule. Of the remaining four, the two quinoid bonds (a and b, see TABLE 3 for definitions) increase, while the other two (b and d) decrease in length with increasing negative charge. We have therefore chosen the ratio $(a + c)/(b + d)$ as a gauge of charge transfer at the four reduced temperatures at which x-ray dimensions are available. The use of linear interpolation between the ratios for $TCNQ^0$ and Rb TCNQ gives values of 0.36 (100°K), 0.21 (60°K), 0.45 (53°K), and 0.31 (45°K). Apart from the variation with temperature, which may not be statistically significant, the most striking result is that the charge transfer appears smaller than values deduced with other methods.

Interpolation between $TCNQ^0$ and Rb TCNQ, as done here, implicitly assumes that in the latter salt a full electron has been transferred. If transfer in Rb TCNQ would be incomplete (as suggested by some charge integration results on Na salts such as NaSCN[21]), the charge transfer in TTF-TCNQ would be proportionally reduced.

For the bond-length analysis to be valid the data should be reasonably accurate. Thus, the results on *N*-methylphenazinium-TCNQ which were based on photographic data,[18] are probably inadequate. For the complex with *N,N,N',N'* tetramethyl-*p*-phenylenediamine [TMPD(TCNQ)$_2$][19] a transfer of 0.45e is obtained, which confirms that the charge on TCNQ in this salt is intermediate between those in Rb TCNQ and TCNQ^0.

Comparison with other Experimental Results

A number of recent results are summarized in Table 4. Considering the different assumptions involved in the derivations of charge from experimental measurement, agreement is reasonable. This is partly due to the considerable experimental errors associated with most results. Nevertheless, it appears well established that

Table 4

Recent Values for Charge Transfer in TTF-TCNQ

Technique	Charge Transfer (electrons)	References
Charge Integration	0.47(15)	Table 2*
Bond Lengths	0.31	Table 3
ESCA	0.8 ± 0.2	†
ESCA	0.56 – 0.67	‡
Diffuse Scattering and	0.53 – 0.56	§
Satellite Reflections	0.59 ± 0.02	¶

*Coppens, P. 1975. Phys. Rev. Lett. **35:** 98.

†Swingle II, R. S., R. B. Groff & B. M. Monroe. 1976. Phys. Rev. Lett. **35:** 452.

‡Grobman, W. D. & B. D. Silverman. 1976. Solid State Commun. **19:** 319.

§Denoyer, F., R. Comes, A. F. Garito & A. J. Heeger. 1975. Phys. Rev. Lett. **35:** 445; Kagoshima, S., H. Anzai, K. Kajimura & T. Ishiguro. 1975. J. Phys. Soc., Japan **39:** 1143.

¶Pouget, J. P., S. K. Khanna, F. Denoyer, R. Comes, A. F. Garito & A. J. Heeger. 1976. Phys. Rev. Lett. **37:** 437.

the charge transfer per formula unit is within the range of 0.40–0.65 electrons. There is no evidence for a temperature dependence of the charge transfer in the information surveyed here.

References

1. Bader, R. F. W. & P. M. Beddall. 1973. J. Am. Chem. Soc. **95:** 305; Bader, R. F. W. 1975. MTP Int. Rev. Science, Phys. Chem. Series II, Vol. **1:** 43; Bader, R. F. W. 1975. Accts. Chem. Res. **8:** 34.
2. Bats, J. W., 1973. MSc. Thesis. Twente University of Technology, Enschede, The Netherlands.
3. Hirshfeld, F. L. 1977. Theor. Chim. Acta **44:** 129.
4. Coppens, P., Y. W. Yang & P. Becker. To be published.
5. Bentley, J. & R. F. Stewart. 1974. Acta Cryst. **A30:** 60; Groenewegen, P. P. M., J. Zeevalkink & D. Feil. 1971. Acta Cryst. **A27:** 487.

6. STEWART, R. F. 1976. Acta Cryst. **A32:** 565.
7. HAREL, M. & F. L. HIRSHFELD. 1975. Acta Cryst. **B31:** 162.
8. HANSEN, N. K. & P. COPPENS. 1976. ACA Abstr. Ser. 2. **4:** 54.
9. KURKI-SUONIO, K. S. 1969. Charge density in crystals as a superposition of spherical atoms. Reports in Physics. University of Helsinki, Helsinki, Finland.
10. P. COPPENS, 1978. Isr. J. Chem. In press.
11. COULSON, C. A. 1961. Valence. 2nd edit. Oxford University Press. Oxford, England.
12. CLEMENTI, E. & D. L. RAIMONDI. 1963. J. Chem. Phys. **38:** 2686.
13. STAUDENMANN, J. L. 1976. Thesis. Université de Genève. Geneva, Switzerland.
14. COPPENS, P. 1975. Phys. Rev. Lett. **35:** 98.
15. JOHANSEN, H. 1975. Int. J. Quantum Chem. **9:** 459.
16. GROBMAN, W. D. & B. D. SILVERMAN. 1976. Solid State Commun. **19:** 319.
17. HERBSTEIN, F. H. 1971. *In* Perspectives in Structural Chemistry. J. D. Dunitz and J. A. Ibers, Eds. 4th edit.: 166. HOEKSTRA, A., T. SPOELDER & A. VOS. 1972. Acta Cryst. **B28:** 14.
18. FRITCHIE, JR., C. J. 1966. Acta Cryst. **20:** 892.
19. HANSON, A. W. 1968. Acta Cryst. **B24:** 768.
20. STAUDENMANN, J. L., P. COPPENS & J. MULLER. 1976. Solid State Commun. **19:** 29.
21. BATS, J. W., P. COPPENS & Å. KVICK. 1977. Acta Cryst. **B33:** 1534.

DISCUSSION

ROBERT METZGER: A different histogram was devised for the correlation between bond length and charge transfer by S. C. Nyburg and J. A. Potworowski (U. of Toronto, Toronto, Canada). Instead of adding two or looking at only one bond distance at a time they compared the *p*-quinodimethane "molecular lengths" for TCNQ salts. Their histogram yields 0.50 ± 0.05 for the charge transfer in (TTF)-(TCNQ).

COPPENS: I believe that the most sensitive measure is the ratio of the lengthened bond to that of the shortened bond. [**Note added in proof:** For an extensive survey of charges derived from bond lengths, see FLANDROIS, S. & D. CHASSEAU. 1977. Acta Cryst **B33:** 2744.]

REFLECTION SPECTRA AND ELECTRONIC STRUCTURES OF METALLIC TCNQ COMPLEXES*

Jiro Tanaka, Masashi Tanaka, Chizuko Tanaka, and Teruaki Ohno

Department of Chemistry, Faculty of Science
Nagoya University
Chikusa, Nagoya 464, Japan

Teruhiro Takabe

Department of Chemistry, Faculty of Science and Technology
Meijo University
Tenpaku, Nagoya 468, Japan

Hiroyuki Anzai

Electrotechnical Laboratory
Mukodai 5-4-1
Tanashi, Tokyo 188, Japan

In a previous paper[1] we discussed the electronic structure of TCNQ complexes from the assignment of the electronic spectra of these single crystals. The spectra were measured by a transmission technique with very thin crystals, and it was difficult to estimate accurately the absolute intensity of each band. In this paper we will present the reflection spectra of several metallic TCNQ complexes and discuss the electronic structures and charge distributions of the TCNQ and cation columns.

One of the conclusions in the previous paper is a classification of TCNQ complexes into three types: dimeric, alternant, and island (FIGURE 1). Although we believe that such terminology may be useful, too much simplication must be avoided, and we will present our view on the electronic structure of TTF(TCNQ) in this paper.

EXPERIMENTAL

The single crystals of TTF(TCNQ), Q(TCNQ), NMP(TCNQ)(I) (triclinic), and NMP(TCNQ)(II) (monoclinic) were grown from a purified acetonitrile solution in a vacuum-sealed tube. The crystalline axes and faces were confirmed by x-ray photographs. The reflectivities of these crystals were measured at room temperature in the range of 3700 cm^{-1} ~ 30000 cm^{-1} with a polarized light passed through a MgF_2 polarizer. A Carl-Zeiss double monochromator was used with a PbS detector and a HTV 446 photomultiplier tube. A specially designed microscope with a Carl-Zeiss ultrafluar lens and a rotatable crystal mount were used to

*Manuscript received June 6, 1977.

0077-8923/78/0313-0256 $1.75/1 © 1978, NYAS

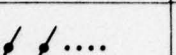
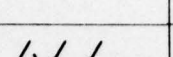
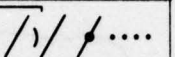
Donors	Ratios of Donor to Acceptor	Electron Configurations	Types of Interactions
Rb,K,Li,Mor	1:1		Dimer Type
NMP	1:1		Alternant Type
Q,Ac,TMPD	1:2		
Cs,Mor	2:3		Island Type
TEA,MTPP	2:4		

FIGURE 1. Electronic configurations of TCNQ complexes and types of interactions.

concentrate the light beam onto the crystalline surface, and a reflectivity was obtained by comparison with a standard of SiC crystal.

The crystals of Q(TCNQ) were needles with a flat (100) surface, and the reflectivity was measured along the *b*- and *c*-axes. The result is shown in FIGURE 2. The crystals of TTF(TCNQ) were thin plate or tabular developing (001) and (100) faces. The reflectivity below 3700 cm^{-1} shown in FIGURE 3 is taken from the data of Tanner *et al.*[2] and joined with our data above 3700 cm^{-1}. The crystals of

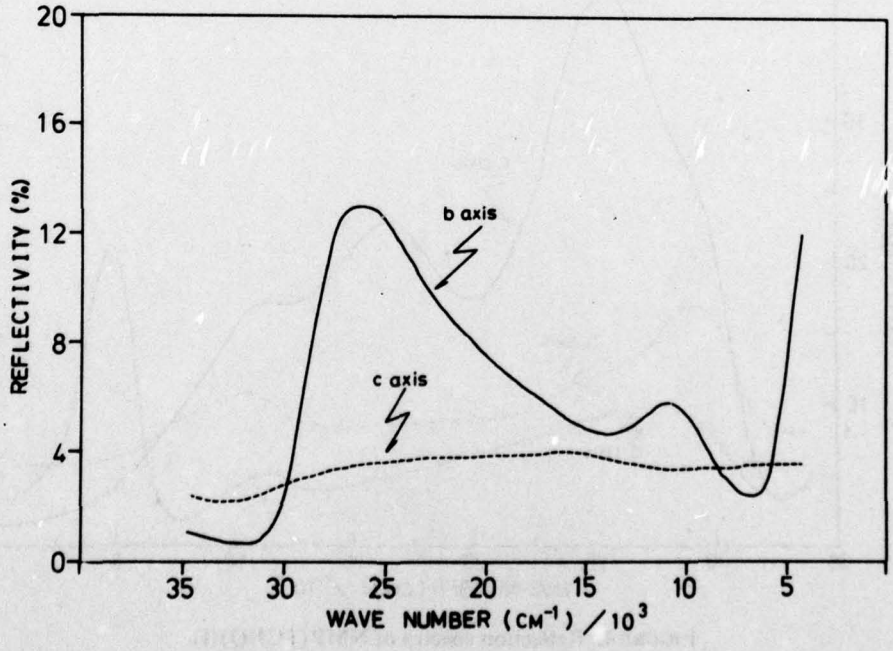


FIGURE 2. Reflection spectra of $Q(TCNQ)_2$.

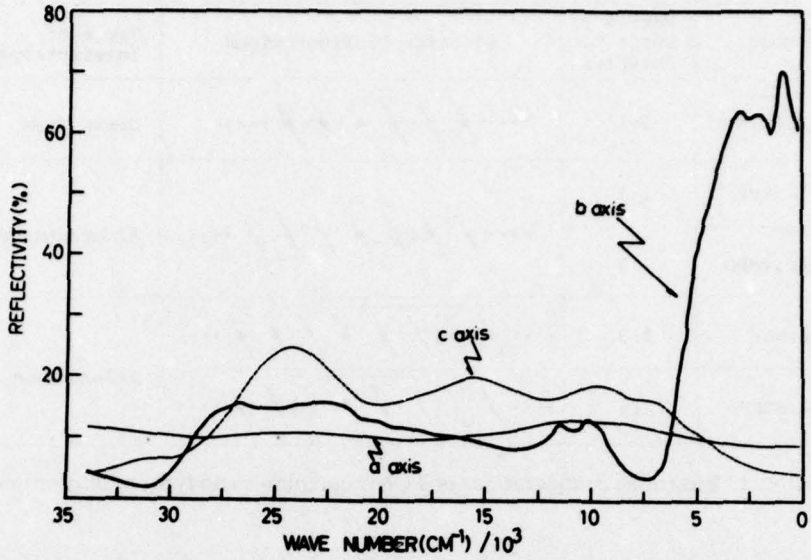


FIGURE 3. Reflection spectra of TTF(TCNQ). The data below 3700 cm^{-1} is from Tanner *et al.*[2]

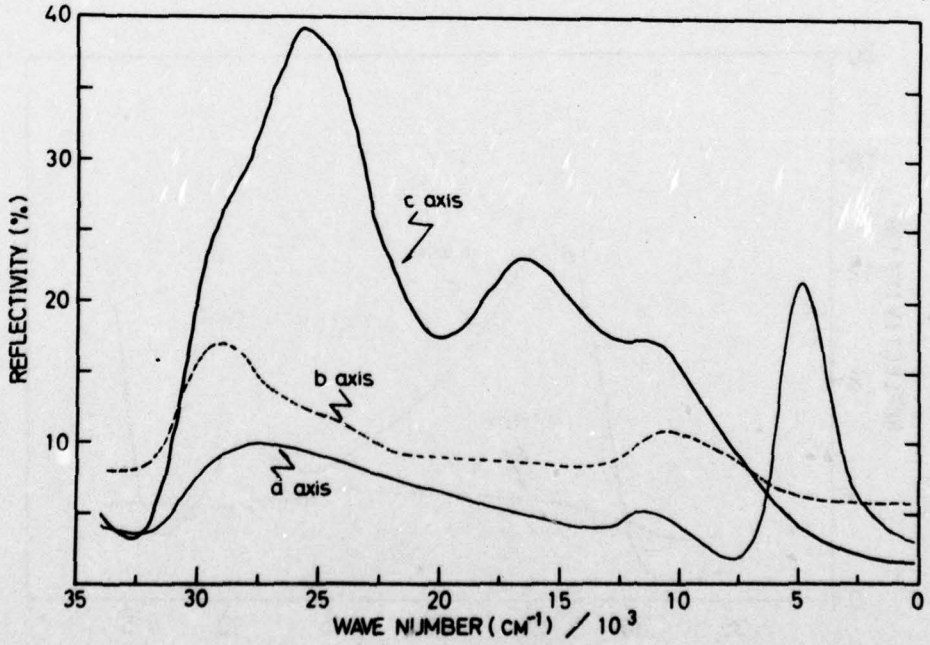


FIGURE 4. Reflection spectra of NMP(TCNQ)(I).

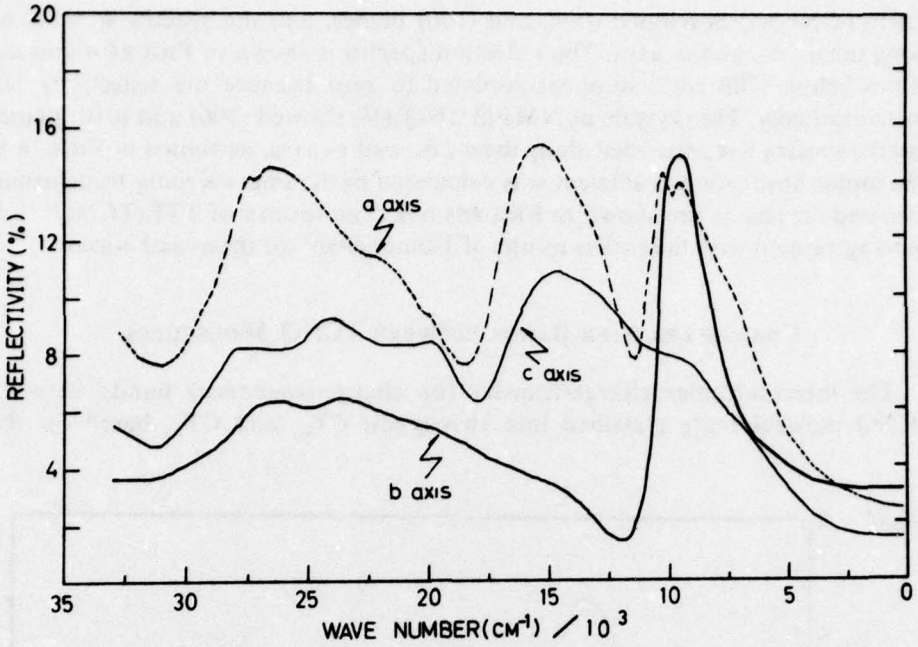


FIGURE 5. Reflection spectra of NMP(TCNQ)(II).

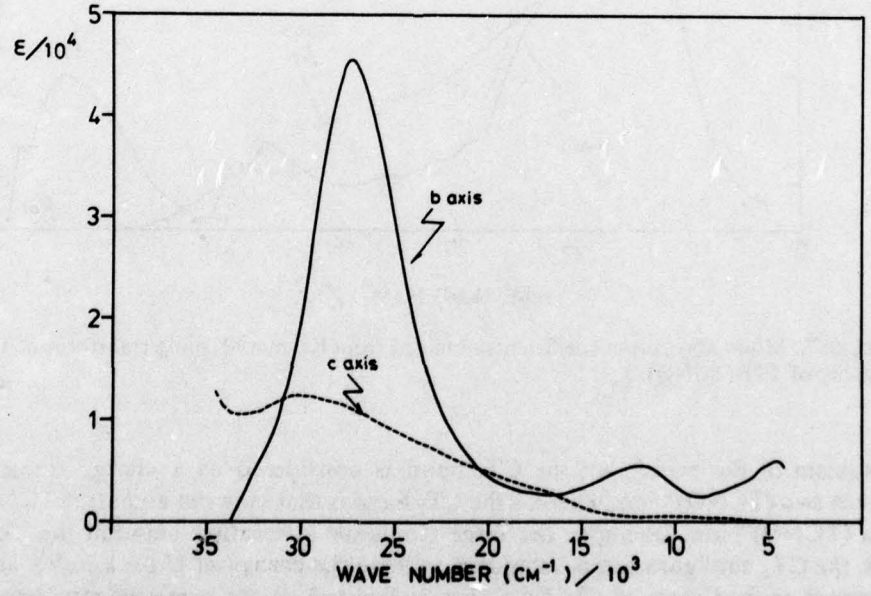


FIGURE 6. Molar absorption coefficients obtained from Kramers-Kronig transform of the reflectivity of $Q(TCNQ)_2$.

NMP(TCNQ)(I) developed (001) and (100) planes, and the spectra were taken along the *a*-, *b*-, and *c*- axes. The reflection spectra is shown in FIGURE 4 and the values below 3700 cm^{-1} were extrapolated to zero because the reflectivity fell down gradually. The crystals of NMP(TCNQ)(II) showed (100) and (010) planes and the spectra were recorded along the *a*-, *b*-, and *c*- axes, as shown in FIGURE 5. The molar absorption coefficient was calculated by Kramers-Kronig transformation, and the results are shown in FIGURES 6–9. The spectra of TTF(TCNQ) is in good agreement with the earlier results of Tanner *et al.*[2] for the *a*- and *b*-axes.

CHARGE-TRANSFER BANDS BETWEEN TCNQ MOLECULES

The intermolecular charge-transfer (or charge-resonance) bands between TCNQ molecules are classified into two types, CT_1, and CT_2, based on the

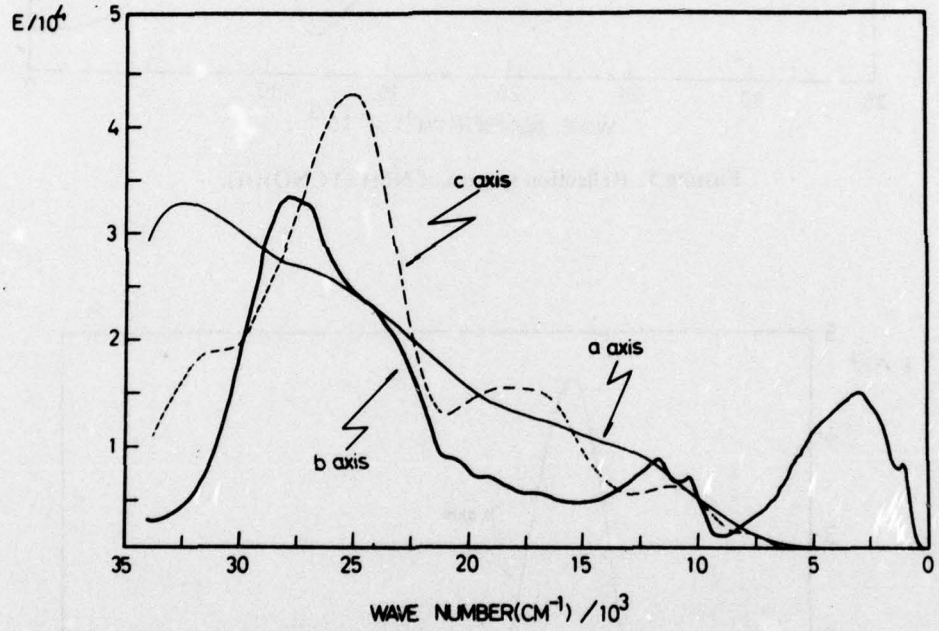


FIGURE 7. Molar absorption coefficients obtained from Kramers-Kronig transform of the reflectivity of TTF(TCNQ).

mechanism of the transition; the CT_1 band is considered as a charge transfer between two $(TCNQ)^-$ ion, whereas the CT_2 band is that between a neutral TCNQ and a $(TCNQ)^-$ ion. Owing to the large Coulomb interaction between the electrons, the CT_1 configuration is estimated to have the energy of U (~1.5 eV), and the lowest excited state of $(TCNQ)^-$ ion is located at the same energy region of 1.5 eV (LE_1). The configuration interaction between the CT_1 and LE_1 levels results in the splitting of the energy levels, and the direction of the transition moments is modified from a pure CT and a geniune LE transition. The coupled

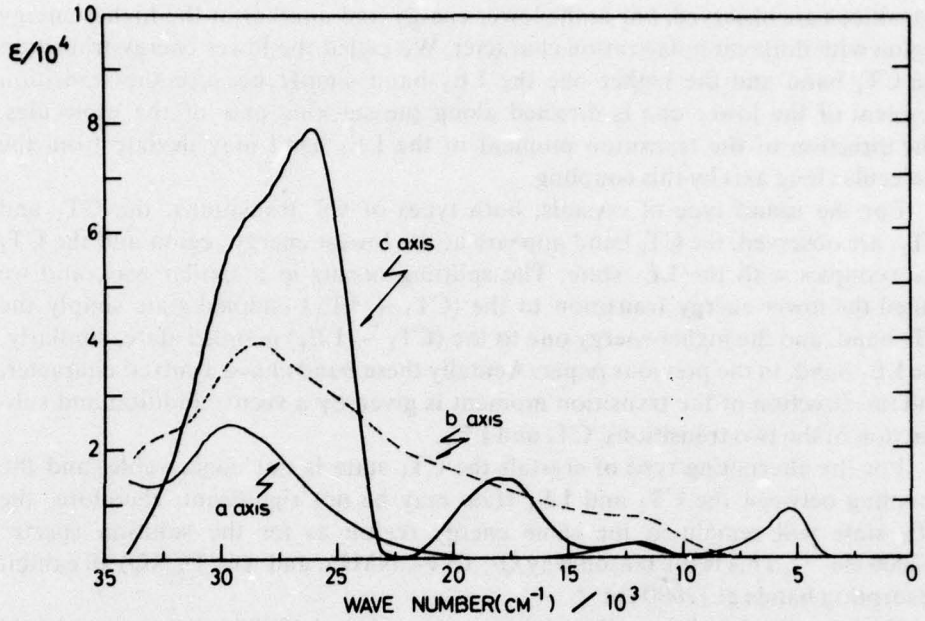


FIGURE 8. Molar absorption coefficients obtained from Kramers-Kronig transform of the reflectivity of NMP(TCNQ)(I).

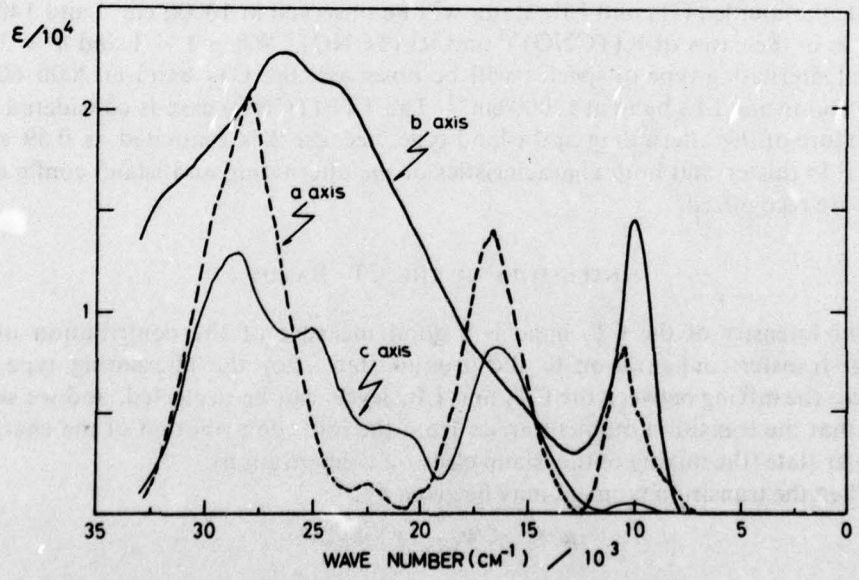


FIGURE 9. Molar absorption coefficients obtained from Kramers-Kronig transform of the reflectivity of NMP(TCNQ)(II).

transitions are observed, one at the lower energy and another at the higher energy region with different polarization character. We called the lower energy transition the CT_1 band and the higher one the LE_1 band simply because the transition moment of the lower one is directed along the stacking axis of the molecules. The direction of the transition moment of the LE_1 band may deviate from the molecular long axis by this coupling.

For the island type of crystals, both types of CT transitions, the CT_1 and CT_2, are observed; the CT_2 band appears at the lowest energy region and the CT_1 state couples with the LE_1 state. The splitting occurs in a similar way, and we called the lower energy transition to the $(CT_1 + LE_1)$ coupled state simply the CT_1 band, and the higher energy one to the $(CT_1 - LE_1)$ coupled state, similarly, the LE_1 band, in the previous paper. Actually these bands have a mixed character, and the direction of the transition moment is given by a vector addition and subtraction of the two transitions, CT_1 and LE_1.

For the alternating type of crystals the CT_1 state is not conceivable, and the coupling between the CT_2 and LE_1 state may be not significant; therefore, the LE_1 state will remain at the same energy region as for the solution spectra ($12000\ cm^{-1}$). This is the reason why Q-, TTF-, NMP-, and Ad-(TCNQ) all exhibit absorption bands at $12000\ cm^{-1}$.

Torrance[3] claimed that all transitions appearing at $12000\ cm^{-1}$ region should be the CT_1 band (his B band); however, the mechanism of the electronic transition is different with each crystalline type. We therefore believe that the $12000\ cm^{-1}$ band in the alternating type of crystal must be assigned to the LE_1 band.

The crystalline spectra have been shown to be useful in the analysis of the electronic structure of these TCNQ complexes. For instance the degree of an electron transfer in $D^{+\delta}(TCNQ^{-\delta/n})_n$ may be guessed from the pattern of the CT_2, CT_1, and LE_1 bands appearing in the crystalline spectra. That is if $\delta = 1$ and $n = 1$, the coupled CT_1 and LE_1 states will be observed at $10000\ cm^{-1}$ and $14000\ cm^{-1}$ as in the cases of K(TCNQ)[4,5] and Rb(TCNQ).[1] When $\delta = 1$ and $n = 2$, a typical alternating type of spectra will be observed: the CT_2 band at 3000–6000 cm^{-1} region and LE_1 band at $12000\ cm^{-1}$. The TTF(TCNQ) case is considered an admixture of the alternating and island type, because δ is estimated as 0.59 and $n = 1$. In this crystal both characteristics of the alternating and island configurations are recognized.

Intensities of the CT_2 Bands

The intensity of the CT_2 band is a good measure of the contribution of a charge-transfer configuration to the ground state. For the alternating type of crystals the mixing between the CT_2 and LE_1 levels can be neglected, and we suppose that the transition moment arises from the ionic contribution of the charge-transfer state (the mixing of the island electron configuration).

Then the transition moment may be given by

$$\mu \simeq \langle \Psi_{CT_2} | r | \Psi_0 \rangle$$

and

$$\Psi_0 = a\psi_A + b\psi_I$$
$$\Psi_{CT_2} = a\psi_I - b\psi_A$$

where the charge-transfer state is written as ψ_I (island-type electron configuration) and the ground state is given by ψ_A (alternating type structure). Here ψ_I represents the state where the cation charges are still fixed and only an electron is transferred from one site to a neighbour site.

Then

$$\mu = abR$$

where R is the distance between the centers of two TCNQ molecules. The experimental oscillator strengths are estimated from the crystalline spectra by a formula that $f = 4.32 \times 10^{-9} \int \epsilon d\tilde{\nu}$. A theoretical value of the oscillator strength for the one-dimensional oscillator is given by

$$f = 3 \times 1.085 \times 10^{-5} \times \tilde{\nu}\mu^2 (\cos \beta)^2$$

where $\cos \beta$ is the angle between the transition moment and the crystalline axis. The transition moment will be large when the charge-transfer configuration mixes with the alternant ground configuration; an equal mixing of both state ($a = b =$

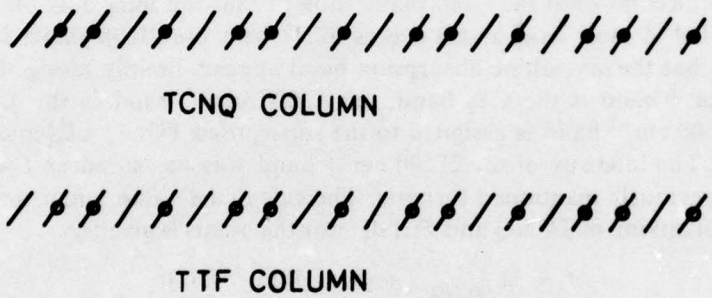


FIGURE 10. Electronic structure of $TTF^{\delta+}(TCNQ)^{\delta-}$ ($\delta = 0.59$).

$1/\sqrt{2}$) gives a maximum value. The observed f values clearly show that the TTF(TCNQ) involves the charge-transfer configuration to the largest extent in the ground state.

For TTF(TCNQ) crystal the estimated transition moment from the observed spectra is 1.75 Å, which is nearly a maximum value of this type of transition. Here we took the direction of the transition moment along the *b*-axis. By using this number the ground-state wave function is estimated as $0.84 \psi_A + 0.54 \psi_I$. Moreover, by this mixing there will be produced vacant sites where more electrons may flow in, and nearly equal mixing of the alternating and island configuration will be produced (FIGURE 10). This configuration corresponds to electron transfer of $\delta = 0.59$.

For Q(TCNQ) and NMP(TCNQ)(I) the estimated wave functions are

$$0.98 \psi_A + 0.21 \psi_I \quad \text{(Q(TCNQ))}$$

$$0.98 \psi_A + 0.18 \psi_I \quad \text{(NMP(TCNQ))}.$$

LE_2 Bands of TCNQ Molecule and TCNQ Ion

In this section we advance a discussion of the spectral consideration of the electronic structure with the shorter wavelength LE_2 band. The absorption spectra of TCNQ molecule and $TCNQ^-$ ion in solution show strong bands at 25000 cm^{-1} region; $\epsilon(TCNQ)_{24500\,cm^{-1}} = 64400$ ($f = 0.76$) and $\epsilon(TCNQ^-)_{24000\,cm^{-1}} = 24000$ ($f = 0.48$). The latter band is the transition to the second locally excited state of $(TCNQ)^-$, which is polarized along the long axis, and we call it LE_2 band. By using the same notation we call the band at the same position for the neutral TCNQ molecule the LE_2° band, which is also polarized along the long axis. The peak intensity and the oscillator strength are apparently much larger for the neutral TCNQ molecule than for the $TCNQ^-$ ion; therefore, the crystalline absorption spectra in this region may be utilized in estimating the degree of an electron transfer.

$Q(TCNQ)_2$

The crystal of Q(quinolinium)(TCNQ) is typical of an alternant type. The projection of molecules onto the (100) plane showed that the long axis of TCNQ is nearly parallel to the *b*-axis, and it makes 32.9° with the (010) plane. It is quite reasonable that the crystalline absorption band appears mainly along the *b*-axis; the 4500 cm^{-1} band is the CT_2 band, the 12000 cm^{-1} band is the LE_1 band, and the 27500 cm^{-1} band is assigned to the superposed TCNQ LE_2° and $TCNQ^-$ LE_2 bands. The intensity of the 27500 cm^{-1} band was measured as $f = 1.01$ by using the previously mentioned formula. The calculated value under an assumption of equal mixing of TCNQ and $TCNQ^-$ for the b-axis is given by

$$f = 3(f_{TCNQ^-} + f_{TCNQ})(\cos 57.1°)^2$$

$$= 1.10.$$

The contribution of the quinolinium ion will not be significant, since its solution spectra exhibit a band centering at 32000 cm^{-1} with $\epsilon_{max} = 4700$. The band appearing at 30000 cm^{-1} along the *c*-axis may be assigned to the quinolinium long-axis polarized transition. Thus the assumption of the charge distribution of $Q(TCNQ)_2$ crystal as an alternant type is confirmed by the intensity measurement in the 25000 cm^{-1} region.

TTF(TCNQ)

From analysis of the previous section, the ground-state configuration of this crystal involves a large amount of the CT configuration, and we take the electronic structure as $TTF^{+0.59}TCNQ^{-0.59}$. The absorption intentisy in the 25000 cm^{-1} region due to TCNQ species may be estimated by this model as

$$f = 3 \times (0.41 f_{TCNQ} + 0.59 f_{TCNQ^-})(\cos \beta)^2$$

where β is the angle between the transition moment and the crystalline axis. The

calculated value is 0.59 for the *b*-axis and 1.20 for the *c*-axis, and these values may be compared with the observed value of 0.85 for the *b*-axis and 1.12 for the *c*-axis. However, the TTF^+ ion also absorbs in this region, and actually, we have separated the 23000 cm^{-1} band along the *b*-axis as due to TTF^+ ion, and the above-mentioned agreement must be further investigated after determining the absorption intensities of TTF cation in the crystalline state.

In the region around 17000 cm^{-1}, a strong band is observed along the *c*-axis, and it may be due to the coupled (LE_1 – CT_1) state of the island-type of electron configuration of the TCNQ column. The transition moments are deviated from the pure LE_1 or CT_1 bands because of the coupling of these levels. The TTF^+ ion

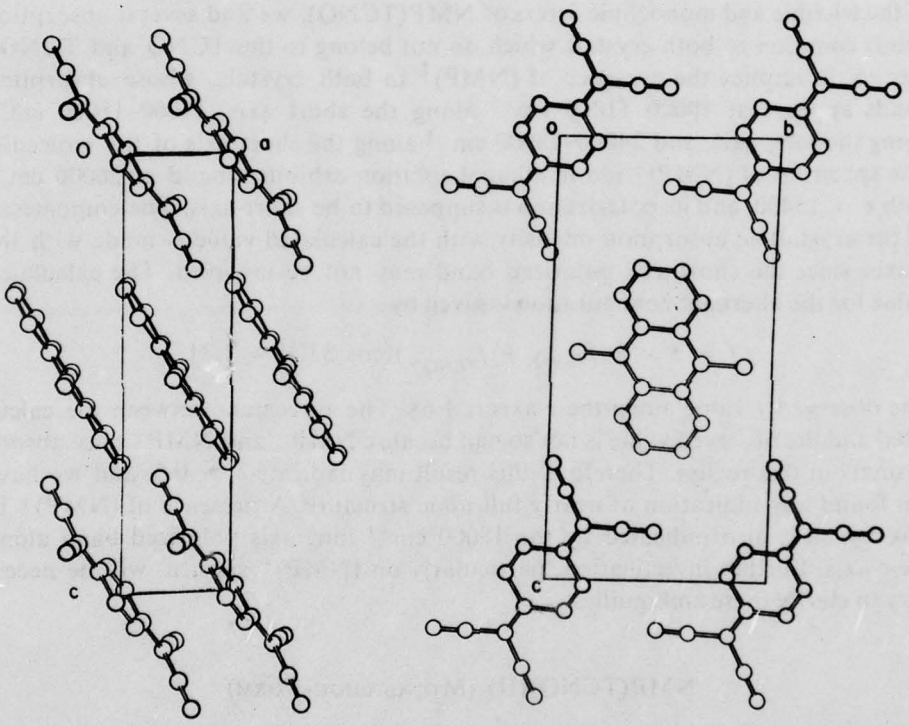


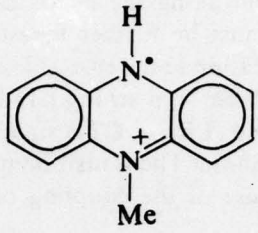
FIGURE 11. Projection of NMP(TCNQ)(I) crystal onto the crystalline plane after Fritchie.[6]

may also absorb in this region; however, its intensities are still not accurately determined and further analysis cannot proceed.

NMP(TCNQ)(I) (TRICLINIC FORM)

The crystalline structure of this form was determined by Fritchie,[6] and the projection of the molecules is shown in FIGURE 11. Electronic spectra of crystals of NMP(TCNQ) are not simple, because the absorption spectra of $(NMP)^+$ radical is not fully investigated. Butler *et al.*[7] proposed a partial charge transfer

in this crystal that $\delta = 0.96$ and $n = 1$. However, a recent x-ray study by Morosin[8] indicated that the NMP cation in the monoclinic crystal (form (II)) has a structure of $(NMPH^+)\cdot$ of 15 π electron system. By comparing the spectra



of the triclinic and monoclinic forms of NMP(TCNQ), we find several absorption bands common to both crystals which do not belong to the TCNQ and $TCNQ^-$ species. It implies the presence of $(NMP)^+$ in both crystals, whose absorption bands appears at 10000–11000 cm^{-1} along the short axis, 17000–18000 cm^{-1} along the long axis, and 24000–28000 cm^{-1} along the short axis of the molecule. The spectrum of $(NMP)^+$ ion in ethanol solution exhibits a band at 26000 cm^{-1} with $\epsilon = 15400$, and its polarization is supposed to be short-axis. The comparison of the crystalline absorption intensity with the calculated value is made with the *c*-axis, since the short-axis polarized band may not be involved. The calculated value for the alternant configuration is given by

$$f = 3 \times \tfrac{1}{2}(f_{TCNQ} + f_{TCNQ^-})(\cos 33°)^2 = 1.31.$$

The observed f value along the *c*-axis is 1.68. The agreement between the calculated and the observed value is not so bad because NMP^+ and $NMP^\dagger$ may absorb strongly in this region. Therefore, this result may indicate $\delta \simeq 0.5$, and we have not found any indication of nearly full ionic structure. A presence of $(NMP)^\dagger$ in this crystal is also indicated by the 18000 cm^{-1} long-axis polarized band along the *c*-axis. Further investigation, particularly on $(NMP)^\dagger$ spectra, will be necessary to clarify these ambiguities.

NMP(TCNQ)(II) (Monoclinic Form)

The crystalline structure of this form was recently analyzed by Morosin[8] and the structure was corrected by his informal information. The *N*-methylphenazyl cation was actually a protonated form, having 15 π electron in the ring. The projection of molecules onto the crystalline face is shown in Figure 12.
We must consider the absorption spectra of this crystal by this revised form.

The CT band between $(TCNQ)^-$ and $(NMPH)^\dagger$ is expected to appear strongly along the stacking *c*-axis. Actually, a band whose polarization is solely along the *c*-axis is found at the 20000–22000 cm^{-1} region; hence we tentatively assign this band as the CT band (a kind of back CT band). Another characteristic of this crystal is that the short molecular axes of both $(TCNQ)^-$ and $(NMPH)^\dagger$ are oriented along the *b*-axis. Therefore, the short-axis polarized band of $(NMPH)^\dagger$ should appear strongly along the *b*-axis, and the 10000 cm^{-1} band ($f = 0.12$) and 25000 cm^{-1} band ($f = 0.95$) should be assigned to this species.

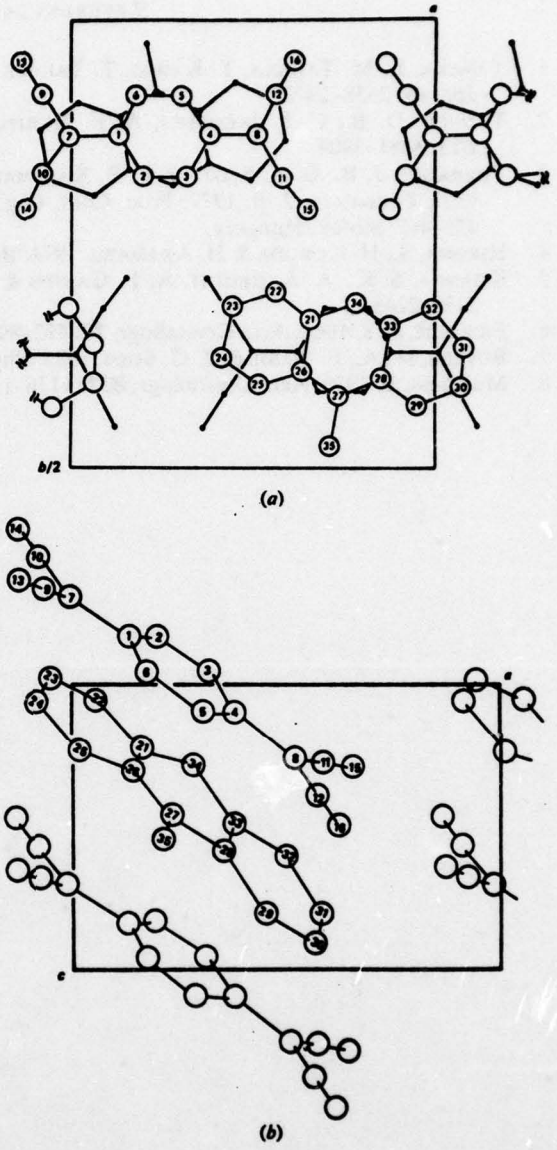


FIGURE 12. Projection of NMP(TCNQ)(II) crystal onto the crystalline plane after Morosin.[8]

The absorption due to $TCNQ^-$ ion should appear both along the *a*- and *c*-axes. The band at 12000 cm^{-1} along the *a*-axis is the LE_1 band and the band at 28000 cm^{-1} (f_a = 0.39, f_c = 0.23) is the LE_2 band of $TCNQ^-$. The dichroic intensity ratio is in agreement with the value calculated from the oriented gas model, but the *f* value estimated from the solution spectra is twice that of the observed values. Along the *a*- and *c*-axes the long-axis polarized $(NMPH)^+$ band is expected, and the band at 16500 cm^{-1} (f_a = 0.18, f_c = 0.12) is assigned to this origin.

The present crystal provides useful information on the spectra of $(NMPH)^+$ as well as its complex with $TCNQ^-$.

REFERENCES

1. TANAKA, J., M. TANAKA, T. KAWAI, T. TAKABE & O. MAKI. 1976. Bull. Chem. Soc. Jpn. **49:** 2358–2373.
2. TANNER, D. B., C. S. JACOBSEN, A. F. GARITO & A. J. HEEGER. 1976. Phys. Rev. **B13:** 3381–3404.
3. TORRANCE, J. B., B. A. SCOTT & F. B. KAUFMAN. 1975. Solid State Commun.: 1369–1373; TORRANCE, J. B. 1977. Proc. Conf. Organic Conductors and Semiconductors: 453–467. Siofok, Hungary.
4. HIROMA, S., H. KURODA & H. AKAMATU. 1971. Bull. Chem. Soc. Jpn. **44:** 9–15.
5. KHANNA, S. K., A. A. BRIGHT, A. F. GARITO & A. J. HEEGER. 1974. Phys. Rev. **B10:** 2139–2143.
6. FRITCHIE, C. J. 1966. Acta Crystallogr. **20:** 892–898.
7. BUTLER, M. A., F. WUDL & Z. G. SOOS. 1975. Phys. Rev. B.: 4708–4719.
8. MOROSIN, B. 1976. Acta Crystallogr. **B32:** 1176–1179.

SOLID-STATE REACTIONS IN ORGANIC CONDUCTORS AND THEIR TECHNOLOGICAL APPLICATIONS*

Susumu Yoshimura and Mutsuaki Murakami

Matsushita Research Institute Tokyo, Inc.
Ikuta, Tama-ku, Kawasaki 214, Japan

INTRODUCTION

Recent extensive investigations on conducting organic solids have developed a new branch of solid-state chemistry,[1,2] opening up the possibility of designing and synthesizing unique properties of both fundamental and technological interest. Research on organic semiconductors peaked around 1960 and was partly motivated by an anticipation of realizing organic counterparts of typical semiconductor devices, as reviewed by Hermann[3] and Gutmann and Lyons.[4] But an "organic transistor" has not been made so far, and the organic conductors are still in the early stages of development. While the unstable nature of organic materials has hampered their practical use in most cases, it may have been a misunderstanding[2] to expect them to function as mere substitutes for inorganic semiconductors. However, in line with recent progress in the understanding of the physical properties of organic solids, there have been several approaches to making organic solids technologically fascinating, directed toward the properties peculiar to organic materials; for instance, a high efficiency of charge transfer between molecules, surface catalytic or electrochemical activities, sensitivity to various stimuli, or low dimensionality.

In this paper we present some topics on the technological application of organic conductors based on solid-state reactions and discuss the scope of future advances in this field. This paper is divided into two parts. The next section reviews various speculations and actual examples of the use of organic conductors. There we go into details of the development of a new type of solid electrolytic capacitor[5] having an organic conductor counterelectrode of 7,7,8,8-tetracyanoquinodimethane (TCNQ) ion radical salts.[6] The potential effects of the solid-state electrochemical properties and the metallic nature of the TCNQ salts on the capacitor performance are described. The section CONTROL OF PHASE TRANSITIONS BY SOLID-STATE CHEMICAL METHODS introduces a new family of TCNQ salts based on substituted pyridinium[7] and thiazolium cations, which underwent characteristic phase transitions with sharp conductivity changes above room temperature. We revealed a possibility of modifying and designing the phase transition, and the result is thought to be helpful for providing potentially useful organic conductors.

TECHNOLOGICAL APPLICATIONS OF ORGANIC CONDUCTORS

First of all, it should be noticed that the discovery of unique materials or properties has always been followed by a proposal of practical use. For example,

*Manuscript received June 10, 1977.

0077-8923/78/0313-0269 $1.75/1 © 1978, NYAS

the discovery of the highly conducting TCNQ ion-radical salts[6,8] immediately led to patents disclosing electrochemical devices, a solid primary cell,[9] and a solid electrolytic capacitor.[10] Tetrathiafulvalene (TTF) TCNQ appeared on the scene carrying a proposal of a thermoelectric device in its hand.[11] The former devices are now identifying their own area of use in somewhat modified ways,[5,12] and the latter will turn out to be a good conception, because in a one-dimensional system there is a possibility that the Wiedemann-Franz law[13] does not hold and a large figure of merit for the thermoelectric conversion is obtained.

Junction Devices

A simple analogy of inorganic semiconductor devices may be an organic *p-n* junction.[4] Although the low mobility of the organic conductors limits their use at high frequencies, the junction devices still have a great significance in view of their useful electronic circuit applications; signal detection, amplification, memory, energy conversion, and so on. Various proposals have been made on both the preparation of junctions[14–16] and their uses,[11,17,18] and the modification of the conduction mechanisms by doping[16,19–21] remains a major complex problem yet to be solved. It appears, however, that our understanding of the electronic behavior of organic conductors has not reached the stage where we can modify their electronic properties physically and construct a well-defined junction between dissimilar systems.

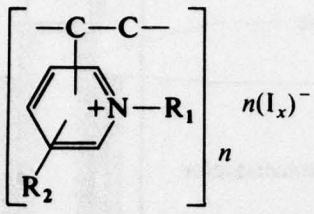
Recently Aviram and Patner[22] and Aviram *et al.*[23] have presented one possibility for realizing a molecular rectifier based on a simple concept of a charge-transfer complex. The device consists of a donor π system and an acceptor π system separated by a sigma-bonded tunneling bridge and may be constructed as a two-dimensional array, using a monolayer technique.[24] Another suggestion is that of a junction between polymorphic modifications of phthalocyanine.[25] These examples seem to introduce a sophisticated approach in providing an organic junction, depending upon a simple knowledge available at present.

Electrochemical Cells

Organic charge-transfer complexes are active electrochemically, and various solid-state electrochemical devices have been proposed: primary cells,[9] electrolytic capacitors,[10] and ion-selective electrodes.[26,27]

Electrochemical cells can be constructed with organic conductors like TCNQ salts or iodine complexes, acting as either an electrolyte[28] or cathode,[26,29] and the iodine complexes have shown reasonable promise of development of a solid cell. An original prototype devised by Gutmann *et al.*,[28,30] with Ba, Ca or Mg as an anode metal and halogen complexes as an electrolyte, offered an attractive possibility of a high-power density battery. Schneider *et al.*[12,31] have developed a lithium-lithium iodide cell that can be used for a pace-maker power source or in electronic watches.[12,32] In this cell, the cathode comprises a poly(vinylpyridine)-I_2 complex, which at the same time serves as an iodine source of a cell reaction: $2Li + I_2 \rightarrow 2LiI$, the reaction product functioning as a solid electrolyte *in situ*.

The energy density of the cell is reported to be 120 Wh/kg, which is considerably higher than that of a Mg-I_2-complex cell, 22 Wh/kg, or a lead acid cell, 30 Wh/kg. Very recently Kondo *et al.*[33] have synthesized quaternary donor polyiodide complexes typically formulated as



The iodine molecules are very strongly bound in this complex, resulting in a low vapor pressure in contrast to the case of a weak charge-transfer complex, which may possibly lead to a further improvement of the lithium-lithium iodide cell.

Solid Electrolytic Capacitors

The replacement of MnO_2 in solid electrolytic capacitors[34] with organic conductors is an old concept for improving both the capacitor performance and manufacturing processes.[10] Several newly developed materials have been examined as candidates for the solid electrolyte; for example, nitrogen-containing polymer-TCNQ system[35,36] or ionene polymer-TCNQ.[37,38] The major problems that hampered the realization of such a capacitor were 1) the lack of a technique that would give a uniform and adherent film of the organic conductor suitable for capacitor application, and 2) the lack of detailed information of the electrochemical properties of the TCNQ salts. We have developed, on a laboratory scale, a solid-aluminum electrolytic capacitor having an electrolyte layer of a TCNQ salt, such as quinolinium$(TCNQ)_2$, Q$(TCNQ)_2$, for example,[5] FIGURE 1. A thin electrolyte film was deposited from a solution of the TCNQ salt and polymer, where the polymer was suitably chosen to retard the crystal growth and effect the adsorption of the crystals during the film formation.[5]

Solid-State Anodic Oxidation.[39] The solid electrolyte layer (FIGURE 1) is a substantial cathode or counterelectrode of the capacitor, and it should also function as a protective layer for the very thin anodic oxide. The self-healing action of the conventional solid electrolytic capacitor has been understood on the basis of either a thermal transformation of the counterelectrode[40] or a solid-state anodic oxidation of the valve metal[41] (FIGURE 1).

In order to obtain an insight into the electrochemical properties of the organic conductors, we studied the electrical properties of an electrode system consisting of a fresh aluminum bar (0.5 mm in diameter) in contact with a pressed pellet of various TCNQ salts. FIGURE 2 shows the current-voltage (I-V) characteristics for Q$(TCNQ)_2$, *N-n*-propylquinolinium$(TCNQ)_2$ ((NPQ)$(TCNQ)_2$), *N*-methylacridinium$(TCNQ)_2$ ((NMA)$(TCNQ)_2$), and MnO_2 systems measured at a relative humidity of 50% RH, using a constant-rate-of-voltage increase (CRVI) method.[42] For the anodic polarization, all the electrode systems exhibited a well-known passivation curve with a current peak at voltages, V_p^+, between 2.5 and

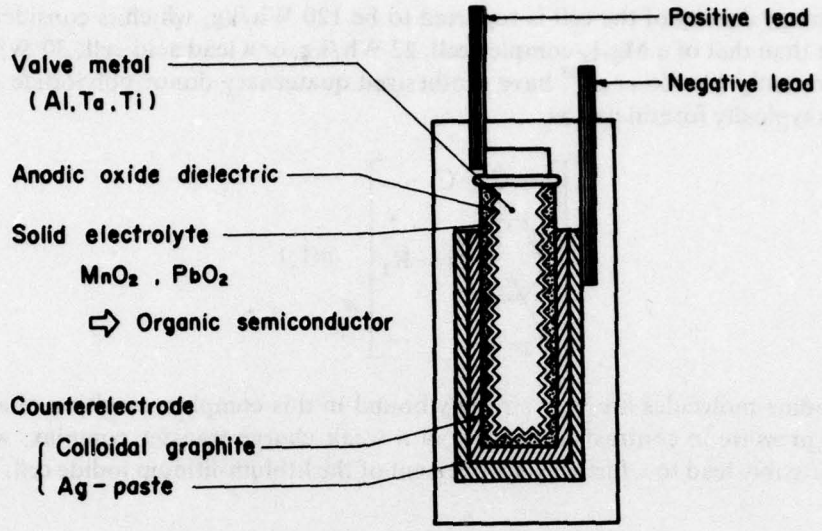


FIGURE 1. Construction of solid electrolytic capacitor.

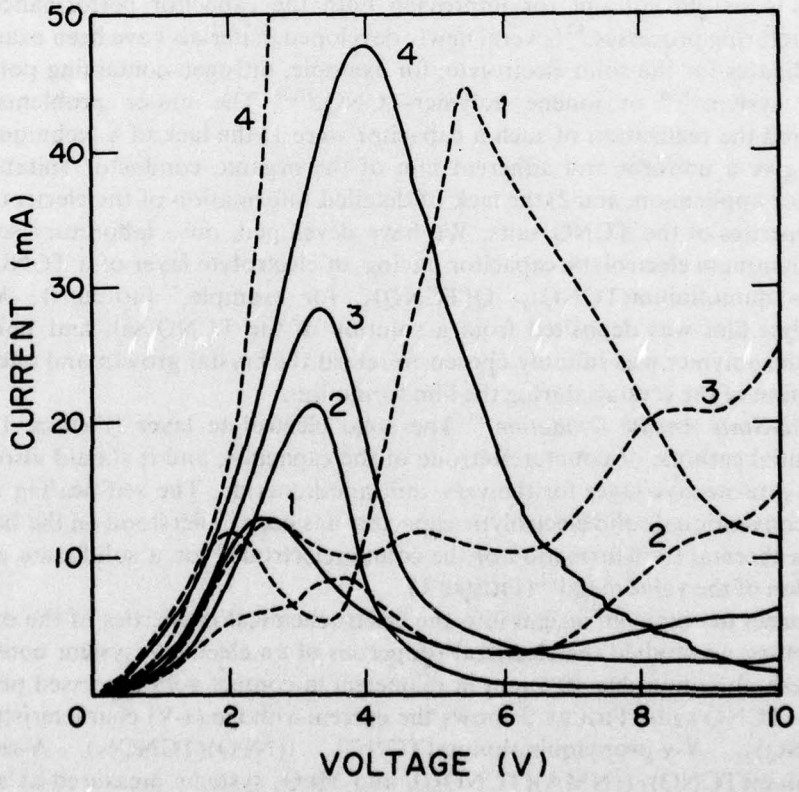


FIGURE 2. Current-voltage characteristics at 1/24 V/sec and 50% RH of Al electrode systems for anodic (solid lines) and cathodic (dotted lines) polarizations. 1. $Q(TCNQ)_2$; 2. $(NPQ)(TCNQ)_2$; 3. $(NMA)(TCNQ)_2$; 4. MnO_2.

4.5 V, and the current fell to as low as 10^{-5} amps in cases at higher voltages. The major difference in the I-V curves between the organic conductor and MnO_2 systems was that the former has very smooth curves without any discontinuous jumps in current and the degree of the passivation was much higher. Below 20% RH and/or when a noble metal electrode was used, the current diverged to infinity at about 8 V, while for the valve metal system the minimal current density at voltages higher than about 2 V_p^+ markedly decreased with increasing humidity. The passivation at about $V = V_p^+$ was essentially not altered by the relative humidity or by the use of the nobe metal electrode. These results suggest that both thermal

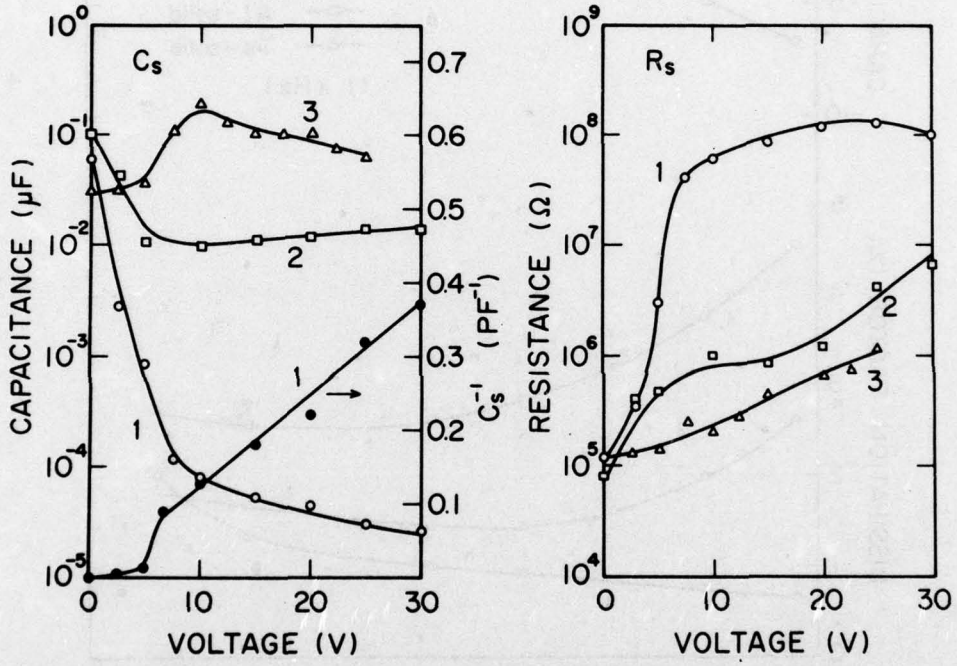


FIGURE 3. Equivalent series capacitance and resistance of an Al/Q(TCNQ)$_2$ system as a function of applied voltage. 1. Anodic polarization at about 70% RH; 2. Anodic polarization in dry oxygen; 3. Cathodic polarization in the room air.

and electrochemical reactions are involved in the anodic passivation, the former being replaced by the latter at a voltage of about 2 V_p^+ in the presence of water.

FIGURE 3 shows the equivalent series capacitance (C_s) and resistance (R_s) of the Al/Q(TCNQ)$_2$ system as a function of applied voltage. The measurements were made at 1 kHz after the current reached a steady state for a sequential application of voltage. For the anodic polarization in humid air (about 70% RH), C_s decreased and R_s increased strongly with increasing voltage. The inverse of C_s obeyed a linear dependence on voltage at voltages in excess of about 6 V, the voltage roughly corresponding to that at which the I-V curve reached a steady state ($V = V_p^+$). This result strongly indicates the formation of the anodic oxide

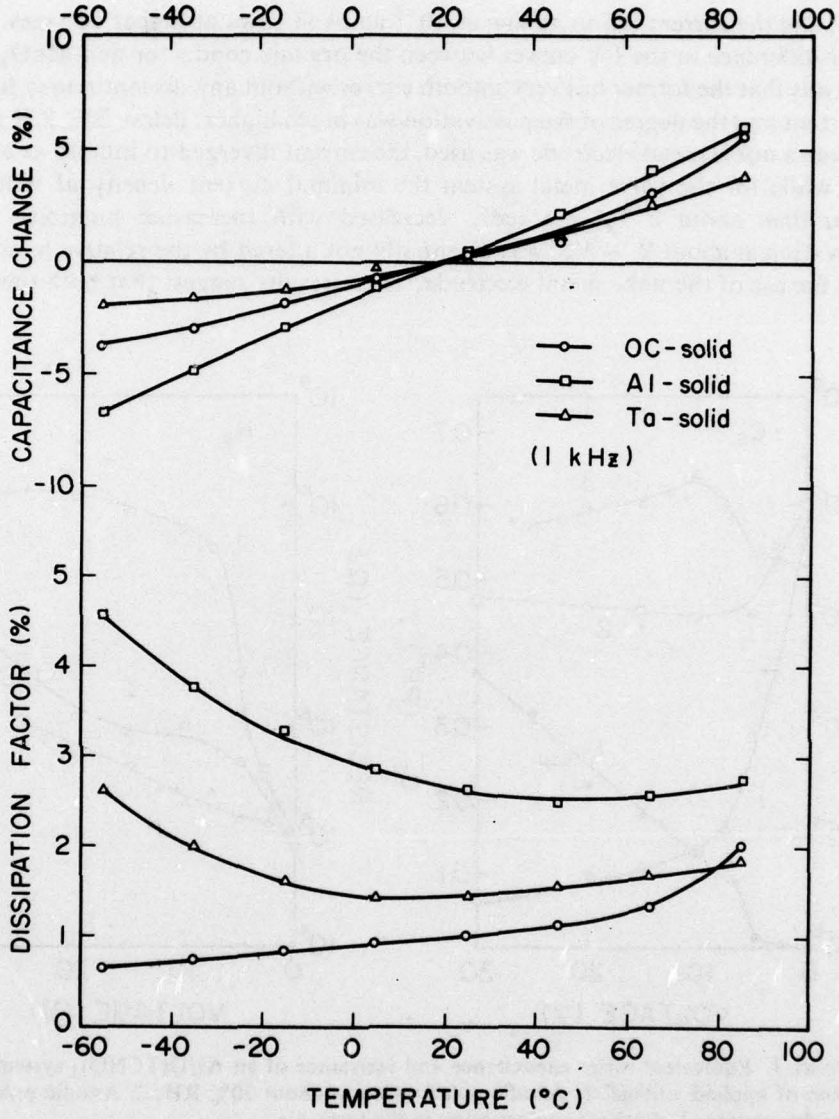


FIGURE 4. Capacitance change and dissipation factor as a function of temperature.

on Al, and a measured capacitance-voltage product, $C_sV = 0.44\ \mu F\ V/cm^2$, compares fairly well with the theoretical value, $CV = 6.45\ \mu F\ V/cm^2$, obtained from the anodization of Al in liquid electrolytes.[43] It was also made evident that the initial passivation was caused by a thermal transformation in organic conductors that proceeded at temperatures between 80 and 150°C, resulting in a non-stoichiometric composition with excess neutral TCNQ molecules. The transformed layer presumably acts as an electrolyte *in situ* to facilitate ionic conduction and electrolytic rectification.

The current efficiency of the anodic oxidation was obtained with use of the

CRVI results.[42] The results at 50% RH were: 0.053% for $Q(TCNQ)_2$, 0.62% for $(NPQ)(TCNQ)_2$, and 0.10% for $(NMA)(TCNQ)_2$, which are considerably higher than published data on a Ta/MnO_2 system (0.01–0.001%).[41] At higher relative humidities, the efficiency was still higher: for example, 2.1% and 1.5% for $Q(TCNQ)_2$ and $(NMA)(TCNQ)_2$, respectively, at 98% RH. Not all the TCNQ salts were good anodizing electrolytes; for example, the simple salts with metallic cations, with the single exception of $Cu(TCNQ)_2$,[44] did not exhibit the anodizing ability. *N*-methylphenazinium (NMP)TCNQ, which is known to exhibit a partial charge transfer between NMP and TCNQ,[45] had an anodization efficiency of 0.2% at 50% RH, which is comparable to that of complex salts. We conclude that the existence of the neutral TCNQ molecules both in the starting and the transformed salt is essential for the anodic oxidation, and the TCNQ may behave like a catalyst in electron transfer processes in a cell reaction: $2Al + 3H_2O \rightarrow Al_2O_3 + 6H^+ + 6e$.

Capacitor Characteristics. Much improvement was realized in capacitor characteristics by the use of the organic-conductor solid electrolyte: the low leakage current, the extended ratio of breakdown-to-formation voltage, and stable frequency characteristics.[46] The temperature dependence of the capacitance and dissipation factor is shown in FIGURE 4, where the data for the conventional solid Ta and Al electrolytic capacitors are also included. One of the striking differences from the conventional capacitors is that the dissipation factor decresed with decreasing temperature, which is undoubtedly ascribed to the metallic nature of the organic conductor.[47]

The improved capacitor performance over the MnO_2-based capacitors, especially in the low-temperature and high-frequency characteristics, may extend the applicability of the electrolytic capacitor from the ordinary low-frequency use. A thin film capacitor with a screened organic-conductor electrolyte is currently being developed by Itoh *et al.*,[48] interfacing with an application to an audio frequency and high-voltage capacitor.

Transducers

Some of the organic solids are very sensitive to physical or chemical stimuli, and a variety of organic transducers have been found feasible. The flexibility, moldability, and mechanical properties of polymeric substances may also be utilized in these applications.[49]

Elastomeric or flexible conductors have recently found an extensive utility in integrated or display circuitry, as connector, junction, leads, switches, and so on. Hermann *et al.*[50,51] have prepared elastomeric TCNQ salts that have striking differences in electrical behavior from carbon-filled polymers. The elastomeric complexes had either unchanged conductivities or increased conductivities with elongation, suggestive of a stress-induced molecular orientation. A flexible channel electron multiplier employing NaTCNQ or carbon fillers has been developed and used for photon detection in space.[52,53] The photoconductive polymer poly(vinylcarbazole) (PVK) has accepted much attention as a display and printing medium. A charge-transfer complex of PVK with trinitrofluoroenone[54] has been

used by IBM in an electrophotographic copier.[55] An automatic slide processer has been manufactured by Matsushita, using dye-sensitized substituted PVK;[56] the technology has been recently extended to making a color slide film.[57] A high quantum efficiency of charge transfer between PVK and Se has been reported by workers at Xerox[58] and by Matsushita,[59] which seems to be particularly interesting because a junction between organic and inorganic solids is an attractive subject[60] to be studied.

Related to transducers or sensors is a colorimetric indication of various substances based on charge-transfer reactions. TCNQ is useful in characterizing amines and amino acids on chromatograms,[61] in determining the critical micelle concentrations of surfactants,[62] and in qualifying the catalytic activity of inorganic catalysts.[63] This line of unique applications may have to be developed further, so that the use of the organic conductors will be called for as an electronic detector that may implement the detection of, say, gases[18,64] or ions,[26] at low cost and with sharp selectivity.

Since the temperature is one of the most important physical variables to be sensed, the application of organic conductors to a resistance thermometer has naturally been considered. For example, Yamamoto *et al.*[65] have developed a "plastic thermistor" using various filled polymers, which is actually used for the temperature regulation of flexible heating elements. Materials with high-temperature coefficient of resistivity, suitable resistivity, and good thermal stability have been explored, and TCNQ salts with metallic cations[66] and cationic ionene polymers[67] were found to be advantageous to the device. Organic conductors that display reversible[68–70] or irreversible[71,72] phase transitions offer another attractive possibility as a temperature transducer or a temperature-sensitive switch. In particular, there appear to be many organic conductors that have a sharp metal-insulator (M-I) transition as demonstrated in (TTF)(TNAP) at 185 K[73] (TNAP-11,11,12,12-tetracyanonaphtho-2,6-quinodimethane), TTF-$(I)_n$ between 200 and 270°K,[74] $(TTF)_{12}(SCN)_7$ at 167°K,[75] $(TTF)_{12}(SeCN)_7$ at 173°K,[75] $(NPPy)(TCNQ)_x$ between 371 and 381°K[7] (NPPy is *N-n*-propylpyridinium cation), and (NPTh)$(TCNQ)_x$ between 340 and 405°K[76] (NPTh is *N-n*-propylthiazolium cation; see the following section). For the present these compounds cannot compete with vanadium oxides[77] as a critical temperature resistor (CTR)[78] because of their instability upon temperature cycling or insufficient magnitude of the resistivity change at the transition point. However, use of these and related systems could be reconsidered if the phase transition could be modified molecularly that the transition temperature is varied over a wide range and the resistivity change is as large as that of VO_2,[79] (TTF)(TCNQ)[80] or TTF-I_n.[74] Resistors with the positive temperature coefficient of resistance (PTCR)[81,82] may favorably be used in simple temperature-regulating circuits. The first, interesting discovery of such PTCR characteristics in the organic conductors, viz. $(NBPy)(TCNQ)_x$ and $(NBTh)(TCNQ)_x$ (where NBPy and NBTh are *N-n*-butylpyridinium and *N-n*-butylthiazolium cations, respectively), will now be reported.

Control of Phase Transitions by Solid-State Chemical Methods

One of the most fascinating features of the organic conductors may be that their physical properties can be modified by synthetic or solid-state chemical

methods, which seems to be the major driving force of the development of this field. In this section we will present the recent results on the solid-state chemical control of transition reactions[83] in a new family of organic conductors; (NPPy)$(TCNQ)_x$, (NBPy)$(TCNQ)_x$, (NPTh)$(TCNQ)_x$, (NBTh)$(TCNQ)_x$ and their alloys.

Substituted Pyridinium TCNQ Salts

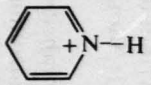
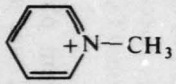
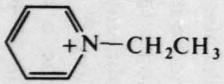
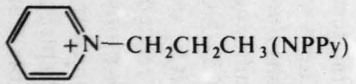
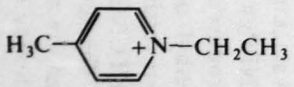
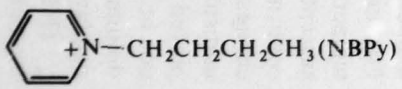
Because of the low-dimensional nature, the TCNQ salts are featured by instabilities toward structural distortions[86] both in the solid state and in solutions as a growing crystal,[84,85] which might be an origin of the appearance of polymorphism,[87] nonstoichiometry,[88] and various phase transitions.[89] It has been shown[7,90] that the substituted pyridinium TCNQ system provides a variety of new solid-state chemical phenomena. Particularly, as shown in TABLE 1, (NPPy)$(TCNQ)_x$ and (NBPy)$(TCNQ)_x$ displayed both crystallization anomalies (dimorphism and nonstoichiometry) and characteristic phase transitions. Since the TCNQ-to-cation ratio was dependent on crystallization conditions and could not be assigned to an integral number, the molecular formula will be provided hereafter with a subscript x or y on TCNQ.

(NPPy)$(TCNQ)_x$ (II) crystallized in a triclinic $P\bar{1}$ symmetry with crystal data: $a = 7.80$ Å, $b = 13.86$ Å, $c = 14.04$ Å, $\alpha = 95.72°$, $\beta = 108.54°$, and $\gamma = 101.09°$. Referring the crystal structures of the TCNQ salts with related cations, such as (NPQ)$(TCNQ)_2$,[91] (DEBP)$(TCNQ)_4$[92] (DEBP is *N*,*N*′-diethyl-4,4′-bipyridinium), or (DEPE)$(TCNQ)_4$ (DEPE is 1,2-di(*N*-ethyl-4-pyridinium)ethylene),[93] it is plausible that the molecular arrangement in (NPPy)$(TCNQ)_x$ or its related salts is such that the TCNQ molecules are stacked in a face-to-face manner with a tetrameric period and the pyridinium cations are piled in the channel surrounded by four TCNQ columns forming a chain in a head-to-head or tail-to-tail manner. We note here that the anomalies appearing at the specific length of cation is presumably caused by an incompatibility[94] between the cation length and the stacking spacings of TCNQ and/or by the variety in arrangement of the substituents. The temperature dependence of the resistivity for (NPPy)$(TCNQ)_x$ (II) is shown in FIGURE 5. The resistivity underwent a sharp M-I transition at 376 K, the high-temperature phase having temperature-independent resistivity and paramagnetic susceptibility expected for a metallic system. The x-ray and DSC measurements confirmed that the transition is a first-order transition with crystallographic changes, and the IR results suggest that the high-temperature modification had an undistorted stacking of TCNQ molecules in the column. The M-I transition displayed by (NPPy)$(TCNQ)_x$ seems to be inherent to the NPPy cation, for it could not be reproduced by related cations, such as *N*-ethylpyridinium, *i*-propylpyridinium, *N*-ethyl- or *N*-*n*-propylpicolinium cations (TABLE 1), though some of them displayed irreversible phase transitions.[90]

(NBPy)$(TCNQ)_x$ displayed quite a different phase transition as shown in FIGURE 6. The reversible transition at 407 K was a semiconductor-to-semiconductor transition accompanied by an increase in resistivity toward higher temperatures, which may be the first finding of reversible PTCR characteristics[81] in the TCNQ ion-radical salt. The striking differences in the nature of the transition be-

TABLE 1

STOICHIOMETRY AND ELECTRICAL PROPERTIES OF SUBSTITUTED PYRIDINIUM-TCNQ COMPLEX SALTS

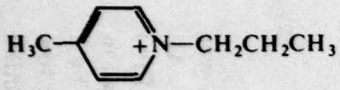
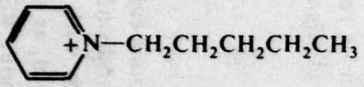
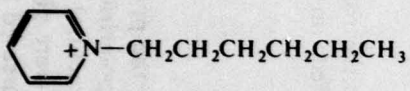
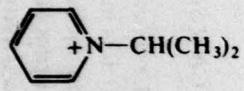
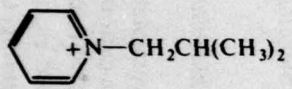
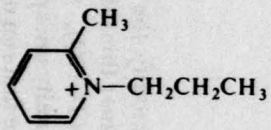
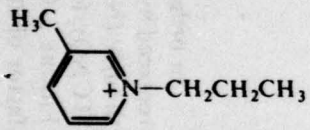
Cation	Salt I			Salt II			Remarks*
	TCNQ/Cation	ρ(Ωcm)	E_A (eV)	TCNQ/Cation	ρ(Ωcm)	E_A (eV)	
	1.65	0.16	0.07	2.09	14	0.10	I
				1.96	2600	0.28	
				1.92	2900	0.33	
	2.45	1.4	0.08	1.88	2000	0.34	I, R
	2.51	2.0	0.14	1.46	120	0.29	
	1.86	7.0	0.05	1.67	50	0.14	I, R

AD-A065 304 NEW YORK ACADEMY OF SCIENCES N Y F/G 7/2
SYNTHESIS AND PROPERTIES OF LOW-DIMENSIONAL MATERIALS,(U)
1978 J S MILLER, A J EPSTEIN N00014-77-C-0374
UNCLASSIFIED NL

4 OF 9
AD
A065304




OF
5304

	2.91	14	0.15	1.50	1200	0.36	I
				1.96	230	0.15	I
				2.11	7.5	0.08	I
				1.97	60	0.11	I
				1.86	200	0.14	I
				2.00	1200	0.26	I
				2.00	950	0.28	I

*I = irreversible transition; R = reversible transition.

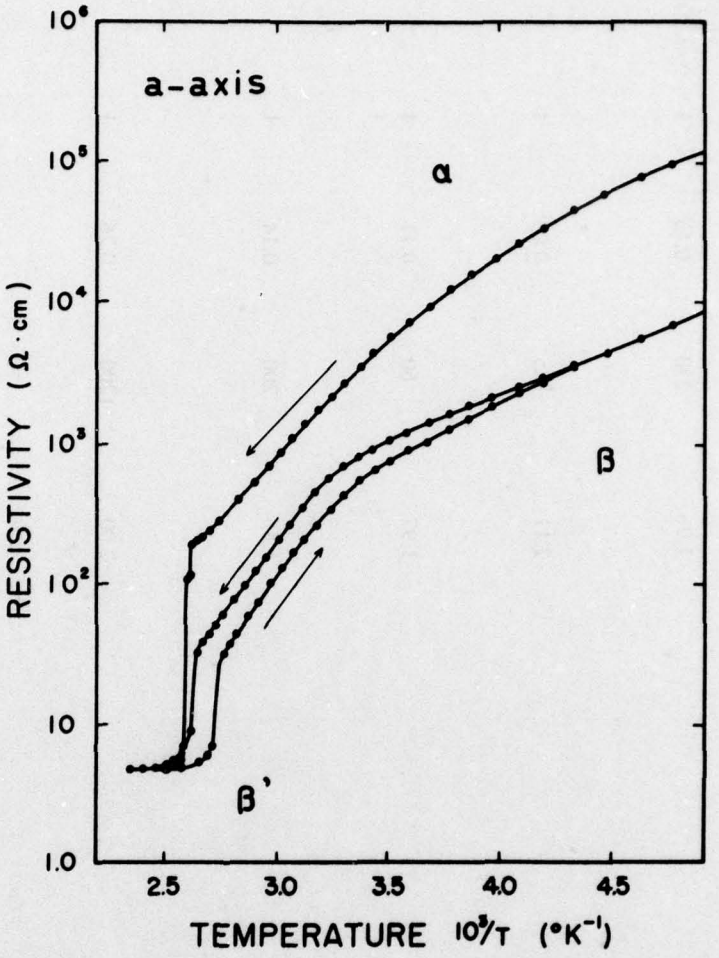


FIGURE 5. Temperature dependence of the electrical resistivity of $(NPPy)(TCNQ)_x$ (II) single crystal.

tween the NPPy and NBPy salts strongly suggest that the rotation or rearrangement of the linear substituents has an important effect on the changes in the stacking mode of the TCNQ molecules.

Thiazolium TCNQ Salts

In order to modify the reversible M-I transition, the pyridinium cation was replaced by a planar thiazolium cation, which is more polarizable and smaller. Although $(NPTh)(TCNQ)_x$ was obtained in an isostructural form with $(NPPy)(TCNQ)_x$ (II), totally unexpected electrical properties were observed, as shown in FIGURE 7. On the first run of heating, the resistivity decreased at about 402 K by a factor of 200, but upon cooling, it showed a very large hysteresis and a very low rate of transition below about 330 K. On the following heating run, the transition

temperature shifted to 405 K, implying the existence of both irreversible and reversible transitions.

Latent heat was observed at the transition temperature on heating, T_H (ΔH = 2.7 kcal/mol for the first run), but, on cooling the sample, exothermic signals which should be observed at the lower transition temperature, T_l, could not be detected. Instead, we measured the latent heat at T_H after the sample was maintained at a lower temperature for a predetermined period so that we assume the heat to be that associated with the slow exothermic reaction. Results are shown in FIGURE 8, from which several important features of the transition were deduced; 1) the hysteresis indeed exists and T_l is 340°K; 2) the fraction of transformed volume has a maximum at 300–320°K; and 3) the fraction tends to increase again at temperatures below 270°K.

The NBTh salt exhibited almost the same features of the transition as the

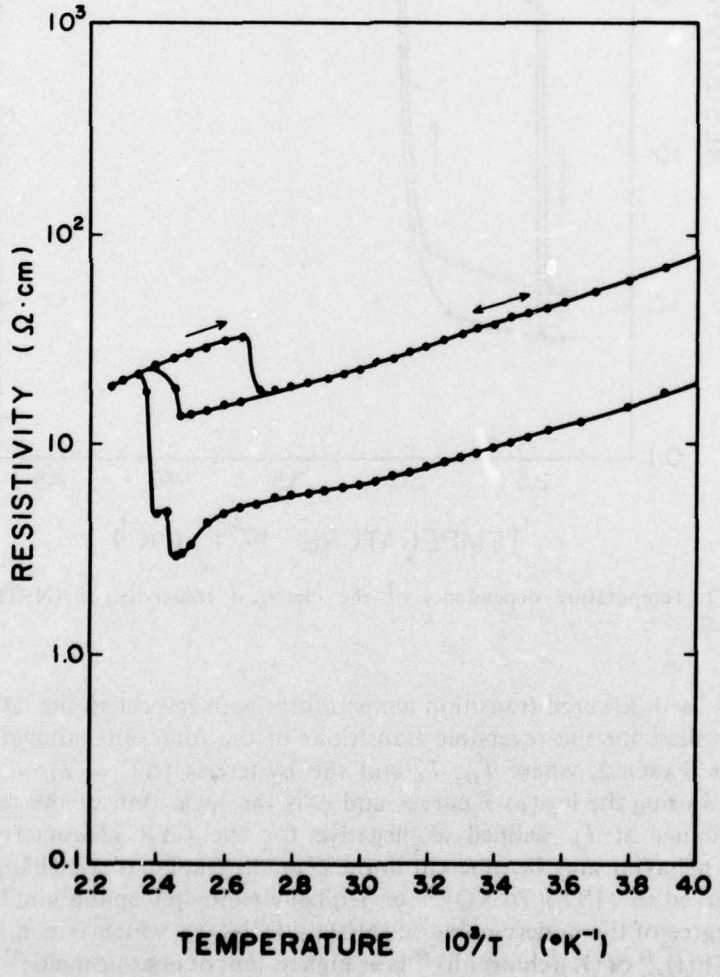


FIGURE 6. Temperature dependence of the electrical resistivity of (NBPy)(TCNQ)$_x$ (II) single crystal.

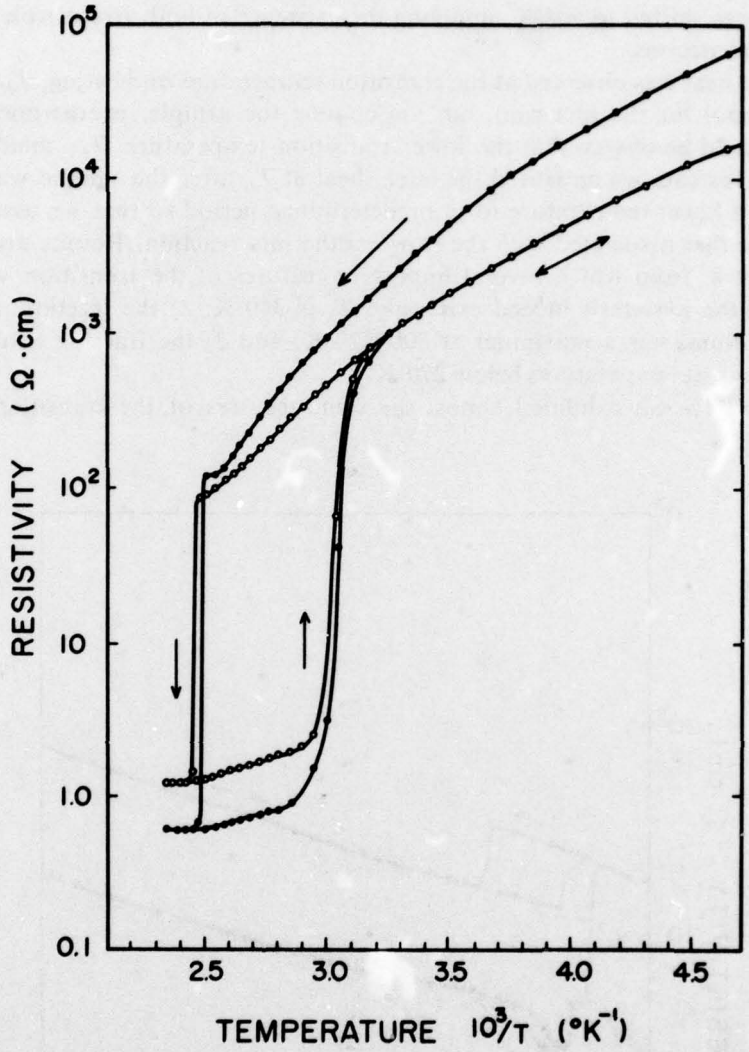


FIGURE 7. Temperature dependence of the electrical resistivity of $(NPTh)(TCNQ)_x$ single crystal.

NBPy salt, with lowered transition temperatures with respect to the latter. Characteristic values for the reversible transitions of the four salts studied are summarized in TABLE 2, where T_H, T_l and the hysteresis ($\Delta T = T_H - T_l$) were determined using the $\log(\rho)$-T curves and ψ is the logarithm of the ratio of resistivity change at T_H defined as negative for the CTR characteristics. The hysteresis behavior may be inherent in the crystallographic phase change, as has been observed in (TTF)(TCNQ),[95] or triphenylmethylphosphonium$(TCNQ)_2$,[70] but the degree of the undercooling of $(NPTh)(TCNQ)_x$, which is comparable to that of $TTF(I)_n$[74] or (K)(chloranil),[96] is as high as that of organic melts.[97]

In an attempt to account for the large hysteresis, we considered the following simple model: The high-temperature modification is stable below T_H because the

free energy of the system is not decreased on account of a surface energy created at the interface between the two phases. If we assume that a spherical nucleus of r in diameter is created at a temperature T, the free-energy change $\Delta G(r)$ is expressed as

$$\Delta G(r) = -\frac{4\pi}{3} r^3 \frac{\Delta\mu}{\nu} + 4\pi r^2\sigma \tag{1}$$

where $\Delta\mu$ is the chemical potential, ν the molecular volume and σ the interfacial energy. Differentiating (1) shows that there is a critical radius r^* above which the nucleus grows. The total free energy G^* for the critical nucleus is given by

$$\Delta G^* = \frac{16\nu^2\sigma^3 T_H^2}{3(\Delta H)^2(\Delta T)^2}. \tag{2}$$

The undercooling temperature ΔT is viewed as that which is obtained setting $\Delta G^* = kT$, so that,

$$(\Delta T)^3 - T_H(\Delta T)^2 + \frac{16\nu^2\sigma^3 T_H^2}{3k(\Delta H)^2} = 0 \tag{3}$$

which has a solution in the range $0 \leq \Delta T \leq (2/3)T_H$. Using (3) with experimental data on ΔT and ΔH and estimated data on ν, we obtained a rough esti-

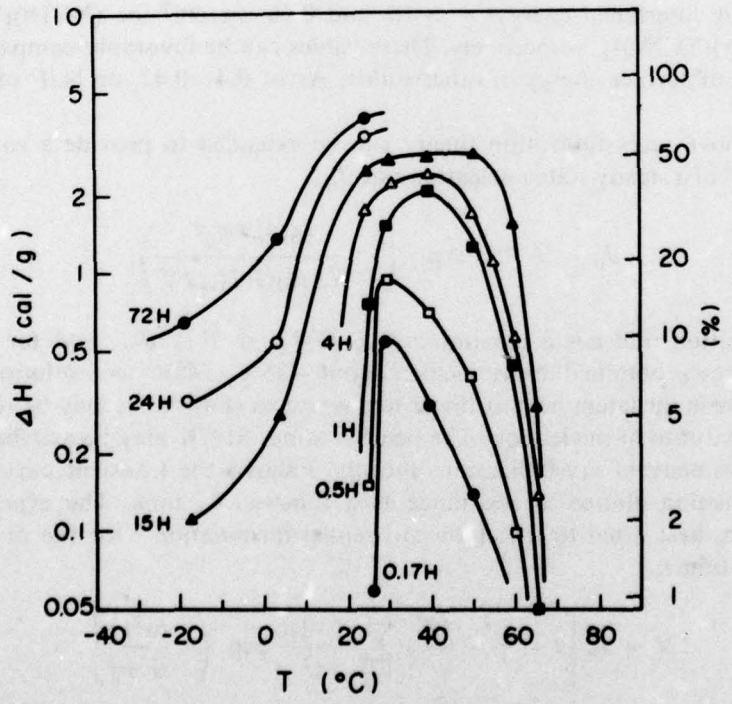
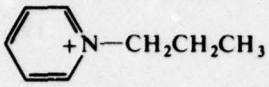
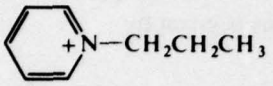
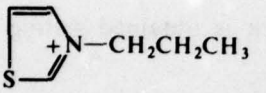
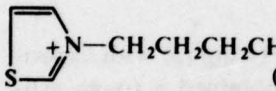


FIGURE 8. Heat associated with the transition at T_H of $(NPTh)(TCNQ)_x$ as a function of the temperature at which the sample was stood for a period cited.

TABLE 2
CHARACTERISTIC DATA ON THE REVERSIBLE TRANSITIONS

Cation	Trans. Temp. (K) T_H	T_1	ΔT (K)	ψ	ΔH^* (cal/g)
 (NBPy)	376	370	6	−0.62	4.5
 (NBPy)	407	384	23	+0.17	2.5
 (NPTh)	405	340	65	−1.49	5.4
 (NBTh)	371	351	20	+0.23	3.6

mate of the interfacial energy; σ = 1.8 and 0.46 erg/cm^2 for (NPTh)(TCNQ)$_x$ and (NPPy)(TCNQ)$_x$, respectively. These values can be favorably compared with the values of surface energy of other solids; Ar of 0.41–0.42, or NaF of 2.1–6.4 erg/cm^2.[97]

The above recrystallization theory can be extended to provide a rough formulation[98] of a steady state nucleation rate J_0:

$$J_0 = A\,T^{1/2} \exp\left(-\frac{16\nu^2\sigma^3 T_H^2}{3(\Delta H)^2 RT(\Delta T)^2}\right). \tag{4}$$

The nucleation rate has a maximum at $(1/3)T_H \leq T \leq T_H$, and for (NPTh)(TCNQ)$_x$ the σ obtained above yielded about −25°C (248K) as a solution. Thus, the increase in the latent heat at lower temperatures (FIGURE 8) may be related to the maximal rate of nucleation. The peak at about 313°K may be ascribed to the maximal velocity of crystallization. FIGURE 9 shows the transient curve of the phase transition plotted as resistance as a function of time. The experimental points were best fitted to a Zeldovich-Frenkel formulation[98] for the number of nucleus at time t,

$$N = J_0\left[t - \tau - \frac{12}{\pi^2}\tau\sum_{s=1}^{\infty}\frac{(-1)^s}{s^2}\exp\left(-\frac{6s^2 t}{\pi^2\tau}\right)\right] \tag{5}$$

where τ is an induction time that depends on the diffusion rate and stacking probability of molecules in transition. The excellent agreement between experi-

ment and theory confirms that the rate-determining step of the solid solid reaction in $(NPTh)(TCNQ)_x$ is the nucleation process.

The difference in the interfacial energy between $(NPTh)(TCNQ)_x$ and $(NPPy)(TCNQ)_x$ suggests that the motion of the cation rings also plays an important role in the nucleation. This agrees well with the fact that the picolinium salts (TABLE 1) displayed no reversible transition. An S—S interaction in the cation chain or an interaction between S and the acceptor N atoms may be postulated. The effect of the S atom was less significant in the *n*-butyl-substituted system, so that the PTCR characteristics may be dominated by a rearrangement of the butyl group.

Alloys

Another approach to the modification of the M-I transition of $(NPPy)(TCNQ)_x$ was made by doping or alloying with $(NBPy)(TCNQ)_x$ or $(NPTh)(TCNQ)_x$. Various procedures for the preparation of alloys[21] were surveyed, and a rapid coprecipitation yielded well-defined alloys with great ease. Two components, $(NPPy)(TCNQ)_x$ and $(NBPy)(TCNQ)_x$, for example, were dissolved in *N,N'*-dimethylformamide at 80°C in the desired proportions, and the solution was transferred into cold water drop by drop. After the precipitates were collected, alloy formation was confirmed by the DSC measurements; the heat associated with the transition of each component could not be detected. FIGURES 10 and 11 show the resistivity-temperature characteristics of the alloys $(NPPy)_{1-x}(NBPy)_x(TCNQ)_y$ and $(NPPy)_{1-x}(NPTh)_x(TCNQ)_y$, respectively.

One of the striking features is that the hysteresis behavior that is quite similar to that observed in $(NPTh)(TCNQ)_x$ occurred in $(NPPy)_{1-x}(NBPy)_x(TCNQ)_y$ for x between 0.15 and 0.85. The latent heat associated with the transition was detectable at both T_H and T_1, indicative of a relatively high rate of transition in this case. The hysteresis behavior may be regarded as a stabilization of the metallic

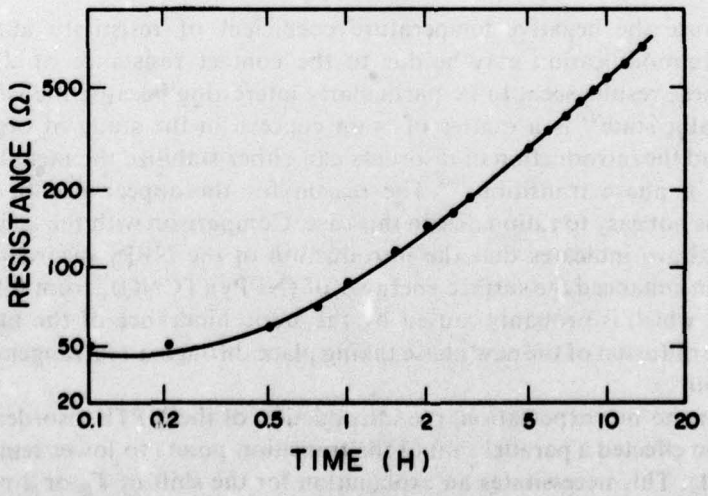


FIGURE 9. Transient phenomenon of the resistivity increase at 40°C for $(NPTh)(TCNQ)_x$ disc.

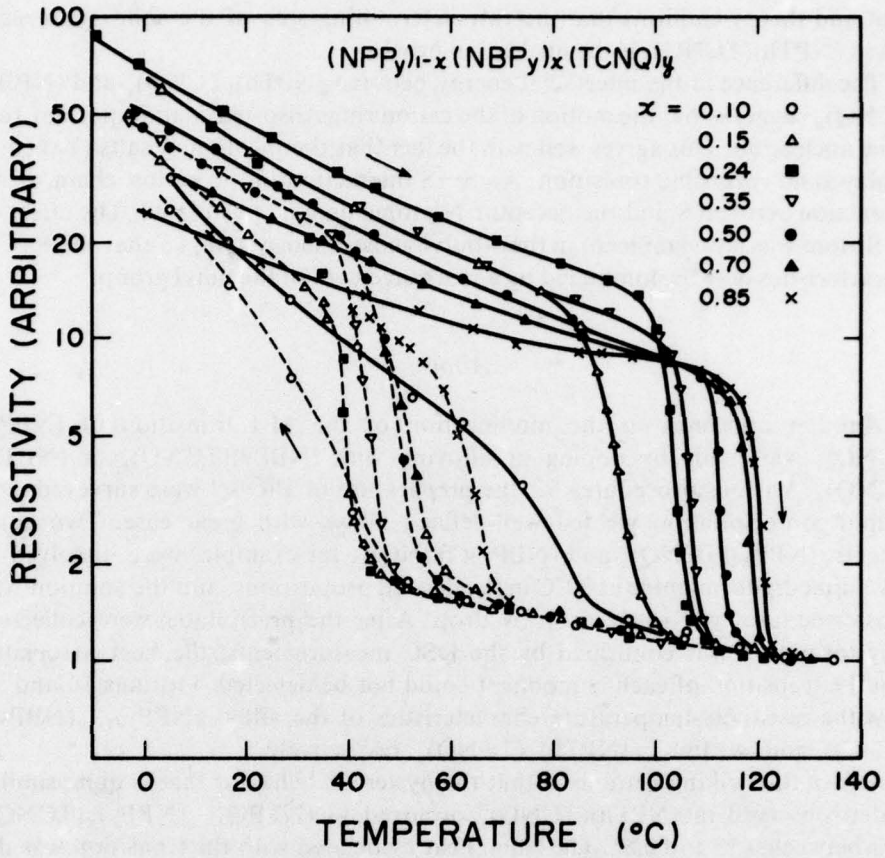


FIGURE 10. Temperature dependence of the electrical resistivity of alloys, $(NPPy)_{1-x}(NBPy)_x(TCNQ)_y$.

state, because the negative temperature coefficient of resistivity at the high-temperature modification may be due to the contact resistance of the powder sample. These results seem to be particularly interesting because the stabilization of the metallic state[99] is a matter of main concern in the study of organic conductors, and the introduction of disorders can either stabilize the metallic state or smear out a phase transition.[100] The reason for the appearance of the large hysteresis is not easy to rationalize in this case. Comparison with the simple model described above indicates that the introduction of the NBPy disorders into the NPPy chain enhanced the surface energy σ of $(NPPy)(TCNQ)_x$ from 0.5 to about 2 erg/cm^2, which is probably caused by the steric hindrance of the butyl group against the diffusion of the new phase taking place through a rearrangement of the cation chain.

Contrary to our expectation, the introduction of the NPTh disorders into the NPPy chain effected a parallel shift of the transition points to lower temperatures. (FIGURE 11). This necessitates an explanation for the shift of T_H or a mechanism of the M-I transition at T_H which may be driven by the excess entropy of soft-

phonon modes. The hysteresis may also be understood on the basis of the recrystallization theory, for (3) implies that ΔT tends to decrease as T_H decreases.

Possibilities

In this section it was shown that we can control the phase transition in the TCNQ ion radical salts through combination of very simple systems. The transition temperatures, the temperature hysteresis, and the rate of the transition were modified to vary over a wide range of interest, and the striking hysteresis behavior found in a variety of compositions may be peculiar to organic materials. Although the unique phase transitions should be examined more fundamentally, they are potentially useful for practical purposes. Especially, the sluggish nature of the transition may possibly be used to implement various timing circuits at low cost. Heating the sample in a form of pressed disc, either directly or indirectly, facilitates the control of the timer, and the electrical resistance may be read as an output signal. The temperature dependence of the rate of transition may be used for the regulation of the increase rate of resistance or the operation time of the timer.

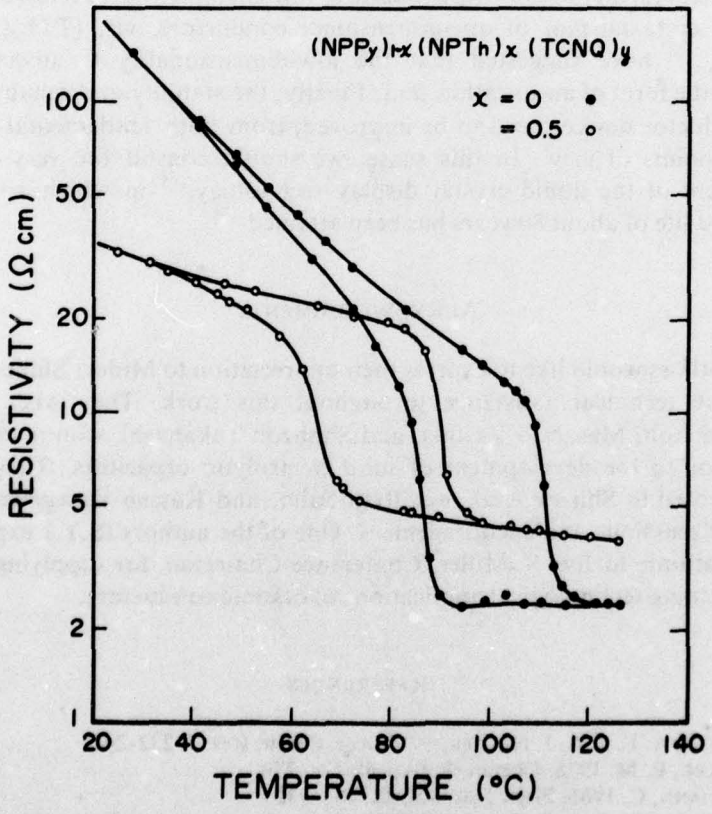


FIGURE 11. Temperature dependence of the electrical resistivity of alloys, $(NPPy)_{1-x}(NPTh)_x(TCNQ)_y$.

Conclusion

Although there have been some guidelines for the molecular design[1,101] of novel materials with unique physical properties, we would point out that there may be two opposing approaches to the successful presentation of such materials; one is to make the system simple and the other to make it complex. Silicon technology is the result of the former approach, and the ceramic (or oxides) and liquid crystal technologies are good examples of the latter. Which direction the study of organic conductors should take may be open to argument, but we suggest that the latter approach has a great possibility, as shown in Control of Phase Transitions by Solid-State Chemical Methods, and furthermore, multiple component systems should be investigated.

Besides exploring novel compounds with unique physical properties, it appears that we need to pay more attention to applied technology, which seems to have been a crucial breakthrough in most applications. Since most of the organic conductors cannot be obtained as large single crystals with good mechanical properties, techniques such as epitaxy, evaporation, grinding, or compressing are essential to their practical applications. It is to be desired that we develop such a technology that not only restores the original properties of starting materials[102] but also offers further interesting properties. For example, the successful evaporation of an epitaxial film of one-dimensional conductors, viz, (TTF)(TCNQ)[103] and $(SN)_x$,[104] have suggested that the low-dimensionality is advantageously utilized in the form of an ultrathin film. Finally, the stability and reliability of organic-conductor devices need to be improved, from both fundamental and technological points of view. In this sense, we should consult the very successful development of the liquid crystal display technology,[105] in which an extended operational life of about 80 years has been attained.[106]

Acknowledgments

The authors would like to express their appreciation to Midori Shinoda for her enthusiastic technical assistance throughout this work. They wish to thank Yoshimasa Itoh, Masahito Yasuda, and Shohzoh Takahashi, who made a major contribution to the development of solid electrolytic capacitors. They are also much indebted to Shirow Asakawa, Reiji Sano, and Katsue Hasegawa for their valuable discussions and encouragement. One of the authors (S.Y.) expresses his sincere gratitude to Joel S. Miller, Conference Chairman, for supplying information concerning technological applications of organic conductors.

References

1. Garito, A. F. & A. J. Heeger. 1974. Acc. Chem. Res. 7: 232–240.
2. Engler, E. M. 1976. Chemtech. (April): 274–279.
3. Hermann, C. 1965. Phys. Stat. Sol. 12: 483–532.
4. Gutmann, F. & L. E. Lyons. 1967. Organic Semiconductors: 632–650. John Wiley and Sons. New York, N.Y.

5. YOSHIMURA, S., Y. ITOH, M. YASUDA, M. MURAKAMI, S. TAKAHASHI & K. HASEGAWA. 1975. IEEE Trans. Parts, Hybrids, Packg. PHP-11(4): 315–321.
6. MELBY, L. R., R. L. HARDER, W. R. HERTLER, M. MAHLER, R. E. BENSON & W. E. MOCHEL. 1962. J. Am. Chem. Soc. **84:** 3374–3387.
7. MURAKAMI, M. & S. YOSHIMURA. 1975. Abstract 7th Mol. Cryst. Symp.: 193–196. Nikko, Japan.
8. ACKER, D. S., R. J. HARDER, W. R. HERTLER, W. MAHLER, L. R. MELBY, R. E. BENSON & W. E. MOCHEL. 1960. J. Am. Chem. Soc. **82:** 6408–6409.
9. WOLFE, W. R., JR. 1963. U.S. Patent 3,110,630 (Nov. 12).
10. ROSS, S. D., R. C. PETERSON & M. FINKELSTEIN. 1965. U.S. Patent 3,214,648 (Oct. 26). ROSS, S. D. & R. C. PETERSON. 1965. U.S. Patent 3,214,650 (Oct. 26).
11. MILES, M. G., J. D. WILSON & M. H. COHEN. 1973. U.S. Patent 3,779,814 (Dec. 18).
12. SCHNEIDER, A. A., W. GREATBATCH & R. MEAD. 1974. Proc. Int. Power Sources Conf.: 651–659.
13. SALMON, M. B., J. W. BRAY, G. DEPASQUALI & R. A. CRAVEN. 1975. Phys. Rev. B. **11**(2): 619–622.
14. WAHLIG, C. F. 1966. U.S. Patent 3,225,392 (June 7).
15. LAUTMAN, R. G. 1967. U.S. Patent 3,321,681 (May 23).
16. KRIKORIAN, F. & R. J. SNEED. 1969. J. Appl. Phys. **40**(5): 2306–2314.
17. KATON, J. E. 1966. U.S. Patent 3,267,115 (Aug. 16).
18. MEINHARD, J. E. 1969. U.S. Patent 3,428,892 (Feb. 18).
19. MEIER, H., W. ALBRECHT & U. TSCHIRWITZ. 1969. Ber. Bunsenges. Phys. Chem. **73** (8–9): 795–805.
20. HOVE, M. J., B. M. HOFFMAN & R. J. LOYD. 1972. J. Phys. Chem. **76**(13): 1849–1853.
21. BARLOW, W. A., G. R. DAVIS, E. P. GOODINGS, R. L. HAND, G. OWEN & M. RHODES. 1976. Mol. Cryst. Liq. Cryst. **33:** 123–148.
22. AVIRAM, A. & M. A. PATNER. 1974. Chem. Phys. Lett. **29**(2): 277–283.
23. AVIRAM, A., M. J. FREISER, P. F. SEIDEN & W. R. YOUNG. 1976. U.S. Patent 3,953,-874 (Apr. 27).
24. KUHN, H. & D. MOBIUS. 1971. Agnew. Chem. Int. edit. **10**(9): 620–637.
25. TSUZAKI, T. 1975. Japan. Kokai 50-93565 (July 25).
26. SHARP, M. & G. JAHANSSON. 1971. Anal. Chim. Acta. **54:** 13–21; Sharp, M. 1976. Anal. Chim. Acta. 85: 17–30.
27. LOEBEL, E., M. SHPORER, O. KEDEM & R. BLOCH. 1975. Israeli Patent 39,996 (Apr. 25).
28. GUTMANN, F., A. M. HERMANN & A. REMBAUM. 1967. J. Electrochem. Soc. **114**(4): 323–329; 1968. J. Electrochem. Soc. **115**(4): 359–362.
29. WEIDENTHALER, P. & E. PELINKA. 1969. Collect. Czech. Chem. Commun. **34**(5): 1482–1490.
30. GUTMANN, F., A. M. HERMANN & A. REMBAUM. 1972. Japan. Patent 47-30769 (Aug. 10).
31. MOSER, J. R. 1972. U.S. Patent 3,660,163 (May 2); Moser, J. R. & A. A. SCHNEIDER. 1972. Japan. Kokai 47-14626 (Aug. 11).
32. WADA, T. 1974. Japan. Kokai 49-56132 (May 31).
33. KONDO, S., M. FUKAI & N. YOSHIIKE. 1977. U.S. Patent to be issued.; 1976. Abstr. 34th Ann. Mtg. Chem. Soc. Jpn. (I): 196.
34. MCLEAN, D. A. & F. S. POWER. 1965. Proc. IRE. **44:** 872–878.
35. LUPINSKI, J. H. 1967. G. E. Report (No. 67-C-094) (Mar.).
36. SHARBAUGH, H. 1969. U.S. Patent 3,483,438 (Dec. 9).
37. MIZOGUCHI, K., E. TSUCHIDA & I. SHINOHARA. 1975. Hyomen **13**(10): 559–587.
38. TABATA, A. & M. KITAJIMA. 1974. Japan. Kokai 49-67153 (June 28).
39. YOSHIMURA, S. & M. MURAKAMI. 1977. Bull. Chem. Soc. Jpn. **50**(12): 3153–3157.
40. PARISI, G. I. 1972. IEEE Trans. Parts, Hybrids, Packag. PHP-8: 33–38.
41. SMITH, D. M. 1966. J. Electrochem. Soc. **113**(1): 19–24.
42. DUNN, C. G. 1968. J. Electrochem. Soc. **115**(2): 219–226.
43. BERNARD, W. J. & J. W. COOK. 1959. J. Electrochem. Soc. **106**(8): 643–646.

44. IKEMOTO, I., J. M. THOMAS & H. KURODA. 1973. Bull. Chem. Soc. Jpn. **46:** 2237–2238.
45. FLANDROIS, S. & P. CHASSEAU. 1977. Acta Cryst. B33 (9): 2744–2750.
46. ITOH, Y. & S. YOSHIMURA. 1977. J. Electrochem. Soc. **124**(7): 1128–1133.
47. SHCHEGOLEV, I. F. 1972. Phys. Stat. Sol. (a) **12:** 9–45.
48. ITOH, Y., S. TAKAHASHI & R. SANO. 1977. In preparation.
49. GOODINGS, E. P. 1975. Endeavor **34:** 123–130.
50. SOMOANO, S., S. P. S. YEN & A. REMBAUM. 1970. Polym. Lett. **8:** 467–479.
51. HERMANN, A. M., S. P. S. YEN, A. REMBAUM & R. F. LANDEL. 1971. Polym. Lett. **9:** 627–633.
52. HAYASHI, T., M. HASHIMOTO, K. YAMAMOTO, W. SHIMOTSUMA, H. MORIGA & T. SHIMIZU. 1970. Ger. Offen. 1,964,665 (July 2).
53. HAYASHI, T. & M. HASHIMOTO. 1972. Shinku **15**(11): 390–396.
54. GILL, W. D. 1972. J. Appl. Phys. **43**(12): 5033–5040.
55. SCHAFFERT, R. M. 1971. IBM Res. Develop. **15**(1): 75–89.
56. MORIMOTO, K. & M. YOKOYAMA. 1974. Imaging (**13**): 17–22.
57. YASUBA, M., M. UMEDA & Y. HAYASHI. 1976. Natl. Tech. Rept. **22**(6): 895–904.
58. MORT, J. & I. CHEN. 1975. Appl. Solid State Sci. **5:** 69–149.
59. HAYASHI, Y. 1976. Natl. Tech. Rept. **22**(6): 818–825.
60. SEYKORA, E. J. 1976. Appl. Phys. Lett. **28**(7): 377–379.
61. GUYER, JR., M. & E. SAMIKI. 1970. Anal. Chim. Acta **49:** 182–184.
62. DEGUCHI, K. & K. MEGURO. 1972. J. COLLOID. Interface Sci. **38**(3): 596–600.
63. HOSAKA, H., N. KAWASHIMA & K. MEGURO. 1972. Bull. Chem. Soc. Jpn. **45:** 3371–3375.
64. ANDERDICE, D. & M. CALVIN. 1976. J. Chem. Soc. Faraday Trans. **II**(10): 1916–1919.
65. YAMAMOTO, K., H. MORIGA, W. SHIMOTSUMA & T. SHIMIZU. 1972. U.S. Patent 3,632,526. (Jan. 4).
66. KISHIMOTO, Y. & F. ODA. 1976. Japan. Kokai 51-22092 (Feb. 21).
67. TABATA, A. 1974. Japan. Kokai 49-61698 (June 14).
68. VEGTER, J. G., T. HIMBA & J. KOMMANDEUR. 1969. Phys. Lett. **3**(6): 427–428.
69. BAILEY, J. C. & D. B. CHESNUT. 1969. J. Chem. Phys. **51**(11): 5118–5128.
70. IIDA, Y. 1973. J. Chem. Phys. **59**(4): 1607–1612.
71. FLANDROIS, S., P. DELHAES & J. C. GIUNTINI. 1973. Phys. Lett. A **45**(4): 339–340.
72. MURAKAMI, M. & S. YOSHIMURA. 1975. J. Phys. Soc. Jpn. **38**(2): 488–492.
73. BERGER, P. A., D. J. DAHM, G. R. JOHNSON, M. G. MILES & J. D. WILSON. 1975. Phys. Rev. B **12**(10): 4085–4089.
74. WARMACK, R. J. & T. A. CALLCOTT. 1975. Phys. Rev. B **12**(8): 3336–3338.
75. SOMOANO, R. B., A. GUPTA, V. HADEK, M. NOVOTNY, M. JONES, T. DATTA, R. DECK & A. M. HERMANN. 1977. Phys. Rev. B **15**(2): 595–601.
76. MURAKAMI, M. & S. YOSHIMURA, 1976. Proc. Symp. Mol. Struc.: 480–481. Tokyo.
77. MORIN, F. J. 1959. Phys. Rev. Lett. **3**(1): 34–36.
78. FUTAKI, H. 1965. Jap. J. Appl. Phys. **4:** 28–41.
79. MOTT, N. F. 1974. Metal-Insulator Transitions. Tayler & Francis Ltd. London, England.
80. HEEGER, A. J. & A. F. GARITO. 1975. *In* Low-Dimensional Cooperative Phenomena, H. J. Keller, ed. Plenum Publishing Co. New York, N.Y.
81. ANDRICH, E. 1969. Philips Tech. Rev. **30:** 170–177.
82. RUTT, T. C., F. C. FULSON & G. B. LAUGHLAN. 1975. Proc. 25th IEEE Electronic Components Conf. May 12–14. Washington, D.C.
83. YAMAGUCHI, G. 1975. Solid-solid reactions. *In* Reactivity of Solids. Kagaku Sosetsu (No. 9): 87–114.
84. MURAKAMI, M. & S. YOSHIMURA. 1975. Bull. Chem. Soc. Jpn. **48**(1): 157–162.
85. FLANDROIS, S., P. LIBERT & P. DUPUIS. 1975. Phys. Stat. Sol. a**28:** 411–415.
86. THOMAS, J. M. 1973. Nature Phys. Sci. **244:** 56–57.
87. MAPLUNOV, M. G., D. N. FEDUTIN, M. L. KHIDEKEL, I. F. SHCHEGOLEV, E. R. YAGUBSKII & R. B. LYUBOVSKII. 1972. Zh. Obshch. Khim. **42**(10): 2295–2301.

88. KISTENMACHER, T. J., T. E. PHILLIPS, D. O. COWAN, J. P. FERRARIS, A. N. BLOCH & T. O. POELER. 1976. Acta Cryst. B32(2): 539–547.
89. SAITO, Y. 1975. Abstr. 7th Mol. Cryst. Symp.: 185–188. Nikko, Japan.
90. MURAKAMI, M. & S. YOSHIMURA. 1977. Chem. Lett. (8): 929–932.
91. SUNDARESAN, T. & S. C. WALLWORK. 1972. Acta Cryst. B28(4): 1163–1169.
92. ASHWELL, G. J., D. D. ELEY, S. C. WALLWORK & M. R. WILLIS. 1975. Proc. R. Soc. Lond. A. 343: 461–475.
93. ASHWELL, G. J., D. D. ELEY, R. J. FLEMING, S. C. WALLWORK, & R. M. WILLIS. 1076. Acta Cryst. B32(11): 2948–2952.
94. BONNIFACE, D. W., M. J. BRAITHWAITE, D. D. ELEY, R. G. EVANS, R. PETHIG & M. R. WILLIS. 1971. Discus. Faraday Soc. (No. 51): 131–138.
95. COMES, R., G. SHIRANE, S. M. SHAPIRO, A. F. GARITO & A. J. HEEGER. 1976. Phys. Rev. B14(6): 2376–2383.
96. ANDRE, J. J. & G. WEILL. 1971. Chem. Phys. Lett. 9(1): 27–30.
97. BRICE, J. C. 1973. The Growth of Crystals from Liquids. North-Holland Publishing Co. Amsterdam, The Netherlands.
98. TOSCHEV, S. 1973. Homogeneous nucleation. *In* Crystal Growth: An Introduction. P. Hartman, Ed.: 1–49. North-Holland Publishing Co. Amsterdam, The Netherlands.
99. BECKGAARD, K., D. O. COWAN & A. N. BLOCH. 1975. Proc. 4th Int. Symp. Org. Solid State. (Paper No. 71.) July 16–18. Bordeaux, France.
100. ETEMAD, S. 1976. Phys. Rev. B13(6): 2254–2261.
101. BLOCH, A. N., D. O. COWAN & T. O. POELER. 1974. *In* Energy and Charge Transfer in Organic Semiconductors: 167–174. Plenum Press. New York, N.Y.
102. YOSHIMURA, S., M. MURAKAMI, Y. ITOH & K. HASEGAWA. 1972. Chem. Lett. (9): 835–838.
103. CHAUDHARI, P., A. S. SCOTT, R. B. LAIBOWITZ, Y. TOMKIEWICZ & J. B. TORRANCE. 1974. Appl. Phys. Lett. 24(9): 439–442.
104. BRIGHT, A. A., M. J. COHEN, A. F. GARITO & A. J. HEEGER. 1975. Appl. Phys. Lett. 26(11): 612–615.
105. HEILMEIER, G. H. 1976. IEEE Trans. Electron Devices ED-23(7): 780–785.
106. CHANG, T. S. 1976. Am. Electrochem. Soc. Extended Abstr. (Oct.): 507–509.

DISCUSSION

PAUL GRANT (IBM–San Jose): Electrolytic capacitors are generally the first components to fail in modern solid state circuitry. Have you run any experiments on the lifetime of these components?

YOSHIMURA: We tested the lifetime. They last over two thousand hours, which is suitable for home appliances.

GRANT: Electrolytic capacitors are used in space, where they are subjected to large temperature variations and a great deal of radiation. How did the organic electrolyte stand up to these types of environmental constraints versus the inorganic ones?

YOSHIMURA: The temperature characteristics are quite sufficient, as compared to conventional aluminum. Organic conductors are very sensitive to moisture, and we must be careful to package the sample. We have not examined the effect of radiation.

PERLSTEIN: A photoreceptor currently in use is an organic photoconductor. In fact, the composition is such that it contains low-dimensional interacting

molecules which, we believe, accounts for the very high quantum efficiency for charge generation.

METZGER: K. Tamaru, of the University of Tokyo, has claimed that many of his donor-acceptor complexes are very good catalysts for typical H_2–D_2 exchange and H D exchange with C_2D_2-hydrogen-containing DA complex, which are typical model reactions in heterogeneous catalysis. The problem seems to be that the experiments are hard to do and to duplicate. Preliminary work at the University of Mississippi has failed to substantiate Tamaru's claim, at least for metal-free DA complexes.

N. P. ONG (*Univ. of Southern California, Los Angeles, Calif.*): One aspect of charge-density wave materials that shows promise in technological applications is the nonlinear effects that some of these materials show. It is known that (TTF) (TCNQ) in the semiconductor phase shows strongly nonohmic behavior. In the metallic $NbSe_3$ we have found that it is highly nonohmic. For example, the application of a 0.5V across a hundred-ohm sample will drop the resistance by a factor of two. This probably shows some promise in applications in microelectronics. (Ong, N.P. & P. Monceau, 1977. Phys. Rev. B, **16:** 3443. **Added in proof.**)

TORRANCE: It has been shown at IBM that the UV-induced reaction between TTF and CCl_4 leads to the formation of the metallic salt $TTF(Cl)_{\sim 0.9}$. If a piece of paper is dampened by a CCl_4 solution of TTF (yellow) and then irradiated by UV light through a mask, the pattern of the mask is reproduced on the paper as a red conducting ink, (U.S. Patent No. 4,036,648).

ROBERT SOMOANO (*Jet Propulsion Laboratory, Pasadena, Calif.*): I wish to point out several examples of products currently in commercial use that were discovered as a result of a basic research program involving the study of organic (and polymeric) conductors. A variation of the electrochemical cell discovered by A. Rembaum at the Jet Propulsion Laboratory, which you described, has been developed. This modified electrochemical cell contains iodine, poly(vinylpyridine), and lithium metal and forms an efficient and effective battery that is currently finding widespread use in cardiac pacemakers. It appears that a greater percentage of the future pacemakers will utilize this organic cell. Second, during the course of an investigation of highly conducting polymers at JPL, Rembaum developed a series of high charge-density polymers called "ionenes." Reaction of the ionenes with TCNQ yielded semiconducting polymers with relatively good electrical conductivity. However, the ionenes themselves were found to have high biological activity and to function as model flocculation polyelectrolytes. These materials are being considered for use in large-scale water-purification systems.

ORGANIC METALS: BASIC CRYSTAL-GROWTH TECHNIQUES*

Jan R. Andersen† and Edward M. Engler

IBM Thomas J. Watson Research Center
Yorktown Heights, New York 10598

Klaus Bechgaard

H. C. Oersted Institute
Copenhagen DK-2100, Denmark

During recent years, much effort has been devoted to the design and synthesis of new materisls with potentially interesting solid-state properties.[1] Many such compounds, however, have been discarded or are slowly decomposing on laboratory shelves because the last crucial step in the preparation—the growth of single crystals suitable for conductivity measurements, structure determination, and so on—has failed. In this paper we present some methods successfully employed in our laboratories for growing crystals of charge-transfer salts of the TTF-TCNQ type. The paper is based chiefly upon personal experiences, supplemented with observations from others. We recognize that our views may not be new and that different techniques used elsewhere may work equally well. The techniques to be covered are diffusion, evaporation, cooling, viscous media diffusion, precipitation, and vapor-phase growth. Before we begin a description of these, we should like to make some general remarks.

The materials—i.e., the neutral donors and acceptors used in the crystal-growing experiments—should be pure. In some cases it is more beneficial to start from a microcrystalline powder of the charge-transfer salt, but since that is normally[2] made from the neutral constitutents, the same considerations apply. Multiple gradient sublimations were proposed by McGhie *et al.*[3] as a proper means of purification. This was later challenged by the Johns Hopkins group, which found no advantage in gradient sublimation compared to normal sublimation techniques.[4] In the latter report it was also claimed that crystalline imperfections seem to have a greater impact on the conductivity behavior of TTF-TCNQ than does chemical purity. In our opinion, a thorough cleanup of the constituents—e.g. by multiple recrystallizations followed by gradient sublimation—should always be performed, although we also have observed that limited amounts of impurities do not significantly affect the electrical properties of the charge-transfer salt. However, for other purposes, such as low-temperature magnetic measurements, the purity of the sample is very important.

The careful purification of the solvents used for crystal growing is important, since even very small amounts of impurities in the solvent, in relation to the amount of material employed in a typical crystal-growing experiment, are sig-

*Manuscript received June 6, 1977.

†IBM postdoctoral fellow. Present address: Chemistry Department, Research Establishment RISO, DK-4000, Roskilde, Denmark.

0077-8923/78/0313-0293 $1.75/1 © 1978, NYAS

nificant. Furthermore, all crystal growing experiments should be performed under an inert atmosphere.

The key solvents for growing these charge-transfer salts are all organic. Some polarity seems to be a necessity, although that does not exclude nonpolar solvents such as hexane used as a "mixer" to decrease polarity. Solvents typically chosen are MeCN, CH_2Cl_2, $CHCl_3$, THF, EtOAc or mixtures thereof, and for high temperature experiments, PhCl.

During crystal growth, care should be taken to avoid undue exposure to light, since photochemical reactions have often been observed[5] and, in one instance, described.[6] This problem can be conveniently overcome by wrapping the whole growing apparatus in aluminum foil. It is also useful to choose a relatively vibrationless place for the experiment, since vibrations can cause rapid nucleation to occur, resulting in microcrystalline powders or, at best, many small crystals. Furthermore, for most of the techniques it is advantageous to control the temperature during the experiment by immersing the apparatus into a thermostated bath.

Glass apparatus apparently leach small amounts of ferromagnetic impurities,[7] and presumably alkali-metal ions as well, into the solution during crystal growth. This problem can be minimized by use of a quartz- or Teflon®-coated apparatus;[7] however, for most purposes leaching does not appear to be important. If there is concern, Teflon coating of a glass apparatus[4] may be the better solution, since even high-quality quartz leaches to a small extent.

Some knowledge about the system for which crystals are to be grown is important in determining the conditions. The electron affinity and the ionization potential of acceptor and donor, respectively, and their solubilities, should always be at least estimated. With these entities known, the process of choosing a medium with the proper polarity and appropriate "solubility power" is facilitated, and it is also easier to determine what particular experimental setup and what temperature to employ for the crystal growth.

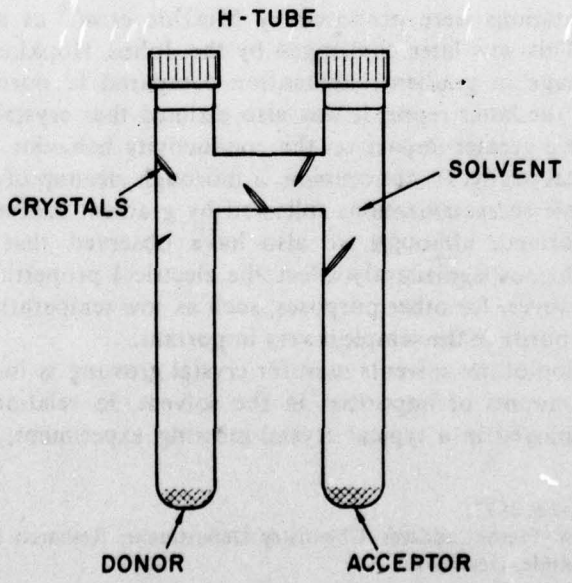


FIGURE 1.

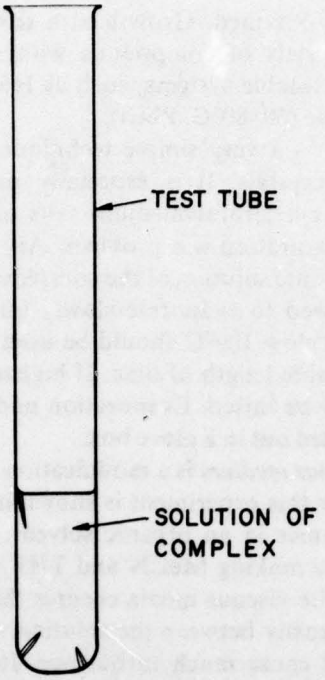


FIGURE 2.

We present below some crystal-growing techniques we have found to work well for a wide variety of TTF-TCNQ derivatives. They are listed in descending order in approximate accordance with their versatility and ease of use.

The diffusion technique, in connection with organic metals, has been described before.[8,9] The variant currently in use in our laboratories, the H-tube, is shown in FIGURE 1. This design allows a solution of, or the solid acceptor itself, to be placed in one leg and the donor, likewise, in the other. Solvent is then carefully added to fill the tube, and the components diffuse together at a rate determined by the temperature and the solvent. A variety of modifications of the basic diffusion tube, such as the incorporation of a central solvent chamber[8] or the use of porous frits between compartments to slow down diffusion,[9] are possible. To our mind, however, the less sophisticated H-tube is less troublesome to work with, and, more importantly, it gives crystals of equal quality.

If there is a large difference in solubility between the components, solutions of the solids are preferred over the solids themselves in order to ensure that the charge-transfer salt does not precipitate on undissolved crystals of the more insoluble component. When this is not convenient, e.g. if the donor or acceptor is too insoluble to allow enough material into a small amount of solvent, then the following procedure has been found useful: The more insoluble component is crushed and placed in the H-tube as a powder, while large, chunky crystals of the other component are selected for the experiment. Because of the much larger surface area of the "insoluble" component, it will dissolve more rapidly. On the other hand, the more soluble component dissolves more slowly for the opposite reason.

By making these kinds of adjustments, crystals of a wide variety of charge-

transfer salts can be obtained. Growth at a temperature in the vicinity of 30°C often gives good crystals of compounds with solubilities comparable to TTF-TCNQ. For more insoluble systems, such as HMTSF-TCNQ, a higher temperature is often preferable (60–80°C, PhCl).

Slow evaporation is a very simple technique, which, in many instances, give astonishingly good crystals. It is especially useful for rather soluble charge-transfer salts such as heterofulvalenium salts of alkylated TCNQ analogs or in systems where oversaturation is a problem. All the experiment requires is a test tube (FIGURE 2). A dilute solution of the complex in question is placed in the tube. Solvent is then allowed to evaporate slowly until crystals are formed. Solvents with boiling points below 100°C should be used in order to complete the experiment within a resonable length of time. If higher boiling solvents are a necessity, the temperature may be raised. Evaporation under an inert atmosphere can most conveniently be carried out in a glove box.

Growth from viscous medium is a modification of the diffusion technique, and a typical apparatus for this experiment is shown in FIGURE 3. The viscous liquid is a solution of a polymer in an organic solvent. We have used polymethylmethacrylate (PMMA) for making MeCN and THF viscous, and polystyrene (PS) for aromatic solvents. The viscous media ensures that the diffusion is very slow and that differences in density between the solution near to a nucleation site and the surroundings do not cause much turbulence. In this respect, the viscous media technique imitates a zero-gravity experiment.

The presence of chemically inert polymers[10] such as PMMA and PS during the crystal growth do not appear to contaminate the crystals grown. For example, crystals of TTF-TCNQ grown in the presence and absence of PMMA[11] have identical x-ray patterns and very similar electrical properties. The only difference appears to be that the crystals grown from the viscous medium were thicker (more growth in the a and c directions) and had a higher room-temperature value of the conductivity (ca 1000 (ohm cm)$^{-1}$) than normally observed for this material. No differences were noticed in the position of T_{max}, the sharpness of the phase transition or the ratio $\sigma_{Tmax}/\sigma_{RT}$ (ca 15). The only inconvenience of this technique is that a very careful washing of the crystals is necessary to avoid deposits of the polymer on the crystal surfaces. This is a limitation, since only fairly insoluble crystals can survive this treatment. Viscous media-diffusion growth was tested successfully on TTF-TCNQ, and we have been able to produce fair crystals of

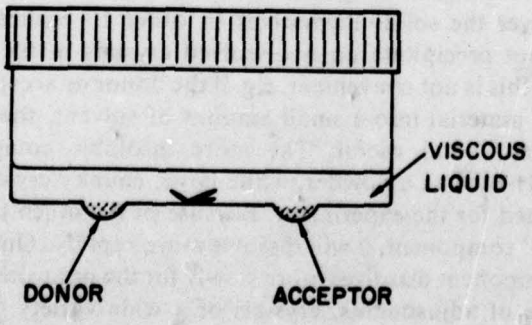


FIGURE 3.

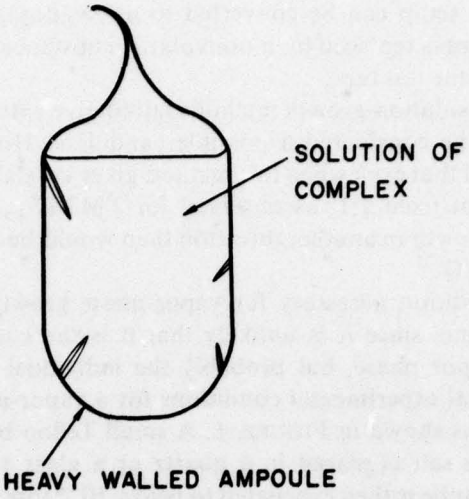


FIGURE 4.

DTTSF-TCNQ[12] (DTTSF = Di-(2,5-dihydrothieno)-[3,4-b, 3,4-h]-1,4,5,8-tetraselenafulvalene), a system where other methods failed.

The slow cooling technique has in the past been shown to be very useful for growing crystals of solid solutions of charge-transfer salts e.g. TTF_xTSeF_{1-x}-TCNQ[13] and for doping experiments.[14,15] Since solubility and diffusion-rate differences between the host and the dopant are minimized by this method, we feel that more reproducible and uniform solid-solution distributions can be realized this way in comparison to a diffusion technique. We have used two different experimental setups: one for very insoluble and a second for moderately soluble systems. The first consists of a heavy-walled ampoule (FIGURE 4) in which the constituents and a suitable solvent are placed. The ampoule is closed and heated until a clear solution results. It is then placed in a programmable, hot, thermostated bath and allowed to cool very slowly to ambient temperature. In this way crystals of the organic alloy $HMTTF_xHMTSF_{1-x}$-TCNQ,[16] together with HMTSF-TCNQ doped with small amounts of MTCNQ,[17] were obtained.

The second setup is a flask, in which a boiling solution of the desired salt is placed. The flask is then stoppered, placed hot into a pre-heated Dewar and packed with warm glass wool. Overnight standing normally causes precipitation to occur. Crystals of TTF_xTSeF_{1-x}-TCNQ,[13] TTF-$TCNQ_xMTCNQ_{1-x}$,[14] and TSeF-$TCNQ_xMTCNQ_{1-x}$[15] have been grown in this manner. The advantage of the second method is that it is completed overnight. It is not, however, applicable for all systems, and the more tedious and time-consuming ampoule method serves well in many such cases.

The precipitation method is the least investigated of the methods presented here. It is only known to work for TTF-TCNQ[18] and for the TTF-halides.[19] The experiment is also, in this case very easy to conduct. A bottom layer of a volatile, low-polarity solvent is placed in a vial (FIGURE 5). Into this is immersed a little test-tube containing a nearly saturated solution of the complex. The vial is closed with a tight, screw cap, and as the solvents begin to equilibrate through the vapor phase, crystals begin to form.

The same setup can be converted to an evaporation experiment, if the low polarity solvent is replaced by a nonvolatile substance that absorbs or reacts with the solvent in the test tube.

When the solution-growth methods fail to give satisfactory results, *vapor-phase growth* may be considered a possible candidate. However, it should always be borne in mind that even when this method gives crystals, they can have a stoichiometry different from 1:1, as observed for $TMTTF_{1.3}$-$TCNQ_2$[20] and $TMTTF_{1.66}$-$TCNQ_2$[21]. Growth in another direction than would be expected has been observed for TTF-TCNQ.[22]

It is a condition necessary for vapor-phase growth that both constituents be able to sublime, since it is unlikely that it is the charge-transfer salt itself that enters the vapor phase, but probably the individual donor and acceptor molecules.[19] Typical experimental conditions for a vapor-phase crystal-growth experiment can be as shown in FIGURE. 6. A small Teflon boat containing a powdered sample of the salt is placed in a quartz or a glass tube coated with Teflon or Kapton. The tube is then evacuated to below 10^{-6} torr and closed. It is placed in a temperature gradient with the powdered sample in the hot end, and the temperature is increased until a deposit of solid is observed at a colder position. Separation of donor and acceptor is sometimes observed, but after a while they normally diffuse together at an intermediate position to form the charge-transfer salt.

Quartz or coated glass may be necessary in this experiment, since decomposition of donors and acceptors on glass surfaces has been observed under experimental conditions similar to these.[3]

In order to characterize properly the solid-state properties of new charge-transfer salts, single crystals are necessary. Fortunately, these crystals do not have to be very large. For example, four-probe dc conductivity measurements can be carried out on crystals as small as a couple of mm in length. In lieu of single crystals, certainly a conductivity measurement on a compacted powder can be carried out in order to decide, whether it is worth spending the time and work necessary for crystal-growing experiments. A more informative measurement is probably the recording of the electronic spectrum of the material in a KBr pellet.[23] Characteristic absorption bands in the infrared region—around 2.5μ for

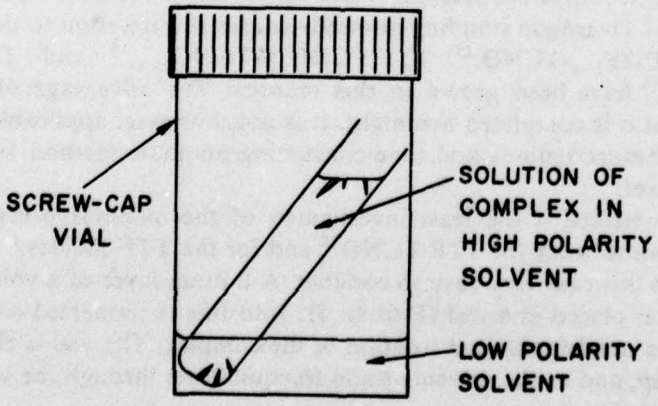
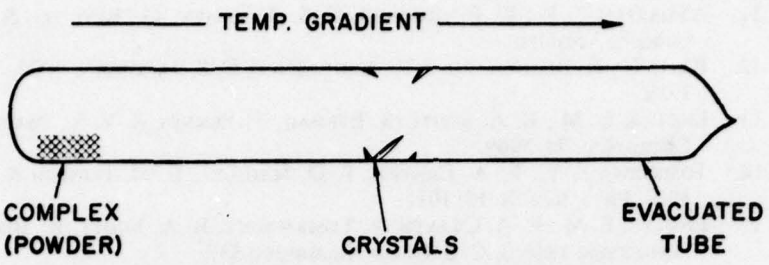


FIGURE 5.

FIGURE 6.



TCNQ salts—are a signature of the mixed valence segregated-stack structure necessary for high conductivity in the material.

Multiple phases of these charge-transfer salts are not uncommon. Thus, if a new material forms an insulating phase under a particular set of crystal-growing conditions, other conditions should be tried to establish the possibility of a conducting crystal habit. For example, with the systems TMTSF-TCNQ[24] and DEDMTSF-TCNQ,[25] the polarity of the solvent used in the growth experiment determined whether a conducting or insulating phase was obtained. For the first material, seeding with small crystallites of the conducting phase was also employed in order to improve crystal quality. The temperature at which nucleation begins can also determine whether an insulator or conductor is formed. For example, slow evaporation at 25°C gave the conducting form of TSeF-DETCNQ, whereas rapid cooling from the same solvent gave the insulation isomer.[26]

Crystal growth of these charge-transfer salts is an unpredictable and sometimes frustrating task. Perseverance is a valuable quality for anyone working in this area, and often decides the difference between success and failure.

NOTES AND REFERENCES

1. For reviews, see GARITO, A. F. & A. J. HEEGER. 1974. Accounts Chem. Res. **7**: 232; BLOCH, A. N., D. O. COWAN & T. O. POEHLER. 1974. *In* Energy and Charge Transfer in Organic Semiconductors. K. Masuda & M. Silver, Eds. Plenum Press. New York, N.Y.; HEEGER, A. J. & A. F. GARITO in Low Dimensional Cooperative Phenomena. 1975. H. J. Keller, Ed. Plenum Press. New York, N.Y.; ENGLER, E. M. 1976. Chem. Technol. **6**: 274; NARITA, M. & C. U. PITTMAN, JR. 1976. Synthesis: 489.
2. Some compounds have so far been produced only by metathetical reactions. See, for example: WUDL, F. 1962. J. Amer. Chem. Soc.: 97. 75. Also, when this is the case, the crude charge-transfer salt should be carefully purified before crystal growth is attempted.
3. MCGHIE, A. R., A. F. GARITO & A. J. HEEGER. 1974. J. Cryst. Growth **22**: 295.
4. GEMMER, R. V., D. O. COWAN, T. O. POEHLER, A. N. BLOCH, R. E. PYLE & R. H. BANKS. 1975. J. Org. Chem. **40**: 3544.
5. ANDERSEN, J. R., E. M. ENGLER & K. BECHGAARD. Unpublished results.
6. SCOTT, B. A., F. B. KAUFMAN & E. M. ENGLER. 1976. J. Amer. Chem. Soc. **98**: 4342.
7. SCOTT, J. C., A. F. GARITO & A. J. HEEGER. 1974. Phys. Rev. B. **10**: 3131.
8. ANZAI, J. 1976. J. Cryst. Growth **33**: 185.
9. KAPLAN, M. L. 1976. J. Cryst. Growth **33**: 161.
10. The polymer used for crystal growth should be as pure as possible. We have prepared the polymers used in our experiments by radiation-induced polymerization of the monomer. Care was taken to remove all of the inhibitor present in the commercial available monomers before polymerization.

11. ANDERSEN, J. R., K. BECHGAARD, C. S. JACOBSEN, G. RINDORF & H. SOLING. Unpublished results.
12. BERG, C., K. BECHGAARD, J. R. ANDERSEN & C. S. JACOBSEN. 1976. Tetrahedron Lett. 1719.
13. ENGLER, E. M., B. A. SCOTT, S. ETEMAD, T. PENNEY & V. V. PATEL. 1977. J. Amer. Chem. Soc. **99:** 5909.
14. TOMKIEWICZ, Y., R. A. CRAVEN, T. D. SCHULTZ, E. M. ENGLER & A. R. TARANKO. 1977. Phys. Rev. B. **15:** 1011.
15. ENGLER, E. M., R. A. CRAVEN, Y. TOMKIEWICZ, B. A. SCOTT, K. BECHGAARD & J. R. ANDERSEN. 1976. J. C. S. Chem. Commun.: 337.
16. See paper by ANDERSEN, J. R., *et al.* This annal.
17. BECHGAARD, K. C. S. JACOBSEN & J. R. ANDERSEN. Unpublished results.
18. ANDERSEN, J. R. Unpublished results.
19. SCOTT, B. A. Personal communication.
20. KISTENMACHER, T. J., T. E. PHILLIPS, J. P. FERRARIS, D. O. COWAN, A. N. BLOCH & T. O. POEHLER. 1976. Acta. Cryst. **B32:** 539.
21. EHRENFREUND, E., S. K. KHANNA, A. F. GARITO & A. J. HEEGER. 1977. Solid State Commun. **22:** 139.
22. COHEN, M. J., L. B. COLEMAN, A. F. GARITO & A. J. HEEGER. 1974. Phys. Rev. B. **10:** 1298.
23. TORRANCE, J. B., B. A. SCOTT & F. B. KAUFMAN. 1975. Solid State Commun. **17:** 1369.
24. BECHGAARD, K., T. J. KISTENMACHER, A. N. BLOCH & D. O. COWAN. 1977. Acta Cryst. **B33:** 417.
25. ANDERSEN, J. R., C. S. JACOBSEN, K. BECHGAARD, G. RINDORF & H. SOLING. To be published.
26. ANDERSEN, J. R., R. A. CRAVEN, J. E. WEIDENBORNER & E. M. ENGLER. 1977. J. C. S. Chem. Commun. 526.

INSTRUMENTAL ANALYSIS FOR PURITY DETERMINATION OF TTF-TCNQ CRYSTALS*

A. R. McGhie,† P. J. Nigrey,† F. G. Yamagishi†‡
and A. F. Garito§

† *The Laboratory for Research on the Structure of Matter*
§ *Department of Physics*
University of Pennsylvania
Philadelphia, Pennsylvania 19104

Considerable progress has been made in the experimental understanding of 1-D conductors, especially in the case of tetrathiafulvalene-tetracyano-quinodimethane (TTF-TCNQ).[1,2] Of critical importance to these studies are the degrees of sample purity and perfection, since it is now generally agreed that many important solid state properties are sample dependent.[3] These properties can be ascribed to differences in chemical purity or physical perfection rather than to differences in experimental methods or handling techniques, since crystals prepared by us have given similar results when measured in different laboratories.

We wish to report the results of standard instrumental methods of analysis for determining the chemical purity of TTF-TCNQ samples obtained by different synthetic and purification techniques.

TTF was prepared according to Melby *et al.*,[4] except that the final coupling reaction utilized the perchlorate salt rather than the phosphorus hexafluoride. TCNQ was prepared by the method of Acker and Hertler.[5] Details of both preparations have been reported elsewhere.[6]

Purification of both TTF and TCNQ was accomplished by primary recrystallization, TTF from cyclohexane and TCNQ from acetonitrile, followed by multiple gradient sublimation.[7]

Crystals of TTF-TCNQ were grown by the three chamber-diffusion technique previously described by Nigrey.[8]

Chemical analysis of TTF-TCNQ crystals has been carried out only by elemental analysis for C, H, N, and S and found to be accurate within the error of the measurement.[9] Because of low solubility, most of the analyses we performed have been on pure neutral samples of TTF and TCNQ. The reactive nature of both neutral components is such that only a limited number of instrumental analytical methods are available for examining the very high levels of purity required in this work. We have concentrated primarily on two nonrelated techniques—thermal analysis and chromatography.

THERMAL ANALYSIS

The melting behavior of a known material can be a useful guide to the degree of purity achieved, and when taken to the extreme has been used to characterize

*This work was supported by the National Science Foundation, MRL Program, under grant no. DMR76-00678. Manuscript received June 15, 1977.
‡Current Address: Hughes Research Laboratories, Malibu, California 90265.

0077-8923/78/0313-0301 $1.75/1 © 1978, NYAS

TABLE 1
MELTING POINT OF TTF SAMPLES*

Source	Forefraction (C)	Main Fraction (C)
Aldrich		
A: as received	(117.3–119)	
B: 1 × G.S.	ND	119.3–119.5
Synthesized		
A: R	(118–119)	
B: R + 1 × G.S.	119.0–119.3	119.3–119.5
C: R + 2 × G.S.	119.3–119.4	119.3–119.5
D: R + 3 × G.S.	ND	119.4–119.5
E: R + 1 × G.S.	118.5–119.3	119.3–119.6
F: R + 1 × G.S.	ND	119.3–119.4

*R = Recrystallized from Cyclohexane; G.S. = gradient sublimed; ND = not determined.

standard materials to 99.999% purity.[10] We have routinely measured the melting point or melting range of samples of TTF subjected to various purification treatments using a Mettler FP5/FP52 hot-stage microscope. High-purity benzoic acid, >99.99%, m.p. 122.4°C, was used to calibrate the hot stage. The melting point was obtained by heating the sample at 3°C/min to 117°C, then at 0.2°C/min, until melting was complete. TABLE 1 lists the results obtained for TTF samples purified either by recrystallization or recrystallization plus gradient sublimation. Two sources of TTF were examined: a) commercially supplied TTF from Aldrich Chemical Co. and b) synthetic material prepared in our laboratory. In both cases the recrystallized only materially gave a broad melting range and lower melting point than the gradient-sublimed material. Most of this effect was presumed to be due to occluded solvent in the crystals, because the forefractions of the gradient-sublimed material gave a high melting point, though not as high as the main fraction. After two gradient sublimations it was observed that the forefraction and the main fraction were of similar purity, indicating that little, if any, decomposition had taken place during the sublimation.

Attempts to determine the melting point of TCNQ by the same technique were unsuccessful because of rapid sublimation and reaction with the adjacent glass coverslip. With use of a unique nonreactive sample holder,[11] it was possible to determine the melting ranges of TCNQ samples. For the purest samples prepared by multiple gradient sublimation in Teflon® it was possible to go through several melting cycles and obtain the same melting range each time, 292–294°C, indicating that TCNQ is relatively melt-stable. This fact enabled us to determine the purity of TCNQ by the more quantitative technique of differential scanning calorimetry.

Both TTF and TCNQ have been analyzed by differential scanning calorimetry (DSC).[12] This is a well-established technique that gives a measure of the total impurity concentration rather than that of specific impurities. The technique is normally restricted to impurities that form eutectics and is not applicable either where solid solutions are formed or where rapid thermal decomposition occurs. Fortunately, most organic systems are eutectic formers.

The total impurity concentration is obtained from a modification of the Van't

Hoff Equation, as applied to dilute solutions, and is given by the equation

$$T_s = T_0 - \frac{(RT_0^2X_2)}{\Delta H_f} \cdot \frac{1}{F}$$

where

ΔH_f = heat of fusion of pure major component (cal/mole),
R = gas constant (1.987 cal/mole/°K),
T_s = sample temperature (°K),
T_0 = melting point of pure major component (°K),
X_2 = mole fraction impurity,
F = fraction of sample melted at T_s.

A plot of T_s versus $1/F$ yields a line of slope

$$-\frac{RT_0^2X_2}{\Delta H_f}.$$

The ΔH_f may be obtained directly from the DSC scan or from the literature. The mole-fraction impurity can then be calculated. This analysis is suitable for materials of purity 98–99.99%, with an error of ±0.02%.

The procedure employed was that described by Barrall and Johnson,[12] with one exception. As we were examining high-purity materials it was felt essential to obtain the most appropriate value for the thermal lag constant of the cell. In order to take into account the fact that organic materials have a thermal conductivity which is ~500 times smaller than that of metals, the thermal lag constant was obtained by using high-purity organic standards whose melting points were close to those of the materials under investigation. The standard materials chosen were benzoic acid, m.p. 122.4°C, and chrysene 256°C. Benzoic acid was purified from ACS certified material (Fisher Scientific, sublimed) by zone melting (12 zone passes at 1 inch/hr on a Sloan-McGowan zone melter), which is known to result in ultrahigh-purity benzoic acid of >99.995%.[10] Chrysene (Aldrich Puriss.) was purified by a combination of sublimation, zone melting (100 zone passes) and liquid chromatography.[13] Purity, as determined by HPLC and G.C., resulted in material >99.99%. Both of these materials yielded thermal lag constants slightly higher than that of the pure metals recommended for those temperature regions. These corrections affected only slightly the results for materials of highest purity. The values obtained are summarized in TABLE 2. The melting points of benzoic

TABLE 2

THERMAL LAG CONSTANTS OBTAINED FOR STANDARD REFERENCE MATERIALS

Material	MP (C)	Thermal Lag Const.	Heating Rate C/min
Benzoic Acid	122.4	0.72	1
Indium	156.6	0.55	1
Tin	231.9	0.80	1
		0.40	2
Chrysene	256	0.43	2

acid, indium, tin, and lead were also used to calibrate the temperature scale of the calorimeter.

DSC runs were carried out with a DuPont 990 thermal analysis system. Purity was determined by computer analysis of the DSC scan after manual calculation showed good agreement. The program yielded the following information: 1) mole fraction of impurity, 2) ΔH_f, 3) T_0, and 4) fractional area correction required for linearization. The data were analyzed only in the region 5–40% fraction melted.

DSC Analysis of TCNQ

Initial DSC runs were carried out in both aluminum crimped and hermetically sealed pans and resulted in decomposition of TCNQ due either to reaction with the pan or decomposition in the melt. Castro[14] reported running TCNQ in gold pans as a means of avoiding decomposition. Initial attempts with crimped gold pans resulted in sublimation of the TCNQ from the cell. Success was achieved by evaporating thin layers of gold (300–500 Å) on the inside of hermetically sealed aluminum pans. With these pans the sample could be melted, recrystallized, and remelted without apparent decomposition. In fact, the interesting observation was made that higher purity was measured when high-purity crystalline samples were run for the second time. This was due to the fact that after melting, a thin film configuration was achieved resulting in better thermal contact with the pan. Samples introduced as powders did not show this effect and impure samples tended to give lower values on the second run, presumably due to thermal decomposition.

The raw DSC data obtained are shown in Figure 1 for two samples of widely differing purity. The analytical results obtained for a variety of TCNQ samples of varying purity are included in Table 3. From these results it can be observed that material of the highest purity, >99.95%, was obtained only after two gradient sublimations. Commercially available TCNQ from two separate sources yielded material of much lower purity after identical purification procedures. The fore-fractions of gradient-sublimed material were consistently less pure than the main

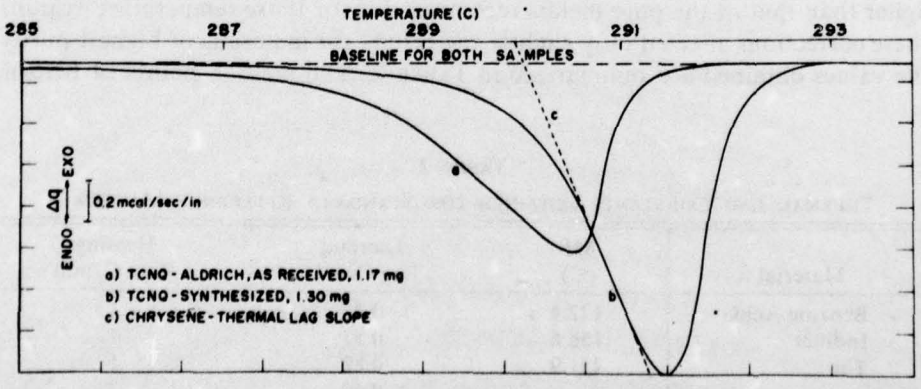


Figure 1. DSC thermograms for two samples of TCNQ. a: TCNQ, as received (Aldrich Chem. Co.); b: TCNQ, synthesized, recrystallized and ×2 gradient sublimed.

TABLE 3
DSC DETERMINATION OF PURITY FOR TCNQ FROM VARIOUS SOURCES

Source	Mole % Purity 1st Run	2nd Run	M. Pt. (C)
As Received			
Aldrich, Sample A	99.64	99.66	289.4
Sample B	99.90	99.91	289.6
Eastman	99.59	99.47	288.7
Synthesized and Recrystallised	99.07	98.65	288.6
Gradient Sublimed			
Synthesized, Forefraction Sample A	98.86	99.01	288.6
Synthesized, Forefraction Sample B	99.51	N.D.	289.3
Eastman, 2 × G.S. Main Fraction	99.77	N.D.	289.8
Aldrich, 2 × G.S. Main Fraction	N.D.	99.85	288.9
Synthesized, 1 × G.S. Main Fraction	99.88	99.93	290.4
Synthesized, 2 × G.S. Main Fraction Sample A	99.95	99.98	290.1
Synthesized, 2 × G.S. Main Fraction Sample B	99.91	99.96	290.4
Synthesized, 2 × G.S. Main Fraction Sample C	99.90	99.95	290.1

fraction, indicating that this procedure removed a more volatile impurity. In general, the calculated melting point increased with purity, the scatter in the data being due to the inaccuracy of the temperature sensor, ±0.5°C.

Accuracy of these results was reduced by using a relatively fast heating rate, 2°C/min, to minimize the time that TCNQ existed in the molten state.

It must be emphasized, however, that the purities quoted in this table cannot be considered absolute measures of purity due to the restrictions discussed previously, but can be considered as a consistent set of relative values.

DSC ANALYSIS OF TTF

The foregoing discussion of the applicability of DSC to analysis of TCNQ holds also for TTF, except that TTF appeared to be thermally stable in the melt and hence was run in regular crimped aluminum pans. FIGURE 2 illustrates the variation in DSC thermograms for samples of widely differing purity.

To check the reproducibility of the DSC technique, six samples were run from the same batch of TTF. The results are shown in TABLE 4. Excellent reproducibility was obtained for TTF first-run data in purity, T_0, ΔH_f, and fractional area correction, with the following average values obtained: purity = 99.99 ± 0.01%, m.p. 119.4°C, ΔH_f = 4.28 Kcal/mole.

Second-run data for this series were interesting in that they showed consistently lower values of all quantities measured together with a larger fractional area correction for the least pure samples. These results indicated that slight decomposition of the sample had taken place on melting. Subsequent repeat runs on a high-purity TTF sample in a hermetically sealed pan confirmed the fact that TTF decomposes slowly in the melt. The results obtained above indicate that this

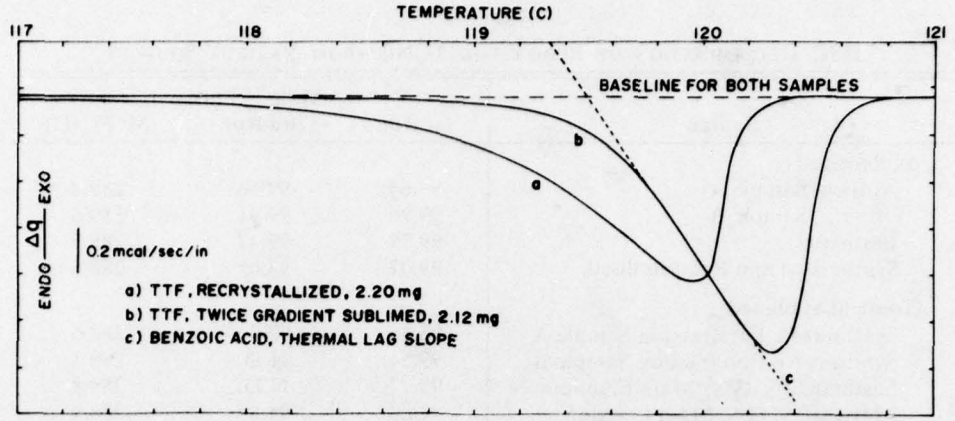


FIGURE 2. DSC thermograms for two samples of TTF. a: TTF synthesized and recrystallized; b: TTF synthesized, recrystallized and ×2 gradient sublimed.

is not a serious analytical problem, provided the sample is melted for the minimum time possible. Thermal decomposition of TTF was also observable by gas chromatographic analysis.

The results of DSC purity analyses for our synthesized TTF at different stages of purification are shown in TABLE 5. The highest measurable purity was obtained only after two gradient sublimations. Samples a), b), and c) were prepared by three different chemists using the same synthetic route. Samples d) and e) were from the same batch in which two polymorphs were obtained in the forends of the sublimation. Both samples behaved identically, with only a small difference in

TABLE 4

REPRODUCIBILITY OF DSC DETERMINATION OF PURITY IN TTF

Sample	Wt. (mg.)	Purity %	T_0 (C)	ΔH_f (Kcal/mole)	% Area Correction
1st Run					
1	2.15	99.99	119.5	4.35	0
2	2.11	99.99	119.4	4.31	0
3	2.11	99.99	119.5	3.97	0.55
4	2.02	99.98	119.4	4.63	0
5	2.10	99.98	119.5	4.33	0
6	2.12	99.99	119.3	4.11	0
		99.99	119.4	4.28	
2nd Run					
1	2.15	99.96	119.5	4.21	2.31
2	2.11	99.98	119.4	4.40	0
3	2.11	99.95	119.5	3.86	4.6
4	2.02	99.97	119.4	4.41	0
5	2.10	99.94	119.5	4.09	5.18
6	2.12	99.98	119.4	3.97	0
		99.96	119.4	4.16	

purity being observed. As expected, sample f), the forend of a once-gradient-sublimed sample, is less pure than samples a), b), and c), and sample g), recrystallized only, gave the lowest measured purity.

TTF has recently become commercially available (Aldrich Chemical Co.) and preliminary work with it indicates that high purity is easily achievable by gradient sublimation.

Liquid Chromatography

Chromatography is a technique in which completely different mechanisms of purity determination are used and represents a method of identification complimentary to thermal analysis. In this technique individual molecular species can be detected.

High-pressure liquid chromatography (HPLC) has recently been developed[15]

Table 5

DSC Determination of Purity for TTF from Various Sources*

Source	Purity %	T_0 (C)	ΔH_f (Kcal/mole)	% Area Correction
A: R + 2 × G.S.	99.99	119.6	4.36	0
B: R + 2 × G.S.	99.99	119.6	4.42	0
C: R + 2 × G.S.	99.99	119.6	4.22	1.5
D: R + 2 × G.S. Forend (yellow)	99.97	119.6	4.72	2.0
E: R + 2 × G.S. Forend (red)	99.90	119.7	4.52	6.55
F: R + 1 × G.S. Forend	99.86	—	—	—
G: R	99.79	119.3	3.78	6.8

*R = Recrystallized; G.S. = gradient sublimed.

to the stage where it can equal the speed and sensitivity of gas chromatography for nonvolatile species that cannot be examined by GC.

Both neutral TTF and TCNQ and TTF-TCNQ have been studied with a DuPont 830 liquid chromatograph with a standard 254 nm UV detector. Initially, HPLC columns utilizing adsorption, normal partition, and reversed phase partition separation mechanisms were used. Column packings included one meter lengths of Permaphase® bonded ODS®, PSP®, ANH®, and ETH® (2 meters) on Zipex® support, 0.25 m ODS® on Zorbax®, and 0.25 m Zorbax-Sil (all E. I. DuPont and Co. trademarks), and a one-foot Partisil M9 ODS column (Whatman). All of these columns were tried with solvents ranging in polarity from hexane to methanol. In no case was an acceptable chromatogram obtained due either to nonretention or degradation on the column. In the case of column degradation, similar degradation patterns were observed for all samples and no additional peaks were observed that could be attributed directly to an impurity. In the cases where no retention of the main component took place, there was no evidence for impurities with longer retention times.

Some degree of success was achieved by yet another method of separation, steric exclusion chromatography[16] (also known as gel permeation chromatography). In this technique, which was primarily developed for separation of polymer molecules according to their molecular weight, a column is packed with porous particles having a closely controlled pore diameter. Molecules passing through the column are separated on the basis of their molecular size. Large molecules cannot enter the pores and are not retained on the column. Smaller molecules enter the pores and are held on the column, having retention times inversely proportional to their size. There is, however, a limiting retention time at which every molecule below a certain size will be eluted. This is dependent on the average pore diameter. Columns have recently been developed with very small pores, enabling molecules with molecular weights of less than 100 to be separated.[17]

The system used for separation of TTF and TCNQ was a 2 ft × 3/8 in 100 Å microstyragel column (Waters Associates) adapted to the DuPont 830 LC. The solvent used was tetrahydrofuran (THF). This system has also been used by Gemmer *et al.*[18]

It was imperative that the THF used be as pure as possible, since spurious peaks were observed when reagent grade solvents were used. THF (Burdick and Jackson, distilled in glass) was further dried and purified by treatment with lithium aluminum hydride followed by slow fractional distillation under nitrogen and used immediately or stored in a well-stoppered flask in the dark.

The results of steric exclusion chromatography are best illustrated by the chromatograms obtained. FIGURE 3 shows the chromatogram of TTF-TCNQ-

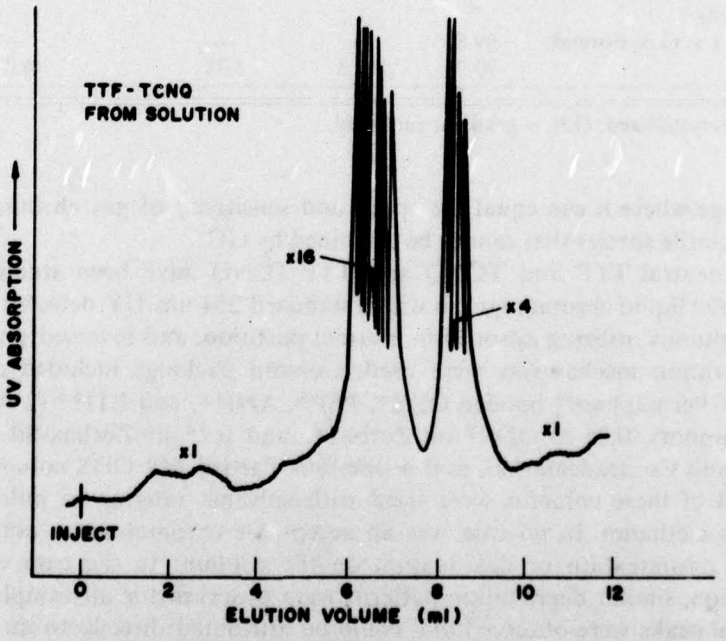


FIGURE 3. Liquid chromatogram of TTF-TCNQ salt run on a 100 Å μ Styragel column eluted with tetrahydrofuran.

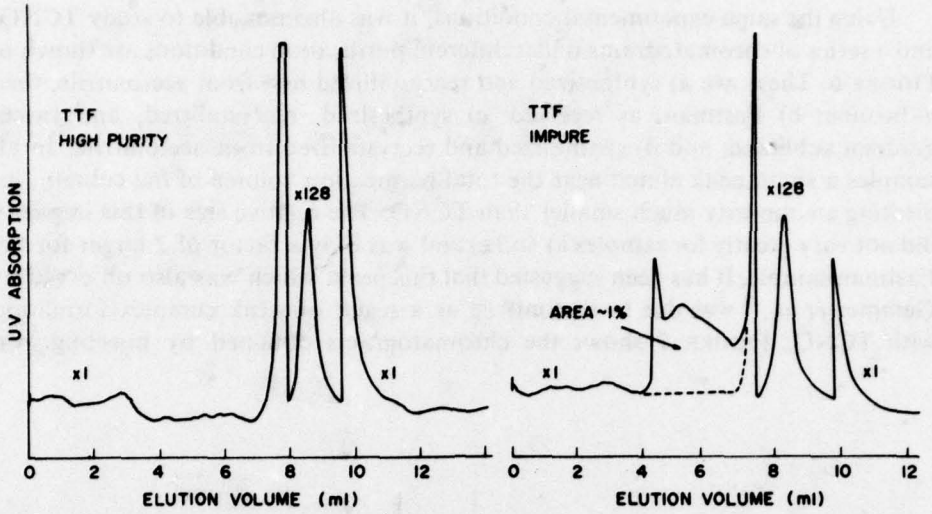


FIGURE 4. Liquid chromatograms of neutral TTF run on a 100 Å μ Styragel column eluted with tetrahydrofuran. a: Synthesized, recrystallized, ×2 gradient sublimed; b: second crop recrystallized from Acetonitrile.

saturated solution in THF. It appears that the complex dissociates into its primary components, which are completely separated. The relatively low signals obtained were caused by our limiting injection volume, 10 $\mu\ell$. No impurities can be detected at this concentration. In an attempt to see trace level impurities we studied the pure components TTF and TCNQ. FIGURE 4 shows chromatograms of two samples taken from the same preparation of TTF. Sample a) was gradient-sublimed three times and showed no detectable impurities, whereas sample b) from the second crop of recrystallized-only material showed significant quantities of impurities totalling ~1% on an area basis. (Since a UV detector was used, it is impossible to calculate the exact concentration of an impurity unless its extinction coefficient at 254 nm is known). These impurities were of higher molecular weight than TTF but were not characterized further, since they are readily removed by gradient sublimation to an undetectable level (less than 10^{-4} mole fr.). The impure sample of ~1% impurity concentration by area can be compared with the DSC determined value for recrystallized-only material of 0.2 mole %.

Unfortunately, TTF eluted near the total permeation volume of the cell; hence molecules smaller than TTF cannot be detected. In fact, this technique can detect only impurity molecules that are significantly larger than TTF. This is illustrated in FIGURE 5, which is a chromatogram of 2,3-dimethyl-TTF (ATTF) on which the chromatogram of TTF has been superimposed. The overlap is such that it would be impossible to distinguish the presence of both components in the same sample. Note, however, that a small impurity peak of high molecular weight was easily distinguishable in ATTF. This may be a telomeric species formed by partial polymerization in solution. The sensitivity of this technique is such that impurity concentrations less than 10^{-4} mole fraction should be detected, providing they have an extinction coefficient at least equal to that of TTF.

Using the same experimental conditions, it was also possible to study TCNQ, and a series of chromatograms under different purification conditions are shown in FIGURE 6. These are a) synthesized and recrystallized first from acetonitrile, then *p*-dioxane; b) Eastman, as received; c) synthesized, recrystallized, and twice-gradient sublimed; and d) synthesized and recrystallized from acetonitrile. In all samples a small peak eluted near the total permeation volume of the column, indicating an impurity much smaller than TCNQ. The relative size of this impurity did not vary greatly for samples a) and c) and was only a factor of 2 larger for the Eastman sample. It has been suggested that this peak, which was also observed by Gemmer *et al.*,[18] was due to acetonitrile as a result of weak complex formation with TCNQ. FIGURE 7 shows the chromatograms obtained by injecting two

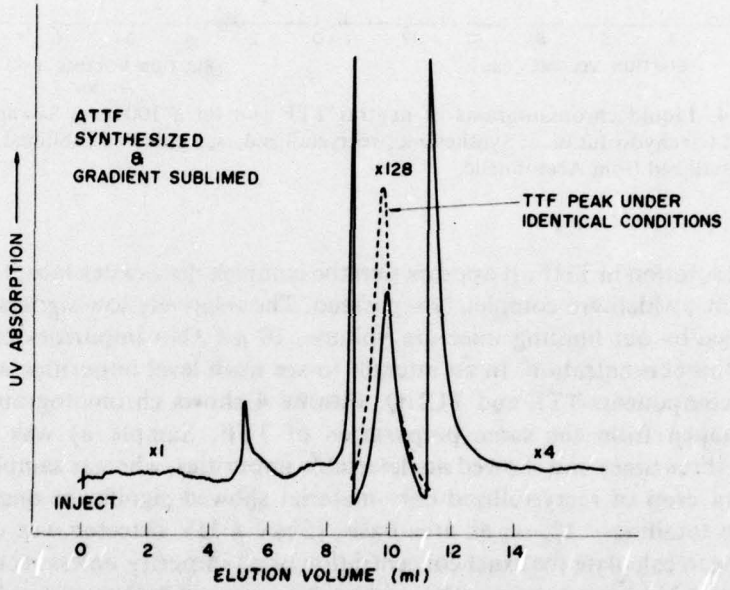


FIGURE 5. Liquid chromatogram of 2,3-dimethyl-TTF (ATTF) run on a 100 Å μ Styragel column eluted with tetrahydrofuran.

samples of pure acetonitrile. In addition to calibrating for the total permeation volume of the column, (~8.5 mℓ) it was observed that even at high injection concentration the UV detector response was only on the x 1 scale and was due not to UV absorption but to a change in the refractive index of the liquid in the cell. Hence acetonitrile cannot cause the small peaks observed in FIGURE 6 a), b), and c), and especially not the peak observed in d), which is more likely caused by small molecule impurities in this sample. The continued presence of this small peak after purification may be due to column degradation caused by impurities in the THF. FIGURE 8 shows a chromatogram of the same material used in FIGURE 6 c), except that the THF used had previously been cycled through the column and then re-purified by $LiAlH_4$ treatment and distillation. The major TCNQ peak has been

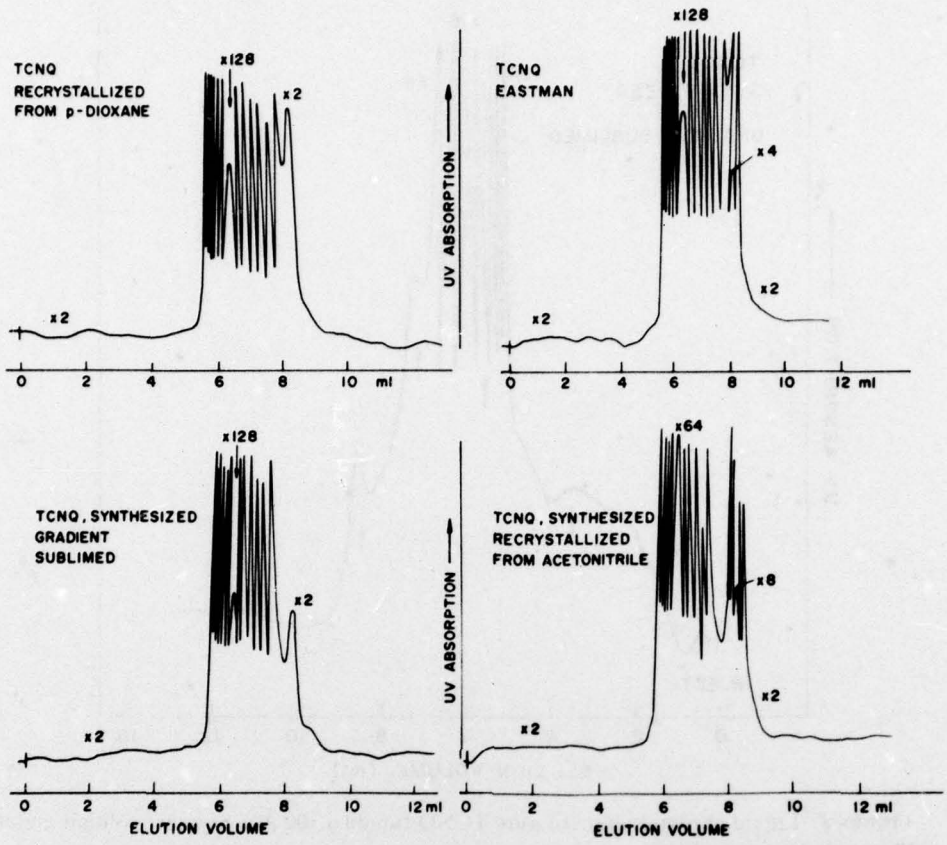


FIGURE 6. Liquid chromatograms of TCNQ run on a 100 Å μ Styragel column. a: Synthesized, recrystallized from Acetonitrile and p-Dioxane; b: Eastman, as received; c: synthesized, recrystallized and $\times 2$ gradient sublimed; d: synthesized and recrystallized from Acetonitrile.

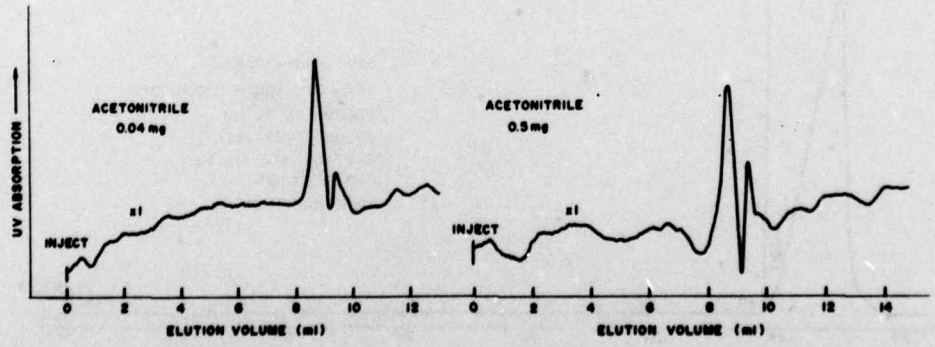


FIGURE 7. Liquid chromatograms of acetonitrile run on a 100 Å μ Styragel column eluted with Tetrahydrofuran.

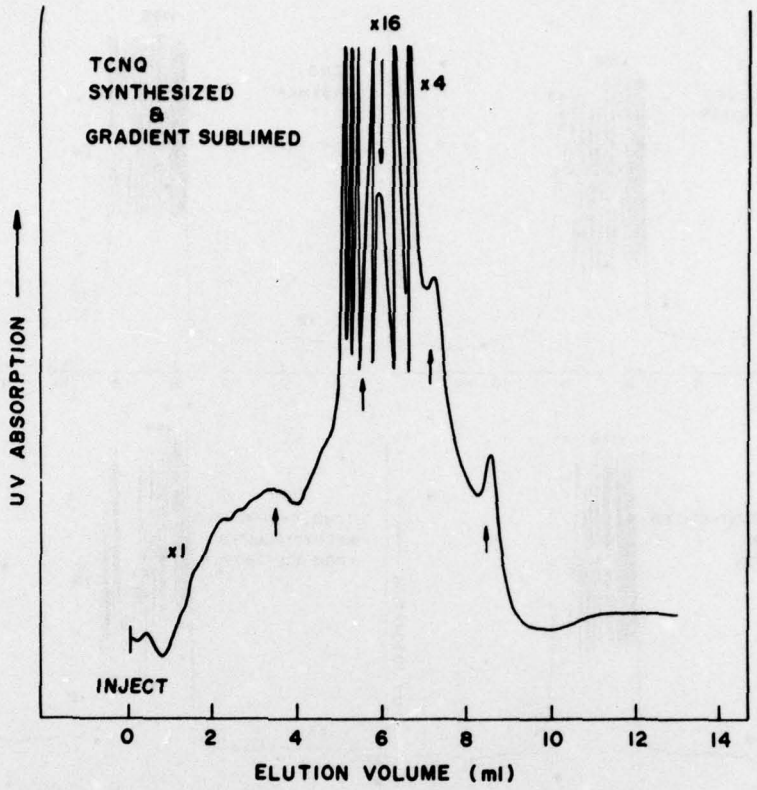


FIGURE 8. Liquid chromatogram of pure TCNQ run on a 100 Å μ Styragel column eluted with impure tetrahydrofuran.

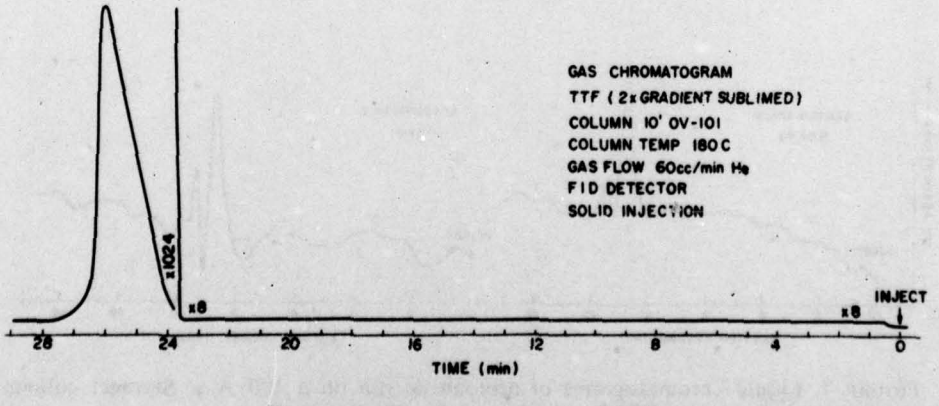


FIGURE 9. Gas chromatogram of TTF.

greatly reduced in intensity, and three other peaks appeared in the chromatogram. These effects were due solely to the use of impure solvent. Hence it does not seem unreasonable to consider the impurity peak in TCNQ as a solvent-related effect. In addition, it should be noted that the TCNQ peaks in FIGURE 6 are skewed: This should not be the case for a pure steric exclusion mechanism which yields symmetrical peaks and may be caused by either an additional adsorption mechanism, which would increase the retention time, or a continuing degradation on the column, which would also give a skewed peak.

In conclusion, we would say that within the acknowledged limits of the steric exclusion separation technique the purification of both TTF and TCNQ, which have been carefully synthesized, recrystallized, and multiply gradient-sublimed, results in materials whose purity approaches the detection limit of the technique.

GAS CHROMATOGRAPHY

The usefulness of gas chromatography was impaired by the thermal decomposition of both TTF and TCNQ. Decomposition of TTF, however, was sufficiently slow that acceptable chromatograms could be obtained. FIGURE 9 shows a chromatogram of twice gradient-sublimed TTF injected as a solid sample. Only one peak was observed whose asymmetry is believed due to slow thermal decomposition on the column yielding a more volatile species which elutes more rapidly. A sample of commercially available TTF gave identical peak shape plus two impurity peaks eluting with retention times of ~one minute, presumably the recrystallization solvent.

TABLE 6

G. C. RETENTION TIMES OF TTF AND RELATED MOLECULES*

Molecule	Retention Time (minutes)
CH_3CH (Acetonitrile)	0.5
TTF	13.0
THTTF (Tetrahydro-TTF)	21.3
ATTF (Dimethyl-TTF)	23.0
TMTTF (Tetramethyl-TTF)	48.0
TPTTF (Tetrapropyl-TTF)	5.0 (decomposition)
$C_3S_3H_2$ (1,3Dithiole-2-Thione)	2.5

*Conditions: P.E. 900 gas chromatograph. Dual column 10 ft × 1/16 in S. S. containing 10% OV-101 on 100/120 GCQ injector 240°C, column 200°C, manifold 230°C injection solvent-acetonitrile. He flow rate 40 cc/min. Flame ionization detector.

The efficiency of the column was checked by comparing the retention times of TTF with those of other TTF derivatives and synthetic precursors. These are included in TABLE 6 in which excellent resolution of all samples examined was achieved. It appears, therefore, that any impurity that does not elute with the same retention time as TTF would be detected in concentration ~ 10^{-4}–10^{-5} mole fraction unless it, too, underwent thermal degradation on the column, resulting in significant broadening of the peak which prevented detection.

Miscellaneous Instrumental Techniques

In addition to the techniques described, other instrumental analyses have been made from which additional information has been obtained. No exhaustive studies, however, have been carried out.

Analysis for metallic impurities in TCNQ was made by standard atomic absorption spectroscopy. TCNQ was analyzed for the presence of sodium, using NaTCNQ as calibration standard. It was concluded that no detectable sodium was present, i.e., <5 ppm. This has been additionally confirmed by E.S.R. and magnetic susceptibility measurements and extended to include all paramagnetic impurities.

Analysis for impurities with different half-wave potentials was made by differential pulse polarography while determining the half-wave potentials of TTF and TCNQ. In neither case could additional impurity peaks be observed.

Preliminary mass-spectral studies have given no indication of easily detectable impurities; however, further detailed studies are required.

Finally, in studies of the optical properties of TTF-TCNQ crystals and the neutral species, no impurity effects were observed in high-purity crystals.

Conclusion

In general, our instrumental analyses have demonstrated that the TTF-TCNQ samples do not contain impurities greater than 10^{-4}–10^{-5} mole fraction. These findings corroborate the early results from a variety of physical measurements,[19] that the impurity levels in the TTF-TCNQ samples are low, and support the finding that intrinsic properties can be measured in these materials when they are prepared, purified, and handled in accordance with the procedures previously described.

It has been a general observation that large, well-formed crystals of TTF-TCNQ are obtained only when high-purity donor and acceptor are used and that small dendritic fibers result from impure materials. It is clear therefore that the physical perfection of TTF-TCNQ crystals is dependent both on the chemical purity of the reactants and the growth conditions.

Notes and References

1. Coleman, L. B., M. J. Cohen, D. J. Sandman, F. G. Yamagishi, A. F. Garito & A. J. Heeger. 1973. Solid State Commun. **12:** 1125.
2. Ferraris, J., D. O. Cowan, V. Walatka, Jr. & J. H. Perlstein. 1973. J. Am. Chem. Soc. **95:** 948.
3. Khanna, S. K., E. Ehrenfreund, A. F. Garito & A. J. Heeger. 1974. Phys. Rev. B **10:** 2205.
4. Melby, L. R., W. R. Hartzler & W. A. Sheppard. 1974. J. Org. Chem. **39:** 2456.
5. Acker, D. S. & W. R. Hertler. 1962. J.A.C.S. **84:** 3370.
6. Yamagishi, F. G., D. J. Sandman, A. F. Garito & A. J. Heeger. 1974. 167th ACS Nat. Mtg. Paper ORGN 012. Los Angeles, Calif.
7. McGhie, A. R., A. F. Garito & A. J. Heeger. 1974. J. Cryst. Growth **22:** 295.
8. Nigrey, P. J. J. 1977. J. Cryst. Growth. **40:** 265.

9. Elemental Analyses performed by Galbraith Laboratories, Knoxville, Tenn.
10. SCHWAB, F. W. & E. WICHERS. 1940. J. Res. Nat. Bureau Standards **25:** 747.
11. MCGHIE, A. R. 1976. J. Chem. Ed. **53:** 637.
12. BARRALL, E. M., JR. & J. F. JOHNSON. 1970. *In* Thermal Characterization Techniques. P. E. Slade and L. T. Jenkins, Ed.: 28. Marcel Dekker, N.Y. N. Y.
13. MCGHIE, A. R. 1974. Mol. Cryst. Liquid Cryst. **27:** 437.
14. G. CASTRO. Private communication.
15. See, e.g., KIRKLAND, J. J., Ed. 1971. Modern Practice of Liquid Chromatography. Wiley-Interscience. New York, N.Y.
16. MOORE, J. C. 1964. J. Polymer Sci. Part A **2:** 835.
17. KRISHEN, A. & R. G. TUCKER. 1977. Anal. Chem. **49:** 898.
18. GEMMER, R. V., D. O. COWAN, T. O. POEHLER, A. N. BLOCH, R. E. PYLE & R. H. BANKS. 1975. J. Org. Chem. **40:** 3544.
19. See, e.g., Lecture notes in Physics **34:** 1975. One Dimensional Conductors. Springer. New York, N.Y., or COLEMAN, L. B. 1976. Ph.D. Dissertation. Univ. of Pennsylvania. Philadelphia, Pa.

DISCUSSION

CHARLES B. DUKE (*Xerox Webster Research Center, Rochester, N.Y.*): In a previous paper you reported high-temperature drift mobilities. The classic problem for people trying to make measurements on molecular solids, such as TTF or TCNQ, is that chemical methods of determining purity are just insufficient to characterize these materials. Could you comment on purity levels?

MCGHIE: We are talking of impurity levels of much less than 100 ppm and, with the standard instrumental methods, we have been unable to detect them.

J. KOMMANDEUR (*Univ. of Groningen, Groningen, The Netherlands*): There may be a relation between the low-temperature magnetic susceptibility—that is, the so-called Curie peak—at very low temperature, and the purity of your sample.

CRYSTAL PERFECTION AND THE PHYSICAL PROPERTIES OF TTF-TCNQ*

Lawrence B. Coleman

Department of Physics
University of California, Davis
Davis, California 95616

The temperature dependence and absolute value of the dc conductivity of tetrathiofulvalene tetracyanoquinodimethan (TTF-TCNQ) have been the most exhaustively studied properties of this compound. They have also been the most controversial, because of the wide range of results reported by the many research groups active in the field. This controversy sprung from two sources of experimental uncertainty. The first, which is the subject of this presentation, is the variable level of crystal perfection from sample to sample (and laboratory to laboratory). The second problem is the well-known difficulty inherent in measuring the conductivity of highly anisotropic materials. Discussed at length in the literature,[1-5] the problem will not be discussed here.†

The central question is, what is the intrinsic dc conductivity of TTF-TCNQ? Room-temperature conductivities have been measured between 100 and 1000 $(\Omega\text{-cm})^{-1}$, and the spread in the temperature dependence of the conductivity is demonstrated in FIGURES 1 and 2. We maintain that this varied behavior is due to widely different levels of crystal perfection (both chemical and structural) from sample to sample. Because the perfect crystal of TTF-TCNQ has yet to be produced, we must determine the intrinsic conductivity by first exploring the effects of imperfection and then using this information to extract the conductivity from the measured values.

To accomplish this, a two-pronged attack was launched. First, an effort was made to produce higher quality samples, both chemically (this effort is reported on in the previous talk[6]) and physically by an investigation of the crystallization of TTF-TCNQ, which led to a model of the crystal growth and the production of larger and more perfect single crystals. Secondly, conductivity studies using samples of various levels of macroscopic crystal perfection and purity were made, to elucidate their effects on the conductivity.

CRYSTAL-GROWTH MODEL

Presented in this section is a model of the growth of TTF-TCNQ crystals. Although it is not a microscopic theory on the molecular level,[7] it has proved useful

*This work was done with the financial support of the National Science Foundation, Laboratory for Research on the Structure of Matter. Manuscript received June 13, 1977.

†The data presented here are the result of careful measurements, made with full knowledge of the problems of the anisotropic conductor; they are believed to be the intrinsic conductivity of the individual samples.

0077-8923/78/0313-0316 $1.75/1 © 1978, NYAS

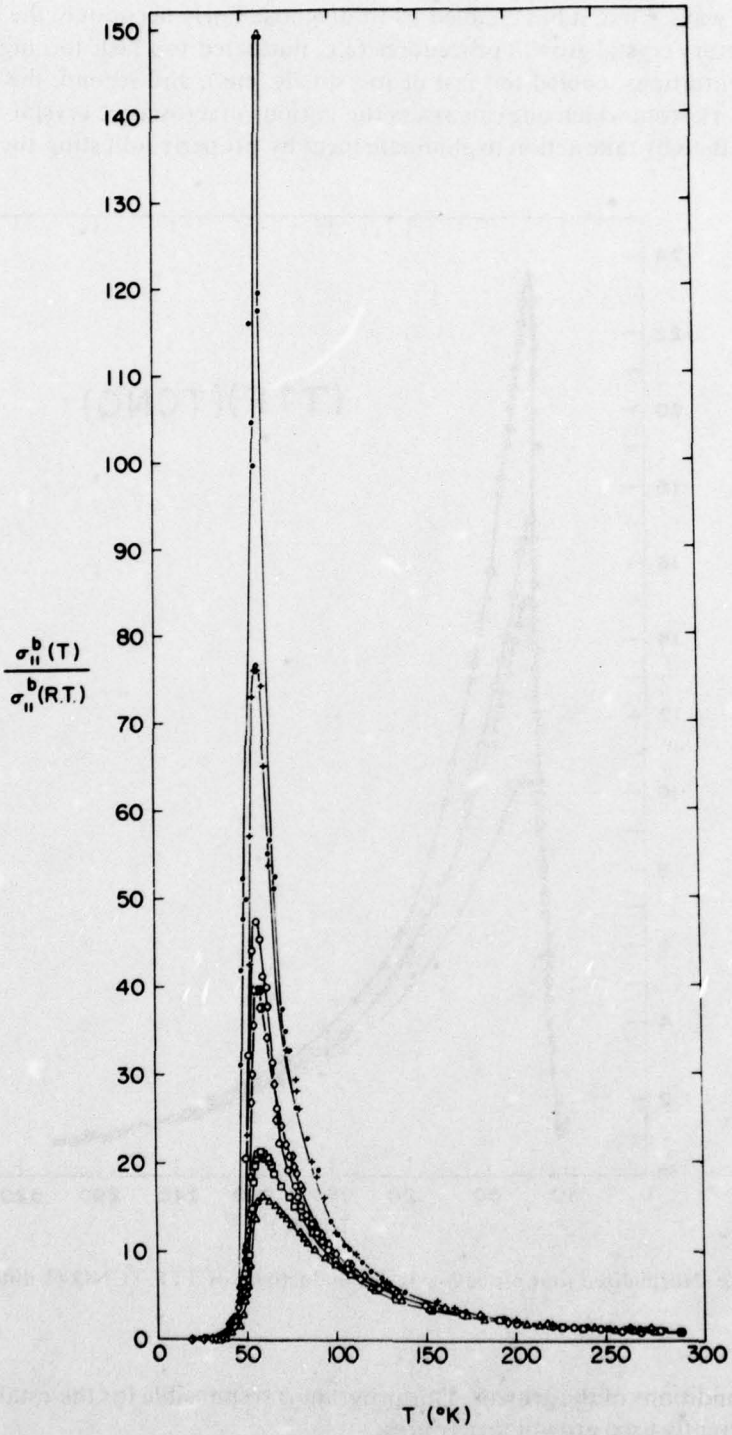


FIGURE 1. Normalized four probe *b*-axis dc conductivity of TTF-TCNQ (6 different samples).

in several ways. First, it has enabled us to diagnose fairly accurately the causes of unsatisfactory crystal growth procedures (e.g. nucleated too fast, too high, or too low concentrations, cooled too fast or too slowly, etc.), and second, the model is a framework from which one can assess the various macroscopic crystal imperfections and thereby take action to eliminate them by properly adjusting the environ-

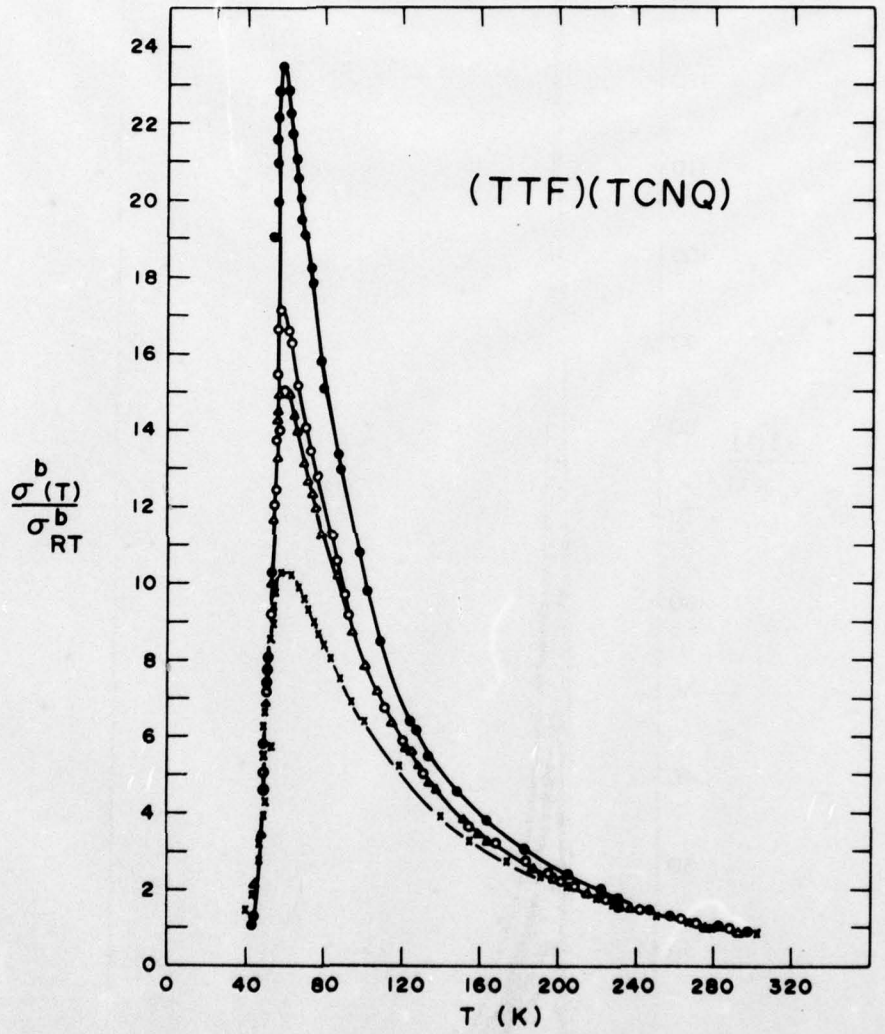


FIGURE 2. Normalized four probe *b*-axis dc conductivity of TTF-TCNQ (4 different samples).

mental conditions of the growth. This program is responsible for the establishment of the currently used growth procedures.

The growth of crystals is controlled by the environmental conditions in the mother liquor. TTF-TCNQ crystals are grown by a combination of solution diffusion and slow cooling; the exact procedure is described elsewhere.[5,8] In this pro-

cedure, both the temperature of the solution and the concentration of the solute are time dependent. In addition, the concentration of the two components, TTF and TCNQ, are spatially dependent. Therefore, at the center of the diffusion apparatus, the concentration is increasing while the temperature is decreasing. It is unlikely that the diffusion rates for the two molecules are equal; therefore, we expect that the initial nucleation will not occur in the center of the apparatus or in an equal concentration of TTF and TCNQ molecules. In fact, the location of the first crystals to appear varies, depending on the manner in which the experiment is prepared and subsequently handled. The dynamic situation that exists in the crystal-growing apparatus is thus completely different from that in the usual methods described in the literature for growing large single crystals, where the temperature and concentration are held as constant as possible. As a result, the crystal growth process in TTF-TCNQ is not expected to be a steady, uniform growth of crystals.

The crystal-growth model was produced by examining (reflectance and transmission optical microscopy, and scanning electron microscopy) large numbers of crystals from many different growth procedures, including several that were aborted early, or were undersaturated so as to reproduce the conditions at the early stages of growth. In addition, through close cooperation with P. J. Nigrey (who was responsible for the preparation and maintenance of the crystal-growing experiments), new preparations were examined and notes made of the initial conditions and life history of the mother liquor; hence, growth peculiarities and the level of crystalline perfection could be correlated with the growth parameters. This procedure resulted in the ability to diagnose problems in the crystal-growing method from an examination of the products.

Several empirical findings were produced in this manner. The relative growth rates of the (100) and (010) faces are concentration dependent. In supersaturated solutions, the growth rate in the *b* direction is faster than that in the *a* direction, whereas in less concentrated solutions the opposite is true. This observation is the key to the crystal growth model as presented below, and explains the creation of the transverse habit in low-concentration solution or vapor-growth procedures. In addition, it was found that the most perfect crystals in a given batch were produced in close proximity to the TCNQ flask of the diffusion apparatus. Several possible explanations of this behavior can be proposed. The TCNQ may be acting as a "counter impurity" to negate the effects of an impurity in the solution; or, in a TCNQ-rich solution the amount of ionized TTF may be greater, leading to more perfect growth (this following the results of Chaudhari, *et al.*[9]); or, the TCNQ may be acting as a poison, being absorbed on the faces and slowing crystal growth down sufficiently for more orderly growth to take place. An attempt was made to improve the overall perfection of the crystal growth by increasing the concentration of the TCNQ solution; however, no significant or observable general increase in crystal perfection was seen.

A flow-chart of the growth of a TTF-TCNQ crystal is displayed in FIGURE 3.

While the intricacies of nucleation remain a mystery, the visual evidence indicates that the neonatal crystallite is a needle-shaped object, elongated *b*. At this stage of the diffusion process the concentration of solutes is still small; therefore, growth is primarily in the *a* direction. If the concentration remains low, the growth will continue primarily along *a*. This accelerating growth in the *a* direction results

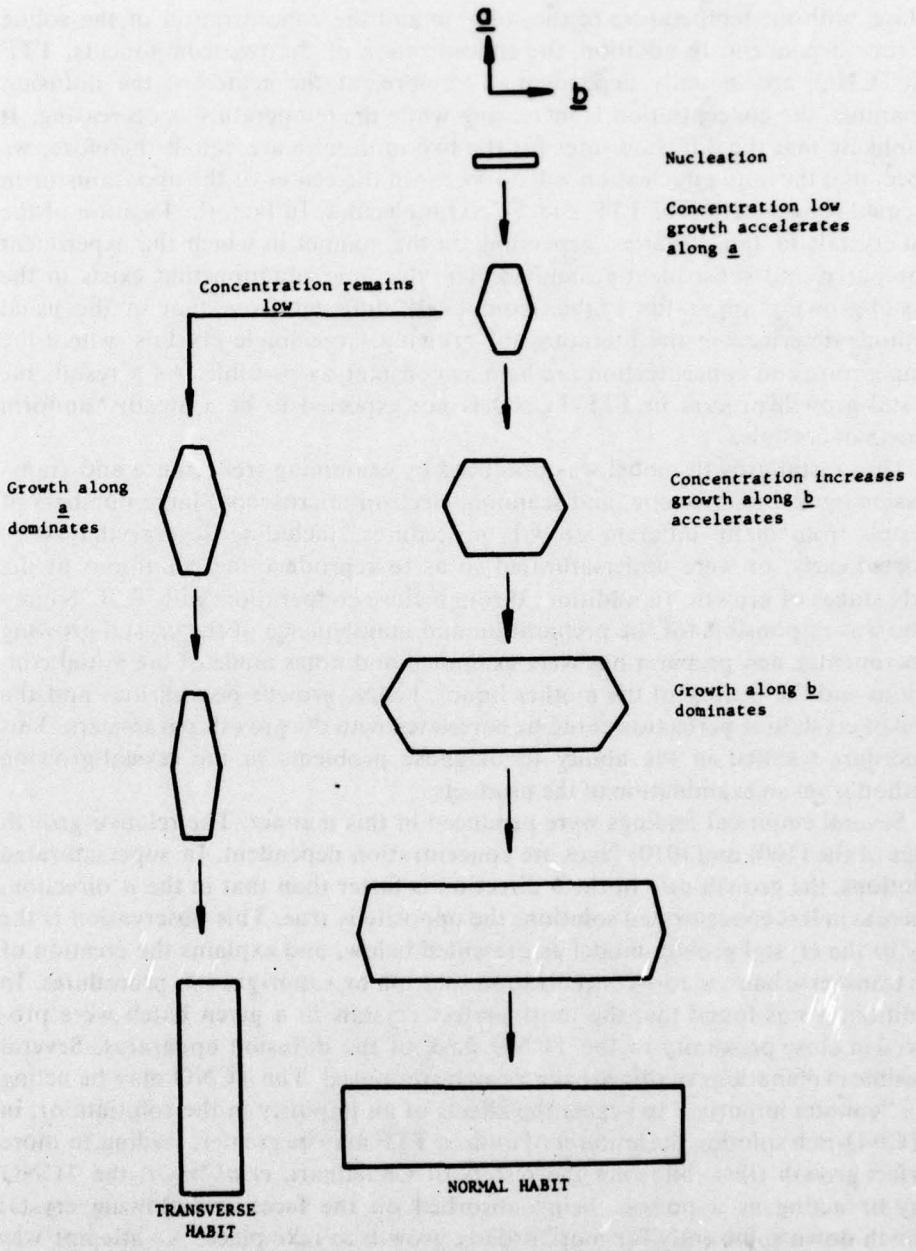


FIGURE 3. Flow diagram of crystal growth process in TTF-TCNQ, for perfect crystal growth.

in the formation of approximately hexagonal-shaped crystals (see FIGURE 4). If the concentration remains small, the growth will continue primarily along *a*; the hexagonal shape will become elongated along *a*, resulting in the creation of a transverse habit crystal. If, however, as usually occurs, the concentration steadily increases, the growth rate along *b* will accelerate, the hexagonal shape will then

elongate in the *b* direction, and the normal habit will result. Growth along the c^* direction appears to be slow (compared to that along *b* and *a*) and uniform, increasing the crystal thickness to the final value.

Conditions, however, are rarely perfect, and as a result, neither are the crystals.

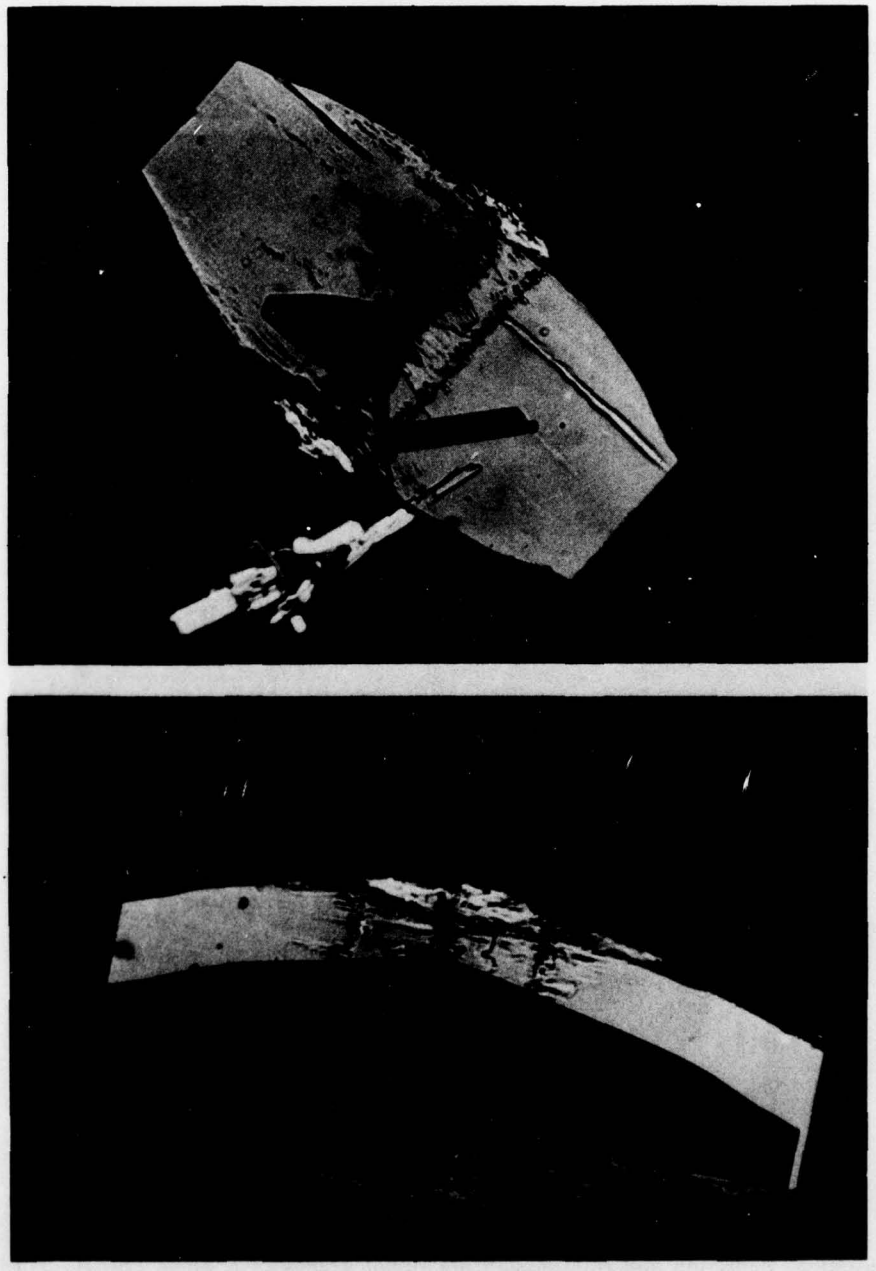


FIGURE 4. Transmission microphotograph of TTF-TCNQ single crystals in early stages of growth. × 430.

Fluctuations or rapid changes in temperature or concentration, along with impurities, will cause modifications of this growth process. Many of these modifications are catastrophic and produce grossly defective crystals or crystals with a variety of growth abnormalities. (Examples of such pathological cases are discussed elsewhere.[5]) Fortunately, the growth of the majority of carefully grown crystals deviates only slightly from the scheme described in the previous section.

In most cases, the nucleation process does not result in the creation of a perfect seed crystal. Photographs of several crystals early in the growth process are shown

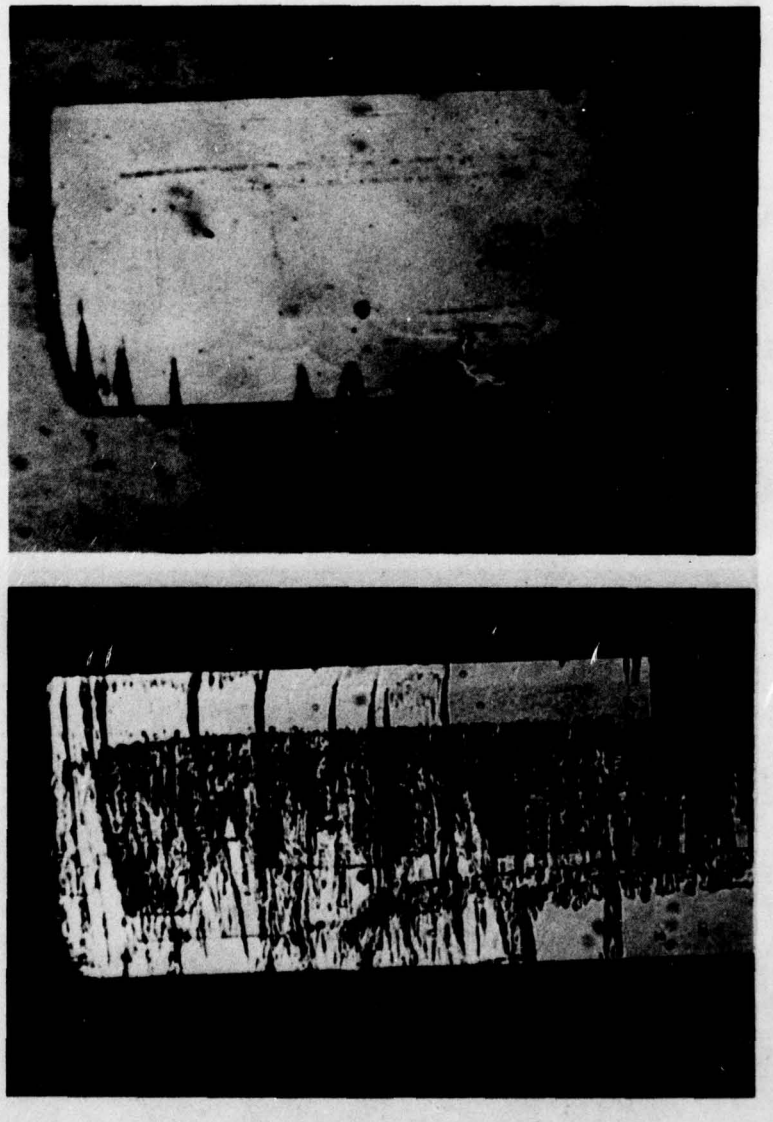


FIGURE 5. Reflection and transmission microphotographs of a single crystal of TTF-TCNQ demonstrating a high level of surface perfection, with large-scale interior defects. × 380.

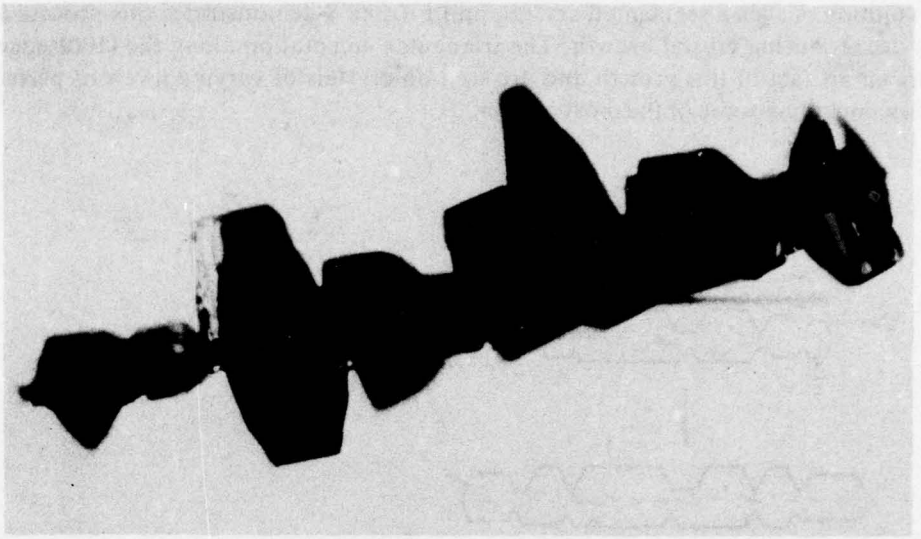


FIGURE 6. Transmission microphotograph of TTF-TCNQ neonatal crystallite, showing common defect. × 480.

in FIGURE 4. As can be seen, although the growth in the *a* direction has resulted in almost perfect regions in the crystal, a clearly defined band of imperfection exists in the center of the crystallite, with the boundaries of the band parallel to the *b* axis. These areas of gross imperfection appear in the exact center of the crystal, and are the result of too rapid an initial nucleation and growth caused by either too high an initial concentration or too rapid a cooling rate. Since rapid growth along the *b* axis occurs on nucleation and during higher concentration situations, this portion of the crystal is more likely to be defected, as opposed to low-concentration growth along the *a* axis (recalling that more perfect growth will usually occur in lower concentrations). When crystals are nucleated slowly, and with no interference, the amount of macroscopic imperfection is minimal.

This tendency for the center of a crystal to be highly defected while the surface may appear of high quality complicates the sample-selection process by demanding transmission microscopic examination. FIGURE 5 is a graphic example of the situation.

Another deviation from perfect growth, while easily observed, is not totally understood. The early manifestation of this growth modification is shown in FIGURE 6. What is seen is a series of roughly hexagonal crystallites growing from the central "nucleation needle," this as opposed to the entire needle taking on a hexagonal shape as growth along *a* accelerates. Several plausible arguments regarding the cause of the segmented growth can be made. The adsorption or entrapment of an "inert" particle could cause a cessation of growth at a point on the needle, as could a dislocation or other imperfection. Another possibility is the existence of large concentration gradients along the needle. Whatever the cause, this deviation is extremely common and residual macrostructure resulting from such growth is seen in almost every crystal examined. FIGURE 7 schematically describes the

evolution of such a segmented crystal, and FIGURE 8 demonstrates this process as it occurs during crystal growth. The triangular indentation along the (100) edges are an artifact of this growth and are seen on crystals of varying levels of perfection, including some of the most perfect.

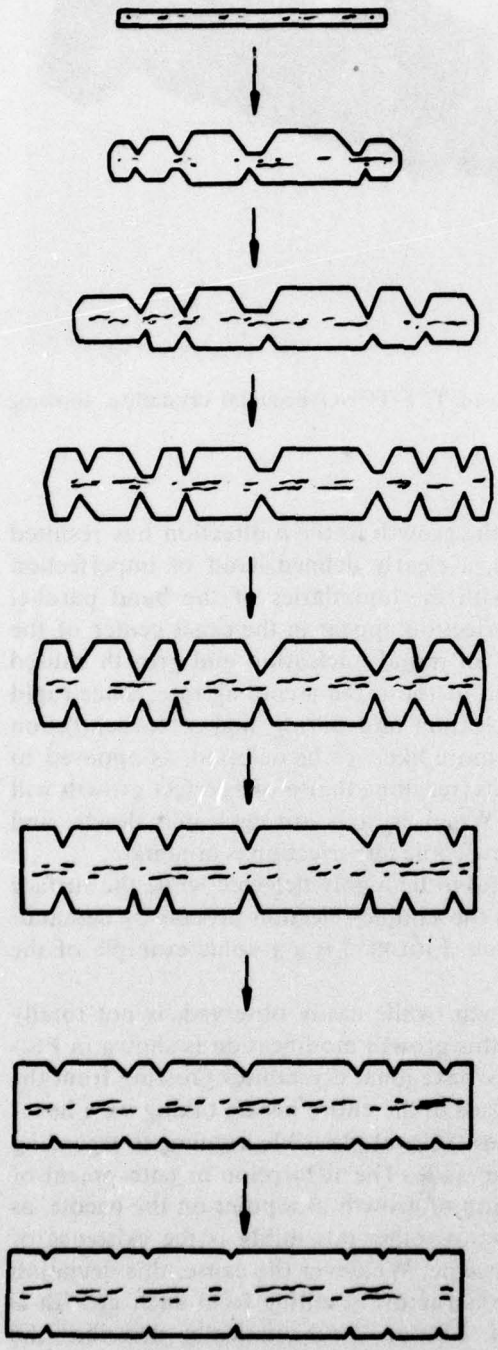


FIGURE 7. Flow diagram of crystal growth process for typical crystal of TTF-TCNQ.

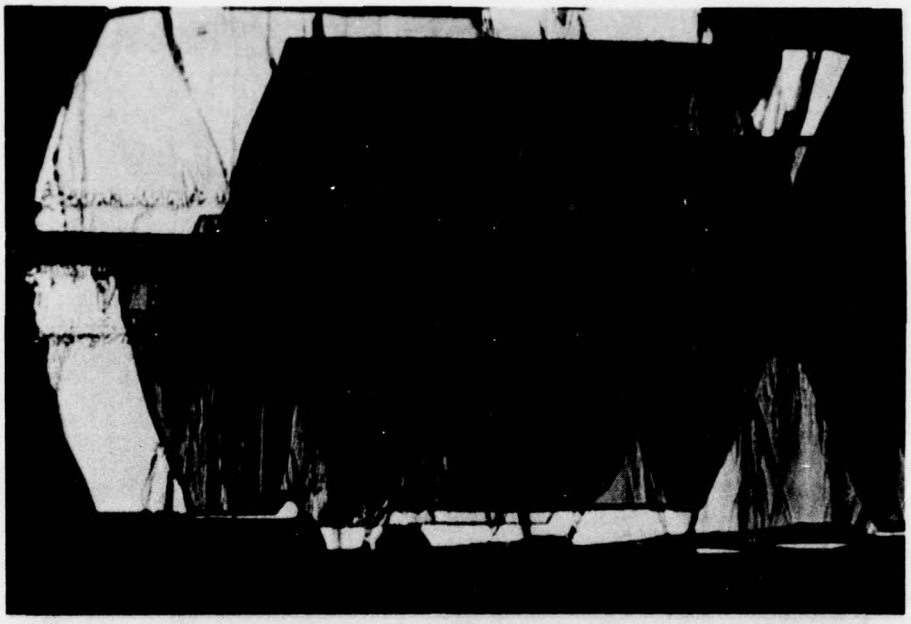


FIGURE 8. Transmission microphotograph of TTF-TCNQ single crystal during growth process. × 310.

Other crystal-growth abnormalities include profuse twinning and layering (along c^*).

The laboratory-to-laboratory universality (or geographic independence) of this model was checked by examining crystals of TTF-TCNQ from other laboratories. A large number of crystals were examined during a visit to the Thomas J. Watson Research Center of the IBM Corporation, and several crystals, kindly supplied by the group at Johns Hopkins University, Baltimore, Md., were also examined; in both cases, the crystals showed the artifacts of the model.

CRYSTAL PERFECTION AND THE *b*-AXIS CONDUCTIVITY

The transmission microphotographs of three crystals of increasing macroscopic crystalline perfection in FIGURE 9 demonstrate the range of crystal quality one is likely to obtain from "naked eye" selection of samples. It is not surprising, therefore, that the dc conductivity in FIGURES 1 and 2 vary over such a wide range.

The evolution of $\sigma_b(T_M)/\sigma_b(RT)$ and T_M (the temperature at which the conductivity maximum occurs) reported in the literature over the past three years is a further indication of the relationship between sample perfection and $\sigma_b(T)$.[3-5]

From a careful study of the macroscopic crystal perfection, it was found possible to *routinely* select samples whose normalized *b*-axis conductivity would exceed 15. It is not possible to predict whether or not a crystal of the level of perfection shown in FIGURE 9c would show a measured conductivity maximum greater

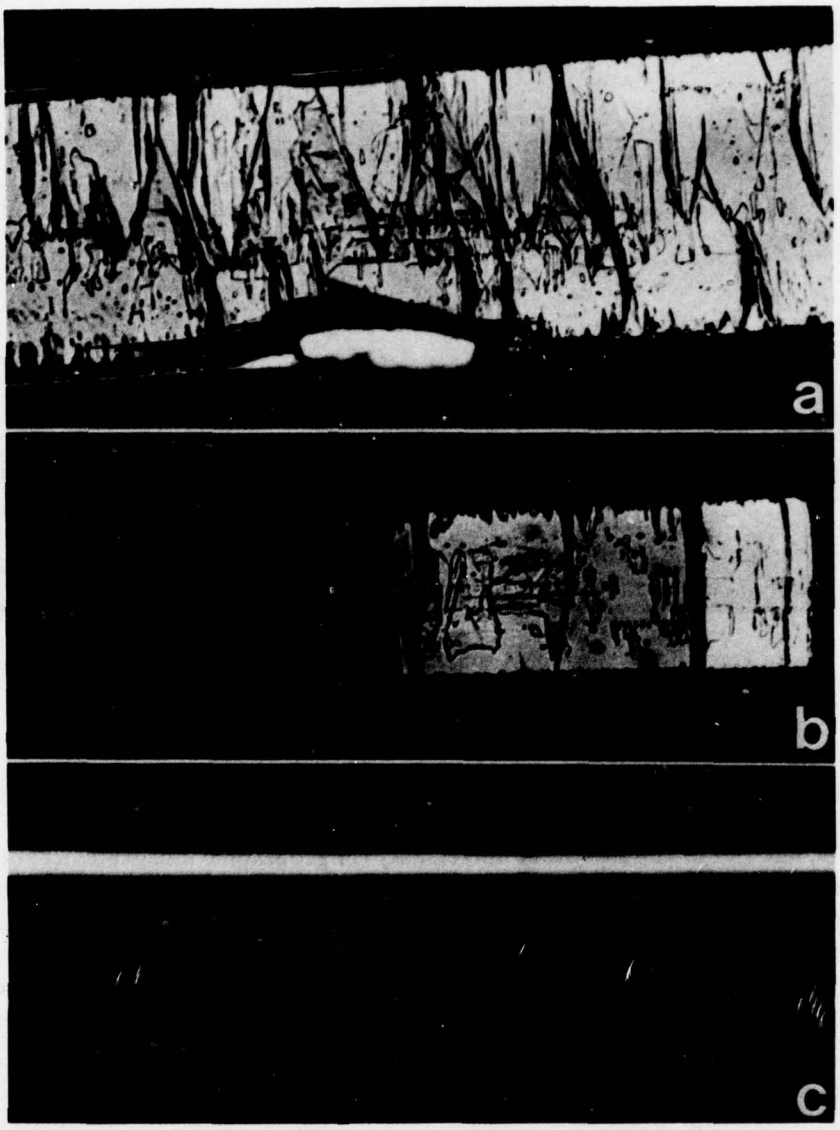


FIGURE 9. Transmission microphotographs of single crystals of varying levels of perfection. a: crystal selected at random; b: crystal selected carefully by "naked eye"; c: crystal selected by transmission microscopy. This crystal is of the highest level of crystalline perfection seen. *a* and *b*, × 240; *c*, × 670.

than 100, but the conductivity maximum of such a crystal would (if carefully handled and mounted) most likely exceed 20. However, crystals with such high levels of imperfection as seen in FIGURES 9a and 9b would certainly display conductivity maxima between 3 and 10. As a result, while conductivity maxima varying in magnitude from 3 to 180 times the room-temperature value have been seen, with careful selection and handling of samples, the majority will show conductivity maxima between 15 and 25 times the room-temperature value.

A variety of experiments were carried out in order to discover how the level of crystal perfection affects the room-temperature conductivity, conductivity maximum, and overall temperature dependence above the metal-semiconductor transition. (With the discovery of nonohmic effects at low temperatures,[10] the effects of impurities on the low-temperature conductivity are complicated and will not be discussed here). Some of the experiments carried out were as follows.

1. A series of impure samples was prepared and $\sigma_b(T)$ studied.
2. Single crystal samples with up to six potential contacts were produced for the study of the variation of $\sigma_b(T)$ over a single sample.
3. Samples were repeatedly thermally cycled so that the effects of added strains and flaws could be studied.
4. Samples were mounted, studied, and then exposed to laboratory air for long periods of time; then $\sigma_b(T)$ was remeasured.
5. Several annealing experiments were attempted.

The effects of nonspecific chemical impurities on $\sigma_b(T)$ were studied by producing a series of samples of varying impurity level. Single crystals of (TTF)(TCNQ) were grown outside the normally used argon-filled glove box, using a variety of starting materials, including only once gradiently sublimed TTF and TCNQ, only once recrystallized Eastman TCNQ, TTF which showed an inferior analysis, nonpurified solvents, and solvents to which a small amount of water had been added. These purposely impure samples exhibited normalized conductivities with maxima ranging from 5.5 to 13.

More important, however, is the relationship between the location of the conductivity maxima (T_M) and the purity of the sample. We have found that in the purest samples, T_M = 57–59 K. While it has been observed that in samples with small values of $\sigma_b(T_M)/\sigma_b(RT)$, T_M is of order 60–62, in impure samples values of T_M as high as 70 K have been observed. Gemmer *et al.*[11] also report an increase in T_M in their experiments involving the addition of small amounts of NaCl to the crystallization solution.

An increase in the value of T_M is also seen when small amounts of TTF and TCNQ derivatives are added, forming solid solutions. The addition of 3% TSeF to (TTF)(TCNQ) results in T_M = 60–64 K[18] and the addition of a small amount (less than 10%) of $TCNQF_4$ to (TTF)(TCNQ) raises T_M to 80 K.[5]

In order to separate the effects of impurity from those caused by imperfection, sample aging studies were performed. In these experiments, single-crystal samples were mounted in the four-probe configuration and $\sigma_b(T)$ measured. Upon return to room temperature, values were remeasured and the samples were removed from the cryostat and stored in the laboratory air for periods up to several weeks. After 48 days in laboratory air, one sample showed no appreciable decrease in $\sigma_b(RT)$; however, the value of T_M had increased 3 K (from 59 to 62 K). In samples where $\sigma_b(T_M)/\sigma_b(RT)$ was initially above 15, decay of the peak value was also seen.

Repeated thermal cycling of a sample mounted for four-probe conductivity measurement adds stress- and strain-created imperfections while leaving the chemical purity constant. The results of a typical experiment are shown in FIGURES 10 and 11. The increased level of imperfections resulted in a precipitous drop in the room-temperature conductivity and maximum conductivity, as well as a shift of T_M from 58 to 130 K.

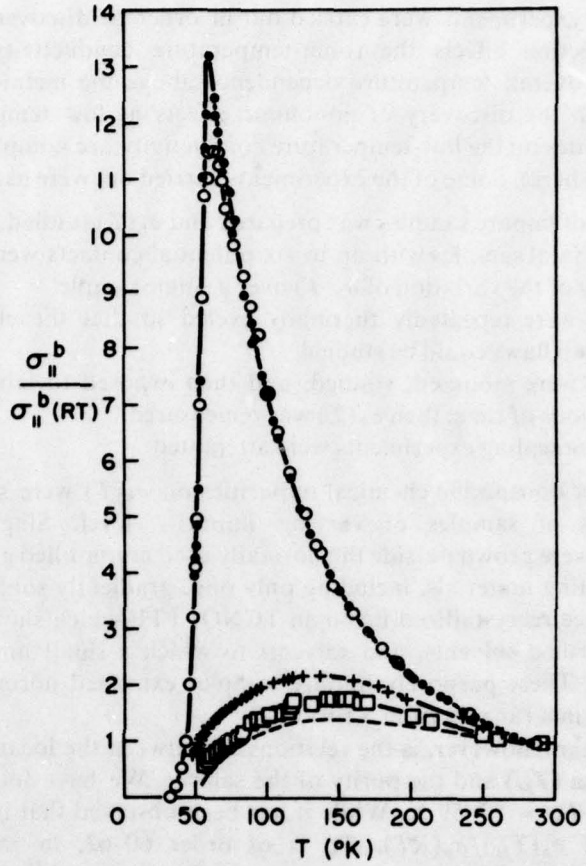


FIGURE 10. Cycling experiment showing degradation of the conductivity maximum: ·–·–· = first cycle; – 0 – 0 – 0 = fourth cycle; + – + – + = sixth cycle; – □ – □ – □ = eighth cycle; – – – – = polycrystalline compaction data.

Recently, more qualitative studies have been completed[12] with use of 8 MeV deuterons to create defects in single crystals of TTF-TCNQ. The results of this controlled addition of imperfections are in agreement with the earlier studies. A dose of radiation which created an estimated defect level of 1000 ppm (0.1%) halved the room-temperature conductivity and increased T_M from 58 to 68 K.

In all the experiments, the 53 K transition was broadened with increasing imperfection level.‡

Attaching multiple pairs of voltage contacts to a single crystal allowed for sampling of $\sigma_b(T)$ over different regions of the crystal. The spread in room-temperature conductivities (usually near 20%) is indicative of the measurement errors;[5] the spread in normalized peak conductivity (usually between 5% and 10%) indicates the reliability of the measurement and the uniformity of the sample.

‡A detailed report of the effects of imperfection on the phase transitions in TTF-TCNQ can be found in Reference 13.

Annealing of samples by heating in an inert atmosphere for eight to ten hours had no observable effect on the conductivity.

To summarize our findings:

1. Chemical impurities and physical defects appear to have the same effects on the conductivity.
2. The temperature at which the conductivity maximum, T_M, occurs is a sensitive measure of the level of imperfection, increasing by a few degrees with small amounts of impurities to as much as 130 K for a large density of defects.
3. The room-temperature conductivity and the maximum conductivity are sensitive to the level of crystal perfection, with only the purest, most physically perfect samples having a conductivity maximum over 25.

To date, analysis of the role of imperfections on the conductivity (or resistivity) has followed the example of metals, fitting the resistivity data to a power law of

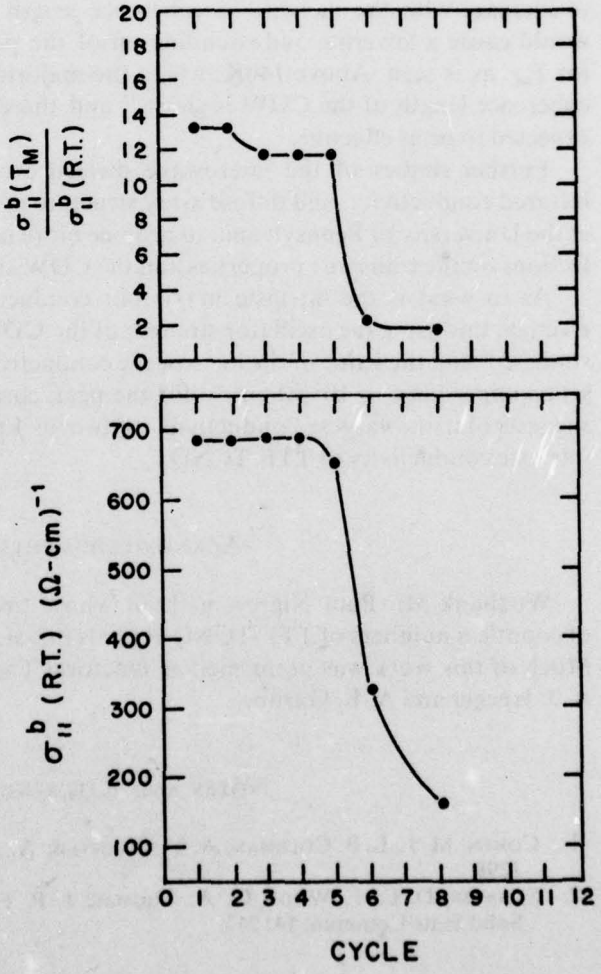


FIGURE 11. Effects of repeated thermal cycling on room-temperature conductivity (lower segment) and $\sigma_b(T_M)/\sigma_b(RT)$ (upper segment).

the form

$$\rho(T) = \rho_0 + \rho_1 T^{\lambda}$$

where ρ_0 is the residual resistance and is expected to contain all the effects of crystalline imperfection. TTF-TCNQ, however, is not simply metallic, and the collective behavior as well as the high anisotropy must be taken into account.

From a simple view, the high anisotropy could be seen as adding small amounts of σ_a and σ_{c^*} to the measured b-axis conductivity whenever an imperfection blocked conduction along a chain. Computer simulations using a variety of temperature dependences for the imperfection contribution to $\sigma_b(T)$ were carried out,[5] and it was found possible to exactly mimic actual data including the increase in T_M with increased imperfection level. However, such computational exercises are probably misleading and do not supply any insight into the microscopic processes that produce the high conductivity.

The lowering of the peak conductivity and shift of T_M to higher temperature can be understood in terms of the collective nature of the charge-density wave (CDW) mechanism. Pinning of the CDW to defects and impurities has been shown to increase with the increase in coherence length of the CDW.[14] Such pinning would cause a lowering and rounding off of the peak along with a higher value for T_M, as is seen. Above 140K, where the majority of data agree quite well, the coherence length of the CDW is short,[15] and therefore pinning by defects is not expected to be as effective.

Further studies of the microwave dielectric constant and conductivity, far infrared conductivity, and diffuse x-ray structure of irradiated samples are planned at the University of Pennsylvania to provide more insight into the effects of imperfections on the transport properties and the CDW state in TTF-TCNQ.

As to what is the intrinsic maximum conductivity of TTF-TCNQ, we can estimate this using the oscillator strength of the CDW found from the far infrared studies[5,16] and the value of the microwave conductivity.[17] From these data, we can set an upper limit of 10^5 $(\Omega\text{-cm})^{-1}$ for the peak conductivity of TTF-TCNQ. This suggests that the largest conductivity shown in FIGURE 1 is indeed close to the intrinsic conductivity of TTF-TCNQ.

ACKNOWLEDGMENTS

We thank Mr. Paul Nigrey, without whose tireless efforts in the production of countless numbers of TTF-TCNQ crystals this study could not have been made. Much of this work was performed as Doctoral Thesis research under Professors A. J. Heeger and A. F. Garito.

NOTES AND REFERENCES

1. COHEN, M. J., L. B. COLEMAN, A. F. GARITO & A. J. HEEGER. 1974. Phys. Rev. **B10:** 1298.
2. SCHAFER, D. E., F. WUDL, G. A. THOMAS, J. P. FERRARIS & D. O. COWAN. 1974. Solid State Commun. **14:** 347.

3. COHEN, M. J., L. B. COLEMAN, A. F. GARITO & A. J. HEEGER. 1976. Phys. Rev. **B13:** 5111.
4. THOMAS, G. A., D. E. SCHAFER, F. WUDL, P. M. HORN, D. RIMAI, J. W. COOK, D. A. GLOCKER, M. J. SKOVE, C. W. CHU, R. P. GROFF, J. L. GILLSON, R. C. WHELAND, L. R. MELBY, M. B. SALAMON, R. A. CRAVEN, G. DEPASQUALI, A. N. BLOCH, D. O. COWAN, V. V. WALATKA, R. E. PYLE, R. GEMMER, T. O. POEHLER, G. R. JOHNSON, M. G. MILES, J. D. WILSON, J. P. FERRARIS, T. F. FINNEGAN, R. J. WARMACK, V. F. RAAEN & D. JEROME. 1976. Phys. Rev. **B13:** 5105.
5. COLEMAN, L. B. 1975. Ph.D. Thesis. Univ. Pennsylvania. Philadelphia, Pa. Unpublished.
6. MCGHIE, A. This volume.
7. THOMAS, J. H. 1973. Nature **244:** 56.
8. NIGREY, P. J. 1977. Int. J. Crystal Growth. To be published. Contains the procedure for the growth of deuterated TTF-TCNQ crystals. The technique used to produce normal TTF-TCNQ single crystals is similar but not identical.
9. CHAUDHARI, P., B. A. SCOTT, R. B. LALBOWITZ, Y. TOMIEWICZ & J. B. TORRENCE. 1974. Applied Phys. Lett. **37:** 1500.
10. COHEN, M. J., P. R. NEWMAN & A. J. HEEGER. 1976. Phys. Rev. Lett. **37:** 1500.
11. GEMMER, R. V., D. O. COWAN, A. N. BLOCH, R. E. PYLE & R. H. BANKS. 1975. J. Org. Chem. **40:** 3544.
12. CHIANG, C. K., M. J. COHEN, P. R. NEWMAN & A. J. HEEGER. 1977. Preprint.
13. CHIANG, C. K., Y. W. PARK & A. J. HEEGER. To be published.
14. LEE, P. A., T. M. RICE & P. W. ANDERSON. 1974. Solid State Commun. **14:** 703; FUKUYAMA, H., T. M. RICE & C. M. VARMA. 1974. Phys. Rev. Lett. **33:** 305.
15. POUGET, J. P., S. K. KHANNA, F. DENOYER, R. COMÉS, A. F. GARITO & A. J. HEEGER. 1976. Phys. Rev. Lett. **37:** 437; KHANNA, S. K., J. P. POUGET, R. COMÉS, A. F. GARITO & A. J. HEEGER. 1977. Phys. Rev. **B16:** 1468.
16. COLEMAN, L. B., C. R. FINCHER, JR., A. F. GARITO & A. J. HEEGER. 1976. Phys. Stat. Solidi. **B77:** 239.
17. KHANNA, S. K., E. EHRENFREUND, A. F. GARITO & A. J. HEEGER. 1974. Phys. Rev. **B10:** 2205.
18. ETEMAD, S. 1976. Phys. Rev. **B13:** 2254.

DISCUSSION

CHARLES B. DUKE: Would you indicate the evidence for splitting the conductivity between charge-density wave and single-particle contribution.

ALAN HEEGER: We really do not know. If you look at the conductivity in the far IR, the conductivity in the range from 20 to 100 cm^{-1} is about 50–100 $ohm^{-1}cm^{-1}$. This provides an estimate of the single-particle contribution. There are ideas around for some low-frequency increase in $\sigma(\omega)$ due to phonon-assisted hopping, and so on, so the single particle contribution could be slightly larger. But I think that it is very difficult to understand the dc conductivity and IR data unless most of the dc conductivity in the vicinity of the peak is collective. At room temperature the two contributions might be comparable.

DUKE: The important experiment that convinces you that it is charge-density waves is that when you compare the ac to the dc conductivity, you notice that as you get close to this peak in the conductivity in temperature, that difference diverges and you find no other way to explain that difference other than by this charge-density wave hypothesis.

HEEGER: Yes; also, there is a structural aspect. The coherence length in the diffuse x-ray studies show that the conductivity is proportional to the growth of coherence and a single-particle contribution should go just the other way.

AARON BLOCH (*Johns Hopkins Univ., Baltimore, Md.*): The resistivity can be decomposed crudely into a constant term which is sample dependent plus another term or series of terms with a power function of temperature, T^{α}, with α being a constant. As one dopes or puts in defects and controlled disorder, does this kind of fit persist? And what maximum conductivity would it alone predict as the intrinsic maximum?

COLEMAN: Yes, one can produce fits to the resistivity data that, by including a temperature-dependent impurity/defect resistivity, do follow the rise in T_M and decrease in maximum conductivity with increased imperfection level (see text and Ref. 5). Such fits do predict maximum conductivities as high as 10^5 $(\Omega\text{-cm})^{-1}$; however, these exercises do not supply any additional insight into the physical processes involved, and I hestitate to put much stock in them.

STRUCTURAL RELATIONSHIPS IN THE HETEROFULVALENE-TCNQ FAMILY OF ORGANIC CONDUCTORS*

Thomas J. Kistenmacher

Department of Chemistry
The Johns Hopkins University
Baltimore, Maryland 21218

INTRODUCTION

The synthesis and structural and electronic properties of organic charge-transfer salts have been the subject of numerous investigations over the past few years. In this laboratory, we set out some time ago to study the structural systematics of such compounds, particularly with regard to derivatives and analogs of the charge-transfer salt formed from TTF (2,2′-bis-1,3-dithiole) and TCNQ (7,7,8,8-tetracyanoquinodimethane). Such charge-transfer salts have been classified as quasi-one-dimensional organic conductors. This generic classification itself deserves some attention. First, the compounds are taken as organic in that they contain only the common, nonmetallic elements C, N, H, S, and Se, arranged into heterocyclic ring systems (FIGURE 1); one of the heterocyclic ring systems functions as a donor and one as an acceptor in an electronic charge-transfer process. Second, the materials are known as quasi-one-dimensional because they have been found to exist in the solid as linear, homogeneous columnar stacks of donor and acceptor molecules. These linear arrays dominate the physical properties of such systems, leading to a highly anisotropic response to external stimuli. The fact, however, that such cationic and anionic chains can be "cocrystallized" into a common three-dimensional lattice causes them to be classified as only quasi-one-dimensional. Lastly, it is commonly observed that the conductivity along the direction of propagation of the linear cationic and anionic chains is substantial, nominally on the order of several hundred $\Omega^{-1}\,cm^{-1}$ at room temperature.

Historically, there are several unusual and interesting antecedents to the subset of materials we will discuss here. For our purposes, however, we will presume that a significant advancement was rendered by the synthesis of what is a most unusual organic conductor, TTF-TCNQ.[1] One of the most important aspects of this material is that both the donor molecule TTF and the acceptor molecule TCNQ are capable of being chemically modified to produce analogs and derivatives that can be systematically and thoroughly studied.

It was with TTF-TCNQ that our structural studies were initiated in 1973. Since that time, we have determined the structural properties of several systems, mainly relying on chemical modification of the TTF molecule. We believe that our studies have laid the groundwork for some general structural relationships that aid in the

*Research supported by the Petroleum Research Fund, administered by the American Chemical Society, the National Science Foundation, and the Advanced Research Projects Agency. Manuscript received May 23, 1977.

0077-8923/78/0313-0333 $1.75/1 © 1978, NYAS

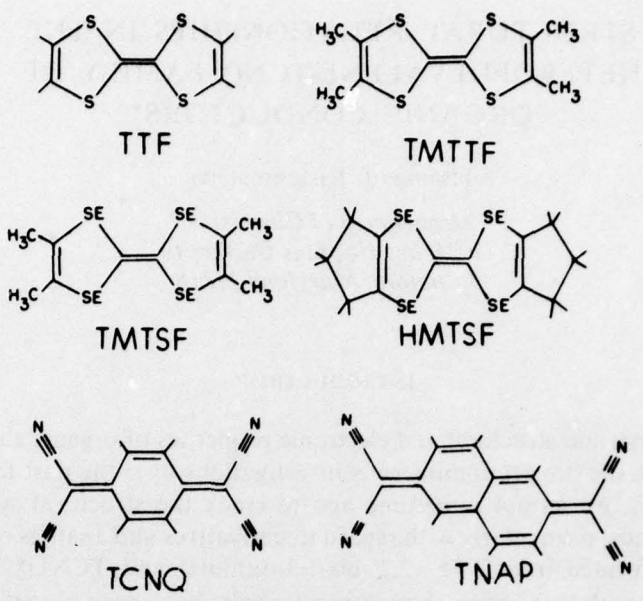


FIGURE 1. Illustrations of the molecular structures for the neutral donor molecules TTF[2,2′-bis-1,3-dithiole], TMTTF[4,4′,5,5′-tetramethyl-2,2′-bis-1,3-dithiole], TMTSF [4,4′,5,5′-tetramethyl-2,2′bis-1,3-diselenole], HMTSF[2,2′-bis(4,5-trimethylene)-1,3-diselenole] and the neutral acceptor molecules TCNQ[7,7,8,8-tetracyano-p-quinodimethane] and TNAP[*11,11,12,12-tetracyanonaphtho-2,6-quinodimethane*].

classification and the determination of the underlying requirements for high conductivity in this class of materials. The common features of these organic salts are as follows: (1) the existence of uniform, separate stacks of cations and anions, (2) and a significant degree of molecular overlap within the cationic and anionic stacks. The differentiation among structures lies primarily in the mode of interchain interactions in the solid state.

It is with these thoughts in mind that we will proceed to review and correlate the accumulated crystallographic information.

MATERIALS

Illustrations of the neutral donor and acceptor molecules we have employed are presented in FIGURE 1. Most of the derivatives are formed, in principle, by the replacement of the exocyclic protons on TTF by methyl groups or, as in HMTSF, by a ring-forming trimethylene bridge. In all cases it is possible to prepare both the thiofulvalene(S) as well as the selenafulvalene(Se) compounds. It should be noted that all of the materials discussed here were prepared in the laboratory of Professor D. O. Cowan, unless otherwise noted. Suitable references can be found in any number of places, including Professor Cowan's paper in these transactions.[2] We will employ, throughout the rest of this paper, the molecular terminology given in FIGURE 1.

Crystallographic Parameters

Important crystallographic parameters for some quasi-one-dimensional, heterofulvalene salts are collected in Table 1. This table covers only materials studied in this laboratory. First, it is clear that in each case there is a fundamental crystallographic cell constant that is on the order of 3.8–3.9 Å. In all cases, this crystallographic axis (or its reciprocal space analog) parallels the direction of propagation of the linear arrays of cationic and anionic constituents and the direction of high conductivity. An interesting parameter to note is the normalized unit-cell volume defined by the ratio of the unit-cell volume(V) to the number of formula units per unit cell(Z). This parameter ranges from a minimum of 420Å^3 for TTF-TCNQ, which contains the smallest cationic and anionic components, to a maximum for HMTSF-TNAP, 607Å,^{3} which contains the largest molecular constituents. The implication is that the volume per asymmetric unit is basically determined by the size of the molecular constituents; however, there is no clear relationship between the normalized unit-cell volume and the degree of interchain coupling which is electronically significant.

Results

We will now describe some of the more important structural aspects of some heterofulvalene charge-transfer salts.

Thiofulvalene Systems

TTF-TCNQ. The crystal structure of TTF-TCNQ is dominated by homologous stacks of cations and anions parallel to the crystallographic *b* axis of a monoclinic cell.[3] A packing view down [010] is presented in Figure 2A. The normal to the TTF molecular plane is tilted 24.5° with respect to the *b* axis. The stacking mode in the TTF columns is illustrated in Figure 3C; the mean distance between molecular planes is 3.47 Å. This observed stacking distance is some 0.15 Å less than has been determined for neutral TTF,[4] where a similar but less symmetric

Table 1

Some Crystallographic Parameters in Quasi-One-Dimensional Organic Conductors

Structure	Crystal System	Space Group	Z*	Stacking Axis Length (Å)	Unit-Cell Volume (Å^3)
TTF-TCNQ	Monoclinic	$P2_1/c$	2	3.819(2)	839.9
TMTTF-TCNQ	Monoclinic	$P2/c$	2	3.850(1)	1061.6
TMTSF-TCNQ	Triclinic	$P\bar{1}$	1	3.883(1)	544.0
HMTSF-TNAP	Triclinic	$P\bar{1}$	1	3.919(2)	606.6
HMTSF-TCNQ	Monoclinic	$C2/m$	2	3.890(1)	1075.9

*Z = number of formula units per unit cell.

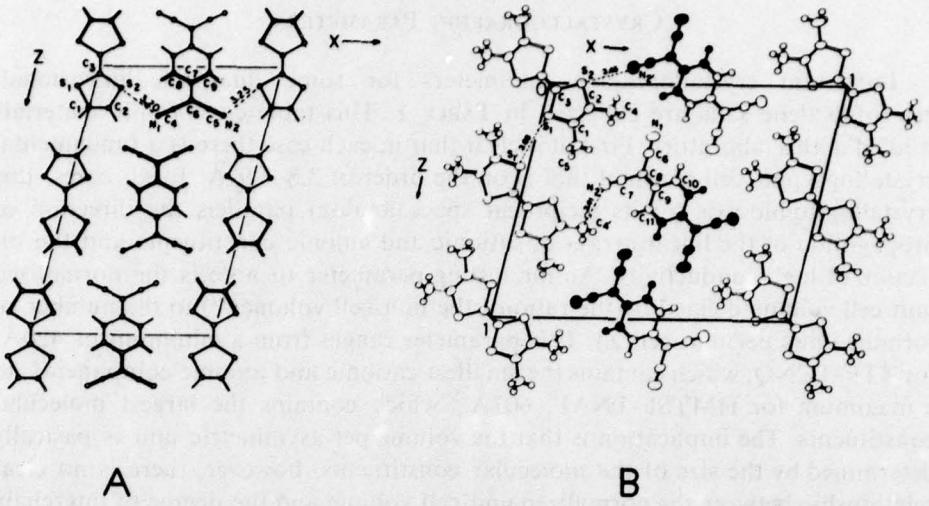


FIGURE 2. A comparison of the crystal structures of TTF-TCNQ(A) and TMTTF-TCNQ(B).

molecular overlap is found (FIGURE 3A). The tilt of the TCNQ molecular plane with respect to the *b* axis is 34.0° and opposite in direction to the tilt of the TTF cation, yielding an interleaving herringbone packing of the molecular components. The TCNQ interplanar stacking distance at 3.17 Å is still the shortest mean separation observed for such a columnar arrangement of TCNQ actions and is 0.28 Å

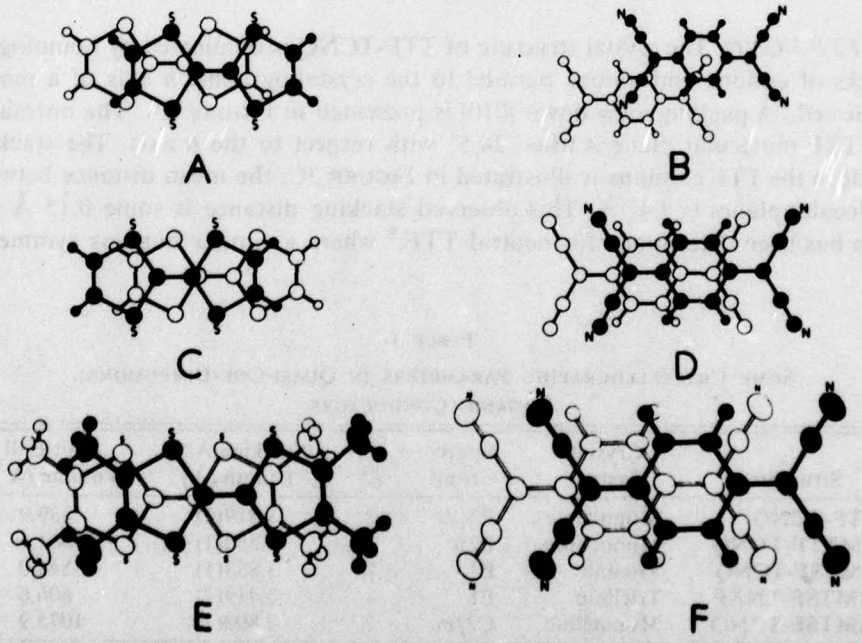


FIGURE 3. Molecular overlap drawings: (A) TTF°, (B) TCNQ°, (C) TTF in TTF-TCNQ, (D) TCNQ in TTF-TCNQ, (E) TMTTF in TMTTF-TCNQ, (F) TCNQ in TMTTF-TCNQ.

less than in neutral TCNQ.[5] The molecular overlap of the TCNQ anions in TTF-TCNQ (FIGURE 3D) is substantially different than has been found in TCNQ° (FIGURE 3B).

The principal interchain contacts along the *a* axis involve the S atoms of TTF and the N atoms of TCNQ (TABLE 2). Both of these S···N contacts are considerably less than the sum of their van der Waals radii[6] (TABLE 2). There is a substantial electrostatic component to these S···N interactions. The interchain coupling along the *c* axis is probably weaker than along the *a* axis; however, it is expected (FIGURE 2A) that there is significant electrostatic coupling along this axis, also. It has been determined by various means[7] that the degree of charge transfer in TTF-TCNQ is about 0.5 e.

TABLE 2

ELECTRONICALLY SIGNIFICANT INTERCHAIN CONTACTS IN QUASI-ONE-DIMENSIONAL ORGANIC CONDUCTORS

Structure	Contact	Distance (Å)	N*	van der Waals Distance (Å)	Figure
TTF-TCNQ	S(2)···N(1)[a]	3.20	2	3.35	2A
	S(1)···N(2)[b]	3.25	2	3.35	2A
	N(1)···C(4)[c]	3.28	2	3.10	2A
	N(1)···C(5)[c]	3.29	2	3.10	2A
TMTTF-TCNQ	S(2)···N(2)[d]	3.45	2	3.35	2B
	S(1)···S(1)[e]	3.66	2	3.70	2B
TMTSF-TCNQ	Se(2)···N(2)[f]	3.36	2	3.50	4A
	Se(1)···Se(1)[g]	3.98	2	4.00	4A
	Se(1)···Se(1)[h]	4.04	2	4.00	4A
HMTSF-TNAP	Se(1)···N(1)[f]	3.05	2	3.50	4B
	Se(2)···Se(2)[i]	3.77	2	4.00	4B
HMTSF-TCNQ	Se···N[f]	3.16	4	3.50	6

*N = number of contacts per molecule.

Symmetry transforms: [a] $x, -1+y, z$; [b] $-1+x, -1+y, z$; [c] $1-x, 1/2+y, 1/2-z$; [d] $x, -y, -1/2+z$; [e] $-x, y, 1/2-z$; [f] x, y, z; [g] $-x, -1-y, -z$; [h] $1-x, -1-y, -z$; [i] $-1-x, -y, -z$.

It is known that the Se analog TSF-TCNQ is isostructural[8] with TTF-TCNQ.

TMTTF-TCNQ. In the structure of TMTTF-TCNQ, the longitudinal axes of both the cations and anions lie in the $(10\bar{1})$ plane (FIGURE 2B).[9] The molecular overlap in the cationic column is illustrated in FIGURE 3E. As in TTF-TCNQ, the stacking is nominally of the ring double bond type.[10] The mean stacking distance is 3.53 Å and is measurably longer than the separation ot TTF planes, 3.47 Å, in TTF-TCNQ. The increased stacking distance is primarily due to the addition of the bulky methyl substituents to the thiofulvalene framework, although there may be some contribution from a different degree of charge transfer and packing effects. The molecular overlap in the TCNQ columns is shown in FIGURE 3F and is essentially identical to that found for the TCNQ columns in TTF-TCNQ. There is, however, a noticeable difference in the mean stacking distances: 3.17 Å in TTF-

TCNQ vs. 3.27 in TMTTF-TCNQ. This result cannot be as simply related to chemical modification as in the cation column.[9]

As is indicated in FIGURE 2B and TABLE 2, the interchain interactions are substantially weaker in TMTTF-TCNQ relative to TTF-TCNQ. The rotation of the stacks to accommodate the methyl substituents on the cationic column completely alters the interchain coupling mode (compare FIGURES 2A and 2B). The strong S···N contacts in TTF-TCNQ of 3.20 and 3.25 Å have been replaced by one moderate S···N contact of 3.45 Å (TABLE 2). Some compensation may be gained by a S···S contact of 3.66 Å. The apparent weakness of the interchain coupling in TMTTF-TCNQ has led us to suggest that it may be the most "one-dimensional" of this family of organic charge-transfer salts.[9]

Selenafulvalene Systems

TMTSF-TCNQ. TMTSF-TCNQ, like its sulfur analog and TTF-TCNQ, contains homologous columns of cations and anions FIGURE 4A.[11] The molecular

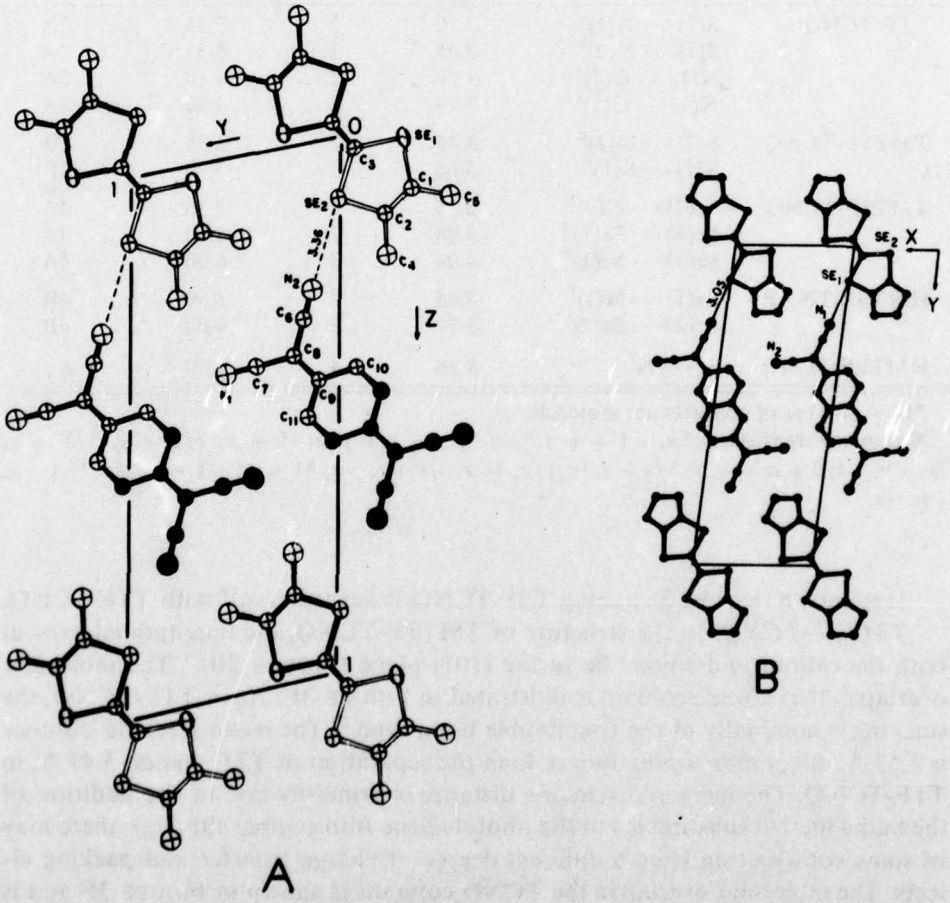


FIGURE 4. A comparison of the crystal structures of TMTSF-TCNQ (A) and HMTSF-TNAP (B).

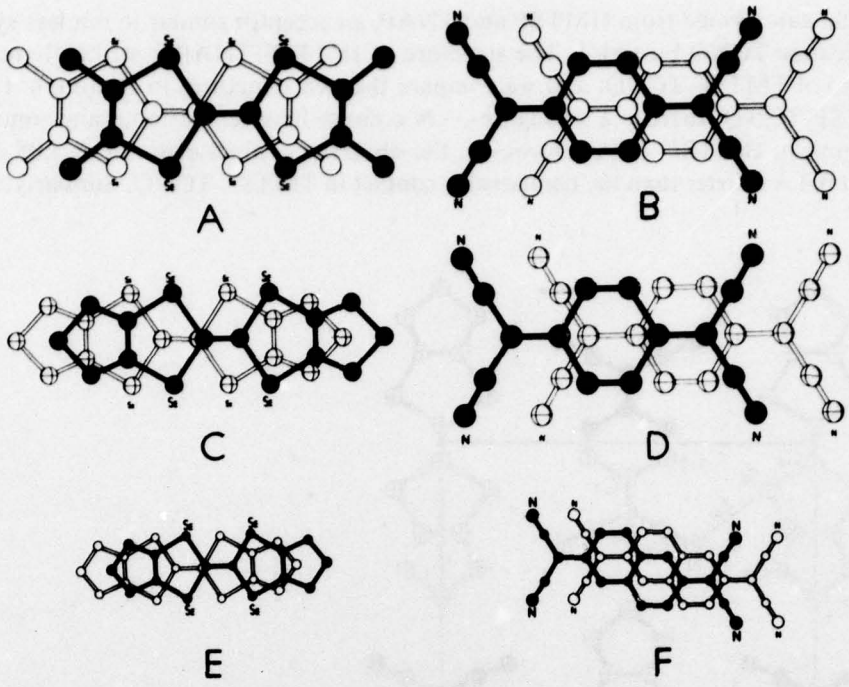


FIGURE 5. Molecular overlap drawings: (A) TMTSF in TMTSF-TCNQ; (B)-TCNQ in TMTSF-TCNQ, (C) HMTSF in HMTSF-TCNQ, (D) TCNQ in HMTSF-TCNQ, (E) HMTSF in HMTSF-TNAP, (F) TNAP in HMTSF-TNAP.

overlaps within these columns are illustrated in FIGURES 5A and 5B. The interplanar spacing in the cationic column at 3.59 Å is the largest encountered thus far, being 0.12 Å longer than in TTF-TCNQ and 0.06 Å longer than in TMTTF-TCNQ. The interplanar spacing in the TCNQ column, 3.26 Å, is longer than in TTF-TCNQ, 3.17 Å, but comparable to the 3.27 Å separation found in TMTTF-TCNQ. Again, these elongated stacking distances are very likely a consequence of the derivatization of the cationic column, the degree of charge transfer, and the mode of interchain coupling.

TMTSF-TCNQ contains one Se · · · N contact that is analogous to the S · · · N contact in TMTTF-TCNQ; however, in TMTSF-TCNQ, the Se · · · N contact is shorter than the van der Waals contact distance by about 0.14 Å, indicating a significant coupling via this contact (TABLE 2). The cationic columns are coupled by Se · · · Se contacts (like the S · · · S contact in TMTSF-TCNQ) which approach the expected van der Waals distance (TABLE 2). It is likely, considering the collection of contacts given above, that the interchain coupling in TMTSF-TCNQ is considerably stronger than in TMTTF-TCNQ and on the same order of magnitude as TTF-TCNQ.

We have also noted[11] that the relative simplicity of the TMTSF-TCNQ structure (there is only one cation-anion pair per unit cell; TABLE 1) may be responsible for the occurrence of only a single metal-insulator phase transition in place of the multiple phase transitions in TTF-TCNQ.[12]

HMTSF-TNAP. Very recently, we[13] determined the structure of a new charge-

transfer salt formed from HMTSF and TNAP, an acceptor similar to but less symmetric than TCNQ FIGURE 1. The structure of HMTSF-TNAP is strikingly reminiscent of TMTSF-TCNQ, and we compare the two structures in FIGURE 4. Like TMTSF-TCNQ, there is a strong Se · · · N contact between cationic and anionic columns; in HMTSF-TNAP, however, the observed contact distance of 3.05 Å is about 0.3 Å shorter than the comparable contact in TMTSF-TCNQ. Similarly, the

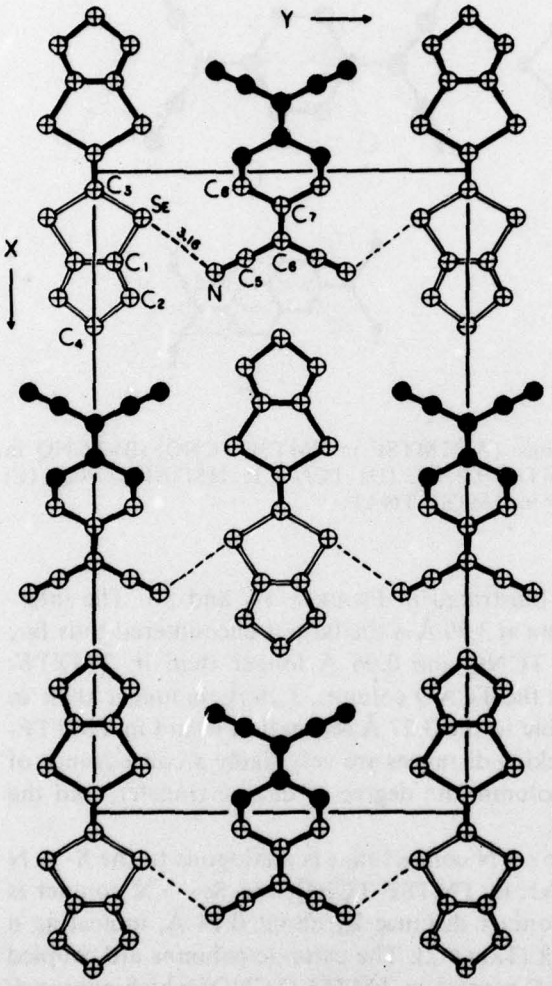


FIGURE 6. The crystal structure of HMTSF-TCNQ.

Se · · · Se contact in HMTSF-TNAP is about 0.25 Å shorter than in TMTSF-TCNQ (TABLE 2). Both of these results suggest that the interchain coupling in HMTSF-TNAP is substantially stronger than in TMTSF-TCNQ, and for that matter, stronger than any of the other salts we have studied.

The intracolumn stacking modes (FIGURES 5E and 5F), are now recognized as typical. The interplanar spacings, 3.58 Å in the cation column and 3.28 Å in the

anion column, are also reasonably standard. The cationic spacing is somewhat long, since the HMTSF molecule is less planar than TTF and the methylated-TTF derivatives.[13]

HMTSF-TCNQ. The structure of HMTSF-TCNQ[14] is illustrated in FIGURE 6. Like all the structures we have discussed, HMTSF-TCNQ contains homologous stacks of cations and anions, with molecular overlaps (FIGURES 5C and 5D) and molecular stacking distances, 3.6 for the cations and 3.2A for the anions, which are consistent with the degree of planarity of the cation and the normal mode of stacking of the anion.

The interchain coupling, however, resembles none of those we have discussed above. As can be seen in FIGURE 6, there are strong Se · · · N contacts at 3.16 Å that secure the structure along the *b* axis. Along the *a* axis, however, there are only dispersive interactions. Indeed, the coupling is so weak along the *a* axis, that stacking faults are a serious problem, and only about 80% of the unit cells are aligned as shown in FIGURE 6. Thus, HMTSF-TCNQ appears to be the most "two-dimensional" conductor of the quasi-one-dimensional organic salts. The degree of charge transfer in HMTSF-TCNQ[15] has been determined by diffuse x-ray scattering to be approximately 0.74 e.

The thiofulvalene analog HMTTF-TCNQ has been prepared and its structure determined.[16] The structure of the sulfur derivative is somewhat similar but considerably less disordered than the present system.

SUMMARY

A variety of structural data leads to the suggestion that the mode of interchain coupling in quasi-one-dimensional organic conductors plays a significant role in determining the systematics of such systems. In order of increasing interchain coupling, our studies suggest that the five compounds described here should be ranked as follows: TMTTF-TCNQ < TMTSF-TCNQ ~ TTF-TCNQ < HMTSF-TCNQ < HMTSF-TNAP. This trend is consistent with electrical and spin resonance data on these materials.[12,17]

ACKNOWLEDGMENT

We wish to acknowledge our coworkers Professor A. N. Bloch, Professor D. O. Cowan, Dr. T. O. Poehler, Dr. T. E. Phillips, Miss Miriam Rossi, Mr. W. F. Urmey, Dr. J. P. Ferraris, Dr. K. Bechgaard, and others who have contributed so much to the success of these endeavors.

NOTES AND REFERENCES

1. FERRARIS, J., D. O. COWAN, V. WALATKA & J. PERLSTEIN. 1973. J. Amer. Chem. Soc. 95: 948–949; COLEMAN, L. B., M. J. COHEN, D. J. SANDMAN, F. G. YAMAGISHI, A. F. GARITO & A. J. HEEGER. 1973. Solid State Commun. 12: 1125–1131.
2. COWAN, D. O. This volume.

3. KISTENMACHER, T. J., T. E. PHILLIPS & D. O. COWAN. 1974. Acta Cryst. **B30:** 763–768.
4. COOPER, W. F., N. C. KENNEY, J. W. EDMONDS, A. NAGEL, F. WUDL & P. COPPENS. 1971. Chem. Commun: 889–890.
5. LONG, R. E., R. A. SPARKS & K. N. TRUEBLOOD. 1965. Acta Cryst. **18:** 932–939.
6. PAULING, L. 1960. The Nature of the Chemical Bond. Cornell Univ. Press. Ithaca, N.Y.
7. DENOYER, F., R. COMES, A. F. GARITO & A. J. HEEGER. 1975. Phys. Rev. Lett. **35:** 445–449; COPPENS, P. 1975. Phys. Rev. Lett. **35:**98–100; COMES, R., S. M. SHAPIRO, G. SHIRANE, A. F. GARITO & A. J. HEEGER. 1975. Phys. Rev. Lett. **35:**1518–1521; KAGOSHIMA, S., H. ANZAI, K. KAJIMURA & T. ISHIGURO. 1975. J. Phys. Soc. Japan **39:** 1143–1147.
8. ENGLER, E. M. & V. V. PATEL. 1974. J. Amer. Chem. Soc. **96:** 7376–7378.
9. PHILLIPS, T. E., T. J. KISTENMACHER, A. N. BLOCH, J. P. FERRARIS & D. O. COWAN. 1977. Acta Cryst. **B33:** 422–428. We have also determined the structure of a non-stoichiometric, vapor-grown phase of TMTTF and TCNQ $(TMTTF)_{1.3}(TCNQ)_2$ (see KISTENMACHER, T. J., T. E. PHILLIPS, D. O. COWAN, J. P. FERRARIS, A. N. BLOCH & T. O. POEHLER. 1976. Acta Cryst. **B32:** 539–547).
10. HERBSTEIN, F. H. 1971. Perspect. Struct. Chem. **4:**166–395.
11. BECHGAARD, K., T. J. KISTENMACHER, A. N. BLOCH & D. O. COWAN. 1977. Acta Cryst. **B33:** 417–422.
12. BLOCH, A. N., T. F. CARRUTHERS, T. O. POEHLER & D. O. COWAN. 1977. Proc. NATO Conf. Chemistry and Physics of One-Dimensional Metals. Plenum Press. New York, N.Y.
13. KISTENMACHER, T. J., W. F. URMEY & M. ROSSI. 1977. Unpublished data.
14. PHILLIPS, T. E., T. J. KISTENMACHER, A. N. BLOCH & D. O. COWAN. 1976. Chem. Commun.: 334–335.
15. WEYL, C., E. M. ENGLER, S. ETEMAD, K. BECHGAARD & J. JEHANNO. 1976. Solid State Commun. **19:** 925–930.
16. GREENE, R. L., J. J. MEYERLE, R. SCHUMAKER, G. CASTRO, P. M. CHAIKIN, S. ETEMAD & S. J. LAPLACA. 1976. Solid State Commun. **20:**943–946.
17. BLOCH, A. N. & T. F. CARRUTHERS. 1977. Unpublished data.

SYNTHETIC APPROACHES TO THE STUDY OF ORGANIC METALS*

Edward M. Engler, Vishnu V. Patel, Jan R. Andersen,†
Yaffa Tomkiewicz, Robert A. Craven, Bruce A. Scott,
and Shahab Etemad‡

IBM Thomas J. Watson Research Center
Yorktown Heights, New York 10598

Since the discovery of metallic conductivity in TTF-TCNQ[1] (**2a-1**), intense research efforts have been under way to understand the properties of this novel material.[2] The origin of the metallic state in TTF-TCNQ derives from the presence of a segregated-stacked crystal structure in which incomplete charge-transfer has occurred.[2-4] This stacking must be uniform, and the distance between adjacent molecular sites must be close enough to allow overlap of their π-orbitals into an energy band. Further, because of the directionality of the π-molecular orbitals, overlap is strongest along the stacking axis and weak in the other crystallographic directions. Both donor and acceptor stacks in TTF-TCNQ are involved in the metallic properties, having partially filled bands of approximately equal width.[5] In the transverse crystallographic direction (i.e., perpendicular to the stacking axis) the conductivity is diffusive.[6] These weak interactions between stacks have been found to play an important role in determining the number and the temperatures at which the phase transitions in TTF-TCNQ and related materials occur, and their influence upon transport properties has been investigated.[7-10]

Attempts to correlate how modifications of the electronic properties of the molecular constituents[11] affect the metallic state in TTF-TCNQ are complicated by accompanying changes in the steric or structural requirements of the solid, and this often leads to different crystal packings. Both factors contribute to the overall changes in solid-state properties observed (Scheme 1). Qualitatively, we can group these changes in solid-state properties due to molecular modifications into two general categories: electronic effects and steric effects. Electronic effects are defined as involving changes in the π-molecular orbitals making up the respective donor and acceptor bands. Heteroatom substitution or expansion or contraction of the band-forming π-molecular orbitals are examples. These effects not only perturb the overlap along a given kind of stack (donor or acceptor), but also influence interactions between stacks. Steric effects, on the other hand, act in a more passive way; they control the packing of the molecular constituents in the solid without altering the character of the band-forming orbitals.

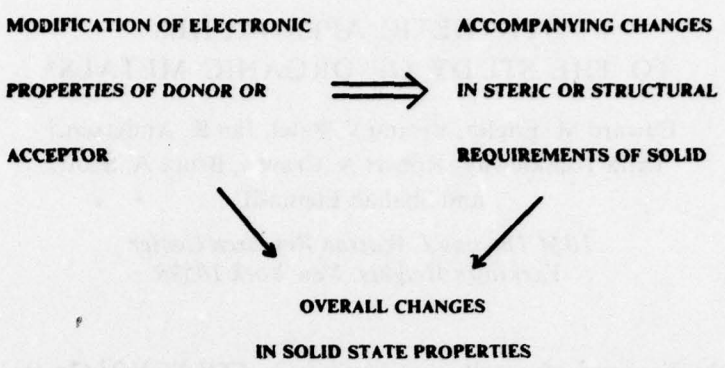
We describe below some of our synthetic efforts aimed at probing these two contributions to the overall solid state properties in TTF-TCNQ derivatives.

*Manuscript received June 6, 1977.

†IBM Postdoctoral Fellow. Permanent address: Chemistry Department, Research Establishment RISØ, DK-4000, Denmark.

‡Present address: Department of Physics, Arya-Mehr University of Technology, P. O. Box 3406, Tehran, Iran.

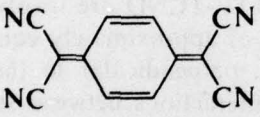
0077-8923/78/0313-0343 $1.75/1 © 1978, NYAS



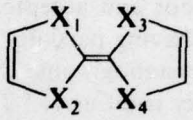
SCHEME 1.

ELECTRONIC EFFECTS

In TTF-TCNQ, heteroatom substitution of the sulfur atoms of the donor appeared to be an ideal means of perturbing electronic properties while keeping steric contributions relatively constant. To this end, the selenium

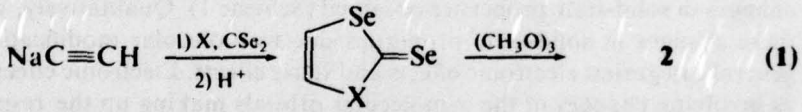


1



2a: X_{1-4}=S
2b: X_{1-4}=Se
2c: $X_{1,3}$=S, $S_{2,4}$=Se; $X_{1,4}$=S, $X_{2,3}$=Se

analogs of TTF (e.g. tetraselenafulvalene,[12] TSeF, **2b** and *cis/trans*-diselenadithiafulvalene,[13] DSeDTF, **2c**)[14] were prepared, by the route outlined in Equation 1.



The TCNQ salts of TTF, DSeDTF, and TSeF are isostructural, with only a slight expansion of the unit cell parameters as expected because of the incorporation of the larger selenium atom.[10] TABLE 1 summarizes these parameters as well as other data on these materials.

Not only does the close structural similarity between TTF-TCNQ and TSeF-TCNQ simplify the task of deciphering the relation of molecular to solid-state properties in these charge-transfer salts, but it also permits the formation of solid solutions: $TTF_xTSeF_{1-x}TCNQ$ where x can vary from 0 to 1, analogous to the alloying of two metals. These "organic alloys" provide a unique probe for the systematic modification of solid-state properties in which the character of the donor stack can be continuously varied from TTF to TSeF.[10]

The substitution of selenium for sulfur in TTF-TCNQ led to a number of important changes in solid-state properties (see TABLE 1). For example, not only is TSeF-TCNQ more conducting than TTF-TCNQ, but the metallic phase has

been stabilized to a lower temperature. Also, in contrast to the multiple-phase transitions seen in TTF-TCNQ, TSeF-TCNQ has apparently only a single-phase transition.[8] FIGURE 1 plots the logarithm of the resistivity versus the reciprocal of the temperature for TTF-TCNQ and TSeF-TCNQ. Two transitions in TTF-TCNQ are easily seen as two sharp rises in resistivity at 53°K and 38°K. These points are emphasized in the insert, which plots the slope of lnR versus T. The two transitions manifest themselves as two sharp peaks over a smooth background. In contrast to TTF-TCNQ, TSeF-TCNQ has a minimum at lower temperature and only a single anomally at 28°K.[8,10,23]

The reason for these changes in going from TTF-TCNQ to TSeF-TCNQ,

TABLE 1
PROPERTIES OF THE TCNQ SALTS OF TTF, DSeDTF, TSeF

Property	TTF-TCNQ	DSeDTF-TCNQ	TSeF-TCNQ
Unit Cell Constants*			
a(Å)	12.298	12.405	12.514
b(Å)	3.819	3.842	3.876
c(Å)	18.468	18.486	18.511
β	104.5°	104.3°	104.2°
Conductivity†			
σ_{RT}(ohm-cm)$^{-1}$	500	550	800
T_p(°K)	58	64	40
T_c(°K)	53	44	28
EPR linewidth‡ (gauss)	5	220	550
Thermal electric power§ (μV/°K, 298°K)	−30	+10	+3

*X-ray diffraction of powdered crystals. Data from Reference 10.

†Four-probe single crystalline dc measurements. σ_{RT} = room temperature conductivity. T_p = temperature of the peak in conductivity, T_c = phase transition temperature. See References 8 and 10 for details.

‡Single-crystal measurement; see Reference 9 for details.

§Data from P. M. Chaikin, R. L. Greene, S. Etemad & E. M. Engler. 1976. Phys. Rev. B 13: 1627.

although not completely understood at present, appear to be due to the greater orbital extent of selenium relative to sulfur. This permits stronger overlap both along the donor stack and with the acceptor stack. A variety of solid-state measurements[15] all indicate a greater contribution of the donor stack to overall solid-state properties in TSeF-TCNQ than in TTF-TCNQ.[10] The increased electronic interaction between donor and acceptor stacks in TSeF-TCNQ is believed to be important in the lowering of the phase-transition temperature relative to TTF-TCNQ.[9,16] Many factors are undoubtedly involved in controlling the phase transition, but the role of inter-stack electronic coupling can be understood qualitatively as follows: The phase transitions in TTF-TCNQ and TSeF-TCNQ

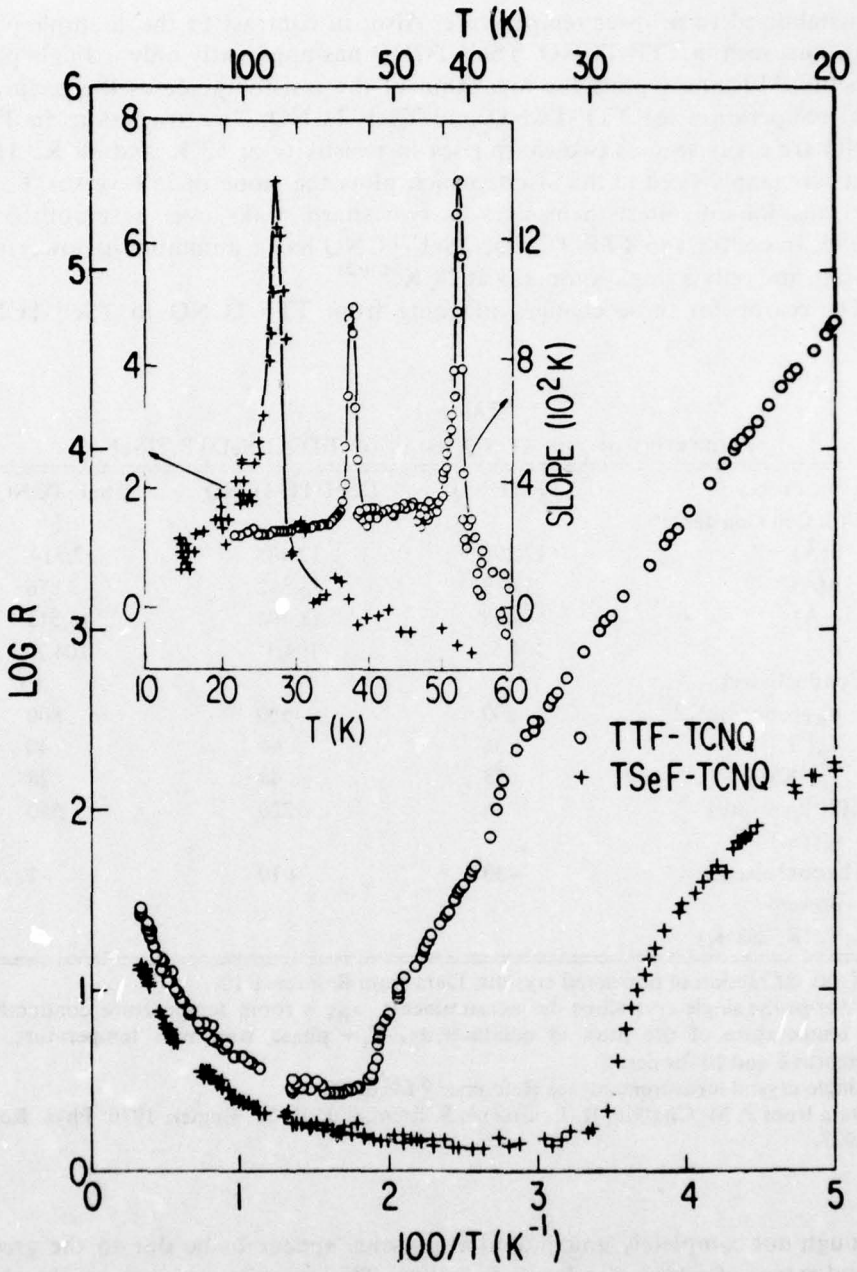


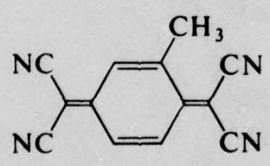
FIGURE 1. Plot of the log resistivity of TTF-TCNQ (0) and TSeF-TCNQ (+) versus inverse temperature (°K). Insert plots slope of log resistivity versus temperature.

involve the interplay of dynamic lattice distortions (i.e., charge-density waves) which occur on both donor and acceptor stacks. It is the building up of three-dimensional ordering of these charge density waves in certain phase relationships which brings about the transitions.[10,17-19] The energy gain for undergoing the phase transition is associated with the 1-dimensional-like character of these materials

(e.g. the Peierls instability). By making the system *less* 1-dimensional, through enhanced donor and acceptor stack electronic overlap, the energy gain for this transition to occur should be less and the transition shifted to lower temperature.[10,16]

The enhanced electronic overlap between donor and acceptor stacks in TSeF-TCNQ may not only be involved in the lowering of T_c relative to TTF-TCNQ, but may also account for the apparent single transition that is observed in TSeF-TCNQ, as opposed to multiple transitions seen in TTF-TCNQ. Considerable evidence has accumulated[7] that indicates that donor and acceptor stacks are weakly interacting in TTF-TCNQ, and that the metal-insulator transition at 53°K affects primarily the TCNQ stacks. The lower transitions at 49°K and 38°K involve interactions of both donor and acceptor stacks.[18,20,21] With stronger interstack interaction in TSeF-TCNQ as well as enhanced overlap along the donor stack, both stacks apparently undergo their transition together.[10]

The effects of introducing small amounts of TSeF in TTF-TCNQ has been shown to be consistent with the above roles of the donor and acceptor stacks in the 53°K and 38°K phase transitions.[8] Since the 53°K transition is believed to involve mainly the TCNQ stacks, it should be relatively unperturbed by a small amount of donor stack doping. On the other hand, the 38°K transition, which involves both donor and acceptor stacks, should be more sensitive to alloy formation. This is indeed the result: three percent incorporation of TSeF into TTF-TCNQ completely obscures the 38°K transition, while the 53°K transition remains relatively sharp.[8] By contrast, doping of the acceptor stack with a similar amount of methyl TCNQ (MTCNQ), **3**) considerably broadens the 53°K transition.[22] FIGURE 2 shows the effect of donor and acceptor stack doping on the phase transitions as seen in the conductivity data.



3

Doping experiments are an excellent probe of electronic effects in these charge-transfer salts and provide useful insights about the character of the phase transitions and the coupling between donor and acceptor stacks.[23] As described above, donor and acceptor stacks are weakly coupled in TTF-TCNQ with the TCNQ stack driving the phase transition at 53°K. The doping behavior of TTF-TCNQ in FIGURE 2 is consistent with such an interpretation. In TSeF-TCNQ, on the other hand, the donor and acceptor stacks are more strongly coupled. Thus, we would expect this material to be more sensitive to donor doping, which is observed: three percent TTF doped in TSeF-TCNQ not only broadens the phase transition at 28°K but also shifts its position[10a,23] (see FIGURE 3). Acceptor doping in TSeF-TCNQ also produces greater changes in the conductivity-temperature profile, compared to similar amounts of MTCNQ in TTF-TCNQ.[24] This is consistent with greater donor-acceptor interaction, which results in a smaller gap opening at the phase transition and, therefore, a corresponding greater sensitivity to doping.[24]

Steric Effects

Whereas the isostructurality of TTF-TCNQ and TSeF-TCNQ facilitated the study of their comparative solid-state properties, it is important to understand how modifications in the crystal packing alters such properties. Introduction of alkyl groups in these materials appeared to us to be an effective means of modify-

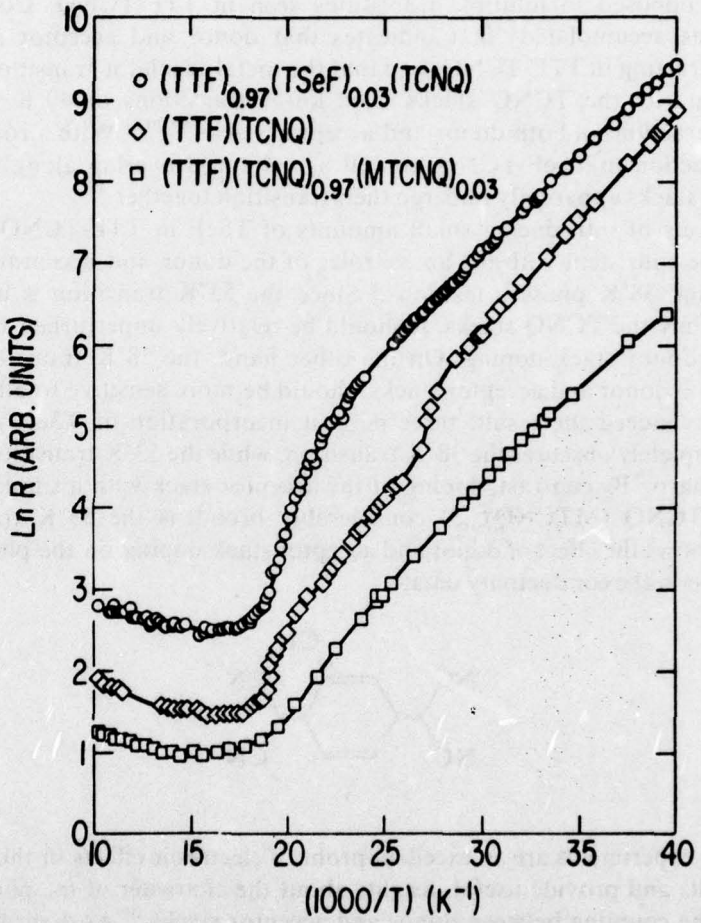


Figure 2. Plots of log resistivity versus inverse temperature (°K) for donor and acceptor stack doping in TTF-TCNQ.

ing interstack coupling in an identifiable manner. Alkyl groups, being sigma bonded, should not significantly perturb the π-framework and therefore should serve mainly as *steric* "spacers"; i.e., to push donor and acceptor stacks apart.

From our studies on TSeF-TCNQ, stronger donor-acceptor overlap in this system compared to TTF-TCNQ was observed and considered a major factor involved in lowering the phase-transition temperature. The rather large increase in EPR linewidth in going from TTF-TCNQ to TSeF-TCNQ (Table 1) was considered evidence for this enhanced donor-acceptor stack interaction.[9] After cor-

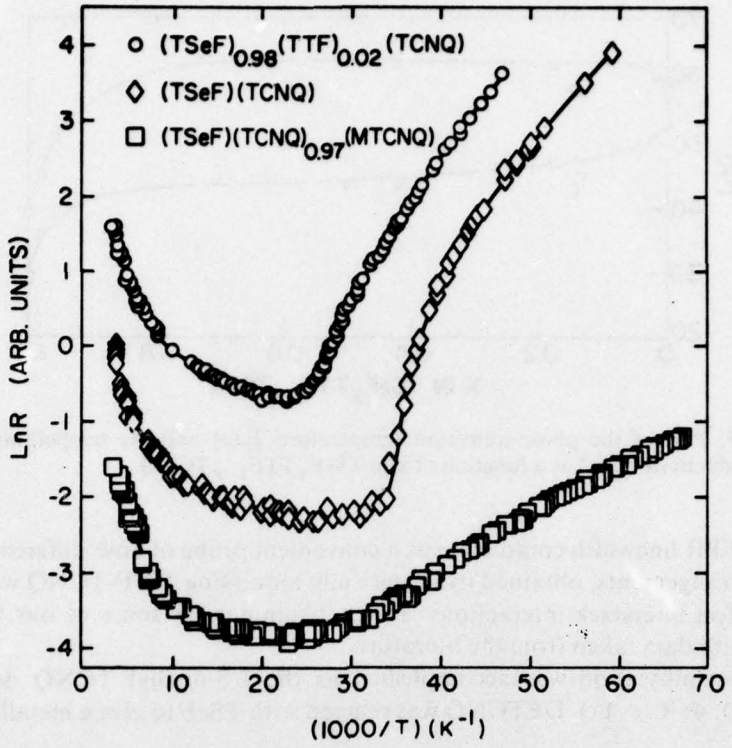


FIGURE 3. Plots of log resistivity versus inverse temperature (°K) for donor and acceptor stack doping in TSeF-TCNQ.

recting for the contribution of greater spin orbit coupling in selenium, considerable, additional relaxation of the signal remained at the high TSeF alloy compositions $x = 0.95, 0.98$, and 1.00 in $TSeF_xTTF_{1-}TCNQ$.[9] FIGURE 4 shows the variation of EPR linewidth as a function of alloy composition. This behavior closely parallels the sharp decrease in the phase-transition temperature noted for the high TSeF composition[10] (see FIGURE 5).

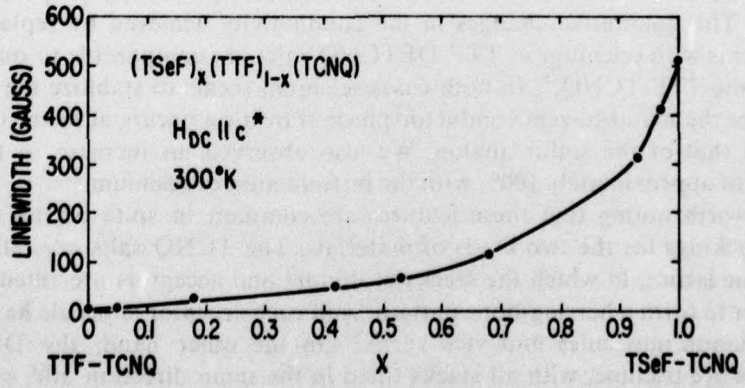


FIGURE 4. Plot of EPR single-crystal linewidth as a function of x in $TSeF_xTTF_{1-x}$-TCNQ.

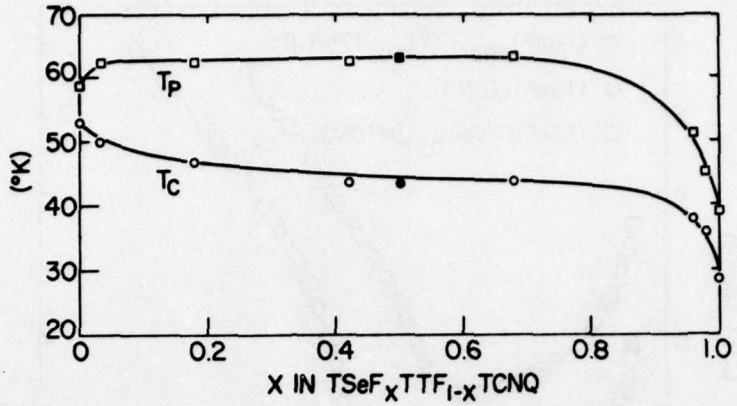
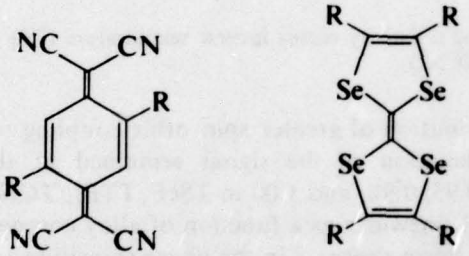


FIGURE 5. Plot of the phase-transition temperature T_c(○) and the temperature of the peak in conductivity T_p(□) as a function of x in $TSeF_xTTF_{1-x}TCNQ$.

Thus, EPR linewidth could serve as a convenient probe of how different crystal packing arrangements, obtained from sterically modifying TSeF-TCNQ with alkyl groups, affect interstack interactions. TABLE 2 summarizes some of our findings, together with data taken from the literature.

Acceptor alkylation was accomplished as the 2,5-diethyl TCNQ derivative (DETCNQ, **4**: R = Et). DETCNQ was reacted with TSeF to give a metallic



4 **5**

charge-transfer salt[25] which is isostructural with the previously prepared sulfur analog.[26] The qualitative changes in the conductivity achieved by replacing the sulfur atoms with selenium in TTF-DETCNQ salts are comparable to our earlier work on the TTF-TCNQ.[10] In both cases selenium seems to stabilize the metallic state, since the metal-to-semiconductor phase transition occurs at lower temperature than that of the sulfur analog. We also observed an increase in the conductivity of approximately 100% with the introduction of selenium.[26,27]

It is worth noting that these features are common in spite of the different crystal packings for the two kinds of materials. The TCNQ salts crystallize in a monoclinic lattice, in which the stacks of donors and acceptors are tilted against each other to form a herring-bone pattern, with each acceptor molecule having two nearest donor molecules and vice versa.[3] On the other hand, the DETCNQ analogues are triclinic, with all stacks tilted in the same direction and with each acceptor being surrounded by four nearest donors.[26]

The alkyl groups in TSeF-DETCNQ increase the interstack separations and as

a result decrease electronic interactions, as evidenced by the more narrow EPR linewidth (TABLE 2). This decrease in donor-acceptor overlap is accompanied by an increase in the phase transition temperature relative to TSeF-TCNQ. Donor alkylation in TSeF-TCNQ (e.g. TMTSeF, **5**: R = R′ = CH_3)[28] also leads to a decrease in the EPR linewidth[29] and an increase in the phase-transition temperature (see TABLE 2). However, in TMTSeF-DMTCNQ,[30] where both the donor and acceptor stacks are alkylated, this trend ends. The EPR linewidth for this material is 50 gauss and is one of the narrowest so far observed in a TSeF-charge-transfer salt.[31] This suggests weak donor-acceptor overlap, yet the phase transition is at a lower temperature than observed for both TSeF-DETCNQ and TMTSeF-TCNQ. While the reason for this behavior is obviously a combination of many factors not yet well understood, some interesting qualitative insights emerge. It was discussed earlier that the phase transition in these materials involve the build up of 3-dimensional order of charge-density waves on the donor and acceptor stacks. By increasing donor and acceptor stack electronic overlap, we decrease the energy gain for this transition to occur and shift the transition to lower temperature. Alkylation can push donor and acceptor stacks apart (see for example Se...N distances in TABLE 2), thereby decreasing their interaction and raising the phase transition temperature. This, however, tends to make the stacks more and more 1-dimensional, and the ability of the charge density waves to 3-dimensionally lock should decrease. Thus, at some point, this effect may take over and lead to a lowering of the phase-transition temperature. These interpretations are highly speculative at present, and more work is required to establish their validity.

It should be mentioned that alkylation does not always have to decrease electronic overlap between donor and acceptor. For example, the alkylated charge-transfer salt HMTSeF-TCNQ[32] (HMTSeF: **5**, R/R′=$(CH_2)_3$) adopts a crystal

TABLE 2

DATA ON ALKYL DERIVATIVES OF TSeF-TCNQ

Compound	T_c[a] (°K)	EPR Linewidth (gauss)	Se...N[b] Distance
TSeF-TCNQ	28	550	3.17[c]
TSeF-DETCNQ[d]	~100	175	—
TMTSeF-TCNQ	~ 57[e]	120[f]	3.36[e]
TMTSeF-DMTCNQ	~ 42[g]	50[h]	3.49[i]
HMTSeF-TCNQ	~16[j]	>2000[k]	3.10[l]

[a] Phase-transition temperature from the single-crystal conductivity measurements.
[b] Shortest Se...N distance in the solid.
[c] S. J. LaPlace & P. W. Cornfield. Unpublished work.
[d] Data from Reference 25.
[e] Data from K. Bechgaard, T. J. Kistenmacher, A. N. Bloch & D. O. Cowan. 1977. Acta Cryst. B 33: 417.
[f] Data from Reference 29.
[g] Data from Reference 30.
[h] Data from Reference 31.
[i] K. Bechgaard, J. R. Andersen, G. Rindorf, H. Soling & C. S. Jacobsen. To be published.
[j] Very broad phase transition. See reference 35 for details.
[k] Data from Reference 32.
[l] Data from Reference 33.

structure[33] that positions the donor and acceptor very close (as judged by Se...N distance in the solid, TABLE 2) to permit strong overlap. The result is an EPR linewidth too broad to measure and a phase transition at 16°K (see TABLE 2).[34,35]

CONCLUSION

The attempt to correlate modifications of the molecular constituents with the resulting solid-state properties of their charge transfer salts is a complex task fraught with many difficulties. Many interconnected parameters are involved with each modification. We have presented our initial approach to this problem. It is aimed at trying to disentangle some of these parameters in terms of electronic and steric effects.

Electronic modifications of TTF-TCNQ were studied with use of the selenium analogs of TTF-TCNQ. Enhanced donor-acceptor stack interaction was considered an important factor in lowering the phase transition from 53°K in TTF-TCNQ to 28°K in TSeF-TCNQ. Alloys of these isostructural organic metals and selective donor and acceptor stack doping experiments provided useful insights concerning the character of the phase transitions and the interactions between donor and acceptor stacks.

Steric effects were studied in TSeF-TCNQ analogs with alkyl groups as electronically insulating "spacers" that can push donor and acceptor stacks apart, leading to new crystal packing arrangements and reduced interstack interactions. EPR linewidth measurements were found to be a convenient probe of these interactions. As the charge-transfer salt is made more and more 1-dimensional through alkylation, as judged by EPR linewidth narrowing, the phase transition first increases and then decreases.

NOTES AND REFERENCES

1. FERRARIS, J., D. O. COWAN, V. WALATKA, JR. & J. H. PERLSTEIN. 1973. J. Amer. Chem Soc. **95**: 948; COLEMAN, L. B., M. J. COHEN, D. J. SANDMAN, F. G. YAMAGISHI, A. F. GARITO & A. J. HEEGER. 1973. Solid State Commun. **12**: 1125.
2. Reviews: GARITO, A. F. & A. J. HEEGER. 1974. Accounts Chem. Res. **7**: 232; BLOCH, A. N., D. O. COWAN & T. O. POEHLER. 1974. *In* Energy and Charge Transfer in Organic Semiconductors. K. Masuda & M. Silver, Eds. Plenum Press. New York, N.Y.; HEEGER, A. J. & A. F. GARITO. 1975. *In* Low Dimensional Cooperative Phenomena. H. J. Keller, Ed. Plenum Press. New York, N.Y. BERLINSKY, A. J. 1976. Contemp Phys. **17**: 331; ENGLER, E. M. 1976. Chem. Technol. **6**: 274.
3. KISTENMACHER, T. J., T. E. PHILLIPS & D. O. COWAN. 1974. Acta Cryst. **B30**: 763.
4. GROBMAN, W. O., R. A. POLLAK, D. E. EASTMAN, E. T. MAAS, JR. & B. A. SCOTT. 1974. Phys. Rev. Lett. **32**: 534; TORRANCE, J. B., B. A. SCOTT & F. B. KAUFMAN. 1975. Solid State Commun. **17**: 1369; TORRANCE, J. B. & B. D. SILVERMAN. 1976. Phys. Rev. B **15**: 788; LaPlaca, S. J., P. W. CORFIELD, R. THOMAS & B. A. SCOTT. 1975. Solid State Commun. **17**: 635.
5. WELBER, B., P. M. GRANT, P. E. SEIDEN & E. M. ENGLER. 1977. Bull. Am. Phys. Soc. **22**: 287.
6. For a recent discussion of the electrical properties of TTF-TCNQ from two points of view, see: THOMAS, G. A. *et al.* 1976. Phys. Rev. B **13**: 5105; COHEN, M. J., L. B. COLEMAN, A. F. GARITO & A. J. HEEGER. 1976. Phys. Rev. B **13**: 5111.
7. TOMKIEWICZ, Y., A. R. TARNAKO & J. B. TORRANCE. 1976. Phys. Rev. Lett. **36**: 751;

RYBACZEWSKI, E. F., A. F. GARITO, A. J. HEEGER & E. EHRENFREUND. 1975. Phys. Rev. Lett. **34:** 524; RYBACZEWSKI, E. F., L. S. SMITH, A. F. GARITO & A. J. HEEGER. 1976. Phys. Rev. B **14:** 2746; BARMATZ, M., L. R. TESTARDI, A. F. GARITO & A. J. HEEGER. 1974. Solid State Commun. **15:** 1299.

8. ETEMAD, S. 1976. Phys. Rev. B **13:** 2254. For the second transition in TTF-TCNQ see also references cited therein.
9. TOMKIEWICZ, Y., E. M. ENGLER & T. D. SCHULTZ. 1975. Phys. Rev. Lett. **35:** 456.
10a. ETEMAD, S., E. M. ENGLER, T. PENNEY, B. A. SCOTT & T. D. SCHULTZ. Phys. Rev. B. In press.
10b. ENGLER, E. M., B. A. SCOTT, S. ETEMAD, T. PENNEY & V. V. PATEL. 1977. J. Amer. Chem. Soc. **99:** 5909.
11. Review of TTF modifications: NARITA, M. & C. U. PITTMAN, JR. 1976. Synthesis: 489. Some recent TCNQ-modifications: WHELAND, R. C. & E. L. MARTIN. 1975. J. Org. Chem. **40:** 3101; see also BESPALOV, B. P. & V. V. TITOV. 1975. Russian Chem. Rev. **44:** 1091.
12. ENGLER, E. M. & V. V. PATEL. 1974. J. Amer. Chem. Soc. **96:** 7376.
13. ENGLER, E. M. & V. V. PATEL. 1975. Chem. Commun. 671.
14. Alternate syntheses of TSeF and DSeDTF have appeared: LAKSHMIKANTHAN, M. V. & M. P. CAVA. 1976. J. Org. Chem. **41:** 882; LAKSHMIKANTHAM, M. V., M. P. CAVA & A. F. GARITO. 1975. Chem. Commun. 383.
15. See Reference 10b for leading references on these measurements.
16. TOMKIEWICZ, Y. & T. D. SCHULTZ. To be published.
17. RICE, M. J. & S. STRÄSSLER. 1975. Solid State Commun. **13:** 1385; LEE, P. A., T. M. RICE & P. W. ANDERSON. 1973. Phys. Rev. Lett. **31:** 462.
18. SCHULTZ, T. D. & S. ETEMAD. 1976. Phys. Rev. B **13:** 4928.
19. SCHULTZ, T. D. 1977. Solid State Commun. **22:** 189.
20. BAK, P. & V. J. EMERY. 1976. Phys. Rev. Lett. **36:** 978.
21. For recent x-ray and neutron scattering measurements of these lattice distortions: DENOYER, F., R. COMÉS, A. F. GARITO & A. J. HEEGER. 1975. Phys. Rev. Lett. **35:** 445; KAGOSHIMA, S., H. ARZAI, K. KAJIMURA & T. ISHIGURO. 1975. J. Phys. Soc. Japan **39:** 1143; COMÉS, R., S. M. SHAPIRO, G. SHIRANE, A. F. GARITO & A. J. HEEGER. 1975. Phys. Rev. B **35:** 1518; COMÉS, R., G. SHIRANE, S. M. SHAPIRO, A. F. GARITO & A. J. HEEGER. 1976. Phys. Rev. B **14:** 2376.
22. TOMKIEWICZ, Y., R. A. CRAVEN, T. D. SCHULTZ, E. M. ENGLER & A. R. TARANKO. 1977. Phys. Rev. B **16:** 3643.
23. CRAVEN, R. A., Y. TOMKIEWICZ, E. M. ENGLER & A. R. TARANKO. 1977. Solid-State Commun. **23:** 429.
24. ENGLER, E. M., R. A. CRAVEN, Y. TOMKIEWICZ, B. A. SCOTT, K. BECHGAARD & J. R. ANDERSEN. 1975. Chem. Commun. 337.
25. ANDERSEN, J. R., R. A. CRAVEN, J. E. WEIDENBORNER & E. M. ENGLER. 1977. Chem. Commun. 526.
26. SHCULTZ, A. J., G. D. STUCKY, R. A. CRAVEN, M. J. SCHAFFMAN & M. B. SALAMON. 1976. J. Amer. Chem. Soc. **98:** 5191.
27. ANDERSEN, J. R., K. BECHGAARD, C. BERG & C. S. JACOBSEN. 1977. *In* Lecture Notes in Physics. Proc. Conf. Organic Conductors and Semiconductors. Aug. 29–Sept. 4. Siofok, Hungary. Springer-Verlag.
28. BECHGAARD, K., D. O. COWAN & A. N. BLOCH. 1974. Chem. Commun.: 937.
29. POEHLER, T. O., J. BOHANDY, A. N. BLOCH & D. O. COWAN. 1976. Bull. Am. Phys. Soc. **21:** 287.
30. ANDERSEN, J. R., C. S. JACOBSEN, G. RINDORF, H. SOLING & K. BECHGAARD. 1975. Chem. Commun. 883.
31. TOMKIEWICZ, Y., J. R. ANDERSEN, A. R. TARANKO. Phys. Rev. B. In press.
32. BLOCH, A. N., D. O. COWAN, K. BECHGAARD, R. E. PYLE, R. H. BANKS & T. O. POEHLER. 1975. Phys. Rev. Lett. **34:** 1561.
33. PHILLIPS, T. E., T. J. KISTENMACHER, A. N. BLOCH & D. O. COWAN. 1976. Chem. Commun.: 334.
34. For some recent references on HMTSeF-TCNQ: COOPER, J. R., M. WEGER, D. JÉROME, D. LEFUR, K. BECHGAARD, A. N. BLOCH & D. O. COWAN. 1976. Solid

State Commun. **19:** 749; WEGER, M. 1976. Solid State Commun. **19:** 1149; SODA, G., D. JÉROME, M. WEGER, K. BECHGAARD & E. PEDERSEN. 1976. Solid State Commun. **20:** 107.

35. The detection of this phase transition appears to be dependent on the conditions of crystal growth. On room-temperature diffusion-grown crystals we have observed an anomaly in the conductivity at 16°K. ENGLER, E. M. & R. A. CRAVEN. Unpublished work. See also References 32, 34.

DISCUSSION

JAN KOMMANDEUR (*Univ. Groningen, Groningen, The Netherlands*): Do you know the structure of the insulating dimethyl derivative?

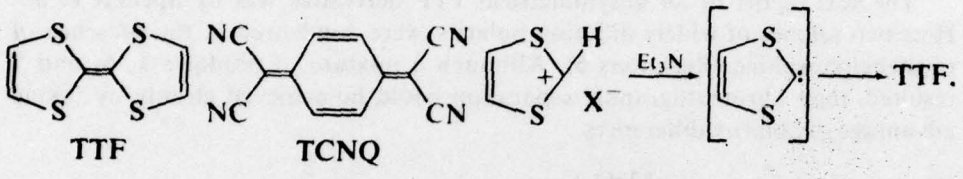
ENGLER: No. It apparently is DA if one believes the optical spectrum taken in KBr.

UNSYMMETRICAL TETRATHIAFULVALENES*

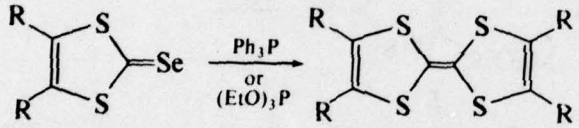
M. P. Cava and M. V. Lakshmikantham

Chemistry Department
University of Pennsylvania
Philadelphia, Pennsylvania 19104

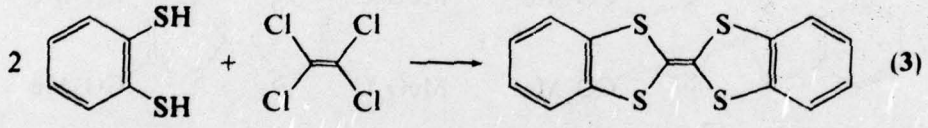
Since the first report of unusually high electrical conductivity in charge-transfer complexes of tetrathiafulvalene-tetracyanoquinodimethane (TTF)-(TCNQ),[1] many analogs of the donor molecules have been reported.[2] In the synthesis of these compounds, a final coupling step is generally involved, giving rise to the generation of symmetrical derivatives (Reactions 1 & 2). There are several syntheses (Reactions 3 & 4) not involving coupling reactions, but these are of limited scope and are essentially symmetrical condensations.[3,4]



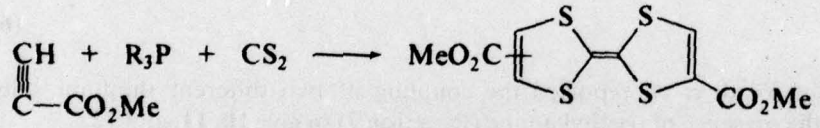
(1)



(2)



(3)



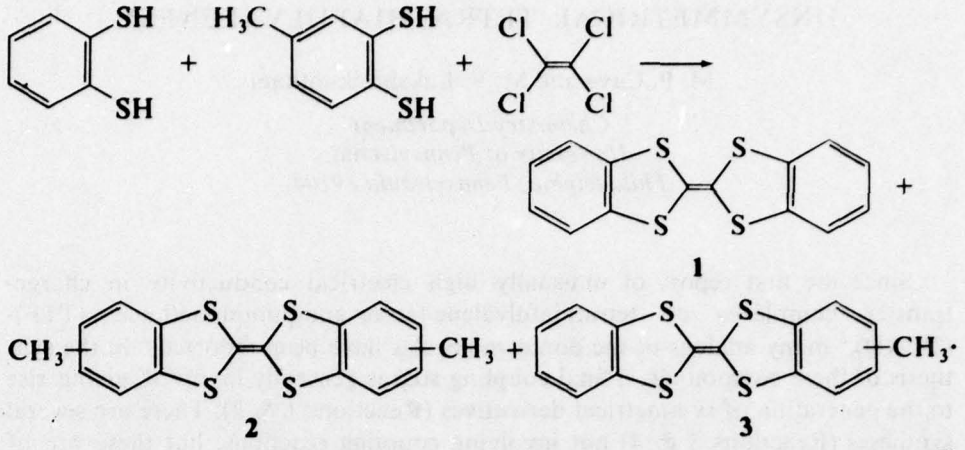
(4)

Until recently no unsymmetrical analogs of TTF were known. These compounds are desirable for the ascertainment of the effects of asymmetry in the π-donor on the solid-state properties of the corresponding TCNQ complex.

Bajwa *et al.* reported the synthesis of an unsymmetrical TTF derivative **3**, using a mixture of vicinal thiols and tetrachloroethylene, in which the desired unsymmetrical product **3** crystallized in preference to the symmetrical products **1** and **2**.[5]

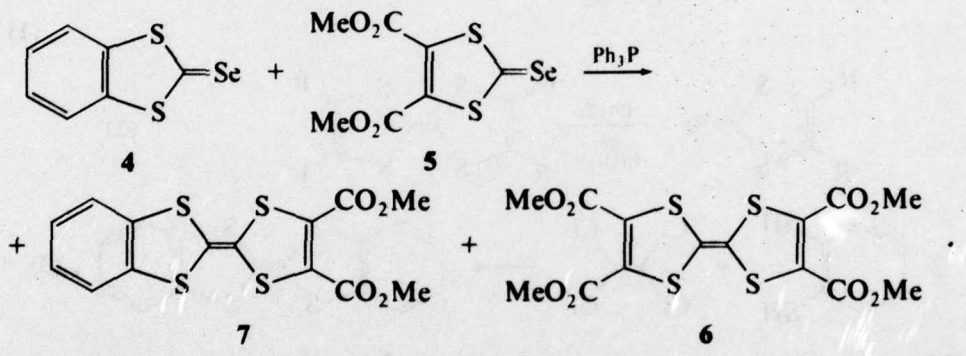
*Supported by the National Science Foundation MRL program under grant DMR 76-00678. Manuscript received June 13, 1977.

0077-8923/78/0313-0355 $1.75/1 © 1978, NYAS



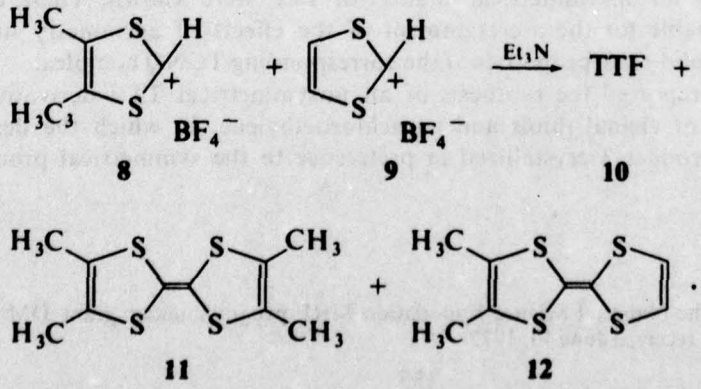
(5)

The next report of an unsymmetrical TTF derivative was by Spencer *et al.*[6] Here two selones of widely differing polarity were condensed in the presence of triphenylphosphine (Reactions 6). Although a mixture of products **1, 6,** and **7** resulted, their chromatographic separation could be achieved cleanly by taking advantage of polarity differences.



(6)

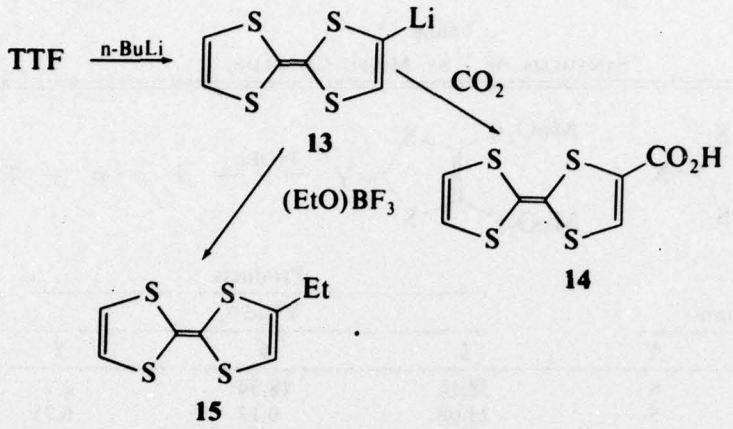
Recently, Wudl *et al.* reported the coupling of two different thiolium salts **8** and **9** in the presence of triethyl amine (Reaction 7) to give **10, 11,** and **12.**[7]



(7)

Here again, the unsymmetrical product **12** was separable by fractional crystallization.

Very recently Green reported the lithiation of TTF and the conversion of the resulting lithio compound **13** into several monosubstituted TTF derivatives (**14, 15**; Reaction 8).[8]

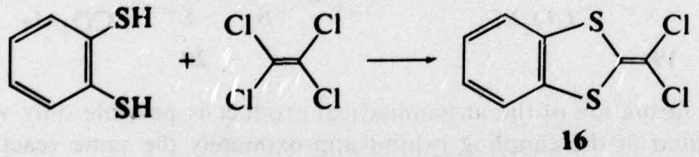


(8)

All of these methods have certain limitations and drawbacks, and none is of general applicability.

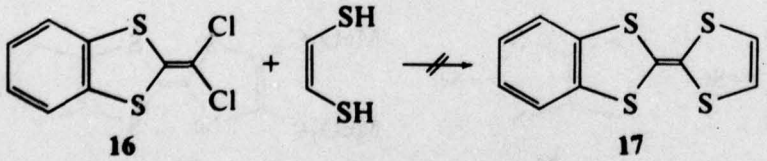
The route employed by Bajwa *et al.*, based upon the original synthesis of dibenzotetrathiafulvalene by Hurtley and Smiles,[3] (Reaction 3), has two serious drawbacks. First, vicinal dithiols are not generally readily available. Second, and more important, the isolation of the unsymmetrical product depends upon fortuitious crystallization.

In a recent reinvestigation of this reaction in our laboratory, a stable geminal dichloro intermediate **16** has been isolated (Reaction 9).[9]

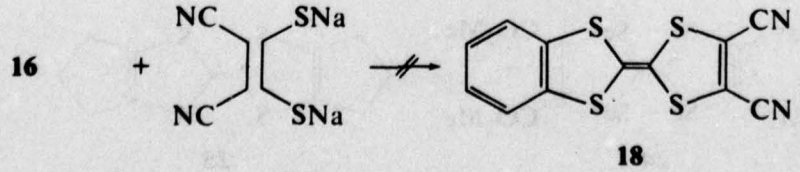


(9)

Intermediate **16** gave dibenzotetrathiafulvalene (**1**) upon treatment with more benzenedithiol. However, reaction of **16** will either ethenedithiol or disodium 1,2-dicyano-ethenedithiolate did not lead to the expected unsymmetrical monobenzotetrathiafulvalences **17** and **18** (Reaction 10.)[9]



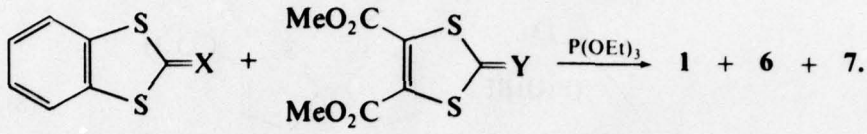
(10)



A more detailed investigation of the coupling of **4** and **5** (Reaction 6) has revealed several interesting features. Optimum yields of the unsymmetrical **7** are obtained only when selones are used, rather than the more readily available thiones.[10] (See TABLE 1).

TABLE 1*

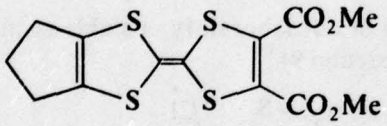
SYNTHESIS OF 7 BY MIXED COUPLING



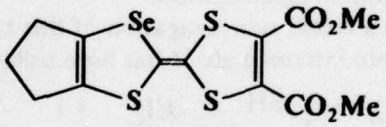
Reactants		Products		
		Yield %		
X	Y	1	6	7
S	S	38.16	18.34	2.7
Se	S	23.68	9.17	6.75
S	Se	10.53	30.28	31.35
Se	Se	4.60	9.17	56.27

*Compare with Reaction 6.

With use of this approach, unsymmetrical TTF derivatives **19** and **20** were prepared, albeit in low yield.[11]

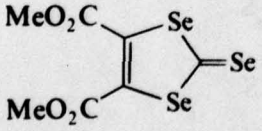


19

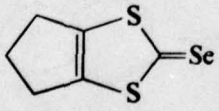


20

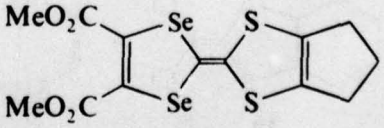
However, the formation of the unsymmetrical product is possible only when the two selones used in the coupling exhibit approximately the same reactivity toward the phosphorus reagent.[11] When the highly reactive diester selone **21** was used in conjunction with **22**, no trace of mixed product **23** was obtained, the only products being the symmetrical derivatives **24** and **25**.



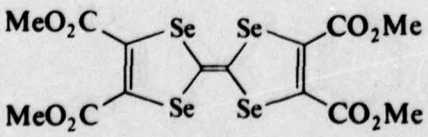
21



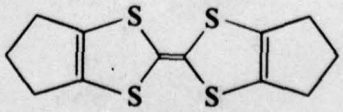
22



23



24



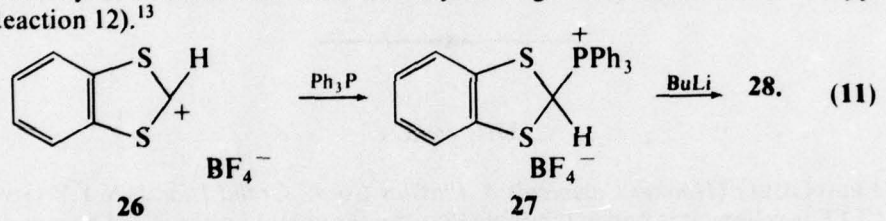
25

Thus this method is limited to selones of comparable coupling reactivity, and involves a laborious optimization of experimental conditions for each set of reactants studied. Furthermore, a final decarbomethoxylation step is involved to obtain the unsymmetrical products for use as donor molecules. Although this has been achieved readily in the case of **7**, this may present problems in the case of more sensitive compounds.

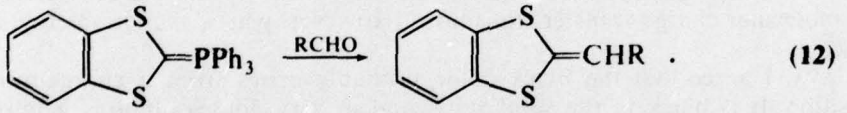
The success of the approach used by Wudl *et al.*[7] depended upon the fortuitious crystallization of the desired unsymmetrical product **12**. This method, however, will always produce a mixture of three TTF derivatives which, if of comparable polarity, may be virtually inseparable chromatographically.

Recently a fundamentally new TTF synthesis has been developed in our laboratory that should allow the preparation of a wide variety of unsymmetrical TTF derivatives from two different 1,3-dithiolium cations without the concomitant formation of symmetrical analogs.[12]

Ishikawa *et al.* recently reported the formation of the heterocyclic Wittig reagent **28** by the low-temperature deprotonation of the phosphonium salt **27**, which in turn was formed readily by reacting triphenylphosphine with the dithiolium salt **26** (Reaction 11); the existence of the unstable phosphorane **28** was proved by its reaction with various aldehydes to give dithiafulvenes of the type **29** (Reaction 12).[13]

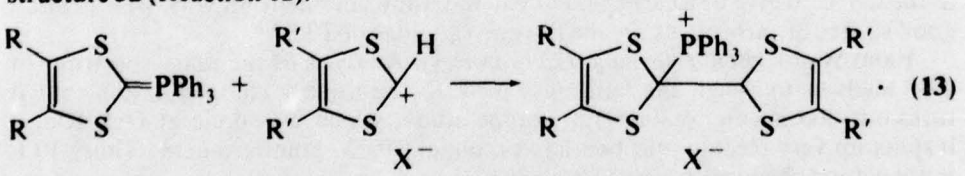


26 **27**



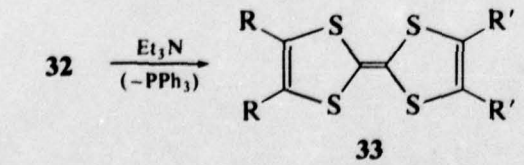
28 **29**

We have now found that phosphoranes of the type **30** (including **28**) react with 1,3-dithiolium salts **31**, giving intermediate phosphonium salts of general structure **32** (Reaction 12).[13]



30 **31** **32**

Deprotonation of **32** leads to triphenylphosphine elimination and the formation of the desired unsymmetrical TTF derivative **33** (Reaction 14).



33

The application of this novel approach to the synthesis of a variety of unsymmetrical π-donors is currently under active investigation in our laboratory.

References

1. Garito, A. F. & A. J. Heeger. 1974. Acc. Chem. Res. **7:** 218 and references cited therein.
2. Narita, M. & C. U. Pittman, Jr. 1976. Synthesis **6:** 489.
3. Hurtley, W. R. H. & S. Smiles. 1926. J. Chem. Soc.: 2263.
4. Melby, L. R., H. D. Hartzler & W. A. Sheppard. 1974. J. Org. Chem. **39:** 2456.
5. Bajwa, G. S., K. D. Berlin & H. A. Pohl. 1976. J. Org. Chem. **41:** 145.
6. Spencer, H. K., M. P. Cava & A. F. Garito. 1976. J.C.S. Chem. Commun.: 966.
7. Wudl, F., A. A. Kruger, M. L. Kaplan & R. S. Hutton. 1977. J. Org. Chem. **42:** 768
8. Green, D. 1977. J.C.S. Chem. Commun.: 161.
9. Mizuno, M. Unpublished observations.
10. Spencer, H. K. Unpublished observations.
11. Lakshmikantham, M. V. Unpublished observations.
12. Gonnella, N. Unpublished observations.
13. Ishikawa, K., K. Akiba & N. Inomoto. 1976. Tetrahedron Lett.: 3695.

Discussion

Fred Goetz (*Hooker Chemicals & Plastics Corp., Grand Island, N.Y.*): Given that TTF is yellow, it is understandable that the thiomethyl ester is red because of intramolecular charge-transfer transitions. However, why is the tetramethyl ester black?

Cava: I agree that the black color probably arises from a charge-transfer transition. It is black in the solid state, and in very dilute solutions it is really yellow or yellow brown; I think this color intensity increases with concentrations, but in the crystalline state it is quite striking—it looks like (TTF)(TCNQ).

A. R. Siedle (*National Bureau of Standards*): We have looked very hard for products derived from TTF and organometallics that would correspond to rupture of the C=C to give us a carbene. Do you have any comment on why TTF is not a good source of carbene, as are the nitrogen analogs of TTF?

Fred Wudl (*Bell Telephone Laboratories*): Analysis of the mass spectrum of TTF leads us to assign the half-mass peak to the doubly charged cation, but it turns out that if you do a careful isotope study, which was done at Oak Ridge, it splits up very cleanly into two halves, under 70 eV bombardment. Thus, TTF is not a good chemical source of carbenes.

NEW SYNTHETIC PROCEDURE FOR THE PREPARATION OF MONOSUBSTITUTED TETRATHIAFULVALENES*

Dennis C. Green

IBM Thomas J. Watson Research Center
Yorktown Heights, New York 10598

Since the discovery of tetrathiafulvalene (TTF),[1] with its unique electron-donating properties, many modifications of the molecule have been attempted through the preparation of various substituted TTF derivatives. A recent review by Pittman[2] outlines eight different methods for the synthesis of disubstituted and tetrasubstituted tetrathiafulvalenes. All of these methods, however, yield only symmetrical substitution in the 2,6; 2,7; or 2,3,6,7 positions. More recently the unsymmetrical 2,3-dimethyltetrathiafulvalene,[3] 2,3-benzotetrathiafulvalene,[2] and 2,3-benzo-6,7-di(methoxycarbonyl)tetrathiafulvalene[2] have been reported by mixed-coupling techniques. There are disadvantages, however, to the mixed coupling method that limit its use as a general method for the preparation of monosubstituted or unsymmetrical multisubstituted TTF derivatives, as shown in FIGURE 1. There are separation problems due to the multiple products that are formed, especially when R and R′ are similar. Conversely, when R and R′ are very different, the reactivities of the starting compounds are often affected such that the self-coupled products are favored. Furthermore, the versatility of the method is limited by the nature of the substituents R and R′ so that they must be inert to the coupling reagents. Thus, many functional groups such as the aldehyde, carboxylic acid, or hydroxymethyl, are not readily compatible with the reagents used in the coupling method.[5]

Most reagents for direct substitution on TTF such as bromine[1] or mercuric chloride[6] result only in oxidatitive attack to yield the radical cation or dication salts. As a consequence, the chemistry of TTF has been ignored except for the preparation of its various salts. We have found, however, that butyl lithium metalates TTF[7,8] at low temperature to provide a route to many new mono- and multisubstituted TTF derivatives, some of which are shown in FIGURE 2 and, later, FIGURE 5. This route has a number of advantages over previous methods:

1. It is the first general method for the preparation of monosubstituted and multisubstituted (symmetric and asymmetric) tetrathiafulvalenes.
2. The starting material is commercially available.
3. The yields are generally good. Initial results have given yields of 35–65 percent for the monosubstituted derivatives.
4. There are few separation problems. The exception to this is the case of alkylated derivatives such as methyl TTF. The reaction of LiTTF with Me_2SO_2 yields methyl TTF plus small amounts of TTF and dimethyl TTF, which presents a difficult purification problem. Importantly, though, the hydroxymethyl TTF is

*Manuscript received June 6, 1977.

0077-8923/78/0313-0361 $1.75/1 © 1978, NYAS

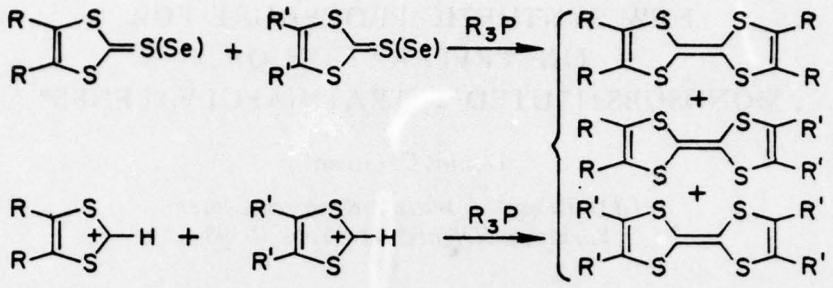


FIGURE 1. The mixed coupling method.

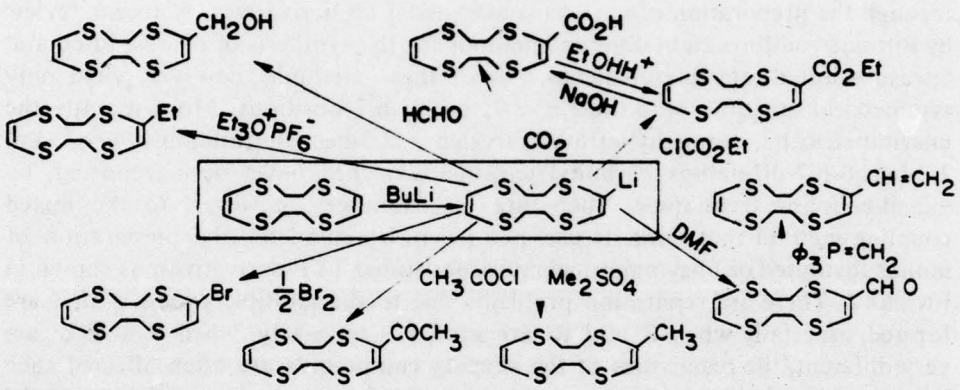


FIGURE 2. Some reactions of tetrathiafulvalenyl lithium.

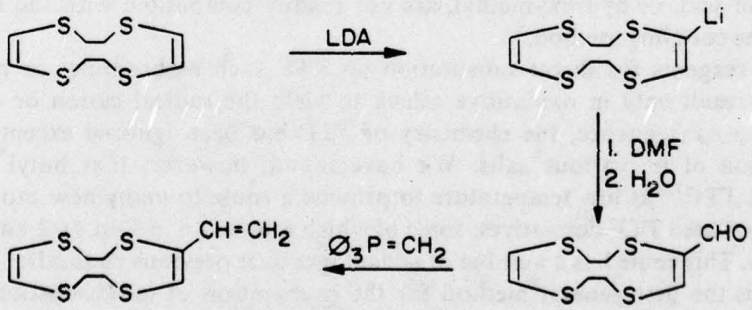


FIGURE 3. Synthesis of vinyl TTF.

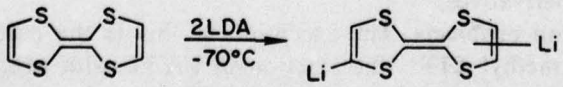
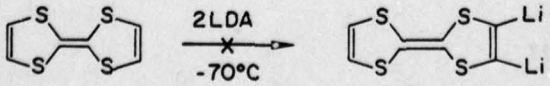


FIGURE 4. Dilithiation.



purified with ease, and work is currently under-way to reduce this to the methyl derivative.

5. The method offers increased versatility over previous methods. For instance, the hydroxymethyl derivative is easily prepared by reaction of LiTTF with formaldehyde gas. This had not been made previously by a direct method. The di(hydroxymethyl) TTF has been made, although, by the indirect method of reduction of the dicarbonylchloride of dicarboxy TTF with lithium tri- *tert* -butoxyaluminum hydride[9] and by reaction of dicarboxy TTF with B_2H_6[10]. In addition, no aldehyde derivative of TTF had been previously reported. Formyl TTF, though, is easily prepared by reaction of LiTTF with dimethylformamide followed by an aqueous workup. The ability to prepare TTF derivatives with functional groups such as the formyl, hydroxymethyl, and others as substituents is of considerable importance because of the additional chemistry that can be carried out utilizing the functional group. For instance, formyl TTF undergoes a Wittig reaction with methylene triphenylphosphorane to yield vinyltetrathiafulvalene, as in FIGURE 3.

TABLE 1

ELECTROCHEMICAL OXIDATION POTENTIALS* OF TETRAHETEROFULVALENES

Compound	E_1	E_2
TTF[13]	0.34	0.71
$TTFCO_2H$	0.47	0.83
$TTFCO_2Et$	0.47	0.83
$TTF(CO_2Et)^2$	0.60	0.94
$TTF(CO_2Me)^4$	0.80	1.08
TTFEt	0.33	0.70
TTF Me	0.33	0.70
TTF Vi	0.42	0.77
$TTFCOCH_3$	0.47	0.83
TTF CHO	0.53	0.89
TTF Me CO_2Et	0.45	0.81
TTF Me_2CO_2Et	0.43	0.79
TTF $Me(CO_2Et)_2$	0.54	0.87
TSeF[13]	0.48	0.76
TSeF CO_2H	0.63	0.90

*Peak potentials vs. SCE.

6. Monofunctionalization can be achieved by this method. Since most functional groups are electron withdrawing, the presence of such functional groups detract from the unique electron-rich character of TTF. The importance of monofunctionalization is demonstrated in the table of electrochemical oxidation potentials. The previously reported tetracarboxy and dicarboxy tetrathiafulvalenes have oxidation potentials of 0.80 V and 0.60 V[11] (respectively as their ester derivatives) and have not been reported to form conducting charge-transfer salts with tetracyanoquinodimethane (TCNQ), whereas the monocarboxytetrathiafulvalene has an oxidation potential of 0.47 V (compared with 0.34 V for TTF) and forms a highly conducting charge-transfer salt with $TCNQ^-$. Thus monofunctionalized tetrathiafulvalenes retain the unique electron-donating ability of TTF and have the

additional advantage of possessing a functional group that can be used to attach TTF to other systems such as electrode sulfaces[12] and other chemical systems.

7. The method is a more direct route to some TTF derivatives. As an example, the carboxytetrathiafulvalenes have not been prepared directly. It has instead, been necessary to first prepare the ester derivative and perform the subsequent saponification. Carboxy TTF, however, can be prepared directly from LiTTF by reaction with CO_2. A further example of the directness of this method is the previously mentioned preparation of hydroxymethyl TTF.

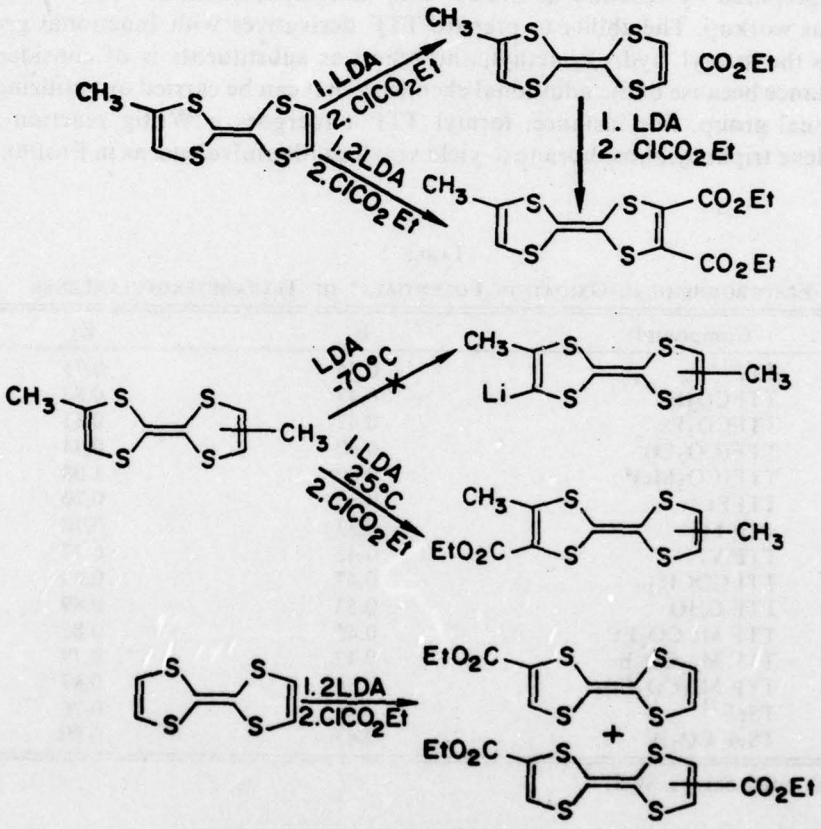


FIGURE 5. Multisubstitution.

Thus, a number of monosubstituted tetrathiafulvalenes have already been prepared, and further, more interesting derivatives can be envisioned. The bromotetrathiafulvalene, as shown in FIGURE 1, has not yet been prepared, since an initial attempt failed, but milder conditions are being pursued in order to obtain this compound.

The synthesis of vinyl TTF shown in FIGURE 3 is of potential value in the preparation of polymer systems with interesting electronic properties. Vinyl TTF has been found to polymerize slowly at room temperature even under inert at-

mosphere dry-box conditions. Controlled polymerization studies are currently under way.

Multisubstitution of TTF can be achieved by the lithiation route, either by multilithiation or by sequential substitution. For these purposes lithium diisopropylamide (LDA) was used in place of BuLi in order to have a less nucleophilic lithiation reagent. Dilithiation yielded the 2,6(7) substitution pattern with no evidence of 2,3 substitution occurring, as shown in FIGURE 4.

For sequential substitution, (see FIGURE 5), electron-donating substituents were found to decrease the acidity of the adjacent allylic proton, resulting in 2,6(7) substitution, whereas electron-withdrawing substituents increased the acidity of the adjacent proton with the consequent predominance of the 2,3 substitution. Furthermore, 2,6(7) dimethyl tetrathiafulvalence was found to be unreactive with LDA at $-70°C$ but would react at 25°C. From these results one can readily extrapolate the considerable flexibility and substituent control that is offered through sequential substitution toward the custom engineering of specified properties into new TTF systems.

In conclusion, the metalation method for introduction of substituents onto TTF provides tremendous potential for the preparation of new mono- and multisubstituted TTF derivatives. This metalation method also demonstrates that, although long ignored, chemistry can be affected on TTF and should be further explored.

NOTES AND REFERENCES

1. WUDL, F., G. M. SMITH & E. J. HUFNAGEL. 1970. Chem. Commun.: 1453.
2. NARITA, M. & C. U. PITTMAN, JR. 1976. Synthesis: 489.
3. WUDL, F., A. A. KRUGER, M. L. KAPLAN & R. S. HUTTON. 1977. J. Org. Chem. **42:** 768.
4. SPENCER, H. K., M. P. CAVA & A. F. GARITO. 1976. Chem. Commun.: 966.
5. It is recognized that these groups may be protected, but this involves additional synthetic steps and possible incompatibility of the protecting reagent with the parent compound itself.
6. GREEN, D. C. Unpublished data.
7. GREEN D. C. 1977. Chem. Commun.: 161.
8. TTF was obtained from the Aldrich Chemical Co.
9. HERTLER, W. R. 1976. J. Org. Chem., **41:** 1412.
10. PITTMAN, C. U., Jr. 1976. J. Org. Chem. **41:** 2855.
11. Oxidation potentials are reported as peak potentials vs. SCE: Pt electrode: 0.1 M tetraethylammonium perchlorate: CH_3CN.
12. MURRAY, R. W., P. R. MOSES, & D. C. GREEN. To be published.
13. ENGLER, E. M., F. B. KAUFMAN, D. C. GREEN, C. E. KLOTS & R. N. COMPTON. 1975 J. Amer. Chem. Soc. **97:** 2921.

A NEW π-DONOR FOR THE STUDY OF ORGANIC METALS*

William P. Krug, Aaron N. Bloch, Theodore O. Poehler, and Dwaine O. Cowan†

Department of Chemistry
The Johns Hopkins University
Baltimore, Maryland 21218

Considerable synthetic effort has been devoted to the preparation of congeners of the donor molecule tetrathiafulvalene[1] (TTF). These π-donors can yield highly electrically conducting charge-transfer salts when oxidized by the acceptor TCNQ. The conducting members of the TTF-TCNQ family[2] consist of separate stacks of radical cations and radical anions with fractional charge-transfer per formula unit and strong intermolecular coupling, principally in the stacking direction. These quasi-one-dimensional organic conductors typically undergo transitions from metallic to insulating phases as the temperature is lowered. An exception is the TCNQ charge-transfer salt of hexamethylenetetraselenafulvalene, HMTSF-TCNQ **1**,[3] the first organic substance whose conductivity remains metallic in magnitude to very low temperature (0.045°K). It is in the interchain coupling that **1** contrasts sharply with other members of the class. Along one transverse axis, the intermolecular Se · · · N contacts[4] are unusually short. Along the other, the interactions are weak, and the structure heavily disordered. In combination, these effects suppress the Peierls transition and may render HMTSF-TCNQ family.

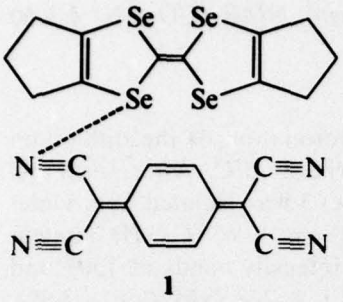
To further probe the steric and electronic factors controlling the Peierls instability,[5] we have synthesized the donor 3. We anticipate that a complex of **3** with TCNQ could have even greater interchain coupling and more metallic low-temperature behavior than HMTSF-TCNQ **1**. The procedure we utilized was developed in our preparation[6] of the previously known compound **2**.[7] The dimerization of the alkylated thione **6** closely parallels Wudl's convenient route[8,9] to unsubstituted TTF. All other schemes to dimerize **5** proved ineffective.[1] The electrochemically formed dithiolate **4**[10] reacts with excess methylene iodide in ethanol to give thione **5**‡ in 38% yield after chromatography (based on current passed) as a bright orange microcrystalline solid, with the following results: mp 159–161°C (from hexanes-methylene chloride); ir: strong (C=S) stretch at 1033 cm^{-1} and weak (C=C) at 1463 cm^{-1}; NMR ($CDCl_3$) δ 4.95 (s); UV (CH_2Cl_2) 252–270 NM (log ϵ 3.79–3.74), 350 (3.04), 429 (4.02); mass spectrum M/E 210 (M^+, 100), 166, (M^+—CS, 8), 164, (M^+—CHS_2, 4) 146 (M—S_2, 15), 134, (M^+—CS_2, 7), (100, C_3S_2, 4), 90 ($C_2H_2S_2$, 21), 88 (C_2S_2, 100), 76 (CS_2, 26). **5** was methylated by $(CH_3O)_2CHPF_6$ in 91% yield to afford orange crystal-

*Supported by National Science Foundation (DMR 76-84238) and the Material Science Office, Advanced Research Projects Agency, Department of Defense. Manuscript received Nov. 7, 1977.

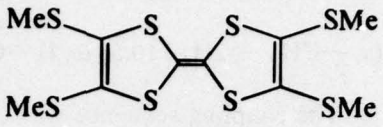
†Visiting scholar, Stanford University, 1977–1978, Stanford, California 94305.

‡Compounds **3**, **5**, **6**, and **7** gave satisfactory C and H analyses.

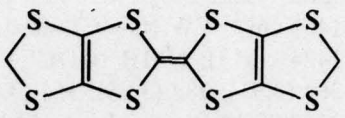
0077-8923/78/0313-0366 $1.75/1 © 1978, NYAS



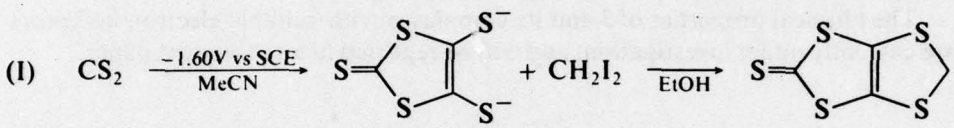
1



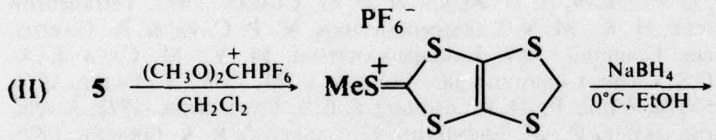
2



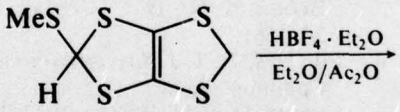
3



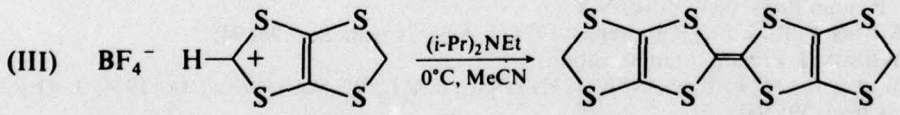
4 5



6



7



8 3

line solid **6** MP 156–157°C. Subsequent reduction of **6** with excess sodium borohydride at 0°C in ethanol gave the 2-s-methyl-1,3-dithiole **7** as a pinkish-orange solid in 93% yield, MP 71–74°C; NMR ($CDCl_3$) δ 2.27 (s, 2-S—CH_3, 3H), δ 4.70 (d, J = 10 Hz, 1 H of —CH_2—), δ 4.97 (d, J = 10 Hz, 1 H of —CH_2), δ 6.42 (S, H—CS_3, 1 H). Acidification of **7** in a diethyl ether-trace acetic anhydride solution by a fluoboric acid: diethyl ether complex generated the desired di-

thiolium salt **8** as a yellow-orange powder in 88%, yield, NMR (CD_3CN) δ 5.50 (s, $-CH_2-$, 2H) δ 10.53 (s, H—C(⊕)(S⁻)(S⁻) 1 H).

The coupling sequence was completed by a deprotonation of the dithiolium salt **8** with N,N-diisopropylethylamine in acetonitrile at 0°C. After silica gel column chromatography (hexanes-methylene chloride) **3** was isolated as a violet solid, yield 50%, MP 154–156°C, IR (KBr) (2921 cm^{-1} W (C—H) stretch, 1463 cm^{-1} VW (C=C) vibration; there are medium intensity bands at 1301 and 1424 cm^{-1}); NMR ($CDCl_3$) δ 4.97 (s), UV (CH_2Cl_2)§ 242 NM (log ϵ 3.99), 264 (3.91), 282 (3.88), 354 (3.69), 542 (3.61); mass spectrum M/E 355.8072 (calc. 355.8079); low resolution M/E (fragment, intensity), 356 (M^+, 33), 312 (M^+—CS, 33), 266 ($C_6H_2S_6$, 23), 234 ($C_6H_2S_5$, 12), 222 ($C_5H_2S_5$, 69), 178 ($M^+/2$, 15), 100 (C_3S_2, 41), 90 ($C_2H_2S_2$, 19), 88 (C_2S_2, 79), 76 (CS_2, 100).

The physical properties of **3** and its complexes with suitable electron acceptors are currently under investigation, and will be reported in a subsequent paper.

References

1. Narita, M. & C. U. Pittman. 1976. Synthesis: 489. A review.
2. Ferraris, J. P., T. O. Poehler, A. N. Bloch & D. O. Cowan. 1973. Tetrahedron Lett.: 2553; Spencer, H. K., M. V. Lakshmikantham, M. P. Cava & A. Garito. 1975. J.C.S. Chem. Commun.: 867; Lakshmikantham, M. V., M. Cava & A. Garito. 1975. J.C.S. Chem. Commun.: 383; Engler, E. M. & V. V. Patel. 1974. J. Am. Chem. **96:** 7376; Wudl, F., D. Wubschall & E. J. Huffnagel. 1972. J. Am. Chem. **94:** 670; Schumaker, R., M. Ebenhahn, G. Castro & R. L. Greene. 1975. Bull. Amer. Phys. Soc. **20:** 495.
3. Bechgaard, K., D. O. Cowan & A. N. Bloch. 1975. J.C.S. Chem. Commun.: 671; Bloch, A. N., D. O. Cowan, R. E. Pyle & R. H. Banks. 1975. Phys. Rev. Lett. **34:** 1561.
4. Phillips, T., T. J. Kistenmacher, A. N. Bloch & D. O. Cowan. 1976. J.C.S. Chem. Commun.: 334.
5. Jerome, D. & M. Weger. 1977. *In* Proc. NATO Conf. Chemistry and Physics of One-Dimensional Metals. H. J. Keller, Ed. Plenum Press. New York, N.Y.
6. Cowan, D. O., P. Shu, W. Krug, T. Carruthers, T. Poehler & A. N. Bloch. 1977. *In* Chemistry and Physics of One-Dimensional Metals. H. J. Keller, Ed. Plenum Press. New York, N.Y.
7. Moses, P. R. & J. Q. Chambers. 1974. J. Amer. Chem. Soc. **96:** 945.
8. Wilson, J. Private communication.
9. Wudl, F., M. P. Kaplan, E. J. Huffnagel & E. W. Southwick, Jr. 1974. J. Org. Chem. **39:** 3608.
10. Wawzonek, S. & S. Heilmann. 1974. J. Org. Chem. **39:** 511; Bontempelli, G., F. Nago, G. Mazzochin & R. Seeber. 1975. J. Electroanalyt. Chem. Interfacial Electrochem. **63:** 231.

§All U.V. absorptions are very broad and shoulderlike; visible absorption is sharp.

CRYSTAL CHEMISTRY OF MIXED-VALENCE TTF SALTS*

B. A. Scott, S. J. LaPlaca, J. B. Torrance†
B. D. Silverman, and B. Welber

IBM Thomas J. Watson Research Center
Yorktown Heights, New York 10598

INTRODUCTION

A necessary structural condition for the occurrence of the "metallic state" in the organic charge-transfer salts is the segregation of the constituent π-donor and acceptor ions into their own stacks within these pseudo-one-dimensional compounds. This arrangement of charged donors and acceptors would appear to be inherently unstable, due to strong intrastack repulsive coulombic forces. To understand the factors that stabilize such a structure we have investigated the crystal chemistry of the π-donor tetrathiafulvalene (TTF) with strong electron acceptors —the halogens (Z).[1,2] Such systems produce compounds having structures with single, conducting, donor stacks combined with nonconducting (closed shell) Z^- anion chains. Moreover, the salts $(TTF)Z_\rho$ are mixed valency phases; i.e., the oxidation state ρ of the donor is nonintegral and, usually, $\rho < 1$. The beauty of these compounds is that the measurement of ρ can be carried out routinely by chemical analysis. Much greater effort is required to deduce this important quantity in the two-stack systems such as (TTF)(TCNQ).[3-5] As we shall see, such a trivial measurement as stoichiometry yields important information regarding the factors that stabilize the segregated-stack crystal structure, and in so doing provides a simple framework in which to understand the origin of the organic metallic state.

METHODS AND MATERIALS

The phases isolated in the TTF-halide systems were systematically prepared by three different chemical methods: (1) Titration of TTF with solutions of halogen in acetonitrile and CCl_4[1d] (2) electrochemical oxidation of TTF to predetermined values of ρ followed by the addition of halide[6], and (3) photochemical oxidation of TTF in CCl_4 or CBr_4 solutions by UV-light.[7]

RESULTS AND DISCUSSION

Crystal Chemistry

Phases prepared in the three TTF-halogen systems are summarized diagrammatically in FIGURE 1. Their crystallographic details have been presented sepa-

*Manuscript received June 6, 1977.
†Present address: IBM Research Laboratory, San José, Calif.

0077-8923/78/0313-0369 $1.75/1 © 1978, NYAS

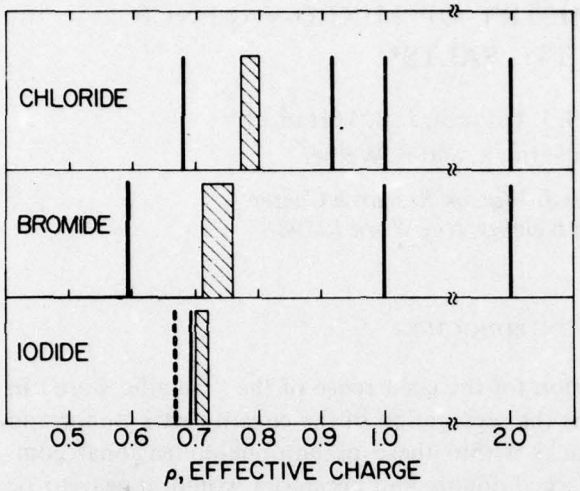


FIGURE 1. Phases observed in the (TTF)-halide (Z) systems plotted as $(TTF)Z_\rho$, where ρ is the halogen content defining the effective (or averaged) charge per cation site, as discussed in the text. The dashed line corresponds to "$(TTF)I_2$", as explained in the text.

rately,[1] and only the major structural features will be discussed here. Lattice constants for all the relevant phases are given in TABLE 1. The observed phase compositions are delineated in terms of the effective cation charge parameter ρ, defined as above by the results of chemical analysis of the pure phases (the halide content of their lattices). This parameter therefore provides a measure of degree of oxidation of the TTF chains in the compounds formed, or the degree of charge transfer from the donor stack to the acceptors, which are fully charged. Summarizing the results briefly, we find two kinds of $(TTF)Z_\rho$ phases: the insulating isovalence cation phases with $\rho = 1$ and 2, and the conducting mixed-valence segregated-stack compounds where ρ is fractional and <1. These latter compounds can be further divided into disordered and ordered halide sublattice phases, where we

TABLE 1

UNIT CELL DATA FOR THE TTF-HALIDES*

	Chlorides	Bromides		Iodides	
Monocation Salts	(TTF)Cl $a = 11.073$ $b = 11.218$ $c = 13.95$	(TTF)Br $a = 11.242$ $b = 11.366$ $c = 14.143$		not observed	
Ordered Mixed-Valence Salts	TTF $Cl_{0.77}$ $a = 10.77$ $b = 3.56$ $c = 22.10$	$(TTF)Br_{0.76}$ sublattice		$(TTF)I_{.72}$ sublattice	
		TTF	Br	TTF	I
		$a = 15.617$	17.368	15.998	8.19
		$b = 15.627$	15.623	16.114	16.11
		$c = 3.572$	4.538	3.558	4.871
		$\beta = 91.23°$	116.01°	90.96°	102.82°
Disordered Mixed-Valence Salts	$(TTF)Cl_{0.68}$ $a = 11.12$ $c = 3.595$	$(TTF)Br_{0.59}$ $a = 11.05$ $c = 3.562$		$(TTF)I_{0.69}$ $a = 11.34$ $c = 3.77$	

*In Å units. Compounds shown in FIGURE 1 but absent here are discussed in Ref. 1d.

find $0.7 < \rho$ (ordered) < 0.8 and ρ (disordered) < 0.7. Distinct homogeneity ranges were determined[1] for the ordered phases as shown in FIGURE 1. Note that in all subsequent discussion we use "degree of oxidation" and "degree of charge transfer" interchangeably for the mixed-valence phases.

Of the two isovalence salts, only the fully charge-transferred ($\rho = 1$), isomorphic, and insulating[1d] salts (TTF)Cl and (TTF)Br are of interest, since the dication salts contain no free radicals. As shown in FIGURE 2, the orthorhombic unit cell of (TTF)Br contains eclipsed free-radical TTF^+ dimers, tilted $\sim 24°$ with respect to the c-axis, with an intradimer spacing of 3.34 Å. The dimers are interspersed with pairs of bromine ions with an interhalide distance of 4.15 Å. The halide

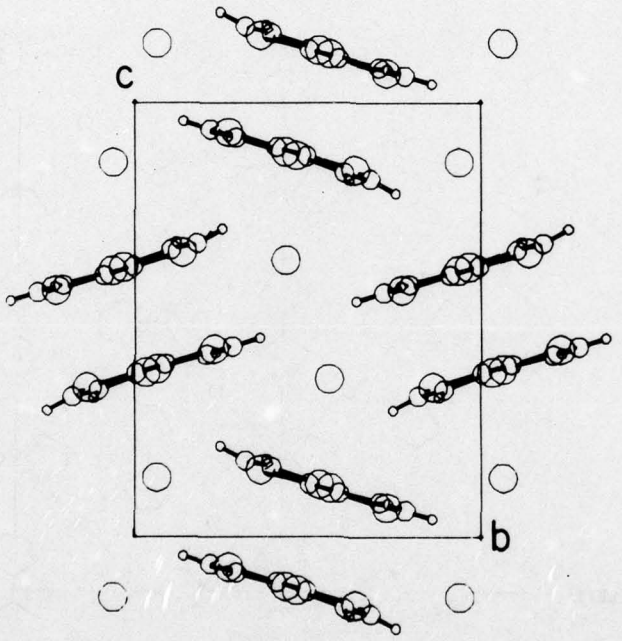


FIGURE 2. Bounded (*a*-axis) projection of the orthorhombic crystal structure of (TTF)Cl and (TTF)Br.

ions and the center of the TTF^+ molecules, shown in the a-axis bounded projection of FIGURE 2, lie nearly in the bc plane. Thus, the structure of (TTF)Br exhibits nearly complete isolation of the $(TTF^+)_2$ dimers along the c-axis. This is reflected in its electrical conductivity: $\sigma_c < 10^{-6}$ $(\Omega\text{-cm})^{-1}$, some eight orders of magnitude smaller than the mixed-valence phases.

The prominent mixed-valence TTF-halides are the ordered phases $(TTF)Z_\rho$ whose compositions fall in the range $0.7 < \rho < 0.8$. We have previously reported[1] the two-subcell structure and homogeneity range of $(TTF)Br_{0.71\text{–}0.76}$. The projection of this structure encompassing four of the monoclinic (pseudotetragonal) unit cells is shown in FIGURE 3. The structure consists of two separate, *ordered,* incommensurate, monoclinic sublattices for TTF and Br, with an equal

number of TTF and Br stacks running along the c-axis. The TTF-TTF distance within the donor stacks is fixed (z_0 = 3.57 Å), while the interhalide distance is constant (z_1) and composition dependent in the ordered mixed valence phases ($\rho = z_0/z_1$; cf. FIGURE 4). A full analysis of the actual three-dimensional modulated structure only recently has been carried out by Johnson *et al.*[8a] for the isomorphic $(TTF)I_{0.70-0.72}$ salt. By contrast, the ordered chloride phase exhibits the closely related orthorhombic structure given by the largest dashed cell of FIGURE 3.

If the halide stacks in the ordered phases are disordered, the unit cell collapses to the smallest tetragonal cell in FIGURE 3 (dashed), and the composition shifts to values of $\rho < 0.7$. The composition shift is largest for the bromide phase (0.71 → 0.59) and smallest for the iodide (0.70 → 0.69), although as previously pointed

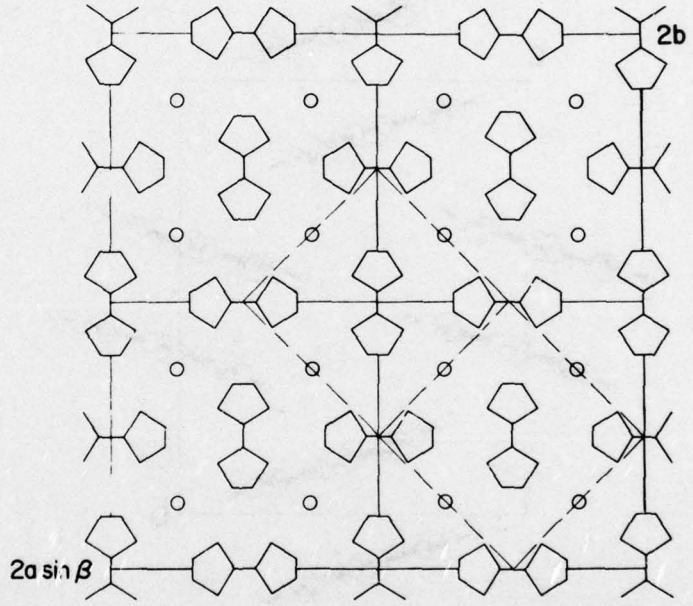


FIGURE 3. Projection parallel to the *c*-stacking axis of the crystal structures of all mixed-valence $(TTF)Z_\rho$ phases ($\rho < 1$), with the exception of $(TTF)Cl_{0.92}$. The various unit cells are given in TABLE 1.

out,[1d] the disordered iodide could contain I_3^- and other polyiodide species so that the actual extent of charge transfer from the TTF stacks is not measurable by chemical analysis. This effect is more clearly exemplified by the disordered compound $(TTF)I_2$ first reported by Johnson and coworkers[8b] and more explicitly written $(TTF^\circ)(TTF^+)_2(I_3^-)_2$. Although at first sight it would appear to be a dication phase, it is shown properly as the dotted phase at ρ = 0.67 in FIGURE 1.

The major point to be understood, of course, is why do the halides adopt the various compositional and structural features shown in FIGURES 1–3? In FIGURE 4 we have outlined these features schematically, beginning with a hypothetical fully charge-transferred, segregated stack, (TTF)Br in FIGURE 4(b). Such a structure has not been observed; indeed, the fully charge-transferred salt is stable at ρ = 1

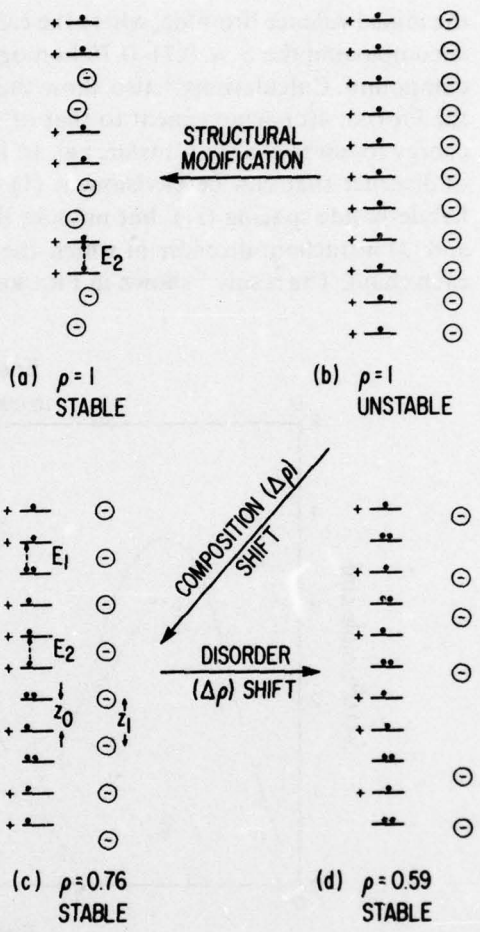


FIGURE 4. Schematic representation of phase and structure stability relationships among the TTF-halides. The structure in (b) is hypothetical, undergoing the "transformations" outlined in *Crystal Chemistry*. The IR transitions E_1 and E_2 expected in these systems are also shown in (a) and (c) and discussed in *Optical Properties*. For the ordered phases in (*c*), the ratio z_0/z_1 defines the composition parameter ρ, with z_0 = 3.57 Å.

only in the integrated stack-dimerized arrangement of FIGURE 4 (a). For the segregated form to be stable, a composition, or charge transfer, shift (FIGURE 4 (c)) must occur to ρ = 0.76 (for the Br^- salt). The reason for this is that the electrostatic binding energy favors the mixed-valence state as shown in FIGURE 5. From this figure, which summarizes the results of detailed Madelung energy calculations,[1d,2] it is clear that the ρ = 1 structure of FIGURE 4 (b) is 25% less bound than

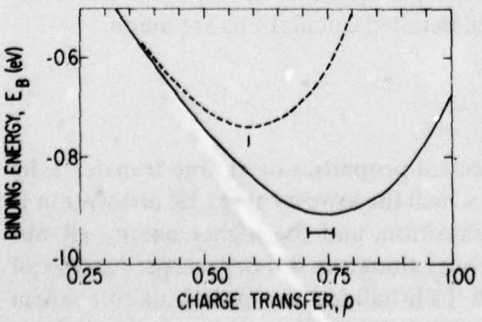


FIGURE 5. Calculations showing binding energy of ordered $(TTF)Br_\rho$ as a function of composition, or degree of oxidation, ρ (solid curve) and the effect of disorder on the binding energy (dashed curve). Band energies have been included in the calculations. Bars indicate the observed composition ranges.

the mixed valence bromide, where the calculations show a broad energy minimum encompassing the $\rho = 0.71$–0.76 homogeneity range we have determined for this compound. Calculations[1d] also show that disordering of the halide subcell from the FIGURE 4(c) arrangement to that of FIGURE 4(d) shifts the maximum binding energy to lower charge transfer, i.e., to lower halide content. There are two types of disorder that can be envisioned: (1) interchain disorder, which preserves the halide-halide spacing (z_1), but unlocks the phase of the chains from cell to cell, and (2) intrachain disorder in which the halide-halide spacing is variable within each chain. The result[1d] shown in FIGURE 5 for the more easily calculated case (2)

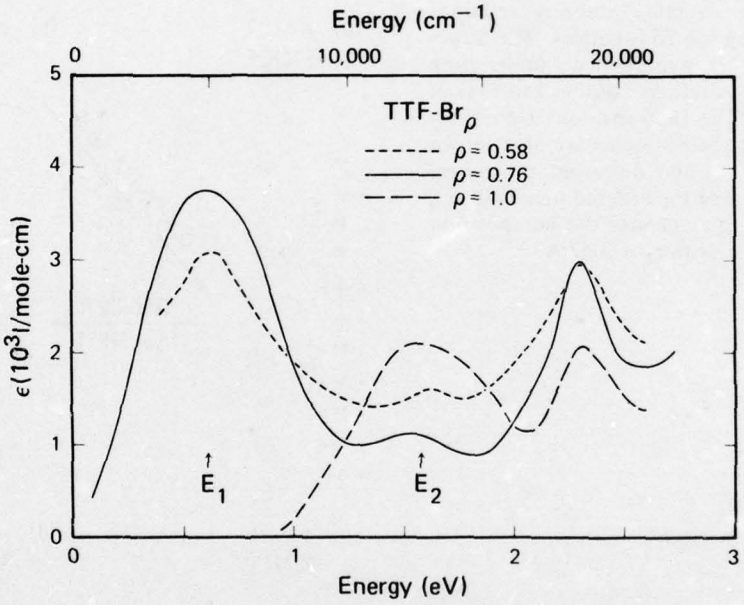


FIGURE 6. Infrared absorption spectra of (TTF)Brρ compounds with $\rho = 0.59$, 0.76 and 1.0, showing the effect of the degree of oxidation. The spectra were taken on pelletized dispersions (1 wt percent concentrations) of each compound in KBr or KCl matrices ($\rho = 0.76$, 1.0), or thin films ($\rho = 0.59$)[1d,10].

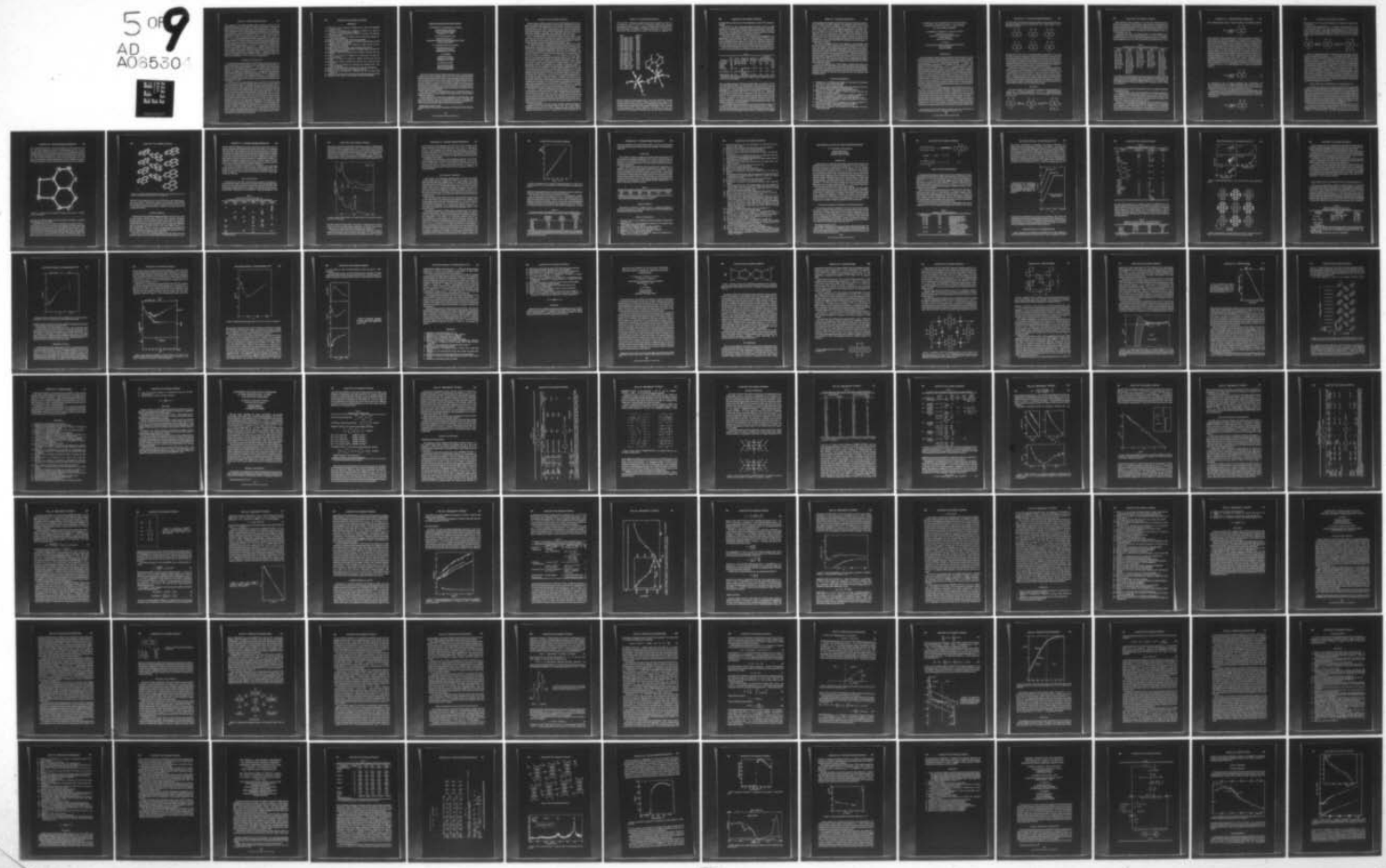
gives excellent agreement with the composition of the disordered mixed valence halide. Although it is this type of disorder which would seem, intuitively, from simple coulomb arguments,[1d] to affect the composition the most, we can not completely rule out interchain disorder (1) until detailed calculations are made.

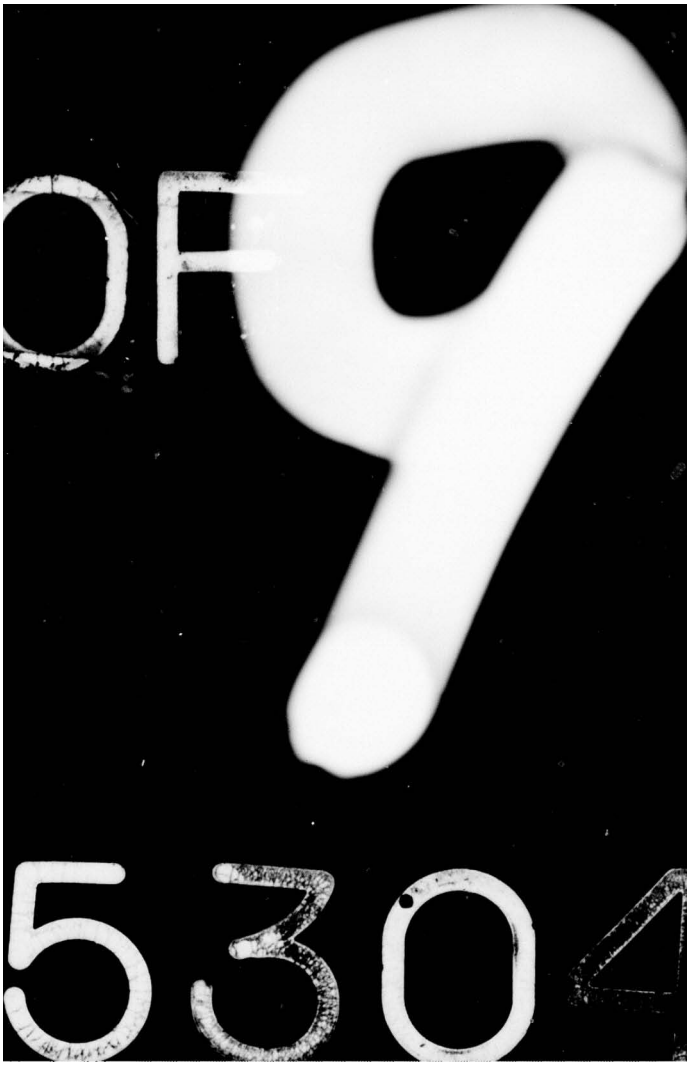
Optical Properties

In previous work[9] we described the optical properties of charge-transfer salts of TCNQ, using a Hubbard-like model in which the lowest energy IR absorption is assigned to a mixed-valence, intraband transition, and the higher energy IR absorption to interband excitations (isovalence) along the donor/acceptor stacks of these compounds. The simple single-stack TTF-halides now permit us to confirm

AD-A065 304 NEW YORK ACADEMY OF SCIENCES N Y F/G 7/2
SYNTHESIS AND PROPERTIES OF LOW-DIMENSIONAL MATERIALS,(U)
1978 J S MILLER, A J EPSTEIN N00014-77-C-0374
UNCLASSIFIED NL

5 OF 9
AD
A065304




OF 9
5304

these assignments. The powder absorption spectra are shown in FIGURE 6. By comparison with these more complex, two-chain, TCNQ systems, we assign the spectra of FIGURE 6 for the mixed-valence TTF-bromides with $\rho = 0.58$ and $\rho = 0.76$ to analogous transitions in these single-stack compounds.[10] Thus, the absorption centered at $E_1 = 0.6$ eV can be interpreted (see FIGURE 4(c)) as an intervalence charge-transfer transition of the type $(TTF^{\circ}, TTF^{+}) \rightarrow (TTF^{+}, TTF^{\circ})$, and the band at $E_2 = 1.55$ eV, as an isovalence transition of the type $(TTF^{+}, TTF^{+}) \rightarrow (TTF^{++}, TTF^{\circ})$. Such assignments are entirely consistent with our single-crystal reflectivity results.[1d,10] There we found that both transitions are polarized along the stacks; also, both E_1 and E_2 transitions would be expected in the highly conducting subhalide compositions $\rho = 0.58$ and 0.76, but only the higher energy transition at E_2 should be observed in the $\rho = 1$ sample, since it contains only $(TTF^{+})_2$ isolated dimers. This is indeed the case, as shown in FIGURE 6 and confirmed in signal crystal studies. We have previously related the transition at E_2 to the Coulomb intermolecular correlation energy, U, associated with the repulsion of two charges on a given molecule.[9,10] Thus, as discussed in detail elsewhere,[10] we estimate that $U \approx E_2 = 1.5$ eV at near-IR frequencies.

SUMMARY AND CONCLUSIONS

Crystal chemical and phase studies of the TTF-halide systems show the existence of mixed-valence donor-halide salts having segregated stack structures, in addition to the fully charge-transferred $\rho = 1$ and 2 phases. The mixed-valence phases occur with both ordered and disordered halide sublattices, and ρ(disordered) < ρ(ordered). The stability of the $\rho < 1$ mixed-valence compounds is directly related to the greater Madelung binding of the subhalide compounds compared to their hypothetical, fully charge-transferred ($\rho = 1$), segregated-stack structures. Additionally, the near IR spectra of the mixed and isovalence compounds permitted an estimate to be made of the intramolecular Coulomb correlation energy, $U \approx 1.5$ eV.

As we have seen, the crystal-binding energy is optimized for single organic stack structures such as the TTF subhalides by forming a mixed-valence stack. In this case, the mixed valency is achieved by adopting a halide-deficient structure. In the case of the two-stack charge-transfer salts of TCNQ, such deficiencies in the donor or acceptor stacks would be sterically unfavorable, but the ability of TCNQ (like TTF) to exist as either neutral molecules of singly charged ions in a crystal permits the two stack systems to adopt mixed valence states on both donor and acceptor stacks to optimize E_B. In this case, the mixed-valence state is achieved by incomplete transfer of charge from the donor to TCNQ. This effect not only maximizes E_B, but is also of paramount importance to the attainment of high electrical conductivity in the entire class of segregated stack TCNQ salts. High conductivity results because U is effectively avoided for $\rho < 1$ through the existence of sites for electrons (or holes) to reside that are not already populated; e.g., $(TCNQ^{-}, TCNQ^{\circ}) \rightarrow (TCNQ^{\circ}, TCNQ^{-})$. Thus, the electrostatic need for mixed valency creates a physically stable ground state in which there exist nearly optimum conditions for high electrical conductivity in these segregated stack, pseudo-one dimensional, organic charge-transfer salts.

REFERENCES

1a. LAPLACA, S. J., P. W. R. CORFIELD, R. THOMAS & B. A. SCOTT. 1975. Solid State Commun. **17**: 635.

1b. SCOTT, B. A., J. B. TORRANCE, S. J. LAPLACA, P. CORFIELD, D. C. GREEN & S. ETEMAND. 1975. Bull. Am. Phys. Soc. **203**: 496.

1c. LAPLACA, S. J., J. E. WEIDENBORNER, B. A. SCOTT & P. CORFIELD. 1975. Bull. Am. Phys. Soc. **203**: 496.

1d. SCOTT, B. A., S. J. LAPLACA, J. B. TORRANCE, B. D. SILVERMAN & B. WELBER. 1977. J. Am. Chem. Soc. **99**: 6631.

2a. TORRANCE, J. B. & B. D. SILVERMAN. 1977. Phys. Rev. **B15**: 788.

2b. TORRANCE, J. B. 1976. Proc. Conf. Organic Conductors and Semiconductors. Siofok, Hungary. August. To be published.

3a. GROBMAN, W. D., R. A. POLLAK, D. E. EASTMAN, E. T. MASS, JR. & B. A. SCOTT. 1974. Phys. Rev. Lett. **32**: 534.

3b. GROBMAN, W. D. & B. D. SILVERMAN. 1976. Solid State Commun. **19**: 319.

3c. CARDONA, M. & L. LEY, Eds. Photoemission from Organic Molecular Crystals. 1977. Springer Heidelberg, Germany.

4a. EPSTEIN, A. J., N. O. LIPARI, P. NIELSON & D. J. SANDMAN. Phys. Rev. Lett. 1975. **34**: 914.

4b. RITSKO, J. J., N. O. LIPARI, P. C. GIBBONS & S. E. SCHNATTERLY. 1976. Bull. Am. Phys. Soc. **21**: 311.

5a. DENOYER, F., R. COMES, A. F. GARITO & A. J. HEEGER. 1975. Phys. Rev. Lett. **35**: 445.

5b. KAGOSHIMA, S., H. ANZAI, K. KAJIMURA & T. ISHIGURO. 1975. J. Phys. Soc. Japan **39**: 1143.

6. KAUFMAN, F. B., E. M. ENGLER, D. C. GREEN & J. Q. CHAMBERS. 1976. J. Am. Chem. Soc. **98**: 1596.

7. SCOTT, B. A., F. B. KAUFMAN & E. M. ENGLER. 1976. J. Am. Chem. Soc. **98**: 4342.

8a. JOHNSON, C. K. & C. R. WATSON. 1976. J. Chem. Phys., **64**: 2271.

8b. JOHNSON, C. K., C. R. WATSON & R. J. WARMACK. 1975. Am. Cryst. Assoc. Mtg. (abst) **3**: 19.

9. TORRANCE, J. B., B. A. SCOTT & F. B. KAUFMAN. 1975. Solid State Commun. **17**: 1369.

10. TORRANCE, J. B., B. A. SCOTT, F. B. KAUFMAN & B. WELBER. To be published.

METALLOTETRATHIAETHYLENES*

A. R. Siedle,† G. A. Candela and T. F. Finnegan

National Bureau of Standards
Institute for Materials Research
Washington, D.C. 20234

R. P. Van Duyne and T. Cape

Northwestern University
Department of Chemistry and Materials Research Center
Evanston, Illinois 60201

G. F. Kokoszka and P. M. Woyciesjes

State University of New York
Department of Chemistry
Plattsburgh, New York 12901

J. A. Hashmall

Georgetown University
Department of Chemistry
Washington, D.C. 20007

M. Glick and W. Ilsley

Wayne State University
Department of Chemistry
Detroit, Michigan 48202

Discovery of unusual electrical transport properties of the 1:1 donor-acceptor complex formed from tetrathiafulvalene (TTF) and tetracyanoquinodimethane (TCNQ) has stimulated an intense study of materials prepared from other cyanocarbon acceptors. Less, however, is known about the complex chemistry of TTF, and only recently has a series of metal dithiolene derivatives such as $(TTF)_2[(C_2H_2S_2)_2Ni]$ been reported.[1,2] To obtain further insight into the fundamental chemistry of such tetrathiaethylenes, we have carried out an extensive study of their complexes with transition metal halides. Several types of materials have been prepared, and they are surveyed here.

Metal halide complexes of tetrathiaethylenes may be considered members of three general classes: (1) crystal complexes, (2) charge-transfer or donor-acceptor complexes, and (3) salts.

Crystal complexes may be formed by cocrystallization of the thiacarbon with some metal derivatives. The x-ray powder diffraction patterns are unique, but optical and vibrational spectroscopic properties are the sum of minimally perturbed component molecules. Such materials are usually insulators.

*Manuscript received Nov. 17, 1977.

†Present Address: Central Research Laboratories, 3M Company, St. Paul, Minnesota 55101.

0077-8923/78/0313-0377 $1.75/1 © 1978, NYAS

Donor-acceptor complexes comprise a broad and fascinating class of materials. We consider them complexes in which low energy-excited states, formed by electron transfer from the thiaethylene to a metal center, is mixed with a neutral, uncharged ground state. These compounds have new infrared and electronic-spectroscopic properties relative to the starting materials. They are usually semiconductors, although, in favorable cases, rather high conductivity may be observed. TTF-TCNQ is probably the most spectacular member of this class.

Salts of tetrathiaethylenes are formed by complete electron transfer to the thiocarbon and so are ionic in character. Some cation-anion interaction, in addition to electrostatic forces, may be observed. Microwave conductivity of pressed powdered samples is usually in the semiconductor-insulator range.[3]

The reaction chemistry of conjugated tetrathiaethylenes, notably TTF, which forms a stable cation radical, is dominated by electron-transfer processes. This is illustrated by a comparison of the products formed from mercuric chloride and TTF or 4,4′,5,5′-tetrahydrotetrathiafulvalene, (H_4TTF). TTF is oxidized by mercuric chloride in acetonitrile to afford the cation radical salt $TTF^{+}HgCl_3^{-}$ and mercurous chloride. Two-probe conductivity measurements on single crystals of this salt reveal that it is an insulator, $\sigma = 1 \times 10^{-7}$ (ohm cm)$^{-1}$ at room temperature. An x-ray structure determination reveals two kinds of TTF cation radical dimers and polymeric $HgCl_3$ chains. The magnetic susceptibility χ_C^M is 300×10^{-6} cm^{3}mole^{-1} at 51°K, or about 4% of the value expected for a simple radical salt. Strong coupling between oxidized TTF moieties appears to be a general phenomenon, at least in compounds that crystallize in segregated stacks, c.f. TTF-TCNQ[4] and TTF subhalides.[5,6] Cooling solutions containing H_4TTF and excess mercuric chloride produces, in contrast, $(H_4TTF)(HgCl_2)_3$. The structure of this material has been determined by x-ray diffraction methods. It is a crystal complex containing molecules of H_4TTF and polymeric $HgCl_2$ units (FIGURE 1). The shortest Hg—S distance is 3.133 Å. The electronic spectrum shows absorption maxima at 33,560, 36,200, and 44,400 cm^{-1}, compared with 40,480 cm^{-1} in the starting thioethylene, confirming minimal interactions between the lattice components. The structure of this compound is important because it demonstrates the ability of TTF analogs to form crystal complexes and discloses that the sulfur atoms in these molecules have a surprisingly low nucleophilicity. The 1:1 complex (TTF) $[Pd(C_5H_7O_2)_2]$, formed by slow evaporation of solutions of TTF and palladium bis(acetylacetonate), appears to be another member of this class.

The TTF-Cu^{++} system is interesting and has yielded several novel materials. The detailed course of the reactions of TTF with CuX_2 depends on both the nature of X and the solvent. Addition of TTF to $CuCl_2 \cdot 2H_2O$ in ethanol yields $(TTF)_3(CuCl_2)_5$, about which more will be said later; recrystallization of this compound from acetonitrile produces $(TTF)_2CuCl_4$. The influence of the solvent on the course of the reaction, demonstrated by the isolation of $(TTF)CuCl_4$ from $CuCl_2 \cdot 2H_2O$ and TTF in acetonitrile, arises from the stronger solvation of Cu^{+} by acetonitrile than ethanol.

Raman spectroscopy has proved extremely valuable in studying metallotetrathiaethylenes. Of the seven Ag normal modes in TTF, the ν_3 mode, which is predominantly the central C=C stretch, undergoes the largest frequency shift on oxidation and shifts from 1515 cm^{-1} in neutral TTF to 1413 and 1323 cm^{-1} in

TTF^{+} and TTF^{++} derivatives, respectively. This mode is observed at 1419 cm^{-1} in $(TTF)_2CuCl_4$ and at 1313 cm^{-1} in $(TTF)CuCl_4$. Electron spin resonance parameters for the former are $g \parallel 2.323(5)$; $g \perp 2.053(5)$, $\Delta H \parallel 43$ G; $\Delta H \perp 41$ G. For $(TTF)CuCl_4$, $g \parallel 2.476(5)$; $g \perp 2.123(6)$; $\Delta H \parallel 69$ G; $\Delta H \perp 175$ G. The relatively narrow lines and spread of g values in $(TTF)_2CuCl_4$ are suggestive of a

Angle	Degree(°)
Cl(1)--Hg(1)--Cl(1')	180.00
Cl(1)--Hg(1)--Cl(6)	93.71
Cl(1)--Hg(1)--Cl(6')	86.29
Cl(1)--Hg(1)--Cl(2)	83.52
Cl(1)--Hg(1)--Cl(2')	96.48
Cl(6)--Hg(1)--Cl(2)	86.15
Cl(2)--Hg(1)--Cl(6')	93.85
Cl(6)--Hg(1)--Cl(2')	93.85
Cl(6')--Hg(1)--Cl(2')	86.15
Cl(6)--Hg(2)--S(3)	84.85
Cl(6)--Hg(2)--S(4)	96.19
Cl(6)--Hg(2)--Cl(2)	170.04
Cl(6)--Hg(2)--Cl(1)	93.66
Cl(6)--Hg(2)--Cl(1')	78.14
Cl(6)--Hg(2)--Cl(2')	92.34
S(3)--Hg(2)--S(4)	62.71
S(3)--Hg(2)--Cl(2')	70.43
Cl(2')--Hg(2)--Cl(1')	71.41
Cl(1')--Hg(2)--Cl(1)	84.31
S(4)--Hg(2)--Cl(1)	73.96

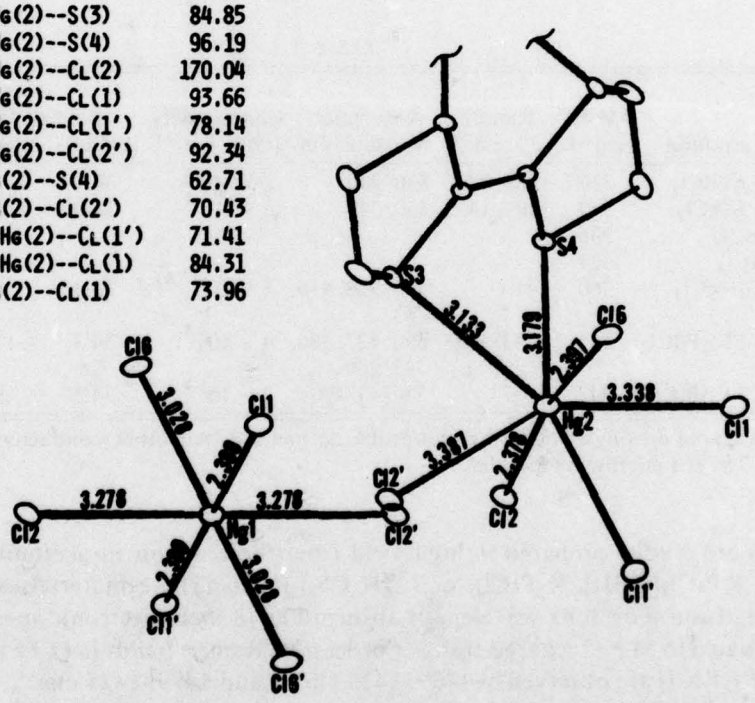


FIGURE 1.

parallel arrangement of square planar $CuCl_4^{2-}$ units, but in $(TTF)CuCl_4$, the data are more consistent with a flattened tetrahedral geometry about copper. From these data and the experimental values of Θ, exchange fields of about 10^4 G were calculated, based on three dimensional magnetic interactions.[7,8] Thus, in contrast to $[(CF_3)_2C_2S_2]_2Cu(TTF)$, where evidence for the presence of linear, one-dimensional antiferromagnetic Heisenberg chains has been adduced,[9] significant

exchange fields are observed in all three dimensions in these TTF tetrachlorocuprates.

$(TTF)_3(CuCl_2)_5$ is only weakly paramagnetic and does not show an ESR spectrum at room temperature. Its Raman spectrum reveals bands at 1456, 1422, and 1306 cm^{-1} and the material therefore contains both the dication and cation radical of TTF. We suggest that this compound is a mixed-valence salt containing chlorine bridged copper(I) centers, c.f. (paraquat) $(CuCl_2)_2$.[10]

Formation of ionic complexes from TTF and metal halides appears to be a general reaction, and as additional examples, $(TTF)(TiCl_4)_2$, $(TTF)_2SnCl_6$, and $(TTF)_2FeCl_4$ prepared from $TiCl_4$, $SnCl_4$, and $FeCl_3$, respectively, may be mentioned. Cobalt(II) chloride represents an unusual case: acetonitrile solutions of TTF and anhydrous $CoCl_2$ yield no solid product, but when air is injected into the system, crystals separate, the analysis of which corresponds to $(TTF)_{2.4}CoCl_3$.

Group VIII metal-halide-TTF complexes of the type $(TTF)_2MX_2$ (M=Pd, Pt; X=Cl, Br) are particularly interesting and have been studied in some detail.

TABLE 1

Compound	νM-Cl cm^{-1}	Raman $\Delta\nu$, cm^{-1}	Absorption Maxima, nm	Conductivity $(ohm, cm)^{-1}$	Core Level Binding Energies, eV Δ(Cl-S)	Δ(S-M)	Δ(Cl-M)
$(TTF)_2PdCl_2$	330	1489, 1425	830, 240	2×10^{-4}	34.1	−137.6	−139.5
$(TTF)_2PtCl_2$	340	1499, 1425	550, 340	6×10^{-4}	34.0	91.6	125.6
K_2PdCl_4	336	—	—	—	—	—	−139.6
K_2PtCl_4	321	—	—	—	—	—	126.1
$(TTF)HgCl_3$	360	1419	530, 380, 410, 280	$1 \times 10^{-7(A)}$	33.4	63.8	97.2
$(H_4TTF)_2PdCl_2$	345	1543, 1528	650, 427, 380, 345, 280	4×10^{-4}	34.3	−173.9	−139.6
$(H_4TTF)_2PtCl_2$	342	1537	530(w), 400	2×10^{-4}	34.5	91.2	125.7

Measured on single crystal by two-probe dc method. All other conductivities were obtained by the microwave method.[3]

They are readily prepared in high yield from the reaction in acetonitrile of TTF with $KPtCl_3(C_2H_4)$, K_2PtCl_4, or $(C_6H_5CN)_2PdCl_2$. These materials are intensely colored and show long wavelength absorptions in their electronic spectra that are attributed to M ← L charge-transfer processes. Raman bands in $(TTF)_2PdCl_2$, and $(TTF)_2PtCl_2$ are observed at 1489, 1425 cm^{-1}, and 1499, 1425 cm^{-1}, respectively. These, therefore, are mixed-valence compounds in that they contain both TTF^0 and TTF^+. In the platinum chloride compound, an absorption in the far infrared at 340 cm^{-1} is observed. This band shifts on substitution of bromine for chlorine and is thus assigned to $\nu_{Pt\text{-}Cl}$. These results exclude the otherwise attractive formulation $[(TTF)_2Pt]^{++}Cl_2$ which might have been anticipated from earlier work on metal complexes of 2,2′-biimidazolyl.[11]

X-ray photoelectron spectroscopy (ESCA) has provided additional insight into the nature of these materials, and some of these results are shown in TABLE 1. Core-level binding energies are expressed in terms of differences between $Cl_{2p}S_{2p}$, S_{2p}-metal, and Cl_{2p}-metal energies so that shifts due to charging of the samples,

a severe problem with the K_2PdCl_4 and K_2PtCl_4 references, will be less important. In the TTF-$PdCl_2$ and $PtCl_2$ complexes, the separation between the Cl_{2p} and Pd $3d_{5/2}$ or Pt $4f_{7/2}$ levels is changed by only a small amount relative to the MCl_4^{2-} salts. Further, the sulfur 2p binding energies fall in the range 162.6–163.5 eV (relative to C_{1s} from the graphite sample holder at 284.0 eV), compared with 163.9 eV in the salt TTF^+ $HgCl_3^-$. These data indicate that small changes in the M—Cl bond polarity have resulted from the interaction of the MCl_2 unit with TTF and that in the cases studied, the sulfurs are less positively charged than in TTF^+. These data appear consistent with the formulation of the palladium(II) and platinum(II) chloride-TTF compounds and donor-acceptor or charge-transfer complexes.

The present, incomplete, picture of the bonding in these palladium and platinum complexes of TTF involves stacks of TTF molecules with linear MX_2 units in the channels. Weak sulfur-metal coordination through the lone pair of electrons on sulfur or back bonding into the ligand π system may also be possible. Partial electron transfer from TTF to the metal center generates mixed-valence materials (on the Raman time scale) containing $TTF^{0,+1}$, but the precise degree of electron transfer has yet to be established. The electrons involved in the charge-transfer process are delocalized over the ten-atom TTF moiety and have only a small effect on the sulfur core-level energies. These are dominated by localized lone electron pairs, as is illustrated by comparison of the ESCA data for $(TTF)_2PdCl_2$ and $(H_4TTF)_2PdCl_2$.

It is clear that additional data will be needed to delineate the structure and bonding in these TTF-metal complexes. The scope and diversity of the chemistry is extremely large. It is probable that within the donor-acceptor class of complexes, gradations in bonding features will continue to be observed among different metal complexes, and that new materials will emerge that have novel chemical and physical properties.

Notes and References

1. Interrante, L. V., K. W. Browall, H. R. Hart, Jr., I. S. Jacobs, G. D. Watkins & S. H. Wee. 1975. J. Amer. Chem. Soc. **97**: 889.
2. Wudl, F. 1977. J. Amer. Chem. Soc. **97**: 1962.
3. Unless otherwise noted, conductivities reported herein were measured by the microwave cavity perturbation method on thin compressed pellets.
4. Scott, J. C., A. F. Garito & A. J. Heeger. 1974. Phys. Rev. **B10**: 3131.
5. Somoano, R. B., A. Gupta, V. Hadek, M. Jones, T. Datta, R. Deck & A. M. Hermann. 1977. Phys. Rev. **B15**: 595.
6. Wudl, F., D. E. Schafer, W. M. Walsh, Jr., L. W. Rupp, F. J. DiSalvo, J. V. Waszczak, M. L. Kaplan & G. A. Thomas. 1977. J. Chem. Phys. **66**: 377.
7. Gaura, R., G. Kokoszka, K. Hyde & R. Lancione. 1976. Coord. Chem. **5**: 105.
8. Kokoszka, G. 1974. *In* Low Dimensional Cooperative Phenomena. H. J. Keller, Ed.: 171. Plenum Press. New York, N.Y.
9. Bray, J. W., H. R. Hart, Jr., L. V. Interrante, I. S. Jacobs, J. S. Kasper, G. D. Watkins, S. H. Wee & J. C. Bonner. 1975. Phys. Rev. Lett. **35**: 744.
10. Prout, C. K. & P. Murray-Rust. 1969. J. Chem. Soc. (A): 1520.
11. Kaiser, S. W., R. B. Saillant, W. M. Butler & P. G. Rasmussen. 1976. Inorg. Chem. **15**: 2681, 2688.

SYNTHESIS AND PROPERTIES OF CHALCOGEN-BRIDGED NAPHTHALENES: A NEW SERIES OF ELECTRON DONORS*

D. Dauplaise,† J. Meinwald,† J. C. Scott,‡ H. Temkin‡

†*Department of Chemistry*
‡*Laboratory of Atomic and Solid State Physics*
Cornell University
Ithaca, New York 14853

J. Clardy

Ames Laboratory-USERDA and Department of Chemistry
Iowa State University
Ames, Iowa 50010

INTRODUCTION

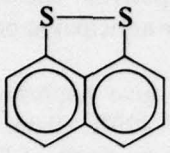
The recent interest in organic charge-transfer salts has been aroused, to a large extent, by the possibility of achieving high conductivity in a novel class of solids.[1,2] To date, the most widely studied open-shell anion and cation radicals have been tetracyanoethylene[3-6] (TCNE), tetracyanoquinodimethane[1,2,4-8] (TCNQ) and tetracyanonaphthoquinodimethane[5,6,9,10] (TNAP) and their derivatives, and members of the tetrathiafulvalene (TTF)[1,2] tetraselenafulvalene[11,12] (TSeF) families respectively. A major problem in the preparation of such complexes is that the physical properties cannot, for the most part, be predicted. It has been suggested that various molecular criteria, such as small size, high polarizability, symmetry, and molecular orbitals perpendicular to the plane of the molecule are necessary to achieve metallic conductivity.[4] However, characteristics that cannot be predetermined—for example, crystal structure and intermolecular atomic interactions—also play a crucial role.[6] In most examples of charge-transfer complexes prepared to date, the molecular properties of interest have not been predictable. Part of this problem lies in the fact that data have been lacking on a large family of closely related chemical structures.[13]

In order to address some of these difficulties, we have undertaken the study of a new class of donors: *peri*-bridged naphthalene dichalcogenides (NDC's). These compounds incorporate within their structure a planar-fused heterocyclic ring containing seven delocalizable electrons, and are expected to have low ionization potentials and to function as electron donors in charge-transfer complexes.[14-16] The first NDC to be described was naphtho[1,8-*cd*]-1,2-dithiole (I), in which a disulfide linkage bridges naphthalene's *peri* positions.[17,18] Zweig and Hoffmann[19] showed that I is a good electron donor, as evidenced by its half-wave oxidation potential (0.95 V vs. s. c. e.) and its ability to form charge-transfer complexes with acceptors such as chloranil and TCNE. Until recently, I was the only known mem-

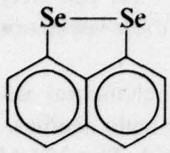
*Partly supported by the National Science Foundation, grant no. CHE 76-82122, and the Cornell Materials Science Center. Manuscript received June 13, 1977.

0077-8923/78/0313-0382 $1.75/1 © 1978, NYAS

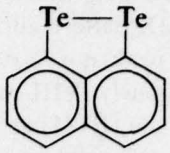
ber of this series. We felt that the remaining members, in which larger and more polarizable chalcogen atoms are substituted for sulfur, might function as even better electron donors.



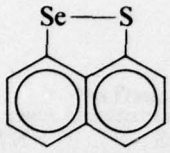
I



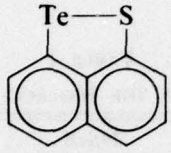
II



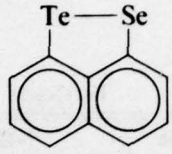
III



IV



V



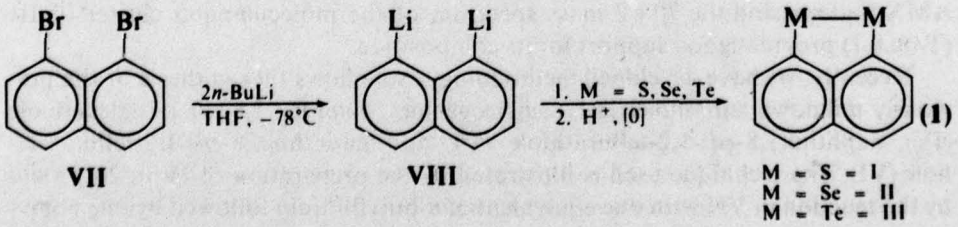
VI

Synthesis of the entire series of chalcogen-bridged naphthalenes (I–VI) would provide a unique set of compounds in which the electron donor properties could be studied and related to the effects of heteroatom substitution. Since there are, in all, six possible combinations of the bridging atoms, we believe that this constitutes the largest group of electron donors that are so closely related by heteroatom substitution. Studies of this series of donor molecules should provide insight into the effect of such heteroatomic substitution on physical properties.

In addition to a description of the synthesis of all six naphthalene dichalcogenides, we wish to report preliminary results of our physical measurements. An x-ray diffraction study was undertaken on one of the donors, naphtho[1,8-*cd*]-1,2-selenathiole (IV), and the results are reported in section CRYSTAL STRUCTURES.... We have measured the resistivity of single crystals of complexes of the NDC's with elemental iodine, where possible. Raman spectroscopy of the NDC's and their iodide complexes lends some insight into the molecular structure of these complexes. Magnetic susceptibility measurements have been made on all six neutral molecular solids, and on the NDSe-iodide complex.

SYNTHESIS

Our initial synthesis of the symmetrical naphthalene dichalcogenides[20] proceeded from 1,8-dibromonaphthalene[21] (VII) via 1,8-dilithionaphthalene (VIII),[22-24] which is conveniently produced in one step by halogen metal exchange as shown in (1).



VII VIII

When elemental sulfur is allowed to react with VIII, naphtho[1,8-*cd*]-1,2-dithiole (I) is produced in 35–40% yield (1). The properties of I obtained in this way are in good agreement with those of an authentic sample of I prepared by the method of Zweig and Hoffmann.[19] Its 220 MHz PMR spectrum shows the expected AMX pattern and its 70 eV mass spectrum shows the anticipated parent ion as its base peak at *m/e* 190.

Analogously, VIII reacts with elemental selenium to give naphtho[1,8-*cd*]-1,2-diselenole (II) (1) as lustrous purple needles, m. p. 127–129°C (from hexane/methylene chloride), in 18–22% yield. The 220 MHz PMR spectrum of II bears a close resemblence to that of I and the characteristic ion intensity ratios of the

TABLE 1

INTENSITY RATIOS OF THE MOLECULAR ION CLUSTERS*

NDSe	NDTe	NSeS	NTeS	NTeSe
278 4 (4)	373 2 (2)	232 2 (2)	280 7 (7)	324 1 (1)
279 5 (5)	374 7 (6)	233 0 (0)	281 2 (3)	325 1 (1)
280 18 (20)	375 5 (5)	234 19 (18)	282 14 (13)	326 5 (5)
281 10 (14)	376 17 (17)	235 18 (17)	283 22 (21)	327 6 (5)
282 47 (51)	377 16 (15)	236 49 (49)	284 56 (55)	328 20 (19)
283 32 (31)	378 36 (36)	237 7 (8)	285 8 (7)	329 16 (15)
284 88 (88)	379 26 (25)	238 100 (100)	286 93 (91)	330 40 (40)
285 23 (15)	380 67 (66)	239 12 (12)	287 11 (11)	331 27 (27)
286 100 (100)	381 30 (28)	240 22 (23)	288 100 (100)	332 83 (81)
287 19 (11)	382 100 (100)	241 3 (3)	289 12 (12)	333 23 (21)
288 39 (32)	383 12 (12)	242 1 (1)	290 5 (5)	334 100 (100)
289 5 (4)	384 92 (93)			335 12 (11)
	385 9 (10)			336 76 (77)
	386 50 (51)			337 8 (9)
	387 5 (6)			338 12 (13)
				339 1 (1)

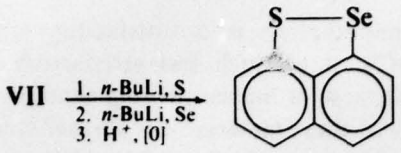
**m/e* Intensity observed (calculated). The observed spectra were obtained on an AEI MS-902 instrument. The calculated mass spectra were obtained by use of the MASH computer program, which is a local version of ISOW, developed by W. A. G. Graham, University of Alberta, Edmonton, Canada, and modified by R. C. Winterton and R. S. Weber, Cornell University.

parent molecular ions in its 70 eV mass spectrum (TABLE 1) confirms the presence of two selenium atoms.

The reaction between VIII and elemental tellurium (1) produces naphtho[1,8-*cd*]-1,2-ditellurole (III) as greenish grey needles, m. p. 212–214°C (from hexane/carbon disulfide) in 8–12% yield. Once more the PMR spectrum consists of an AMX pattern, and the 70 eV mass spectrum of the molecular ion cluster of III (TABLE 1) provides good support for its composition.

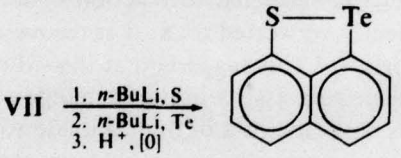
Recently, we have developed methodology that allows the synthesis of the previously unknown unsymmetrical dichalcogenides, naphtho[1,8-*cd*]-1,2-selenathiole (IV), naphtho[1,8-*cd*]-1,2-tellurathiole (V), and naphtho[1,8-*cd*]-1,2-tellураselenole (VI). The technique used is illustrated by the preparation of IV in 24% yield by the reaction of VII with one equivalent of *n*-butyllithium followed by one equiv-

alent of elemental sulfur, then by a second equivalent of *n*-butyllithium followed



IV (2)

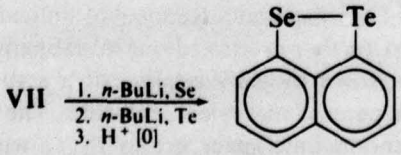
by one equivalent of elemental selenium (**2**). The crude product is isolated as a dark red solid by column chromatography on silica gel with hexane as eluent. Analysis of this product by glc[25] reveals it to be a mixture of I, II, and the desired IV in a ratio of 1:7:8. When the order of addition of sulfur and selenium is reversed, the results obtained are qualitatively similar, although IV is produced in 29% yield. Once again, I and II are also produced, but in this case the latter is the major impurity. All three products of this reaction are well separated on an analytical scale by glc and can be obtained pure on preparative scale by use of medium-pressure liquid chromatography. The formation of these symmetrical by-products probably results from reaction of elemental sulfur and selenium with 1,8-dilithionaphthalene present in the reaction mixture. Naphtho[1,8-*cd*]-1,2-selenathiole is a dark red crystalline solid, m. p. 121–122°C, whose spectral properties closely resemble those of the previously synthesized, symmetrical chalcogen bridged naphthalenes.[19,20] The characteristic ion-intensity ratios of the molecular ion cluster of IV in its 70 eV mass spectrum are in accord with expectations (TABLE 1).



V (3)

As summarized in (**3**), VII reacts analogously with *n*-butyllithium and elemental sulfur, followed by *n*-butyllithium and elemental tellurium, to give V as dark bronze filaments (m. p. 214–216°C) although in only 2% yield. The spectral properties of V are consistent with the proposed structure (TABLE 1).

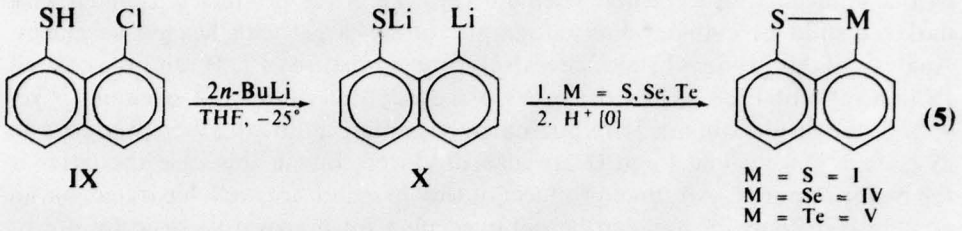
The reaction of VII with *n*-butyllithium followed by elemental selenium, then *n*-butyllithium followed by elemental tellurium gives the last member of this series, naphtho[1,8-*cd*]-1,2-telluraselenole (VI), as shiny black flakes (m. p. 193–195°C) in 4% yield (**4**).



VI (4)

The structure of VI is once again confirmed by its characteristic spectral properties (TABLE 1).

While 1,8-dibromonaphthalene is a satisfactory starting material for the three symmetrical NDC's, it is much less satisfactory for the unsymmetrical cases. We have, therefore, sought higher yielding syntheses for IV–VI in an effort to obtain a better supply of these materials for further study. One solution to this problem, which allows efficient syntheses of IV and V, as well as of I, is outlined in (5).



8-Chloro-1-naphthalenethiol (IX)[26] is treated with two equivalents of *n*-butyllithium in tetrahydrofuran solution at −25°C, generating the dilithio salt (X), which after reaction with elemental sulfur gives I in 44% yield. Under analogous conditions, treatment of X with elemental selenium gives IV in 65% yield, whereas reaction of X with elemental tellurium allows isolation of a 60% yield of V. From the results obtained above, it is apparent that 8-chloro-1-naphthalenethiol undergoes efficient halogen metal exchange. This is unusual, since aryl chlorides are not normally good substrates for halogen metal exchange reactions. Thus, when 1-chloronaphthalene is subjected to reaction conditions identical to those under which IX is efficiently converted to X, it is recovered unchanged, in agreement with previous reports.[27,28] This suggests that the -SLi substituent on one *peri* position of the naphthalene ring assists in the exchange of the chlorine at the adjacent *peri* position. This novel use of a lithium thiolate to enhance halogen metal exchange across *peri* positions may prove useful in the synthesis of other interesting chalcogen-bridged aromatic systems.

CRYSTAL STRUCTURE OF NAPHTHO[1,8-*CD*]-1,2-SELENATHIOLE IV

As a prelude to an examination of the solid-state properties of charge-transfer complexes of the dichalcogenides with suitable acceptors, we have examined the crystal structure of IV by x-ray diffraction.[29] We chose IV as a representative of the NDC class of compounds because the dissymmetry of the chalcogen bridge permits determination of any structural disorder that may exist and because early experiments showed that IV and II were isostructural. Knowledge of the crystal structure would rule out any possibility that these systems are dimeric, and also establish the planarity of the molecule. Reports of difficulty in refinement of the crystal structure of I have further prompted our investigations.[30]

A crystal of IV was grown by slow cooling of a saturated solution of IV in hexane containing a few percent methylene chloride. The long, dark red needles obtained belong to the monoclinic space group $P2_1/c$ with **a** = 15.417 (6), **b** = 4.244 (2), **c** = 16.596 (7) Å and β = 129.11(6)°. Density measurements indicated

four molecules per unit cell or one per asymmetric unit. All unique data with $2\theta \leq 114°$ were collected on a Syntex P_{21} diffractometer with use of monochromated Cu Kα (1.54178 Å) radiation. A total of 1331 reflections was surveyed, and after correction for Lorentz, polarization, and background effects, 1083 (81%) were used in the final refinements ($F_0^2 \geq 3\sigma(F_0^2)$). The selenium atom was located by a three-dimensional Patterson synthesis and the nonhydrogen atoms were located on subsequent selenium-phased electron density syntheses. Full-matrix least-squares refinement, with anisotropic temperature factors for the nonhydrogen atoms and omitting hydrogen atoms, has presently converged to a standard crystallographic residual of 0.080.

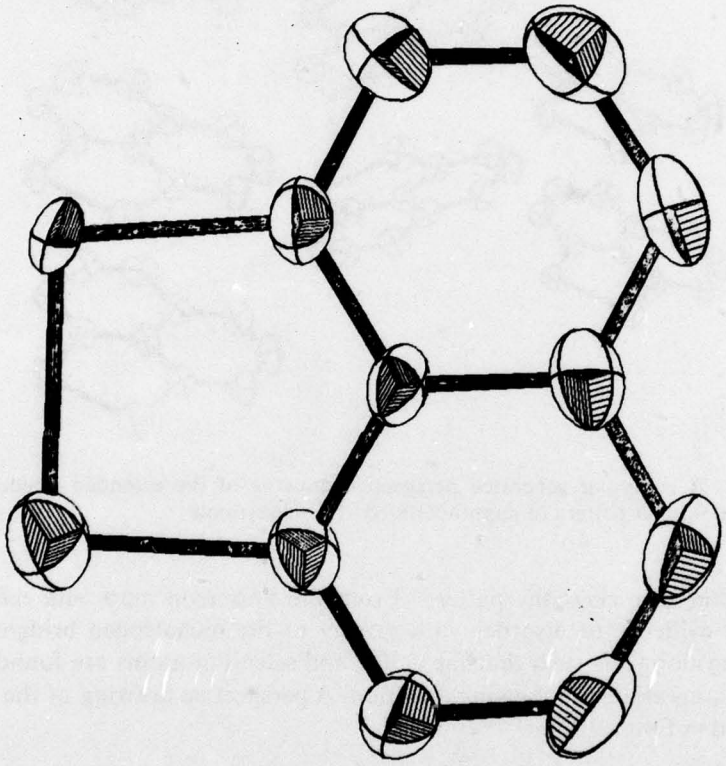


FIGURE 1. A computer generated perspective drawing of the structure of naphtho-[1,8-*cd*]-1,2-selenathiole.

A drawing of the final x-ray model of the molecule is presented in FIGURE 1. The compound is seen to be monomeric; bond distances and bond angles agree well with generally accepted values. The sulfur-selenium bond distance is found to be 2.246 (5) Å and the sulfur-carbon and selenium-carbon are 1.80 (2) Å and 1.88 (2) Å respectively. The bond lengths and bond angles within the naphthalene ring of IV show no serious distortion from those in naphthalene itself.[31] The planar molecules are tilted at 25° and stacked along the *b*-axis. The stacks are

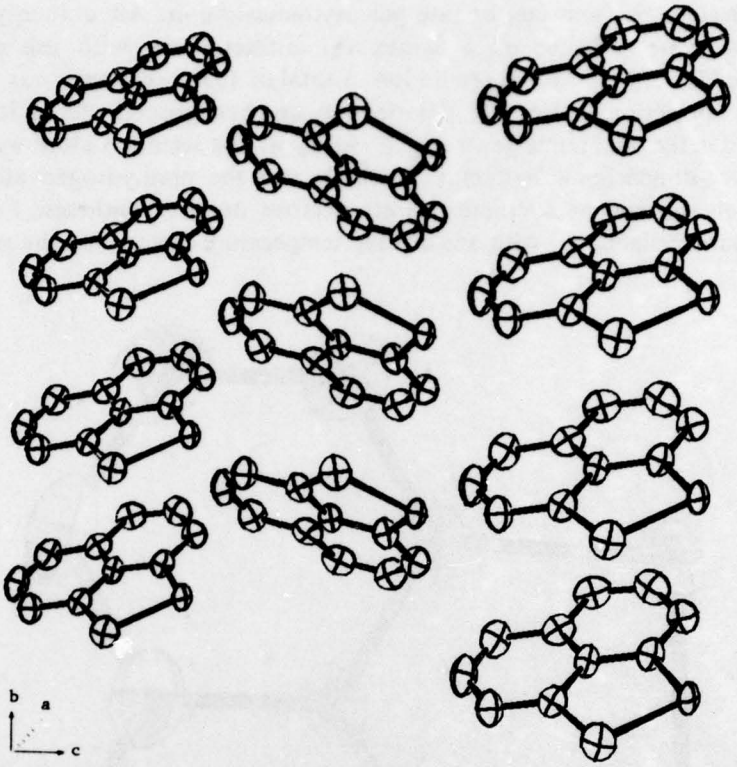


FIGURE 2. A computer generated perspective drawing of the extended structure, illustrating the molecular pattern of naphtho[1,8-*cd*]-1,2-selenathiole.

interleaved in a herringbone pattern. From the Patterson map, and refinement, there is no evidence of disorder with respect to the dichalcogen bridge; indeed, the stacking along *b* is such that the sulfur and selenium atoms are found to exist in linear chains along the stacking direction. A perspective drawing of the unit cell is presented in FIGURE 2.

COMPLEX FORMATION

The three symmetrical chalcogen-bridged naphthalenes were all found to form 1:1 donor-acceptor complexes with TCNQ.[20] A thermal gradient sublimation apparatus similar to the one described by McGhie and coworkers[32] was used in the final purification step for both the donors and the TCNQ. The compaction conductivities for these materials were measured at room temperature. The results show an interesting trend: NDS · TCNQ = 10^{11} Ω cm, NDSe · TCNQ = 2×10^{7} Ω cm and NDTe · TCNQ = 50 Ω cm. It is apparent that in the symmetrical NDC · TCNQ series, as one goes to larger, more polarizable chalcogens, the conductivity of the TCNQ complexes increases dramatically.

In an effort to find more interesting complexes involving these donors, we decided to explore the use of another acceptor, elemental iodine. Buravov *et al.*[33]

and Isett and Perez-Albuerne[34] have shown that iodine proved to be a good acceptor in complexes with tetrathiatetracene (TTT). All six NDC's form complexes with this acceptor. The complexes are formed by mixing solutions of the NDC and iodine in a suitable solvent (usually acetonitrile) and allowing the complexes to crystallize. By using the technique that has been developed for TTF · TCNQ,[35] we were able to produce large crystals in the case of NDSe-iodide. These shiny metallic grey crystals were found to correspond to a stoichiometry of $NDSe_1$-$I_{1.82}$. Elemental microanalysis revealed that this ratio of NDSe to iodine was reproducible over a number of independently prepared samples. The physical properties of this system are discussed in THE ELECTRONIC PROPERTIES.

Up to now, we have been unsuccessful in our attempts to grow large single crystals of either the TCNQ or iodine complexes of the remaining NDC's. This has been due, to a large extent, to the poor solubility characteristics of these compounds. Our efforts to find a suitable solvent system for growth of large single crystals are continuing.

RAMAN SPECTROSCOPY

The Raman data on the NDC's and their iodine complexes were collected using the Spex 1401 double monochromator with photon counting and digital data storage. Various excitation lines were obtained from argon and dye lasers. With the exception of single crystal data on I, all data were obtained on polycrystalline spinning pellets. Complete data in the 100–2000 cm^{-1} range were obtained for I and

TABLE 2
RAMAN FREQUENCIES CHARACTERISTIC OF
FIVE-MEMBERED HETEROCYCLIC RINGS CONTAINING TWO CHALCOGENS

NDS	NDSe	NDTe	NSeS	NTeS	NTeSe
	128			129	
					146
170		168			190
		197			207
				220	224
	238		241	241	
				254	
					261
	278	267	274		
	316		292		296
345				352	
391*		393*	374	400*	
			411		
				440	432
473*			470*	464*	
511*					
			523		
531		528			534
570			556		

*Naphthalene mode.

IV and shows a very strong resemblance to the Raman spectrum of naphthalene,[36] in that the line shifts are not greater than 10 cm^{-1}. This is indicative of a low degree of distortion of the naphthalene nucleus. The new lines that are observed can be attributed to various vibrations and/or deformations of the five-membered heterocyclic ring. We collected data on all six dichalcogenides in the 100–600 cm^{-1} frequency region, which is characteristic of chalcogen-chalcogen and carbon-chalcogen bonds. The energies obtained (TABLE 2) are in general agreement with

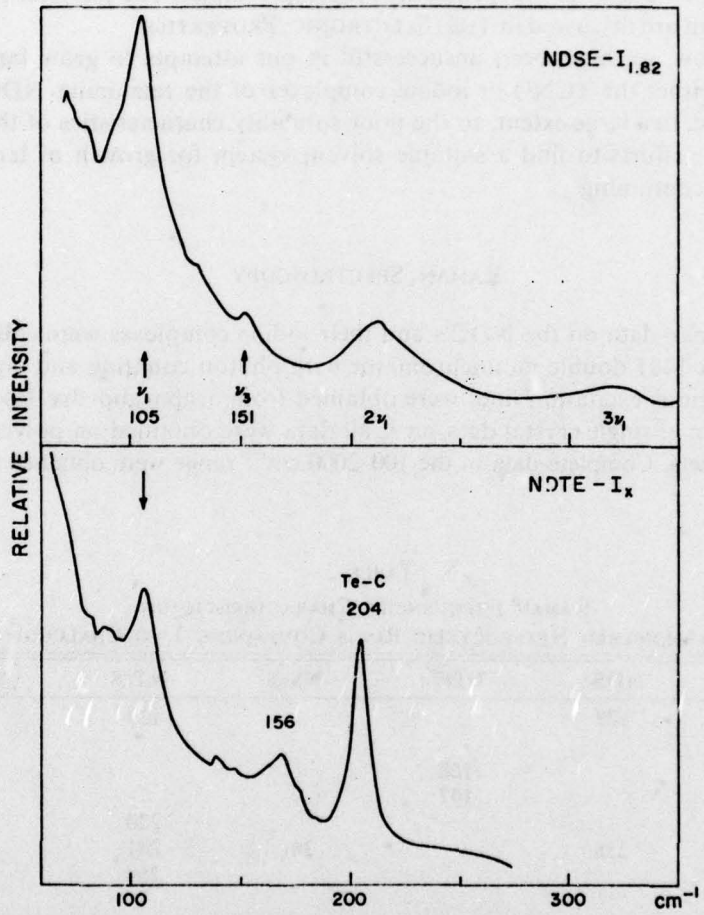


FIGURE 3. Raman scattering spectra of a) NDSe-iodide and b) NDTe-iodide complexes taken with 5145 Å laser line.

the values reported for these bonds.[37] The values we obtained cannot be rationalized on the basis of simple isotopic substitution. A computer force constant calculation now in progress should permit definitive mode assignments.

In the absence of structural data on the NDC-iodine complexes, we have examined their molecular state *via* Raman spectroscopy. The resonant Raman spectrum of the NDSe-iodide complex shows a strong band at 105 cm^{-1}, FIGURE 3

(*top*), characteristic of the symmetric (ν_1) mode of I_3^-.[38] Two overtones of this mode can be seen (5145 Å excitation line) at 211 and 318 cm^{-1}. A weak feature at 151 cm^{-1} can be assigned to the asymmetric (ν_3) mode of the I_3^-. The relative weakness of this mode, even away from the resonance, indicates little deviation from the symmetric ($D_{\infty h}$) triatomic molecule. The preliminary single-crystal data are consistent with a structure in which the triiodide molecules are oriented along the stacking axis of the crystal.

The Raman data obtained on a microcrystalline compaction of the NDTe-iodide complex (FIGURE 3, *bottom*) shows a similar band of 105 cm^{-1}, but no overtones. A strong band at 166 cm^{-1} would indicate a large deviation from the symmetric form of the I_3^- molecule. The band at 204 cm^{-1} is assigned to the carbon-tellurium[39] mode which is shifted up from its position at 198 cm^{-1} in uncomplexed NDTe.

THE ELECTRONIC PROPERTIES

The complexes of the naphthalene dichalcogenides with iodine are all shiny crystalline solids with colors ranging from silvery grey to black. Only NDSe-iodide and NSeS-iodide form needlelike crystals of a length suitable for performing four-probe resistivity measurements. However, as yet we have been able to make suitable contacts only on the diselenide complex. Silver paint with a variety of solvents, indium-mercury amalgam and aquadag all produced two-probe resistances with crystals and compactions of the other complexes of order 10^{11} Ω. Since such impedances were unsuitable for the voltmeters and current sources at our disposal, we are unable to say whether this value is the intrinsic resistance or contact resistance.

With the complex NDSe-iodide, however, we have been able to make contact to both single crystals and compactions using indium-mercury amalgam. Even in this case the contact resistance is disturbingly high, at $\sim 10^6$ Ω. The resistivity of NDSe-iodide compactions was $\sim 10^4$ Ω cm, and of single crystals ~ 10 Ω cm. The temperature dependence of the single-crystal resistance revealed an exponentially activated behavior, with a semiconducting energy gap of (0.46 ± 0.05) eV (see FIGURE 4).

The magnetic susceptibility of NDSe-iodide was measured from 4°K to 300°K, using a Faraday balance. Apart from a small Curie-like tail, which we attribute to about 0.1% concentration of impurities and defects, the susceptibility is temperature independent, $(-2.48 \pm 0.04) \times 10^{-4}$ emu/mole, consistent with the behavior expected for a semiconductor with the above band gap. Since the value obtained is considerably more diamagentic than the prediction of Pascal's constants (-2.14×10^{-4} emu/mole),[40] we made room-temperature measurements on all six neutral donors (TABLE 3). It is apparent that this extra diamagnetism is present in all the neutral donors, particularly the mixed ones. Such departure from the prediction of Pascal's constants can be attributed to the five-atom hetero-ring, for which no corrections are available. The large excess diamagnetism in the mixed species (NSeS, NTeS, and NTeSe) might possibly be due to electron delocalization from the orbitals of the heavier atom, into unfilled orbitals of the

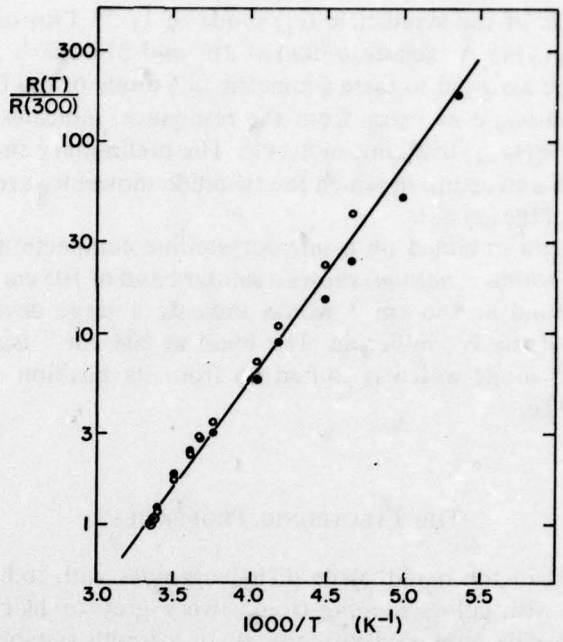


FIGURE 4. The resistance of two crystals of NDSe-iodide, plotted as the ratio of the room-temperature value vs. inverse temperature. The line corresponds to an energy gap of 0.46 eV.

lighter one. Until detailed molecular orbital calculations are done for these materials this hypothesis cannot be put on a theoretical foundation.

The ionization half-wave potentials of certain of the naphthalene dichalcogenides were obtained by cyclic-voltammetry vs. s.c.e. in acetonitrile solution. The results are summarized in TABLE 4. There is a clear trend to reduced ionization potential with heavier heteroatoms, and the value for the mixed dichalcogenide NSeS lies between those of the disulfide and the diselenide. NTeS and NTeSe are not sufficiently soluble in acetonitrile to obtain results for comparison, and other

TABLE 3

THE STATIC MAGNETIC SUSCEPTIBILITIES OF THE SIX NEUTRAL DONORS: NDC*

Compound	Measured Susceptibility χ (meas.)	Pascal Prediction χ (Pascal)	Discrepancy χ (meas.) $-\chi$ (Pascal) $= \Delta\chi$
NDS	−1.51	−1.15	−0.36
NDSe	−1.54	−1.31	−0.23
NDTe	−1.88	−1.59	−0.23
NSeS	−1.71	−1.23	−0.48
NTeS	−1.83	−1.37	−0.46
NTeSe	—	−1.45	—

*The measured results are compared with the predictions of Pascal's constants[40] showing an excess diamagnetism which is attributed to electron delocalization in the heteroatom ring. (All in units of 10^{-4} emu/mole.)

solvents are being tried. The results of these studies, as well as of other physical measurements on this series of neutral donors and complexes, will be presented at a later date.

Conclusion

The six NDC's comprise a complete set of closely related organic donors. We have outlined novel synthetic procedures for five of the six compounds that enable them to be produced in good yields. X-ray structural analysis shows that naphtho[1,8-*cd*]-1,2-selenathiole packs with the molecules stacked face-to-face in an eclipsed configuration.

Clearly, physical characterization beyond the preliminary conductivity, susceptibility, and vibrational spectroscopy described here are desirable. We are currently pursuing these measurements as well as the structures of the neutral materials remaining and their iodine complexes. These and other data are being accumulated in the hope of gaining a coherent picture of how heteroatomic substitutions in donor molecules affect the crystal structures and solid-state properties of charge-transfer salts. We are also exploring the generality of the synthetic techniques used in the preparation of the chalcogen bridged naphthalenes, in an effort to obtain other novel electron donors.

Table 4

The Half-Wave Oxidation Potentials for the Naphthalene Dichalcogenides*

NDS	NDSe	NDTe	NSeS	NTeS	NTeSe
0.86	0.76	0.45	0.80	—†	—†

*The half-wave potentials were measured vs. s.c.e. in acetonitrile.
†These materials are not sufficiently soluble in acetonitrile.

Acknowledgments

We thank Dr. F. Wudl, Dr. R. Hadden, and Dr. J. J. Hauser of the Bell Laboratories for measurement of compaction conductivities of the TCNQ adducts and for oxidation potential measurements.

Notes and References

1. Keller, H. J., Ed. 1975. Low Dimensional Cooperative Phenomena. Plenum Press. New York, N.Y.
2. Schuster, H. G., Ed. 1975. One Dimensional Conductors. G. P. S. Summer School Proc. Springer-Verlag. Berlin, Germany.
3. Acker, D. S. & W. R. Hertler. 1962. J. Am. Chem. Soc. **84**: 3370.
4. Garito, A. F. & A. J. Heeger. 1974. Acc. Chem. Res. **7**: 232.
5. Wheland, R. C. & J. L. Gillson. 1976. J. Am. Chem. Soc. **98**: 3916.
6. Wheland. R. C. 1976. J. Am. Chem. Soc. **98**: 3926.
7. Melby, L. R., R. J. Harder, W. R. Hertler, W. Mahler, R. E. Benson & W. E. Mochel. 1974. J. Am. Chem. Soc. **84**: 3374.

8. For brevity we refer to an early review by Shchegolev, I. F. 1972. Phys. Stat. Sol. A **12:** 9, and to Refs. 1 and 2.
9. DIEKMANN, J., W. R. HERTLER & R. E. BENSON. 1963. J. Org. Chem. **28:** 2719.
10. SANDMAN, D. J. & A. F. GARITO. 1974. J. Org. Chem. **39:** 1165.
11. ENGLER, E. M. & V. V. PATEL. 1974. J. Am. Chem. Soc. **96:** 7376.
12. ETEMAD, S., T. PENNEY, E. M. ENGLER, B. A. SCOTT & P. E. SEIDEN. 1975. Phys. Rev. Lett. **34:** 741.
13. With the exception of TTF, DTDSeF, and TSeF, none of the derivatives of the molecules mentioned involves simple heteroatom substitution.
14. STREITWIESER, A., JR. 1961. Molecular Orbital Theory for Organic Chemists: Chap. 10. John Wiley & Sons, Inc. New York, N.Y.
15. HARRISON, A. G., L. R. HONNEN, H. J. DAUBEN, JR. & F. P. LOSSING. 1963. J. Am. Chem. Soc. **82:** 5593.
16. THRUSH, B. A. & J. J. ZWOLENIK. 1962. Proc. Chem. Soc.: 339.
17. LANFREY, M. 1911. Compt. Rend. **152:** 92.
18. PRICE, W. B. & S. SMILES. 1928. J. Chem. Soc.: 2372.
19. ZWEIG, A. & A. K. HOFFMANN. 1965. J. Org. Chem. **30:** 3997.
20. MEINWALD, J., D. DAUPLAISE, F. WUDL & J. J. HAUSER. 1977. J. Am. Chem. Soc. **99:** 255.
21. The 1,8-dibromonaphthalene used in this study was prepared in 50–60% yield by direct tetraazotization of 1,8-diaminonaphthalene followed by treatment with cuprous bromide/hydrobromic acid.
22. LETSINGER, R. L., J. A. GILPIN & W. J. VULLO. 1962. J. Org. Chem. **27:** 672.
23. LETSINGER, R. L. & J. A. GILPIN. 1964. J. Org. Chem. **29:** 243.
24. LETSINGER, R. L., J. M. SMITH, J. A. GILPIN & D. B. MACLEAN. 1965. J. Org. Chem. **30:** 807.
25. A Hewlett Packard 5720 A gas chromatograph equipped with a flame ionization detector and nitrogen carrier gas was used for all analyses. Satisfactory separation was obtained with a 1.5-m × 4-mm glass column packed with 4% OV-1 on 60/80 Chromosorb W operating isothermally at 160°C.
26. DIKSHIT, V. K. & B. D. TILAK. 1951. Proc. Indian Acad. Sci. Sect. A **33:** 78.
27. JONES, R. G. & H. GILMAN. 1951. Organic Reactions. Vol. VI: Chap. 7, pp. 339–366.
28. GILMAN, H. & F. MOORE. 1940. J. Am. Chem. Soc. **62:** 1843.
29. The following library of crystallographic programs was used: BUSING, W. R., K. O. MARTIN & H. A. LEVY. 1965. A Fortran Crystallographic Least Squares Program. USAEC Report ORNL-TM-305. Oak Ridge Nat. Lab. Oak Ridge, Tenn.; BUSING, W. R., K. O. MARTIN & H. A. LEVY. 1964. ORFFE: A Fortran Crystallographic Function and Error Program. Report ORNL-TM-306. Oak Ridge Nat. Lab. Oak Ridge, Tenn.; JOHNSON, C. K. 1965. ORTEP: A Fortran Thermal Ellipsoid Plot Program for Crystal Structure Illustrations. Report ORNL-TM-3794. Oak Ridge Nat. Lab. Oak Ridge, Tenn.
30. SANDMAN, D. J. Personal communication, Xerox Corp. Rochester, N.Y.
31. CRUICKSHANK, D. W. J. 1957. Acta Crystallogr. **10:** 504.
32. MCGHIE, A. R., A. F. GARITO & A. J. HEEGER. 1974. J. Crystal Growth **22:** 295.
33. BURAVOV, L. I., G. I. ZVEREVA, V. F. KAMINSKII, L. P. ROSENBERG, M. L. KHIDEKEL, R. P. SHIBAEVA, I. F. SHCHEGOLEV & E. B. YAGUBSKII. 1976. Chem. Comm.: 720.
34. ISETT, L. C. & E. A. PEREZ-ALBUERNE. 1977. Solid Stat. Commun. **21:** 433.
35. COLEMAN, L. B. 1975. Ph.D. Thesis. Univ. Penn.
36. SUZUKI, M., T. YOKOYAMA & M. ITO. 1968. Spectrochim. Acta **24A:** 1091.
37. For a review see JENSEN, K. A., L. HENRIKSEN & P. H. NIELSEN. 1973. *In* Organic Selenium Compounds: Their Chemistry and Biology. D. L. Klayman and W. H. H. Gunther, Eds. John Wiley & Sons, Inc. New York, N.Y.
38. MAKI, A. G. & R. FORNEIRS. 1967. Spectrochim. Acta **23A:** 867.
39. DANCE, N. S. & W. R. MCWHINNIE. 1975. J. Chem. Soc. Dalton Trans. 43.
40. KONIG, E. 1966. Numerical Data and Function Relationships in Science and Technology. Group II, Vol. 2. Magnetic Properties of Coordination and Organo-Metallic Transition Metal Compounds. H. H. Hellwege and Landolt-Bornstein, Eds. Springer Verlag. Berlin.

ION-RADICAL SALTS OF TETRATHIOTETRACENE*

L. C. Isett and E. A. Perez-Albuerne

Research Laboratories
Eastman Kodak Company
Rochester, New York 14650

INTRODUCTION

A large number of conducting cation-radical salts have been prepared with tetrathiotetracene (TTT). The synthesis and purification of TTT are reviewed in this paper, and some new single-crystal resistivity data on TTT are reported; single-crystal resistivity values as large as 1×10^7 ohm-cm have been obtained by several gradient sublimitations. The series of TTT-X (X = Cl, Br, I, SCN) shows interesting systematic trends in compressed powder resistivity and infrared absorption spectra suggesting some of the important chemical parameters in the synthesis of highly conducting organic solids. Detailed studies of single-crystal samples of TTT_2I_3, including crystal structure, electrical resistivity, static magnetic susceptibility, and thermoelectric power, show that it is an organic metal ($\rho(300°K) \sim 10^{-3}$ Ω-cm), yet does not exhibit the full metal-insulator transition characteristic of other organic metals ($\rho(10°K) \simeq 5 \times 10^{-3}$ Ω-cm). These observations are related to lattice disorder and interchain coupling.

Tetrathiotetracene† (TTT) is an organic donor molecule that forms highly conducting, cation-radical salts with many acceptors. The properties of TTT place it in the class of "building blocks" of organic metals along with tetrathiofulvalene (TTF), tetracyanoquinodimethane (TCNQ), and TNAP (tetracyanonaphthoquinodimethane). In comparison with TTF and TCNQ, less work has been reported on TTT to date, but interest is increasing because of the availability of single crystals of a number of highly conducting TTT cation-radical salts.

SYNTHESIS AND PHYSICAL PROPERTIES OF TETRATHIOTETRACENE

TTT was first synthesized by Marschalk[1] and may be prepared rather simply by a number of different routes,[2] the most obvious being a direct reaction of sulfur and tetracene in boiling trichlorobenzene. Two alternative approaches are indicated in FIGURE 1. TTT is obtained as a green, relatively insoluble powder that may be recrystallized from trichlorobenzene or nitrobenzene. It may be purified by vacuum sublimitation, either gradient or direct. The molecular structure of TTT proposed by Marschalk and Stumm[2] has been confirmed by x-ray diffraction studies of TTT[3] and two cation radical salts of TTT.[4-6]

*Manuscript received June 13, 1977.

†The naming of tetrathiotetracene has continued to pose problems in the literature. The accepted IUPAC nomenclature is naphthaceno[5,6-cd:11,12-c'd']bis[1,2]dithiole, from which one group has generated NBDT.[6] Tetrathionaphthacene (abbreviated as TTN)[17] has also been used to describe the same molecule. Marschalk used the name tetrathiotetracene, and it seems reasonable to follow his lead.

0077-8923/78/0313-0395 $1.75/1 © 1978, NYAS

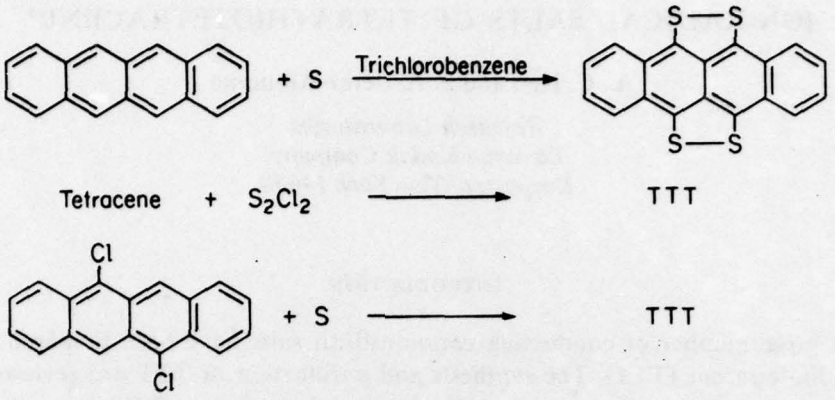


FIGURE 1. Synthesis of tetrathiotetracene.

Marschalk and Niederhauser[7] prepared several cation-radical salts, but it was Matsunaga[8] who first noticed that highly conducting cation-radical salts could be prepared based on TTT and also observed that TTT itself was surprisingly conductive ($\rho \sim 1 \times 10^4$ Ω-cm). Matsunaga suggested that this high conductivity may be due to the presence of cation radical TTT^+ formed by oxidation with air. The activation energy for conductivity in TTT was quite low (~0.23 eV) in these initial observations, consistent with the presence of acceptor levels that are producing the cation radical TTT^+.

TABLE 1 lists some of the measurements of the resistivity of TTT. The data are divided into classes based on measurements on compressed power, vapor-deposited thin films, and single crystals. Very high resistivities ($\sim 10^{10}$ Ω-cm) have been claimed for thin-film configurations,[11] but the observations of Silins and Taure[12] suggest that these very high values are due to the formation of blocking TTT-metal contacts. In the absence of any information, it must be assumed that the thin-film measurements were of the two-probe variety.

In the hope of monitoring the purification by recrystallization and vacuum sublimation of TTT we have measured the single-crystal resistivity of TTT grown

TABLE 1

RESISTIVITY OF TETRATHIOTETRACENE

ρ(300°K) ohm-cm	E_a, eV	
5.6×10^4	0.32	compressed (powder) Ref. 9
1.0×10^4	0.23	compressed powder, Ref. 8
8.5×10^3	0.22	compressed powder, Ref. 11
2.0×10^4	0.21	compressed powder, Ref. 10
1.3×10^6	0.29	thin film, Ref. 11
1.5×10^5	0.35	single crystal, recrystallized from nitrobenzene, this work
3.0×10^6	0.37	single crystal, recrystallized from nitrobenzene, two gradient sublimations, this work
1.0×10^7	0.45	single crystal, three gradient sublimitations, this work

from solvent recrystallization (nitrobenzene) and gradient sublimation. The results of this work are also shown in TABLE 1 and FIGURE 2. An unfortunate complication is that powder diffractometer data from our materials suggest a mixture of two crystal structures different from the published crystal structure,[3] but in agreement with the work of Marschalk. Marschalk identified two crystal structures of TTT from x-ray powder patterns.[13] There exist, therefore, at least three crystal structures of TTT, only one of which has been fully determined. Our data show that significant improvement in purity is achieved by multiple-gradient sublimation, as indicated by the resistivity. The highest values of resistivity and activation energy are obtained for TTT in which the recrystallization step was

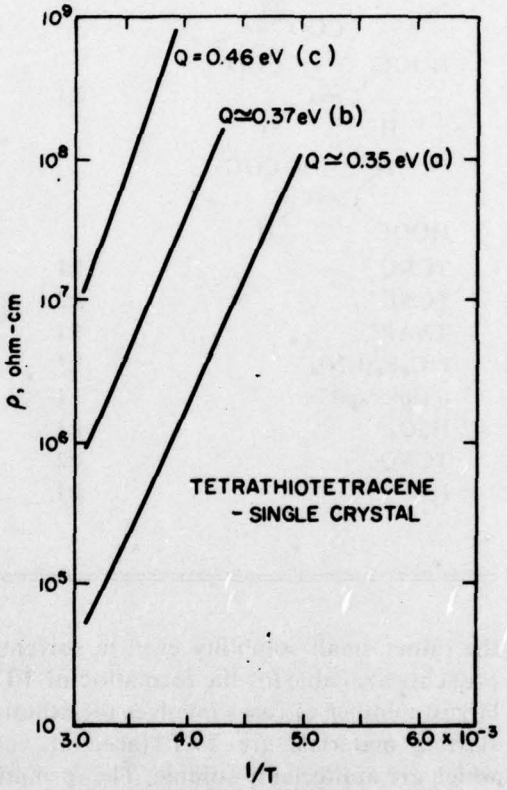


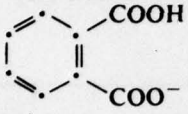
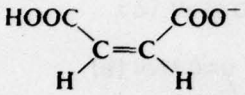
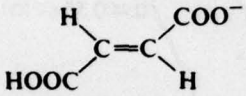
FIGURE 2. Resistivity of single-crystal tetrathiotetracene. (a): Recrystallized from nitrobenzene; (b): recrystallized from nitrobenzene, two direct sublimations, one gradient sublimation; (c): raw tetrathiotetracene, three gradient sublimations.

omitted and only sublimation was employed for purification. This value is still considerably smaller than the band gap determined from optical measurements or photoemission (1.7 eV–2.0 eV).[14,15] Although we believe that much of the increase in the resistivity is due to the increased purity of the TTT samples, a contribution because of changes in crystal structure cannot be ruled out.

ION-RADICAL SALTS OF TETRATHIOTETRACENE

Many conducting, cation-radical salts containing TTT have been synthesized, and some representative data are listed in TABLE 2. The low solubility of TTT and

TABLE 2
REPRESENTATIVE POWDER RESISTIVITY DATA

Anion	Cation:Anion	ρ, ohm-cm	Reference
Cl^-	1:1	2.3×10^3	9
Br^-	1:1	5.0×10	9
I^-	1:0.88	0.7	9
SCN^-	1:0.7	4.3	9
SO_4^-		1.7×10^3	16
$Fe(CN)_6^{-3}$	3:1	$2,0 \times 10^2$	16
	1:1	4.0×10	16
	2:1	4.0×10	16
		5.0×10	16
$TCNQ^+$	1:1	1.5	17
$TCNE^+$	3:2	10^2	17
$TNAP^+$	1:1	0.3	17
$PtC_4S_4(CN)_4^-$	1:1	3	17
o-Chloranil$^-$	3:1	3	8
HSO_4^-	1:1	1.0×10^2	10
$TCNQ^-$	1:2	1	19
I_3^-	2:1	10^{-3} (single crystal)	21 6

the rather small solubility even in solvents in which it is soluble limit the approaches available for the formation of TTT salts. The method that works in the largest number of cases involves metathesis of TTT and acceptor salts. Suitable starting materials are TTT^+(acetate)$^-$ and TTT^+(dichloroacetate)$^-$, both of which are appreciably soluble. The formation of TTT salts by direct reaction is possible in some cases, although reactions reported to date involved nitrobenzene or trichlorobenzene.

TABLE 3
RESISTIVITY, ACTIVATION ENERGY, AND THERMOPOWER OF TETRATHIOTETRACENE HALIDE AND PSEUDOHALIDE SALTS*

	ρ(300°K)	E_a(eV)	S(μV/K)
TTT-Cl	2.3×10^3	0.29	−210
TTT-Br	5.0×10	0.11	+10
TTT-I	2.1×10^1	0.06	+80
TTT-SCN	4.3	0.06	+40

*$\rho = \rho_0 \exp(E_a/kT)$.

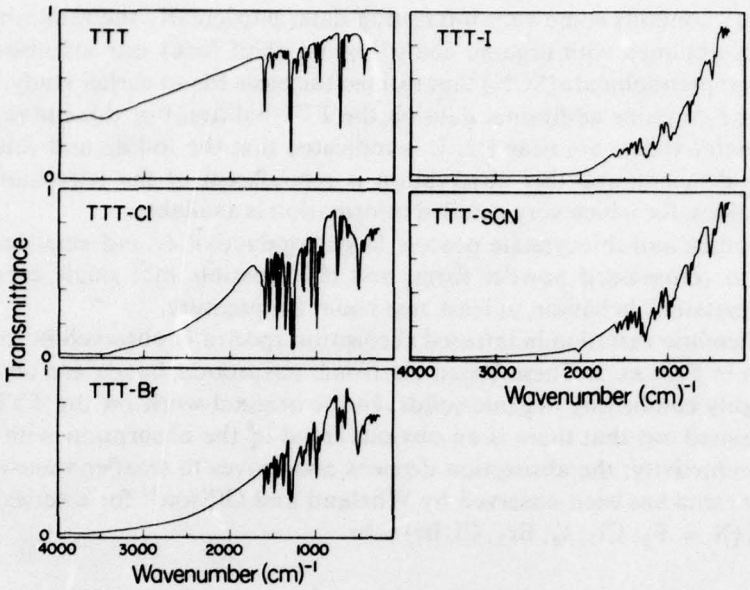


FIGURE 3. Infrared absorption spectra of TTT, and TTT-X (X = Cl, Br, I, SCN) (KBr wafers).

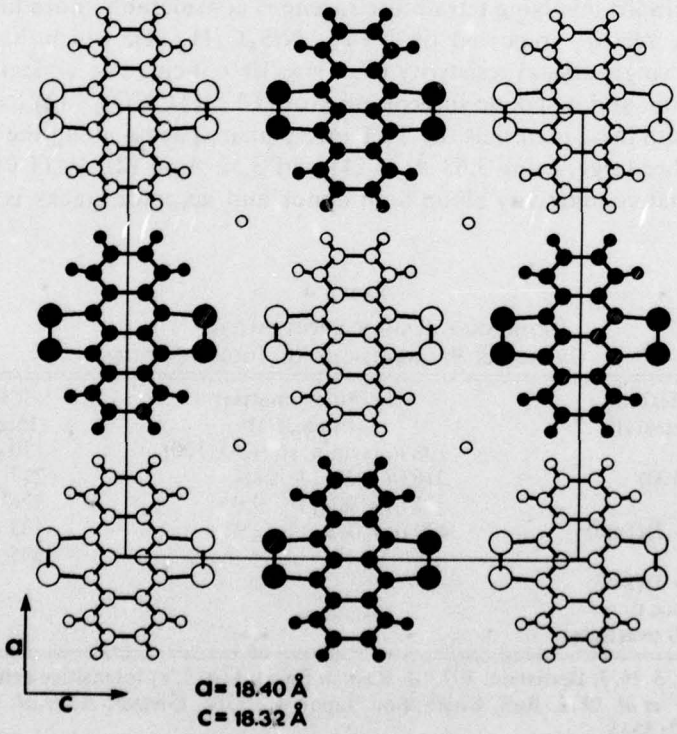


FIGURE 4. (010) projection of the crystal structure of TTT_2I_3 as determined by Smith and Luss.[5] Note the short S-S contact which may provide interchain coupling.

TABLE 2 contains some very interesting data, particularly the rather high conductivities obtained with organic acids, but we shall focus our attention on the halides and pseudohalide (SCN) that formed the basis for an earlier study.[9]

TABLE 3 contains additional data on the TTT-halides. For these materials the stoichiometry values are near 1:1. It is indicated that the iodide and thiocyanate are anion-deficient, and this observation is reminiscent of the tetrathiofulvalene (TTF) halides, for which very detailed information is available.

The iodide and thiocyanate possess large conductivities and small activation energies in compressed powder form, and it is possible that single crystals will exhibit "metallic" behavior, at least near room temperature.

A systematic variation in infrared absorption spectra is observed in this series, as shown in FIGURE 3. These broad electronic absorption bands are observed in many highly conducting organic solids. In the original work on the TTT-halides it was pointed out that there is an obvious trend in the absorption with changes in the conductivity; the absorption deepens and moves to smaller wave-numbers. A similar trend has been observed by Wheland and Gillson[17] for a series of TTT-TCNQX (X = F_2, Cl_2, I_2, Br_2, Cl, Br) salts.

SINGLE-CRYSTAL DATA ON ION-RADICAL SALTS OF TETRATHIOTETRACENE

Data such as described above, obtained on powder samples, are interesting but generally defy detailed interpretation and understanding. Information on single-crystal salts involving tetrathiotetracene is considerably more limited. Bray *et al.*[18] have recently reported on $TTT_{1.2}$ $NiS_4C_4H_4$ (**1**), which has a room-temperature single-crystal resistivity of $\sim 3 \times 10^{-2}$ Ω-cm. The crystal structure,[4] resistivity data, and magnetic susceptibility of $(TTT)(TCNQ)_2$[19] (**2**) have been reported. In both these materials the TTT interplanar spacing along the conducting stacks is rather large, being 3.63 Å in (**1**) and 3.52 Å in (**2**). In $(TTT)(TCNQ)_2$ it is likely that conductivity along both donor and acceptor stacks is important.

TABLE 4

RESONANCE RAMAN SPECTRA (cm^{-1}) OF OVERTONE PROGRESSIONS OF IODINE SPECIES

I_2 (Hexane) (Intensity)*	I_3^- (PVA matrix) (Intensity)†	TTT_2I_3 (Intensity)‡
—	108 ν_1 (symm. stretch) (100)	10 g (100)
211 ν_1 (100)	216 ($n = 2, \nu_1$) 28.4	217 (29.2)
	322 ($n = 3, \nu_1$) 9.9	326 (9.4)
422 ($n - 2$)(56.6)	430 ($n = 4, \nu_1$) 3.9	433 (3.5)
	—	545 (1.6)
631 ($n = 3$)(24.3) plus out to $n = 20$ overtones	—	

*Kiefer, W. & H. J. Bernstein. 1973. J. Raman Spect. **1**: 417. ν_1 intensities defined as 100.

†Inagaki, F. *et al.* 1972. Bull. Chem. Soc. Japan **45**: 3384. Gleizes, A. *et al.* 1975. J. Am. Chem. Soc. **97**: 3545.

‡This work; 4880 Å laser excitation. Trotter, P. J. Unpublished.

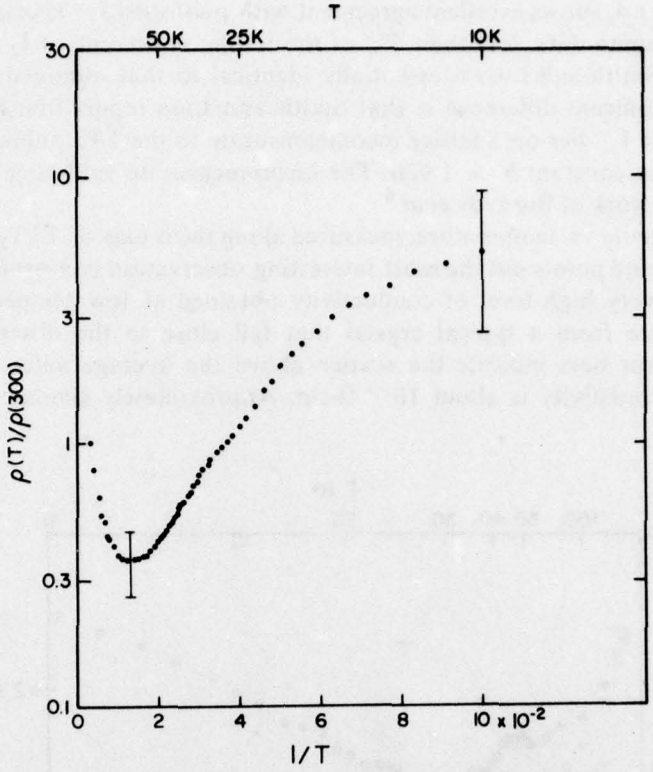


FIGURE 5. Resistivity of TTT_2I_3 along *b* axis, plotted as log of normalized resistivity $\rho(T)/\rho(300)$ vs. $1/T$, for a typical crystal; error bars indicate observed scatter.

Samples of (2) show a great deal of disorder; magnetic susceptibility data indicate a 3–4% spin ½ Curie term at low temperatures.[19,20]

A mixed-valence, TTT-halide compound, $(TTT)_2I_3$, has attracted the interest of several research groups, and at present this is the best characterized (TTT) conducting salt. TTT_2I_3 has been prepared by two synthetic approaches: (1) direct reaction in nitrobenzene,[6,21] and (2) reaction of TTT and I_2 in the vapor phase.[22] Preliminary comparisons indicate significant differences between TTT_2I_3 prepared by these two methods. Buravov *et al.*[6] have reported obtaining TTT^+I^- by direct reaction in nitrobenzene, but give few details.

PROPERTIES OF TTT_2I_3

An (010) projection of the crystal structure of TTT_2I_3, as determined by Smith and Luss,[5] is shown in FIGURE 4. The TTT interplanar spacing in this structure is 3.32 Å. The closest sulfur-sulfur distance on adjacent molecules is 3.73 Å, and a short S...S (3.37 Å) contact may provide some interchain coupling. The iodine atoms lie in chains parallel to b. The iodine sublattice is disordered by a statistically random mutual shift of the iodine columns along their longitudinal axes. The iodine atoms are present as triiodide anions. Resonance Raman data,

listed in TABLE 4, shows excellent agreement with published I_3^- spectra. From the resonance Raman data, less than 2% of the iodine is present as I_2. The crystal structure of Smith and Luss is essentially identical to that obtained by Buravov *et al.* The significant difference is that Smith and Luss report that a substantial fraction of the I_3^- lies on a lattice incommensurate to the TTT sublattice, having a b axis lattice constant $b' = 1.92b$. The incommensurate sublattice was not reported in the work of Buravov *et al.*[6]

The resistivity vs. temperature, measured along the b axis of TTT_2I_3, is shown in FIGURE 5, and points out the most interesting observation concerning $TTT_2I_3^-$, namely, the very high level of conductivity obtained at low temperatures. The data given are from a typical crystal that fall close to the observed average behavior. Error bars indicate the scatter above the average value. The room-temperature resistivity is about 10^{-3} Ω-cm. Approximately similar results have

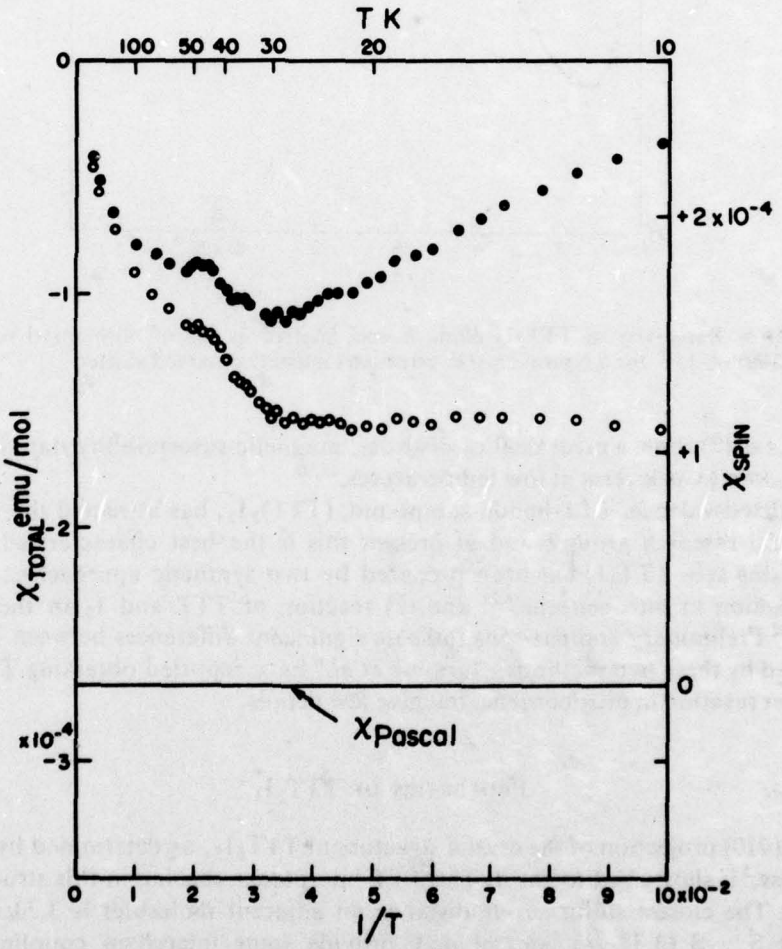


FIGURE 6. Static magnetic susceptibility of TTT_2I_3, plotted vs. $1/T$. Scale on left gives the total measured χ; scale on right gives χ corrected for core diamagnetism ● = raw data; ○ = corrected for Curie tail due to ~0.25% spin-½ impurities.

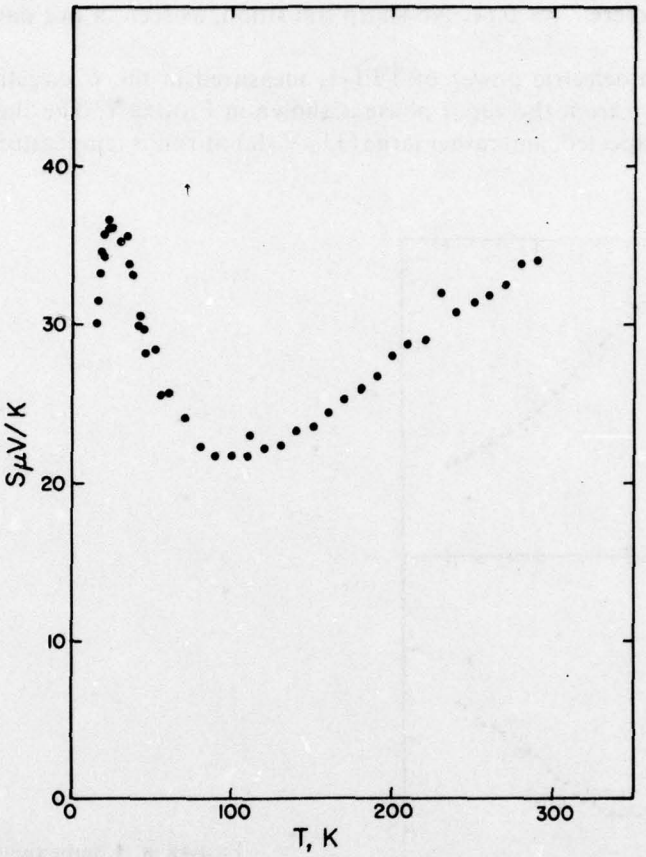


FIGURE 7. Measured *b*-axis thermoelectric power of TTT_2I_3 as a function of temperature.

been obtained on solution-grown crystals by Mihaly and coworkers,[21] although their crystals are consistently more resistive at low temperature and show a smaller value of $\rho(300)/\rho_{min}$. It was the very high conductivity at low temperature which led us to suggest that no metal-insulator transition occurs in TTT_2I_3.

Recent measurements of the magnetic susceptibility and thermoelectric power demonstrate that at low temperatures TTT_2I_3 is behaving in an anomalous manner. The magnetic susceptibility of TTT_2I_3, measured with a Faraday balance, is shown in FIGURE 6, where the magnetic susceptibility is plotted as a function of $1/T$. The susceptibility is roughly constant for $100K < T < 300°K$, and at about 50°K exhibits a definite change in slope, followed by a minimum and a Curie-like tail at low temperatures. The low-temperature Curie tail may be removed to yield the data shown, implying that at $T = 0$ TTT_2I_3 is still paramagnetic. The Curie-tail corresponds to about 0.25% spin ½ impurities. A similar paramagnetic term at low temperatures has been reported in the magnetic susceptibility of TTF_{1-x} $TSeF_xTCNQ$.[24] Magnetic susceptibility measurements on TTT_2I_3 synthesized from nitrobenzene (Mihaly, private communication), shows quite different behavior from our data, and in particular for $T < 30°K$ show

$\chi = A/T^{\alpha}$ where $\alpha \simeq 0.61$. No sharp transition, as seen in our data at ~50°K, is observed.

The thermoelectric power of TTT_2I_3 measured in the *b* direction on single crystals grown from the vapor phase is shown in FIGURE 7. The thermopower is positive, as expected, and rather large (33 μV/K) at room temperature, decreasing

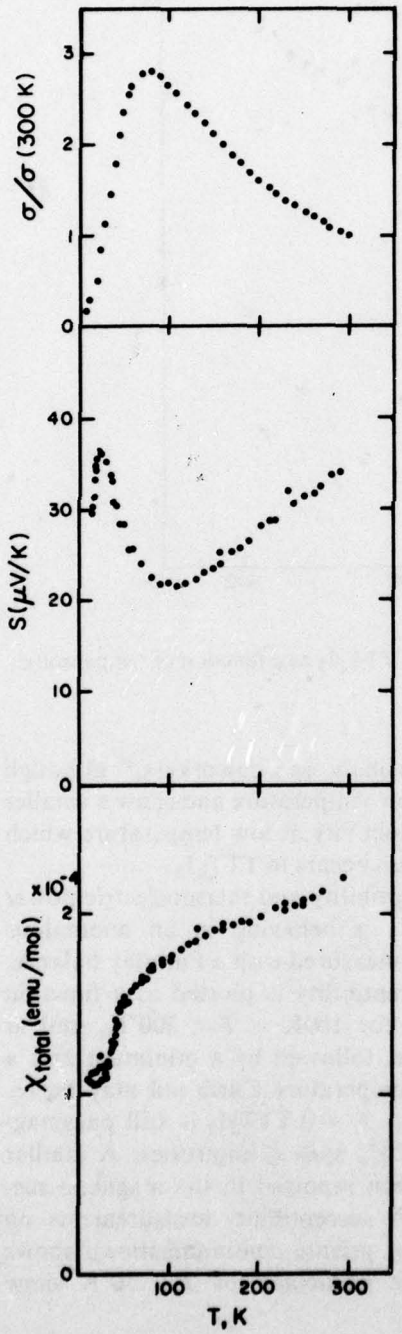


FIGURE 8. Conductivity, thermoelectric power, and magnetic susceptibility for TTT_2I_3 shown on a common temperature scale.

roughly linearly through a broad minimum at $T \sim 100°K$ and passing through a maximum at $T \simeq 25°K$. In the temperature range studied, no sharp breaks characteristic of a metal-insulator transition are observed.

It is worth mentioning that in the thermoelectric power and the magnetic susceptibility data the largest differences between samples of TTT_2I_3 prepared by various techniques are observed. The differences in magnetic susceptibility between the vapor-phase material and solution-grown crystals have already been mentioned. The thermoelectric power of TTT_2I_3 crystals grown from nitrobenzene is positive ($\sim 20\ \mu V/K$ at $T = 300°K$)[21,25] and essentially constant in the range $100°K < T < 300°K$. The most obvious possible difference between samples is in the iodine concentration. The crystal structure of Smith and Luss implies a range $(TTT \cdot I_x)$ with $1.50 < x < 1.56$ for the vapor-grown crystals. Elemental analysis of vapor-grown crystals favors $x = 1.50$, while values of $x = 1.5$,[6] 1.6,[21] and 1.7[26] have been reported for crystals recrystallized from nitrobenzene.

An interesting and related problem in TTT_2I_3 concerns the magnitude of the electron mobility along the triiodide chain. One might anticipate that as x increases above 1.5, and the number of iodine-iodine contacts shorter than 3.64 Å between triiodide anions observed by Smith and Luss increases, increased electron mobility on the triiodide chain would be possible. The change in thermopower between the vapor-grown crystals and solution-grown crystals is consistent with this hypothesis.

An understanding of the low-temperature behavior of TTT_2I_3, and in particular the presence of phase transitions, will require considerably more experimental data. This is best seen in FIGURE 8, where we have arranged the magnetic susceptibility, conductivity, and thermoelectric power to reveal any common features. The very clear feature in the magnetic susceptibility data at 50°K is completely missing in both resistivity and thermoelectric power data. This is in contrast to most other organic metals, e.g. TTF-TCNQ, TTF_x-SCN_y,[27] and TSeF-TCNQ, where sharp breaks are observed in both ρ vs. T and χ vs. T at the same temperature.

REFERENCES

1. MARSCHALK, C. 1939. Bull. Soc. Chim. Fr. **6**: 1122.
2. MARSCHALK, C. & C. STUMM. 1948. Bull. Soc. Chim. Fr. **15**: 418.
3. DIDEBERG, O. & J. TOUSSAINT. 1974. Acta Cryst. **B30**: 2481.
4. SHIBAEVA, R. P. & L. P. ROZENBERG. 1975. Kryst. **20**: 943.
5. SMITH, D. L. & H. R. LUSS. 1977. Acta Cryst. **B33**: XXX. In press.
6. BURAVOV, L. I., G. I. ZVEREVA, V. F. KAMINSKII, L. P. ROSENBERG, M. L. KHIDEKEL, R. P. SHIBAEVA, I. F. SHCHEGOLEV & E. B. YAGUBSKII. 1976. J. Chem. Soc. Chem. Comm. 720.
7. MARSCHALK, C. & P. NIEDERHAUSER. 1952. Bull. Soc. Chim. Fr. **19**: 151.
8. MATSUNAGA, Y. 1965. J. Chem. Phys. **42**: 2248.
9. PEREZ-ALBUERNE, E. A., H. JOHNSON, JR., & D. J. TREVOY. 1971. J. Chem. Phys. **55**: 1547.
10. GOODINGS, E. P., D. A. MITCHARD & G. OWEN. 1972. J. Chem. Soc. Perkin Trans. I: 1310.
11. INOKUCHI, H., M. KOCHI, Y. HARADA. 1967. Bull. Soc. Chem. Japan. **40**: 2695.
12. SILINS, E. & L. TAURE. 1970. Latvijas PSR Tinatnu tkaet. vest., Fix. Tehn. Teir Ser. (1): 18.
13. MARSCHALK, C. 1952. Bull. Soc. Chem. Fr. **19**: 800.

14. SHIROTANI, I., K. KAWADA & H. INOKUCHI. 1970. Bull. Chem. Soc. Japan. **43:** 2381.
15. BAIWIR, M. & O. DIDEBERG. 1969. Bull. Soc. Roy. Sci. Liege **38:** 485.
16. PEREZ-ALBUERNE, E. A., H. JOHNSON, JR. & D. J. TREVOY. Private communication.
17. WHELAND, R. C. & J. L. GILLSON. 1976. J. Am. Chem. Soc. **98**(13): 3916.
18. BRAY, J. W., H. R. HART, JR., L. V. INTERRANTE, I. S. JACOBS, J. S. KASPER, P. A. PIACENTE & G. D. WATKINS. 1977. Preprint.
19. BURAVOV, L. I., O. N. EREMENKO, R. B. LYUBOVSKII, L. P. ROZENBERA, M. L. KHIDEKEL, R. P. SHIBAERVA, I. F. SCHCHEGOLER & E. B. YAGUBSKII. 1974. JETP Lett. **20**(7): 208.
20. DELHAES, P., S. FLANDROIS, G. KERYER & P. DUPIS. 1975. Mat. Res. Bull. **10:** 825.
21. MIHALY, G., A. JANOSSY & G. GRÜNER. Preprint.
22. ISETT, L. C. & E. A. PEREZ-ALBUERENE. 1977. Solid State Commun. **21:** 433.
23. TROTTER, P. Private communication.
24. SINGER, K. T., V. VEI & A. F. GARITO. 1977. Bull. Am. Phys. Soc. **22**(3): 395.
25. HERMAN, A. M. Private communication.
26. KARIMOV, YU. S., G. I. ZVEREVA & E. B. YAGUBSKII. 1977. JETP Lett. **25**(5): 254.
27. WUDL, F., D. E. SCHAFER, W. M. WALSH, JR., L. W. RUPP, F. J. DISALVO, J. V. WASZCACK, M. L. KAPLAN & G. A. THOMAS. 1977. J. Chem. Phys. **66**(2): 377.

DISCUSSION

ROBERT COMÈS: X-ray diffuse scattering by the Shchegolev group on $(TTT)_2I_3$ reveals at least two types of 1-D ordering of the iodines, with a repeat distance close to that expected for I_3^- molecules. It means that the iodines are ordered within each channel, but with little coupling between channels.

MOLECULAR DESIGN OF SOLID-STATE SYSTEMS. ORGANIC-METAL COMPLEX π-DONOR-ACCEPTOR COMPOUNDS*

L. V. Interrante, J. W. Bray, H. R. Hart, Jr.,
J. S. Kasper, P. A. Piacente

General Electric Corporate Research & Development
Schenectady, N.Y. 12301
and

G. D. Watkins

Physics Department
Lehigh University
Bethlehem, Pennsylvania 18051

Continuing interest in the physics and chemistry of quasi-one dimensional (1-D) systems has prompted recent efforts in a number of laboratories to prepare and characterize new examples of such materials and to develop theoretical and empirical guidelines that will enable their directed synthesis. As the papers in this volume demonstrate, considerable progress has been made in both areas. Nonetheless, it is clear that there is still much to be learned about the nature of these materials and particularly how to prepare them in a directed manner.

Our approach to this problem of achieving the directed synthesis of quasi-1-D materials has been largely an empirical one and has focused on the identification of characteristics associated with individual molecules that might be used in a predictive way to determine the likelihood of forming a quasi-1-D conductor. We have chosen, as a focal point for our synthesis efforts, crystalline π-donor-acceptor (π-D-A) compounds, where columnar stacking of the constituent planar molecules can result in extended π-orbital interactions along one direction in the solid. As the π-acceptor unit for these studies, we have used a homologous series of planar metal-organic compounds known as the bis-dithiolene metal complexes (FIGURE 1).[1] In addition to an overall planar molecular geometry, these compounds exhibit a number of characteristics that make them particularly attractive as π-acceptor units for such a study. These include an ability to undergo reversible electron-transfer reactions to yield stable species with unpaired electrons in highly delocalized orbitals of π-symmetry, the existence of species with sufficiently high electron affinity to remove an electron from a wide variety of organic donors, and, in general, good solubility and stability in organic solvents. Perhaps most importantly, however, these complexes possess a considerable degree of structural flexibility, available through changes in the metal (M) and the ligand substituent (X), which can be varied in a systematic way to study the effects of molecular features on solid state structure and properties.

*Supported in part by a grant from the Air Force Office of Scientific Research (AFSC), United States Air Force, under contract F 44620-76-C-0006. Manuscript received June 13, 1977.

0077-8923/78/0313-0407 $1.75/1 © 1978, NYAS

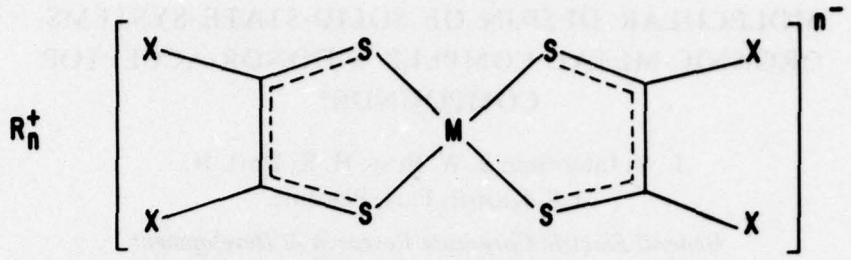


FIGURE 1. Molecular structure of the bis(ethylene-1,2-dithiolene) metal complexes, where *M* can be a variety of elements from the d transition series, *X* = various ligand substituents such as H, CH_3, C_6H_5, CF_3, CN, etc., R^+ = organic or inorganic cations, and $n = 0, 1, 2$.

Our efforts to explore the consequences of such variations are still in progress; however, the results that we have obtained thus far do indeed suggest that profound changes in both the crystal structure and properties of the D-A compound can be produced by relatively subtle variations in these molecular features. In particular, it appears that substituent groups on either the donor or acceptor molecules can influence the crystal structure and solid-state properties not only by determining the way in which the molecules can pack together most efficiently but also by their effect on the tendency of the molecules to give up or accept electrons in the solid-state environment (i.e., the effective D ionization potential and A electron affinity). In the case of the *bis*-dithiolene metal complexes, it is possible to vary the electron affinity, as measured by solution redox potential data,[1] over a wide range through changes in the ligand substituents and thereby to study the effect of this parameter in a fairly controlled manner. Our preliminary results seem to support previous suggestions[2] that a close balance between the effective, *in situ*, ionization potential of the donor and the *in situ* electron affinity of the acceptor is needed in order to obtain highly conductive, 1:1, π-D · A compounds and suggest further that solution redox potential data might serve as a useful guide to the choice of appropriate D-A pairs. This possibility is currently being explored further in experiments with other D-A combinations.

In the course of this study we have prepared a number of new π-D · A compounds that exhibit interesting structural, magnetic, and electronic characteristics.[3–9] These include the first 1-D antiferromagnetic systems to exhibit the theoretically predicted spin-Peierls instability, a lattice dimerization that is apparently driven by the 1-D magnetic spin system.[7]

$TTT_{1.2}NiS_4C_4H_4$

The most recent addition to this family of organic donor-*bis*-dithiolene metal complex acceptor compounds is a material obtained from the interaction of tetrathiotetracene (TTT) and nickel bis(ethylene-1,2-dithiolene) ($NiS_4C_4H_4$) which has the empirical formula $TTT_{1.2}NiS_4C_4H_4$.[9] Tetrathiotetracene (FIGURE 2) is an organic donor molecule that has been shown to react with various organic and metal complex acceptors to yield π-D · A compounds with widely varying

conductivity characteristics. It has been combined with the *bis*-dithiolene complex $NiS_4C_4(CF_3)_4$ to give a material with a 1:1 D:A stoichiometry.[10] The properties of this compound are suggestive of a simple salt containing the TTT^+ and $NiS_4C_4(CF_3)_4^-$ with essentially localized unpaired electrons on each unit. The conductivity is extremely low, measured at $<10^{-10}$ ohm^{-1} cm^{-1} as a pressed pellet.

With TCNQ, TTT gives both 1:1 and 1:2 [$TTT(TCNQ)_2$] derivatives.[11,12] The conductivity of the former has been reported to be ~ 1 ohm^{-1}cm^{-1}, whereas the 1:2 derivative gives somewhat higher value (20–160 ohm^{-1}cm^{-1}) at room temperature (σ_{RT}) which increases on cooling to maximum of $\sim 2 \rightarrow 3.5 \times \sigma_{RT}$ at around 90°K. The structure of this latter compound has been determined and shows separate stacks of TTT and TCNQ units with a 3.52 Å intrastack separation for the TTT units.

Various compounds of TTT with halogens and pseudohalogens have also been prepared which exhibit conductivities up to 1.4 ohm^{-1}cm^{-1} as pressed pellets.[13] Recently one of these compounds, TTT_2I_3, has been obtained in the form of single crystals and has been characterized structurally and by means of conductivity and magnetic susceptibility measurements.[14,15] The conductivity at room temperature (~ 1000 ohm^{-1}cm^{-1}) is among the highest yet observed for an organic system. It increases further on cooling to $\sim 3 \times \sigma_{RT}$ in the vicinity of 60°K, whereupon it goes through a broad maximum and gradually decreases at lower temperature. The crystal structure solution shows an apparently uniform stacking arrangement of TTT units with an interstack separation of 3.32 Å.

As such, TTT is one of the newest and most promising organic systems to receive attention as a potential source of 1-D conductor materials and a much more thorough investigation is its behavior with various π-acceptors is clearly called for.

The compound $TTT_{1.2}NiS_4C_4H_4$ was prepared both by direct combination of the neutral components in organic solvents and by a metathesis reaction in acetonitrile using $(TTT)_x^+SbF_6^-$ and $(C_2H_5)_4N^+ NiS_4C_4H_4^-$. The latter procedure also can be used to obtain the analogous Pd and Pt derivatives that appear to be isostructural with $TTT_{1.2}NiS_4C_4H_4$ (on the basis of x-ray powder diffraction data) and to have similar magnetic and electrical properties; however, attempts to prepare single crystals of these derivatives thus far have been unsuccessful. Likewise, several attempts were made to obtain the analogous $TTT_{1.2}CuS_4C_4H_4$ compound using the above metathesis procedure, but in each case conversion to TTT^0 and unidentified $CuS_4C_4H_4^-$ oxidation products was evidenced.

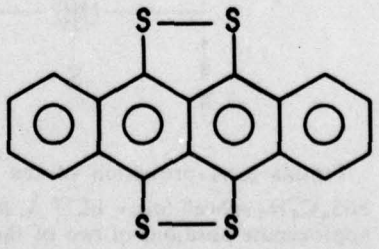


FIGURE 2. Molecular structure of tetrathiotetracene (TTT).

Single crystals of the $TTT_{1.2}NiS_4C_4H_4$ compound measuring typically 1.0 × 0.1 × 0.02 (mm) were prepared by slow cooling of hot chlorobenzene solutions containing a 1:2 molar proportion of TTT to $NiS_4C_4H_4$. Higher proportions of TTT to $NiS_4C_4H_4$ gave another phase which had a higher ratio of TTT and a much lower conductivity ($\sim 10^{-3}$ohm^{-1}cm^{-1}, for a crystal). Solutions containing a further excess of $NiS_4C_4H_4$ gave only mixtures of the $TTT_{1.2}NiS_4C_4H_4$ phase and $NiS_4C_4H_4^0$. Crystals of $TTT_{1.2}NiS_4C_4H_4$ were also successfully obtained from a controlled current (0.75 μamp) electrolysis at a Pt cathode of a 1:1 mixture of $(TTT)_x^+SbF_6^-$ and $NiS_4C_4H_4^0$ in acetonitrile using $(n\text{-butyl})_4N^+AsF_6^-$ as a supporting electrolyte. In our hands, this method yielded crystals poorer in quality and smaller in size than those obtained by slow cooling from chlorobenzene solution.

This new material has been studied by means of x-ray diffraction, magnetic susceptibility, EPR, dc conductivity, and thermopower measurements and shows some features that appear to be unique among TTT derivatives and π-D · A compounds in general.

The crystal structure (see FIGURE 3) may be conveniently viewed as involving two separate orthorhombic subcells for the two molecules with $a_T = 2a_N$ (T ≡ TTT and N ≡ $NiS_4C_4H_4$), $b_T = 2b_N$, and $c_T = c_N/2.4$. Thus, in any given crystal volume there are 1.2 T molecules for every N molecule. The complete structure has not yet been refined, but the structural parameters are known sufficiently well to specify the molecular arrangement. A projection of this structure on the *ab* plane is shown in FIGURE 3 in terms of the smaller subcell appropriate for N, for

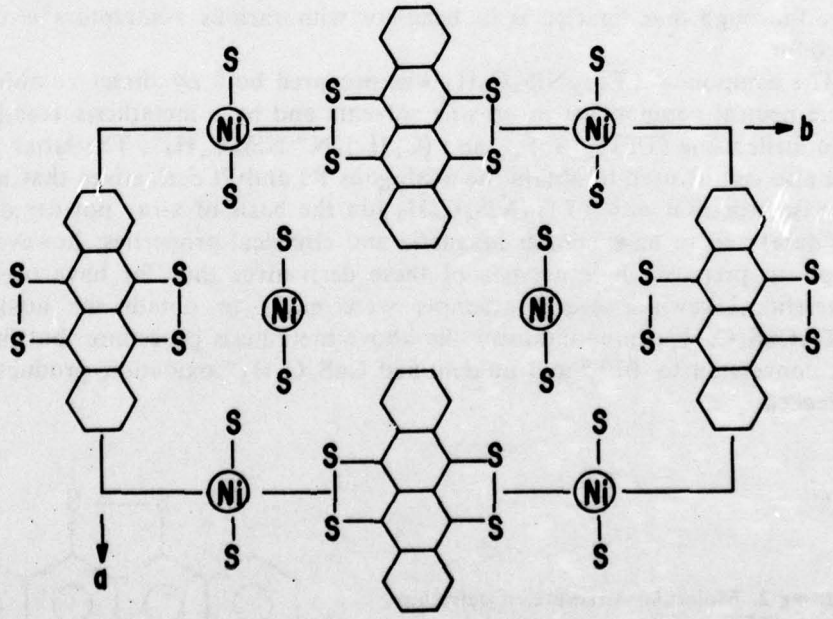


FIGURE 3. A projection of the $TTT_{1.2}NiS_4C_4H_4$ structure on the ab plane of the $NiS_4C_4H_4$ subcell (a_N = 12.73 Å, b_N = 22.13 Å). (Ni) indicates positions of the Ni and the approximate positions of two of the S atoms of the $NiS_4C_4H_4$ unit. These S atoms lie, respectively, above and below the Ni in the actual structure.

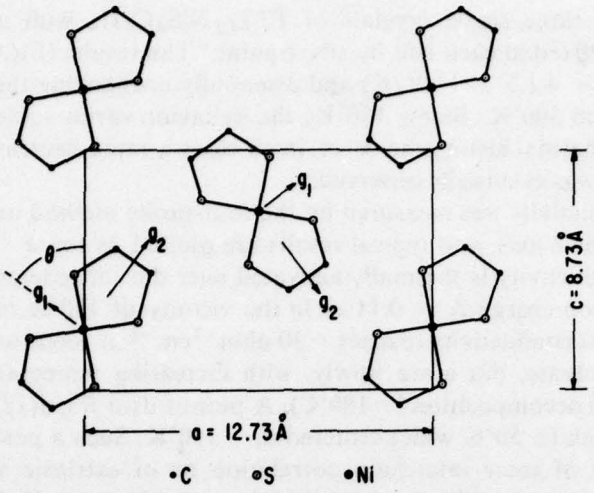


FIGURE 4. A projection of the N^- subcell on the ac plane showing the relative orientation of the $NiS_4C_4H_4^-$ units within this plane. The directions of the principal g values, g_1 and g_2, characteristic of the individual N^- units are indicated; g_3 lies perpendicular to the plane of the molecules and parallel to the crystallographic b axis.

which a_N = 12.73 Å, b_N = 22.12 Å, and c_N = 8.73 Å, space group $C222_1$, with Z = 4 N's and 4.8 T's. The T molecules are stacked along the c axis with uniform spacing c_T = 3.6 Å and are almost parallel to the ab plane. The N molecules are parallel to the ac plane as indicated in FIGURE 4. There is no stacking of N molecules, nor are there any close contacts between them. The T chains are separated by at least 4.4 Å (closest carbon-carbon distance in a direction). The needle axis of these crystals is coincident with the c axis (TTT stacking direction).

The magnetic susceptibility χ was measured by the Faraday method on an unoriented collection of these crystals. The results show Curie-Weiss paramagnetic behavior with an antiferromagnetic Weiss constant $\Theta \cong -5.5$°K, indicative of localized spins. The magnitude of the Curie constant C is essentially that expected for one g = 2, S = ½ electron per $TTT_{1.2}NiS_4C_4H_4$ formula unit. Since the T and N molecules have closed-shell electronic structures, complete one-electron transfer should produce unpaired spins on both the resultant T^+ and N^- ions. Therefore, the magnitude of C indicates that only half of these spins appear as paramagnetic spins.

The location of these spins on the N^- units is suggested by the results of EPR measurements carried out on a single crystal of this compound. A single, intense EPR signal was observed over the temperature range ~300°K → 1.7°K. The principal values of the g-tensor are essentially temperature independent over this range and are completely consistent with expectations for weakly exchange coupled N^- units in the two orientations found in the crystal-structure determination (FIGURE 4). There is no evidence of any contribution from T^+ unpaired spins, either as a separate signal or via exchange coupling with the N^- spins. We conclude from these measurements and the crystal structure that complete charge transfer has occurred in the solid state from the T to the N units but that only the N^- subsystem contributes to χ.

The absolute thermopower S was measured along the c-axis as a function of

temperature on three single crystals of $TTT_{1.2}NiS_4C_4H_4$ with a gold-advance thermocouple affixed to each end by silver paint.[4] The results (FIGURE 5) indicate a very small ($S = +1.5 \pm 1\ \mu V/K$) and essentially unchanging thermopower between ~180° and 300°K. Below 180°K, the behavior varies somewhat with the sample and its thermal history; however, in all cases a rapid decrease of S to large negative values was eventually observed.

The dc conductivity was measured by the four-probe method on several single crystals along the *c*-axis, and typical results are plotted as log σ vs. 1/T in FIGURE 6. The conductivity is thermally activated over the entire temperature range, with an activation energy $\Delta \simeq 0.11$ ev in the vicinity of 150°K (denoted by the dashed line). The conductivity reaches ~30 $ohm^{-1}cm^{-1}$ at room temperature and continues to increase, but more slowly, with increasing temperature up to the point of thermal decomposition (~180°C). A plot of $d(\ln R)/d(1/T)$ vs. T shows a very broad peak (~50°K wide) centered at ~150°K. Such a peak may indicate the onset either of some interchain correlation or of extrinsic semiconducting behavior due to defects and impurities (which would decrease Δ). The breadth of this peak plus the absence of a peak in $d(R)/d(1/T)$ vs. T repudiate the existence of any true 3-D phase transition.

We believe that the concept of a periodic distortion of the TTT chains at all temperatures best explains these observations. One likely source of such periodic chain distortion is the Peierls instability,[17] which we may characterize for our system as follows. Because there are 1.2 T molecules for each N molecule and there is complete charge transfer from T to N, on the average each of the T molecules has lost $\frac{5}{6}$ of an electron. Assuming that the usual tight-binding band with two

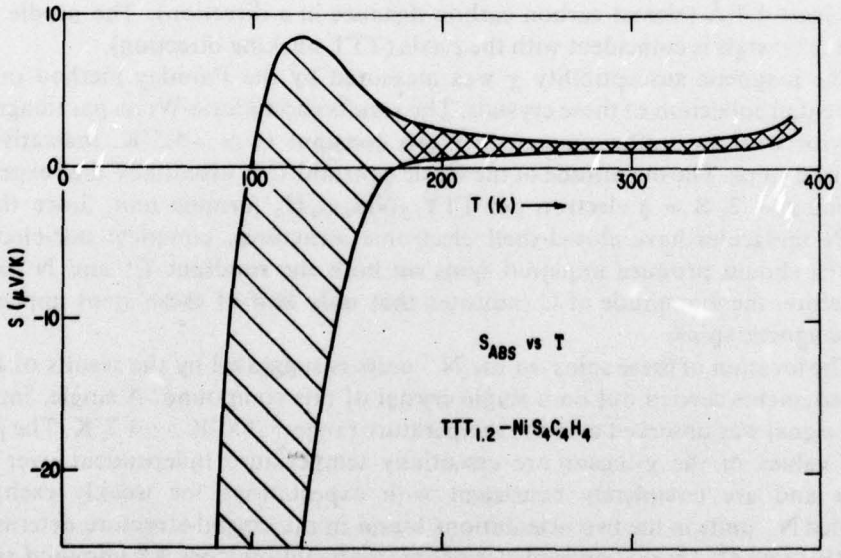


FIGURE 5. The absolute thermoelectric power, or Seebeck coefficient, for $TTT_{1.2} \cdot NiS_4C_4H_4$ (*c*-axis). The hatched area included all the values obtained for three samples. The spread indicated at lower temperatures includes both sample-to-sample variations and changes that occurred upon heating the sample and its silver-paint contacts above room temperature.

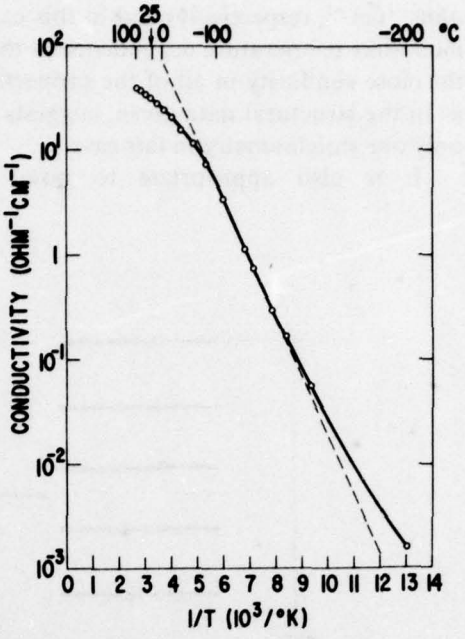


FIGURE 6. Conductivity (σ) along the c-axis direction of a typical $TTT_{1.2}NiS_4C_4H_4$ crystal as a function of temperature. The dashed line denotes the region of maximum slope of log σ vs. 1/T, with an activation energy $\Delta = 0.11$ eV.

states/molecule is responsible for conduction along the T chains, the band is thus $\frac{7}{12}$ filled. Since a Peierls distortion of periodocity mc_T (where c_T is the undistorted chain periodicity) creates gaps at band fillings n/m ($n = 1, 2, \ldots, m-1$), a Peierls distortion would have periodicity $12c_T$ in this system. We also note that since $c_N/c_T = 2.4$, the N and T subsystems are in registry along the c axis at every twelfth T molecule (i.e., the true cell has a c-axis dimension of $12c_T$) (See FIGURE 7). The periodic crystal field associated with this registry periodicity could also produce a distortion of this same period in the T chains. This effect and the Peierls instability certainly reinforce each other and probably contribute to lowering the attainable conductivity of this system.

There are apparently very few other instances of equivalence of Peierls and crystal structure (registry) periodicities among the known examples of 1-D conductors. One possible example is a compound of tetrathiafulvalene (TTF) and thiocyanate (SeCN) with the reported formula $TTF_{11}(SeCN)_6$.[18] An examination of the crystal-structure data given for this material indicates that the TTF and SeCN substructures should be in registry at every eleventh TTF unit along the stacking direction (the true unit cell presumably contains 11 TTF units along the stacks). The same kind of analysis of the expected band filling as we have made for $TTT_{1.2}NiS_4C_4H_4$ would predict a Peierls periodicity also of eleven for this system. It is perhaps notable that this compound does not exhibit a "metallic" conductivity temperature dependence and has a conductivity at 280°K of ~13 ohm^{-1}cm^{-1}. This is about a factor of 50 lower than that of the closely related $(TTF)_{12}(SeCN)_7$ compound,[19] where our analysis indicates a 2:1 ratio of the Peierls and structural periodicities.

The difference in the reported conductivities of the presumably analogous 11:6 and 12:7 TTF:SCN compounds is not quite so large ($\sigma_{298°K} = 250$[18] and 550[19]

ohm^{-1}cm^{-1}, respectively) and in this case both compounds apparently exhibit a metal-like temperature dependence in the vicinity of room temperature; however, the close similarity in all of the properties reported for these two phases, as well as in the structural data given, suggests the possibility that there may in fact be only one stoichiometry in this case.

It is also appropriate to point out the striking similarities between

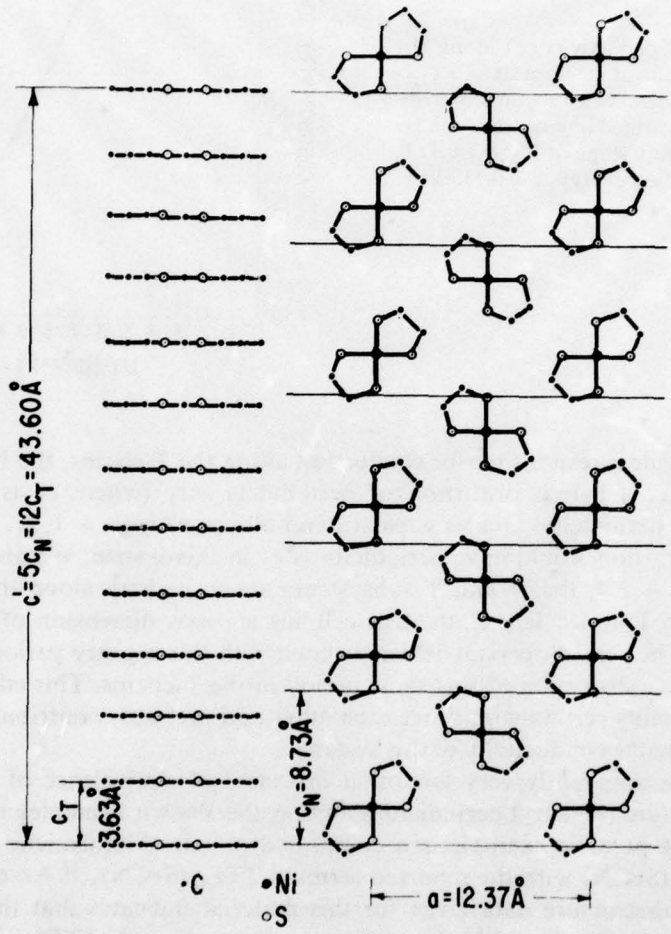


FIGURE 7. A view of the two subcells in the $TTT_{1.2}NiS_4C_4H_4$ structure normal to the ac plane, showing the coincidence of the $NiS_4C_4H_4$ and TTT subcells at $5c_N \approx 12c_T$.

$TTT_{1.2}NiS_4C_4H_4$ and the well-known quasi-1-D conductor $K_2Pt(CN)_4Br_{0.3} \cdot 3H_2O$ (KPC). After subtracting out the N^- contribution in $TTT_{1.2}NiS_4C_4H_4$ the susceptibility of both is quite small or diamagnetic.[20] In each case the thermopower[21] is small and temperature independent above ~180°K, and decreases rapidly to negative values at low temperatures. The conductivity behavior is also very similar, except that KPC peaks at an accessible temperature.[22]

KPC has been found via x rays and neutron scattering[23,24] to have a Peierls distortion with a well-developed intrachain correlation at room temperature. Its interchain correlation commences at ~130°K and increases, but remains incomplete at T → 0°K. It is reasonable to suggest that the same behavior may be observable with x-ray or neutron scattering in our material, with an onset of interchain ordering at ~150°K. A broad bump in the specific heat should then be present around 150°K, also in analogy with KPC.[25]

In conclusion, we believe $TTT_{1.2}NiS_4C_4H_4$ to be a quasi-1-D, periodically distorted conductor with great similarity to KPC. This material offers an interesting opportunity to study the Peierls distortion in a commensurate crystal field. Further studies are in progress to clarify its structure in order to assess further its relationship to other 1-D conductors such as KPC.

References

1. McCleverty, J. A. 1968. Progr. Inorg. Chem. **10:** 49.
2. Torrance, J. B. & B. D. Silverman. 1977. Phys. Rev. **15:** 788.
3. Interrante, L. V., K. W. Browall, H. R. Hart, Jr., J. S. Jacobs, G. D. Watkins & S. H. Wee. 1975. J. Am. Chem. Soc. **97:** 889.
4. Kasper, J. S., L. V. Interrante & C. A. Secaur. 1975. J. Am. Chem. Soc. **97:** 890.
5. Interrante, L. V. 1976. Adv. Chem. **150:** 1.
6. Kasper, J. S. & L. V. Interrante. 1976. Acta Cryst. B **32:** 2914.
7. Jacobs, J. S., J. W. Bray, H. R. Hart, Jr., L. V. Interrante, J. S. Kasper, G. D. Watkins, D. E. Prober & J. C. Bonner. 1976. Phys. Rev. B **14:** 3036.
8. Jacobs, J. S., H. R. Hart, Jr., L. V. Interrante, J. W. Bray, J. S. Kasper, G. D. Watkins, D. E. Prober, W. P. Wolf & J. C. Bonner. 1977. Physica B **86:** 655.
9. Interrante, L. V., J. W. Bray, H. R. Hart, Jr., J. S. Kasper & P. A. Piacente. 1977. J. Am. Chem. Soc. **99:** 3523.
10. Geiger, Jr. W. E. 1973. J. Phys. Chem. **77:** 1862.
11. Perlstein, J. H., J. P. Ferraris, V. V. Walatka, D. O. Cowan & G. A. Candela. 1972. AIP Conf. Proc. **10:** Pt. 2. Magnetism and Mag. Materials; 1973. Amer. Inst. Phys.: 1494.
12. Buravov, L. J., O. N. Eremenko, R. B. Lyubovskii, L. P. Rozenberg, M. L. Khidekel, R. P. Shibaeva, I. F. Schchegolev & E. B. Yagubskii. 1974. JETP Lett. **20:** 208.
13. Delhaès, P. 1975. S. Flandrois, G. Keryer & P. Dupuis. 1975. Mats. Res. Bull. **10:** 825.
14. Perez-Albuerne, A. E., H. Johnson, Jr. & D. J. Trevoy. 1971. J. Chem. Phys. **55:** 1547.
15. Buravov, L. I., G. I. Zvereva, V. F. Kaminski, L. P. Rosenberg, M. L. Khidekel, R. P. Shibaeva, I. F. Shchegolev & E. B. Yagubskii. 1976. J.C.S. Chem. Comm.: 720.
16. Isett, L. C. & E. A. Perez-Albuerne. 1977. Sol. State Commun. **21:** 433.
17. Peierls, R. E. 1955. Quantum Theory of Solids: 108. Oxford Univ. Press. Oxford, England.
18. Wudl, F., D. E. Schafer, W. M. Walsh, Jr., L. M. Rupp, F. J. DiSalvo, J. V. Waszczak, M. L. Kaplan & G. A. Thomas. 1977. J. Chem. Phys. **66:** 377.
19. Somoano, R. B., A. Gupta, V. Hadek, M. Novotny, M. Jones, T. Datta, R. Deck & A. M. Hermann. 1977. Phys. Rev. B **15:** 595.
20. Kuindersma, P. I. & G. A. Sawatzky. 1973. Solid State Commun. **13:** 39.
21. Kuse, D. & H. R. Zeller. 1972. Solid State Commun. **11:** 355.
22. Zeller, H. R. 1973. Festkorperprobleme **13:** 31.
23. Comes, R., M. Lambert, H. Launois & H. R. Zeller. 1973. Phys. Rev. B **8:** 571.

24. LYNN, J. W., M. IIZUMI, G. SHIRANE, S. A. WERNER & R. B. SAILLANT. 1975. Phys. Rev. B 12: 1154.
25. FRANULOVIS, K. & D. DJUREK. 1975. Phys. Lett. 51A: 91.

DISCUSSION

ARTHUR J. EPSTEIN: For the bis(maleonitrile-dithiolate) compounds, what orbital does the unpaired electron reside in and does this orbital have considerable extension perpendicular to the molecular plane?

INTERRANTE: It is the b_{2g} π orbital, which is about a $\sim 50\%$ combination of a d_{xy} orbital and a ligand π orbital. It is clearly a π orbital and does have considerable spatial extent perpendicular to the plane.

EPSTEIN: The degree of mixing of the ligand π orbital with the metal d-orbitals is important, because it does not mix with the d_{z^2} orbital, though it does mix with the d_{xz} and d_{yz} orbitals which extend perpendicular to the molecular plane. A large in-plane component of this orbital implies a small extension perpendicular to the molecule which would decrease overlap and hence decrease transport along the stacks.

INTERRANTE: True. But the orbital has considerably more spacial extension perpendicular to the molecular plane than the b_{2g} orbital of TCNQ, which, of course, produces highly conductive 1-D stacks.

EPSTEIN: The conductivity at high temperatures for $(TTT)_{1.2}Ni(S_2C_2H_2)_2$ becomes less activated. That type of behavior is also quite consistent with a decrease in mobility of the materials and a constant energy gap. I would like to point out that $(NMe_3H)(I)(TCNQ)$, with a lattice periodicity commensurate with the Peierls periodicity, displays "metal-like" conductivity at temperatures above 240°K, yet is actually a semiconductor with an activated carrier concentration and a temperature-dependent mobility.

LAWRENCE ISETT: We have discovered $(NH_4)Ni(S_2C_2(CN)_2)_2 \cdot H_2O$, which exhibits a powder conductivity of about 1 ohm^{-1}cm^{-1} at room temperature and a static magnetic susceptibility consistent with a metallic state. Thus, it appears to be possible to transport charge along stacks of the $Ni(MNT)_2^{Z-}$ units.

ELECTRONIC AND STRUCTURAL PROPERTIES OF SOME BIPYRIDYLIUM^{2+} $(TCNQ)_4^{2-}$ AND RELATED COMPLEXES*

D.D. Eley, G.J. Ashwell, S.C. Wallwork,
M.R. Willis, and J. Woodward

Chemistry Department
Nottingham University
Nottingham, United Kingdom

The first paper[1] describing the simple $M^+(TCNQ)^-$ and complex $M^+(TCNQ)_2^-$ anion radical salts of tetracyanoquinodimethane, TCNQ, mentioned a compaction of the complex salt of the 2,2′-bipyridylium cation as having a room-temperature electrical conductivity of $\sigma_{RT} \sim 2$ S cm^{-1}. Later Rembaum *et al.*[2] described the preparation and properties of the simple and complex TCNQ salts of the mono- and di-N-methyl derivatives of 1,2-bis(4-pyridyl)ethylene and 1,2-bis(4-pyridyl)ethane. Compactions of the simple salts gave $\sigma_{RT} \sim 10^{-5}$ S cm^{-1} and the complex salts $\sigma_{RT} \sim 0.2$ S cm^{-1}, polymeric derivatives giving somewhat smaller values than the monomers. In several instances Hall and Seebeck measurements were made, which indicated positive holes as majority carriers with mobilities around 0.1 cm^{2}V^{-1}s^{-1}. Electron spin resonance showed the paramagnetism of the simple salts to conform to the singlet-triplet excitation model, whereas some of the more highly conducting complex salts showed the temperature-independent (Pauli) paramagnetism which characterizes metals. These findings on the di-cation salts agree with the earlier electric and magnetic studies on the monocation salts, described by Siemons *et al.*[3] and by Kepler *et al.*[4]

The bipyridylium di-cations offer many possibilities for chemical modification, and form the basis of our present programme, in which, wherever possible, attention is concentrated on obtaining single crystals, for x-ray structural, electric, and magnetic studies. It does appear, however, that some of the complex salts, especially the semimetallic ones, tend to give only microcrystalline products, in which case our electrical and magnetic work has been limited to compacted powders. The theoretical study of W. Little,[5] and the more recent discovery of the semimetallic properties of tetrathiofulvalene (TTF)-TCNQ,[6,7] has given a considerable stimulus to the program. Our objectives are to relate conductivity to structure, in this series, and the present paper reviews some of our progress toward this end.

Methods and Materials[8]

The complexes were prepared from commercially available pure chemicals by either[1] reacting an aqueous solution of the di-cation dibromide or dichloride with stoichiometric quantities of LiTCNQ and TCNQ, or reacting the di-iodide di-

*Manuscript received June 13, 1977.

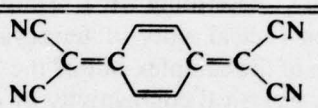
0077-8923/78/0313-0417 $1.75/1 © 1978, NYAS

rectly with neutral TCNQ. In both cases the solvent used for the reaction, and subsequent recrystallization, was warm acetonitrile. The crystals of the radical ion salt were washed with toluene and ether to remove unreacted TCNQ, the stoichiometry being established by chemical analysis. The $TCNQ^-/TCNQ$ ratio was determined by the absorbances at 395 and 842 nm.[1] The first complex in TABLE 1, $BP(TCNQ)_2$ was prepared not only by direct mixing of 4,4′-dipyridyl and TCNQ, but also by thermal degradation of the hydro, propyl and butyl diquaternary 4,4′-bipyridylium salts.[9]

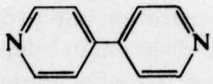
TABLE 1

COMPOUNDS AND NOMENCLATURE

TCNQ, Tetracyanoquinodimethane

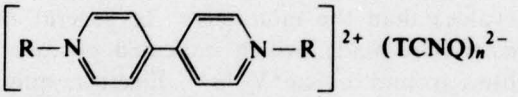


I, $BP(TCNQ)_2$, 4,4′Bipyridylium$(TCNQ)_2$



$(TCNQ)_2$

II$(DABP)^{2+}(TCNQ)_n^{2-}$ (N,N′-dialkyl-4,4′-Bipyridylium)$^{2+}(TCNQ)_n^{2-}$



$(TCNQ)_n^{2-}$

IIa $n = 4$, R = methyl, CH_3 $(DMBP)^{2+}(TCNQ)_4^{2-}$

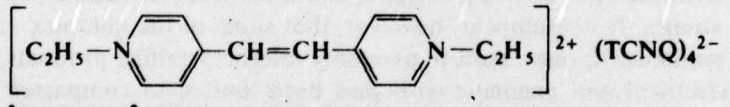
IIb $n = 4$, R = ethyl, C_2H_5 $(DEBP)^{2+}(TCNQ)_4^{2-}$*

IIe $n = 4$, R = propyl, C_3H_7 $(DPrBP)^{2+}(TCNQ)_4^{2-}$*

IId $n = 4$, R = *i*-propyl, *i*-C_3H_7 $(DiPrBP)^{2+}(TCNQ)_4^{2-}$

IIe $n = 4$, R = benzyl, $C_6H_5CH_2$ $(DBzBP)^{2+}(TCNQ)_4^{2-}$*

III $(DEPE)^{2+}(TCNQ)_4^{2-}$ (1,2-di(N-ethyl-4-pyridinium)ethylene)$^{2+}(TCNQ)_4^{2-}$



$(TCNQ)_4^{2-}$

$(DEPE)^{2+}(TCNQ)_4^{2-}$ I is the metallic form

$(DEPE)^{2+}(TCNQ)_4^{2-}$ II is the semiconducting form*

*Crystal structures determined on these complexes.

The space group and cell dimensions were obtained initially from oscillation and Weissenberg photographs by Cu Kα radiation. Subsequently the cell dimensions were refined on a Hilger and Watts computer-controlled, four-circle diffractometer. Intensities were collected from crystals about 0.5 × 0.2 × 0.1 mm with a $\theta/2\theta$ scan, a scintillation counter, and Mo Kα radiation. In each case about 3000 reflections were measured, and intensities were corrected for Lorentz and polarization factors, but not adsorption. The structures were solved from three-dimensional Patterson syntheses and refined by block diagonal least squares. X-ray powder photographs were taken on polycrystalline specimens.

The electrical measurements presently reported comprise two-electrode dc conductivity measurements on compressed discs, and along the *a*, *b*, and *c* axes of single crystals where available, and thermoelectric power (Seebeck) measurements on compressed discs. The compressed discs were formed by compressing microcrystals in a previously evacuated die to 75 MPa for six minutes. The single crystals were attached via Acheson Electrodag 915 high-conductivity paint electrodes to copper leads. Crystals and compactions were evacuated at 350°K and 10^{-6} Torr for 16 hours in the conductivity or Seebeck cell, and the cell was then filled with 10 Torr He gas for heat transfer, before starting measurements. In the case of the organic metal $(DEPE)^{2+}(TCNQ)_4^{2-}$-I, conductivity measurements were made down to 2°K, and the specimens were then transferred to the Science Research Council's Rutherford Laboratory, Harwell, Berkshire, U.K., for measurements in the range of 4°K to 30m°K.

Optical band gaps in some instances were calculated from infrared absorption spectra taken on a KBr disc containing the complex.[10]

Electron spin resonance studies on polycrystalline powders and single crystals were made with a Decca X3 spectrometer operating at 9.27 GHz with 100 kHz modulation, equipped with an Oxford Instrument's cryostat working over 300–4.2°K, with a temperature control $< \pm 0.2$°K. Single crystals were mounted on a well-annealed silica or a nylon rod, attached to a goniometer head. The polycrystalline specimens were pumped out to $<10^{-5}$ Torr and sealed under vacuum in silica tubes.

Results and Discussion

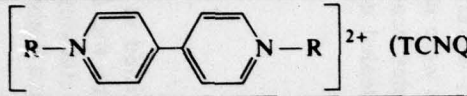
Compounds and Crystal Structures

The complexes and their shorthand nomenclature are listed in Table 1. In most cases the single crystals examined were platelets, with the *b* axis of the monoclinic or triclinic unit cell, which is parallel to the stacking axis of the TCNQ molecules, perpendicular to the platelet surface. Table 2 gives the crystal structure data.

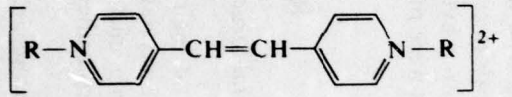
Figure 1 shows projections along the *a* and *c* axes of $(DEBP)^{2+}(TCNQ)_4^{2-}$, a typical example of one of our semiconducting complexes, of "intermediate conductivity" in the original nomenclature.[1,3] There is a segregated stack of TCNQ molecules, grouped in tetrads, along the *b* axis. However, although the molecular overlap between tetrads is much less than within tetrads, since no other molecule intervenes between two tetrads, we think, in terms of Dahm's nomenclature,[11] that the stack is more homosoric than nonsoric, and suggest that pseudohomosoric might be an appropriate designation. The TCNQ overlaps within the tetrad both approximate to the ideal, ring-external bond (R—EB) overlap[12] as shown in Figure 2 for the typical case of $(DEBP)^{2+}(TCNQ)_4^{2-}$, and in Table 2 are given the corresponding interplanar spacings for the TCNQ's, which are AA', 3.16 Å, and AB 3.22 Å. The symbol *X* for the third, or intertetrad, spacing denotes there is only a small area of overlap between the end TCNQ's B and B' of the two tetrads in this case, irrespective of the contact distances between them. The BB' interplanar spacings are not given in the table, since they can be calculated only when the end TCNQ's are parallel, which is not always the case. However, for

TABLE 2

CRYSTALLOGRAPHIC DATA



	R (cation)	Cell dimensions (Å; deg)	TCNQ ⊥'r spacings (Å)	Length of stacking axis: No. of TCNQ along axis	TCNQ grouping: *L* or *D*	Space group: complexes per cell
IIb	C_2H_5	*a* 13.077 α 90°		25.316		$P2_1/c$
	(DEBP)	*b* 25.316 β 92.66°	3.16(3.16),3.22(3.19),	8	tetrads	2
	M	*c* 7.838 γ 90°	*X*		*D*	
IIc	C_3H_7	*a* 13.334 α 90°		25.954		$P2_1/c$
	(DPrBP)	*b* 25.954 β 93.66°	3.20(3.21),3.23(3.22),	8	tetrads	2
	M	*c* 7.877 γ 90°	*X*		*D*	
IIe	$C_6H_5CH_2$	*a* 7.15 α 99.5°		16.82		$P\bar{1}$
	(DBzBP)	*b* 16.82 β 83.8°	3.24(3.17),3.16(3.20),	4	tetrads	1
	T	*c* 12.10 γ 91.8°	*X*		*L*	



III–II	C_2H_5	*a* 7.964 α 123.46°		15.549	pairs of dimers	$P\bar{1}$
	(DEPE)	*b* 15.549 β 125.55°	3.29(3.32),3.24(3.15),	4	*D*	1
	T	*c* 16.200 γ 76.00°	*X*			

**L* = Localized; *D* = Delocalized electrons on TCNQ's; *M* = Monoclinic; *T* = Triclinic. Spacings: The first figure is between whole TCNQ molecular planes, and the following figures in brackets is between quinonoid ring planes. *X* denotes no appreciable overlaps between tetrads.

$(DBzBP)^{2+}(TCNQ)_4^{2-}$ we can quote BB′ = 3.62 Å, and for $(DEPE)^{2+}$. $(TCNQ)_4^{2-}$-II, BB′ = 3.14 Å, since here the planes are parallel.

Referring to FIGURE 1 we see for the DEBP complex that the TCNQ's are arranged in the *bc* plane with the *a* direction across the cation sheets, and this is so for all the monoclinic crystals determined so far. For the triclinic crystals, however, the choice of axes has been such that the TCNQ's are arranged in the *ab* plane and *c* is the cell direction across the cation sheets.

There is a significant difference between the bond lengths in $TCNQ^0$ [13] and $TCNQ^-$,[8] and this enables us to define when and where charge localization occurs within the tetrad, denoted by *L* in TABLE 2 for $(DBzBP)^{2+}(TCNQ)_4^{2-}$, where

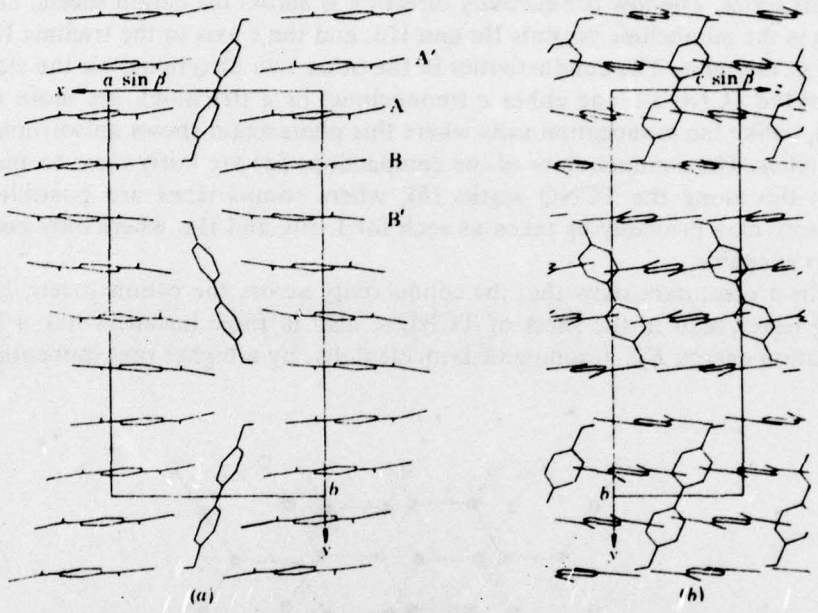


FIGURE 1. Crystal structure of $(DEBP)^{2+}(TCNQ)_4^{2-}$. (a): Projection along the *c* axis; (b): projection along the *a* axis.

the two charges are localized on the two innermost A,A′ TCNQ molecules of the tetrad. Where molecules BAA′B′ are shown with similar intermediate bond lengths, characteristic of $TCNQ^{1/2-}$, as in $(DEBP)^{2+}(TCNQ_4)^{2-}$ we have denoted the charge as delocalized, D.[8] However, crystallographic data cannot distinguish between true mobile delocalized charges and a random distribution of localized charges over all the TCNQ's in the stack in the crystal,[14] but the evidence can be used in support of other evidence, when present, for delocalization.

A difference in crystal structures between the $(DEPE)^{2+}(TCNQ)_4^{2-}$ semiconducting II and metallic I forms was established by powder diffraction diagrams, as shown in TABLE 3.

Electrical Properties

If we refer to Table 4, we note that in some cases it was impossible to grow suitable single crystals, so only data on compactions (p) are recorded. If we examine the single-crystal conductivities, determined from four complexes, we see that the room-temperature values show a certain degree of anisotropy, a factor of perhaps 20 separating the highest and lowest values. This anisotropy is smaller than the usual 100–1000 given by monocationic radical ion salts.[1,3] The reproducibility from crystal to crystal allows us to eliminate electrode-placing errors, and in any case, the technique used here has given an anisotropic factor of 200 for the complex,[15] $(DQMBn)^{2+}(TCNQ)_3^{2-}$ 1,4-di(N-quinolinium-methyl)·benzene$^{2+}(TCNQ)_3^{2-}$, so we may regard the factor 20 as correct in magnitude for this series. The low conductivity direction is across the cation sheets, i.e., the a axis in the monoclinic crystals IIc and IId, and the c axis in the triclinic IIf and III-II in the table. The conductivities in the other two directions, viz the stacking axis of the TCNQ's b and either c (monoclinic) or a (triclinic), are more nearly equal, unlike the monocation salts where this plane again shows anisotropic conductivities. The conductivities of the compactions (p) are fairly close to the conductivities along the TCNQ stacks (b), where comparisons are possible, and therefore may probably be taken as such for I, IIe, and IIa, where only compaction is available.

The present data show that the conductivity across the cation sheets, besides being lower than in the sheet of TCNQ's, also in three instances has a higher activation energy E_A, accompanied, incidentally, by a higher preexponential fac-

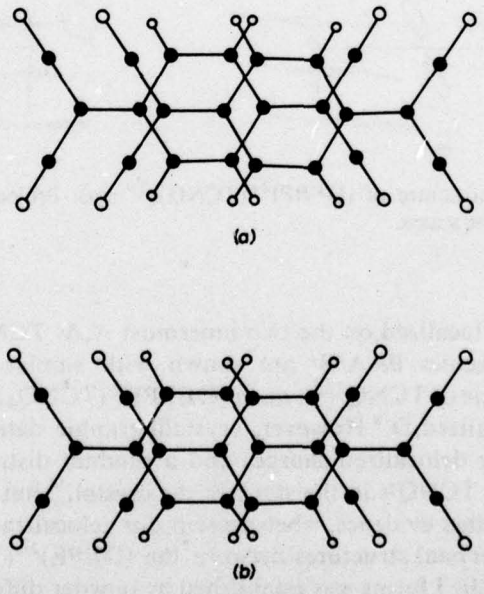


Figure 2. Types of TCNQ overlap in $(DEBP)^{2+}(TCNQ)_4^{2-}$. (a): Molecule A on B; (b) molecule A on A′ (cf. Figure 1). ● = carbon; ○ = hydrogen; ○ = nitrogen.

TABLE 3

POWDER DIFFRACTION DATA FOR THE TWO FORMS OF $(DEPE)^{2+}(TCNQ)_4^{2-}$*

Form I, Metallic		Form II, Semiconducting	
2θ	Intensity	2θ	Intensity
6.7	*m*	6.8	*mw*
7.2	*w*	7.8	*m*
8.2	*m*	11.4	*mw*
11.3	*m*	13.7	*s*
13.15	*w*	14.6	*s*
14.0	*vs*	15.95	*m*
14.55	*s*	18.2	*mw*
16.4	*w*	19.6	*ms*
17.7	*w*	20.85	*m*
19.1	*vw*	21.2	*w*
20.1	*m*	23.55	*mw*
21.0	*w*	24.4	*ms*
22.65	*w*	25.4	*ms*
23.45	*mw*	26.1	*w*
24.9	*ms*	26.55	*ms*
25.7	*w*	27.6	*vs*
27.0	*vs*	29.25	*w*
28.2	*m*	30.3	*vw*
29.2	*mw*	31.2	*mw*
30.0	*vw*	32.4	*m*
30.95	*w*	33.9	*mw*
32.9	*m*	34.9	*mw*
34.35	*mw*	36.8	*vw*
36.05	*mw*	37.7	*vw*
37.55	*m*	38.7	*m*

*λ = 1.5418 Å; estimated error in $2\theta = \pm 0.1°$; *vw* = very weak; *w* = weak; *m* = medium; *s* = strong; *vs* = very strong.

tor σ_0, in $\sigma = \sigma_0 \exp(-E_A/kT)$. However, in $(DEBP)^{2+}(TCNQ)_4^{2-}$, E_A is isotropic in all three directions, (cf. FIGURE 3) and another instance of this behavior is the $(DQMBn)^{2+}(TCNQ)_3^{2-}$.[15] This situation is complicated; Siemons *et al.*[3] have reported that three complexes, including the triethylammonium salt $TEA^+(TCNQ)_2^-$, with strongly anisotropic conductivities, still have isotropic activation energies, although Brau and Farges[16] and Farges[17] have reported that $TEA^+(TCNQ)_2^-$ has a higher activation energy, surprisingly enough, in the direction of highest conductivity. Shchegolev[18] has remarked that an isotropic activation energy is scarcely understandable, with an anisotropic conductivity, and attributes the result to a possible effect of inaccurate electrode placings, or dislocations. In the next section we shall argue for a probable (narrow) band conduction in the sheet of the TCNQ's. Reference to the typical example in FIGURE 1 (a) shows that TCNQ overlap across the sheets of cations is too small to give rise to band conduction, a much more likely mechanism being hopping or tunneling.[8] In this case, although clearly one can predict a lower conductivity, the relative magnitudes of E_A and σ_0 are more difficult to predict. These observations all refer to conduction in the intrinsic region, i.e., for $(DEBP)^{2+}(TCNQ)_4^{2-}$, above 215°K. Although the single crystal results of FIGURE 3 (a) are all above this

TABLE 4

ELECTRICAL DATA ON BIPYRIDYLIUM COMPLEXES [$\sigma = \sigma_0 \exp(-E_A/kT)$]*

No., Complex, Axis		σ(300°K) S cm^{-1}	E_A eV	σ_0 (300°K) S cm^{-1}	x ($\sigma_0 = \beta T^x$)	Q(RT) $\mu V K^{-1}$	μ_e, μ_h (300°K) cm^2 V^{-1} s^{-1}
I,	BP(TCNQ)$_2$, *p*	2.3 × 10^{-2}	0.042	0.15	3.1	−200	0.02 ($\propto T^{1.6}$) 0.01 ($\propto T^{1.5}$)
IIe,	(DiPrBP)$^{2+}$ (TCNQ)$_4^{2-}$, *p*	2.5 × 10^{-3}	0.15 (>300°K)	0.9	—	—	—
IIa,	(DMBP)$^{2+}$ (TCNQ)$_4^{2-}$, *p*	7.1 × 10^{-2}	0.21	246	−2.0	−150	53 ($\propto T^{-3.5}$) 38 ($\propto T^{-3.5}$)
IIc,	(DEBP)$^{2+}$ (TCNQ)$_4^{2-}$, *p*	2.2 × 10^{-3}	0.27 (>260°K)	72	~0	−440	10–25 ($\propto T^{-1.6}$) 4–8 ($\propto T^{-1.1}$)
	M *a*	1.2 × 10^{-4}	0.25	1.9			
	b	2.5 × 10^{-3}	0.28	129			
	c	3.2 × 10^{-3}	0.27 (I.R. 0.54)	110			
IId,	(DPrBP)$^{2+}$ (TCNQ)$_4^{2-}$, *p*	1.3 × 10^{-3}	0.22	6.4	~0		
	M *a*	3.0 × 10^{-4}	0.36	329			
	b	5.9 × 10^{-3}	0.22	289			
	c	1.2 × 10^{-3}	0.30	132			
IIf,	(DBzBP)$^{2+}$ (TCNQ)$_4^{2-}$ *a*	8 × 10^{-5}	0.20	0.18	—		
	b	2 × 10^{-4}	0.20	0.46			
	T *c*	2 × 10^{-5}	0.32 (I.R. 0.4)	5.4			
III–II	(DEPE)$^{2+}$ (TCNQ)$_4^{2-}$, *p*	1.4 × 10^{-3}	0.26	33.0	—	−150	—
	T *a*	1.0 × 10^{-3}	0.25	16.0			
	b	7.0 × 10^{-4}	0.26	16.5			
	c	3.0 × 10^{-4}	0.35	231			

*p denotes a compressed disc of microcrystals. a, b, and c-the crystallographic axes of a single crystal. The conductivity is $\sigma = \sigma_0 \exp(-E_A/kT)$. Q-the thermoelectric power, determined on a compressed disc, leading to mobilities of electron μ_e and hole μ_h. I.R. denotes the infrared absorption maximum. M & T denote monoclinic and triclinic.

temperature, the transition is apparent in conductivity results on a compaction in FIGURE 3 (b) and the thermoelectric power results of FIGURE 3 (c).

The arguments for applying band theory to semiconductivity in the sheet of the TCNQ's rests on our interpretation of the combined conductivity and Seebeck results for IIc, (DEBP)$^{2+}$(TCNQ)$_4^{2-}$ in terms of broad-band theory, resulting in mobility values, and mobility-temperature coefficients that fit in with this theory. The temperature dependence of the thermoelectric power (compaction) over 100–350°K is typical of a *p*-type semiconductor at low temperatures becoming intrinsic at 215°K. By combining the equations of band theory[19]

$$\sigma = e(\mu_e + \mu_h)2\left(\frac{2\pi m^* kT}{h^2}\right)^{3/2} \exp(-E_G/2kT) \qquad (1)$$

and
$$Q = -\frac{k}{e}\left(\frac{\mu_e - \mu_h}{\mu_e + \mu_h}\right)\left[\frac{E_G}{2kT} + 2\right] \quad (2)$$

and assuming the energy gap $E_G = 2E_A$, and the average effective mass of the two charge carriers is the free electron mass, we were able to deduce μ_e and μ_h, the mobilities for electron and hole shown in FIGURE 4. These mobilities, μ_e = 10–25 and μ_h = 4–8 $cm^2 V^{-1} s^{-1}$ yield mean free paths $L = 3\mu(2\pi m^* kT)^{1/2}/4e$, greater than the intertetrad spacing, and therefore satisfy the Ioffé criterion for band conduction.

Band-theory calculations provide two formulae of relevance (see, e.g.,

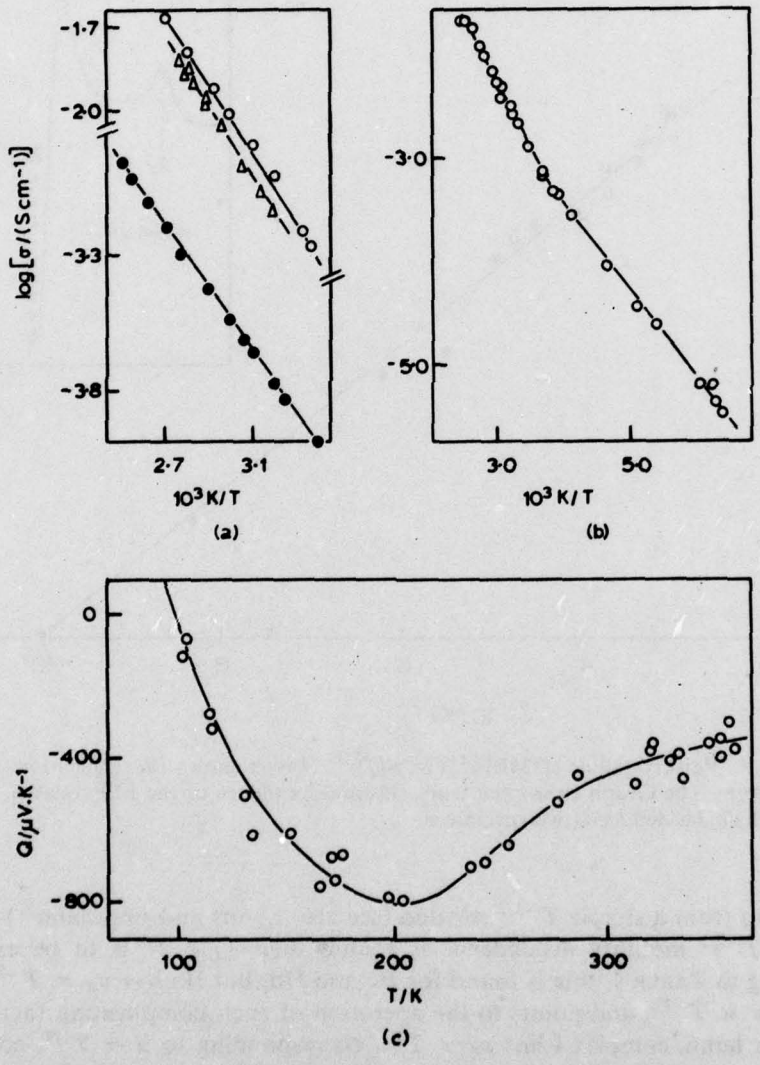


FIGURE 3. DEBP^{2+}$(TCNQ)_4^{2-}$. (a): Temperature dependence of single-crystal conductivity. ● = *a* axis; △ = *b*; ○ = *c*. (b): Polycrystalline compaction. (c): Thermoelectric power of a compaction.

Ziman[20]). Where the dominant scattering mechanism for charge carriers is lattice phonons, then $\mu \propto T^{-3/2} m^{*-5/2}$ and where it is ionized impurities, then $\mu \propto T^{3/2} m^{*1/2}$. So the results obtained here, $\mu_e \propto T^{-1.6}$ and $\mu_h \propto T^{-1.1}$, fit in well with the idea that the intrinsic conductivity in $(DEBP)^{2+}(TCNQ)_4^{2-}$ is controlled by excitation of electrons over a band gap E_G into a two-dimensional conduction band where the dominant scattering process is by acoustic phonons. This is perhaps surprising, since the band width concerned must be of order kT, and for such narrow bands m^* must depend on T, and there are other factors that may cause

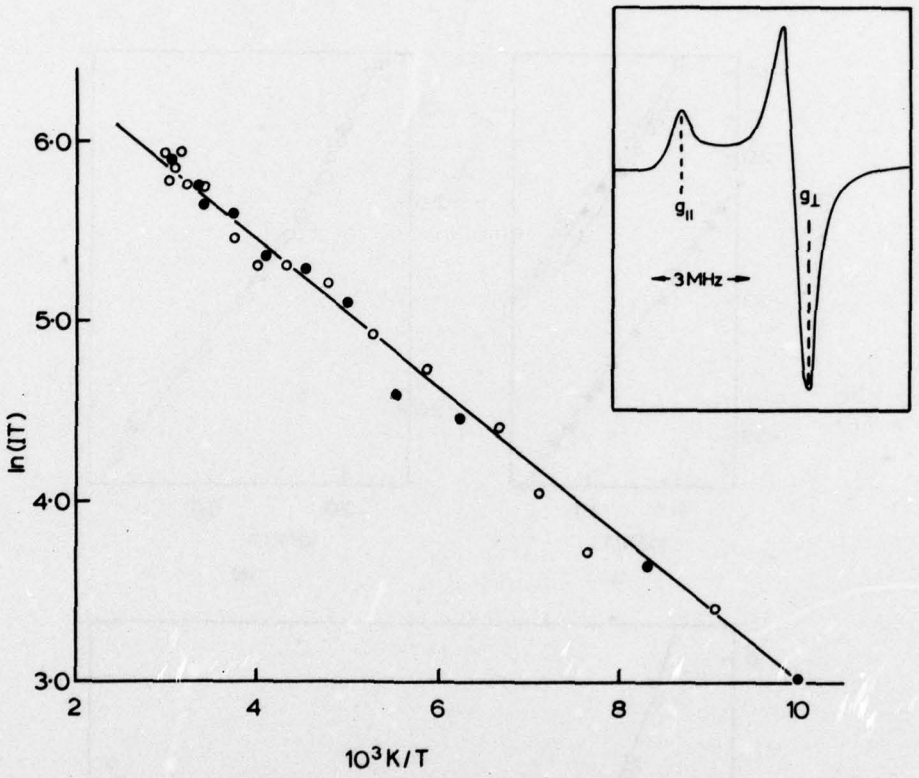


FIGURE 4. Polycrystalline $(DMBP)^{2+}(TCNQ)_4^{2-}$. Insert shows the ESR room-temperature spectrum. The Graph shows the temperature dependence of the ESR relative intensity I, from which J is deduced (two specimens).

deviations from a simple $T^{-3/2}$ relation (see also Lyons and Gutmann[21]). Where a strict $T^{-3/2}$ mobility dependence is found, then $\sigma_0 \propto T^0$ is to be expected. Referring to TABLE 4, this is found for IIc and IId, but IIa has $\sigma_0 \propto T^{-2}$, which implies $\mu \propto T^{-3.5}$, and points to the operation of such complicating factors. On the other hand, complex I has $\sigma_0 \propto T^{3.1}$, corresponding to $\mu \propto T^{3/2}$, consistent with ionized impurity scattering. It should be noted that although both results refer to compressed discs, the fact that the deviations in the two cases are in opposite directions suggests that we may neglect any intergranular scattering

effects, and the temperature exponents are characteristic of the crystal behavior, in agreement with our earlier remarks about the equivalence of compaction and *b*-axis single-crystal conductivities.

In two cases, IIc and IIf, we list the energy of the infrared absorption maximum for the complex, and this approximates closely to the energy gap $E_G = 2E_A$, supporting the idea of an intrinsic energy band conductivity.[10] Furthermore, the σ_0 values for IIa, IIc, IId, and III-II, interpreted in terms of band theory with the free-electron mass, yield mobility values ($\sigma_0 \sim 4\mu$ at room temperature) consistent with the presence of energy bands. This clearly does not apply to IIf, $DBzBP^{2+}(TCNQ)_4^{2-}$, where the correspondingly calculated μ values are <1 cm^2 V^{-1} s^{-1}. Here it seems possible that hopping or tunneling is the conduction mechanism. The same conclusion probably applies to I, $BP(TCNQ)_2$, where the σ_0 value is also low.

Electron Spin Resonance Measurements

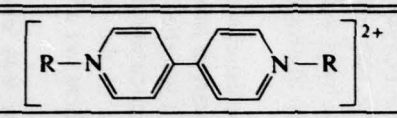
Our ESR studies of di-cation complexes are based on the earlier studies of monocation complexes by Chesnut and coworkers,[22-24] and Kepler.[4] A study of $DBzBP^{2+}(TCNQ)_4^{2-}$ has recently appeared[25] which is relevant to the present work. In our work the *x* direction is the long dimension of the TCNQ molecules, *y* the short direction, and *z* perpendicular to the plane of the TCNQ, these dimensions being related to the crystallographic *a*, *b*, *c* directions by a study of the dipolar splittings of the triplet signal as a function of the three angles for a single crystal.[23]

We refer to our results in Table 5. All samples showed the usual single $g \sim 2$ line, over 4–50°K, which obeyed the Curie-Weiss Law, disappearing around 50°K. By a careful comparison the intensity of this line with that of a weighed sample of DPPH of known purity, it was possible in the usual way to calculate the number of spins from the Curie Law constant, the result being given in the last column of the table. These spins are generally agreed to arise from chemical and physical defects, and will not be discussed further.

At temperatures >50°K a characteristic triplet spectrum was observed, increasing with temperature according to a law determined by the singlet-triplet excitation energy *J*. In the case of polycrystalline specimens, double integration of the derivative signal with an analog integrator[26] gave the relative intensity of the signal I, *J* being derived from a plot of $\ell n(IT)$ vs. T^{-1} (see below). The signals themselves (see Figure 4) were those characteristics of cylindrical symmetry, and were characterized by $g_\parallel$ and $g_\perp$, where $g_\perp$ refers to two equal *g* values at right angles.

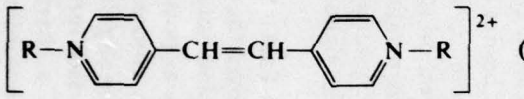
In the case of a single crystal, two lines were observed at 110°K (Figure 5), the midpoint *g* value being studied as a function of angle around the 3 crystal axes, giving principal values g_x, g_y, g_z. A study of the angular variation of the dipolar splitting gives the parameters *D* and *E*; in addition, the temperature variation of the dipolar splitting as the two lines collapse and the width of the resultant single broad line, give the activation energy ΔE_e for spin exchange, which is equal to $J + \Delta E_m$, where ΔE_m is the activation energy for triplet migration. This in outline comprises the measurements taken on the single crystals of Table 5.

TABLE 5
ESR RESULTS ON TCNQ COMPLEXES



$(TCNQ)_4^{2-}$

Cation (R)	Form	g_x, g_y, g_z, or $g_\perp, g_\parallel$			Magnetic State	J kJ mol^{-1}	W kJ mol^{-1}	D MHz	E MHz	ΔE_m kJ mol^{-1}	$\chi(RT)$ emu cm^3 mol^{-1}	Curie Law (<50°K) spin mol^{-1}
DMBP ($R = CH_3$)	*p*	2.0024	2.0035		D.E.	5.4	4.1	—	—		1.1×10^{-3}	5.9×10^{21}
DEBP ($R = C_2H_5$)	*s*	2.0037	2.0043	2.0032	L.E. (partial D.E.?)	7.2	—	±130	±14.2	1.2	0.9×10^{-3}	1.6×10^{22}
DBzBP ($R = C_6H_5CH_2$)	*s*	2.0048	2.0040	2.0033	L.E.	7.2	—	±202	∓36	5.9	0.47×10^{-3}	7.8×10^{21}



$(TCNQ)_4^{2-}$

DMPE ($R = CH_3$)	*p*	2.0024	2.0034		D.E.	5.1	3.3	—	—	—	1.2×10^{-3}	1.4×10^{22}
DEPE I	*p*				Pauli						2.1×10^{-3}	
II ($R = C_2H_5$)	*s*	2.0036	2.0041	2.0030	L.E.	2.8		±63 ±34	±30 ±16	1.5	1.6×10^{-3}	

*The specimens are measured as powder(*p*) or single crystal(*s*). The magnetic states are D.E., delocalized triplet excitons; L.E. localized excitons and Pauli paramagnetism. χ and Curie Law spins determined on polycrystalline specimens with the exception of $(DEPE)^{2+}(TCNQ)_4^{2-}$, where single crystals were used.

If we look in more detail at the polycrystalline $DMBP^{2+}(TCNQ)_4^{2-}$, we see that (FIGURE 4) $\ell n(IT)$ vs. T^{-1} is linear over a wide temperature range, including 300°K, where the $\ell n\sigma$ vs. T^{-1} graph was found to curve toward the T^{-1} axis. The magnetic linearity strongly supports the interpretation already given to the conductivity, that the nonlinearity arises from a temperature dependence of mobility, rather than reflecting the onset of a metal-semiconductor transition, the explanation chosen by Farges to explain a similar nonlinear $\ell n\sigma$ vs. T^{-1} plot in triethylamine$^+(TCNQ)_2^-$.

In interpreting this susceptibility χ-temperature relation we adopt the model of spins on a linear lattice, in which the spin $2j$ interacts with its neighbor $2j + 1$ with an exchange integral J, and with its other neighbor $2j - 1$ with an exchange integral γJ, the so-called Heisenberg antiferromagnet, γ being the alternation parameter. Bulaevski[28] (cf. Etemad[29]) has given an approximate solution to the Hamiltonian for this model, valid over $0.033 < T/J < 0.25$ and $\gamma < 0.5$. This gives for χ (proportional to I)

$$\chi T = \frac{Ng^2\mu_B^2 S(S+1)}{K} a(\gamma) \exp\left[-J\Delta(\gamma)/kT\right] \qquad (3)$$

The slope of FIGURE 4 thus gives $J\Delta(\gamma) = 3.7$ kJ mol^{-1}.

A Faraday balance value of $\chi = 1.1 \pm 0.3 \times 10^{-3}$ e.m.u. cm^3 mol^{-1} at 293°K gives us a calibration for I, and hence allows us to derive a value for the intercept in FIGURE 4 as the preexponential factor in (3) above. This yields $a(\gamma) = 0.5 \pm 0.1$, which (following Bulaevski) leads to $\gamma = 0.5 \pm 0.1$, hence $\Delta(\gamma) = 0.7 \pm 0.1$ and finally $J = 5.29$ kJ mol^{-1}, which suggests our analysis is only valid up to 150°K. An iterative procedure then yields best values $\gamma = 0.6 \pm 0.1$ $\Delta(\gamma) = 0.7 \pm 0.1$, $J = 5.4 \pm 0.9$ kJ mol^{-1}, and a bandwidth $W = 4.1 \pm 0.6$ kJ mol^{-1}, using the graphs in Etemad's[29] thesis. The value $\gamma = 0.6$ puts the equation outside its strict range of validity, but the linearity of FIGURE 4, also observed by other workers[30] in a magnetic balance study yielding similar values of the parameters, suggests the treatment holds to a good approximation, and we may safely conclude (since $\gamma > 0$) that the triplet excitons are delocalized in this complex. In support of this, we note that $g_\perp$ being close to the free spin value (2.00232) suggests delocalization in two-dimensions, here the two-dimensional array of TCNQ's. The form of the spectrum suggests that the zero-field parameters are negligible, also consistent with delocalization, since electron-electron separations will on average be larger than for localized excitons.

There is more than one crystal habit for $DBzBP^{2+}(TCNQ)_4^{2-}$. There are the small platelets, used in our x-ray work,[31] and by Shields for ESR studies.[25] The crystals used in the present work were more needle-like, but a full study (to be published[32]) shows the same structure for both habits, in each case somewhat similar to that illustrated earlier in this paper for $DEBP^{2+}(TCNQ)_4^{2-}$. Using three single crystals, the angular variation of the 100°K spectrum of FIGURE 5 established the g_x, g_y, g_z, D and E values in TABLE 5. A computerized curve-fitting procedure was used to fit the well-known equations for dipolar splitting d and g values[23] and derive the best values of these parameters, for each crystal, the result being the average over three crystals. The D and E values, according to an approximate treatment,[33] correspond to an average separation of the two electrons

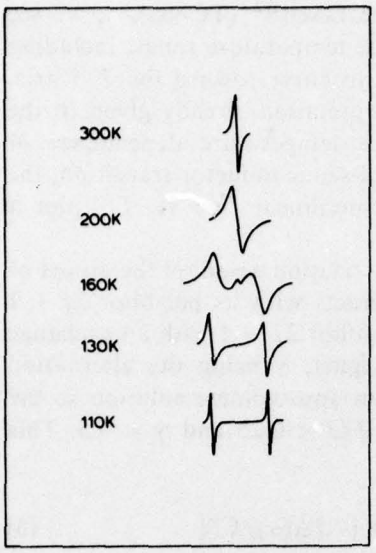


FIGURE 5. Single-crystal $(DBzBP)^{2+} \cdot (TCNQ)_4^{2-}$. Effect of temperature on the line-shape, line-width and peak separation for a given orientation.

making up the triplet exciton of 0.49 ± 0.08 nm. This may be compared with the TCNQ spacings within the tetrad of 0.316 nm and 0.324 nm, which gives 0.64 nm as corresponding to an average separation if the triplet exciton electrons were delocalized within the tetrad. In fact, the result is more in agreement with the x-ray indication[32] that the electrons are localized on the two central TCNQ's of the tetrad.

The well-known equation for the susceptibility due to localized triplet excitons is

$$\chi = \frac{2N\mu_B^2 g^2}{kT}(3 + \exp J/kT)^{-1}. \quad (4)$$

This equation also follows from (3), when the alternation factor $\gamma = 0$. A plot of $\ell n(IT)$ vs T^{-1} at low (<110°K) and high (>200°K) temperatures, outside the region where electron exchange is collapsing the dipolar splitting, gave a value of $J = 7.2$ kJ mol^{-1} independent of both temperature and orientation. Equation 4 gave, for room temperature, $\chi = 0.48 \times 10^{-3}$ e.m.u. cm^3 mol^{-1} and (3) with $\gamma \to 0$, gave 0.56×10^{-3} e.m.u. cm^3 mol^{-1}, and the agreement with the experimental value of $\chi = 0.47 \pm 0.15 \times 10^{-3}$ e.m.u. cm^3 mol^{-1} again supports the idea of localized excitons.

The frequency of spin exchange ν in the fast and slow regimes was derived from line-width measurements.[34]

$$\text{Slow regime } \nu = \sqrt{3}(\Delta H - \Delta H_0) \quad (5)$$

$$\text{Fast regime } \nu = \frac{d_0^2}{2\sqrt{3}}(\Delta H - \Delta H_0)^{-1} \quad (6)$$

where d_0 is the limiting dipolar splitting at low temperatures for the particular orientation under consideration, ΔH the linewidth and ΔH_0 the limiting high-

temperature line-width. A plot of log ν vs. T^{-1} in FIGURE 6 gives, for the fast regime, ΔE_e = 12.5 ± 1.2 kJ mol^{-1} ν_0 (THz) = 2.2 ± 1.4, and for the slow regime ΔE_e = 13.7 ± 0.7 kJ mol^{-1}, ν_0 (THz) = 2.5 ± 0.3, in the equation

$$\nu = \nu_0 \exp(-\Delta E_e/kT). \quad (7)$$

This allows us to calculate ΔE_m, the activation energy for spin exciton migration, as $\Delta E_e - J$ = 5.9 kJ mol^{-1}.

There are some differences in the behavior of $(DEBP)^{2+}(TCNQ)_4^{2-}$. At room temperature a single narrow resonance was observed for each crystal and its angular variation studied, from which g_x, g_y, and g_z were calculated. An orientation for maximum or minimum g was chosen and its line width and intensity studied as a function of temperature. The plot of $\ell n(IT)$ vs. T^{-1} showed a negative slope at "high" temperatures corresponding to a singlet-triplet equilibrium with J = 7.2 kJ mol^{-1} changing abruptly at c. 130°K to a positive slope taken to indicate a low-temperature Curie law species. Inserting the J value into (4) yields a susceptibility of 0.48 × 10^{-3} e.m.u. cm^3 mol^{-1} at 300°K, while into (3), taking the localized spin limit, yielded 0.56 × 10^{-3} e.m.u. cm^3 mol^{-1}, to be compared with the experimental value of 0.9 × 10^{-3} e.m.u. cm^3 mol^{-1} at 300°K. If we assume delocalized excitons in (3) we should obtain an even lower value, so they would seem on this basis to be excluded. However, the rather high experimental value for J could indicate that it is temperature dependent, in which case we cannot decide whether the excitons are localized or non-localized, from the room-temperature susceptibility. The Curie law signal yields a value of 1.6 ± 0.7 × 10^{22} spins mol^{-1}, but this is possibly an overestimate. On cooling to 70°K, a dipolar splitting was observed that remained constant as the temperature de-

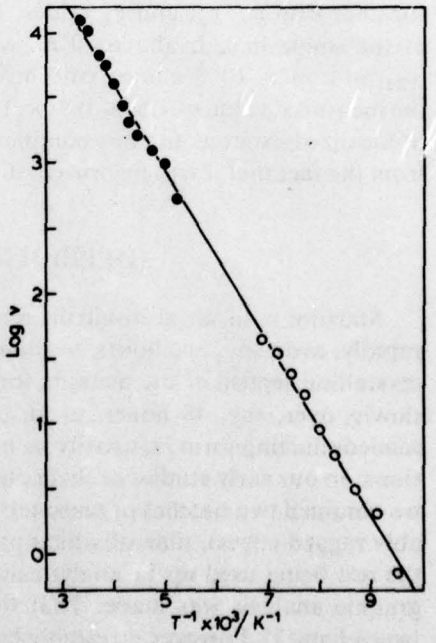


FIGURE 6. Single crystal $(DBzBP)^{2+}$. $(TCNQ)_4^{2-}$. Effect of temperature on the exchange rate ν of triplet excitons.

creased further. This splitting, however, could not be observed when the magnetic field was parallel to the z axis of each TCNQ molecule, possibly a masking effect of the Curie law signal. As a result, approximate values of D and E had to be estimated by equating the splitting when $H_0//x$ to $D - 3E$, and $H_0//y$ to $D + 3E$. The D and E values using the previous method[33] give an average electron-electron separation in the triplet exciton of 0.64 ± 0.06 nm, indicative of an even charge distribution over each tetrad of TCNQ's. A temperature dependence of line-width above 150°K (where the Curie law signal can be neglected) gave evidence of exciton exchange with ΔE_e = 8.4 ± 0.6 kJ mol^{-1}, giving ΔE_m = 1.2 ± 1.0 kJ mol^{-1}. There remains an unusual dependence of line width at 300°K observed for the case when $H_0 \perp z$, which is similar to one observed earlier[35] for 3,3′-diethyl-2,2′-oxocarbocyanine$^+$(TCNQ)$_2^-$, and there associated with collapse of fine structure in a two-dimensional conductor. This observation, together with the low ΔE_m value, leads us to classify (DEBP)$^{2+}$(TCNQ)$_4^{2-}$ as localized excitons, with a possible partial delocalization.

Coming to (DEPE)$^{2+}$(TCNQ)$_4^{2-}$-II, three crystals were studied, one for each orientation, and each exhibited a single resonance line at room temperature, which developed fine structure on cooling to 30°K, there being one central line, and two sets of outer lines due to dipolar splitting. On cooling below 30°K the outer lines all decreased in intensity, but there was no change in the splitting and the central line increased in intensity. It was concluded that the central line arose from a species obeying the Curie law, and the outer lines were dipolar splitting caused by the presence of triplet excitons. The outer lines began to saturate at a microwave attenuator setting of 10db, while maximum microwave power was required to saturate the central line. We were unable to measure the temperature dependence of these signals, but the angular variations of the two dipolar splittings were measured at 30°K, resulting in the two values of D and E in TABLE 5, together with g_x, g_y, and g_z values. The temperature dependence of the intensity of the single line, I, above 70°K, was used to calculate J = 2.8 kJ mol^{-1} and χ_{RT} = 1.66 × 10^{-3} e.m.u. cm^3 mol^{-1}, using (4), in excellent agreement with the measured value of 1.6 ± 0.9 × 10^{-3} e.m.u. cm^3 mol^{-1} supporting the concept of localized excitons for this complex. The rather large error in this value arises from the fact that it was measured on a single crystal, rather than a powder.

(DEPE)$^{2+}$(TCNQ)$_4^{2-}$-I AND II[36]

Starting with an acetonitrile solution of the complex at c. 60°C, if we cool rapidly, over, say, two hours, to room temperature we normally get a black microcrystalline deposit of the metallic form, I of (DEPE)$^{2+}$(TCNQ)$_4^{2-}$, but if we cool slowly, over, say, 48 hours, to an ambient temperature of 40°C, we obtain the semiconducting form II, usually as black plates, around 5 × 1 × 0.2 mm dimensions. In our early studies of this complex, for reasons we still do not understand, we obtained two batches of reasonably sized single crystals of form I (with noticeably ragged edges), nine of which provided the conductivity data described here, the rest being used up in analytical procedures, before a proper x-ray crystallographic analysis was made. That there are significant structural differences between I and II, however, is established by the powder-diffraction results of TABLE

3. We shall in this section compare the properties of I and II, in spite of some repetition of data regarding II.

We deal first with the electrical properties of I and II in that order, then with the magnetic properties (cf. Ref. 36).

Electrical Properties

In FIGURE 7 we show the resistivity/temperature relation for I and II, the conductivity for I being measured across the short direction of the platelets, which, at least in the semiconductor complexes of similar habit, correspond to the stacking axis of the TCNQ's. The comparative data are summarized in TABLE 6. It was checked that the electrode resistivity was insignificantly small, and that no short circuit occurred. At 300°K the nine single crystals of I gave conductivities in the range 150–2200 S cm^{-1}, compared with a value for the compressed pellet of microcrystals of I of 3 ± 2 S cm^{-1}. A sample of microcrystalline metal I also shows a very marked lowering of Q when placed in the ESR cavity. The single-crystal conductivity increases monotonically with decrease of temperature by a factor 3.7 at 35 mK, with no sign of any metal-semiconductor transition.[37] Above 340–50°K,

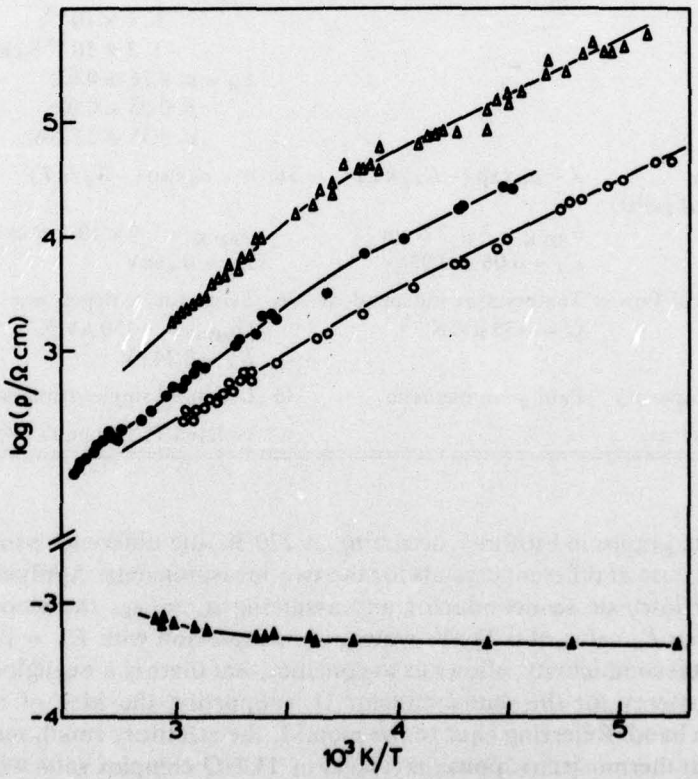


FIGURE 7. Temperature dependence of the conductivity of single crystals of $(DEPE)^{2+}\cdot(TCNQ)_4^{2-}$, I ▲, and $(DEPE)^2(TCNQ)_4^{2-}$ II △ = long, here c, axis; ○ = intermediate, a axis; ● = short, b axis.

the temperature variation of single crystals of I followed $\sigma/\sigma_{RT} = 23T^{-0.55}$, and below 50°K a weaker dependence still on T. This temperature exponent of −0.55 is considerably less marked than the exponents found for other organic metals, viz −2.33 for TTF-TCNQ[38,39] and −2.39 for HMTSF-TCNQ.[39] The compaction of microcrystals, by comparison, had a very small activation energy of 0.06 eV, no doubt arising from electron transport across intergranular boundaries.

In FIGURE 8 we compare the thermoelectric power of II (single-crystal, short axis = b), with a compaction of microcrystalline I. The curve for II is typically that for a semiconductor, being very similar to that for $(DEBP)^{2+}(TCNQ)_4^{2-}$ in FIGURE 3. The inset plot of Q vs T^{-1} for II shows a transition at 220°K, probably due to a change from extrinsic to intrinsic conduction, a similar transition in the

TABLE 6

A SUMMARY OF THE ELECTRICAL, MAGNETIC AND CRYSTALLOGRAPHIC DATA ON THE METALLIC (I) AND SEMICONDUCTING FORMS (II) OF $(DEPE)^{2+}(TCNQ)_4^{2-}$

	$(DEPE)^{2+}(TCNQ)_4^{2-}$–I	Ref.	$(DEPE)^{2+}(TCNQ)_4^{2-}$–II	Ref.
Conductivity (single crystal)	$\sigma/\sigma_{RT} = 23T^{-0.55}$ (50–340°K) $\sigma_{300\,K}$ = 150–2200 S cm^{-1}	37	$\sigma = \sigma_0 \exp(-E_A/kT)$ $\sigma_{300°K}$ = a, 7×10^{-4}; b, 1×10^{-3}; c, 3×10^{-4} S cm^{-1} E_A = a, 0.26 ± 0.02; b, 0.25 ± 0.02; c, 0.35 ± 0.02eV.	36
Conductivity (compacted pellet)	$\sigma = \sigma_0 \exp(-E_A/kT)$ $\sigma_{300°K} = 3 \pm 2$ S cm^{-1} $E_A = 0.06 \pm 0.02$eV	36	$\sigma = \sigma_0 \exp(-E_A/kT)$ $\sigma_{300°K} = 1.4 \times 10^{-3}$ S cm^{-1} E_A = 0.26eV	36
Thermoelectric Power	Temperature independent $Q = -35\,\mu$V K^{-1}	36	Temperature dependent $Q_{300°K} = -150\,\mu$V K^{-1} E_A = 0.24 eV	36
Magnetic Properties	Pauli paramagnetic	36	Localized singlet-triplet model	36
Crystal Structure	—		Isolated TCNQ pairs of dimers	47

conductivity graphs in FIGURE 7 occurring at 270°K, the difference probably arising from the use of different crystals for the two measurements. Applying (2) for a two-carrier intrinsic semiconductor and assuming $\mu_e \gg \mu_h$, the slope of Q vs T^{-1} yields an E_a value of 0.24 eV, which, on comparison with E_A = 0.26 eV for single-crystal conductivity, allows us to conclude that there is a negligible mobility activation energy for the semiconductor II, supporting the idea of a (narrow) conduction band. Referring back to the metal I, the relatively small, temperature-independent thermoelectric power is typical of TCNQ complex salts with metallic conductivity.[18] Chaikin and Beni[40] have treated such cases by considering correlated charge carriers in a narrow-band system, localized by a strong on-site electron-electron Coulomb repulsion, obtaining for the thermoelectric power Q,

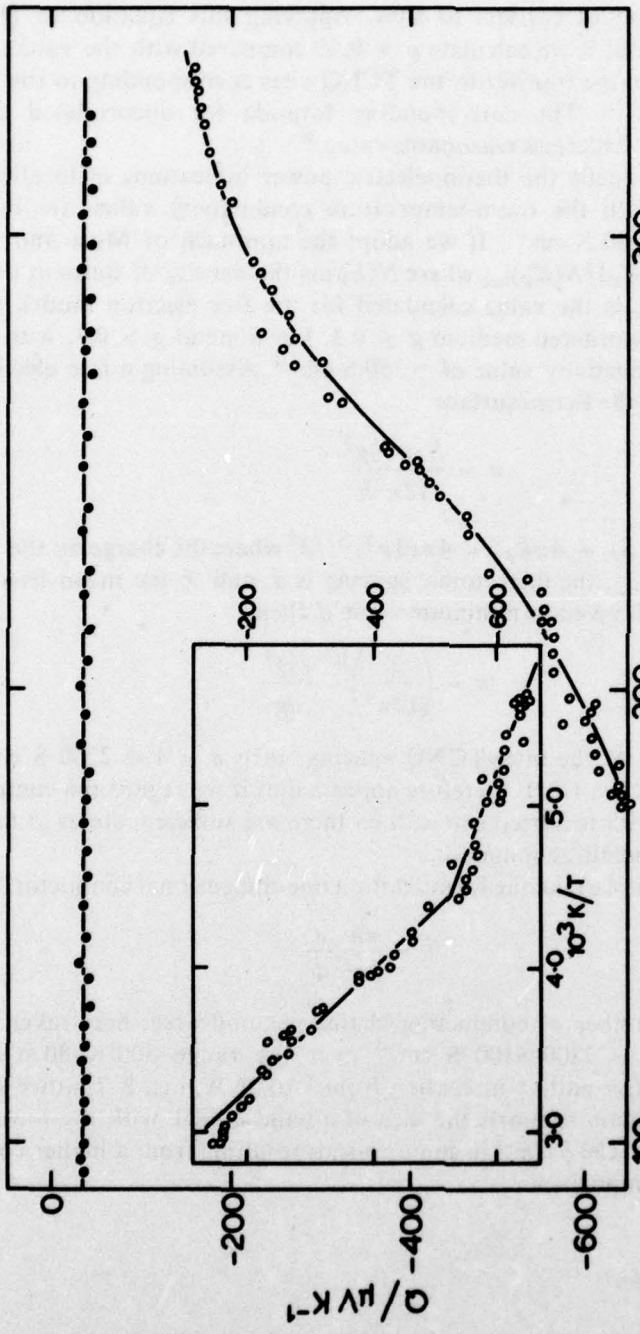


FIGURE 8. Temperature dependence of the thermoelectric power of $(DEPE)^{2+}(TCNQ)_4^{2-}$ I (●) and $(DEPE)^{2+}$. $(TCNQ)_4^{2-}$ II (○). Inset: variation of the thermoelectric power of II with reciprocal temperature.

$$Q = -\frac{k}{e} \ell n \left[\frac{2(1-\rho)}{\rho}\right] \tag{8}$$

where ρ is the ratio of carriers to sites. Applying this equation to $Q = -35$ $\mu V\ K^{-1}$ for the metal I, we calculate $\rho = 0.57$ compared with the value $\rho = 0.5$ for the complete charge transfer to the TCNQ sites corresponding to the formula $(DEPE)^{2+}(TCNQ)_4^{2-}$. The corresponding formula for uncorrelated electrons would require $\rho = 0.8$, a less reasonable value.[36]

We have to reconcile the thermoelectric power indications of localized (correlated) carriers with the room-temperature conductivity values (in the single crystals) of 150–2200 S cm^{-1}. If we adopt the approach of Mott and Davis,[41] and define $g = N(E_F)/N(E_F)_{free}$ where $N(E_F)$ is the density of states at the Fermi level, and $N(E_F)_{free}$ is the value calculated for the free electron model, then for localization in a disordered medium $g \leq 0.3$. For a metal $g > 0.3$, with a minimum metallic conductivity value of ~350 S cm^{-1}. Assuming a free electron gas, with S_F the area of the Fermi surface

$$\sigma = \frac{S_F e^2 \ell g^2}{12\pi^3 h}$$

and, substituting $S_F = 4\pi k_F^2 = 4\pi(3\pi^2)^{2/3}/d^2$ where the charge on the "atom," here the TCNQ, is $\frac{1}{2}$, the interatomic spacing is d, and ℓ the mean free path of the charge carrier is given its minimum value d, then

$$\sigma = \left(\frac{1}{12\pi^2}\right)^{1/3} \frac{e^2 g^2}{dh}$$

and, with $d = 3.3$ Å, the inter-TCNQ spacing, then $\sigma = 150$–2200 S cm^{-1} corresponds to $g = 0.3$ to 1.2. It therefore appears that if we regard the complex as a disordered solid with localized states, then there are sufficient states at the Fermi level to give semimetallic conduction.

Alternatively, if we take the formula for a one-dimensional conductor,[42]

$$\ell = \frac{\pi h}{2e^2} \frac{\sigma}{\Phi}$$

where Φ is the number of conducting chains per unit area, here taken as $\Phi = 0.02$ $Å^{-2}$, then $\sigma = 2200$–8100 S cm^{-1} over the range 300°K–30 m°K corresponds to a mean free path ℓ increasing from 7 to 26 Å; i.e., 2–7 lattice spacings, on cooling. This again supports the idea of a band model, with the lower values observed of $\sigma_{RT} \sim 150$ S cm^{-1} in some crystals resulting from a higher concentration of defects or impurities.

Magnetic Properties

We have already referred to the evidence for localized triplet excitons in $(DEPE)^{2+}(TCNQ)_4^{2-}$-II. In FIGURE 9 we show the paramagnetic susceptibilities of I and II determined from E.S.R. intensity measurements over 4–300°K. The two forms have very different behavior, that for I remaining largely constant with

temperature from 300 to 20°K, that for II starting from a similar value at 300°K, and falling to a value about $\frac{1}{20}$ that of the metallic form I at 70°K. Intensity measurements on II were discontinued below 70°K as the signal became very small and exhibited structure (Figure 3 in Reference 36 contains a printer's error in the ordinate, here corrected in FIGURE 9). The temperature-independent susceptibility for I is consistent with the Pauli paramagnetism expected for metals and found in other highly conducting TCNQ salts.[2,4,43] The departure from a temperature-independent susceptibility for I that occurs at lower temperatures is probably to be associated with defects, where both simple and activated Curie law behavior[44,45] is known to occur. A combination of these two effects is perhaps a more likely

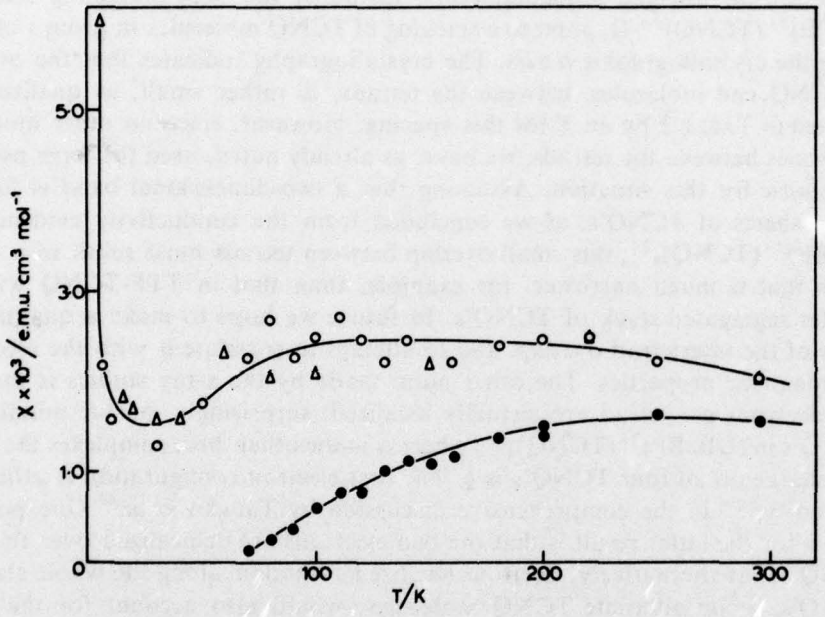


FIGURE 9. Temperature dependence of the paramagnetic susceptibility of $(DEPE)^{2+}\cdot(TCNQ)_4^{2-}$ I (○, △) and $(DEPE)^{2+}(TCNQ)_4^{2-}$ II (●).

explanation than that proposed for a similar phenomenon in quinolinium$^+$ $(TCNQ)_2^-$,[46] which equates the susceptibility to a sum of an impurity signal ($\chi \propto T^{-0.6}$) and a singlet-triplet contribution with a spread of J values. The latter explanation would require spin correlation, which is inappropriate for a complex showing metallic conductivity. Using

$$\chi_m = 64 \times 10^{-6} N(E),$$

substituting $\chi_m = 2.1 \pm 0.9 \times 10^{-3}$ e.m.u. cm^3 mol^{-1}, we obtain a density of states $N(E) = 32 \pm 14$ eV^{-1} molecule^{-1}, by taking $(DEPE)^{2+}(TCNQ)_4^{2-}$ as one molecular unit. This corresponds to 16 states per eV per $(TCNQ)_2^-$ unit, which is similar to values obtained[43] for quinolinium$^+(TCNQ)_2^-$ which range from 2.3 to 24 states per eV. We regard this value as an upper estimate, as χ_m is enhanced by electron-electron screening effects in metals, and by magnetism associated with the defects already mentioned.

Conclusions

A main difficulty in this field of bipyridylium radical ion salts is the crystallization process. Some complexes such as $BP(TCNQ)_2$, and $(DiPrBP)^{2+}(TCNQ)_4^{2-}$ have so far only yielded microcrystalline preparations, and in our most important case, the semimetal $(DEPE)^{2+}(TCNQ)_4^{2-}$-I, we ran out of our original two batches of single crystals before attempting a single-crystal x-ray analysis, and subsequently have been successful only in making microcrystalline preparations. Clearly we are left here with a problem that can be overcome only by further work, and in this connection earlier studies on metastable phases in N-methylquinolinium-TCNQ are relevant.[48] But the structures we have derived for these complexes, which are all low-gap semiconductors, including the semiconducting form of $(DEPE)^{2+}(TCNQ)^{2-}$-II, point to a stacking of TCNQ molecules in groups of four along the crystallographic *b* axis. The crystallography indicates that the overlap of TCNQ end molecules, between the tetrads, is rather small, as qualitatively denoted in Table 2 by an *X* for this spacing. However, since no other molecule intervenes between the tetrads, we have, as already noted, used the term pseudo-homosoric for this situation. Assuming that a two-dimensional band is formed in the sheets of TCNQ's, as we concluded from the conductivity evidence for $(DEBP)^{2+}(TCNQ)_4^{2-}$, this small overlap between tetrads must result in a bandwidth that is much narrower, for example, than that in TTF-TCNQ with its regular segregated stack of TCNQ's. In future we hope to make a quantitative study of the intertetrad overlap, and to attempt to correlate it with the electrical and magnetic properties. The other point made by the x-ray studies is that the two electrons per tetrad are virtually localized, surprisingly, on the middle two TCNQ's in $(DBzBP)^{2+}(TCNQ)_4^{2-}$, whereas in the other three complexes the effective charge on all four TCNQ's is $\frac{1}{2}$. The first electron configuration is called the "island type" in the comprehensive discussion by Tanaka *et al.*[49] One possible reason for the latter result is that the two electrons are delocalized over the four TCNQ's, but alternatively, electrons localized at random along the whole stack of TCNQ's, or on alternate TCNQ molecules, would also account for the x-ray results.

If we turn now to the magnetic data, the available evidence points to localized triplet excitons in $(DBzBP)^{2+}(TCNQ)_4^{2-}$ and $(DEPE)^{2+}(TCNQ)_4^{2-}$, localized excitons with a possible partial degree of delocalization in $(DEBP)^{2+}(TCNQ)_4^{2-}$, and delocalized excitons in $(DMBP)^{2+}(TCNQ)_4^{2-}$ and $(DMPE)^{2+}(TCNQ)_4^{2-}$, although studies on the latter two complexes were limited to polycrystalline specimens only.

It is interesting that the complex $(DBzBP)^{2+}(TCNQ)_4^{2-}$ where x-ray evidence points to localization of electrons at room temperature, and magnetic evidence points most definitely to localization in the triplet (excited) state, is also the complex with the lowest values for the single-crystal conductivity. The origin of these differences, however, is obscure. Why should two electrons be localized on average on adjacent TCNQ's in the centre of the tetrad, when Coulombic effects would rule otherwise? The main difference from the other complexes is the relatively high activation energy for exciton mobility over the stack of TCNQ's, and this may in some way be linked to the relatively large intertetrad distance of 3.62 Å, although the intertetrad overlap (still to be expressed quantitatively)

may in fact be even more unfavorable in the other complexes. The relatively low σ_0 values for $(DBzBP)^{2+}(TCNQ)_4^{2-}$ suggest a possible change over from two-dimensional narrow band conduction in the sheet of TCNQ's we suggested for $(DEBP)^{2+}(TCNQ)_4^{2-}$, to an intertetrad electron tunneling process.

Le Blanc[50] used the Mott-Hubbard model, which equates the energy gap $2E_A$ to $C - \Delta$, where C is the on-site Coulombic repulsion energy and Δ the bandwidth, to discuss the metal-semiconductor transition in radical ion-salts. Le Blanc emphasized that an excess electron in the "complex" salt where it corresponds to $TCNQ^-TCNQ^-$ neighbors has a much lower Coulombic energy than in the corresponding simple salt where it is $TCNQ^-$. He also emphasized the role played by polarizable aromatic cations in reducing C, to the extent that $C = \Delta$ and an organic metal results. In more recent terminology[51] for a linear conductor $2E_A = U - 4t$, with U the on-site repulsion energy and t the intermolecular transfer integral, which lowers the energy of the system and allows the electrons to delocalize into a one-dimensional band. In the case where there is lattice polarization[52] U is replaced by $U^* = U - 2E_B$, where E_B is the polaron-binding energy per electron, and t is reduced to $t^* = te^{-\gamma}$, where $\gamma \sim 1.0$, and the Mott-Hubbard gap is now $2E_A = U^* - 4t^*$. Le Blanc[50] had stressed the polarizability of the cation in determining E_B, and hence the energy gap $2E_A$. Bloch[6] has stressed the role of permanent moments on the cation. A typical E_B is 0.8 eV, and for the R-EB overlap for the TCNQ's $t \sim 0.11$ eV.[53] These considerations are such as to lead to zero gap and metallic behavior down the linear TCNQ stacks in TTF-TCNQ and NMP-TCNQ. Here we have made a case for a two-dimensional sheet of TCNQ molecules, grouped in tetrads along the b axis, where we presumably have several different transfer integrals to consider, with a reasonable certainty that between the tetrads $t \ll 0.11$ eV. On the other hand, the U^* value will refer to electrons on neighboring TCNQ molecules within the tetrad and will therefore be determined by the intratetrad spacings. However, if the semiconducting properties of these complexes relate to a *two-dimensional* sheet of TCNQ's, presumably the energy gap should be written as $2E_A \sim U^* - 8t^*$, where t^* is an average value for the sheet, which may well explain the result that the $2E_A$ values observed are still relatively small, ~0.4 eV, in spite of low t^* values. Then any slight rearrangement of crystal structure to equalize the TCNQ spacings to values around 3.2 Å might be expected to raise t^* to a value sufficient to reduce $2E_A$ to zero. We might suppose this to be the case for the metal $(DEPE)^{2+}(TCNQ)_4^{2-}$-I, where, additionally, disorder remains a factor to be assessed. All such speculations must await the proper x-ray analysis, which we shall carry out as soon as further suitable single crystals become available.

References

1. Melby, L. R., R. J. Harder, W. R. Hertler, W. Mahler, R. E. Benson & W. E. Mochel. 1962. J. Amer. Chem. Soc. **84**: 3374.
2. Rembaum, A., A. M. Hermann, F. E. Stewart & F. Gutmann. 1969. J. Phys. Chem. **73**: 513.
3. Siemons, W. J., P. E. Bierstedt & R. G. Kepler. 1963. J. Chem. Phys. **39**: 3523.
4. Kepler, R. G. 1963. J. Chem. Phys. **39**: 3528.
5. Little, W. 1964. Phys. Rev. **A134**: 1416.

6. BLOCH, A. N. 1973. Energy and Charge Transfer in Organic Semiconductors. K. Masuda and M. Silver, Eds.: 159, 167. Plenum Press. New York, N.Y.
7. GARITO, A. F. & A. J. HEEGER. 1974. Accounts of Chemical Research. **7:** 232.
8. ASHWELL, G. J., D. D. ELEY, S. C. WALLWORK & M. R. WILLIS. 1975. Proc. R. Soc. Lond. **A343:** 461.
9. ASHWELL, G. J., D. D. ELEY & M. R. WILLIS. 1975. J.C.S. Faraday Trans. **71:** 1227.
10. IIDA, Y. 1969. Bull. Chem. Soc. Japan. **42:** 637.
11. DAHM, R. J., P. HORN, G. R. JOHNSON, M. G. MILES & J. D. WILSON. 1975. J. Cryst. Mol. Struct. **5:** 27.
12. HERBSTEIN, F. H. 1971. Perspectives in Structural Chemistry. Vol. 4. J. D. Dunitz and J. A. Ibers, Eds.: 166. John Wiley & Sons, New York, N.Y.
13. LONG, R. E., R. A. SPARKS & K. N. TRUEBLOOD. 1965. Acta Cryst. **18:** 932.
14. HANSON, A. W. 1968. Acta Cryst. **B24:** 768.
15. ASHWELL, G. J., D. D. ELEY, S. C. WALLWORK, M. R. WILLIS, G. F. PEACHEY & D. B. WILKOS. 1977. Acta Cryst. **B33:** 843.
16. BRAU, A. & J. P. FARGES. 1972. Phys. Lett. **41A:** 179.
17. FARGES, J. P. 1973. Phys. Lett. **43A:** 161.
18. SHCHEGOLEV, I. F. 1972. Phys. Stat. Sol. (a) **12:** 9.
19. JOHNSON, V. A. & K. LARK-HOROVITZ. 1953. Phys. Rev. **93:** 226.
20. ZIMAN, J. 1964. Principles of the Theory of Solids.: 188, 194. Cambridge Univ. Press Cambridge, England.
21. LYONS, L. E. & F. GUTMANN. 1967. Organic Semiconductors. John Wiley & Sons. New York, N.Y.
22. CHESNUT, D. B., H. FOSTER & W. D. PHILLIPS. 1961. J. Chem. Phys. **34:** 684.
23. CHESNUT, D. B. & W. D. PHILLIPS. 1961. J. Chem. Phys. **35:** 1002.
24. CHESNUT, D. B. & P. ARTHUR. 1963. J. Chem. Phys. **39:** 3528.
25. SHIELDS, L. 1974. J.C.S. Faraday Trans. II. **70:** 1372.
26. RANDOLPH, M. L. 1960. Rev. Sci. Inst. **31:** 949. (Modified to suit the Decca ESR output).
27. FARGES, J. P., A. BRAU & F. GUTMANN. 1972. J. Phys. Chem. Solids **33:** 1723.
28. BULAEVSKI, L. N. 1969. Soviet Phys. (Solid State) **11:** 921.
29. ETEMAD, S. 1972. Ph.D. Thesis. Univ. Pennsylvania. Philadelphia, Pa.
30. SOMOANO, R., V. HADEK, S.P.S. YEN & A. REMBAUM. 1975. J. Chem. Phys. **62:** 1061.
31. SUNDARESAN, T. & S. C. WALLWORK. 1972. Acta Cryst. **B28:** 2474.
32. ASHWELL, G. J. *et al.* To be published.
33. HIBMA, T. 1974. Ph.D. Thesis. Univ. Groningen. Groningen, The Netherlands.
34. JONES, M. T. & D. B. CHESNUT. 1963. J. Chem. Phys. **38:** 1311.
35. TAKAGI, S. & K. KAWABE. 1976. Sol. Stat. Comm. **18:** 1476.
36. ASHWELL, G. J., D. D. ELEY, M. R. WILLIS & J. WOODWARD. 1977. Phys. Stat. Sol. **b79:** 629.
37. ASHWELL, G. J., D. D. ELEY & M. R. WILLIS. 1976. Nature **259:** 201.
38. GROFF, R. P., A. SUNA & R. E. MERRIFIELD. 1974. Phys. Rev. Lett. **33:** 318.
39. BLOCH, A. N., D. O. COWAN, K. BECHGAARD, R. E. PYLE & R. H. BANKS. 1975. Phys. Rev. Lett. **34:** 1561.
40. CHAIKIN, P. M. & G. BENI. 1976. Phys. Rev. **B13:** 647.
41. MOTT, N. F. & E. A. DAVIS. 1971. Electronic Processes in Noncrystalline Materials.: 36, 71. Oxford Univ. Press. Oxford, England.
42. THOMAS, G. A. *et al.* 1976. Phys. Rev. **B13:** 5015.
43. DELHAES, P., F. ALY & P. DUPUIS. 1973. Sol. Stat. Commun. **12:** 1099.
44. BAILEY, J. C. & D. B. CHESNUT. 1969. J. Chem. Phys. **51:** 5118.
45. MUNNOCH, P. J. & J. D. WRIGHT. 1975. VII Molecular Crystal Symposium. Nikko, Japan.
46. MILJAK, M., A. JANOSSY & G. GRÜNER. 1975. KFKI (Reports) 75.
47. ASHWELL, G. J., D. D. ELEY, R. J. FLEMING, S. C. WALLWORK & M. R. WILLIS. 1976. Acta Cryst. **B32:** 2948.
48. MURAKAMI, M. & S. YOSHIMURA. 1975. Bull Chem. Soc. Japan **48:** 157.
49. TANAKA, J., M. TANAKA, T. KAWAI, T. TAKABE & O. MAKI. 1976. Bull. Chem. Soc. Japan **49:** 2358.

50. LeBlanc, Jr., O. H. 1965. J. Chem. Phys. **42**: 4307.
51. Epstein, A. J., S. Etemad, A. F. Garito & A. J. Heeger. 1972. Phys. Rev. B. **5**: 952.
52. Chaikin, P. M., A. F. Garito & A. J. Heeger. 1973. J. Chem. Phys. **58**: 2336.
53. Berlinsky, A. J., J. F. Carolan & L. Weiler. 1974. Solid State Commun. **15**: 795.

Discussion

Lawrence Coleman (*Univ. California, Davis, Calif.*): The measurement technique that you described cannot really be called four-probe in the sense that you have only two contacts. If you evaluate the room-temperature conductivity that you quote and the size of the crystal, it seems that your contact resistance must have been incredibly small. Did you make any attempt to see if perhaps you had some filaments of silver paint, or other problems?

Eley: We made a special point of that. I think those measurements were okay.

Coleman: If you look at the crystal structure of the other phase done by the group at Jet Propulsion Lab., and Tulane [New Orleans, La.], and compare it to your powder data of the metallic phase, there seems to be a good match.

Eley: Those are probably identical, but maybe those single crystals we have are something different again. It may be disorder or a different phase.

Robert Somoano (*Jet Propulsion Laboratory, Pasadena, Calif.*): We also have obtained two crystalline phases of (DEPE)$(TCNQ)_4$. However, both of our phases were found to be semiconducting by electrical studies on single crystals in which the electrical resistivity was measured as a function of temperature along all three crystallographic directions by the four-probe and Montgomery techniques. We have also ground up crystals from both phases and compared our x-ray powder 2θ values with those reported by Eley *et al.* for their metallic and semiconducting phases. We find that our semiconducting phase I is identical to their reported metallic phase. Similarly, our second semiconducting phase is identical to Eley's semiconducting phase. Thus, we believe that the reported stable metallic state is either an experimental artifact resulting from the unusual electrode geometry used in the resistivity measurements or that the crystals used in the electrical measurements are not the same phase as the microcrystalline powder used in the x-ray studies by Eley *et al*:

PHENAZINE CATION RADICAL SALTS: CHARGE-TRANSFER COMPLEXES WITH TCNQ*

Z. G. Soos

Department of Chemistry
Princeton University
Princeton, New Jersey 08540

H. J. Keller, W. Moroni, and D. Nöthe

Anorganisch-Chemisches Institut der Universitat Heidelberg
D-6900 Heidelberg 1, West Germany

Partial Charge Transfer

The first systematic study[1] of the conductivities of tetracyanoquinodimethane (TCNQ) salts with closed-shell, diamagnetic M^+ cations identified the importance of single-crystal work and the generally higher conductivities of complex salts such as $M_2(TCNQ)_3$ or $M(TCNQ)_2$ in comparison to simple 1:1 salts like M(TCNQ). Chemical purity and crystal perfection have remained obvious and difficult goals in all subsequent studies of organic conductors or, indeed, of other organic molecular solids. The implication that complex stoichiometry helps in achieving high conductivity has been less widely recognized, at least until recently. This is due in part to the fact that it is not the stoichiometry itself, but rather the degree of ionity γ and the packing arrangement in the structure that are important. When M^+ is a diamagnetic inorganic ion, the complex salt $M_2(TCNQ)_3$ clearly has $\gamma = \frac{2}{3}$ on the $TCNQ^{-\gamma}$ stacks when all sites are crystallographically equivalent and has two ionic $TCNQ^-$ and one neutral TCNQ site when the sites are very different. On the other hand, the simple salt M(TCNQ) contains only $TCNQ^-$ ions and has $\gamma = 1$.

The semiconduction observed in simple salts with $\gamma = 1$ is associated with a correlation energy U for producing doubly occupied $TCNQ^{-2}$ sites.[2] Either empty TCNQ or doubly occupied $TCNQ^{-2}$ sites are carriers in an ionic lattice. Charge carriers can be formed without creating $TCNQ^{-2}$ sites for $\gamma < 1$, when there are fewer electrons than sites in the singly filled molecular orbital (MO) of $TCNQ^{-1}$. The major features of the magnetic, optical, and electric properties of molecular solids based on π-electron donors (D) and acceptors (A) can in fact be understood[2] by pursuing the implications of strong electron-electron correlations in these quasi-one-dimensional systems. Indeed, all highly conducting inorganic and organic systems in which there is no direct covalent bonding along the chain appear[3] to be based on fractional charges, or mixed valency in inorganic terminology, with a uniform value of γ at each site.

The importance of electron-electron correlations in narrow-band organic D and A crystals should not be surprising, since the triplet spin excitons found in

*Supported by the National Science Foundation for the work at Princeton, and for Heidelberg, by DFG and Fonds der Chemischen Industrie. Manuscript received July 5, 1977.

0077-8923/78/0313-0442 $1.75/1 © 1978, NYAS

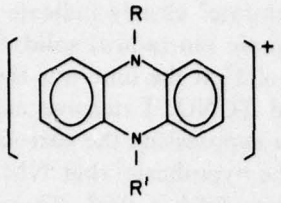
dimerized TCNQ salts[4] and in Wurster's blue perchlorate[5] clearly indicate that correlations dominate the magnetic properties of organic ion-radical solids.[6] On the other hand, the most highly conducting organic solid[7] at the time was the 1:1 system N-methylphenazinium (NMP^+ or MP^+) and TCNQ. Extensive experimental and theoretical arguments[8] were developed for suppressing the correlation energy U. NMR evidence[9] subsequently confirmed the hypothesis[2] that $NMP^{+\gamma}$-$TCNQ^{-\gamma}$ shows incomplete charge transfer, with $\gamma = 0.94 \pm 0.02$. There are fewer electrons than sites, and no doubly occupied $TCNQ^{-2}$ site is required for conduction. Incomplete charge transfer is also indicated by optical,[10] thermopower[11] and resonant Raman studies.[12] Strong electron-electron correlations are increasingly being postulated in models for organic conductors.[13]

Conductors like TTF-TCNQ which have partial charge transfer crystallize in segregated stacks of D and A sites. They resemble ion-radical salts in having the same open-shelled chemical specie forming the one-dimensional array. Solid charge-transfer (CT) complexes, by contrast, crystallize in mixed stacks based on face-to-face arrays of the type $\ldots D^{+\gamma}A^{-\gamma}D^{+\gamma}A^{-\gamma}\ldots$. Weak donors, with high ionization potential I_D, and weak acceptors, with low electron affinity A_A, form neutral ($\gamma = 0$) complexes. These diamagnetic insulators have a low-lying CT excitation polarized along the stack. Strong D and A molecules can be stabilized by the crystal electrostatic, or Madelung, energy M as paramagnetic ion-radical solids with $\gamma \sim 1$. In the limit of zero overlap (zero bandwidth) there is a sharp separation[14] into neutral complexes for $I_D - A_A > M$ and ionic complexes for $I_D - A_A < M$. Such a separation is consistent with a variety of experimental data on solid state complexes.[2,6]

The degree of charge transfer, or of ionicity, in mixed DA stacks depends sensitively on the bandwidth, since virtual excitations to the CT state stabilize either neutral or ionic complexes. We have recently found[15] that the substituted phenazines shown in FIGURE 1 form a series of cation radicals D^+ whose 1:1 complexes with TCNQ are close to the neutral-to-ionic separation. The 1:1 TCNQ complex with ethylmethylphenazine (MEP), with diethylphenazine (E_2P), and with diisopropylphenazine (Pr_2P) can also be prepared[16] and provides a series of increasingly bulky donors. As shown below, the solid-state complexes probably exhibit nonintegral charges and the dimethylphenazine (M_2P) complex may undergo a reversible transition from a primarily neutral to a primarily ionic form around 370°K.

Systematic studies of partial charge transfer have been restricted to segregated stacks such as found in the TTF-TCNQ family[17] or the TTF halides.[18] Truly large variations in γ are apparently possible in mixed-valence organometallic stacks,[19] and some of these segregated stack systems can now be crystallized. The phenazine-TCNQ family discussed here is a mixed stack system in which γ can be varied by suitably choosing the donor. M_2P-TCNQ may well be the first complex in which γ can be varied by changing temperature. Such mixed stacks lead predominantly to semiconductors, except possibly at the neutral-to-ionic separation. The demonstration of such transitions and their theoretical description should become clearer as more information is obtained on phenazine-TCNQ complexes.

We summarize below recent observations on the structure and physical properties of phenazine cation radical salts and of phenazine-TCNQ complexes. The



	Cation Radical
R = R′ = H	H_2P^+
R = H; R′ = CH_3	HMP^+
R = R′ = CH_3	M_2P^+
R = CH_3; R′ = CH_2CH_3	MEP^+
R = R′ = CH_2CH_3	E_2P^+
R = R′ = $CH(CH_3)_2$	Pr_2P^+

FIGURE 1. NN′-alkyl-substituted phenazine cation radicals.

geometry of the phenazine radicals and the packing arrangements show considerable variety, once again underlining the very limited extent to which structures can be predicted or "engineered" in advance. The neutral-ionic interface for mixed DA stacks is examined in DIMER APPROXIMATION FOR THE NEUTRAL-IONIC INTERFACE in terms of a dimer embedded in the lattice. The qualitative features of the M_2P-TCNQ complex can be treated, especially below the transition, as excitations of a largely neutral stack.

PHENAZINE CATION RADICALS

Elementary bonding considerations indicate that dialkyl phenazines (RR′P) in FIGURE 1 are bent along the N-N axis, whereas the 14 π-electron aromatic molecule P is planar and isoelectronic with anthracene. Ionization of RR′P leads to slightly bent 15 π-electron cation radicals. In addition, alkylhydrophenazines (HRP) can lose H to form 15 π-electron neutral radicals. The oldest and most extensively studied[20] is the R = CH_2CH_3 derivative, or EP, which crystallizes as a free radical solid. The paramagnetic species associated with phenazines are shown in FIGURE 2 for the HMP to MP^+ sequence. The versatility and biochemical importance of phenazines is related to their ability to act as one-electron oxidants and reductants and also as proton donors and acceptors.

Both the structure of the phenazine moiety and the stacking patterns in solids depend on the electron population, or the ionicity. The planar, diamagnetic 14 π-electron specie MP^+ forms[21] segregated stacks in $MP^{+\gamma}TCNQ^{-\gamma}$, with γ = 0.94 deduced from NMR.[9] Closed-shell molecular ions do not overlap appreciably, but show van der Waals contacts. The spacing (3.36 Å) along the $MP^{+\gamma}$ stack is in fact substantially greater than along the $TCNQ^{-\gamma}$ stack and approaches the van der Waals separation of about 3.5 Å. The more closely spaced (3.16 Å) TCNQs provide the open-shelled subsystem responsible for the quasi-one-dimensional physical properties.

The addition of an H to MP^+ leads to an open-shell cation radical HMP^+. Now a mixed stack with $TCNQ^-$ occurs naturally, as in many other organic DA systems.[2] The slight bending[22] (by 5.6°) of the HMP^+ about the N-N axis (FIGURE 1) and the mixed stacking suggested to us that the originally reported[23] "second

phase" of MP-TCNQ was in fact HMP-TCNQ, with the MP^+ inadvertently changed to HMP^+ by addition of H. Direct x-ray evidence[24] has now confirmed this hypothesis, as the electron density associated with the additional H can readily be found. The ability of MP^+ to abstract H has also been noted during electrolytic reductions when, instead of the anticipated MP radical, the epr spectrum associated with the hyperfine pattern of HMP^+ was found.[25] The structure of MP radicals is not known in detail, although their existence is established spectroscopically,[26] because solid MP has so far not been prepared. Solid EP is a stable, free radical solid, as has already been mentioned.

Although HMP^+ is bent along the N-N axis, Morosin[24] finds that in $HMPC10_4$ it is twisted to form a propeller, with an angle of 2.1° between the two benzene rings in FIGURE 1. The 15 π-electron HMP^+ ions again deviate slightly from planarity, but in $HMPC10_4$ crystallize as expected in segregated stacks. The occurrence of magnetically inequivalent HMP^+ stacks offers the usual test[2] for magnetic one-dimensionality. $HMPC10_4$ has sufficient interchain coupling to prevent separate electron spin resonance (*epr*) lines in applied fields of 330 G (X band). Bulkier substituents and/or higher applied fields may be needed to decouple the stacks, as in various $TCNQ^-$ systems.[2,6]

A final structural comment has to do with the N-ethylphenazine (EP)-TCNQ complex. This highly insulating material crystallizes[27] in a mixed stack, with $TCNQ^-$ ions in adjacent stacks forming localized, σ-bonded $(TCNQ)_2^{-2}$ dimers. These dimers are closely related to the first σ-bonded $(TCNQ)_2^{-2}$ dimers reported,[28] in the very different salt of *bis*(dipyridyl)platinum (II). The EP bond lengths and structure suggest[27] an ionic specie. The contrast with the conducting, segregated-stack $MP^{+\gamma}$-$TCNQ^{-\gamma}$ system is quite remarkable. The change from a

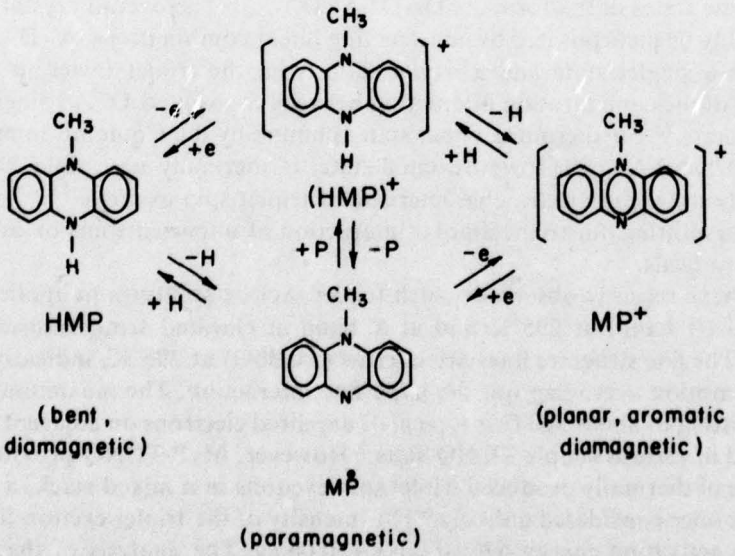


FIGURE 2. Diamagnetic and paramagnetic species in the series HMP, HMP^+, MP, and MP^+.

CH_3 to a CH_2CH_3 substituent on the phenazine completely alters the mode of crystallization and induces a rare σ-bonded dimerization of the $TCNQ^-$ ions. The addition of an H to MP^+ to form HMP^+ also changes segregated stacking in the TCNQ complex to mixed stacking, but that structural change can be rationalized as going from a closed-shell cation to an open-shell cation radical. The enormous structural variety found in the CT complexes of TCNQ and closely related phenazines strongly suggests that there are multiple minima in these systems and that the actual structure represents a very delicate balance between crystal forces.

We turn next to the physical properties[15] of mixed stack HMP-TCNQ and M_2P-TCNQ. Except for an N-H vibration around 3200 cm^{-1}, the infrared spectrum of HMP-TCNQ shows vibrational features that are superimposable on those of conducting MP-TCNQ. Thus both materials contain predominantly ionic species. Also, HMP-TCNQ has a single, exchange-narrowed *epr* absorption, which is a common feature of ionic $\ldots D^+A^-D^+A^- \ldots$ systems.[29] The best formulation for the charge distribution is thus $HMP^{+\gamma}TCNQ^{-\gamma}$, with $\frac{1}{2} < \gamma < 1$. *Complete* charge transfer ($\gamma = 1$) is probably not achieved, as can be argued from a more careful analysis of the magnetic susceptibility.

The M_2P molecule has a dihedral angle[30] of 165° in M_2P-TCNQ, indicative of a neutral specie. A weak *epr* signal at 300°K around the $TCNQ^-$ *g*-values can probably be associated with impurities, since it can be almost completely suppressed in good single crystals.[31] Heating produces a strong, reversible onset of paramagnetism around 370°K at a *g* value which is intermediate between the M_2P^+ and the $TCNQ^-$ resonances.[15] Grinding M_2P-TCNQ under an inert atmosphere also produces paramagnetism, although not reversibly. Above 390°K, the *epr* signal is typical of mixed ionic stacks, whereas the neutral diamagnetic phase around 300°K is best represented as $M_2P^{+\gamma}TCNQ^{-\gamma}$ with $0 < \gamma < \frac{1}{2}$.

The elementary CT excitations[14] of a neutral ($\gamma = 0$) $\ldots$ DADA $\ldots$ lattice are degenerate states of the form $\ldots DAD^+A^-DA \ldots$. The overall crystal symmetry can readily be incorporated by constructing linear combinations. A (D^+A^-) dimer contains a singlet state and a triplet state, with the triplet lower in energy on account of the configuration interaction between the excited D^+A^- singlet and the ground state.[2,6] Furthermore, either state is bound by the Coulomb interaction between D^+ and A^-. The lowest excited state, *if* thermally accessible, should consequently show *epr* spectra characteristic of triplet spin excitons,[4,5,6,29] with a fine structure splitting due to the dipolar interaction of unpaired spins on adjacent D^+ and A^- radicals.

We have recently observed[32] such triplet exciton splittings in applied fields of 12,000G (*Q* band) at 295°K and at *X* band at elevated temperatures of about 330°K. The fine structure lines are narrow (<0.50G) at 295°K, indicative of rapid exciton motion averaging out the hyperfine interaction. The maximum fine-structure splitting of about 300 G is typical of unpaired electrons on adjacent molecules, as found in various simple TCNQ salts.[2] However, M_2P-TCNQ provides the first example of thermally produced triplet spin excitons in a mixed stack, a possibility that was once considered unlikely.[6] The intensity of the triplet exciton lines can be fit to an activation energy ΔE_ρ of 0.60 ± 0.06 ev. The analysis of the fine structure lines, including their broadening with heating and their sudden collapse into a single line around 390°K, will be published elsewhere.[32] Here we simply note

that the collapse is qualitatively different than expected from exciton-exciton collisions.[4,5] These magnetic effects probably reflect a neutral-ionic transition.

Separating the charges in the D^+A^--excited states produces charge carriers. Both D^+ and A^- are stabilized by interactions with the partially charged lattice. The activation energy ΔE_c for semiconduction for five different single crystals of M_2P-TCNQ was 0.50 ± 0.03 ev below 350°K and increased to about 1.0 ± 0.1 ev in the high-temperature region.[33] Extrapolation of the low- and high-temperature data led to a remarkably constant transition temperature of T_c = 365 ± 2°K for all samples, which is somewhat lower than suggested by *epr*. The main points here are, first, that comparable energies $\Delta E_c \simeq \Delta E_p$ point to a largely neutral lattice and, second, that reproducible T_c suggests intrinsic, rather than impurity, conduction.

We are not aware of direct measurements of the CT excitation ΔE_{CT} in M_2P-TCNQ. This optical transition would further characterize the reversibly conversion from a predominantly neutral low-temperature form to a predominantly ionic high-temperature lattice. The borderline nature of neutral M_2P-TCNQ is also emphasized by the low energies for ΔE_c and ΔE_p. In more typical neutral DA complexes, optical excitation[33] is needed to produce the triplet state D^+A^- via intersystem crossing.

Triplet spin excitons have also been observed[32] at the Q band in the Pr_2P-TCNQ system, with smaller activation energy ΔE_p. It remains to be seen whether the many RR'P species in FIGURE 1 form 1:1 TCNQ complexes with similar structures. Although they all probably crystallize in mixed stacks, there may be significant differences in the packing. Furthermore, the structural variety exhibited by MP-TCNQ, EP-TCNQ, and HMP-TCNQ suggest that small changes at the phenazine can produce striking changes. The cation radicals MEP^+, E_2P^+, and Pr_2P^+ also form ClO_4^-, I^-, and other salts.[16] Segregated $RR'P^+$ stacks are expected when the counterions are closed-shell inorganic ions. The structure and probable one-dimensional magnetic properties of these phenazine cation radical salts have yet to be explored.

The simple H_2P-TCNQ complex has been conspicuously absent from our discussion of phenazine-TCNQ CT crystals. Although various H_2P^+ free radical salts are known,[15] the 1:1 TCNQ complex has yet to be prepared. The usual approach leads[16] to reduction of TCNQ to H_2TCNQ and oxidation of H_2P to P, instead of the desired CT complex.

Dimer Approximation for the Neutral-Ionic Interface

The preceding discussion of phenazine-TCNQ complexes indicates that they are close to the neutral-ionic separation, with HMP-TCNQ largely ionic and M_2P-TCNQ largely neutral at 300°K. The evaluation of partial charge transfer in mixed stacks is a many-electron problem for which even simplified models, such as the modified Hubbard model,[35,2] have not been solved exactly. We begin by considering a single DA dimer and then turn to an improved analysis of the electronic states of mixed stacks $\ldots D^{+\gamma}A^{-\gamma}D^{+\gamma}A^{-\gamma}\ldots$ for nonintegral γ.

The highest occupied molecular orbital (HOMO) of a donor and the lowest unoccupied molecular orbital (LUMO) of an acceptor have energies ϵ_D and ϵ_A,

respectively, in FIGURE 3. These energies can be taken as representative of free molecules or, formally, of molecules slightly perturbed by the solid.[36] Such a molecular exciton approximation has been central for elucidating the qualitative features of the magnetic, optical, and electric properties of ionic π-molecular solids.[2] Electron-electron correlations, including those with core electrons, are represented for simplicity by the same parameter U. As seen from FIGURE 3, the energy of a neutral DA dimer is $E(DA) = 2\epsilon_D + U$ and corresponds to a singlet state in which the two electrons are spin-paired in the normalized HOMO Φ_D

$$|DA> = \Phi_D(1)\Phi_D(2)2^{-1/2}\{\alpha(1)\beta(2) - \beta(1)\alpha(2)\} \quad (1)$$

The ionic state D^+A^- then has energy $E(D^+A^-) = \epsilon_D + \epsilon_A$ and can have either a singlet or a triplet total spin. The singlet state is

$$^1|D^+A^-> = 2^{-1}\{\Phi_D(1)\Phi_A(2) + \Phi_D(2)\Phi_A(1)\}\{\alpha(1)\beta(2) - \beta(1)\alpha(2)\} \quad (2)$$

where Φ_A is the normalized LUMO of A and the overlap between Φ_A and Φ_D has been neglected for simplicity. The corresponding triplet states $^3|D^+A^->$ have

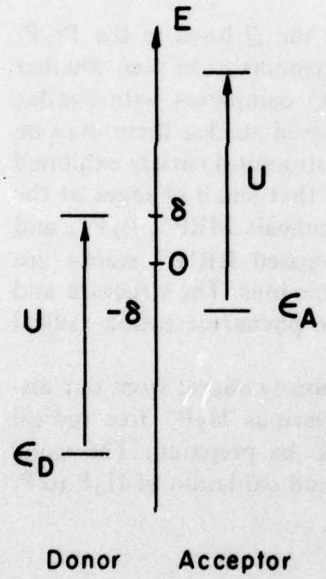


FIGURE 3. Schematic representation of the energy levels ϵ_D and ϵ_A for D and A sites, with a correlation energy U for doubly occupying either ϵ_D or ϵ_A.

space-antisymmetric and spin-symmetric wave functions. The high-energy, doubly ionized singlet state $|D^{+2}A^{-2}>$ has energy $2\epsilon_A + U$ and will be neglected. It should be emphasized that the energetics for these dimer states can be developed rigorously, without using the simple basis states in (1) and (2).

If there is overlap between D and A, then the Mulliken CT matrix element t must also be included,

$$t = <D^+A^-|\mathcal{H}|DA>. \quad (3)$$

Although t is small,[37] of the order of 0.1–0.3 ev, it mixes the singlet excited state $^1|D^+A^->$ and the ground state and thus makes a CT transition possible. The

stabilization of the ground state is relatively less important.[38] In zeroth order ($t = 0$), the CT excitation $\Delta E_{CT}^{(0)}$ is given by

$$\Delta E_{CT}^{(0)} = E(D^+A^-) - E(DA) - M_1 \approx I_D - A_A - \frac{e^2}{R}. \qquad (4)$$

The difference $E(D^+A^-) - E(DA)$ contains other terms than $I_D - A_A$, which nevertheless is the leading term and is of the order of 4 ev even for strong π-donors and π-acceptors. The Coulomb interaction M_1 in the ionic state must, of course, be evaluated for a delocalized π-electron distribution and is considerably smaller than the approximation e^2/R for point charges separated by R. Typical values[39] of M_1 are about 4 ev. The observed CT excitation[2] in many systems is in fact around 1 ev. More elaborate quantum mechanical descriptions can be developed for the DA dimer.

The infinite DA stacks and the long-range (three-dimensional) Coulomb interactions encountered in solid CT complexes cannot be treated so easily, as even the enumeration of states becomes prohibitive. McConnell, et al,[14] were the first to rationalize the observed separation of 1:1 complexes into essentially neutral ($\gamma \sim 0$) and ionic ($\gamma \sim 1$) solids. Their model begins with the assumption of zero differential overlap, and consequently $t = 0$ in (3). The energy needed to transfer an electron from $N/2$ donors to $N/2$ acceptors is $N(I_D - A_A)/2$, again neglecting other contributions to $E(D^+A^-) - E(DA)$. The resulting ionic lattice has a Madelung, or electrostatic, energy of $-MN/2$ and, for most lattices, M exceeds the nearest neighbor term M_1. In mixed DA stacks, Metzger[39] finds $M \sim 5$ ev. The overall energy balance leads to a neutral lattice for $I_D - A_A < M$ and an ionic lattice for $I_D - A_A > M$. Furthermore, since the Madelung contribution is quadratic in γ, the energy minimum always occurs[6,14] at either $\gamma = 0$ or $\gamma = 1$ in the limit $t \to 0$. Of course, a similar argument holds for the second ionization potential and electron affinity to form a doubly charged lattice. Also, the argument remains fundamentally unchanged if the $I_D - A_A$ and M terms are generalized to include any other differential energies that go as γ and γ^2, respectively.

The difference $|I_D - A_A - M|$ will usually be of the order of electron volts, whereas t is an order of magnitude smaller. Thus, corrections to the small t limit will rarely be important, especially for the more common neutral complexes. Strebel and Soos[35] have included finite t for mixed stacks, while retaining a Hartree approximation for the electrostatic interactions. Now finite values of the charge transfer γ in the ground state are possible, but a discontinuous change from small to large γ still occurs as U increases (FIGURE 3) sufficiently to make D^+A^- be energetically more favorable than DA. The nature of the optical gap at the crossover, which in FIGURE 3 corresponds to $\delta = 0$, has been further examined by Krivnov and Ovchinnikov,[40] still in a molecular field approximation. They find a finite gap, and thus semiconduction, even at $\delta = 0$. Since even simplified models involve severe mathematical approximation, the physical approximations of neglecting various polarization, Coulomb exchange, and relaxation contributions cannot be readily assessed.

As a first step in improving the phenomenological model[14] for the neutral-ionic interface, we consider a DA dimer embedded in a crystal. Self-consistency is imposed by forcing all dimers to be alike in the crystal ground state, which again amounts to a Hartree approximation for the long-range electrostatic con-

tributions. A number of advantages can immediately be noted: (1) the CT interaction and ΔE_{CT} within a simer can be treated exactly; (2) the Coulomb interaction M_1 is explicitly included; and (3) the ionic dimer is a dipole, with a reduced electrostatic interaction with the other dimers.

Again neglecting the doubly ionized state $D^{+2}A^{-2}$ we construct a normalized linear combination of (**1**) and (**2**) for the gound state of each dimer,

$$|\xi> = \cos\xi\,|DA> - \sin\xi\,{}^1|D^+A^->. \tag{5}$$

The parameter $0 < \xi < \pi/2$ describes the relative admixture of the two singlets. A neutral ground state corresponds to $\xi = 0$, an ionic ground state to $\xi = \pi/2$, and equal admixtures to $\xi = \pi/4$. The degree of charge transfer in the ground state is clearly given by $\gamma = \sin^2\xi$. The energy difference between $E(D^+A^-)$ and $E(DA)$ can be written as

$$2\epsilon = I_D - A_A - M_1 \tag{6}$$

and would simply by $\Delta E_{CT}^{(0)}$ in (**4**) for a neutral ($\gamma = 0$) lattice. The Madelung energy $2m$ of a dimer, which includes all Coulomb interactions except the intradimer term M_1, is simply

$$m = M - M_1 \tag{7}$$

and is generally a small positive number for mixed stacks. The additional stabilization of the ionic state in a crystal with $\gamma = \sin^2\xi$ is thus $-2m\sin^2\xi$. The occurrence of ξ in both the wavefunction $|\xi>$ and the energy leads to a self-consistent computation.

The CT matrix element t in (**3**) between the singlet states $|DA>$ and ${}^1|D^+A^->$ in (**1**) and (**2**), respectively, is $\sqrt{2}\,t$. Each dimer self-consistently embedded in the solid is consequently described by the 2×2 Hamiltonian matrix

$$\mathcal{H} = \begin{pmatrix} 0 & \sqrt{2}t \\ \sqrt{2}t & 2\epsilon - 2m\sin^2\xi \end{pmatrix}. \tag{8}$$

The ground state energy is

$$E_- = -\sqrt{2}t\tan\xi \tag{9}$$

where ξ is defined self-consistently by

$$\tan 2\xi = \frac{\sqrt{2}t}{\epsilon - m\sin^2\xi}. \tag{10}$$

A simple physical interpretation is shown in FIGURE 4. Taking $t > 0$ for simplicity, we see that ξ is small when $\epsilon - m\sin^2\xi$ is large and positive. This describes a neutral lattice, with $\gamma = \sin^2\xi \sim 0$. Conversely, we have $\xi \to \pi/2$ for $\epsilon - m\sin^2\xi$ large and negative, which corresponds for an ionic lattice. An equal admixture of neutral and ionic states occurs for $\xi = \pi/4$, the dashed line in FIGURE 4, where we have $2\epsilon = m$. Comparison with (**6**) and (**7**) shows that $2\epsilon = m$ is equivalent to $I_D - A_D = M$. The present dimer model reduces naturally to the previous $t = 0$ results, while generalizing them to include intradimer charge transfer exactly.

In order to solve (**10**) graphically, we rearrange to

$$\epsilon - m \sin^2 \xi = \sqrt{2}t \cot 2\xi \qquad (11)$$

and plot each side a function of ξ in FIGURE 5. Three different regimes occur. For $\epsilon > m$ (curve A) only a single solution with $\xi < \pi/2$ is found; in this case, (**6**) and (**7**) yield $I_D - A_A > M + m$ and even the lattice energy is insufficient to stabilize the ionic form. For $\epsilon < 0$ (curve B) the dimer is already ionic and only a single solution with $\xi > \pi/2$ is found; this corresponds from (**6**) to $I_D - A_A < M_1$. The most interesting solutions, such as curve *C*, occur in the region $-m < I_D - A_A - M < m$ where multiple roots are possible. According to (**9**), the most ionic (largest ξ) solution then has the lowest energy. For completeness, we note that $m < 0$, which corresponds to destabilizing collective interactions, lead to at most one solution which is always less ionic than the $m = 0$ result for an isolated

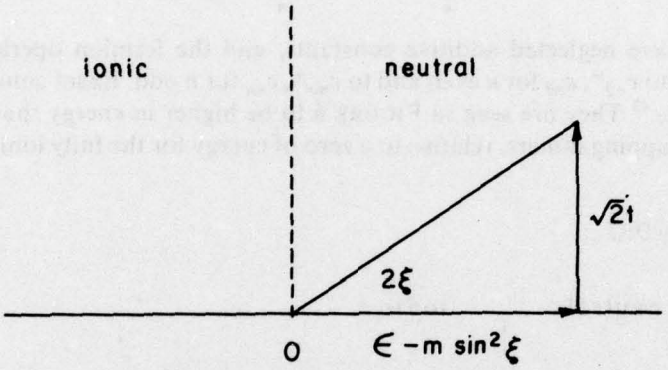


FIGURE 4. Definition of the angle ξ determining the degree of charge transfer on either side of the neutral-ionic interface at $\xi = \pi/4$.

dimer. Also, as t increases the possibility for multiple solutions decreases, since even curve *C* then has only one intersection with $\sqrt{2}t \cot 2\xi$.

Although the dimer model is very simple, it can readily be shown to be superior to more elaborate many-body treatments of mixed stacks. For example, the modified Hubbard model for a mixed stack can be rewritten in an electron-hole representation[41] as

$$\mathcal{H}_{eh} + UN/2 = N\delta - \delta \sum_{n\sigma} c_{n\sigma}^{+} c_{n\sigma} + \sum t(c_{n\sigma}^{+} c_{n+1\bar{\sigma}}^{+} + c_{n+1\bar{\sigma}} c_{n\sigma})$$

$$+ U \sum_{n} c_{n\alpha}^{+} c_{n\beta}^{+} c_{n\beta} c_{n\alpha}. \qquad (12)$$

The energy levels $\epsilon_D = -U + \delta$ and $\epsilon_A = -\delta$ are shown in FIGURE 3. The limit $U \to \infty$ then excludes D^{+2} or A^{-2} sites, and such sites are excluded in the dimer model as well. The fermi operators $c_{n\sigma}^{+}$, $c_{n\sigma}$ create and annihilate electrons on even n sites and holes on odd n sites. Overall electrical neutrality is guaranteed by solving (**12**) for equal numbers of electrons and holes,

$$\sum_{\substack{n\sigma \\ \text{even}}} c_{n\sigma}{}^{+} c_{n\sigma} = \sum_{\substack{n\sigma \\ \text{odd}}} c_{n\sigma}{}^{+} c_{n\sigma}. \tag{13}$$

The solution to (12) with no electrons or holes, which in general is *not* the ground state, is the neutral lattice ... DADA ... with $\gamma = 0$. Its energy $N(2\epsilon_D + U)/2 = -N(U - 2\delta)/2$ corresponds simply to the energy of $N/2$ D sites.

The $U \rightarrow \infty$ limit of (12) reduces to noninteracting dimers when every other t term along the chain is neglected. Alternatively, the $U \rightarrow \infty$ limit can be approximated by allowing only excitations with β spin on A sites and α spin on D sites (or vice versa) for the entire chain. We call this the Néel state because, for $\delta \gg t$, there is in fact an array like ... $A^{-}(\beta)D^{+}(\alpha)A^{-}(\beta)D^{+}(\alpha)$.... In this approximation, (12) reduces[41] to

$$\mathcal{H}_N = N\delta - \delta \sum_n f_n{}^{+} f_n + t \sum_n (f_n{}^{+} f_{n+1}{}^{+} + f_{n+1} f_n) \tag{14}$$

where we have neglected additive constants, and the fermion operators $f_n{}^{+}$, f_n correspond to $c_{n\beta}{}^{+}$, $c_{n\beta}$ for n even and to $c_{n\alpha}{}^{+}$, $c_{n\alpha}$ for n odd. Exact solutions to (14) are available.[42] They are seen in FIGURE 6 to be higher in energy than the energy of nonoverlapping dimers, relative to a zero of energy for the fully ionic state.

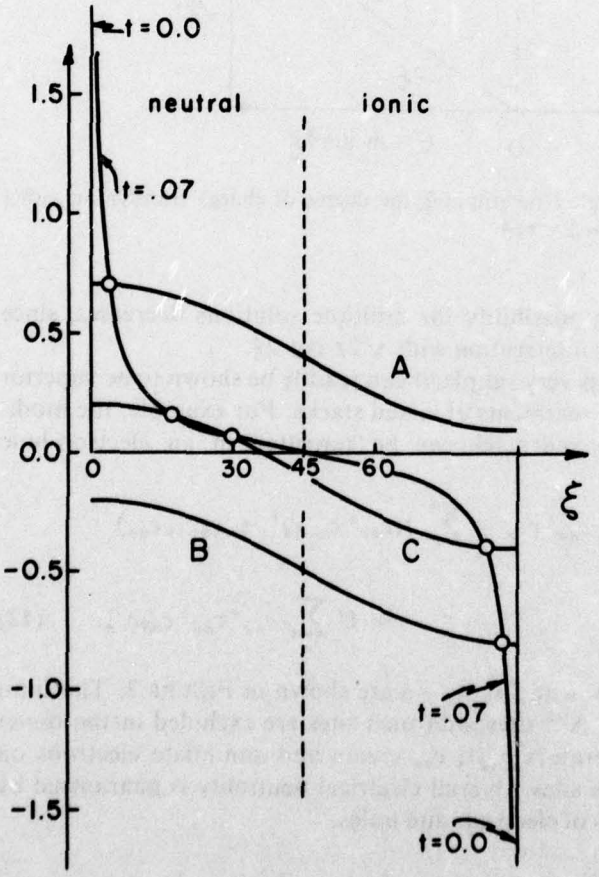


FIGURE 5. The indicated intersections are solutions to (12) determining the self-consistent value of ξ. The different cases A, B, and C are discussed in text.

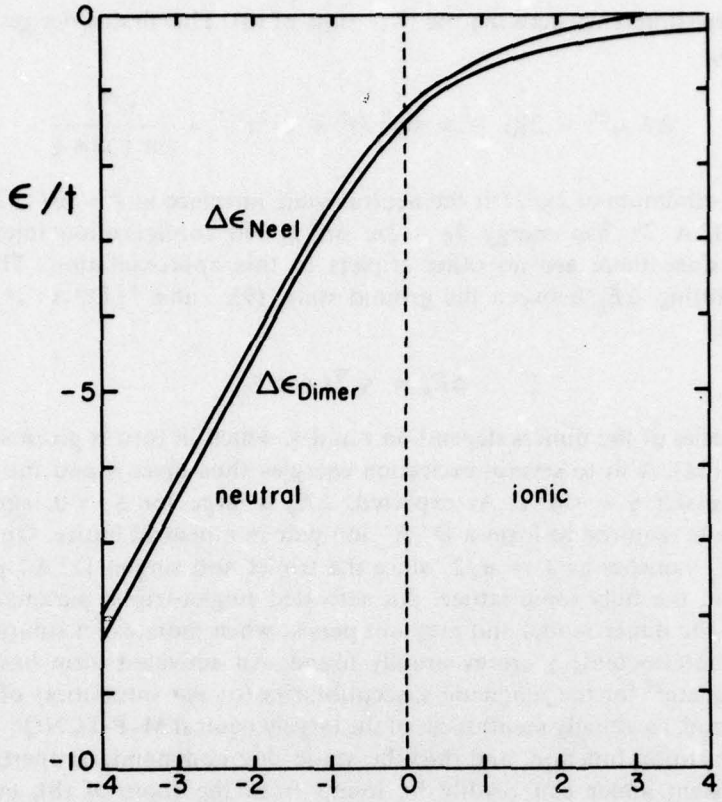


FIGURE 6. Comparison of the ground-state energies of the self-consistent dimer and the Néel approximations in the limit of strong correlations, with the zero of energy for the ionic lattice.

Self-consistent treatments of (12) for finite U reduce, in the limit $U \rightarrow \infty$, to (14) and are thus inferior to the simple dimer limit.[41] It appears than an exact treatment of the correlations U within a dimer is superior, at least for $U \gg t$ and $\gg 2\delta$, to including delocalization within the entire stack and treating correlations approximately. The explicit demonstration in FIGURE 6 of the lower energy of dimers is an example of the use of cluster expansions,[43] which are often preferable to band models when the bands are narrow (small t). The weakness of the dimer approximation is that it initially neglects CT between dimers, even though in a regular mixed stack the same t occurs both within and between dimers. Thus some care must be taken with applications. An exact solution to (12), even in the special case of $\delta = 0$ and $U = \infty$, would be quite valuable.

DISCUSSION

The simplicity of the self-consistent dimer approximation and its superiority over band models in the limit of small CT integrals t encourages further applications. Each dimer has a CT excitation connecting the two singlet states, whose

energy is the difference between the two roots of (**8**). This first-order result yields, using (**10**),

$$\Delta E_{CT}^{(0)} = 2\{(\epsilon - m \sin^2 \xi)^2 + 2t^2\}^{1/2} = \frac{\sqrt{2}t}{\sin \xi \cos \xi} \qquad (15)$$

and has a minimum of $2\sqrt{2t}$ at the neutral-ionic interface at $\xi = \pi/4$. The triplet state $^3|D^+A^->$ has energy $2\epsilon - 2m \sin^2 \xi$. No configuration interaction is possible, since there are no other triplets in this approximation. The singlet-triplet splitting ΔE_p between the ground state, (**9**), and $^3|D^+A^->$ is, again using (**10**),

$$\Delta E_p = \sqrt{2}t \cot \xi. \qquad (16)$$

All properties of the dimers depend on t and ξ, which in turn is given self-consistently by (**11**). A fit to several excitation energies thus gives ξ and the degree of charge transfer $\gamma = \sin^2 \xi$. As expected, ΔE_p is large for $\xi \to 0$, since an energy of 2ϵ is required to form a D^+A^- ion pair in a neutral lattice. On the other hand, ΔE_p vanishes as $\xi \to \pi/2$, since the triplet and singlet D^+A^- pair is degenerate in the fully ionic lattice. An activated singlet-triplet paramagnetism is built into the dimer model and may not persist when more exact solutions in the region of intermediate γ are eventually found. An activated form has generally been adequate[29] for the magnetic susceptibilities (or *epr* intensities) of ionic CT complex and, as already mentioned, of the largely neutral M_2P-TCNQ.

The partition function, and thus the static thermodynamic properties, of the self-consistent dimer can readily be found from the roots of (**8**), even if the $D^{+2}A^{-2}$ singlet is included. We are computing free energies $G(T)$ to test the extent to which spin entropy favors the paramagnetic ion state.[15] By contrast, the thermodynamics of molecular field solutions are often difficult to generate. We are fortunate that the dimer approximation is probably superior for the actual narrow-band DA stacks.

Extensions of the dimer limit can also be tested, especially if comparison with experiment is favorable. For example, we have neglected CT matrix elements connecting D and A sites in adjacent dimers. Such matrix elements further improve the dimer energy in FIGURE 6 by stabilization through virtual excitations and also provide a mechanism for transporting excitations along the stack. Another class of improvements is to treat explicitly the changes in electrostatic interactions of the ground and excited states by considering a single excited dimer in the lattice. We have naturally focused on ground-state properties in discussing the neutral-ionic interface, but could include excited dimers.

The major physical improvement of the dimer approximation is the explicit treatment of the important Coulomb interaction M_1 between adjacent D^+A^- pairs. Thus the energy for creating a D^+A^- pair in (**6**) is $2\epsilon = I_D - A_A - M_1$, which is approximately $\Delta E_{CT}^{(0)}$ in a neutral lattice, or neglecting solvent effects, in solution. Conversely, the excess stabilization of the ionic solid in (**7**) depends on $m = M - M_1$. Physically, this is the energy that can potentially interconvert a largely neutral molecular dimer into a largely ionic solid. The interplay between ϵ, m, and t then determines the various degrees of charge transfer γ

in the ground state, as has already been discussed in connection with FIGURE 5. It is worth emphasizing that once M_1 is included, both ϵ and m can be relatively small (order of 1 ev or less) and can easily be comparable to t. Thus in borderline cases like phenazine-TCNQ complexes, it is quite possible to have intermediate values of γ around $\frac{1}{2}$ in the solid as shown schematically in curve *C* of FIGURE 5.

The series of HMP-TCNQ, M_2P-TCNQ, MEP-TCNQ, E_2P-TCNQ, and Pr_2P-TCNQ may afford other tests of the model, expecially if they turn out to have similar structures. For example, increasing the size of the alkyl groups should decrease I_D. The puzzling fact that at 300°K HMP-TCNQ is ionic while M_2P-TCNQ is largely neutral may eventually be related to a larger M_1 for the more compact HMP. Similarly, the value of $m = M - M_1$ will depend on both the overall packing and the nearest-neighbor overlap, in a complicated but readily computable way from the crystal structure. Large donors like Pr_2P could well reduce m significantly, thus favoring a more neutral lattice. Although the overall energy balance of comparing $I_D - A_A$ and M for estimating the relative stabilities of the neutral and ionic forms has not been changed, the self-consistent dimer model offers additional intermediate cases and shows how changes in the CT interaction t may affect the ionicity γ.

The structures of HMP-TCNQ[22,24] and of M_2P-TCNQ[30] both have a small but unmistakable dimerization along the mixed stack, with closer contact within a DA pair than with either neighbor. The Wurster's blue cation, NNN'N'tetramethyl-p-phenylenediamine (TMPD), apparently forms mixed regular stacks in TMPD-TCNQ[44] and TMPD-chloranil,[45] although the former structure presents some puzzling features.[46] All CT matrix elements t in a mixed regular stack are equal, whereas dimerization allows for alternating t_1 and t_2 along the stack. Dimerization might be expected on the basis of various instabilities of one-dimensional arrays. The alternating stack lends itself naturally to a dimer approximation, since the larger t can be associated with the intradimer CT. Also, an activated paramagnetism is then expected, whereas the finite ΔE_ρ found in regular stacks like TMPD-TCNQ or TMPD-chloranil has been difficult to understand theoretically.[29,42] The occurrence of both regular and alternating mixed DA stacks has not been appreciated in previous work, and this structural possibility merits further attention.

In summary we have shown that the low-temperature properties of M_2P-TCNQ are qualitatively understood as excitations of a largely neutral stack and provide the first observation of thermally activated triplet spin excitons in mixed stacks. The self-consistent dimer model rationalizes the occurrence of intermediate charge transfer γ in molecular solids close to the neutral-ionic interface. The model allows explicit inclusion of the bandwidth $4t$ and nearest neighbor Coulomb interaction M_1, and it is sufficiently simple to yield thermodynamic properties. The physical properties of ionic mixed stacks like HMP-TCNQ or M_2P-TCNQ at high temperature are still poorly understood, but may become clearer for dimerized mixed stacks. A more quantitative analysis of the probable temperature dependence of $\gamma(T)$ in M_2P-TCNQ remains a major experimental and theoretical goal. The great flexibility of phenazine cation radicals has clearly been demonstrated. Both interesting new systems and systematic investigations can be anticipated.

ACKNOWLEDGMENTS

Z. G. Soos is grateful to the Anorganisch-Chemisches Institut, Heidelberg, for hospitality as a visiting professor in 1976 and to NSF for support of this work at Princeton. The work at Heidelberg was supported by DFG and Fonds der Chemischen Industrie.

REFERENCES

1. SIEMONS, W. J., P. E. BIERSTEDT & R. G. KEPLER. 1963. J. Chem. Phys. **39:** 3523.
2. SOOS, Z. G. 1974. Ann. Rev. Phys. Chem. **25:** 121; SOOS, Z. G. & D. J. KLEIN. 1975. Charge transfer in solid state complexes. *In* Molecular Association. R. Foster, Ed.: 1–119. Academic Press. New York, N.Y.
3. SOOS, Z. G. & H. J. KELLER. 1977. Comparison of columnar and inorganic solids. *In* Chemistry and Physics of One-Dimensional Metals. H. J. Keller, Ed.: 391–412. Plenum Press. New York, N.Y.
4. CHESNUT, D. B. & W. D. PHILLIPS. 1961. J. Chem. Phys. **35:** 1002.
5. THOMAS, D. D., H. J. KELLER & H. M. MCCONNELL. 1963. J. Chem. Phys. **39:** 2321.
6. NORDIO, P. L., Z. G. SOOS & H. M. MCCONNELL. 1966. Ann. Rev. Phys. Chem. **17:** 237.
7. MELBY, L. R. 1965. Can. J. Chem. **43:** 1448.
8. EPSTEIN, A. J., J. A. COHEN, A. F. GARITO & A. J. HEEGER. 1972. Phys. Rev. **B5:** 952; HEEGER, A. J. & A. F. GARITO. 1975. The electronic properties of TTF-TCNQ. *In* Low-Dimensional Cooperative Phenomena. H. J. Keller, Ed.: 89–123. Plenum Press. New York, N.Y.
9. BUTLER, M. A., F. WUDL & Z. G. SOOS. 1975. Phys. Rev. **B12:** 4708.
10. TORRANCE, J. B., B. A. SCOTT & F. KAUFMAN. 1975. Solid State Commun. **17:** 1369.
11. KWAK, J. F., G. BENI & P. M. CHAIKIN. 1976. Phys. Rev. **B13:** 641.
12. VAN DUYNE, R. P. 1977. Private communication.
13. TORRANCE, J. B. 1977. The role of Coulomb interactions in TTF-TCNQ. *In* Chemistry and Physics of One-Dimensional Metals. H. J. Keller, Ed.: 137–166. Plenum Press. New York, N.Y.
14. MCCONNELL, H. M., B. M. HOFFMAN & R. M. METZGER. 1965. Proc. Nat. Acad. Sci. USA **53:** 46.
15. SOOS, Z. G., H. J. KELLER, W. MORONI & D. NÖTHE. 1977. Cation radical salts of phenazine. J. Amer. Chem. Soc. **99:** 504.
16. MORONI, W. F. 1977. Kristallisierte, Planare Radikal- and Übergangsmetallkomplexe mit Anisotropen. Physikalischen Eigenschaften. Ph.D. Thesis. Heidelberg University. Heidelberg, Germany. Unpublished.
17. BLOCH, A. N., T. F. CARRUTHERS, T. O. POEHLER & D. O. COWAN. 1977. The organic metallic state: some physical aspects. *In* Chemistry and Physics of One-Dimensional Metals. H. J. Keller, Ed.: 47–85. Plenum Press. New York, N.Y.
18. SOMOANO, R. B., A. GUPTA, V. HADEK, T. DATTA, M. JONES, R. DECK & A. M. HERMANN. 1970. J. Chem. Phys. **63:** 4970; LA PLACA, S. J., P. W. R. CORFIELD, R. THOMAS & B. A. SCOTT. 1975. Solid State Commun. **17:** 635; WUDL, F., D. E. SCHAFER, W. M. WALSH, JR., L. W. RUPP, F. J. DISALVO, J. W. WASZCZAK, M. L. KAPLAN & G. A. THOMAS. 1977. J. Chem. Phys. **66:** 377.
19. MARKS, T. J., D. F. WEBSTER, S. L. RUBY & S. SCHULTZ. 1976. J. Chem. Soc. Chem. Commun. 444; HOFFMAN, B. M. 1977. Private Communication.
20. MCILWAIN, H. 1937. J. Chem. Soc. 1704; HAUSSER, K. H. & J. N. MURRELL. 1957. J. Chem. Phys. **27:** 500; SAKATA, T. & S. NAGAKURA. 1969. Bull. Chem. Soc. Japan 1497; SERAFIMOW, O., H. ZIMMERMANN, B. Bunsenges. 1972. Phys. Chem. **76:** 904.
21. FRITCHIE, C. J. 1965. Jr. Acta Cryst. **20:** 892; MOROSIN, B. 1975. Phys. Lett. **53A:** 455.
22. MOROSIN, B. 1976. Acta Cryst. **B32:** 1176.

23. COLEMAN, L. B., S. K. KHANNA, A. F. GARITO, A. J. HEEGER & B. MOROSIN. 1972. Phys. Lett. **42A:** 15.
24. MOROSIN, B. 1978. Acta Cryst. In press.
25. WUDL, F., J. H. MARSHALL & Z. G. SOOS. 1975. Unpublished work.
26. DOBLOWSKI, J. & W. RUBASZEWSKA. 1976. Rocz. Chem. **50:** 1435; RUBASZEWSKA, W. & Z. R. GRABOWSKI. 1975. J. Chem. Soc. Perkin Trans. **2:** 417.
27. MOROSIN, B., H. J. PLASTAS, L. B. COLEMAN & J. M. STEWART. 1978. Acta Cryst. In press.
28. DONG, V., H. ENDRES, H. J. KELLER, W. MORONI & D. NÖTHE. 1977. Acta Cryst. **833:** 2428.
29. SOOS, Z. G. 1975. Magnetic interactions in linear chain crystals. *In* Low-Dimensional Cooperative Phenomena. H. J. Keller, Ed.: 45–64. Plenum Press. New York, N.Y.
30. GOLDBERG, I. & U. SHMUELI. 1973. Acta Cryst. **B29:** 421.
31. NÖTHE, D. 1977. Unpublished work.
32. NÖTHE, D., W. MORONI, H. J. KELLER, S. MAZUMDAR & Z. G. SOOS. 1978. Solid State Commun. *In* press.
33. BELMONT, A. 1977. Conductivity of M_2P-TCNQ. Senior Thesis. Princeton Univ. Unpublished.
34. KEIJZERS, C. P. & D. HAARER. 1977. J. Chem. Phys. **67:** 925. IWATA, S., J. TANAKA & S. NAGAKURA. 1967. J. Chem. Phys. **47:** 2203.
35. STREBEL, P. J. & Z. G. SOOS. 1970. J. Chem. Phys. **53:** 4077.
36. KLEIN, D. J. & Z. G. SOOS. 1971. Mol. Phys. **20:** 1013.
37. MULLIKEN, R. S. & W. B. PEARSON. 1969. Molecular Complexes, A Lecture and Reprint Volume; 127. John Wiley & Sons. New York, N.Y.; BERLINSKY, A. J., J. F. CAROLAN & L. WEILER. 1974. Solid State Commun. **15:** 795.
38. HANNA, M. W. & J. L. LIPPERT. 1973. Theory of the ground state structure of molecular complexes. *In* Molecular Complexes. Vol. 1. R. Foster, Ed.: 1–48. Crane, Russak & Co. New York, N.Y.
39. METZGER, R. M. 1972. J. Chem. Phys. **57:** 1876.
40. KRIVNOV, V. Y. & A. A. OVCHINNIKOV. 1973. Soviet Physics-Solid State **15:** 118.
41. SOOS, Z. G. 1977. Eighth Molecular Crystal Symp.: 355–362. Santa Barbara, Calif.
42. KRUGLER, J. I., C. G. MONTGOMERY & H. M. MCCONNELL. 1964. J. Chem. Phys. **41:** 2421; KATSURA, S. 1962. Phys. Rev. **127:** 1508; LIEB, E. H., T. D. SSHULTZ & D. C. MATTIS. 1961. Ann. Phys. **16:** 407.
43. KLEIN, D. J. & M. A. GARCIA-BACH. 1976. Mol. Phys. **31:** 797. KLEIN, D. J. 1977. Preprint.
44. HANSON, A. W. 1967. Acta Cryst. **19:** 610.
45. DEBOER, J. L. & A. VOS. 1968. Acta. Cryst. **B24:** 1066.
46. HERBSTEIN, F. H. 1971. Crystalline π-molecular compounds. *In* Perspectives in Structural Chemistry. Vol. IV. J. D. Dunitz and J. A. Ibers, Eds.: 344–345. John Wiley & Sons. New York, N.Y.

DISCUSSION

JEROME H. PERLSTEIN (*Eastmas Kodak, Rochester, N.Y.*): You raised a very interesting question about whether (NMP)(TCNQ) is mixed valent. Is there back charge transfer to NMP^+? And if there is, does transport occur along the NMP stack as well as along the TCNQ stack? Have you tried to make NMP complexes in which the anion is not carrying any charge, as in NMP thiocyanate?

Soos: The NMP^+ spacing is larger than the TCNQ, and the type of transport one expects when there are fewer charges is less. But certainly, any two-stacked system always has this question, of trying to tie down for sure to what extent each

stack is involved in the transport. The NMP neutral radical is quite a difficult thing to work with. In solution it has been stabilized; however, I suspect that the quality of the crystals of solid NMP° would be poor.

AARON BLOCH (*Johns Hopkins Univ., Baltimore, Md.*): Is there any evidence for small amounts of hydrogen in (NMP)(TCNQ)?

SOOS: Small amounts of hydrogen—for example, six percent or so—is probably outside of what you could reliably get by elemental analysis. The fact that the hydrogen cation radicals form a different structure raises a possibility of alloys; however, the answer is not presently known.

ARTHUR J. EPSTEIN: There is direct evidence against transport along the NMP stacks. When we replace NMP^{+} with phenazine in the stack we are strongly disordering the NMP^{+} stack, and we do not see a sharp decrease in the conductivity which is expected if this were the major source of conduction path. Thus, the NMP^{+} chain is not the major path for charge transport.

ESTHER CONWELL (*Xerox Webster Research Center, Webster, N.Y.*): You make the statement that you found a 94% charge transfer in (NMP)(TCNQ). How many samples were measured, and what are the errors? Certainly there are large differences in the magnetic susceptibility at low temperature that can be attributed to differences in charge transfer.

SOOS: We have done the CH_3 and CD_3 measurements on probably a half-dozen samples and three samples, respectively. If there are significant changes in the degree of partial electron transfer from sample to sample, there are more serious difficulties with the reproducibility of the magnetic susceptibility than observed.

LAWRENCE COLEMAN (*Univ. California at Davis, Davis, Calif.*): In regard to the hydrogen in the (NMP)(TCNQ): when working on that material, we found that you could go from one phase to the other simply by heating the solution approximately five degrees warmer than for the conducting phase. It seems remarkable that such a small difference is enough to protonate.

SOOS: When we tried to prepare NMP electrolytically we found that we picked up a hydrogen essentially every time. This equilibria between NMP's and the hydro-forms are apparently very fast. There is an enormous biochemical literature that focuses on precisely this point, and these materials are important just because of their ability to be electron donors and acceptors, and also to transfer hydrogen. We do not understand this.

THE CHEMICAL AND PHYSICAL PROPERTIES OF THE REACTION PRODUCT BETWEEN TRIMETHYLAMMONIUM IODIDE AND TCNQ. A TERNARY 1-D SEMICONDUCTOR WITH "METAL-LIKE" CONDUCTIVITY*

M. A. Abkowitz,† J. W. Brill,‡ P. M. Chaikin,§ A. J. Epstein†
M. F. Froix,†** C. H. Griffiths,† W. Gunning,¶ A. J. Heeger,¶
W. A. Little,‡ J. S. Miller,†‡‡ M. Novatny,‡ D. B. Tanner,‖
and M. L. Slade†

†*Xerox Webster Research Center, Rochester, New York 14644.*
‡*Department of Physics, Stanford University, Stanford, California 94305*
§*Department of Physics, University of California, Los Angeles, California 90024*
¶*Department of Physics, University of Pennsylvania, Philadelphia, Pennsylvania 19174*
‖*Department of Physics, The Ohio State University, Columbus, Ohio 43210*

The study of linear-chain organic and inorganic anisotropic compounds has emphasized those systems with high "metal-like" conductivity.[1-3] Such systems typically have one donor and one acceptor. Recently, Cougrand *et al.*[4] reported that 7,7,8,8-tetracyano-*p*-quinodimethane, TCNQ, reacts with $NMe_3H^+I^-$ ($Me{=}CH_3$) to form a novel ternary component material of $(NMe_3H)(I)(TCNQ)$ stoichiometry with one cation and two different segregated acceptor chains, presumably only one of which, TCNQ, is conducting.

Herein we indicate the initial results of extensive physical studies undertaken on this system. These studies include elemental analysis, x-ray diffraction, thermal gravimetric analysis (TGA), differential scanning calomimetry (DSC), Raman scattering, polarized reflectance, anisotropic dc conductivity, microwave conductivity, dielectric constant, electron-spin resonance (ESR), proton magnetic resonance (^1H NMR), thermoelectric power (TEP), and Young's Modulus (E). These results show the large highly conducting metallic green-appearing crystals to be $(NMe_3H^+)(I_3^-)_{1/3}(TCNQ)^{2/3-}$, a thermally stable compound that undergoes a semiconductor-semiconductor transition at 150°K.

The elemental analysis of 13 samples (TABLE 1) shows[5] that all samples are equivalent and that 1.00:1.00:1.00 ratio exists for NMe_3H^+:TCNQ:I. This conclu-

*Manuscript received Nov. 14, 1977. Correspondence to A. J. Epstein or Joel S. Miller. JWB, WAL, and MN acknowledge support in part by NSF grant DMR76-82087-A01, NASA JPL grant 953752, and Stanford Center for Materials Research NSF grant DMR-72-03022.

**Present address: Celanese Research Corporation, Summit, New Jersey 07901.

‡‡Present address: Science Center, Rockwell International, 1049 Camino Dos Rios, Thousand Oaks, Calif. 91360.

0077-8923/78/0313-0459 $1.75/1 © 1978, NYAS

TABLE 1
ELEMENTAL ANALYSIS FOR TCNQ TRIMETHYLAMMONIUM IODIDE REACTION PRODUCT

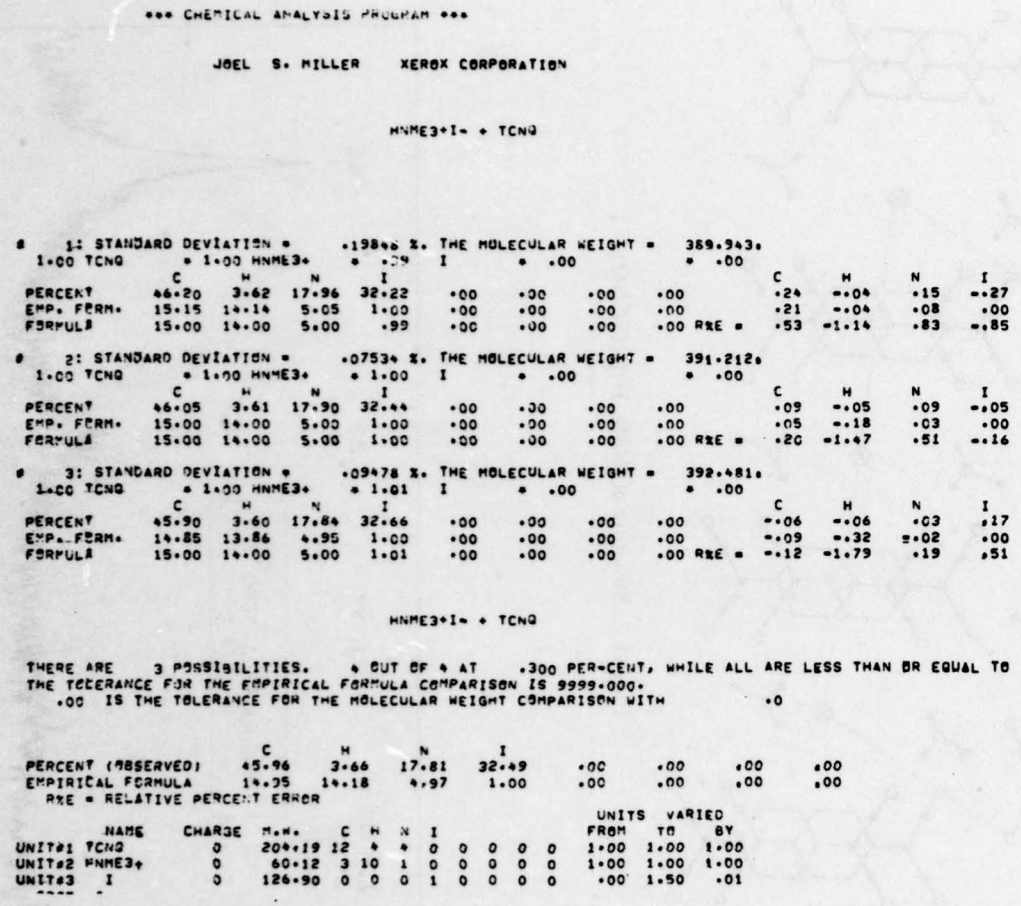
Formulation	Analyst*	%C	%H	%N	%I	Total
$(NMe_3H)(I)(TCNQ)$, (Calc)		46.05	3.61	17.90	32.44	100.00
Sample 1	G	46.00	3.70	17.84	32.40	99.94
	G	45.93	3.75	17.86	32.60	100.14
Sample 2	G	46.06	3.60	17.87	32.54	100.07
	G	45.91	3.68	17.79	32.61	99.96
Sample 3	S	45.88	3.75	17.84	32.31	99.78
	G	46.03	3.61	17.88	32.44	99.96
Sample 4	G	46.04	3.64	17.89	32.47	100.04
	G	45.96	3.52	17.60	32.77	99.85
	S	45.78	3.75	17.84	32.31	99.78
Sample 5	G	46.02	3.60	17.90	32.43	99.95
	G	45.78	3.78	17.96	32.29	99.81
Sample 6	G	46.07	3.70	17.77	32.45	99.99
Sample 7	S	45.97	3.78	17.80	32.23	99.78
Mean (Standard Deviation)		45.96(10)	3.66(9)	17.81(11)	32.49(18)	99.92(15)

*G = Galbraith Laboratories; S = Spang Microanalytical Laboratory.

sion is reinforced by evaluation of computer analysis of the average microanalytical data [45.96(10) C, 3.66(9) H, 17.81(11) N, and 32.49(18) I] (FIGURE 1). The printout shows that the formulation with the lowest sum of root mean square deviations for the C, H, N, and I analyses is of 1.00:1.00:1.00 stoichiometry.

The oxidation state of iodine, and, consequently, the degree of charge transfer is assigned from interpretation of Raman scattering data. The Raman active mode at 105 cm^{-1} (FIGURE 2) is assigned to I_3^-. Thus, conservation and stoichiometry suggest the charge-transfer formulation to be $(NMe_3H)^+(I_3^-)_{1/3}(TCNQ)^{2/3-}$, **1**. Consequently, there is a one-third filled band on the TCNQ chain for this one-dimensional complex.[5] Differential scanning calorimetry (DSC) and thermal gravimetric analysis (TGA) data characterize **1** to be thermally stable with respect to iodine loss up to 225°C; however, in open vessels, decomposition to NMe_3(g), HI(g), and TCNQ° occurs at higher temperatures.[5] Refinement of 25 x-ray reflections from a single crystal reveal that **1** possesses a monoclinic unit cell [a = 13.874(9), b = 6.441(3), c = 19.084(6) Å, β = 105.85(4)°, and V = 1640.7(5) $Å^3$].[5] In diffuse x-ray work, Delhaes *et al.* reported[6a] a one-dimensional (1-D) superlattice ascribed to a periodic distortion on the iodine chain, consistent with I_3^-. Cougrand *et al.*,[4] in their preliminary note, discuss the structure as being comprised of 1-D chains of TCNQ and iodine with uniform 3.22 Å (interplanar) spacings between the TCNQ (FIGURE 3) and 2.97 Å and 3.47 Å intra- and intermolecular iodine separations.[6b]

The room-temperature four-probe dc conductivity in the stack (b-axis) direction of **1**, σ, is ~20 $ohm^{-1}cm^{-1}$ and the anisotropic conductivity ratio (σ_b/σ_a), is



```
*** CHEMICAL ANALYSIS PROGRAM ***

        JOEL  S. MILLER    XEROX CORPORATION

                        HNME3+I- + TCNQ

#    1: STANDARD DEVIATION =      .19846 %. THE MOLECULAR WEIGHT =    389.943.
  1.00 TCNQ       * 1.00 HNME3+     *  .99    I        *  .00             *  .00
                  C        H        N        I
PERCENT       46.20    3.62    17.96    32.22     .00      .00      .00      .00          C     H     N     I
EMP. FORM.    15.15    14.14     5.05     1.00     .00      .00      .00      .00          .24  -.04   .15  -.27
FORMULA       15.00    14.00     5.00      .99     .00      .00      .00      .00 RAE =    .53 -1.14   .83  -.85

#    2: STANDARD DEVIATION =      .07534 %. THE MOLECULAR WEIGHT =    391.212.
  1.00 TCNQ       * 1.00 HNME3+     * 1.00    I        *  .00             *  .00
                  C        H        N        I
PERCENT       46.05    3.61    17.90    32.44     .00      .00      .00      .00          C     H     N     I
EMP. FORM.    15.00    14.00     5.00     1.00     .00      .00      .00      .00          .05  -.18   .03  -.00
FORMULA       15.00    14.00     5.00     1.00     .00      .00      .00      .00 RAE =    .20 -1.47   .51  -.16

#    3: STANDARD DEVIATION =      .09478 %. THE MOLECULAR WEIGHT =    392.481.
  1.00 TCNQ       * 1.00 HNME3+     * 1.01    I        *  .00             *  .00
                  C        H        N        I
PERCENT       45.90    3.60    17.84    32.66     .00      .00      .00      .00          C     H     N     I
EMP. FORM.    14.85    13.86     4.95     1.00     .00      .00      .00      .00          -.06  -.06   .03   .17
FORMULA       15.00    14.00     5.00     1.01     .00      .00      .00      .00 RAE =   -.09  -.32   .02   .00
                                                                                          -.12 -1.79   .19   .51

                        HNME3+I- + TCNQ

THERE ARE    3 POSSIBILITIES.    4 OUT OF 4 AT    .300 PER-CENT, WHILE ALL ARE LESS THAN OR EQUAL TO    .300 PER-CENT.
THE TOLERANCE FOR THE EMPIRICAL FORMULA COMPARISON IS 9999.000.
   .00  IS THE TOLERANCE FOR THE MOLECULAR WEIGHT COMPARISON WITH          .0

                        C        H        N        I
PERCENT (OBSERVED)    45.96    3.66    17.81    32.49     .00      .00      .00      .00
EMPIRICAL FORMULA     14.95    14.18     4.97     1.00     .00      .00      .00      .00
  RAE = RELATIVE PERCENT ERROR

                                                                          UNITS  VARIED
        NAME     CHARGE  M.W.     C  H  N  I                             FROM   TO    BY
UNIT#1 TCNQ         0    204.19  12  4  4  0  0  0  0  0                 1.00   1.00  1.00
UNIT#2 HNME3+       0     60.12   3 10  1  0  0  0  0  0                 1.00   1.00  1.00
UNIT#3  I           0    126.90   0  0  0  1  0  0  0  0                  .00   1.50   .01
```

FIGURE 1. Computer analysis of the elemental analysis of $(NMe_3H)(I)(TCNQ)$.

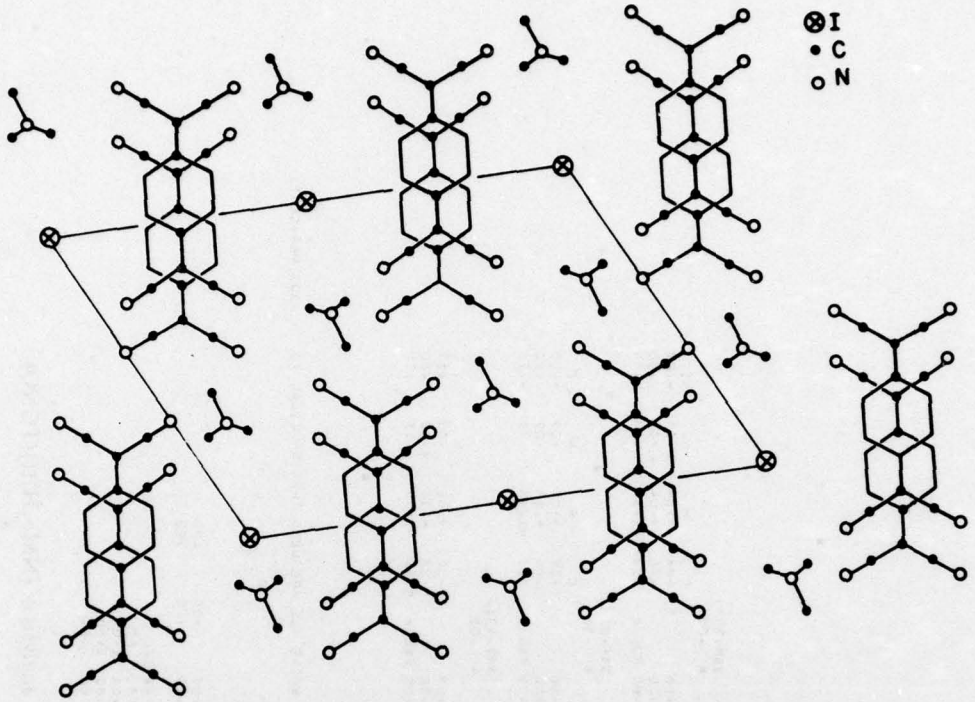


FIGURE 2. Structure of $(NMe_3H)(I)(TCNQ)$.[4]

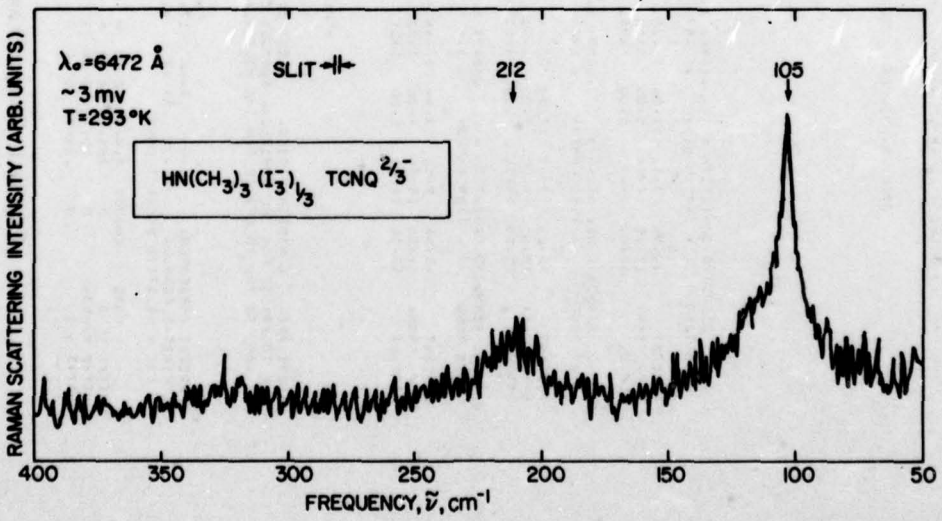


FIGURE 3. Raman-scattering intensity vs. frequency shift from unscattered beam (λ_0 = 6472 Å).

~400. The temperature, T, dependence[5] of σ is shown in FIGURE 4. The conductivity parallel to the needle axis of these crystals increases as the temperature is decreased below room temperature, reaching a maximum of 1.08 $\sigma_{\parallel}$(295°K) at ~240°K. It then decreases until 160 ± 1°K, when it begins to decrease continuously at a much more rapid but continuous rate. A maximum in $-\mathrm{d} \log \sigma/\mathrm{d}(T^{-1})$ is observed[7] at 150°K. These results indicate a metal-like behavior above 240°K and an abrupt but reversible change at 150°K. In accord with the perspective of Epstein *et al.*,[8-10] the transition at 150°K appears to be a semiconductor to semiconductor transition, i.e., metal-like variations in $\sigma(T)$ for $T > 160$°K can be accounted for by thermally excited carriers with a temperature-dependent mobil-

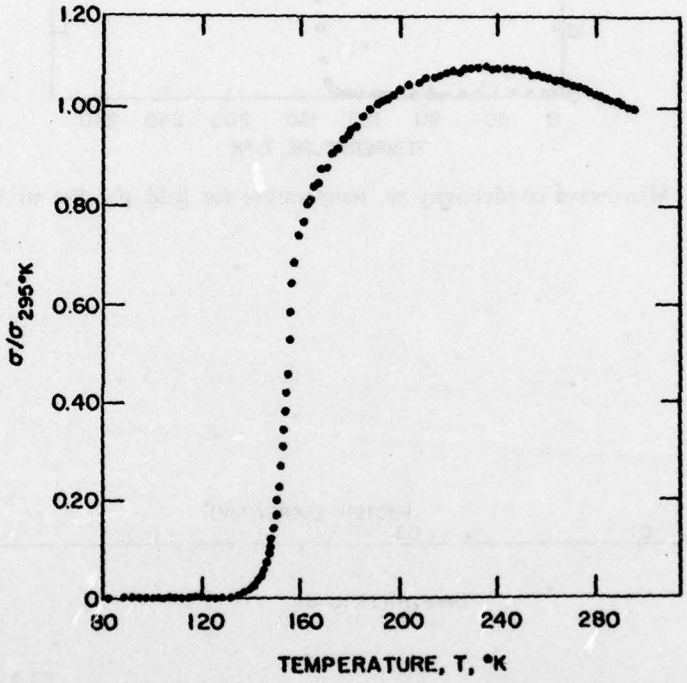


FIGURE 4. Four-probe dc conductivity vs. temperature, for current parallel to TCNQ chain axis.[5]

ity.[5,7] The mobility is determined by scattering of the charge carriers by the intramolecular vibrations. Variation from sample to sample is probably due to scattering from sample-dependent defects and impurities.

Temperature-dependent microwave conductivity measurements[11] (FIGURE 5) closely parallel the dc conductivity features. A microwave dielectric constant of ~40 is measured at low temperature (<60°K), which increases as the temperature is increased, consistent with the decreasing low-temperature gap.[11]

Room-temperature polarized reflectance data[12] (FIGURE 6) provide direct confirmation of the existence of a semiconducting gap in the metal-like regime. Analysis[12] of data ranging from 20 cm^{-1} to 25,000 cm^{-1} yields an optical gap of 0.2 eV (consistent with analysis[7] of dc conductivity data) and a plasma frequency

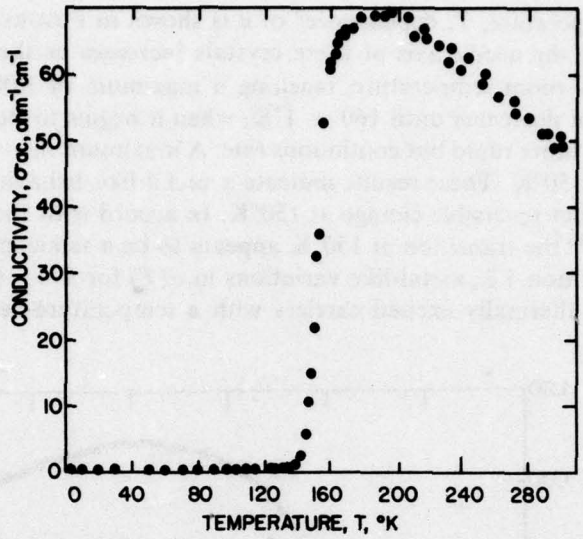


FIGURE 5. Microwave conductivity vs. temperature for field parallel to TCNQ chain axis.[11]

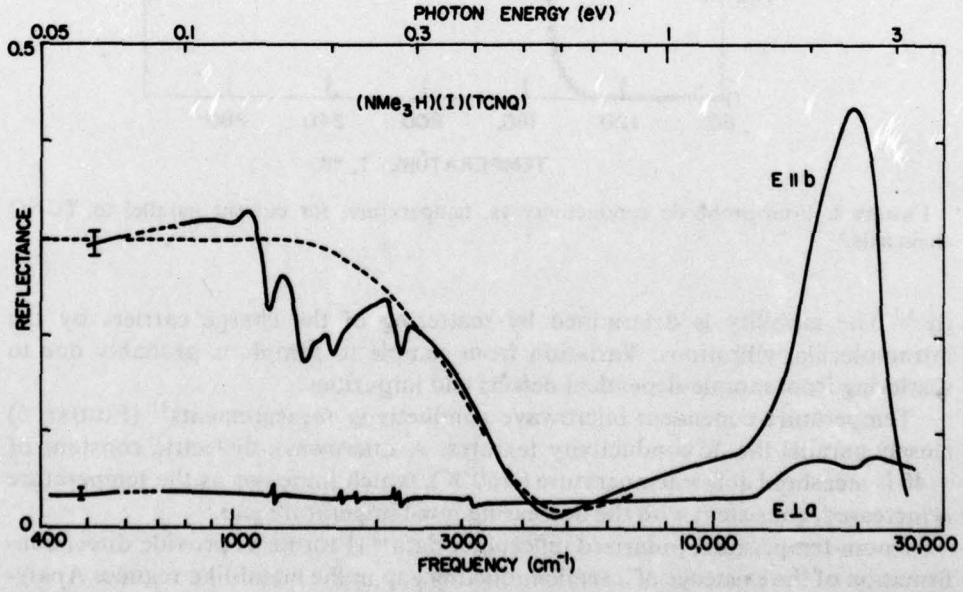


FIGURE 6. Reflectance vs. energy for light polarized parallel to *b*-axis (TCNQ chain axis) and also *a*-axis.[12]

of 0.63 eV. Prominent vibrational structure is in evidence for light polarized parallel to the chain axis,[12] as expected for a semiconducting state as a consequence of electron-molecular vibration coupling.[13]

The temperature-dependent thermoelectric power,[14] $S(T)$, further supports the model of semiconductor behavior in the metal-like regime. Above 150°K, the thermoelectric power is proportional to T^{-1} as expected for semiconductors (FIGURE 7).

The ESR linewidth[5] monotonically decreases as the temperature is lowered until 160°K, below which it broadens rapidly, in agreement with the conductivity data. The ESR derivative peak-to-peak linewidth is ~225 mG at 160°K and ~500 ± 50 mG at 295°K. The isotropic nearly free electron g value (g = 2.003 ± 0.0005), however, appears to remain temperature independent.[5] No corresponding change at 150°K is observed in the protonic relaxation time.[15]

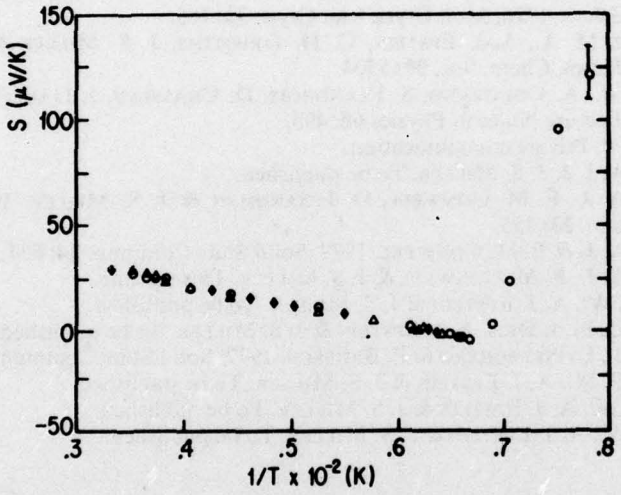


FIGURE 7. Absolute thermoelectric power parallel to chain axis vs. T^{-1}.[13]

Young's modulus data[16] confirms this transition, as a small anomaly is observed at 150°K. A large anomaly is also observed at T ~ 89°K, which may be associated with the methyl rotation. This 89°K anomaly may be the source of the thermally activated relaxation process which is observed in the proton resonance spin-lattice (T_1) and spin-spin (T_2) relaxation times.[15]

These experimental data show this thermally stable system to be of (NMe_3H^+)-$(I_3^-)_{1/3}(TCNQ)^{-2/3}$ composition. The complex exhibits properties that suggest an energy gap exists at the Fermi energy at room temperature. This gap probably arises from a periodic potential at the TCNQ chains induced by the distortion on the (I_3^-) chains. This gap is consistent with the interpretation of the conductivity in terms of an exponentially temperature-dependent, thermally excited charge-carrier concentration in extended states, and a large, strongly temperature-dependent charge carrier mobility, determined mainly by interaction with molecular vibrations. The presence of semiconducting energy gap, despite the metal-like

dc and microwave conductivity, is confirmed with polarized reflectivity and thermoelectric power studies. Other measurements confirm the semiconductor-semiconductor transition at 150°K and suggest a second transition, probably associated with methyl group rotations, at 89°K.

References

1. PÁL, L., G. GRÜNER, A. JÁNOSSY & J. SÓLYOM, Eds. 1977. Lecture Notes in Physics **65.** Proc. Int. Conf. Organic Conductors and Semiconductors. Siófok, Hungary. 1976. Springer-Verlag. Berlin, Germany; NATO Advanced Study Institute Series 1977. **B25.** (Lectures presented at NATO Advanced Study Institute on Chemistry and Physics of One-Dimensional Metals. Bolzono, Italy. 17–29 August 1976. H. J. Keller, Ed. Plenum Press. New York, N.Y.
2. MILLER, J. S. This volume.
3. MILLER, J. S. & A. J. EPSTEIN. 1976. Prog. Inorg. Chem. **20:** 1.
4. COUGRAND, A., S. FLANDROIS, P. DELHAES, P. DUPUIS, D. CHASSEAU, J. GAULTIER & J. L. MIANE. 1976. Mol. Cryst. Liq. Cryst. **32:** 165.
5. ABKOWITZ, M. A., A. J. EPSTEIN, C. H. GRIFFITHS, J. S. MILLER & M. L. SLADE. 1977. J. Am. Chem. Soc. **99:** 5304.

6a. DELHAES, P., A. COUGRAND, S. FLANDROIS, D. CHASSEAU, J. GAULTIER & C. HANN. 1977. Lecture Notes in Physics **65:** 493.

6b. DELHAES, P. Private communication.

7. EPSTEIN, A. J. & J. S. MILLER. To be published.
8. EPSTEIN, A. J., E. M. CONWELL, D. J. SANDMAN & J. S. MILLER. 1977. Solid State Commun. **23:** 355.
9. EPSTEIN, A. J. & E. M. CONWELL. 1977. Solid State Commun. **24:** 627.
10. EPSTEIN, A. J., E. M. CONWELL & J. S. MILLER. This volume.
11. GUNNING, W., A. J. EPSTEIN & J. S. MILLER. To be published.
12. TANNER, D. B., J. DEIS, A. J. EPSTEIN & J. S. MILLER. To be published.
13. RICE, M. J., L. PIETRONERO & P. BRÜESCH. 1977. Solid State Commun **21:** 757.
14. CHAIKIN, P. M., A. J. EPSTEIN & J. S. MILLER. To be published.
15. FROIX, M. F., A. J. EPSTEIN & J. S. MILLER. To be published.
16. BRILL, J. W., A. J. EPSTEIN & J. S. MILLER. To be published.

CHEMICAL PREPARATION AND PHYSICAL PROPERTIES OF A METALLIC ORGANIC CHARGE-TRANSFER COMPLEX: HMTTF-TCNQ*

P. Delhaes, S. Flandrois, J. Amiell, and G. Keryer

Centre de Recherches Paul Pascal (C.N.R.S.)
Université de Bordeaux I
33405 Talence - France

E. Toreilles, J. M. Fabre, and L. Giral

Laboratoire de Chimie Structurale Organique (U.S.T.L.)
34060 Montpellier - France

C. S. Jacobsen

Physics Laboratory III
Technical University of Denmark
DK 2800 Lyngby, Copenhagen, Denmark

K. Bechgaard

Chemistry Laboratory II
H. C. Oersted Institute
University of Copenhagen
Copenhagen DK 2100 - Denmark

These last years a new class of materials has appeared: the II type of organic charge transfer complexes which present a metallic behavior. As part of these studies we want to report here the synthesis and the physical properties of a compound belonging to the TTF (tetrathiofulvalenium) family. The TTF-TCNQ charge-transfer complex has been intensively studied, but the interest has recently spread to other similar complexes, in particular the selenium analogs, among them HMTSF-TCNQ, which has been found to be a conductor down to 1°K[1] and semimetallic under pressure.[2] In order to get a better knowledge of the general behavior of this class of organic materials it is therefore of great interest to study the sulfur analog: HMTTF-TCNQ.

Chemical Preparation and Structure

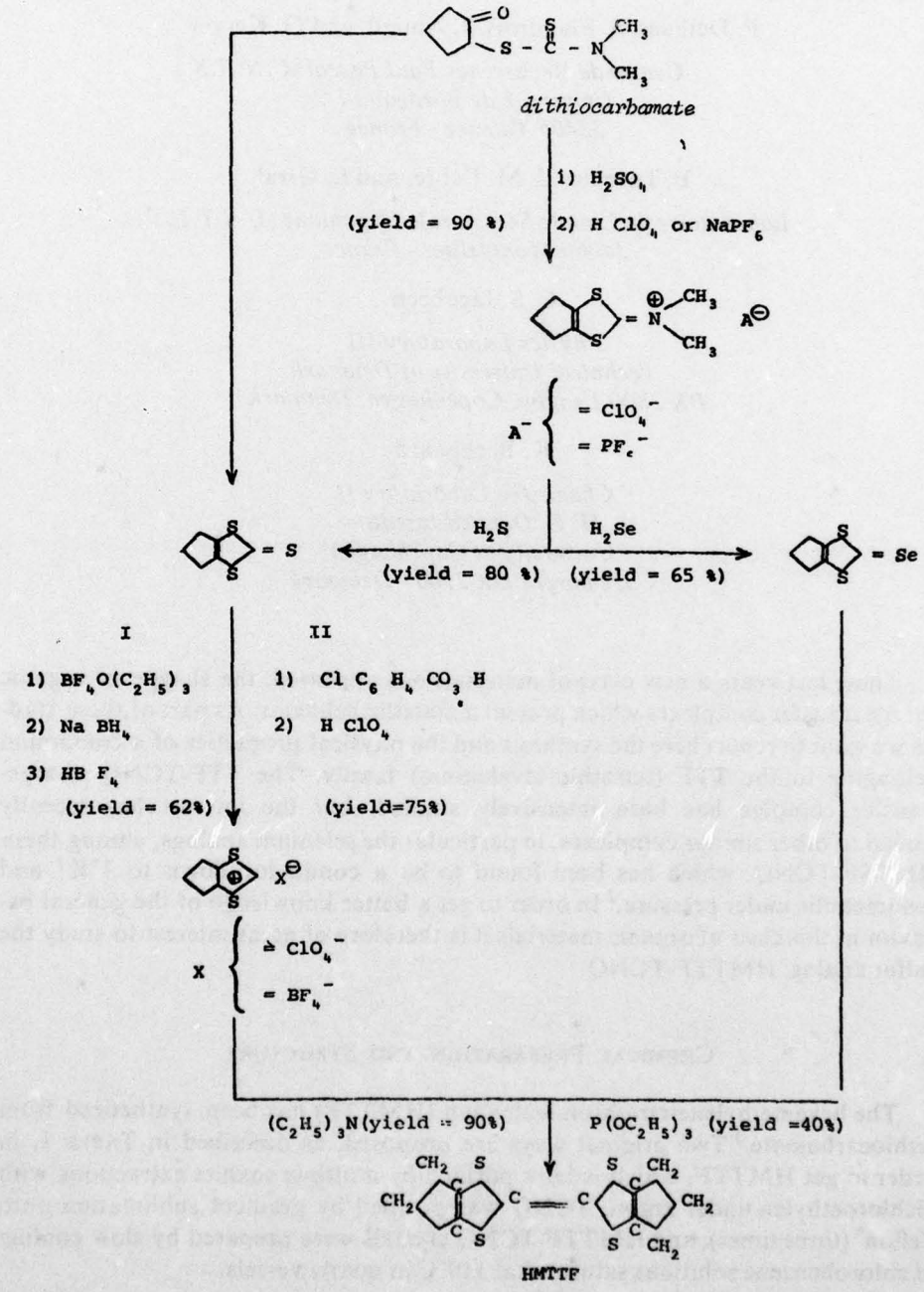
The hexamethylenetetrathiofulvalenium (HMTTF) has been synthetized from dithiocarbamate.[3] Two original ways are proposed, as described in Table 1, in order to get HMTTF, which is later purified by multiple soxhlet extractions with dichloroethylen under argon. TCNQ was purified by gradient sublimation onto Teflon® (three times), and HMTTF-TCNQ crystals were prepared by slow cooling of chlorobenzene solutions saturated at 110°C in quartz vessels.

It has been verified[4] by x-ray diffraction at room temperature that a simple salt

*Manuscript received June 6, 1977.

0077-8923/78/0313-0467 $1.75/1 © 1978, NYAS

TABLE 1


dithiocarbamate
1) H_2SO_4
2) $H ClO_4$ or $NaPF_6$
(yield = 90 %)
A^- = ClO_4^- = PF_6^-
H_2S
H_2Se
(yield = 80 %)
(yield = 65 %)
= S
= Se
I
1) $BF_4O(C_2H_5)_3$
2) $NaBH_4$
3) HBF_4
(yield = 62%)
II
1) $Cl C_6H_4 CO_3H$
2) $H ClO_4$
(yield=75%)
X^- = ClO_4^- = BF_4^-
$(C_2H_5)_3N$(yield = 90%)
$P(OC_2H_5)_3$ (yield =40%)
HMTTF

similar to that recently described by Greene and colleagues[5] was prepared. Furthermore, the classical x-ray diffuse scattering at 2 k_F has been detected,[6] indicating a charge-transfer of 0.72.

Physical Properties

Electrical Conductivity

The absolute value at room temperature and the thermal variation of dc electrical conductivity along the needle axis indicate a similar behavior, as previously published[5] (Figure 1). About 75°K, a broad conductivity maximum occurs, fol-

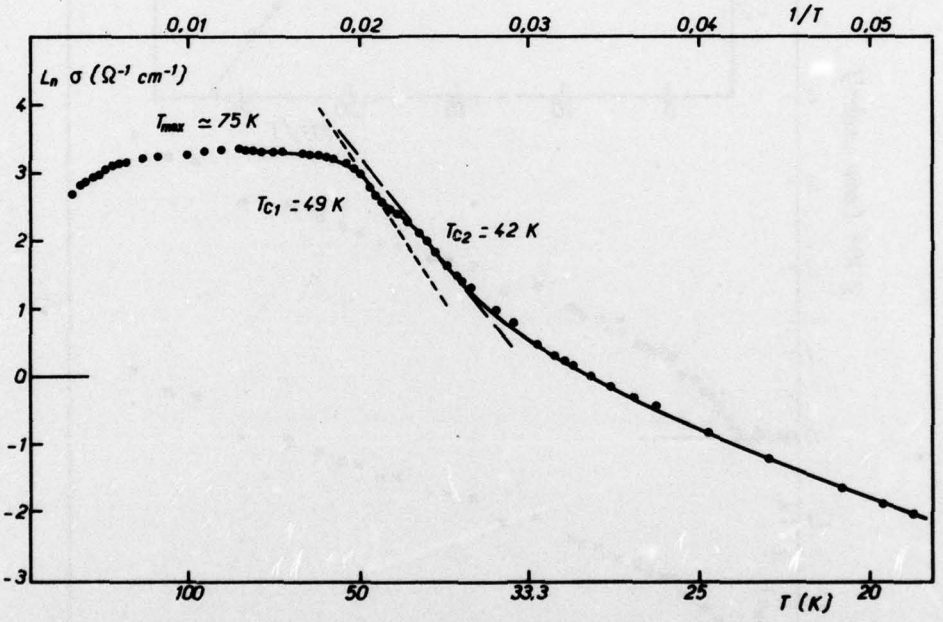


Figure 1. Thermal variation of dc conductivity in reduced values versus T^{-1}; the absolute dc conductivity at room temperature is $\sigma \simeq 550\ (\Omega\text{cm})^{-1}$.

lowed by two sharp transitions at $T_{c1} = 49 \pm 1$ K and $T_{c2} = 43 \pm 1$°K when the temperature is going down. Above the transitions a square dependence on temperature is observed, as in other metallic charge-transfer complexes[1,2] that we will analyze.

Static Susceptibility

The temperature variation of the static susceptibility obtained by the Faraday method is shown in Figure 2. Below 30°K the susceptibility follows a Curie law: a plot of χ_{exp} versus T^{-1} gives a straight line whose slope is the Curie constant $C \simeq 14.7 \times 10^{-4}$ emu K/mole (corresponding to 3.9×10^{-3} paramagnetic

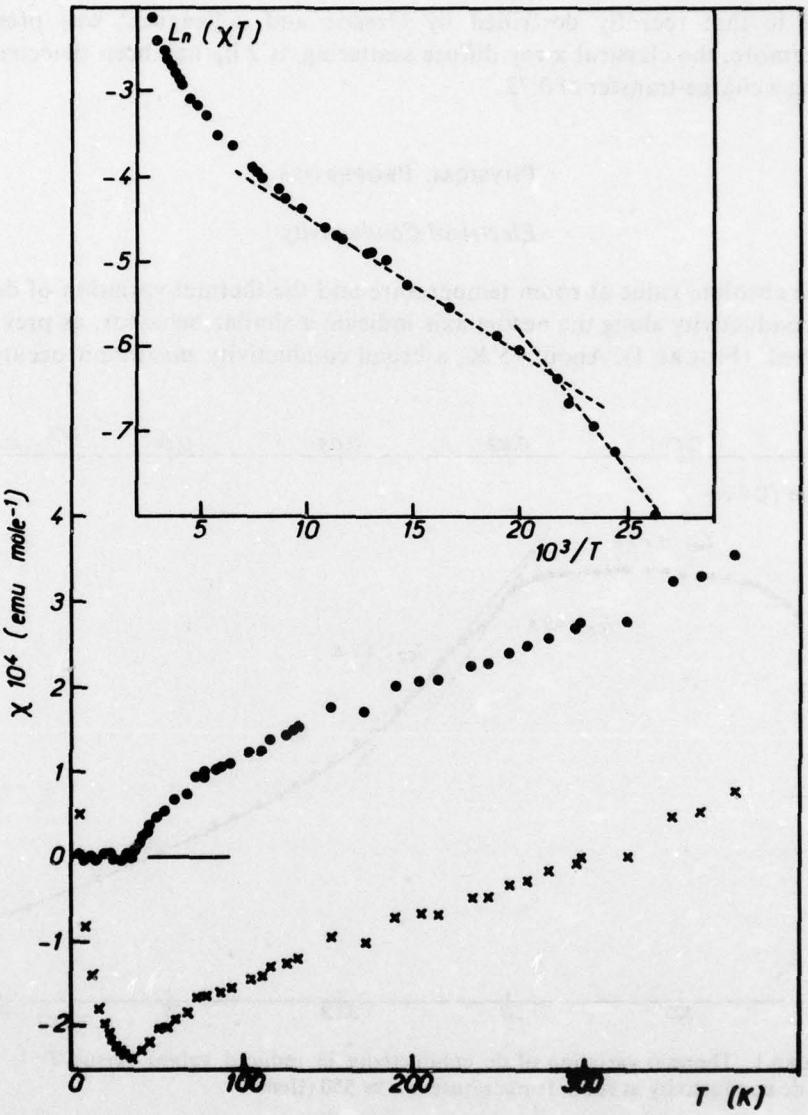


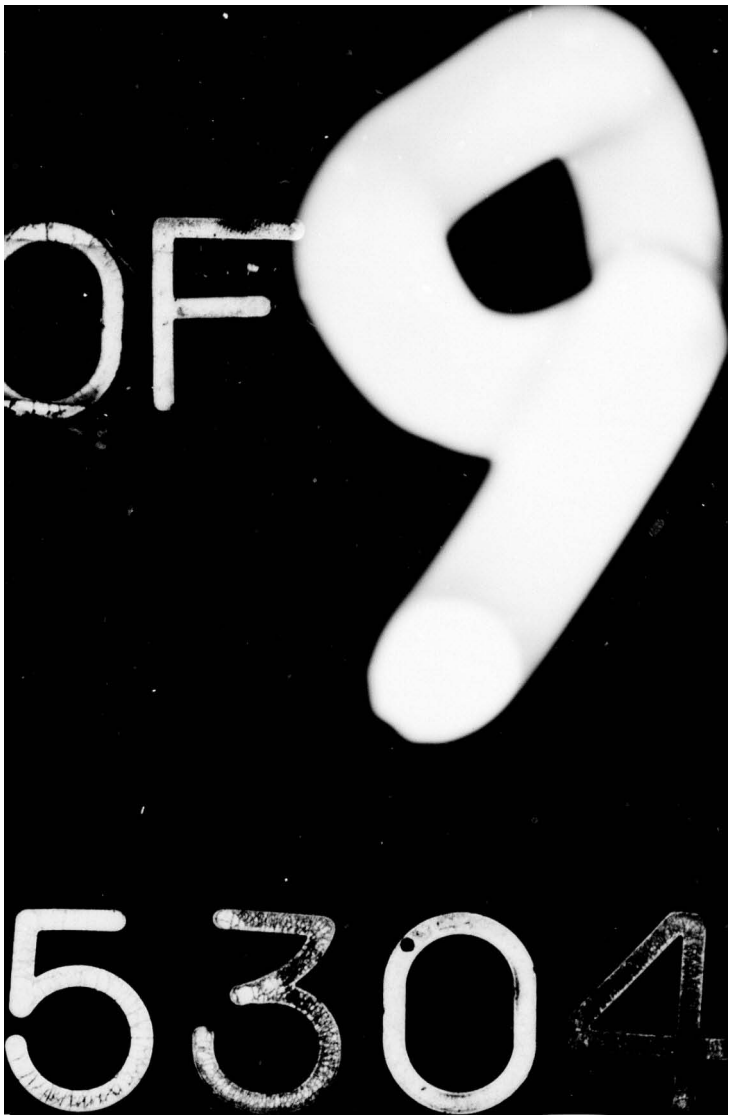
FIGURE 2. Thermal variation of magnetic susceptibility. The experimental points (crosses) are shown at bottom; intrinsic paramagnetism (dots) obtained after corrections for core diamagnetism and Curie paramagnetism are shown center; top shows a plot of ln (χT) versus T^{-1}.

centers per mole, assuming $g = 2$ and $S = \frac{1}{2}$). The extrapolation to $T^{-1} \Longrightarrow 0$, gives $\chi = -2.8 \times 10^{-4}$ emu/mole, which is in good agreement with the diamagnetism calculated from Pascal's constants (-2.7×10^{-4} emu/mole).[7] After substracting the Curie part and the core diamagnetism from the observed susceptibility, the residual part is obtained. The thermal variation of paramagnetism, although looking regular at first view, seems to present a slope change around 44°K if $\ln(\chi T)$ is plotted versus T^{-1} (FIGURE 2).

AD-A065 304 NEW YORK ACADEMY OF SCIENCES N Y F/G 7/2
SYNTHESIS AND PROPERTIES OF LOW-DIMENSIONAL MATERIALS,(U)
1978 J S MILLER, A J EPSTEIN N00014-77-C-0374
UNCLASSIFIED NL

6 OF 9
AD A065304




OF 9
5304

EPR Investigation

Experiments were carried out on single crystals with a Varian X and Q bands spectrometer equipped with home-made (below 78°K) and standard (78–400°K) thermal-variation accessories.

From the structure determination[4,5] we know that this charge-transfer complex crystallizes in the orthorhombic system. By rotation diagrams at 295°K we checked that the *g*-factor and the line-width between inflection points (*S*) of the unique line are frequency independent in spite of some experimental differences. Besides, they behave as second-order tensors with the principal axes in agreement with the crystallographic ones (FIGURE 3). For the three defined positions, we studied the thermal variations of the EPR line between 5° and 400°K as indicated on FIGURE 4. The labeling of the *g*-factor and line-width was done following Greene's work;[5] without morphologic indications *X* and *Z* directions are indiscernible; they were attributed by analogy with Tomkiewicz and colleagues'[8] experiments on TTF-TCNQ because of the similarities of behavior except for the *g*-factor thermal variation (FIGURE 4b).

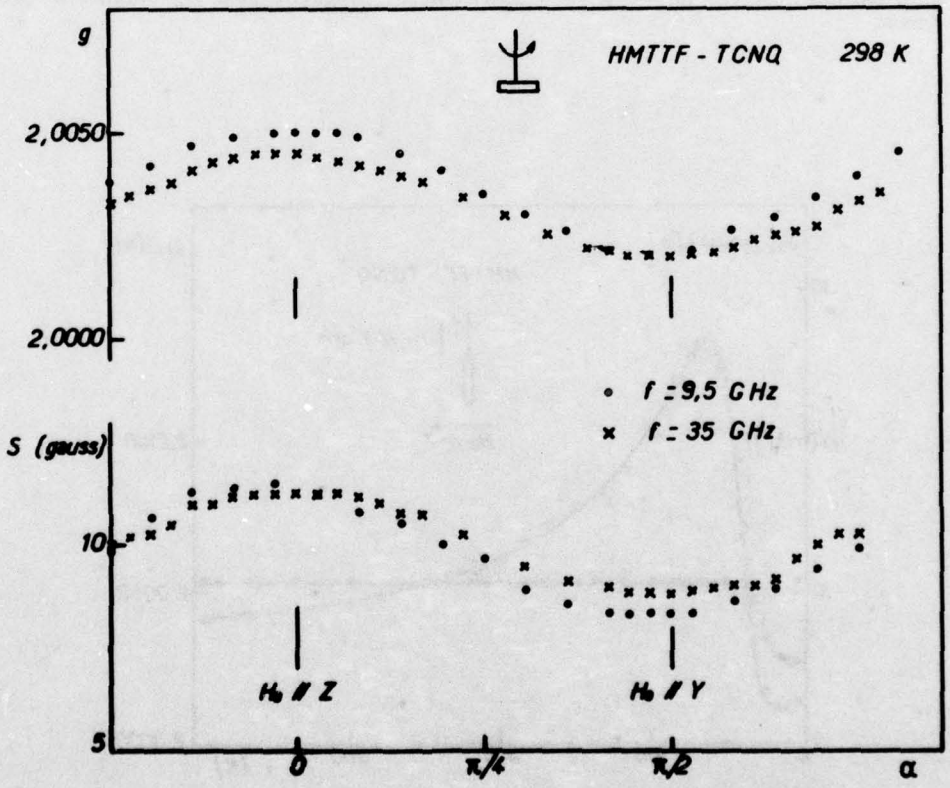


FIGURE 3. EPR rotation diagrams at 295°K in the (*Y Z*) cristallographic planes: α is the angle between *Z* axis and the applied magnetic field H_0; *g* is the *g*-factor and *S* the line-width between inflection points.

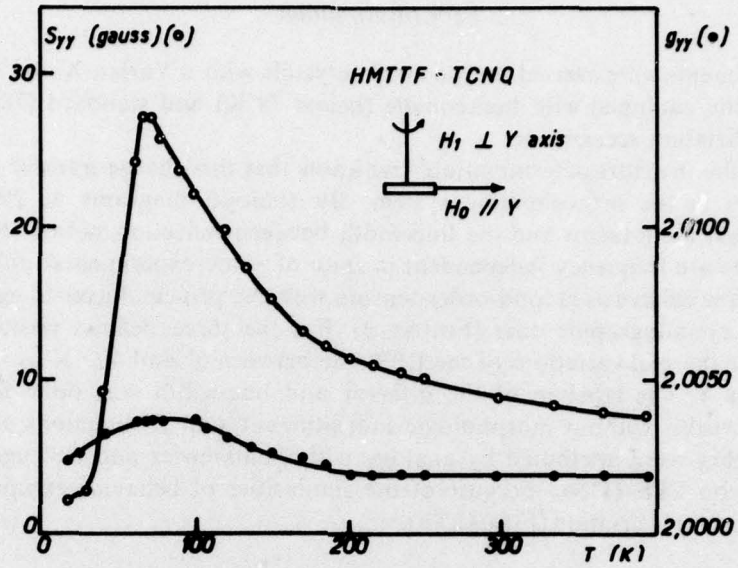


FIGURE 4a. Thermal variations of the diagonal terms of the *g*-factor (•) and line-width *S* (○) tensors observed in the *X*-band spectrometer. Magnetic field H_0 parallel to the *Y* axis.

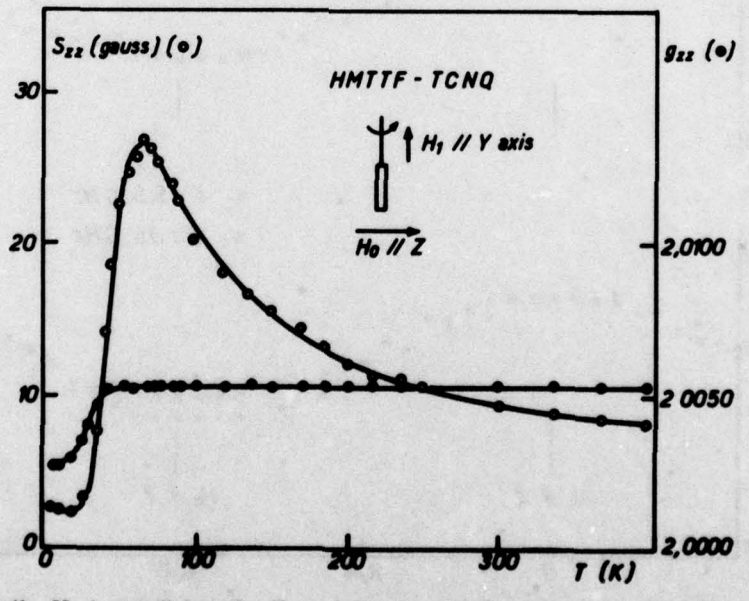


FIGURE 4b. H_0 is parallel to the *Z*- and *X*-axis, and the microwave field H_1 is parallel to the needle axis *Y*. See legend for FIGURE 4a.

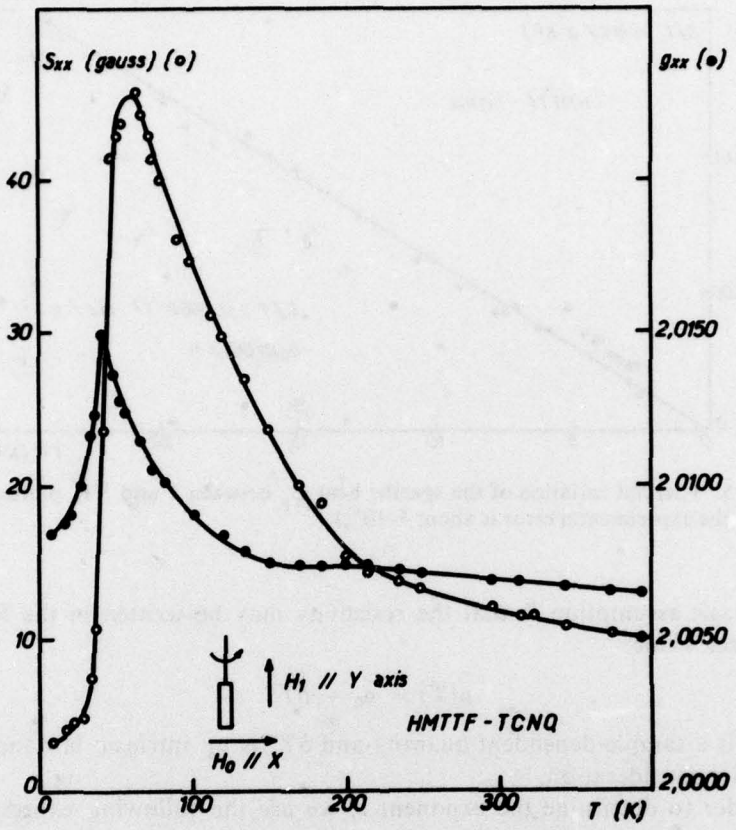


FIGURE 4c. See legend for FIGURES 4a and 4b.

The observed line-width is Lorentzian in these two directions (X and Z) but slightly asymmetric, due to a small skin effect, in the Y direction.

Specific Heat Measurements

Experiments were carried out between 1.5° and 10°K with an adiabatic calorimeter. The sample was a pellet weighing about 100 mg, placed on an alumina support as described elsewhere.[9] The specific heat of HMTTF-TCNQ is shown on FIGURE 5, where we can see that an ordinary cubic term appears that allows us to calculate the Debye temperature (θ_D = 86°K). This result can be compared to the low temperature specific heat of TTF-TCNQ (θ_D = 89.5°K).[10]

ANALYSIS AND INTERPRETATION

Conductivity Behavior

The dc conductivity is similar to the previously known result.[5] To compare these results the data are plotted in the form suggested by Groff *et al.*[11] and used by Isett and Perez-Albuerne.[12]

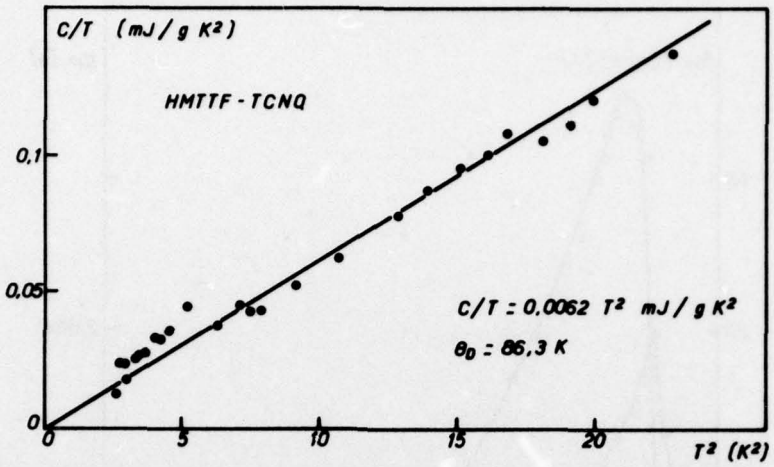


FIGURE 5. Thermal variation of the specific heat C_p between 1 and 5°K plotted as C_p/T versus T^2 (the experimental error is about 5–10%).

The basic assumption is that the resistivity may be written in the form of a Matthiessen's rule:

$$\rho(T) = \rho_0 + bT^{\nu} \tag{1}$$

where ρ_0 is a sample-dependent quantity and bT^{ν} is an intrinsic law for the material under consideration.

In order to determine the exponent ν, we use the following expression (see FIGURE 6):

$$\ln \frac{R_0 - R}{R_0 - R_1} = \text{cste} + \log \left[1 - \left(\frac{T}{T_0}\right)^{\nu}\right] \tag{2}$$

where R is the measured resistance at T, R_0 the value at $T_0 \simeq 290$°K, and R_1 the value at $T_1 = 110$°K.

We find that the best fit is obtained with $\nu = 2.2 \pm 0.2$ and $\rho = 0.3\ 10^{-3}\Omega$cm. From the results of Greene *et al.*,[5] the same analysis furnishes a slightly smaller value: $\nu = 1.8 \pm 0.2$. It seems, therefore, that an exponent of the order of 2 is correct for this compound. In the TTF and HMTSF-TCNQ compounds larger values of ν have been found ($\nu \simeq 2.3$–2.4),[1,11] but some discrepancy might be due to the measurement techniques.

A macroscopic model has been proposed by Phillips[13] to explain such a relationship, but the problem of the metallic conductivity temperature dependence does not appear to be clarified.

Furthermore, we observed a rounded maximum which is separated from the first transition temperature by about 25°K (see FIGURE 1). Following the arguments given by Horn and Rimai[14] for TTF-TCNQ, this behavior indicates resistive fluctuations in quite a large domain, as are supposed to occur in a one-dimensional electronic system.

Phase-Transitions Analysis and Magnetic Behavior

The specific heat in the helium temperature range (FIGURE 5) is characterized by the absence of a linear term which indicates a nonmagnetic ground state and confirms that a metal-insulator transition has taken place at higher temperatures on the two chains.

The *g*-factor anisotropy and the mean value reported in FIGURE 7 furnish a first insight into this phenomenon. As shown on the thermal variation, the g-value reaches a maximum about 43°K with a value ($\bar{g}$ = 2.0077), near the accepted

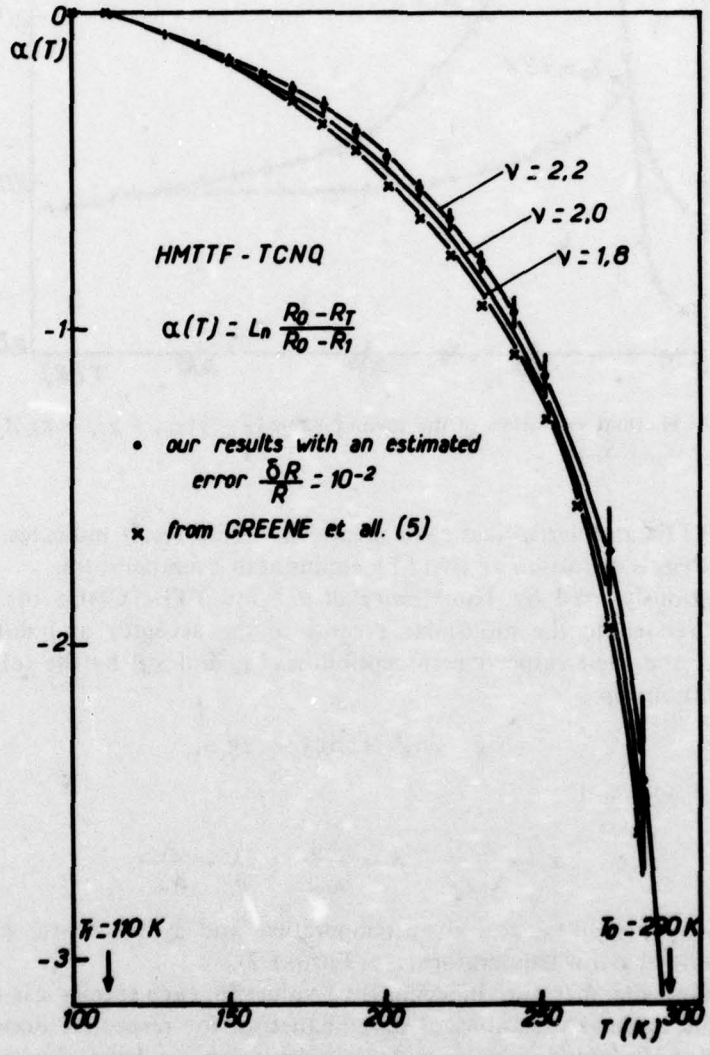


FIGURE 6. $\alpha(T) = \ln R_0 - R_T/R_0 - R_1$ versus T in high-temperature region from T_0 = 290°K to T_1 = 110°K, for two crystals of HMTTF-TCNQ. Comparison with calculated curves for different temperature exponent values defined in (1).

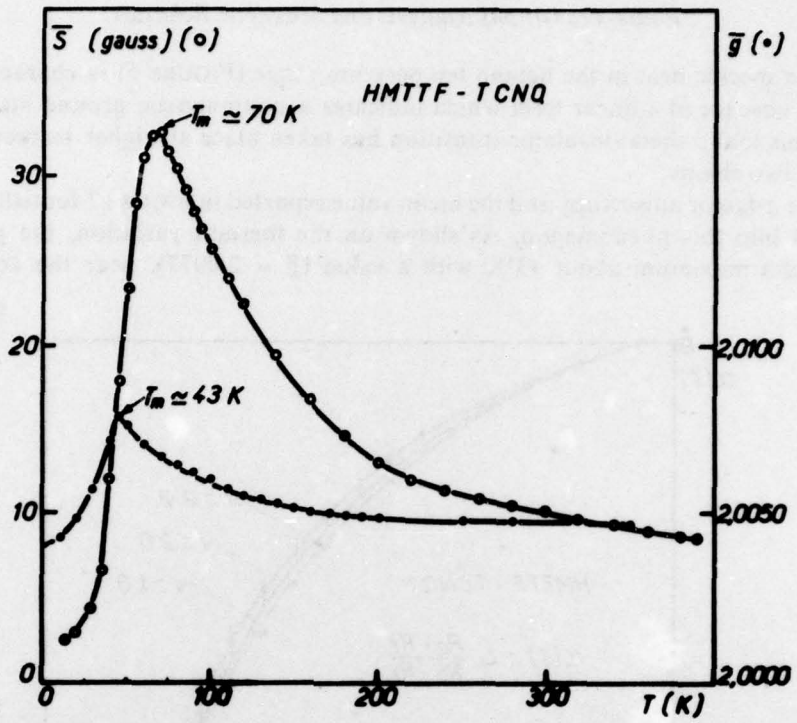


FIGURE 7. Thermal variations of the mean $\bar{g}$-value ($\bar{g} = \frac{1}{3}(g_{xx} + g_{yy} + g_{zz})$) and $\bar{S}$ value ($\bar{S} = \frac{1}{3}(S_{xx} + S_{yy} + S_{zz})$).

value for TTF^+ and derivatives radical-cations.[15] This result indicates the occurrence of a Peierls distortion on HMTTF chains at that temperature.

As previously used by Tomkiewicz *et al.*[8] for TTF-TCNQ, the measured g-value is related to the molecular g-value of the acceptor and donor stacks (g_a and g_d) and their respective susceptibilities (χ_a and χ_d) by the following additivity relationship.

$$\bar{g} = \alpha g_a + \beta g_d + \gamma g_c \qquad (3)$$

with $\alpha + \beta + \gamma = 1$

$$\alpha = \frac{\chi_a}{\chi_{tot.}} \qquad \beta = \frac{\chi_d}{\chi_{tot.}} \qquad \lambda = \frac{\chi_c}{\chi_{tot.}}$$

$\chi_{tot.} = \chi_a + \chi_d + \chi_c$ at a given temperature and χ_c the Curie paramagnetism determined at low temperatures (see FIGURE 2).

By assuming temperature-independent g-values for each species it is possible to calculate the thermal variations of paramagnetism for respective donor and acceptor stacks. In order to carry out this calculation we have chosen for $g_a = g_{TCNQ} = 2.0025$, as previously determined;[8] $g_d = g_{HMTSF} = 2.0084$; the g-value of $HMTTF^+$ in solution is unknown, but it is reasonnable to assume it similar to the TTF^+ and substituted analogs[15] because the spin-orbit coupling on sulphur atoms should be the same.

g_c = 2.0042. This is the extrapolated value at zero Kelvin from the thermal variation at very low temperatures where the paramagnetic localized centers affect the g-value (FIGURE 7).

A remark must be made about this value: If we assume that the localized spins are equally distributed to each stack, whatever the charge-transfer amount is, we might observe a larger figure, about 2.0054; actually, this discrepancy is not understood.

The thermal variations of paramagnetism are presented in FIGURE 8. We observe that the donor stacks of HMTTF are predominant at low temperatures where we can detect the second transition temperature T_{c2} concerning the acceptor stacks of TCNQ. Our experiments do not appear accurate enough to show the first transition temperature T_{c1}. However, the associated paramagnetism is temperature dependent in a large range, as predicted by Lee *et al.*[16] with a model where the interactions between stacks are weak and the 1-D fluctuation effects are dominant.

Line-Width Behavior and 3-D Interactions

The line-width is anisotropic and characterized by the ratio S_{xx}/S_{yy} or S_{xx}/S_{zz}, which increases at low temperatures, but it is always lower than two. This is in agreement with Yafet's theory[17] for free-charge carriers in anisotropic solids when the motionnal narrowing is complete, which predicts also that $T_2 < 2\ T_1$ (T_1 and T_2 are respectively the spin lattice and spin-spin relaxation times).

From an argument given by T.D. Schultz and quoted in Reference 8, the relaxation processes in electron-spin resonance are more and more efficient when the departure from the unidimensionality for the electronic system becomes larger.

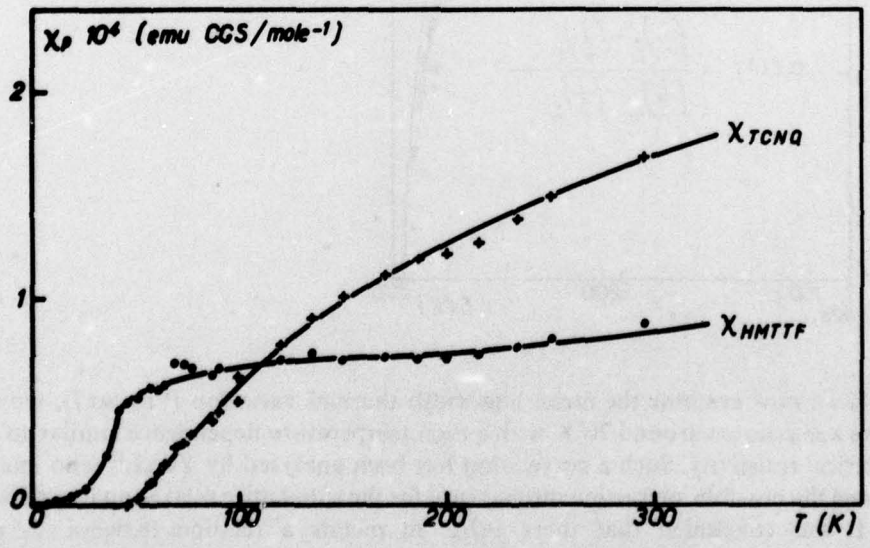


FIGURE 8. Thermal variations of paramagnetic susceptibilities attributed to donor stacks (χ_{HMTTF}) and to acceptor stacks (χ_{TCNQ}).

The relaxation times T_1 and T_2 are shorter and the line-widths larger when the interchains electronic coupling are more efficient. In this compound the line-widths, at a given temperature, are twice as large as in TTF-TCNQ with a similar temperature dependence, because more influent 3-D couplings must exist. It is noteworthy to point out that spin-lattice relaxation-time measurement at 295°K on TTF-TCNQ have shown that $T_1 \simeq T_2 = 0.019\ 10^{-6}$ s. If no anisotropic relaxation times seem to exist on TTF-TCNQ, a similar result might occur in HMTTF-TCNQ, too.

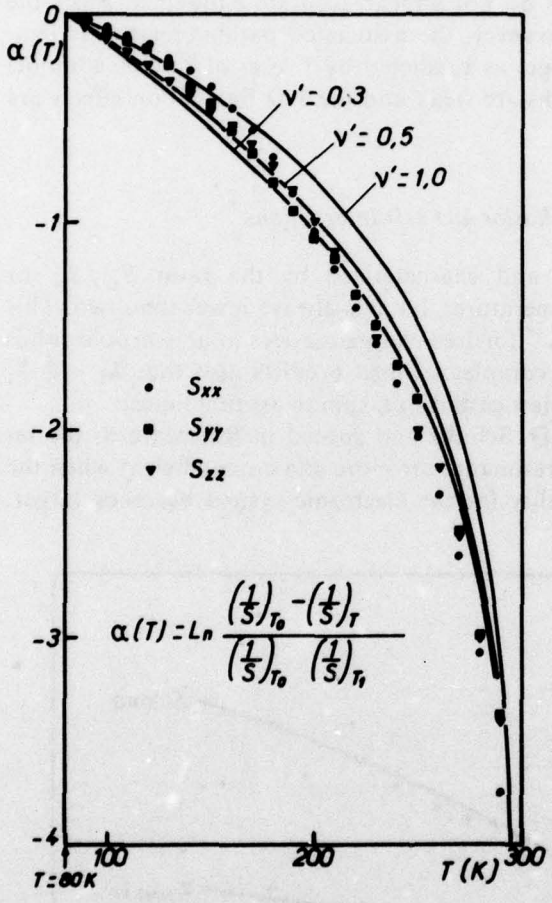


FIGURE 9. $\alpha(T) = \ln(S_{T_0}^{-1} - S_T^{-1}/S_{T_0}^{-1} - S_{T_1}^{-1})$ versus T in high-temperature region from $T_0 = 300$°K to $T_1 = 80$°K for the three components of the line-width tensor and comparison with the theoretical relation (3).

If we now examine the mean line-width thermal variation (FIGURE7), we observe a maximum around 70°K with a high temperature dependence similar to the electrical resistivity. Such a correlation has been analyzed by Yafet,[17] who has reviewed the possible interaction mechanisms for the spin-lattice relaxation in metals.

It was concluded that there exists in metals a relation between T_1 and the electrical resistivity if the relaxation rate due to the modulation of the spin-orbit coupling by lattice vibrations is the most effective process. Such a relation-

ship might exist in anisotropic materials such as HMTTF-TCNQ. To look for this point we assume that:

the line-width S is proportionnal to T_2, in absence of saturation effects, and to T_1 because $T_2 \simeq T_1$;
the thermal variation of the inverse of the line-width is equal to

$$S^{-1} = S_0^{-1} + cT^{\nu'} \tag{4}$$

with use of a similar form as for resistivity (see (1)), where $cT^{\nu'}$ is the intrinsic term.

S_0 is the line-width that we attribute to the scattering by impurities and defects.

By using the same plot as previously (see (2)), we examine the temperature dependence of the inverse of the line-width between $T_0 = 300°K$ and $T_1 = 80°K$ (FIGURE 9). This picture indicates that:

the three line-widths follow the same temperature dependence, which does not obey the presumed law ($\nu' \cong 2$);
a unique temperature dependence is not followed in the observed range. Qualitatively, around 200°K, a change is detected.

It can be due to either a different interaction mechanism or a change in the ratio T_2/T_1, which depends on the anisotropic electron-phonon interactions.

It therefore appears that the intrinsic thermal variation of the line-width is not correctly understood in the metallic range of this material.

CONCLUSION

Comparison with the properties of similar charge-transfer complexes—namely, HMTSF-TCNQ and TTF-TCNQ—is interesting. Similar crystallographic structure with HMTSF-TCNQ with a charge transfer amount quasiidentical is seen.[4,5,6,19] The physical properties, as previously pointed out by Greene and colleagues,[5] behave the same way. After 90°K, the thermal variation of paramagnetism is parallel with a larger value for HMTTF ($+1.2 \times 10^{-4}$ emu CGS/mole). This comparison indicates a narrower bandwidth in the sulfur compound than in the selenium one with a free carrier mobility estimated to be smaller. No semimetallic state exists at low temperature, and we do not detect any Landau diamagnetism.[20] Compared to TTF-TCNQ, several differences are noted relative to the maximum of d.c. conductivity, the *g*-factor thermal variations, and the 3-D electronic interactions between stacks. They must be related to differences in crystallographic structure and charge-transfer amounts.

In conclusion, this study has shown that the magnetism of HMTTF is predominant at low temperatures; these chains undergo a PEIERLS transition at 43°K. In that frame, the anomaly of conductivity detected around 49°K is connected to the TCNQ chains distortion. From the paramagnetism attributed to each chain (FIGURE 8) we can assume that the high-temperature domain where resistive fluctuations exist must be correlated to the TCNQ stacks if the decreasing susceptibility is associated with the existence of a pseudogap more characteristic of 1-D

behavior. However, for a definite interpretation it will be necessary to resolve the conflicting point between these 1-D fluctuation effects and the 3-D interstack interactions indicated by the line-width values.

Notes and References

1. Bloch, A. N., D. O. Cowan, K. Bechgaard, R. P. Pyle, R. H. Banks & T. O. Poehler. 1975. Phys. Rev. Lett. **34**(25): 1561.
2. Jerome, D. & M. Weger. 1976. Proc. NATO Adv. Study Inst. Chemistry and Physics of 1-D metals. August. Bolzano, Italy.
3. Campaigne, E. & N. W. Jacobsen. 1964. J. Org. Chem. **29:** 1703; Bechgaard, K., D. O. Cowan, A. N. Bloch & L. Henriksen. 1975. J. Org. Chem. **40:** 746.
4. Hauw, C. Private communication.
5. Greene, R. L., J. J. Mayerle, R. Schumaker, G. Castro, P. M. Chaikin, S. Etemad & S. J. Laplaca. 1976. Solid State Commun. **20:** 943.
6. Comes, R. Private Communication.
7. Flandrois, S., P. Dupuis, P. Delhaes, J. Amiell & J. Neel. 1972. J. Chim. Phys. Biol. **69:** 1305. In that publication the diamagnetism of the TCNQ molecule has been measured and found to be equal to -1.00×10^{-4} emu CGS/mole; this is the value used for this calculation.
8. Tomkiewicz, Y., B. A. Scott, L. J. Tao & R. S. Title. 1974. Phys. Rev. Lett. **32**(24): 1363; Tomkiewicz, Y., A. R. Taranko & E. M. Engler. 1976. Phys. Rev. Lett. **37:**1705; Tomkiewicz, Y., A. R. Taranko & J. B. Torrance. 1977. Phys. Rev. **B15**(2): 1017.
9. Keryer, G., J. P. Manceau & P. Delhaes. To be published.
10. Wei, T., S. Etemad, A. F. Garito & A. J. Heeger. 1973. Phys. Lett. **A45**(4): 269.
11. Groff, R. P., A. Suna & R. E. Merrifield. 1974. Phys. Rev. Lett. **33:**418.
12. Isett, L. C. & E. A. Perez-Albuerne. 1977. Solid State Commun. **21:**433.
13. Phillips, J. C. 1976. Phys. Stat. Sol. (b) **78:** 471.
14. Horn, P. M. & D. Rimai. 1976. Phys. Rev. Lett. **36**(14): 809.
15. Wudl, F., G. M. Smith & E. J. Hufnagel. 1970. J. Chem. Soc., Chem. Commun.: 1453; Wudl, F., A. A. Kruger, M. L. Kaplan & R. S. Hutton. 1977. J. Org. Chem. **42**(4): 770.
16. Lee, P. A., T. M. Rice & P. M. Anderson. 1973. Phys. Rev. Lett. **31:**462.
17. Yafet, Y. 1963. Solid State Phys. **14:** 67.
18. Berthet, G., J. P. Blanc, J. Gallice, H. Robert, G. Thibaut, J. M. Fabre & L. Giral. Solid State Commun. To be published.
19. Weyl, C., E. M. Engler, K. Bechgaard, G. Jehanno & S. Etemad. 1976. Solid State Commun: **19:** 225.
20. Soda, G., D. Jerome, M. Weger, K. Bechgaard & E. Pedersen. 1976. Solid State Commun. **20:** 107.

PART III. INORGANIC MATERIALS

ELECTRONIC COUPLING MECHANISMS IN MIXED-VALENCE MOLECULES*

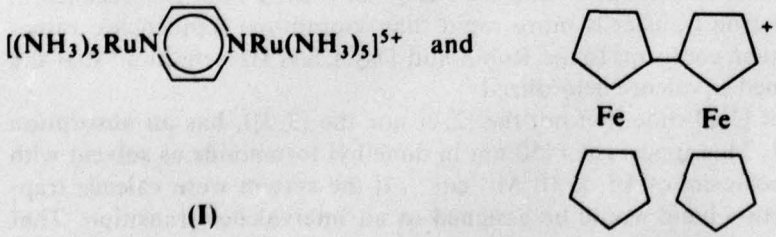
Henry Taube

Department of Chemistry
Stanford University
Stanford, California 94305

Interaction between metal ions in close contact or separated at most by a single atom or ion have been described for numerous systems. By contrast, little has been done explicitly on the electronic coupling mechanism and on the changes in properties attending the interactions for metal ions separated by several bond distances. A means of studying electronic coupling in such cases is afforded by the substitution-inert (robust) mixed-valence molecules. Substitution inertia is important for two reasons: it provides for preparative control, and ensures that structure and composition are maintained in solution. The fact that molecules rather than three-dimensional structures are being investigated also leads to a number of advantages: the restraints placed on composition inherent in the latter kinds of systems are greatly alleviated, and systematic changes in composition can readily be introduced. Also, properties in solution as well as in the solid can be determined, among them the electrochemical and other chemical behavior. Finally, as will be seen, the properties of mixed-valence species, important among them the light absorption associated with inter-ion charge transfer,[1,2] provide a rather direct, though at this stage still qualitative, means of learning about communication between the metal ions and how this is affected by changes in structure and composition.

Some of the advantages of working with molecules rather than with interconnected solid arrays have been pointed out, but it must be acknowledged that at the same time, important advantages are lost when interest is limited to molecular species. Thus, direct measurement of the mobility of the charge carriers is possible for solids, but not for the discrete units which will be dealt with. Many of the observations for the two regimes are complementary, but, if the hopes of those working with the molecular species are realized, elaboration from the two- or three-center species to large molecular weight units, possibly extending through a crystal, will be achieved.

The systematic synthesis of the robust mixed valence molecules



(I) (II)

were reported in 1969[3] and 1970,[4] and since then a large number of additional

*Manuscript received June 13, 1977.

0077-8923/78/0313-0481 $1.75/1© 1978, NYAS

compositions have been described. This paper will be devoted mainly to species related to (I), that is those based on the Ru(III)-Ru(II) couple. These ions, low-spin d^5 and d^6, respectively, form complexes that are substitution-inert even in a solvent as nucleophilic as water. Among the ligands, which, when attached to Ru(III) and Ru(II), undergo substitution slowly are ammonia, nitrogen heterocyclics, nitriles, cyanide ion, thioethers, phosphites, and phosphines. The binuclear complexes in the totally reduced or [2, 2] state can usually be formed simply by mixing an ion such as $Ru(NH_3)_5H_2O^{2+}$, from which H_2O is readily replaced by any of the ligands just mentioned, in a 2:1 ratio with the bifunctional ligand. The mixed-valence, or [3, 2] state can then be formed by oxidation.

Strong Coupling

In summarizing the salient results, a number of molecules that appear to be valence delocalized[5] will be described first,[6a,6b] beginning with the cyanogen complex:

$$[(NH_3)_5RuN{\equiv}C{-}C{\equiv}NRu(NH_3)_5]^{5+}.$$

(III)

It should be noted that cyanogen is an extremely strong π acid, a point that will become especially important when the coupling mechanism in (III) is considered. That there is strong $d\pi \rightarrow \pi^*$ delocalization from Ru(II) to the ligand is shown by the change in the C—N stretching frequency from 2150 cm^{-1} in the free ligand to 1960 cm^{-1} in the [2, 2] complex analogous to (III) (for the Raman active band the change is 2330 cm^{-1} to 2185 cm^{-1}). For the [3, 3] species, the IR active band was determined only in the solid (bromide) and it appears at 2330 cm^{-1}; as expected on the basis of other experience, there is little back-bonding from Ru(III) to π acid ligand.

In the mixed-oxidation state, a single IR frequency is observed at 2210 cm^{-1}, that is, intermediate between those registered for [2, 2] and [3, 3].

If, in (III), a particular state with one ruthenium explicitly 3+ and the other 2+ had a lifetime long compared to that corresponding to the difference in vibrational frequency, two IR bands would be expected, because Ru(II) and Ru(III), as has been documented above, and earlier in the literature,[7] interact differently with the nitrile group. Thus the specific rate for electron transfer must be greater than the frequency difference between 1960 and 2330 cm^{-1} or greater than 10^{13} $seconds^{-1}$. It is because electron transfer is more rapid than vibrational frequencies, rather than that the system conforms to the Robin and Day Class III definition[2] that the system is described as valence delocalized.

The mixed or [3, 2] state (but not the [2, 2] nor the [3, 3]), has an absorption band in the NIR. This appears at 1450 nm in dimethyl formamide as solvent with an extinction coefficient of $4.1 \times 10^2 M^{-1}cm^{-1}$. If the system were valence trapped, this absorption band would be assigned to an intervalence transition. That the valence-trapped description is not appropriate is shown not only by the IR evidence but also by the fact that the NIR band is much narrower than is predicted by the Hush equation[1] (1.6 kK obs. vs. 4.0 calc.). The conclusion finds additional

support in the observation that the band energy, far from following expectation[1] based on charge trapping by solvent orientation, is essentially independent (variation less than ±2%) of the dielectric properties of the solvent. These assertions must be considered in the context of results to be presented later for systems in which the valences are trapped, where it is usual that the band width at half height is somewhat greater than the Hush Equation predicts, and where the variation of band energy with dielectric properties does obey the relation $E \propto (1/n^2 - 1/D)$ (n^2 measures the high-frequency dielectric constant and D the static) with as much as a 20% range in energy when the solvent is changed.

The relatively narrow NIR bands are characteristic of molecules, which, on the basis of other evidence, appear to be valence delocalized. For such systems the bands are also relatively insensitive to solvent properties. The latter observation is easy to understand; if the rate of electron transfer is rapid compared to rotation of solvent molecules (ca. $10^{11}\,sec^{-1}$), and this seems to be the case for (**III**), the solvent will not participate in charge trapping by molecular reorientation.

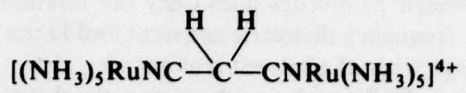
The oxidation-reduction potentials for the separate stages of oxidation of the bi- and polynuclear species studied can and rather routinely have been determined by cyclic voltammetry. These measurements lead to determinations of the stability of the mixed oxidation state with respect to reaction with itself (disproportionation) to produce the fully reduced and fully oxidized species. Making use of such data, a lower limit on the conproportionation constant, K_c, for (**III**)

$$[2,2] + [3,3] = 2[3,2]$$

of 10^{13} in DMSO is set. Because this value is so much greater than that of the statistical value of 4, a value that corresponds to no interaction between the metal ions, there is a temptation to ascribe the stability of the mixed-oxidation state relative to the [2, 2] + [3, 3] to delocalization of the unpaired electron. This delocalization, however, does not appear to be an important factor in the interaction.

In this connection, the relatively low value of the extinction coefficient for the NIR band needs to be taken into account, a value not significantly higher than that observed for some valence-trapped systems (*vide infra*). In considering the electronic structure of the molecule, it is clear that the orbitals extending along the molecular axis (denoted as the z axis) are stabilized by back bonding into the two mutually perpendicular π^* orbitals of the ligand, at least in the [2, 2] state. Because of the extra stabilization of the yz and zx orbitals, on oxidation, an electron will not be lost from them but rather from an xy orbital. Owing to the large distance separating the metal ions, the xy orbitals interact only weakly. The energy needed to make the coordination spheres about the metal ions equivalent is presumably derived from the extra stabilization arising when the yz and zx electrons can delocalize over the whole Ru—N≡C—C≡NRu framework, rather than being constrained mainly to a RuNCCN unit, as would be the case for valence trapping. On this basis, the unpaired electron, instead of contributing substantially to stabilization of the ground state by delocalization, may take advantage of the stabilization provided by delocalization of electrons in the *yz* and *zx* orbitals. Thus, there is no particular mystery about the fact that the "intervalence" transition is weak, even though there is a rather strong interaction between the electronic systems of the metal ions.

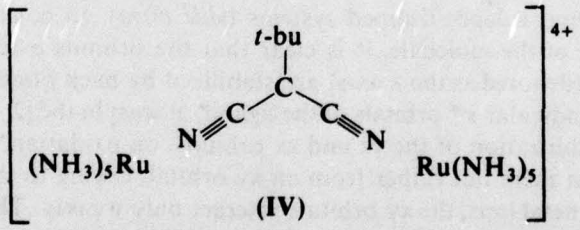
If the goal is to elaborate the two-center system into a useful linear conductor, the results obtained for (III) are disappointing. The particular shortcoming of (III) for such purposes is absent from a class of molecules to be described which have a different mechanism for electronic interaction. These molecules have limitations of their own based on their chemical properties as well as the basic ones inherent in "linear" conductors. Molecules of the general type:



are readily synthesized. The results, which will be cited, were obtained[8a,8b] with the particular derivative with R = *t*-butyl. This composition, rather than the simple malonitrile, was chosen for practical reasons. The molecules, particularly in the [2, 3] and [3, 3] state, undergo decomposition reactions, but the rates of these undesirable reactions are much slower for R = *t*-butyl than for many of the related bridging ligands that were investigated.

The pK_a value of the free ligand is 13.2, but when doubly ligated by $Ru(NH_3)_5^{2+}$ $pK_a > 15$. The increase in pK_a for the ligand on being attached to the metal ion has precedent in other systems, and is a response to net flow of electron density from Ru(II) to the ligand by $\pi d - \pi^*$ backbonding. The foregoing results are cited to provide a basis for gauging the effect of withdrawing one electron from the molecule. When the [2, 2] state is converted to the [3, 2], the pK_a value of the proton on the middle carbon falls to 2.4. Were oxidation limited to the ruthenium centers, and were *Ru(III) to exert a purely inductive effect, a decrease in* pK_a *of* at most two units would be expected for the proton, which, it should be noted, is on a carbon three atoms removed from the metal. The enormous decrease in pK_a registered shows that on oxidation, substantial electron density is removed also from the central carbon, or in other words, the electron hole created on oxidation is not limited to the metal ion (ions) but is distributed over the molecule.

In contrast to the case of (III), in (IV)



(IV)

(since the ligand is deprotonated, the mixed valence species now bears charge of 4+ rather than 5+) the NIR absorption band has a very high intensity, $\epsilon > 10^4$-$M^{-1}cm^{-1}$, the highest thus far reported for a mixed-valence molecule. The band appears at 1260 nm in DMF and 1170 in D_2O. It is again narrower than is calculated by the Hush Equation (2.72 kK obs. vs. 4.44 calc.).

A fundamental difference between a system such as (III) and one such as (IV) is that whereas in the former, where $\pi d - \pi^*$ interactions are in question, the electron hole is not in an orbital directly involved in electron delocalization along the axis connecting the metal ions, in (IV), where $\pi d - \pi$ delocalization seems to obtain, the orbital containing the electron hole embraces both metal ions. In this

case, then, the delocalization involving the electron hole probably plays a prominent part in stabilizing the ground state. Unfortunately, the evidence supporting valence delocalization for (IV), using a criterion based on infrared frequencies can be applied only with the greatest difficulty, owing to the fact that a solid phase containing the mixed-valence ion has not been obtained. In addition, the criterion based on the solvent dependence of the NIR band is not applicable in this case. Because of the geometry of (IV), a solvent dependence is expected even for a valence-delocalized structure, if only there is a change in the electron distribution between ligand and the metal ions attending the transition.

The three items of evidence cited—namely, the profound effect of $1e^-$ oxidation on pK_a for the ligand, the narrowness of the NIR band, and its large extinction coefficient—do support the conclusion that (III) is valence delocalized. It is somewhat bolstered by the fact that the conproportionation constant is again large. The value of K_c for the reaction

$$2[2, L^-, 2] + [3, L^-, 3] = 2[3, L^-, 2]$$

is greater than 10^{10} in water (only a lower limit can be set because only a lower limit on pK_a for the [2, L, 2] state has been observed). As will be shown later, caution must be exercised in using the values of K_c to reach conclusions about the strength of coupling in the mixed-valence state. A large value of K_c may reflect an interaction destabilizing the [2, 2] and/or [3, 3] rather than an intrinsic stabilization of the [2, 3] by electron delocalization.

The difference in the interaction of ruthenium ions with a π-acid such as $N{\equiv}C{-}C{\equiv}N$ on the one hand, and a π donor such as $[N{\equiv}C{-}\overset{\displaystyle R}{\underset{|}{\ddot{C}}}{-}C{\equiv}N]^-$ on the other, is reflected in differences in the absorption spectra in the visible region. It is typical of Ru(II) in combination with π acids to show strong absorption corresponding to a $\pi^* \leftarrow \pi d$ transition.[9] For many nitrogen heterocyclics this appears in the visible region of the spectrum; for the [2, 2] complex with cyanogen as bridging group it appears at 360 nm ($\epsilon = 6.9 \times 10^4 M^{-1}cm^{-1}$). Since the [3, 3] complex is rather unstable in solution, spectra for it have not been obtained. It is typical, however, for the π-acid ligand class that $\pi^* \leftarrow \pi d$ transitions are shifted to higher energies when the metal ion is oxidized. By contrast, the [3, 3] state based on $[N{\equiv}C{-}\overset{\displaystyle R}{\underset{|}{\ddot{C}}}{-}C{\equiv}N]^-$ shows a very strong band at 786 nm ($\epsilon \sim 3 \times 10^4$). This is ascribable to the interaction between the electron hole on Ru(III) and the π electron pair set free on the middle carbon when it is deprotonated. In the limit corresponding to localization of the electron hole on the metal ion, it would be described as a $\pi d \leftarrow \pi$ transition.

The first system of the general class under discussion which was shown[10] to be valence delocalized according to the criterion used in this article was

$$[Cl(NH_3)_4Os{-}N{\equiv}N{-}Os(NH_3)_4Cl]^{3+}$$

(V)

It is introduced last because despite there being two intervening nitrogen atoms, the osmium ions may still be close enough for direct orbital overlap, and thus (V)

may not belong to the category to which this article is devoted. Nevertheless, the observations are of such interest as to merit mention. Because the composition is simpler, the results[11] for (VI):

$$[(NH_3)_5OsN_2Os(NH_3)_5]^{5+}$$

(VI)

will be outlined, rather than those for (V), but it should be noted that the two species have quite similar properties.

As is expected on the basis of other experience, when N_2 is coordinated to Os(II), the N≡N stretching frequency is significantly lower than when it is attached to Os(III) – 2037 cm^{-1} for $(NH_3)_5OsN_2^{2+}$ [12] and 2217 cm^{-1} for $(NH_3)_5OsN_2^{3+}$.[13] However, in (VI), the N≡N stretch is virtually inactive in the IR, although it does appear in the Raman spectrum (1993 cm^{-1} in bromide salt). The observation that (VI) has a center of symmetry on the IR time scale places a lower limit of $\sim 10^{13}$ sec^{-1} on the rate of electron transfer. The evidence to be adduced suggests that the system is so strongly delocalized that the "rate of electron transfer" has lost physical meaning.

Electrochemical measurements on the system giving rise to (VI) yield the following results for E_f:

$$[3,3] \xrightarrow{> 1.04} [3,2] \xrightarrow{-0.16\,V} [2,2].$$

These values place a lower limit on the conproportionation constant of 10^{20}; i.e., the osmium ions, far from acting independently, interact strongly enough to stabilize 2[3, 2] with respect to [2, 2] by [3, 3] more than 26 kcal. That there is in this case an intrinsic stabilization of the [3, 2] state is shown by the fact that whereas $(NH_3)_5OsN_2^{3+}$ loses N_2 in aqueous solution at room temperature at a specific rate of 2×10^{-2} sec,[14] the dinitrogen-osmium bonds in (VI) and related species are indefinitely stable ((V) is produced in a solution heated at 70° for 36 hr). Thus Os(III) character has been lost from the osmium ions, and a new chemical entity is being dealt with.

In contrast to the systems described earlier, and others to be introduced, for both (V) and (VI) the NIR region is rich in transitions, at least 4 bands being discernable in the spectrum of (VI) between 1000 and 2100 nm. In addition, there is a strong band at 700 nm ($\epsilon = 4.0 \times 10^3$ mol^{-1} cm^{-1}), as well as bands at 260 (shoulder) and 238 nm. Most of the features of the spectrum that have been mentioned remain to be understood.

Intermediate Coupling

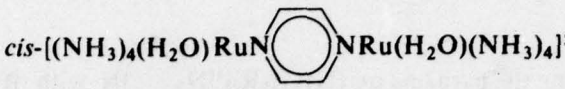
Even though species (I) is not fully understood, several significant observations have been made in the course of the numerous studies devoted to it and to related species.

Whatever the detailed nature of (I), it seems certain that the rate of electron transfer is rapid compared to solvent reorientation. This follows because the energy of the NIR band, which appears at 1580 nm in D_2O, is virtually independent of the nature of the solvent. Furthermore, vibration frequencies, which

ordinarily are distinct for Ru(II) and Ru(III) ammines, are averaged in (I). This was observed for the symmetric NH_3 rocking frequency by Creutz, and more thoroughly and convincingly documented by Beattie *et al.*[15] for a number of other frequencies.[16]

These observations appear to set a lower limit on the lifetime of a [3, 2] state of between 10^{-12} and 10^{-13} seconds. Finally, it should be mentioned that in common with the systems mentioned earlier, and in contrast to others, still to be mentioned, which are clearly valence trapped, the band is again abnormally narrow.

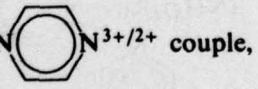
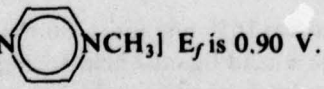
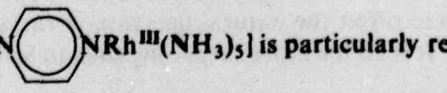
Even though, using the vibrational criterion, the system is valence delocalized, it appears that the interaction between the metal ions is quite weak; i.e., delocalization of the valences has done little to stabilize or modify the ground state. Thus the substitution lability[17] of H_2O in



is virtually the same as it is in

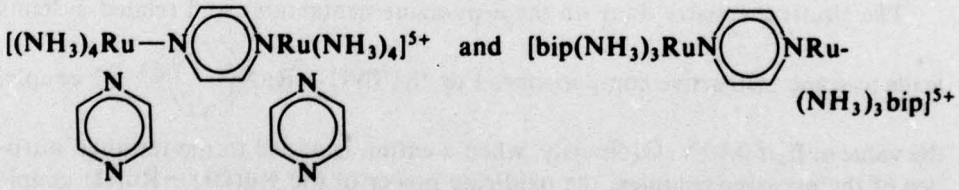


In the second case there is no possibility of modifying the properties of Ru(II) by valence delocalization (Rh(III) is in a low spin d^6 state and the species is very difficult to oxidize). Substitution in Ru(III) takes place much less rapidly than in Ru(II) and if Ru(II) in the *bis*-ruthenium ion acquired substantial Ru(III) character, a marked reduction in substitution rate would be expected. In this connection, it is important to remember that the uncertainty broadening for a lifetime even as short as 10^{-13} sec is only a fraction of a kilocalorie. Thus a system may be valence-delocalized in a practical sense, as is the case if the lifetime of a particular valence assignment is less than that corresponding to vibrational frequencies involved in charge trapping, and yet not have gained much in the way of electronic stabilization.

The electrochemistry done on the μ-pyrazine pentaamine and related systems leads to some instructive comparisons. For the  couple, the value of E_f is 0.49 V. Ordinarily, when a cation is added to the terminal nitrogen of the pyrazine complex, the oxidizing power of the Ru(III)—Ru(II) couple increases; thus for  E_f is 0.90 V. The measurement made with  is particularly relevant to assessing the interactions between the metal ions in the Ru—Ru case. Rhodium(III) is a d^6 system, and both the $Rh^{4+/3+}$ and $Rh^{3+/2+}$ couples are outside the range of poten-

tials being considered here, the former very strongly oxidizing and the latter, strongly reducing. The $Ru^{3+/2+}$ couple for the rhodium(III)-capped species has a value of E_f of 0.79 V, whereas E_f for the couple $[(NH_3)_5RuN\bigcirc NRu(NH_3)_5]^{6+/5+}$, which is identical to the rhodium(III)-capped couple, but now with an electron hole in the πd system, is 0.74. Thus the difference between the two systems suggests that the stabilization in the bis-ruthenium case ascribable to the presence in it of the electron hole amounts to only 0.05 volts or ca. 1.2 kcal. The value of E_f for the rhodium-bearing complex can usefully be compared also to the value for the $[(NH_3)_5RuN\bigcirc NRu(NH_3)_5]^{5+/4+}$ couple, measured as 0.37. If the effect of capping the pyrazine on $(NH_3)_5Ru^{II}N\bigcirc N$ with $Ru^{II}(NH_3)_5$ were simply a matter of positive charge, a value of perhaps 0.60 for the 5+/4+ couple would be expected (0.71 for the $Rh^{III}(NH_3)_5$-capped case). The fact that it is easier by more than 0.200 volt to extract an electron from the [2, 2] system than a purely inductive influence would allow suggests that there are electronic interactions that destabilize the [2, 2] state. This is shown more directly by the fact that Ru(II) is unique among the cations mentioned in lowering the reduction potential of the $(NH_3)_5RuN\bigcirc N^{3+/2+}$ couple from 0.49 to 0.37 V. An obvious source of these is the electronic repulsion that arises on delocalizing πd electrons from two centers into a common orbital on the π acid ligand. Thus the large value of K_c for (I)—4×10^6—appears to be less a matter of an inherent stability of the [3, 2] state than it is of an intrinsic instability of the [2, 2] (and perhaps the [3, 3]).

On partial substitution of NH_3 in (III) by π acid ligands, the character of the NIR band remains unchanged, but the band moves to lower energies. Thus for

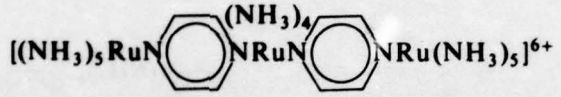


the band maxima are at 1650 nm and 1720 nm, respectively.[3b] This is in the direction expected if the π acid ligands help to make the coordination spheres about the ions equivalent; back-bonding, which is more important for the 2+ than for the 3+ state, tends to offset the natural decrease in radius accompanying increase in cationic charge. It is all the more surprising then to learn that



is a valence-trapped species.[18] The NIR band in D_2O has its maximum at 1240 nm. It is about 16% broader than the value calculated from Hush's Equation.[1] The band energy nicely follows the property $(1/n^2 - 1/D)$ for the five solvents studied and changes about 10% over the range of solvents used (lowest energy in $C_6H_5NO_2$, highest in D_2O), and thus the rate of electron transfer would appear to be less than 10^{12} sec^{-1}. Also significant for the issue of valence trapping is the observation that the centrosymmetric pyrazine stretch absent in [2,2] and [3,3] appears in the [3,2] species. This then sets an upper limit of $10^{12} - 10^{13}$ sec^{-1} on the rate of electron transfer. It is not clear at this stage whether valence trapping is a consequence of having four π acid groups on Ru(II) competing with the bridging ligand for πd electron density (this is expected to diminish the coupling between the centers) or whether it is a result of having chloride ion in the coordination sphere. The Ru(II)—Cl^- distance is expected to be considerably larger than the Ru(III)—Cl^- distance, and this may be an important factor in valence trapping.

Considerable work has been done with μ-pyrazine polynuclear species, which has included the synthesis of a linear hexanuclear molecule.[19] The only results obtained with such species that will be mentioned are some which bear on the question of electron transfer through a metal ion. The species



(VII)

shows[19] three oxidation stages.

$$[3,3,3] \xrightarrow{0.95} [3,2,3] \xrightarrow{0.51} [3,2,2] \xrightarrow{0.40} [2,2,2].$$

This assignment of oxidation states is unambiguous on the major point, that the central ruthenium is the last to be oxidized: this ruthenium bearing as it does two π acid ligands is expected to be 0.4–0.5 volts more difficult to oxidize than are the terminal ones, which are associated with a single π acid ligand. The NIR spectrum for the singly oxidized species is shown in FIGURE 1. It is quite clear that the band is composite when measured in D_2O as a solvent, and the rough resolution into two components attempted places one maximum at 8.7 kK and another at 5.9 kK. There is little doubt that the higher energy band corresponds to the unsymmetrical transition:

$$[2,3,2] \leftarrow [3,2,2]$$

The energy is high because to the Franck-Condon barrier must be added the difference in the equilibrium stability of the two species. This then leaves the low-energy transition as related to the symmetrical change

$$[2,2,3] \leftarrow [3,2,2].$$

We then have an example of electron transfer through a metal ion, despite the fact that the central Ru(II) has a rather stable closed electronic structure (πd^6 low spin). The point, however, is that the system is only "rather" stable. The state [2,3,2] lies only ca. 0.4 to 0.5 volts above the ground state [3,2,2] (or [2,2,3])

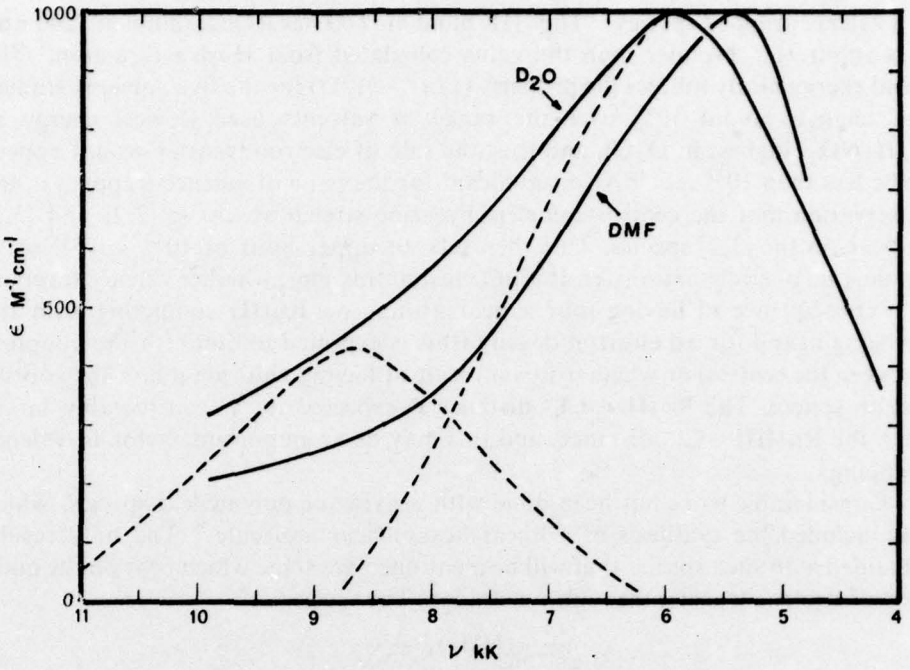


FIGURE 1. NIR absorption for $[(NH_3)_5RuN\langle\bigcirc\rangle N\ Ru\ N\langle\bigcirc\rangle NRu(NH_3)_5]^{7}$ in solvents as indicated. Dotted line represents attempt to resolve band for D_2O into two components.

and therefore can contribute significantly by mixing with the ground state. Supporting this interpretation are the observations made[20] with

$$[(NH_3)_5RuN\langle\bigcirc\rangle NRuN\langle\bigcirc\rangle NRu(NH_3)_5]$$

(VIII)

In this case there is no evidence of absorption for the 7+ in the NIR region at low energies. An essential difference between (VII) and (VIII) is that the central ruthenium in (VIII) is much harder to oxidize than in (VII). Thus the contribution of the state [2,3,2] to the ground state is less for the latter, diminishing the interaction between the terminal ruthenium cations, and the intensity of the end-to-end intramolecular transition.

WEAK COUPLING

One example of a valence-trapped system has already been described. The results for a rather extensive series of interrelated molecules, which provide some constructive comparisons, are presented in TABLE 1.

The intervalence bands are in each case of "normal" width, i.e., somewhat broader than calculated by the Hush Equation. The energies of the bands are solvent dependent, this variation being shown in FIGURE 2 for three bridging ligands that provide for equal separations of the metal ions. As far as the data go, they conform well to the requirements of theory for valence-trapped systems. It is especially gratifying that the slopes of the lines in FIGURE 2 are approximately equal, as theory requires if the metal-to-metal separations are the same in the three different molecules. Finally, in outlining group properties it should be mentioned that for none of the systems does the conproportionation constant exceed about 20, an observation consistent with the view that the coupling is weak in each of the separate stages of oxidation.

In general, the relative intensities of the NIR bands follow expectation, if for strong coupling, a conjugated bond system connecting the centers is important. Among the first four entries, the lowest intensity is observed for the third ligand

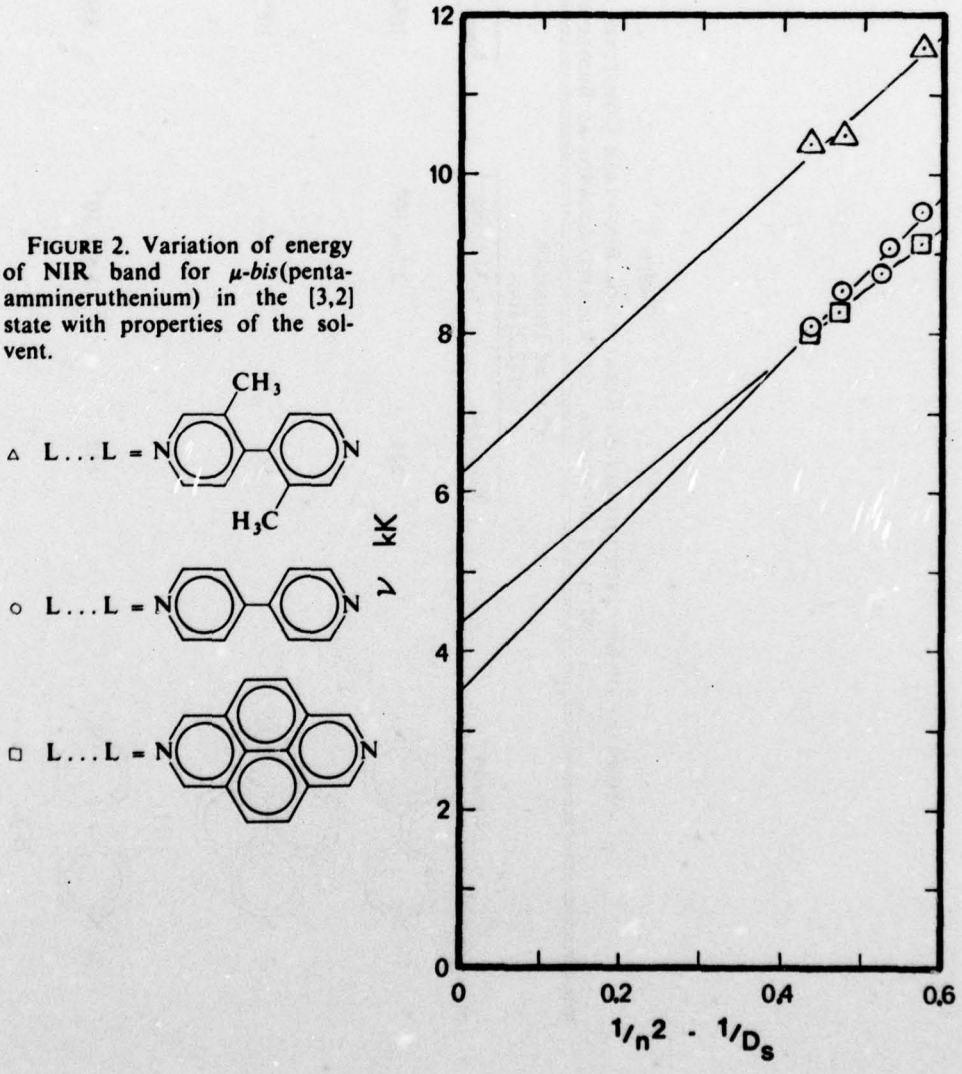
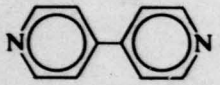
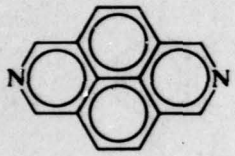
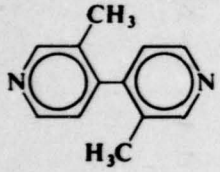
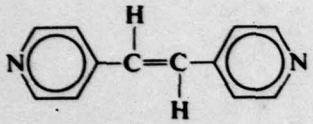
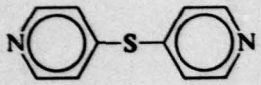
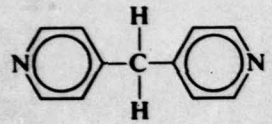
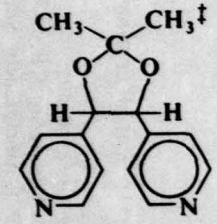


FIGURE 2. Variation of energy of NIR band for *μ-bis*(pentaammineruthenium) in the [3,2] state with properties of the solvent.

TABLE 1

SUMMARY OF SPECTROPHOTOMETRIC RESULTS FOR BINUCLEAR COMPLEXES OF RUTHENIUM AMMINES WITH 4,4′-BIPYRIDINE AND RELATED LIGANDS AS BRIDGING GROUPS

Ligand	$\pi^* \leftarrow \pi d$ Transition for [2,2] Ions		Intervalence Transition for [,3] Ions		Ref.
	λ_{max}, nm	ϵ, $M^{-1}\,cm^{-1}$	λ_{max}, nm	$\epsilon\dagger$, $M^{-1}\,cm^{-1}$	
1. 	521	2.7×10^4	1050	400	21
2. 	511	—	1090	450	22
3. 	437	1.6×10^4	860	90	22

4. 	547	2.9×10^4	960	400	22
5. 	465	2.2×10^4	855	70	22
6. 	—	—	825	~5	23
7. 	427	1.6×10^4	950	~6	24

†Calculated assuming that in an equimolar mixture of [2,2] and [3,3], the [2,3] species is formed to completion.
‡Meso form, which brings the metal atoms closer together than the alternate form.

shown, where, because of the location of the methyl groups, the two rings are obliged to be almost perpendicular. The diazapyrene system calls for special comment. The ligand was chosen because it was felt that being planar, the lowest unoccupied π^* orbital would be below that in 4,4′-bipyridine, where the rings are not coplanar. In the light of this expectation, the results summarized were astonishing but became less to when it was shown[25] that the lowest unoccupied π^* orbital for diazapyrene has the wrong symmetry to interact with the filled $d\pi$ orbitals of Ru(II). The lowest orbital of appropriate symmetry has an energy approximately that of 4,4′-bipyridine, with the rings at a torsional angle of 60°.

Where conjugation is interrupted by a saturated link—entries 5, 6, and 7—there is a substantial decrease in the intensity of the intervalence band, but an intervalence band still appears, and the mechanism by which electronic coupling takes place in such systems is a matter of interest. In the case of —S— bridging the two pyridine rings, at least three mechanisms come to mind: two invoke particular properties of the sulfur atom (i) contribution to the ground state by electron transfer from a p orbital of S to Ru(III), (ii) back-bonding, using unoccupied orbitals of appropriate symmetry on S; the third mechanism (iii) would involve direct ring-to-ring interactions. The fact that the intensity of the intervalence band is about as great for 7 as for 6 suggests that mechanism (iii) can operate. Coupling by a mechanism analogous to (i) would be strongly attenuated in 7 as compared to 6, and by mechanism (ii) would also be strongly attenuated, and mechanism (ii) in any case seems unrealistic for saturated carbon centers. Direct interaction between ruthenium ions needs to be considered but cannot apply to both 6 and 7. The Ru—Ru separation in 6, assuming normal bond angles is about 10 Å, while in 7 it is 7 Å.

Considerable effort is being expended currently in studying weak interactions.[26] These are interesting in their own right, and when sufficient data are collected, may be amenable to theoretical analysis. They are relevant also to concern with the role of bridging groups reactions involving net electron transfer, i.e., in oxidation reduction reactions.[22] Effort is being devoted to uncovering other systems analogous to malononitrile; *bis*-(4-pyridyl)methane may behave in a similar fashion if the oxidizing power of the $Ru^{3+/2+}$ couple is increased.[27] If the goal of preparing high molecular-weight species is to be achieved, the synthetic strategy used for the work outlined, which involves small sequential changes in structure, becomes inappropriate. What is needed is a planar metal containing unit, which is substitution labile in the 5th and 6th axial positions. Porphyrins meet these requirements but are often rather intractable preparatively. Other macrocycles may fill the stated need, and complexes with ruthenium(II) and (III) are being studied.[28]

Notes and References

1. Hush, N. S. 1967. Prog. Inorg. Chem. **8:** 391.
2. Robin, M. B. & P. Day. 1967. Adv. Inorg. Chem. Radiochem. **10:** 247.
3a. Creutz, C. & H. Taube. 1969. J. Amer. Chem. Soc. **91:** 3988.
3b. Creutz, C. & Taube, H. 1973. J. Amer. Chem Soc. **95:** 1086.
4. Cowan, D. O. & F. Kaufman. 1970. J. Amer. Chem. Soc. **92:** 219.
5. The criterion that will be used for valence delocalization is that the lifetime of a particular mixed valence state be shorter than the vibrational timescale.

6a. Tom, G. 1975. Ph.D. Thesis. Stanford Univ., Stanford, Calif.
6b. Tom, G. & H. Taube. 1975. J. Amer. Chem. Soc. **97:** 5310.
7. Ford, P. C. & R. E. Clarke. 1968. Chem. Commun. 1109.
8a. Krentzien, H. 1976. Ph.D. Thesis. Stanford Univ., Stanford, Calif.
8b. Krentzien, H. & H. Taube. 1976. J. Amer. Chem. Soc. **98:** 6379.
9. Ford, P. C., R. Gaunder, De F. P. Rudd & H. Taube. 1968. J. Amer. Chem. Soc. **90:** 1187.
10. Magnuson, R. H. & H. Taube. 1972. J. Amer. Chem. Soc. **94:** 7213.
11. Sen, J. To be published.
12. Allen, A. D. & J. R. Stevens. 1967. Chem. Commun. 1147.
13. J. Buhr. Research in progress.
14. Elson, C. M., J. Gulens, I. J. Itzkovitch & J. A. Page. 1970. Chem. Commun. 875.
15. Beattie, J. K., N. S. Hush & P. R. Taylor. 1976. Inorg. Chem. **15:** 992.
16. But see results of resonance Raman work: Strekas, T. C. & T. G. Spiro. 1976. Inorg. Chem. **15:** 974.
17. Isied, S. & H. Taube. 1976. Inorg. Chem. **15:** 3070.
18. Callahan, R. W. & T. J. Meyer. 1976. Chem. Phys. Letters **39:** 82.
19. von Kameke, A., G. Tom & H. Taube. 1978. Inorg. Chem. **17:**. In press.
20. Powers, M. J., R. W. Callahan, D. J. Salmon & T. J. Meyer. Inorg. Chem. **15:** 894.
21. Tom, G. M., C. Creutz & H. Taube. 1974. J. Amer. Chem. Soc. **96:** 7827.
22. Fischer, H., G. M. Tom & H. Taube. 1976. J. Amer. Chem. Soc. **98:** 5512.
23. Rieder, K. & H. Tuabe. 1977. J. Amer. Chem. Soc. **99:** 789.
24. Brown, G. M. Unpublished results.
25. Jacobs, R. & B. S. Hudson. Private communication.
26. Stein, C. Work in progress on cyclic *dithia* species.
27. Sutton, J. Research in progress.
28. Walker, D. & Y. Hung. Research in progress.

Discussion

Robin Clark (*University College, London, England*): The resonance Raman data on the ruthenium pyrazine mixed-valence dimer is now interpreted to imply that the compound is valence-delocalized.

Peter Day: I think that even in the pyrazine compound charge is trapped on some time-scale, possibly faster than the IR time scale in the sense that there is a visible transition that you briefly alluded to which is certainly the Ru^{II} to π^* charge transfer. Of course, that is an optical time-scale which is faster than the ^{IR} time-scale, and the existence of that band suggests that on this more rapid time-scale the Ru valence is trapped. Presumably, one should go to even faster time-scale measurements and higher energies and more closely reassess the XPS data to see whether the Ru valence is also trapped on that time-scale.

Taube: The XPS spectra obtained by Citrin [Citrin, P. H. 1973. J. Am. Chem. Soc. **95:** 6472.]† have been taken to indicate that two different kinds of ruthenium are present in the Creutz ion. Hush challenges this [Hush, N. S. 1975. Chem. Phys. **10:** 361.]† and points out that even in cases where the metals are equivalent you can have splitting of the state that is created when the electron is removed, and thus see two signals in the XPS.

†References added.

DESIGN AND SYNTHESIS OF MIXED-VALENCE COMPLEXES*

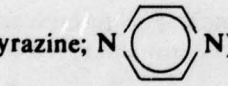
Thomas J. Meyer

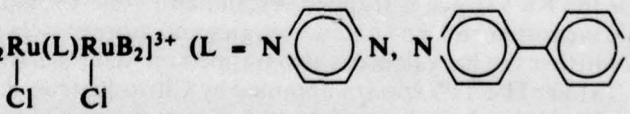
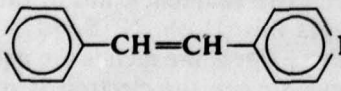
Department of Chemistry
The University of North Carolina
Chapel Hill, North Carolina 27514

INTRODUCTION

Many methods are known for preparing compounds where two or more metal sites are held together by strong chemical bonds (metal-metal or metal-ligand-metal). Mixed-valence compounds appear when a nonintegral number of electrons is reversibly gained or lost either from individual redox sites or from delocalized molecular orbitals. In mixed-valence compounds, the HOMO or redox levels are only partly occupied and intramolecular charge transfer between sites becomes of interest, as does the possibility of long-range intramolecular transfer in mixed-valence oligomers. The chemical bridge between sites usually provides the orbital pathway for electron transfer and it is established and can be varied systematically during the preparation of the material. In contrast to materials that rely on stacking or other solid-state effects, intramolecular transfer is determined mainly by the properties of the bridge and of the redox sites and can be controlled chemically. Environmental effects are important, but to a lesser degree.

PROPERTIES OF MIXED-VALENCE COMPLEXES

The review articles by Robin and Day[1] and by Hush[2] and Hush *et al.*[3] and the interest generated by the Creutz and Taube ion, $[(NH_3)_5Ru(pyz)Ru(NH_3)_5]^{5+}$ (pyz is pyrazine; ),[4] and by the biferrocenium ion $[(C_5H_5)Fe(C_5H_4—C_5H_4)Fe(C_5H_5)]^+$, studied initially by Cowan and his coworkers,[5] set the stage for further developments in mixed-valence chemistry. Much of the interest in the area has remained on these spin-paired d^5-d^6 systems because of their synthetic versatility. The work of my own group on these and other mixed-valence compounds has been summarized in three recent accounts.[6]

In the complexes $[B_2Ru(L)RuB_2]^{3+}$ (L =  ,  ; B is 2,2′-bipyridine), good evidence has

*Supported by the Army Research Office, Durham (N.C.) and by the National Science Foundation. Manuscript received June 13, 1977.

0077-8923/78/0313-0496 $1.75/1© 1978, NYAS

been obtained for discrete Ru(II) and Ru(III) sites having properties of related monomeric complexes of Ru(II) and Ru(III).[7,8] The appearance of Intervalence Transfer (IT) bands[2] (Equation 1) in the near infrared provides evidence for a slight electron delocalization from Ru(II) to Ru(III) in the ground state.

$$B_2ClRu^{II}(L)Ru^{III}ClB_2^{3+} \xrightarrow{h\nu} B_2ClRu^{III}(L)Ru^{II}ClB_2^{3+*} \qquad (1)$$

From the dependence of IT band energies on such factors as solvent environment[7,9] and distance between Ru(II) and Ru(III) sites,[8] it has been possible to show that the semiclassical theories developed by Marcus[10] and Hush[11] for thermal electron transfer and by Hush[2] for intervalence transfer work well for these systems. The barrier to electron transfer arises because metal-ligand bond strengths and distances commonly vary with oxidation state, and outer-sphere solvation energies are dependent on ion charge. In the absence of nuclear tunneling effects, differences in coordination environments between oxidation states require reorganization of outer and inner coordination spheres before electron transfer can occur.

The situation is similar in unsymmetrical complexes like $[(NH_3)_5Ru^{III}$-  $-Ru^{II}ClB_2]^{4+}$ where the site of oxidation is localized at the more easily reduced site.[12] However, the oxidation-state asymmetry induced by the differences in the inner coordination spheres makes electron transfer from Ru(II) to Ru(III) thermodynamicaliy unfavorable, which increases the barrier to electron transfer.

The extent of metal-metal interaction can be changed dramatically by variations in bridging or nonbridging ligands. The ion $[B_2ClRuORuClB_2]^{2+}$ undergoes reversible electron transfer to give mixed-valence +1 and +3 ions, but electron transfer occurs to and from delocalized levels rather than from individual Ru sites. Taube and his coworkers have concluded that delocalization is complete in the dimeric ions $[(NH_3)_5RuNCCNRu(NH_3)_5]^{5+}$ [13] and $[(NH_3)_5RuNCC(R)CNRu(NH_3)_5]^{4+}$ [14] and the pyrazine-bridged ion $[(NH_3)_5RuN$  $N-Ru(NH_3)_5]^{5+}$ is delocalized, or nearly so.[7,15]

Similar observations have been made in ferrocene chemistry.[16] In ions like $[(C_5H_5)Fe(C_5H_4-C\equiv C-C_5H_4)Fe(C_5H_5)]^+$ there appear to be localized redox sites and well-defined IT bands,[17] whereas the +1 and +2 *bis*(fulvalene) diiron cations are delocalized.[16,18]

The extent of delocalization represents a balance between the delocalization energy and the reorganizational energy required to make the two redox sites equivalent. For spin-paired d^5-d^6 systems, reorganizational barriers are characteristically low (e.g., 5–6 kcal/mole for $B_2ClRu^{II}N$  $NRu^{III}ClB_2^{3+}$ in acetonitrile[7]). Relatively subtle changes in the molecular structure are sufficient to change

the extent of delocalization and cause the transitions between localized and delocalized cases in closely related compounds.

If delocalization is slight, the rate constant for thermally activated intramolecular electron transfer is given by Equation 2.[19] In the absence of nuclear tunneling effects, the origin of the activation barrier can be

$$k = \nu_{et} \exp(-E_a/RT) \tag{2}$$

understood in terms of the treatments given by Marcus and Hush,[10,11,19] and E_a can be estimated from the energies of IT bands ($E_{op} \sim 4E_a$).[2] The frequency factor for electron transfer, ν_{et}, will depend on orbital overlap and the extent of delocalization, whether treated as a surface crossing, resonance, or electron tunneling process.

If there is unsymmetrical counterion packing in the solid state because of different charge types ($Ru^{II}—Ru^{III}$), there will be an additional contribution to E_a (and to E_{op}). Electron transfer then becomes an unsymmetrical process because of the "frozen" nature of the outer coordination spheres in the lattice. Similar effects are observed for higher mixed-valence oligomers in solution. In twice-oxidized 1,1′-terferrocene $(Fc—Fc—Fc)^{2+}$, the IT band is at higher energy than for $(Fc—Fc)^{+}$.[20] The transition (eq. 3) is energetically unsymmetrical because of unfavorable interactions between adjacent ferrocenium groups.[20] In $(Fc—Fc—Fc)^{2+}$ and in ions like $[(NH_3)_5Ru^{III}(pyz)Ru^{II}(bpy)_2(pyz)\text{-}Ru^{III}(NH_3)_5]^{8+}$,[21] intramolecular

$$Fc^+—Fc—Fc^+ \xrightarrow{h\nu} Fc^+—Fc^+—Fc^* \tag{3}$$

electron transfer along the chain must occur by electron hopping (2, 2, 3 → 2, 3, 2 → 2, 2, 3) where the first step, which is endergonic, is rate determining.

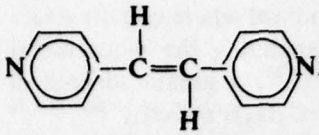
If delocalization is extensive, but not complete, localized oxidation state sites may exist, but the effects of delocalization must be taken into account. Delocalization amounts to partial charge transfer, and the oxidized and reduced sites become more nearly alike. Modified forms of the Marucs-Hush theory may apply to intramolecular electron transfer, but as the sites become more nearly alike, the activation barrier becomes "thinner" and the probability of electron transfer by quantum mechanical tunneling through the barrier must increase.

In delocalized compounds, a hole exists in the highest redox level, and since it is delocalized over both sites, there is no thermal barrier to electron transfer. Low-energy absorption bands can appear, but their origin is in electronic transitions between molecular levels and not in electron transfer between different sites. It is the latter feature which characterizes IT transitions.

Redox Sites

The building blocks for mixed-valence compounds are chemical sites which can both undergo reversible redox changes and be linked chemically. Several features emerge from the work on spin-paired d^5-d^6 ions which are of general value in the design of mixed-valence compounds.

In localized systems, the appearance of IT bands shows that directed, optical electron transfer can occur, even over long distances as in ions like $[B_2ClRu^{II}$-



.[8] The appearance of IT bands also provides evidence for the existence of the related thermally activated process.

There is a close connection between electron transfer processes and the properties of mixed-valence ions. The same factors that decrease activation barriers for intramolecular electron transfer will increase the probability of a delocalized description. Activation barriers can be minimized in two ways. For cases like the spin-paired d^5-d^6 ions, the inner coordination sphere environments are similar because there is no occupation of metal-based antibonding (e_g) orbitals. Contributions from inner-sphere reorganizations are small.[22] Large barriers will exist where there are changes in coordination number between different oxidation states (Cu(II)—Cu(I)) or where spin changes occur (Co(III)—Co(II)) which lead to significant differences in metal-ligand bond distances.[22] Contributions from outer-sphere reorganization can be minimized by using large ions and short internuclear separations between sites.[8] Delocalized cases will be favored when reorganizational energies are low and electronic interactions between the redox orbitals on different sites are high.

Stable mixed-valence complexes will be favored for second- and third-row transition metals where complexes are substitution-inert and where greater d-orbital extension can lead to stronger metal-metal interactions. The exception is in low oxidation state organometallic complexes where strong ligand fields lead to spin-pairing and coordinative stability even for first-row complexes, and some spectacular examples of reversible electron transfer behavior are known, e.g., $Cr(NCR)_6^{-/0/+/2+}$.[23]

Many chemical systems exhibit mixed-valence properties. They can differ in the nature of the chemical bridge, in the nature of the redox sites, or in the probable orbital pathway for intersite electronic interactions. All have their distinctive features, and several different types are discussed below, frequently with examples from my own work for convenience.

Metal-Metal Bonds

In compounds like $(CO)_5Mn—Mn(CO)_5$ there is a direct metal-metal bond between the metals. The bond strengths for typical metal-metal single bonds appear to fall in the range ~20–50 kcal/mole and the thermal chemistry of these compounds, including their redox reactions, is dominated by the metal-metal bond.[24] In structurally simple systems the metal-metal bond acts as both the chemical bridge and the site of redox, and oxidation-reduction processes frequently occur in net two electron changes with a breakdown in primary structure (Equation 4).

$$[(\pi\text{—}C_5H_5)Fe(CO)_2]_2 \xrightarrow[+2S]{-2e^-} 2(\pi\text{—}C_5H_5)Fe(CO)_2S^+ \qquad (4)$$

$$[(\pi\text{—}C_5H_5)Fe(CO)_2]_2 \xrightarrow{+2e^-} 2(\pi\text{—}C_5H_5)Fe(CO)_2^-$$

(S is solvent)

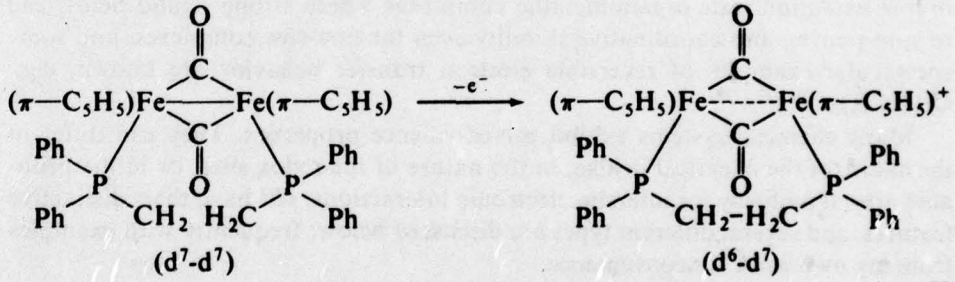
One-electron, mixed-valence compounds have been stabilized where certain structural features are present, including: a ligand bridge spanning the metal-metal bond as in $[(\pi\text{—}C_5H_5)Fe(CO)]_2(Ph_2PCH_2CH_2PPh_2)^{+/0}$ [25]; a greater degree of metal-metal bonding as in the tetrahedral cluster $[(\pi\text{—}C_5H_5)Fe(CO)]_4^{-/0/+/2+}$,[26] or in the multiple Re-Re bond in $Re_2Cl_8^{2-/3-}$;[27] or by stacking between square planar units in a crystal lattice.

There are many examples of reversible redox behavior based on metal-metal bonds even for first-row transition metal dimers like $[Fe(CO)_3P(CH_3)_2]_2^{0/-/2-}$ and $[(\pi\text{—}C_5H_5)Co(SCH_3)]_2^{+/0/-}$.[24,28] The relative contributions from metal-metal and metal-ligand orbitals to the redox levels are not always clear. However, the design of mixed-valence materials based on metal-metal bonds is very promising. Metal-metal bonds can be linked by chemical bridges (Equation 5),[29]

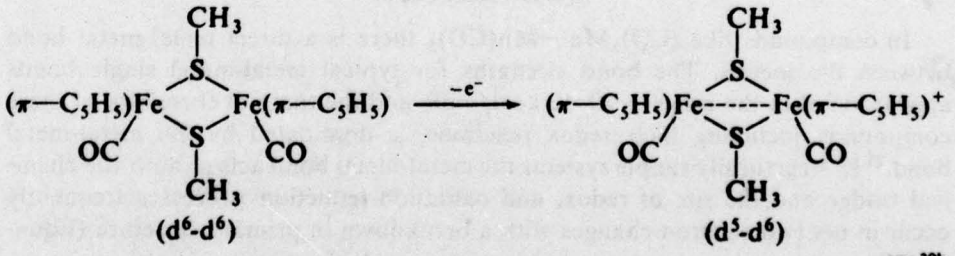
$$2(\pi\text{—}C_5H_5)_2Fe_2(CO)_4 + Ph_2PC{\equiv}CPPh_2 \rightarrow$$

$$(\pi\text{—}C_5H_5)_2Fe_2(CO)_3(Ph_2PC{\equiv}CPPh_2)Fe_2(CO)_3(\pi\text{—}C_5H_5) + 2CO \quad (5)$$

and metal-metal bonded compounds can have an extensive reversible redox chemistry, as shown by the five different redox forms of the tetrahedral cluster $[(\pi\text{—}C_5H_5)FeS]_4^{3+/2+/+/0/-}$.[30a] They are very flexible as redox sites in that electrons can be gained or lost from either metal-metal bonding or antibonding orbitals to give delocalized, mixed-valence ions in which there is a partial metal-metal bond (Equations 6, 7).



(6)[25]



(7)[30b]

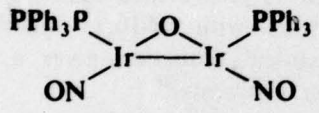
Small Inorganic Ions or Molecules as Bridges

The properties of oxo-bridged dimers like $[B_2ClRuORuClB_2]^{2+}$ and its +1(2, 3) and +3(3, 4) mixed-valence forms can be understood in terms of a

molecular orbital scheme involving delocalized levels having both $d\pi$(Ru) and p(O) character.[31] In this scheme the redox levels are antibonding and largely Ru in character. The strong Ru—Ru interaction is like a metal-metal bond in that it results in significant changes in chemical and physical properties compared to related monomers.[31] Higher aggregates containing oxo-bridges are known including the linear ruthenium red trimer $[(NH_3)_5RuORu(NH_3)_4ORu(NH_3)_5]^{6+}$ and its brown +7 form[32] and the multiple oxidation state clusters $[Ru_3O(CH_3CO_2)_6L_3]^{3+/2+/+0/-1}$ in which there are bridging acetates and an oxo-group bridging three rutheniums.[33,34]

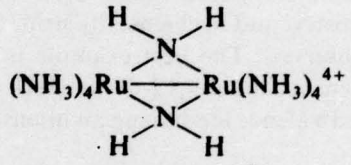
The extent of interaction between metal sites can depend critically on the metal and its orbital properties. Stronger interactions should occur for second- and third-row transition metals where the d orbital extension is greater. As examples, Magnuson and Taube have concluded that the mixed-valence ion *cis*-$[Cl(NH_3)_4OsN_2Os(NH_3)_5]^{4+}$ is delocalized even using dinitrogen as the bridging ligand,[35] whereas in oxo-bridged Fe(III)—Fe(III) dimers like $[B_2ClFeOClB_2]^{2+}$,[36,37] the interaction is significantly less than for Ru.[31] In the face-shared chloro-bridged dimers $M_2Cl_9^{3-}$, there is a weak intermetallic interaction for M = Cr (Cr—Cr = 3.1Å), a strong M—M bond for M = W (W—W = 2.4Å) and the molybdenum case is intermediate between the two others (Mo—Mo = 2.8Å).[38]

It is not always clear whether reversible redox processes and the orbital description of mixed-valence ions are metal-ligand-metal or metal-metal based. There are both ligand bridges and strong metal-metal bonds in the dimers I and II below.



(Ir-Ir 2.56 Å)

I



(Ru-Ru 2.62 Å)

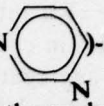
II

In the interesting "Ruthenium Blue" ions like $[(NH_3)_3RuCl_3Ru(NH_3)_3]^{+/2+/3+}$, the nature of the metal-metal interaction remains unclear in the absence of structural information.[41]

Aromatic Ligands as Bridges

Ligands like pyridine and its derivatives have lowlying π^* orbitals, and $d\pi \rightarrow \pi^*$ backbonding can be of importance in their complexes. The effect is well documented in pyridine complexes of Ru(II).[42-44] In bifunctional pyridines the π^* orbitals provide a pathway for interaction between redox sites. In mixed-valence Ru(II)—Ru(III) systems, the key to the interaction appears to be the extent of delocalization from Ru(II) to Ru(III) by $d\pi$ mixing with π^* orbitals of the bridging ligand.

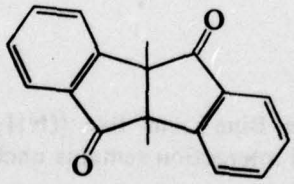
$d\pi$-π^* mixing is strongly affected by competitive backbonding to nonbridging ligands as shown by the much greater delocalization in $[(NH_3)_5Ru(pyz)Ru\cdot(NH_3)_5]^{5+}$ compared to $[B_2ClRu(pyz)RuClB_2]^{3+}$.[7] The importance of the orbital

properties of the bridging ligand can also be demonstrated.[45] Molar extinction coefficients at the IT λ_{max} in acetonitrile are 455 for $[B_2ClRu^{II}(pyz)Ru^{III}ClB_2]^{3+}$ but only ~20 for the analogous pyrimidine ()-bridged dimer.[46] For the latter ion, the Ru—Ru distance is shorter, but the nodal properties at the *meta*-positions of the bridging ligand are unfavorable for delocalization from Ru(II) to Ru(III).

In biferrocene, $(C_5H_5)Fe(C_5H_4—C_5H_4)Fe(C_5H_5)$, and its mixed-valence ion, ligand π and metal $d\pi$ levels are close in energy and π(ligand) → $d\pi$(metal) interactions are of importance, especially at oxidized ferrocenium sites.[16,18] For $[(C_5H_5)Fe(C_5H_4—C_5H_4)Fe(C_5H_5)]^+$ the situation is reversed from the $d\pi - \pi^*$ case in that delocalization effects depend on electron hole delocalization from the oxidized to the reduced site. This may be important, for example, for Ru-bpy complexes, which owe their stability and easily controllable synthetic chemistry (next section) to their electron-deficient nature. With the right bridging ligand it may be possible to change the nature of the interaction from electron to electron hole delocalization, and so to prepare delocalized Ru-bpy polymers.[47]

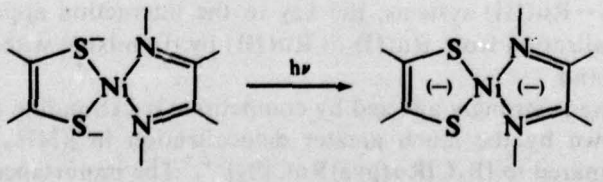
Ligands as Redox Sites

In the design of mixed-valence compounds, there has been a bias toward the use of metal-based redox sites. There is an extensive reversible organic redox chemistry, and in chemically bridged systems, typical mixed-valence behavior can be observed. The best example is from Mazur's work with *cis*-10,11-dimethyl-diphensuccindan-9,12-dione (**III**) where electrochemical reduction gives a −1 mixed-valence ion having an intense IT band in several solvents.[48]



III

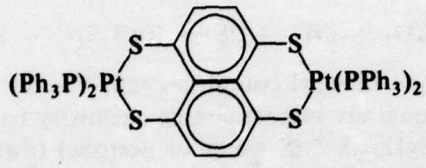
In fact, in appropriate metal complexes, the function of redox site and bridge may be reversed. In mixed dithiolene-α,α-diimine complexes of nickel, low-energy absorption bands appear that can be assigned to intraligand CT transitions with the metal ion used as bridge between electron donor and acceptor sites. (Equation 8).[49]



(8)

In the mercaptide-bridged trimer $[B_2ClRu(SPh)RuB_2(SPh)RuClB_2]^{2+}$ oxidation to the +3 and +4 mixed-valence ions has only a slight effect on both uv-visible spectra and on the Ru $3d_{5/2}$ binding energy by ESCA both of which are known to respond to oxidation of Ru(II) to Ru(III).[50] The mercaptide-bridged system may be similar to $[B_2ClRuORuClB_2]^{+/2+/3+}$ except with ligand- rather than metal-based orbitals lying highest. The question of a localized or delocalized description or of rates of intramolecular electron transfer must then depend on the extent of the interaction of the mercaptide groups through ruthenium, and not vice versa.

The extent of ligand-based, multiple redox chemistry can be extraordinary. The bridged tetrathiolene complex (IV) has been found to undergo four reversible one-electron oxidations which are based largely on the ligand as shown by epr.[51]

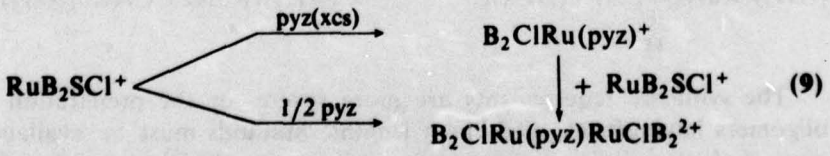


IV

Synthesis

The chemical variety in known mixed-valence systems is impressive, and clearly, many new compounds are accessible with the use of known synthetic chemistry. In most cases the key synthetic step is formation of the chemical bridge between redox sites. There seem to be nearly as many reactions and synthetic approaches as there are chemical systems, and I will limit my discussion to reactions that have proved useful in my own work. It is hoped they will illustrate strategies that may be of general value in the design and synthesis of new mixed-valence materials.

Synthetic control where one of the oxidation state sites is labile can be extremely difficult. Unless macrocyclic ligands are used, the inner coordination sphere around the labile site will be determined by its equilibrium properties in solution and not by prior synthesis. Spin-paired d^6 complexes (Ru(II), Co(III), Rh(III)....) avoid this problem, since they are usually substitution-inert. By incorporating labile solvent molecules, controlled substitutions can be carried out under mild conditions. For example, in (9) the solvent molecule (acetone or methanol) in RuB_2SCl^+ is weakly bound and is selectively displaced by added pyrazine



(9)

to give $RuB_2(pyz)Cl^+$. The pyrazine complex is itself a ligand and can react further with RuB_2SCl^+ to give the dimer. The dimer can also be prepared by a direct

coupling reaction when ½ the stoichiometric amount of pyrazine is added to the solvent-complex.

A number of reactions have been developed for d^6 complexes that lead to synthetically useful solvent complex intermediates. They include photoejection of CO, oxidation of metal-metal bonds (**10**), and reactions of coordinated ligands including the Ru-bpy examples shown below (**12–14**).

$$(\pi\text{—}C_5H_5)_2Fe_2(CO)_4 + 2S \xrightarrow{-2e^-} 2(\pi\text{—}C_5H_5)Fe(CO)_2S^+ \quad (10)^{52}$$

$$Co(NH_3)_5N_3^{2+} + S + NO^+ \rightarrow Co(NH_3)_5S^{3+} + N_2 + N_2O \quad (11)^{53}$$

$$RuB_2(NO)Cl^{2+} + N_3^- + S \rightarrow RuB_2SCl^+ + N_2 + N_2O \quad (12)^{54}$$

$$RuB_2(N_3)_2^+ + S \rightarrow RuB_2(N_3)S^+ + 3/2\,N_2 \quad (13)^{55}$$

$$RuB_2CO_3 + 2H^+ + 2S \rightarrow RuB_2S_2^{2+} + H_2O + CO_2 \quad (14)^{56}$$

The reaction involving nitrosyl complexes (**12**) has been especially useful in Ru-bpy chemistry. Of equal use in pentaamine chemistry have been displacement reactions based on $Ru(NH_3)_5S^{2+}$ (S water or acetone) (Equations 15, 16) which have been exploited most notably by Taube's group.

$$2Ru(NH_3)_5H_2O^{2+} + N\bigcirc\!\!\bigcirc N \rightarrow (NH_3)_5RuN\bigcirc\!\!\bigcirc NRu(NH_3)_5^{4+} + 2H_2O \quad (15)^4$$

$$2Ru(NH_3)_5S^{2+} + RuB_2(pyz)_2^{2+} \rightarrow (NH_3)_5Ru(pyz)RuB_2(pyz)Ru(NH_3)_5^{6+} + 2S \quad (16)^{21}$$

Labile Ru(II) intermediates have also been of value in the oxidative preparation of oxo-bridged dimers (**17**). In some systems a metal-metal electronic interaction can

$$4Ru(NH_3)_5S^{2+} + O_2 \rightarrow 2(NH_3)_5RuORu(NH_3)_5^{4+} \quad (17)^{57}$$

be "turned-on" or enhanced by reactions at the bridge following dimer formation as in reactions 18 and 19 from Taube's work.

$$(NH_3)_5RuNH_2CH_2CH_2NH_2Ru(NH_3)_5^{4+} \xrightarrow{-4e^-} (NH_3)_5RuNCCNRu(NH_3)_5^{4+} + 4H^+ \quad (18)^{13}$$

$$(NH_3)_5RuNC(R)CNRu(NH_3)_5^{5+} \xrightarrow{-H^+} (NH_3)_5RuNCCCNRu(NH_3)_5^{4+} \quad (19)^{14}$$

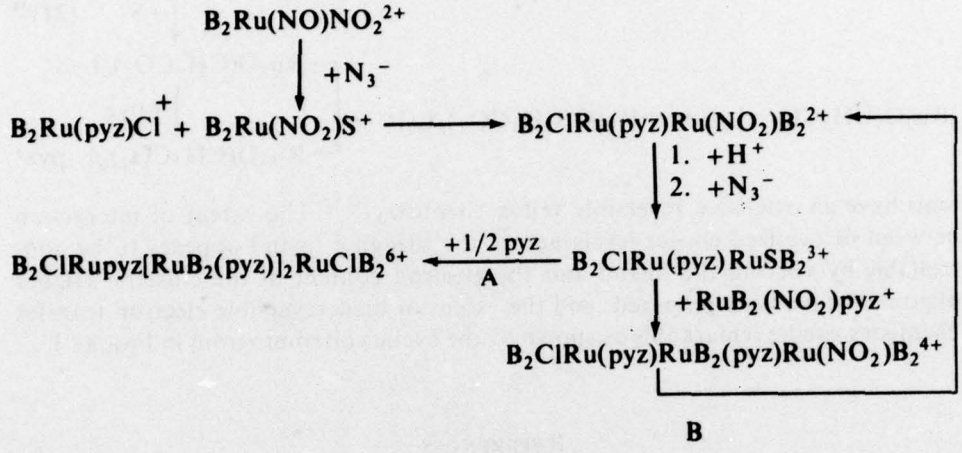
(R = H)

The synthetic requirements are more severe for the preparation of higher oligomers having controlled chain lengths. Methods must be available for the sequential, stepwise preparation of complexes in which substitution at two coordination sites can be controlled independently. For Ru-bpy complexes, the combination of reaction 12 and the known conversion of bound nitro into nitrosyl groups by acid (**20**) provide the necessary synthetic chemistry for activating co-

ordination sites to stepwise substitution.

$$2H^+ + RuB_2NO_2Cl \rightarrow RuB_2(NO)Cl^{2+} + H_2O. \qquad (20)^{58}$$

As shown in the scheme below, a series of ligand-bridged Ru-bpy polymers have been prepared based on the nitronitrosyl chemistry.[59] Polymer chain lengths can be increased by direct coupling of solvent complex intermediates (reaction A in the Scheme) or by coupling reactions using $RuB_2(NO_2)pyz^+$; the attached $Ru\text{-}NO_2$ group can always be recycled through the scheme (reaction B).



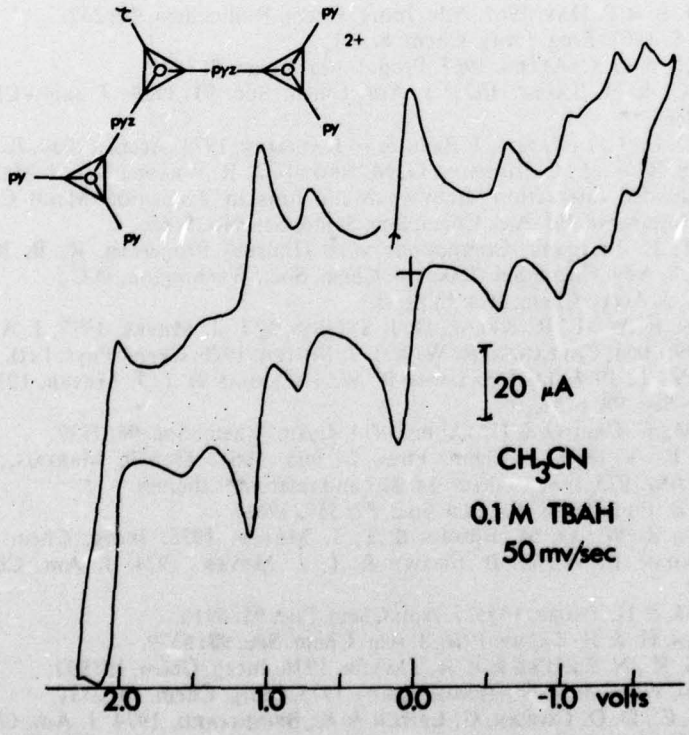
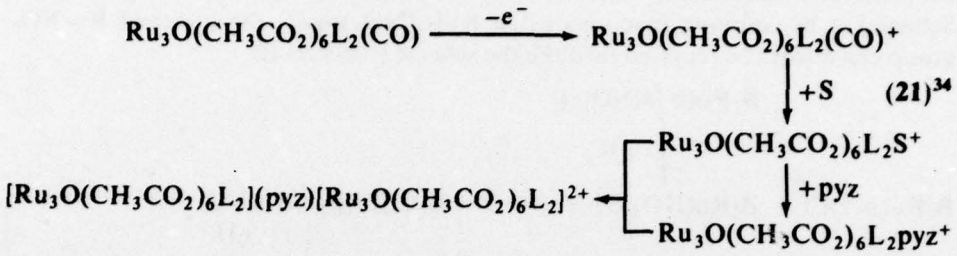


FIGURE 1. Cyclic voltammogram of $[(py)_2Ru_3O(CH_3CO_2)_6(pyz)Ru_3O(CH_3CO_2)_6(CO)(pyz)Ru_3O(CH_3CO_2)_6(py)_2]^{2+}$ in acetonitrile.

Complexes containing as many as six ruthenium sites have been prepared using related sequences of reactions.[59]

Similar methods have been applied to the triangular, oxo-bridged clusters $Ru_3O(CH_3CO_2)_6L_3$. CO is firmly bound in the neutral clusters but easily lost in the +1 ions which provides the basis for the reactions in (**21**). The cluster sys-



tems have an extensive reversible redox chemistry.[34,57] The extent of interaction between delocalized cluster levels across the bridging ligand appears to be controllable by varying the ligand and the electron content of the clusters. Higher oligomers have been prepared, and the extent of their reversible electron transfer chemistry can be remarkable as shown by the cyclic voltammogram in FIGURE 1.

REFERENCES

1. ROBIN, M. B. & P. DAY. 1967. Adv. Inorg. Chem. Radiochem. **10:** 247.
2. HUSH, N. S. 1967. Prog. Inorg. Chem. **8:** 391.
3. HUSH, N. S. & G. C. ALLEN. 1967. Prog. Inorg. Chem. **8:** 357.
4. CREUTZ, C. & H. TAUBE. 1973. J. Am. Chem. Soc. **91:** 3988; J. Am. Chem. Soc. **95:** 1086.
5. COWAN, D. O., C. LEVANDA, J. PARK & F. KAUFMAN. 1973. Accts. Chem. Res. **6:** 1.

6a. CALLAHAN, R. W., E. C. JOHNSON, G. M. BROWN, T. R. WEAVER & T. J. MEYER. 1975. *In* Extended Interactions Between Metal Ions in Transition Metal Complexes. L. V. Interrante, Ed. Am. Chem. Soc. Symp. Ser. No. **5:** 66;

b. MEYER, T. J., Inorganic Compounds with Unusual Properties, R. B. King, Ed.: Chap. 7. Adv. Chem. Ser. **150.** Am. Chem. Soc., Washington, D.C.;

c. MEYER, T. J. Accts. Chem. Res. In press.

7. CALLAHAN, R. W., F. R. KEENE, D. J. SALMON & T. J. MEYER. 1977. J. Am. Chem. Soc. **99:** 1064; CALLAHAN, R. W. & T. J. MEYER. 1976. Chem. Phys. Lett. **39:** 82.
8. POWERS, M. J., 1976. D. J. SALMON, R. W. CALLAHAN & T. J. MEYER. 1976. J. Am. Chem. Soc. **98:** 6731.
9. TOM, G. M., C. CREUTZ & H. TAUBE. 1974. J. Am. Chem. Soc. **96:** 7827.
10. MARCUS, R. A. 1956. J. Chem. Phys. **24:** 966; 1965. **43:** 679; MARCUS, R. A. & N. SUTIN. 1975. Inorg. Chem. **14:** 213 and references therein.
11. HUSH, N. S. 1961. Trans. Faraday Soc., **57:** 557 (1961).
12. CALLAHAN, R. W., G. M. BROWN & T. J. MEYER. 1975. Inorg. Chem. **14:** 1443; CALLAHAN, R. W., G. B. BROWN & T. J. MEYER. 1974. J. Am. Chem. Soc. **96:** 7829.
13. TOM, G. M. & H. TAUBE. 1975. J. Am. Chem. Soc. **91:** 5310.
14. KRENTZIEN, H. & H. TAUBE. 1976. J. Am. Chem. Soc. **98:** 6379.
15. BEATTIE, J. K., N. S. HUSH & P. R. TAYLOR. 1976. Inorg. Chem. **15:** 992.
16. MORRISON, W. H. & D. N. HENDRICKSON. 1975. Inorg. Chem. **14:** 2331.
17. LEVANDA, C., D. O. COWAN, C. LEITCH & K. BECHGAARD. 1974. J. Am. Chem. Soc. **96:** 6789.

18. KIRCHNER, R. F., G. H. LOEW & U. T. MUELLER-WESTERHOFF. 1976. Inorg. Chem. **15:** 2665.
19. SUTIN, N. 1973. *In* Inorganic Biochemistry. Vol. 2. G. L. Eichhorn, Ed.: 611. Elsevier. New York, N. Y.
20. BROWN, G. M., T. J. MEYER, D. O. COWAN, C. LEVANDA, F. KAUFMAN, P. V. ROLING & M. D. RAUSCH. 1975. Inorg. Chem. **14:** 506.
21. POWERS, M. J., R. W. CALLAHAN, D. J. SALMON & T. J. MEYER. 1976. Inorg. Chem. **15:** 894.
22. HAIR, N. J. & J. K. BEATTIE. 1977. Inorg. Chem. **16:** 245.
23. ESSENMACHER, G. J. & P. M. TREICHEL. 1977. Inorg. Chem. **16:** 800.
24. MEYER, T. J. 1975. Prog. Inorg. Chem. **19:** 1.
25. FERGUSON, J. A. & T. J. MEYER. 1972. Inorg. Chem. **11:** 631; FERGUSON, J. A. & T. J. MEYER. 1971. Chem. Commun. 1544; HAINES, R. J. & A. L. DUPREEZ. 1972. Inorg. Chem. **11:** 330.
26. FERGUSON, J. A. & T. J. MEYER. 1972. J. Am. Chem. Soc. **94:** 3409.
27. COTTON, F. A. & E. PEDERSEN. 1975. Inorg. Chem. **14:** 383.
28. DESSEY, R. E. & L. A. BARES. 1972. Accts. Chem. Res. **5:** 415 and references therein.
29. CARTY, A. J., A. EFRATY, T. W. NG & T. BIRCHALL. 1970. Inorg. Chem. **9:** 1263.
30a. TRIN-TOAN, B. K. TEO, J. A. FERGUSON, L. F. DAHL & T. J. MEYER. 1977. J. Am. Chem. Soc. **99:** 408 (1977);
30b. CONNELLY, N. G. & L. F. DAHL. 1970. J. Am. Chem. Soc. **92:** 7472.
31. WEAVER, T. R., T. J. MEYER, S. A. ADEYEMI, G. M. BROWN, R. P. ECKBERG, W. E. HATFIELD, E. C. JOHNSON, R. W. MURRAY & D. UNTEREKER. 1975. J. Am. Chem. Soc. **97:** 3039.
32. EARLY, J. E. & T. FEALEY. 1973. Inorg. Chem. **12:** 323.
33. SPENCER, A. & G. WILKINSON. 1972. J. Chem. Soc. Dalton Trans: 1570.
34. WILSON, S. T., R. F. BONDURANT, D. J. SALMON & T. J. MEYER. 1975. J. Am. Chem. Soc. **97:** 2285.
35. MAGNUSON, R. H. & H. TAUBE. 1977. J. Am. Chem. Soc. **94:** 7213.
36. LEWIS, J., F. E. MABBS & A. RICHARDS. 1967. J. Chem. Soc. A: 1561.
37. MURRAY, K. S. 1976. Coord. Chem. Rev. **12:** 1.
38. SAILLANT, R. & R. A. D. WENTWORTH. 1968. Inorg. Chem. **7:** 1606.
39. CARTY, P., A. WALKER, M. MATTHEWS & G. J. PALENIK. 1969. Chem. Commun. 1374.
40. FLOOD, M. T., R. F. ZIOLO, J. E. EARLY & H. B. GRAY. 1973. Inorg. Chem. **12:** 2153.
41. MERCER, E. E. & L. W. GRAY. 1972. J. Am. Chem. Soc. **94:** 6476.
42. TAUBE, H. 1973. Survey Prog. Chem. **6:** 1.
43. BOWDEN, W. L., W. F. LITTLE, D. J. SALMON & T. J. MEYER. 1975. J. Am. Chem. Soc. **97:** 6897.
44. SALMON, D. J. 1976. Ph.D. Dissertation. University of North Carolina. Chapel Hill, N. C.
45. FISCHER, H., G. M. TOM & H. TAUBE. 1976. J. Am. Chem. Soc. **98:** 5512.
46. POWERS, M. J. & T. J. MEYER. Inorg. Chem., in press.
47. SULLIVAN, B. P. In preparation.
48. MAZUR, S., C. STREEKUMAR & A. H. SCHROEDER. 1976. J. Am. Chem. Soc. **98:** 6713.
49. MILLER, T. R. & I. G. DANCE. 1973. J. Am. Chem. Soc. **95:** 6970.
50. JOHNSON, E. C. 1975. Ph.D. Dissertation. University of North Carolina. Chapel Hill, N. C.
51. TEO, B. K., F. WUDL, J. H. MARSHALL & A. KRUGER. 1977. J. Am. Chem. Soc. **99:** 2349.
52. JOHNSON, E. C., N. WINTERTON & T. J. MEYER. 1972. Inorg. Chem. **10:** 1673; BROWN, M. L., J. L. CRAMER, J. A. FERGUSON, N. WINTERTON & T. J. MEYER. 1972. J. Am. Chem. Soc: **94:** 8707.
53. HURST, J. K. & H. TAUBE. 1968. J. Am. Chem. Soc. **90:** 1174.
54. MILLER, F. J. & T. J. MEYER. 1971. J. Am. Chem. Soc. **93:** 1294; ADEYEMI, S. A., F. J. MILLER & T. J. MEYER. 1972. Inorg. Chem. **11:** 994.
55. BROWN, G. M., R. W. CALLAHAN & T. J. MEYER. 1975. Inorg. Chem. **14:** 1914.
56. SULLIVAN, B. P. & S. A. ADEYEMI. Unpublished results.
57. BAUMANN, J. In preparation.

58. GODWIN, J. B., N. WINTERTON & T. J. MEYER. 1970. Chem. Commun. 872; GODWIN, J. B. & T. J. MEYER. 1971. Inorg. Chem. **10:** 2150.
59. ADEYEMI, S. A., J. N. BRADDOCK, G. M. BROWN, J. A. FERGUSON, F. J. MILLER & T. J. MEYER. 1972. J. Am. Chem. Soc. **94:** 300; ADEYEMI, S. A., E. C. JOHNSON, F. J. MILLER & T. J. MEYER. 1973. Inorg. Chem. **12:** 2371.

SYNTHESIS, STRUCTURE, AND CONDUCTIVITY OF NEW ONE-DIMENSIONAL TETRACYANOPLATINATES CONTAINING FLUORINE*

Jack M. Williams and Arthur J. Schultz

Chemistry Division, Argonne National Laboratory
Argonne, Illinois 60439

The numerous experimental and theoretical studies of inorganic one-dimensional conductors in the past eight to ten years have, for the most part, concentrated on the metal-chain systems containing platinum.[1] The focus of this work has been the prototype, "linear" chain conductor, $K_2[Pt(CN)_4]Br_{0.3} \cdot 3H_2O$, KCP(Br).[2] The corresponding "cation deficient" tetracyanoplatinate (TCP) salt $K_{1.75}[Pt(CN)_4] \cdot 1.5H_2O$, K(def)TCP, contains a "bent" Pt atom chain. We have studied both KCP(Br)[2] and K(def)TCP[3] by neutron diffraction methods and have reviewed the overall field elsewhere.[1] The partially oxidized TCP systems all exhibit high electrical conductivity parallel to the Pt chain ($\sigma \simeq 100 - 830$ $\Omega^{-1}\,cm^{-1}$) but show gradual conductivity loss as the temperature is lowered.

A major difficulty that has plagued investigators in this field has been the genuine paucity of new materials available for study. In the case of square-planar platinum complexes, with electron-rich cyanide ligands, no new derivatives have been reported since the work of Levy[4] more than 65 years ago.

It has been our aim to attempt preparation of new TCP complexes with Pt-Pt distances less than those previously known [2.87 Å in KCP(Cl)[5]] and with degrees of partial oxidation outside of the narrow range of 0.25–0.30 enclosed by K(def)TCP and KCP(Cl). In addition to studying the relative electrical conductivities of these materials, other properties, such as interchain coupling and its effect on the metal-insulator transition temperature, could also be investigated. To this end we will discuss our synthetic, structural, and electrical conductivity research into totally new TCP systems which contain bifluoride $(FHF)^-$ and fluoride F^- ions in the crystal lattice. The newly prepared systems are summarized in TABLE 1 and are unique in that within the K^+, Rb^+, and Cs^+ series, (1) the *DPO* can vary from 0.19 to 0.40 and at *DPO* = 0.40 the shortest Pt-Pt spacings [2.80 Å in Rb^+ and 2.83 Å in Cs^+] yet observed in any POTCP salt are obtained, (2) *different* Pt-Pt chain distances may be produced while maintaining the *same* anion $(FHF)^-$ and cation (Cs^+ or Rb^+), and (3) the first *anhydrous* POTCP salts have been prepared which may promote the use of these materials in practical applications.

$Rb_2[Pt(CN)_4](FHF)_{0.40}$, RbCP(FHF)

The preparative methods and the crystal and molecular structure for *anhydrous* $Rb_2[Pt(CN)_4](FHF)_{0.40}$ are given below.

*Research performed under the auspices of the Division of Basic Energy Sciences of the U.S. Department of Energy. The work of A.J.S. was partly supported by the National Science Foundation (grant CHE76-07409). Manuscript received June 13, 1977.

0077-8923/78/0313-0509 $1.75/1© 1978, NYAS

TABLE 1
NEW FLUORINE-CONTAINING PARTIALLY OXIDIZED TETRACYANOPLATINATE ONE-DIMENSIONAL CONDUCTORS

Compound	Pt(*DPO*)*	Pt-Pt Distance (Å)	Color	Reference
$K_2[Pt(CN)_4](FHF)_{0.30} \cdot 3H_2O$	0.30	2.92	reddish-bronze	7
$Rb_2[Pt(CN)_4](FHF)_{0.40}$	0.40	2.80	gold	8
$Rb_2[Pt(CN)_4](FHF)_{0.26} \cdot 1.67H_2O$	0.26	2.89	greenish-bronze	9
$Cs_2[Pt(CN)_4](FHF)_{0.39}$	0.39	2.83	reddish-gold	10
$Cs_2[Pt(CN)_4](FHF)_{0.23}$	0.23†	2.87	reddish-bronze	11
$Cs_2[Pt(CN)_4]F_{0.19}$	0.19†,‡	2.88	reddish-gold	12

*Degree of partial oxidation.

†Based on the Pt-Pt separation, the *DPO* determined by elemental F analyses appears anomalous both with respect to the trend observed in other TCP complexes and to the values calculated for the *DPO* by using Pauling's Equation.[6]

‡This is the first known preparation of a F^- containing POTCP salt, and the structure determination is presently under way.

Preparation. Anhydrous RbCP(FHF) has been prepared to date by an electrolytic[8] procedure only. In this procedure[8] 1.08 g of $Rb_2[Pt(CN)_4] \cdot 1.5H_2O$, 3 ml of concentrated HF, and 2.0 g of RbF are added to 6 ml of distilled H_2O. The solution is electrolyzed at 1.5 V in a polyethylene beaker with Pt electrodes over a period of 24 hours. Needle-shaped crystals of RbCP(FHF) up to 5 mm in length are grown in this manner. The lustrous metallic gold-colored crystals have been shown to be anhydrous by thermal gravimetric analysis and as a result of the crystal structure determination (*vide infra*).

Crystal and Molecular Structure. The crystal structures of $M_2[Pt(CN)_4](FHF)_{\sim 0.40}$, M = Cs and Rb, have been determined by x-ray diffraction.[13] These

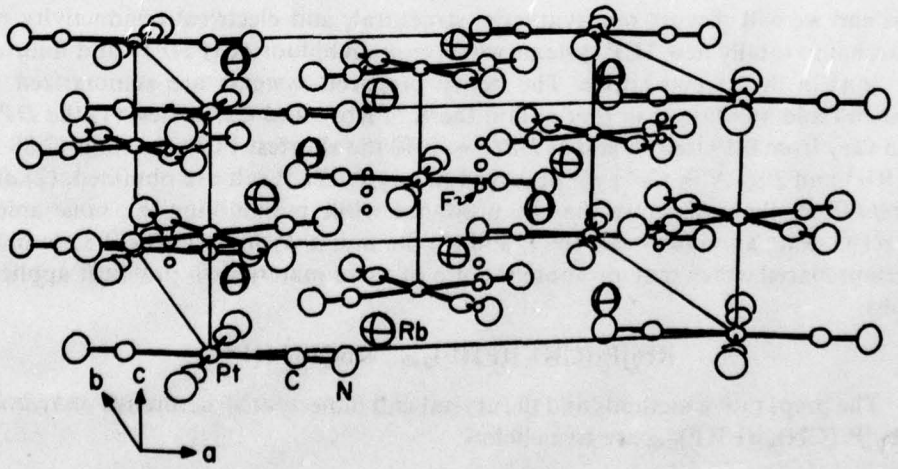


FIGURE 1. A perspective view of the unit cell of $Rb_2[Pt(CN)_4](FHF)_{0.40}$. The small circles are the partially occupied fluorine positions. The thermal ellipsoids of the other atoms are drawn with a scale of 50% probability.

two materials are isostructural, crystallize in the body-centered tetragonal space group *I4/mcm*, and are structurally *different* from KCP(Br, Cl) (space group *P4mm*). They constitute new structure types in the POTCP-KCP(X) series and in addition are the first to contain a triatomic anion, $(FHF)^-$.

The crystal structures, as shown in FIGURE 1, consist of columnar chains of square-planar $Pt(CN)_4^{-1.60}$ groups that stack parallel to *c*. The derived Pt-Pt distance (*c*/2) of 2.798(1) Å for M = Rb and 2.833(1) Å for M = Cs are the

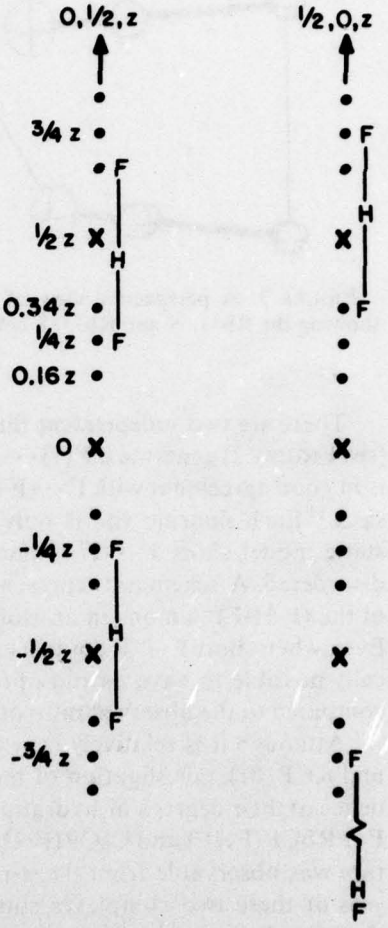


FIGURE 2. Schematic representation of the possible positions and orientations of $(F\text{-}H\text{-}F)^-$ anions along two parallel chains. The positions of the hydrogen atoms have not been located from the x-ray data. Therefore, the linearity of the $(F\text{-}H\text{-}F)^-$ ion or the symmetrical location of H between F atoms has not been experimentally determined. The dots represent all partially occupied F sites; the crosses indicate only the coordinates where $z = 0, \pm 1/2$.

shortest of any known POTCP salt and are very close to the 2.77 Å internuclear separation in Pt metal itself. In KCP(Br)[2] and KCP(Cl)[5] the Pt-Pt separations are 2.88 ± 0.01 Å and the torsion angle between neighboring TCP groups is constrained by symmetry to be 45°. At this angle, steric interactions between cyano ligands on neighboring TCP groups are minimized, although in RbCP(FHF) the torsion angle is 49.2(6)°. Therefore, intermolecular ligand-ligand repulsion is *not* the limiting factor in the case of this short Pt-Pt separation of 2.80 Å, and it is conceivable that this distance could be reduced even further.

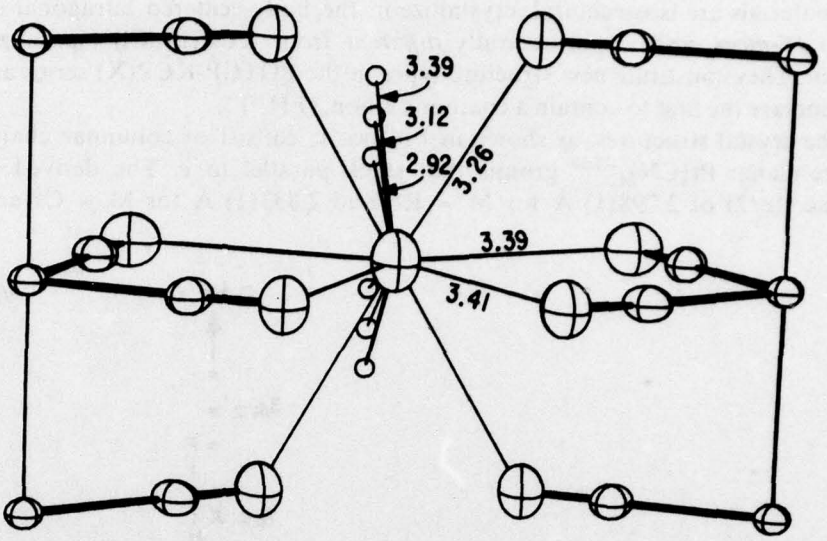


FIGURE 3. A perspective view of the coordination sphere about the rubidium cation, showing the Rb···N and Rb···F contacts.

There are two independent fluorine positions such that symmetry-related sites (see FIGURE 2) generate a F(1)···F(2) distance of 2.27(8) Å in RbCP(FHF). This is in good agreement with F···F distances found in simple alkali metal bifluoride salts.[14] Each fluorine site is only partially occupied, and since for any assumed static model short F···F contacts must be prohibited, the $(F\text{-}H\text{-}F)^-$ group is disordered. A schematic representation of the possible positions and orientations of the $(F\text{-}H\text{-}F)^-$ anions in an isolated region of the crystal is shown in FIGURE 2. Even when short F···F contacts are excluded, however, it is still crystallographically possible to have a ratio of $(FHF)^-$ anions to Pt atoms as high as 0.5:1, as compared to the observed ratio of 0.4:1.

Although it is relatively easy to grow large, well-formed crystals of KCP(Cl) and KCP(Br), investigation of their physical properties is hindered by the dependence of their degrees of hydration on atmospheric and temperature conditions.[15] For RbCP(FHF) and CsCP(FHF), no evidence of a water site in the crystal structure was observable from the x-ray data. Furthermore, thermogravimetric analyses of these two complexes show no evidence for the presence of water. We therefore believe that these materials are the first known POTCP complexes that are completely anhydrous, and this property may facilitate their use for practical applications.

In the absence of interchain hydrogen bonding as a means for crystal stabilization, the binding force must be due to the stronger $Rb^+\cdots X^-$ Coulombic interactions. The short contacts shown in FIGURE 3 range from 3.26 Å to 3.41 Å for Rb···N and 2.92 Å to 3.39 Å for Rb···F.

Polarized Specular Reflectance and Electrical Conductivity. From polarized specular reflectance measurements on single crystals of RbCP(FHF) and CsCP(FHF), it has been established[16] that a well-defined plasma edge exists and that they are indeed one-dimensional metals. Although very preliminary, our four-

probe conductivity measurements at room temperature indicate that the conductivity of CsCP(FHF) could be approximately twice that of KCP(Cl). Low-temperature conductivity measurements now in progress[17] show that CsCP(FHF) does not exhibit the same rapid conductivity decrease with decreasing temperature as do KCP(Br) and KCP(Cl). It therefore appears that, as one might expect, among the POTCP complexes increased conductivity parallels shortening in the Pt-Pt intrachain distance.

$$K_2[Pt(CN)_4](FHF)_{0.30} \cdot 3.0H_2O, \quad KCP(FHF)$$

The preparation and crystal structure of KCP(FHF) are presented below.

Preparation. Hydrated KCP(FHF) may be prepared either by hydrogen peroxide oxidation or by electrolysis.[7] Using the electrolytic procedure, 1.55 g of $K_2[Pt(CN)_4] \cdot 3H_2O$, 1.51 g of KF, and 3 ml of conc. HF are added to 6 ml of distilled water. After electrolysis for ~ 2 hours at 1.5 V, long, needle-shaped crystals are produced. The crystals have a metallic reddish-bronze luster and are stored over a saturated NaCl solution to prevent dehydration.

Crystal and Molecular Structure. From an x-ray diffraction single-crystal structure investigation[18] of hydrated KCP(FHF), we have determined that the K salt is *not* isostructural with the analogous Cs^+ or Rb^+ bifluoride salts (space group *I4/mcm*), but is nearly isomorphous with KCP(Br, Cl) in which case the common space group is *P4mm*. The molecular structure, which again consists basically of parallel chains of $Pt(CN)_4^{-1.7}$ groups and disordered $(FHF)^-$ ions, is presented in FIGURE 4. The crystallographically independent Pt-Pt distances are 2.928(1) Å and 2.918(1) Å, which may be compared to 2.88(1) Å in KCP(Br, Cl). Neighboring TCP groups are required to possess a staggered configuration with a torsion angle of 45°.

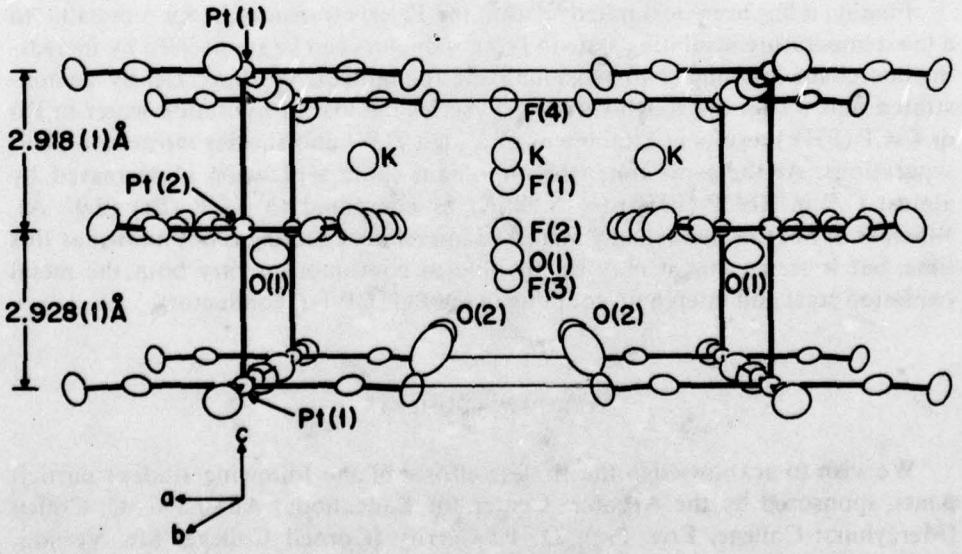


FIGURE 4. A drawing of the unit-cell contents of $K_2[Pt(CN)_4](FHF)_{0.3} \cdot 3H_2O$. The crystallographically independent Pt-Pt spacings are ~0.04 Å longer than those in $K_2[Pt(CN)_4]Br_{0.3} \cdot 3H_2O$. The $(F\text{-}H\text{-}F)^-$ anions are aligned parallel to the Pt chains which lie along *c*. Thermal ellipsoids are scaled to 50% probability.

The (presumed) linear bifluoride ions are aligned parallel to *c*, i.e., parallel to the Pt chain. The fluorine atom coordinates, which have proved difficult to refine by least-squares methods due to the low site occupancy and imposed disorder, are all of the type (0.5, 0.5, *z*). At the present highly satisfactory level of refinement [$R(F_0^2) = 0.033$] we are attempting to locate the $(FHF)^-$ ion precisely, but this may have to await a neutron-diffraction investigation. Although we have located the oxygen atoms, a neutron study will also be required to locate the water molecule H atoms in order to provide an understanding of the H-bonding in $KCP(FHF) \cdot 3H_2O$.

Conductivity. Although we have been unable to prepare crystals of satisfactory dimensions for four-probe measurements, it seems likely that the conductivity comparison will be KCP(FHF) < KCP(Br, Cl) because of the longer average Pt-Pt separation (~ 0.04 Å) of KCP(FHF) over KCP(Br, Cl).

Discussion

In the preceding sections, we discussed the basic crystal structures associated with a new series of partially oxidized alkali metal tetracyanoplatinate conducting salts. Thus, for the first time, it has been demonstrated that within the same series of Cs^+ or Rb^+ with $(FHF)^-$, for the POTCP salts formed it is possible to *vary* the degree of partial oxidation (and Pt-Pt spacing) by changing only the preparative conditions. This is in marked contrast to prototype $K_2[Pt(CN)_4]Br_{0.3} \cdot 3H_2O$, where only one stoichiometry is apparently produced regardless of the initial conditions.[19] It was also possible to prepare the first *anhydrous* POTCP salts, in the case of $M_2[Pt(CN)_4](FHF)_{0.40}$, M = Cs or Rb, the consequences of which may be new technical applications.

Finally, it has been postulated[20,21] that the Peierls transition from a metallic to a low-temperature insulating state in 1-*D* conductors can be suppressed by increasing interchain coupling (3-dimensionalizing the lattice). We have clearly demonstrated that within the *K*-Rb-Cs $(FHF)^-$ series the loss of hydration water in Rb or CsCP (FHF) results in attainment of a high *DPO* and shorter *intra*chain Pt-Pt separations. At the same time, the *inter*chain chain separation is decreased by almost 1 Å in RbCP (FHF) (~ 8.98 Å) as compared to KCP (Br) (9.91 Å). Whether or not this has actually increased interchain coupling is not known at this time, but it seems that it may be possible to continuously vary both the metal oxidation state and interchain coupling in the POTCP 1-*D* conductors.

Acknowledgments

We wish to acknowledge the tireless efforts of the following student participants, sponsored by the Argonne Center for Educational Affairs: C. C. Coffey (Mercyhurst College, Erie, Pa.); D. P. Gerrity (Cornell College, Mt. Vernon, Iowa); G. C. Lee (St. Mary-of-the-Woods College, St. Mary-of-the-Woods, Ind.); T. J. Lynch (Marist College, Poughkeepsie, N. Y.); and K. L. Stearley (Illinois State University, Normal, Ill.).

Notes and References

1. For reviews, see Stucky, G. D., A. J. Schultz & J. M. Williams. 1977. Ann. Rev. Mater. Sci. **7**: 301; Miller, J. S. & A. J. Epstein. 1976. Prog. Inorg. Chem. **20**: 1.
2. Williams, J. M., J. L. Petersen, H. M. Gerdes & S. W. Peterson. 1974. Phys. Rev. Lett. **33**: 1079; Williams, J. M., F. K. Ross, M. Iwata, J. L. Petersen, S. W. Peterson, S. C. Lin & K. D. Keefer. 1975. Solid State Commun. **17**: 45; Williams, J. M., M. Iwata, F. K. Ross, J. L. Petersen & S. W. Peterson. 1975. Mater. Res. Bull. **10**: 411; Peters, C. & C. F. Eagen. 1976. Inorg. Chem. **15**: 782; Deiseroth, H. J. & H. Schulz. 1974. Phys. Rev. Lett. **33**: 963.
3. Williams, J. M., K. D. Keefer, D. M. Washecheck & N. P. Enright. 1976. Inorg. Chem. **15**: 2446; Keefer, K. D., D. M. Washecheck, N. P. Enright & J. M. Williams. 1976. J. Amer. Chem. Soc. **98**: 233.
4. Levy, L. A. 1912. J. Chem. Soc. 1081.
5. Williams, J. M., M. Iwata, S. W. Peterson, K. A. Leslie & H. J. Guggenheim. 1975. Phys. Rev. Lett. **34**: 1653.
6. For a discussion, see Williams, J. M. 1976. Inorg. Nucl. Chem. Lett. **12**: 651; Reis, Jr., A. H. & S. W. Peterson. 1976. Inorg. Chem. **15**: 3186, and references therein.
7. Gerrity, D. P., T. J. Lynch & J. M. Williams. 1977. Inorg. Synth. Submitted for publication.
8. Coffey, C. & J. M. Williams. 1977. Inorg. Synth. Submitted for publication.
9. Stearley, K. L. & J. M. Williams. 1977. Inorg. Synth. Submitted for publication.
10. Gerrity, D. P. & J. M. Williams. 1977. Inorg. Synth. Submitted for publication.
11. Lee, G. C., K. L. Stearley & J. M. Williams. 1977. Inorg. Synth. Submitted for publication.
12. Lee, G. C., K. L. Stearley & J. M. Williams. 1977. Inorg. Synth. Submitted for publication.
13. Schultz, A. J., C. C. Coffey, G. C. Lee & J. M. Williams. 1977. Inorg. Chem. **16**: 2129.
14. Carell, H. L. & J. Donohue. 1972. Isr. J. Chem. **10**: 195.
15. Cahen, D. 1973. Sol. State Commun. **12**: 1091.
16. Novotny, M. & W. A. Little. Work in progress.
17. Underhill, A. & J. M. Williams. Work in progress.
18. Brown, R. K., P. L. Johnson, T. J. Lynch & J. M. Williams. 1977. Acta Crystallogr. In press.
19. Saillant, R. B. & R. C. Jaklevic. 1974. *In* Extended Interactions between Metal Ions in Transition Metal Complexes. L. V. Interrante, Ed: 376–381. Amer. Chem. Soc. Symposium Series No. 5.
20. Thielemans, M., R. Deltour, D. Jerome & J. R. Cooper. 1976. Solid State Commun. **19**: 21.
21. Horovitz, B. & A. Birnboim. 1976. Solid State Commun. **19**: 91.

PREPARATION, STRUCTURE, AND ELECTRICAL CONDUCTION PROPERTIES OF KCP-TYPE COMPOUNDS*

A. E. Underhill and D. J. Wood

School of Physical and Molecular Sciences
University College of North Wales
Bangor, Gwynedd, Wales, UK

The great interest over the past few years in metal atom chain complexes that exhibit one-dimensional metallic properties was initially concentrated on one compound, $K_2Pt(CN)_4Br_{0.3},3.2H_2O$(KCP). Although a considerable number of complexes of this type has been known for many years and reviewed by Krogmann[1] in 1969, KCP was studied almost exclusively and in great detail because it was possible to obtain relatively easily large crystals of good quality for physical measurements. These studies on KCP have produced a wealth of new ideas, theories, and results.[2] Many of the ideas and theories can be tested only by studying a series of compounds in which regulated changes have been made to the lattice. In this way the effect of the lattice constituents, cations, anions, and water molecules on both the lattice forces and the electronic properties of the crystal can be studied. Therefore, a series of compounds is required in which a controlled change has been made to the lattice. Such a study demands the careful preparation of a series of chemically and structurally well-characterized compounds in the form of high-quality crystals of a size suitable for physical measurements.

Studies on KCP-Type Compounds $M_2[Pt(CN)_4]Cl_{0.3},3H_2O$

The crystal structure of KCP is well established[3] and consists of a columnar stacked array of planar $[Pt(CN)_4]$ units to form a chain of Pt atoms with a short Pt-Pt separation of 2.894 Å. The distance between the chains in the tetragonal unit cell is 9.890 Å. The Br^- occupies 60% of the sites in the center of the unit cell. Water molecules form a hydrogen-bonded network between the CN^- ligands and the K^+ ions and effectively cross-link the $[Pt(CN)_4]$ chains. The importance of the water molecules in the lattice has been emphasized by the fact that small changes in the degree of hydration can produce very large differences in the specific conductivity in the platinum atom chain direction.[4]

In the present work it was decided to investigate the effect of changing the cation and hence altering the lattice forces between the one-dimensional strands of platinum atoms on both the structure and electrical conduction properties of this type of compound. In order to keep other alterations to the lattice to a minimum it was decided to concentrate on monovalent cations that formed the KCP-type structure. A preliminary survey indicated that well-formed crystals of the K, NH_4, and Rb compounds of general formulae $M_2Pt(CN)_4Cl_{0.3}$, $3H_2O$ could be prepared. Preliminary x-ray powder studies[5] showed that $Rb_2Pt(CN)_4Cl_{0.3}$, $3H_2O$-

*Manuscript received June 13, 1977.

0077-8923/78/0313-0516 $1.75/1© 1978, NYAS

(RCP-Cl) and $(NH_4)_2Pt(CN)_4Cl_{0.3}, 3H_2O$(ACP-Cl) had similar structures to one another and to $K_2Pt(CN)_4Cl_{0.3}, 3H_2O$(KCP-Cl). The full structure of the NH_4 compound has now been determined in detail by neutron diffraction studies.[6]

Experimental

Preparation of Compounds

$K_2Pt(CN)_4Cl_{0.3}, 3H_2O$ was prepared as previously described.[7]

$(NH_4)_2Pt(CN)_4Cl_{0.3}, 3H_2O$

K_2PtCl_4 (Johnson Matthey and Co. Ltd.) was twice recrystallized from water and then converted with KCN to $K_2Pt(CN)_4, 3H_2O$. The $K_2Pt(CN)_4$ was converted to $H_2Pt(CN)_4$ under N_2 with use of a Dowex 50W-X8 cation exchange resin. The acid was rotary-evaporated to an oil, with only gentle warming (<30°C) to avoid decomposition. The acid was then neutralized with dilute ammonia solution (analytical grade), and one sixth of the solution was saturated with chlorine. Both this solution and the remaining five sixths of the original solution were then separately evaporated to dryness, with gentle heating (<30°C) to remove excess chlorine and ammonia, respectively. The resulting solids were dissolved in a little water to give almost saturated solutions.

The concentrated solutions were mixed and filtered without suction through a no. 4 sinta glass crucible.

Small-sized crystals were obtained by the slow evaporation of the concentrated aqueous solution. Analysis of these crystals showed the composition to be $(NH_4)_2Pt(CN)_4Cl_{0.3}, 3H_2O$ (Found Total Pt, 47.9; Pt^{IV}, 7.0; C, 12.3; N, 20.2; NH_4, 8.85; Cl, 2.65, H_2O, 12.5, Calculated Total Pt, 48.35; Pt^{IV}, 7.25; C, 11.9; N, 20.8; NH_4, 8.9; Cl, 2.6; H_2O, 14.3%). Crystals of much higher quality and size (up to 1.7 × 0.6 × 0.6 cm) were obtained by adding NH_4Cl to the solution prior to filtration through a Millex 0.45 μm filter followed by slow evaporation at 20°C. The solution was initially made 3.7 M in NH_4Cl and 0.5 M in $(NH_4)_2Pt(CN)_4 \cdot Cl_{0.3}, 3H_2O$ (Found Total Pt 48.18; Pt^{IV}, 6.7; C, 12.7; N, 22.0; NH_4, 8.94; Cl, 3.50%). A preliminary report[8] that crystals grown in this manner contain excess NH_4^+ ions in the lattice has now been shown to be in error, and that essentially the same product is obtained even from saturated NH_4Cl solution. However, a chloride analysis consistently higher than expected (~3.5%) is obtained for crystals grown from NH_4Cl solution compared with aqueous solution (~2.65%). The reason for this is still being investigated.

The presence of the ammonium chloride in the crystallizing solution not only encourages the growth of large well-formed crystals but also suppresses side reactions that cause the crystallizing solution to become cloudy.

$Rb_2Pt(CN)_4Cl_{0.3}, 3H_2O$

This compound was prepared by a method analogous to that previously described for the ammonium complex. Crystals of the product were grown from a

solution containing 10 g of product and 10 g of RbCl in 100 cm^3 of water (0.81 M in RbCl). (Found Total Pt, 36.06; Pt^{IV}, 5.88; C, 9.02; N, 9.78; Rb^+, 31.9; Cl, 2.7; H_2O, 9.86%: $Rb_2Pt(CN)_4Cl_{0.33}$, $3H_2O$ requires Total Pt, 36.39; Pt^{IV}, 6.00; C, 8.96; N, 10.50; Rb^+, 31.88; Cl^-, 2.19; H_2O, 10.08%).

Analyses

Chloride analyses were performed by Dr. F. B. Strauss, Microanalytical Laboratories, Oxford, and Dr. F. Pascher, Mikroanalytisches Laboratorium, Bonn, Germany. Platinum was determined by Dr. F. Pascher and at Johnson Matthey and Co. Ltd. NH_4^+ was determined by micro-Kjeldahl technique, C and total N by microanalysis, Rb and K gravimetrically as the insoluble tetraphenylborate or by flame photometry.

Electrical Measurements

All measurements were performed with a four-probe technique. Gold wires were attached to the crystals by means of a graphite dag or by gold paste. The crystals and contacts were encapsulated in "Quickmount." In all cases the crystal was checked for ohmic behaviour and reversibility of the current flow prior to the experiment. In general, the experiment could be repeated the following day with good reproducibility.

TABLE 1

COMPARISON OF STRUCTURAL DATA FOR $M_2Pt(CN)_4Cl_{0.33}3H_2O$

Cation	K^+	NH_4^+
space group	P_4mm	P_4mm
$a = b$, Å	9.883	10.048
c, Å	5.748	5.861
Pt-Pt distance, Å	2.87	2.903
Reference	*	†

*WILLIAMS, J. M., M. IWATA, S. W. PETERSON, K. A. LESLIE & H. J. GUGGENHEIM. 1975. Phys. Rev. Lett. 34: 1653.

†WILLIAMS, J. M., P. L. JOHNSON, A. E. UNDERHILL & D. J. WOOD. Unpublished results.

RESULTS AND DISCUSSION

Structural Studies

The three compounds studied possess very similar tetragonal structures. TABLE 1 summarizes the results of single-crystal structural determinations. It can be seen that both the interchain distance and the Pt-Pt distance have increased on replacing K with NH_4^+ ions. This series of compounds is particularly interesting for two reasons. First, Rb^+ and NH_4^+ are of the same size, 1.48 Å, but con-

siderably larger than K^+ (1.33 Å).[9] Second, it would be expected that the presence of NH_4^+ ions compared with K^+ or Rb^+ would increase the effect of interchain coupling between the Pt chains through NH_4^+ hydrogen bonding interactions. Thus, by studying this series of compounds it should be possible to distinguish between steric and H-bonding effects on the lattice and conduction properties.

Electrical Conduction Studies

In 1974 Zeller and Beck reported a detailed study of the dc electrical conductivity of KCP.[10] They stressed the importance of using crystals of the correct geometry to obtain the correct anisotropy of conduction. In KCP, where the ratio of the specific conductivity parallel to the platinum atom chain direction ($\sigma_{\parallel}$) to the specific conductivity perpendicular to the chain direction ($\sigma_{\perp}$) is $\sim 10^5$, measurements of $\sigma_{\parallel}$ should be made on crystals with a ratio of length (ℓ) to width (a) of $\sqrt{10^5} \sim 300$. The results reported for KCP were for crystals where $\ell/a \sim 100$.

Unfortunately, the crystals obtained for the Rb and NH_4 compounds were much more chunky than those formed by KCP and ℓ/a were typically < 10. Thus the value of the anisotropy $\sigma_{\parallel}/\sigma_{\perp}$ as determined by 4-probe dc measurements, and indeed the value obtained for $\sigma_{\parallel}$ itself is likely to be too low. However, this is unlikely to affect the temperature dependence of the conductivity, since approximately the same behavior is observed for both $\sigma_{\parallel}$ and $\sigma_{\perp}$ for KCP.[10]

We have observed a wide variation of the temperature dependence of $\sigma_{\parallel}$ for different batches of crystals of ACP-Cl. Initially it was thought[8] that these differences arose from the incorporation of additional NH_4^+ and Cl^- ions into the lattice. This has now been proved not to be the case, and a reasonably consistent temperature behavior of $\sigma_{\parallel}$ has been observed for good quality crystals grown from both aqueous solution and from solutions containing various concentrations of NH_4Cl. This temperature behavior is shown for $\sigma_{\parallel}$ in FIGURE 1. It can be seen that there is a linear portion with an activation energy of 0.125 ± 0.015 ev, from 100 to 165°K. Above this temperature the variation of $\sigma_{\parallel}$ with temperature is complicated, but by room temperature the conductivity is almost temperature independent. Although, as indicated above, a range of activation energies has been observed for the linear regions at low temperatures, all the curves are in excellent agreement above 170°K. However, batches of crystals have also been obtained that exhibit quite different temperature behavior but for which chemical analysis still indicates the same compound. One batch of poor quality crystals obtained from aqueous solution exhibited a much lower activation energy of ~ 0.09 ev. On the other hand, batches of crystals grown from NH_4Cl solution and which may have been contaminated with NH_4Cl on their surfaces, exhibited a much steeper temperature dependence with activation energies as high as 0.19 ev. Thus it can be seen that the conduction properties of ACP-Cl are very susceptible to both crystal quality and possibly to trace amounts of contaminents.

FIGURE 1 also shows the temperature dependence of $\sigma_{\perp}$ for ACP-Cl. It can be seen that the value of $\sigma_{\perp}$ at room temperature is close to that reported for KCP[10] ($\sim 10^{-3}\Omega^{-1}cm^{-1}$), but the value of $\sigma_{\parallel}$ is much less. This may be due in part to the low ℓ/a rates discussed earlier.

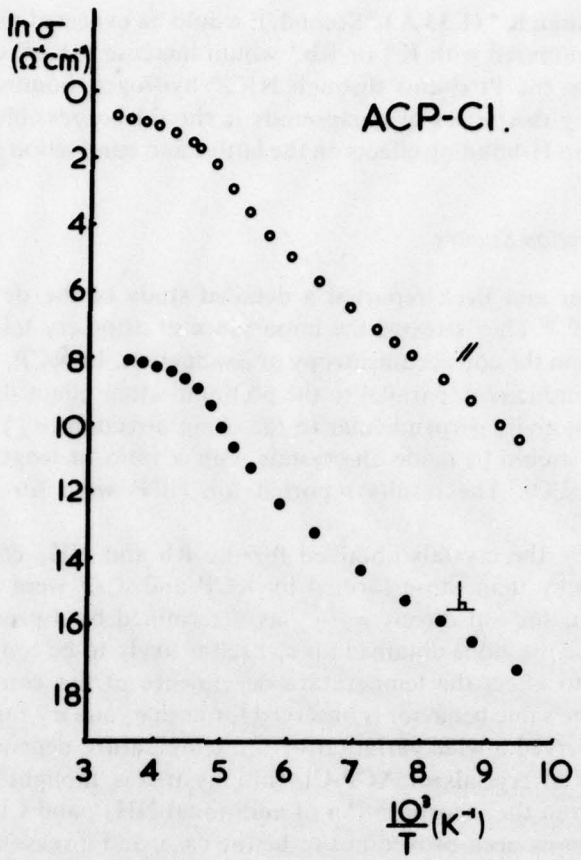


FIGURE 1. Specific conductivity of $(NH_4)_2Pt(CN)_4Cl_{0.3}$, $3H_2O$ (ACP-Cl) parallel (∥) and perpendicular (⊥) to the platinum atom chains.

The same variation of conductivity with temperature is observed for both $\sigma_{\parallel}$ and $\sigma_{\perp}$. This similarity in temperature behavior, which has also been observed for KCP,[10] may at first sight seem surprising for such an anisotropic material. It is considered, however, that the charge-carrier generation process, which is a temperature-dependent process, is the same in both directions. The temperature-independent mobility of carriers will be very different in the two directions, thus resulting in the observed temperature behavior and anisotropy.

FIGURE 2 compares the temperature behavior of $\sigma_{\parallel}$ for $K_2Pt(CN)_4Cl_{0.3}$, $3H_2O$ (KCP-Cl), $Rb_2Pt(CN)_4Cl_{0.3}$, $3H_2O$ (RCP-Cl) and ACP-Cl. The temperature profiles of the Rb and K compounds are very similar to one another, but that of the NH_4 compound is different. The behavior of the ACP-Cl is qualitatively similar, however, to that reported[10] for KCP over the much wider temperature range 26 to 320°K, (see FIGURE 3). In KCP a correlated pseudostatic Peierls distortion has been shown to exist at low temperatures (< 77K) with a correspondingly weakly pinned charge-density wave (CDW).[2] At higher temperatures the CDW becomes unpinned and there is a rapid decrease in the correlation

length between the platinum atom chains. The conductivity data for the ammonium compound suggests that in this compound the static Peierls distorted state exists to a much higher temperature ($\sim$ 160°K). If this is the case, and further structural studies are in progress, then the difference in behavior cannot be due to the different size of the cation, since NH_4^+ is very similar in size to Rb^+. It is more likely that the differences are due to the unique properties of the NH_4^+ ion. The NH_4^+ ion could influence the temperature at which the transition from the predominantly static to the dynamic state occurs (T_c) in either or both of two ways. The presence of additional H-bonding between the Pt strands may raise T_c by coupling the Pt atom chain more firmly together. Alternatively, the greater polarizability of the NH_4^+ ion, compared with K^+ or Rb^+, may increase the extent of electronic coupling between correlated strands at low temperatures and hence again raise T_c.

In an attempt to probe the H-bonding effect of the NH_4^+ in the lattice, a fully deuterated crystal of ACP-Cl was grown from D_2O/ND_4Cl solution. However,

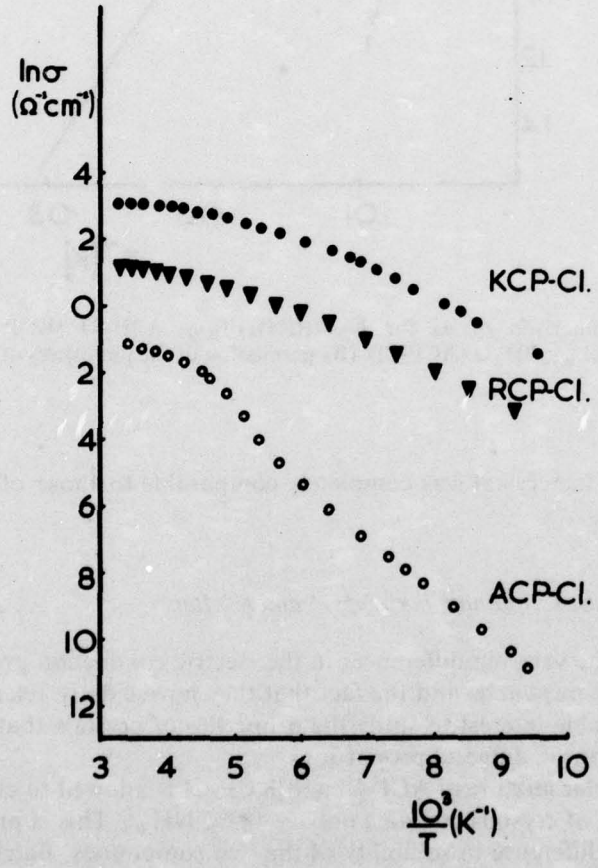


FIGURE 2. Comparison of $\sigma_{\parallel}$ for $K_2Pt(CN)_4Cl_{0.3}$, $3H_2O$ (KCP-Cl), $Rb_2Pt(CN)_4Cl_{0.3}$, $3H_2O$ (RCP-Cl), and $(NH_4)_2Pt(CN)_4Cl_{0.3}$, $3H_2O$ (ACP-Cl).

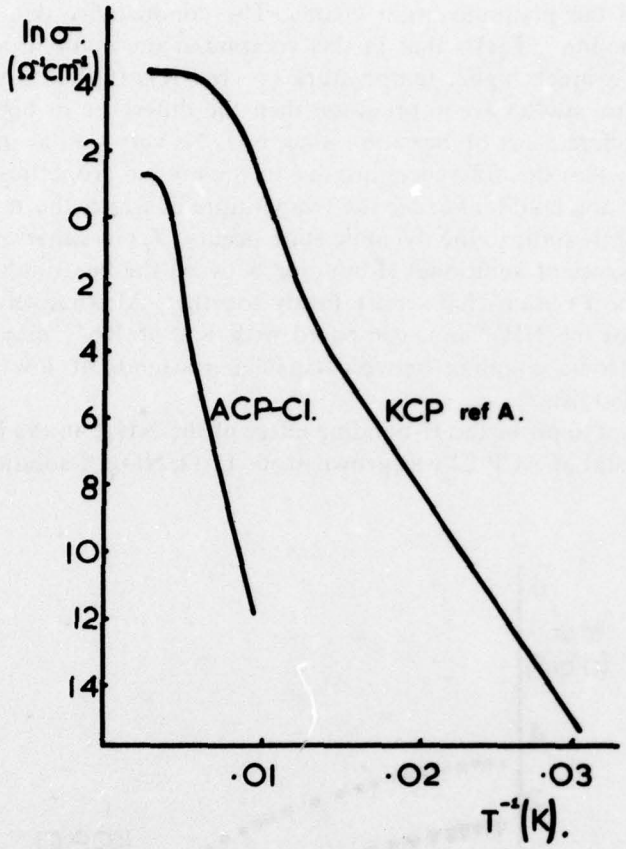


FIGURE 3. Comparison of $\sigma_{\parallel}$ for $K_2Pt(CN)_4Br_{0.30}$, $3.2H_2O$ (KCP Ref. 10) and $(NH_4)_2Pt(CN)_4CL_{0.3}$, $3H_2O$ (ACP-Cl). (By permission of the publishers of J. Phys. Chem. Solids.[10])

the behavior of the crystal was completely comparable to those of the hydrogen form.

Studies of Crystals Containing both NH_4^+ and K^+ Ions

Because of the very big differences in the electric conduction properties of the K^+ and NH_4^+ compounds and the fact that they have closely related structures, it is of considerable interest to study the properties of crystals that contain both K^+ and NH_4^+ ions in different proportions.

If an equimolar mixture of ACP-Cl and KCP-Cl is allowed to crystallize, then the initial batch of crystals contains only ~ 0.3% NH_4^+. This is presumably due to the very big difference in solubility of the two compounds. Batches of crystals having a NH_4:K ratio of 1:1.78 and 1:0.67 have been obtained from solutions containing a 5:1 and a 10:1 NH_4:K mole ratio, respectively. The variation of $\sigma_{\parallel}$ with $1/T$ for these crystals is shown in FIGURE 4 together with those observed

for KCP-Cl and ACP-Cl for comparison. It can be seen that in those crystals in which 40% of the NH_4^+ cations has been replaced by K^+, the approximate shape of ln σ vs. $1/T$ dependence of ACP-Cl is retained, but that the low-temperature activation energy is much lower than in ACP-Cl. This curve is similar to those obtained for the ACP-Cl crystal of poor quality described previously. Crystals containing approximately 64% K^+ cations exhibit a temperature dependence very similar to KCP-Cl itself.

Discussion

In ACP-Cl it has been proposed that the low-temperature correlated state involving a pinned Frohlich charge density wave (CDW) exists up to ~ 150°K compared with only approximately 70°K in the potassium analog. It has been shown that the activation energy for ACP-Cl in the low-temperature region is much larger than that observed for KCP (ΔE = 0.057 ev) and is very strongly de-

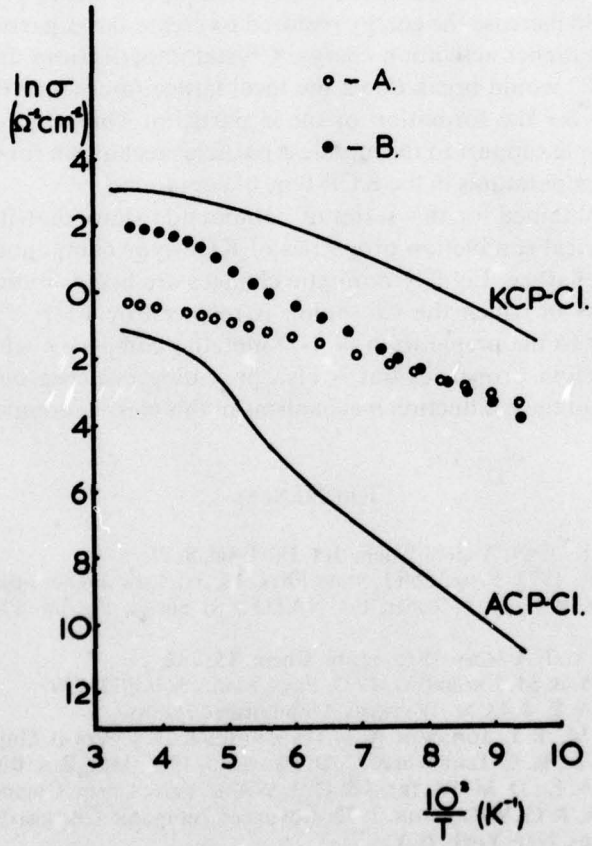


Figure 4. Comparison of $\sigma_{\parallel}$ for crystals having NH_4:K ratio of 1:1.78(o) and 1:0.67 (•) with those of $(NH_4)_2Pt(CN)_4Cl_{0.3}$, $3H_2O$ (ACP-Cl) and $K_2Pt(CN)_4Cl_{0.3}$, $3H_2O$ (KCP-Cl).

pendent on crystal perfection and the substitution of NH_4^+ by K^+ ions. It has been considered by some workers that the low-temperature activation energy of KCP corresponds to excitation of electrons across the Peierls gap in the insulating material and has been correlated with the occurrence of an absorption band in the i.r. spectrum at 0.2 ev.[2] More recently,[11] the observed activation energy has been attributed to the creation of ϕ particles corresponding to propagation of localized compression or rarefactions in the local condensed electron density.

In the former case it might be expected that stiffening the lattice by the replacement of K^+ by NH_4^+, with the consequential increase in hydrogen bonding between the Pt chains, would enhance correlation interactions and hence would raise the transition temperature (as observed). However, since the Peierls distortion is a balance between the energy required to distort the lattice and the gain in electronic energy upon distortion, it might be expected that this stiffening of the lattice would lead to a reduction in the extent of the distortion and result in a smaller band gap and lower activation energy. This is contrary to the observed behavior.

If, however, the low-temperature conductivity is due to mobile ϕ particles, it might be expected that the increased interaction in the lattice on replacing K^+ with NH_4^+ would increase the energy required to create the ϕ particles and result, as observed, in a higher activation energy. Crystal imperfections and replacement of NH_4^+ with K^+ would break down the local lattice forces and thus reduce the energy required for the formation of the ϕ particles. Thus the results reported here may give some support to the mobile ϕ particle mechanism for the conduction process at low temperatures in the KCP-type of compound.

The results obtained for this series of compounds show that it is possible to modify the electrical conduction properties of KCP-type compounds by changing the cation in the lattice. Equally dramatic changes are being found in work currently in progress in which the Cl^- anion is replaced by FHF^-.[12] This work is leading not only to the preparation of 1-*D* metallic complexes with a variety of electrical conduction properties but is also providing evidence on which to test current theories of the conduction mechanisms in this class of compound.

References

1. Krogmann, K. 1969. Angew. Chem. Int. Ed. Engl. **8:** 35.
2. Zeller, H. R. 1973. Prog. Solid. State Phys. **13:** 31; Low Dimensional Co-operative Phenomena. 1975. H. J. Keller, Ed. NATO ASI Series. Plenum Press. New York, N.Y.
3. Peters, C. & C. F. Eagen. 1976. Inorg. Chem. **15:** 782.
4. Drosdziok, S. & M. Engbrodt. 1975. Phys. Status Solidi **72:** 739.
5. Underhill, A. E. & D. M. Watkins. Unpublished results.
6. Williams, J. M., P. L. Johnson, A. E. Underhill & D. J. Wood. Unpublished results.
7. Saillant, R. B., R. C. Jaklevic & C. D. Bedford. 1974. Mat. Res. Bull. **9:** 289.
8. Underhill, A. E., D. M. Watkins & D. J. Wood. 1976. Chem. Commun.: 805.
9. Cotton, F. A. & G. Wilkinson. 1972. Advanced Inorganic Chemistry. 3rd edit. John Wiley & Sons. New York, N.Y.
10. Zeller, H. R. & A. Beck. 1974. J. Phys. Chem. Solids **35:** 77.
11. Rice, M. J., A. R. Bishop, J. R. Krumhansl & S. E. Trullinger. 1976. Phys. Rev. Lett. **36:** 432.
12. Underhill, A. E., J. M. Williams & D. J. Wood. Unpublished results.

PHYSICAL AND STRUCTURAL PROPERTIES OF TWO CONDUCTING ONE-DIMENSIONAL MATERIALS: GUANIDINIUM (GCP) TETRACYANOPLATINATE BROMIDE HYDRATE AND BARIUM VANADIUM TRISULFIDE*

Galen Stucky, C. Putnik, and J. Kelber

Department of Chemistry and Materials Reserach Laboratory
University of Illinois
Urbana, Illinois 61801

M. J. Schaffman, M. B. Salamon, and G. Pasquali

Department of Physics and Materials Research Laboratory,
University of Illinois
Urbana, Illinois 61801

and

A. J. Schultz, J. Williams, T. F. Cornish,
D. M. Washecheck, and P. L. Johnson

Chemistry Division
Argonne National Laboratory
Argonne, Illinois 60439

INTRODUCTION

One of the most important and, at the same time, difficult questions to resolve in the study of quasi-one-dimensional materials is the specific nature of the 3-d interactions that are responsible for the coherent phasing of physical properties associated with individual 1-d stacks or chains. In the partially oxidized tetracyanoplatinates,[1-4] hydrogen bonding and the acid-base interactions between the cation and the cyanide nitrogen atom lone-pair electrons define the structure in a three-dimensional sense and are apparently responsible for the type of periodicity obtained in the insulating state.[5-7] The most studied of the partially oxidized tetracyanoplatinates, in terms of both structural and physical properties, is $K_2[Pt(CN)_4]Br_{0.3} \cdot 3H_2O$(KCP(Br)). This compound undergoes a very gradual transition from metallic to insulating behavior[2] and displays evidence of an infrared active Fröhlich mode[8-9] at low temperatures. Theorizing, in accordance with the well-known theorem of Landau[10] that the phase transition in KCP(Br) might be sharper if there were more cross linking between the platinum chains to enhance the three-dimensional nature of the system, we have substituted the large

*Supported by National Science Foundation grants DMR-7601058 (University of Illinois) and CHE 76-07409 (Argonne National Laboratory). The support of the Division of Physical Research of ERDA at Argonne National Laboratories is also acknowledged. Manuscript received June 14, 1977.

0077-8923/78/0313-0525 $1.75/1© 1978, NYAS

organic cation guanidinium, $C(NH_2)_3^+$, for the potassium ion in KCP(Br). The results of our studies on the structural and conducting properties of this new compound, GCP(Br), are reported in this paper.

An entirely different class[11] of 1-d compounds is represented by $BaVS_3$, which undergoes a metal-to-insulator phase transition at a reduced temperature. Whereas the partially oxidized tetracyanoplatinate complexes and TTF-TCNQ derivatives crystallize as columnar stacks of the planar molecules to give conduction bands via the interaction of orbitals with large extensions perpendicular to the molecular planes (e.g. d_{z2}, p_z or π type orbitals) $BaVS_3$ may be viewed as consisting of infinite linear chains of face-sharing VS_6^{8-} octahedra separated from neighboring chains by the Ba^{2+} cations. Alternatively, the structure can be described as a hexagonal stacking of ordered, close-packed BaS_3^{4-} layers with the V^{4+} ions filling linear arrays of near-octahedral sites along the stacking direction.

The initial report of $BaVS_3$[11] showed the conductivity of pressed pellets to be $\sim 10^2$ mho cm^{-1} at room temperature and to increase with decreasing temperature to a maximum at 130°K. At lower temperatures the conductivity decreased such that a total decline of twelve orders of magnitude was observed between 130 and 5°K, with the region of sharpest change near 80°K. This report also showed a structural transition to begin near 180°K and to proceed continuously through 77°K, at which it was thought to be incomplete. The precise transition temperature was undefined. In order to continue the characterization of this material we have examined the metal-to-insulator transition by means of magnetic susceptibility and heat-capacity measurements, and have extended the magnetic measurements to liquid helium temperatures with surprising results.

Crystal Structure of $[C(NH_2)_3]_2[Pt(CN)_4]Br_{0.25} \cdot H_2O$, GCP(Br)

Crystals of $[C(NH_2)_3]_2[Pt(CN)_4]Br_{0.25} \cdot H_2O$, GCP(Br) were prepared by slow evaporation from an aqueous solution of $[C(NH_2)_3]_2[Pt(CN)_4]$ and $[C(NH_2)_3]_2[Pt(CN)_4Br_2]$ in a 5:1 ratio. The initial guanidinium tetracyanoplatinate salt, originally reported in the literature in 1907,[12] was obtained by metathesis between $Ba[Pt(CN)_4] \cdot 4H_2O$ and $[C(NH_2)_3]_2CO_3$. Elemental analysis indicates that there is one water of hydration per formula weight of GCP(Br), and this was verified by thermal gravimetric analysis.[13]

Diffraction data were measured with x-radiation and with neutrons. The x-ray data set is beset by the problem of obtaining suitable intensity measurements of the very weak $l = 2n + 1$ reflections, since the very strongly scattering Pt atoms have a repeat of $c/2$. This particular problem is not encountered with neutron diffraction, and data were collected on a 1.9 mg crystal sealed in a lead-glass capillary to avoid possible loss of water. A second data set was also obtained on a larger crystal, for which our attempt to deuterate had apparently been only partially successful. Since we were not able to satisfactorily locate and refine the hydrogen atoms, it appeared that with partial deuteration the negative scattering amplitudes of the protons and the positive scattering amplitudes of the deuterium atoms effectively canceled one another. Therefore, only the results obtained from the small protonated crystal are described here.

The lattice parameters for the tetragonal cell were determined from a least-

TABLE 1

POSITIONAL AND THERMAL PARAMETERS FOR $[C(NH_2)_3]_2[Pt(CN)_4]Br_{0.25} \cdot H_2O$ AND ROOT-MEAN-SQUARE THERMAL DISPLACEMENTS (IN Å) OF ATOMS ALONG THEIR PRINCIPAL ELLIPSOIDAL AXES.*

	10^4x	10^4y	10^4z	$10^4\beta_{11}$	$10^4\beta_{22}$	$10^4\beta_{33}$	$10^4\beta_{12}$	$10^4\beta_{13}$	$10^4\beta_{23}$	$10^3\mu_1$	$10^3\mu_2$	$10^3\mu_3$
Pt	0	0	0	29(2)	29(2)	94(28)	0	0	0	127(19)	188(7)	188(7)
C(1)	1182(5)	489(5)	−139(52)	28(3)	55(4)	137(23)	−2(3)	12(20)	−8(25)	145(23)	191(20)	262(10)
N(1)	1861(4)	747(4)	73(58)	38(3)	69(4)	337(25)	−18(2)	27(19)	−53(22)	191(11)	209(19)	331(16)
C(2)	1655(22)	6655(22)	5528(106)	87(14)	87(14)	1329(405)	61(14)	−113(57)	−113(57)	178(36)	358(37)	532(55)
N(2)	3303(25)	8303(25)	3255(101)	62(15)	62(15)	1336(183)	12(21)	41(37)	41(37)	248(61)	294(42)	484(34)
N(3)	1008(11)	2956(9)	−9(73)	120(10)	80(6)	551(48)	−41(7)	87(42)	0(33)	232(26)	311(28)	438(34)
H(1)	668(53)	2800(66)	454(209)	265(64)	416(94)	4323(1011)	−221(57)	916(220)	−1220(281)	149(75)	364(67)	1196(129)
H(2)	802(39)	2403(39)	−680(221)	184(45)	222(42)	1459(784)	−186(40)	214(177)	−176(170)	136(43)	444(120)	734(92)
H(3)	1513(71)	3050(39)	4042(297)	100(72)	105(29)	5495(2702)	39(39)	−428(397)	−499(227)	262(50)	283(72)	1024(249)
Br	5000	0	681(408)	59(25)	59(25)	1133(1834)	−46(40)	0	0	128(152)	362(87)	441(360)

*The estimated standard deviations in parentheses for this and all subsequent tables refer to the least significant figure. The form of the temperature factor is $\exp\{-(\beta_{11}h^2 + \beta_{22}k^2 + \beta_{33}l^2 + 2\beta_{12}hk + 2\beta_{13}hl + 2\beta_{23}kl)\}$. Atoms in special positions were restricted as required by symmetry.

squares fit of the angles on the four-circle diffractometer at the CP-5 reactor and are a = 15.621(5) Å, c = 5.816(2) Å, and V_c = 1419.2 Å.[3] The crystal density of 2.16 g/cm^3 determined by flotation agrees well with the calculated value of 2.14 g/cm^3 based on four formula weights per unit cell. Although systematic absences allowed a choice among three space groups, the structure was refined in space group I4cm, since refinements in the remaining two were unsatisfactory. Data were collected out to a maximum $(\sin\Theta)/\lambda$ = 0.59 in four octants, corrected for absorption (μ = 1.94 cm^{-1}) and averaged. The present discrepancy indices, based on 369 independent data, are $R(F_0)$ = 0.148, $R(F_0^2)$ = 0.133 and $R_w(F_0^2)$ = 0.192. The positional and thermal parameters are presented in TABLE 1.

The structure consists of linear stacks of very nearly square planar $Pt(CN)_4^{-1.75}$ moieties stacking along the c-axis, channels of Br^- ions along 0, 1/2, z and guanidinium cations whose molecular planes are oriented perpendicular to the

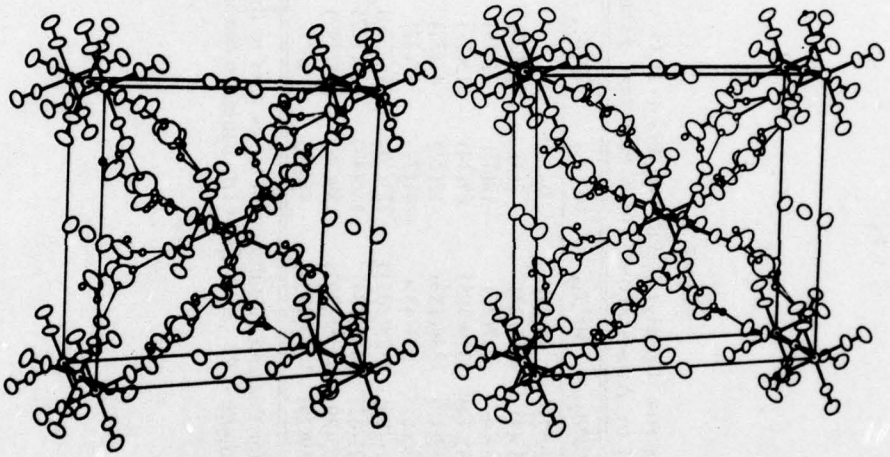


FIGURE 1. A stereoscopic view of the unit cell of GCP(Br). The hydrogen atoms are shown as small circles, for clarity. The ellipsoids for all other atoms are scaled to enclose 50% probability.

$Pt(CN)_4$ planes (see FIGURE 1). The Pt-Pt separation along the chain is 2.908(2) Å, and all Pt-Pt distances are required by symmetry to be equivalent. As seen from the bond angles given in TABLE 2, the $Pt(CN)_4$ moiety is slightly distorted from being perfectly square planar. The torsion angle between neighboring $Pt(CN)_4$ groups is 45°.

Major difficulties were encountered in the refinement of the coordinates of the bromine anion and the guanidinium cation. In the case of Br^-, it appeared that it is disordered along 1/2, 0, z such that satisfactory convergence was never obtained. As seen in TABLE 2 the guanidinium cation geometry is grossly distorted from the expected N—C—N angles of 120° and C—N distances of 1.33 Å.[14] The unrealistic parameters obtained are partly due to the large thermal motion of the guanidinium cation, which is particularly pronounced for the hydrogen atoms

TABLE 2

SELECTED BOND DISTANCES AND ANGLES FOR $[C(NH_2)_3]_2[Pt(CN)_4]Br_{0.25} \cdot H_2O$

Atoms	Distance (R)	Atoms	Angle (deg)
Pt—Pt	2.908(2)	C(1)—Pt—C(1)′	89.91(7)
Pt—C(1)	2.002(7)	C(1)—Pt—C(1)″	175(2)
C(1)—N(1)	1.136(9)	Pt—C(1)—N(1)	175(2)
C(2)—N(2)	1.59(8)	N(2)—C(2)—N(3)	106(3)
C(2)—N(3)	1.22(4)	N(3)—C(2)—N(3)′	139(4)
N(2)—N(3)	0.67(13)		
N(3)—H(1)	0.64(7)		
N(3)—H(2)	1.00(6)		
N(1)···H(3)	2.27(10)		
N(1)···H(2)	2.59(5)		
N(1)···N(1)	2.67(7)		
N(1)···H(2)	2.70(12)		

(see r.m.s. displacements in TABLE 1). The guanidinium cations lie on a mirror plane that contains C(2) and N(2) and bisecting N(3) and symmetry-related N(3)′.

The location of the water molecule still remains a mystery. There are two extra Fourier peaks in the vicinity of the guanidinium cation, so that it is possible there is some type of site disorder between H_2O and $C(NH_2)_3^+$. In fact, the apparent Br^- disorder along 0, 1/2, *z* may also be due to a site disorder with H_2O. However, no satisfactory model for disorder would refine successfully, and no evidence for an independent water site was observed.

As shown in FIGURE 2, there is extensive hydrogen bonding between the cyanoligands and the guanidinium protons. This network of hydrogen bonds appears to couple the chains together and should increase the three-dimensional nature of the

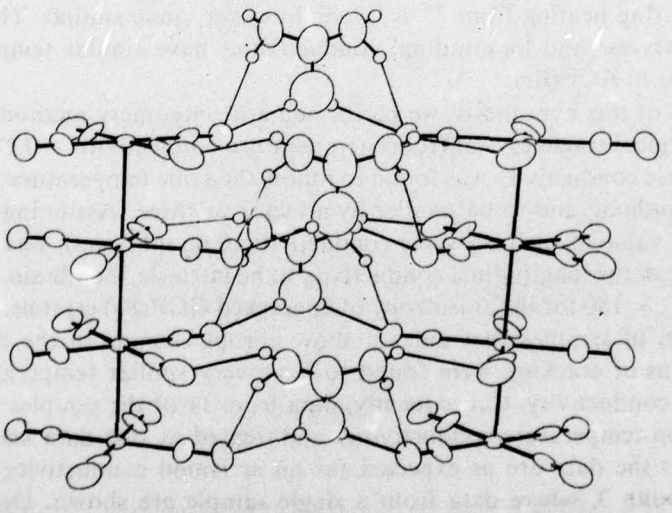


FIGURE 2. View of two neighboring $Pt(CN)_4$ chains showing the extensive hydrogen-bonding interactions.

system. It is also seen in FIGURE 2 that neighboring $Pt(CN)_4$ moieties within the same chain are linked together by hydrogen bonds to the guanidinium cations.

Direct evidence for the existence of a superlattice at room temperature has been observed in an x-ray diffuse scattering photograph.[15] The diffuse lines correspond to a superlattice of $7.9 \pm 0.5c'$, where c' is the Pt-Pt separation, and are indicative of a Peierls distortion as seen in KCP(Br) and related compounds.[15,16] Peierls distortions are associated with superlattices corresponding to phonons of wave-vector $2k_F$, twice the Fermi wave-vector. In GCP(Br) the presence of the bromine acceptors leads to a conduction band 88% full, giving a Fermi wave-vector k_F of $0.88\pi/c' \simeq \pi/c'(1-1/8)$. Thus one would expect a Kohn-Peierls instability to lead to a superlattice of approximately $8c'$, which is in agreement with our observations.

TRANSPORT PROPERTIES OF $[C(NH_2)_3]_2[Pt(CN)_4]Br_{0.2} \cdot H_2O$, GCP(Br)

The dc electrical conductivity was measured by the standard four-probe method on single crystals of GCP(Br). Contact with the crystals was made by cementing 90% gold-10% copper wires, 25 μm diameter, to the crystals with Microcircuits *R*-01 Very Low Resistance Paint, a graphite suspension. Care was taken to make the voltage contacts reach around the crystals; the current contacts were extended over the ends of the crystals.

Considerable variation was found in the room-temperature conductivity of GCP(Br) crystals, the best being ~ 11 mho/cm with 0.1 mho/cm as a typical value. In addition, the conductivity of good samples tended to decrease, sometimes abruptly, upon thermal cycling. Microscopic (140×) examination of the crystals after thermal cycling showed that a large number of cracks appear that run transverse to the *c*-axis. Such cracks tend to force the current path in the transverse direction, decreasing the apparent conductivity. The temperature dependence of the conductivity of crystals with widely varying room-temperature values and measured during heating from 77°K, were, however, quite similar. This indicates that the transverse and longitudinal conductivities have similar temperature dependences, as in KCP(Br).

As a test of this hypothesis, we performed a Montgomery method[17] measurement on a typical single crystal (room-temperature conductivity ~ 0.17 mho/cm). The transverse conductivity was found to follow the same temperature dependence as the longitudinal, and to be smaller by a factor of three. Assuming this room-temperature value of the transverse conductivity (0.06 mho/cm), and taking our largest value of the longitudinal conductivity to be intrinsic, we obtain an estimate of $\sigma_{\parallel}^{\max}/\sigma_{\perp} \approx 180$ for the anisotropy of uncracked GCP(Br) crystals.

A number of samples that did not show abrupt changes in the conductivity or visual signs of cracking were found to have very similar temperature dependence of the conductivity. Consequently, data from 11 of the samples were scaled by their room-temperature conductivities and treated as one data set. At higher temperatures the data are as expected for an activated conductivity as may be noted in FIGURE 3, where data from a single sample are shown. Data from all samples generally fall within ± 0.08 vertical divisions of the data shown.

We have attempted to fit the low-temperature data to two proposed functional forms: the interrupted strand model,[18-20] for which

$$\sigma = \sigma_0 \exp [-A/T)^x], \tag{1}$$

and where x is in the range $1/3 \leq x \leq 1/2$; and an activation model, for which

$$\sigma = \sigma_0(B/T)^y \exp (-E_0/k_B T). \tag{2}$$

For a one-dimensional semiconductor, y should be less than unity. We have fitted both (1) and (2) to our combined data. Using (1), we require $x \simeq 1.2$, which eliminates the possibility of an interrupted strand model for GCP(Br). Equation 2, which gives a slightly better fit, leads to $y = 1.50 \pm 0.06$ and $E_0/k_B = 370 \pm 8°K$. The latter fit is shown as a solid line in FIGURE 3.

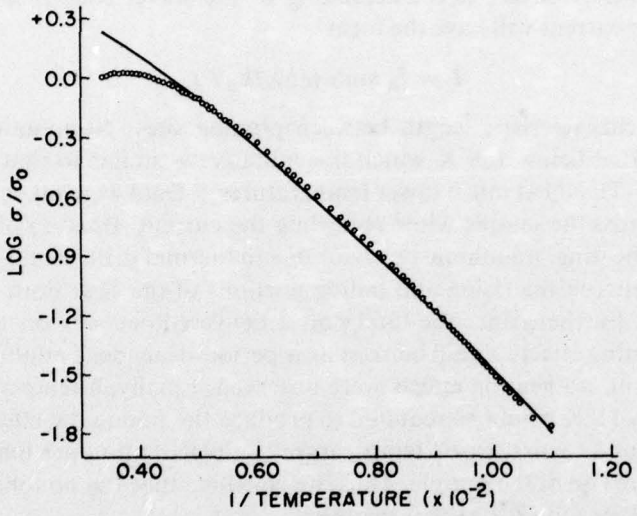


FIGURE 3. The ratio of the conductivity to the room-temperature conductivity vs. inverse temperature for a typical GCP crystal is given by the circles. The solid line is the fit to the conductivities of 11 crystals, given by Equation 2 with $y = 1.5$ and $E_0 = 370°K$.

Our data for GCP(Br) thus seem to rule out both a simple hopping model and normal one-dimensional semiconductivity. Recently, however, Rice *et al*[21] proposed a theory in which the conductivity arises from the excitation of solitary waves in a weakly pinned charge-density wave condensate. For such a theory to hold, the system must be far below the Peierls transition temperature T_p, so that collective effects dominate. That this may be the case is indicated by what appears to be the partial coalescence into spots of the diffuse sheets observed in the x-ray studies.[15] Further, we have measured the susceptibility of GCP(Br) and found that it is temperature independent between 77°K and 200°K.[22] Since it has been suggested[23] that the susceptibility of such materials first becomes temperature independent below about one fourth of the mean field transition temperature, our results seem to indicate a very high Peierls temperature.

According to the soliton model,[21] the low-temperature conductivity is given by

$$\sigma = [4\mathrm{Ne}^2\omega_F L(E_0 k_B T)^{-1/2}(n_s/n)^2] \exp[-E_0/k_B T], \quad (3)$$

where ω_F is the pinning frequency; L, the soliton mean free path; n_s/n, the fraction of electrons in the condensed state; and N, the density of chains. If we assume that the mean free path is dominated by phonon scattering, then $L \propto T^{-1}$ and the overall temperature dependence of (3) agrees with (2) with $y = 1.5$. Further, the gap E_0 is much smaller than estimates of 3.5 $k_B T_P$, as noted above. Finally, comparing our largest longitudinal conductivity with (3) and taking $\omega_F = 10^{12}$ sec^{-1} (see below), we obtain $L = 600$ Å$/T$ when all the electrons are in the condensed state. This seems to indicate that the mean free path is longer than several Pt-Pt distances at low temperatures, and that we are not in the hopping regime.

Another characteristic of pinned charge-density wave models is the possibility of nonohmic behavior due to the depinning of the wave. Rice *et al.*[24] have suggested that the current will have the form

$$I = I_0 \sinh(eE\lambda/k_B T), \quad (4)$$

where λ is a characteristic length between pinning sites. Nonohmic behavior is observed in GCP below 160°K which is qualitatively similar to that recently observed in TTF-TCNQ at much lower temperatures.[25] Data were taken by sweeping the voltage across the sample while recording the current. Because of the cumulative effects of heating, nonohmic behavior due to thermal drift would appear as an asymmetry between the rising and falling portions of the saw-tooth sweep. None was observed. Further, since the total power delivered depends on the period of the sweep, heating effects would be seen as a period-dependent nonlinearity in the response. Again, no heating effects were observed. Finally, a temperature rise of approximately 11°K would be required to produce the nonohmic effects observed. Our estimate of a "worst case" temperature rise places an upper limit of 2°K on the temperature rise of the sample. Thus, we conclude that the nonohmic behavior of GCP(Br), shown in FIGURE 4, is intrinsic.

We have fitted the data of FIGURE 4 to expression (4) and find that $\lambda = 6000$ Å at 77°K, an unreasonably large number. A similar analysis of the recent data for TTF-TCNQ[25] gives a similarly large value $\lambda = 2000$ Å at 4.2°K. We conclude that (4) is inappropriate for such pinned CDW's. We have analyzed our data in the same way as in Reference 25 and find that the activation energy tends toward zero as the field increases, vanishing at $E_c \cong 1000$ V/cm. This is to be compared with $E_c = 150$ V/cm for TTF-TCNQ. Our estimate of the pinning frequency for GCP(Br) results from the observation[22] of a decrease in *IR* transmission near 30 cm^{-1} which we attribute to the optical mode. Then, using the argument[23] that $\omega_F \simeq 0.2\ \omega_{LO}$, we conclude that ω_F is on the order of 6 cm^{-1}. This is approximately a factor of three larger than estimates for TTF-TCNQ,[25] which, through the quadratic dependence of the E_c on ω_F, is consistent with our observed critical field.

In summary, we have shown that GCP(Br) is a new example of a quasi-one-dimensional compound of the platinum chain type. Because of a tendency for cracks to form normal to the conducting axis, a definitive value of the longitudinal conductivity was not obtained. The overall temperature dependence, however, is

strongly suggestive of a soliton mechanism for the low-temperature conductivity. The presence of nonohmic behavior also seems to be evidence against a simple depinning model for the conductivity due to the unreasonably long coherence lengths required. We speculate that the structure of GCP(Br) tends to shield the Pt chains from Br^--ion disorder, thus accounting for the differences between GCP(Br) and KCP(Br).

$BaVS_3$: Experimental

Crystalline $BaVS_3$ was prepared as described previously.[11] Analysis by the analytical facility of our chemistry department showed the crystals to be stoichiometric within the limit of detection ($\pm 0.03\%$) and indicated that any chloride ion

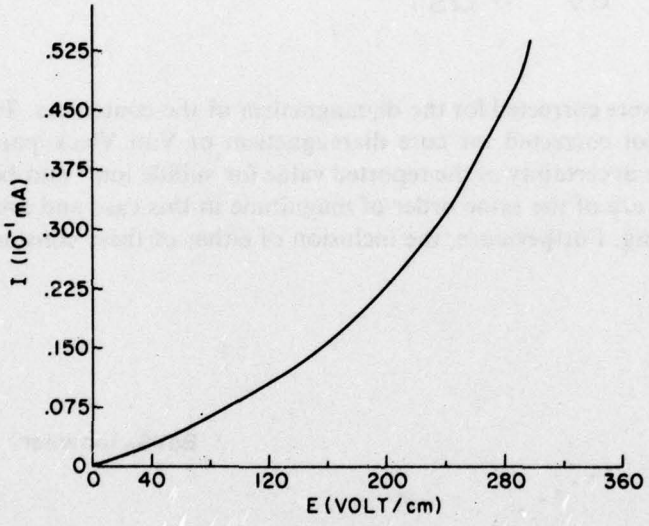


FIGURE 4. Current vs. electric field for a single crystal of GCP at 77°K.

inclusion from the $BaCl_2$ growth flux was at or below this limit. Further identification of the compound was accomplished by determination of the crystalline properties of several single crystals from x-ray diffraction photographs and automated diffractometer measurements. The results agreed with the previous report showing the material to crystallize in the hexagonal space group $P6_3/mmc$ with a = 6.725(2) Å and c = 5.614(2) Å (see FIGURE 5).

Since the crystals obtained were small (typically 0.75 × 0.25 × 0.25 mm), the magnetic measurements were performed on powdered samples produced by mechanically grinding the small single crystals. Magnetic susceptibilities were determined by the Faraday method employing Cahn electrobalance force recording and a superconducting solenoid. Metallic copper was used as a calibrating standard.

The samples were suspended in high-purity quartz containers, and the mea-

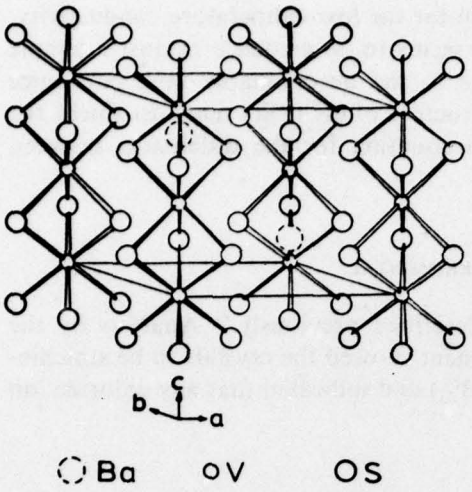


FIGURE 5. Perspective view of the room-temperature, hexagonal unit cell of $BaVS_3$.

sured values were corrected for the diamagnetism of the containers. The measurements were not corrected for core diamagnetism or Van Vleck paramagnetism because of the uncertainty of the reported value for sulfide ion[26] and because these contributions are of the same order of magnitude in this case and are thus essentially off-setting. Furthermore, the inclusion of either of these constant contribu-

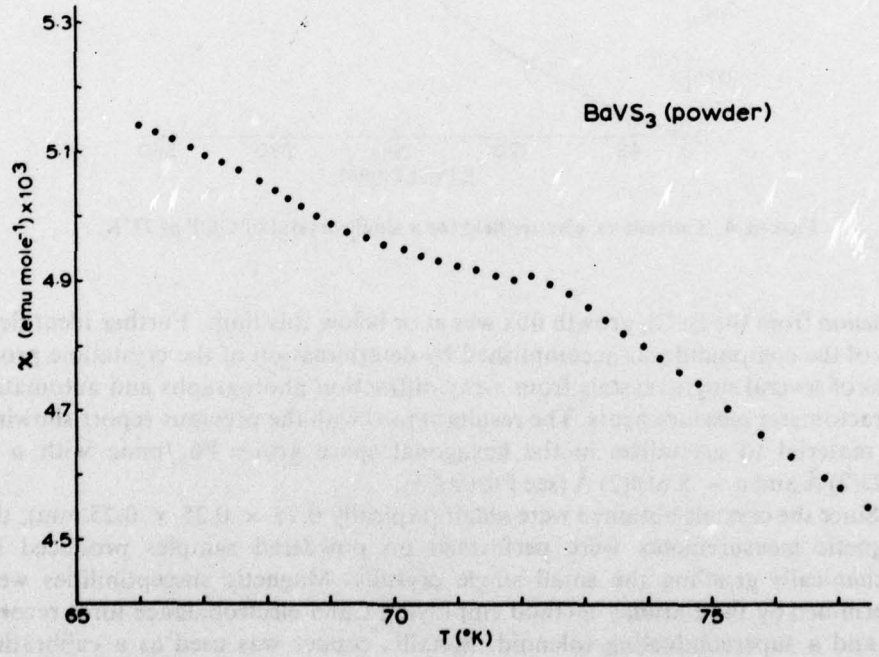


FIGURE 6. The magnetic susceptibility of $BaVS_3$ powder in the temperature region of the metal-to-insulator transition.

tions would change measured values by 1% or less, and this is also the level of uncertainty in our measurements.

Susceptibility measurements were made between 5° and 80°K with the regions between 65° and 80°K and 5° and 30°K examined closely. Temperature was monitored with a calibrated germanium resistance thermometer and with a calibrated carbon-glass resistance thermometer. At five-degree intervals within the measured temperature range, measurements were made at several applied field strengths to determine the field dependence of the susceptibility. Measured susceptibilities were found to be independent of the applied field above 15°K. Below 15°K a net ferromagnetic ordering was observed.

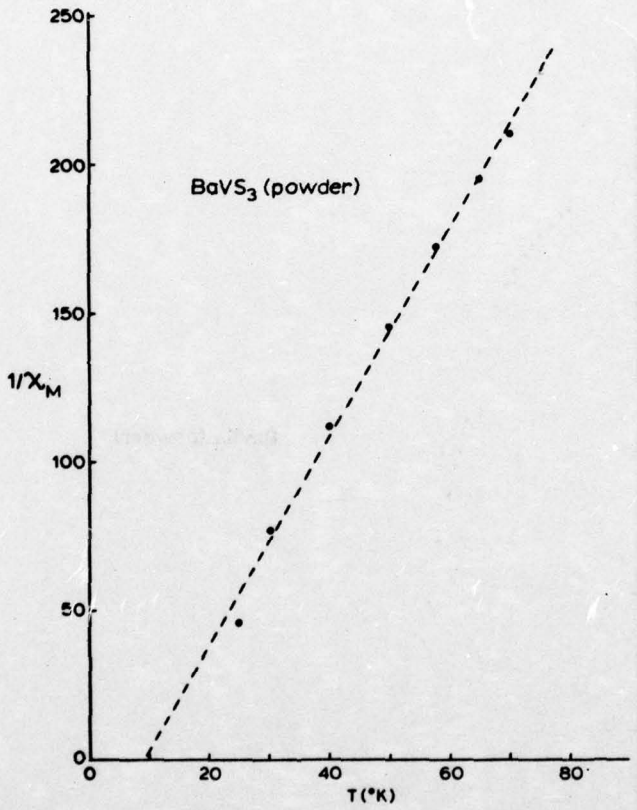


FIGURE 7. Plot of the inverse susceptibility vs. temperature in the insulating phase. Measured data are represented as dots and the least squares "best fit" as the dashed line.

$BaVS_3$: RESULTS

The behavior of the magnetic susceptibility, χ, in the region of the metal insulator phase transition reported by Wold[11] is presented in FIGURE 6. The critical point of the transition is evident as the anomalous peak in the susceptibility near 72°K. AC heat-capacity measurements indicated a second-order transition at

69.8 ± 0.2°K. The magnitude of the susceptibility in this region suggests a strong contribution from Curie paramagnetism above and below the critical point of the transition. The temperature-dependent paramagnetism observed above and below the 72°K critical point of the metal to insulator transition reveals several facets of the process. The Curie type of behavior above the critical point indicates that the observed decrease in conductivity below 130°K is accompanied by a decreasing density of states associated with the conduction band, with the displaced electrons filling localized paramagnetic states. Thus there is a continuous increase in the Curie type of contribution to the susceptibility from 130° to 72°K, in accord with the second-order nature of the process.[27]

Measurements extended to lower temperatures show the susceptibility in the

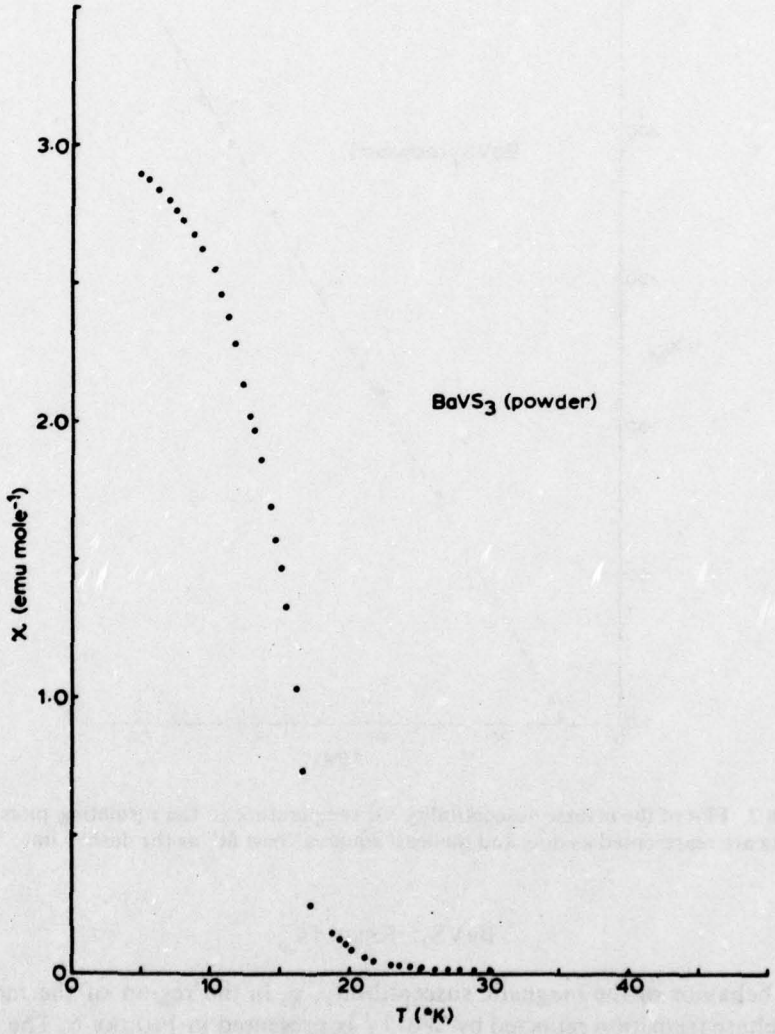


FIGURE 8. The magnetic susceptibility of $BaVS_3$ powder in the temperature region of the magnetic phase transition.

insulating phase to obey the Curie-Weiss law between 70 and ~25°K (FIGURE 7). The best fit was obtained by linear-regression, least-squares analysis for a Curie constant of 0.280 emu °K mole^{-1} and a Weiss constant of +9.865°K. Below 25°K, marked deviation from Curie-Weiss behavior is observed as the susceptibility increases by three orders of magnitude between ~20 and 5°K, with the largest increase taking place near 15°K (FIGURE 8). The downward curvature of the $1/\chi$ versus T curve and the anomalously small magnetic moment at 4.2°K may be indicative of ferrimagnetic behavior.

Additional experiments concerning the low-temperature structural, electrical, and magnetic properties of single crystals of $BaVS_3$ are currently under way in the laboratories of Dr. C. K. Chakraverty of the Centre National De La Recherche Scientifique (CNRS), Paris, France, and the University of Illinois.

ACKNOWLEDGMENT

The authors gratefully acknowledge the assistance of Dr. R. J. Miller in obtaining the magnetic measurements.

NOTES AND REFERENCES

1. SCHEGOLEV, I. F. 1972. Phys. Stat. Sol. (a) **12:** 9–45.
2. ZELLER, H. R. 1973. Fest. Körperprobleme **13:** 31–58.
3. KELLER, H. J., Ed. 1975. *Low-Dimensional Cooperative Phenomena.* Plenum Press. New York, N.Y.
4. SCHUSTER, H. G. 1975. One-Dimensional Conductors. Springer Company. Berlin, West Germany.
5. STUCKY, G., A. SCHULTZ & J. WILLIAMS. 1977. Structural aspects of one-dimensional conductors. *In* Annual Reviews of Materials Science **7:** 301–339.
6. KEEFER, K. D., D. N. WASHECHECK, N. P. ENRIGHT & J. M. WILLIAMS. 1976. J. Am. Chem. Soc. **98:** 233–234.
7. WILLIAMS, J. M., K. D. KEEFER, D. N. WASHECHECK & N. P. ENRIGHT. 1976. Inorg. Chem. **15:** 2446–2454.
8. FROHLICH, H. 1954. Proc. R. Soc. London, Ser. A. **223:** 296–305.
9. BRUSECH, P. & H. I. ZELLER. 1974. Solid State Commun **14:** 1037–1039.
10. LANDAU, L. D. & E. M. LIFSHITZ. 1969. Statistical Physics: 478. J. D. Sykes and M. J. Kearsley, trans. Addison-Wesley. Reading, Mass.
11. GARNER, R. A., M. VALSSE & A. WOLD. 1969. Acta Cryst. Sect. **B25:** 781–787.
12. LEVY, L. A. 1907. Proc. Camb. Phil. Soc. **14:** 159–160.
13. On samples prepared at Illinois, it is seen that between 70° and 120°C KCP(Br) has a weight loss equivalent to 3 H_2O, and GCP(Br) loses one H_2O. (Gunggenberger, L. J. DuPong Central Research Dept. Private communication).
14. ADAMS, J. M. & V. RAMDAS. 1976. Acta Cryst. **B32:** 3224–3227.
15. SCHULTZ, A. J., G. D. STUCKY, J. M. WILLIAMS, T. R. KOCH & R. L. MAFFLEY. 1977. Solid State Commun. **21:** 197–200.
16. RENKER, B. & R. COMES. 1975. Low-Dimensional Cooperative Phenomena. H. J. Keller, Ed.:235–258. Plenum Press. New York, N.Y.
17. MONTGOMERY, H. C. 1971. J. Appl. Phys. **42:** 2971–2975.
18. MOTT, N. F. 1969. Philos. Mag. **19:** 835–852.
19. BLOCH, A., R. B. WEISMAN & C. M. VARMA. 1972. Phys. Rev. Lett. **28:** 753–756.
20. BERNASCONI, J., D. KUSE, M. J. RICE & H. R. ZELLER. 1972. J. Phys. **C5:** L127–L130.
21. RICE, M. J., A. R. BISHOP, J. A. KRUMHANSL & S. E. TRULLINGER. 1976. Phys. Rev. Lett. **36:** 432–435.

22. Measurements on the Faraday balance at the University of Illinois Materials Research Laboratory gave constant values of $\chi = 0.38 \pm 01$ μemu/g parallel to the *c*-axis and $\chi = -0.50 \pm .01$ emu/g perpendicular to the *c*-axis. (Schaffman, M. 1977. Ph.D. Thesis. Univ. Illinois. Urbana, Ill.)
23. LEE, P. A., T. M. RICE & P. W. ANDERSON. 1973. Phys. Rev. Lett. **31:** 462–463.
24. RICE, M. J., S. STRASSLER & W. R. SCHNEIDER. 1975. One-Dimensional Conductors. H. G. Schuster, Ed.: 307–329. Springer. Berlin, Germany.
25. COHEN, M. R., P. R. NEWMAN & A. J. HEEGER. 1976. Phys. Rev. Lett. **37L:** 1500–1503.
26. SELWOOD, P. W. 1956. Magnetochemistry. 2nd edit.: 92–93. Interscience. New York, N.Y.
27. Heat capacity measurements in the region of the metal-to-insulator transition corroborate the critical temperature and show the transition to be second order. Putnik, C. F., G. D. Stucky & M. B. Salamon. To be published.)

DISCUSSION

M. COLER, (*Coler Engineering, New York, N.Y.*): Can you give us some idea of the conductivity of the $BaVS_3$?

STUCKY: The conductivity is $\sim 10^3$ ohm^{-1}cm^{-1} at room temperature and decreases by about five or six orders of magnitude at the first transition.

JERRY TORRANCE: Did you find any changes in the conductivity on the excess sulfur samples?

STUCKY: There is little difference at room temperature; however, there is structure present in the resistivity versus temperature plot at 105°K in the excess sulfur samples which is not present in the undoped samples. There also appears to be a peak in the resistivity versus temperature plot at 16°K in the "stoichiometric" $BaVS_3$, which is not present in the excess sulfur sample. In the insulating, low-temperature regime the resistivity of the excess sulfur sample is slightly lower.

TORRANCE: Some of the features of $BaVS_3$ are very similar to those found in magnetic semiconductors.

BRIAN HOFFMAN, (*Northwestern Univ., Evanston, Ill.*): The susceptibility of your "pure" material still exhibited a little deviation. Do you think it could actually be a little excess sulfur that is giving you the high conductivity?

STUCKY: Our chemical analyses indicate that we are within one percent of having stoichiometric $BaVS_3$. There are problems, however, in the analysis for sulfur, and I do not feel that we have eliminated the possibility of excess sulfur's being present.

PHILLIP COPPENS: You should also look at the angles of the S—N and Se—N interaction with the other bonds, because there are other examples for bonds where there is S—S interaction which is not electrostatic, and there may be something very similar going on in these compounds that would be interesting to elucidate.

KISTENMACHER: In (HMTSeF)(TCNQ), where the molecular planes are roughly parallel, there probably is a significant amount of π contribution to the Se—N contact. We feel that many of the Se—Se and the S—S contacts, especially the ones that are quite short relative to van der Waals radii there, are probably significant.

SPECTROSCOPIC STUDIES OF $M_x[Pt(CN)_4] \cdot yH_2O$*

Hartmut Yersin and Günter Gliemann

Institut fur Chemie
Universität Regensburg
8400 Regensburg, Germany

INTRODUCTION

Square planar $[Pt(CN)_4]^{2-}$ complexes tend to crystallize in columnar structures. The distances between the molecular units along the columnar axis are short, compared with the separations from column to column. This structure type is expected to exhibit some interesting physical properties. One compound ($K_2[Pt(CN)_4]Br_{0.3} \cdot 3.2H_2O$(KCP · $X_{0.3}$)) of the relatively large series of the tetracyanoplatinates has become famous mainly because of its extremely anisotropic conductivity.[1-3] However, most members of the tetracyanoplatinates are nonconducting compounds. This might be the reason why these have not attracted as many scientific investigations.

TABLE 1 shows a list of the tetracyanoplatinates (MCP) which crystallize in columnar structures. The Pt-Pt-distances R in the direction of the column can be varied according to the choice of the cations M and/or the crystal water content y from R = 3.67 Å to 3.09 Å. This allows the "adjustment" of the intermolecular interaction in the direction of the chains over a large range. This adjustment by the chemical substitution method, however, is discontinuous. Application of high pressure, on the other hand, permits "tuning" the in-chain interaction to any intermediate value. Consequently, the spectroscopic properties can be tuned continuously, as well.

The purpose of the present paper is, first, to summarize recent results found by spectroscopic investigations with polarized light under ambient conditions, at high pressure, and at low temperature. A correlation between the transition energies and structural properties is pointed out. Mainly R-dependent trends are discussed, and the results of an electronic band structure calculation are presented. In the second part of the paper the influence of the immediate surrounding on the $[Pt(CN)_4]^{2-}$ columns is discussed. For this purpose, rare earth cations (e.g. $M = Sm^{3+}$) with energy levels near the excited column states are used as "probe" ions. *Energy transfer* from the tetracyanoplatinate columns (donors) to Sm^{3+} (acceptor) is observed. Thus, a new system for energy-transfer investigations is presented that exhibits interesting aspects because of the tuneability of the donor states.

POLARIZED SPECTROSCOPY

The optical spectroscopy represents an appropriate method for investigating the physical properties of the tetracyanoplatinates(II), since the dominant transi-

*Manuscript received June 16, 1977.

0077-8923/78/0313-0539 $1.75/1 © 1978, NYAS

TABLE 1

TETRACYANOPLATINATES WITH DIFFERENT METAL-METAL-DISTANCES IN THE DIRECTION OF THE COLUMNS (AT ROOM TEMPERATURE)

$M_x[Pt(CN)_4] \cdot yH_2O$ (MCP)	Pt-Pt-distance R [Å]	Reference
$Na_2[Pt(CN)_4] \cdot 3H_2O$	3.67	4
$Sr[Pt(CN)_4] \cdot 5H_2O$	3.60	5
$Cs_2[Pt(CN)_4] \cdot H_2O$*	3.54	6
$K_2[Pt(CN)_4] \cdot 3H_2O$	3.48	7
$Rb_2[Pt(CN)_4] \cdot 1.5H_2O$	3.42	8
$Ca[Pt(CN)_4] \cdot 5H_2O$	3.38	5
$Sm_2[Pt(CN)_4]_3 \cdot 18H_2O$	3.35†	36
$K_2Sr[Pt(CN)_4]_2 \cdot 6H_2O$	3.33	5
$Ba[Pt(CN)_4] \cdot 4H_2O$	3.32	4, 5, 9
$(NH_4)_2[Pt(CN)_4] \cdot 2H_2O$	3.26	10
$KNa[Pt(CN)_4] \cdot 3H_2O$	3.25	10
$KLi[Pt(CN)_4] \cdot 2H_2O$	3.20	11
$Y_2[Pt(CN)_4]_3 \cdot 21H_2O$	3.18	12
$Mg[Pt(CN)_4] \cdot 7H_2O$	3.15	5
$Sr[Pt(CN)_4] \cdot 3H_2O$	3.09	5
$K_2[Pt(CN)_4]Br_{0.3} \cdot 3.2H_2O$ ($KCP \cdot X_{0.3}$)	2.89	13

*Helix structure.
†Spectroscopic estimate.

tions of these compounds lie in the energy range between the near ultraviolet and the infrared. Further, most of the spectroscopic properties such as oscillator strengths, transition energies, and emission properties, including lifetime, show a very anisotropic behavior, as is expected for the columnar structure type. Therefore, important additional information is gained if methods of *polarized* spectroscopy are applied.

Spectroscopic Properties under Ambient Conditions

An investigation of the properties of the tetracyanoplatinates requires the application of various methods of optical spectroscopy. The transitions that are polarized with the electric field vector E parallel to the columnar axis (*c*-axis) have extremely high oscillator strengths. These are therefore appropriately investigated by single-crystal reflectivity measurements.[19] The transitions polarized with $E \perp c$, on the other hand, are relatively weak and should be detected by single-crystal absorption techniques. All the tetracyanoplatinates (II) exhibit a very strong emission. Consequently, the measurements of the polarized emission represent a further important source of information.

FIGURE 1 shows the polarized emission spectra of some tetracyanoplatinate(II) single crystals with different in-chain Pt-Pt-distances R. The spectra are recorded under ambient conditions (295°K, 1 atm) with E parallel and perpendicular to the chain axis, respectively. All the compounds show two differently polarized

transitions. It is seen from FIGURE 1 that the emission properties change systematically with a variation of R:

The transitions shift to lower energy with decreasing R. This effect is attributed to a decrease of the band-gap energy caused by an increase of the in-chain interaction. For further discussion see ENERGY BANDS.

The relative intensities $I(\mathbf{E} \parallel c)/I(\mathbf{E} \perp c)$ invert with reduction of R. A similar inversion of the relative intensities is observed with temperature decrease and can be understood in a first approximation applying a Boltzmann distribution to the two emitting states (*Low-Temperature Investigations*).

FIGURE 2 summarizes the peak energies of the emission and reflectivity spectra versus R^{-3}. The experimental data follow a R^{-n} power law[17,18] (with $n = 3.0 \pm 0.3$).

Reflectivity and emission peak energies with $\mathbf{E} \parallel c$ undergo the same red shift with decreasing R (constant Stokes shift), because they are connected with the same interband transitions. These are fully allowed (very high oscillator strengths) and can be assigned to transitions between one-electron hybrid molecular states

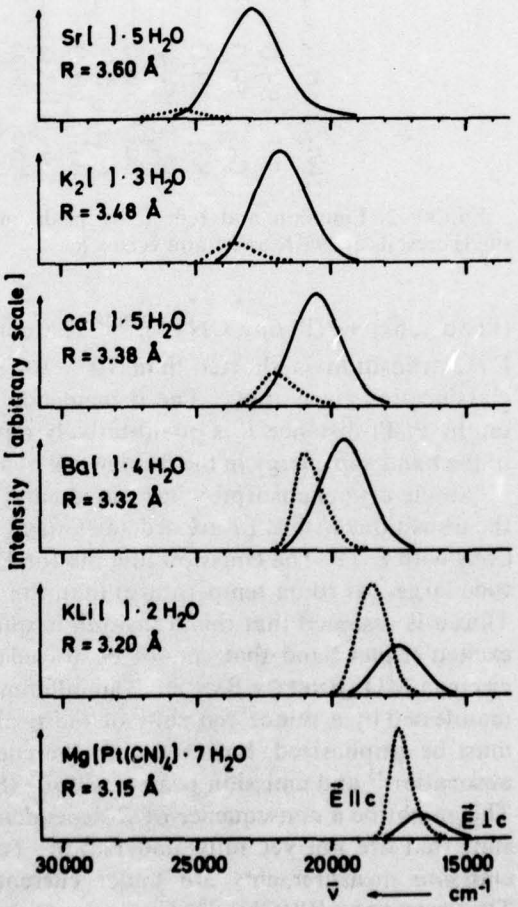


FIGURE 1. Polarized emission spectra of different tetracyanoplatinate (II) single crystals at 295 K and 1 atm. The intensities are not comparable for different compounds and the spectra are not corrected for the response of the apparatus, which is described in Reference 15 (for additional details see Reference 16). Spectral resolution: 10 cm^{-1}. The excitation energies are chosen to be about 2–3 × 10^3 cm^{-1} above the emission peak energies. Some of the compounds are discussed in detail elsewhere: BaCP,[16] KLiCP,[11] MgCP.[20]

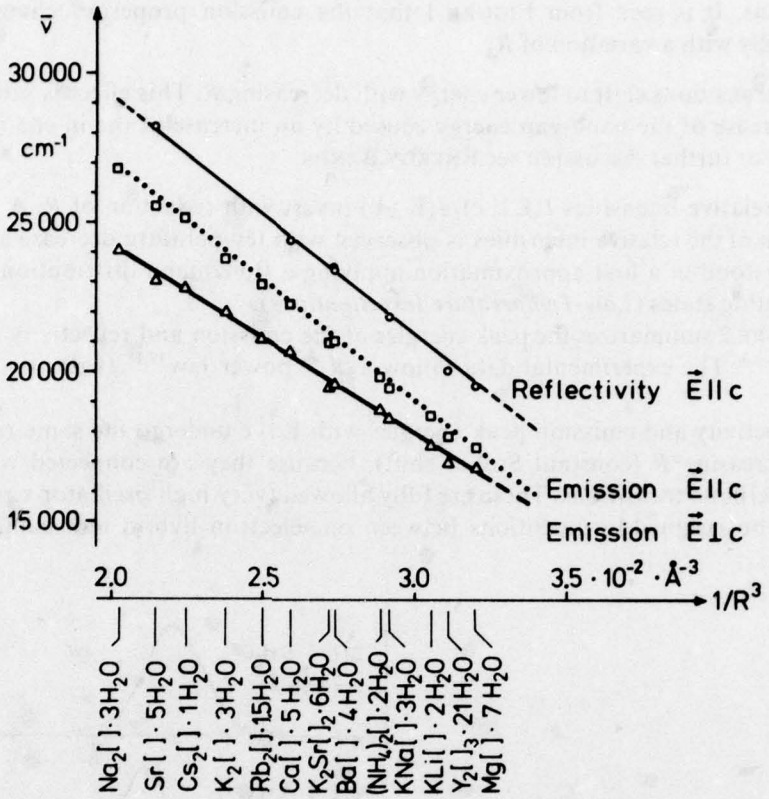


FIGURE 2. Emission and reflectivity peak energies of different $M_x[Pt(CN)_4] \cdot yH_2O$ single crystals at 295°K and 1 atm versus R^{-3}.

$(Pt\ 5d_{z^2}, 6s) \leftrightarrow (Pt\ 6p_z, CN\pi^*)$.[20,21] The emission lifetime corresponding to the $\mathbf{E} \parallel c$ transition is shorter than 10^{-8} to 10^{-9} seconds,[22] thus confirming the classification given above. The dependence of the transition energy (with $\mathbf{E} \parallel c$) on the Pt-Pt-distance R is quantitatively reproduced by one-electron calculations of the band gap energy in the framework of a two-band model (ENERGY BANDS).

Single-crystal absorption measurements[14] show that the oscillator strengths of the transitions with $\mathbf{E} \perp c$ are orders of magnitude smaller than those of the transitions with $\mathbf{E} \parallel c$. The emission lifetime for $\mathbf{E} \perp c$ is at least two orders of magnitude larger (at room temperature) than the lifetime of the parallel component.[22] Thus it is assumed that this transition is spin-forbidden and is connected with an excited triplet band that cannot be traced back simply to one dominant one-electron MO (ENERGY BANDS). The different origin of the $\mathbf{E} \perp c$ emission is also manifested by a minor red shift of the peak energies versus R^{-3} (FIGURE 2). It must be emphasized, however, that the energy difference between single-crystal absorption[14] and emission peak positions (Stokes shift) is also a function of R. This might be a consequence of R-dependent relaxation properties in the excited state that are not yet fully understood. To enlighten this effect, time-resolved emission measurements are under current investigation.[22] (See also ENERGY TRANSFER FROM $[Pt(CN)_4]^{2-}$ COLUMNS TO Sm^{3+}.)

Structural Correlation

The systematic dependence of the emission peak energies on the in-chain Pt-Pt-distance R for columnar structures of the tetracyanoplatinates(II) represents a useful correlation that may be applied to determine structural parameters.

The correlation of the emission peak energies $\bar{\nu}$ (in cm^{-1}) with the Pt-Pt-distances R (in Å) can be expressed (at 295°K) by the empirical equations[11] (FIGURE 2)

$$\mathbf{E} \parallel c: \bar{\nu}_{\parallel} = 42.9 \cdot 10^3 - 8.0 \cdot 10^5 R^{-3} \quad (1)$$

$$\mathbf{E} \perp c: \bar{\nu}_{\perp} = 36.8 \cdot 10^3 - 6.3 \cdot 10^5 R^{-3} \quad (2)$$

A determination of R has been achieved for the columnar structure compound KLiCP, using polarized emission peak energies. Conventional x-ray methods confirmed the result.[11]

The application of the correlation to CsCP represents an interesting example and will be discussed in more detail. The CsCP emission peak energies $\bar{\nu}_{\parallel} = 25200\ cm^{-1}$ and $\bar{\nu}_{\perp} = 22800\ cm^{-1}$ (at 295°K) fulfill Equations 1 and 2 independently at $R = (3.56 \pm 0.02)$ Å. This value is not equal to $c/6$ ($Z = 6$) (with

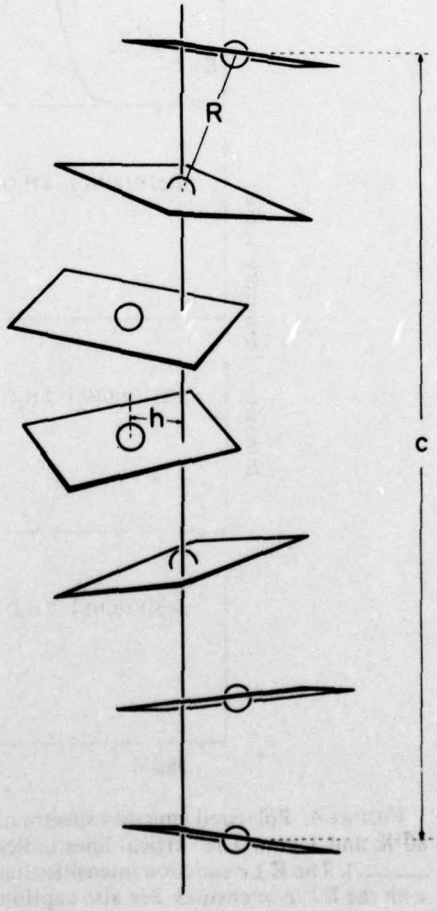


FIGURE 3. Helix of the $[Pt(CN)_4]^{2-}$ units in $Cs_2[Pt(CN)_4] \cdot H_2O$. (Space group: C_6^2-$P6_1$).[6,23]

the lattice constant c = 19.336 Å [6a]), which would be expected if the platinum atoms of the $[Pt(CN)_4]^{2-}$ units were located just on the c-axis. The first structure predictions,[6a] however, suggest a helical arrangement of the complex units lying a distance h apart from the sixfold screw axis. This implies a larger Pt-Pt-distance. If the spectroscopically determined R is assumed to be correct, it follows h = (1.50 ± 0.04) Å. Crystal structure determination confirms the values found for h and R.[6b,23] (FIGURE 3).

In spite of the lateral displacement of the $[Pt(CN)_4]^{2-}$ units, the application of Equations 1 and 2 still yields the correct Pt-Pt-distance (within limits of experimental error). This implies that the transition energies are not essentially altered. On the other hand, the energies react very sensitively to small changes of the intermolecular interaction, which is determined by the wave-function overlap. An appreciably smaller overlap would be suggested for a helix structure type unless the wavefunctions are widely spread out over the whole molecular units (although the complexes are tilted toward each other (FIGURE 3)). A calculation of the

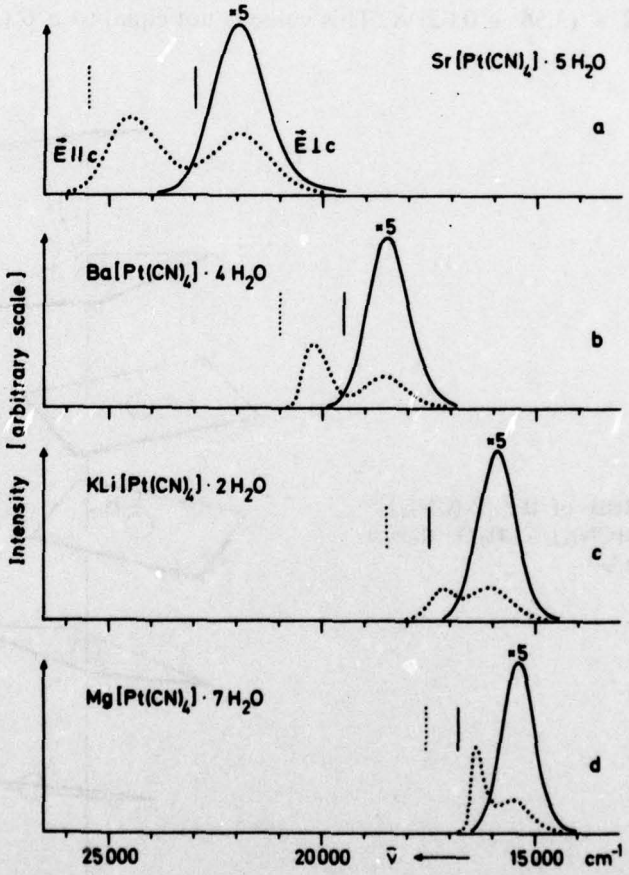


FIGURE 4. Polarized emission spectra of different tetracyanoplatinate(II) single crystals at 80°K and 1 atm. The vertical lines indicate the peak energies at 295°K (E ∥ c: . . . , E ⊥ c: ———). The E ⊥ c emission intensities have to be multiplied by a factor of 5 for comparison with the E ∥ c-intensities. See also caption for FIGURE 1.

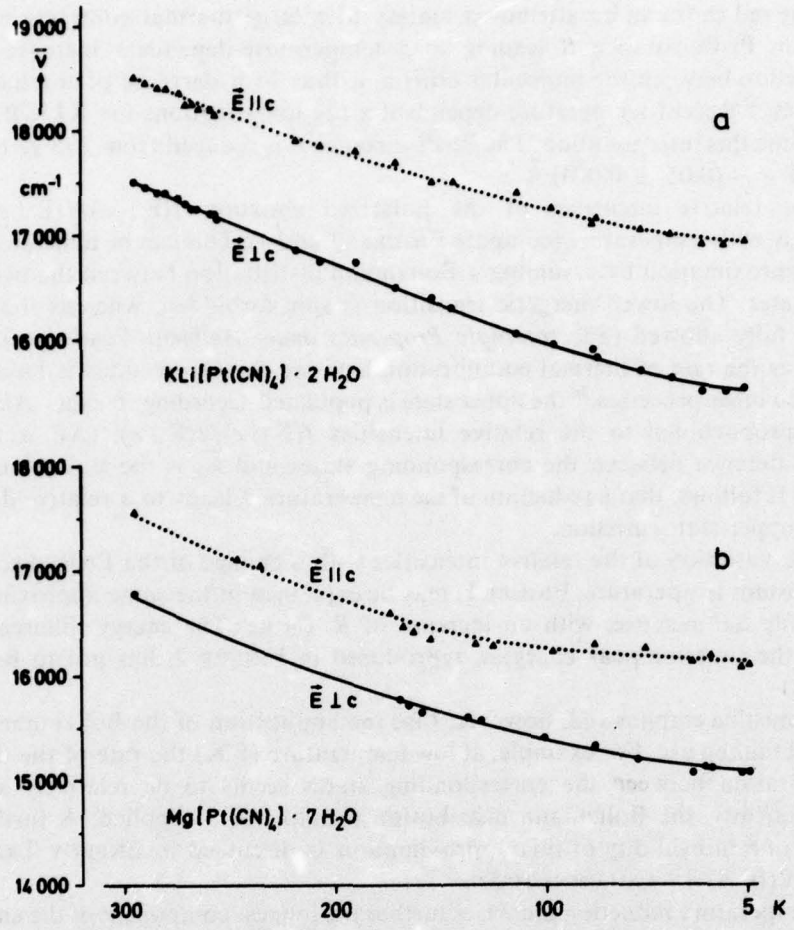


FIGURE 5. Energetic positions of the polarized single-crystal emission maxima versus temperature for KLiCP[11] and MgCP.[20]

wavefunction distribution carried out by Interrante and Messmer confirms this overall diffuseness.[24]

Low-Temperature Investigations

Temperature variation causes obvious changes of the spectroscopic properties of the tetracyanoplatinates. Thus these investigations represent a source of further information.

FIGURE 4 shows some 80°K emission spectra.* The transition energies undergo a large red shift which is also observed for the single-crystal absorption data.[14,20] FIGURE 5 reproduces the peak energies of the polarized emission versus temperature for the two compounds KLiCP[11] and MgCP.[20]

*The relative intensities of the low energetic $\mathbf{E} \parallel c$ emission peaks depend strongly on the quality of the crystals. The half-widths and peak energies are approximately the same as those of the $\mathbf{E} \perp c$ emission peaks. Therefore, the low energetic $\mathbf{E} \parallel c$ emission peaks are mainly attributed to a polarization error being about 5%.

The red shift can be attributed mainly to a large thermal contraction of the in-chain Pt-Pt-distance R leading to a temperature-dependent increase of the interaction between the molecular units and thus to a decrease of the band gap energies.[20] Recent temperature-dependent x-ray investigations for KLiCP clearly underline this interpretation. The Pt-Pt-distance R is reduced from 295°K to 80°K by $\Delta R = -(0.05 \pm 0.004)$ Å.[25]

The relative intensities of the polarized emission $I(\mathbf{E} \parallel c)/I(\mathbf{E} \perp c)$ vary strongly with temperature (compare FIGURES 1 and 4). This can be understood in a first approximation by assuming a Boltzmann distribution between the two emitting states. The lower energetic transition is spin-forbidden, whereas the higher one is fully allowed (*Spectroscopic Properties under Ambient Conditions*). Thus, as far as the rate of thermal equilibration between these two states is large compared to other processes,[26] the upper state is populated according to $\exp(-\Delta E/k_B T)$, being proportional to the relative intensities $I(\mathbf{E} \parallel c)/I(\mathbf{E} \perp c)$. ($\Delta E$ is the energy difference between the corresponding states and k_B is the Boltzmann constant.) It follows, that a reduction of the temperature T leads to a relative decrease of the upper-state emission.

The variation of the relative intensities with a change of the Pt-Pt-distance R (at constant temperature, FIGURE 1) may be explained in the same approximation. Probably ΔE increases with an increase of R. (Note: The energy difference between the emission peak energies, reproduced in FIGURE 2, has not to be equal to ΔE.)

It must be emphasized, however, that the application of the Boltzmann law is only of limited use. For example, at low temperature (5°K) the rate of the thermal equilibration between the corresponding states seems to be relatively small.[22] Consequently, the Boltzmann distribution should not be applied. A further example of a nonvalidity of this approximation is discussed in ENERGY TRANSFER FROM $[Pt(CN)_4]^{2-}$ COLUMNS TO Sm^{3+}.

Temperature reduction increases further the longest component of the emission lifetime by some orders of magnitude.[22] It also causes an appreciable half-width reduction of the emission spectra (FIGURES 1 and 4). These effects are not further discussed in this paper.

Phase Transformation in $Y_2[Pt(CN)_4]_3 \cdot 21H_2O$

Structural phase transformations that are connected with changes of the Pt-Pt-distance can be detected by monitoring the emission spectra (*Structural Correlation*). $Y_2[Pt(CN)_4]_3 \cdot 21H_2O$ (YCP) represents an informative example.[12] Between $T = 295$°K and $T > T_c = (218.5 \pm 1)$°K the YCP emission properties are equivalent to those of other tetracyanoplatinates (phase I) (FIGURE 6). *Slow* temperature reduction below T_c (≈ 10°K/*h*) causes a jump of the transition energies by about 10^3 cm^{-1} (phase II). Further temperature decrease leads again to typical emission properties (lower two branches of FIGURE 6, a). This behavior is attributed to a phase transformation. The columnar structure is preserved but the in-chain distance R is reduced by $\Delta R = (0.05 \pm 0.005)$ Å, determined spectroscopically from Equations 1 and 2, and also confirmed by temperature-dependent x-ray diffraction methods.[25]

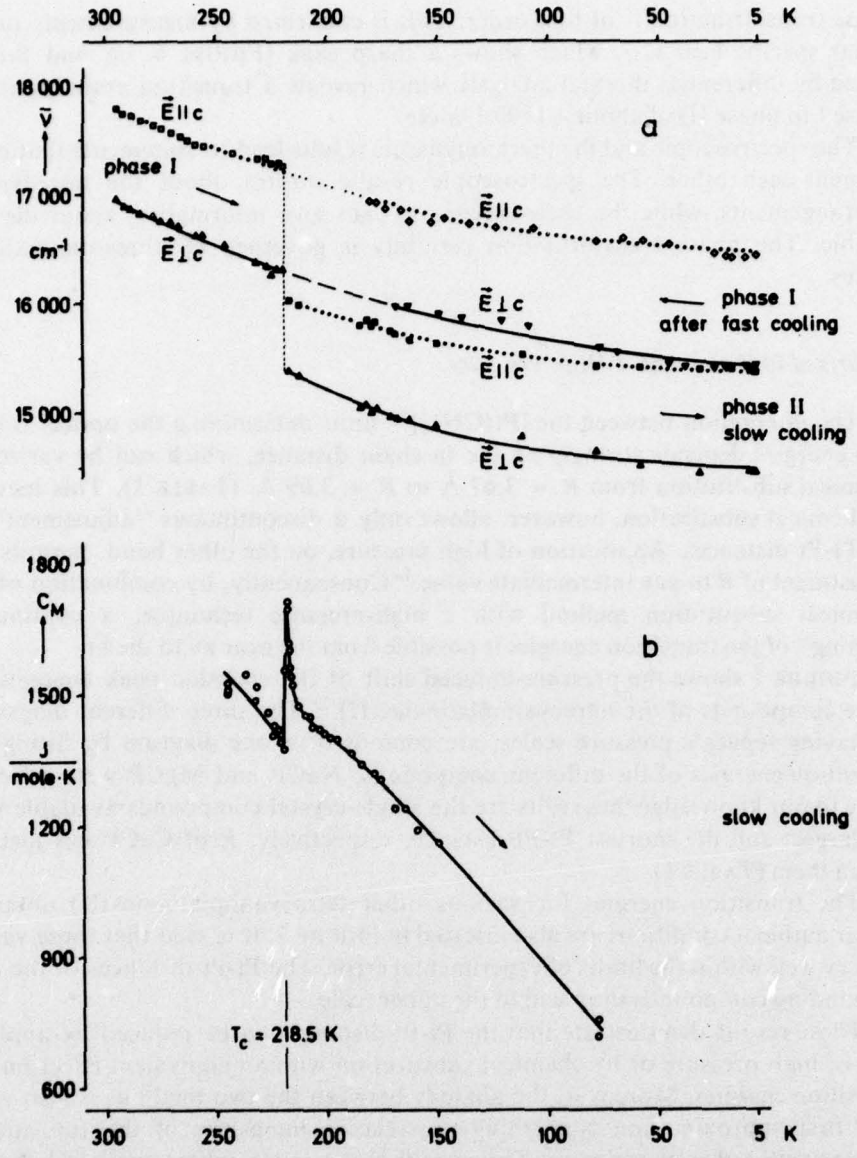


FIGURE 6. Energetic positions of the single-crystal emission maxima (a) and molar specific heat C_M (b) of $Y_2[Pt(CN)_4]_3 \cdot 21H_2O$ (YCP) versus temperature. The arrows give the direction of the temperature variation. Specific heat measurements were accomplished by a relaxation technique.[12,28]

A *fast cooling* procedure to 5°K (≈30°K/min) and subsequent measurements on slowly warming up results in emission properties of the YCP compounds as if no phase transformation had occurred (upper two branches of FIGURE 6, a, including the extrapolated temperature range). It is assumed that the fast-cooling procedure leads to a supercooled phase I.[27]

The spectroscopic properties, discussed above, allow the conclusion that the

phase transformation is of first order. This is confirmed by measurements of the molar specific heat C_M, which shows a sharp peak (FIGURE 6, b), and further stated by differential thermal analysis which reveals a transition enthalpy (from phase I to phase II) of about +1500 J/mole.

The spectroscopic and the thermodynamic results lead to statements that complement each other. The spectroscopic results inform about the microscopic rearrangements, while the thermodynamic ones give information about the ensemble. The phase transformation certainly is governed by three-dimensional forces.

Polarized Emission under High Pressure

The interaction between the $[Pt(CN)_4]^{2-}$ units determining the optical transition energies depends strongly on the in-chain distance, which can be varied by chemical substitution from R = 3.67 Å to R = 3.09 Å. (TABLE 1). This method of chemical substitution, however, allows only a discontinuous "adjustment" of the Pt-Pt-distances. Application of high pressure, on the other hand, permits the adjustment of R to any intermediate value.[16] Consequently, by combination of the chemical substitution method with a high-pressure technique, a continuous "tuning" of the transition energies is possible from the near uv to the i.r.

FIGURE 7 shows the pressure-induced shift of the emission peak energies for three compounds of the tetracyanoplatinates(II).[29] The three different diagrams, *all having separate pressure scales, are composed to one diagram* by fitting the transition energies of the different compounds. NaCP and MgCP were selected, since to our knowledge these salts are the single-crystal compounds available with the largest and the shortest Pt-Pt-distance, respectively. R of CaCP lies just between them (TABLE 1).

The transition energies for various other tetracyanoplatinates(II) obtained under ambient conditions are also inserted in FIGURE 7. It is seen that these values fit very well within the limits of experimental error. The Pt-Pt-distances of the corresponding compounds thus lead to the upper scale.

These results demonstrate that the Pt-Pt-distance can be reduced by application of high pressure or by chemical substitution with an equivalent effect on the transition energies. Moreover, the analogy between the two methods is also valid in a first approximation concerning the relative intensities of the transitions. Consequently, this investigation indicates that the outer sphere surrounding one chain is of minor importance for the determination of the transition energies. This is the reason the correlation between pressure (lower scale of FIGURE 7) and Pt-Pt-distance (upper scale of FIGURE 7) can be given.[16] The dependence is not a linear one.

The importance of the actual crystal structure, however, clearly appears in the transition regions of NaCP and CaCP where pressure increase does not shift the emission peak energies within the limits of experimental error. Equivalent behavior has been found for BaCP at nearly the same emission peak energies.[16] The optical data do not allow a conclusive interpretation for this effect, but a reasonable assumption seems to be that phase transformations occur in these regions with no or only small changes of the Pt-Pt-distances.

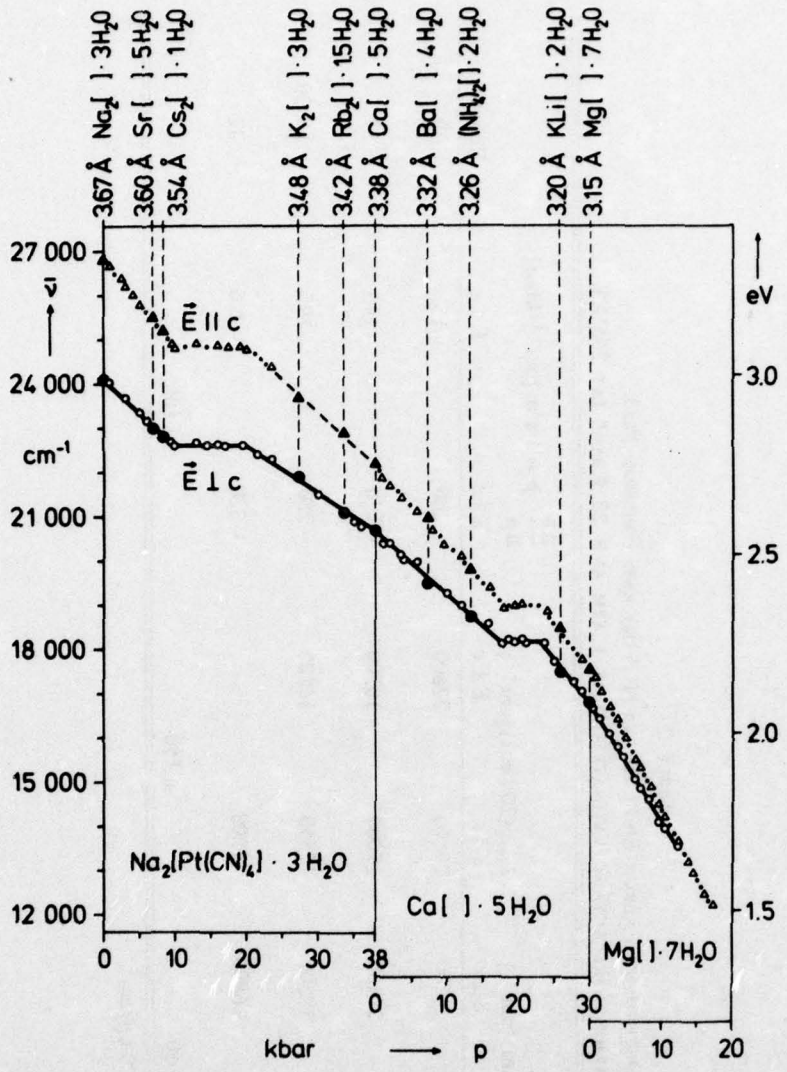


FIGURE 7. Emission peak energies for single-crystal $Na_2[Pt(CN)_4] \cdot 3H_2O$, $Ca[Pt(CN)_4] \cdot 5H_2O$, and $Mg[Pt(CN)_4] \cdot 7H_2O$ versus pressure.[29,42] The emission peak energies for various other $M_x[Pt(CN)_4] \cdot yH_2O$ salts are also inserted ($E \parallel c$▲, $E \perp c$●). The experimental uncertainty is about ±1 kbar and ±100 cm^{-1}.

TABLE 2 summarizes some of the results found by application of high pressure (at 295°K). It includes the peak energies of the polarized emission at 1 atm and 20 kbar, and the slopes $\Delta\bar{\nu}/\Delta p$ for p = 1 atm. These data belong to the largest values reported until the present.

ENERGY BANDS

An interpretation of essential properties of the tetracyanoplatinates can be given on the basis of a simple model. Because of the exceptional arrangement of

TABLE 2

PRESSURE-DEPENDENT ENERGY SHIFT $\Delta\bar{\nu}/\Delta p$ (1 ATM) AND EMISSION PEAK ENERGIES FOR VARIOUS TETRACYANOPLATINATES(II) AT 1 ATM AND 20 KBAR* (AT 295°K).

Compound	$\bar{\nu}_{max}$ (1 atm) [cm^{-1}]		$\bar{\nu}_{max}$ (20 kbar) [cm^{-1}]		$\frac{\Delta\bar{\nu}}{\Delta p}$ p = 1 atm [cm^{-1}/kbar]		Reference
	E ∥ c	E ⊥ c	E ∥ c	E ⊥ c	E ∥ c	E ⊥ c	
$Na_2[Pt(CN)_4] \cdot 3H_2O$ R = 3.67 Å	26750	24100	24800	22600	−200	−155	29
$Ca[Pt(CN)_4] \cdot 5H_2O$ R = 3.38 Å	22250	20700	19000	18200	−170	−140	29
$Ba[Pt(CN)_4] \cdot 4H_2O$ R = 3.32 Å	21000	19500	17550	16800	−280	−195	16, 30
$Mg[Pt(CN)_4] \cdot 7H_2O$ R = 3.15 Å	17550	16800	11200	—	−320	−270	42
Experimental Error	± 50		± 150		± 10%		

*1 kbar = 10^9 dyn/cm^2 = 986.9 atm = 1020 kp/cm^2.

the molecular units in crystals with columnar structure the intermolecular coupling within every column is much stronger than the coupling between different columns. This has been stated by the high-pressure investigations (*Polarized Emission under High Pressure*). Therefore, as a rough model it seems possible to regard only a linear chain of $[Pt(CN)_4]^{2-}$-complexes.

In the case of very large intermolecular distances R, we have a system of single-oriented complex ions, without mutual coupling. The relevant one-electron states of such single complex-ions are shown schematically in FIGURE 8. It is of great importance that the ($CN\pi^*$)-states of the CN-system lie energetically in the neighborhood of the (Pt-5d/6p)-states. By coupling with the metal (Pt $6p_z$)-

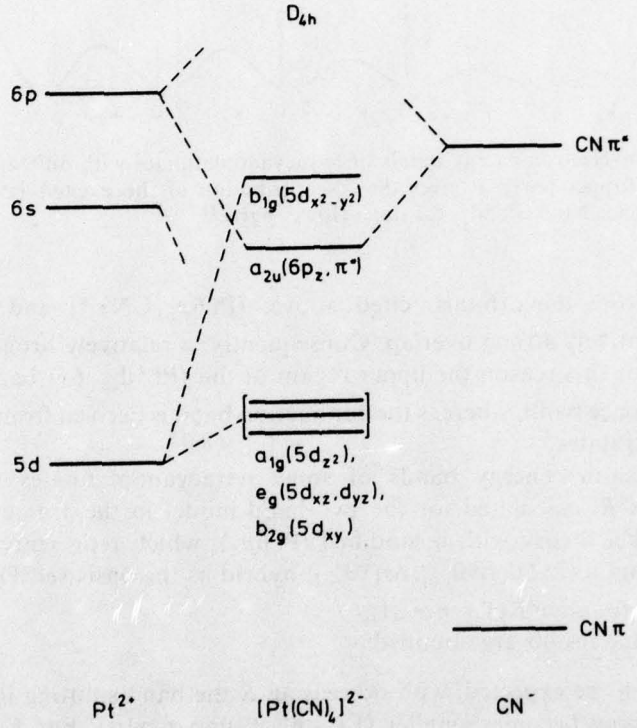


FIGURE 8. Simplified one-electron molecular orbital level diagram for $[Pt(CN)_4]^{2-}$.

orbital, a mixed molecular state (Pt $6p_z$, $CN\pi^*$) results which is located *below* the metal (Pt $5d_{x^2-y^2}$)-state, and which leads to the first excited state $^1A_{2u}$ (D_{4h}).† The ground state $^1A_{1g}$ (D_{4h}) results from the occupied (Pt $5d_{xy}$, $5d_{z2}$, $5d_{xz}$, $5d_{yz}$)-orbitals being mixed with ligand orbitals.[24,31-33] The $5d_{z^2}$ orbital may also be modified by additional Pt 6s admixtures.

If the Pt-Pt spacing R decreases, orbitals of neighboring molecular units will show increasing overlap, especially those orbitals pointing directly to the adjacent

†This is in contrast to the tetrahalogenoplatinate (II) ions, where the π^*-ligand orbitals are very high above the (Pt 5d)-levels.[14]

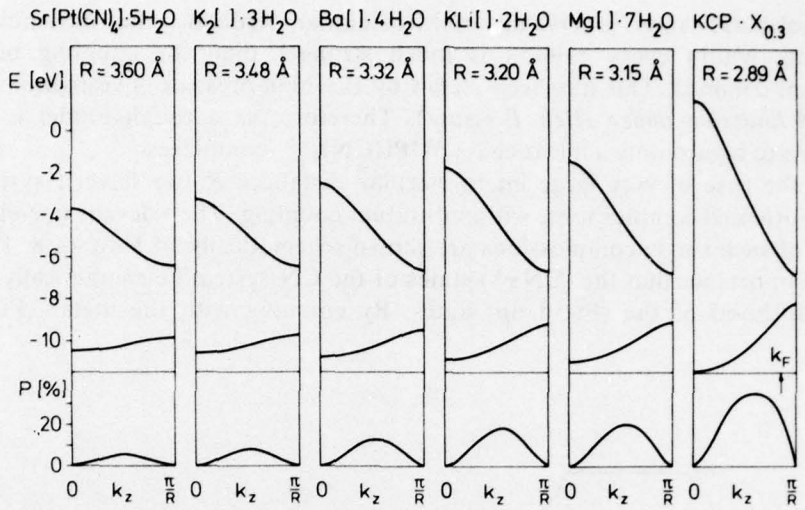


FIGURE 9. One-electron energy bands of tetracyanoplatinates with different in-chain Pt-Pt-distances R (upper part). P gives the %-contribution of the excited (Pt $6p_z$, CNπ^*) states to the valence band (Pt $5d_{z^2}$ 6s) states (lower part).[21]

metal ions. From the orbitals, cited above, (Pt $6p_z$, CNπ^*) and (Pt $5d_{z^2}$, $6s$) will have a relatively strong overlap. Consequently, a relatively broad band splitting results. For this reason the upper region of the (Pt $5d_{z^2}$, $6s$) band forms the edge of the valence band, whereas the conduction band is derived from the coupled (Pt $6p_z$, CNπ^*) states.

FIGURE 9 shows energy bands of some tetracyanoplatinates for different Pt-Pt-distances R, calculated for the two-band model in the framework of the extended Hückel theory with a modified (Pt $6p_z$), which represents the (Pt $6p_z$, CNπ^*) state and a (Pt $5d_{z^2}$[90%], $6s$[10%])-hybrid as the basis set. Details of the calculation are found in Reference 21.

The following results are obtained:

As was to be expected, with decreasing R the band splitting increases and the gap energy becomes smaller (FIGURE 9, upper part). For $k_z = \pi/R$ the calculated gap energy agrees well with the R^{-3} law obtained from optical experiments for $\mathbf{E} \parallel c$ (see FIGURE 10).

The conformity between experimental and theoretical results seems to allow an extrapolation to $R \rightarrow \infty$ ($R^{-3} \rightarrow 0$). This leads to the most prominent absorption peak of the $[Pt(CN)_4]^{2-}$ aqeuous solution,[17,18] which is assigned to correspond mainly to the (Pt $5d_{z^2}$, $6s$) $\rightarrow$ (Pt $6p_z$, CNπ^*) one-electron transition.[24,31-33,43]

An extrapolation of the experimental data to R = 2.89 Å being realized in the partially oxidized KCP · $X_{0.3}$ (FIGURE 10) leads to an energy gap of about 10^4 cm^{-1}, which corresponds to the calculated band gap energy for R = 2.89 Å. Approximately the same value has been found by Messmer and Salahub.[34]

The (Pt $6p_z$, $CN\pi^*$)-orbital and the (Pt $5d_{z^2}$, $6s$)-hybrid mix for $0 < k_z < \pi/R$, with the wave-vector k_z along the chain axis. For decreasing R the amount of (Pt $6p_z$, $CN\pi^*$) contribution to the (Pt $5d_{z^2}$, $6s$)-valence band increases and the contribution maximum shifts toward the edge of the Brillouin zone at $k_z = \pi/R$ (see bottom of FIGURE 9). The increasing contribution of (Pt $6p_z$, $CN\pi^*$) produces an increasing delocalization of ground state charge perpendicular to the chain axis, caused by the charge structure of the (Pt $6p_z$, $CN\pi^*$)-hybrid. These results have important consequences concerning three-dimensional interactions, as, for example, the interchain coupling or the properties of energy transfer to the rare-earch cations being located between the columns.

The results of the band calculations are supported by qualitative considerations in the many-electron-scheme. Starting from the many-electron states of an isolated complex ion, by coupling along the chain, the molecular singlet $^1A_{2u}$ (D_{4h}) and the molecular triplets $^3A_{2u}$, ^3E_u, $^3B_{1u}$ (primarily) generate the first excited singlet band and the lowest triplet band, respectively. Group theoretical analysis taking into account spin-orbit coupling by introducing the corresponding double group[35] (D'_{4h}) shows that the transition between the ground state and the first excited singlet band is $\mathbf{E} \parallel c$ polarized. This transition corresponds mainly to the one-electron (Pt $5d_{z^2}$, $6s$) $\leftrightarrow$ (Pt $6p_z$, $CN\pi^*$) transition. The triplet band containing admixtures of the molecular ^1E_u (D_{4h}) state (by spin orbit coupling) is allowed $\mathbf{E} \perp c$.[20]

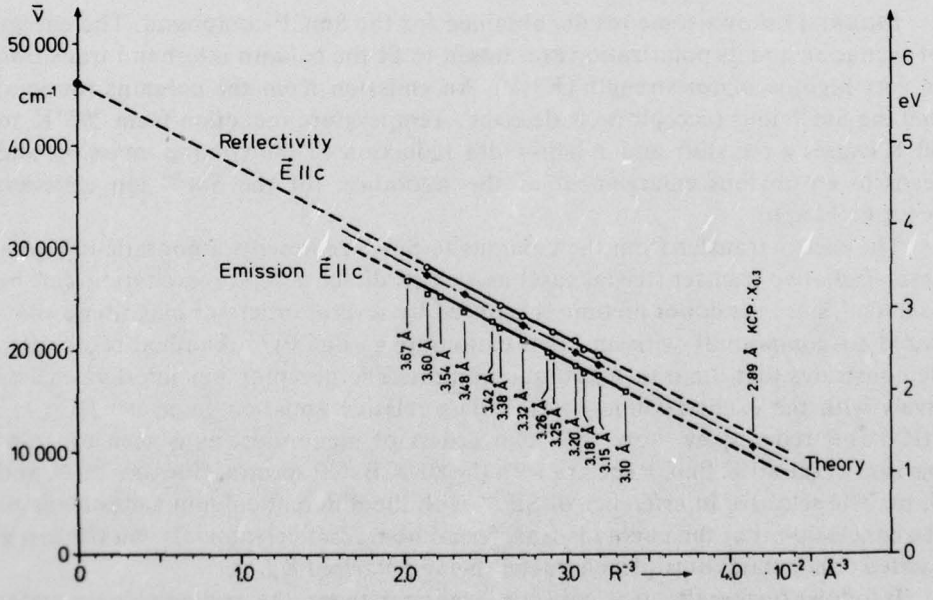


FIGURE 10. Emission and reflectivity peak energies ($\mathbf{E} \parallel c$) versus R^{-3} for various tetracyanoplatinates with different in-chain Pt-Pt-distances R at 295°K. The compounds are listed in TABLE 1. The emission peak energy at 3.10 Å is taken from Reference 42 and the point at $R^{-3} = 0$(●) represents the peak energy of the corresponding transition in solution.[17,18] The theoretical points are the band gap energies at $k_z = \pi/R$ from FIGURE 9.[21]

Because of the different charge structure of the generating molecular states, a decrease of R should produce a greater band splitting and therefore a stronger reduction of the gap energy for the singlet than for the triplet band. This is a qualitative interpretation of the different red shift of the transitions polarized $\mathbf{E} \parallel c$ and $\mathbf{E} \perp c$, respectively. The R-dependent red shift of the *emission* peak energies possibly is additionally modified by different relaxation properties in the excited states (POLARIZED SPECTROSCOPY).

ENERGY TRANSFER FROM $[Pt(CN)_4]^{2-}$ COLUMNS TO Sm^{3+}

The stacks of the tetracyanoplatinates are not isolated in the crystal. Three-dimensional interactions, not as yet studied systematically, are very important, especially the influence of the immediate surrounding on the $[Pt(CN)_4]^{2-}$ columns. For investigations of these interactions, cations having energy levels near the excited column states can yield useful information. Suitable "probe" ions are chosen out of the rare earth series (e.g. Ln = Pr^{3+}, Nd^{3+}, Sm^{3+}, Eu^{3+}). The $Ln_2[Pt(CN)_4]_3 \cdot xH_2O$ compounds also crystallize in columnar structures.[36]

The results of the spectroscopic measurements reveal important additional aspects for further investigating the LnCP systems. Radiationless energy transfer from the columns to the rare earth ions is observed. Since the excited states of the columns can be "tuned" over a large energy range by chemical substitution methods and/or applications of high pressure the tetracyanoplatinates(II) represent an exceptional donor system.

FIGURE 11 shows some results obtained for the SmCP-compound. The energy of excitation and its polarization are chosen to fit the column interband transition of very high oscillator strength ($\mathbf{E} \parallel c$). An emission from the columns (donors) *and* the Sm^{3+} ions (acceptors) is detected. Temperature reduction from 295°K to 80°K causes a red shift and a half-width reduction of the column emission and leads to an obvious enlargement of the resolution for the Sm^{3+} ion emission (FIGURE 11 a, b).

The energy transfer from the columns to Sm^{3+} represents a nonradiative process. Radiative transfer (trivial case) as well as direct acceptor excitation can be excluded, since the donor lifetime is reduced by several orders of magnitude compared to compounds with inactive cations (e.g. BaCP).[22] Another result also demonstrates that the transfer is radiationless. The acceptor ion interferes selectively with the excited column states. The relative emission intensity $I(\mathbf{E} \perp c)/I(\mathbf{E} \parallel c)$ is reduced by more than two orders of magnitude, as is seen by comparison of the 80°K SmCP spectra with the 80°K BaCP spectra. (FIGURE 11, b, and 4, b). The selective interference of Sm^{3+} with the different column states leads to the conclusion that the energy is transferred nonradiatively, mainly via the lower excited donor states of triplet character (being polarized $\mathbf{E} \perp c$).

It follows further that thermal equilibration between the excited column states (of E'_u- and A'_{2u}-character in D'_{4h}) is less efficient than energy transfer to the acceptor, otherwise the relative change of the polarization would not occur. A relatively slow relaxation between the different excited column states is also indicated by investigations of time-resolved spectroscopy.[22] This possibly points to an involvement of exciton traps in the dynamics of the column emission and transfer pro-

cesses.[36] The relaxation mechanism is not fully understood; however, the results reveal the restrictions to an application of a Boltzmann distribution between the excited column states, if transfer to the acceptor represents a competitive process.

The acceptor state is not exactly known but presumably is one of the Sm^{3+} ion quartet states (FIGURE 12, a). The acceptor emission, however, can be classified to transitions from $^4G_{5/2}$ to the ^6H_J ground-state manifold.[37,38]

The mechanism of the energy transfer is not easily determined. Nevertheless, the spatial proximity of donor and acceptor favors the Dexter-exchange[39] mecha-

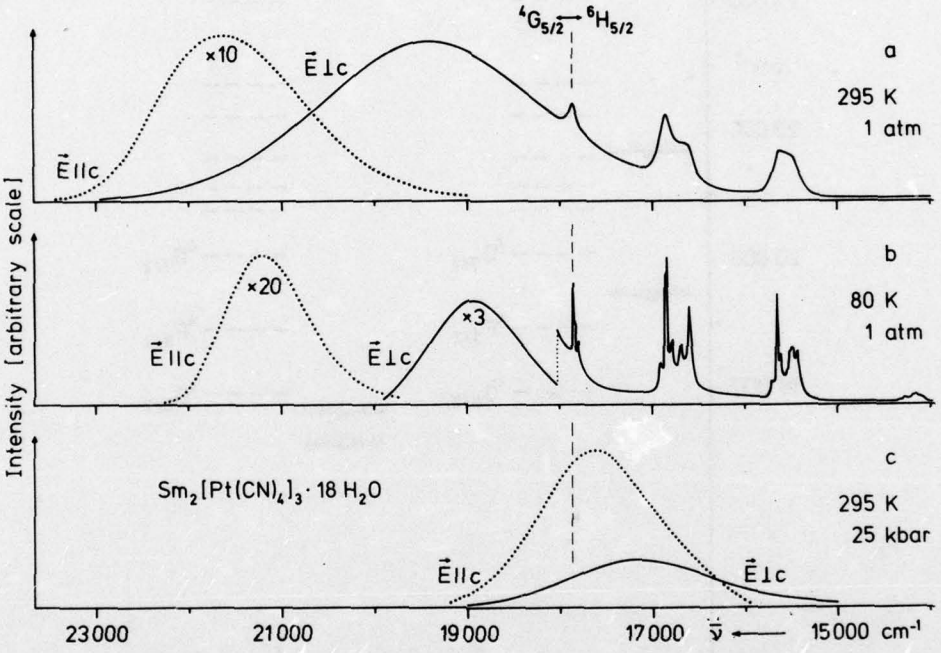


FIGURE 11. Polarized emission of single-crystal $Sm_2[Pt(CN)_4]_3 \cdot 18H_2O$ (SmCP) under different conditions.[36,42] The dashed line indicates the energy of the Sm^{3+} $^4G_{5/2} \leftrightarrow {}^6H_{5/2}$ transition. For clarity, the Sm^{3+} line-emission ($\mathbf{E} \parallel c$) is omitted. Note that for comparison of the intensities the spectra have to be multiplied by the factors given in the diagram. The intensities of spectra obtained at different temperature and pressure are not comparable.

nism. An inspection of crystal structures actually known[4-13] shows that nitrogen atoms of the $[Pt(CN)_4]^{2-}$ units are in the first coordination sphere of the cations. The corresponding distance is only of the order of 3 Å. Further, the $[Pt(CN)_4]^{2-}$ wave-functions are spread out over the whole complex unit with substantial amplitude even beyond the nitrogens.[24] Consequently, the wave-function overlap with the $4f$ orbitals may be considerable. Only a rough estimate of the transfer rate is possible, and in reference[36] it is pointed out that the exchange transfer presumably predominates the Coulomb transfer mechanism. Further, it is shown that the Wigner spin selection rules[40] for an exchange transfer from the excited triplet column state to the quartet Sm^{3+} state are fulfilled.

Energy transfer from the columns to the rare earth ions can be detected only if the energetic position of the emitting acceptor states is low enough that even a phonon-assisted back-transfer to the donor states can be excluded. This has been established not only for SmCP but also for various other compounds (e.g. EuCP, PrCP, and TbCP).[36] Crosby *et al.* discussed this rule investigating a large series of rare earth chelates.[41] Consequently, it seems to be possible that the Sm^{3+} emis-

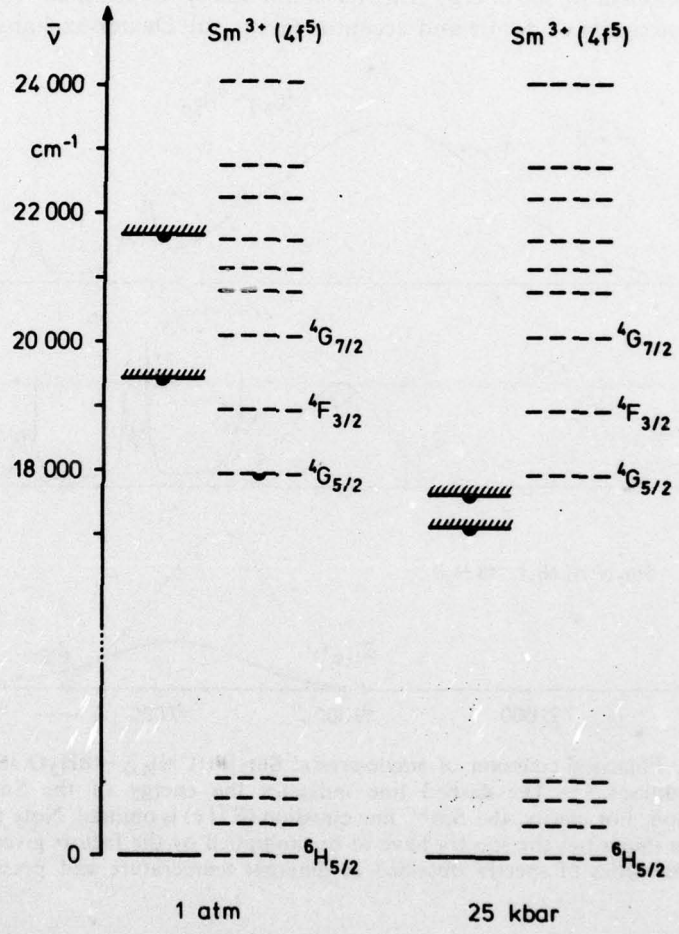


FIGURE 12. Energy level schemes for $Sm_2[Pt(CN)_4]_3 \cdot 18H_2O$ at 1 atm and 25 kbar at 295°K. The shaded bars represent the emission maxima of the $[Pt(CN)_4]^{2-}$ columns. The dashed lines represent the Sm^{3+} levels.[37,38] The black half circles indicate emitting states.

sion (of SmCP) can be quenched if the excited column states are shifted to lower energy. This is demonstrated in FIGURE 11, c.[42] Application of 25 kbar results in a red shift of the column states by several thousand wave-numbers and leads to the expected disappearance of the Sm^{3+} emission. Connected with this quenching the relative intensity of the polarized column emission $I(\mathbf{E} \perp c)/I(\mathbf{E} \parallel c)$ is changed to the same ratio as if the cations were inactive.

In FIGURE 12 the relevant energy-level diagram for SmCP under ambient con-

ditions is compared to that under 25 kbar. The disappearance of the Sm^{3+} emission seems to be connected with a change of the spectral overlap integral[39] between the $\vec{E} \perp c$ donor-emission and $^4F_{3/2}$ acceptor-absorption.[36]

Conclusion

The tetracyanoplatinates(II) represent an exceptional class of compounds due to the arrangement of the $[Pt(CN)_4]^{2-}$ units in quasilinear stacks. The special structure leads to very strong intermolecular interactions in the direction of the columns and relatively weak interchain interactions. As a consequence of this structure type, the physical properties are very anisotropic. Methods of polarized spectroscopy with special emphasis on polarized emission spectroscopy represent adequate techniques for studying these compounds. The transitions follow different selection rules and can be classified group-theoretically. The transition energies are determined essentially by one parameter, the in-chain Pt-Pt-distance. The energy dependence can be reproduced quantitatively (for the highly allowed transition with $\mathbf{E} \parallel c$) by one-electron band structure calculations. These, as well as spectroscopic predictions, permit the determination of band-gap energy for the partially oxidized tetracyanoplatinate (e.g. $K_2[Pt(CN)_4]Br_{0.3} \cdot 3.2H_2O$).

It has further been demonstrated that the in-chain Pt-Pt-distance can be adjusted by chemical substitution (cation exchange) or application of high pressure having an equivalent effect on the energies of the electronic transitions. Regarding these properties, the compounds behave as being pseudoone-dimensional. Of importance is that transition energies can be "tuned" almost continuously from the near uv to the near i.r.. The possibility of tuning the excited column states may imply some future technical applications.

Interactions of the columns with their immediate surroundings have been studied by incorporation of "probe" ions selected of the series of the rare earth ions (Ln^{3+}). For $Sm_2[Pt(CN)_4]_3 \cdot 18H_2O$ (SmCP), it could be shown that a radiationless energy transfer from the columns (donors) to SM^{3+} (acceptor) occurs. The investigations reveal that the energy transfer rate is much larger than the thermal relaxation rate between the excited column states. This possibly points to an involvement of exciton traps in the dynamics of the column-emission process.

The main importance of the LnCP compounds, however, does not seem to be the "probing" effect of the Ln^{3+} ions but the new possibilities existing for energy transfer investigations with *tunable donor states*. Thus it has been shown for SmCP that the high pressure-induced red shift of the donor (column) states leads to a quenching of the SM^{3+} emission.

References

1. Interrante, L. V., Ed. 1974. Extended Interactions Between Metal Ions in Transition Metal Complexes. ASC Symposium. Washington, D.C.
2. Keller, H. J., Ed. 1975. Low-Dimensional Cooperative Phenomena. Plenum Press. New York, N.Y.
3. Miller, J. S. & A. J. Epstein. 1976. Prog. Inorg. Chem. **20:** 1.
4. Moreau-Colin, M. L. 1972. Struct. Bonding **10:** 167.
5. Krogmann, K. & D. Stephan. 1968. Z. Anorg. Allgem. Chem. **362:** 290.

6a. Otto, H. H., W. Holzapfel, H. Yersin & G. Gliemann. 1976. Z. Naturforsch. Teil b. **31:** 528.

6b. OTTO, H. H., SCHULZ, K. H. THIEMANN, H. YERSIN & G. GLIEMANN. 1977. Z. Naturforsch. Teil b. **32:** 127.
7. WASHECHECK, D. M., S. W. PETERSON, A. H. REIS & J. M. WILLIAMS. 1976. Inorg. Chem. **15:** 74.
8. KOCH, T. R., P. L. JOHNSON & J. M. WILLIAMS. 1977. Inorg. Chem. **16:** 640.
9. MAFFLY, R. L., P. L. JOHNSON & J. M. WILLIAMS. 1977. Acta Cryst. **B33:** 884.
10. MOREAU-COLIN, M. L. 1968. Bull. Soc. Mineral. Cristallogr. **91:** 332.
11. HOLZAPFEL, W., H. YERSIN, G. GLIEMANN & H. H. OTTO. 1978. Ber. Bunsenges. Phys. Chem. **82:** (Heft 2). In press.
12. YERSIN, H., G. GLIEMANN & H.-S. RÄDE. 1978. Chem. Phys. Lett. In press.
13. KROGMANN, K. & H. D. HAUSEN. 1968. Z. Anorg. Allgem. Chem. **358:** 67.
14. TUSZYNSKI, W. & G. GLIEMANN. Unpublished.
15. YERSIN, H. & G. GLIEMANN. 1972. Meßtechnik **80:** 99.
16. STOCK, M. & H. YERSIN. 1976. Chem. Phys. Lett. **40:** 423.
17. YERSIN, H. & G. GLIEMANN. 1975. Ber. Bunsenges. Phys. Chem. **79:** 1050.
18. DAY, P. 1975. J. Am. Chem. Soc. **97:** 1588, and Ref. 1, p. 234.
19. MONCUIT, C. & H. POULET. 1962. J. Phys. Rad. **23:** 353.
20. YERSIN, H. & G. GLIEMANN. 1975. Z. Naturforsch. **30b:** 183.
21. YERSIN, H., G. GLIEMANN & U. RÖSSLER. 1977. Solid State Comm. **21:** 915.
22. GERHARDT, V. & W. v. AMMON *et al.* (Regensburg.) Unpublished.
23. GLIEMANN, G., W. HOLZAPFEL, H. H. OTTO & H. YERSIN. Inorg. Chim. Acta. Submitted.
24a. INTERRANTE, L. V. & R. P. MESSMER. Ref. 1. p. 382.
24b. INTERRANTE, L. V. & R. P. MESSMER. 1974. Chem. Phys. Lett. **26:** 225.
25. DANIELS, W. Diplomarbeit (Regensburg.) Unpublished.
26. YERSIN, H., H. OTTO & G. GLIEMANN. 1974. Theor. Chim. Acta **33:** 63.
27. GREEN, H. S. & C. A. HURST. 1964. Order-Disorder Phenomena. Wiley Interscience. New York, N.Y.
28. RÄDE, H.-S. 1975. Meßtechnik **83:** 230.
29. STOCK, M., I. HIDVEGI *et al.* (Regensburg.) Unpublished.
30. YERSIN, H. & M. STOCK. 1976. Proceedings XVIIIth ICCC: 103. Hamburg, Germany.
31. PIEPHO, S. B., P. N. SCHATZ & A. J. MCCAFFERY. 1969. J. Amer. Chem. Soc. **91:** 5994.
32. ISCI, H. & W. R. MASON. 1975. Inorg. Chem. **14:** 905.
33. MARSH, D. G. & J. S. MILLER. 1976. Inorg. Chem. **15:** 720.
34. MESSMER, R. P. & D. R. SALAHUB. 1975. Phys. Rev. Lett. **35:** 533.
35. SCHLÄFER, H. L. & G. GLIEMANN. 1969. Basic Principles of Ligand Field Theory. Wiley Interscience. New York, N.Y.
36. YERSIN, H. 1976. Ber. Bunsenges. Phys. Chem. **80:** 1237; J. Chem. Phys. Submitted.
37. DIEKE, G. H. 1968. Spectra and Energy Levels of Rare Earth Ions in Crystals. Wiley Interscience. New York, N.Y.
38. STEIN, G. & E. WÜRZBERG. 1975. J. Chem. Phys. **62:** 208.
39. DEXTER, D. L. 1953. J. Chem. Phys. **21:** 836.
40. LAMOLA, A. A. 1969. *In* Energy Transfer and Organic Photochemistry. A. A. Lamola and N. J. Turro, Eds.: 17. Wiley Interscience. New York, N.Y.
41. CROSBY, G. A., R. E. WHAN & R. M. ALIRE. 1961. J. Chem. Phys. **34:** 743.
42. YERSIN, H. & M. STOCK. Submitted for publication.
43. COWMAN, C. D. & H. B. GRAY. Inorg. 1976. Inorg. Chem. **15:** 2823.

DISCUSSION

PETER DAY: There are two different starting points from which one could set out to describe the electronic structure of molecular materials. One is the route

that you took in your tight-binding one-electron band-structure calculation. The other approach for a molecular solid would be to assume that there was essentially zero electron exchange between the constituent molecules, and then discuss the optical properties in terms of tightly bound excitons. Have any of the experiments that you have described actually enabled one to distinguish which is the better model for these substances? The most direct evidence that you could expect to have, at least for the excited states, would be if one detected photoconductivity. We attempted to detect photoconductivity, and to a very good approximation did not find any.

YERSIN: The electronic properties of the tetracyanoplatinates(II) along the stacking direction presumably lie in between these extreme limits. However, the wavefunctions overlap in chain direction is large, leading to delocalized Bloch-functions. The band-structure calculation based on this model quantitatively describes the transition energies for $\mathbf{E} \parallel c$. The measurement of photoconductivity can be obscured by many effects. Possibly trapping effects prevent the detection of photocurrents.

JACK WILLIAMS: The disodium tetracyanoplatinate trihyrate has a zig-zag chain and three different platinum-platinum separations. Which separation do you use in your calculations?

YERSIN: In most cases the emission comes from the lowest excited states, and this would lead to the shortest metal-metal distance. However, the error bars for the spectroscopic metal-metal distance determination is rather large in the corresponding UV emission range.

JERRY TORRANCE: If you extrapolate your energy as a function $1/R^3$ to infinite separation, you get an energy for that transition. How does that compare to what you find in solution?

YERSIN: The formal extrapolation leads to the energy value of the corresponding transition observed in solution.

STRUCTURE AND OXIDATION STATES OF Ir AND Pt ONE-DIMENSIONAL INORGANIC COMPLEXES*

Arthur H. Reis, Jr. and Selmer W. Peterson

Chemistry Division, Argonne National Laboratory
Argonne, Illinois 60439

INTRODUCTION

The field of one-dimensional anisotropically conducting inorganic complexes has been recently reviewed.[1] Since publication of that review article, significant contributions to the understanding of the anisotropic physical properties in these inorganic salts have been made by means of synthesis of new materials and their characterization by single crystal x-ray and neutron diffraction methods. Concomitantly, several classical 1-D materials, although first synthesized a number of years ago, had never been structurally characterized, and this appears to have retarded their physical and theoretical study. This paper will describe our attempts to accurately characterize several of these classical materials. We will present structural data on $K_2Pt(CN)_4 \cdot 3H_2O$, $K_{1.75}Pt(CN)_4 \cdot 1.5H_2O$, $K_{1.6}Pt(C_2O_4)_2 \cdot 1.2H_2O$, and $Ir(CO)_3Cl$. In our discussion of these diverse 1-D materials, emphasis is placed on the relationship of the structural properties, metal-metal distance and ligand conformation, and the partial oxidation state of the metal.

$K_2Pt(CN)_4 \cdot 3H_2O$ (KTCP)

The preparation of partially oxidized 1-D salts of the type $K_2Pt(CN)_4Br_{0.30} \cdot 3H_2O$, KCP(Br), and $K_2Pt(CN)_4Cl_{0.32} \cdot 3H_2O$, KCP(Cl), and the cation-deficient compound $K_{1.75}Pt(CN)_4 \cdot 1.5H_2O$, KDEF, requires the partial oxidation of the starting material, $K_2Pt(CN)_4 \cdot 3H_2O$, KTCP. The latter compound crystallizes as clear needles, noticeably dichroic, reflecting yellow light perpendicular to the needle axis and blue light along the axis. The conductivity is $\approx 10^{-9}$ that of KCP(Br).[2] We have investigated the three dimensional structure of KTCP by neutron diffraction.[3]

KTCP is orthorhombic, space group, *Pbcn*, with unit cell axes, $a = 13.426(5)$, $b = 11.848(4)$, $c = 6.956(2)$ Å and $Z = 4$. The crystal structure, shown in FIGURE 1, consists of nearly square planar $Pt(CN)_4^{2-}$ groups stacked parallel to the *c* axis of the crystal, thus forming *linear* Pt atom chains. A single Pt-Pt distance of 3.478(1) Å is observed along the linear chain, indicative of a weak metal-metal interaction. Even though this chain interaction is very weak, in accord with the lack of metallic properties, each $Pt(CN)_4^{2-}$ group influences those groups above and below it along the chain. As is shown in FIGURE 2, the CN ligands are staggered 15.7(1)° and 16.7(1)°. Since in this material the d^8 Pt is not partially oxidized, any electronic interaction between Pt atoms along the chain arises, as is

*Supported by the Division of Physical Research of the United States Energy Research and Development Administration. Manuscript received May 23, 1977.

0077-8923/78/0313-0560 $1.75/1© 1978, NYAS

shown in FIGURE 3(a) through the repulsion of a_{1g}–a_{1g} bonding and a_{2u}–a_{2u} antibonding MO's.[4] The stacks of $Pt(CN)_4^{2-}$ groups are further stabilized by hydrogen-bonded water molecules which link CN^- groups within a stack and also cross-link between CN^- groups of adjacent stacks (see FIGURE 1).

It is interesting to compare what happens to the KTCP lattice upon partial oxidation by the addition of Br^- or Cl^- to the lattice forming the familiar KCP(Br) and KCP(Cl) lattices,[5] shown in FIGURE 4. The point group symmetry is changed from mmm to 4mm and thus from centrosymmetric to noncentrosymmetric. The site symmetry of Pt is changed from $\bar{1}$ to 4mm. The $Pt(CN)_4^{2-}$ group is nearly square planar in KTCP, whereas it is square but distinctly nonplanar in KCP(Br). The K^+ ion and H_2O are distributed in opposite halves of the cell in the noncentrosymmetric KCP(Br), but they are symmetrically distributed in KTCP. The most striking changes are the shortening of the Pt-Pt separation from 3.478(1) to 2.890(1) Å (KCP(Br)), and the configurational change of the vertically stacked

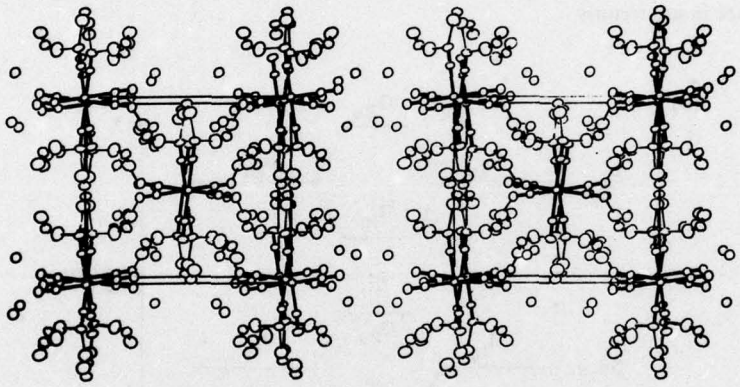


FIGURE 1. Stereopacking drawing of $K_2Pt(CN)_4 \cdot 3H_2O$ viewed down *c*. The *a* axis is horizontal and *b* is vertical. Hydrogen bonds are indicated by the lighter lines.

$Pt(CN)_4^{2-}$ groups from a staggered 16° torsion angle to a 45° configuration. In addition, while the four Pt atoms in the cell of KTCP are equivalent, there are two distinct Pt atoms in KCP(Br) with essentially equal separations. The shortened Pt-Pt separation has been previously explained to be due to a partial removal of $d_{Z}2$ electrons from Pt upon oxidation, which allows substantially improved $d_{Z}2$ orbital overlap and stronger metal-metal bonding (see FIGURE 3). The $Pt(CN)_4^{2-}$ group configurational change is undoubtedly due to the increased π-orbital repulsion of the CN^- groups brought into closer contact in KCP(Br).

In many respects the structures of KTCP and KCP(Br) are quite similar, in spite of the symmetry differences. The K^+ ions in KTCP have sevenfold coordination with four N and three O near neighbors, while in KCP(Br) the neighbors are Br plus four N and three O atoms, giving an eightfold antiprism coordination. There are two kinds of H_2O molecules in each structure. The $H_2O(1)$ molecules link $Pt(CN)_4^{2-}$ groups lying along the cell edges, and the $H_2O(2)$ molecules cross-link essentially along cell diagonals between nonequivalent CN^- ions at-

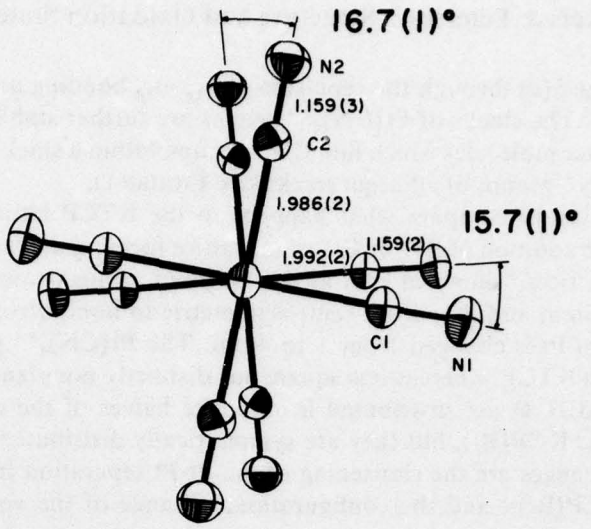


FIGURE 2. Stacking configuration of the $Pt(CN)_4^{2-}$ ions. View is down the *c* axis. Bond distances are in angstroms.

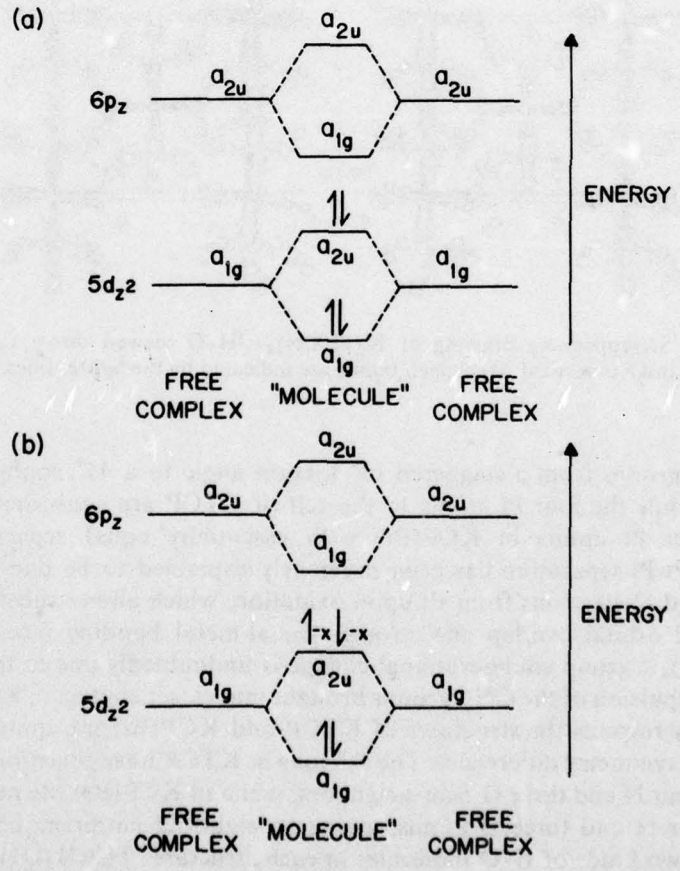


FIGURE 3. (a): Molecular orbital diagram of a complex formed between two $Pt^{2.0+}$ ions. (b): Molecular orbital diagram of a complex formed between two $Pt^{(2+x)+}$ ions.

tached to the $Pt(CN)_4^{2-}$ groups located diagonally across the cell. In both cases H_2O is given up readily.

$$K_{1.75}Pt(CN)_4 \cdot 1.5H_2O(KDEF)$$

Unlike the subtle yet electronically important lattice changes that occur when KTCP is partially oxidized to the anion excessive KCP(x), $x = Br^-$ or Cl^- materials, the partial oxidation of KTCP to $K_{1.75}Pt(CN)_4 \cdot 1.5H_2O$, (KDEF), with the removal of cations, has a drastic disruptive effect in the lattice. KDEF crystallizes in the triclinic space group $P\bar{1}$ with a = 10.323(14), b = 9.285(13), c = 11.865(17) Å, α = 77.31(3), β = 114.85(5), γ = 73.84(2)° and Z = 4. The

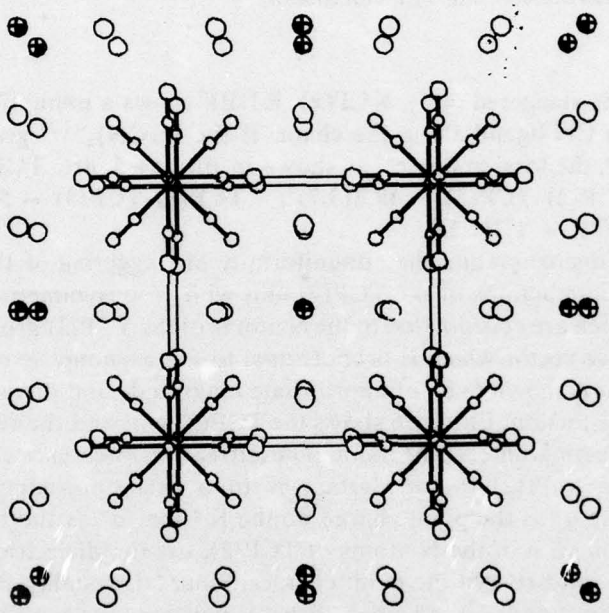


FIGURE 4. A unit cell of $K_2Pt(CN)_4 \cdot Cl_{0.32} \cdot 3H_2O$ viewed down the c axis.

most striking feature of the crystal structure of KDEF is the nonlinear zigzag chain of Pt atoms, Pt(1)-Pt(2)-Pt(3) = 173.21(2)° (see FIGURE 5), which arises from the transverse displacement (0.198(1) Å) of one of the three nonequivalent Pt atoms within the asymmetric unit. X-ray[6] and neutron[7] structural studies agree well on the magnitude and direction of this chain distortion and that its origin is not electronically caused or related to a Peierls distortion. Even though there are three nonequivalent Pt atoms, there appears to be only a single Pt-Pt distance; thus x-ray results[6] give Pt(1)–Pt(2) = 2.967(1) and Pt(2)–Pt(3) = 2.976(1), while neutron results[7] give Pt(1)-Pt(2) = 2.961(1) and Pt(2)-Pt(3) = 2.965(1) Å. The Pt-Pt distances are of the order of 0.1 Å longer than those found in KCP(Br) and KCP(Cl), and, as we shall discuss later in this paper, they appear to correlate with the smaller oxidation state of Pt in KDEF. Unlike the more eclipsed (~ 16°)

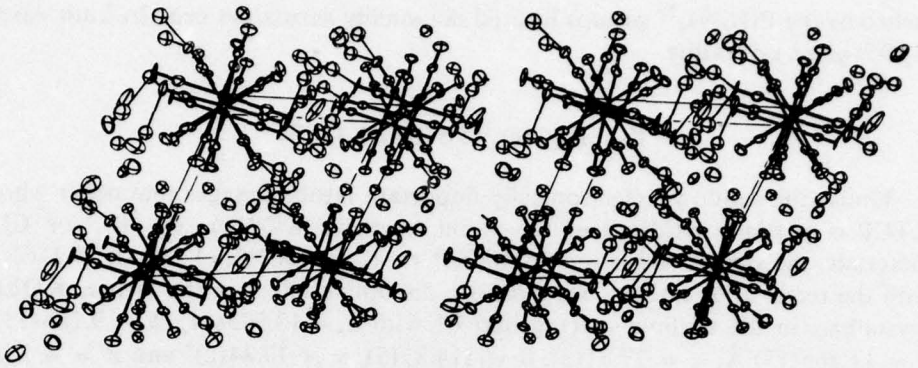


FIGURE 5. Stereopacking drawing of $K_{1.75}Pt(CN)_4 \cdot 1.5H_2O$ viewed down the *c* axis showing hydrogen bonding and TCP unit rotation.

KTCP, and the staggered (45°), KCP(*x*), KDEF shows a nonuniformity of staggering of each CN ligand along the chain. If the $Pt(CN)_4^{-1.75}$ groups are represented as TCP, the torsion angles, as shown in FIGURE 5, are: TCP(1)–TCP(2) = 45.3(5)°, TCP(2)–TCP(3) = 49.8(3.7)°, TCP(1)–TCP(3) = 5.1(2.1)°, and TCP(2)–TCP(2)′ = 1.7(1.1)°.

The chain distortion and the nonuniformity of staggering of the TCP groups are caused by interactions of the TCP(2) unit with an unsymmetrical distribution of K^+ ions which are coordinated to the N atoms of the TCP(2) group. A resultant coulombic force vector which is proportional to the asymmetric charge distribution of K^+ ions is shown to be of appropriate magnitude and direction to account for the Pt(2) distortion. FIGURE 6 shows the TCP(2) unit and the resultant K^+ ion point charges acting on each N atom. The attractive force exerted by a K^+ ion coordinated to a Pt(2) cyanide group is to a first approximation given by $q^+q^-/\epsilon r^2$ where q^+ is the point charge on the K^+ ion, q^- is the formal −0.4375 point charge on each of the N atoms of TCP(2), ϵ is the dielectric constant, and *r* is the separation between the point charges. Since *r* is roughly the same for all K^+-N interactions and ϵ is assumed to be a constant, the net force on Pt(2) is approximately proportional to the net K^+ ion point charge distribution and may be obtained by summing over all potassium ion-TCP(2) interactions. The sums of the K^+ ion charge components in the direction of the Pt-N vectors are 1.378, 0.994, 1.511, and 0.000 for N(1)′, N(2)′, N(3)′, and N(4)′, respectively (see FIGURE 6). The components along the *x* and *y* crystal axes of the resultant charges are then 0.601 and −1.215, which should be directly proportional to the forces exerted along these directions. These unbalanced point charges acting on the Pt(2) tetracyanoplatinate unit would be expected to displace it until restoring forces set up a new equilibrium. The actual displacement of Pt(2) observed in this study has *x* and *y* components of 0.096 and −0.198 Å, respectively. The ratio of the magnitudes of the resultant point charges along the *x* and *y* axis is −0.495; the ratio of the Pt(2) shift components in the *x* and *y* directions is −0.485. Clearly this simplified model is in good agreement with the observed direction and relative ratio of the displacement in the *x* and *y* directions. It is also possible to show very

approximately that the chief restoring force is the stretching of the Pt(1)—Pt(2) and Pt(2)—Pt(3) bonds.

Degree of Partial Oxidation—Bond Distance Correlations

As we have stated in the previous section, the decrease in the partial oxidation state in KDEF to $Pt^{2.25}$ appears to correspond to an increase in Pt-Pt distance when compared to the KCP(x) materials. Contrary to previous data showing only a few partial oxidation states being stabilized, a number of partial oxidation states have been reported for 1-D salts (Table 1) where the basic bonding unit, the polymeric $[Pt(CN)_4]_x$ or $[Pt(C_2O_4)_2]_x$ chain is present in all known structures. In order to establish a physical correlation among these partially oxidized materials, a partial oxidation—bond distance correlation may be adopted.[8,9]

Some years ago, Pauling[10] introduced the resonating valence bond theory of metals (RVBM) and used it to assign metallic valences and to successfully correlate a vast amount of data concerning structure and interatomic distances in metals. The theory assumes the existence of a fractional metallic orbital, formally empty, which makes possible unsynchronized resonance of electron-pair bonds between adjacent metal atoms. The resulting resonance stabilization leads to the characteristic metal bond and other metallic properties. The dependence of metal-metal distances on bond numbers was formulated as $D_n = D_0 - 0.600 \log n$, where D_n and D_0 are metallic distances applicable to bond numbers n and 1, respectively, with $n \leq 1$. Bond number refers to the number of electron pairs involved in a bond and is assigned by means of a relation equating the valence of an atom to the sum of the bond numbers for all bonds to a given atom. The

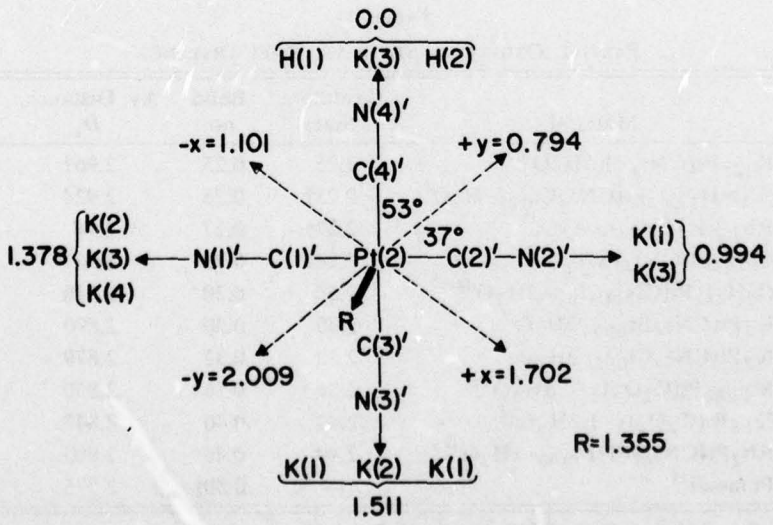


Figure 6. TCP unit 2 showing the resultant K^+ point charges acting on the various CN^- ligands and the resultant Pt chain deformation.

bond between the metal atoms is strengthened, if electrons are removed from the a_{2u} antibonding molecular orbitals (FIGURE 3) by partial oxidation of the metal. FIGURE 3 describes a simplified M.O. description of $Pt^{2.0+}$ complex which has been partially oxidized to a $Pt^{(2+x)+}$ state. Here x electrons per atom are removed from the a_{2u} antibonding molecular orbitals; the bonding stabilization is therefore related to $2x$, the number of bonding electrons, and the metallic valence = x for 1-D chain bonding. Since the oxidation state of Pt is $(2 + x)^+$ the bond number is equal to the increase (x) in oxidation state due to partial oxidation. Using this approach and the equation $D_n = D_0 - \alpha \log n$ where D_n is the average metal-metal distance in a 1-D partially oxidized Pt complex, D_0 = 2.590 Å a Pt-Pt single bond distance,[11] and n the fractional part of the partial oxidation state which is equal to the bond number, TABLE 1 gives calculated values of α for eleven different 1-D metallic complexes and Pt metal. α varies over a small range from 0.527 in $Rb_2Pt(CN)_4(FHF)_{0.40} \cdot xH_2O$[14b] to 0.640 for $K_{1.6}Pt(C_2O_4)_2 \cdot 1.2H_2O$;[15] however, in these two materials the stoichiometries are still doubtful. A least-squares fit of these twelve values of α gives an average value of 0.59 ± 0.03, which is surprisingly similar to that determined by Pauling 30 years ago for 3-D metals. Therefore, the degree of partial oxidation appears to be directly related to the metal-metal distance in at least a closely related series of compounds such as these partially oxidized Pt 1-D materials. The relation, since it holds for both free metals and the 1-D metal complexes, implies a metallic bond involving resonance stabilization, which is common to both types of materials.

$$K_{1.6}Pt(C_2O_4)_2 \cdot 1.2H_2O\,(KDOX)$$

The two complexes $Mg_{0.82}Pt(C_2O_4)_2 \cdot 5.3H_2O$[13] and $K_{1.6}Pt(C_2O_4)_2 \cdot$

TABLE 1

PARTIAL OXIDATION STATE VS. Pt-Pt DISTANCE

No.	Material	Oxidation State	Bond no.	Av. Distance, D_n	α*
1	$K_{1.75}Pt(CN)_4 \cdot 1.5H_2O$[6,7]	2.25	0.25	2.967	0.626
2	$[C(NH_2)_3]_2Pt(CN)_4Cl_{0.25} \cdot H_2O$[12]	2.25†	0.25	2.924	0.555
3	$Rb_{1.73}Pt(CN)_4 \cdot xH_2O$[17]	2.27†	0.27	2.94	0.616
4	$Cs_{1.72}Pt(CN)_4 \cdot xH_2O$[17]	2.28†	0.28	2.88	0.524
5	$(NH_4)_2Pt(CN)_4Cl_{0.3} \cdot 3H_2O$[14a]	2.30	0.30	2.910	0.612
6	$K_2Pt(CN)_4Br_{0.30} \cdot 3H_2O$[5]	2.30	0.30	2.890	0.573
7	$K_2Pt(CN)_4Cl_{0.32} \cdot 3H_2O$[5]	2.32	0.32	2.879	0.584
8	$Mg_{0.82}Pt(C_2O_4)_2 \cdot 5.3H_2O$[13]	2.36	0.36	2.850	0.586
9	$K_{1.6}Pt(C_2O_4)_2 \cdot 1.2H_2O$[15]	2.40	0.40	2.845	0.640
10	$Rb_2Pt(CN)_4(FHF)_{0.40} \cdot xH_2O$[14b]	2.40	0.40	2.800	0.527
11	Pt metal[16]	—	0.50‡	2.775	0.614

*$D_n = D_0 - \alpha \log n$, D_0 = 2.590 Å. $\alpha_{av} = 0.59 \pm .03$.

†Values of the partial oxidation state obtained from diffuse scattering measurements.

‡Pt metal is assigned a metallic valence of 6 and has 12 near neighbors; hence the bond number is 0.5.

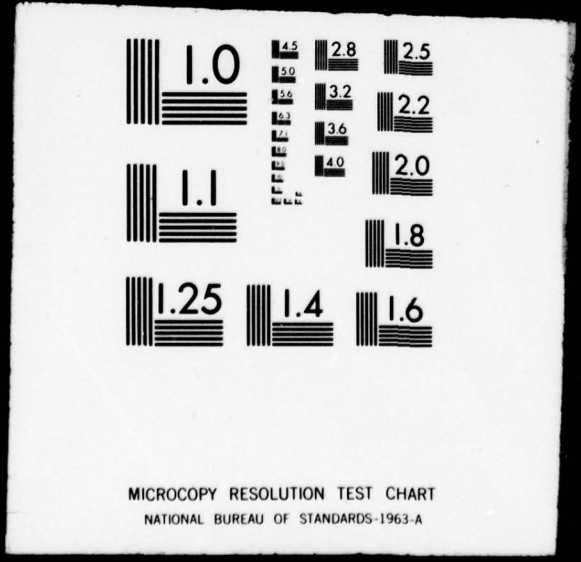
AD-A065 304 NEW YORK ACADEMY OF SCIENCES N Y F/G 7/2
SYNTHESIS AND PROPERTIES OF LOW-DIMENSIONAL MATERIALS.(U)
1978 J S MILLER, A J EPSTEIN N00014-77-C-0374
UNCLASSIFIED NL

7 OF 9
AD A065304



7 OF 9

AD
A065304



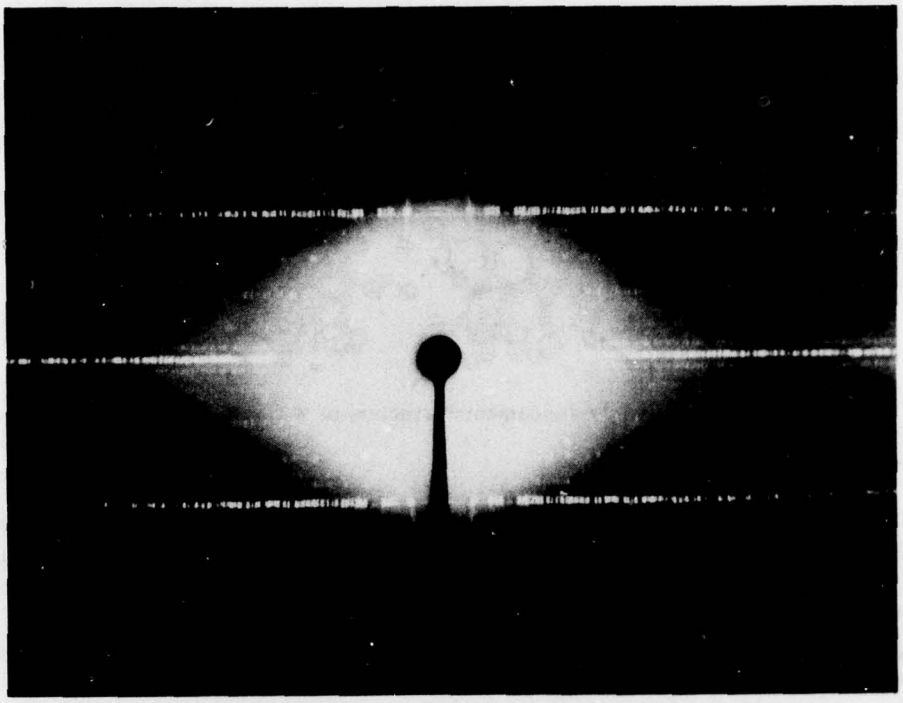


FIGURE 7. A rotation photograph of a crystal of $K_{1.6}Pt(C_2O_4)_2 \cdot 1.2H_2O$ mounted along the c axis showing the metal lattice (c_m), the intermediate cell ($4 \times c_m$), and the incommensurate metal superlattice ($10.25 \times c_m$).

$1.2H_2O$,[15] KDOX, are the only partially oxidized platinum oxalate complexes to have their structures characterized by x-ray diffraction. In many aspects the chemistry and physical properties of these oxalate salts are very similar to those one-dimensional CN salts which we have described earlier; however, in other aspects, especially the existence of several phases for each salt, their chemistry is quite different. Within this section we will present a detailed description of the $K_{1.6}Pt(C_2O_4)_2 \cdot 1.2H_2O$, (KDOX), phase and compare it structurally with $Mg_{0.82}Pt(C_2O_4)_2 \cdot 5.3H_2O$ and the cationic deficient CN complexes.

FIGURE 7 shows an x-ray rotation photograph of a crystal of KDOX mounted along the c axis. The KDOX lattice may be described in terms of three cells that differ in their c axis length. The smallest cell (most intense reflection spacing on the photograph) represents a metal-metal spacing along the c axis of 2.844 Å (c_m), the intermediate cell (weak commensurate levels on the photograph) a spacing of exactly $4 \times c_m$, which is indicative of the ligand repeat and transverse chain distortion; and the largest cell (weak incommensurate levels bracketing the most intense lattice reflections) a spacing of $10.25 \times c_m$, which may be indicative of sinusoidal displacements of the metal-ligand groups. Ignoring the superlattice incommensurate data at this time, we will discuss only the fundamental structure of KDOX, which is shown in FIGURE 8.

KDOX crystallizes in the triclinic space group, $P\bar{1}$, with unit cell constants, $a = 9.744(12)$, $b = 10.700(13)$, $c = 11.377(14)$ Å, $\alpha = 80.23(6)°$, $\beta = 77.97(7)°$,

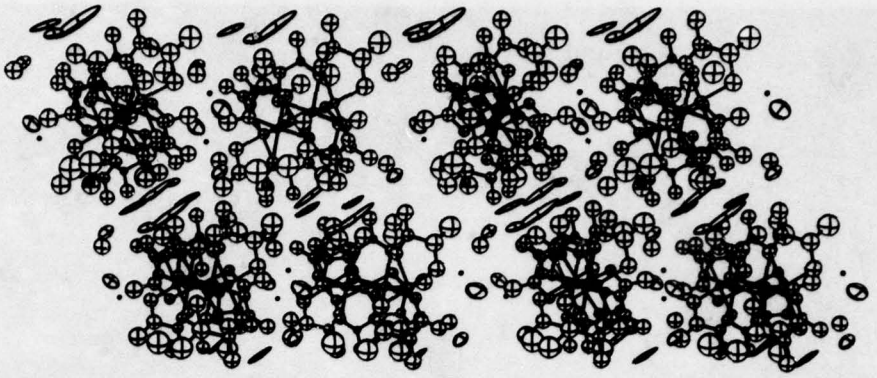


FIGURE 8. A stereoview of the fundamental structure of $K_{1.6}Pt(C_2O_4)_2 \cdot 1.2H_2O$ viewed down the *c* axis of the lattice.

$\gamma = 115.87(3)^\circ$ and $Z = 4$. The structural properties of the fundamental structure of this 1-*D* compound are quite similar to those observed for $K_{1.75}Pt(CN)_4 \cdot 1.5H_2O$, KDEF. They include: (1) The formation of parallel zig-zag Pt atom chains aligned along the *c* axis. (2) A transverse Pt atom displacement of 0.056(5) Å (somewhat smaller than in KDEF), and a Pt(1)-Pt(2)-Pt(3) bond angle of 177.8(2)°. (3) Three nonequivalent Pt atoms in the chain and two Pt-Pt distances, 2.857(2) and 2.833(2) Å. (4) The oxalate ligands are bidentate and are staggered (~ 45°) with respect to the ligands directly above and below it in the chain (see FIGURE 9). However, all Pt(2) oxalate ligands are eclipsed (~ 5°), whereas Pt(1) and Pt(3) oxalate ligands are staggered (~ 90°), giving a staircase effect to the ligands. (5) Except for a single K^+ ion, all other K^+ ions and water molecules are positionally disordered. There are five K^+ ion sites and five H_2O sites in the asymmetric unit. (6) K^+ ion and water molecule interactions cause the exterior oxygens of the oxalate ligands to be bent from planarity. (7) An oxidation state of 2.4 for Pt is indicated by the crystallographic stoichiometry and is in good agreement with that found by chemical analysis.[18]

Both KDOX and KDEF materials are triclinic and the platinum atom sites are such that in each structure two of the Pt atoms are at centers of symmetry and the third at a general position. This arrangement allows displacement of Pt atoms in the general positions giving rise to nonlinear zigzag chains of Pt atoms in both structures. The driving force behind the chain distortion in KDEF is the asymmetric distribution of K^+ ions around Pt(2). KDOX also has an asymmetric K^+ ion distribution around Pt(2), and the chain distortion is in the direction of the shortest O–K^+ interaction. The displacement amplitude, however, is only 0.056(5) Å compared to the 0.198(1) Å displacement found in KDEF. This is attributed to the greater shielding effect of the larger and more complex oxalate ligand and to an increase in the π bonding due to the overlap of oxalate molecular orbitals of like symmetry.

The Pt-Pt bond distances in KDOX are inequivalent and differ by 0.024 Å ± .003. However, the Pt-Pt separations given above should not be taken as definitive, since the noncommensurate superlattice intensities were not included in the calculation. These superlattice reflections persist to very high 2θ angles (160° Cu$K\alpha$),

giving evidence of their origin in scattering from Pt atoms. The supercell becomes commensurate with the intermediate cell at 116.19 Å, which delineates a 41 Pt atom repeat. The average Pt-Pt distance of 2.845 Å is quite consistent with the experimental oxidation state of 2.4 for Pt determined crystallographically from the K^+ ion site occupancies.

Finally, we wish to comment on the interesting and unique ligand conformation in KDOX. In the previously characterized $Mg_{0.82}Pt(C_2O_4)_2 \cdot 5.3H_2O$, the $Pt(C_2O_4)_2^{-1.64}$ units show a repeat of two units staggered by 60°. In the KDOX chain, three units are staggered by 45° and 90° from the first. Recent intermolecular orbital calculations[19] have accounted for the 60° rotation in $Mg_{0.82}Pt(C_2O_4)_2 \cdot 5.3H_2O$ in that for this rotation a maximum number of attractive versus repulsive orbital overlaps occur between the HOMO and LUMO of appropriate symmetry. By similar calculations for KDOX, the staircase configuration is easily justified in that 12 favorable overlaps occur between each of the two consistent pairs of HOMO and LUMO orbitals of appropriate symmetry[20] (see FIGURE 10). The conformations that are observed for the $Mg_{0.82}Pt(C_2O_4)_2 \cdot 5.3H_2O$ and for KDOX appear quite different. From the M.O. results, however, they are indeed very similar. In KDOX the third oxalate ligand is rotated 90° to the first and 45° to the second; however, if it were rotated to be eclipsed with the first ligand (still staggered 45° to the second) the same number of orbital overlaps will result because of a mirror plane passing through the C—C bonds of the LUMOS. Now this hypothetical arrangement is quite similar to the $Mg_{0.82}Pt(C_2O_4)_2 \cdot 5.3H_2O$

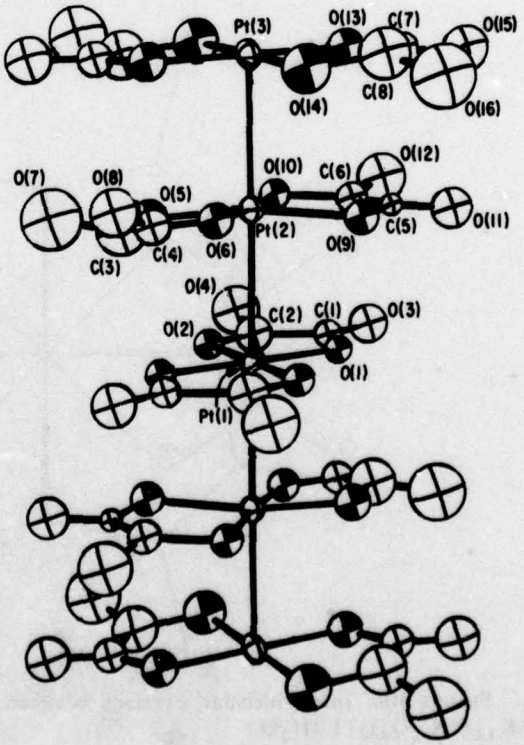


FIGURE 9. A single wavelength of the Pt chain showing the ligand conformation in $K_{1.6}Pt(C_2O_4)_2 \cdot 1.2H_2O$.

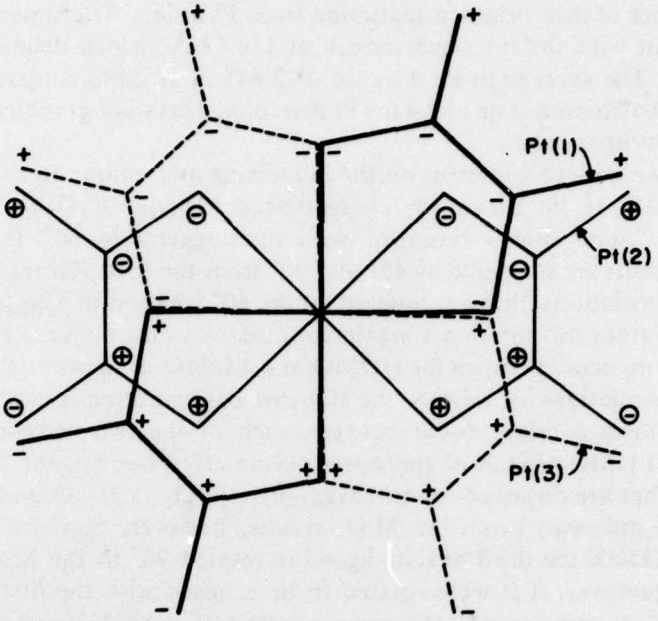


FIGURE 10a. Intermolecular overlaps between the LUMO, b_{2g}, and HOMO, b_{3g}, in $K_{1.6}Pt(C_2O_4)_2 \cdot 1.2H_2O$.

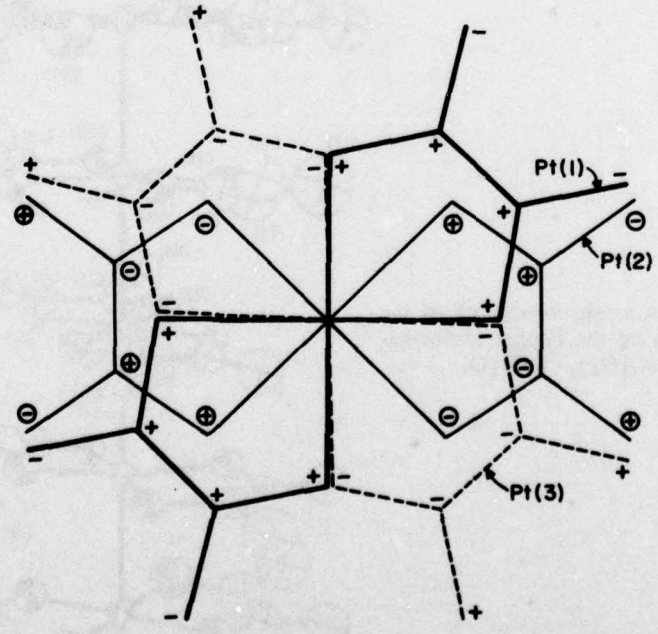


FIGURE 10b. Intermolecular overlaps between the LUMO, b_{1u}, and HOMO, a_u, in $K_{1.6}Pt(C_2O_4)_2 \cdot 1.2H_2O$.

conformation except for a 15° rotation difference. A very shallow energy barrier might be assumed between the 45° and 60° conformation, where packing restrictions will determine the final configuration of the polymer chain.

$Ir(CO)_3Cl$

Recently, controversy has arisen concerning the 1-D chain compound originally characterized as $Ir(CO)_3Cl$[21,22] and later reported to be nonstoichiometric, $Ir(CO)_{2.93}Cl_{1.07}$[23] or $Ir(CO)_3Cl_{1.1}$.[24] A preliminary report on the x-ray structure of the Ir compound gave the stoichiometry as $Ir(CO)_{2.93}Cl_{1.07}$ based on an unpublished chemical analysis.[23] Since the structure of this compound involved stacked square planar groups and short Ir-Ir distances, it was described as similar to the partially oxidized cyanoplatinate compounds which share similar physical properties and structures. The reported chemical formulation was rationalized by suggesting that a small amount of $Ir(CO)_2Cl_2$ was incorporated into the crystal. Others[24] have concluded that the excess Cl^- ion must reside interstitially within the crystalline lattice on the basis of Ir^{193} Mössbauer data, which suggest Ir is present in a single-valence state and also magnetic susceptibility data, which rules out the presence of Ir^{+2}. It is well known, however, that this material sublimes readily at 150°C in a stream of CO, which seems to be inconsistent with an ionic state. A quite different objection to the formulation $Ir(CO)_3Cl_{1.1}$ is that it implies an $Ir^{1.1}$ oxidation state, suggesting a very weak Ir-Ir bond of bond number 0.1[8,9] and an expected Ir-Ir bond distance of 3.16 Å. The observed distance, 2.844 Å, corresponds to a stronger bond of bond number ~ 0.3 with an oxidation state of $Ir^{1.3}$. Thus, a much larger amount of Cl^- ion is expected to be present if this material is to be described similarly to the Pt 1-*D* materials. The class of anionic iridium carbonyl halide complexes[25,26] $R_xIr(CO)_2Cl_2$ (x = 0.38 – .52), which are partially oxidized and have higher oxidation states are cases in point. We have therefore concluded based on our structural data and other physical measurements that $Ir(CO)_3Cl$ is stoichiometric.[27]

$Ir(CO)_3Cl$ prepared by the method of Fischer and Brenner[22] and sublimed at 150°C in a CO stream resulted in long copper-brown orthorhombic needle crystals. The space group is C_{mcm}, and the cell dimensions are a = 5.687(2), b = 15.168(5), c = 12.909(7) Å, and Z = 8. The chemical analysis of this material is shown in TABLE 2 along with the calculated values for $Ir(CO)_3Cl_{1.1}$ and $Ir(CO)_3Cl$. Single x-ray sized crystals were used for one of the determinations to eliminate impurities as far as possible. This table clearly indicates that the stoichiometry of our samples is $Ir(CO)_3Cl$, showing no excess halide. In the structure solution all atoms were refined anisotropically to a final R_F2 = 0.019 for 581 reflections with no reflections considered unobserved. This very low discrepancy index reflects the high accuracy of our structural model and the completeness of our refinement.

The chief structural findings which relate directly to the one-dimensional character are: (1) Two crystallographically different Ir atoms at $(0, 0.083, \frac{1}{4})$ and $(0, 0.581, \frac{1}{4})$ and a single Ir-Ir bond distance of 2.844(1) Å and a Ir(1)-Ir(2)-Ir(1) bond angle of 178.53(2)°. (2) Staggered planar $Ir(CO)_3Cl$ molecules are stacked parallel to the a axis (see FIGURE 11) (3) A stacking disorder of

TABLE 2

ELEMENTAL ANALYSIS OF $Ir(CO)_3Cl$ SAMPLE*†

	% Ir	% C	% Cl
Calculated $Ir(CO)_3Cl_{1.1}$	60.97	11.43	12.37
Calculated $Ir(CO)_3Cl$	61.67	11.56	11.37
Single Crystal Sample‡ Two Sublimations in CO	61.92	11.36	10.90
Powder Sample, Two Sublimations in CO	61.98	11.20	11.11

*Elemental analysis performed by Galbraith Laboratories, Inc., Knoxville, Tenn. 37921.
†% O_2 cannot be determined in the presence of Ir, C, and Cl.
‡The calculated stoichiometry determined from the single-crystal sample and based on integral CO is $Ir_{1.02}(CO)_3Cl_{0.98}$.

$Ir(2)(CO)_3Cl$ groups results in a close overlap of the Cl and one CO ligand (see FIGURE 12). The 50% positional disorder was completely resolvable because of the excellent refinement. When refinement of the multipliers of each of the disordered atoms were included as variables, no change from the 50% weighting initially assumed was found. This result precludes the existence of $Ir(CO)_2Cl_2$ groups within the chains, which is in agreement with the previous Mössbauer and magnetic data.[24] (4) The bond distances of the ligands bonded to Ir(1) and Ir(2) are shown in FIGURE 12. The Ir-CO distances indicate multiple bond character. The Ir(1)-CO bond which is *trans* to the Cl bond is 0.071(8) Å shorter than the *cis* Ir-CO distance. This is consistent with a strong *trans* bond and a large backbonding d-π_{z^*} contribution. (5) Unlike the Pt 1-D materials where water molecules and counter ions fit into holes or channels in the lattice, $Ir(CO)_3Cl$ crystallizes in a close-packed lattice where all intermolecular contacts except for the Ir-Ir bond are at normal van der Waals distances. This leaves no room for interstitial Cl^- sites, as can be verified by inspection of FIGURE 11.

Our recent time of flight mass spectral data gives an indication of the source of the 50% Cl-CO disorder about one of the Ir atoms and the mechanism for the

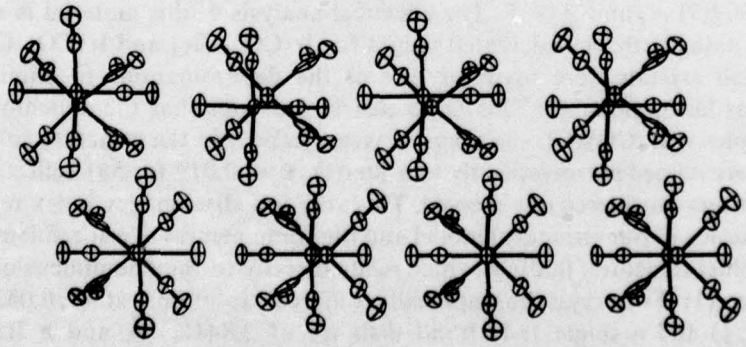


FIGURE 11. A stereoview of a unit cell of $Ir(CO)_3Cl$ viewed down the *a* axis. The close packing of $Ir(CO)_3Cl$ units is easily observed.

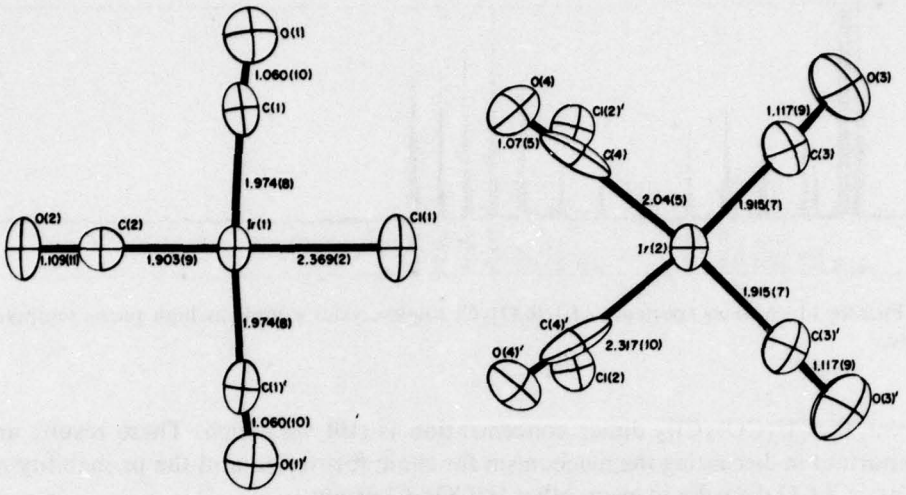


FIGURE 12. The two different $Ir(CO)_3Cl$ units with atom labeling and bond distances.

formation and disruption of the metal chain. FIGURE 13 shows a mass spectrum of a powdered $Ir(CO)_3Cl$ sample at a low probe temperature which has three distinct mass areas corresponding to the materials $Ir(CO)_3Cl$, $[Ir(CO)_2Cl]_2$ dimer, and an $Ir_4(CO)_{12}$ impurity. The $Ir_4(CO)_{12}$ is formed in the gas phase $IrCl_3$ + CO reaction and is more highly soluble in H_2O, the solvent used to slurry the $Ir(CO)_3Cl$ onto the probe of the mass spectrometer. The most striking result is the apparent strength of the $[Ir(CO)_2Cl]_2$ dimer, which is believed to be similar to the Rh analog,[28] and the lack of higher polymeric $[Ir(CO)_3Cl]_n$ units. Also, only a very low concentration of the $Ir(CO)_3Cl$ monomer is evident at this temperature. These observations imply that $[Ir(CO)_2Cl]_2$ is probably very volatile and is formed by the destruction of the polymeric chains. FIGURE 14 shows a mass spectrum taken over the same mass range but for a single-crystal sample of $Ir(CO)_3Cl$ at a higher probe temperature. The concentration of $Ir_4(CO)_{12}$ in this sample is negligible compared to the other mass fragments. Also, the concentration of the apparent $Ir(CO)_3Cl$ monomer has increased at this higher temperature. This may either be due to monomer $Ir(CO)_3Cl$ fragments being volatilized at the probe or to reaction of CO + $[Ir(CO)_2Cl]_2$ dimer in the mass spectrometer. In any

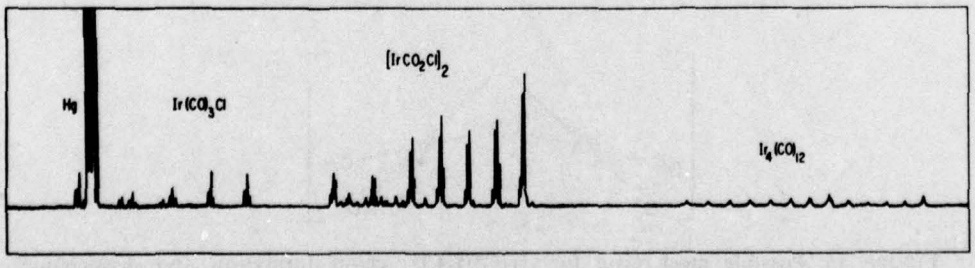


FIGURE 13. A mass spectrum of $Ir(CO)_3Cl$ powder sample at low probe temperature.

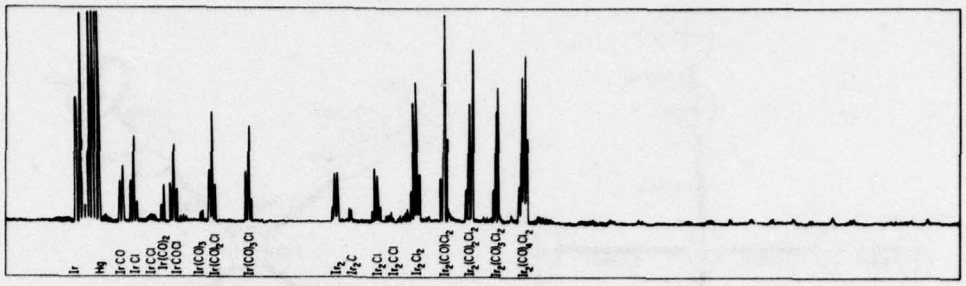


FIGURE 14. A mass spectrum of $Ir(CO)_3Cl$ single-crystal sample at high probe temperature.

event, the $[Ir(CO)_2Cl]_2$ dimer concentration is still very high. These results are important in discussing the mechanism for chain formation and the probability of a 50% Cl-CO disorder in every other $Ir(CO)_3Cl$ group.

We and others[21-24] have pointed out that $Ir(CO)_3Cl$ can be purified by subliming the material in a stream of CO. We have tried to sublime this material in a stream of high-purity N_2 without success; instead, a deep blue material results which is highly insoluble and which has not been characterized. A possible mechanism for chain formation is shown in FIGURE 15. Upon heating, the weak

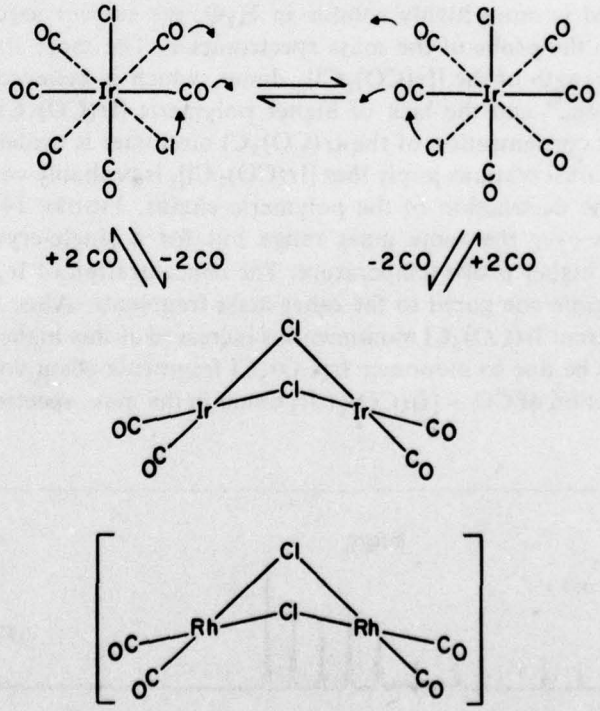


FIGURE 15. Possible mechanism for $[Ir(CO)_3Cl]_n$ chain formation and dissociation to the $[Ir(CO)_2Cl]_2$ dimer, which is similar to the known $[Rh(CO)_2Cl]_2$ dimer.

metal-metal bonds are assumed to be broken and the $Ir(CO)_3Cl$ units which result are unstable and lose one CO group; this is presumably a CO which is *cis* to Cl and thus less tightly bound (see FIGURE 12). The volatile $Ir(CO)_2Cl$ which is formed is coordination-unsaturated, hence combine in pairs to form dimeric $[Ir(CO)_2Cl]_2$. The dimer, in turn, reacts in the presence of excess CO to reform $Ir(CO)_3Cl$ monomers which then recombine to form $[Ir(CO)_3Cl]_x$ units which eventually form the polymeric crystal. This mechanism also accounts in part for the observed CO-Cl disorder. The close approach of the $Ir(CO)_3Cl$ groups in the chain polymer requires, in order to reduce steric hindrance, a staggered arrangement in which each Cl atom lies between two CO ligands in the groups directly above and below it in the chain. Thus, assuming the observed ordering of the $Ir(1)(CO)_3Cl$ units in the chain, the incoming $Ir(2)(CO)_3Cl$ groups can select either of the two equally likely staggered orientations. The expected result is, of course, the observed 50% Cl-CO disorder. It is of interest to observe that a mass spectrum of $Na_{0.6}Ir(CO)_2Cl_2 \cdot xH_2O$ (see FIGURE 16) also shows as a dominant feature the $[Ir(CO)_2Cl]_2$ mass peaks.

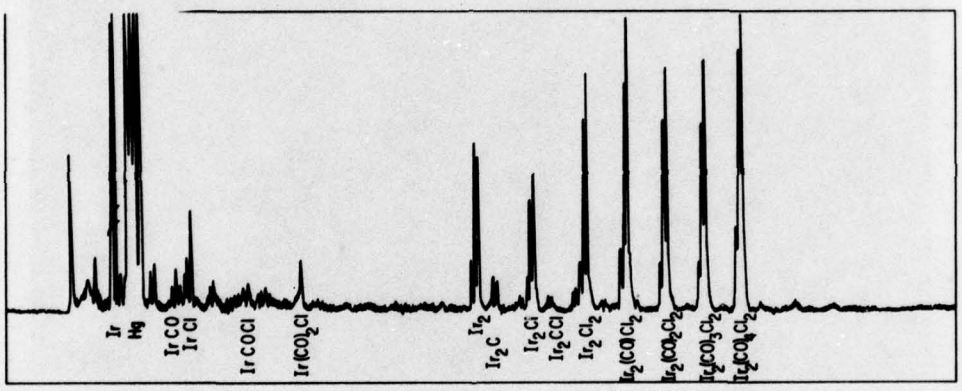


FIGURE 16. A mass spectrum of an $Na_{0.60}Ir(CO)_2Cl_2 \cdot xH_2O$ sample.

Based on the above structural and analytical evidence, we therefore conclude that $Ir(CO)_3Cl$ is indeed stoichiometric and thus cannot be considered to be another example of *partially oxidized* 1-*D* materials. This finding is highly significant in view of the considerable evidence that this material has some of the properties of a metal or semimetal; e.g., its metallic luster, high conductivity, and linear metal chains with very short metal-metal bonds. We are now attempting to examine the implications of this finding, and particularly to explore further the metallic nature of $Ir(CO)_3Cl$ by means of x-ray diffuse scattering photographs, a reexamination of Mössbauer data, and by polarized reflectance measurements that are in progress.

An x-ray diffuse scattering photograph of $Ir(CO)_3Cl$ is shown in FIGURE 17. The sample that was used for this experiment was the same single crystal used in the three-dimensional x-ray analysis. The exposure time for the sample was 48 hours. No diffuse superlattice lines appear for a $2k_f$ distortion. However, diffuse

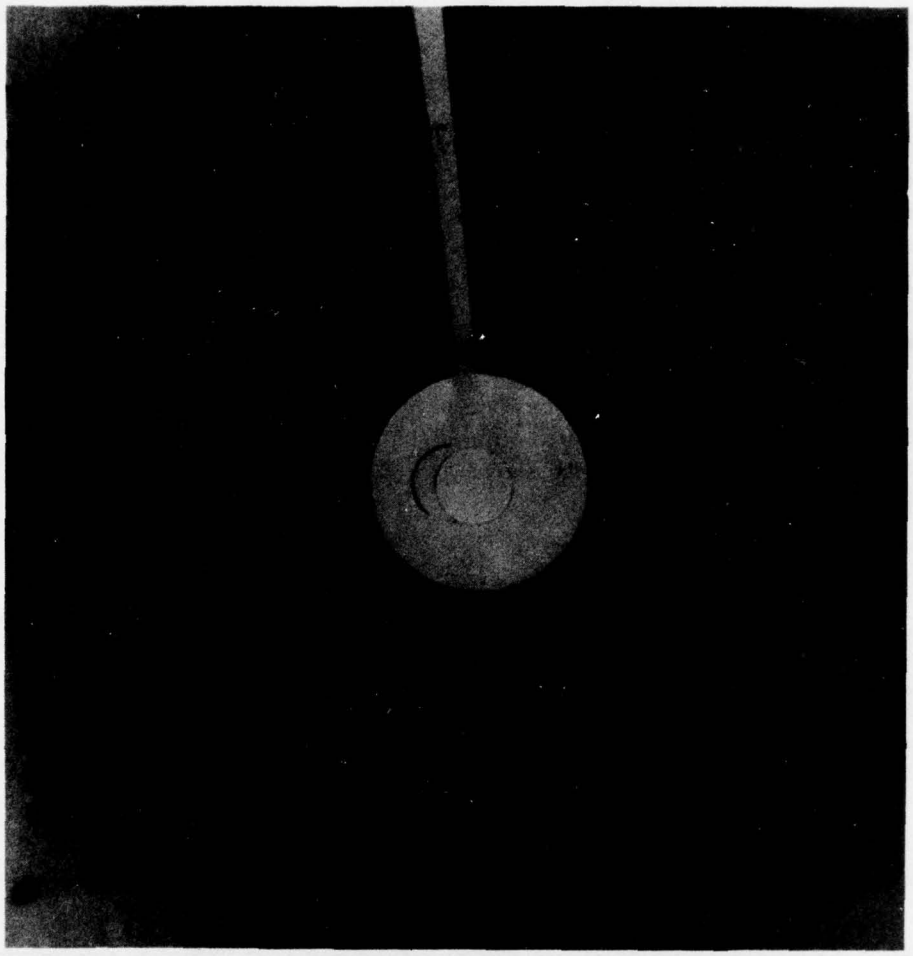


FIGURE 17. A diffuse x-ray scattering photograph of $Ir(CO)_3Cl$.

lines are observed that are commensurate with the Bragg lattice at $n \cdot a/2$ and show intensities increasing with Bragg order. There is no indication of a diffuse line passing through the zero level. This type of diffuse scattering is indicative of a linear disorder.[29] An obvious linear disorder in the structure is that due to the random (supposed) ordering of Cl and CO in columns along a due to the observed Cl(2)-CO(4) disorder. However, the reciprocal spacing of the disordered units is a*, whereas the diffuse pattern spacing is 2a*. The diffuse spacing does correlate however with the Ir atom reciprocal spacing 2a*. Thus, the diffuse planes of scattering would appear to be related to Ir atom, or more probably $Ir(CO)_3Cl$ group-displacements along a. If the latter is the case, it may represent slight displacements of adjacent chains with respect to each other. It is interesting to conjecture alternatively whether the diffuse scattering is evidence for a basic instability such as the Kohn anomaly. The lack of diffuse satellite type scattering would appear to rule out the existence of such an instability. However, if $2k_f$ is very small, which is likely in the case of a semimetal with few carriers, the expected closely

spaced satellite pair of diffuse lines would be unresolved. We estimate that the resolution of the diffuse camera system is sufficient to allow detection of splitting due to $2k_f > 0.03$. Thus we cannot completely rule out a Kohn anomaly, but we apparently can rule out an oxidation state of 1.1 for Ir (and associated band splitting) in $Ir(CO)_3Cl$.

Mössbauer data contain additional information regarding the oxidation of Ir in various 1-*D* materials and thus bear indirectly on the question of metallic character. FIGURE 18 shows ^{197}Ir Mössbauer data[30] compiled for several Ir materials in a plot of oxidation state versus isomer shift (mm/sec). If $Ir(CO)_3Cl$ is not considered at first, a linear plot results for the three materials $(C_6H_5)_4As[Ir(CO)_2Cl_2]$, $K_{0.60}[Ir(CO)_2Cl_2]\cdot 0.5H_2O$, and $[(C_6H_6)_4As]_2\ [Ir_2(CO)_4Cl_6]$. Making use of this relationship, the reported isomer shift of $-.040$ mm/sec for $Ir(CO)_3Cl$ leads to an apparent oxidation state of 1.32 for the Ir, instead of the previous values of 1.10 based on a questionable stoichiometry. The oxidation state of 1.32 is consistent with the value of 1.30 calculated from the Ir-Ir bond distance of 2.844(1) Å. The meaning of this finding is, however, far from clear. The formal oxidation state of Ir is clearly +1. Back-bonding to the CO ligands is expected and the actual charge on the Ir atom may well be greater than 1, which would, of course, be reflected in the s electron density at the nucleus and the so-called oxidation state. This, however should not be equated with the partial oxidation state assumed in the chemical and band models used for the Krogmann salts.

A qualitative model consistent with some of the known properties of $Ir(CO)_3Cl$ involves overlap of the filled $5d_{z^2}$ band with the empty $6p_z$ bands as is shown in the simplified M.O. diagram in FIGURE 19. If the $6p_z$ molecular orbitals are decreased in energy such that the a_{1g} bonding orbital overlaps with the a_{2u} antibonding orbitals of the $5d_{z^2}$ band and x electrons are removed from the a_{2u}

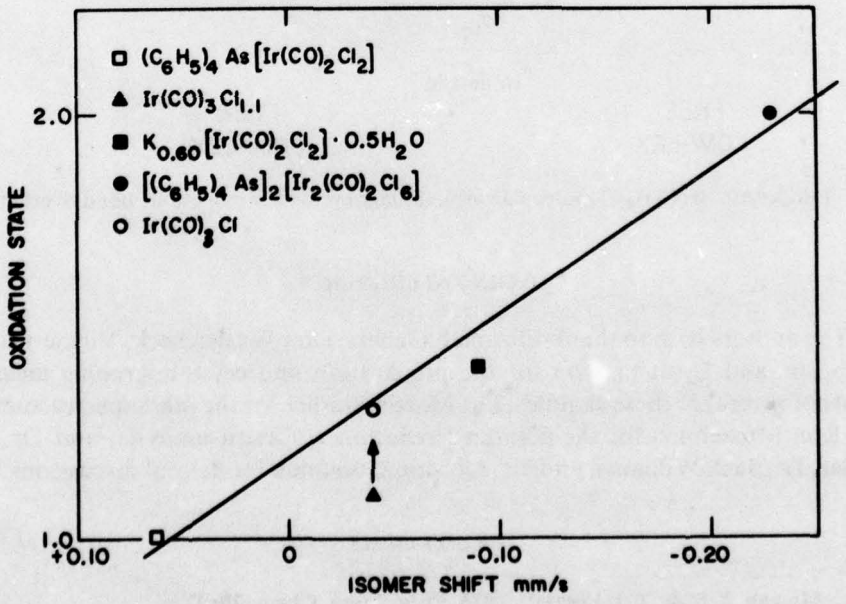


FIGURE 18. Oxidation state vs. isomer shift (mm/sec)[30] for several Ir materials.

and transferred to the a_{1g}, then x is 0.15 e^- per Ir atom to account for apparent bond number of 0.30. This electron transfer results in $2 + 2x$ electrons in the bonding orbitals and $2 - 2x$ electrons in the antibonding orbitals, producing a net bond strength of $4x$ electrons, and if x is equal to 0.15 e^- a bond is formed of bond number 0.30. This model would classify $Ir(CO)_3Cl$ as a semimetal in regard to its 1-*D* properties. The conductivity of $Ir(CO)_3Cl$ measured as 0.2 Ω cm^{-1} [31] does not appear high enough to warrant a metal or semimetal description, but in view of the well-known difficulty in obtaining good crystals, judgment should be suspended. The polarized reflectance measurements, when they become available, should provide some of the crucial data for determination of the metallic nature of this very interesting material.

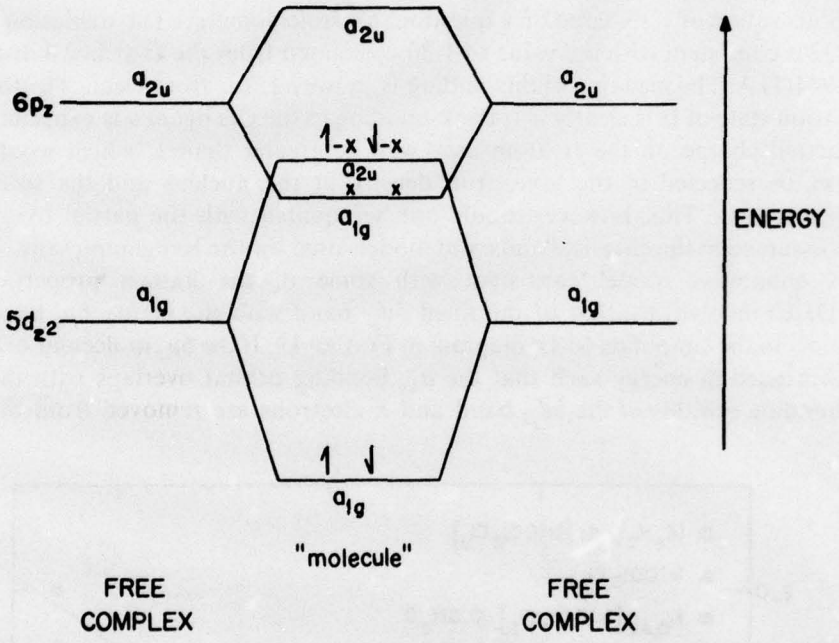


FIGURE 19. $Ir(CO)_3Cl$ molecular orbital diagram for a semimetallic band overlap.

ACKNOWLEDGMENTS

The authors wish to thank Elizabeth Gebert, Don Washecheck, Vickie Hagley, S. C. Lin, and Lynn Preston for the preparation and crystallographic measurements of several of these samples; Dr. Martin Studier for the mass spectra analysis; Dr. Ron Musselman for the polarized reflectance spectra analysis; and Dr. Joel Miller, Dr. Jack Williams, and Dr. Gordon Goodman for helpful discussions.

REFERENCES

1. MILLER, J. S. & A. J. EPSTEIN. 1976. Prog. Inorg. Chem. **20**: 1.
2. MINOT, M. J. & J. H. PERLSTEIN. 1971. Phys. Rev. Lett. **26**: 371.

3. Washecheck, D. M., S. W. Petersen, A. H. Reis, Jr. & J. M. Williams. 1976. Inorg. Chem. **15:** 74.
4. Krogmann, K. 1969. Angew. Chem., Int. Ed. Engl. **8:** 35.
5a. Williams, J. M., J. L. Petersen, H. M. Gerdes & S. W. Peterson. 1974. Phys. Rev. Lett. **33:** 1079.
5b. Williams, J. M., M. Iwata, S. W. Peterson, K. A. Leslie & H. J. Guggenheim. 1975. Phys. Rev. Lett. **34:** 1653.
5c. Deiseroth, H. J. & H. Schulz. 1974. Phys. Rev. Lett. **33:** 963.
6a. Reis, Jr., A. H., S. W. Peterson, D. M. Washecheck & J. S. Miller. 1976. J. Amer. Chem. Soc. **98:** 234.
6b. Reis, Jr., A. H., S. W. Peterson, D. M. Washecheck & J. S. Miller. 1976. Inorg. Chem. **15:**2455.
7a. Keefer, K. D., D. M. Washecheck, N. P. Enright & J. M. Williams. 1976. J. Amer. Chem. Soc. **98:**233.
7b. Williams, J. M., K. D. Keefer, D. M. Washecheck & N. P. Enright. 1976. Inorg. Chem. **15:**2446.
8. Reis, Jr., A. H. & S. W. Peterson. 1976. Inorg. Chem. **15:**3186.
9. Williams, J. M. 1976. Inorg. Nucl. Chem. Lett. **12:**651.
10. Pauling, L. 1947. J. Am. Chem. Soc. **69:**542.
11. Cheung, K. K., R. J. Cross, K. P. Forrest, R. Wandle, & M. Meuer. 1971. Chem. Commun. **875.**
12. Schaffman, M. J., M. B. Salamon, G. De Pasquali, A. J. Schultz & G. D. Stucky. Solid State Commun. Submitted for publication.
13. Krogmann, K. 1968. Z. Anorg. Allg. Chem. **358:**97.
14a. Williams, J. M., P. L. Johnson & A. E. Underhill. 1977. Abstr. Amer. Crystallographic Assoc. HA6. Asilomar, Calif.
14b. Schultz, A. J., C. C. Coffey & J. M. Williams. 1977. Abstr. Amer. Crystallographic Assoc. HA7. Asilomar, Calif.
15. Reis, Jr., A. H., S. W. Peterson & S. C. Lin. 1976. J. Amer. Chem. Soc. **98:**7839.
16. Pauling, L. 1960. The Nature of the Chemical Bond. 3rd edit. Cornell Univ. Press. Ithaca, N.Y.
17. Schultz, A. J., G. D. Stucky, J. M. Williams, T. R. Koch & R. L. Maffly. 1977. 1977. Solid State Commun. **21:**197.
18. Krogmann, K. & P. Dodel. 1966. Chem. Ber. **99:**3402.
19. Miller, J. S. 1976. Inorg. Chem. **15:**2357.
20. Reis, Jr., A. H. 1977. Inorg. Nucl. Chem. Lett. **13:** 231.
21a. Hieber, W. & H. Lagally. 1940. Z. Anorg. Allg. Chem. **245:**321.
21b. Hieber, W., H. Lagally & H. Mayr. 1941. Z. Anorg. Allg. Chem. **246:**138.
22. Fischer, E. O. & K. S. Brenner. 1962. Z. Naturforsch. B. **17:** 774.
23. Krogmann, K., W. Binder & H. D. Hausen. 1968. Angew. Chem. Int. Ed. Engl. **7:** 812.
24. Ginsberg, A. P., R. L. Cohen, F. J. Di Salvo & K. W. West. 1974. J. Chem. Phys. **60:** 2657.
25. Krogmann, K. & H. P. Geserich. 1974. Extended Interactions Between Metal Ions in Transition Metal Complexes. L. V. Interrante, Ed. Amer. Chem. Soc. Washington, D.C.
26. Ginsberg, A. P., J. W. Koepke, J. J. Hauser, K. W. West, F. J. Di Salvo, C. R. Sprinkle & R. L. Cohen. 1976. Inorg. Chem. **15:** 514.
27. Reis, Jr., A. H., V. S. Hagley & S. W. Peterson. 1977. J. Amer. Chem. Soc. In press.
28. Dahl, L. F., C. Martell & D. L. Wampler. 1961. J. Amer. Chem. Soc. **83:**1761.
29. Comes, R., M. Lambert & A. Guinier. 1968. C. R. Acad. Sci. Paris, B. **266:** 959.
30. Ginsberg, A. P., J. W. Koepke, R. L. Cohen & K. W. West. 1976. Chem. Phys. Lett. **38:**310.
31. Lecrone, F. N., M. J. Minot & J. H. Perlstein. 1972. Inorg. Nucl. Chem. Lett. **8:** 173.

THE SYNTHESIS AND CHARACTERIZATION OF SOME LINEAR CHAIN COMPLEXES CONTAINING ISOCYANIDE LIGANDS*

J. G. Gordon II

IBM Research Laboratory
San Jose, California 95193

R. Williams, C.-H. Hsu, E. Cuellar, S. Samson, K. Mann, and H. B. Gray

California Institute of Technology
Pasadena, California 91125

V. Hadek and R. Somoano

Jet Propulsion Laboratory
Pasadena, California 91103

During the past decade, several organic materials and inorganic coordination complexes have been discovered that exhibit high, nearly metallic conductivity.[1,2] The electrical, optical, and other physical properties are highly anisotropic, and the compounds are frequently referred to as one-dimensional. It is particularly intriguing that these properties are the manifestation of extended electronic interactions in materials that one would naïvely consider to be simple molecular solids.

There are several classes of such materials, but we will consider, here, only those derived from d^8 square planar coordination complexes. The essential feature of these compounds is that the planar complex ions stack along an axis perpendicular to the coordination plane to form linear chains of metal atoms. The electronic interactions between the metal atoms, primarily through d_{z^2} orbitals, play a dominant role in determining the solid-state properties. Despite the intense scrutiny of KCP ($K_2Pt(CN)_4Br_{0.3} \cdot 3H_2O$) and related compounds, it is not yet understood how this interaction, and hence the physical properties, is affected by such parameters as the metal-metal distance, the metal atom in the chain, or the nature of the coordinating ligands. Such questions can be answered only by systematic comparison of several different one-dimensional materials. We have therefore tried to synthesize a series of complexes in which some of these parameters might be varied.

In order to generate one-dimensionally conducting crystals, several conditions must be fulfilled:[3-5] First, the structure must be consistent with long-range electronic delocalization. This generally means monadic linear chains. Second, the intermolecular orbital interaction should be large. It is maximized by a short metal-metal separation and large orbital extension perpendicular to the coordina-

*This work was supported, in part, by the National Science Foundation, by NASA Contract NAS7-100, and by the donors of the Petroleum Research Fund, administered by the American Chemical Society. This is contribution No. 5601 from the Arthur Amos Noyes Laboratory of Chemical Physics, California Institute of Technology, Pasadena, Calif. Manuscript received June 13, 1977.

0077-8923/78/0313-0580 $1.75/1© 1978, NYAS

tion plane. The ligands should be small and probably cylindrical, so that a staggered configuration can further decrease ligand-ligand repulsions. Carbonyl, cyanide and isocyanide are obvious choices. To be sufficiently large, the metal atom should be from the second or third row and in a low oxidation state. The preferred order for d^8 metal atoms would be $Os^0 > Ru^0 \sim Ir^I > Rh^I \sim Pt^{II} > Pd^{II}$. Third, there must be free carriers, either holes or electrons. These can be produced in several ways, including thermal excitation, partial oxidation, creating holes in a filled band, partial reduction, putting electrons in an empty band, or by the overlapping of filled and empty bands, as in a semimetal. Only partial oxidation has been observed in the highly conducting platinum and iridium complexes known to date.

We report, here, some of the results of our ongoing study of tetrakis(isocyanide) rhodium (I) salts, $[Rh(CNR)_4]X$, R = phenyl, vinyl, ethyl, methyl, X = Cl, PF_6, BF_4, ClO_4. These complexes satisfy the above requirements and present a less formidable synthetic problem than Os(0) or Ru(0) complexes. The isocyanide ligand, in addition to being small and π-accepting, enables us to systematically produce gross or subtle changes through variation of the substituent, R. Other features of the isocyanide complexes that make them particularly useful for elucidating the nature of the metal-metal interaction, and how it and the solid-state properties are affected by the composition of the complex ion, will be pointed out below.

Solution Behavior

The tetrakis(isocyanide)Rh(I) complexes were prepared by reacting $[Rh(1,5\text{-}COD)Cl]_2$ with an excess of the appropriate isocyanide in acetonitrile or methanol. In some cases, *tris*(isocyanide)haloRh(I) complexes could be obtained if the Rh:ligand ratio was 1:3. Dilute solutions in nonpolar solvents are yellow, and their absorption spectra are similar to those of other square planar Rh(I) complexes with π-accepting ligands. The spectra, however, do not follow Beer's Law, and concentrated solutions in polar solvents, as well as the solids, can be any color from yellow to deep purple or black. Representative spectra for three different concentrations of $[Rh(CNPh)_4](PF_6)$ in acetonitrile are shown in Figure 1. The bands at 361, 411, and 468 nm which dominate the low-concentration spectrum are assigned to the monomeric $[Rh(CNPh)_4]^+$ cation. As the total Rh(I) concentration is increased, two new bands grow in, first at 568 and then at 727 nm, while the relative intensity of the higher energy bands decreases. Quantitative analysis of their concentration dependence clearly demonstrates that the new bands must be assigned to a dimeric (568) and trimeric (727 nm) species, respectively.[6]

Because infrared spectra reveal no evidence for bridging isocyanides, the most reasonable model for the dimer consists of face-to-face monomer units held together by a metal-metal bond. The electronic spectral properties of $[Rh(CNPh)_4]_2^{2+}$ may be understood in terms of the orbital interactions diagrammed in Figure 2. The $a_{1_g}(d_{z^2})$ and $a_{2_u}(p_z, \pi^*[CNPh])$ orbitals that project perpendicular to the molecular plane will interact most strongly. The low-energy band at 568 is then a spin-allowed transition from $1b_2$ to $2a_1$ in the dimer. Mixing

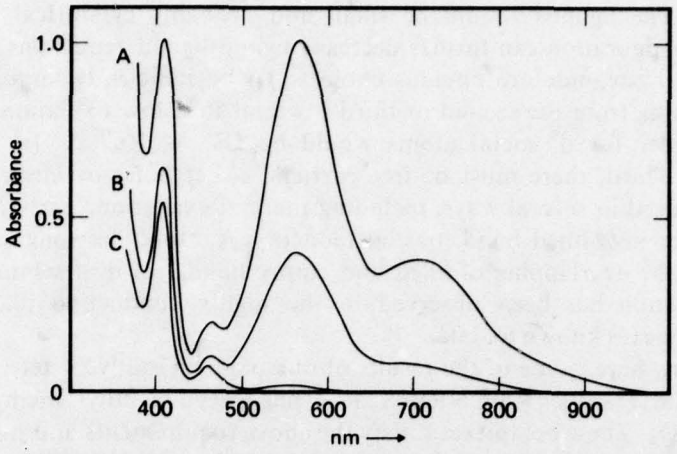


FIGURE 1. Electronic absorption spectra of $[Rh(CNPh)_4](PF_6)$ in acetonitrile at 25°C (cell pathlength): A, 5.7×10^{-2} M (0.066 mm); B, 2.7×10^{-2} M (0.06 mm); C, 6.3×10^{-4} M (0.75 mm). (By permission of the American Chemical Society.[6])

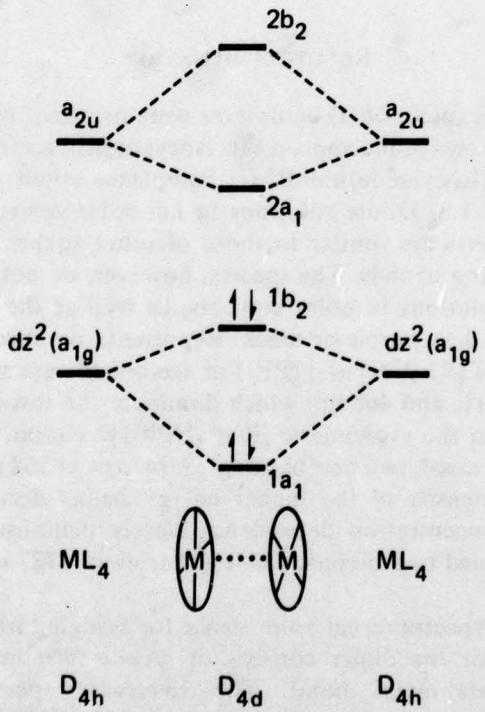


FIGURE 2. Relative energies of the molecular orbitals derived from $a_{1g}(d_{z^2})$ and a_{2u} monomer functions in D_{4d} for $[Rh(CNPh)_4]_2^{2+}$.

of the two a_1 and the two b_2 orbitals must provide the attractive interaction that stabilizes the dimeric structure.

This model for the structure of the dimer is supported by the crystal structure of $[Rh_2(CNPh)_8](BPh_4)_2$.[7] The deep-purple crystals contain discrete dimers, composed of planar $Rh(CNPh)_4^+$ units held face-to-face by a direct metal-metal bond. (See FIGURE 3.) The ligands are staggered to permit a metal-metal distance of 3.19 Å. This material has an absorption band in the solid at 560 nm, which is nearly the same wavelength as the dimer band in solution, and suggests that the metal-metal distance in solution is also about 3.2 Å.

A similar analysis applied to the trimer leads to the assignment of the 727 nm band to a $2a_1$ to $2b_2$ transition. As the chain gets longer, this transition will move to lower energy. Extrapolation from the dimer and trimer frequencies using a

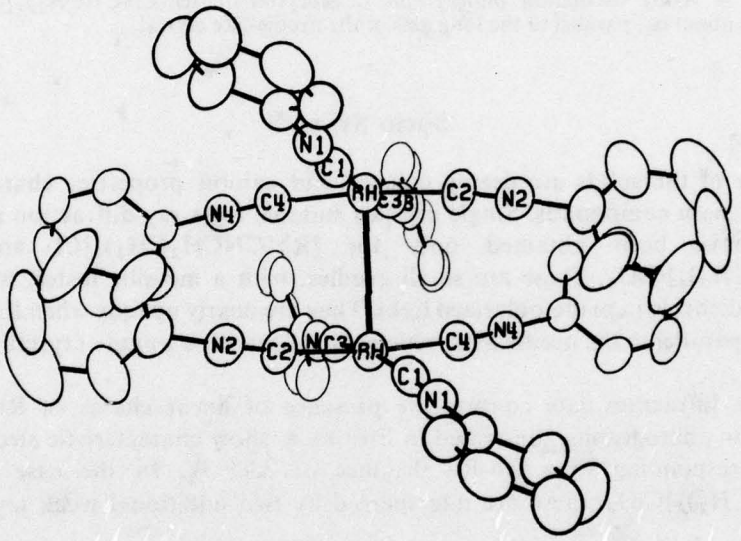


FIGURE 3. Molecular structure of $[Rh(CNPh)_4]_2(BPh_4)_2$.

simple Hückel model places this absorption at 900 nm (11,000 cm^{-1}) for an infinite chain length. This seems quite reasonable, inasmuch as the solid-state band in $Rh(CO)_2acac$ occurs at 526 nm (19,100 cm^{-1}) and this compound has both a longer Rh-Rh distance, 3.26 Å, and a larger $d_{z^2} - (p_z - \pi^*)$ separation in the monomeric unit.[8]

Reversible oligomerization seems to be a general characteristic of the rhodiumisocyanide complexes, applying equally to alkyl and to aromatic isocyanides. That similar oligomerization is not observed in the case of $Pt(CN)_4^{2-}$ is presumably due to the much higher electrostatic repulsion caused by the platinocyanides' higher charge. Indeed, $pt(CN)_4^-$ apparently does form a face-to-face complex with $Pt(CNCH_3)_4^{2+}$ which has a new low-energy absorption at 355 nm (29,800 cm^{-1}).[9]

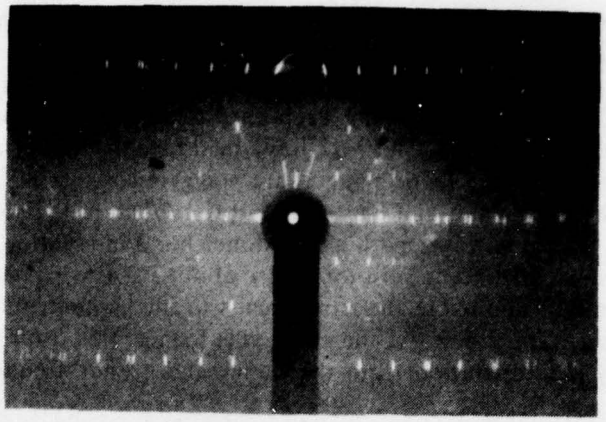


FIGURE 4. X-ray oscillation photograph of a crystal of $[Rh(CNCHCH_2)_4]ClO_4$. Oscillation is about a_0, parallel to the long axis of the needle-like crystal.

SOLID STATE

Many of the solids are deeply colored and exhibit properties characteristic of linear chain compounds. Single crystals suitable for x-ray diffraction measurements have been obtained only for $[Rh(CNCH_2CH_3)_4]Cl$ and $[Rh(CNCHCH_2)_4]ClO_4$. These are small needles, with a metallic luster, which are strongly dichroic in plane-polarized light. They are nearly opaque when the electric vector is parallel to the needle axis, which coincides with a unique crystallographic direction.

X-ray diffraction data confirm the presence of linear chains of Rh atoms. Oscillation photographs, illustrated in FIGURE 4, show characteristic strong layer lines corresponding to a Rh-Rh distance of 2.95 Å. In the case of $[Rh(CNCHCH_2)_4]ClO_4$, these are interspersed by two additional weak layer lines,

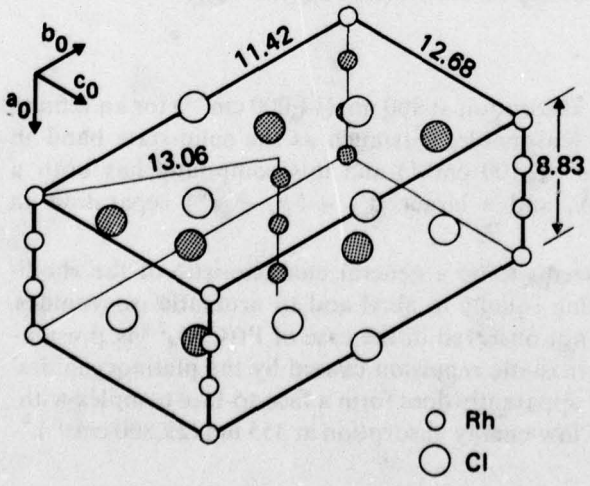


FIGURE 5. Unit cell of $[Rh(CNCHCH_2)_4]ClO_4$.

TABLE 1

THE LENGTHS OF THE UNIT-CELL EDGES IN ÅNGSTRÖMS FOR RHODIUM ISOCYANIDE COMPLEXES*

Compound	a_0	b_0	c_0	S	a_0/S
$[Rh(CNCHCH_2)_4]ClO_4$	8.823(1)	22.843(3)	12.677(1)	3	2.94
$[Rh(CNCH_2CH_3)_4]Cl$	11.82(2)	22.83(4)	12.83(2)	4	2.96
$[Rh(CNCH_2CH_3)_4]ClO_4$	11.77(2)	23.54(3)	12.97(2)	4	2.94
$[Rh(CNCH_2CH_3)_4]PF_6$	11.81(2)	24.06(5)	13.21(2)	4	2.95

*The crystal system is orthorhombic. S is the number of subcells stacked along a_0.

whereas for $[Rh(CNCHCH_2CH_3)_4]Cl$ there are three. The actual unit-cell lengths in this direction are thus three and four times the average Rh-Rh distance, respectively.

The structure of the vinyl compound has been partially solved. A schematic of the atomic arrangement is illustrated in FIGURE 5. It has a body-centered orthorhombic unit cell (dimensions in TABLE 1) with chains of rhodium atoms along the 100 direction, which coincides with the needle axis of the crystals. At the present stage of refinement, all of the Rh-Rh distances are equal at 2.95 Å. The orientations of the ligands are still unknown.

Other salts did not yield suitable single crystals and were characterized by Guinier powder-diffraction photographs. The powder patterns are nearly identical with those of the above two complexes and it is quite certain that the compounds have similar structures, containing Rh chains parallel to the a_0 axis. The Rh-Rh distances vary from 2.93 to 2.96 Å. It is noteworthy that the Rh-Rh distance is insensitive to changes in the ligand or counterion. This is illustrated by the data in TABLE 1, which lists unit cell parameters for several salts of $[Rh(CNCH_2CH_3)_4]^+$. As the counterion is changed from Cl^- to ClO_4^- to PF_6^-, a_0 (the length of the stacking axis) remains constant and only b_0 and c_0, which corresponds to interchain directions, change significantly.

Electrical conductivities, measured on powders, are reported in TABLE 2. As expected, $[Rh_2(CNPh)_8](BPh_4)_2$ is an insulator. The other complexes show ap-

TABLE 2

ELECTRICAL CONDUCTIVITIES, OXIDATION STATES AND METAL-METAL DISTANCES OF RHODIUM ISOCYANIDE COMPLEXES

Compound	σ Powder ($\Omega^{-1}cm^{-1}$)	Oxidation State	Rh-Rh Distance (Å)
$[Rh_2(CNPh)_8](BPh_4)$	7.2×10^{-11}	1.00	3.19
$[Rh(CNCH_3)_4]Cl$	3.3×10^{-2}		
$[Rh(CNCH_3)_4]BF_4$	2.2×10^{-2}		2.94
$[Rh(CNCH_2CH_3)_4]Cl$	6.7×10^{-4}		2.95
$[Rh(CNCH_2CH_3)_4]ClO_4$	5.1×10^{-4}	1.00	2.94
$[Rh(CNCH_2CH_3)_4]PF_6$	3.9×10^{-5}	1.25	2.95
$[Rh(CNCHCH_2)_4]Cl$	2.9×10^{-4}	1.01	
$[Rh(CNCHCH_2)_4]ClO_4$	5.6×10^{-3}	1.04	2.94
$[Rh(CNCHCH_2)_4]PF_6$	5.6×10^{-4}		2.96

preciable conductivity and contain infinite chains. The room-temperature conductivity of single crystals of $[Rh(CNCHCH_2)_4]ClO_4$, the only compound for which sufficiently large crystals were obtained, is 2 $ohm^{-1}cm^{-1}$. This is lower than that of the best KCP samples, but comparable to that of partially oxidized iridium carbonyl halides.[10]

Analytical data suggest that many of the complexes are partially oxidized, although the degree of oxidation is generally small. Apparent oxidation states, calculated from the anion:rhodium ratios, are given in TABLE 2. Low partial oxidation and high conductivity are also observed in some of the iridium carbonyl halides.

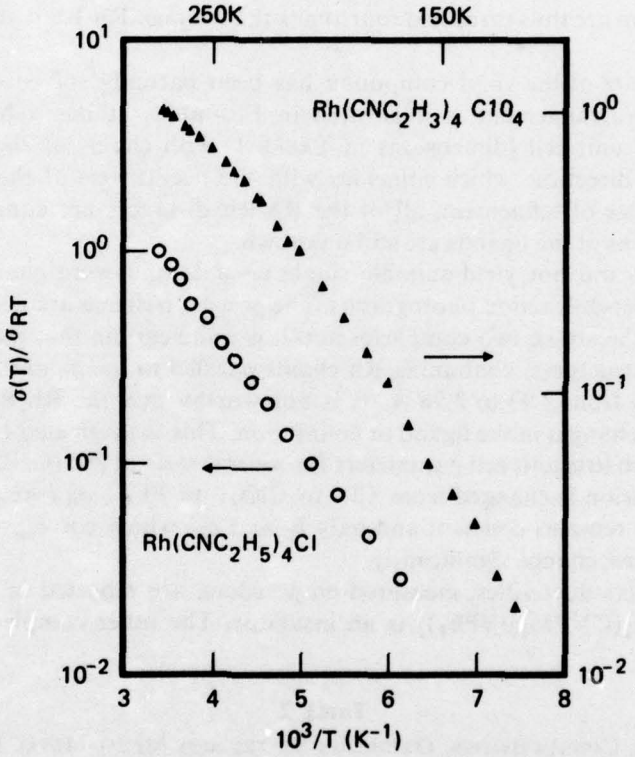


FIGURE 6. Temperature dependence of the conductivity of a single crystal of $[Rh(CNCHCH_2)_4]ClO_4$ and of $[Rh(CNCH_2CH_3)_4]Cl$ powder.

The temperature dependence of the conductivity of $[Rh(CNCH_2CH_3)_4]Cl$ powder and of a single crystal of $[Rh(CNCHCH_2)_4]ClO_4$ is shown in FIGURE 6. The interesting curvature in $\sigma(T)$ at high temperatures is suggestive of an analogous feature observed in the conductivity of KCP and some iridium carbonyl halides.[10,11] It is the type of behavior expected on the low-temperature side of a metal-insulator transition. However, the samples were heated to 330°K, where decomposition sets in, without any indication of a metallic state. The curves in FIGURE 6 can be fit to ln σ vs $1/T$, yielding apparent activation energies of .10

and .086 eV for the vinyl and ethyl compounds, respectively. They can be fit equally well to $\sigma = \sigma_0 \exp(-T_0/T)$ with $T_0 \sim 3.2 \times 10^4$K. This latter form is characteristic of charge transport via a hopping process.

It is clearly impossible to say with certainty, at this stage, what the mode of conduction is in these compounds. In light of the short metal-metal distance, low activation energy, and apparent partial oxidation, it is tempting to believe that they are one-dimensional metals in which metallic behavior has been quenched by crystalline disorder and imperfections. One must not ignore the possibility, however, that at least some of the complexes may have an integral oxidation state, in which case one may have a small band gap intrinsic semiconductor or an extrinsic semiconductor in which the conductivity is dominated by Rh(II) "impurities."

The information presented here and in the previous paper suggests that study of rhodium isocyanide complexes may be particularly fruitful in relating the electronic properties of the molecular unit to those of the solid linear chain compound. It is the only system we are aware of in which one has access to both long and short metal-bonded chains in both integral and fractional oxidation states.[12]

References

1. Miller, J. S. & A. J. Epstein. 1976. *In* Progress in Inorganic Chemistry. S. J. Lippard, Ed. Vol. **20:** 1.
2. Zeller, H. R. 1973. Adv. Solid State Phys. **13:** 31.
3. Aderjan, R., D. Baumann, H. Breer, H. Endres, W. Gitzel, H. J. Keller, R. Lorentz, W. Moroni, M. Megnamisi-Bélombé, D. H. Nöthe & H. H. Rupp. 1974. Extended Interactions between Metal Ions. ACS Symposium Series 5. L. V. Interrante, Ed.: 314.
4. Krogmann, K. 1974. *In* Low-Dimensional Cooperative Phenomena. H. J. Keller, Ed. Nato Advanced Studies Inst. Ser. Vol. **7B:** 315. Plenum Press. New York, N.Y.
5. Underhill, A. E. 1974. *In* Low-Dimensional Cooperative Phenomena. H. J. Keller, Ed. Nato Advanced Studies Inst. Ser. Vol. **7B:** 287. Plenum Press. New York, N.Y.
6. Mann, K. R., J. G. Gordon II & H. B. Gray. 1975. J. Amer. Chem. Soc. **97:** 3553.
7. Mann, K. R., N. S. Lewis, R. M. Williams, H. B. Gray & J. G. Gordon II. 1978. Inorg. Chem. **17:**.
8. Dessent, T. A., R. A. Palmer & S. A. Horner. 1974. *In* Extended Interactions between Metal Ions. ACS Symposium Series 5. L. V. Interrante, Ed: 301.
9. Isci, H. & W. R. Mason. 1974. Inorg. Chem. **13:** 1175.
10. Ginsberg, A. P., J. W. Koepke, J. J. Hansen, K. W. West, F. J. DiSalvo, C. R. Sprinkle & R. L. Cohen. 1976. Inorg. Chem. **15:** 514.
11. Zeller, H. R. & A. Beck. 1974. J. Phys. Chem. Solids. **35:** 77.
12. Balch, A. This volume.

THE SOLUTION PHOTOCHEMICAL PROPERTIES OF OLIGOMERIC IRIDIUM ISOCYANIDE COMPLEXES*

Gregory L. Geoffroy, Mark G. Bradley, and Mark E. Keeney

Department of Chemistry
The Pennsylvania State University
University Park, Pennsylvania 16802

INTRODUCTION

In 1972 an interesting report[1] appeared in the chemical literature that described the photochemical reactions of $[Ir(CNCH_3)_4]^+$. The complex was isolated in the form of its chloride salt as a blue-black air-sensitive solid. In the absence of oxygen the complex gave deep-blue solutions (λ_{max} = 610 nm; ϵ = 22,000) that were stable for days in the dark, but rapidly turned red or orange when irradiated. It was noted that the photoreaction in methanol solution was reversible. On the basis of slight shifts in the NMR spectrum during photolysis, it was suggested[1] that photoinduced association of solvent occurred to give a five-coordinate complex, (1).

$$[Ir(CNCH_3)_4]^+ + S \overset{h\nu}{\rightleftharpoons} [Ir(CNCH_3)_4(S)]^+$$

$$S = (CH_3)_2CO,\ CH_3CN,\ CH_3OH. \qquad (1)$$

In support of this proposal it was shown that aqueous solutions of $[Ir(CNCH_3)_4]^+$ did not react with CO or excess CH_3NC in the dark but did so under irradiation. The corresponding $[Ir(CNCH_3)_5]BPh_4$ and $[Ir(CNCH_3)_4CO]BPh_4$ adducts were isolated as orange solids and characterized by their NMR and infrared spectra. The authors stated[1] that this represented the first example of a true photoinduced association reaction.

There are two puzzling aspects of this report which aroused our curiosity. The first is the observation that the complex showed no tendency to add $CNCH_3$ or CO in the dark, yet gave stable five-coordinate complexes upon photolysis. It was highly unlikely that a large thermal activation barrier should exist for this process, since other Ir^1L_4 complexes are known to be very susceptible to addition and oxidative-addition. The most difficult-to-rationalize aspect of the reported study, however, was the blue-black color of the initial complex. We know from several previous studies[2-4] that square-planar complexes of Ir(I) which possess π-accepting ligands like CH_3NC should not be blue-black but rather yellow or orange in color. This coloration has been shown to arise from metal-to-ligand charge-transfer transitions that lie in the visible spectral region, and a typical spectrum is that of *trans*-$[IrCl(CO)(PPh_3)_2]$, shown in FIGURE 1. Importantly, all the Ir^1L_4 complexes examined showed a similar three-band pattern, and furthermore, the bands showed only slight spectral shifts as the ligands were varied.[2-4]

*Supported by the National Science Foundation. Manuscript received May 31, 1977.

0077-8923/78/0313-0588 $1.75/1 © 1978, NYAS

In 1973, in a study[5] of arylisocyanide complexes of Ir(I), $[Ir(CNAr)_4]^+$, (R = *p*-$CH_3C_6H_4$ and *p*-$CH_3OC_6H_4$), Kawakami *et al.* noted that these materials were dark green in color and were also light-sensitive. The photoreaction was, however, markedly slower than that of $[Ir(CNCH_3)_4]^+$, and these workers found no evidence of solvated $[Ir(CNAr)_4S]^+$ complexes. Molecular weight measurements and the electronic absorption spectra of the complexes which showed bands with maxima at about 720 nm ($\epsilon \approx 10^4$) led these workers to suggest that the complexes existed as oligomers, even in solution.[5] Most important, they suggested that the photochemical reaction was cleavage of the iridium-iridium interaction.[5]

It is our intention in this article to demonstrate that the suggestions of Kawakami *et al.*[5] are correct. We first show that $[Ir(CNCH_3)_4]^+$ does indeed

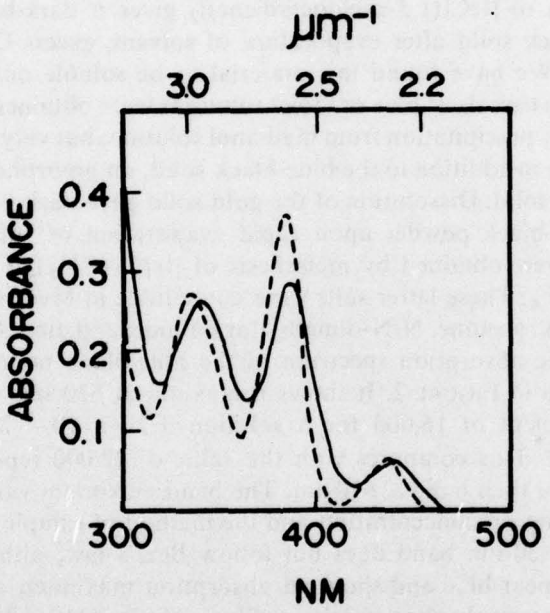


FIGURE 1. Electronic absorption spectrum of $[IrCl(CO)(PPh_3)_2]$ in EPA (5:5:2 ethyl-ether-isopentane-ethyl alcohol) solution at 298° (——) and 77°K (----).[3]

exist as oligomeric $[Ir(CNCH_3)_4]_n^{n+}$ in solution, and second that the photochemical reaction is not an association reaction as suggested by Bedford and Rouschias,[1] but rather is photoinduced cleavage of the solution oligomers to give monomeric $[Ir(CNCH_3)_4]^+$. It is then monomeric $[Ir(CNCH_3)_4]^+$ which reacts with excess $CNCH_3$ or with CO to give the stable five-coordinate complexes.

Precedence does exist for the solution oligomerization of isocyanide complexes of d^8 metals. Isci and Mason[6] have provided spectral evidence for cation-anion association in solution for $[Pt(CNR)_4][Pt(CN)_4]$ (R = CH_3, C_2H_5, *t*-C_4H_9). Mann and coworkers[7] have studied the solution oligomerization of $[Rh(CNPh)_4]^+$ and have provided spectral evidence for $[Rh(CNPh)_4]_2^{2+}$ and $[Rh(CNPh)_4]_3^{3+}$.

The rhodium-isocyanide complexes are in equilibrium in solution, and the measured equilibrium constants are shown in (2).

$$3[Rh(CNPh)_4]^+ \overset{K = 16}{\rightleftharpoons} [Rh(CNPh)_4]_2^{2+}$$

$$+ [Rh(CNPh)_4]^+ \overset{K = 16}{\rightleftharpoons} [Rh(CNPh)_4]_3^{3+}. \quad (2)$$

The rhodium system rapidly responds to any concentration perturbation, suggesting rapid kinetics for the oligomerization and deoligomerization processes.

Results and Discussion

Preparation of $[Ir(CNCH_3)_4]Cl$ by the addition of excess $CNCH_3$ to a CH_2Cl_2 solution of [IrCl(1,5-cyclooctadiene)]$_2$ gives a dark-blue solution that yields a blue-black solid after evaporation of solvent, excess $CNCH_3$, and 1,5-cyclooctadiene. We have found this material to be soluble only in MeOH and H_2O, and in each case dark-blue or violet solutions were obtained. The compound can be purified by precipitation from methanol solution, but very slow evaporation of methanol gave in addition to the blue-black solid, an amorphous highly reflecting gold-colored solid. Dissolution of the gold solid gave dark-blue solutions that yielded the blue-black powder upon rapid evaporation of solvent. Other salts (BPh_4^-, BF_4^-) were obtained by metathesis of $[Ir(CNCH_3)_4]Cl$ in MeOH with $NaBPh_4$ or $NaBF_4$. These latter salts were not soluble in MeOH or H_2O but dissolved in CH_3CN, acetone, N,N-dimethylformamide, and dimethylsulfoxide.

The electronic absorption spectrum of the blue-black material in methanol solution is shown in Figure 2. It shows a maxima at 630 nm with an apparent extinction coefficient of 16,000 for a solution 1.77×10^{-3} M in monomeric $[Ir(CNCH_3)_4]Cl$. This compares with the value of 22,000 reported by Bedford and Rouschias for their band at 610 nm. The band maximum varies between 600–650 nm, depending on concentration and the method of sample preparation. The intensity of the 630-nm band does not follow Beer's law, although very dilute solutions still appear blue and show an absorption maximum at about 610 nm. The complex is extremely photosensitive, dilute solutions (10^{-4} M) turning orange within seconds of irradiation. The color change can be induced by fluorescent room light, sunlight, flashlight irradiation, or photolysis with $\lambda \leq 650$ nm. The spectral changes which obtain during irradiation are complex, but after five minutes' photolysis using $\lambda \geq 525$ nm, the dashed spectrum shown in Figure 2 is obtained and no further changes are observed. This final spectrum shows bands at 490, 425, 370, and 305 nm and is exactly the type of spectrum expected for an Ir^1L_4 complex with π-accepting ligands.

If *t*-butylisocyanide is employed in place of $CNCH_3$ in the preparation, a yellow-orange solid, rather than a blue-black material, is isolated. The infrared spectrum of the solid is identical to that obtained by Dart *et al.*[8] for a complex formulated as $[Ir(CNBu^t)_4]PF_6$. The electronic absorption spectrum of the *t*-butylisocyanide complex in methanol solution is virtually identical to that shown in Figure 2 for irradiated $[Ir(CNCH_3)_4]^+$, showing bands at 490, 423, 372, and 303 nm; furthermore, it is the type of spectrum shown by the other square-planar

Ir(I) complexes previously studied.[2-4] Thus $[Ir(CNBu^t)_4]^+$ behaves exactly as expected for a monomeric Ir^IL_4 complex.

On the basis of the established tendency of rhodium(I) isocyanide complexes to oligomerize in solution, the molecular weight measurements of Kawakami *et al.*, the color of the blue-black $[Ir(CNCH_3)_4]Cl$ material, its absorption spectrum, which is *not* that expected for monomeric $[Ir(CNCH_3)_4]^+$, and our ability to obtain reflecting gold-colored material by slow precipitation, we propose that $[Ir(CNCH_3)_4]^+$ does not exist as monomers but rather as oligomers in both solution and the solid state. The oligomers presumably form through stacking of the planar Ir^IL_4 units. The electronic absorption spectrum of the solution obtained after photolysis, which is virtually identical to that of $[Ir(CNBu^t)_4]^+$, which

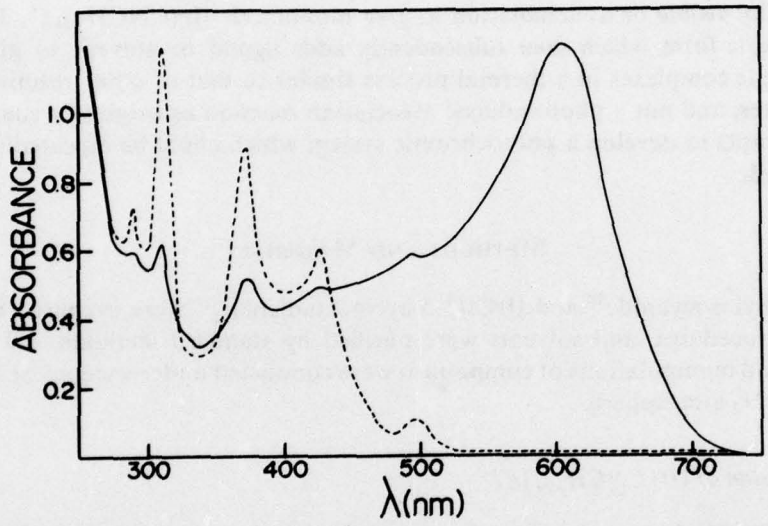


FIGURE 2. Electronic absorption spectrum of a 4.02×10^{-5} M MeOH solution of $[Ir(CNCH_3)_4]Cl$ before (——) and after (----) 5 min irradiation with $\lambda > 525$ nm.

does not oligomerize, strongly suggests that photolysis induces cleavage of the oligomers to generate monomeric $[Ir(CNCH_3)_4]^+$, (3).

$$[Ir(CNCH_3)_4]_n^{n+} \xrightarrow{h\nu} [Ir(CNCH_3)_4]^+. \quad (3)$$

We have observed, like Bedford and Rouschias,[1] that the photoreaction can be partially reversed. Storage of the orange-irradiated solutions in the dark results in a return of the blue color but never to the original extent. The rate of return is highly dependent on conditions, occurring faster the greater the original complex concentration, and faster at elevated temperatures. The system can be cycled only through the photoinduced deoligomerization-thermal oligomerization process two to three times before it fails to yield any more oligomers. Although we have no firm experimental evidence, it is likely that the monomeric $[Ir(CNCH_3)_4]^+$ units react with methanol solvent adding across the CN bonds, much as has been

demonstrated[9] for other isocyanide complexes. We find that the $[Ir(CNCH_3)_4]\cdot BPh_4$ and $[Ir(CNCH_3)_4]BF_4$ salts in CH_3CN, DMF, and DMSO solutions are also photosensitive, changing from dark blue to red-orange upon irradiation. These reactions, however, are not at all reversible, and the electronic absorption spectra of the irradiated solutions are not those of square-planar Ir^IL_4 complexes but resemble that of $[Ir(CNCH_3)_5]^+$, which, like Bedford and Rouschias,[1] we find can be prepared by photolysis in the presence of excess $CNCH_3$. It appears, then, that photolysis in these donor solvents, and also in the presence of excess $CNCH_3$, gives first cleavage of the oligomers and generation of monomeric $[Ir(CNCH_3)_4]^+$, which then thermally adds $CNCH_3$ or solvent to give stable five-coordinate complexes.

In summary, we have shown that $[Ir(CNCH_3)_4]Cl$ exists as oligomeric $[Ir(CNCH_3)_4]_n^{n+}$ in solutions and that the solution oligomers can be readily cleaved by visible or uv irradiation to give monomeric $[Ir(CNCH_3)_4]^+$. It is the monomeric form which then subsequently adds ligand or solvent to give five-coordinate complexes in a thermal process similar to that of other reactive Ir^IL_4 complexes, and not a photoinduced association reaction as originally suggested.[1] All attempts to develop a photochromic system which could be repeatedly cycled has failed.

Methods and Materials

Methyl isocyanide[10] and $[IrCl(1,5\text{-cyclooctadiene})]_2$[11] were prepared by published procedures, and solvents were purified by standard methods. All experiments and manipulations of compounds were conducted under vacuum or under a purified N_2 atmosphere.

Preparation of $[Ir(CNCH_3)_4]Cl$

Excess CH_3NC was distilled into a Schlenk tube containing $[IrCl(1,5\text{-cyclooctadiene})]_2$ (0.30 g; 0.4 mmol) in 20 ml of CH_2Cl_2, and the mixture was stirred for one hour. The solvent, excess $CNCH_3$, and 1,5-cyclooctadiene were removed under vacuum. The crude product was dissolved in methanol and filtered, followed by evaporation of solvent to give a blue-black solid. Other salts (BPh_4^- and BF_4^-) were prepared by metathesis in methanol solution with $NaBPh_4$ and $NaBF_4$. These salts are insoluble in methanol and precipitate out of solution during the metathesis.

General Irradiation Procedures

Irradiations were conducted with a 450-W Hanovia medium-pressure Hg lamp in a quartz well equipped with a Corning Glass 3–70 cut-off filter ($\lambda \geq 525$ nm). The complex to be studied was placed in an evacuable quartz UV cell or a Schlenk tube, and after degassing on a vacuum line the appropriate solvent was distilled onto the sample. Solutions for infrared studies were transferred in an inert-atmosphere glove box to 0.5 mm NaCl solution infrared cells. Samples for NMR analysis were similarly prepared and sealed under vacuum. Lamp intensities were measured by ferrioxalate actimometry.

Spectral Measurements

Infrared spectra were recorded on a Perkin-Elmer 621 grating infrared spectrometer. Electronic absorption spectra were recorded with a Cary 17 spectrophotometer using 0.1 or 1.0 cm quartz cells.

References

1. Bedford, W. M., & G. Rouschias. 1972. *Chem. Communun.*: 1224.
2. Geoffroy, G. L., M. S. Wrighton, G. S. Hammond & H. B. Gray. 1974. J. Amer. Chem. Soc. **96:** 3105.
3. Brady, R., B. R. Flynn, G. L. Geoffroy, H. B. Gray, J. Peone, Jr., & L. Vaska. 1976. Inorg. Chem. **15:** 1485.
4. Geoffroy, G. L., H. Isci, J. Litrenti & W. R. Mason. 1977. Inorg. Chem. **16:** 1950.
5. Kawakami, K., M.-A. Haga & T. Tanaka. 1973. J. Organometal. Chem. **60:** 363.
6. Isci, H. & W. R. Mason. 1977. Inorg. Chem. **13:** 1175.
7. Mann, K. R., J. G. Gordon & H. B. Gray. 1975. J. Am. Chem. Soc. **97:** 3553.
8. J. W. Dart, M. K. Lloyd, R. Mason & J. A. McCleverty. 1973. J. Chem. Soc. Dalton Trans. 2039.
9. Ugi, I., Ed. 1971. Isonitrile Chemistry. Academic Press. New York, N.Y.
10. Schuster, R. E., J. E. Scott & J. Casanova, Jr. 1973. Org. Synth. Coll. Vol. 5: 772.
11. Herde, J. L., J. C. Lambert & C. V. Senoff. 1974. Inorg. Synth. **15:** 18.

Discussion

Joseph Gordon (*IBM, San Jose, Calif.*): There is only one band in the iridium isocyanide spectrum at long wavelengths. Do you think that it is for a dimer, long chain, or do you think there is a mixture of chains in solution?

Geoffroy: The photochemically prepared monomer has this kind of absorption spectrum, and if we then turn off the light and observe the oligomerization, what we see is a progressive growth of bands that end up as shoulders on a larger band. We see this progression of shoulders throughout the oligomerization process until we finally get to the final spectrum. Thus, it must go through a fairly high degree of oligomerization in solution.

George C. Stanley (*Texas A.&M., College Station, Texas*): Could you regenerate the blue color upon thermal treatment of the yellow solvent adduct?

Geoffroy: We observe that, but we never got the same extent of blue color as we had originally. It usually would come back about two thirds or half. Each time you do this you drain it away, and after two or three cycles you just cannot do it any more.

Stanley: If you let a fairly concentrated solution (e.g. 1 mM) of $Ir(CNMe)_4Cl$ stand protected from air, after a few months a precipitate will form. We took this to mean that you do have a certain equilibrium favoring the longest oligomers which eventually will precipitate out of solution. Likewise, if you take the same clear solution with the dark solid at the bottom and shake it up, part of it will redissolve and go back to the lower oligomer forms, which are soluble. However, you still have an appreciable amount of solid that will not redissolve into the methanol.

RATIONAL SYNTHESIS OF NEW UNIDIMENSIONAL SOLIDS: CHEMICAL AND PHYSICAL STUDIES OF MIXED-VALENCE POLYIODIDES*

Tobin J. Marks

Department of Chemistry and the Materials Research Center
Northwestern University
Evanston, Illinois 60201

INTRODUCTION

There has recently been intense interest on the part of chemists and physicists in the solid-state properties of materials that contain strong unidimensional structural and electronic interactions.[1] The reason for this interest is that such one-dimensional and quasi-one-dimensional systems sometimes exhibit rather spectacular and highly anisotropic electrical, magnetic, and optical properties.[1] Several materials (e.g. TTF-TCNQ, $(SN)_x$) have stimulated much activity in solid-state science.[1,2] New organic and coordination compounds with quasimetallic characteristics have forced a constant reevaluation and improvement of both theoretical models and experimental expectations for cooperative phenomena in solids. Clearly these studies are leading to a deeper understanding of the nature and magnitude of those fundamental factors which control electron transport in solids. This recent activity has also stimulated an exciting new field of chemical science that concentrates contemporary synthetic expertise on the goal of tailoring new molecules for specific (in this case solid state) properties: "molecule engineering." The practical outcome of these efforts may be an entirely new generation of electronic materials[2,3] and possibly even high-temperature superconductors.[4]

A number of features are generally believed[1,2,5] to facilitate electron transport in stacked organic, inorganic, and metal-organic systems such as Krogmann's salt $[K_2Pt(CN)_4Br_{0.30} \cdot 3H_2O]$, TTF-TCNQ, and others (including some which do not undergo a low-temperature transition to the semiconducting state[6]). In the Hubbard terminology,[1] it is desirable to minimize U (the site electron correlation energy) and to maximize t (the charge-transfer integral). The most reasonable approach to these requirements is to choose for stacking, highly delocalized, polarizable molecules (*vide infra*). It is assumed, of course, that the stacked moieties occupy crystallographic sites that are as similar as possible. Another closely related, crucial feature which only recently has been widely recognized as extremely important is mixed valency; i.e., the molecular entities which are connected in series must have fractionally occupied electronic valence shells.[1c,7] A crucial test of solid-state theory and a challenge to chemical methodology

*Supported by the Northwestern Materials Research Center (NSF-DMR 72-0319A06), the U.S. Office of Naval Research (N00014-17-C-0231), and the Paint Research Institute. The author is a Camille and Henry Dreyfus Teacher-Scholar. Manuscript received May 31, 1977.

0077-8923/78/0313-0594 $1.75/1© 1978, NYAS

would be to devise a rational synthesis of such "mixed valence" lattices. One plausible approach we have pursued is to cocrystallize stacks of planar (to promote stacking) conjugated donor molecules, D, with an appropriate acceptor system A,

$$\begin{matrix} D & A \\ D & A \\ D & A \\ D & A \\ D & A \\ D & A \end{matrix} \rightarrow \begin{bmatrix} D \\ D \\ D \\ D \\ D \\ D \end{bmatrix}^{+q} \quad \begin{bmatrix} A \\ A \\ A \\ A \\ A \\ A \end{bmatrix}^{+q}$$

D = donor; A = acceptor.

which would remove a nonintegral amount of electronic charge per D unit. Ideally, the A moiety should also be polarizable and must be sufficiently compact to be easily incorporated into the lattice of $(D)_n$ stacks. To promote "partial oxidation" of the D units, the A must form stable polynuclear anions, A_n^{-1}. Thus in $AD_{1.0}$ each A would increase the formal oxidation state of each D by the fraction $+1/n$. It will be seen that this simple stragegy is impressively effective when the donor units are a variety of readily accessible and chemically flexible organic and metal-organic macrocycles and when the acceptor, A, is iodine. Because of the high stability of polyiodides such as I_3^{-1} and I_5^{-1} in nonpolar environments[8] (lattices composed principally of organic functional groups), and because their shape allows them to occupy relatively narrow channels in one-dimensional lattices, polyiodide acceptors are favorably suited for introducing mixed valency. In a solid of stoichiometry $DI_{1.0}$, if iodine is present as I_3^{-1}, then D has increased its formal oxidation state by +0.33. Furthermore, iodine-containing acceptors are readily amenable to spectroscopic characterization. The powerful combination of resonance Raman[9] and iodine-129 Mössbauer[10] spectroscopy readily identifies the form of the iodine present in the lattice, i.e., I_2, I^{-1}, I_3^{-1}, I_5^{-1} or a combination thereof, and thus allows a direct and accurate estimation of the extent of electronic charge transfer from D to A.[11] This technique is easily applied to even noncrystalline and severely disordered materials. Such charge-distribution information is of great importance in refining present theories of electron transport and has never before been acquired with such ease or for such a wide range (*vide infra*) of materials.

The purpose of this article is to briefly survey some of the recent research that has been conducted at Northwestern University on rationally synthesizing mixed-valence materials by the strategy outlined above, and on studying the various physicochemical properties of the resulting products. The physical basis of the resonance Raman/iodine-129 Mössbauer technique of charge-distribution measurement will first be discussed, then results will be reviewed in the areas of partially oxidized metal bisdioximates and phthalocyanines.

Resonance Raman/I-129 Mössbauer Measurement of Charge Distribution in Mixed Valence Lattices

Resonant Raman scattering[9] provides valuable information on polyiodide molecular and electronic structure.[12] As will be seen, each type of iodine-containing species gives rise to a characteristic scattering spectrum. Moreover, the intensities of iodine-centered spectral features are vastly enhanced when a laser-excitation source is brought into resonance with molecular electronic transitions. Unlike simple infrared absorption, the resonance Raman scattering is not obscured by other, frequently extraneous, normal modes of vibration. The intensity of a Raman transition, $I(\nu_r)$, averaged over all molecular orientations, is related to the Raman scattering tensor, $R_{\rho\sigma}$, as given in equation (1). Here $I(\nu_0)$ is the intensity

$$I(\nu_r) = \frac{2^7\pi^5}{3^2c^4}\,\nu_r^4 I(\nu_0) \sum_{\rho\sigma} |R_{\rho\sigma}|^2 \tag{1}$$

of the exciting laser source (at ν_0), ν_r is the frequency of the Raman scattered light, and c is the speed of light. Quantum mechanical descriptions of $R_{\rho\sigma}$ have recently been derived that take account of both Herzberg-Teller coupling and Born-Oppenheimer nonadiabatic coupling.[9,13] $R_{\rho\sigma}$ can be expressed as the sum of two contributions (2), which describe

$$R_{\rho\sigma} = A + B \tag{2}$$

scattering arising from Franck-Condon allowed transitions involving a single excited electronic state (A), and those which derive intensity *via* vibronic coupling between two or more excited electronic states (B). General expressions for the A and B terms are presented in (3) and (4).

$$A = \frac{1}{h}\sum_{e,v}\left[\frac{(g^0|\mu_\rho|e^0)(e^0|\mu_\sigma|g^0)\langle gj|ev\rangle\langle ev|gi\rangle}{\nu_{ev,gi} - \nu_0 + i\Gamma_{ev}} + \frac{[\rho \leftrightarrow \sigma]}{\nu_{ev,gj} + \nu_0 + i\Gamma_{ev}}\right] \tag{3}$$

$$B = \frac{-1}{h^2}\sum_{e,v}\sum_{s,u}{}'$$

$$\left[\frac{(g^0|\mu_\rho|s^0)(s^0|(\partial H/\partial\text{-})_0|e^0)(e^0|\mu_\sigma|g^0)\langle gj|su\rangle\langle su|Q|ev\rangle\langle ev|gi\rangle}{(\nu_{su,gi} - \nu_0 + i\Gamma_{su})(\nu_{ev,gi} - \nu_0 + i\Gamma_{ev})}\right.$$

$$\left. + \frac{[\rho \leftrightarrow \sigma]}{(\nu_{su,gj} + \nu_0 + i\Gamma_{su})(\nu_{ev,gj} + \nu_0 + i\Gamma_{ev})}\right]. \tag{4}$$

These describe a transition from vibrational state i to j in the ground-state electronic level (gi to gj). Here $|e^0)$ is the adiabatic electronic wave function of excited electronic state e, evaluated at the equilibrium nuclear positions of the ground electronic state, μ is the dipole transition operator, $|ev\rangle$ is the wave function for the vth vibrational level of electronic state e. In the denominators the terms $\nu_{ev,gi}$ are the frequency separation between vibronic levels, and the

Γ_{ev} are damping terms that describe the radiative widths of the vibronic states *ev*. The term *s* refers to another excited electronic state (other than *e*), the prime on the summation excludes terms where $s = e$, and $(\partial H/\partial Q)_0$ is the vibronic coupling operator describing the change in the electronic Hamiltonian with displacement along normal mode Q. $(\partial H/\partial Q)_0$ is evaluated at the ground-state nuclear coordinates and transforms as normal mode Q. The second term in each of the above expressions refers to the nonresonant regime. For *A* terms, only the totally symmetric normal modes of molecular vibration should be resonant-enhanced, while for *B* terms only those modes which vibronically couple *s* and *e* states will exhibit this behavior. In principal these effects can be distinguished *via* the excitation profiles.

As can be readily appreciated, Equations 3 and 4 contain a wealth of information about molecular and electronic structure. For the present discussion of charge-distribution analysis, the emphasis will be on deriving structural information about polyiodides from resonance Raman studies. Since Equations 3 and 4 provide no information on empirical quantities such as force and interaction constants (and indeed whether useful structural deductions will be possible) it is necessary first to investigate model systems. FIGURE 1A illustrates a solution spectrum of I_2, and 1B a solid state spectrum of a material containing isolated I_3^{-1} units $[(C_6H_5)_4As^+I_3^-]$[14]; besides the extremely intense fundamental vibrations (205 and 114 cm^{-1}, respectively) characteristic overtone scattering is observed.[15] In I_3^{-1}, only the totally symmetric vibration is seen to be appreciably enhanced. The actual I—I stretching frequency in I_3^{-1}, i.e., the average of the symmetrically (110 cm^{-1}) and antisymmetrically (145 cm^{-1})[8] coupled normal modes, is 128 cm^{-1}. This represents a considerable lowering of the force constant from that in I_2 and illustrates an important feature of polyiodide electronic structure that is evident in the vibrational spectroscopy and also in the metrical data: I_2 acts as a Lewis acid and the coordination to Lewis bases; e.g., I^{-1} decreases the I—I bond order. The I—I distance in I_2 is 2.72 Å, whereas in I_3^{-1} it is ca. 2.92 Å.[8] Approximate molecular orbital calculations[16] on I_3^{-1} show that the highest occupied molecular orbital has I—I antibonding character.

Turning now to further examples in the solid state, it is seen that resonance Raman spectra of more complex polyiodides of known structure can also be readily assigned. In no case to date does factor group splitting (correlation field effects) introduce a series problem in the spectral interpretation. FIGURE 1C presents the spectrum of $(C_6H_5CONH_2)_2H^+I_3^-$, which structurally[17] is known to consist of one-dimensional chains of symmetrical (equal I—I distances) I_3^- units. The resonance Raman spectrum clearly shows that the compound is composed of I_3^{-1} units. Because of strong lattice forces, the triiodide units in CsI_3 are distorted (I—I = 2.83(2) and 3.03(2) Å)[14]; this is readily apparent in the Raman spectrum (FIGURE 1D) where the lowered symmetry gives rise to two ν_{I-I} emissions (further split by solid state effects). For the characterization of mixed valence polyiodides it is also reasonable to inquire whether the presence of I_2 and I_3^{-1} together could be recognized by the resonance Raman technique. The answer is affirmative. FIGURE 2 presents spectra and schematic structural diagrams for the model compounds $(Cs^+)_2(I_3^{-1})_2 \cdot I_2$,[18a] $(\text{phenacetin})_2H^+I_3^{-1} \cdot I_2$,[18b] and $(C_2H_5)_4N^+I_3^{-1} \cdot 2I_2$;[18c] it is clear that both I_2 and I_3^{-1} are present. The dotted

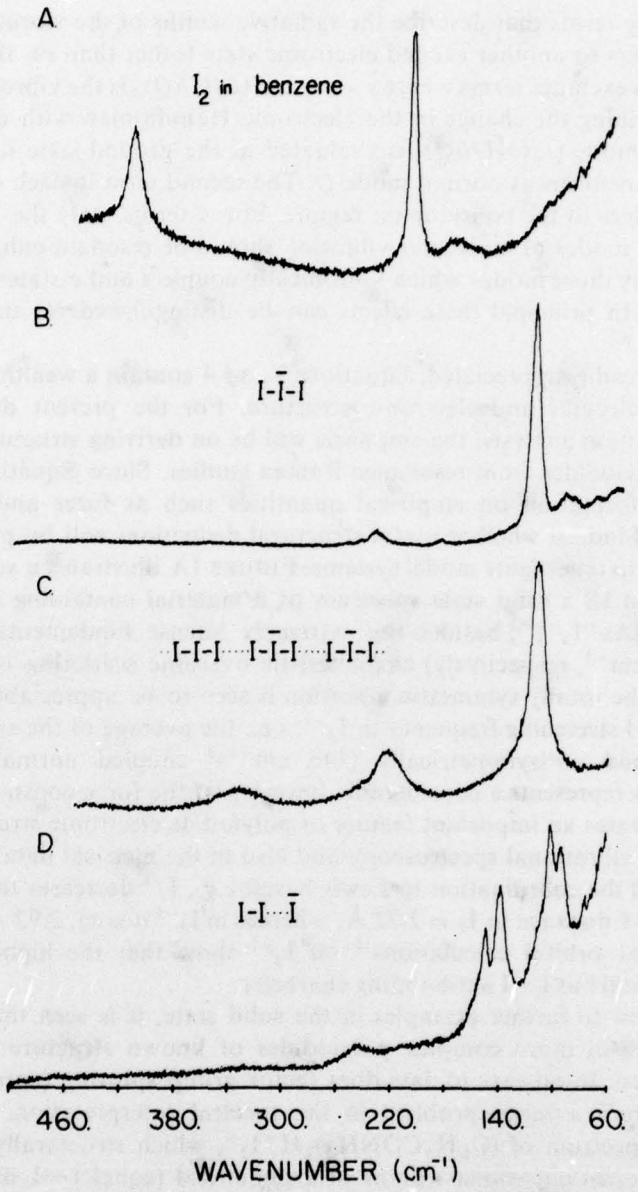


FIGURE 1: Resonance Raman spectra of A: I_2 in benzene solution. B: $(C_6H_5)_4As^+I_3^-$ solid. C: $(C_6H_5CONH_2)_2H^+I_3^-$ solid. D: CsI_3 solid. In all cases ν_0 = 5145 Å.

lines in the structures indicate weak interactions on the order of 3.42–3.55 Å. These cause a slight lengthening of the "I_2" I—I distances in the above three compounds to 2.83(2), 2.748(2), and 2.735(3) Å, respectively, and a roughly commensurate drop in the observed "I_2" ν_{I-I} frequencies to 171,187, and 183 cm^{-1}, respectively. Distortions in the I_3^{-1} units appear to give rise to a second band in the ca. 150 cm^{-1} region. This band is relatively weak in relation to the ca. 110 cm^{-1} transition except in Cs_2I_8, where the triiodide is rather severely dis-

torted (triiodide I—I = 2.84(2) and 3.00(2) Å).[18a] Although it is premature to draw quantitative conclusions, it can also be seen that the ν_{I-I} scattering increases in intensity relative to the I_3^{-1} scattering as the proportion of I_2 in the lattice increases. Another significant feature of these spectra is the presence not only of overtone bands, but also of combination bands between the various I_2 and I_3^{-1} modes. These transitions are assurance of the physical proximity of the oscillators

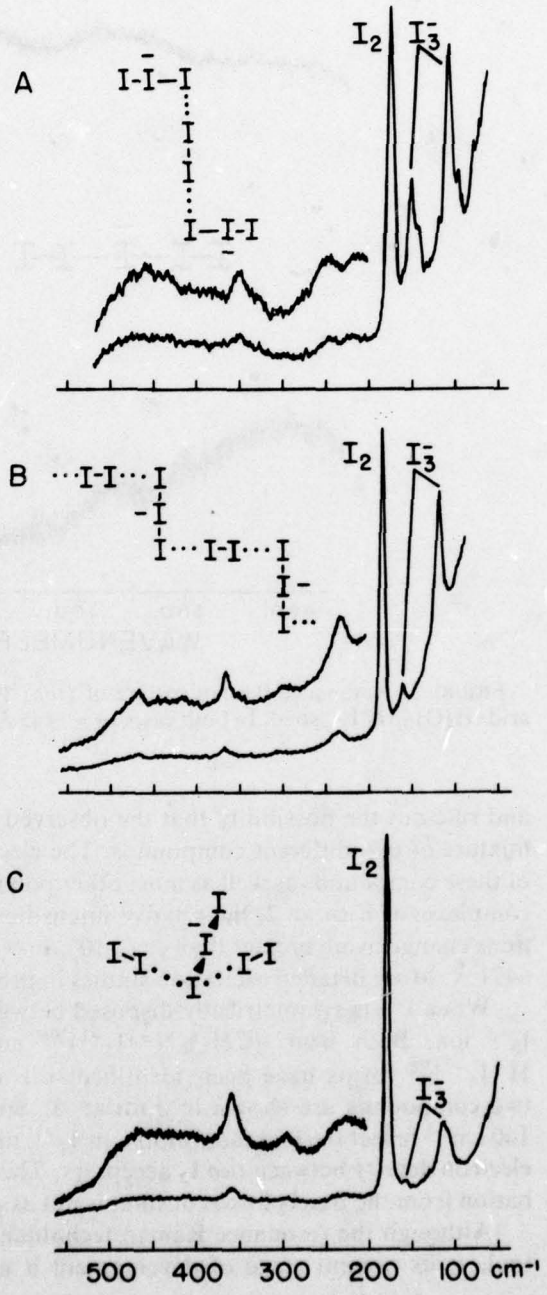


FIGURE 2. Resonance Raman spectra of A: $(Cs^+)_2(I_3^-)_2 \cdot I_2$ solid. B: $(phenacetin)_2H^+I_3^- \cdot I_2$ solid. C: $(C_2H_5)_4N^+I_3^- \cdot 2I_2$ solid. In all cases ν_0 = 5145 Å.

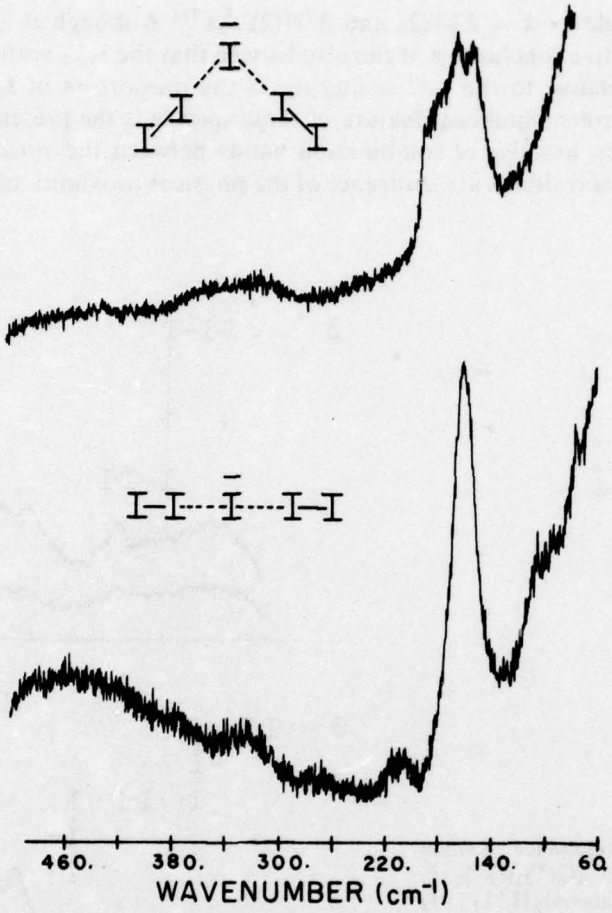


FIGURE 3. Resonance Raman spectra of (*top*) $(CH_3)_4N^+I_5^-$ solid; (*bottom*) (trimesic acid $\cdot H_2O)_{10}H^+I_5^-$ solid. In both cases $\nu_0 = 5145$ Å.

and rule out the possibility that the observed spectrum arises from a mechanical mixture of two different compounds. The electronic transitions in the solid state of these compounds as well as most other polyiodides are rather broad.[12,19] For the complexes of FIGURE 2, the relative intensities of the various fundamental transitions change by no greater than ca. ±10% on varying the exciting line from 4880 to 6471 Å. More detailed excitation studies in progress.

When I^{-1} is symmetrically disposed between two I_2 moieties, the result is the I_5^{-1} ion. Both bent $((CH_3)_4N^{+1}I_5^{-1})$[20a] and linear [(trimesic acid $\cdot H_2O)_{10} \cdot H^+I_5^{-1}$][20b] forms have been identified; the resonance Raman spectra of these two compounds are shown in FIGURE 3. Stretching vibrations centered at ca. 160 cm^{-1} reflect the fact that, unlike in I_3^{-1}, the I^{-1} in I_5^{-1} must now distribute its electron density between *two* I_2 acceptors. The first-order result is that the perturbation from the free I_2 force constant is not as drastic as in I_3^{-1}.

Although the resonance Raman technique is obviously a powerful structural tool, at its present stage of development it is limited with respect to quantita-

tively analyzing the relative amounts of various polyiodide species. Furthermore, it cannot detect isolated I^{-1} ions. For these reasons a complementary spectroscopic technique, also immune to crystallographic disorder and noncrystallinity, has been applied to charge-density measurements in mixed valence polyiodides: iodine-129 Mössbauer spectroscopy. This method of recoiless nuclear gamma ray spectroscopy[10] involves transitions between ground and excited nuclear states. For I-129 these have nuclear spin quantum numbers of 7/2 and 5/2, respectively. FIGURE 4 illustrates the maximum of 8 allowed transitions for this particular nucleus and the appearance of a typical spectrum when iodine is in an axially

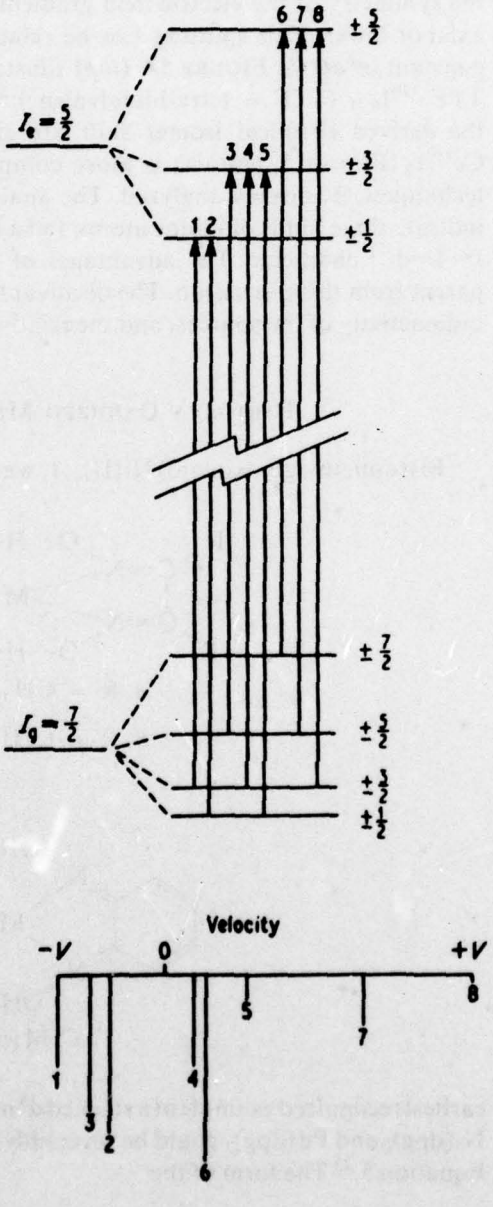


FIGURE 4. Iodine-129 Mössbauer transitions and a stick plot of a typical spectrum for the nucleus in a noncubic environment.

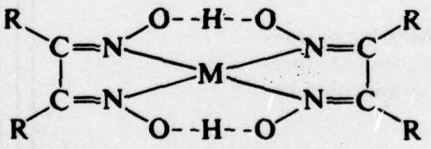
symmetric environment. The chemical isomer shift (δ) is a hyperfine term that reflects the s electron density at the iodine nucleus (relative to the gamma ray source) and affects the overall velocity position of the Mössbauer spectrum. In equation 4, Z is the atomic number, ϵ_0 the

$$\delta = \frac{1}{5\epsilon_0} Ze^2R^2\frac{\delta R}{R}\left(|\Psi_s(0)\text{absorber}|^2 - |\Psi_s(0)\text{source}|\right) \qquad (4)$$

permitivity of a vacuum, R is the nuclear radius, and δR is the change in R on making a transition to the excited state. The quadrupole splitting (QS) reflects the energy differences that arise between nuclear-spin angular momentum states when the symmetry of the electric field gradient at the nucleus descends from cubic to axial or lower. This splitting can be related to the nuclear quadrupole coupling constant, e^2qQ/h. FIGURE 5A (*top*) illustrates the I-129 Mössbauer spectrum of TTF $^{129}I_{0.71}$ (TTF = tetrathiafulvalene);[21] the lack of quadrupole splitting and the derived chemical isomer shift are characteristic of I^{-1}. The spectrum of $Cs^{129}I_3$ (FIGURE 5, *bottom*) is more complex, but by using computer simulation techniques, it is easily analyzed. The analysis agrees well with x-ray data[14] which indicate three kinds of iodine atoms and a long I—I bond which lends appreciable $I—I{=}I^{-1}$ character. The advantages of I-129 Mössbauer spectroscopy are apparent from this discussion. The disadvantages include the expense of ^{129}I, the high radioactivity of the sources, and the relatively low recoiless fractions.

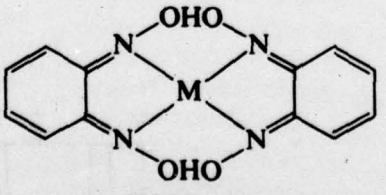
PARTIALLY OXIDIZED METAL BIS(DIOXIMATES)

Bis(dimethylglyoximato)Ni(II), *A*, was the



A, R = CH_3: M(dmg)$_2$

B, R = C_6H_5: M(dpg)$_2$



C, M(bqd)$_2$

earliest recognized example of a stacked d^8 metal complex[22]. Early work revealed that Ni(dpg)$_2$ and Pd(dpg)$_2$ could be reversibly iodinated (or brominated), as shown in Equation 5.[23] The form of the

$$M(dpg)_2 + \tfrac{1}{2}I_2 \rightleftharpoons M(dpg)_2I \qquad M = Ni, Pd \qquad (5)$$

iodine in these complexes was variously formulated as I_2(i.e. Ni^{+2}), I_3^{-1} (i.e., $Ni^{+2.33}$), and I^{-1} (i.e. Ni^{+3}). Since the golden-olive colored halogenated products were reported to be diamagnetic and to be more electrically conductive (pressed

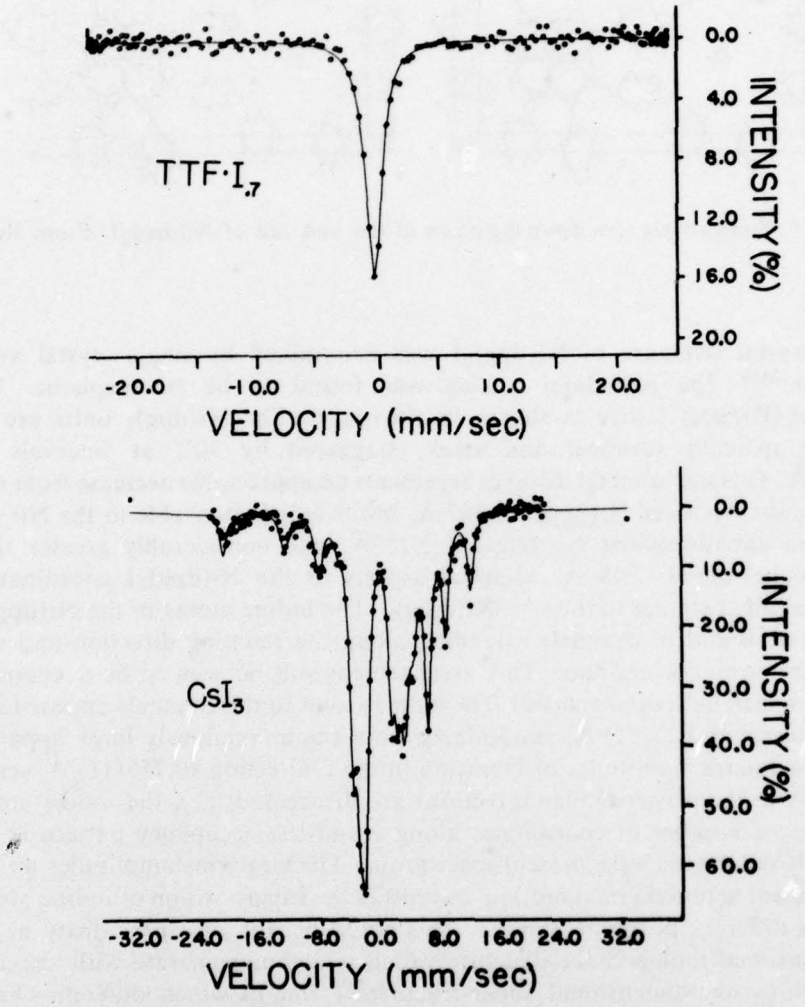


FIGURE 5. Iodine-129 Mössbauer spectra of (*top*) tetrathiafulvalene · $I_{0.7}$; (*bottom*) CsI_3.

pellet measurements) than the starting $M(dpg)_2$ materials by a factor of 10^3 – 10^4,[24] it was of great interest to investigate these complexes in more detail as the first prototypes of mixed valence materials synthesized *via* the polyiodide strategy. The reports by Endres *et al.*,[25] which demonstrated that Ni and Pd *bis*(benzoquinonedioximates), *C*, were chemically similar added further impetus to the efforts.

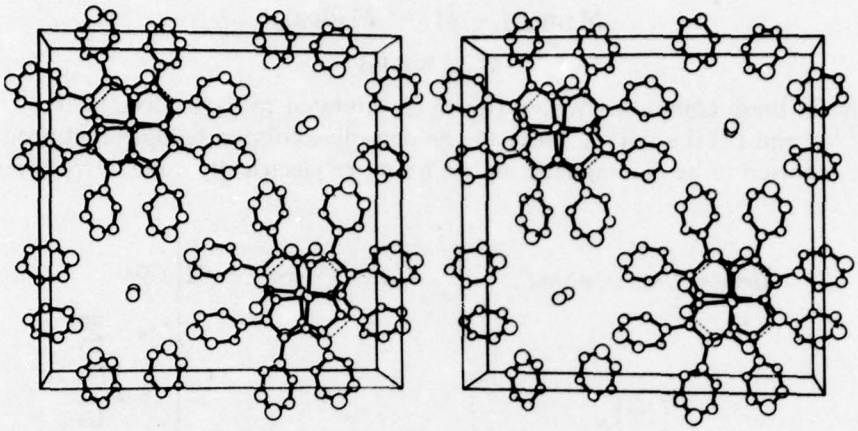


FIGURE 6. Stereoscopic view down the *c* axis of the unit cell of $Ni(dpg)_2I$. From Reference 26.

The crystal structure of $Ni(dpg)_2I$ was determined by single crystal x-ray diffraction.[26,27] The palladium analog was found to be isomorphous. The tetragonal (P4/ncc) lattice is shown in FIGURE 6. The $Ni(dpg)_2$ units are all crystallographically identical and stack, staggered by 90°, at intervals of 3.271(1) Å. This metal-metal distance represents an appreciable decrease from that found in unhalogenated $Ni(dpg)_2$, 3.547 Å, but is still comparable to the Ni—Ni distance in unhalogenated $Ni(dmg)_2$,[22] 3.25 Å, and considerably greater than that in nickel metal, 2.49 Å. Metrical aspects of the $Ni(dpg)_2I$ coordination sphere are rather similar to those of $Ni(dmg)_2$. The iodine atoms in the $Ni(dpg)_2I$ structure are found in channels extending along the stacking direction and surrounded by aromatic residues. This arrangement will be seen to be a common pattern for such lattices (*vide infra*). The iodine atoms in the channels appear to be equally spaced at 3.271(1) Å, and judging from the anomalously large apparent root-mean-square amplitudes of vibration in the *c* direction (0.756(11) Å versus 0.234(4) Å in the perpendicular direction) are disordered; i.e., the iodine atoms can occupy a number of coordinates along *c* and the occupancy pattern is not adequately described by the present space group. The large rms amplitudes do not then represent actual thermal motion, but rather the superposition of iodine atoms in slightly different positions along *c*. This could be due to a periodicity in the one-dimensional iodine chain structure which is incommensurate with the unit cell length (a one-dimensional superstructure[28]) and in which different chains may or may not be in registry, or it may simply reflect random positioning of the iodine moieties in the channel. In optimum cases it is possible to make additional structure inferences (or to test certain models) if diffuse x-ray scattering reflections can be located between the Bragg lines, and analyzed.[28]

The resonance Raman/I-129 Mössbauer technique was next applied to deducing the form(s) of iodine present in the $M(dpg)_2I$ materials.[26,27] The resonance Raman spectrum of $Ni(dpg)_2I$ (FIGURE 7) clearly rules out the presence of either free I_2 or symmetrical I_3^{-1}. Though a highly and unprecedentedly distorted I_3^{-1} moiety was at first considered as an explanation for the intense I—I stretch at

160 cm^{-1} and the weaker one at 107 cm^{-1}; the reason for such an unusual distortion in this particular lattice is not at all clear, or physically reasonable. Furthermore, the agreement between the spectra of the model I_5^{-1} compounds (FIGURE 3) and that of $Ni(dpg)_2I$ is extremely close, arguing persuasively for the I_5^{-1} formulation. In addition to the Raman results, the fully refined I-129 Mössbauer data[27] (FIGURE 7) indicate site populations in excellent agreement with the 1:2:2 ratios expected for I_5^{-1}. Based on the conservative estimates, there is less than ca. 5% I_2 or I^{-1} present and less than ca. 5–10% I_3^{-1}. Raman and Mössbauer data for

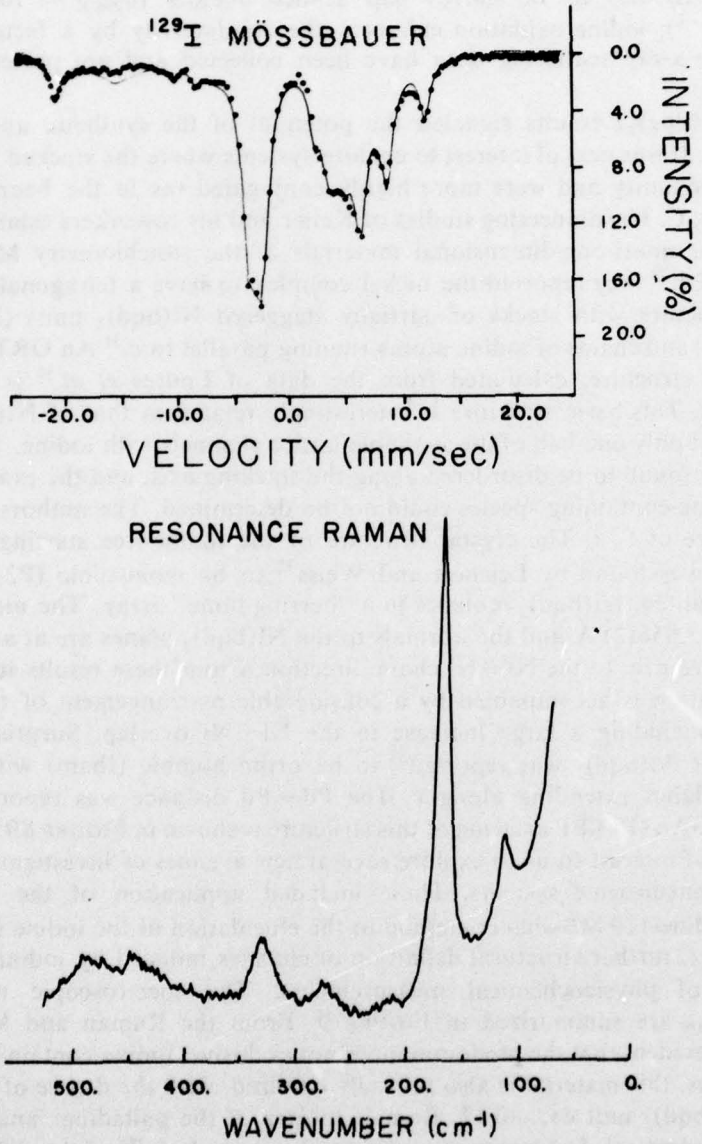


FIGURE 7. Iodine-129 Mössbauer and resonance Raman spectra (ν_0 = 5145 Å) of $Ni(dpg)_2I$.

$Pd(dpg)_2I$ are identical to those for $Ni(dpg)_2I$. Thus, this work represents the first conclusive proof that the $M(dpg)_2I$ materials are partially oxidized, mixed-valence compounds and that the iodine oxidation strategy is viable. The formal fractional oxidation state of the metal units has thus increased by ca. +0.20 upon iodination.

In addition to the Raman and Mössbauer spectral results, it has recently been possible to grow large enough single crystals of $Ni(dpg)_2I$ and $Pd(dpg)_2I$ to allow, for the first time, both four-probe dc conductivity[29] and diffuse x-ray scattering measurements[30] to be performed. We find the partially oxidized bisdiphenylglyoximates to be narrow-gap semiconductors ($\sigma_{298°K} \approx 10^{-3} - 10^{-2}$ ohm^{-1} cm^{-1}); iodine oxidation enhances the conductivity by a factor of 10^8! The diffuse x-ray scattering data have been collected and are presently being analyzed.

The $M(dpg)_2I$ results signaled the potential of the synthetic and spectral techniques. It was next of interest to explore systems where the stacked units were in close proximity and were more highly conjugated, as in the benzoquinonedioximates, *C*. The pioneering studies of Keller and his coworkers established the existence of quasi-one-dimensional materials of the stoichiometry $M(bqd)I_{0.5}$, M = Ni, Pd;[25] they reported the nickel complex to have a tetragonal (P4/mcc) crystal structure with stacks of partially staggered $Ni(bqd)_2$ units (Ni—Ni = 3.153(3) Å) and chains of iodine atoms running parallel to *c*.[31] An ORTEP drawing of this structure, calculated from the data of Endres *et al.*[31] is shown in FIGURE 8A. This basic structure is interestingly related to that of $Ni(dpg)_2I$ by the filling of only one-half of the available lattice channels with iodine. The iodine atoms were found to be disordered along the stacking axis, and the exact identity of the iodine-containing species could not be determined. The authors proposed the presence of I_3^{-1}. The crystal structure of the iodine-free starting material, $Ni(bqd)_2$, was found by Leichert and Weiss[32] to be monoclinic ($P2_1/n$), with stacks of canted, $Ni(bqd)_2$ moieties in a "herring bone" array. The nickel-nickel distance is 3.856(2) Å and the normals to the $Ni(bqd)_2$ planes are at an angle of 61.8° with respect to the Ni—Ni chain direction. From these results it appeared that iodination is accompanied by a considerable rearrangement of the crystal structure, including a large increase in the Ni—Ni overlap. Surprisingly, the structure of $Pd(bqd)_2$ was reported[33] to be orthorhombic (Ibam) with stacked $Pd(bqd)_2$ planes extending along *c*. The Pd—Pd distance was reported to be 3.202(1) Å. An ORTEP drawing of this structure is shown in FIGURE 8B.

It was of interest to us to explore several new avenues of investigation in the benzoquinonedioxime systems. These included application of the resonance Raman/iodine-129 Mössbauer method to the elucidation of the iodine identity in $M(bqd)_2I_{0.5}$, further structural definition of changes induced by iodination, and extension of physicochemical measurements. The spectroscopic results on $Ni(bqd)_2I_{0.5}$ are summarized in FIGURE 9. From the Raman and Mössbauer data[11] it is evident that the predominant, if not exclusive, iodine-containing species is I_3^{-1}. Thus, this material is also partially oxidized, with the degree of oxidation of the $Ni(bqd)_2$ unit ca. +0.17. Raman spectra of the palladium analogue are essentially identical. Independent of this work, an analysis[28b] of the diffuse x-ray scattering pattern arising from the iodine chain structure in $Ni(bqd)_2I_{0.5}$ reached exactly the same conclusion as to the form of the iodine: I_3^{-1}.

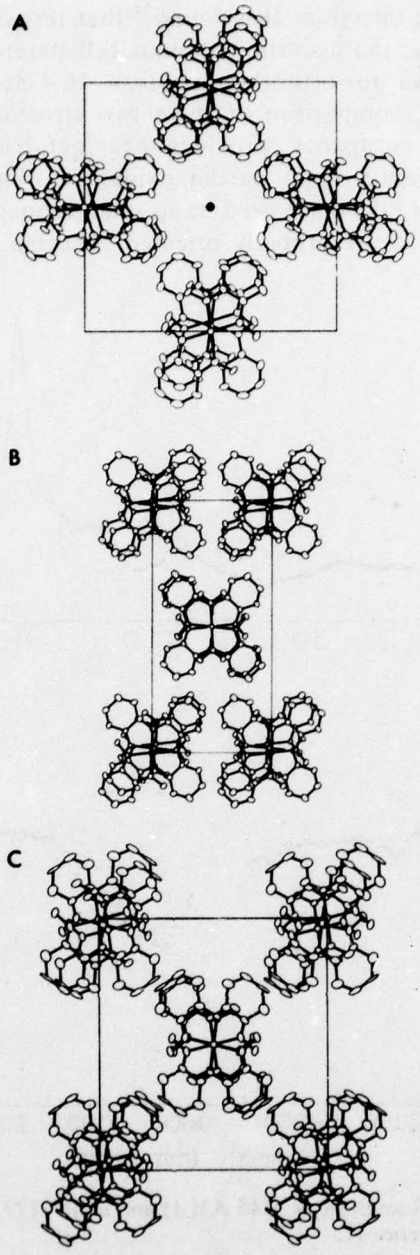


FIGURE 8. View down the *c* axis of the unit cells of A: $Ni(bqd)_2I_{0.5}$. B: $Pd(bqd)_2$. C: orthorhombic $Ni(bqd)_2$. From Reference 36.

In the course of studying the reactions of $Ni(bqd)_2$ under various iodination conditions, it was discovered[34] that small amounts of iodine promoted the crystallization of an orthorhombic (P4/mcc) modification of $Ni(bqd)_2$. The extraordinary crystal structure of this compound is presented in FIGURE 8C. The most striking feature of the lattice geometry is the presence of large, empty channels

parallel to the stacking direction. It is found[34] that this $Ni(bqd)_2$ is structurally similar to $Ni(bqd)_2I_{0.5}$; the distortion of unit cell parameters from tetragonal ($a = b = 15.553(4)$ Å) to orthorhombic ($a = 16.438(4)$, $b = 14.759(3)$ Å) is rather small. Thus, comparison of these two structures, which differ principally in the channel occupancy, provides meaningful insight into the spatial reorganization that occurs upon partial oxidation. What is most surprising is that the changes that take place need be so small in magnitude for this system when the $Ni(bqd)_2$ units are properly oriented. The major alteration in going

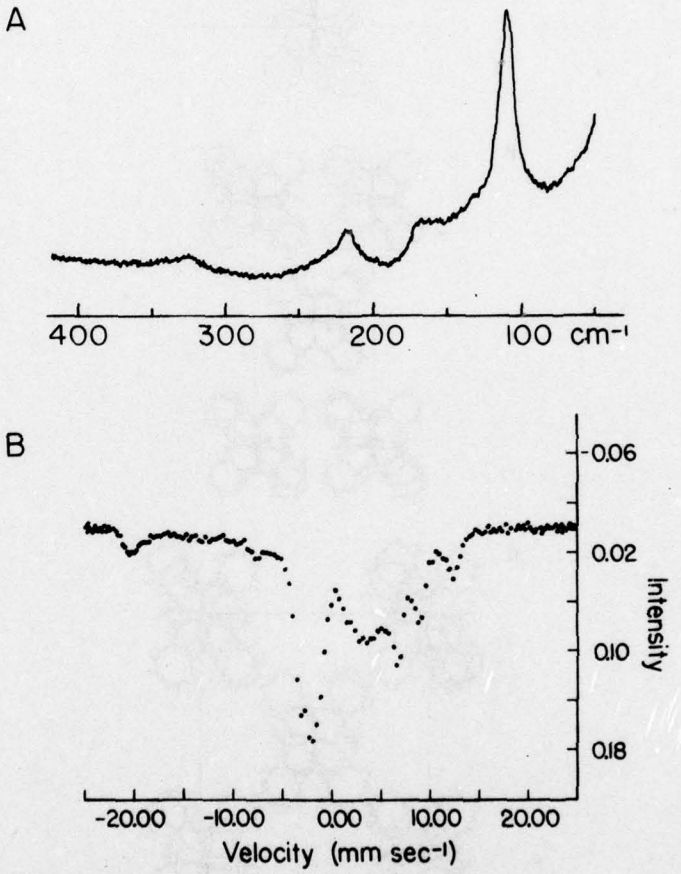


FIGURE 9. Resonance Raman ($\nu_0 = 5145$ Å)(*A*) and iodine-129 Mössbauer (*B*) spectra of $Ni(bqd)_2I_{0.5}$. From Reference 11.

from $Ni(bqd)_2$ to $Ni(bqd)I_{0.5}$ is in the stacking distance, which contracts from 3.180(1) to 3.153(3) Å upon oxidation—a 0.027 Å change. The relative orientation of the adjacent $Ni(bqd)_2$ units in a stack is apparently not dictated in this case by the symmetries of the ligand molecular orbitals.[35] Optimum overlap of highest occupied and lowest unoccupied molecular orbitals in $Ni(bqd)_2$ is expected to require a different orientation that optimum overlap of the highest occupied molecular orbitals in $Ni(bqd)_2I_{0.5}$. It is seen that these factors are not structure-determining in the present situation.

It was also of interest to investigate structurally the response to iodination of the $Pd(bqd)_2$ system. We find $Pd(bqd)_2I_{0.5}$ and $Ni(bqd)_2I_{0.5}$ to be isomorphous.[36] Indeed, even the diffuse scattering pattern of the palladium compound is identical to that reported for the nickel analogue.[28] The Pd—Pd separation in $Pd(bqd)_2I_{0.5}$ is 3.184(1) Å, which represents a 0.019 Å contraction upon iodination. This is, as in the $Ni(bqd)_2$ lattice, a relatively small contraction compared to the $M(dpg)_2I$ system. The other major change that takes place in the $Pd(bqd)_2$ structure upon iodination can be readily appreciated in FIGURE 8 and is a spreading out of the lattice in the plane perpendicular to *c*, to provide space for the iodine channels. The relative orientation, i.e., angle of staggering of adjacent $Pd(bqd)_2$ groups in a stack does not change upon oxidation.

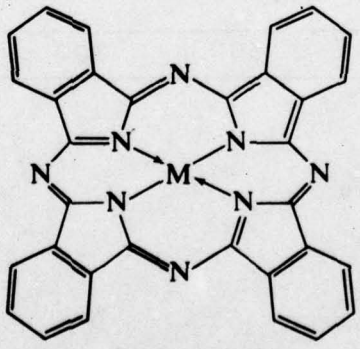
Sufficiently large single crystals of the $M(bqd)_2$ and $M(bqd)_2I_{0.5}$ materials have now been grown to allow four-probe dc conductivity studies.[29] An approximately 10^6 increase in electrical conductivity takes place upon partial oxidation. The mixed-valence crystals are narrow-gap semiconductors, with room temperature conductivities in the range $10^{-3} - 10^{-2}$ ohm^{-1} cm^{-1}. These values are close to those found for the $M(dpg)_2I$ compounds, which have a ca. 0.10 Å greater metal-metal separation.

PARTIALLY OXIDIZED PHTHALOCYANINE MATERIALS

The highly conjugated (in comparison to the dioximates) flat structures, the presence of multiple redox states, and the inherent chemical flexibility of phthalocyanines suggested attractive donor molecules for the construction of mixed valence lattices, with use of the iodine method. It was found[37] that the oxidation of metallophthalocyanines (MPc) or the metal-free macrocycle (PcH_2) by iodine vapor or solutions results in an extensive new class of very highly conductive "molecular metals," as shown in Equation 6. The

$$MPc + \chi/2I_2 \rightleftharpoons (MPc)(I)_x \qquad (6)$$

$M = Fe, Co, Ni, Cu, Zn, Pt, H_2$



= MPc

exact stoichiometry obtained depends on the reaction procedure and can be systematically varied. The iodination is reversible, and heating under vacuum regenerates the starting phthalocyanines. That these new materials are partially oxidized, mixed-valence solids is supported by resonance Raman/iodine-129 spectroscopy. In FIGURE 10 are shown Raman spectra of typical samples. The strong

fundamental and vibrational progression of I_3^{-1} are readily evident. For $x \lesssim 3$ there is no evidence of I_2, which the aforementioned model studies (*vide supra*) indicate should be readily detectable. The ^{129}I Mössbauer spectrum of $NiPcI_{2.16}$ is illustrated in FIGURE 11. It is also indicative of a symmetrical I_3^{-1} molecule, i.e., δ = 1.34 and 0.27 mm/sec vs. ZnTe, and the ^{129}I e^2qQ = −1667 and −862 MHz. Any I_2 present must, by these measurements, be less than 10% of the total iodine, and any I^{-1} is less than 5%.

Single crystals of a number of partially oxidized phthalocyanines can be grown by temperature-gradient diffusion methods. The crystal structure of $NiPcI_{1.0}$ has

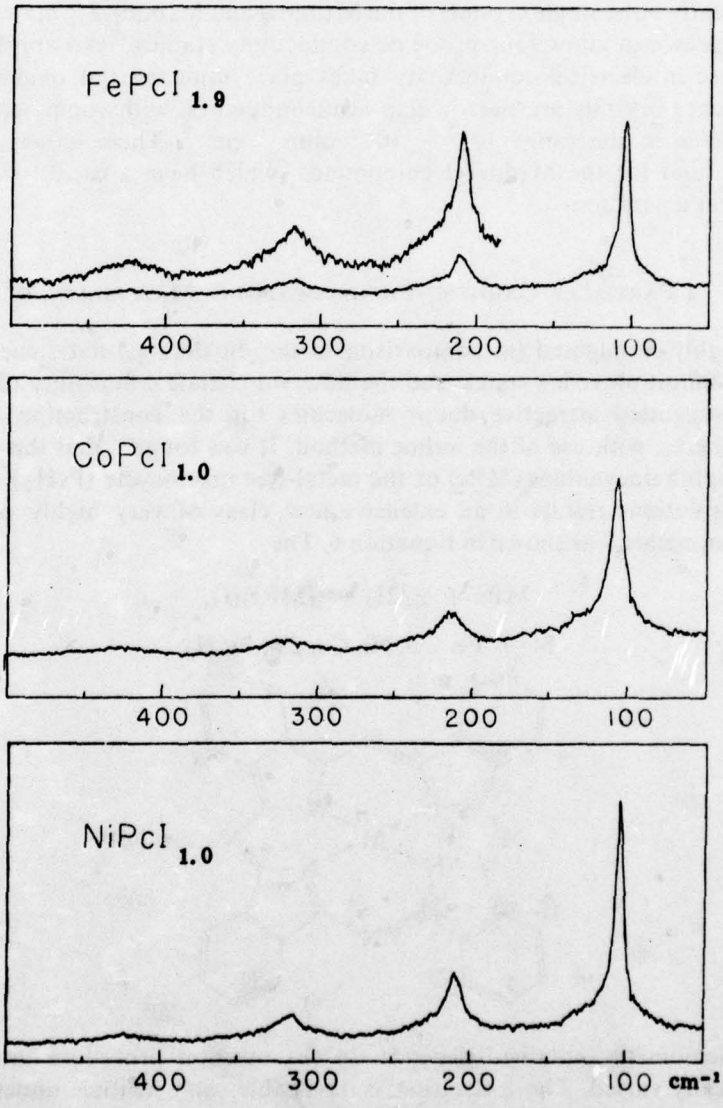


FIGURE 10. Resonance Raman spectra of partially oxidized metal phthalocyanine materials with 5145 Å excitation.

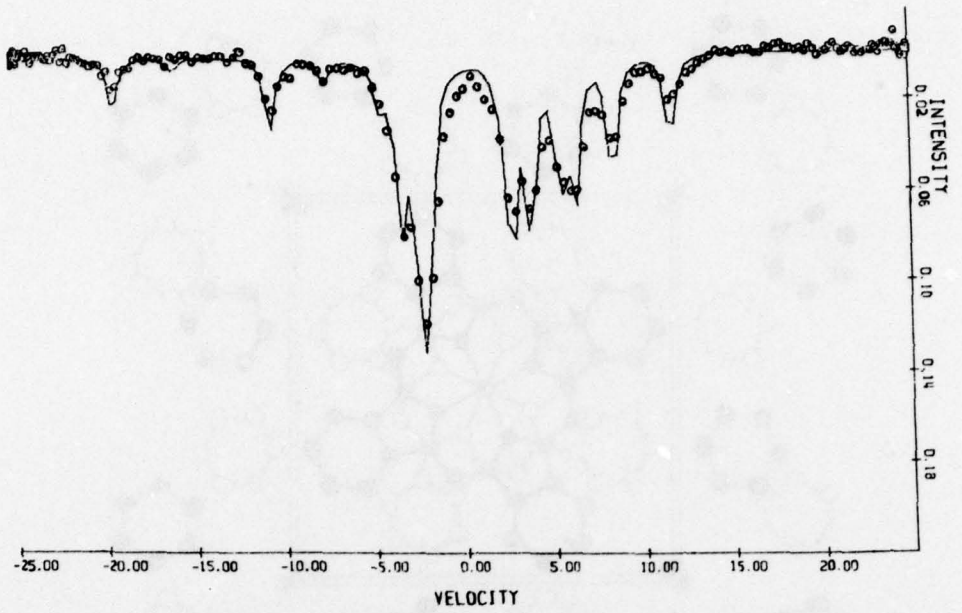


FIGURE 11. Iodine-129 Mössbauer spectrum of $Ni(Pc)I_{2.16}$. From Reference 38.

been determined by x-ray diffraction and is shown in FIGURE 12.[38] The overall packing is typical of these kinds of materials: tetragonal (P4/mcc) with stacks of donors and chains of iodine atoms extending parallel to the *c* direction. The stacking repeat distance for the NiPc units is 3.244(3) Å, which is somewhat longer than in the partially oxidized nickel and palladium benzoquinonedioximates. The individual NiPc groups are staggered by 39.5° with respect to adjacent units in stack. Bond distances and angles within the NiPc molecule are comparable to those of other planar metal phthalocyanines.[39] The iodine atoms of $NiPcI_{1.0}$ give rise to diffuse scattering in the diffraction photographs. Analysis of the positions and intensities of these extra lines yields a structural model consisting of chains of I_3^{-1} units with I—I bond distances of 3.00(2) Å and spacings of 3.72(2) Å between the I_3^{-1} units.[38] This result is in excellent accord with known polyiodide structures.[8] More importantly, it reinforces the conclusions drawn from the Raman/Mössbauer studies that these are indeed mixed-valence materials. For $NiPcI_{1.0}$, the D → A charge density transfer is thus 0.33 electron per NiPc unit.

Powder-diffraction studies of other $MPcI_x$ and PcH_2I_x compounds indicate that all have similar crystal structures.[37,38] It seems plausible that the various stoichiometries are related by the degree of iodine occupation of the various channels in the lattice that run parallel to *c*. By eclipsing the PcNi units in the $PcNiI_{1.0}$ structure, four additional channels are created at 1/2, 0, *z* and symmetry-related positions. Complete filling of all channels would produce a tetragonal cell of comparable dimensions and the stoichiometry $NiPcI_{3.0}$. At this time insufficient data are available on any of the new materials to rigorously determine whether *x* varies continuously from 0 to 3 or whether mixtures of discrete phases with fixed *x* or *x* ranges are present. Preliminary iron-57 Mössbauer studies on the

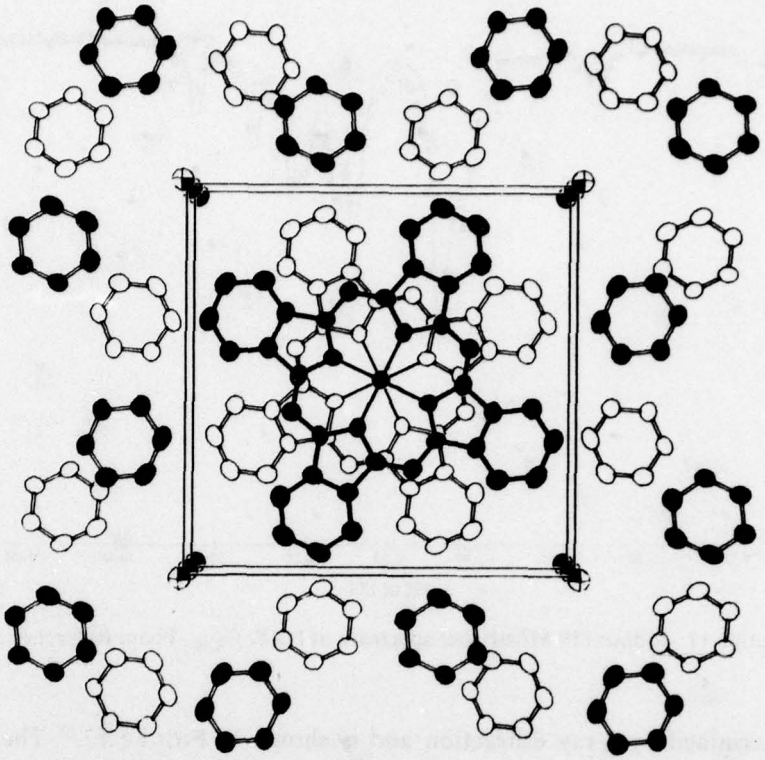


FIGURE 12. View down the *c* axis of the unit cell of $NiPcI_{1.0}$. From Reference 38.

$FePcI_x$ series[40] indicate that in this case x does not vary continuously, but that several $FePcI_x$ species exist. The distribution of phases is a function of the stoichiometry and the preparative methodology (including the solvent). XPS (x-ray photoelectron spectroscopy) studies[41] of $NiPcI_x$ and $PtPcI_x$ materials ($x < 3$) have been conducted at low temperature with careful monitoring of the I 3d 5/2 signal (to insure no I_2 was being lost from the surface) and in several instances with ion-sputter cleaning of the surface. In all cases only a single kind of nickel or platinum ion could be distinguished.[41]

The electron-transport properties of the new phthalocyanine materials were initially investigated with pressed pellets by four-probe conductivity techniques.[37] Remarkably, it is found that iodine oxidation causes a 10^9–10^{10} increase in the electrical conductivity. Representative plots of conductivity as a function of temperature are illustrated in FIGURE 13. It is seen that the best $MPcI_x$ conductors are comparable to (quinolinium)$(TCNQ)_2$ pressed pellets in electron-transport characteristics (TCNQ = 7,7,8,8-tetracyanoquinodimethane).[37] Generally, pressed-pellet specimens are found to be ca. 10^2 less conductive than single-crystal values in these types of materials. The room-temperature electrical conductivity of $NiPcI_{1.0}$ crystals, in the stacking (*c*) direction, is *ca.* 200–650 ohm^{-1} cm^{-1} and increases on lowering the temperature to 100°K.[42] Further evidence for the quasimetallic electronic structure of the $PcNiI_x$ derivatives is provided by magnetic

susceptibility studies. Faraday balance measurements from 100–298°K show weak, temperature-independent paramagnetism.[37] The fact that the PcH_2I_x compounds have conductivities comparable to the partially oxidized metallophthalocyanines strongly implies that electron transport takes place largely through the highly conjugated ligand π electron clouds, rather than through metal-metal overlap. The new partially oxidized phthalocyanine materials are unique for two important reasons. First, they possess a great chemical flexibility in terms of metal and ligand which offers the opportunity to "fine tune" solid state properties. Second, unlike the starting materials for other highly conductive molecular solids, phthalocyanines are today produced on a millions of pounds per year scale by the pigment industry and are thus extremely inexpensive.

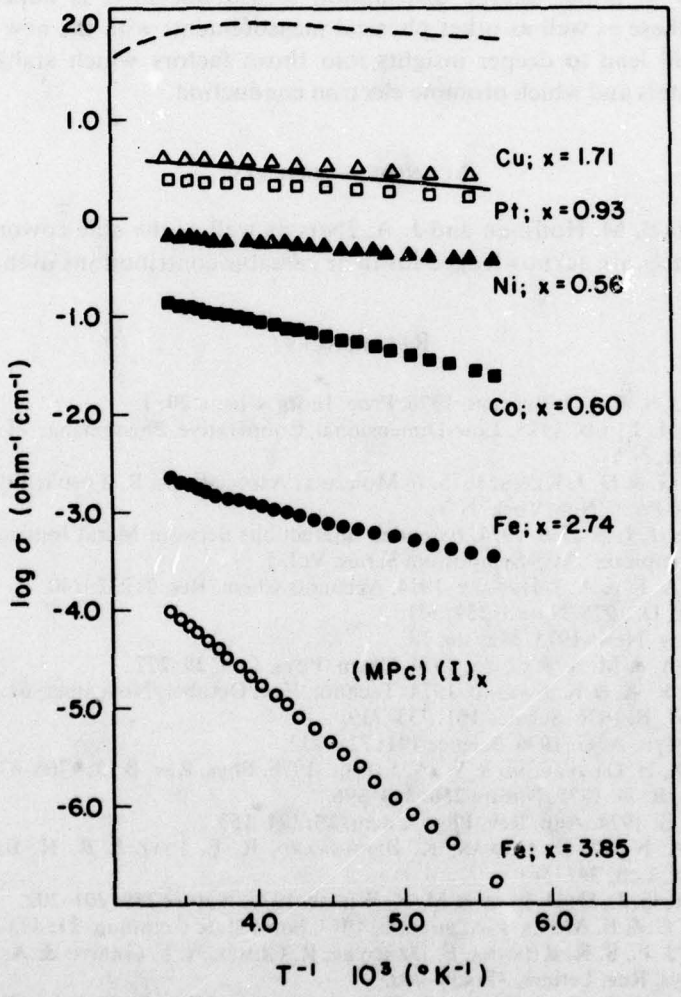


FIGURE 13. Electrical conductivity as a function of temperature for pressed-pellet samples of various partially oxidized metal phthalocyanines, $MPcI_x$. Powder (——) and single crystal (-----) data for (quinolinium)$(TCNQ)_2$ are also presented. (From Reference 37.)

Conclusions and Prospects

It is apparent that the iodine-oxidation procedure has considerable efficacy in the construction of quasi-one-dimensional mixed-valence lattices. It should also be obvious that the scope of this procedure, as of most chemical syntheses, has certain bounds, dictated by the intrinsic molecular properties of the reactants. For example, we[27] (and others[23a]) have found that $Pt(dpg)_2$ is oxidized to $Pt(dpg)_2I_2$; also, perchlorophthalocyanines cannot be oxidized under normal conditions.[38] Despite these limitations, the variety of new and unusual partially oxidized compounds already produced by this method suggests a broad scope, and that considerable refinement in the design and synthesis of highly conductive unidimensional materials is possible. The other major advantage of using iodine as an acceptor lies in the applicability of resonance Raman and iodine-129 Mössbauer spectroscopy to lattice charge distribution measurement. It is hoped that the coupling of these as well as other physical measurements with the new solid-state chemistry will lead to deeper insights into those factors which stabilize quasi-metallic crystals and which promote electron conduction.

Acknowledgments

Professors B. M. Hoffman and J. A. Ibers as well as the able coworkers listed in the references are acknowledged for their valuable contributions to this work.

References

1a. Miller, J. S. & A. J. Epstein. 1976. Prog. Inorg. Chem. **20:** 1.
b. Keller, H. J., Ed. 1975. Low-Dimensional Cooperative Phenomena. Plenum Press. New York, N.Y.
c. Soos, Z. G. & D. J. Klein. 1975. *In* Molecular Associations. R. Foster, Ed.: Chapt. 1. Academic Press. New York, N.Y.
d. Interrante, L. V., Ed. 1974. Extended Interactions Between Metal Ions in Transition Metal Complexes. ACS Symposium Series. Vol. 5.
2a. Garito, A. F. & A. J. Heeger. 1974. Accounts Chem. Res. **7:** 232–240.
b. Yoffe, A. D. 1976. Nature **259:** 171.
c. Chem. Eng. News 1975. May 26: 18.
3a. Aviram, A. & M. A. Ratner. 1974. Chem. Phys. Lett. **29:** 277.
b. Laudise, R. A. & K. Nassau. 1974. Technol. Rev. October/November: 61.
c. Hillig, W. B. 1976. Science **191:** 733–739.
d. Chynoweth, A. G. 1976. Science **191:** 725–732.
4. Davis, D., H. Gutfreund & W. A. Little. 1976. Phys. Rev. B **13:** 4766–4779.
5a. Haddon, R. D. 1975. Nature **256:** 394–396.
b. Soos, Z. G. 1974. Ann. Rev. Phys. Chem. **25:** 121–153.
6a. Bloch, A. N., D. O. Cowan, K. Bechgaard, R. E. Pyle & R. H. Banks. 1975. Phys. Rev. Lett. **34:** 1561.
b. Ashwell, G. J., D. D. Eley & M. R. Willis. 1976. Nature **259:** 201–202.
c. Isett, L. C. & E. A. Perez-Albuerne. 1977. Solid State Commun. **21:** 433–435.
7a. Pouget, J. P., S. K. Khanna, F. Denoyer, R. Comès, A. F. Garito & A. J. Heeger. 1976. Phys. Rev. Letters, **37:** 438–440.
b. Torrance, J. B., B. A. Scott & F. B. Kaufman. 1975. Solid State Commun. **17:** 1369–1373.
c. Butler, M. A., F. Wudl & Z. G. Soos. 1975. Phys. Rev. B **12:** 4708–4719.
d. Coppens, P. 1975. Phys. Rev. Lett. **35:** 98–100.

8. Popov, A. I. 1972. *In* MTP International Review of Science. Inorganic Chemistry. Ser. One. Vol. 3, V. Gutmann, Ed. Chapt. 2, and references therein. University Park Press. Baltimore, MD.
9a. Johnson, B. B. & W. L. Peticolas. 1976. Ann. Rev. Phys. Chem. **27:** 465–91.
b. Tang, J. & A. C. Albrecht. 1970. *In* Raman Spectroscopy. H. A. Szymanski, Ed. Vol. 2, Chapt. 2. Plenum Press. New York, N.Y.
c. Spiro, T. G. & P. Stein. 1977. Ann. Rev. Phys. Chem. **28:** 501–21.
10. Gibb, T. C. 1976. Principles of Mössbauer Spectroscopy. Chapman and Hall. London, England.
11. Marks, T. J., D. F. Webster, S. L. Ruby & S. Schultz. 1976. J. Chem. Soc. Chem. Commun. 444–445.
12. Kalina, D. W., T. J. Marks, D. R. Stojakovic & R. C. Teitelbaum. Submitted for publication.
13a. Mingardi, M. & W. Siebrand. 1975. J. Chem. Phys. **62:** 1074–1085.
b. Nafie, L. A., R. W. Pastor, J. C. Dabrowiak & W. H. Woodruff. 1976. J. Amer. Chem. Soc. **98:** 8007–8014.
c. Johnson, B. B., L. A. Nafie & W. L. Peticolas. 1977. Chem. Phys. **19:** 303–311.
14. Runsink, J., S. Swen-Walstra & T. Migchelsen. 1972. Acta Cryst. **B28:** 1331–1335.
15. Kiefer, W. 1974. Appl. Spectrosc. **28:** 115–134.
16. Gabes, W. & M. A. M. Numan-Meester. 1973. Inorg. Chem. **12:** 589–592.
17. Reddy, J. M., K. Knox & M. B. Robin. 1964. J. Chem. Phys. **40:** 1082–1089.
18a. Havinga, E. E., K. H. Boswijk & E. H. Wiebenga. 1954. Acta Cryst. **7:** 487.
b. Herbstein, F. H. & M. Kapon. 1972. Nature (London) **239:** 153–154.
c. Havinga, E. E. & E. H. Wiebenga. 1958. Acta. Cryst. **11:** 733–737.
19. Gabes, W. & D. J. Stugkens. 1974. Spectrochim. Acta **30A:** 1835–1841.
20a. Hach, R. J. & R. E. Rundle. 1951. J. Amer. Chem. Soc. **73:** 4321–4324.
b. Herbstein, F. H. & M. Kapon. 1972. Acta Cryst. **A28:** S74, and private communication.
21. Marks, T. J., R. C. Teitelbaum & S. L. Ruby. In preparation.
22. Williams, D. E., G. Wohlauer & R. E. Rundle. 1959. J. Amer. Chem. Soc. **81:** 755–756.
23a. Miller, J. S. & C. H. Griffiths. 1977. J. Amer. Chem. Soc. **99:** 749–755.
b. Mehne, L. F. & B. B. Wayland. 1975. J. Amer. Chem. Soc. **14:** 881–885.
c. Keller, H. J. & K. Seibold. 1971. J. Amer. Chem. Soc. **93:** 1309–1310.
d. Foust, A. S. & R. Soderberg. 1967. J. Amer. Chem. Soc. **89:** 5507–5508.
24. Underhill, A. E., D. M. Watkins & R. Pethig. 1973. Inorg. Nucl. Chem. Lett. **9:** 1269–1273.
25. Endres, H., H. J. Keller, M. Mégnamisi-Bélombé, W. Moroni & D. Nöthe. 1974. Inorg. Nuclear Chem. Lett. **10:** 467.
26. Gleizes, A., T. J. Marks & J. A. Ibers. 1975. J. Amer. Chem. Soc. **97:** 3545–3546.
27. Cowie, M. A., A. Gleizes, G. W. Grynkewich, D. W. Kalina, R. P. Scaringe, R. C. Teitelbaum, S. L. Ruby, T. J. Marks & J. A. Ibers. Submitted for publication.
28a. Renker, B. & R. Comès. 1975. *In* Low-Dimensional Cooperative Phenomena. H. J. Keller, Ed.: 235–258. Plenum Press, New York, N.Y.
b. Endres, H., H. J. Keller, M. Mégnamisi-Bélombé, W. Moroni, H. Pritzkow, J. Weiss & R. Comès. 1976. Acta Cryst. **A32:** 954–957.
29. Kalina, D. W., M. McClure, C. R. Kannewurf & T. J. Marks. In preparation.
30. Kalina, D. W., R. P. Scaringe, T. J. Marks & J. A. Ibers. In preparation.
31. Endres, H., H. J. Keller, W. Moroni & J. Weiss. 1975. Acta Cryst. **B31:** 2357–2358.
32. Leichert, I. & J. Weiss. 1975. Acta Cryst. **B31:** 2877–2878.
33. Leichert, I. & J. Weiss. 1975. Acta Cryst. **B31:** 2709–2710.
34. Brown, L. D., D. W. Kalina, T. J. Marks & J. A. Ibers. Submitted for publication.
35. Miller, J. S. 1977. Inorg. Chem. **16:** 957–960.
36. Brown, L. D., D. W. Kalina, T. J. Marks & J. A. Ibers. In preparation.
37. Peterson, J. L., C. S. Schramm, D. R. Stojakovic, B. M. Hoffman & T. J. Marks. 1977. J. Amer. Chem. Soc. **99:**286–288.
38. Peterson, J. L., C. S. Schramm, R. P. Scaringe, D. R. Stojakovic, B. M. Hoffman, J. A. Ibers & T. J. Marks. Submitted for publication.
39. Day, V. W., T. J. Marks & W. A. Wachter. 1975. J. Amer. Chem. Soc. **97:** 4519–4527.

40. KIM, K., C. S. SCHRAMM, D. R. STOJAKOVIC, B. M. HOFFMAN, T. J. MARKS & L. H. SCHWARTZ. In preparation.
41. GRYNKEWICH, G. W. 1976. Unpublished results at Northwestern Univ., Evanston, Ill.
42. SCHRAMM, C. S., D. R. STOJAKOVIC, B. M. HOFFMAN & T. J. MARKS. 1978. Science. in press.

DISCUSSION

JEROME PERLSTEIN (*Eastman Kodak, Rochester, N. Y.*): Have you tried to make these mixed-valence phthalocyanine materials with Br_2 or Cl_2?

MARKS: Yes, bromine and IBr work. We have looked at a lot of Raman spectra. When you use the mixed halogens the Raman spectra seem to indicate we have got almost every conceivable polyhalide present. The trouble with bromine is that it goes in more easily, but it also comes out more easily. A lot of complexes lose bromine on standing.

PERLSTEIN: Is there a possibility that transport may occur along an iodine chain?

MARKS: We have looked at several polyiodine complexes. The perylene complex is partially oxidized. But there are classical compounds that have chains of I_3^-, I_2, I_3^- alternating, and they are narrow-gap semiconductors. In fact, iodine itself is a semiconductor. But we do not see the high conductivity that we see in the phthalocyanine complexes.

JOEL S. MILLER: We tried to oxidize the $Ni(dpg)_2$ with thiocyanogen, which is intermediate in oxidation potential between bromine and iodine and did not form a complex. But other people have formed thiocyanogen complexes of TTF, and the conductivity is comparable to that of the iodide complexes of TTF. This suggests that the conductivity is along the cation chain.

LEONARD INTERRANTE: Your choice of metal and halogen oxidation states implictly assume that the electron comes from the metal. Could these be metal-stabilized cation radicals (i.e., ligand oxidation)?

BRIAN HOFFMAN: All the evidence on the basis of the EPR is that it is indeed a cation radical. I think the metal is altering the properties of ligand in some sense, just as a substituent might do.

BIS(α,β-DIONEDIOXIMATO)METAL COMPLEXES: SOLID-STATE DESIGN BY MOLECULAR ENGINEERING*

H. Endres, H. J. Keller, R. Lehmann,
H. van de Sand, and Dong Vu

Anorganisch-Chemisches Institut
Universität Heidelberg
Heidelberg, Germany

and

Arnulfo Poveda

Departimento de Chimica
Universidad Nacional
Bogota, Colombia

INTRODUCTION

This paper deals with special *synthetic* efforts in the field of linear-chain transition metal complexes. The recent chemical and physical investigations into these materials (a full account of the pertinent references as well as a synopsis of the historical background is included in Dr. J. S. Miller's paper in this volume) make clear that there is a great need for new materials which could be prepared in a more systematic way. This is especially true of investigations related to the model compound of a high-temperature superconductor proposed by W. A. Little[1] and Gutfreund and Little.[2] The primary proposal[1] of a one-dimensional excitonic superconductor was surely one of the greatest contributors to the explosive development of linear-chain chemistry. Very recently a complicated platinum complex was used as a model compound.

For a chemist interested in transition metal chemistry this latter proposal raises the question of whether such complicated structures are stable at all and if so, whether they could be prepared in a systematic way. We are engaged in finding an answer to this question as far as the chemical problems are concerned. This seems reasonable not only in the hope of finding new highly conducting materials. The elaboration of synthetic routes for the preparation of a *Little* model compound would additionally lead to more *general rules* for the preparation of distinct linear-chain matrices. On this basis practically any other tailor-made linear-chain compound with strong intermolecular interactions could be synthesized in a directed way. Apart from any connection to an excitonic superconductor the synthesis of new one-dimensional, crystallizable materials and investigations of their physical and chemical properties are of rather general importance. Some of them (if intermolecular interactions are strong) behave very like crystallized linear polymers ($Ir(CO)_3CL$, e.g.) and therefore merit interest in many respects (topo-

*Supported by grant no. Ke 135/17 from Deutsche Forschungsgemeinschaft, Bonn-Bad Godesberg, Germany. Manuscript received June 13, 1977.

0077-8923/78/0313-0617 $1.75/1© 1978, NYAS

chemical reactions on linear matrices, binding of chemical species, anisotropic physical properties.

Selection of Materials

The Little Model requires a conducting spine and polarizable ligands closely attached to it. One possible way to build up such a system is—as proposed by Gutfreund and Little[2]—to use the ability of some planar transition metal complexes to crystallize in columnar stacks. It is a well-known fact that certain planar transition metal complex molecules are "pancaked" one on top of the other upon crystallization in such a way that linear metal chains result. Known for a long time are some "classical" examples like the tetracyanoplatinates(II),[3] tetrachloroplatinate(II),[4] and bis(2,3-butanedionedioximato)nickel(II).[5]

Following the Little concept one has to find other appropriate *planar* species that crystallize in stacks, and one has to check whether these stacks contain strongly interacting metal ions. A huge amount of planar molecules has been described in the literature and one has to answer the question which of them might be best suited for the mentioned purpose.

Omitting planar complexes with those ligands which "force" the metal ions—without regard to their "electronic ability"—in a planar geometry (phthalocyanine, porphyrins, and other tetra-aza-macrocycles, etc.), and omitting some rather exotic examples like *tris*(triphenylphosphin)-palladium(O) and -platinum(O) or the *tris*[*bis*(trimethylsilyl)amid] metal(III) compounds as well as the few planar main-group compounds like $[ICl_4]^-$ and XeF_4, planar species are found only in the chemistry of the fourcoordinate d^7, d^8, and d^9 transition metal ions.

There are only a few planar d^7 compounds and, moreover, only some exceptional cases which crystallize in columns and which would fit into this program, at least theoretically. These are some d^7 cobalt(II) species such as the N_4S_4 derivative $Co(N_2S_2)_2C_4H_9NO$, which could be obtained by the reaction of *bis*(S-amino-dithionitrito)cobalt(II) with ammonia, formaldehyde, and methanol[6] or some of the oxygen carriers such as N,N′-ethylene *bis*(salicylideneaminato)-cobalt(II), but none of them stacks with directly interacting metal ions.[7] Other d^7 ions (Rh(II) and Ir(II), e.g.) do not form planar species under reasonable experimental conditions. The experimental fact that there are only a few planar d^7 species is surely connected with the Lewis acidity of planar four-coordinate complexes with less than 8 d electrons. All of them tend to add axial donor ligands. But the possibility of stacking disappears for these five- or six-coordinate species.

The d^9 ion copper(II) forms numerous planar complexes, but the few that have been found to crystallize in stacks with directly interacting metal ions show only minor intermolecular interactions. They behave like antiferromagnetic isolators.[8]

The most extensive chemistry of planar fourcoordinate complexes is connected with the d^8 metal ions rhodium(I), iridium(I), nickel(II), palladium(II), platinum(II), and gold(III). Numerous compounds of these ions are obtained in columnar stacks upon crystallization, and appreciable intermolecular interactions occur along the chains in many of these solids.[9] Very strong interactions are found in those chains which contain complex molecules with small ligands such as CN^- or CO. Whether strong interactions could be retained after introducing huge,

highly polarizable dye molecules is certainly one of the main questions connected with the realization of the Little-Gutfreund model. In order to answer this question one has to investigate the change of solid-state properties by using more and more bulky ligands. In following up such a complicated matter it seems reasonable to start with well-known and thoroughly investigated species and add distinct features of the model step by step.

We therefore started the project by looking for appropriate planar d^8 compounds which contain highly versatile and more or less bulky ligands and which, additionally, have been shown to contain linear metal chains.

Stacks of Planar d^8 Transition Metal Complexes with Versatile Ligands

Of the many groups of linear-chain d^8 transition metal complexes which have been proved to contain directly interacting metal ions, only a few actually contain versatile organic ligands. These are mainly the dicarbonychelatoiridium(I) and rhodium(I) compounds,[10] the tetrakis(isonitrile)-iridium(I) and rhodium(I) cations[11,12] and the *bis*(α,β-dionedioximato)metal(II) compounds of the d^8 ions nickel(II), palladium(II), and platinum(II).[13] A few other species such as the α-modification of bis(N-methylsalicylaldiminato)-nickel(II),[14] the *bis*(pyridine-2-methylcarboxaldoximinato)-platinum(II)[15] and N,N'-ethylenebis(1,1,1-trifluoroacetyl-acetoneiminato)nickel(II)[16] have been shown to contain directly interacting linear metal ion chains, but nothing is known about the changes in solid-state properties if the central metal or the ligands are varied over a wide range. We therefore decided to select one of the former three groups of complexes for our investigation. The results described here are related to the *bis*(α,β-dionedioximato)metal(II) compounds only.

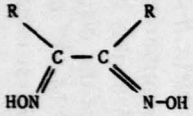
The reasons for using this type of complex are additionally their chemical stability, versatility, possibility of oxidation without destroying the ligand, and finally, the fact that all of these materials prepared and investigated so far have been shown to crystallize in columnar stacks either with direct metal-metal interactions or in a modification in which the ions interact via neighboring ligand atoms.[17]

Bis(α,β-Dionedioximato)metal(II) and Bis(α,β-Dionedioximato)-Metal(II,IV) Complexes

Recent structural and chemical data on *bis*(α,β-dionedioximato)-metal complexes of the ions Ni^{2+}, Pd^{2+}, and Pt^{2+} are summarized in Table 1. Not included are most of the compounds investigated thoroughly by Banks and Barnum[30] and discussed by Thomas and Underhill.[17] All of the *bis*(α,β-dioximato) compounds investigated so far crystallize in columns. "M-M" modification designates such stacks in which the M-M distance is the shortest intermolecular distance (Figure 1 a). "M-L-M" form means that the closest intermolecular contact occurs between the central metal ion of one molecule and a ligand atom of a neighboring species (Figure 1 b).

TABLE 1

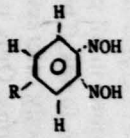
STRUCTURAL, CHEMICAL, AND PHYSICAL DATA OF *Bis*(α,β-DIONEDIOXIMATO) METAL COMPLEXES

Ligand (Abbreviation)	Metal-Complex	Preparation and physical data - Color	M-M distance in Å	Crystal System	Structural type (M-M or M-L-M)
					
R_1=R_2=H (GH_2)	$Ni(GH)_2$	ref. 18, red brown, after heating to 160°C black violet, (explosive transition at 170°C)	4.196(ref.18a) 4.21 (ref.18b)	monoclinic	M-L-M
	$Pd(GH)_2$	ref. 19, yellow-orange	3.558(ref.19)	triclinic	M-L-M
	$Pt(GH)_2$	ref. 20, brown violet, dichroic	3.504(ref.20)	monoclinic	M-L-M
	$Pd(GH)_2I$	black, metallic	3.244(ref.25)	tetragonal	M-M
R_1=CH_3, R_2=C_2H_5 (EMGH) preparation ref. 21	α-$Ni(EMG)_2$	ref. 22, density: 1.58 g/cm^3	4.747	monoclinic	M-L-M
	β-$Ni(EMG)_2$	ref. 23 density: 1.47 g/cm^3	3.44	orthorhombic	M-M

	$Pd(EMG)_2$	ref. 23	3.4 (ref.23) 3.44 (ref.24)	orthorhombic	M-M
	$Pt(EMG)_2$	ref. 23	3.42 (ref.23 and this work)	orthorhombic	M-M
R_1=CF_3, R_2=CH_3 (MTFMGH) preparation ref. 26	α-$Ni(MTFMG)_2$	yellow			
	ß-$Ni(MTFMG)_2$	ref. 26 and this work dark red, dichroid	3.25		M-M
	α-$Pd(MTFMG)_2$	yellow density: 2.07 g/cm^3	5.08	triclinic	M-L-M
	ß-$Pd(MTFMG)_2$	yellow density: 2.03 g/cm^3	3.27	orthorhombic	M-M
	$Pt(MTFMG)_2$	brown violet			
	$Pt(MTFMG)_2$	yellow orange			
R_1=CH_3, R_2=$COOC_2H_5$ (MCEGH) preparation ref. 27	$Ni(MCEG)_2$	red brown, metallic lustre	3.26	c-axis of unit cell= four M-M distances	M-M
	$Pd(MCEG)_2$	yellow orange	3.26		M-M
R_1=R_2=$COOC_2H_5$ (DCEGH) preparation ref. 28	$Ni(DCEG)_2$	bright red			M-L-M
	$Pd(DCEG)_2$	yellow	5.39		M-L-M
	α-$Pt(DCEG)_2$	brown	5.38		M-L-M
	ß-$Pt(DCEG)_2$	blue-violet	3.30		M-M

TABLE 1 (*continued*)

Ligand (Abbreviation)	Metal-Complex	Preparation and physical data - Color	M-M distance in Å	Crystal System	Structural type (M-M or M-L-M)
$R_1=R_2=Cl$ (DCGH) preparation ref. 29	$Pd(DCG)_2$	two modifications			
	$Pt(DCG)_2$		3.198	monoclinic	M-M
$R_1=R_2=C_6H_5$ (DPGH)	$Ni(DPG)_2$	ref. 30,31, red	3.547	orthorhombic	M-M
	$Pd(DPG)_2$	ref. 30,31, yellow	3.517	orthorhombic	M-M
	$Pt(DPG)_2$	ref. 30, deep red, dichroic	3.50	orthorhombic	M-M
	$Ni(DPG)_2X_y$	ref. 31,32,33	(a) 3.36(ref.33) 3.28(ref.31)	tetragonal "	M-M M-M
	X=(a)Br	$y_a \lesssim 1.14$	(b) 3.271(ref.32)	"	M-M
	X=(b)I	$y_b \lesssim 1.02$	3.28 (ref.31,33)	"	M-M
	$Pd(DPG)_2X_y$	ref. 31,32,33	(a) 3.28 (ref.33)	"	M-M
	X=(a)Br	$y_a \lesssim 1.08$	3.29 (ref.31)	"	M-M
	X=(b)I	$y_b \lesssim 1.02$	(b) 3.26 (ref.31,33)		
	$Pt(DPG)_2ClO_4$	reddish-brown density: 1.93 g/cm^3	3.259	tetragonal	M-M

$R_1=R_2=p\text{-}CH_3O\text{-}C_6H_4$ (PMBDH) preparation ref. 34	$Ni(PMBD)_2$		9.36 or 4.68	monoclinic	M-L-M
	$Pt(PMBD)_2$		3.32	orthorhombic	M-M
$R_1=R_2=m\text{-}Cl\text{-}C_6H_4$ (MCBDH)	$Ni(MCBD)_2$		3.32	orthorhombic	M-M
$R_1=R_2=p\text{-}NO_2\text{-}C_6H_4$ (PNBDH) preparation ref. 35	$Ni(PNBD)_2$		3.7	monoclinic	
	$Ni(BCD)_2$	black-green	3.86 (ref.36)	monoclinic	M-L-M
	$\alpha\text{-}Pd(BCD)_2$		3.77		M-L-M
	$\beta\text{-}Pd(BCD)_2$	black	3.202(ref.37)	orthorhombic	M-M
	$Pt(BCD)_2$	violet, black lustrous	3.20	orthorhombic (isomorphous with $\alpha\text{-}Pd(BCD)_2$)	M-M
R=H (BCDH) preparation ref. 38	$Ni(BCD)_2 0{,}51$	*golden lustrous*	3.153 (ref.39)	tetragonal	M-M
	$Pd(BCD)_2 0.51$	golden lustrous	3.153	tetragonal	M-M
	$Pt(BCD)_2 \cdot 0.5\ AgClO_4$	blue-black, dichroic	3.386(ref.40)	monoclinic	between M-M and M-L-M (Pt-Pt distance shortest intermolecular distance)

In discussing these results, one has to remember one of the basic points of this type of investigation. Whether a certain complex crystallizes in columnar stacks with strong intermolecular interactions or not cannot be controlled by the crystal-growing process. Generally, certain molecules inevitably do stack, others do not, whatever the crystallization conditions are. This means that one has to adjust certain *molecular* parameters in such a way that the molecules tend to stack or, in other words, one has to introduce an "instruction for stacking" chemically by building appropriate *molecules*.

The investigations on the *bis*(α,β-dionedioximato)metal complexes have

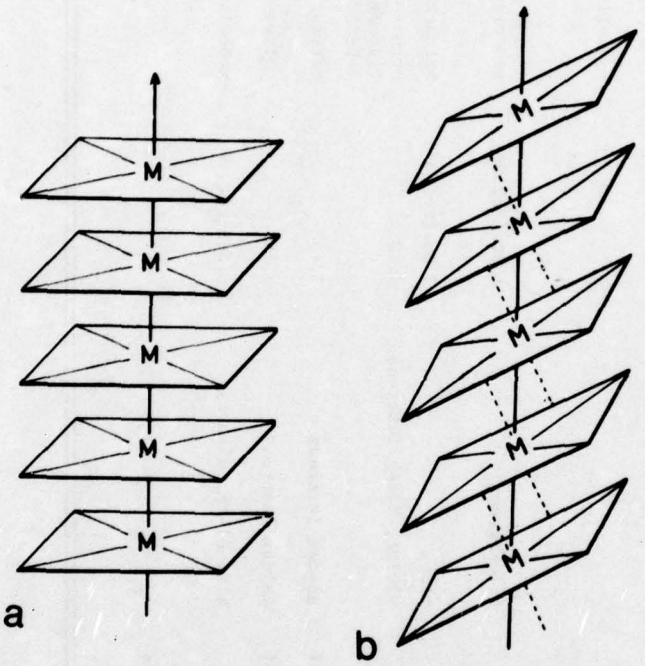


FIGURE 1. Schematic presentation of "M-M" stacks (1a) and "M-L-M" stacks (1b) of square planar transition metal complexes.

shown that this "instruction for stacking" is incorporated to the best in molecules which have the highest ability for metal-metal bonding. Appreciable metal-metal bonds are a prerequisite to stabilize the "M-M" type of structure.

One evidence for this comes from a comparison between the physical data, e.g. the densities, of those complexes which are able to crystallize in two modifications. This hints to the fact that the M-M modifications in all cases investigated so far have the lower density compared to the M-L-M forms. This is valid for other similar compounds too.[41] This means that the directly interacting M-M forms are less densely packed than other possible modifications. Only if metal-metal bond energies in the less dense M-M phases counterbalance the favorable packing in the M-L-M or similar phases the crystallization results in the desired directly interact-

ing linear-chain system. A systematic synthesis of solids with strongly interacting planar transition metal compounds—as demanded in the Little model—starts, therefore, with the search for molecules with a high ability for metal-metal bonding. Possibly this problem can be solved by investigating the dependence between certain molecular parameters, like size and oxidation state of the central metal ion, type of ligand, and so on, and the ability of the complex molecule to form metal-metal bonds.

On the basis of the structural investigation into *bis*(α,β-dionedioximato)metal compounds and on the assumption that the metal-metal distances in comparable chains reflect the strength of the metal-metal interactions between molecules, the following relations hold for this special class of compounds:

1. In complexes with one and the same ligand, the interactions increase if the 3-d metal ion nickel(II) is substituted by the 4-d or 5-d ions palladium(II) and platinum(II).
2. The metal-metal interactions increase with increasing "electron-withdrawing" capability of the ligands.
3. A decrease in interactions along the spine is observed if bulky ligands are used. This result is rather trivial, since everyone expects such a relation.
4. A considerable increase in metal interactions occurs upon partial oxidation of the compounds. (Decreasing repulsion between nonbonding electrons along the chain?).

This summary merits a few comments.

To 1:

This finding means that platinum complexes (or in the neighboring group the iridium species) are better suited if strongly interacting metal chains are needed. This is actually valid for all other classes of linear chain transition metal complexes and is certainly the reason that the Little model compound contains platinum.

To 2:

The data in TABLE I show without any doubt that substituents such as Cl, CN, etc., help to increase the interactions along the spine. In the chemistry of *bis*(dioximato)metal complexes adding electron withdrawing groups has, on the other hand, severe consequences on the stability of the compounds. If the oxime protons are too much acidified by the electron withdrawing groups, the complexes are not stable any more. (Dicyanoglyoximato compounds could not be prepared so far). Additionally, most dyes—which are needed in the Little model—are not electron withdrawing. Although this is a very effective method of increasing metal interactions, it is not of too much importance with respect to excitonic systems.

To 4:

Most efficient in increasing metal interactions is the partial oxidation of the compounds. As has been shown, this can be achieved by reaction of some *bis*(dioximato)metal(II) species with molecular iodine. In some cases the

M-L-M form is converted into a M-M modification upon oxidation. This might be a consequence of pure *packing* advantages, since similar structural changes are observed in the TTF and TTT iodides too.[42] Triiodide ions are incorporated into the lattice[43] and the formal oxidation state of the metal depends on the iodide content of the lattice.

For the *bis*(diphenylglyoximato)nickel(II, IV)[32] [$Ni(DPGH_2)I_x$] and for the *bis*(glyoximato)palladium(II, IV)[25] the lattices of which contain only crystographically identical channels, the obtained compounds have M : I ratios around 1.0.[31] If the lattice contains channels of different size as in the *bis*(1,2-benzoquinonedioximato)nickel(II,IV) and palladium(II,IV)[39] species, at least two phases, one with M : I = 1.0 and another with M : I = 0.5, can be obtained. This gives a formal oxidation number of 2.16 for the central metal in the latter solid, the structure of which is shown in FIGURE 2. Smaller differences in the *degree* of *partial oxidation* seem to have only minor or no effects on the M-M interactions in the compounds of this type.

In the case of the platinum compounds which should be best suited for intermolecular interactions, this method of partial oxidation does not work. The treatment of *bis*(dioximato)-platinum(II) species with iodine leads to oxidative addition products with halide in the axial positions. But these halides can be removed by reaction with $AgClO_4$ in nonpolar solvents. In the case of the *bis*(diphenylglyoximato)platinum(II), the reaction with molecular iodine proceeds at 40°C in dichloromethane to give diiodobis(diphenylglyoximato)platinum(IV). Reaction of this compound with $AgClO_4$ in benzene at 80°C results in the formation of a dark, reddish-brown solid with stoichiometry $(DPG)_2PtClO_4$.

Bis(diphenylglyoximato)platinum(II) perchlorate crystallizes in the tetragonal

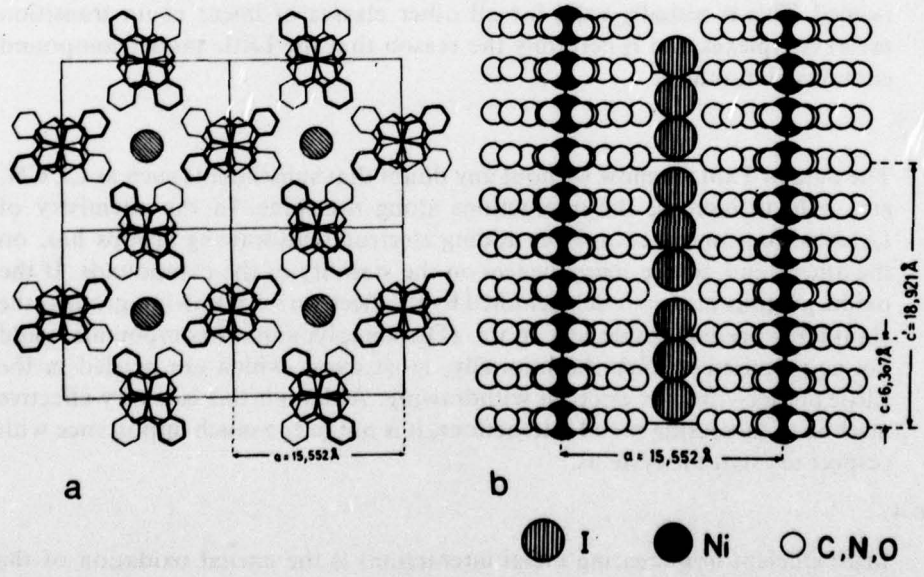


FIGURE 2. Structure of *bis*(1,2-benzoquinonedioximato)-nickel(II,IV) iodide projected along the *c*-axis (*a*) and along the *b*-axis (*b*).

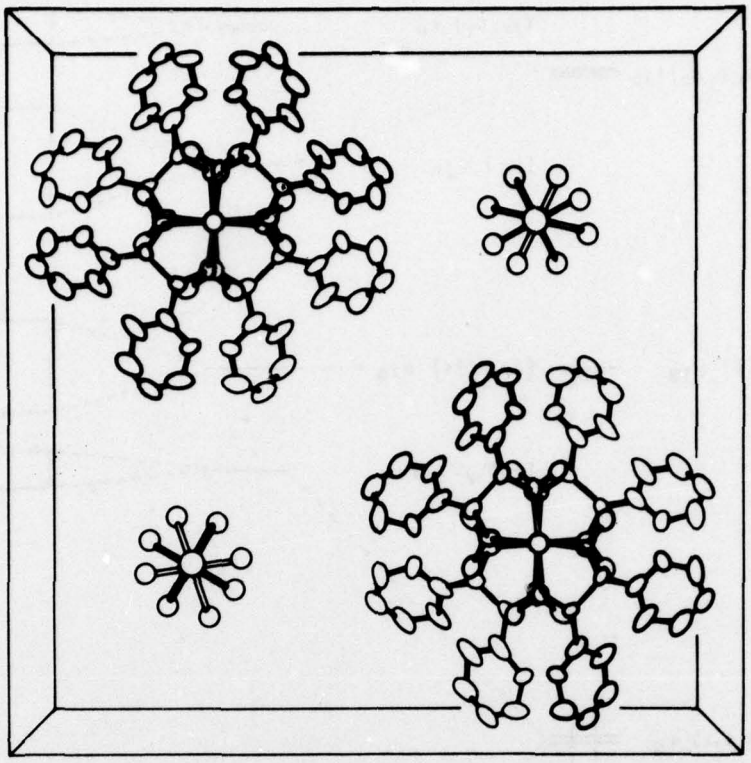


FIGURE 3. Structure of complex stacks in $(DPG)_2PtClO_4$ projected along the *c*-axis.

space group $P_4/ncc\text{-}D_{4h}^8$ with unit-cell parameters $a = b = 20.325(6)$ Å and $c = 6.518(5)$ Å.

The structure of the compound resembles very much the structure of the triiodide nickel(II,IV) and palladium(II,IV) derivatives,[32] with the exception that tetrahedral ClO_4^- ions are incorporated into the lattice instead of the linear triiodides (FIGURE 3). This leads to the formal oxidation state of 3.0 for the platinum and to a formally half-filled d_z2-band. As would be expected, the linear chain for this oxidation state is considerably distorted, giving a kind of dimerization along the chains.

ENERGY LEVEL DIAGRAM: A "WORKING" MODEL

If one needs a qualitative physical explanation for these findings, one could argue as follows.

The interactions along the chains are brought about mainly by overlap between *metal* orbitals but with the ligands contributing minor effects. Well suited for the "linear" overlap are the n d_z2, the $(n + 1)p_z$ and $(n + 1)s$ orbitals. This means that, in a first approximation, a metallic state might arise if one of the bands made up of these orbitals is only partially filled.

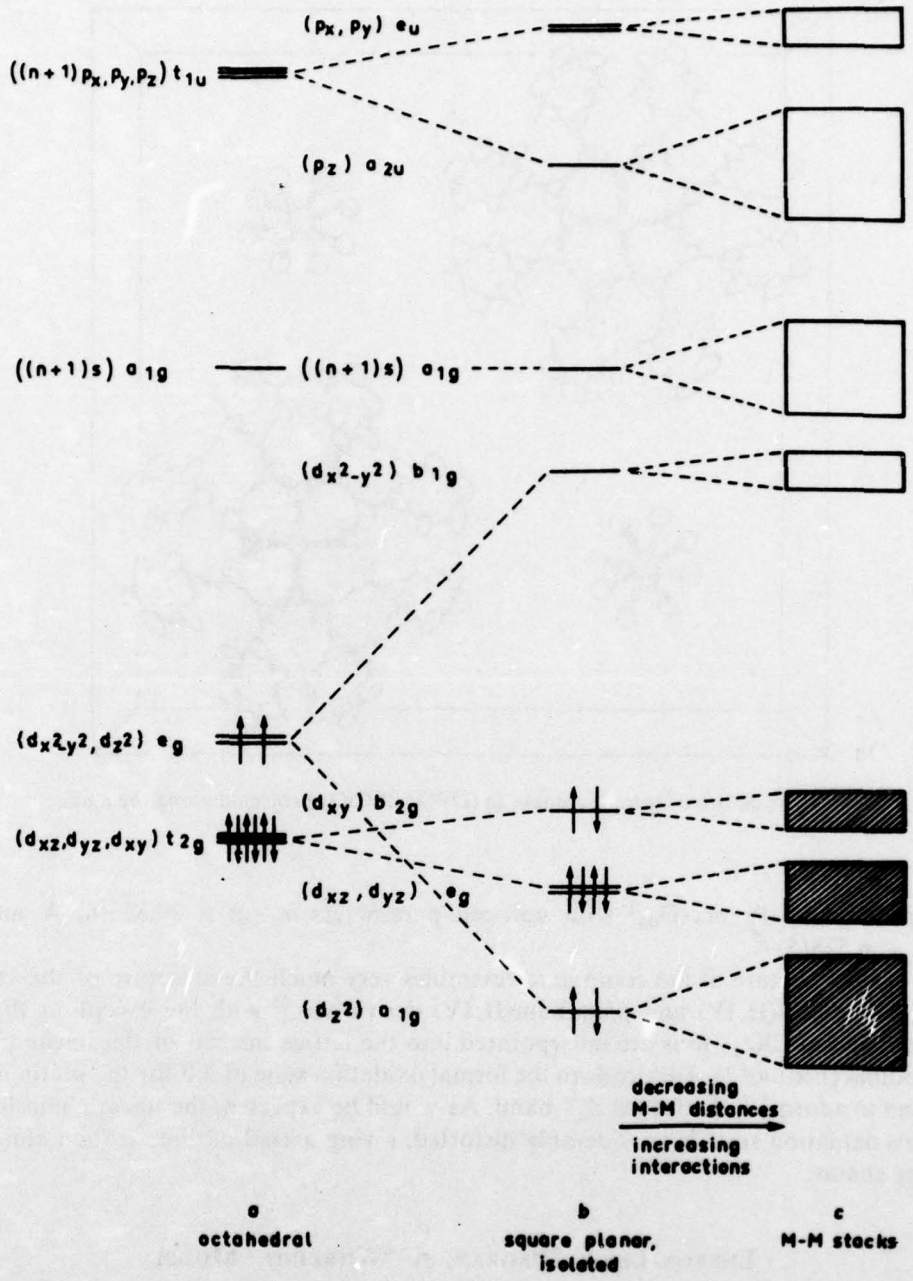


FIGURE 4. Schematic energy level diagram for a d^8 transition metal ion in: a) octahedral ligand field, b) tetragonal field (square planar complex), and c) stacks of strongly interacting metal ions.

One way to fulfill this condition is to start with planar transition metal complex molecules with unpaired electrons in one of the nd_z2, $(n + 1)p_z$ or $(n + 1)s$ orbitals. But as mentioned above, these types are rather exceptional cases in the chemistry of *planar* transition metal compounds.

Nevertheless, partially filled bands, which are a basic prerequisite for a conducting spine, could result if the other energetically available metal orbitals are taken into account. The energetic gradation of the metal orbitals in an octahedral and tetragonal (square planar) ligand field is depicted in FIGURES 4a and 4b.

In an isolated planar four-coordinate compound the d_z2 orbital is probably the lowest one, but its energy is raised by the introduction of "axial" ligands which are actually the metal ions of the neighboring molecules in the stack. The crystal field picture of a metal ion in a stack should therefore be somewhere between the situations shown in FIGURES 4a and 4b. If the electronic exchange interactions along the spine are "turned on," bands result that are shown in FIGURE 4c for the square planar crystal field. A qualitative impression of the bandwidths is given in FIGURE 4c, too. It indicates which of the above mentioned metal orbitals are regarded as best suited for overlap. Without discussing the energy level diagram in a more quantitative way, at least one simple conclusion is evident.

Overlap of one of the broad d_z2, $(n + 1)p_z$ or $(n + 1)s$ bands with one of the other narrow bands is almost *inevitable* if interactions are strong and the crystal field situation of the single ion is "somewhere between octahedral and square planar." In fact, it is difficult to draw a "nonoverlapping situation" (as in FIGURE 4c) if the tetragonal crystal field splittings are small. In the case of stacks with short metal-metal distances one has therefore to *expect* overlap between filled and empty bands. This, in any case, leads to a partially filled band and, if this is broad, gives possibly metallic conductivity even in compounds with *even electron numbers*.

On the basis of the simple scheme depicted in FIGURE 4 and the fact that all complexes discussed here and most other complexes with columnar structures contain d^8 central metal ions overlapping partially filled bands could be (and have been) explained by different authors with different models. Two possibilities are mentioned here.

1. If the metal ions in the stacks are sitting in a more or less octahedral field (exerted by the four "equatorial" ligand donor atoms and the two axially arranged neighboring metal ions in the stack), then the d_z2 and $d_x2_{-y}2$ orbitals for the individual molecules are almost degenerate. Since the d^8 system has a filled d_z2 but an empty $d_x2_{-y}2$ band, a broad partially d_z2 band results if the $d_z2 - d_x2_{-y}2$ energy difference is less than half the d_z2 bandwidth. Even in the case of a very sharp $d_x2_{-y}2$ band, as depicted in FIGURE 5 (drawn with an arbitrary but small $d_z2 - d_x2_{-y}2$ energy differ-

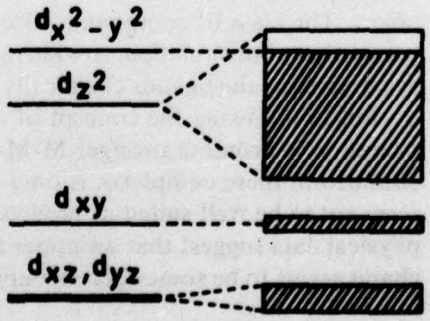


FIGURE 5. Schematic presentation of overlap between d-orbitals in a tetragonal field with axial metal-metal bonds.

ence and omitting the *s* and *p* orbitals for simplicity), a partially filled broad d_z2 band could result.

2. If the energy of one of the energetically higher bands involved ($(n + 1)p_z$ or $(n + 1)s$) is lowered by the interaction along the spine, or if their width is increased above the crystal field energy differences in the individual molecules, again band overlap occurs.

The latter model is more often used to explain the solid-state properties of linear chain d^8 complexes. But one has to take into consideration that both models discussed here are very much simplified. The important orbitals involved (like the $d_x2_{-y}2$, d_z2 or $(n + 1)p_z$) are actually not simple metal AO's but complicated admixtures between metal and ligand orbitals. Which one of the above models is in fact used to explain the collective properties is therefore more a question of taste, in our opinion. This type of argument is nevertheless very helpful for a preparative chemist because it predicts that in *strongly interacting* linear chain "*even-electron*" systems, overlapping partially filled bands should be quite common, and if the Peierls instability could be suppressed, a 1-d metallic state could occur. This reduces the complexity of the Little model, which demands linear-chain "mixed valence" solids, originally. The sensitivity of some of these systems to oxidation would otherwise introduce severe problems.

Conclusions

The results suggest that the collective electron properties of d^8 linear-chain solids can be changed systematically over a wide range approaching almost a 1-d metallic state by "adjusting" the M-M distances "chemically." Other examples for this statement are found in the tetracyanoplatinates.[44] Whether this is explained by overlap of the filled d_z2 with the empty $d_x2_{-y}2$ or with a broadening, energetic decrease and, finally, overlap of the $(n + 1)p_z$ band does not matter too much for a chemist. He has to look for strongly interacting molecules, since both effects, "the crystal field effect" and the "broadening effect," are brought about by strong metal-metal interactions along the chain.

The tetracyanoplatinates have the disadvantage that the parameters which govern the occurrence of long or short M-M distance along the chains are not known at all. But most important in the search for new 1-d conducting spines is the problem to find the relevant molecular parameters that govern the ability of a certain planar metal complex to form linear chains with short metal-metal distances. The class of compounds discussed here is especially well suited to the investigation of this relation. A wide range of metal-metal distances can be obtained by controlling the ligands chemically.

But in following the concept of strongly electron withdrawing ligands and/or oxidation to promote stronger M-M-interactions, the lowest metal-metal distance obtained in these complexes is only 3.15 Å. Because of this result these materials seem not to be well suited as models for an excitonic superconductor, since other physical data suggest that an upper M-M limit for 1-d *metallic* behavior of metal chains seems to be somewhere around 2.9 Å.

References

1. Little, W. A. 1964. Phys. Rev. **134**(6A): A 1416–A 1424.
2. Gutfreund, H. & W. A. Little. 1977. Prospects of excitonic superconductivity. *In* Highly Conducting One Dimensional Solids. Plenum Press. New York, N.Y.
3. Bozorth, R. M. & L. Pauling. 1932. Phys. Rev. **39:** 538.
4. Dickinson, R. G. 1922. J. Amer. Chem. Soc. **44:** 2404–2411.
5. Godycki, L. E. & R. E. Rundle. 1953. Acta Cryst. **6:** 487.
6. Thewalt, U. 1974. Z. Naturforsch. **29b:** 308–311.

7a. Brückner, S., M. Calligaris, G. Nardin & L. Randaccio. 1969. Acta Cryst. **25B:** 1671–1674.

7b. Schaefer, W. P. & R. E. Marsh. 1969. Acta Cryst. **25B:** 1675–1682.

8. Bartkowski, R. R. & B. Morosin. 1972. Phys. Rev. **B6**(11): 4209–4212.
9. Miller, J. S. & A. J. Epstein. 1976. *In* Progress In Inorganic Chemistry. Vol. **20:** 1–151. Interscience Press. New York, N.Y.
10. Aderjan, R., H. J. Keller, H. H. Rupp, F. E. Wagner & U. Wagner. 1976. J. Chem. Phys. **64**(9): 3748–3752 and references cited therein.
11. Balch, A. L. & M. M. Olmstead. 1976. J. Amer. Chem. Soc. **98:** 2354–2356.
12. Baumann, D, H. J. Keller, D. Nöthe, H. H. Rupp & G. Uhlmann. 1976. Z. Naturforsch. **31b:** 912–921.
13. Endres, H., H. J. Keller, R. Lehmann, A. Poveda, H. H. Rupp & H. van de Sand. 1977. Z. Naturforsch. **32b:** 516–527.
14. Fox, M. R. & E. C. Lingafelter. 1967. Acta Cryst. **22:** 943–944.
15. Phelps, D. W., W. F. Little & D. J. Hodgson. 1976. Inorg. Chem. **15:** 2263–2266.
16. Scaringe, R. P. & D. J. Hodgson. 1976. Inorg. Chem. **15**(5): 1193–1196.
17. Thomas, T. W. & A. E. Underhill. 1972. Chem. Soc. Rev. **1:** 99–120.

18a. Calleri, M., G. Ferraris & D. Viterbo. 1967. Acta Cryst. **22:** 468–475.

18b. Murmann, R. K. & E. O. Schlemper. 1967. Acta Cryst. **23:** 667–669.

19. Calleri, M., G. Ferraris & D. Viterbo. 1967. Inorg. Chem. Acta **1:** 297–302.
20. Ferraris, G. & D. Viterbo. 1969. Acta Cryst. **B25:** 2066–2070.
21. Diels, O. & G. Plaut. 1905. Chem. Ber. **38:** 1917–1921.
22. Bowers, R. H., C. V. Banks & R. A. Jacobsen. 1972. Acta Cryst. **B28:** 2318–2322.
23. Sharpe, A. G. & D. B. Wakefield. 1957. J. Chem. Soc. (London): 281–285.
24. Egneus, G. 1969. Anal. Chimica Acta. **48:** 291–307.
25. Endres, H., H. J. Keller, R. Lehmann & J. Weiss. 1976. Acta Cryst. **32B**(2): 627–628.

26a. Belcher, B., A. Sykes & J. C. Tatlow. 1957. J. Chem. Soc. (London): 2393–2397.

26b. Sykes, A., J. C. Tatlow & C. R. Thomas. 1956. J. Chem. Soc. (London): 835–839.

27. Bouveault, L. & A. Wahl. 1905. Chem. Ber. **38:** 926–931.
28. Anschütz, R. & E. Parlato. 1892. Chem. Ber. **25:** 1975–1980.
29. Ponzio, G. & F. Baldracco. 1930. Gazz. Chim. Ital. **60:** 415.
30. Banks, C. V. & D. W. Barnum. 1958. J. Amer. Chem. Soc. **80:** 3579–3582; 4767–4772.

31a. Miller, J. S. & S. Z. Goldberg. 1975. Inorg. Chem. **14:** 2294–2296.

31b. Miller, J. S. & C. H. Griffiths. 1977. J. Amer. Chem. Soc. **99**(3): 749–755.

32. Gleizes, A., T. J. Marks & J. A. Ibers. 1975. J. Amer. Chem. Soc. **97:** 3345–3546.
33. Foust, A. S. & R. H. Soderberg. 1967. J. Amer. Chem. Soc. **89:** 5507–5508.
34. Stierlin, R. 1889. Chem. Ber. **22:** 376–383.
35. Brydówna, W. 1939. Chem. Zentralblatt II: 2065 and 1938. Roczniki Chem. **18:** 396.
36. Leichert, I. & J. Weiss. 1975. Acta Cryst. **B31:** 2877.
37. Leichert, I. & J. Weiss. 1975. Acta Cryst. **B31:** 2709.
38. Ladd, E. C. & W. P. Ter Horst. 1943. U.S. Patent No. 23 336 941.
39. Endres, H., H. J. Keller, M. Megnamisi-Bélombé, W. Moroni, H. Pritzkow, J. Weiss & R. Comès. 1976. Acta Cryst. **32A:** 954–957.
40. Endres, H., M. Megnamisi-Bélombé, H. J. Keller & J. Weiss. 1976. Acta Cryst. **32B:** 457–460.
41. Lingafelter, E. C., B. Morosin & G. L. Simmons. 1960. Acta Cryst. **13:** 1025.
42a. Daly, J. J. & F. Sanz. 1975. Acta Cryst. **B31:** 620–621.

42b. Buravov, L. I., G. I. Zvereva, V. F. Kaminskii, L. P. Rosenberg, M. L. Khidekel,

R. P. SHIBAEVA, I. I. SHCHEGOLEV & E. B. YAGUBSKII. 1976. J. Chem. Soc. Chem. Comm.: 720–721.

42c. IISETT, L. C. & E. A. PEREZ-ALBUERNE. 1977. Solid State Commun. **21**: 433–535.

43. MARKS, T. J., D. F. WEBSTER, S. L. RUBY & S. SCHULTZ. 1976. J. Chem. Soc. Chem. Comm. 444–445.

44. YERSIN, H., G. GLIEMANN & U. RÖSSLER. 1977. Solid State Commun. Preprint.

1,2-BENZOQUINONEDIOXIME (bqdH) AS A VERSATILE LIGAND SYSTEM FOR THE SYNTHESIS OF NEW ONE-DIMENSIONAL COMPOUNDS*

Michel Mégnamisi-Bélombé

Department of Physics
Stanford University
Stanford, California 94305

INTRODUCTION

It has been found that transition metal compounds, which preferentially crystallize in a stacking structure, almost exclusively involve d^8 metal ions.[1] These ions are coordinated to the ligands in such a way that square planar complex molecules are formed which then stack face-to-face in parallel columns, linking the metal ions in extended linear chains throughout the crystal lattice. This structural arrangement imposes the requirement that the ligand be sufficiently small and/or flat in order to minimize steric hindrance between neighboring molecules within a columnar stack.

In 1969 Krogmann first demonstrated experimentally the evidence for one-dimensional metallic behavior in stacked square planar complexes based on platinum with nonintegral oxidation numbers.[2] This discovery has catalyzed a widespread scientific interest among solid-state researchers throughout the world. Despite the multiple efforts devoted since then, however, the success in the synthesis of new Krogmann analogs has remained extremely meager, obviously, because of the small number of metal ions and, most importantly, due to the extremely limited choices of ligand systems that may favor the columnar structure in the solid. In other words, the selection of an appropriate ligand system to be combined with d^8 ions appears to constitute the key step toward a successful synthesis of linear metal-chain compounds.

During the past few years our research efforts have been mainly directed toward the design, synthesis, and study of new Krogmann-type compounds.[3,4] Thus, the synthetic work was based essentially on the divalent d^8 metal ions Ni^{2+}, Pd^{2+}, and Pt^{2+}; the electrophilic aromatic molecule 1,2-benzoquinonedioxime (bqdH) was selected as a ligand system outstandingly suited to preferentially favor the stacking structure in the solid. Moreover, bqdH appears to be a very flexible molecule that may be easily converted into a highly polarizable dye-like system by proper chemical substitutions, thus justifying the hope that this ligand system might open a new route for the synthesis of an excitonic high-temperature superconductor in accord with the model of Little.[5a,5b] The purpose of this contribution is first to emphasize the intrinsic value of bqdH as a versatile ligand system for the synthesis of one-dimensional compounds. Second, we wish

*Partly supported by National Science Foundation grant DMR-74-00427-A03 and by Deutsche Forschungsgemeinschaft through Prof. H. J. Keller (contract Ke 135-16). Manuscript received June 13, 1977.

0077-8923/78/0313-0633 $1.75/1 © 1978, NYAS

to underline the exceptional chemical flexibility of this ligand system by summarizing all the various new one-dimensional complexes based on it that we have been able to isolate, along with a general discussion of some of the most relevant experimental results that have been obtained so far.

EXPERIMENTS

Synthesis of the Ligands

The benzoquinonedioxime ligands, as summarized in TABLES 1 and 2, were prepared from the corresponding commercially available *o*-nitroanilines: oxidation of the *o*-nitroanilines to the benzofuroxans with basic NaOCl[6a,6b] followed by reduction with aqueous NaHS, according to the method described by E. C. Ladd and W. P. ter Horst,[7a,7b] afforded the benzoquinonedioximes in high yield. Elemental analysis, ir and ^{1}H-nmr spectra were used to verify the identity of the benzofuroxans and to ascertain the purity of the benzoquinonedioximes.

Synthesis of the Complexes (TABLE 3)

Preparation of Ni(bqd)$_2$.[3,8]

A solution of 2.26 g of bqdH dissolved in 300 ml warm aqueous alcohol was filtered and heated to reflux. A solution of 3.50 g $NiCl_2.6H_2O$ in 50 ml water was added slowly, with careful stirring. The color of the mixture deepened immediately, and a dark-brown solid precipitated; when the addition was complete, the acidic mixture was neutralized with dilute ammonia. Stirring was continued for another hour to ensure completeness of the reaction. Most of the solvent was removed by evaporation. The mixture was allowed to stand overnight, and the precipitate was filtered, washed with cold water until the washings were neutral,

TABLE 1

1,2-BENZOQUINONEDIOXIME (BQDH; SEE FIGURE 1) AND ITS DERIVATIVES

Molecular formula	Substituent at position 3	4	5	6	Melting point (°C)	Color	Ref.
$C_6H_6N_2O_2$ (bqdH)	—	—	—	—	144–0.5	yellow	7
$C_7H_8N_2O_2$ (MebqdH)	—	CH_3	—	—	128–30	bright-yellow	3
$C_7H_8N_2O_3$ (MeObqdH)	—	CH_3O	—	—	161–3.5	yellow	3
$C_6H_5N_2O_2Cl$ (ClbqdH)	—	Cl	—	—	110–12	orange-yellow	7a
$C_6H_4N_2O_2Cl_2$ (Cl_2bqdH)	—	Cl	Cl	—	142–3	orange-yellow	this work
$C_8H_{10}N_2O_2$ (Me_2bqdH)	—	CH_3	CH_3	—	157–9	yellow	this work

TABLE 2
ELEMENTAL ANALYSES OF BQDH DERIVATIVES*

Compound	Element%			
	C	H	N	Cl
bqdH	52.46	4.60	20.24	—
	(52.20)	(4.32)	(20.24)	—
MebqdH	55.28	5.37	18.25	—
	(55.30)	(5.30)	(18.40)	—
MeObqdH	50.08	5.02	16.46	—
	(50.00)	(4.75)	(18.26)	—
ClbqdH	41.88	3.04	14.95	20.18
	(41.71)	(2.91)	(16.25)	(20.57)
Cl_2bqdH	35.42	2.06	12.99	33.58
	(34.81)	(1.95)	(13.53)	(34.25)
Me_2bqdH	57.83	6.10	16.90	—
	(57.82)	(6.07)	(16.85)	—

*Calculated values in parentheses.

and then dried in air. The final washing was with two 150 ml portions of cold anhydrous ether. The solid was dried in a desiccator over $CaCl_2$. The reaction afforded 2.90 g (95%) of analytically pure $Ni(bqd)_2$.

The remainder of the $M(bqd)_2$ complexes (TABLE 3) were prepared in the same general manner as $Ni(bqd)_2$. Since ethanol and methanol tend to reduce Pt(II) to Pt(0), acetone was used as the solvent in the preparation of the platinum(II) derivatives.

Oxidation Products of Some Metal(II) Dioximates

Preparation of $Ni(bqd)_2I_x$[3,4,9] ($x \sim 0.5$). 333 mg $Ni(bqd)_2$ are dissolved in 150 ml of warm 1,2-dichlorobenzene (99%+). The solution is filtered and kept at about 80°C. With efficient stirring, an iodine solution is added, which was prepared as follows: 1.87 g of I_2 are dissolved in 50 ml of warm 1,2-dichlorobenzene and filtered; a few drops of a dilute solution of highest purity KI or LiI in methanol or acetonitrile are added (to initiate the formation of I_3^-). After dropwise addition of this iodine solution to the $Ni(bqd)_2$ solution the temperature is raised to about 100°C and the mixture is stirred for 24–30 hours, after which it is filtered into another flask, which is placed into the 100°C bath. About one hour later, the heater is turned off, and after a few days, long needles with a golden luster form. The crystals are separated by filtration, dried on the filter paper at ambient, and treated with a little cold water (to wash off KI or KI_3 that might still be present) and again dried in air. The final washings are with cold petrol ether and with a little ether. The crystals are then dried in a desiccator over $CaCl_2$. The reaction may also be carried out in nitrobenzene or chloroform.

$Pd(bqd)_2I_x$. This compound was prepared in the same manner as $Ni(bqd)_2I_x$. Elemental analyses of various samples of these two compounds indicate that x ranges from 0.5 to 0.7.

TABLE 3

1,2-BENZOQUINONEDIOXIME COMPLEXES OF Ni, Pd, Pt, AND THEIR ELEMENTAL ANALYSES*

Complex	Element %						
	C	H	N	Br	Cl	I	M
$Ni(bqd)_2$	43.68	3.05	16.76	—	—	—	17.33
	(43.29)	(3.03)	(16.83)	—	—	—	(17.63)
α-(β-)$Pd(bqd)_2$	37.80	2.63	14.65	—	—	—	27.50
	(37.87)	(2.65)	(14.72)	—	—	—	(27.85)
$Pt(bqd)_2$	31.05	2.30	11.93	—	—	—	41.30
	(30.71)	(2.15)	(11.94)	—	—	—	(41.57)
$Ni(bqd)_2I_x$	33.39	2.87	12.81	—	—	15.47	12.60
(for $x = 1$)	(31.33)	(2.20)	(12.81)	—	—	(27.65)	(12.77)
$Ni(bqd)_2TCNQ$	53.44	2.62	20.86	—	—	—	10.85
	(53.67)	(2.63)	(20.86)	—	—	—	(10.93)
$Ni(Mebqd)_2$	46.48	3.61	15.24	—	—	—	—
	(46.62)	(3.88)	(15.53)	—	—	—	—
$Ni(MeObqd)_2$	42.78	3.77	14.33	—	—	—	14.60
	(42.78)	(3.59)	(14.26)	—	—	—	(14.94)
$Ni(Me_2bqd)_2$	49.18	4.52	14.43	—	—	—	14.80
	(49.40)	(4.66)	(14.40)	—	—	—	(15.10)
$Ni(Clbqd)_2$	35.80	2.00	13.92	—	17.73	—	14.40
	(35.87)	(2.01)	(13.94)	—	(17.65)	—	(14.61)
$Ni(Cl_2bqd)_2$	30.90	1.20	11.87	—	29.40	—	—
	(30.62)	(1.28)	(11.90)	—	(30.13)	—	—
$Pd(Mebqd)_2$	40.91	3.45	13.78	—	—	—	25.60
	(41.14)	(3.45)	(13.71)	—	—	—	(26.03)
$Pd(MeObqd)_2$	38.11	3.22	12.63	—	—	—	23.70
	(38.15)	(3.20)	(12.71	—	—	—	(24.14)
$Pd(Me_2bqd)_2$	43.60	4.14	12.82	—	—	—	—
	(44.00)	(4.15)	(12.83)	—	—	—	—
$Pd(Clbqd)_2$	32.00	1.76	12.34	—	15.82	—	23.20
	(32.06)	(1.79)	(12.46)	—	(15.77)	—	(23.67)
$Pd(Cl_2bqd)_2$	27.85	1.07	10.90	—	26.03	—	—
	(27.81)	(1.17)	(10.81)	—	(27.35)	—	—
$Pd(bqd)_2TCNQ$	49.08	2.61	19.25	—	—	—	—
	(49.29)	(2.42)	(19.16)	—	—	—	—
$Pt(bqd)_2I_2$	19.99	1.48	6.98	—	—	—	—
	(19.95)	(1.39)	(7.75)	—	—	—	—
$Pt(bqd)_2Br_2$	22.92	1.49	8.52	25.43	—	—	—
	(22.91)	(1.60)	(8.91)	(25.40)	—	—	—
$Pt(bqd)_2(AgClO_4)_{0.5}$	25.94	1.96	9.07	—	—	—	—
	(25.40)	(1.78)	(9.85)	—	—	—	—
$Pt(MeObqd)_2$	30.49	2.75	9.76	—	—	—	—
	(31.70)	(2.66)	(10.60)	—	—	—	—
$Pt(Me_2bqd)_2$	36.57	3.46	10.72	—	—	—	—
	(36.58)	(3.45)	(10.66)	—	—	—	—
$Pt(Clbqd)_2$	26.30	1.65	9.51	—	—	—	—
	(26.80)	(1.51)	(10.42)	—	—	—	—
$Pt(Cl_2bqd)_2$	25.14	1.01	9.56	—	23.35	—	—
	(23.74)	(1.07)	(9.23)	—	(23.35)	—	—
$Pt(Me_2bqd)_2I_2$	24.74	2.17	6.91	—	—	32.42	—
	(24.66)	(2.33)	(7.19)	—	—	(32.57)	—
$Pt(Me_2bqd)_2Br_2$	26.99	2.49	7.57	25.97	—	—	—
	(28.04)	(2.65)	(8.17)	(23.32)	—	—	—
$Pd(bqd)_2I_x$	34.48	2.64	11.11	—	—	12.51	20.5
(for $x = 1$)	(28.40)	(1.99)	(11.04)	—	—	(25.00)	(20.96)

Oxidation of Pt(II) dioximates

Preparation of $Pt(bqd)_2I_2$.[3] 470 mg of $Pt(bqd)_2$ are dissolved in 350 ml hot 1,2-dichlorobenzene. A filtered solution of 1.0 g of I_2 in 50 ml of *o*-dichlorobenzene is added slowly and stirred at 140°C. A reflux cooler is used to prevent excessive escape of the iodine. When the addition is complete, the mixture is stirred overnight at 100°C. It is then filtered into another flask, which is placed into a bath and kept at 150°C for a time. The heater is turned off, and the flask is sealed and left undisturbed for a few days at ambient temperature. Rhombohedral crystals form, which exhibit a strong but isotropic luster. They are filtered off, washed with cold acetone and then with ether, and dried under vacuum.

Preparation of $Pt(bqd)_2Br_2$, $Pt(dmbqd)_2I_2$, $Pt(dmbqd)_2Br_2$. This was done in a manner similar to $Pt(bqd)_2I_2$.

Addition Reactions

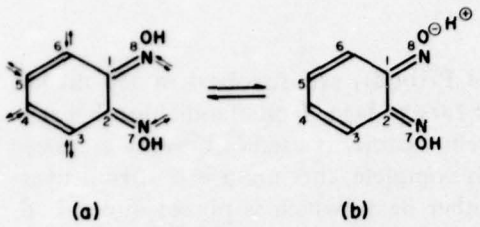
Preparation of $Pt(bqd)_2(AgClO_4)_{0.5}$[3a,10] 160 mg of $Pt(bqd)_2$ are dissolved in 120 ml of hot 1,2-dichlorobenzene and treated with a solution of 210 mg anhydrous silver perchlorate in 50 ml benzene. The reaction mixture is stirred overnight at 140°C under reflux. The dirty black-brown powder that has formed during this time is filtered off and washed with 20 ml hot *o*-dichlorobenzene. The combined filtrates are kept at 120°C for a while, and then the heater is turned off. Two days later, needle-like blue-black crystals form which exhibit a marked dichroism and lustrous sheen. The crystals are filtered off, washed with benzene and then with a little water, again with benzene, and finally with ether. They are dried over $CaCl_2$. The product is very stable in air but decomposes with explosion when heated above 200°C (caution!).

Preparation of $Pd(bqd)_2TCNQ$. To a suspension of 130 mg of $Pd(bqd)_2$ (α- and/or β-modification)[12] in 250 ml chloroform plus 60 ml *o*-dichlorobenzene was added a solution of high-purity TCNQ (150 mg in 50 ml chloroform). The mixture was refluxed with stirring for about 48 hours, after which the green solution was filtered and concentrated to 150 ml by slow evaporation. Dark blue, shiny, and slightly dichroic platelets formed. They were filtered off, washed with cold $CHCl_3$ and petrol ether, and dried overnight at 90°C. Concentration of the mother liquor to 70 ml afforded an additional portion of flat crystals, which were washed as above. Total yield: 195 mg (97.5%) of analytically pure $Pd(bqd)_2 \cdot$ TCNQ.

Preparation of $Ni(bqd)_2TCNQ$. 111 mg of $Ni(bqd)_2$ were treated in the same manner as $Pd(bqd)_2$ to yield the analogous $Ni(bqd)_2$ TCNQ (90%). Both products appear to exhibit similar properties.

Results and Discussion

The aromatic compound 1,2-benzoquinonedioxime (bqdH) shown in Figure 1 has been known for a long time.[7b] In contrast to a large number of other 1,2-dionedioximes,[34] however, very little attention has been paid to this bidentate



(a) (b)

FIGURE 1. Schematic molecular structure of bqdH. (a): the arrow pairs indicate the positions across which electron density may be *pushed into* or *pulled from* the benzoquinone ring; (b): the acidic character (predominantly monovalent) of bqdH is emphasized.

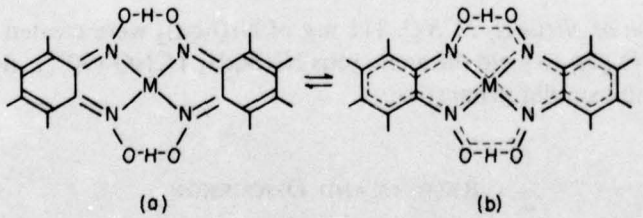
ligand with respect to the synthesis of stacked compounds. The failure for the most extensively used aliphatic dionedioxime ligands to yield solids with dramatic one-dimensional properties obviously explains the neglect of bqdH, whose outstanding value in this regard has thus been overlooked or underestimated.

The molecular structure of bqdH (FIGURE 1) shows that this compound is a strictly flat molecule, due to its benzoquinonoid nature. Because of this benzoquinonoid structure, bqdH is an electrophilic aromate whose electronic "household" may be influenced in two ways: first, by substitution of the benzene ring with appropriate groups; second, by coordination to a metal ion through the *N* atoms, in which case the resulting "backbonding"[13] provides a mechanism for the metal electron "cloud" to be delocalized on the electron-poor ligand (nephelauxetic effect). The flatness of the molecule combined with this electronic effect causes the uniqueness of bqdH.

The reaction of 1,2-benzoquinonedioxime ligands (TABLE 1) with the metal ions Ni^{2+}, Pd^{2+}, or Pt^{2+}, according to the equation

$$2\text{bqdH} + M^{2+} \xrightarrow{-2H^+} M(\text{bqd})_2,$$

affords extremely stable, intensely colored neutral products. In the case of the unsubstituted bqdH as the ligand (FIGURE 2), x-ray structural studies on numerous derivatives have shown the complex molecules to be completely coplanar. In addition, the intramolecular O—H—O bridges (evidenced by ir spectra, FIGURE 3),[3b] the chelate effect, and the mesomerism of the delocalized π-electron system, contribute jointly to enhance the stability of $M(\text{bqd})_2$. The observed planarity of the complex molecules minimizes steric hinderances between neighboring units of a stack and thus favors the stacking arrangements.



(a) (b)

FIGURE 2. Schematic molecular structure and mesomeric π-electron delocalization in a $M(\text{bqd})_2$ complex unit. The π-electrons are obviously not localized as in (a), but delocalized as in (b).

Impact of the Nephelauxetic Effect on Cooperative Properties of a Metal Atom Chain

When bqdH coordinates a transition metal ion, as in FIGURE 2, the first step of bond formation consists in the formation of a dsp-σ bond for which both

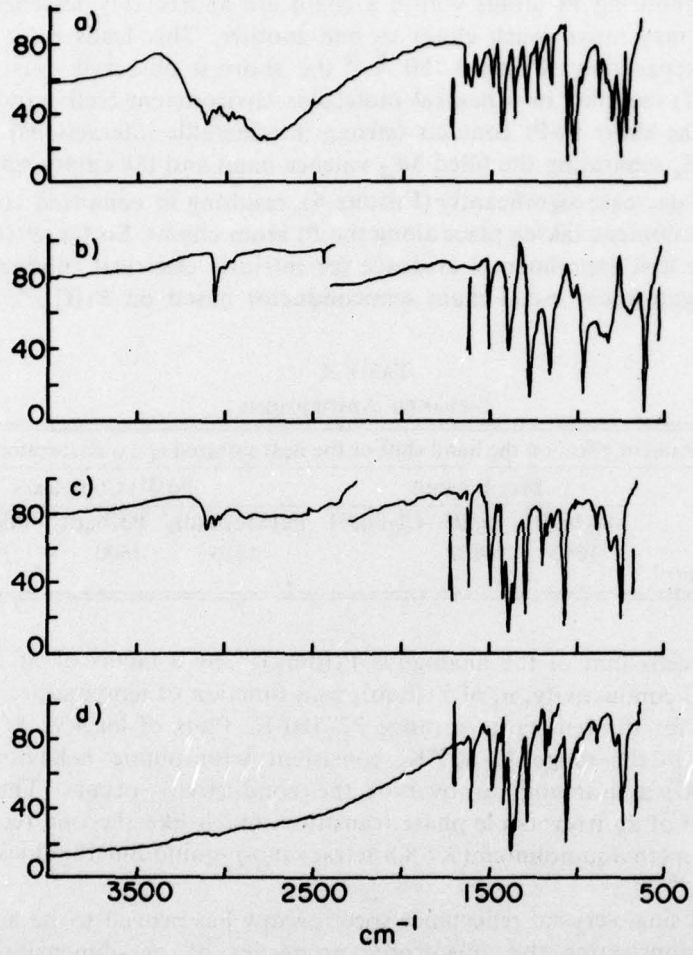


FIGURE 3. Near infrared spectra of (a): bqdH (free ligand) with evidence for a broad ν_{O-H} absorption band at 3500–2500 cm^{-1}; (b) $Ni(bqd)_2$ (c) $Pd(bqd)_2$ and (d) $Pt(bqd)_2$: The formation of strong and symmetric O—H—O bridges is evidenced by the disappearance of the ν_{O-H} band.

electrons are provided by the nitrogen atom. However, there exists the possibility of finite overlap between filled orbitals of the central metal and empty π^* orbitals of the coordinating *N* atoms. Thus, the second step of bond formation consists in a "backdonation" of metal *d* electron density to the ligands, provided the *d*-shell involved is sufficiently polarizable. The 5-*d* electron shell of Pt(II) is more polarizable than the more rigid 4-*d* shell of Pd(II) or even the much more rigid

3-*d* shell of Ni(II). Therefore, the nephelauxetic effect induced by electronic properties of the ligands is expected to have a much more dramatic impact on the *d*-electron density of Pt(II) than on that of Pd(II) and Ni(II). As a consequence, the electron "clouds" of the Pt atoms are appreciably delocalized on the spheres of the electron-poor ligands. The delocalization is equivalent with a partial reduction in *d*-shell electron density at the Pt sites. Consequently, van der Waals repulsions between neighboring Pt atoms within a chain are appreciably lessened so that these atoms may move much closer to one another. This leads to a relatively short Pt-Pt separation of only 3.180 Å,[14] the shortest observed thus far for a stacked Pt(II) complex in a neutral molecular environment (cell parameters in TABLE 5). The short Pt-Pt contacts (strong intermetallic interactions) cause the energy gap E_g separating the filled $5d_{z^2}$ valence band and the empty $6p_z$ conduction band to decrease significantly (FIGURE 4), resulting in enhanced cooperative transport phenomena taking place along the Pt atom chains. So far, $Pt(bqd)_2$ had provided the first experimental evidence for intrinsic electrical conduction in a small band gap linear metal-chain semiconductor based on Pt(II).[14] This conductivity exceeds that of the analogous $Pt(dmg)_2$[15] by a factor of at least 10^9. The electrical conductivity, σ, of $Pt(bqd)_2$ as a function of temperature is shown in FIGURE 5 for the temperature range 77–550°K. Plots of $\log\sigma$ vs $1/T$ yield a straight line in the range 77–300°K, consistent with ohmic behavior. Above 380°K (110°C) a dramatic turnover of the conductivity occurs. This change is reminiscent of an irreversible phase transition, much like the one recently observed in *N*-methylquinolinium(7,7,8,8-tetracyano-*p*-quinodimethanide)$_2$, NMeQn(TCNQ)$_2$.[16]

TABLE 4

INFRARED ABSORPTIONS

Substituent effect on the band shift or the near infrared $\nu_{C=N}$ absorption						
	Free Ligands			Pd(II) Complexes		
	Me_2bqdH	bqdH	Cl_2bqdH	$Pd(Me_2bqd)_2$	$Pd(bqd)_2$	$Pd(Cl_2bqd)_2$
$\nu_{C=N}$ absorpn. in cm^{-1}	1640	1630		1610	1600	1565

Polarized single-crystal reflectance spectroscopy has proved to be a powerful tool for demonstrating the anisotropic properties of one-dimensional materials.[17–17c] The reflectance spectra of $Pt(bqd)_2$ are displayed in FIGURE 6.[14] The band centered at 0.85 eV and polarized along the stacking direction is reminiscent of an interband electronic transition, reasonably associated with the optical $5d_{z^2}$ to $6p_z$ transition in a direct process.[17a] The disappearance of this band when the reflected light is polarized perpendicular to the stacking direction of the molecules demonstrates the one-dimensional character of $Pt(bqd)_2$.

Finally, the observed diamagnetism in $Pt(bqd)_2$ (negative susceptibilities, χ_m, no epr signal) excludes the possibility of an "extrinsic" conduction, i.e., a conduction dominated by small amounts (in ppm concentrations) of Pt(III) impurity ions doped into the Pt(II) chains of the host lattice, as has been found recently in the most extensively studied Magnus Green Salt (MGS), $Pt(NH_3)_4\,PtCl_4$.[18a,18b]

TABLE 5

LATTICE PARAMETERS OF BQDH COMPLEXES

Complex	Space Group	in Å			in Degree			Z	V in Å^3	Ref.
		a	b	c	α	β	γ			
$Ni(bqd)_2$	$P2_1/n$	3.856	9.461	16.542	90	90.45	90	2	603.5	20
α-$Pd(bqd)_2$	*Imcb*	6.405	9.728	20.649	90	90	90	4	1286	21
$Pt(bqd)_2$	*Imcb*	6.361	9.663	20.837	90	90	90		1280.7	19
$Ni(bqd)_2I_{0.5}$	*P4/mcc*	15.553	15.553	6.307	90	90	90	4	1525.6	23
$Pd(bqd)_2I_{0.55}$	*P4/mcc*	15.977	15.977	6.371	90	90	90	4	1626.2	24
$Pt(bqd)_2I_2$ Modif. I	$P\bar{1}$	7.433	9.515	7.824	121.44	119.08	81.45	1	408.5	31
$Pt(bqd)_2I_2$ Modif. II	$P\bar{1}$	9.653	11.668	7.715	89.77	107.40	94.58	2	826.4	31
$Pt(bqd)_2 \cdot (AgClO_4)_{0.5}$	$P2/n$	6.773	13.635	15.723	90	92.56	90	4	1451	10
$Ni(bqd)_2 \cdot TCNQ$	$P\bar{1}$	9.92	7.88	7.41	105.1	81.0	92.9		552	11
$Pd(bqd)_2 \cdot TCNQ$	$P\bar{1}$	10.251	7.843	7.328	105.54	83.63	92.28	1	465	11

By way of contrast, the analogous derivatives $Pd(bqd)_2$ and $Ni(bqd)_2$, which have larger metal-metal separations, are found to behave like insulators,[4] with conductivities less than $10^{-9}\,\Omega^{-1}\,cm^{-1}$, i.e., too small to be detected with our experimental equipment. Although the three compounds $Ni(bqd)_2$, $Pd(bqd)_2$, and $Pt(bqd)_2$ are characterized by the common stacking structure in the solid, they exhibit specific differences in the molecular arrangement within their respective crystal lattices. Whereas $Pt(bqd)_2$ and $Ni(bqd)_2$ crystallize only in the space groups *Imcb* (or *Ibam*)[14,19] and $P2_1/n$,[20] respectively, $Pd(bqd)_2$ forms two crystalline

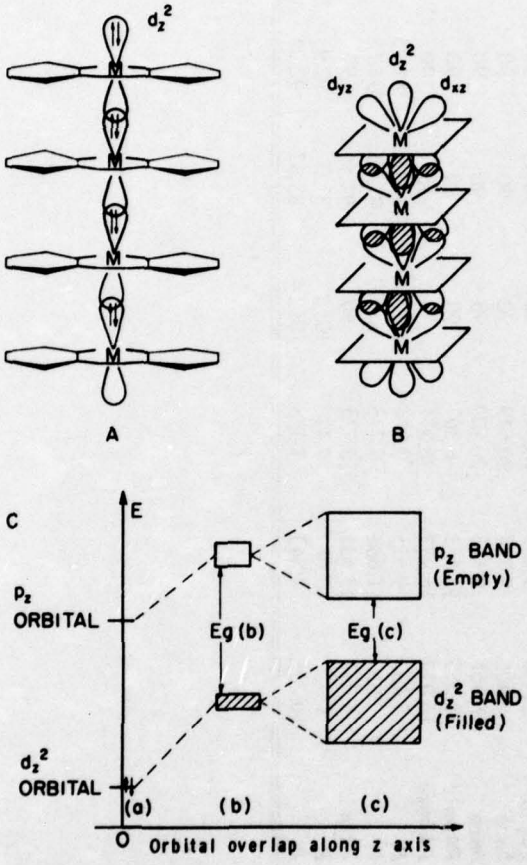


FIGURE 4. Schematic representation of the stacking and energy-band structure in $M(bqd)_2$ complexes. A: Real case of weakly interacting metal orbitals along the z direction (the p_z orbitals have been omitted for clarity); B: Idealized case of maximum interactions, which may result in a *magnetic one-dimensional metallic state*; C: Band gap E_g between the filled d_{z^2} valence and the empty p_z conduction band as a function of orbital interaction along the z-axis (stacking direction). The energy separation between the filled d_{z^2} and the empty p_z orbitals of a single $M(bqd)_2$ complex molecule is sketched in a); for weak intrachain interactions, the corresponding narrow bandwidths and large band gap are represented in b), and the effect of strong intrachain interactions upon the bandwidths and band gap is shown in c).

modifications, α and β. α-$Pd(bqd)_2$ is isostructural with $Pt(bqd)_2$.[21] It forms dark, red-violet, rectangular prisms that exhibit a marked red luster when viewed under light polarized parallel to the long axis of the crystal (stacking direction). β-$Pd(bqd)_2$, by contrast, crystallizes in a system of lower symmetry, as indicated by preliminary precession photographs. The space group of this material (black, lustrous, but not dichroic crystals), however, is currently in the process of being determined accurately.[12] It is to be emphasized that further differences are found in the solid-state properties of the two modifications, in particular with respect to their polarized single-crystal reflectance spectra, their elastic properties,[22] and their

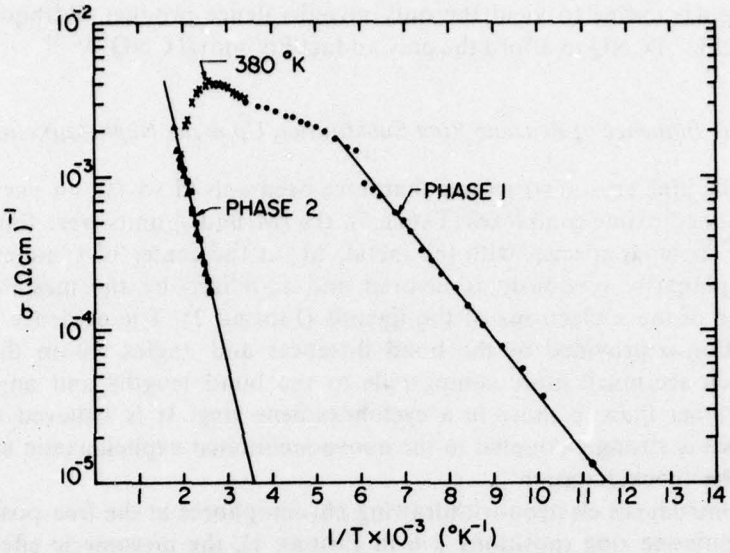


FIGURE 5. Temperature dependence of the dc electrical conductivity of $Pt(bqd)_2$, $\log \sigma$ vs. 1/T. Dots = cooling and heating curve between room temperature and liquid nitrogen; crosses = heating from room temperature to 240°C; squares: Cooling from 240 to 110°C; triangles: heating from 110 to 275°C (crystal decomposes at 278°C). The activation energy is 0.15 eV and 0.55 eV for phase 1 and phase 2, respectively.

solubilities. These divergences are due solely to different stacking patterns of the individual $Pd(bqd)_2$ molecules. Various experimental results provide clear evidence for the conservation of the molecular identity in the solids. In particular, 1) the elemental analysis is the same; 2) the color of solutions is identical (dark green); 3) the near infrared spectra are identical; and 4) the solids equally react

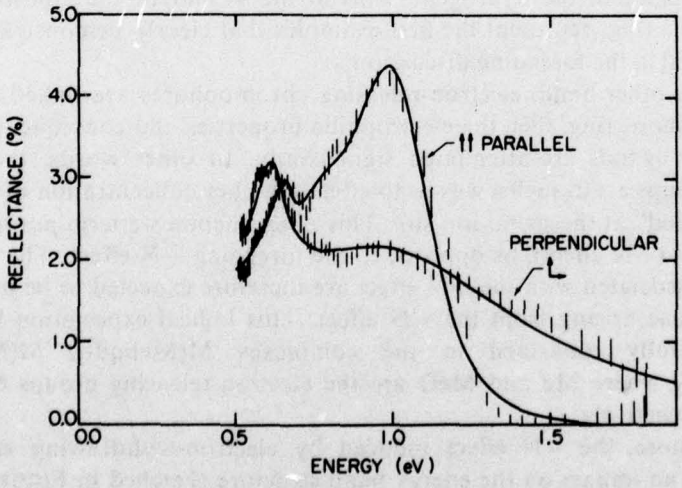


FIGURE 6. Polarized single-crystal reflectance spectra of $Pt(bqd)_2$. Broken lines = experimental data; Solid lines = fitting curves to these data.

with molecular iodine to yield the only mixed-valence product, $Pd(bqd)_2I_x$,[4] or with molecular TCNQ to afford the only adduct $Pd(bqd)_2TCNQ$.[11a,11b]

Electronic Influence of Benzene Ring Substitution Upon the Nephelauxetic Effect

In all the nine crystal structures that have been solved so far on various 1,2-benzoquinonedioxime complexes (TABLE 5), the $[M(bqd)_2]$ units were found to be rigorously coplanar species, with the metal, M, at the center of symmetry. This preferred planarity obviously is favored and stabilized by the mesomeric delocalization of the π-electrons of the ligands (FIGURE 2). The evidence for such delocalization is provided by the bond distances and angles within the ligand rings, which are much more comparable to the bond lengths and angles in a benzene, rather than to those in a cyclohexadiene ring. It is believed that this mesomerism is strongly coupled to the above-mentioned nephelauxetic effect (induced by the "back donation").

If one introduces electron-withdrawing chromophores at the free positions of the benzoquinone ring (positions 3–6 in FIGURE 1), the mesomeric effect is expected to act as a handle by means of which these electrophilic chromophores can grip down to the electron "cloud" of the central metal and expand it toward the spheres of the ligands. This partial reduction in *d*-shell electron density of the metal ions we term *negative* nephelauxetic effect (−N effect) in analogy to the negative mesomeric or inductive effects in organic chemistry (−M or −I effect). One expects the most striking manifestation of the −N effect to result in enhancement of the metal-metal interaction in terms of increased orbital overlap of the adjacent metal ions within a chain. The large intermolecular forces that result this way should be markedly reflected, e.g., in the low solubility of the compounds. They manifest themselves also in the more intense colors of the solid compounds, compared to their rather bright colors in dilute solutions. The complexes $M(Clbqd)_2$ and $M(Cl_2bqd)_2$, where the electrophilic chlorine atoms have been introduced in place of the hydrogen atoms at the 4- and/or the 5-position of the benzoquinone ring, represent the first examples that clearly demonstrate the −N effect outlined in the foregoing discussion.

If, on the other hand, electron-releasing chromophores are linked directly to the benzoquinone ring, then the electrophilic properties and consequently the −N effect of the ligands are attenuated significantly. In other words, the electron-releasing groups act in such a way as to effect a higher concentration of the *d*-shell electron "cloud" at the metal ion site. This phenomenon we term *positive* nephelauxetic effect (+N effect), as opposed to the foregoing −N effect. The solid-state properties associated with the +N effect are therefore expected to be just the opposite of those arising from the −N effect. This logical expectation has indeed been beautifully confirmed in the complexes $M(Mebqd)_2$, $M(MeObqd)_2$, $M(Me_2bqd)_2$, where Me and MeO are the electron-releasing groups CH_3- and CH_3O-, respectively.

Furthermore, the −N effect induced by electron-withdrawing substituents should have an impact on the energy band structure sketched in FIGURE 4c so as to reduce the band gap E_g between the filled d_{z^2} valence and the empty p_z conduction band. Thus, it might become possible to gradually enhance the transport

phenomena occurring within the chain to such an extent that, at the uppermost limit, metallic state could be reached if the two bands were to merge. To put it another way, if the coordination geometry around each metal ion in the solid were to approximate a regular octahedron, then the energy difference between the empty b_{1g}^{*} ($d_{x^2-y^2}$) and the filled a_{1g}(d_{z^2}) levels would become so negligible that Hund's rule would require the share of the two d_{z^2} electrons by both degenerate orbitals. Thus, with one electron in each d_{z^2} orbital, the extended d_{z^2} band would be half-filled and would therefore become a pure metallic conduction band. The single electrons in the $d_{x^2-y^2}$ orbitals, by contrast, would remain pinned at the molecular sites, since in the stacking structure with the molecular planes perpendicular to the stacks, the extent of the $d_{x^2-y^2}$ band is so small that these states may be regarded as isolated. The most exciting aspect of this hypothesis is that one now reaches the concept of a fascinating model solid where the metallic transport properties are confined in one direction and the magnetic properties restricted in the orthogonal directions. The unique merit of the bqdH ligands is, at the least, to inspire this prediction of a *magnetic one-dimensional metal*.

In the present work, care has been taken to employ substituents of approximately the same and relatively small specific volume in order to minimize or cancel steric hinderance, so that their inductive (±I) and/or mesomeric (±M) effects may be observed.

IR Evidence for Mesomeric Delocalization

Near infrared (nir) spectra record the characteristic absorption bands of individual molecules and thus furnish accurate information concerning intramolecular vibrations as a function of bond strength. In the present compounds it is important to focus primarily on two types of vibrational modes that appear to be of interest in understanding electronic effects within the complex molecules.

The first characteristic vibration is the O—H stretching mode which absorbes in the frequency region 3600–2400 cm^{-1}. From the intensity and width of the O—H absorption band, it is possible to learn about the symmetry and strength of the O—H—O bridges. In the absence of such bridges a very sharp and intense absorption band characteristic of isolated O—H stretching vibrations is observed at the high-energy side of the above frequency region. If weak and unsymmetric O—H—O bridges are present, this band is broadened and red-shifted (FIGURE 3a). Finally, the presence of very strong and strictly symmetric bridges causes the O—H vibration to become ir-insentitive, and the band to pratically disappear (FIGURES 3b–d).[3a,3b,8] On the evidence of x-ray studies, the presence of symmetric bridges was confirmed by equivalent N—O bond lengths and identical electron densities around the O atoms. It is obvious that the formation of these symmetric bridges favors the planar geometry and contributes to the stability of the complex molecules.

The second vibration of interest is the C=N stretching mode, which generally absorbes around 1600 cm^{-1}. This vibration may provide a very sensitive probe for evaluating, at least qualitatively, the extent of electronic effects induced by substituents linked to the remote parts of the ligands. In TABLE 4 are listed the band

positions of the C=N absorption as a function of substituent effects in the free bqdH ligands as well as in their corresponding complexes. For example, in the ligands Me_2bqdH, bqdH, and Cl_2bqdH, the absorption band is shifted to lower frequencies following this order, which coincides with the increasing electrophilic character. Clearly, electron-withdrawing substituents produce a red-shift of the C=N absorption in contrast to the effect produced by electron-releasing substituents. This is easy to understand from the fact that the electron-deficient benzoquinonoid ring is likely to pull some electron density out of the adjacent C=N bond. This withdrawal of electrons from the carbon-nitrogen double bond results in the weakening of the bond. Consequently, the oscillator frequency which is a direct function of the bond strength decreases, and the frequency of the absorption is red-shifted. The shift is even more dramatic in the complexes where the *N* atoms are quaternized. Thus, the ir experiment appears to offer a powerful and sensitive method to demonstrate that electronic effects induced by chromophoric groups at the ligand sites may be carried via the mesomerism throughout the entire complex molecule down to the direct vicinity of the central metal. The fundamental significance of this finding is primarily associated with the possibility of achieving Little's excitonic high-temperature superconductor for which the extension of ligand polarizability down to the nearest vicinity of the central metal site is a necessary condition.[5]

Derivatives of the 1,2-Benzoquinonedioximates

The flexibility of the coordination chemistry based on 1,2-benzoquinonedioximes is not only restricted to the preparation of, so to speak, first-generation complexes described above, which are formed by the reaction of the free ligands with divalent d^8 metal ions. These first-generation complexes also readily react with various other reagents to afford new and interesting compounds.

The most interesting derivatives of this kind are the partially oxidized linear metal-chain compounds $M(bqd)_2I_x$[3a,3b,4,9] (M = Ni, Pd: $x \simeq 0.5$). Full x-ray structure determinations show that these isostructural crystal lattices[23,24] consist of positively charged (partially oxidized) stacks of $M(bqd)_2$ units and negatively charged (partially reduced) chains of iodine atoms that may be desordered. Within the complex stacks, the metal ions are linked in extended linear chains with a uniform metal-metal separation of 3.153 Å for $Ni(bqd)_2I_{0.5}$ and 3.185 Å for $Pd(bqd)_2I_{0.5}$; these are the shortest metal-metal distances observed so far in Ni and Pd compounds of this type. The iodine chains consist of I_3^- units, as evidenced by resonance Raman and Mössbauer spectroscopy,[25] and by diffuse x-ray scattering analysis;[26] the I_3^- units are linked head-on-tail parallel to the metal atom chains at a distance of about 8 Å. The experimentally assessed degree of partial oxidation indicates a nonintegral oxidation number of +2.17 for the metal ions in these compounds.[25,26] This number corresponds to the removal of an amount of 0.17 electron from each Ni^{2+} or Pd^{2+} ion, which is much less than in the case of Krogmann Salts[2] (>0.3 electron removed from each Pt^{2+}) and even twice as less as in the case of analogous mixed-valence compounds based on glyoxime ligands.[27,28]

Although $Ni(bqd)_2I_{0.5}$ and $Pd(bqd)_2I_{0.5}$ exhibit a golden metallic luster polarized parallel to the stacking direction,[22] their electrical and optical properties

differ markedly from those of the prototypical Krogmann Salt, $K_2Pt(CN)_4 \cdot Br_{0.33} \cdot 3H_2O$ (KCP). This divergence is best explained in terms of the d_{z^2} band filling. Accordingly, the d_{z^2} band in KCP is filled to about 83%. By contrast, the d_{z^2} band in $Ni(bqd)_2I_{0.5}$ or $Pd(bqd)_2I_{0.5}$ is filled to 92%, leaving only 8% of available free room for transport phenomena to occur. In such a narrow space, however, the density of states of "Fermi electrons" is expectedly too small to give rise to "metallic" behavior. Therefore, the materials behave as semiconductors. Nevertheless, there is an enormous increase in electrical conductivity of at least 10^5 when going from the unoxidized $M(bqd)_2$ to their partially oxidized products. Obviously the electrical properties depend predominantly on the extent of metal-metal interactions (measured by metal-metal distances) rather than on the degree of partial oxidation. This statement is supported by the experimental observations made on the analogous glyoxime complexes, $M(dpg)_2I$ (M = Ni or Pd; dpg^- = ion of diphenylglyoxime),[27,30] and $Pd(Glyox)_2I$ ($Glyox^-$ = ion of glyoxime).[28] In these partially oxidized iodine chains-containing compounds, the degree of partial oxidation[27] was found to be twice as much as in the corresponding $M(bqd)_2I_{0.5}$ derivatives. Yet the latter derivatives possess a higher conductivity, due to their much smaller metal-metal distances.

When the Pt(II) complexes of 1,2-benzoquinonedioxime ligands are treated with molecular iodine or bromine, the only products that form are the oxidative adducts exemplified by the derivatives, $Pt(bqd)_2X_2$ ($X = Br^-, I^-$).[3] Here, the resulting Pt(IV) ions are octahedrally coordinated by the four equatorial *N* atoms and the two halides linked axially below and above the plane of the chelate.[31] This type of reaction has also been observed on other 1,2-dionedioximates of Pt(II).[27,32] Worthy of note is the completely different reaction of bromine or chlorine with $Ni(bqd)_2$ and $Pd(bqd)_2$. Presumably because of the higher oxidizing power of these halogens, their action on the Ni(II) and Pd(II) benzoquinonedioximates consists in attacking preferentially the ligand moities which, under destruction of the complex, are probably oxidized to the corresponding benzofuroxans in the manner reported in literature.[33a,33b]

Another interesting addition reaction is the action of silver perchlorate upon $Pt(bqd)_2$, which yields the adduct of stoichiometry $Pt(bqd)_2 \cdot (AgClO_4)_{0.5}$.[3a,3b,10] This adduct is the first example of its kind, since no analogous derivative, i.e., a silver porchlorate-containing linear metal-chain compound, has been previously reported. The presence of $AgClO_4$ in the crystal lattice does not prevent the highly preferred stacking structure of the $Pt(bqd)_2$ molecules, although the Pt-Pt separation of 3.386 Å is significantly increased, compared to 3.180 Å in $Pt(bqd)_2$.[19] This large Pt-Pt distance is obviously caused by steric effects induced by the roomy perchlorate ion, ClO_4^-.

Finally, the attempt to oxidize $Ni(bqd)_2$ and $Pd(bqd)_2$ using the electron acceptor 7,7,8,8-tetracyano-p-quinodimethane, TCNQ, resulted in the formation of the equally interesting 1:1 new adducts, $M(bqd)_2 \cdot TCNQ$[11a,11b] ($M = Ni^{2+}, Pd^{2+}$). The $M(bqd)_2$ and the TCNQ molecules, though packed closely together in the crystal lattice of these adducts, remain individually uncharged, as was evidenced by the absence of an epr signal.[11a] Only diamagnetic and minor electronic properties may be expected in these solids since all the symmetry-related levels of the interacting single molecules are either completely filled or completely empty. This

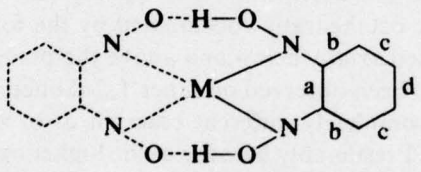
state of affairs imposes that the resulting energy band structure along the stacking direction remain characteristic of an insulator or, at most, of a semiconductor, similar to FIGURE 4C, which is experimentally observed. Future efforts will be aimed at finding proper ways of inducing a partial filling of these energy bands, in which case the solids are suspected to possibly become highly conductive (one-dimensional metals).

X-ray Evidence for the "Backdonation" Effect

In TABLE 5 are displayed the most relevant structural features of all the 1,2-benzoquinonedioxime complexes that have so far been analyzed by means of x-ray techniques. In all cases, the $M(bqd)_2$ entity was found to be a strictly flat species.

It is useful to note the variation of the M—N (metal-nitrogen) bond distance in different complexes of the same metal atom. As shown in TABLE 6, this bond dis-

TABLE 6
COMPARATIVE INTRAMOLECULAR BOND DISTANCE
IN UNOXIDIZED AND OXIDIZED $M(bqd)_2$ COMPLEXES



Complex	Bond distance in Å							
	M—N	C—N	N—O	*a*	*b*	*c*	*d*	Ref.
$Ni(bqd)_2$	1.864	1.310	1.32	1.445	1.43	1.35	1.43	20
$Ni(bqd)_2I_{0.50}$*	1.905	1.31	1.33	1.50	1.43	1.37	1.42	23
α-$Pd(bqd)_2$	1.975	1.32	1.335	1.47	1.45	1.36	1.48	21
$Pd(bqd)_2I_{0.55}$*	2.042							24
$Pt(bqd)_2 \cdot (AgClO_4)_{0.5}$	1.98	1.29	1.385	1.48	1.45	1.35	1.475	10
$Pt(bqd)_2I_2$*	2.002	1.32	1.33	1.46	1.43	1.365	1.445	31

*Oxidized.

tance may be regarded as a reliable estimate for the magnitude of the "backdonation" effect discussed earlier. There, it was stated that the M—N bond formation may be thought of as taking place in a two-step or "push-and-pull" mechanism (synergetic effect).[2] In the pushing phase, the N atom *pushes* its free electron pair into the *d*-shell of the central metal to form the σ_{M-N} bond. In the following pulling step, the N atom *pulls* via its π^* orbital a certain amount of electron density out of the filled, symmetry related *d*-orbitals of the metal. Obviously, the total degree of bonding between the nitrogen and the metal atoms is dominated by the extent of this backdonation effect, which, in turn, is directly related to the *d*-shell polariza-

bility, and therefore to the nephelauxetic effect discussed above. When one compares the M—N distances of the unoxidized $M(bqd)_2$ complexes with those of their oxidation products, one notes that these distances are larger (weaker bonding) for the latter than for the former compounds. This difference is understood as the direct result of the oxidation process (removal of *d*-electrons), following which the reduction in *d*-shell electron density is accompanied by an attenuated backdonation effect. The net result is a lengthening of the M—N bond in the oxidized complexes.

Concluding Remarks

It has been shown in the foregoing discussion that, barring large steric effects, the ligand system 1,2-benzoquinonedioxime (bqdH) is outstandingly suited for the synthesis of linear metal-chain compounds, especially of those based on the ions Ni^{2+}, Pd^{2+}, and Pt^{2+}. The nephelauxetic effect (expansion or contraction of the *d*-shell electron "cloud" at the metal site) has been experimentally observed. Thus, using properly substituted 1,2-benzoquinonedioxime ligands, the *d*-shell electron density of the central metal ion may be either lowered somewhat to enhance intermetallic interactions within the chains or may be slightly increased to lower the metal-oxidation potential and render the chains more susceptible to (partial) oxidation.

This partial oxidation (possibly resulting in a one-dimensional metal), along with the possibility of expanding the observed mesomerism of bqdH to a highly polarizable dye-like system, represents the fundamental prerequisite for the construction of an excitonic high-temperature superconductor according to the model proposed by Little.[5a,5b] It is particularly in this connection that the bqdH complex chemistry is expected to have the most exciting impact in years to come.

Acknowledgment

The author thanks Prof. W. A. Little for his encouragement.

Notes and References

1. Miller, J. S. & A. J. Epstein. 1976. Progr. Inorg. Chem. **20:** 1 and literature cited therein.
2. Krogmann, K. 1969. Angew. Chem. Internat. Ed. **8:** 35.
3a. Bélombé, M. M. 1974. Dissertation. Doctoral Univ. of Heidelberg. Heidelberg, Germany.
3b. Bélombé. M. M. 1972. Diplomarbeit (M.S. thesis). Univ. Heidelberg. Heidelberg, Germany.
4. Endres, H., H. J. Keller, M. Megnamisi-Belombe, W. Moroni & D. Nöthe. 1974. Inorg. Nucl. Chem. Lett. **10:** 467.
5a. Little, W. A. 1964. Phys. Rev. **A134:** 1416.
5b. Davis, D., H. Gutfreund & W. A. Little. 1976. Phys. Rev. **B13:** 4766.
6a. Kaufman, J. V. R. & J. P. Picard. 1959. Chem. Rev. **59:** 429.
6b. Mallory, F. B. 1957. Org. Syn. **37:** 1.
7a. Ladd, E. C. & W. P. ter Horst. 1943. U. S. Pat. 2, **336:** 941.

7b. ZINCKE, T. & P. SCHWARZ. 1899. Ann. Chem. **307:** 28.
8. BURGER, K. & I. RUFF. 1966. Acta Chem. Acad. Sci. Hung. **49(1):** 1 and references therein.
9. BUSE, K. D., H. J. KELLER & M. MEGNAMISI-BÉLOMBÉ. 1976. West Germ. Pat. P2510689. Sept.
10. ENDRES, H., M. MEGNAMISI-BÉLOMBÉ, H. J. KELLER & J. WEISS. 1976. Acta Cryst. **B32:** 457.
11a. KELLER, H. J., I. LEICHERT, M. MEGNAMISI-BÉLOMBÉ, D. NÖTHE & J. WEISS. 1977. Z. Anorg. Allg. Chem. **429:** 231.
11b. KELLER, H. J., I. LEICHERT, M. MEGNAMISI-BÉLOMBÉ, W. MORONI, D. NÖTHE & J. WEISS. 1976. Mol. Cryst. Liq. Cryst. **32:** 155.
12. The full structure determination of the β-Pd(bqd)$_2$ by the author and others is currently in progress.
13. See e.g. COTTON, F. A. & G. WILKINSON. 1972. Advanced Inorganic Chemistry. 3rd edit.: chapters 20, 22, 23. John Wiley & Sons. New York, N.Y. See also reference 2.
14. BÉLOMBÉ, M. M. 1977. J. Solid State Chem. **22.** In press.
15. GOMM, P. S., T. W. THOMAS & A. E. UNDERHILL. 1971. J. Chem. Soc. (A) 2154 and references therein.
16. MIHALY, G., K. HOLCZER, G. GRÜNER & L. D. KUNSTELJ. 1976. Solid State Commun. **19:** 1091.
17a. KROGMANN, K. & H. P. GESERISCH. 1974. *In* Extended Interactions Between Metal Ions. ACS Symposium Series 5. L. V. Interrante, Ed.: 354. American Chemical Society. Washington, D.C.
17b. ZELLER, H. R. 1973. Adv. Solid State Phys. **13:** 31.
17c. ANEX, B. G. 1974. *In* Extended Interactions Between Metal Ions. L. V. Interrante, Ed.: 276. ACS Symposium Series 5. Washington, D.C.
18a. INTERANTE, L. V. 1972. J. Chem. Soc. Chem. Comm.: 302, also *In* Low-Dimensional Cooperative Phenomena. 1975. H. J. Keller, Ed. NATO ASI **B7:** 299. Plenum Press. New York, N.Y.
18b. MEHRAN, F. & B. A. SCOTT. 1973. Phys. Rev. Lett. **31:** 99.
19. BÉLOMBÉ, M. M. *et al.* In Preparation.
20. LEICHERT, I. & J. WEISS. 1975. Acta. Cryst. **B31:** 2877.
21. LEICHERT, I. & J. WEISS. 1975. Acta. Cryst. **B31:** 2709.
22. BÉLOMBÉ, M. M., J. BRILL & M. NOVOTNY. In preparation.
23. ENDRES, H., H. J. KELLER, W. MORONI & J. WEISS. 1975. Acta. Cryst. **B31:** 2357.
24. BÉLOMBÉ, M. M., R. OLSON & P. WOLBER. To be published.
25. MARKS, T. J. & D. F. WEBSTER. 1976. J. C. S. Chem. Commun.: 444.
26. COMES, R., H. ENDRES, H. J. KELLER, M. MEGNAMISI-BÉLOMBÉ, W. MORONI, H. PRITZKOW & J. WEISS. 1976. Acta Cryst. **A32:** 954.
27. GLEIZES, A., T. J. MARKS & J. A. IBERS. 1975. J. Amer. Chem. Soc. **97:** 3545.
28. ENDRES, H., H. J. KELLER, R. LEHMANN & J. WEISS. 1976. Acta. Cryst. **B32:** 627.
29. ZELLER, H. R. 1975. *In* Low-Dimensional Cooperative Phenomena. H. J. Keller, Ed. NATO ASI **B7:** 215. Plenum Press. New York, N.Y., and references therein.
30. UNDERHILL, A. E., D. M. WATKINS & R. PETHIG. 1973. Inorg. Nucl. Chem. Lett. **9:** 1269.
31. PRITZKOW, H. 1976. Z. Naturforsch. **31b:** 401.
32. MILLER, J. S. & S. Z. GOLDBERG. 1975. Inorg. Chem. **14:** 2294. See also Ref. 27.
33a. VON ILINSKI, M. 1886. Ber. Deut. Chem. Ges. **19:** 349.
33b. BOYER, J. H. & G. MAMIKUNIAN. 1958. J. Org. Chem. **23:** 1807.
34. CHAKRAVORTY, A. 1974. Coord. Chem. Rev. **13:** 1.

THE CONSTRUCTION OF METAL-METAL BONDS BY REDOX PROCESSES*

Alan L. Balch

Department of Chemistry
University of California
Davis, California 95616

INTRODUCTION

The chemical and physical behavior of low-dimensional materials has been, quite naturally, focused on studies of these materials in the solid state. However, the emphasis on the solid form of these materials has left many chemically intriguing aspects of these substances unexplored. In this article we will be concerned with some of these aspects of the chemistry of linear materials composed, in particular, of chains of transition metal ions. Our emphasis will be on the construction, especially the controlled construction, of metal-metal bonds.

Numerous questions remain unanswered in this area. The mechanism of metal-metal bond formation in columnar materials such as the intensively studied $K_2Pt(CN)_4 \cdot 0.3\,Br \cdot H_2O$[1] and, in fact, in most systems containing metal-metal bonds remains for future exploration. The relative importance of lattice effects versus direct covalent bond in determining the stability of factional oxidation states in such unconventional materials as $K_{1.67}Pt(O_2C_2O_2)_2 \cdot H_2O$[2] and $(cation)_xIr(CO)_2Cl_2$ (x varies from .3 to .6 depending on the cation)[3] have not been ascertained. Rational means of anticipating the synthesis of columnar transition metal complexes remain to be devised.

One of the useful means of constructing metal-metal bonds involves a redox reaction in which metal complexes containing different formal oxidation states of the same metal are allowed to react. This process, however, can lead to a variety of different reactions. These are outlined in TABLE 1. One of these, simple electron transfer between the accessible oxidation states, is of little interest here. A second reaction type leads to the formation of a columar material containing an effectively infinite chain of directly bound metal atoms. An example is the reaction between the square d^8 Pt(II) complex $Pt(CN)_4^{-2}$ and the six-coordinate d^6 Pt(IV) complex $PtCl_2(CN)_4^{-2}$ to form the solid $K_2Pt(CN)_4Cl_{0.32}(H_2O)_3$.[4] Only one product with a unique stoichiometry results from this reaction. During the reaction, halide ions are expelled from the coordination spheres of the platinum centers which originated as $PtCl_2(CN)_4^{-2}$. A reaction type closely related to the preceeding example does not result in halide ion extrusion from the metal coordination sphere. As a result, a chain of directly bound metal centers does not form. Rather, a chain of alternating metal and halide ions ($\cdots M-X-M-X-M-X\cdots$) is obtained. An example is the formation of Wolfram's red salt, $[Pt^{II}(NH_2Et)_4][Pt^{IV}Cl_2 \cdot (NH_2Et)_4]Cl_4$, from square, d^8 $Pt(NH_2Et)_4^{2+}$ and six-coordinate, d^6 $PtCl_2 \cdot (NH_2Et)_4^{2+}$. In another reaction type, a compact metal cluster may be formed in

*Supported by the National Science Foundation. Manuscript received June 13, 1977.

0077-8923/78/0313-0651 $1.75/1© 1978, NYAS

TABLE 1

CLASSIFICATION OF REACTIONS BETWEEN METAL COMPLEXES WITH METALS IN DIFFERENT FORMAL OXIDATION STATES WITH SELECTED EXAMPLES

Electron-Transfer

$Ni[S_2C_2(CN)_2]_2^{-2} + Ni[S_2C_2(CF_3)_2]_2 = Ni[S_2C_2(CN)_2]_2^{-} + Ni[S_2C_2(CF_3)_2]_2^{-}$ [a]

$FeS_4[S_2C_2(CF_3)_2]_4^{-2} + Fe_4S_4[S_2C_2(CF_3)_2]_4 = 2Fe_4S_4[S_2C_2(CF_3)_2]_4^{-}$ [b]

Direct Metal-Metal Bond Formation Linear Chains

$17Pt^{II}(CN)_4^{2-} + 3\ trans\text{-}Pt^{IV}(CN)_4Cl_2^{2-} + 40K^+ = 20K_2Pt(CN)_2X_{0.3}$ [c]

$2Pd^0(CNCH_3)_x + Pd^{II}(CNCH_3)_4^{2+} = Pd_3(CNCH_3)_8^{2+}$ [d]

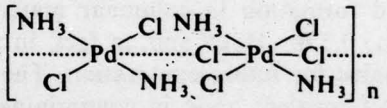
$Hg + Hg^{2+} = Hg_2^{2+}$

Clusters

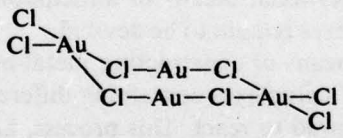
$2[Ir(CO)_4]^- + 2Rh(CO)_2Cl_2^- = Rh_2Ir_2(CO)_{12} + 4Cl^-$ [e]

$Rh_6(CO)_{14}^{4-} + Rh(CO)_2(CH_3CN)_2^+ = [Rh_7(CO)_{16}]^{3-} + 2CH_3CN$ [f]

Ligand Bridge Formation Extended Linear Chains

$Pd^{II}(NH_3)_2Cl_2 + Pd^{IV}(NH_3)_2Cl_4 =$  [g]

Cyclic Chains

$2Au^{I}(CO)Cl + Au_2^{III}Cl_6 =$  $+2CO$

Dimers

$(Et_2NCS_2)_2Mo^{IV}O + (Et_2NCS_2)_2Mo^{VI}O_2 = (Et_2NCS_2)_2Mo(=O)-O-Mo(=O)(S_2CNEt_2)_2$ [e]

[a] DAVISON, A., N. EDELSTEIN, R. H. HOLM & A. H. MAKI. 1963. Inorg. Chem. **2**: 1227.

[b] BALCH, A. L. 1969. J. Am. Chem. Soc. **91**: 6962.

[c] KROGMAN, K. & H. D. HANSEN. 1968. Z. Anorg. Allgem. Chem. **358**: 67.

[d] BALCH, A. L., J. R. BOEHM, H. HOPE & M. M. OLMSTEAD. 1976. J. Am. Chem. Soc. **98**: 7431.

[e] MARTINEGO, S., P. CHINI, V. G. ALBANO, F. CARIATI & T. SALVATORI. 1973. J. Organometallic Chem. **59**: 379.

[f] CHINI, P., G. LONGONI & V. G. ALBANO. 1976. Adv. Organometal. Chem. **14**: 285.

[g] BROSSETT, C. 1948. Arkiv. Kemi. A. **25**: 1.

[h] DELL'AMICO, D. B., F. CALDERAZZO, F. MARCHETTI, S. MERLINO & G. PEREGO. 1977. J. Chem. Soc., Chem. Commun.: 31.

[i] NEWTON, W. E., J. L. CARBIN, D. C. BRAVARD, J. E. SEARLES & J. W. MCDONALD. 1974. Inorg. Chem. **13**: 1100.

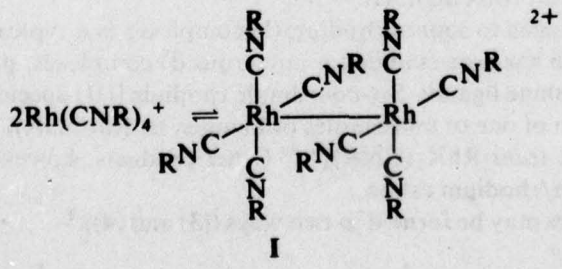
preference to a chain or columnar structure. Such reactions have been used mostly to prepare mixed metal clusters. For example, the reaction of square, d^8 $Rh(CO)_2Cl_2^-$ and tetrahedral d^{10} $Ir(CO)_4^-$ produces the tetrahedral cluster $Ir_zRh_2(CO)_{12}$.[6] The difference between cluster formation in this case and the formation of columns in the previous examples cited in this paragraph cannot be simply correlated with a change in the electronic configuration of the reactants. A related reaction between d^8 Pd(II) and d^{10} Pd(O) isocyanide complexes can produce a linear species $Pd_3(CNR)_8^{2+}$.[7] It is clear that the factors that differentiate between columnar and cluster formation remain to be elucidated. Indeed, the possibility of isomerization between columnar and cluster forms remains a distinct possibility.

Recently, several systems that enable short chains of directly bound metal atoms to be examined in solution have become available. Chains of two, three, four, and more atoms have been observed to exist in solution. The complexes involved include rhodium,[8-11] palladium,[7,12,13] and iridium[14] isocyanide complexes and the platium blues.[15] The discovery of such soluble systems opens up these chains to study by a variety of solution techniques that have been previously unusable. These systems also expand and simplify the synthetic possibilities in this area.

In the sections that follow, we summarize our studies of two systems that produce a rich array of short metal-metal chains that are stable in solution. These systems involve palladium and rhodium with ligands which have been chosen so that they do not sterically interfere with the formation of metal-metal bonds. Among the most versatile of the ligands of this type are isocyanides, carbonyls, and halides.

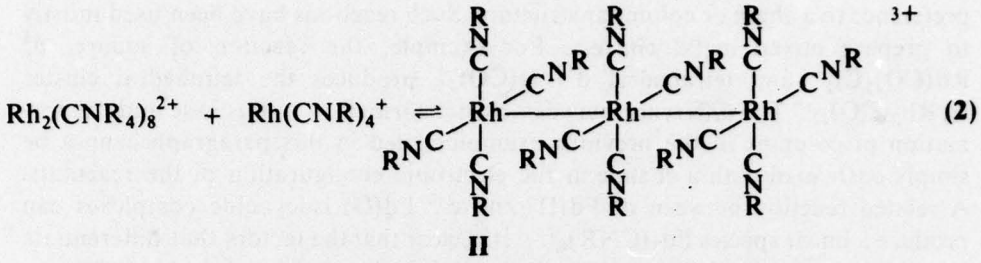
Rhodium Isocyanides

Treatment of a variety of Rh(I) complexes with four or more moles of an isocyanide readily produces the cation $Rh(CNR)_4^+$ (R = alkyl or aryl). Solutions of these cations display a variety of colors that are dependant on the substituent R, the cation concentration, the solvent, and, to a lesser extent, on the anion present. In dilute solutions or with bulky isocyanide substituents these cations are yellow, and they display electronic spectra dominated by metal-to-ligand charge-transfer absorption that are characteristic of planar Rh(I) complexes.[16] More concentrated solutions are red or blue, because of the increase in intensity of new low-energy electronic transitions due to dimeric and trimeric species.[10] The concentration dependence of the intensity of these spectra can be quantitatively analyzed in terms of the Equilibria 1 and 2.[10,17] Although the electronic



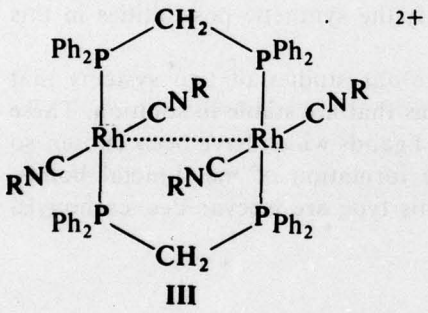
(1)

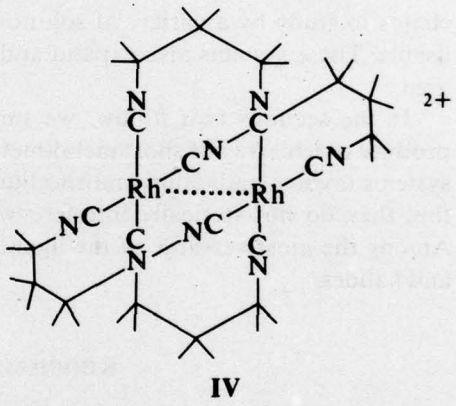
I



(2)

spectra show distinct absorption maxima for both I and II; the infrared absorptions, particularily the CN-stretching frequencies, of the cations remain unaltered by concentration changes. The interpretation of these spectral changes in terms of the formation of dimers and trimers with direct metal-metal bonds is strengthened by the similarity in physical properties of I and of the dimers III and IV, which



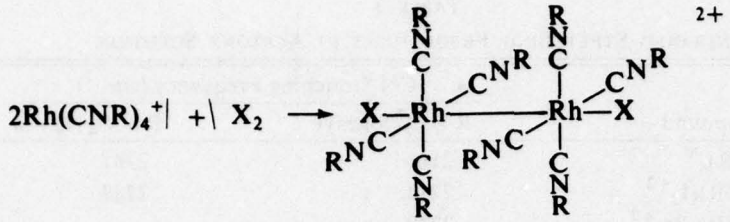


have bridging ligands that constrain the two metal centers to close approach.[8,11]

We have examined the electronic spectra of $Rh(CNCH_2Ph)_4X$ ($X = PF_6^-$ and I^-) in a variety of solvents in order to ascertain the solvent dependence of Equilibria 1 and 2. The thorough study has not been completed, but the following qualitative observations are available. Although solvents and anions do not appreciably alter the position of the electronic band maxima, they do alter the relative band intensities. Consequently, these effects alter the equilibrium constants for Equations 1 and 2 through solvation and ion-pairing effects. The equilibrium constant for Equation 1 decreases in the following order of solvents: chloroform ($K = 5$) > tetrahydrofuran ($K = 3$) > acetonitrile ($K = 1$) ~ methanol ($K = 1$) > acetone ($K = .1$) ~ dichloromethane ($K = .1$).

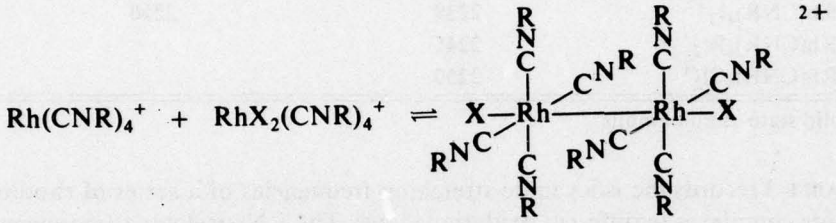
The addition of halogen to square rhodium(I) complexes is a typical oxidative addition reaction which has been studied for numerous d^8 complexes, particularily those containing phosphine ligands. Six-coordinate rhodium(III) species generally are produced. Addition of one or more moles of halogen to $Rh(CNR)_4^+$ in any of its forms does produce *trans*-$RhX_2(CNR)_4^+$.[18] Other products, however, are obtained at lower halogen/rhodium ratios.

Rhodium(II) dimers may be formed in two ways ((3) and (4)).[9]



(3)

V



(4)

V

Reaction 4 is related to the formation of solid $K_2Pt(CN)_4Br_{0.3}(H_2O)_3$ by interaction of $Pt(CN)_4^{-2}$ and $PtBr_2(CN)_4^{-2}$ except that in (4) only one Rh—Rh bond is created and it is stable enough to be maintained in some solutions. The rhodium(II) dimers are rapidly formed by either route. The integrity of these dimers is strongly solvent dependent, since they can rapidly disproportionate by the reverse of reaction 4. TABLE 2 gives the equilibrium constants for reaction 4 in a variety of solvents. Since the equilibrium constants decrease with decreasing dielectric of the solvent, it appears that the ability of the solvent to stabilize the divalent dimer is of major importance in determining the amount of dimer present. Reaction 4 is exothermic; in acetone solution ΔH is +15 kcal/mole for X = I and R = cyclohexyl.[17] In a crude sense this value may be taken as an indication of the Rh—Rh bond energy in V, since the products and reactants of equation 4 differ in number of chemical bonds by the presence or absence of a Rh—Rh bond.

The formation of $Rh_2X_2(CNR)_8^{2+}$ may be readily monitored by either electronic or infrared spectra. Both methods have been used to obtain the equilibrium constants shown in TABLE 2 and good agreement is found between complimentary

TABLE 2

EQUILIBRIUM CONSTANTS FOR THE REACTION

$Rh(CNC_6H_{11})_4^+ + RhX_2(CNC_6H_{11})_4^+ \rightleftharpoons Rh_2(CNC_6H_{11})_8X_2^{2+}$

Solvent	Dielectric Constant	K (at 23°)	
Dimethylsulfoxide	46.7	5.8×10^3	X = I
Acetonitrile	38.8	4.7×10^3	
Nitromethane	35.9	2.8×10^3	
Acetone	20.7	3.2×10^2	
Dichloromethane	8.9	<10	
Chloroform	4.7	<10	
Acetonitrile	38.8	2×10^4	X = Br

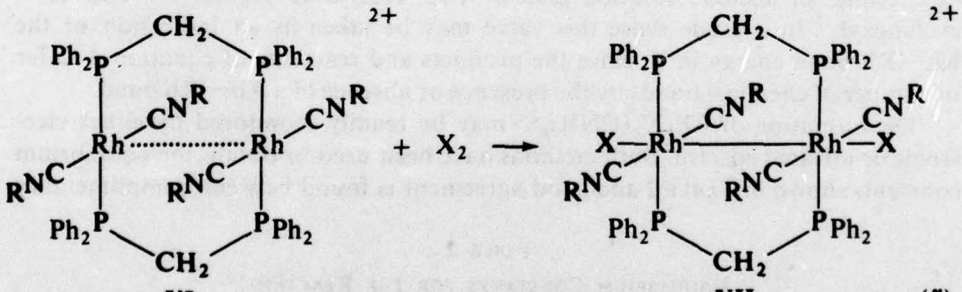
TABLE 3
INFRARED STRETCHING FREQUENCIES IN ACETONE SOLUTION

Compound	CN Stretching Frequency (cm^{-1})	
	R = cyclohexyl	R = $C_4H_9 - n$
$Rh(CNR)_4^+$	2168	2181
$Rh_2(CNR)_8I_2^{+2}$	2214	2228
$Rh_2(CNR)_8Br_2^{+2}$	2220	
$Rh_2(CNR)_8Cl_2^{+2}$	2220	
$Rh(CNR)_4I_{1.66}$	2227, 2205*	2239, 2215*
$Rh(CNR)_4I_2^+$	2239	2250
$Rh(CNR)_4Br_2^+$	2245	
$Rh(CNR)_4Cl_2^+$	2250	

*In solid state as nujol mulls.

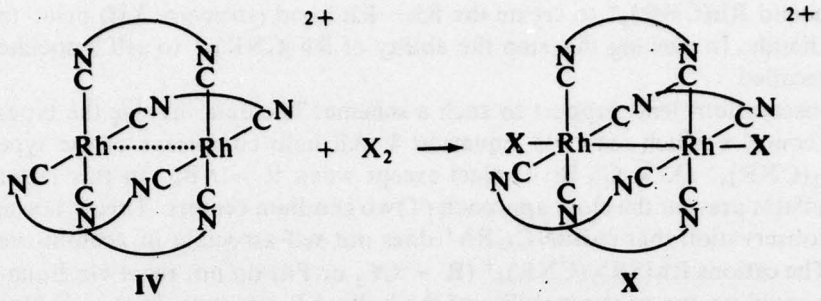
data. TABLE 3 records the isocyanide-stretching frequencies of a series of rhodium isocyanide complexes in different oxidation states. The CN-stretching frequency is a sensitive probe of electron density at the metal centers. As rhodium increases its formal oxidation state, the CN-stretching frequency increases because of reduced π donation from metal to ligand.

The products of Equations 3 and 4 are formulated as dimers with directly bonded rhodium atoms. Although a number of crystalline salts containing these cations have been isolated, no direct x-ray structural data are available on these systems. However, some related chemistry supports these structural assignments. Dimeric Rh(I) species in which the metal centers are held closely by bridging ligands undergo oxidation by halogen according to Equations 5–7.[9,11] Of the species involved



VI VII (5)

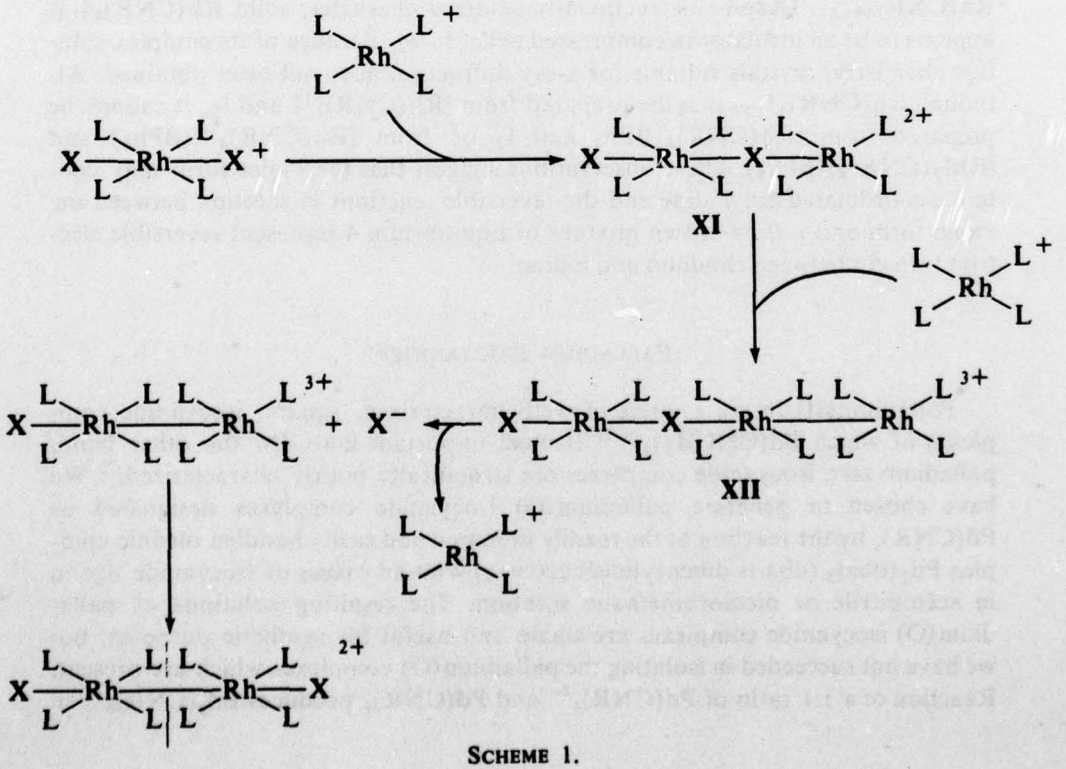
VIII IX (6)



IV X (7)

in these reactions, the structure of $Rh_2(CO)_2Cl_2(Ph_2AsCH_2AsPh_2)_2$ has been determined crystallographically.[9] The electronic and infrared spectra (CN stretching frequencies) of V, VII, and X are similar.

How do Rh(II) dimers of the type $Rh_2(CNR)_8X_2^{2+}$ form? The mechanism of Reaction 4 is intriguing, since it occurs within the time required to mix reagents and yet involves expulsion of a halide ligand from $RhX_2(CNR)_4^+$. The straightforward route for reaction *via* dissociation of a halide from $RhX_2(CNR)_4^+$ appears to be unlikely if the rate of ligand loss from the complex is comparable to the rate of ligand dissociation from other low spin d^6 complexes. Rather we suspect that reaction 4 may occur *via* a path that is related to the Pt(II) catalized mechanism for substitution in Pt(IV) complexes. In the present case a key step may involve the association of a rhodium(I) and rhodium(III) center *via* a linear halo bridge (structure XI) as shown in Scheme 1. This step could be followed by addi-



XI XII

SCHEME 1.

tion of a second $Rh(CNR)_4^+$ to create the Rh—Rh bond (*structure* **XII**) prior to the loss of halide. In viewing this step the ability of $Rh(CNR)_4^+$ to self associate should be recalled.

Some observations lend support to such a scheme. The data involve the types of Rh(III) complex which react via Equation 4. All halo complexes of the type *trans*-$RhX_2(CNR)_4^+$ (X = Cl, Br, I) react except when R = *t*-Bu. In this latter case steric effects prevent the close approach of two rhodium centers. This is borne out by the observation that $(t\text{-BuNC})_4Rh^+$ does not self-associate in acetonitrile solution.[8] The cations $Rh(SR)_2(CNR)_4^+$ (R = CF_3 or Ph) do not react via Equation 4; this could be due to the inability of the bulky SR group to form a bridge (structure **XI**) between two rhodium centers. Additionally $CH_3RhI(CNR)_4^+$ and $CH_3\overset{O}{\overset{\|}{C}}RhCl(CNR)_4^+$ are unreactive in Reaction 4. In these cases, although bridged intermediates could be formed through the halo ligands, the alkyl or acyl groups would not function as leaving groups to allow the reaction cycle to be completed through ligand loss from **XII**. We are investigating the kinetics of Reaction 4 in order to gain more definitive mechanistic information.

Oxidation of $Rh(CNR)_4I$ with $\frac{1}{3}$ mole of I_2 produces a distinct new material $Rh(CNR)_4I_{1.67}$ (or $Rh_3(CNR)_{12}I_5$). This crystalline material contains only terminal isocyanide ligands as shown by the CN-stretching frequencies in TABLE 2. This solid is violet, and it dissolves in most solvents to give transiently violet solutions that become yellow-brown after varying times. These yellow-brown solutions are mixtures of $Rh(CNR)_4^+$, $Rh_2(CNR)_8I_2^{2+}$, and $RhI_2(CNR)_4^+$ governed by Equilibrium 4. Evaporation of these solutions reforms solid violet $Rh(CNR)_4I_{1.67}$. Despite its fractionally oxidized character, solid $Rh(CNR)_4I_{1.67}$ appears to be an insulator in compressed pellet form. Because of its complex solution chemistry, crystals suitable for x-ray diffraction have not been obtained. Although $Rh(CNR)_4I_{1.67}$ may be prepared from $[Rh(CNR)_4]I$ and I_2, it cannot be prepared from $[Rh(CNR)_4]BPh_4$ and I_2 or from $[Rh(CNR)_4^+](BPh_4)$ and $[RhI_2(CNR)_4](BPh_4)$. These observations suggest that the violet form may contain a coordinated polyhalide and the reversible reactions in solution between the violet form and yellow-brown mixture of Equilibrium 4 represent reversible electron transfer between rhodium and iodine.

PALLADIUM ISOCYANIDES

Palladium(II) forms a series of well-characterized, square, isocyanide complexes of which $Pd(CNCH_3)_4^{2+}$ [21] is most important here. On the other hand, palladium zero isocyanide complexes are structurally poorly characterized.[22] We have chosen to generate palladium(O) isocyanide complexes designated as $Pd(CNR)_x$ by the reaction of the readily prepared and easily handled olefinic complex $Pd_2(dba)_3$ (dba is dibenzylideneacetone) with an excess of isocyanide ligand in acetonitrile or dichloromethane solution. The resulting solutions of palladium(O) isocyanide complexes are stable and useful for synthetic purposes, but we have not succeeded in isolating the palladium(O) complexes which are present. Reaction of a 1:1 ratio of $Pd(CNR)_4^{2+}$ and $Pd(CNR)_x$ produces $Pd_2(CNR)_6^{2+}$ in

greater than 90% yield (**8**). The dication derived from methyl isocyanide has been fully

$$Pd(CNR)_4^{2+} + Pd(CNR)_x \rightarrow Pd_2(CNR)_6^{2+} \quad (8)$$

characterized by an x-ray structure determination.[24] The structure, shown in FIGURE 1, consists of a short (2.531 Å) Pd—Pd bond and only terminal isocyanides. An analogous reaction (**9**) between platinum complexes produces a structurally

$$Pt(CNR)_4^{2+} + Pt(CNR)_x \rightarrow Pt_2(CNR)_6^{2+} \quad (9)$$

similar platinum dimer. The palladium dimer is fluxional, but there is no evidence

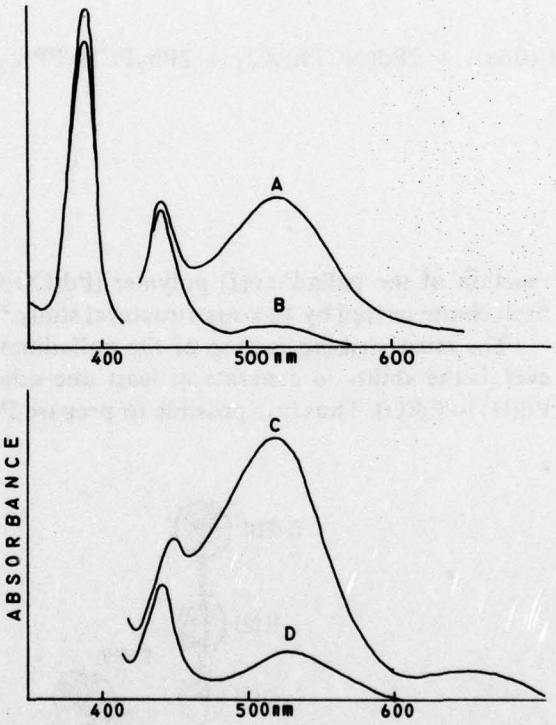


FIGURE 1. The electronic spectrum of $Rh(CNCH_2C_6H_5)_4PF_6$ in various solvents. The solvent concentration and cell-path length are as follows: A, tetrahydrofuran, .01 F, 0.1 cm; B, tetrahydrofuran, .001 F, 1.0 cm; C, chloroform, .01 F, 0.1 cm; D, acetonitrile, .01 F, 0.1 cm.

for fluxional behavior in the platinum compound.[25] The activation energy for axial-equitorial ligand interchange in $Pd_2(CNCH_3)_6^{2+}$ is 13.8 kcal/mole. The process appears to be intraionic and may occur through electronic redistribution in the Pd—Pd bond to give a Pd(O)—Pt(II) intermediate with tetrahedral geometry at one palladium center and planar geometry at the other.

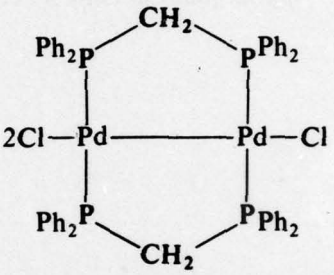
The bond strength in these palladium and platinum dimers must be considerably stronger than in the case of the rhodium(II) dimers discussed in the previous section. No evidence of fragmentation of these cations into radicals has been found. The mixed-metal derivative $PtPd(CNCH_3)_6^{2+}$ is formed in high purity and high yield via Reaction 10. The fact that this mixed-metal species may be

$$Pt(CNCH_3)_4^{2+} + Pd(CNCH_3)_x \rightarrow PtPd(CNCH_3)_6^{2+} \quad (10)$$

prepared essentially free of the homonuclear dimers $Pd_2(CNCH_3)_6^{2+}$ and $Pt_2(CNCH_3)_6^{2+}$ and can be maintained pure in solution for periods of more than a day, attests to the strength of the metal-metal bond.

Other Pd(I) dimers can also be prepared by the reactions of Pd(II) and Pd(O) species in the presence of appropriate ligands. Some examples are shown in equations 11[25] and 12.[26] Product **XIII** has been prepared previously from the

$$Pd_2(dba)_3 + 2PdI_2 + 8PhNC \rightarrow 2Pd_2I_2(CNPh)_4 + 3dba \quad (11)$$

$Pd_2(dba)_3 + 2Pd(NCPh)_2Cl_2 + 2Ph_2PCH_2PPh_2 \rightarrow$ 

XIII (12)

reaction of the palladium(I) polymer $[Pd(CO)Cl]_x$ with $Ph_2PCH_2PPh_2$ and has been characterized by an x-ray structural study.[27]

The most striking feature of the palladium(II)-palladium(O) reactions, however, is the ability to generate at least one other species by altering the ratio of Pd(II) to Pd(O). Thus it is possible to prepare $Pd_3(CNCH_3)_8^{2+}$ by either Reaction

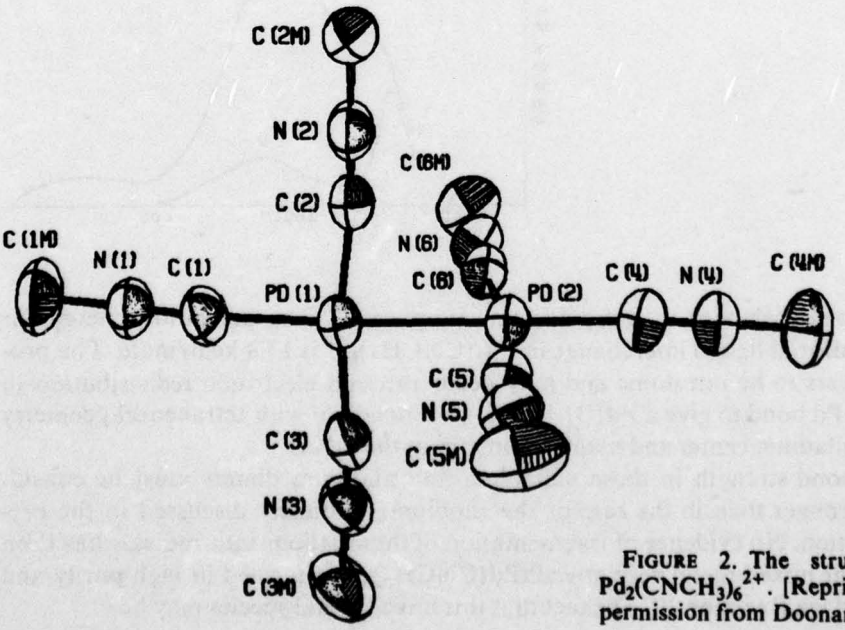


FIGURE 2. The structure of $Pd_2(CNCH_3)_6^{2+}$. [Reprinted with permission from Doonan *et al.*[12]]

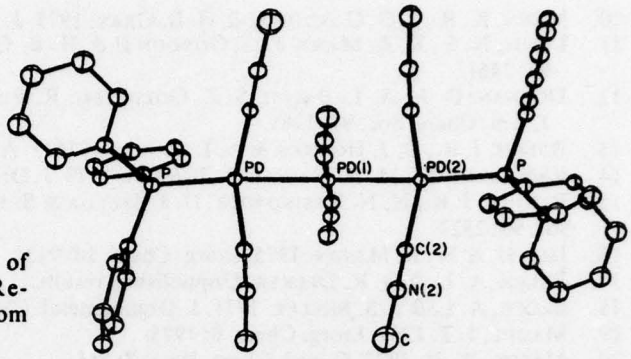


FIGURE 3. The structure of $Pd_3(CNCH_3)_6(PPh_3)_2^{2+}$ [Reprinted with permission from Balch *et al.*[7]]

13 or 14. Like $Pd_2(CNCH_3)_6^{2+}$, which forms the axially substituted

$$Pd(CNCH_3)_4^{2+} + 2Pd(CNCH_3)_x \rightarrow Pd_3(CNCH_3)_8^{2+} \quad (13)$$

$$Pd_2(CNCH_3)_6^{2+} + Pd(CNCH_3)_x \rightarrow Pd_3(CNCH_3)_8^{2+} \quad (14)$$

$Pd_2(CNCH_3)_4(PPh_3)_2^{2+}$ when treated with triphenylphosphine, $Pd_3(CNCH_3)_8^{2+}$ also reacts with triphenylphosphine to yield axially substituted $Pd_3(CNCH_3)_6 \cdot (PPh_3)_2^{2+}$. The last complex has been characterized by an x-ray structural study. Its structure is shown in FIGURE 3.[7] The Pd—Pd distance (2.5921) in this linear tripalladium species is only slightly longer than that distance in $Pd_2(CNCH_3)_6^{2+}$. In other aspects as well, these two cations are structurally related. We are continuing to investigate the possibility of constructing longer palladium and platinum chains by further alterations in the M(II)-M(O) ratio.

ACKNOWLEDGMENTS

I thank my coworkers Marilyn Olmstead, Joel S. Miller, Dan Doonan, John Boehm, Linda Benner, Gerry Delker, and Professor H. Hope for their contributions to this work, and the Matthey Bishop Corporation for a generous loan of precious metal salts.

REFERENCES

1. MILLER, J. S. & A. J. EPSTEIN. 1976. Prog. Inorg. Chem. **20:** 1.
2. KEEFER, K. D., D. M. WESHECHECK, N. P. ENRIGHT & J. M. WILLIAMS. 1976. J. Am. Chem. Soc. **98:** 233; REIS, JR., A. H., S. W. PETERSON, D. M. WASHECHECK & J. S. MILLER. 1976. J. Am. Chem. Soc. **98:** 234.
3. GINSBERG, A. P., J. W. KOEPKE, J. J. HAUSER, K. W. WEST, F. J. D. SALVO, C. R. SPRINKLE & R. L. COHEN. 1976. Inorg. Chem. **15:** 514.
4. KROGMAN, K. & H. D. HAUSEN. 1968. Z. Anorg. Allg. Chem. **358:** 67.
5. CRAVEN, B. M. & D. HALL. 1961. Acta Crystallogr. **14:** 475.
6. MARTINENGO, S., P. CHINI, V. G. ALBANO, F. CARIATI & T. SALVATORI. 1973. J. Organometal. Chem. **59:** 379.
7. BALCH, A. L., J. R. BOEHM, H. HOPE & M. M. OLMSTEAD. 1976. J. Am. Chem. Soc. **98:** 7431.
8. BALCH, A. L. & M. M. OLMSTEAD. 1976. J. Am. Chem. Soc. **98:** 2354.
9. BALCH, A. L. 1976. J. Am. Chem. Soc. **98:** 8049.

10. MANN, K. R., J. G. GORDON II & H. B. GRAY. 1975. J. Am. Chem. Soc. **97:** 3553.
11. LEWIS, N. S., K. R. MANN, J. G. GORDON II & H. B. GRAY. 1976. J. Am. Chem. Soc. **98:** 7461.
12. DOONAN, D. J., A. L. BALCH, S. Z. GOLDBERG, R. EISENBERG & J. S. MILLER. 1975. J. Am. Chem. Soc. **97:** 1961.
13. BOEHM, J. R., D. J. DOONAN & A. L. BALCH. 1976. J. Am. Chem. Soc. **98:** 2129.
14. KAWAKAMI, K., M.-A. HAGA & T. TANAKA. 1973. J. Organometal Chem. **60:** 363.
15. BARTON, J. K., H. N. RABINOWITZ, D. J. SZALDA & S. J. LIPPARD. 1977. J. Am. Chem. Soc. **99:** 2827.
16. ISCI, H. & W. R. MASON. 1975. Inorg. Chem. **14:** 913.
17. BALCH, A. L. & G. R. DELKER. Unpublished results.
18. BALCH, A. L. & J. S. MILLER. 1971. J. Organometal. Chem. **32:** 263.
19. MAGUE, J. T. 1969. Inorg. Chem. **8:** 1975.
20. MASON, W. R. 1972. Coord. Chem. Revs. **7:** 241.
21. MILLER, J. S. & A. L. BALCH. 1972. Inorg. Chem. **11:** 2069.
22. MALATESTA, L. 1955. J. Chem. Soc.: 3924; OTSUKA, S., A. NAKAMURA & Y. TATSUNO. 1969. J. Am. Chem. Soc. **91:** 6994.
23. UKAI, T., H. KAWAZURA, Y. ISHII, J. J. BONNETT & J. A. IBERS. 1974. J. Organometal. Chem. **65:** 253.
24. GOLDBERG, S. Z. & R. EISENBERG. 1976. Inorg. Chem. **15:** 535.
25. BOEHM, J. R. & A. L. BALCH. 1977. Inorg. Chem. **16:** 778.
26. BENNER, L. S. & A. L. BALCH. Unpublished results.
27. HOLLOWAY, R. G., B. R. PENFOLD, R. COLTON & M. J. MCCORMICK. 1976. J. Chem. Soc., Chem. Comm.: 485.

DISCUSSION

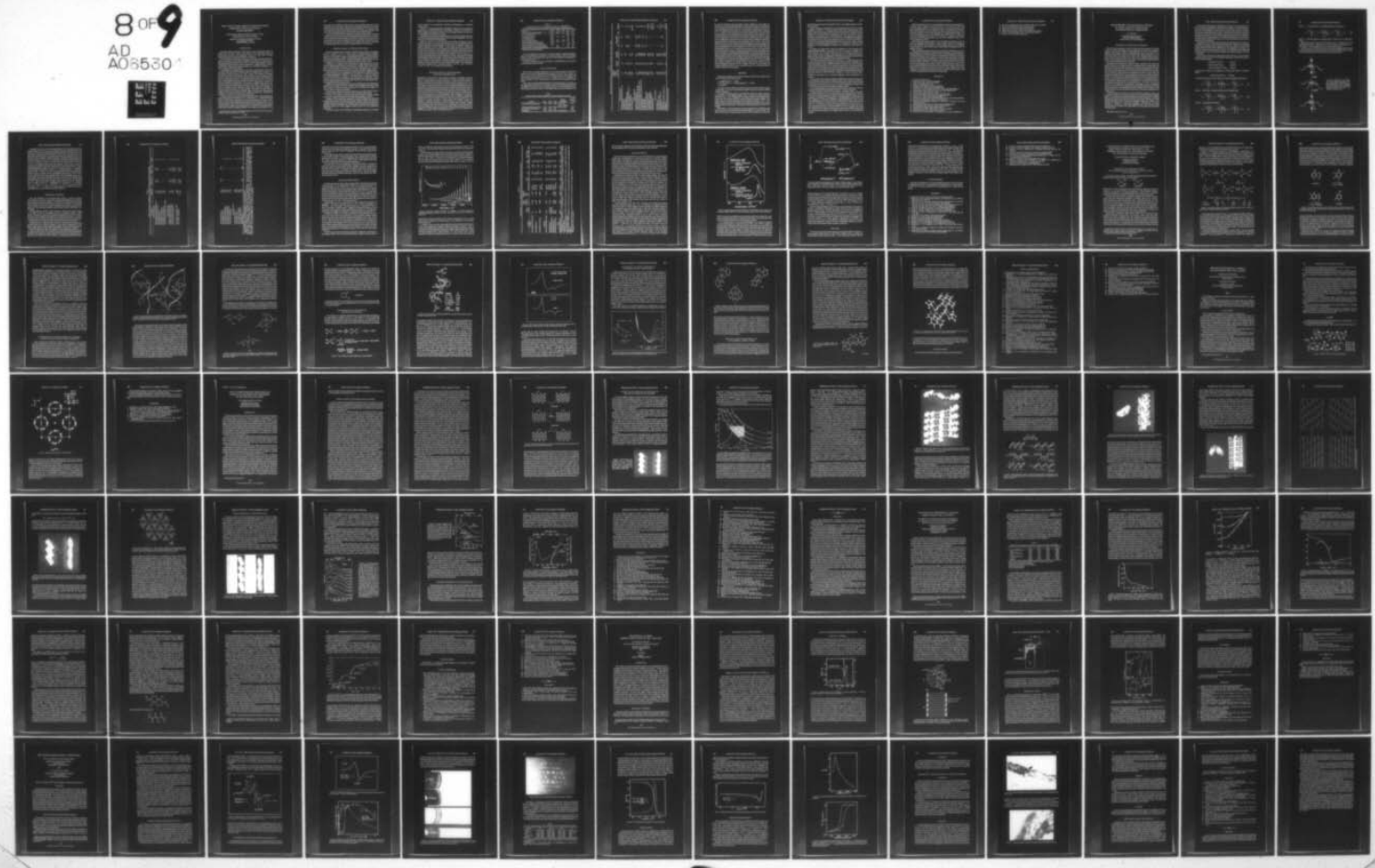
HEIMO KELLER (*University of Heidelberg, Heidelberg, Germany*): What are the arguments for this dimerization of the Rh(II) compound?

BALCH: The monomer formulation would not be diamagnetic; however, nmr spectra and bulk susceptibility measurements indicate that the material is diamagnetic. Also, the physical properties of the phosphine ligand bridged Rh(II) species and $Rh_2(CNR)_8X_2^{2+}$ are similar. Direct molecular weight measurements in solution are not useful, due to the partial dissociation of $Rh_2(CNR)_8X_2^{+}$ into $Rh(CNR)_4^{+}$ and $Rh(CNR)_4X_2^{+}$.

[**Note added in proof:** Recent x-ray crystal structure results on $(p\text{-}CH_3C_6H_4NC)_8 \cdot Rh_2I_2^{2+}$ establish the presence of the linear I—Rh—Rh—I unit. The Rh—Rh bond length is 2.875 Å (M. M. Olmstead & A. L. Balch. 1978. J. Organometal. Chem. 148, C15).]

AD-A065 304 NEW YORK ACADEMY OF SCIENCES N Y F/G 7/2
SYNTHESIS AND PROPERTIES OF LOW-DIMENSIONAL MATERIALS,(U)
1978 J S MILLER, A J EPSTEIN N00014-77-C-0374
UNCLASSIFIED NL

8 OF 9
AD A065304




OF 9
5304

NEW LINEAR CHAIN MIXED-VALENCE PLATINUM COMPLEXES WITH AND WITHOUT HALIDE BRIDGES*

Helmut Endres, Mohammed El Sharif, Heimo J. Keller, Reinhold Martin, and Ulrich Träger

Anorganisch-Chemisches Institut der Universität
Im Neuenheimer Feld 270
D 6900 Heidelberg, Germany

INTRODUCTION

The mixed-valence chemistry of platinum has been arousing the interest of chemists for more than a century, even though it took a long time before the mixed-valence character was recognized. As early as 1842, Knop[1] obtained copper-like crystals on oxidizing $K_2Pt(CN)_4$ with chlorine.

In 1855 Schafarik[2] observed the formation of lustrous substances when handling cyanoplatinates. The oxidation of $K_2Pt(CN)_4$ by HNO_3 to copper-like needles was reported by Weselsky[3] in 1856. Wilm[4] reanalyzed the oxidation product of $K_2[Pt(CN)_4]$ with chlorine and found a composition, $K_2[Pt(CN)_4]Cl_{0.33} \cdot 11H_2O$. In 1896 Werner[5] dealt with oxidation reactions on compounds $K[PtCl_3a]$ (a = NH_3, pyridine) and $K_2[Pt(oxalate)_2]$.

The possibility of oxidizing Peyrone's Chloride, *cis*-$PtCl_2(NH_3)_2$ with air was reported in 1886, followed by a detailed study by Tschugajeff and coworkers[7,8] on the oxidation reactions with O_2, O_3, $S_2O_8^{2-}$, H_2O_2. The reaction of Peyrone's Chloride with sulfuric acid yielding a black substance with incorporated sulfato groups was observed by Drew[9] and reinvestigated by Gillard and Wilkinson.[10] From crystallographic data, the compound was assumed to have a Pt—Pt chain with an intermetallic separation of 3.06 Å. Cahen[11] repeated the oxidation of Peyrone's Chloride by $(NH_4)_2S_2O_8$. The product is different from the one described by Gillard and Wilkinson and contains, from ESCA measurements, two kinds of platinum species. Different products form when the oxidation of Peyrone's Chloride is carried out in the presence of $K_2[PtCl_4]$[5] or $(NH_4)_2PtCl_6$.[11] Coppery needles were obtained, the ESCA spectra of which show only one kind of platinum. It must be noted that all the oxidation reactions of *cis*-$PtCl_2(NH_3)_2$ cited above work with the *cis* form of the complex only.

Oxidation reactions to (presumably) mixed-valence systems have been reported with other platinum compounds, too, e.g. $[Pt(NH_3)_4]^{2+}$,[12] "MGS"$[Pt(NH_3)_4][PtCl_4]$[7,13] and $PtenCl_2$.[7] According to our present knowledge, two types of structures can form on oxidizing platinum(II) compounds if the oxidation does not run straight to Pt(IV). They are chains of directly interacting platinum atoms such as in the partially oxidized tetracyanoplatinates,[14] or chains of alternating Pt(II)–Pt(IV) species linked by bridging halogens, the Wolffram's Salt analogs.[15] In the

*Supported by the Deutsche Forschungsgemeinschaft and by the Fonds der Chemischen Industrie. Manuscript received June 13, 1977.

0077-8923/78/0313-0663 $1.75/1© 1978, NYAS

latter case, the two different oxidation states of the platinum atoms can be distinguished. The compounds are therefore to be grouped in class II of the scheme for mixed-valence compounds proposed by Robin and Day.[16] In the former case, only one kind of platinum can be found, mostly with a nonintegral oxidation number, and the compounds belong to class III of the mixed-valence scheme.

Aiming at the synthesis of new highly anisotropic materials based on platinum complexes, several questions must be answered: Which molecular features and reaction conditions favor the forming of each of the two types of structures, and how can the electronic interactions along the chains in each type of structure be enhanced? For that reason a systematic test of ligands and reaction conditions, crystallizing experiments, and x-ray investigations have to be carried out.

Reactions Leading to Pt-Halogen-Pt Chains

A series of compounds of the general composition $Pt(a\text{-}a)_2XY_2$ was prepared, where X = Cl, Br, I, Y = Br^-, I^-, ClO_4^- and a-a is a diamino ligand. As ligands we used 1,2-diaminoethane (en), 1,2-diaminopropane(dapn), 2,3-diaminobutane-(dabn), and 1,2-diamino-2-methyl-propane(daibn). Some preparative procedures and structural properties of ClO_4^- containing Wolffram's Salt analogues were reported earlier.[15] In the following we describe compounds with X = Br, I.

$Pt(dapn)_2Br_3$ is prepared from $Pt(dapn)_2Cl_2$ by precipitating the chloride ions with Ag_2O and acidifying the basic solution with HBr. One half the aqueous solution of $Pt(dapn)_2Br_2$ is oxidized with bromine to $Pt(dapn)_2Br_4$. The two solutions are poured together and evaporated *in vacuo*. The golden shiny residue is dissolved in methanol and precipitated as a deep-blue powder by adding acetone.

Crystals suited for x-ray investigations can be obtained by a diffusion method described by Guggenheim and Bahnck:[17] the two halves of a U-tube are separated by a Teflon® membrane; a solution of the blue powder in methanol (and an amount of acetone just not sufficient to cause precipitation) is filled into one half the tube, and pure acetone into the other half. After four to six days, golden shiny, strongly dichroic platelets have formed.

$Pt(dabn)_2Br_3$ is precipitated from a solution of $Pt(dabn)_2Br_2$ and $Pt(dabn)_2Br_4$ in glycol by the addition of acetone. The green shiny precipitate becomes red and then colorless on drying. The color change can be reversed by the addition of acetone. Crystals could not be obtained.

$Pt(daibn)_2Br_3$, prepared by the above procedure, is a yellow powder that becomes red on drying *in vacuo*. Exposed to the air, it becomes yellow again.

$Pt(a\text{-}a)_2I_3$. The analogous reactions with iodine instead of bromine yielded only brown to blue-brown powders with unsatisfying elementary analyses.

$Pt(dapn)_2I_3$. When the powder supposed to be mainly $Pt(dapn)_2I_3$ is dissolved in methanol and several ml of *n*-butanol and the solution allowed to evaporate by standing (the butanol slows down the evaporation process), golden shiny, dichroic, platelike crystals form together with a brown powder. X-ray structure analysis and elementary analysis for iodine suggest that the crystals have the composition $Pt(dapn)_2I_3$.

The same procedure with "$Pt(dabn)_2I_3$" yields golden crystals, too, but these

are not suited for x-ray investigations. Starting with $Pt(daibn)_2I_3$, no crystalline product forms.

$PtenCl_3$. As already described by Tschugajeff,[7] *cis*-$PtenCl_2$ can be oxidized by $(NH_4)_2S_2O_8$ to a compound $PtenCl_3$. The oxidation works only if several ml of HCl are added; other acids have no effect. X-ray investigations show that the compound belongs to the Wolffram's Salt type.

If $Pt(dapn)Cl_2$ is used as starting material, two fractions of crystals can be isolated: the unchanged $Pt(dapn)Cl_2$ and the Pt(IV) complex $Pt(dapn)Cl_4$. The same observation can be made with $Pt(dabn)Cl_2$.

$Pten_2X_2 + CuX_2$, X = Cl, Br. The reaction of $CuCl_2$ on $Pten_2Cl_2$ was described by Kurnakow[18] to yield metallic shiny crystals. We repeated the reaction, using the chlorides and the bromides. In both cases we obtained needles, the metallic appearance and the stability of the crystals being more pronounced for the bromo compound. X-ray investigations showed the compounds to be isomorphic and to belong to the hexagonal system. They differ only in the length of the *c*-axis, which is parallel to the needle axis. The length of *c* (10.52 Å for X = Cl, 11.02 for Br) and the characteristic distribution of strong- and weak-layer lines on rotating crystal photographs make it probable that the compounds are analogs of the Wolffram's Salt. A complete structure determination is being carried out mainly to obtain an explanation for the different EPR properties of the two compounds (the chloro compound has a pronounced EPR signal that is missing for the bromo analogue), and to determine whether —Pt—X——Pt——X—Pt— or —Pt—X—Cu—X—Pt-chains occur in the lattice.

Reactions Leading to Chain Structures other than Wolffram's Salt

Oxidation of cis-$PtCl_2(NH_3)_2$. The oxidation of Peyrone's Chloride by $(NH_4)_2S_2O_8$ to a black powder was reported earlier.[7,11] Using a powdered sample of Peyrone's Chloride which has been recrystallized several times, crystals can be obtained that allow the determination of the metal-metal separation by x-rays. The distance was found to be 3.45 Å, and two metal-metal separations give the length of the unit cell in chain direction. Since the oxidation products of Peyrone's Chloride with $(NH_3)_2S_2O_8$ can be stabilized in solution with perchloric acid, we investigated the influence of $HClO_4$ and other substances on the crystallizing properties and the structure of the oxidation product. The oxidation product was dissolved in an aqueous solution containing $HClO_4$, HBF_4, $K_2[PtCl_4]$, or $K_2[PdCl_4]$. Copper-like needles were obtained which, in the case of $K_2[PtCl_4]$, allowed the determination of type of structure and of the metal-metal separation by x-ray methods. In another experiment, *cis*-$PtCl_2(NH_3)_2$ was directly oxidized by $K_2[PtCl_6]$. Analytical data listed in Table 1, together with IR spectra, suggest that the additional ions in the solution are not incorporated into the crystals. The analytical findings show that the substances obtained have practically the same composition. The data might be interpreted by a formulation of the compounds as $Pt(NH_3)_2Cl_{3-x}(OH)_x$, where x varies from 0.27 to 0.7.

TABLE 1

ANALYTICAL DATA OF THE OXIDATION PRODUCTS OF *cis*-$PtCl_2(NH_3)_2$ WITH $(NH_3)_2S_2O_8$ OBTAINED FROM SOLUTIONS CONTAINING ADDITIONAL IONS

Conditions	% Pt	% Cl	% O	% N	% H
Calculated for $Pt(NH_3)_2Cl_2OH$	61.5	22.4	5.1	8.8	2.2
Prep. as in Reference 7	61.6*			8.0	2.75
From $HClO_4$ solution	57.9	23.9	6.82	8.4	2.17
From HBF_4 solution	58.9*			7.8	2.2
From $K_2[PtCl_4]$ solution	61.6	24.6	4.33	8.15	2.27
Oxid. by $K_2[PtCl_6]$ in HCl solution	59.87	25.51	4.23	8.17	1.98
Oxid. by $K_2[PtCl_6]$ in $HClO_4$ solution	62.3*			7.64	2.16
Cahen's product[11] (oxid. by $(NH_3)_2S_2O_3$)	61.6	21.5	5.1	8.0	2.45
Cahen's product[11] (oxid. by $(NH_3)_2[PtCl_6]$		25.4		8.1	2.1

*Residue from N,H determination.

X-ray investigations of the crystals from the solution containing $K_2[PtCl_4]$ show that the compound crystallizes in a columnar structure with a metal-metal distance of 3.06 Å, the length of the unit cell in chain direction comprising four metal-metal separations.

Analogous reactions were tried, starting with *cis*-$PtBr_2(HN_3)_2$, but no mixed-valence product could be isolated.

X-RAY INVESTIGATIONS

Some of the x-ray results, especially for the oxidation products of Peyrone's chloride and its bis(1,2-diaminoethane) analog as well as for the reaction of $Pten_2X_2$ with CuX_2, have been given in the preceding sections. This section will deal with structural problems we have encountered with the Pt—halogen—Pt chain compounds. TABLE 2 contains some crystal data of the compounds investigated.

The compound $[Pt(en)_2][Pt(en)_2Br_2](ClO_4)_4$ was characterized by us earlier as belonging to the monoclinic system. Using a crystal from another preparation for the collection of intensity data, we found the crystal to be orthorhombic with the lattice parameters given in TABLE 2. Nevertheless, the unit cell axis parallel to the

TABLE 2

CRYSTAL DATA OF SOME COMPOUNDS WITH Pt—HALOGEN—Pt CHAIN

Formula	*a*(Å)	*b*(Å)	*c*(Å)	Possible Spacegroups	Pt—Pt Separation (Å)
$[Pt(dapn)_2][Pt(dapn_2)Br_2]Br_4$	5.359	6.882	19.788	Imm2, I222, $I2_12_12_1$, Immm	5.359
$[Pt(dapn)_2][Pt(dapn_2)I_2](ClO_4)_4$	5.726	7.609	19.644	$Pmc2_1$, Pmma	5.726
$[Pt(en)_2][Pt(en_2)Br_2](ClO_4)_4$	10.982	10.18	14.31		5.491
$[Pt(dapn)_2]I_3$	5.770	7.300	19.981	Pnm2, Pnmm	5.770

TABLE 3

CRYSTALLOGRAPHIC FINDINGS OF COMPOUNDS WITH LINEAR —M—X—M— CHAINS

	Repeating Distance in Chain Direction (A)	1-D Superstructure	M-M Separation (A)	Bond Lengths (A) M—X	——M	Reference
Chloro Compounds						
$[Pt(NH_2C_2H_5)_4][Pt(NH_2C_2H_5)_4Cl_2]Cl_4$ "Wolffram's Red"	5.39	yes	5.39	2.26	3.13	20
$[PtenCl_2][PtenCl_4]$	5.481	no	5.481	—	—	21
$[Pd(NH_3)_2Cl_2][Pd(NH_3)_2Cl_4]$	5.21	yes	—	1.99	3.22	22
$[(Pd,Pt)(NH_3)_2Cl_2][Pd,Pt](NH_3)_2Cl_4]$	5.33	yes	—	2.03	3.30	22
$[Pten_2][Pten_2Cl_2](ClO_4)_4$	10.90	no	5.45	—	—	15
$[Pt(en)_2Cl]_6[CuCl_4]_4$*	10.522	no	5.261	—	—	this work
Bromo Compounds						
$[Pt(NH_3)_2Br_2][Pt(NH_3)_2Br_4]$	5.53	yes	5.53	2.50	3.03	23
$[Pt(NH_2C_2H_5)_4][Pt(NH_2C_2H_5)_4Br_2]Br_4$	12.14	yes	6.07	2.42	3.19	24
$[Pt(NH_2C_2H_5)_4][Pt(NH_2C_2H_5)_4Br_2]Br_4 \cdot 4H_2O$	5.586	yes	5.686	2.479	3.139	25
$[Pt(NH_2C_2H_5)_4][Pt(NH_2C_2H_5)_4Br_2]Br_4 \cdot 4H_2O$	5.606	yes	5.606	—	—	26
$[PtenBr_2][PtenBr_4]$	5.60	yes	5.60	2.48	3.125	27
$[PtenBr_2][PtenBr_4]$	5.606	no	5.606	—	—	21
$[Pt(NH_3)_2Br_2][Pt(NH_3)_2Br_4]$	5.54	yes	—	2.17	3.37	22
$[Pten_2][Pten_2Br_2](ClO_4)_4$*	10.982	no	5.491	—	—	this work
$[Ptdapn_2][Ptdapn_2Br_2](ClO_4)_4$	5.64	yes	5.64	—	—	15
$[Ptdapn_2][Ptdapn_2Br_2]Br_4$*	5.359	yes	5.359	—	—	this work
$[Pten_2Br]_3[CuBr_4]_2$*	11.02	no	5.501	—	—	this work
Iodo Compounds						
$[PtenI_2][PtenI_4]$	5.862	no	5.862	—	—	21
$[Pten_2][Pten_2I_2](ClO_4)_4$	6.05	yes	6.05	—	—	15
$[Ptdapn_2][Ptdapn_2I_2](ClO_4)_4$*	5.726	yes	5.726	—	—	this work
$K_4[PtI_4][PtI_6]$	5.74	no	5.74	2.74	3.00	28
$[Pt(NH_2C_2H_5)_4][Pt(NH_2C_2H_5)_4I_2]I_4$	12.732	?	6.366	—	—	26
$[Pt(dapn)_2]I_3$	5.770	yes	5.770	—	—	this work

*Compounds discussed in this paper.

Pt—Br—Pt chains have the same length for both modifications. The length corresponds to two metal-metal separations, whereas normally an axis corresponding to one metal-metal separation is found.[15] In the latter case diffuse layer lines between the Bragg layer lines indicate a one-dimensional superstructure along the Pt—X—Pt chains which comprises two metal-metal separations. This is normally due to a disorder in the halogen positions, which could be easily detected in the structure determinations described in the literature (references are given in TABLE 3). The determination of the structures of the four compounds in TABLE 2 suffers from two difficulties which seem to be new for this class of compounds: although a structural disorder is indicated for the compounds with the "short" unit cell by diffuse layer lines, we are not able to find, from Patterson or Fourier syntheses, the two half-occupied halogen positions typical for Wolffram's Salt compounds. (The structure determination for the compound with the "large" unit cell, $[Pt(en)_2]$-$[Pt(en)_2Br_2](ClO_4)_4$, has not yet advanced far enough to arrive at the same problem). Instead of that we run in a disorder problem connected with the ligand dapn: With the exception of $[Pt(dapn)_2][Pt(dapn)_2Br_2]Br_4$, if the space group I222 is assumed, the platinum atoms occupy positions the point symmetry of which is either higher than the symmetry of the complex molecule or, when the Pt atoms occupy a crystallographic "*m*" position, the complex molecule has no possibility of having a mirror plane coincide with the crystallographic one. Therefore, in order to fulfill the symmetry requirements, a disorder of the complex molecules has to be assumed. Though the occurrence of a Pt—halogen—Pt chain is quite evident, the complete structure could not yet be evaluated because of the disorder problem. Further calculations are in progress.

DISCUSSION

The platinum complexes, the oxidative behavior of which was studied in this work, can be divided into three groups:

1. *cis*-$Pt(NH_3)_2X_2$, X = Cl, Br;
2. *cis*-$Pt(a\text{-}a)X_2$, *a-a* = a diamino ligand, X = Cl, Br, I;
3. $Pt(a\text{-}a)_2X_2$.

All of them can be oxidized to mixed-valence systems. The ease of the reaction, the possibility to isolate characterizable products and their structures depend mainly on the ligand.

The oxidation products always have chain-like structures, either with direct Pt-Pt contacts or with bridging halogen atoms, the latter ones being related to Wolffram's Salt. In our investigations we always obtained metal-halogen-metal chains when the complex molecule contained bidentate diamino ligands, independent from the way of the preparation: by oxidation with $S_2O_8^{2-}$, Cu^{2+}, or by adding a Pt(IV) compound. The chance of isolating characterizable mixed-valence systems depends on the halogen: It decreases with increasing atomic number of the halogen.

Nevertheless, in the cases where we expected products with a Wolffram's Salt type of structure, we worked with bromides and iodides, for, as stated earlier,[15] the electronic interactions along the chains increase with increasing size of the halo-

gen: The metal-metal separation depends mostly on the bridging halogen, increasing with its size.

But this increase is completely due to an elongation of the Pt(IV)—X bond; the length of the Pt(II)——X charge transfer bond remains nearly constant. This leads to a more pronounced overlap of the electronic systems of the metal and the halogen. This increased electronic interaction is shown by the variation in color (normally, Cl-compounds red or grass-green; Br, shiny dark green, I, golden metallic) and enhanced reflectivity. For comparison, crystallographic findings of the compounds of this type are summarized in TABLE 3, where it is interesting to note that the compounds $[Pt(NH_3)_2X_2][Pt(NH_3)_2X_4]$ are the *trans* forms, whereas complexes with bidentate ligands must have *cis* configuration. Wolffram's Salt analogs of *cis*-diamminedihalogen complexes with monodentate amines seem not to exist.

We found an unusual short metal-metal separation in the compound $[Pt(dapn)_2][Pt(dapn)_2Br_2]Br_4$. It amounts to 5.359 Å, instead of, normally, 5.55–5.60 in other Pt—Br—Pt systems. Therefore, there are stronger electronic interactions along the chain, which manifest themselves in the golden metallic appearance of the crystals. The difficulties of finding split bromine positions and the disorder problem of the ligand have been mentioned previously.

The reaction products from $Pten_2X_2$ with CuX_2, X = Cl, Br may have, from the unit cell length in chain direction and from the characteristic distribution of weak and strong layer lines, a Wolffram's Salt-like structure, too, where the length of the unit cell corresponds to two metal-metal separations. The metal-metal separations fit well with the separations normally found for these compounds, but two observations are noteworthy: The compounds belong to the hexagonal system, and both have a golden metallic appearance. At present it cannot be discerned whether the usual —Pt—X——Pt——X—Pt— chains or —Pt—X—Cu—X—Pt— chains occur in the lattice. An x-ray structure analysis to answer this question is in progress.

How strongly the formation of halogen bridged chains is favored in the presence of bidentate diamino ligands is demonstrated by the oxidation of *cis*-$PtenCl_2$ by $(NH_4)_2S_2O_8$. The reaction works only in the presence of HCl, which provides the additional chloride for the Pt—Cl——Pt chain. Acidifying with other acids, e.g. H_2SO_4, does not lead to an identifiable oxidation product.

From these findings we may draw the conclusion that the oxidation of Pt complexes with bidentate diamino ligands leads to Pt—halogen—Pt chains.

Different solids are formed on the oxidation of *cis*-$PtCl_2(NH_3)_2$. The structures obtained depend on reaction conditions and on additional ions in solution. The primary oxidation product of Peyrone's Chloride with $(NH_4)_2S_2O_8$ was formulated by Tschugajeff & Tschernjajeffe[7] as $PtCl_2(OH)(NH_3)_2$, and Robin and Day[16] suggested a formulation $[Pt(HN_3)_2Cl_2(OH)_2][Pt(NH_3)_2Cl_2]$ with a Wolffram's Salt-like structure. In crystals of this compound we found a chain structure with a Pt—Pt distance of 3.45 Å, which is not possible for a linear Pt—X—Pt chain. On the other hand, the distance is longer than that of the unoxidized starting compounds (alternately 3.372 and 3.409 Å[19]), and an elongation of a direct Pt—Pt bond has never been observed upon oxidation. We therefore suggest that the compound does indeed have a bridged chain structure, but with nonlinear bridges.

When the oxidation product is crystallized from a solution containing $[PtCl_4]^{2-}$ or $[PdCl_4]^{2-}$ ions, a structure results with direct Pt—Pt contacts of 3.06 Å and a unit cell length of four Pt—Pt separations. This is exactly the result found by Gillard and Wilkinson[10] for the oxidation product of *cis*-$PtCl_2(NH_3)_2$ with sulfuric acid. They report that their product contains the sulfate group, which is obviously impossible in our case. Our findings are in agreement with Cahen's results.[11] On oxidizing Peyrone's chloride with $[PtCl_6]^{2-}$ he obtains a solid which contains, from ESCA measurements, only one kind of platinum atoms with a Pt—Pt separation of 3.04 Å.

These results lead to the conclusion that two different structures can be obtained on oxidizing *cis*-$PtCl_2(NH_3)_2$: a chain structure with Pt—Pt distance of 3.45 Å and probably with nonlinear Cl or OH bridges and Pt atoms in different oxidation states, or a class III linear chain mixed-valence compound with Pt—Pt distances of 3.06 Å.

After all the puzzling details there remains one question: What governs the different chemistry of *cis* and *trans* complexes and of complexes with monodentate or bidentate ligands? The different behavior seems quite unreasonable for a chemistry in solution. Therefore, we assume that it is the free lattice energy which determines the type of solid formed: The solubility is lowest if the lattice energy is highest, and you will get a Wolffram's Salt analog in cases where its solubility is lower than that of the Pt(II), the Pt(IV), and the species with direct Pt—Pt interactions. Directly interacting Pt chains will form if their solubility is the lowest one. In other cases, oxidation of Pt(II) compounds will only yield Pt(IV) species without a precipitation of a mixed-valence compound. If the free lattice energies and the free enthalpies of solvation could be exactly evaluated, a prediction of the type of solid formed on oxidizing Pt(II) complexes would be possible.

References

1. Knop, W. 1842. Ann. **43:** 111.
2. Schafarik, A. 1855. J. Prakt. Chemie **66:** 385.
3. Weselsky, P. 1856. J. Prakt. Chemie **69:** 276.
4. Wilm, T. 1889. Berichte **22:** 1542.
5. Werner, A. 1896. Z. Anorg. Allg. Chemie **12:** 46.
6. Jörgensen, S. M. 1886. J. Prakt. Chemie **33**(2): 489.
7. Tschugajeff, L. & J. Tschernjajeff. 1929. Z. Anorg. Allg. Chemie **182:** 159.
8. Tschugajeff, L. & W. Chlopin. 1926. Z. Anorg. Allg. Chemie **151:** 253.
9. Drew, H. D. K. 1934. J. Chem. Soc. 1790.
10. Gillard, R. D. and G. Wilkinson. 1964. J. Chem. Soc. 2835.
11. Cahen, D. 1973. Thesis. Northwestern University, Evanston, Ill.
12. Jensen, K. A. 1936. Z. Anorg. Allg. Chemie **229:** 252.
13. Gitzel, W., H. J. Keller, H. H. Rupp & K. Seibold. 1972. Z. Naturforsch. **27b:** 365.
14. Krogmann, K. 1969. Angew. Chemie, Int. Ed. Engl. **8:** 35.
15. Bekaroglu, Ö., H. Breer, H. Endres, H. J. Keller & H. Nam Gung. 1977. Inorg. Chim. Acta **21:** 183.
16. Robin, M. B. & P. Day. 1967. Adv. Inorg. Chem. Radiochem. **10:** 247.
17. Guggenheim, H. J. & D. Bahnck. 1974. J. Cryst. Growth: 29.
18. Kurnakow, N. S. 1898. Z. Anorg. Chemie **17:** 207.
19. Milburn, G. H. W. & R. Truter. 1966. J. Chem. Soc. (A): 1609.
20. Craven, B. M. & D. Hall. 1961. Acta Cryst. **14:** 475.
21. Browall, K. W., J. S. Kasper & L. V. Interrante. 1974. Acta Cryst. **B30:** 1649.

22. WALLEN, J., C. BROSSET & N.-G. VANNERBERG. 1962. Ark. Kem. **A18:** 541.
23. HALL, D. & P. P. WILLIAMS. 1958. Acta Cryst. **11:** 624.
24. CRAVEN, B. M. & D. HALL. 1966. Acta Cryst. **21:** 177.
25. BROWN, K. L. & D. HALL. 1976. Acta Cryst. **B32:** 279.
26. TEXTOR, M. & H. R. STIEGER. 1976. Z. Anorg. Allg. Chem. **423:** 185.
27. RYAN, T. D. & R. E. RUNDLE. 1961. J. Am. Chem. Soc. **83:** 2814.
28. THIELE, G. 1977. Personal communication.

SPECTROSCOPIC AND STRUCTURAL STUDIES OF MIXED-VALENCE LINEAR-CHAIN TRANSITION-METAL COMPOUNDS*

R. J. H. Clark

Christopher Ingold Laboratories
University College London
London WC1H OAJ, United Kingdom

Background and Structural Information

Mixed-valence compounds of class II (using the scheme proposed by Robin and Day[1]) comprise the category of such compounds in which the two different valences remain firmly trapped with distinguishable sites but in which there is sufficient overlap between orbitals on adjacent metal atoms, presumably via the intermediacy of the intervening *s* and *p* orbitals of the bridging halogen atoms, to permit electron transfer between the two sites. Such compounds typically display intense, broad absorption bands in the visible or near-infrared regions which are due to intervalence charge-transfer transitions.

Resonance Raman spectra are obtained when a molecule in the vapor state at high pressure or in a condensed state is irradiated with an exciting beam the frequency of which falls within the contour of an electronic band of the molecule.[2] When the electronic transition is allowed, the resonance Raman spectra are characterized by a large enhancement to the intensity of certain Raman bands (often those arising from totally symmetric fundamentals) and also, in many cases, the appearance of high-intensity overtone progressions in one of the totally symmetric modes. The technique thus provides detailed information about the chromophore, because it is only vibrational modes involving atoms at the absorbing centre in the molecule that display the effect. The intensification of some Raman bands can be so great that compounds at concentrations of 3×10^{-6} M in water can be detected. The technique has thus attracted considerable attention in biological circles, and much information relating to the chromophoric centers of molecules such as cytochrome *c* and hemoglobin has been obtained.[3] The technique is also being used for the remote sensing of small amounts of atmospheric pollutants such as NO_2 and O_3.

Of more fundamental interest is the way in which the technique is being used to probe the nature of the resonant excited state in structurally simple inorganic species.[4] Very striking resonance Raman spectra have been obtained by irradiating high-symmetry (D_{4h}) ions within the contour of the lowest allowed, and axially polarized absorption bands in each case. Examples include the studies on the $[Mo_2Cl_8]^{4-}$,[5] $[Mo_2Br_8]^{4-}$,[6] $[Re_2Cl_8]^{2-}$,[7] $[Re_2Br_8]^{2-}$,[7] $[Ru_2OCl_{10}]^{4-}$,[8] and other $[M_2OX_{10}]^{n-}$[9] species, for which long progressions have been observed under resonance Raman conditions in the metal-metal or metal-oxygen-metal symmetric stretching mode.

*Manuscript received June 17, 1977.

0077-8923/78/0313-0672 $1.75/1 © 1978, NYAS

The intensity enhancement is considered to take place by two mechanisms:[10] First, the single-state mechanism which concerns vibrational modes whose potential surfaces are displaced in the excited state, this leading to intensity enhancement of a totally symmetric mode and its overtones; and second, a two-state mechanism in which enhancement occurs to modes active in vibronic coupling of the resonant (ψ_e) and one or more higher lying excited states (ψ_s). The modes enhanced by this mechanism belong to the irreducible representations contained in the direct product representation $\psi_e\psi_s$; thus nontotally symmetric modes may be enhanced by this mechanism.

The main thrust of the research on mixed-valence compounds in this area is to investigate the nature of any resonance Raman spectra obtained on irradiating mixed-valence halogen-bridged compounds within the contour of the mixed-valence absorption band. We anticipate that the single-state mechanism will dominate, since in the excited state an electron has effectively been transferred from one metal atom site to another, leading to substantial changes in the axial bond lengths.

Of the many mixed-valence compounds of class II known, we have concentrated our attention recently on the halogen-bridged chain compounds of platinum with the general formulae

$$[Pt^{II}L_4][Pt^{IV}L_4X_2]X_4 \qquad \text{(type A)}$$

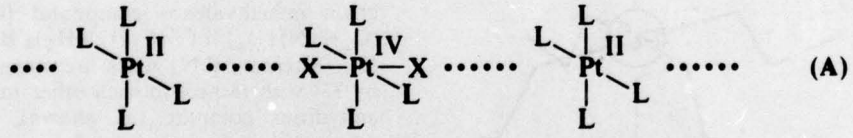
$$[Pt^{II}L_2X_2][Pt^{IV}L_2X_4] \qquad \text{(type B)}$$

$$[Pt^{II}(L\text{-}L)X_2][Pt^{IV}(L\text{-}L)X_4] \qquad \text{(type C)}$$

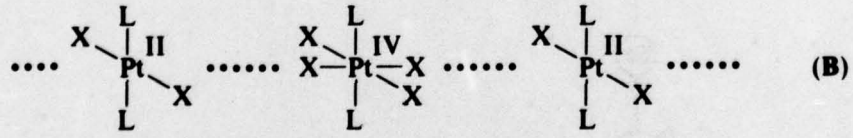
and we hope to extend the investigation to include other types of compound such as

$$K_2[Pt^{II}LX_3][Pt^{IV}LX_5] \qquad \text{(type D)}$$

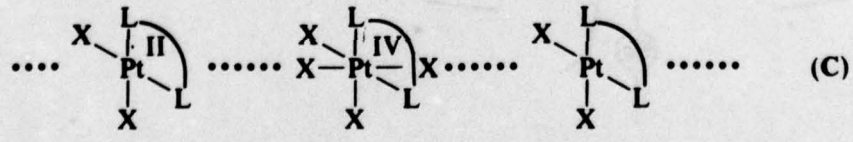
A schematic representation of the structures of these compounds is given below:



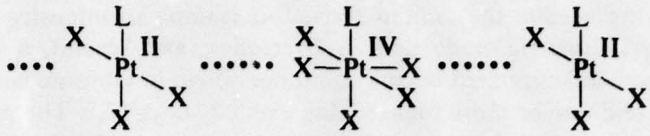
where L = ethylamine or propylamine (positively-charged chain)



where L = ammonia (neutral chain)



where L = 1,2 diaminoethane or 1,2-diaminopropane (neutral chain)



(D)

where L = ammonia (negatively charged chain—structure not yet fully determined.)

The classic examples of type A are Wolffram's red (L = ethylamine, X = Cl) and Reihlen's green (L = ethylamine, X = Br),[11] (FIGURE 1), while type D (L = ammonia, X = Cl) is thought to be a variant on Cossa's red salt.[12]

In all cases, the two metal-atom sites are structurally distinguishable, but may be interconverted by a concerted movement of the axial halogen atoms in phase away from the platinum(IV) atoms toward the platinum(II) atoms.

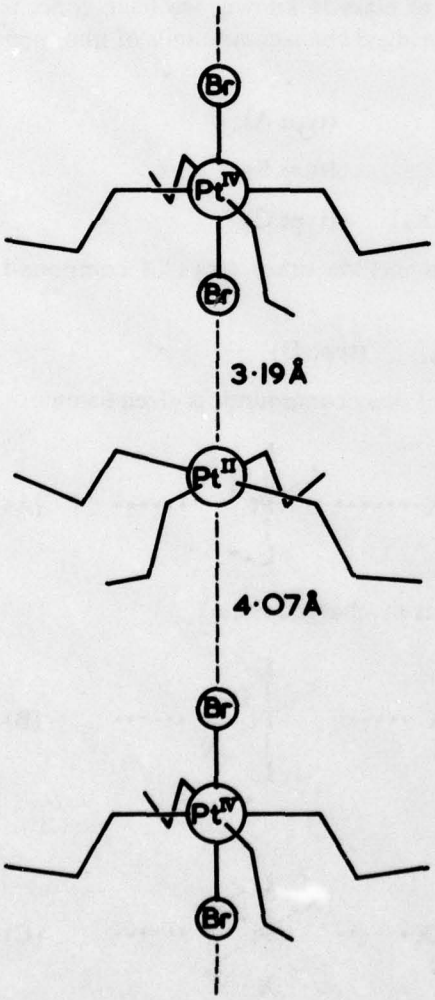


FIGURE 1. Structure of the linear-chain mixed-valence compound $[Pt^{II}\cdot(C_2H_5NH_2)_4]\,[Pt^{IV}(C_2H_5NH_2)_4\,Br_2]\cdot Br_4$. Alternate PtN_4 units are staggered by 37° with respect to each other in the anhydrous complex (as shown), but eclipsed in the hydrated one.

Although there are no direct metal-metal bonds in these complexes, they are strongly dichroic and have a variety of highly anisotropic properties. Thus, their electrical conductivity is typically about 300 times greater in the direction of the chains than in the perpendicular directions.[13] They are thus considered to be one-dimensional semiconductors. A hopping process has been proposed for the conductivity of these complexes at ambient pressures,[14] although at high pressures this localized process may give way to a band-type conduction process because the metal d_{z^2} and ligand p_z orbital interactions increase under pressure.[15] Attempts to remove the bridging halogen atoms with $AgClO_4$ or $HClO_4$, and so to obtain compounds with direct metal-metal bonds, have so far been unsuccessful,[16] anion exchange taking place only to the extent of the interchain anions; i.e., to produce $[Pt(L\text{-}L)_2][Pt(L\text{-}L)_2X_2](ClO_4)_4$, with L-L = 1,2-diaminoethane or 1,2-diaminopropane and X = Cl, Br or I. X-ray investigations have shown that the long axis of such crystals is parallel with the metal-halogen-metal chain. The $Pt^{II}—Pt^{IV}$ distance is found to be, for a given halogen atom, rather independent of the nature of the equatorial groups and to depend mainly on the size of the halogen atom and possibly on the counterions and water content of the lattice. The increased $Pt^{II}—Pt^{IV}$ distance with larger halogen atoms (chlorides 5.27 Å, bromides 5.60 Å, iodides 5.92 Å) is a consequence of increased $Pt^{IV}—X$ distances ($Pt^{IV}—Cl$ = 2.09 Å, $Pt^{IV}—Br$ = 2.42 Å, $Pt^{IV}—I$ = 2.74 Å), there being virtually no change in $Pt^{II}.....X$ distance (3.18 Å) (averages of a variety of x-ray crystallographic data, some of which are included in TABLE 1).

EXPERIMENTAL TECHNIQUES

The main difficulties to be overcome when trying to measure resonance Raman spectra lie in (1) the elimination of thermal decomposition of the sample and, in the case of liquids or solutions, of the thermal lens effect (which interferes with the effectiveness with which the laser beam can be focused in the sample); (2) the making of corrections to allow for absorption processes occurring at the same time as the scattering processes; and (3) the elimination of fluorescence and photolysis.

The first difficulty may be largely overcome by spinning the sample rapidly (at ca. 2000 rev. min^{-1}); the sample may be in the gaseous, liquid, or solid states.[4,17] Alternative devices have also been developed that allow the incident laser beam to scan rapidly over the surface of a solid or liquid, either in a circular or a linear path. In all cases, the object of the procedure is to try to ensure that a molecule is held at the focal point of the laser beam for the least possible time.

Difficulty (2) is not easily overcome, except by reducing the path length of the scattered beam to the absolute minimum, since accurate measurement of the effective path length is nearly impossible for deeply colored scattering materials. Raman difference spectroscopy offers possibilities for solving these problems.[17]

Photolytic effects seem also to be reduced by sample spinning procedures, but the effects of fluorescence can be effectively removed only by time-discrimination procedures. The technique involves excitation of a sample with a pulsed laser, the pulse duration being of the order of nano- or picoseconds, together with time-

TABLE 1

X-RAY STRUCTURAL INFORMATION ON MIXED-VALENCE PLATINUM COMPOUNDS*

Compounds	r(M-M)/Å	$r(M^{IV}-X)$/Å	$r(M^{II}...X)$/Å	Ref.†
Chloro Compounds				
$[(Pt, Pd)(NH_3)_2Cl_2][(Pt, Pd)(NH_3)_2Cl_4]$	5.33	2.03	3.30	a
$[Pt^{II}etn_4][Pt^{IV}etn_4Cl_2]Cl_4.4H_2O$	5.39	2.26	3.13	b
$[Pt^{II}enCl_2][Pt^{IV}enCl_4]$	5.481	—	—	c
$[Pt^{II}en_2][Pt^{IV}en_2Cl_2](ClO_4)_4$	5.45	—	—	d
$[Pt^{II}en_2][Pt^{IV}en_2Cl_2](CuCl_2)_4$	5.261	—	—	d
$K_2[Pt^{II}(NH_3)Cl_3][Pt^{IV}(NH_3)Cl_5].2H_2O$	5.22	—	—	e
Bromo Compounds				
$[Pt^{II}(NH_3)_2Br_2][Pt^{IV}(NH_3)_2Br_4]$	5.53	2.50	3.03	f
$[Pt^{II}(NH_3)_2Br_2][Pt^{IV}(NH_3)_2Br_4]$	5.54	2.17	3.37	a
$[Pt^{II}etn_4][Pt^{IV}etn_4Br_2]Br_4.4H_2O$	5.586	2.479 2.447	3.139 3.107	g
$[Pt^{II}etn_4][Pt^{IV}etn_4Br_2]Br_4.4H_2O$	5.606	—	—	h
$[Pt^{II}etn_4][Pt^{IV}etn_4Br_2]Br_4$	5.61 6.53	2.42 2.46	3.19 4.07	i

$[Pt^{II}enBr_2][Pt^{IV}enBr_4]$	5.60	2.48	3.125	j
$[Pt^{II}enBr_2][Pt^{IV}enBr_4]$	5.606	—	—	c
$[Pt^{II}en_2][Pt^{IV}en_2Br_2](ClO_4)_4$	5.491	—	—	d
$[Pt^{II}en_2][Pt^{IV}en_2Br_2](CuBr_2)_4$	5.561	—	—	d
$[Pt^{II}pn_2][Pt^{IV}pn_2Br_2](ClO_4)_4$	5.64	—	—	d
$[Pt^{II}pn_2][Pt^{IV}pn_2Br_2]Br_4$	5.359	—	—	d
Iodo Compounds				
$[Pt^{II}etn_4][Pt^{IV}etn_4I_2]I_4$	6.366	—	—	h
$[Pt^{II}enI_2][Pt^{IV}enI_4]$	5.862	—	—	c
$[Pt^{II}en_2][Pt^{II}en_2I_2](ClO_4)_4$	6.05	—	—	d
$[Pt^{II}pn_2][Pt^{IV}pn_2I_2](ClO_4)_4$	5.726	—	—	d
$K_4[Pt^{II}I_4][Pt^{IV}I_6]$	5.74	2.74	3.00	k

*etn = ethylamine; en = 1,2-diaminoethane; pn = 1,2-diaminopropane.

†[a]Wallén, J., C. Brosset & N.-G. Vannerberg. 1962. Arkiv Kem. A. **18:** 541–551. [b]Craven, B. M. & D. Hall. 1961. Acta Cryst. **14:** 475–480. [c]Browall, K. W., J. S. Kasper & L. V. Interrante. 1974. Acta Cryst. **B30:** 1649–1650. [d]Ref. 16; also H. Endres & H. Keller. Unpublished work. [e]Ref. 12. [f]Hall, D. & P. P. Williams. 1958. Acta Cryst. **11:** 624–626. [g]Brown, K. L. & D. Hall. 1976. Acta Cryst. **B32:** 279–281. [h]Textor, M. & H. R. Stieger. 1976. Z. Anorg. Allgem. Chem. **423:** 185–192. [i]Craven, B. M. & Hall, D. 1966. Acta Cryst. **21:** 177–180. [j]Ryan T. D. & R. E. Rundle. 1961. J. Am. Chem. Soc. **83:** 2814–2816. [k]G. Thiele. To be published.

adjusted gate electronics to permit temporal resolution of the resonance Raman spectrum from the fluorescence spectrum. Rejection of even short-lived fluorescence by more than three orders of magnitude from the Raman scattering has been achieved.

All resonance Raman spectra reported in this article have been obtained either on the powdered solids (in some cases diluted with a suitable Raman intensity standard such as K_2SO_4) or on alkali halide discs of the mixed-valence compound; the samples have been rotated at ca. 1500 rev min^{-1}. Some spectra have been recorded for samples held at liquid nitrogen temperatures.

All compounds have been prepared by standard procedures. It should be noted that in many cases the mixed-valence compound can also be prepared by grinding together the platinum(II) and platinum(IV) constituent species in the solid state. In particular, it is essential to prepare discs of the mixed-valence compounds with the appropriate alkali salt; otherwise, not only does exchange take place between the interchain and matrix anions but also between the intrachain and matrix anions.

Resonance Raman Spectra

The infrared spectra of mixed-valence compounds of Class II characteristically correspond closely to the superposition of those of the constituent species. The resonance Raman spectra, however, do not. Use of an exciting line whose wavelength falls within the contour of the mixed-valence transition leads to a Raman spectrum dominated by the band associated with the $\nu_1(X—Pt^{IV}—X)$ symmetric stretching fundamental, together with its associated overtone progression. This intense resonance Raman spectrum usually completely overwhelms the rest of the spectrum, although in some cases other weak progressions are also seen, based on one quantum of another Raman-active band. The progression-forming mode is still, however, the $\nu_1(X—Pt^{IV}—X)$ mode in each case.

Initial studies on a wide variety of mixed-valence compounds of platinum,[18] palladium,[18] antimony[19] and lead[19] led to a very detailed investigation of Wolffram's red $[Pt^{II}etn_4][Pt^{IV}etn_4Cl_2]Cl_4.4H_2O$, etn = ethylamine,[20] and its bromo counterpart, Reihlen's green.[21] Single-crystal electronic spectra of these compounds indicate that the broad mixed-valence transition at ca. 21000 cm^{-1} (chloride) and ca. 18000 cm^{-1} (bromide) is polarized parallel to the chain axis.[22,23]

Irradiation of Wolffram's red with an exciting line which falls within the contour of this band leads of the appearance of one extremely intense overtone progression based on the symmetric stretching fundamental $\nu_1(Cl—Pt^{IV}—Cl)$ at 316 cm^{-1} plus a few other very weak features. The progression can be observed as far as $9\nu_1$ when measured at room temperature and with 514.5 nm excitation, but recent studies[24] have indicated that it can be observed as far as $16\nu_1$ when the sample is held at liquid nitrogen temperature. Several other much weaker progressions can be identified in this spectrum, in all of which it is ν_1 which acts as the progression-forming mode. The spectacular nature of this spectrum is illustrated in Figure 2.

All other mixed-valence linear-chain compounds of platinum, involving halogen bridges, studied so far have been found likewise to display resonance Raman

spectra in which the main feature is the overtone progression based on the ν_1 (X—Pt^{IV}—X) symmetric stretching fundamental. Some results are summarized in TABLE 2.

The observation of a large number of overtones of a totally symmetric fundamental, ν_1, of a molecule under resonance Raman conditions makes it possible to determine the harmonic frequency (ω_1) and certain anharmonicity constants x_{11} and x_{1j}. The ω_1 and x_{11} values may be determined by standard procedures[4] from the slope and intercept of the $\nu(v_1)/v_1$ versus v_1 plot (v_1 = the vibrational quantum number of the progression-forming mode). The cross terms x_{1j} may be

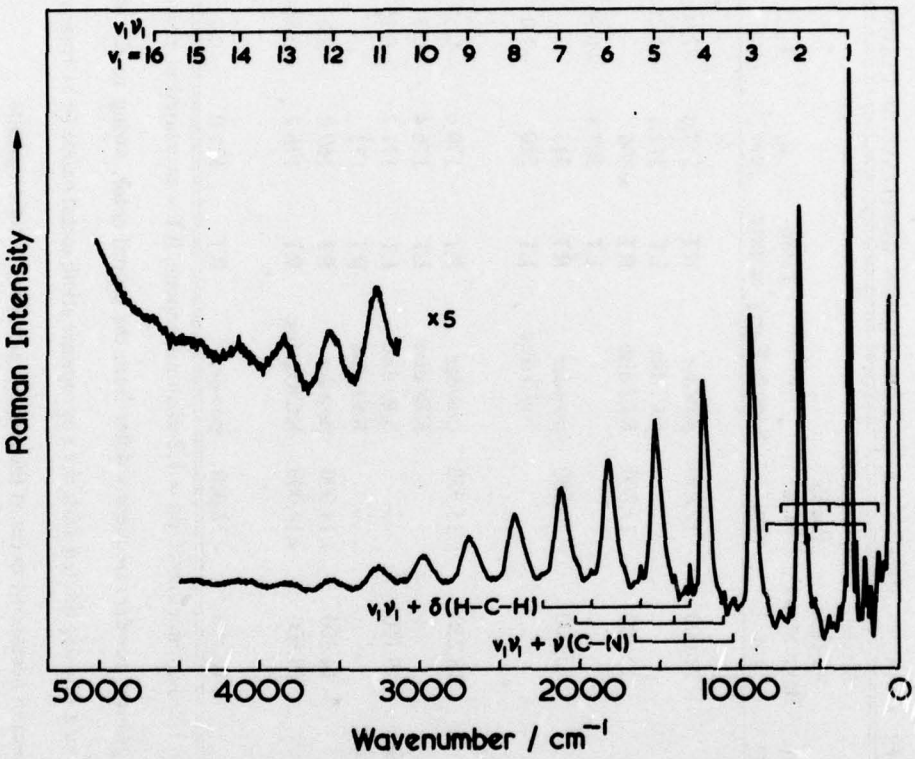


FIGURE 2. Resonance Raman spectrum of Wolffram's red, $[Pt^{II}(C_2H_5NH_2)_4]\cdot[Pt^{IV}(C_2H_5NH_2)_4Cl_2]Cl_4\cdot 4H_2O$ at ca. 80K. Exciting line, 514.5 nm Ar+, spectral slit width 1 cm^{-1}.

determined, by similar procedures, only if further progressions in the ν_1 mode, based upon one quantum of another mode ν_j, are observed in the resonance Raman spectrum.

A summary of the ω_1 and x_{11} values determined as above for the mixed-valence linear-chain compounds of platinum studied are included in TABLE 2. The x_{11} values are invariably small, and become even smaller when measured for samples pressed into an alkali halide disc and held at liquid nitrogen temperatures. Under the latter conditions, the x_{11} values average—1.1, −0.3, and ca. 0 cm^{-1} for the chlorides, bromides, and iodide studied. Thus, in common with other molecules

TABLE 2

SPECTROSCOPIC DATA ON MIXED-VALENCE LINEAR-CHAIN COMPLEXES OF PLATINUM*

Complex	Crystal Colour†	Mixed-Valence Band Max‡ /cm^{-1}	Excitation Profile Max. /cm^{-1}	Sample Form	Temperature	ω_1 /cm^{-1}	x_{11} /cm^{-1}	Progression	$I(2\nu_1)/I(\nu_1)$ Max. Value§	Ref.
Chlorides										
$[Ptetn_4][Ptetn_4Cl_2]Cl_4.4H_2O$	red	21,000	17,450	powder	RT	319.5	−2.00	$9\nu_1$	0.55	20
				KCl disc	LT	312.1	−1.26	$16\nu_1$	1.1	23
$[PtenCl_2][PtenCl_4]$	red	22,500	17,800	KCl disc	RT	≈306	—	$8\nu_1$	0.62	23
					LT	307.8	−0.98	$14\nu_1$	0.96	23
$[Ptpn_2][Ptpn_2Cl_2](ClO_4)_4$	yellow	25,000	≈20,000	powder	RT	315	—	$7\nu_1$	0.40	26
				NaCl disc	LT	310	−1.0	$8\nu_1$	0.47	26
Bromides										
$[Ptetn_4][Ptetn_4Br_2]Br_4.4H_2O$	green	18,250	15,950	powder	RT	179.6	−0.37	$7\nu_1$	0.50	21
				KBr disc	LT	176.4	−0.3	$12\nu_1$	≈0.6	23
$[PtenBr_2][PtenBr_4]$	gold-green	19,150	—	KBr disc	LT	171.7	−0.25	$10\nu_1$	≈0.4	23
$[Pten_2][Pten_2Br_2](CuBr_2)_4$	gold-green	—	—	KBr disc	RT	173	—	$6\nu_1$	0.57	26
$[Ptpn_2][Ptpn_2Br_2]Br_4$	green	14,300	<14,000	powder	RT	169.8	0.0	$5\nu_1$	0.52	26
$[Ptpn_2][Ptpn_2Br_2](ClO_4)_4$	green	18,900	<14,000	$KClO_4$ disc	RT	176.2	−0.54	$7\nu_1$	0.59	26
Iodide										
$[Ptpn_2][Ptpn_2I_2](ClO_4)_4$	gold	12,500	<12,000	powder	RT	121.0	≈0.0	$4\nu_1$	0.35¶	26

*Abbreviations: etn = ethylamine; en = 1,2-diaminoethane; pn = 1,2-diaminopropane; RT = measured at room temperature; LT = measured in a liquid nitrogen cell.

†The colors of the complexes as finely ground powders frequently differ from the crystal color, owing to the differing relative importance of specular and diffuse reflectance.

‡Measured either by diffuse reflectance as a powder diluted with the appropriate alkali metal halide or by transmission as the appropriate alkali halide disc.

§The maximum value of $I(2\nu_1)/I(\nu_1)$ does not necessarily occur at the maximum in the excitation profile.

¶Obtained with 514.5 nm excitation.

and ions found to display the resonance Raman effect,[4] the fundamental displaying the long progression of overtones is mechanically virtually harmonic.

Excitation Profiles

Plots of the frequency dependence of the scattered intensity of a Raman band arising from a fundamental or its overtones are known as excitation profiles. These profiles are beginning to assume an important role in resonance Raman studies, because they appear to indicate clearly which fundamentals of the scattering molecule are coupled vibronically with which electronic transitions. For totally symmetric modes, the exciting frequency for maximum resonance enhancement to the Raman intensity (Stokes band) need not coincide with either the pure electronic transition frequency, ν_{00}, or with $\nu_{00} + \nu_1'$, where ν_1' is the value of ν_1 in the resonant excited state. Indeed, the simplest theories predict that it should maximize at the Franck-Condon maximum,[27] and in practice it seems to do so.[4]

The plotting of excitation profiles has really become possible only since the introduction of tunable dye lasers and a variety of efficient lasing dyes. Only in this way has it become possible to obtain a sufficient number of points to be able to plot an excitation profile closely. The most commonly used and most efficient dye for this purpose is rhodamine 6G (tuning range 575–640 nm, maximum output 4 W at 600 nm for a 21 W argon ion pump, operating all-wave), but other dyes are also commonly used now, viz rhodamine B (615–665 nm), rhodamine 110 (550–590 nm), sodium fluorescein incorporating cyclooctatetraene (540–590 nm), and several different coumarins (430–550 nm). Many of the coumarins are, unfortunately, not only very short-lived (ca. 48 hr) but highly expensive. Other dyes (e.g. nile blue or cresyl violet) can be used to provide tunability in the near infrared, though with relatively low efficiency. Raman band intensities are determined as band areas relative to the band area of a standard that shows no resonance enhancement in the frequency range under study (e.g. the a_1 bands of ClO_4^-, ClO_3^- or SO_4^{2-} ions).

Excitation profiles for the $\nu_1(X—Pt^{IV}—X)$ symmetric stretching fundamental have been measured carefully for a series of mixed-valence compounds, and the maxima are listed in Table 2 together with the maximum (by diffuse reflectance or transmission) of the mixed-valence band in each case. Excitation profiles for the ν_1 bands of Wolffram's red[20] and Reihlen's green[21] are shown in Figure 3. They are typical of the excitation profiles of the ν_1 bands of all the mixed-valence linear-chain compounds studied so far, in that all reach a maximum several thousand wave-numbers to the low-frequency side of the maximum of the broad mixed-valence band. This feature of the excitation profiles is not typical, as indicated earlier, of excitation profiles in general. Thus the results suggest either that there is more than one axially polarized mixed-valence transition of the $d_{z^2}(Pt^{IV}) \leftarrow d_{z^2}(Pt^{II})$ sort in a chain polymer (Figure 4), and that the resonance enhancement of ν_1 is specifically determined by the lowest of these, or that the excitation profiles are a consequence of destructive interference[25] between different terms in the expression for the scattering tensor. This matter is under active study, and remains to be resolved. Circular dichroism studies on the complexes $[Pt(R\text{-}pn)_2][Pt(R\text{-}pn)_2X_2](ClO_4)_4$, X = Cl or Br, are currently under investiga-

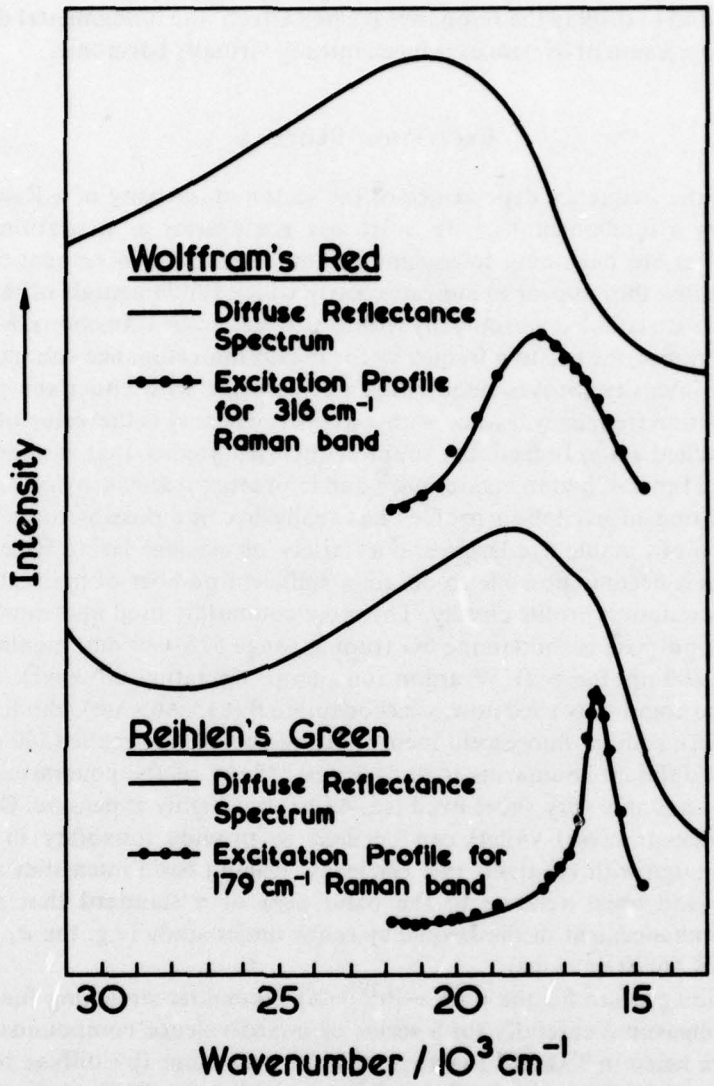


FIGURE 3. Diffuse reflectance spectra of Wolffram's red and Reihlen's green together with excitation profiles for the 316 cm^{-1} band of the former and the 179 cm^{-1} band of the latter.

tion[26] in a search for multiple electronic transitions under the envelope of the intervalence charge-transfer bands. If successful, information on the interactions between the various component transitions could be extracted.

It is considered that, of the various fundamentals of a scattering molecule, the one which displays the resonance Raman effect is that which is capable of transforming the molecule from its ground-state sterochemistry to its excited-state sterochemistry. In the case of the mixed-valence compounds under discussion, the coordinate effective in this respect is clearly the $\nu_1(X—Pt^{IV}—X)$ symmetric stretching mode, in agreement with the resonance Raman observations. Moreover, this normal coordinate seems to be related to the halogen movements involved in the proposed hopping process for the conductivity of these linear-chain mixed-

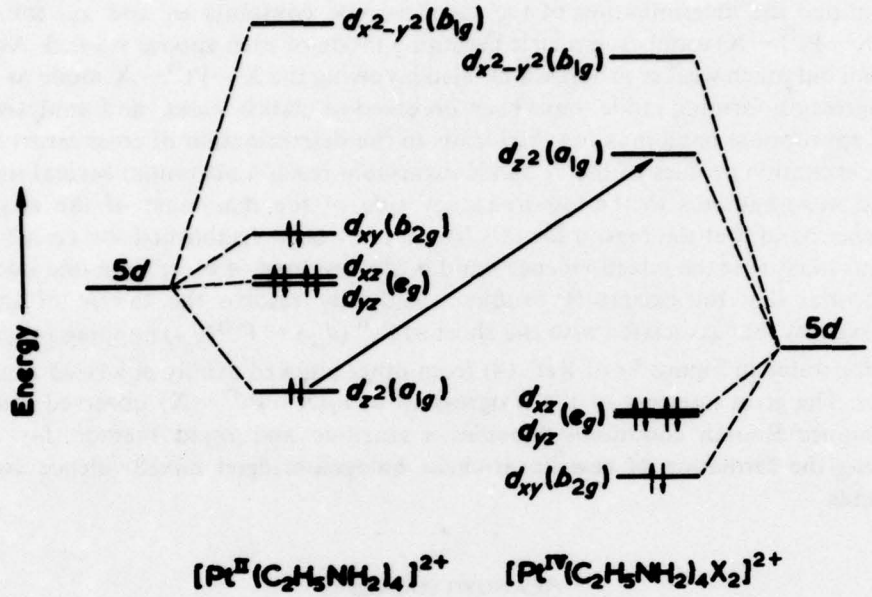


FIGURE 4. Qualitative representation of the relative *d*-orbital energies in the constituent ions of Wolffram's red and Reihlen's green, and of the lowest axially polarized mixed-valence charge-transfer transition $Pt^{IV}(d_{z^2}) \leftarrow Pt^{II}(d_{z^2})$ (ignoring the chain nature of the complex and the effects of the *s* and *p* orbitals of the intervening halogen atoms).

valence compounds.[14] The chain halogen atoms would need to move on average 0.54, 0.38 and 0.22 Å for chlorides, bromides, and iodides, respectively, in order to reach the point midway between the two platinum atoms, i.e., to the situation of a platinum(III) chain. These values differ only by a factor of about two from the mean square amplitudes of vibration of the $\nu_1(X—Pt^{IV}—X)$ vibration, in the $v_1 = 16$ states; these are calculated to be 0.22 Å for X = Cl ($\omega_1 = 319.5\ cm^{-1}$) and 0.20 Å for X = Br ($\omega_1 = 179.6\ cm^{-1}$).

The above distance changes are also similar to those estimated on the basis of the theory of Mingardi and Siebrand,[27] which relates the relative intensities of different members of the overtone progression to the shift in the equilibrium $X—Pt^{IV}—X$ bond lengths on excitation of the molecule from the ground to the resonant excited electronic states. The ratio $I(2\nu_1)/I(\nu_1)$ is about 0.5 at room temperature for the compounds under discussion, but increases as the temperature is lowered, reaching 1.1 at liquid nitrogen temperatures for Wolffram's red (TABLE 2). There is, however, some difficulty in applying the theory to the compounds under discussion, owing to our lack of knowledge regarding the origins of the mixed-valence charge-transfer transition in each case.

CONCLUSION

The mixed-valence linear-chain compounds of platinum display extremely intense resonance Raman spectra on their being irradiated with an exciting line whose frequency falls within the contour of the mixed-valence band. This has

permitted the determination of the spectroscopic constants ω_1 and x_{11} for the $\nu_1(X—Pt^{IV}—X)$ totally symmetric breathing mode of each species studied. Additional but much weaker progressions, also involving the $X—Pt^{IV}—X$ mode as the progression-forming mode, have been observed in certain cases, and analysis of the appropriate band maxima then leads to the determination of cross terms x_{1j}. The excitation profiles of the ν_1 bands invariably reach a maximum several thousand wave-numbers to the low-frequency side of the maximum of the mixed-valence band, but the reason for this has not yet been established for certain; it seems likely that the mixed-valence band is the envelope of more than one transition, and that the excitation profiles specifically resolve the lowest of these (possibility that associated with the shortest $Pt^{IV}(d_{z^2}) \leftarrow Pt^{II}(d_{z^2})$ hopping process, as illustrated in Figure 5a of Ref. 14) from other allowed axially polarized transitions. The great intensity of the progression in $\nu_1(X—Pt^{IV}—X)$ observed under resonance Raman conditions provides a sensitive and rapid method for detecting the formation of new linear-chain halogen-bridged mixed-valence compounds.

Acknowledgments

The author is indebted to Dr. P. Day for helpful discussion, to Prof. H. Keller for supplying some of the 1,2-propanediamine compounds, and to his collaborators Drs. M. L. Franks, B. Stewart, W. R. Trumble and P. C. Turtle on this project.

References

1. Robin, M. B. & P. Day. 1967. Adv. Inorg. Chem. Radiochem. **10**: 247.
2. Behringer, J. 1967. *In* Raman Spectroscopy. H. A. Szymanski, Ed. Vol. **1**: 168–223. Plenum Press. New York, N.Y.
3. Spiro, T. G. 1975. *In* Advances in Infrared and Raman Spectroscopy. R. J. H. Clark & R. E. Hester. Eds. Vol. **1**: 98–142. Heyden. London, England.
4. Clark, R. J. H. 1975. *In* Advances in Infrared and Raman Spectroscopy. R. J. H. Clark & R. E. Hester, Eds. Vol. **1**: 143–172. Heyden. London, England.
5. Clark, R. J. H. & M. L. Franks. 1975. J. Am. Chem. Soc. **97**: 2691–2697.
6. Clark, R. J. H. & N. D'Urso. 1978. J. Am. Chem. Soc. **100**: May 10.
7. Clark, R. J. H. & M. L. Franks. 1976. J. Am. Chem. Soc. **98**: 2763–2767.
8. Clark, R. J. H., M. L. Franks & P. C. Turtle. 1977. J. Am. Chem. Soc. **99**: 2473–2480.
9. Clark, R. J. H. & J. Campbell. 1978. Mol. Phys. In press.
10. Albrecht, A. C. 1961. J. Chem. Phys. **34**: 1476–1484.
11. Reihlen, H. & E. Flohr. 1934. Ber. **67**: 2010–2017.
12. Fanwick, P. E. & D. S. Martin. 1973. Inorg. Chem. **12**: 24–30.
13. Thomas, T. W. & A. E. Underhill. 1971. J. Chem. Soc. (A): 512–515.
14. Interrante, L. V. & K. W. Browall. 1974. Inorg. Chem. **13**: 1162–1166.
15. Interrante, L. V., K. W. Browall & F. P. Bundy. 1974. Inorg. Chem. **13**: 1158–1162.
16. Bekaroglu, O., H. Breer, H. Endres, H. J. Keller & H. Nam Gung. 1977. Inorg. Chim. Acta **21**: 183–186.
17. Kiefer, W. 1977. *In* Advances in Infrared and Raman Spectroscopy. R. J. H. Clark & R. E. Hester, Eds. Vol. **3**: 1–42. Heyden. London, England.

18. CLARK, R. J. H. & W. R. TRUMBLE. 1976. Inorg. Chem. **15:** 1030–1035.
19. CLARK, R. J. H. & W. R. TRUMBLE. 1976. J. Chem. Soc. (Dalton): 1145–1149.
20. CLARK, R. J. H., M. L. FRANKS & W. R. TRUMBLE. 1976. Chem. Phys. Lett. **41:** 287–292.
21. CLARK, R. J. H. & M. L. FRANKS. 1977. J. Chem. Soc. (Dalton): 198–203.
22. YAMADA, S. & R. TSUCHIDA. 1956. Bull Chem. Soc. Japan **29:** 894–898.
23. DAY, P. 1975. *In* Low-Dimensional Cooperative Phenomena. H. J. Keller, Ed.: 191–214. Plenum Press. New York, N.Y.
24. CLARK, R. J. H. & P. C. TURTLE. 1978. Inorg. Chem. In press.
25. STEIN, P., V. MISKOWSKI, W. H. WOODRUFF, J. P. GRIFFIN, K. G. WERNER, B. P. GABER & T. G. SPIRO. 1976. J. Chem. Phys. **64:** 2159–2167.
26. CLARK, R. J. H. & B. STEWART. Unpublished results.
27. MINGARDI, M. & W. SIEBRAND. 1975. J. Chem. Phys. **62:** 1074–1085.

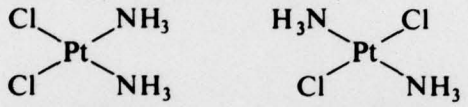
A CRYSTALLINE PLATINUM BLUE: ITS MOLECULAR STRUCTURE, CHEMICAL REACTIVITY, AND POSSIBLE RELEVANCE TO THE MODE OF ACTION OF ANTITUMOR PLATINUM DRUGS*

Jacqueline K. Barton and Stephen J. Lippard†

Department of Chemistry
Columbia University
New York, New York 10027

Background: The Antitumor Activity of *Cis*-dichlorodiammineplatinum(II) and its Binding to DNA and its Constituents

The simple inorganic complex *cis*-dichlorodiammineplatinum(II) (DDP) inhibits the division of bacterial cells with little effect on



cis-DDP *trans*-DDP

their growth.[1,2] It was subsequently shown that DDP has substantial antitumor activity on a wide variety of animal malignancies.[3] These findings stimulated numerous investigations of diammineplatinum(II) complexes both to establish their mode of action and to design more effective antitumor platinum drugs.[4]

The structural characteristics of platinum complexes that exhibit antitumor activity have been empirically established.[5] Complexes with only one relatively labile leaving group, such as $[(dien)PtCl]^+$ (dien = diethylenetriamine), are ineffective. Activity is therefore not derived from monofunctional attachment of the metal ion to a cellular component. Bifunctional complexes with a *trans* configuration, for example *trans*-DDP, are also inactive. These results have suggested to some investigators a geometric fit between *cis*-DDP and its primary target in the tumor cell. Kinetic factors dependent upon the *cis* disposition of chloride ions might also influence the mode of action, as will be discussed later.

The screening of analogs of DDP showed chloride to be the optimal anion. Complexes with poor leaving groups were inactive, whereas those with labile ligands were found to be highly toxic. The mechanism for ligand substitution in square platinum(II) complexes has been thoroughly investigated.[6] The rate laws are consistent with both solvent-assisted (k_1) and second-order (k_2) substitution pathways. Although $k_2 \gg k_1$ in general, the solvent-assisted pathway is probably more important in biological media where the concentrations of potential entering

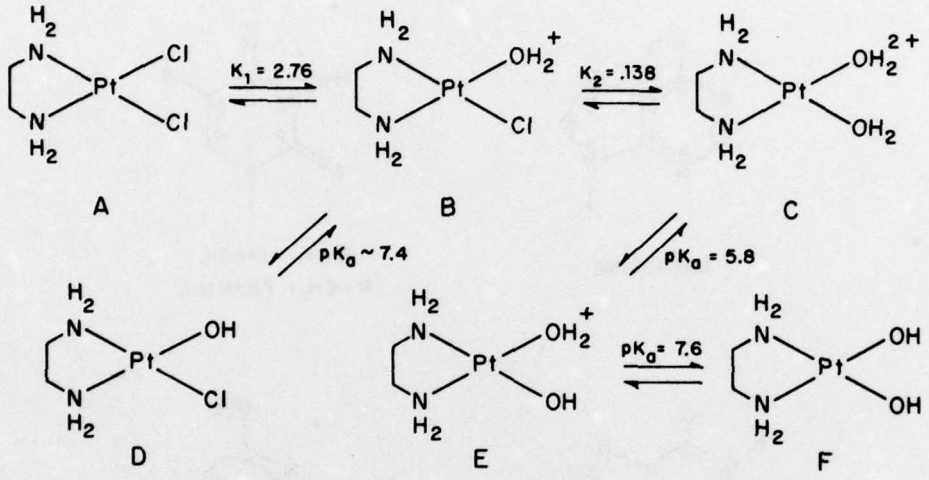
*Supported by National Institutes of Health Research Grant no. CA-15826 from the National Cancer Institute. J.K.B. is the recipient of a Predoctoral Fellowship from the National Science Foundation. Manuscript received July 11, 1977.

†Address correspondence and reprint requests to S.J.L.

0077-8923/78/0313-0686 $1.75/1© 1978, NYAS

ligands are low. The biological reactivity of DDP will therefore be strongly dependent upon the concentration of free chloride ion in solution.

FIGURE 1 summarizes the results of thermodynamic considerations[7] for $[(en)PtCl_2]$ (en = 1,2-diaminoethane) dissolved in media of varying chloride ion concentration. Analogous behavior may be expected for DDP. In plasma, where $[Cl^-]$ = 0.103 M, DDP will be neutral and unreactive. Passive diffusion[8] of the drug across cell membranes exposes DDP to a much lower chloride ion concentration, producing the hydrolysis products shown in FIGURE 1. Since water is an excellent leaving group, the drug is activated for attachment to an intracellular component, following which its antitumor activity can be manifest.



Estimate of Species A-F in a Biological System, pH = 7.4

	$[Cl^-]$	A	B	C	D	E	F
Plasma	103 mM	37.3	1	.00134	1	.053	.033
Cytoplasm	4 mM	1.45	1	.0345	1	1.38	0.86

FIGURE 1. Hydrolysis reactions of antitumor platinum complexes and an estimate of species present in plasma and cytoplasm (cf Ref. 7).

The primary cellular function known to be disrupted by DDP is DNA synthesis. By inhibiting replication the drug prevents cell division and tumor growth. In the presence of low concentrations of DDP, mammalian cells in culture show a marked decrease in uptake of ^{3}H-thymidine, reflecting a selective inhibition of DNA synthesis. Only a slight change in the uptakes of ^{3}H-uridine and ^{3}H-leucine were exhibited, indicating little effect on RNA and protein synthesis, respectively.[9] *In vivo* evidence for the inhibition of replication by DDP was provided by diminished incorporation of ^{3}H-thymidine into the DNA of Ehrlich ascites tumor cells from mice preinjected with the drug.[10]

These results suggest that DDP binds intracellular DNA, altering its template activity, rather than inhibiting the enzymes involved in replication. Various spectroscopic[11-15] and x-ray structural[16-19] studies have therefore been employed to

characterize the binding sites of diammineplatinum(II) complexes with individual nucleic acid components. FIGURE 2 displays the bases normally found in nucleic acids. Both the purine and pyrimidine rings have several potential metal-binding sites, the most probable of which are the heterocyclic ring nitrogen atoms. Through sequential blocking of possible coordination sites by alkylation of nitrogen atoms, followed by spectroscopic measurements, evidence[11] was accumulated indicating N3 as the favored binding site for the pyrimidines and both N7 and N1 for the purines, with N7 being preferred at acid pH. Proton nuclear magnetic resonance studies[12,13] substantiate these assignments. Kinetic measurements[14] show guanosine to react most rapidly with the platinum complexes, suggesting

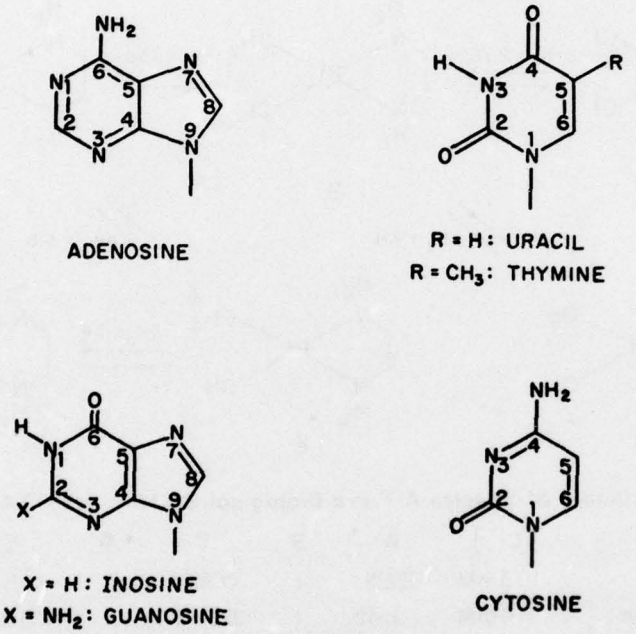


FIGURE 2. The structures and base numbering schemes of the common nucleosides. The sugar ring attachment sites are designated by vertical bonds. Purines are on the left and pyrimidines are on the right.

preferential binding of the metal to DNA rich in G-C base pairs. Raman difference spectroscopy[15] was used to demonstrate the formation of both mono- and bis N7-bound inosine platinum complexes at low pH. At neutral pH the formation of polynuclear complexes was found and platinum was proposed to be bound at both N7 and deprotonated N1 of guanosine. Chelation of inosine through N7 and the exocyclic keto oxygen O6 was not observed. X-ray crystal structure determinations of bis(purine)platinum(II) complexes have, to date, revealed only the presence of Pt-N7 bonds.[17,18]

The inactivation of DNA as a template for replication through the binding of DDP can be achieved in a variety of ways, and studies of the interaction of DDP with polynucleotides have led to some specific proposals of its mode of action.

Monofunctional coordination of the platinum complex to a base on the DNA duplex could sterically block access to the polymerase active site. This model will not, however, account for the selective activity of the *cis* over the *trans* isomer. A more rigid complex, less susceptible to DNA repair mechanisms and blocking polymerase activity, would arise through bidentate coordination of an individual base to the platinum atom. The chelation of guanine at N7 and O6 sites to DDP has been suggested[20,21] as a mode for the activity of the drug. The absence of definitive evidence for N7-O6 chelation in a model system, however, casts doubt on this proposal. X-ray photoelectron spectroscopic results have been interpreted as evidence for O6 coordination to platinum when *cis*- but not *trans*-DDP binds to DNA. Intercalation of DDP to DNA, which would alter the conformation of the duplex, has been ruled out as a binding mode based on the inability of DDP to unwind superhelical DNA or to inhibit competitively the binding of ethidium bromide, a known intercalator.[22] These same experiments suggested that DDP prefers to coordinate to exposed donor sites on the bases, normally involved in base pairing, of locally unwound regions of the duplex. Buoyant density studies using polynucleotides of varying G-C content have shown the preferential binding of DDP to G-C-rich DNAs.[23]

Inter- and intrastrand cross-linking of DNA by a bifunctional platinum reagent would constrain the otherwise flexible polymer duplex, could prevent strand separation, and might account for the antitumor activity of DDP. A selective reduction in the template activity of poly[dAT · dAT] in the presence of DDP led to the proposal that platinum forms interstrand cross-links between opposite and adjacent adenines through the N6 amino nitrogen atom.[24] The proposed involvement of the exocyclic amino group as a coordinating ligand has no precedence in model studies. Interstrand cross-linking has been demonstrated[25] through sedimentation studies using heavy, 5-bromodeoxyuridine-containing DNA of mammalian cells following their treatment in culture with both *cis*- and *trans*-DDP. The frequency of cross-linking did not correlate with the biological activity of the complexes, however. The fact[26] that DDP produces large increases in the buoyant density of poly dG · poly dC and unexpectedly small shifts of poly[dGC · dGC] led to the proposal[27] that DDP cross-links adjacent guanine bases through the N7 site. Various models of the mechanism of action of DDP are summarized in FIGURE 3.

PLATINUM BLUES AND THEIR RELATIONSHIP TO THE BINDING OF DDP TO NUCLEIC ACIDS AND THEIR CONSTITUENTS

While investigating the binding of DDP to polynucleotides it was observed that blue products are formed over several days of incubation of *cis*-diammineplatinum(II) hydrolysis products (cf. FIGURE 1) with poly U. This reaction was subsequently found to occur with thymine, uracil, and an assortment of substituted pyrimidines, leading to the formation of very soluble, deep-blue solid complexes.[28] These "platinum pyrimidine blues" were tested against a broad spectrum of tumor systems, and many were found to have high antitumor activity and low renal toxicity compared to the parent compound DDP.[28,29] The composition and structures of these amorphous blue powders were uncertain, however.

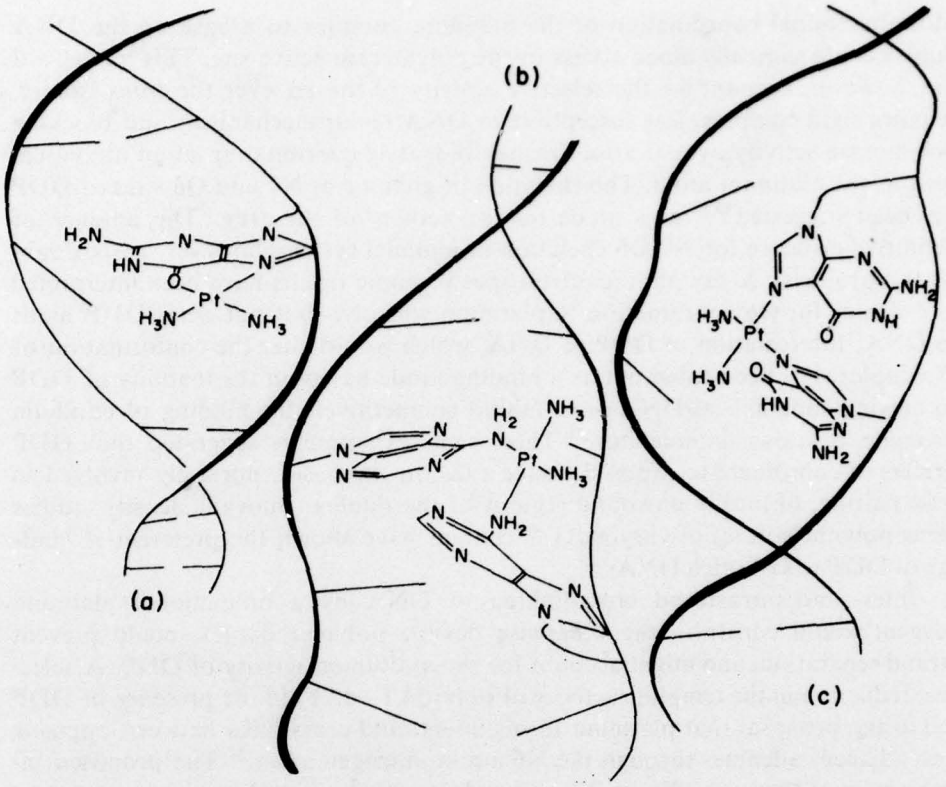


FIGURE 3. Postulated models by which DDP might inhibit DNA replication: (a) chelation at the N7–O6 site of guanine;[20,21] (b) formation of an interstrand crosslink between adenine units;[24] (c) formation of intrastrand crosslinks at adjacent guanine bases. [27]

Blue platinum complexes, although rare, had been observed previously. In 1908 a blue complex was reported[30] to have formed in the reaction of $Pt(CH_3CN)_2Cl_2$ with silver sulfate or silver nitrate. The product, termed "platinblau," was characterized as monomeric $Pt(CH_3CONH)_2 \cdot H_2O$ on the basis of chemical analysis and freezing-point depression measurements. It was later found[31] that platinblau could not be prepared from mixtures of acetamide and platinum salts, although the original synthesis could be repeated. By analogy to postulated structures for a number of deeply colored related platinum complexes, platinblau was proposed to have "a polymeric structure involving acetamido-bridges." More recently, a crystalline blue product was isolated[32] by allowing $Pt(CH_3CN)_2Cl_2$ to react with trimethylacetamide. The crystals were found to be a mixture of three interconvertible species, two of which were yellow and crystalline, the third of which was blue and amorphous. Chemical and spectroscopic analyses of this last component led to its formulation as $Pt[(CH_3)_3CCONH]_2Cl_2$, a platinum(IV) complex with bidentate amidate ligands. X-ray photoelectron spectra[33] of the blue trimethylacetamide complex do not support a platinum(IV) oxidation-state formulation, however, based on the $4f_{7/2}$ platinum electron binding energy. The various proposals for the structure of platinblau are displayed in FIGURE 4.

The finding that platinum pyrimidine blues possess a high degree of antitumor activity generated substantial interest in elucidating their structures as well as that of platinblau. Blue platinum compounds have been synthesized from a number of amides and *cis*-diammine platinum reagents.[28,34-36] Use of the analogous *trans*-diammineplatinum complex in the synthesis does not produce blue compounds. Mass spectrometry,[37] sedimentation analysis,[36,38] and kinetic studies[34] of the formation and decomposition of the unstable blue compounds in solution are consistent with a polymeric chain of platinum atoms. An oxidative titration of the deeply colored purple complex formed upon incubation of 1-methylthymine with dicyclopropylamineplatinum(II) hydrolysis products provided evidence[36] for non-integral formal oxidation state of the platinum atoms in the complex. These properties, polymerization and mixed oxidation states, of the blue complexes resemble those of the solid partially oxidized, one-dimensional platinum chain compounds,[39] one of which, $K_{1.64}Pt(oxalate)_2$, exhibits a blue absorption band in concentrated acidic aqueous solutions.[40] The platinum pyrimidine blues are paramagnetic, judging from magnetic susceptibility[34] and electron-spin resonance[41] measurements, a property that is also consistent with a mixed-valence formulation.

Both biological and chemical investigations of the platinum pyrimidine blues have been hampered by the lack of reproducibility in the preparation of the compounds. It has long been realized that an unambigous determination of the chemical composition and structure of these species requires the isolation of a crystal-

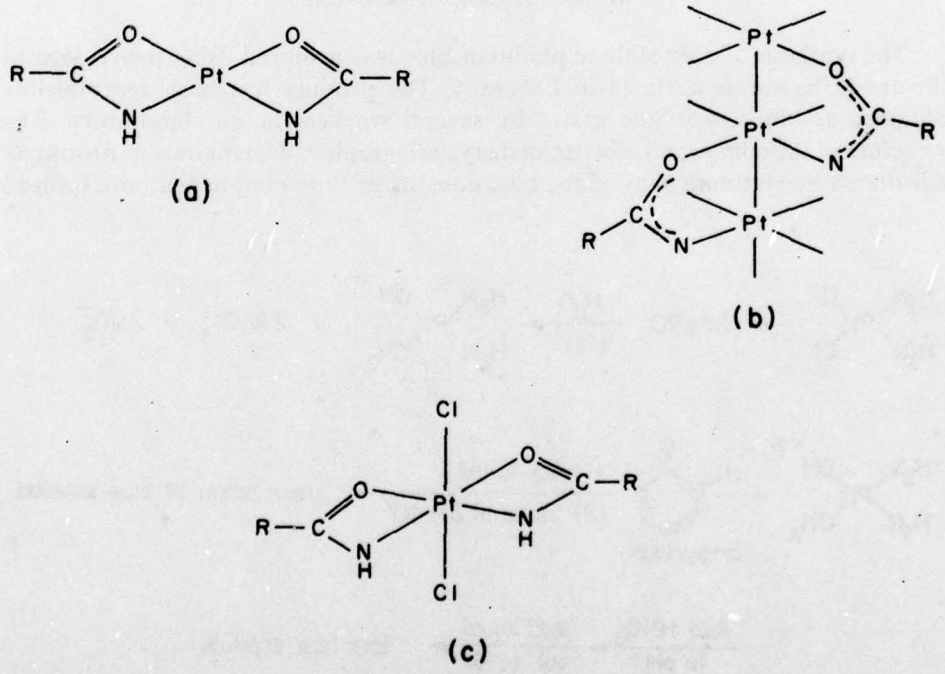
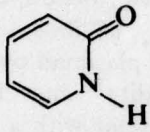


FIGURE 4. Proposals for the structure of platinblau: (a) a monomeric bis(acetamide) complex;[30] (b) a polymeric structure involving acetamido bridges;[31] (c) a platinum(IV) chelating amidate complex.[32]

line blue complex for x-ray crystallographic analysis. Studies in our laboratory, showing the platinum pyrimidine blues to be a mixture of oligomers with varying degrees of stability in solution,[34,38] suggested that single crystals might be obtained under certain conditions. Firstly, an amide ligand with only one nitrogen donor atom would eliminate the formation of mixtures of compounds differing in the site of attachment of the ligand to the metal ion. Secondly, formation of oligomeric mixtures of variable chain length, perhaps the most severe limitation to crystallization, might be avoided by using a sterically hindered amide ligand lacking additional hydrogen-bonding substituents that could stabilize intercomplex interactions in a chain. Finally, the positive charge on the blue complex and its instability to base (hydroxide) required a synthesis employing low pH conditions and high concentration of counterion at the critical, crystallization stage. Using α-pyridone,



α-pyridone

a pyrimidine analog, as the amide ligand and conditions of the kind just described, a crystalline platinum blue was synthesized and its structure determined through x-ray crystallography.[42]

Cis-Diammineplatinum α-Pyridone Blue: The Molecular Structure

The synthesis of a crystalline platinum blue was achieved using α-pyridone as the amide ligand as outlined in Figure 5. The product has been reproducibly obtained as blue crystalline plates by several workers in our laboratory. The structure of the compound, determined crystallographically, is shown in Figure 6. *Cis*-diammineplatinum α-pyridone blue consists of four platinum atoms bridged

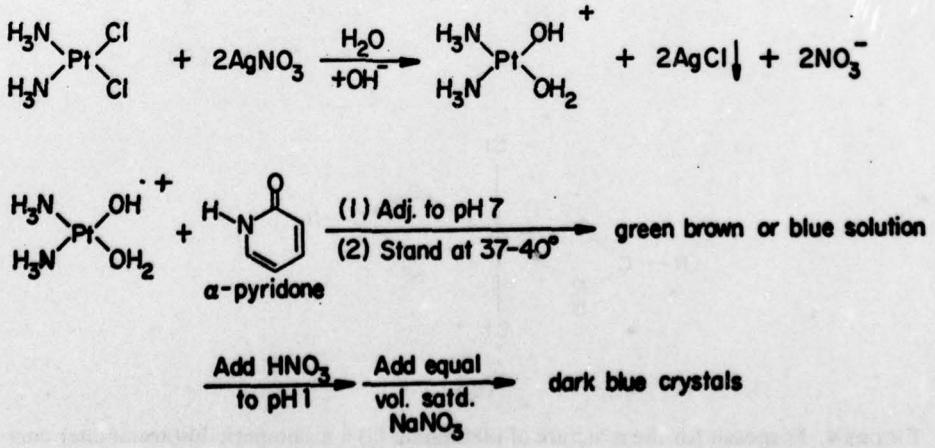


Figure 5. The synthesis of *cis*-diammineplatinum α-pyridone blue.[42]

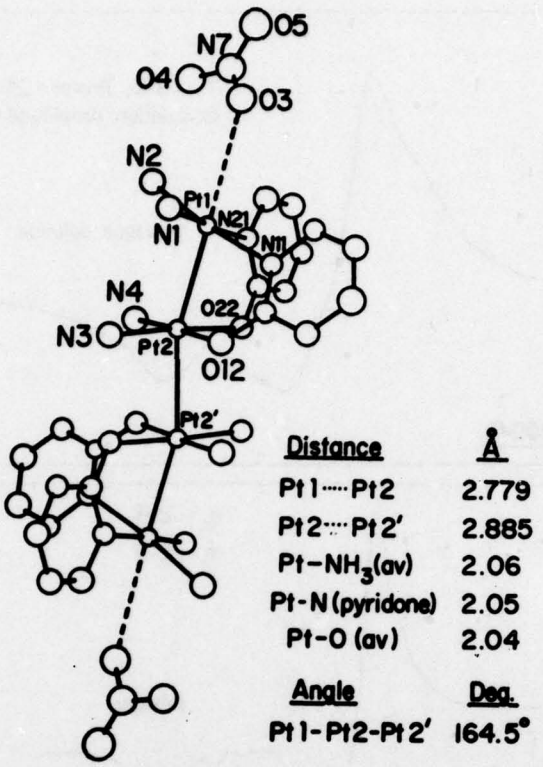


FIGURE 6. The structure[42] of *cis*-diammineplatinum α-pyridone blue showing selected average bond lengths and angles.

by α-pyridonate ligands. The tetramer is composed of two centrosymmetrically related dimers, as required by the space group symmetry. Within each dimer, two *cis*-diammineplatinum units are held together by a platinum-platinum bond (d_{Pt-Pt} = 2.779 Å) and two α-pyridonate bridges. The two platinum coordination planes form a dihedral angle of 28.7° owing to the short N···O bite distance (2.31 Å) of the pyridonate ligands. The ammine groups are in van der Waals contact, with repulsive interactions being minimized by the splaying of the coordination planes and a 23° tortional twist about the platinum-platinum bond axis. The amidate ligands bridge in an identical manner, one coordination plane being comprised of two ammine groups and two deprotonated α-pyridone nitrogen atoms, the other consisting of two ammine groups and two oxygen atoms from the α-pyridonate ligands. The two dimers are further associated by a platinum-platinum bond at a distance of 2.885 Å. This interaction is stabilized by hydrogen bonding between the ammine groups of one dimeric unit and the pyridonate oxygen atoms of the other. The four platinum atoms form a zig-zag chain with a Pt1-Pt2-Pt2′ angle of 164.5°. This value may be compared with the angles found in the one-dimensional platinum chains, 173.08° in $K_{1.75}Pt(CN)_4 \cdot 1.5H_2O$[43] and 177.8° in $K_{1.6}Pt(C_2O_4)_2 \cdot 1.2H_2O$.[44] A channel of nitrate anions and water molecules surrounds the oligomeric complex in the crystal lattice, affording hydrogen-bond acceptors for the ammine ligands. The tetranuclear chain is capped

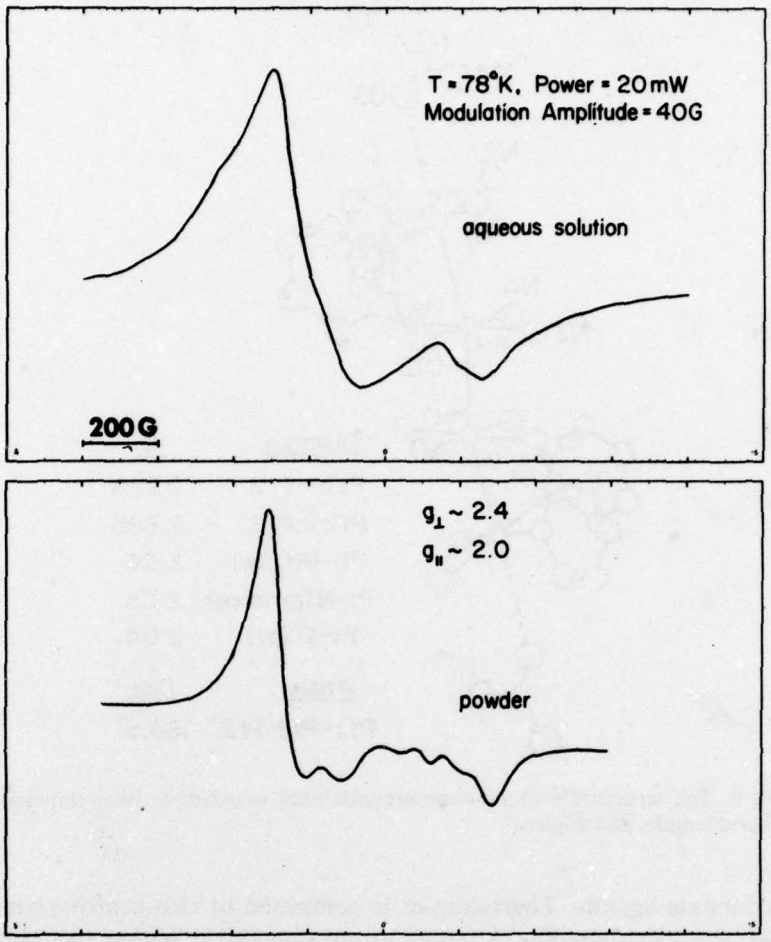


FIGURE 7. ESR spectra of (top) a frozen aqueous solution and (bottom) solid *cis*-diammineplatinum α-pyridone blue. The field is increasing from left to right.

at both ends by weakly bonded nitrate anions (Pt···O distance = 3.29 Å). The elemental and x-ray analyses establish the chemical formulation as $[Pt_2(C_5H_4NO)_2(NH_3)_4]_2(NO_3)_5 \cdot H_2O$. The platinum formal oxidation state is therefore 2.25.

The metal-metal distances (2.779 Å and 2.885 Å) observed in the *cis*-diammineplatinum α-pyridone blue structure reflect the nonintegral formal oxidation states of the platinum atoms. The platinum-platinum distance is shorter than predicted from bond length-oxidation state correlations for the partially oxidized one-dimensional platinum chain complexes.[45] Comparisons with results for $K_2[Pt_2(SO_4)_4(H_2O)_2]$ (Pt-Pt bond distance = 2.446 Å)[46] and $Pt_2(NH_3)_4P_2O_7$ (Pt-Pt bond distances = 3.22 Å and 3.11 Å),[47] two oligomeric bridged platinum complexes, however, reveal a qualitative agreement between the extent of metal-metal bonding and formal oxidation state, 3.0, 2.25, and 2.0 in the sulfate, pyridonate, and pyrophosphate bridged structures, respectively.

Spectroscopic and Chemical Properties of *Cis*-Diammineplatinum α-Pyridone Blue

Additional evidence for the nonintegral formal oxidation state assignment is provided through the electron spin resonance (ESR) spectrum of *cis*-diammineplatinum α-pyridone blue. FIGURE 7 shows the ESR spectra of both solid and frozen aqueous solutions of the compound, characterized by a broad axial signal, $g_\perp \sim 2.4$, $g_\parallel \sim 2.0$. The spectrum is strikingly similar to that reported for the platinum pyrimidine blues[41] and strongly suggests structural similarities. The regular signal pattern at high field observed in the powder spectrum is probably due to ^{195}Pt hyperfine coupling interactions (^{195}Pt has $I = \frac{1}{2}$ and is 33.8% abundant). The magnitude of the g values may be compared to those observed in studies[48] of $K_2Pt(CN)_4Br_{1/3} \cdot 3H_2O$, the spectrum of which was interpreted in terms of d_{z^2}-like hole states. A complete analysis of the ESR spectrum is not possible at present because of poor resolution of a broad signal complicated by the weighting of contributions from ^{195}Pt statistically distributed in the tetranuclear chain. Unlike the partially oxidized one-dimensional conductors, *cis*-diammineplatinum α-pyridone blue exhibits an ESR signal in solution. Integration of a solution spectrum calibrated with a copper(II)-EDTA standard yielded a value of 0.8 ± 0.2 unpaired spins per tetramer unit, in agreement with both the elemental and x-ray crystallographic analyses.

The visible spectrum of *cis*-diammineplatinum α-pyridone blue is given in FIGURE 8. The compound is unstable in aqueous solution as judged by the diminu-

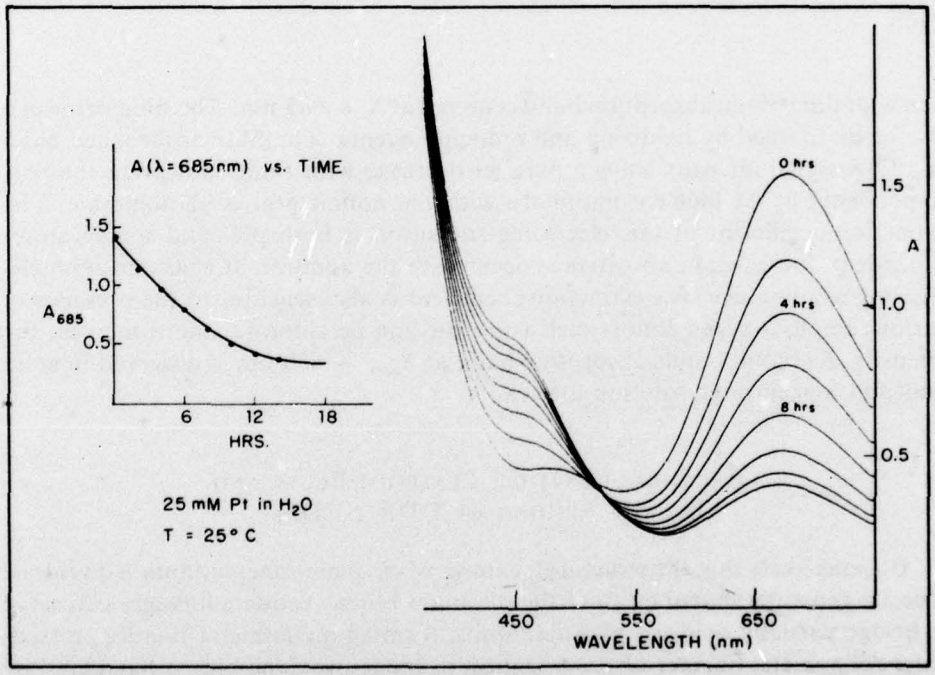


FIGURE 8. Visible spectra of *cis*-diammineplatinum α-pyridone blue in water at 25°C over various time intervals. Inset shows the time dependence of the 685 nm band.

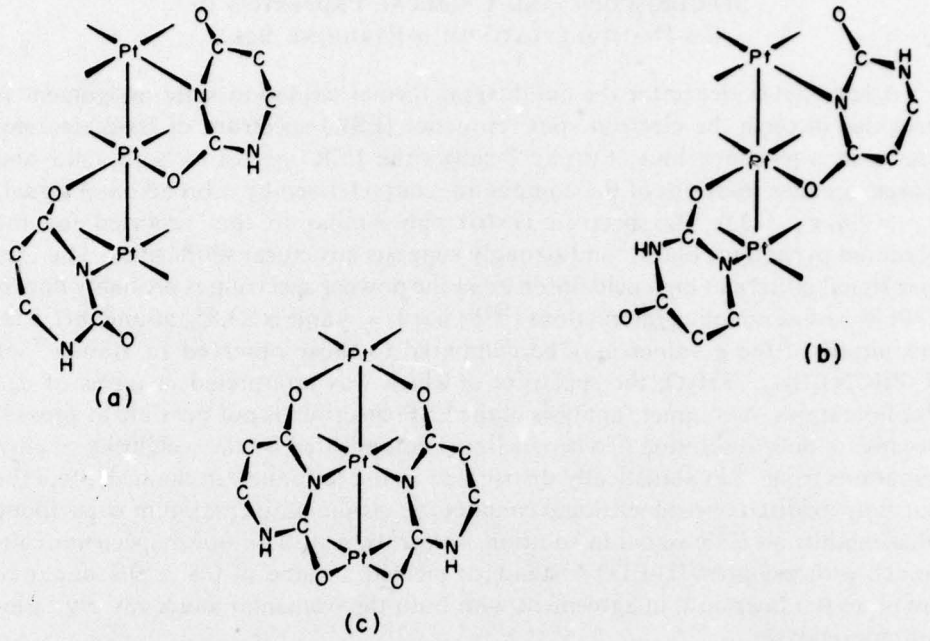


FIGURE 9. Possible structures for platinum uracil blues: (a) alternate singly bridging uracil anions; (b) a mixture of amidate linkages through both deprotonated N1 and N3 nitrogen atoms of uracil; (c) three platinum atoms bridged by two uracil anions through N3 nitrogen atoms and both exocyclic oxygen atoms, O2 and O4. Double bonds are not shown, for clarity.

tion with time of the absorption band centered at λ = 685 nm. The blue color can also be discharged by oxidizing and reducing agents. The blue absorbance band and ESR signal intensity show a parallel decrease with time, indicating the correspondence of the blue chromophore with the nonintegral oxidation state. The extinction coefficient of this electronic transition is both pH- and temperature-dependent. Increases in absorbance occur with the addition of acid and with decreasing temperature. The extinction coefficient is also sensitive to the presence of various anions; oxygen donors such as nitrate and perchlorate anions increase the intensity. A second visible absorption band at λ_{max} = 480 nm is observed in solid mull and concentrated solution spectra.

RELATION TO OTHER PLATINUM BLUES AND TO THE BINDING OF DDP TO DNA

It seems likely that the structural features of *cis*-diammineplatinum α-pyridone blue are generally shared by all of the platinum blues. Amidate linkages can serve to bridge partially oxidized platinum units, forming metal-metal bonded, mixed-valent oligomers. Further oligomerization of the α-pyridone blue is hampered by the steric bulk of the α-pyridonate rings and the lack of hydrogen-bonding groups at the chain ends. FIGURE 9 shows a number of possible configurations that the

platinum pyrimidine blue structures might achieve. Variable chain lengths are likely for those compounds, with alternating singly (rather than doubly) bridged arrangements giving rise to a variety of permutations.[34] The pyrimidines offer a further possibility in choice of amidate-binding site, with both deprotonated N1 and N3 as potential nitrogen donor atoms. The pyrimidines could also form hexamers by the pairing of units in which three platinum atoms are linked through two pyrimidine bridges.

The *cis*-diammineplatinum α-pyridone blue structure suggests new possibilities for the mode of binding of DDP to DNA. DDP binds preferentially to regions rich in G-C content. Recent studies[49] have again raised the possibility that N7 might not be the only, or even the biologically important, binding site of DDP on DNA and suggest the sensitivity of binding site to solution pH and kinetic factors. In neutral solution, the N1 and N7 donor sites show similar tendencies to bind platinum. In double-stranded DNA, the N7 position is more accessible and therefore is likely to be a primary site of attachment. The antitumor activity of DDP, however, may arise through the binding to deprotonated N1, disrupting the normal Watson-Crick hydrogen bonding in the double helix. Evidence for preferential binding of DDP to exposed regions of the duplex has already been mentioned.[22] The platinum blue structure suggests that, in regions of locally high G-C content, guanine bases might link *cis*-diammineplatinum units through amidate bridges using the deprotonated N1 and exocyclic keto oxygen O6; the result would be a tightly bound, stable configuration. FIGURE 10 shows the proposed complex. In this regard it is worth noting the polymeric structure[50] of 1-methylcytosine bound to silver nitrate (*FIGURE 11*) *in which silver ions* are linked by cytosine units through N3 and O2 donor atoms in a fashion strikingly similar to that observed in *cis*-diammineplatinum α-pyridone blue. In the silver complex the metal-metal distance is 3.370 Å, too long for metal-metal bonding. This result demonstrates that deprotonated N1-O6 amidate bridging by guanosine, or a similar bridged structure involving N3 and O4 of cytosine, might occur when DDP binds DNA without necessitating partial oxidation of the platinum.

The chemical reactivity of the platinum blues in solution suggests additional possibilities that might account for the antitumor activity of DDP. The *cis*-diammineplatinum blues are unstable in solution. Elemental analyses of a variety of

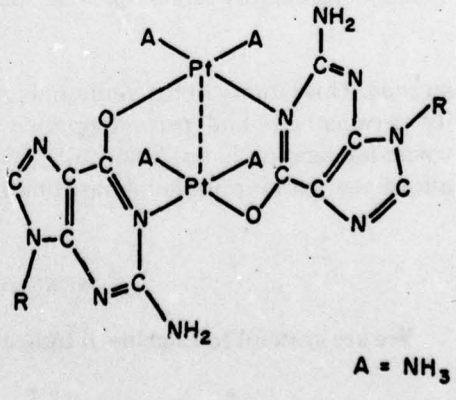


FIGURE 10. A possible complex between *cis*-diammineplatinum units and guanine bases.

platinum-pyrimidine blues,[28] as well as *cis*-diammineplatinum α-pyridone blue, reveal variable, generally low values for the nitrogen content. It is possible that, upon coordination to platinum, the amidate nitrogen atoms might labilize the ammine ligands *trans* to them, facilitating decomposition. The addition of a large excess of ammonium nitrate to aqueous solutions of *cis*-diammineplatinum α-pyridone blue enhances the stability of the blue color over a period of time. This reactivity of the blues, in which ammonia is lost upon binding of the amidate moiety, might have a parallel in the reactivity of DDP with the nucleic acid bases. Binding *cis*-diammineplatinum to the deprotonated nitrogen donors on the bases and possibly to the oxygen atoms might labilize the ammonia ligands, providing third and fourth platinum binding sites for additional cross-linking of the DNA

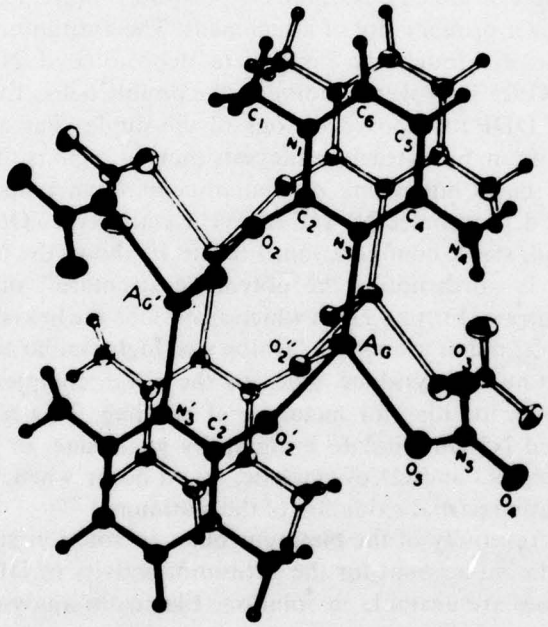


FIGURE 11. The structure of the nitrate salt of the complex formed between silver(I) and 1-methyl cytosine. (By permission of the American Chemical Society.[50])

strands. This lability of the ammonia groups would explain the differences in activity between *cis*- and *trans*-diammine complexes, since the *trans* arrangement, where labilization is not kinetically favored following DNA binding, would not afford new sites for platinum base binding and cross-linking.

ACKNOWLEDGMENT

We are grateful to Engelhard Industries for generous loans of K_2PtCl_4.

Notes and References

1. Rosenberg, B., L. Van Camp & T. Krigas. 1965. Nature **205:** 698.
2. Rosenberg, B., L. Van Camp, E. B. Grimley & A. J. Thomson. 1967. J. Biol. Chem. **242:** 1347.
3. (a) Rosenberg, B., L. Van Camp, J. E. Trosko & V. H. Mansour. 1969. Nature **222:** 385; (b) Rosenberg, B. & L. Van Camp. 1970. Cancer Res. **30:** 1799; (c) For a review, see Hill, J. M., E. Loeb, A. MacLellan, N. O. Hill, A. Khan & J. J. King. 1975. Cancer Chemother. Rep. **59:** 647.
4. (a) Connors, T. A. & J. J. Roberts, Eds. 1974. Platinum Coordination Complexes in Cancer Chemotherapy. Springer-Verlag. New York, N.Y.; (b) Khan, A., Ed. 1977. Proc. Third Internat. Symp. Platinum Coordination Complexes in Cancer Chemotherapy. J. Clin. Hematol. Oncol. Vol. 7.
5. Cleare, M. J. & J. D. Hoeschele. 1973. Bioinorg. Chem. **2:** 187.
6. Langford, C. H. & H. B. Gray. 1965. Ligand Substitution Processes. W. A. Benjamin, Inc., New York, N.Y.
7. Lim, M. C. & R. B. Martin. 1976. J. Inorg. Nucl. Chem. **38:** 1911.
8. Rosenberg, B. 1975. Cancer Chemother. Rep. **59:**589.
9. Harder, H. C. & B. Rosenberg. 1970. Int. J. Cancer **6:** 207.
10. Howle, J. A. & G. R. Gale. 1970. Biochem. Pharm. **19:** 2757.
11. Mansy, S., B. Rosenberg & A. J. Thomson. 1973. J. Am. Chem. Soc. **95:** 1633.
12. Kong, P. C. & T. Theophanides. 1974. Inorg. Chem. **13:** 1167.
13. Kong, P. C. & T. Theophanides. 1974. Inorg. Chem. **13:** 1981.
14. Robins, A. B. 1973. Chem. Biol. Interactions **7:** 11.
15. Tobias, R. S., G. Y. H. Chu & H. J. Peresie. 1975. J. Am. Chem. Soc. **97:** 5305.
16. Terzis, A., N. Hadjiliadis, R. Rivest & T. Theophanides. 1975. Inorg. Chim. Acta **12:** L5.
17. Gellert, R. W. & R. Bau. 1975. J. Am. Chem. Soc. **97:** 7379.
18. Goodgame, D. M. L., I. Jeeves, F. L. Phillips & A. C. Skapski. 1975. Biochem. Biophys. Acta **378:** 153.
19. Lock, C. J. L., R. A. Speranzini & J. Powell. 1976. Can. J. Chem. **54:** 53.
20. Miller, M. M., J. P. Macquet & T. Theophanides. 1975. Biochem. Biophys. Acta **402:** 166.
21. Dehand, J. & J. Jordanov. 1976. J. Chem. Soc. Chem. Commun. 598.
22. Howe-Grant, M., K. C. Wu, W. R. Bauer & S. J. Lippard. 1976. Biochemistry **15:** 4339.
23. Stone, P. J., A. D. Kelman & F. M. Sinex. 1974. Nature **251:** 736.
24. Harder, H. C. & R. G. Smith. 1977. J. Clin. Hematol. Oncol. **7:** 401.
25. Pascoe, J. M. & J. J. Roberts. 1974. Biochem. Pharm. **23:** 1345.
26. Stone, P. J., A. D. Kelman, F. M. Sinex, M. M. Bhargava & H. O. Halvorson. 1976. J. Mol. Biol. **104:** 793.
27. Kelman, A. D., H. J. Peresie & P. J. Stone. 1977. J. Clin. Hematol. Oncol. **7:** 440.
28. (a) Davidson, P. J., P. J. Faber, R. G. Fischer, Jr., S. Mansy, H. J. Peresie, B. Rosenberg & L. Van Camp. 1975. Cancer Chemother. Rep. **59:** 287; (b) Rosenberg, B. 1975. Cancer Chemother. Rep. **59:** 589.
29. Speer, R. J., H. Ridgeway, L. M. Hall, D. P. Stewart, K. E. Howe, D. Z. Lieberman, A. D. Newman & J. M. Hill. 1975. Cancer Chemother. Rep. **59:** 629.
30. Hofmann, K. A. & G. Bugge. 1908. Ber. **41:** 312.
31. Gillard, R. D. & G. Wilkinson. 1964. J. Chem. Soc. 2835.
32. Brown, D. B., R. D. Burbank & M. B. Robin. 1969. J. Am. Chem. Soc. **91:** 2895.
33. Cahen, D. 1973. Ph.D. Dissertation. Northwestern Univ. Evanston, Ill.
34. Lerner, E. I. 1976. Ph.D. Dissertation. Columbia Univ. New York, N.Y.
35. Flynn Jr., C. M., T. S. Viswanathan & R. B. Martin. 1977. J. Inorg. Nucl. Chem. **39:** 437.
36. Thomson, A. J., I. A. G. Roos & R. D. Graham. 1977. J. Clin. Hematol. Oncol. **7:** 242.

37. MACFARLANE, R. D. & D. F. TORGERSON. 1976. Science **191:** 920.
38. LERNER, E. I., W. R. BAUER & S. J. LIPPARD. To be submitted for publication.
39. For a review see MILLER, J. S. & A. J. EPSTEIN. 1976. Prog. Inorg. Chem. **20:** 1.
40. KROGMANN, K. & P. DODEL. 1966. Chem. Ber. **99:** 3408.
41. LIPPERT, B. 1977. J. Clin. Hematol. Oncol. **7:** 26.
42. BARTON, J. K., H. N. RABINOWITZ, D. J. SZALDA & S. J. LIPPARD. 1977. J. Am. Chem. Soc. **99:** 2827.
43. REIS JR., A. H., S. W. PETERSON, D. M. WASHECHECK & J. S. MILLER. 1976. J. Am. Chem. Soc. **98:** 234.
44. REIS JR., A. H., S. W. PETERSON & S. C. LIN. 1976. J. Am. Chem. Soc. **98:** 7839.
45. (a) WILLIAMS, J. M. 1976. Inorg. Nucl. Chem. Lett. **12:** 651; (b) REIS JR., A. H. & S. W. PETERSON. 1976. Inorg. Chem. **15:** 3186.
46. MURAVEISKAYA, G. S., G. A. KUKINA, V. S. ORLOVA, O. N. EVSTAF'EVA & M. A. PORAI-KOSHITS. 1976. Dokl. Akad. Nauk. SSSR. **226:** 596.
47. STANKO, J. A. Results quoted by M. J. Cleare in Ref. **4a:** 24.
48. MEHRAN, F. & B. A. SCOTT. 1973. Phys. Rev. Let. **31:** 1347.
49. LIM, M. C. & R. B. MARTIN. 1976. J. Inorg. Nucl. Chem. **38:** 1915.
50. MARZILLI, L. G., T. J. KISTENMACHER & M. ROSSI. 1977. J. Am. Chem. Soc. **99:** 2797.

PSEUDO-ONE-DIMENSIONAL NIOBIUM CHALCOGENIDES $NbSe_3$ AND $I_{0.33}NbSe_4$*

J. Rouxel and A. Meerschaut

Laboratoire de Chimie Minérale A, Faculté des Sciences
Nantes, France

P. Haen and P. Monceau

C.R.T.B.T.-C.N.R.S.
Centre de Recherches Très Basses Températures
Grenoble, France

$NbSe_3$

The triselenide of niobium was recently prepared and described by A. Meerschaut and J. Rouxel.[1]

$NbSe_3$ is a monoclinic system. The structure was determined from a collection of intensities by an automatic diffractometer Nonius Cad 3. The reliability factor was refined to a minimum value of 0.046 when an anisotropic temperature factor for all the atoms was considered. The atoms are all in position 2e with space-group $P2_1/m$.

$$2e: X\,\tfrac{1}{4}\,Z,\ \bar{X}\,\tfrac{3}{4}\,\bar{Z}$$

FIGURE 1 shows the projection of the structure on the plane XOZ.

Each niobium is surrounded by six seleniums occupying the corners of a trigonal prism. These prisms are stacked along the *b*-axis and give this structure a pseudo-one-dimensional character. The distance between the niobium atoms situated along the *b*-axis is constant and equal to 3,478 Å. The distance between niobium atoms in neighboring chains ranges approximately between 4.40 and 4.60 Å. In the prisms, two of the three selenium atoms at each triangular base are sufficiently close so that one may envision a Se-Se bond.

This structural model is found for the most part in the trichalcogenides of the transition metals and, namely, in $ZrSe_3$, which is well known.[2]

The pseudo-one-dimensionality of the structure led us to undertake a study on the physical properties of this compound. This study was performed at C.R.T.B.T. in Grenoble with Dr. P. Monceau and Dr. P. Haen.

The resistivity along the *b*-axis has been measured on a single crystal of approximate dimensions 7 × 0.05 × 0.01 mm. The conventional four-probe direct current technique was used.[3] The value of 600 $\mu\Omega$cm for the resistivity is comparable to that found for TTF-TCNQ and $(SN)_x$. The variation of ρ with respect to temperature between 1.2°K and 300°K is typical of metallic-type behavior. The essential interest of this curve resides in the presence of two strong anomalies at $T_1 = 125$°K and $T_2 = 49$°K (temperatures for the maxima). The amplitude of these peaks attains, respectively, 10% and 30% of the resistivity at 300°K.

*Manuscript received June 6, 1977.

0077-8923/78/0313-0701 $1.75/1© 1978, NYAS

The phenomena of hysterisis has not been observed upon varying the temperature over the region of the anomalous behavior.

The measurement of specific heat has been performed in an adiabatic calorimeter between 20° and 300°K on a sample size of 0.8 g.[3] The values for specific heat shows an anomaly at the same temperature T_2 that was found in the resistivity data.

We interpreted the previous measurements as the appearance of charge-density wave (CDW) by analogy to the layered dichalcogenides.[4] The formation of CDW depends upon the competition between two terms in the expression for the free energy of the system. The strain energy is increased with distortions of superstructure and the gain in electronic energy resulting from an opening of the gap in the Fermi surface. The last term increases as the temperature decreases, since the edge of the Fermi surface is sharper at low temperatures.

If one applies pressure the rigidity of the lattice increases, with a subsequent increase in the strain energy. The CDW will remain stable at a lower temperature, due to a gain in electronic energy.

The temperature at which anomalies appear changes linearly with pressure. One calculates $dT_0/dP = -4°K/Kbar$. The first anomaly is reduced to 30% of its initial magnitude when subjected to 4 Kbar, the second anomaly disappears after 6 Kbar.[3]

One may add that the critical temperature for superconductivity is increased under pressure, $dT_c/dP \sim 0.4\ K/Kbar$.

The coordination of physical properties described is compatible with the hypothesis of CDW. The observation of an eventual superstructure by electron diffraction will be a proof for the existence of CDW.

$I_{0.33}NbSe_4$

$I_{0.33}NbSe_4$ has been obtained by vapor transport from $NbSe_3$ ($NbSe_3 + I_2$). The crystals obtained have a needle-like shape.

$I_{0.33}NbSe_4$ has tetragonal symmetry. The structure has been determined by a

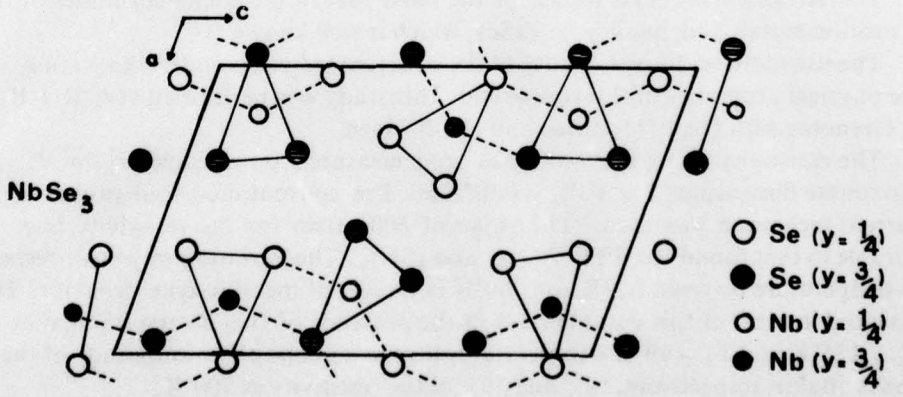


FIGURE 1. Projection of the structure on the plane XOZ.

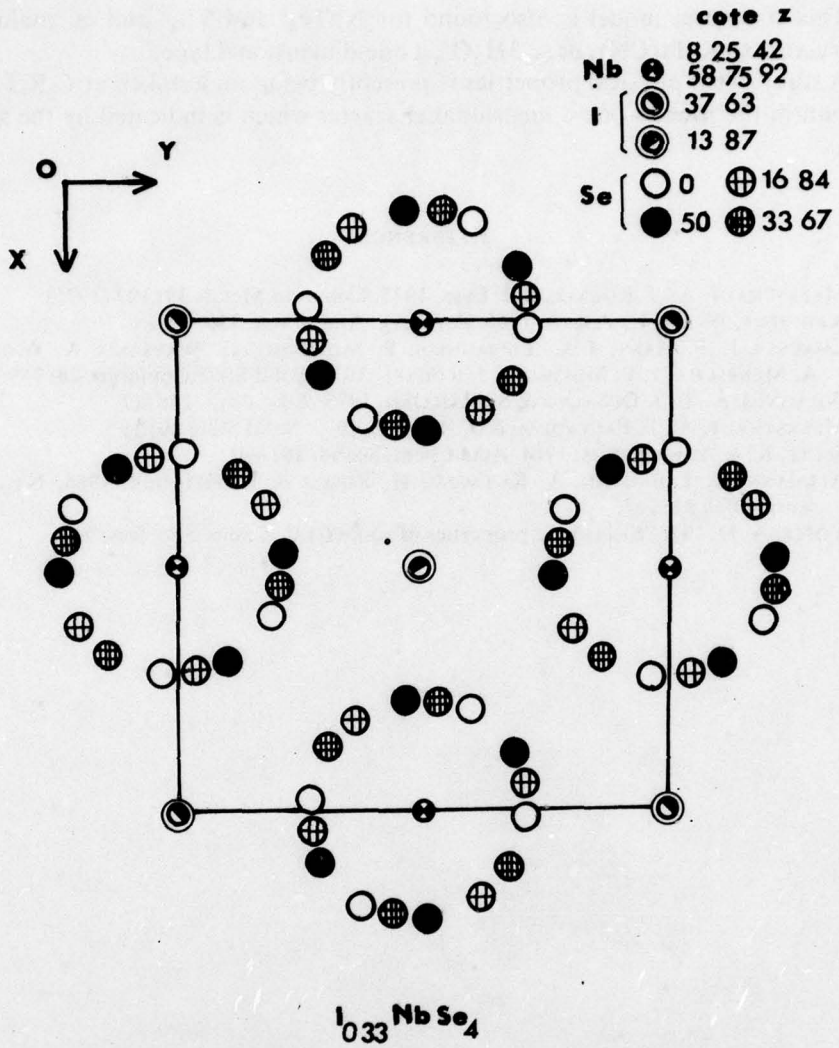


FIGURE 2. Projecture of the structure on the plane XYO.

collection of intensities on an automatic diffractometer Nonius Cad 3. The reliability factor has been refined to an R value of 0.030 after considering the thermal anisotropic temperature factor for all of the atoms.[5]

FIGURE 2 shows the projection of the structure on the plane XYO. Each atom of niobium is surrounded by eight selenium atoms occupying the corners of rectangular antiprism. On such a rectangular base there exist two short Se-Se distances (~2.35 Å) and two longer Se-Se distances (~3.55 Å). The antiprisms are stacked along the *c*-axis in a "helicoîdale" arrangement; two different Nb-Nb distances along this axis are found (3.06 Å and 3.25 Å). Between neighboring chains the Nb-Nb distances are equal to 6.71 Å. The iodine atoms are situated between the chains.

This structural model is also found for $NbTe_4$[6] and VS_4[7] and is analogous in structure to $K_2Pt(CN)_4Br_{0.30}3H_2O$[8], a one-dimensional type.

A study of the physical properties is presently being undertaken at C.R.T.B.T. to confirm the pseudo-one-dimensional character which is indicated by the structure.

References

1. Meerschaut, A., J. Rouxel, & J. Less. 1975. Common Metals **39:** 197 (1975).
2. Kroniert, W. and K. Plieth. 1965. Z. Anorg. Allg. Chem **336:** 207.
3. Chaussy, J., P. Haen, J. C. Lasjaunias, P. Monceau, G. Waysand, A. Waintal, A. Meerschaut, P. Molinié & J. Rouxel. 1976. Solid State Commun. **20:** 759.
4. Wilson, J. A., F. J. Di Salvo & S. Mahajan. 1975. Adv. Phys. **24:** 117.
5. Meerschaut, A., P. Palvadeau & J. Rouxel. 1977. Solid State **20:** 21.
6. Selte, K. & A. Kjekshus. 1964. Acta Chem. Scand. **18:** 690.
7. Allmann, R., I. Bauman, A. Kutaglu, H. Rosch & E. Hellner. 1964. Naturwissenschaffen **51:** 263.
8. Yoffe, A. D. 1976. Electromic properties of some CLC. Chem. Soc. Rev. **5:** 1.

PART IV. COVALENT MATERIALS

FULLY CONJUGATED POLYMER CRYSTALS: SOLID-STATE SYNTHESIS AND PROPERTIES OF THE POLYDIACETYLENES*

R. H. Baughman and R. R. Chance

Materials Research Center
Allied Chemical Corporation
Morristown, New Jersey 07960

INTRODUCTION

The electronic properties of linear polymers have been of research interest for a number of decades.[1,2] However, the gross structural inhomogeneity typical of conventional organic polymers has severely hindered research progress in this area. Conventional organic polymers are morphological jungles. For example, polymer crystallites contained in bulk semicrystalline polymers are typically about 100Å in chain-axis dimension. These crystallites are typically bounded by surfaces at which the polymer chains fold back upon themselves in an accordion fashion to complete the crystal. Defects such as dislocations and chain kinks are contained in the crystallites. Finally, these polymer crystallites are surrounded by a highly disordered matrix and occasionally interconnected by tie molecules that run from one folded-chain crystal to another.[3,4]

It is an awesome challenge to understand the relationships between electronic properties and structure for such complex materials. Many useful polymer properties are highly defect-limited. For these reasons, there has been considerable interest in developing methods for producing large dimension polymer single crystals having high structural perfection.

This work is concerned with the solid-state synthesis and electronic properties of large-dimension crystals of organic polymers. In contrast with the case for organic polymer crystals obtained by conventional methods, there are no intrinsic limitations on the dimensions of these crystals. In fact, it is feasible in principle to obtain these polymers as continuous single-crystal filaments.

These polymer crystals are of special importance for a number of different reasons. First, the large dimensions of these crystals permit the measurement of polymer properties which would be virtually impossible to determine for the extremely small crystals obtainable for conventional polymers. Second, the present polymer crystals have an extended-chain morphology rather than the folded-chain morphology typical of conventional organic polymeric materials. The individual polymer chains do not transverse the entire length of a macroscopic dimension crystal, so that chain-end defects occur within these crystals. Chain ends, however, are generally unsegregated; the effect of these defects on polymer properties is therefore minimized. A third important point is that the polymer crystals of interest here have fully conjugated backbones. As a consequence of this conjuga-

*Manuscript received July 8, 1977.

0077-8923/78/0313-0705 $1.75/1© 1978, NYAS

tion and the high structural perfection obtainable in the polymer crystals, a variety of interesting electronic properties arise.

General Concepts for Polymer Crystal Synthesis

In order to synthesize large-dimension polymer crystals, it is necessary to avoid intermediate states involving highly coiled polymer chain conformations. Kinetic limitations on the crystallization of such high-entropy molecular states essentially preclude the possibility of obtaining large-dimension, extended-chain crystals having high structural perfection.

There are basically two different methods for synthesizing polymer crystals from the monomer without involving highly disordered polymeric intermediate states. The first method involves nearly simultaneous crystallization and polymerization of monomer molecules at a liquid-solid or gas-solid interface. The second method is matrix-controlled solid-state synthesis. The first method, which has been analyzed by Wunderlich[5,6] for both synthetic and biological polymers, is analogous to the crystal growth of nonpolymeric materials from the liquid or vapor phases. The ideal case of simultaneous polymerization and crystallization could be viewed essentially as a crystallization process in which the product crystal phase has an unusually high interaction energy in one direction, corresponding to covalent bonds in the polymer chain. Interesting examples of less ideal processes are provided by Lee and Wunderlich[7] for the synthesis of polydiphenylsilylene from gaseous diphenylsilylene and by Wegner[8] for the growth of polyoxymethylene crystals by monomer insertion at fold surfaces. As is true for the crystal growth of molecular solids, the growth of polymer crystals is best obtained by selecting ambient conditions that result in a small free-energy change on crystal growth. This means that polymerization (crystallization) should be close to the ceiling temperature of the polymer. Difficulties associated with the formation of the initial polymer nuclei, obtaining nearly simultaneous crystallization and polymerization, maintaining active chain ends in the growing crystal, and operating close to equilibrium conditions, place severe constraints on this method.[5-7]

Solid-state polymerization is at present the most successful method known for producing large-dimension polymer single crystals.[9-18] This synthetic method utilizes the three-dimensional periodicity of a crystalline monomer phase as a template to determine the molecular and crystallographic structures of a polymer. In ideal cases, solid-state reaction transforms a monomer single crystal to a polymer single crystal with nearly the same dimensions and similar structural perfection. As mentioned by Adler,[19] solid-state polymerization reactions can be viewed fundamentally as phase transformations in which unusually strong interactions arise in the product phase, corresponding to the covalent bonds in the polymer structure. However, in contrast to the case which was discussed earlier for nearly simultaneous crystallization and polymerization, the solid-state reactions of greatest interest for polymer crystal synthesis do not involve crystallization as a discontinuous process. In the ideal case, the polymer should enter the polymerizing lattice as a solid solution over the entire monomer-to-polymer conversion range, because phase separation, with the associated shear and volume strains, will usually introduce imperfections in the polymerizing monomer.[9-12]

In the ideal case for polymer crystal synthesis by solid-state polymerization, there will exist a one-to-one correspondence between the crystal structure of the monomer and the chemical and crystallographic structure of the polymer. For most solid state synthesis reactions, however, the correspondence will be less than perfect.[19-25] In these cases limited degrees of order in the monomer phase will be preserved in the polymer crystallographic and/or molecular structure.

In the latter cases, either of two related factors can be important for decreasing order in the polymerized phase. First, the monomer lattice may constitute an imperfect template because it does not contain enough information for the required synthesis. This occurs, for example, when several reaction directions are crystallographically equivalent in the monomer phase. This also occurs as a result of structural imperfections in the monomer phase. For example, the periodicity of the monomer phase is disrupted in the vicinity of isolated dislocations or stacking faults. Consequently, near these defects the solid-state reaction either will not occur or will occur in a less ordered fashion than in more perfect regions of the crystal. A second, related point is that molecular packing determines whether a particular monomer phase will be reactive and the reaction mode of polymerizable monomer phases. For this reason different phases of the same monomer molecule often differ enormously in solid-state reactivity. If the structural changes that occur during reaction are too large, the reaction will destroy the perfection of the polymerizing phase. Consequently, the polymerizing phase will lose the ability to serve as a reliable template for further reaction.

When comparing different symmetry-allowed reaction modes that involve similar intramolecular energy changes and variations in similar kinds of intermolecular bonding, it is generally true that the observed reaction mode will be that mode which requires minimum atom displacements. The approximation here, which has important utility for solid-state synthesis, is that the reaction mode that requires the smallest atom displacements in going from a monomer array geometry to the polymer chain geometry will have the lowest activation free energy. Correspondingly, this reaction mode is expected to predominate. This simple least-motion concept has been used successfully to predict the relative reactivities of different monomer phases, the reaction modes of monomers having known structures, the structure of partially polymerized phases, and whether likely packing modes for a particular monomer molecule could result in a desired polymer structure.[10,12,24,25]

The importance of reaction mode in determining the adequacy of a monomer phase as a template for solid-state reaction is illustrated in FIGURE 1. The array of stick figures represent individual monomer molecules in a monomer phase. The polymerization reaction corresponds to the joining hands of the stick figures. The stick figures can potentially polymerize (i.e., join hands) by a number of different modes, three of which are illustrated in this figure. For a real crystal, one can predict the active polymerization mode by asking a simple question: How can the array of monomer molecules polymerize in such a way as to result in the least disruption of the polymerizing phase? Note that two of the three reaction modes pictured in FIGURE 1 are nonunique. In other words, two of these mode reactions are equally likely to proceed via either of two symmetry-related routes to produce distinguishable products. The key point here is that in order for a polymerization reaction (or associated phase transformation) to be unique, that reac-

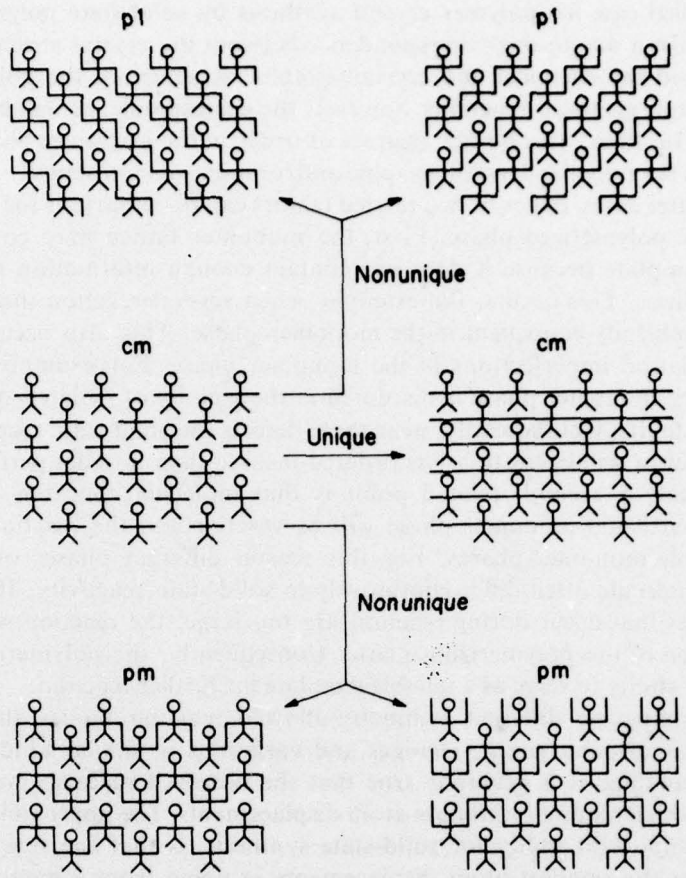


FIGURE 1. Schematic representation of matrix-controlled solid-state polymerization. The array symmetries are indicated above each array.

tion must preserve crystallographically all the symmetry elements of the precursor phase.[12,24,26] The reaction mode illustrated on the top of FIGURE 1 is nonunique because this reaction mode preserves neither the monomer unit mirror symmetry nor the crystallographic glide plane, which relates the monomers in neighboring verticle arrays. Similarly, the reaction mode shown at the bottom of FIGURE 1 is nonunique because only the former lattice symmetry element is preserved. Depending upon the degree of cooperativeness for the solid state reaction, lack of reaction uniqueness can result in molecular scale disorder, twinning, and/or a statistical relationship between parent and product crystal orientations. Note that this disorder will be introduced so as to preserve on a statistical basis those symmetry elements which cannot be retained in a periodic product phase. By knowing the type of reaction nonuniqueness evident for a particular solid-state synthesis reaction, it has been possible to predict the structure of defects.[23,24] This information is important for understanding defect sensitive electronic properties.

Examples of the Versatility and Limitations of Solid-State Polymer Crystal Synthesis

A variety of different organic monomers have been polymerized in the solid state to produce fully conjugated polymers. In most cases, however, the dimensional changes required for polymerization are so large that a highly disordered reaction product results. Nevertheless, lattice effects can still be significant in determining product structure. For example, the irradiation-induced polymerization of acetylene at low temperature gives a *cis* polymer in the liquid phase and a *trans* polymer in the solid phase.[27,28]

One broad class of compounds is exceptionally suitable for the solid-state synthesis of high structural perfection polymer single crystals. These are compounds that contain at least two conjugated acetylene groups. The remainder of this paper will be concerned with specific discussions of the solid-state synthesis and electronic properties of the polydiacetylenes.

For nearly a century it has been known that certain diacetylenes are unstable in the solid state. Typically, the colorless diacetylene crystals become deeply colored and insoluble upon thermal annealing or upon exposure to light. However, it was not until much more recently that this reactivity was correctly interpreted by Wegner as 1,4-addition polymerization.[9] He found that in certain cases this reaction preserves the structural perfection of the polymerizing monomer crystals. This observation constituted a major breakthrough in the area of polymer crystal synthesis.

The solid-state polymerization of a monomer array in a diacetylene crystal is represented in Figure 2 for the usual case that the mutually reacting monomer molecules are related by a lattice translation. Polymerization occurs via 1,4-addition reaction by the coordinated rotation of mutually reacting molecules about their respective centers and a change in the monomer-center to monomer-center separations.[9-12] This reaction in all known cases is "translational-direction

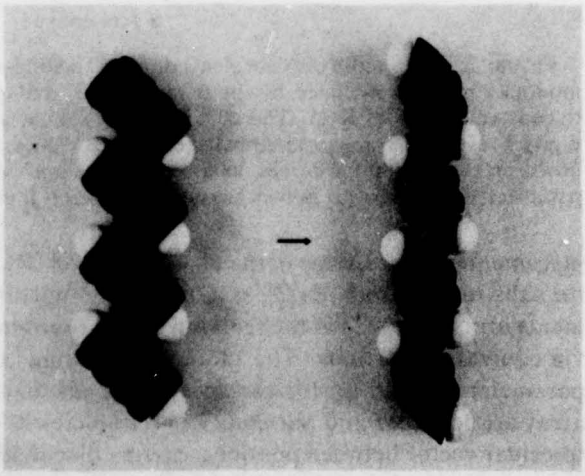


Figure 2. Polymerization of a crystalline array of diacetylene molecules to produce a polydiacetylene chain. The substituent groups, which are typically complex organic functionalities, are indicated by the white balls.

invariant".[12] In other words, during reaction the monomer-center to monomer-center vector potentially changes in length, but not in direction.

Simple least motion and packing arguments allow one to predict which diacetylene monomers are likely to pack in such a way as to be highly polymerizable in the solid state.[10,12,16,29] Although such calculations employ major simplifying assumptions, they have utility for the prediction of the variety of new polymers that can be synthesized by solid-state reaction.

For example, the graph in FIGURE 3 indicates the route mean-square atom dis-

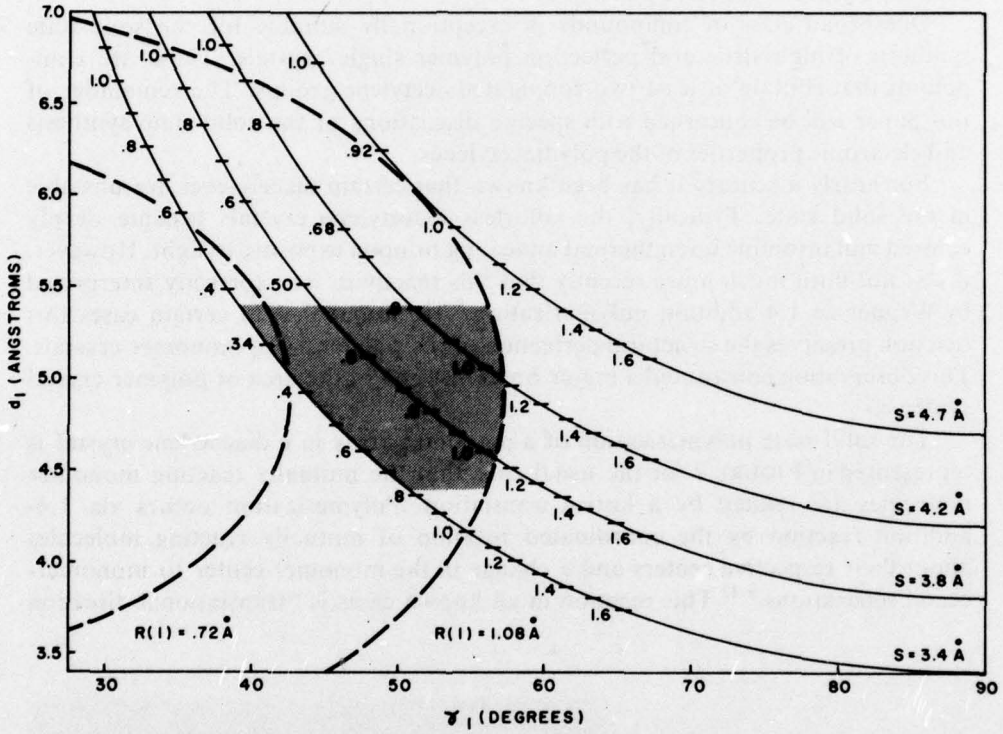


FIGURE 3. RMS atom displacements during the solid-state polymerization of an array of monomer molecules defined by the parameters d_I and γ_I. The dashed curves correspond to constant values of R(1). The d_I and γ_I coordinates to the left of the solid curve for a given value of S are geometrically excluded. Values of R(2) in 0.1 Å increments are denoted on the constant S curves, as are the minimum values of R(2). The range of packing parameters of interest for polymer crystal synthesis is indicated by the shaded region.

placements for the atoms in the diacetylene rod [R(1)] and the first carbon atom in the substituent group [R(2)], as a function of packing coordinates. These displacements are calculated for the reaction of two monomer molecules to initiate a chain via equivalent motions. The monomer packing configuration is defined by two parameters d_I and γ_I for the case where all diacetylenic rods in the monomer array are coplanar and parallel. The parameter d_I is the magnitude of the center-to-center vector between possibly reacting diacetylene groups in neighboring molecules and γ_I is the angle that each diacetylene rod makes with this vector. In the

polymer the corresponding parameter values are d_2 and γ_2, which are, respectively, ~ 4.9Å and ~ 13.4°. During polymerization the monomer-center to monomer-center distance must change by $d_2 - d_1$ and the conjugated rod of each reacting monomer molecule must rotate about its center by an angle of at least $\gamma_2 - \gamma_1$. It is empirically observed[12] that diacetylene phases for which all possible reaction modes require a $R(1)$ larger than ~ 1.08Å are not sufficiently reactive for polymer crystal synthesis. Consequently, the nearest neighbor coordinates d_1 and γ_1, to the right of the curve for $R(1) = 1.08$ Å, should correspond to packing arrays with little reactivity.

A further constraint is placed on the parameter d_1 by the requirement that the chains should propogate without serious disruption of the polymerizing phase. For example, the monomer 2,4-hexadiyne-1,6-diol is polymerizable in the solid state. The polymerizing phase, however, becomes progressively disordered during reaction, and phase separation eventually occurs. This introduction of disorder during polymerization and the eventual phase separation of monomer from the polymerizing phase is probably a consequence of the 8.2% decrease in monomer-center to monomer-center separation required to form an unstrained polymer chain from the monomer array.[10] This monomer is hydrogen bonded and contains small substituent groups, which exaggerates the lattice energy changes corresponding to such dimensional changes. However, in general it is expected that the magnitude of $(d_1 - d_2)/d_2$ should be less than about 0.10 for there to be much likelihood for the synthesis of nearly defect-free polymer single crystals.

For monomers with unknown crystal structures, pairwise close-packing considerations (using molecular models with the appropriate van der Waals radii, bond lengths, bond angles, and energetically realistic molecular conformations) allows determination of permissible values for the coordinates d_1 and γ_1. Reference to FIGURE 3 then permits evaluation of whether a permissible value for these coordinates (which may or may not correspond to an obtainable phase) results in the desired phase reactivity. For parallel diacetylene groups in neighboring molecules that can pack no closer than a distance S, the only permissible values of d_1 are greater than or equal to $S/\sin \gamma_1$. The curves $d_1 = S/\sin \gamma_1$ for S = 3.4A (corresponding to twice the van der Waals radius of carbon, which is the smallest possible value for S) and for S = 4.7Å (corresponding to a bulky substituent group, such as the tertiary butyl group) are shown in FIGURE 3. Note that there is essentially no overlap between the curve for S = 4.7Å and the curve for minimal reactivity (R(1) = 1.08Å). Consequently, no coordinates d_1 and γ_1 consistant with substantial solid-state reactivity are permissible for molecules with such bulky substituent groups. This is in agreement with the observations of Bohlmann.[31]

A model for the structure of the simplest type of diacetylene monomer and polymer is presented in FIGURE 4. Note in this case that all substituent groups ($-(CH_2)_4OCONHC_6H_5$) are identical and nonchiral. Such large substituent groups on the diacetylene increase the liklihood of successful polymer crystal synthesis. The important point here is that the diacetylene polymerization requires about an 18% change in the total van der Waals volume of the backbone associated carbon atoms. By choosing a monomer phase in which there are long flexible sidegroups and/or interstitial molecules, this van der Waals volume

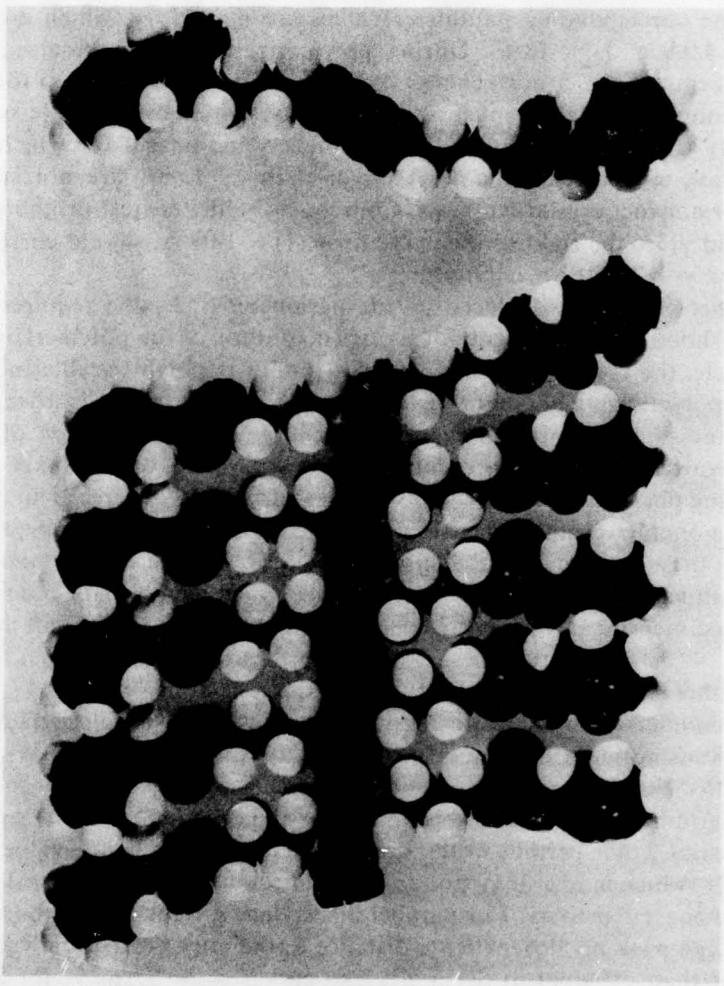


FIGURE 4. Models for the structure of a symmetric diacetylene, where the substituent groups are $-(CH_2)_4OCOC_6H_5$, and the corresponding 1,4-addition polymer. Only the approximate molecular structure is represented.

change on polymerization can most readily be accommodated by the polymerizing phase without resulting in large-dimensional changes and high-lattice strains. The linear and nonlinear spectroscopic properties of polymer crystals of the polymer shown in FIGURE 4, as well as transformations in the structure of the polymer backbone, will be discussed later.

The unsymmetric monomers $R_1{-}C{\equiv}C{-}C{\equiv}C{-}R_2$ provide the simplest examples of diacetylenes for which the chemical structure of the solid-state reaction product, as well as the crystal structure and phase perfection, is dependent upon monomer packing.[16] If all the mutually reacting monomer molecules in a periodic precursor phase are symmetry related and nonchiral, the structure of the 1,4-addition polymer can be either head-to-tail, $[{=}(R_1)C{-}C{\equiv}C{-}C(R_2){=}(R_1)C{-}C{\equiv}C{-}C(R_2){=}]_n$, or head-to-head, $[{=}(R_1)C{-}C{\equiv}$

$C-C(R_2)=(R_2)C-C\equiv C-C(R_1)=]_n$. Independent of the monomer-site symmetry or the symmetry relationship between mutually reacting monomer molecules, a polymer with regular sidegroup alternation will be produced by solid-state reaction unless more than one nonequivalent reaction mode is fortuitously favored for polymerization in some conversion range. It is possible to synthesize monocrystalline polymers having complex structural periodicities from such assymmetric diacetylenes. Depending upon the symmetry of the monomer array, chain-repeat lengths obtainable for orthorhombic or lower symmetry phases include either one monomer length (~ 4.9Å), two monomer lengths (~ 9.8Å), or four monomer lengths (~ 19.6Å). The former polymers can be obtained as chiral and/or noncentric structures that are of interest because of the symmetry allowed electronic properties such as either piezoelectricity, pyroelectricity, or optical activity. Even longer periodicities and more complex structures are obtainable by solid-state polymerization if the molecules in the reacting arrays are not all symmetry related.[16]

Baughman and Yee have reported[14,32] that certain cyclic diacetylenes polymerize in the solid state to produce monocrystalline polymers in which the backbone is reinforced by covalently bonded linkages. The first known example of a backbone-reinforced polydiacetylene was obtained by the γ-ray-induced solid-state reaction of the cyclic diacetylene o, o'-diacetylenyldiphenylglutarate,[14] the structure of which is shown in FIGURE 5. Various possible reaction modes for this monomer are shown in this figure, each of which result in a different polymer

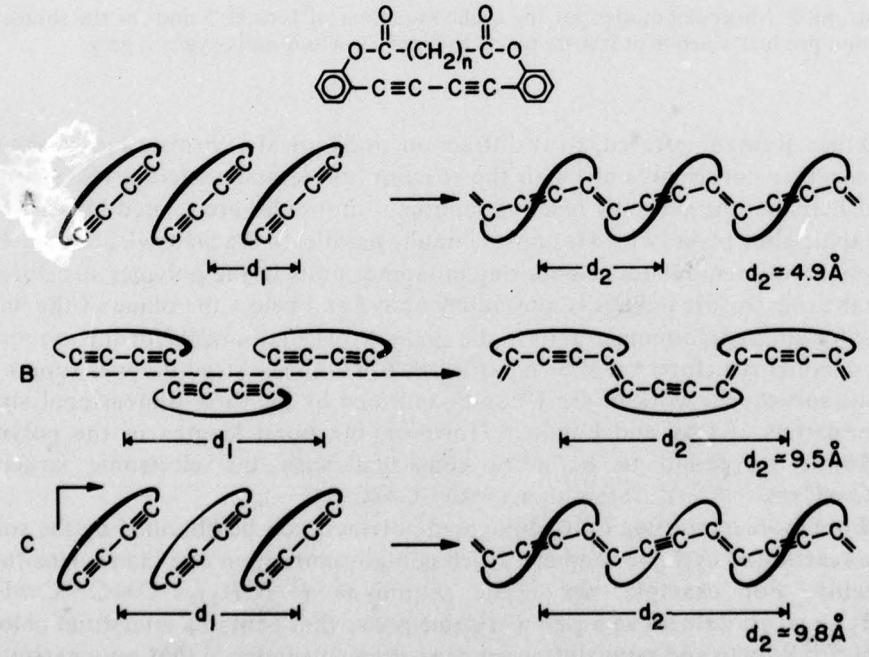


FIGURE 5. Possible packing modes for a cyclic diacetylene and the corresponding structures for the 1,4-addition polymer. The ring closure functionality is represented by the loops in *A*, *B*, and *C*.

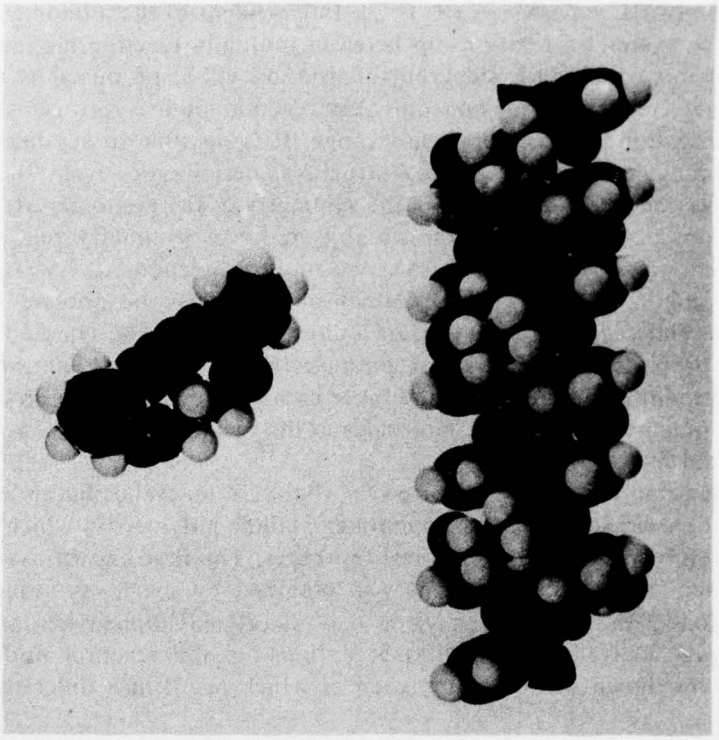


FIGURE 6. Molecular models for the cyclic monomer of FIGURE 5 and for the solid-state reaction product. Carbon atoms are black, hydrogen is white, and oxygen is grey.

structure. Raman, infrared, x-ray diffraction, and optical dichroism measurements are together consistent only with the reaction mode and structure shown in C. Note here that the mutually reacting monomer molecules are related by a crystallographic glide plane, which is approximately parallel to the diacetylene rods. This symmetry element relates neighboring monomer units in the polymer structure so that the ring closure linkage is alternately above and below the plane of the backbone for adjacent monomer units in the chain. Molecular models for the monomer and polymer structures are shown in FIGURE 6. This basic structure was supported by the subsequent work of Graf[33] and confirmed by the three-dimensional structure analysis of Day and Lando.[34] However, the bond lengths in the polymer backbone are found to be more consistent with the electronic structure $(-C=C=C=C-)_n$, rather than $(=C-C\equiv C-C=)_n$.

Even more interesting fully conjugated polymers can be obtained by the solid-state reaction of cyclic monomers which contain more than one diacetylene functionality. For example, the cyclic tetradiyne $(-(CH_2)_2-C\equiv C-C\equiv C-(CH_2)_2-)_4$ crystallizes as a polymerizable phase that contains interstitial chloroform.[29,32] Raman and x-ray diffraction measurements indicate that polymerization occurs by 1,4-addition reaction to produce a polymer phase that is fully chain aligned, but crystallographic only in the chain-axis projection. Such reaction at each of the four diacetylene functionalities in the tetradiyne would produce an

unusual ladder polymer. This polymer would then consist of four fully conjugated chains joined together pairwise via methylene groups to form a cylindrical structure, as shown in FIGURE 7. Fourier transform infrared measurements indicate that most, but not all, diacetylene functionalities are reacted in the insoluble polymer.[35]

Similarly, polymers with multiple connectivity could be synthesized from acyclic monomers containing more than one diacetylene functionality. Consider, for example, a monomer of the form $R_1—C\equiv C—C\equiv C—R_2—C\equiv C—C\equiv C—R_3$. Depending upon monomer packing in the solid state, as well as molecular geometry, such a monomer could polymerize 1) by 1,4-addition reaction at only one diacetylene functionality, 2) by 1,4-addition reaction at both diacetylene functionalities with the diacetylene functionalities in the same neighboring monomer molecules, or 3) by 1,4-addition reaction at both diacetylene functionalities, but with the diacetylene functionalities in different neighboring monomer molecules. The first case is least interesting, since only the normal single-chain polymer results. As shown in FIGURE 8, however, the latter reactions would result in a double-chain ladder polymer and a two-dimensional polymer, respectively. M. Steinbach and G. Wegner[36] have recently proposed that a double-chain ladder polymer results from the solid-state polymerization of the mercury aduct $[CH_3—C\equiv C—C\equiv C—]_2H_g$.

So far, a variety of different types of fully conjugated polymers have been dis-

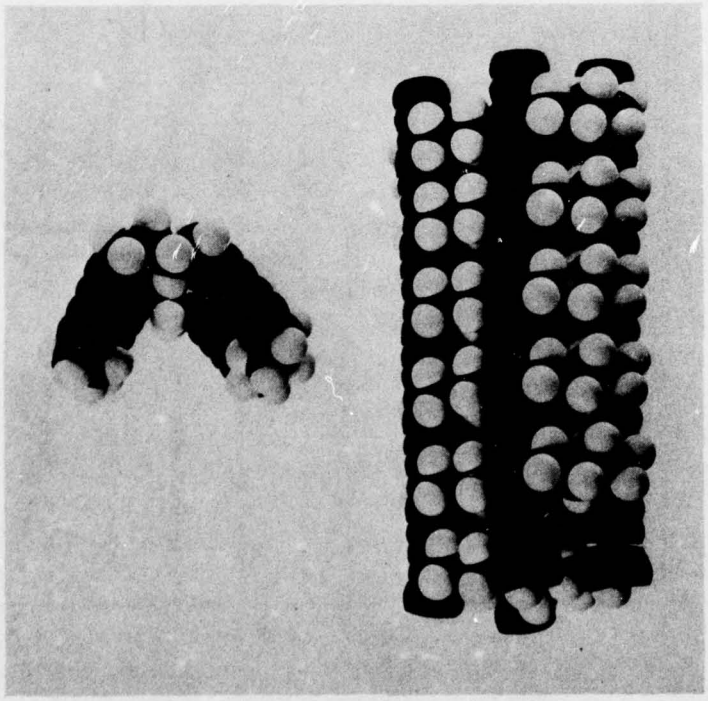


FIGURE 7. Model for the cyclic tetradiyne $(—C\equiv C—(CH_2)_4—C\equiv C—)_4$ and for the ladder polymer resulting from solid-state reaction.

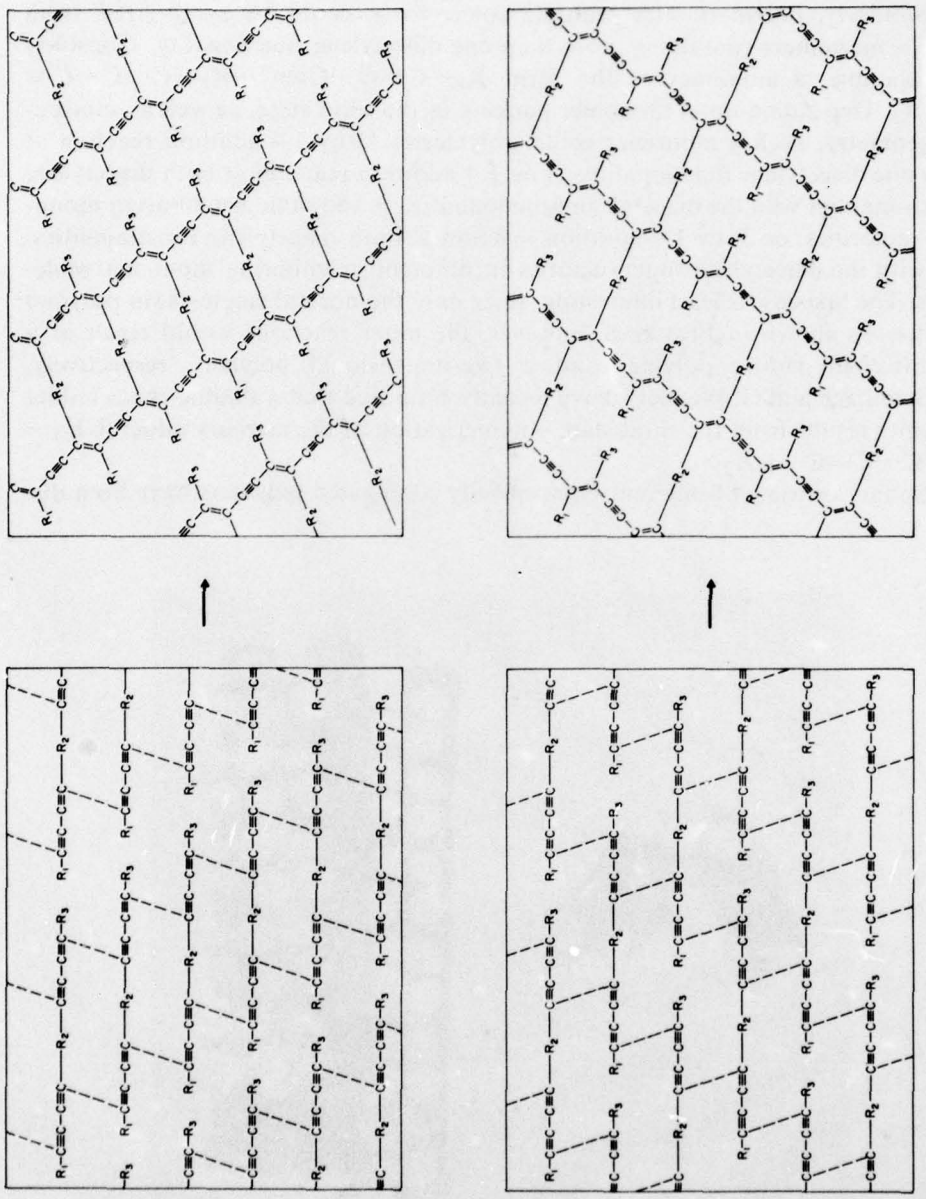


FIGURE 8. Reaction of an acyclic monomer containing two diacetylene functionalities to produce either a ladder polymer or a two-dimensional polymer.

cussed. However, in each case the structure involved a conjugated backbone of the type

$$(=C-C\equiv C-C=)_n \leftrightarrow (-C=C=C=C-)_n$$

Attempts have been made to obtain monocrystalline polymers having backbone structures of the type $(=C\text{-}(\text{-}C\equiv C\text{-})_x C=)_n \leftrightarrow (-C\text{=}(\text{=}C=C\text{=})_x C-)_n$, for $x = 2$ and higher, by the solid-solid state polymerization of triynes $R\text{-}(\text{-}C\equiv C\text{-})_3 R$[13] or tetraynes $R\text{-}(\text{-}C\equiv C\text{-})_4 R$[16]. In each of the observed cases however, the polymer obtained by solid-state reaction was the normal 1,4-addition polymer,

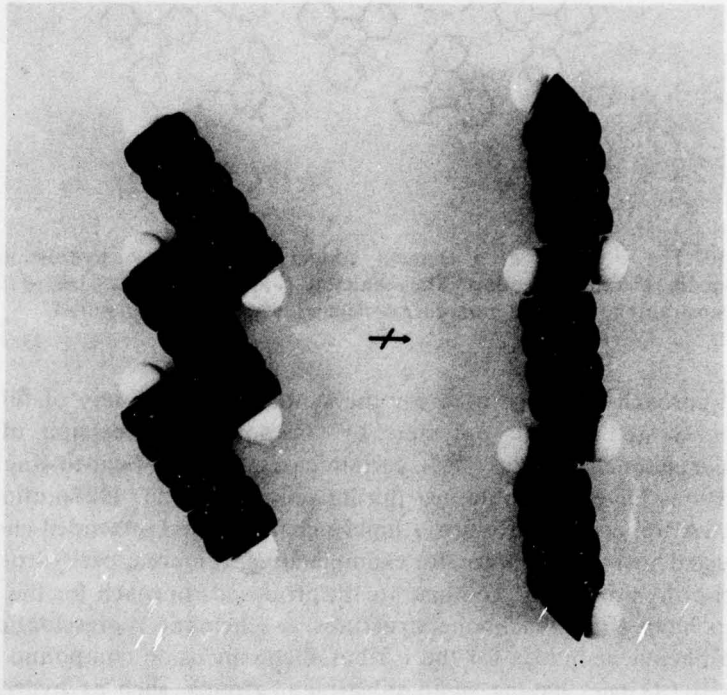


FIGURE 9. Typical packing mode for a triyne, which would result in the 1,4-addition polymer rather than the pictured 1,6-addition polymer. Here and in the following figures the substituent groups, which may be complex organic functionalities, are indicated by the white balls.

having acetylenic functionalities in the sidegroups. Likely packing modes for these compositions result in monomer arrays for which least-motion arguments predict formation of the 1,4-addition polymer.[16] A typical packing mode for a triyne, which would result in the 1,4-addition polymer rather than the desired 1,6-addition polymer, is shown in FIGURE 9.

A reasonable approach, more likely to result in these new polymer backbone structures, would be to crystallize triyne, tetraynes, or higher polynes having small substituent groups (such as hydrogen) in the channels of a channel adduct.

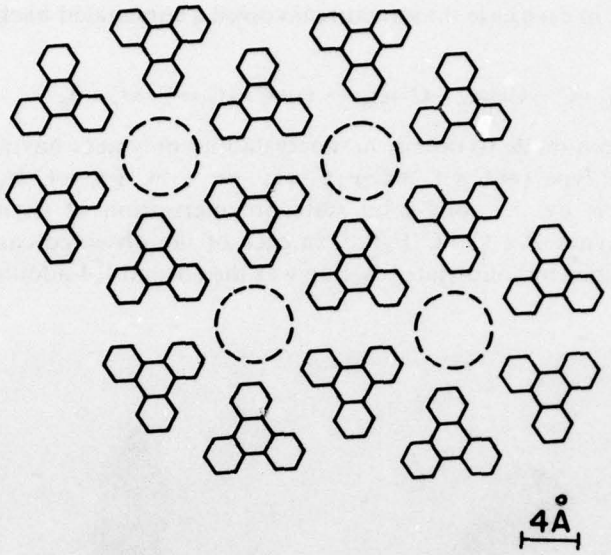


FIGURE 10. The structure of a channel adduct formed by perhydrotriphenylene,[37] viewed down the channel direction. The channels (indicated by the dashed lines) geometrically constrain the enclosed monomer molecules, which are not pictured.

A similar approach has been used for the synthesis of a variety of fully chain-aligned, highly stereoregular polymers by the solid-state reaction of various butadienes in channel adducts.[37-40] In certain cases, single crystal-to-single crystal transformations have been obtained during polymerization. Dissolution of the adduct matrix appears to produce a highly chain-aligned, extended-chain polymer. Suggested host materials are, for example, urea, thiourea, perhydrotriphenylene, and tri-*o*-thymotide.[37-41] To illustrate the proposed approach for the synthesis of polymers having new backbone structures, a schematic representation of the perhydrotriphenylene matrix for the 1,3-butadiene inclusion compound is shown in FIGURE 10. Triynes having small substituent groups, such as hydrogen, can potentially form similar inclusion structures in which this molecule is geometrically constrained in molecular channels. The cross-section of such channels is schematically represented in FIGURE 10, by the dashed circles.[37] An orthogonal view representing a triyne in a channel complex is pictured in FIGURE 11. By suitably choosing the host compound so as to provide channels with the desired geometric constraints, the packing arrangement shown here would result. Note that the end-to-end type of molecular packing, as pictured in the figure, corresponds to a geometric arrangement that is favorable for 1,6-addition polymerization. It seems feasible to cocrystallize different acetylenic compositions in these channels (such as triynes with diynes or triynes with H—C≡C—C≡N) so as to produce a host of otherwise unobtainable homoatomic or heteratomic polymers with fully conjugated backbone structures. These polymers could then be obtained as fully extended chains in single crystals of the adduct.

Optical Properties of the Polydiacetylenes

The optical properties of the polydiacetylenes have been of intense interest principally because of their low dimensionality. Optical data are now available for a number of polydiacetylenes, although PTS [R is $-CH_2SO_3C_6H_4CH_3$] remains the most extensively investigated. The lowest energy optical transition in PTS is located at 2.02 eV at room temperature and is polarized very close to the chain direction.[42-44] At low temperatures this peak splits into two peaks with the same polarization and separated by $\sim 300cm^{-1}$. There has been much discussion in the literature concerning the origin of the splitting.[42,43] It is now apparent that the splitting has its origin in a phase transition that occurs at 170°K and results in a doubling of the unit cell in a direction normal to the chain direction.[45] This results in four molecules per unit cell, i.e., two inequivalent pairs of chains. Therefore, two optical transitions are observed with essentially the same polarization.[46] It has recently been shown that the splitting persists up to room temperature, due presumably to a small admixture of the low-temperature phase.[44] This phase transition is at the present time unique to PTS.

The room-temperature crystal structure reveals that the bonding sequence in PTS can be best represented by the acetylene structure $\dashv RC{-}C{\equiv}C{-}CR \vdash$.[47] On the other hand, a recent x-ray structure determination shows that TCDU

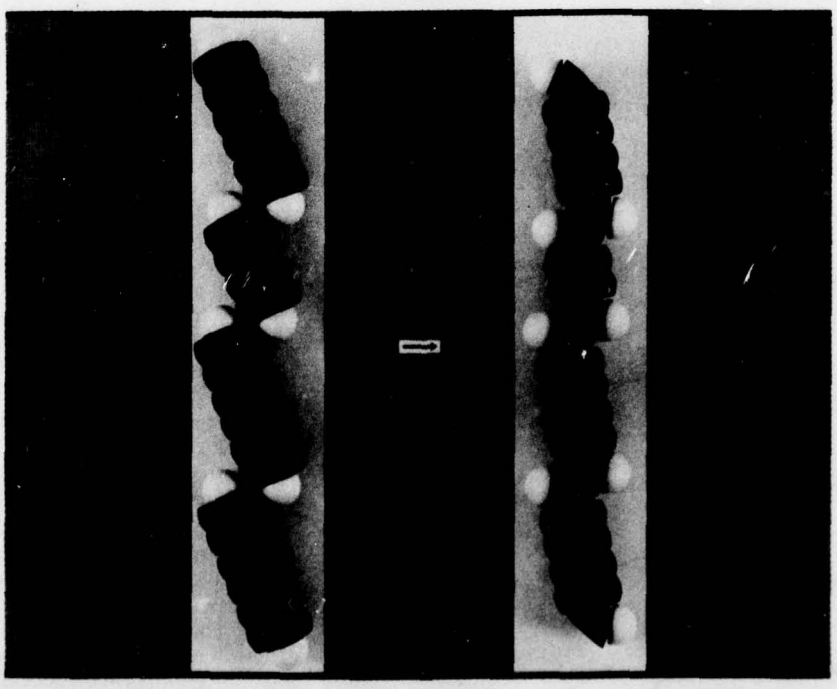


Figure 11. The polymerization of an array of triyne molecules in a channel complex (left) to produce the 1,6-addition polymer (right).

[R is $-(CH_2)_4OCONHC_6H_5$] can be best represented by the butatriene structure $+RC{=}C{=}C{=}CR+$.[48] The optical properties of TCDU contrast greatly with those of PTS.[49,50] The most notable difference is that the lowest energy transition in TCDU is located at 2.3eV; i.e., 0.3eV to the blue of that in PTS. Just the opposite, a substantial red shift, is expected from current theoretical models for the polydiacetylenes,[51,52] including a recent $SCFX_\alpha$ treatment.[53] However, none of these theoretical treatments attempts to include excitonic or electron correlation effects.

A number of polydiacetylenes exhibit reversible color changes in conjunction with a temperature-induced phase transition. Of these thermochromic polydiacetylenes, only ETCD [R is $-(CH_2)_4OCONHC_2H_5$] has been thoroughly investigated.[54–56] The normal incidence reflection spectra of ETCD at various temperatures is shown in FIGURE 12. The phase transition occurs at ~ 120°C. The considerable hysteresis in this phase transition would indicate a first-order transition. The room-temperature reflection spectrum is quite reproducible even after several temperature cycles.

In FIGURE 13 we compare the ETCD spectra, above and below the phase transition, with those of PTS[44] and TCDU.[49] Below the phase transition, the ETCD spectrum is quite similar to that of PTS, which, as indicated in the figure, is best represented by the acetylene structure. Above the phase transition, the ETCD spectrum is quite similar to that of TCDU, which is best represented by the butatriene structure. From this comparison and a similar comparison of Raman

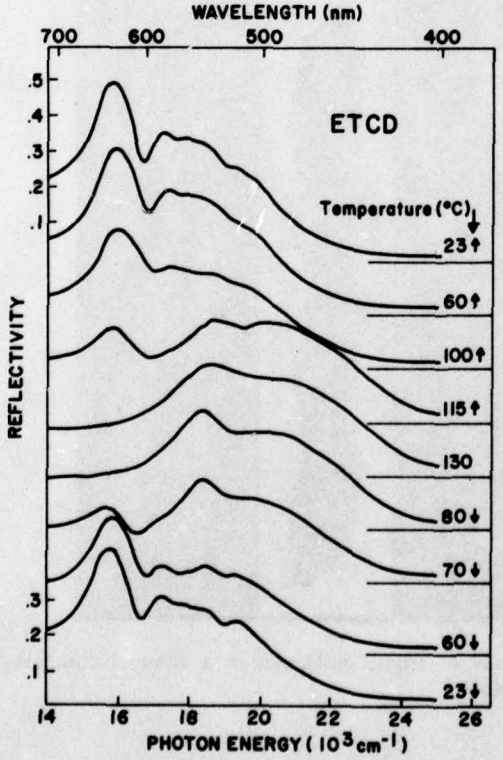


FIGURE 12. Normal incidence reflection spectra of ETCD [R is $-(CH_2)_4OCONHC_2H_5$] as a function of temperature. The uppermost curve is obtained for the as-polymerized material. The reflectivity scales on the left refer to the room temperature spectra. The origin of each spectrum is indicated by the horizontal line on the right. The temperature is controlled to within ± 0.1° at the indicated values. The arrows beside the temperatures are included to indicate position on the hysteresis loop. The incident light is polarized parallel to the chain direction with a bandpass of 50 cm^{-1}. There was no observable structure in the reflection spectra when the incident light was polarized perpendicular to the chain. (After Chance *et al.*[56])

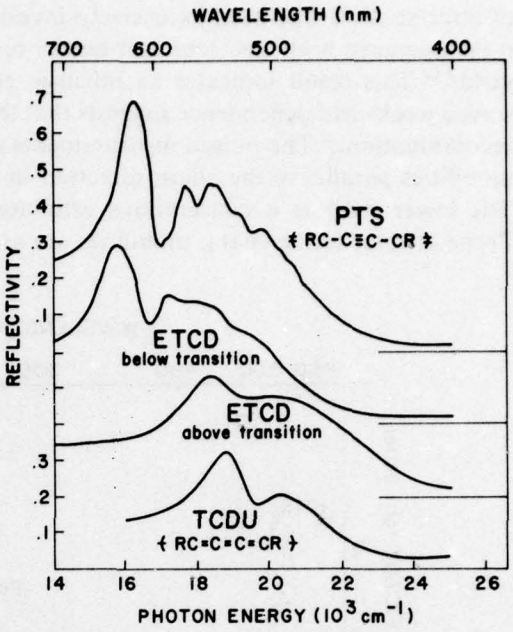


FIGURE 13. Normal incidence reflection spectra for PTS[11], TCDU[12], and ETCD below the phase transition, and ETCD above the phase transition. The observed backbone bonding sequences for PTS and TCDU are shown schematically.[47,48] The ETCD data are the FIGURE 12 curves labeled 23 and 80. The displaced origins of the curves are indicated by the horizontal lines on the right. (After Chance *et al.*[56])

spectra, the electronic structure change at the phase transition is believed to have its origin in an acetylene-to-butatriene transformation. Consistent with this hypothesis, a Raman spectral investigation of TCDU suggests that at low temperatures (< 100K) and/or high pressure (> 5Kbar) TCDU undergoes a butatriene-to-acetylene transformation.[50] X-ray structures are not yet available for the low-temperature phase of TCDU or either phase of ETCD.

One of the most exciting developments in the investigation of the optical properties of the polydiacetylenes has been the nonlinear spectroscopic work of Sauteret *et al.*[57] Measurements on PTS and TCDU show these polydiacetylenes to have the highest $\chi^{(3)}$ values known for any material, including inorganics, with a comparable transparency range in the near infrared. These results, coupled with the observed high damage thresholds, could be useful in picosecond pulse applications such as the construction of four-wave parametric amplifiers, ultrafast light shutters, and optical pulse sharpeners.

ELECTRICAL PROPERTIES OF THE POLYDIACETYLENES

All polydiacetylenes investigated to date would be classified as electrical insulators. Room-temperature conductivities in the range 10^{-16} to 10^{-12} $ohm^{-1}cm^{-1}$ have been reported.[58-60] It is not clear, however, whether any of these measurements actually relates to the intrinsic conductivity of the polydiacetylene crystal. In the case of PTS, for example, a value of $10^{-13}ohm^{-1}cm^{-1}$ can be measured under ambient conditions. However, this value decreases several orders of magnitude to $10^{-16}ohm^{-1}cm^{-1}$ under high-vacuum conditions. These results are typical for the polydiacetylenes as a class.

Photoconductivity in the polydiacetylenes has been the subject of a great deal

of interest. PTS has been extensively investigated. In pulsed photoconductivity measurements, both electrons and holes are observed in approximately the same yields.[61] This result indicates an intrinsic generation mechanism. Also, the observed weak-field dependence suggests that the carrier yield is limited by geminate recombination.[62] The pulsed measurements also yield an estimate for the carrier mobilities parallel to the chain direction in PTS: $3 > \mu_e, \mu_h > 10^{-3}$ cm^2/V-sec. The lower limit is a conservative estimate based on a carrier yield of unity. Perpendicular to the chain, mobilities are at least ten times smaller. Recent tran-

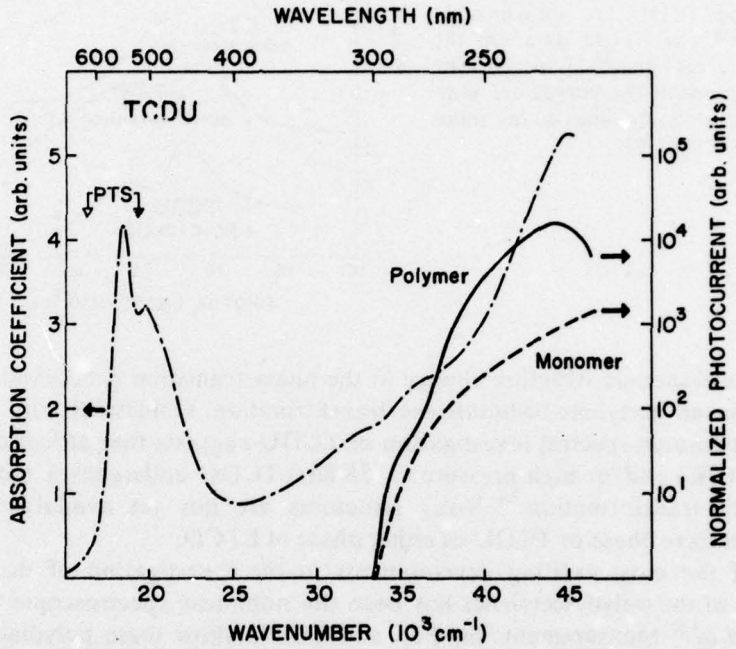


FIGURE 14. Normalized photoconductivity versus excitation energy for TCDU polymer (-) and TCDU monomer(- - -). The absorption spectrum (-·-·-) for TCDU polymer is also shown as the preliminary results from a Kramers-Kronig analysis of the reflectivity data in FIGURE 13. The open and closed arrows (labeled PTS) mark the absorption maximum and photoconduction onset for PTS polymer, respectively. After Müller et al.[49]

sient measurements[63] in PTS, in conjunction with a bulk-recombination model, have yielded $\mu \approx 1$ parallel to the chain and $\mu \approx 0.01$ perpendicular to the chain.[59] These mobilities are much greater than those typically observed for conventional polymers. However, this result can be considered a natural consequence of the high structural perfection of the polydiacetylenes compared to conventional polymers. In fact, the mobilities in PTS are fairly typical of those commonly observed in molecular crystals,[64] although the large anisotropy in the PTS mobilities must be considered unusual in this regard.

The action spectra for photoconduction in the polydiacetylenes show that the onset for photoconductivity is substantially blue-shifted with respect to the lowest energy optical transition.[60] The extreme example of this effect is shown in FIG-

URE 14 for TCDU.[49] Results for PTS[60] are also indicated in the figure. It is clear from the TCDU results that excitation in the lowest energy band system does not lead to any significant free carrier production. With the possible exception of weak charge transfer crystals, this result is characteristic of intrinsic photoconductivity in all organic photoconductors. The explanation is that the lowest energy transition is excitonic in origin in organic solids, including the polydiacetylenes. Frenkel excitons can participate in photocurrent generation only via extrinsic processes[65] and in a manner limited by their lifetime. In the polydiacetylenes the exciton lifetime is apparently quite short ($\tau < 10^{-13}$ sec from the absence of any observable fluorescence from the 2eV state),[66] and extrinsic photocurrents of excitonic origin have not been observed.

The excitonic assignment for the lowest energy optical excitation is supported by the highly structured, vibrational progressions observed in the optical spectra, which would not be expected in a direct band system. Also, Müller and Eckhardt[67] have recently observed weak structure in reflection spectra with polarization normal to the chain direction. This structure can be interpreted as indicating Davydov splitting in the lowest energy, excitonic transition. The exciton assignment casts doubt on the utility of calculations which attempt a *quantitative* explanation of the optical properties of the polydiacetylenes using a simple Huckel model.

References

1. Paushkin, Ya. M., T. P. Vishnyakova, A. F. Lunia & S. A. Nizova. 1974. Organic Polymeric Semiconductors. John Wiley & Sons. New York, N.Y.
2. Mark, H. 1972. Israel J. Chem. **10:** 407–421.
3. Geil, P. H. 1963. Polymer Single Crystals. Interscience Publishers. New York, N.Y.
4. Wunderlich, B. 1973. Macromolecular Physics. Vol. 1. Crystal Structure, Morphology, Defects. Academic Press. New York, N.Y.
5. Wunderlich, B. 1970. Ber. Bunsenges. Phys. Chem. **74:** 768–777.
6. Wunderlich, B. 1968. Adv. Polym. Sci. **5:** 566–619.
7. Lee, C. J., B. Wunderlich. 1977. J. Polym. Sci., Polym. Phys. Ed. **15:** 355–369.
8. Wegner, G. Unpublished material.
9. Wegner, G. 1969. Z. Naturforsch. **24b:** 824–832.
10. Baughman, R. H. 1972. J. Appl. Phys. **43:** 4362–4370.
11. Kaiser, J., G. Wegner & E. W. Fischer. 1972. Israel J. Chem. **10:** 157–171.
12. Baughman, R. H. 1974. J. Polym. Sci., Polym. Phys. Ed. **12:** 1511–1535.
13. Kiji, J., J. Kaiser, G. Wegner & R. C. Schultz. 1973. Polymer. **14:** 433–439.
14. Baughman, R. H. & K. C. Yee. 1974. J. Polym. Sci., Polym. Chem. Ed. **12:** 2467–2475.
15. Wegner, G. 1974. Chimia **28:** 475–484.
16. Baughman, R. H. & K. C. Yee. 1977. J. Macromol. Sci. Rev. Macromol. Chem. In press.
17. Wegner, G. 1971. Makromol. Chem. **145:** 85–94.
18. Schermann, W., G. Wegner, J. O. Williams & J. M. Thomas. 1975. J. Polym. Sci., Polym. Phys. Ed. **13:** 753–763.
19. Adler, G. 1971. Trans. Am. Cryst. Assoc. **7:** 55–67.
20. Colson, J. P. & D. H. Reneker. 1973. J. Appl. Phys. **44:**4293–4302.
21. Morawetz, H. 1966. J. Polym. Sci., Part C. **12:** 79–88.
22. Nakanishi, H., M. Hasegawa & Y. Sasada. 1977. J. Polym. Sci. Polym. Phys. Ed. **15:** 173–191.
23. Thomas, J. M. 1972. Israel J. Chem. **10:** 573–580.
24. Baughman, R. H., R. R. Chance & M. J. Cohen. 1976. J. Chem. Phys. **64:** 1869–1876.

25. BAUGHMAN, R. H. & R. R. CHANCE. 1976. J. Polym. Sci., Polym. Phys. Ed. **14:** 2019–2035.
26. GOUGOUTAS, J. Z. 1972. Israel J. Chem. **10:** 395–407.
27. TABATA, Y., B. SAITO, H. SHIBANO, H. SOBUE & K. OSHIMA. 1963. Makromol. Chem. **76:** 89–98.
28. PEN'KOVSKII. 1964. Russian Chemical Reviews. **33:** 532–549.
29. BAUGHMAN, R. H. 1977. *In* Contemporary Topics in Polymer Science. E. M. Pearce and J. R. Schaefgen, Eds.: 205–233. Plenum Press. New York, N.Y.
30. HADICKE, E., K. PENZIER & H. W. SCHNELL. 1971. Angew Chem. **83:** 1024–1024.
31. BOHLMANN, F. 1953. Chem. Ber. **86:** 657–667.
32. BAUGHMAN, R. H. & K. C. YEE. U.S. Patent 3,923,622. (Dec. 2, 1975).
33. GRAF, H. J. 1974. Diplome Thesis, Univ. Mainz, West Germany. Feskorperpolymerisation eines Cyclischen Diacetylenes.
34. DAY, D. & J. B. LANDO. 1978. J. Polym. Sci., Polym. Phys. Ed. In press.
35. BANERJIE, A. & J. B. LANDO. Unpublished material.
36. STEINBACH, M. & G. WEGNER. 1977. Preprint.
37. COLOMBO, A. & G. ALLEGRA. 1971. Macromolecules **4:** 579–584.
38. FARINA, M., G. AUDISIO & M. J. GRAMEGNA. 1972. Macromolecules **5:** 617–621.
39. CHATANI, Y. & S. NAKATANI. 1972. Macromolecules **5:** 597–604.
40. CHATANI, Y. & S. KOWATA. 1975. Macromolecules **8:** 12–18.
41. BRUNIE, S. & G. TSOUCARIS. 1974. Cryst. Struct. Comm. **3:** 481–484.
42. BLOOR, D., D. J. ANDO, F. H. PRESTON & G. C. STEVENS. 1976. Chem. Phys. Lett. **24:** 37–40.
43. REIMER, B., H. BÄSSLER, J. HESSE & G. WEISER. 1976. Phys. Status Solidi **B73:** 709–716.
44. ECKHARDT, C. J., H. MÜLLER, J. TYLICKI & R. R. CHANCE. 1976. J. Chem. Phys. **65:** 4311–4312.
45. ENKELMANN, V. & G. WEGNER. 1977. MAKROMOL. Chem. **178:** 635–638.
46. SCHOTT, M. 1977. Preprint.
47. KOBELT, D. & E. F. PAULIS. 1973. Acta. Crystallogr. **B30:** 232–233.
48. ENKELMANN, A. & J. B. LANDO. 1977. Preprint.
49. MÜLLER, H., C. J. ECKHARDT, R. R. CHANCE & R. H. BAUGHMAN. 1977. Chem. Phys. Lett. **20:** 22–25.
50. IQBAL, Z., R. R. CHANCE & R. H. BAUGHMAN. 1977. J. Chem. Phys. **66:** 5520–5525.
51. WILSON, E. G. 1975. J. Phys. C. **8:** 727–741.
52. COJAN, C., G. P. AGRAWAL & C. FLYTZANIS. 1977. Phys. Rev. **B15:** 909–925.
53. BOUDREAUX, D. & R. R. CHANCE. 1977. Chem. Phys. Lett. **51:** 273–278.
54. EXARHOS, G. J., W. M. RISEN & R. H. BAUGHMAN. 1976. J. Amer. Chem. Soc. **98:** 481–485.
55. CHANCE, R. R., R. H. BAUGHMAN, A. F. PREZIOSI & E. A. TURI. 1977. Bull. Amer. Phys. Soc. **22:** 408–408.
56. CHANCE, R. R., R. H. BAUGHMAN, H. MÜLLER & C. J. ECKHARDT. 1977. J. Chem. Phys. **67:** 3616–3618.
57. SAUTERET, C., J. HERMANN, R. FREY, F. PRADERE, J. DUCUING, R. H. BAUGHMAN & R. R. CHANCE. 1976. Phys. Rev. Lett. **36:** 956–959.
58. SCHERMANN, W. & G. WEGNER. 1974. Makromol. Chem. **125:** 667–672.
59. REIMER, B. & H. BÄSSLER. 1975. Phys. Status Solidi **32a:** 435–441.
60. CHANCE, R. R. & R. H. BAUGHMAN. 1976. J. Chem. Phys. **64:** 3889–3890.
61. CHANCE, R. R., R. H. BAUGHMAN, P. J. KEUCROFT & K. TAKAHASHI. 1976. Chem. Phys. **13:** 181–185.
62. CHANCE, R. R. & C. L. BRAUN. 1973. J. Chem. Phys. **59:** 2269–2274.
63. REIMER, B. & H. BÄSSLER. 1976. Chem. Phys. Lett. **43:** 81–85.
64. SCHEIN, L. B. 1977. Phys. Rev. **B15:** 1024–1029.
65. CHANCE, R. R. & A. PROCK. 1973. Phys. Status Solidi **B57:** 597–609.
66. BAUGHMAN, R. H. & R. R. CHANCE. 1976. J. Polym. Sci. Poly. Phys. Ed. **14:** 2037–2045.
67. MÜLLER, H. & C. J. ECKHARDT, 1977. J. Chem. Phys. **67:** 5386–5387.

Discussion

Zoltan Soos (*Princeton Univ., Princeton, N.J.*): Do you think the polydiacetylenes are like anthracene but with perhaps a larger mobility because of the covalent bonding?

Baughman: The polydiacetylenes have a mobility in the chain-axis direction that is about the same as anthracene ($\sim$ 1 $cm^2/volt \cdot sec$). Like anthracene, the lowest lying excited state in the polydiacetylenes appears to be excitonic.

Barry Schechtman (*IBM Research Laboratory, San Jose, Calif.*): Would it not be straightforward to distinguish between the acetylenic and the butatriene structures by using IR or Raman spectroscopy?

Baughman: Infrared lines associated with the polymer backbone for symmetrically substituted polydiacetylenes are characteristically weak. In fact, the infrared spectra of the polymers typically look quite similar to those of the monomers. Intense Raman lines are observed at close to the same frequencies in the double and triple bond stretching region for polydiacetylene crystals known to have either the butatriene or acetylenic backbones. Hence, neither IR nor Raman spectroscopy provides a clear means to independently determine the best representation for the backbone structure. For the few cases in which we know the backbone structure from x-ray structure analysis, we can see differences in the vibrational spectroscopy for the two different kinds of polymer backbone. For example, the relative intensity of the Raman line in the triple-bond region, as compared with the Raman line in the double-bond region, appears to be higher for the butatriene backbone than for the acetylene backbone.

Jan Kommandeur (*Groningen Univ., Groningen, The Netherlands*): Were the polymer infinitely long, you would find a much higher mobility. You find what is typically found in molecular crystals, which must mean that the molecules are not infinitely long. (And they cannot be, because you make them at these finite temperatures; so the system is going to make errors as entropy, and the second law of thermodynamics will take over.) Do you have an estimate of chain length? And how many errors are you going to make in a chain, and why do these matter in your case and not in $(SN)_x$?

Baughman: We know that the monomer crystals contain dislocations and impurity concentrations of at least one part in 10^4. Since these imperfections can block the polymerization reaction, the average chain length is expected to be less than about a micron. However, the molecular weight and perfection is sufficiently high that, in certain instances, near theoretical mechanical properties can be obtained. For many of the polydiacetylene crystals of interest, insolubility precludes measurement of molecular weight by conventional techniques.

Even if the chain lengths were essentially infinite, the conjugation length would be interrupted by entropically stabilized point defects. One such defect type, which we call an orbital-flip defect, involves configurational changes leading to a 90° rotation of the sp^2 π-orbitals of two carbon atoms.

The photoconductive properties of the polydiacetylenes, as well as the dc conductivity of $(SN)_x$, are undoubtedly affected by chain defects. Strong interchain coupling in $(SN)_x$ probably explains why such defects do not preclude reasonably high conductivities in this polymer.

SYNTHESIS AND PROPERTIES OF HALOGEN DERIVATIVES OF $(SN)_x$ AND $(CH)_x$*

M. Akhtar,† C.K. Chiang,‡ M.J. Cohen,‡ J. Kleppinger,†
A.J. Heeger,‡ E.J. Louis,† A.G. MacDiarmid,† J. Milliken,†
M.J. Moran,† D.L. Peebles,‡ and H. Shirakawa†

† Department of Chemistry
‡ Department of Physics
Laboratory for Research on the Structure of Matter
University of Pennsylvania
Philadelphia, PA 19104

Polymeric sulfur nitride, polythiazyl, $(SN)_x$, has been of interest in recent years as the first example of a covalent polymer that is a metal even though it contains no metal atoms. Studies of the optical and electronic properties have indicated metallic behavior along the $(SN)_x$ chains[1] with sufficient interchain coupling to give the properties of an anisotropic three-dimensional metal.[2,3]

As part of a continuing study of the properties of $(SN)_x$ we have been investigating its reactions with halogens. In 1969 Patton[4] made brief reference to the fact that $(SN)_x$ reacts with chlorine to give NSCl. Bernard *et al.*[5] have reported recently that $(SN)_x$ reacts with bromine vapor at room temperature to give a gray-blue solid of unknown composition. Independent studies carried out by us[6] and by Street *et al.*[7] involved the characterization of crystals and films of $(SNBr_{0.4})_x$, the first derivative of $(SN)_x$. In this paper we report[8] the initial results of studies of the electrical transport and optical properties of $(SNBr_{0.4})_x$ and the related derivative $(SNBr_{0.25})_x$. We also report studies on $(CH)_x$ and its halogen derivatives.

Samples of polythiazyl bromides, $(SNBr_y)_x$, were prepared by reacting analytically pure $(SN)_x$[9] with bromine vapor. For example, crystals of $(SN)_x$ (*ca.* 1–10 mm^3) in 60 torr of bromine vapor react immediately at room temperature to give shiny black crystals having a lustrous blue-purple tinge. The composition of the brominated material was determined by exposure of a known weight of $(SN)_x$ to the bromine vapor. Excess bromine was then removed from the product by pumping it for 5 to 15 minutes at room temperature. The weight of bromine absorbed was determined by weighing the polythiazyl bromide produced. The time required for the maximum amount of bromine to be absorbed under these conditions was approximately 40 minutes. The composition was confirmed by elemental analysis; compositions varied slightly, but significantly, according to minor variations in experimental procedure, with values obtained for $(SNBr_y)_x$ in the range $0.38 \leq y \leq 0.42$. Two typical analyses are given in TABLE 1. For convenience, this material will be referred to as $(SNBr_{0.4})_x$ in this paper. No unreacted $(SN)_x$ could be detected visually or in the x-ray powder patterns of the

*Supported by the National Science Foundation by MRL program grant DMR 76-00678 and by grant CHE-73-04771-AO3 and by the Office of Naval Research contract no. N10014-75-C-0962. Manuscript received July 5, 1977.

0077-8923/78/0313-0726 $1.75/1© 1978, NYAS

material. Crystals of $(SNBr_{0.4})_x$ appear to react with air to a negligible extent during approximately one hour at room temperature but are tarnished after ten hours, during which time some ammonium bromide is formed.

Other compositions besides $(SNBr_{0.4})_x$ can also be synthesized. Crystals that were weighed under 60 torr of bromine vapor had a bromine content as high as $(SNBr_{0.55})_x$. Material containing only small amounts of bromine, e.g. $(SNBr_{0.05})_x$, was prepared by reacting $(SN)_x$ with bromine for shorter periods and/or at lower bromine vapor pressures. However, some of these compositions may contain some unreacted $(SN)_x$ and will not be discussed further. When crystals of $(SNBr_{0.4})_x$ were pumped at room temperature for 45 hours or more, there was little change in appearance, but the bromine content decreased to as low as $(SNBr_{0.33})_x$. When crystals of $(SNBr_{0.4})_x$ were heated with pumping at approximately 86°C for about 30 hours, they were converted to copper-colored crystals with composition $(SNBr_{0.25})_x$ (see TABLE 1) and density 2.54 ± 0.06 g/cm^3.

TABLE 1

REPRESENTATIVE ELEMENTAL ANALYSES OF SELECTED POLYTHIAZYL BROMIDES*

	%S	%N	%Br	Total
Calc. for $(SNBr_{0.40})_x$†	41.09	17.95	40.96	100.00
Found	40.92	17.93	41.01	99.86
Calc. for $(SNBr_{0.38})_x$‡	41.95	18.32	39.73	100.00
Found	42.10	18.15	39.85	100.10
Calc. for $(SNBr_{0.25})_x$§	48.54	21.21	30.25	100.00
Found¶	48.34	21.06	30.25	99.65
Found‖	48.36	21.42	30.10	99.88

*Analyses performed by Galbraith Laboratories, Inc., Knoxville, Tenn. 37921.
†Shiny, black crystalline form of $(SNBr_y)_x$.
‡Copper-colored crystalline form of $(SNBr_y)_x$.
¶From $(SN)_x$ and bromine.
‖From S_4N_4 and bromine.

Polycrystalline metallic $(SNBr_{0.25})_x$ can also be synthesized directly from S_4N_4 and bromine without the necessity of first synthesizing $(SN)_x$. When finely powdered S_4N_4 is exposed to 180 torr of bromine at room temperature for 16 hours, it is converted to a black powder whose composition from weight gain is $(SNBr_{1.5})_x$. When this material is pumped at room temperature for four hours, bromine is lost and the composition of the black powder remaining is $(SNBr_{0.4})_x$. Preliminary studies on a compressed pellet of this material showed it to have a conductivity considerably lower than the conductivity of $(SNBr_{0.4})_x$ formed by the direct bromination of $(SN)_x$. When the powder is heated at 80°C for four hours with constant pumping, an 82% yield of a dark copper-colored powder of composition $(SNBr_{0.25})_x$ (see TABLE 1) is obtained. Its x-ray powder pattern is identical with that obtained from a sample of $(SNBr_{0.25})_x$ prepared from $(SN)_x$ and bromine. This observation, together with data presented below, leads to the surprising conclusion that the bromination of S_4N_4 to $(SNBr_{0.25})_x$ involves the polymerization of the cradlelike cyclic S_4N_4 molecule.

The density of the $(SNBr_{0.4})_x$ (2.67 ± 0.04 g/cm^3) is significantly greater than

that of $(SN)_x$ (2.30 g/cm^3).[6,7] The volume increase calculated from the formula and density data is 46%, in reasonable agreement with the observed changes in crystal dimensions upon bromination.[6,7] There is no significant change in the length of the crystal in the *b* crystallographic direction (the direction parallel to the $(SN)_x$ polymer chains).[6,7] The entire volume-change results from a swelling of the crystal perpendicular to the chain axis. Although the crystals appear well-formed, x-ray studies show they have very considerable defect structure. The fibrous nature characteristic of $(SN)_x$ crystals when mechanically pulled apart is preserved in $(SNBr_{0.4})_x$.

In order to monitor the kinetics of the chemical reaction and provide definitive data on the change in electrical resistance on bromination, we have measured the resistance along the chain axis during the bromination of a single crystal of $(SN)_x$. The resulting normalized resistance vs. time during the reaction is shown in FIGURE 1. The data were obtained in bromine vapor at a pressure of 20–25 torr. Chemical analysis of crystals brominated in the same experiment showed the reaction had proceeded to give the composition $(SNBr_{0.40})_x$. Contacts to the sample were made with the graphite suspension Electrodag (Acheson Colloid Co., Port Huron, Mich.) in order to avoid reaction of the usual metallic contacts. The measurements were made with four-probe, low-frequency (37 Hz) ac techniques.

The initial reaction proceeds rapidly and results in an obvious decrease in the sample resistance. The resistance eventually falls to a value approximately 0.05 of the initial value, as shown in FIGURE 1. Taking into account the ~ 46% increase in cross-sectional area, we find a final room-temperature conductivity approximately 13 times the initial $(SN)_x$ value. Independent measurements on five samples of $(SNBr_{0.4})_x$ mounted for measurement after the reaction yielded values from

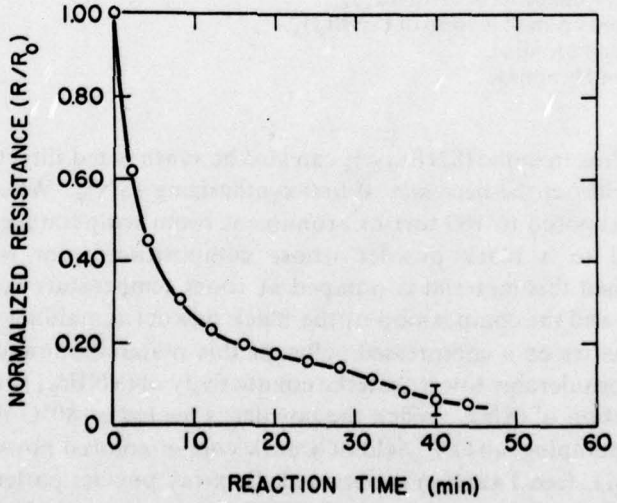


FIGURE 1. Normalized resistance of $(SNBr_y)_x$ during bromination; bromine vapor pressure of 20–25 torr. Chemical analysis of the product indicated $y = 0.4$; see text. The sample conductivity was 1.6×10^3 $(\Omega\text{-cm})^{-1}$ before reaction increasing to 2.2×10^4 $(\Omega\text{-cm})^{-1}$ after reaction. Average value for $(SNBr_{0.4})_x$; $\sigma_{(300K)} = 3.8 \times 10^4$ $(\Omega\text{-cm})^{-1}$ (see text).

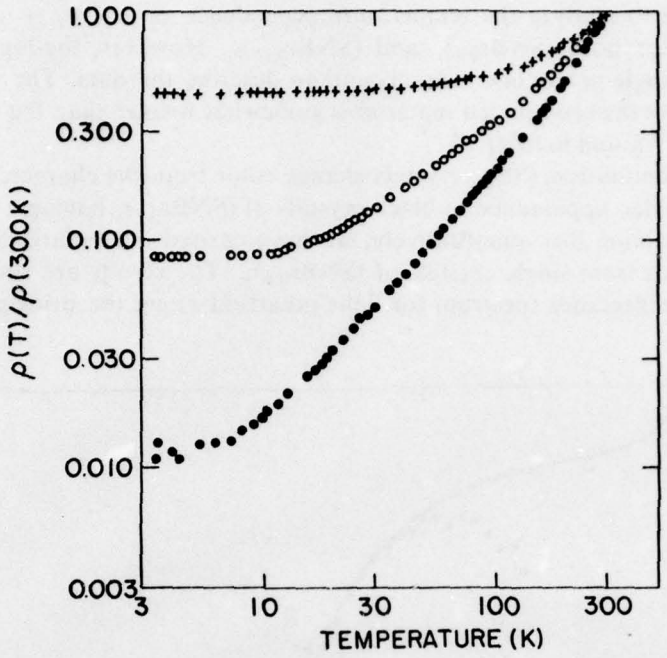


FIGURE 2. Temperature dependence of the resistivity of polythiazyl bromides; ●●● = $(SNBr_{0.4})_x$; ○○○ = $(SNBr_{0.4})_x$; +++ = $(SNBr_{0.25})_x$.

1.4×10^4 to 9.1×10^4 $(\Omega\text{-cm})^{-1}$ with an average room-temperature conductivity, $\sigma_{\parallel}(300\ K) = 3.8 \times 10^4$ $(\Omega\text{-cm})^{-1}$. Room temperature measurements of $\sigma_{\perp}$ yielded 8 $(\Omega\text{-cm})^{-1}$, i.e. comparable to the values obtained for pure $(SN)_x$. However, because of the fibrous nature of the crystals, the value for $\sigma_{\perp}$ is probably not intrinsic but is determined by interfiber contact.

The temperature dependence of the resistivity of $(SNBr_{0.4})_x$ along the chain axis is shown in FIGURE 2. The data were obtained by four-probe dc techniques with Electrodag contacts. The normalized results for two samples shown in FIGURE 2 indicate metallic behavior over the entire temperature range $4 < T < 300$ K. Sample 1 (closed circles) had room-temperature conductivity of 9.1×10^4 $(\Omega\text{-cm})^{-1}$ and a resistance ration $\rho(300\ K)/\rho(4.2\ K) \simeq 90$. Sample 2 (open circles) had room-temperature conductivity of 1.4×10^4 $(\Omega\text{-cm})^{-1}$ and a resistance ratio of approximately 12. Note that sample 2 becomes residual at $T \leq 10$ K whereas the resistivity of sample 1 continued to decrease, becoming residual at a value $\rho_0 \simeq 1.2 \times 10^{-7}$ $(\Omega\text{-cm})$ only well below 10 K.

The temperature dependence of the resistivity of a crystal of $(SNBr_{0.25})_x$ is also shown in FIGURE 2 for comparison. The results again indicate metallic behavior with typically somewhat larger residual resistivity values. Measurements on six samples of $(SNBr_{0.25})_x$ yielded an average room-temperature conductivity of 2×10^4 $(\Omega\text{-cm})^{-1}$, with values ranging from 0.9×10^4 to 5.9×10^4 $(\Omega\text{-cm})^{-1}$. Dark copper-colored compressed pellets of the $(SNBr_{0.25})_x$ formed directly from S_4N_4 and bromine were highly conducting, with a conductivity of *ca.* 1×10^2 $(\Omega\text{-cm})^{-1}$ at 25°C.

Attempts to analyze the temperature dependence as $\rho = \rho_0 + AT^n$ yielded $1 < n < 2$ for both $(SNBr_{0.4})_x$ and $(SNBr_{0.25})_x$. However, log-log plots suggest that a single power law is inadequate to describe the data. The temperature dependence of the brominated material is somewhat weaker than the well-defined T^2 behavior[10] found in $(SN)_x$.

Upon bromination, $(SN)_x$ crystals change color from the characteristic highly reflecting golden appearance to black crystals of $(SNBr_{0.4})_x$ having a blue-purple tinge. To examine this quantitatively, we have carried out polarized reflectance measurements from single crystals of $(SNBr_{0.4})_x$. The results are shown in FIGURE 3. The reflectance spectrum for light polarized along the principal conduct-

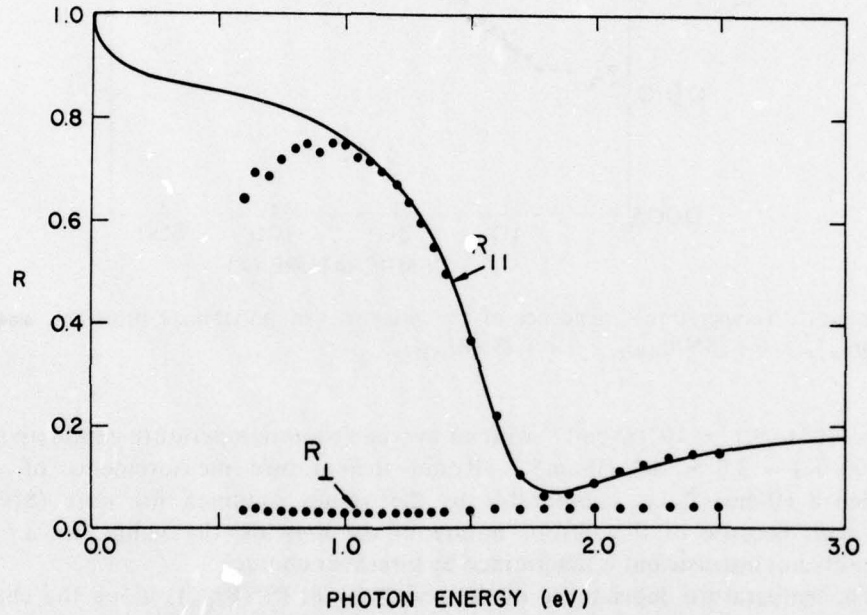


FIGURE 3. Polarized reflectance of $(SNBr_{0.4})_x$ in the spectral range 0.6 eV to 2.5 eV. The solid curve represents a least-square fit arbitrarily restricting the input data to the range above 1.1 eV. The data are plotted with the absolute normalization as determined from the Drude fits.

ing axis ($R_\parallel$) shows a broad minimum in the visible with a plasma edge $\hbar\omega_P/(\epsilon_\infty^{1/2})$ and high reflectivity in the near infrared. The plasma edge is shifted from approximately 2.55 eV in $(SN)_x$ to about 1.65 eV for $(SNBr_{0.4})_x$. For light polarized perpendicular to the principle conducting axis, the reflectance ($R_\perp$) is fiat and featureless, with no sign of metallic behavior ($R_\perp \sim 3\%$ over the entire range). The long wavelength optical anisotropy of $(SNBr_{0.4})_x$ is greater than that of $(SN)_x$, indicating somewhat weaker interchain coupling. Polarized reflectance data have also been obtained from oriented films of brominated $(SN)_x$ on Mylar®. The results are consistent with the single crystal data.

Below 1 eV, $R_\parallel$ decreases, rather than asymptotically approaching 100%, as would be the case for a simple Drude dielectric function. Since the dc conductivity

is high, the most likely explanation involves a relatively strong low-frequency interband transition with corresponding structure in $\epsilon(\omega)$. Similar effects have been observed in graphite intercalation compounds.[11] Alternatively, the decrease may result from structure in $\epsilon(\omega)$ arising from a pseudogap related to the more nearly one-dimensional behavior suggested by the optical anisotropy. Detailed reflectance measurements into the intermediate and far infrared regions will be required to develop a complete picture of the dielectric function. Our initial studies presented here focus on the oscillator strength and comparison of $(SNBr_{0.4})_x$ with $(SN)_x$.

The $(SNBr_{0.4})_x$ reflectance data, $R_\parallel$, were analyzed in the vicinity of the plasma edge, assuming a simple Drude dielectric function

$$\epsilon(\omega) = \epsilon_\infty - \frac{\omega_p^2}{\omega^2 + i\omega/\tau}$$

where ϵ_∞ represents the combined contributions from high-frequency interband transitions and the core atomic polarizabilities, τ is the conduction electron scattering time, $\omega_p = (4\pi Ne^2/m^*)^{1/2}$ is the plasma frequency, and N is the number of conduction electrons per unit volume with optical effective mass m^*. The solid curve on FIGURE 3 represents a least-square fit (weighted by $R^{-1/2}$), arbitrarily restricting the input data to the range above 1.1 eV. The resulting parameters are $\hbar\omega_p = 4.8$ eV, $\epsilon_\infty = 8.7$ and $\hbar/\tau \simeq 0.4$ eV. Because of the clear deviation from Drude behavior below 1 eV, these parameters can be taken only as an indication of overall behavior. Nevertheless, it is instructive to compare the results with the corresponding values for $(SN)_x$, of $\hbar\omega_p = 5.1$ eV, $\epsilon_\infty = 4.2$, and $\hbar/\tau = 0.55$ eV.[12] The small decrease in plasma frequency is more than accounted for by the $\sim 46\%$ increase in sample volume on bromination, indicating that any charge transfer to the bromine acceptor states is weak. The downward shift in plasma edge $\hbar\omega_p/(\epsilon_\infty^{1/2})$ on bromination appears to be due primarily to the larger value for ϵ_∞.[13]

Visual observation of the crystals after reaction suggests that bromination decreases the crystalline quality. X-ray studies confirm these latter observations. The brominated material is crystalline; however, the relatively well-defined x-ray patterns obtained from $(SN)_x$ crystals become broad and diffuse indicative of a significant decrease in crystal quality. Nevertheless, the dc conductivity studies described above demonstrate an increase in the absolute value of conductivity with resistance ratios comparable to those found in relatively high quality $(SN)_x$. The reflectance data from $(SNBr_{0.4})_x$ indicate no significant change in (N/m^*) compared with $(SN)_x$ and a value for $\hbar/\tau$ comparable to that typically found for $(SN)_x(\sigma_{opt} = (1/4\pi)\omega_p^2\tau \simeq 7000\ (\Omega\text{-cm})^{-1})$. These results therefore provide evidence that the fundamental $(SN)_x$ chains remain intact as bromine enters the structure with little or no charge transfer. The combined transport and optical data suggest an analogy with bromine intercalation compounds of graphite.[14]

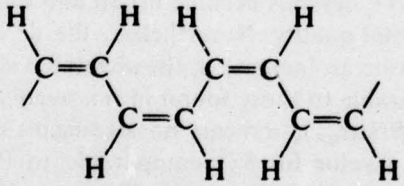
The observation of little or no charge transfer from $(SN)_x$ to bromine is consistent with the known electronegativities. The Pauling electronegativity of bromine (2.8) is equal to the average of the electronegativities of sulfur (2.5) and nitrogen (3.0). The possibility that charge transfer might occur *from* the bromine *to* the $(SN)_x$ chain may even be considered. In this case, the charge transfer would

tend to compensate for the reduction in electron density caused by the increase in volume of the $(SN)_x$ upon bromination. This is consistent with the suggestion from Schottky barrier studies[15] that $(SN)_x$ may be assigned an effective electronegativity of 2.9 or more on the Pauling scale.

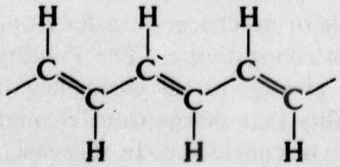
The observation of more than an order of magnitude increase in room-temperature conductivity upon bromination is particularly interesting in the context of the optical properties and the poorer overall crystal quality. Earlier measurements[10] of the temperature dependence of the conductivity of pure $(SN)_x$ indicated that $\rho \propto T^2$ over a wide range of temperatures. Band-structure calculations[16] characterized $(SN)_x$ as a semimetal in which the resistivity may be dominated by electron-electron scattering processes[10,17] leading to a T^2 term in the resistivity with magnitude that is sensitive to detailed features of the electron and hole pieces of the Fermi surface. The higher conductivity and weaker temperature dependence of $(SNBr_{0.4})_x$ compared to $(SN)_x$ imply that the T^2 contribution is smaller in the brominated compound. Evidently the combined effects of a small change in (N/m^*) and the implied decrease in interchain coupling as inferred from the optical studies partially quench the T^2 contribution. Such effects have been predicted from analysis of electron-hole scattering in semimetals[18] and have been observed in nonstoichiometric TiS_2.[19]

In summary, our initial transport and optical studies of this class of brominated derivatives of $(SN)_x$, polythiazyl bromides, demonstrate metallic behavior. The $(SN)_x$ chains appear to remain intact with somewhat weaker interchain coupling as inferred from the optical anisotropy. The bromine evidently enters the structure with little or no charge transfer. The relatively high room-temperature conductivity, $\sigma(300\ K) \simeq 4 \times 10^4\ (\Omega\text{-cm})^{-1}$, in highly defected crystals of $(SNBr_{0.4})_x$ is encouraging from the point of view of the eventual possibility of useful highly conducting synthetic polymers.

In attempting to find a covalent *organic* polymer that would be a metal or at least have a high conductivity, we have focused our attention on the simplest organic polymer, "polyacetylene," $(CH)_x$. In a series of studies, Shirakawa and his coworkers[20-24] have succeeded in synthesizing high quality flexible silver-copper-colored films of the *cis* isomer



and silvery films of the *trans* isomer



of this conjugated polyene from acetylene in the presence of a Ziegler catalyst, and they have developed techniques for controlling the *cis* and *trans* content.[22,23] X-ray diffraction and scanning electron micrograph studies show that films of any *cis* and *trans* composition are crystalline and consist of matted fibrils.[22] These materials are semiconductors;[24] the *trans* isomer, which is the thermodynamically stable form at room temperature, has a higher conductivity ($\sigma_{273K} = 4.4 \times 10^{-5}$ $(\Omega\text{-cm})^{-1}$) than the *cis* isomer ($\sigma_{273K} = 1.7 \times 10^{-9}$ $(\Omega\text{-cm})^{-1}$).[24]

Shirakawa and Ikeda[25] have noted that when $(CH)_x$ films are exposed to bromine or chlorine vapor at room temperature for a few minutes, a dramatic decrease in infrared transmission (4,000 cm^{-1} to 400 cm^{-1}) occurs without any visible change in appearance of the films. Complete halogenation to yield (e.g. $(CHBr)_x$) results again in high infrared transmission with concomitant production of a white film. The initial reduction in infrared transmission suggests that the halogen-doped material might have unusual electronic properties. The results of studies involving the halogenation of films of *trans*-$(CH)_x$ are summarized below.

The conductivity of the $(CH)_x$ films was measured by four-probe dc techniques at room temperature in a glass vessel to which was attached a bulb containing the halogen. This bulb was held at various temperatures to produce known halogen-vapor pressures. When $(CH)_x$ is exposed to 1 torr of bromine vapor at room temperature for 10 min, the conductivity rapidly increases by approximately four orders of magnitude to give silvery films of $(CHBr_{0.05})_x$ having a conductivity of 0.5 $(\Omega\text{-cm})^{-1}$ at room temperature. Longer bromination gives silvery-black films having the composition $(CHBr_{0.23})_x$ and a slightly smaller conductivity ($\sigma_{298K} = 0.4$ $(\Omega\text{-cm})^{-1}$). The films are stable both in vacuum and when exposed to air for at least several hours at room temperature. Qualitatively similar results are obtained with chlorine, but the increase in conductivity is smaller (about three orders of magnitude).

When iodine vapor reacts with $(CH)_x$ at room temperature, the infrared transmission decreases in a manner similar to that described above for bromine. The increase in conductivity, however, is even more remarkable, more than seven orders of magnitude, as shown in FIGURE 4. The maximum conductivity ($\sigma_{298K} =$ 38 $(\Omega\text{-cm})^{-1}$) was observed on a silvery-black film of composition $(CHI_{0.22})_x$.§ The appearance of the $(CH)_x$ film remained essentially unchanged until the approximate composition $(CHI_{0.05})_x$ was reached, after which it began to darken. The stability of the iodinated films is similar to that of the brominated material. Separate measurements of three samples of $(CHI_{0.22})_x$ gave an average conductivity of 30 $(\Omega\text{-cm})^{-1}$. This material has the largest room-temperature conductivity observed for any covalent organic polymer.

We believe that charge-transfer complexes are formed between $(CH)_x$ and halogens when they are permitted to react under certain conditions, as has been observed previously with iodine and polyphenylene.[26] In the case of $(CH)_x$, however, the absolute conductivities obtained are four to five orders of magnitude greater.

The highly conducting polyacetylene bromides and iodides may be charge-

§Analytical data (Galbraith Laboratories, Inc., Knoxville, Tenn. 37921): Calcd. for $(CHI_{0.22})_x$, C, 29.34; H, 2.46; I, 68.20. Found: C, 29.14; H, 2.62; I, 68.26%. (Total = 100.02%).

transfer pi complexes of the type believed to be formed during the halogenation of olefins. Stable, colored compounds that may be charge-transfer and/or carbonium ion complexes of this type have been obtained by the action of bromine on certain substituted ethylenes.[27,28]

We note for comparison that the room-temperature conductivity of a compacted, polycrystalline pellet of the organic charge-transfer metallic salt, (TTF)(TCNQ), is *ca.* 10 $(\Omega\text{-cm})^{-1}$,[29] whereas that of a compressed pellet of polycrystalline $(SN)_x$ at room temperature is ca 20 $(\Omega\text{-cm})^{-1}$.[30] The conductivity of the latter material *decreases* when the temperature is lowered and exhibits an activation energy, E_a, of about 0.02 eV. Later experimental results on *single*

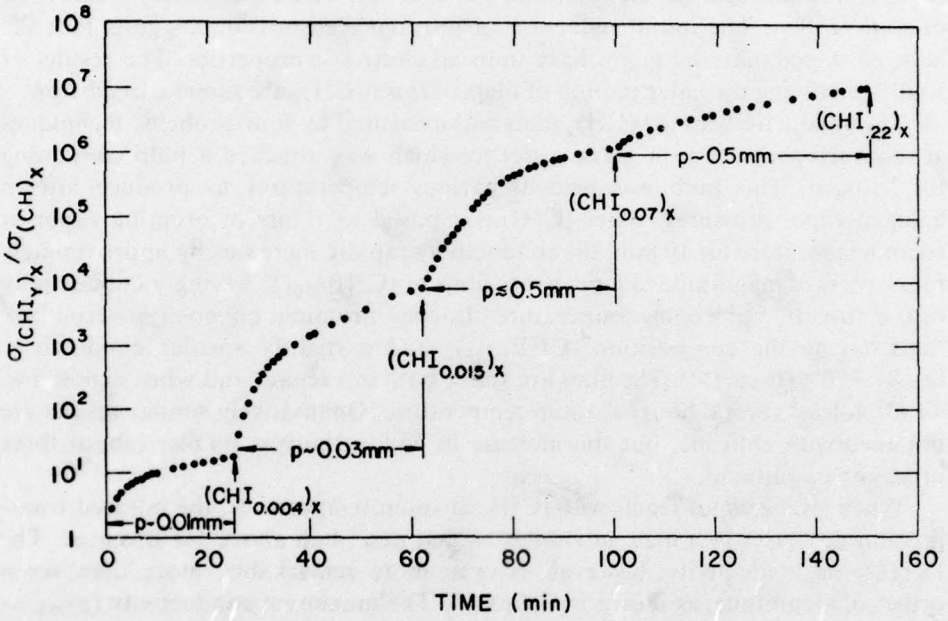


FIGURE 4. Increase in the room-temperature conductivity of *trans*-polyacetylene, $(CH)_x$, as a function of time at fixed iodine vapor pressures. The initial room-temperature conductivity is 3.2×10^{-6} $(\Omega\text{-cm})^{-1}$. (In the last experiment some iodine was sublimed onto the glass walls of the conductivity apparatus in order to promote attainment of the equilibrium vapor pressure of the iodine at room temperature in the vicinity of the film.)

crystals of $(SN)_x$ have shown that the conductivity *increases* with decrease in temperature, ($E_a = 0$), in a manner characteristic of a metal.[1] In the polycrystalline $(SN)_x$ sample, the increase in conductivity on lowering the temperature that occurs within a small, metallic crystal of $(SN)_x$ is apparently more than offset by the decrease in conductivity involved in the passage of electrons from one crystal to another. As with polycrystalline $(SN)_x$, the conductivity of the most highly conducting composition, $(CHI_{0.22})_x$, decreases slowly on temperature decrease ($300\ K > T > 4.2$ k) with an activation energy, $E_a \simeq 0.016$ eV (for comparison the activation energy for *trans*-$(CH)_x$ is $E_a \simeq 0.3$ eV).[24] These results are sug-

gestive of metallic behavior; experiments are under way directed toward clarification of the origin of the very small activation energy.

Although the randomness of the halogenated polyacetylene may be playing an important role, the overall behavior is like that of a series of semiconductors with activation energies that vary with halogen content. However, a detailed study of the temperature dependence of the conductivity indicates that a simple semiconductor model involving a single activation energy is inadequate for the description of the conductivity of the material. We believe that the polyacetylene halides may be the forerunners of a new class of organic polymers with electrical properties, which may be systematically and controllably varied over a wide range by chemical doping.

Acknowledgment

We thank Dr. A. J. Epstein for helpful suggestions on achievement of stable contacts in the presence of bromine.

Notes and References

1. See, for example, Walatka, V. V., Jr., M. M. Labes & J. H. Perlstein. 1973. Phys. Rev. Lett. **31:** 1139; Hsu, C. & M. M. Labes. 1974. J. Chem. Phys. **61:** 4640; Mikulski, C. M., P. J. Russo, M. S. Saran, A. G. MacDiarmid, A. F. Garito & A. J. Heeger. 1975. J. Amer. Chem. Soc. **97:** 6358; Greene, R. L., P. M. Grant & G. B. Street. 1975. Phys. Rev. Lett. **34:** 89. Greene, R. L., G. B. Street & L. J. Suter. 1975. Phys. Rev. Lett. **34:** 577. Cohen, M. J., A. F. Garito, A. J. Heeger, A. G. MacDiarmid, C. M. Mikulski, M. S. Saran & J. Kleppinger. 1976. J. Amer. Chem. Soc. **98:** 3844; Baughman, R. H., P. A. Apgar, R. R. Chance, A. G. MacDiarmid & A. F. Garito. 1977. J. Chem. Phys. **66:** 401; Geserich, H. P. & L. Pintschovius. *In* Festkörperprobleme (Advances in Solid State Physics). J. Treusch Ed. Vol. **XVI:** 65. Vieweg. Braunschweig, Germany.
2. Bright, A. A., M. J. Cohen, A. F. Garito, A. J. Heeger, C. M. Mikulski & A. G. MacDiarmid. 1975. Appl. Phys. Lett. **26:** 612.
3. Chen, C. H., J. Silcox, A. F. Garito, A. J. Heeger & A. G. MacDiarmid. 1976. Phys. Rev. Lett. **36:** 525.
4. Patton, R. L. 1969. Ph.D. Thesis. Univ. California. Berkeley, Calif.
5. Bernard, C., A. Herold, M. Lelaurain & G. Robert. 1976. C. R. Acad. Sci. (Paris) **C, 283:** 625.
6. Akhtar, M., J. Kleppinger, A. G. MacDiarmid, J. Milliken, M. J. Moran, C. K. Chiang, M. J. Cohen, A. J. Heeger & D. L. Peebles. 1977. Chem. Commun.: 473.
7. Street, G. B., W. D. Gill, R. H. Geiss, R. L. Greene & J. J. Mayerle. 1977. Chem. Commun.: 464; Gill, W. D., W. Bludau, R. H. Geiss, P. M. Grant, R. L. Greene, J. J. Mayerle & G. B. Street. 1977. Phys. Rev. Lett. **38:** 1305.
8. A preliminary version of this study was presented as a postdeadline contributed paper at the American Physical Society Meeting, San Diego, Calif., on March 23, 1977. Similar results were reported at the same time by G. B. Street *et al.* (See Ref. 7.)
9. Mikulski, C. M., A. G. MacDiarmid, A. F. Garito & A. J. Heeger. 1976. Inorg. Chem. **15:** 2943.
10. Chiang, C. K., M. J. Cohen, A. F. Garito, A. J. Heeger, C. M. Mikulski & A. G. MacDiarmid. 1976. Solid State Commun. **18:** 1451.
11. Fischer, J. E., T. E. Thompson, G. M. T. Foley, D. Guerard, M. Hoke & F. L. Lederman. 1976. Phys. Rev. Lett. **37:** 769.

12. COHEN, M. J. 1975. Ph.D. Thesis. Univ. Pennsylvania. Similar results have been obtained for $(SN)_x$ by others; see GRANT, P. M., R. L. GREENE & G. B. STREET. 1975. Phys. Rev. Lett. **35:** 1743.
13. This point has been emphasized by W. D. Gill in a private communication.
14. PLATTS, D. A., D. D. L. CHUNG & M. S. DRESSELHAUS. 1977. Phys. Rev. **B 15:** 1087.
15. SCRANTON, R. A., J. B. MOONEY, J. O. MCCALDIN, T. C. MCGILL & C. A. MEAD. 1976. Appl. Phys. Lett. **29:** 46.
16. See, for example, the following: RUDGE, W. E. & P. M. GRANT. 1975. Phys. Rev. Lett. **35:** 1799; BRIGHT, A. A. & P. SOVEN. 1976. Sol. State Commun. **18:** 317; SCHLICTER, M., J. R. CHELIKOWSKI & M. L. COHEN. 1975. Phys. Rev. Lett. **35:** 869; FREISEN, W. I., A. J. BERLINSKY, B. BERGERSEN, L. WEILER & T. M. RICE. 1975. J. Phys. **C8:** 3549.
17. ABRIKOSOV, A. A. 1972. Introduction to the Theory of Metals: 67–73. Academic Press. New York, N.Y.
18. KUKKONEN, C. A. & P. F. MALDAGUE. 1976. Phys. Rev. Lett. **37:** 782.
19. THOMPSON, A. H. 1975. Phys. Rev. Lett. **35:** 1786, and private communication.
20. SHIRAKAWA, H. & S. IKEDA. 1971. Polym. J. **2:** 231.
21. SHIRAKAWA, H., T. ITO & S. IKEDA. 1973. Polym. J. **4:** 460.
22. ITO, T., H. SHIRAKAWA & S. IKEDA. 1974. J. Polym. Sci. Polym. Chem. Ed. **12:** 11.
23. ITO, T., H. SHIRAKAWA & S. IKEDA. 1975. J. Polym. Sci. Polym. Chem. Ed. **13:** 1943.
24. SHIRAKAWA, H., T. ITO & S. IDEKA. 1976. Unpublished results.
25. SHIRAKAWA, H. & S. IKEDA. 1976. Unpublished results.
26. MAINTHIA, S. B., P. L. KRONICK, H. U. E. F. CHAPMAN & M. M. LABES. 1963. Polym. Prepr. Amer. Chem. Soc. Div. Polym. Chem. **4:** (1) April.
27. BUCKLES, R. E. & N. A. MEINHARDT. 1952. J. Amer. Chem. Soc. **74:** 1171.
28. BUCKLES, R. E. & W. D. WOMER. 1958. J. Amer. Chem. Soc. **80:** 5058.
29. COLEMAN, L. B. 1975. Ph.D. Thesis. Univ. Pennsylvania. Philadelphia, Pa.
30. LABES, M. M. 1966. Pure Appl. Chem. **12:** 275.

DISCUSSION

FRED WUDL (*Bell Telephone Laboratories, Murray Hill, N.J.*): Are reflections really sharp, or are they broad in the x-ray powder patterns of $(CH)_x$?

MACDIARMID: These are fairly sharp. There does not appear to be a real amorphous phase.

FRED GOETZ (*Hooker Chemicals & Plastics Corp., Grand Island, N.Y.*): It is not unusual to see conductive complexes of iodine with hydrocarbons.

MACDIARMID: It is not only iodine that causes the conductivity to increase. There are many things, such as BF_3 or a small amount of oxygen, that may do this.

POLYTHIAZYL HALIDES: BROMINE DERIVATIVES OF $(SN)_x$ AND S_4N_4*

G. B. Street, S. Etemad,†
R. H. Geiss, W. D. Gill, R. L. Greene, and J. Kuyper

IBM Research Laboratory
San Jose, California 95193
and

R. D. Smith

Battelle
Richland, Washington 99352

INTRODUCTION

The metallic and superconducting properties of polysulfurnitride have encouraged extensive efforts to prepare analogs or derivatives.[1-3] To date, the most interesting extension of this material is the halogen derivatives.[4-7a] The influence of halogens on the conductivity of $(SN)_x$ has been mentioned by Yoffe,[8] but no details were reported. Bernard *et al.*[4] found that bromine reacts with $(SN)_x$ to give what they believed to be an insertion compound. Independently, we have observed the reaction of $(SN)_x$ crystals and films with bromine and also other halogens[5,6] which indicated that the halogen content of the $(SN)_x$ could be varied widely and continuously. In the case of bromine, the composition ranged between $(SN)_x$ and $(SNBr_{0.6})_x$. In addition, we found that the incorporation of bromine led to an order of magnitude increase in conductivity parallel to the chain axis compared to pristine $(SN)_x$. Similar results have also been reported by others.[7,7a] The thermopower of $(SN)_x$ changes sign on bromination, becoming *p*-type, which is consistent with the bromine acting as an acceptor, and the superconducting transition temperature increases only slightly. Optical reflectivity data show the metallic behavior typical of pristine $(SN)_x$ but with the reflectivity edge shifted toward the red. This shift is due to an increase in the background dielectric constant; the plasma frequency itself is essentially unchanged. These electronic properties of brominated $(SN)_x$ are discussed in detail elsewhere.[6] In this paper the physical and chemical properties of bromine derivatives of $(SN)_x$ will be described together with our current model for their structure.

PREPARATION OF $(SNBr_y)_x$

Treatment of $(SN)_x$ crystals or films with liquid bromine, gaseous bromine, or bromine in solution causes a rapid color change from the gold of $(SN)_x$ to a blue-black. Accompanying this color change is an anisotropic increase in volume,

*Partly supported by the Office of Naval Research. Manuscript received July 22, 1977.
†Permanent address: Dept. of Physics, Aria-Mehr University of Technology, Tehran, Iran.

0077-8923/78/0313-0737 $1.75/1© 1978, NYAS

with almost all of the increase occurring in directions perpendicular to the *b*-axis. This expansion frequently leads to extensive cracking of the crystals. By controlling the bromine concentration and the temperature of the $(SN)_x$ crystals, it is possible to obtain any composition between $(SN)_x$ and $(SNBr_{0.6})_x$. Intermediate compositions may also be obtained by debromination under controlled temperature and pressure. Because the principal discussion in this paper will be restricted to $(SNBr_{0.4})_x$, its preparation will be described in detail. $(SN)_x$ crystals at room temperature are exposed to the room-temperature vapor pressure of bromine in a sealed, evacuated (10^{-5} torr) Pyrex® tube. To avoid side products, the bromine should be dry and free from chlorine or hydrogen bromide. In order to ensure that the bromination is complete, the reaction is allowed to preceed for several days. The blue-black crystals, which retain the fibrous nature of pristine $(SN)_x$, are then transferred to a vacuum system without exposure to air. They are then pumped on for about one hour at 10^{-5} torr, during which their composition changes from $\sim (SNBr_{0.5})_x$ to $(SNBr_{0.4})_x$. Although these $(SNBr_{0.4})_x$ crystals are stable in the absence of air, they decompose fairly rapidly in air to give ammonium salts. We will return to this point in the following discussion of the mass spectrometric and infrared data for this material.

Thermal Analysis and Mass Spectrometry of $(SNBr_{0.4})_x$

Bernard *et al.*[4] report that the bromination of $(SN)_x$ is partly reversible. This result is evident from the thermogravimetric analysis (TGA) data (Figure 1(a)) obtained at a heating rate of 5°C/min and under one atmosphere of helium. These data show that under these conditions rapid loss of bromine first occurs at temperatures ~ 125°C, and they do not provide any evidence of preferential stability of intermediate compositions. The differential thermal analysis data shown in Figure 1(b) agrees well with the TGA data. It shows a strong exotherm ~ 165°C associated with the liberation of bromine and exothermic decomposition. Although debromination can lead to compositions intermediate between $(SNBr_{0.6})_x$ and $(SN)_x$, it is not possible to obtain pure $(SN)_x$ in this way because the $(SN)_x$ itself becomes volatile before all the bromine has been driven off.

Phase-angle mass spectrometry in conjunction with electron impact and chemical ionization techniques[9] have identified Br_2 and SNBr as the predominant molecular species obtained on heating $(SNBr_{0.4})_x$ to 80°C in vacuum. The intensity of these two species is time dependent. Initially, Br_2 is the most intense; however, after a period of ~ 3 hours the bromine is almost undetectable, and SNBr becomes the principal bromine-containing peak. Even if the temperature is now raised to 150°, the bromine peak does not reappear. It is also interesting to note that the hydride species, $N_xS_yH_z$, are reduced to ~ 10% of their intensity in pristine $(SN)_x$.[10] This suggests that bromination in some way removes the hydrogen, perhaps forming the HBr which is initially observed in the mass spectra. It is important to realize that $(SNBr_{0.4})_x$ reacts much more rapidly with air than pristine $(SN)_x$. This becomes apparent from the mass spectra of samples exposed to air for one day, which show several additional products NH_3, SO_2, HNSO, S_x, and S_4N_2, as well as increased amounts of HBr and hydrides.

Structure of $(SNBr_{0.4})_x$

Consistent with the observed lack of expansion of the crystals in the *b* directions, Bernard *et al.*[4] showed that the chain axis of $(SN)_x$ did not expand on bromination. We have confirmed this from x-ray precession photographs,[5,6] but the increase in disorder perpendicular and parallel to the chain axis after bromination prevented direct measurement of *a* and *c*.[5,6] However, Baughman[11] concludes that *a* decreases by 7% and *c* increases by 1% on bromination to $(SNBr_{0.4})_x$. From transmission electron diffraction data,[5,6] we believe that the essential chain structure of $(SN)_x$ does not change on bromination. The electron diffraction data confirms the disorder in directions perpendicular to the chain axis and reveals a

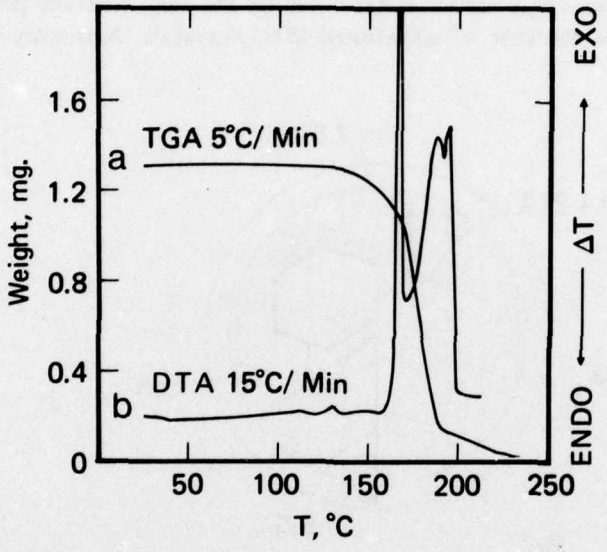
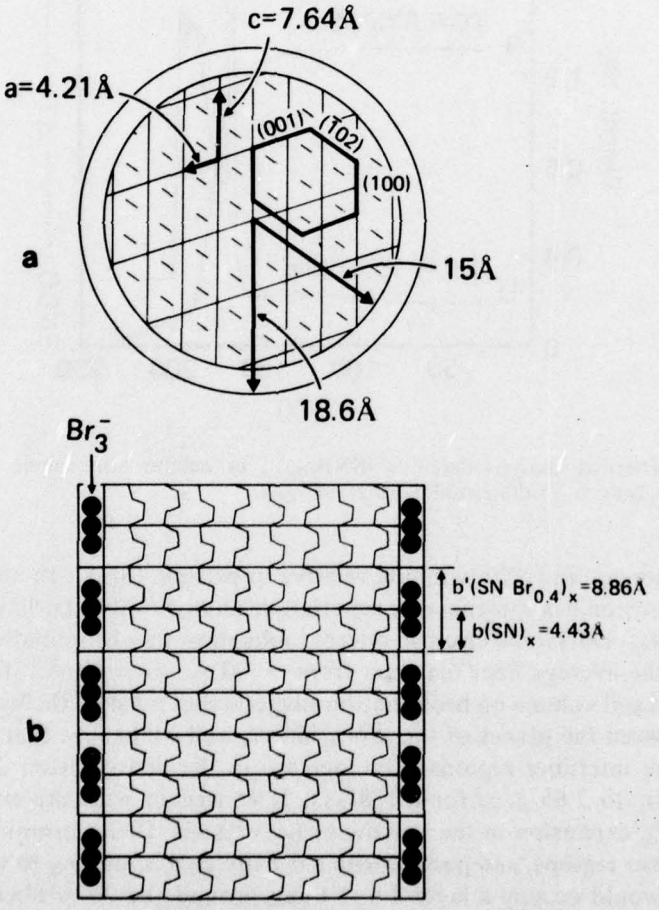


FIGURE 1. Thermal analysis data for $(SNBr_{0.4})_x$ in helium atmosphere. a = Thermogravimetric analysis; b = differential thermal analysis.

noticeable increase in (100) twinning relative to pristine $(SN)_x$. In addition, there is a one-dimensional commensurate superlattice along *b* with a period of twice the *b*-axis of $(SN)_x$. Dark-field electron micrographs show that bromination leads to a decrease in the average fiber diameter from ~ 70 Å to ~ 30 Å.[6] The small decrease in unit cell volume on bromination suggests that most of the bromine is not entering between the planes of the $(SN)_x$ lattice, and we believe that it is present mainly in the interfiber regions. The increase in the density from 2.32 g/cc for pristine $(SN)_x$ to 2.65 g/cc for $(SNBr_{0.4})_x$ is consistent with the experimentally observed 50% expansion in the volume of the crystals. If the bromine is entirely in the interfiber regions, and packed with a density corresponding to that of liquid bromine, it would occupy a layer 3.6 Å thick around the 30 Å fibers, which we assume, for simplicity, are cylindrical, as shown in FIGURE 2a, 2b, and 2c. This 3.6 Å thickness is close to the VDW diameter of a bromine atom,[12] suggesting that

the bromine forms a layer one atom thick around the 30 Å fibers. From Raman studies described elsewhere,[13] it appears that, contrary to our earlier report,[5,6] the bromine is present mainly as a linear, but asymmetric, Br_3^- ions aligned with their axes parallel to the chains of $(SN)_x$. The length of a Br_3^- ion is close to $2b$, and we believe that these ions are responsible for the observed commensurate one-dimensional superlattice of period $2b$. FIGURE 2b shows a cross section of a 30 Å diameter cylindrical fiber (perpendicular to b) containing approximately 25 unit cells of $(SN)_x$, or about 50 chains. The lower part of the diagram also shows the corresponding view of the $(SN)_x$ fibers looking in along c. The $(SN)_x$ chains are shown running along b with the Br_3^- ions arranged on the outside of the fibers. It must be emphasized that this model is an oversimplification in several respects. The fibers are obviously not cylindrical, but would probably have an approximately hexagonal cross section determined by the easy cleavage planes shown in FIGURE 2b, as is the case of untwinned $(SN)_x$ crystals. Normally $(SN)_x$ crystals



FIGURES 2a & 2b. Clad fiber model for $(SNBr_{0.4})_x$. a = Br_3^- ions forming a 3.6 Å monolayer around 30 Å diameter fibers; b = cross section of 30 Å diameter cylindrical fiber (perpendicular to b) showing ~ 25 unit cells, or 50 chains.

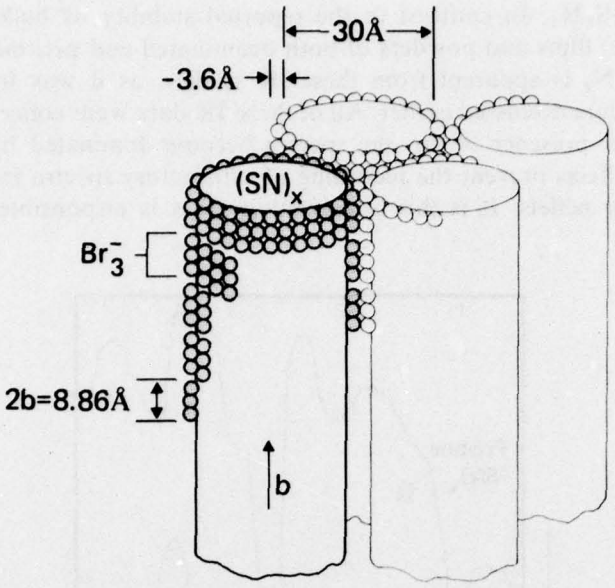


FIGURE 2c. Cylindrical fiber of $(SN)_x$ viewed down the c axis showing $(SN)_x$ chains of period b and Br_3^- ions forming commensurate superlattice of period $2b$.

are twinned, and this would lead to further deviations from cylindrical fibers. It also seems unlikely that the Br_3^- ions would pack randomly around the fibers; it seems more probable that they would exhibit some preferential packing, in addition to being parallel to the $(SN)_x$ chains. Furthermore, the model does not account for the significant increase in twinning observed on bromination.

BROMINATION OF S_4N_4

S_4N_4, a cradle-shaped molecule,[14] is a precursor of $(SN)_x$. It is an orange-yellow molecular solid of high electrical resistivity ($\sigma \sim 10^{14}\Omega$ cm at 25°C). We have observed that the reaction of solid S_4N_4 with bromine, as well as other halogens,[15] destroys the S_4N_4 crystal habit and leads to a voluminous black powder with a conductivity (measured as a compressed pellet) of $32\Omega^{-1}$ cm^{-1} at 25°. The density (2.65 g/cc) and composition $SNBr_{0.4}$ of the bromine derivative are identical to the values obtained for the principal composition of brominated $(SN)_x$ discussed in this paper. The transmission IR spectrum of brominated S_4N_4 is compared with that of $(SN)_x$ and $(SNBr_{0.4})_x$ in FIGURE 3. All the spectra were recorded as films on KBr discs. Bromination causes the 1000 cm^{-1} peak of $(SN)_x$ to almost disappear and the other peaks to shift somewhat in position and relative intensity. A detailed investigation of these spectra is in progress; however, the general similarity of the two spectra supports our conclusion that the $(SN)_x$ chain geometry does not change drastically on bromination. The similarity of the spectra of brominated $(SN)_x$ and brominated S_4N_4 is striking, particularly if one removes the peaks at 545 and 920 cm^{-1} which are due to the presence of some

unbrominated S_4N_4. In contrast to the reported stability of bulk $(SN)_x$,[16] the air sensitivity of films and powders of both brominated and pristine $(SN)_x$[17] and brominated S_4N_4 is apparent from these IR studies, as it was from the mass spectrometric data discussed earlier. All of these IR data were collected under dry nitrogen. In the presence of air, the spectra become dominated by ammonium salts.[18] These effects prevent the recording of satisfactory spectra from powdered material in KBr pellets. It is this air sensitivity that is responsible for many of

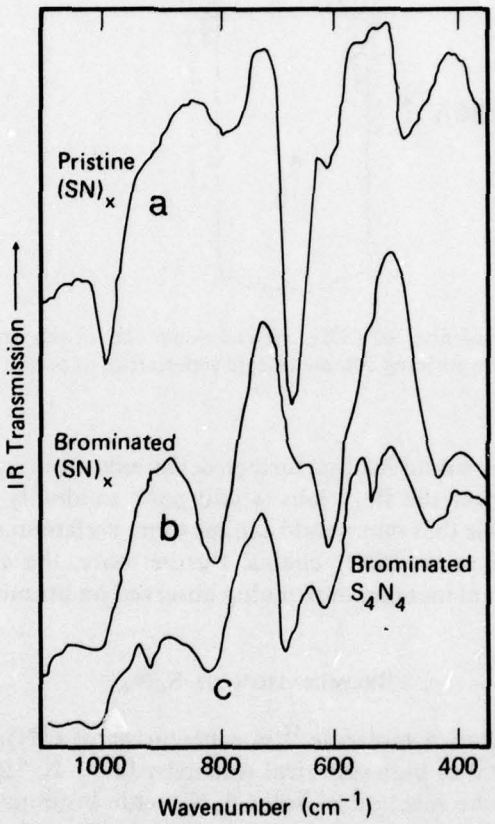


FIGURE 3. Transmission IR spectra on KBr discs of films of a = pristine $(SN)_x$; b = brominated $(SN)_x - (SNBr_{0.4})_x$; c = brominated $S_4N_4 - SNBr_{0.4}$.

the nonintrinsic peaks reported in the early IR spectra of $(SN)_x$[19] rather than non-stoichiometry, as suggested by Stolz *et al.*[20]

From the similarity of the IR spectra of brominated $(SN)_x$ and brominated S_4N_4, we conclude that the latter also contains polymerized sulfur-nitrogen chains. X-ray powder data shows a large broad peak corresponding closely to the $\bar{1}02$ interchain spacing observed for $(SN)_x$.[15] The poorly crystalline nature of brominated S_4N_4 is not unexpected, because the structure of S_4N_4 does not provide as favorable a route for solid-state polymerization as that of S_2N_2.[21] DTA, TGA, and mass spectrometric studies[9] also tend to confirm the essential

similarity of brominated $(SN)_x$ and brominated S_4N_4. These techniques demonstrate that bromine is lost somewhat more readily from the brominated S_4N_4. On sublimation, brominated S_4N_4 gives rise to conducting films similar to those obtained from brominated $(SN)_x$.

Conclusions

The model of brominated $(SN)_x$ presented here assumes that most of the bromine is present as Br_3^- ions which are situated mainly in the interfiber regions and do not enter the $(SN)_x$ lattice in large amounts. In the description of the model we have used twinfree, cylindrical fibers for descriptive simplicity. In reality, the fibers of $(SN)_x$ are heavily twinned and not cylindrical. We have presented a variety of data that suggest such a strong similarity between brominated $(SN)_x$ and brominated S_4N_4 that we believe this latter material also consists of polymerized chains of sulfur and nitrogen atoms. The similarity in composition between these two bromine derivatives, despite the fact that the brominated S_4N_4 does not appear to be fibrous, is puzzling, in view of our model. More work is clearly necessary in order for us to understand fully the structure of these new materials.

Acknowledgments

The many discussions with Professor J. M. Thomas and Dr. G. Wolmershauser are greatly appreciated.

References

1. Geserich, H. P. & L. Pintschovius. 1976. Festkörperprobleme **XVI:** 96.
2. Street, G. B. & R. L. Greene. 1977. IBM J. Res. Develop. **21:** 99.
3. Greene, R. L. & G. B. Street. 1977. Proc. NATO-ASI on Chemistry and Physics of One-Dimensional Metals. Bolzano, Italy, August, 1976. H. J. Keller, Ed. Plenum Press. New York, N.Y.
4. Bernard, C., A. Herald, M. Lelaurain & G. Robert. 1976. C. R. Acad. Sci. [D] (Paris) **C283:** 625.
5. Street, G. B., W. D. Gill, R. H. Geiss, R. L. Greene & J. J. Mayerle. 1977. J. C. S. Chem. Comm. In press.
6. Gill, W. D., W. Bludau, R. H. Geiss, P. M. Grant, R. L. Greene, J. J. Mayerle & G. B. Street. 1977. Phys. Rev. Lett. **38:** 1305.
7. Akhtar, M., J. Kleppinger, A. G. MacDiarmid, J. Milliken, M. J. Moran, C. K. Chiang, M. J. Cohen, A. J. Heeger & D. L. Peebles. 1977. J. C. S. Chem. Comm. In press.

7a. Chiang, C. K., M. J. Cohen, D. L. Peebles, A. J. Heeger, M. Akhtar, J. Kleppinger & A. G. MacDiarmid. To be published.

8. Yoffe, A. D. 1976. Chem. Soc. Rev. **5:** 51.
9. Smith, R. D. & G. B. Street. To be published.
10. Smith, R. D., J. R. Wyatt, J. J. DeCorpo, F. E. Saalfeld, M. J. Moran & A. G. MacDiarmid. 1977. J. Amer. Chem. Soc. **99:** 1726.
11. Baughman, R. H. Private communication.
12. Bondi, A. 1968. Physical Properties of Molecular Crystals, Liquids and Gases. John Wiley & Sons. New York, N.Y.
13. Temkin, H., D. B. Fitchen, W. D. Gill & G. B. Street. 1977. This conference.

14. SHARMA, B. D. & J. DONOHUE. 1963. Acta Cryst. **16:** 891.
15. STREET, G. B., R. L. BINGHAM, J. I. CROWLEY & J. KUYPER. 1977. J. C. S. Chem. Comm. In press.
16. MIKULSKI, C. M., A. G. MACDIARMID, A. F. GARITO & A. J. HEEGER. 1976. Inorganic Chemistry **15:** 2943.
17. MENGEL, P., P. M. GRANT, W. E. RUDGE, B. H. SCHECHTMAN & D. W. RICE. 1975. Phys. Rev. Lett. **35:** 1803.
18. WOLMERSHAUSER, G. 1975. Private communication.
19. CHAPMAN, D. & R. J. WARN. 1964. Trans. Farad. Soc. **60:** 294.
20. STOLZ, H. J., H. WENDEL, A. OTTO, L. PINTSCHOVIUS & H. KAHLERT. 1976. Phys. Stat. Sol. **b78:** 277 (1976).
21. BAUGHMAN, R. H., R. R. CHANCE & M. J. COHEN. 1976. J. Chem. Phys. **64:** 1869.

DISCUSSION

DAVIS (*Temple Univ., Philadelphia, Pa.*): What observations have you been able to make about the properties of the brominated $(SN)_x$ after removal of bromine?

STREET: As the bromine is removed, the conductivity decreases.

MOHAN SARAN (*Hooker Chemical and Plastics Corp., Grand Island, N.Y.*): Is $(SNBr_{0.4})_x$ obtained from S_4N_4 the same as that prepared from $(SN)_x$?

STREET: There is a great deal of evidence that the products of bromination of S_4N_4 and $(SN)_x$ are the same. For example, both give similar results from thermal analysis, mass spectrometry, IR, and Raman spectroscopy, and they also have similar electrical properties.

$(SN)_x$ GROWN UNDER UNUSUAL CONDITIONS*

P. Love, G. Myer, H. I. Kao, and M. M. Labes

Departments of Chemistry and Geology
Temple University
Philadelphia, Pennsylvania 19122

and

W. R. Junker and C. Elbaum

Department of Physics and Metals Research
Brown University
Providence, Rhode Island 02912

Growth of $(SN)_x$ from Three Different Thermolysis Products

Introduction

In the preparation of S_2N_2 from S_4N_4, it has often been observed that several colored by-products are formed.[1-3] The pyrolysis conditions are usually adjusted to attempt to minimize these products, or the growth of S_2N_2 crystals conducted so as to effectively reject them. An examination of the early literature reveals that in 1925[4] Usher noted that a ruby-red precursor could be obtained from S_4N_4 silver-wool pyrolysis, and that it eventually formed a thin blue film which he assumed was identical to the $(SN)_x$ prepared by Burt in 1910.[5] These observations led us to speculate that the colored by-products accompanying S_2N_2 might indeed be isolable and polymerizable. Their color suggests that they might be free radical species such as SN· or higher analogs. Therefore, the likelihood of their crystal structure being identical to S_2N_2 seems remote, and the possibility of their polymerizing to unusual forms of $(SN)_x$ needed investigation.

Pyrolysis, Isolation, and Polymerization Techniques

The products from the silver-wool pyrolysis of S_4N_4 that had been purified by fractional sublimation were condensed on a liquid-nitrogen cold finger. Typically, the S_4N_4 was heated to 80–100°C, while the silver-wool zone was kept at 250–300°C at a vacuum of 10^{-6} torr, with continual pumping. The total product was then transferred to another liquid-nitrogen trap by allowing the pyrolysis cold finger to warm up to room temperature.

By high-vacuum fractionation procedures, three main products were isolated: a dark-brown material, a colorless material (S_2N_2), and a deep-red material. The relative volatility of the freshly prepared materials is red > brown > S_2N_2. A

*This work was supported by the National Science Foundation under grants DMR-74-24202 and DMR 77-01055. The work on clathration of $(SN)_x$ was also supported by the Jet Propulsion Laboratory under Contract Number 954326. Manuscript received June 13, 1977.

0077-8923/78/0313-0745 $1.75/1 © 1978, NYAS

typical set of conditions involves sublimation from trap 1 (−9°C) to trap 2 (−31°C) to trap 3 (−196°C). Appropriate fraction cutting leaves brown material and S_2N_2 in trap 1, and red monomer in trap 2. The brown material is then separated from S_2N_2 by rapid fractionation from a trap at 0°C to a liquid-nitrogen trap.

The fractionation conditions and temperatures of the traps employed were, however, found to vary from preparation to preparation, presumably depending on local pressure, flow rate, and relative amounts of the mixed products. In several preparations, multiple fractionations had to be conducted in order to achieve effective separations.

Mass spectral analysis of the red monomer was conducted at the Naval Research Laboratory by an electron-impact quadrupole mass spectrometer.[6] By observing the relative mass ratios as red and colorless materials were volatized, and by observing the clear predominance of the mass 46 peak for red material, an assignment of the structure SN· was made.[7] The monomer vapor pressures were ~0.035 torr for red and ~.021 torr for S_2N_2 at 0°C. No assignment could be made for brown material, which polymerizes extremely rapidly.

During trap-to-trap transfer, and/or in subsequent transfer of isolated fractions, crystals of "red" and "brown" materials were grown and allowed to polymerize. These crystals polymerized to golden, lustrous $(SN)_x$ crystals at rates that are appreciably different from S_2N_2 polymerization. We will refer to these crystals of $(SN)_x$ as red, brown, and normal (from S_2N_2), even though the color of all the polymer crystals are identically golden. The rates of the initial polymerization at room temperature (as observed by the formation of a golden luster) are of the order of hours, minutes, and days, respectively. To complete the polymerizations, long-term storage at room temperature of all of these crystals was conducted, and most crystals were annealed at 75°C prior to determination of their properties.

Crystal size and quality of red $(SN)_x$ was adequate for conductivity measurements, but brown $(SN)_x$ crystals large enough for such studies have not as yet been obtained. Elemental analysis of red $(SN)_x$ was extremely satisfactory (%N 30.46, %S 69.52), but brown $(SN)_x$ contained some impurities (%N 29.26, %S 67.91). The theoretical values are %N 30.40, %S 69.60.

Magnetic Properties of Red and Brown Precursors

S_2N_2 is known to be diamagnetic; during the polymerization, a paramagnetic species is formed and subsequently decays as the polymerization proceeds.[8] To study the nature of the red and brown precursors and their relative rates of polymerization, electron paramagnetic resonance (EPR) spectra were determined by a Varian V-4502 spectrometer operating in the X-band microwave region, recording spectra at −118°. For the time-dependent polymerization studies, samples were warmed to room temperature and then quenched to −118° again to record the EPR trace. Because of the difficulties in separation of pure red and brown materials from S_2N_2, the spectra were obtained on polycrystalline samples containing approximately 50–70% of red or brown material admixed with S_2N_2.

The EPR spectrum of the red monomer is shown in FIGURE 1, and is consistent

with the structure being SN·. The center of the two main peaks of this pattern is at $g = 2.013$. The asymmetry is presumably due to an anisotropic g tensor. This initial signal decays as soon as the sample is warmed, and is replaced by a signal that appears to be characteristic of partially polymerized material with a g value of 2.005.

As opposed to this behavior, the brown precursor is diamagnetic. Upon warming, an EPR signal is obtained that is essentially identical to partially polymerized red $(SN)_x$, although the line width is slightly broader for the brown material

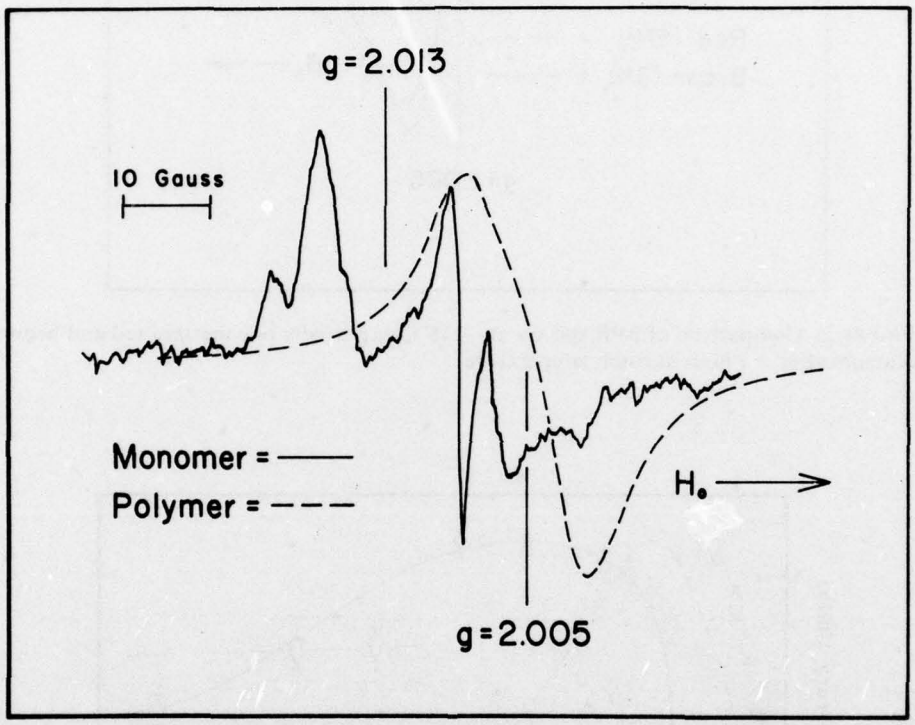


FIGURE 1. EPR spectra at −118°C of red monomer SN·, and of partially polymerized red monomer after warming to room temperature for ~ 1 hour.

(FIGURE 2). A comparison of the relative rates of polymerization can be seen in FIGURE 3. We have not as yet done our own comparison of these rates of polymerization with S_2N_2; data from the University of Pennsylvania group on S_2N_2 are given in FIGURE 3. The rate of polymerization can be quite variable from sample to sample, and one suspects that some free radical quenching processes may be involved.

X-Ray Diffraction Unit Cell Data on Red, Brown, and Normal $(SN)_x$

Powder diffraction films were produced by the Gandolfi-randomizer technique with indexing checked by precession (Buerger) camera films from the same crystal.

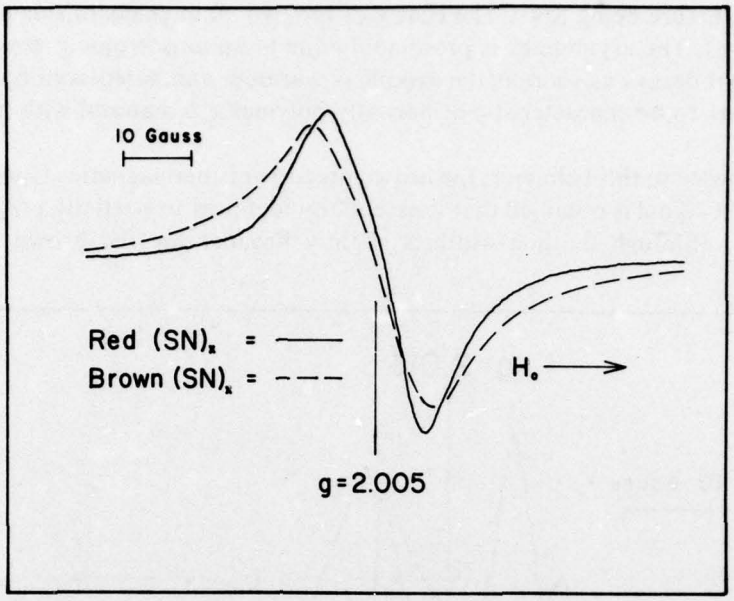


FIGURE 2. Comparison of EPR spectra at −118°C of partially polymerized red and brown precursors after ~ 1 hour at room temperature.

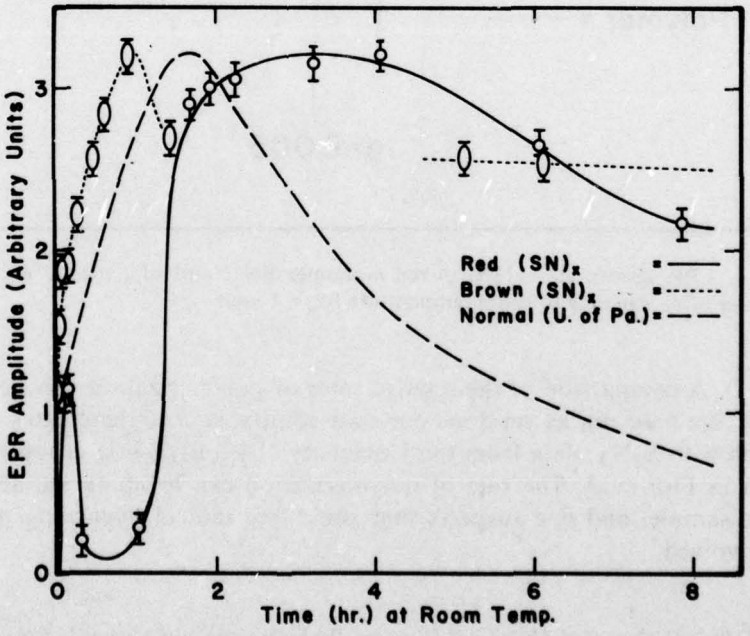


FIGURE 3. Relative rates of polymerization of red and brown monomers as indicated by the amplitude of the EPR signals. Data from University of Pennsylvania on S_2N_2 polymerization are shown for comparison purposes.[8]

Typical exposures of 72–100 hours recorded 48 reflections (for polymers from red and S_2N_2 precursors), of which 21 were sharp enough for least-squares refinement of unit cell values. FIGURES 4 and 5 present some of the powder-diffraction films and a typical precession photograph. Unit-cell parameters are indicated in TABLE 1, and are compared with data from the Molecular Structure Corporation-University of Pennsylvania structure determination.

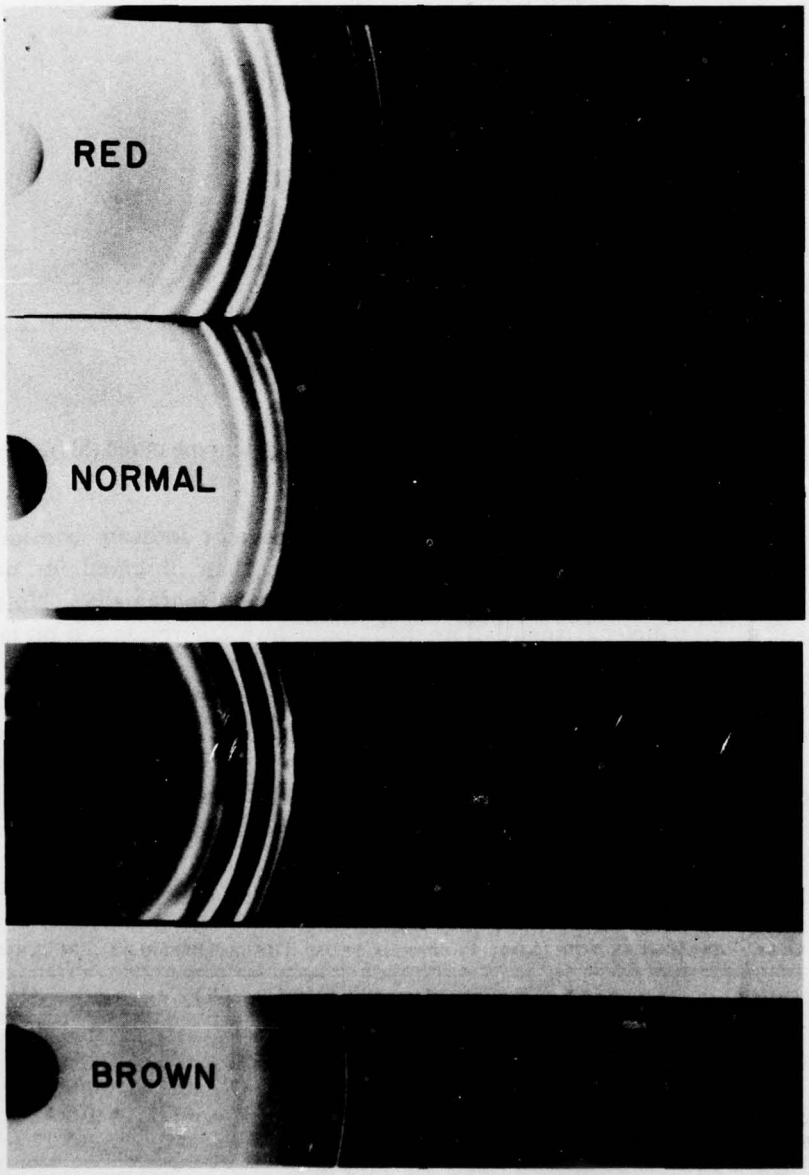


FIGURE 4. X-ray powder difffraction patterns produced from single crystals via the Gandolfi-randomizer technique of (top) red and normal $(SN)_x$, and (bottom) red and brown $(SN)_x$. Back reflections allow film-shrinkage corrections.

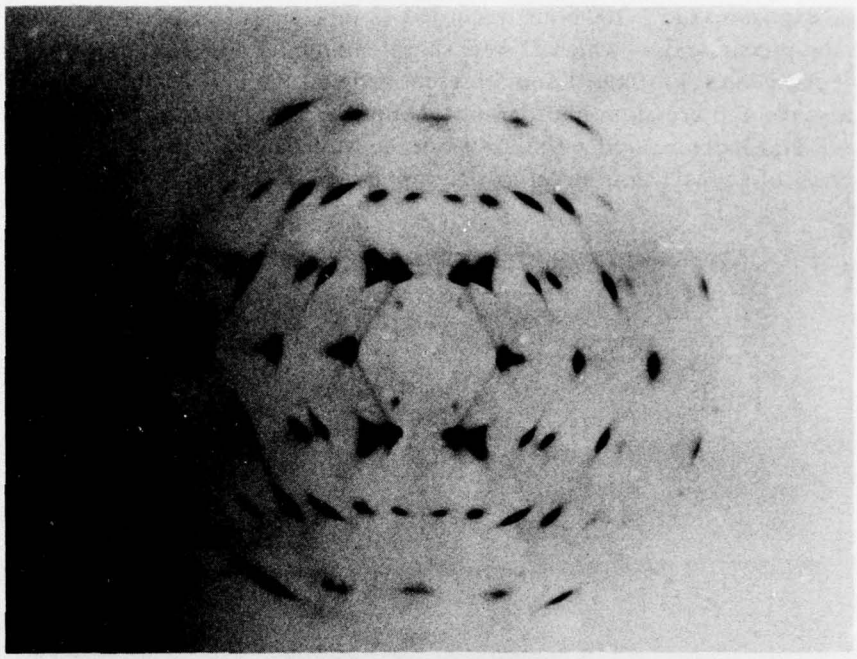


FIGURE 5. Zero level x-ray (MoKα) precession photograph of red $(SN)_x$.

The results on crystals grown from the red precursor indicate considerably sharper reflections and smaller standard deviations than observed for normal $(SN)_x$, but the crystals have essentially the same unit cell parameters. Note that the Penn "*c*" parameter is slightly larger than our own determination on normal $(SN)_x$, or on red $(SN)_x$. The brown precursor, on the other hand, forms polymer crystals with identical *b* and *c* parameters, but the *a* parameter is well outside the standard deviation.

As discussed by Baughman *et al.*,[9] polymerization of S_2N_2 may occur by one point cleavage of S_2N_2, in which case the solid-state polymerization must be nonunique, and disorder must be introduced into the polymerizing phase. If, on

TABLE 1

UNIT CELL PARAMETERS FOR $(SN)_x$ PREPARED FROM THREE DIFFERENT PRECURSORS*

Precursor	a (Å)	b (Å)	c(Å)	β°
Red No. 1	4.151 ± .002	4.439 ± .001	7.586 ± .004	109.35 ± .03
Red No. 2	4.132 ± .002	4.427 ± .001	7.592 ± .003	109.43 ± .02
S_2N_2	4.144 ± .008	4.427 ± .003	7.587 ± .012	109.5 ± .1
S_2N_2 (Penn)†	4.153 ± .006	4.439 ± .005	7.637 ± .012	109.7
Brown	4.302 ± .002	4.423 ± .001	7.576 ± .002	108.19 ± .03

*All the unit cell data are reported on single crystals of $(SN)_x$ of monoclinic symmetry, space group $P2_1/c$.

†Mikulski, C. M., P. J. Russo, M. S. Saran, A. G. MacDiarmid, A. F. Garito & A. J. Heeger. 1975. J. Amer. Chem. Soc. **97**: 6358.

the other hand, S_2N_2 cleaves into two SN radicals which react in separate chains, the polymerization may occur as a unique reaction, introducing less disorder in the polymerizing phase. The differences in the behavior of $(SN)_x$ generated from SN· and S_2N_2 at various stages in the polymerization will be interesting to examine in this context, and indeed the quality and properties of $(SN)_x$ grown from the red precursor may undergo further changes as the purity and crystal growth of polymer are further explored. As to brown $(SN)_x$, its crystal structure appears to be different. It is our intent to examine the crystal structure of the precursor phases at low temperature and the dynamics of the structural changes during polymerization in order to understand the topochemical aspects involved.

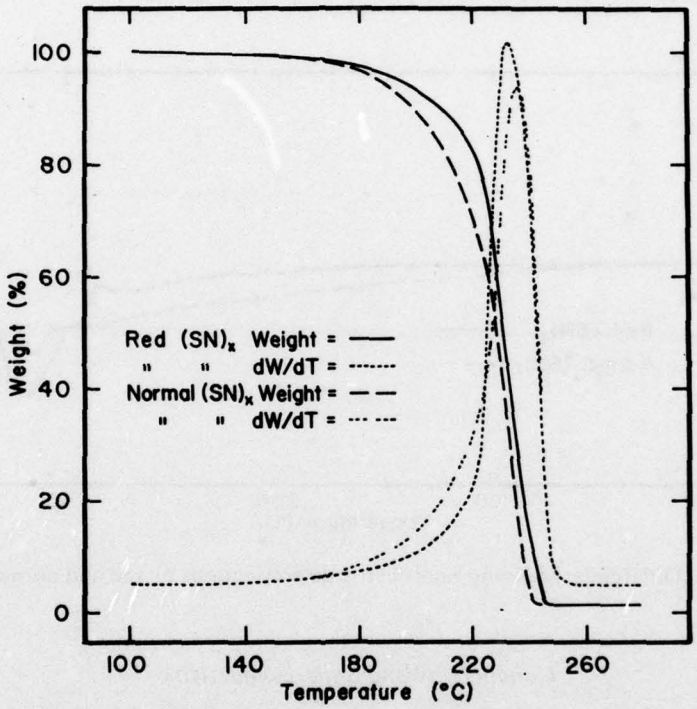


FIGURE 6. Thermogravimetric analyses of red and normal $(SN)_x$.

Thermal Properties

Thermogravimetric analysis (TGA) was conducted on a DuPont 990 TGA system (at Princeton University), which was carefully purged with helium for two hours prior to a TGA scan.[10] Polymer samples of red and normal $(SN)_x$ of comparable particle size and weight were chosen, and the TGA curves are given in FIGURE 6. From the equation $dW/dT = Ae^{-\Delta E/RT}(1 - W)^n$, which gives the change in sample weight W with temperature in terms of the activation energy for sublimation ΔE, a distinct difference in ΔE for normal (29 ± 3 Kcal mole^{-1}) and red (52 ± 3 Kcal mole^{-1}) was observed. The value of ΔE for normal $(SN)_x$

agrees well with that obtained via field desorption mass spectral measurements of 29.0 ± 0.5 Kcal mole^{-1}.[6]

This difference in thermal property is also seen in differential scanning calorimetry (DSC) studies, employing a Perkin-Elmer DSC-1B. Two-hour purges with helium gas of sample and sample housing prior to a scan were conducted, and the data are given in FIGURE 7. Normal $(SN)_x$ appears to start subliming (decomposing) at ~140°C, whereas red $(SN)_x$ does not begin sublimation until ~175°C. Both normal and red samples, however, show the major endotherm at 248°C.

In light of the identity of the crystal structures of red and normal $(SN)_x$, these differences in thermal stabilities must involve a macroscopic property associated with the degree of order (or disorder) in the respective crystals.

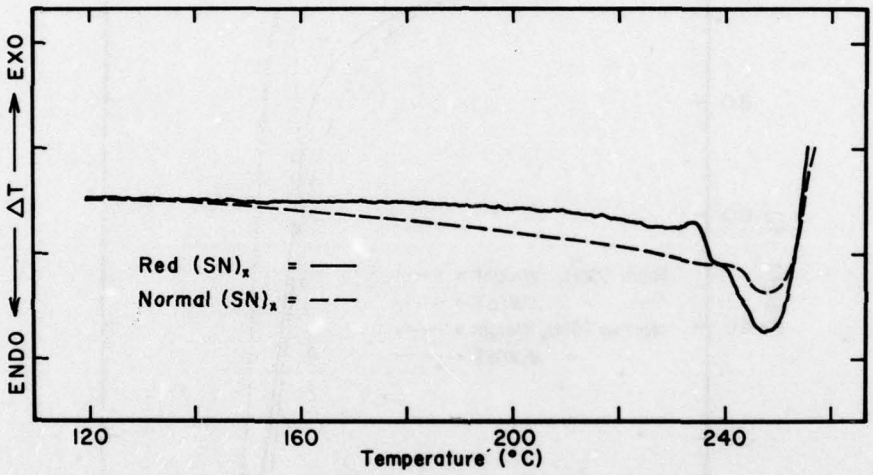


FIGURE 7. *Differential scanning calorimetric determinations on red and normal* $(SN)_x$.

Conductivity and Superconductivity

We have succeeded in obtaining crystals of red $(SN)_x$ of sufficient quality and size to evaluate the normal and superconductivity, but have not succeeded with brown $(SN)_x$. Their physical perfection and normal conductivity is reminiscent of the early measurements on normal $(SN)_x$.[11,12] The red crystals are highly striated and have a room-temperature conductivity of ~1200 $\Omega^{-1}cm^{-1}$. They show a weak conductivity maximum ~2 times the room temperature value at ~50°K (FIGURE 8). The conductivity at 1°K is ~1.3 times the room temperature conductivity. For red $(SN)_x$ having a $\sigma_{1°K}$ of 1500 $\Omega^{-1}cm^{-1}$, the midpoint of the superconducting resistive transition is ~220°mK (FIGURE 9). As observed in poor normal $(SN)_x$ crystals, there is a large residual resistance in the red $(SN)_x$ sample which undoubtedly reflects a high density of fiber-segment junctions.[13,14]

Because the unit cell parameters of brown $(SN)_x$ appear to differ from red and normal $(SN)_x$, further efforts to achieve crystal growth and determine normal and superconductivity are under way.

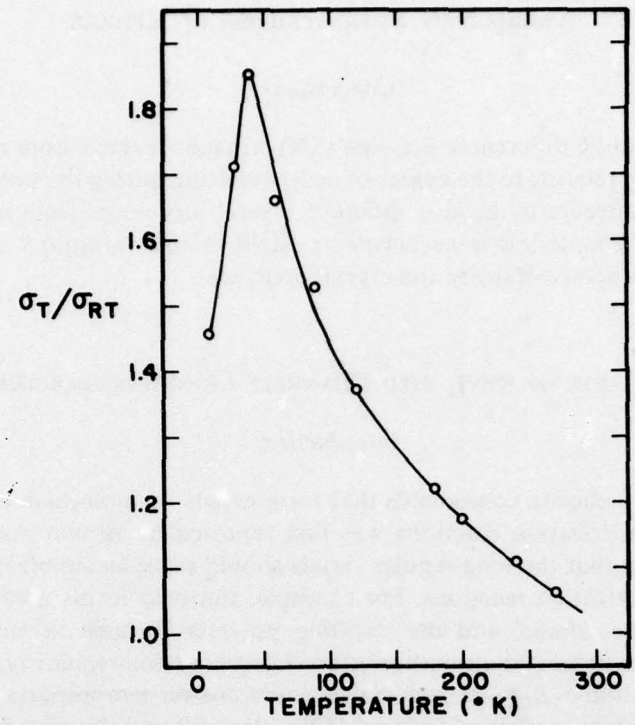


FIGURE 8. Temperature dependence of the conductivity of red $(SN)_x$ normalized to room temperature.

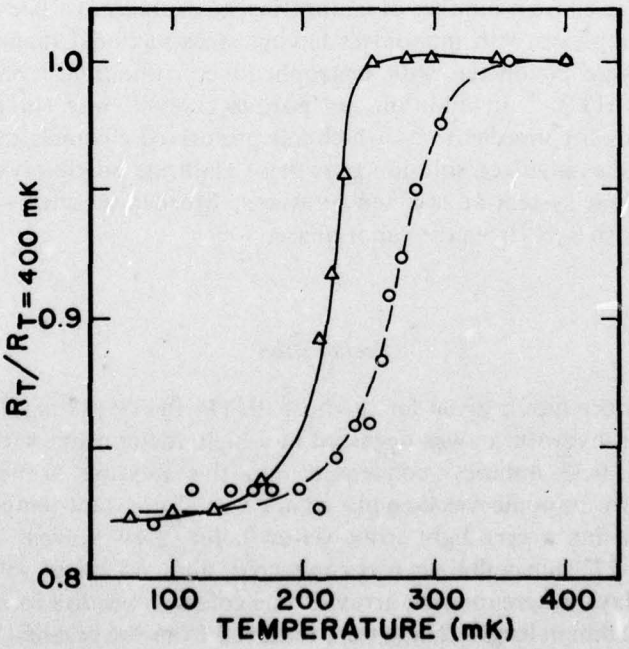


FIGURE 9. Superconducting, resistive transition of red $(SN)_x$ (——). Measurements were made at a current level of 1×10^{-6} A. For comparison purposes, data are shown on a poor quality normal $(SN)_x$ crystal (- - - -) having a large residual resistance and relatively low superconducting transition.

Conclusions

There are subtle differences between $(SN)_x$ crystals formed from red $SN\cdot$ and S_2N_2, probably relating to the degree of order resulting during the polymerization. Brown $(SN)_x$ appears to have a different crystal structure. Isolation of better crystals of both materials is necessary to establish the variations in properties associated with degree of order and crystal structure.

Incorporation of $(SN)_x$ into Channels of Molecular Dimension

Introduction

The use of inclusion compounds that form canals of molecular dimension as hosts for polymerization reactions was first reported by Brown and White,[15,16] their idea being that the long regular canals should serve as templates for stereospecific polymerization reactions. For example, thiourea forms a canal complex with 1,3-cyclohexadiene, and the resulting polymer formed on irradiating the complex with ionizing radiation showed considerable stereoregularity.

Polymerization of S_2N_2 in such canals could answer two important questions: (1) What are the properties of isolated $(SN)_x$ strands? and (2) what are the possibilities that conducting strands in a properly chosen dielectric matrix would fulfill the structural requirements of the Little model for high-temperature superconductivity?[17]

We therefore chose a number of clathrating hosts that have been reported to form canal complexes with monomers having cross-sectional diameters ≥ 6 Å. Experiments were conducted with benzophenone,[18] thiourea,[15] and perhydrotriphenylene (PHTP).[19] In addition, a "porous crystal" was studied—a single crystal of the zeolite mordenite[20]—which has preformed channels of ~ 6 Å. The clathration studies involved solution growth of clathrate single crystals from an S_2N_2-host-solvent system at low temperatures. Mordenite single crystals were allowed to adsorb S_2N_2 from the vapor phase.

Preparation

A typical procedure is given for the host PHTP. PHTP (88 mg, 0.36 mmoles) in 12 ml of tetrahydrofuran was degassed in a high vacuum line (10^{-6} torr) and S_2N_2 (31 mg, 0.33 mmoles) condensed into this mixture at liquid-nitrogen temperature. The ampoule was then placed in a $-15°C$ constant-temperature bath, the solution having a very light straw-yellow color. Slow solvent transpiration *in vacuo* to a $-27°$ side container was conducted, and ~ 5 ml of solvent was removed in six days, whereupon an array of fine colorless needles formed, some of which were ~ 2 mm in length. These were removed from the residual solution in a nitrogen-purged glove box. Some of these crystals appeared to have dark filaments running along the needle axis. Additional crystals were harvested by further solvent removal *in vacuo* from the apparatus. These crystals were stored for various

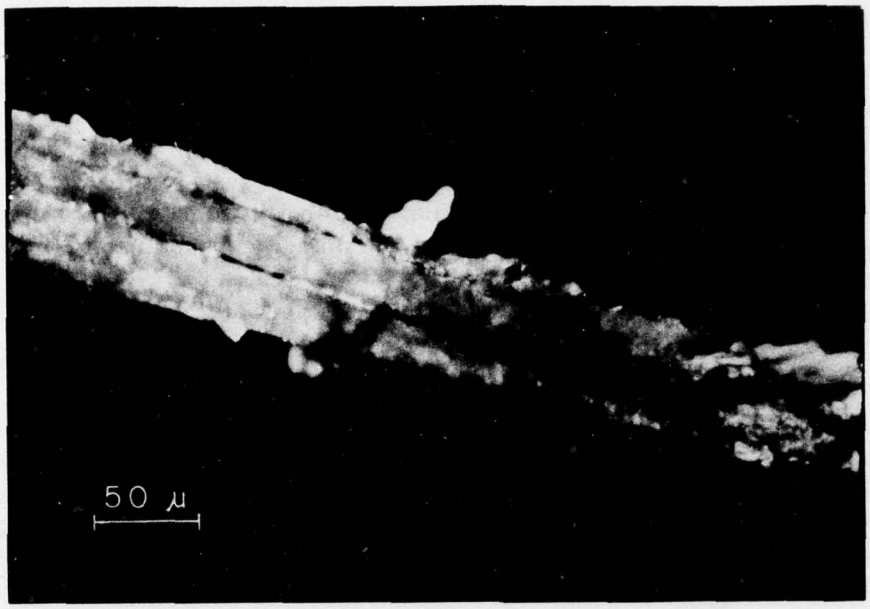


FIGURE 10. Photomicrograph taken between crossed polarizers of a perhydrotriphenylene-$(SN)_x$ crystal.

periods of time up to eleven months *in vacuo* at room temperature. The black filamentary lines observable in many of these crystals are shown in FIGURE 10.

In the case of benzophenone, growth of $(SN)_x$ single crystals of macroscopic dimensions in a polycrystalline benzophenone matrix was observed (FIGURE 11). For thiourea, needle-like crystals of clathrate formed, but this was accompanied

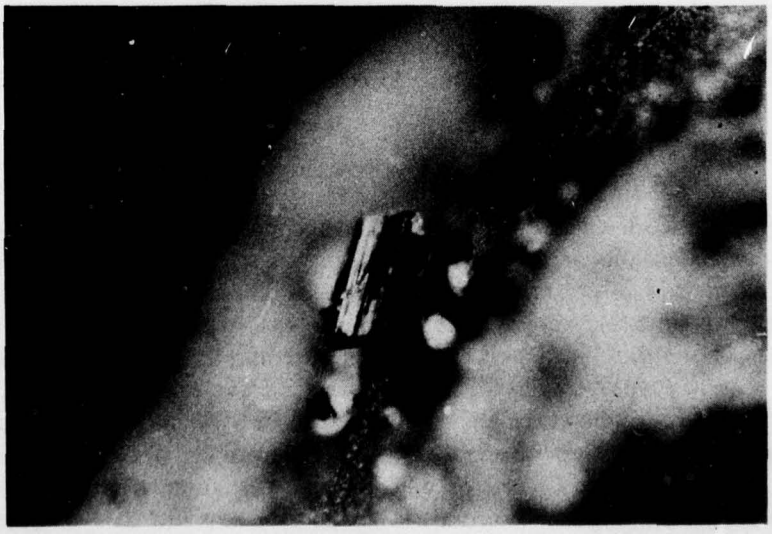


FIGURE 11. Photomicrograph of an $(SN)_x$ crystal growing in a benzophenone matrix.

by color formation in solution; a deep cherry-red color formed rapidly at $-15°$. A few needle-like crystals were removed, but no observation of filaments, as in the PHTP preparations, could be made. This system seems complicated by side reactions between S_2N_2 and thiourea.

Mordenite single crystals were placed in a vacuum of 10^{-6} torr, dehydrated at 500°, and exposed to S_2N_2 vapor. Immediately, the transparent needle-shaped crystals developed a light-yellow coloration. After one or two days, dark filaments appeared to form along the needle axis. After storage for one to three months, these filaments lightened or disappeared.

Properties

Microprobe analyses were conducted (E. F. Fullam, Inc.) on the PHTP-$(SN)_x$ crystals to confirm that the dark filamentary lines observed optically were indeed $(SN)_x$. By presetting the x-ray detector to the sulfur Kα peak and conducting a line-scan through the filament, a strong signal for sulfur was obtained as the beam passed through the filamentary zone. Mordenite crystals also contained sulfur, but the concentrations are too low to determine the sulfur distribution in the crystals.

The filamentary zones in the PHTP crystals are of the order of one to two μ in diameter in crystals of ~ 60 μ diameter. These zones can either be macroscopic inclusions as the crystals grow, or true clathrates. The number of such zones, the quality of the crystals, and the continuity of these filamentary zones all present problems in evaluating their properties. All attempts, to date, to measure any significant conductivities along the filaments have failed.

Conclusions

$(SN)_x$ can be incorporated into channel-like hosts; the polymeric strands are highly interrupted and spatial distribution is irregular. It is, therefore, not clear whether $(SN)_x$ is incorporated into macroscopic inclusions or is truely clathrated.

$(SN)_x$ Crystals Grown from Solution

During the work on clathration of S_2N_2, techniques were developed for preparing stable solutions of S_2N_2 in solvents such as tetrahydrofuran. Accompanying the formation of crystals of host-containing clathrated or included $(SN)_x$, single crystals of $(SN)_x$ were also obtained. Growth of S_2N_2 crystals in pure solvent systems (without "host") have also been attempted. Both programmed cooling and solvent evaporation can lead to well-formed single crystals of S_2N_2.

We have recently observed that these crystals of S_2N_2 in tetrahydrofuran are stable *in the dark* at temperatures below $-25°$. However, upon irradiation with a weak tungsten source (a microscope illuminator), these transparent crystals attain a dark color within 30 seconds at temperatures as low as $-60°$; i.e., *polymerization is photo-induced.* The polymerization rates at these low temperatures

after this irradiation are, of course, very slow. At −35°, a golden luster starts to form on these crystals after several weeks, but complete polymerization at these temperatures will undoubtedly require several months of storage. Variations in either degree of order or crystal structure as compared to normal $(SN)_x$ will be evaluated in these crystals in the near future.

Acknowledgments

We are indebted to Professor M. Farina for furnishing us with a sample of PHTP, and to Professor J. V. Smith for samples of mordenite fibers.

References

1. Patton, R. L. 1969. Ph.D. Thesis. Univ. California. Berkeley, Calif.
2. Mikulski, C. M., P. J. Russo, M. S. Saran, A. G. MacDiarmid, A. F. Garito & A. J. Heeger. 1975. J. Amer. Chem. Soc. **97:** 6358.
3. Kahlert, H., & B. Kundu. 1976. Mater. Res. Bull. **11:** 967.
4. Usher, F. L. 1925. J. Chem. Soc. **127:** 730.
5. Burt, F. P. 1910. J. Chem. Soc. **97:** 1121.
6. Smith, R. D., J. R. Wyatt, J. J. DeCorpo, F. E. Saalfeld, M. J. Moran & A. G. MacDiarmid. 1977. J. Amer. Chem. Soc. **99:** 1726.
7. Allen, W., P. Love, J. J. DeCorpo & M. M. Labes. Unpublished results.
8. Cohen, M. J., A. F. Garito, A. J. Heeger, A. G. MacDiarmid, C. M. Mikulski, M. S. Saran & J. Kleppinger. 1976. J. Amer. Chem. Soc. **98:** 3844.
9. Baughman, R. H., P. A. Apgar, R. R. Chance, A. G. MacDiarmid & A. F. Garito. 1977. J. Chem. Phys. **66:** 401.
10. Love, P., F. Rogers & M. M. Labes. To be published.
11. Walatka, V. V., Jr., M. M. Labes & J. H. Perlstein. 1973. Phys. Rev. Lett. **31:** 1139.
12. Hsu, C. & M. M. Labes. 1974. J. Chem. Phys. **61:** 4640.
13. Civiak, R. L., C. Elbaum, W. Junker, C. Gough, H. I. Kao, L. F. Nichols & M. M. Labes. 1975. Solid State Commun. **17:** 1573.
14. Civiak, R. L., C. Elbaum, L. F. Nichols, H. I. Kao & M. M. Labes. 1976. Phys. Rev. B **14:** 5413.
15. Brown, J. F., Jr. & D. M. White. 1960. J. Amer. Chem. Soc. **82:** 5671.
16. White, D. M. 1960. J. Amer. Chem. Soc. **82:** 5678.
17. Little, W. A. 1964. Phys. Rev. **135:** A1416.
18. Seigle, J. 1939. Chimie et Industrie **42:** 99.
19. See, for example, Farina, M., G. Audiso & M. T. Gramegna. 1972. Macromolecules **5:** 617.
20. For a review of the properties of "porous crystals" see Barrer, R. M. 1973. Adv. Chem. **121:** 1.

Discussion

Alan G. MacDiarmid: Have you observed either red species or brown species acting as a catalyst for the polymerization of S_2N_2? We found, for example, that if we do not purify the S_2N_2 very well from these other species, one can get a very rapid polymerization to $(SN)_x$, whereas if one takes a crystal that has been poly-

merizing for a couple of days and pumps out the S_2N_2, one can get S_2N_2 which can remain colorless at room temperature for several hours. So it would appear that some of these other species are probably catalysts for the polymerization of S_2N_2 itself, and we have even wondered if S_2N_2 if absolutely pure would indeed polymerize spontaneously.

LABES: The colored species can act as catalysts for the polymerization of S_2N_2. This is indicated in FIGURE 3 by the more rapid appearance of the EPR signals for the red and brown monomer mixtures with S_2N_2 as compared to pure S_2N_2. High-purity crystals of S_2N_2 are considerably more stable at room temperature than those which contain impurities.

RICHARD FOREMAN (National Bureau of Standards): We have been able to prepare the same brown and red phases from S_4N_4 under high pressure, i.e., 60–110 Kbar. We have some Raman data that does differentiate the various red and brown phases under pressure. It is not a clean experiment, because we have pentane/*iso*-pentane in the cells to provide a pressure medium. If you run the cell ungasketted with no pressure-transmitting fluid, S_4N_4 will detonate.

BRYAN STREET: If, during the preparation of S_2N_2, the pressure is allowed to rise (e.g., by increasing the rate of vaporization of the S_4N_4), the resulting S_2N_2 crystals become contaminated and can vary in color between red and brownish red. These well-faceted crystals never completely polymerize, and unlike pure S_2N_2, they partially melt if allowed to warm to 21°C. Mass spectrometry shows they contain S_4N_2. If the remaining S_2N_2 is allowed to polymerize, copper-colored rather than golden crystals of $(SN)_x$ are obtained, and these crystals have inferior electrical properties.

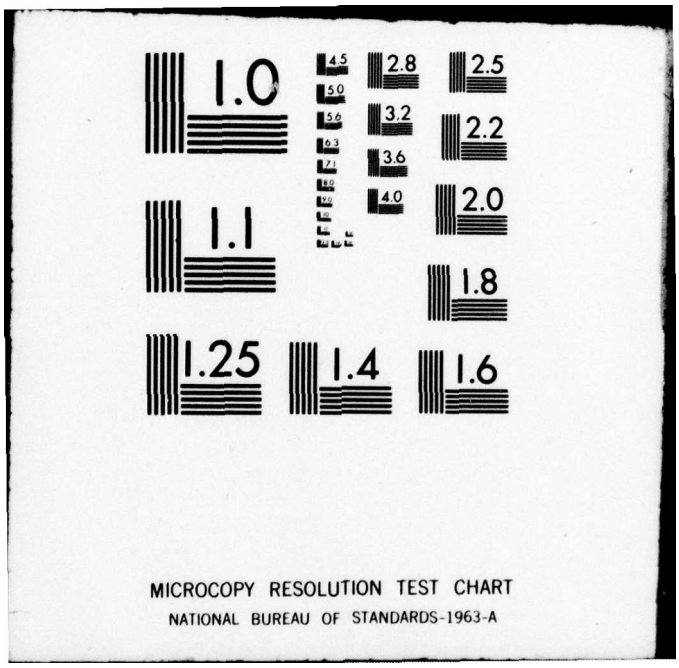
LABES: You are correct in stating that S_4N_2 can be formed in the preparation of S_2N_2 at high rates of S_4N_4 sublimation. However, the red monomer discussed above is not S_4N_2, the properties of which are well known. It differs from S_4N_2 in terms of magnetic properties, physical properties at room temperature, and vapor pressure. The red SN· monomer is paramagnetic, whereas S_4N_2 is reported to be diamagnetic. The red monomer is a crystalline solid that polymerizes rapidly at room temperature. Tetrasulfur dinitride is an unstable liquid that evolves gas at room temperature. The SN· monomer is more volatile than S_2N_2; S_4N_2 is much less volatile. Indeed, S_4N_2 has a vapor pressure greater than but comparable to that of S_4N_4.

AD-A065 304 NEW YORK ACADEMY OF SCIENCES N Y F/G 7/2
SYNTHESIS AND PROPERTIES OF LOW-DIMENSIONAL MATERIALS,(U)
1978 J S MILLER, A J EPSTEIN N00014-77-C-0374
UNCLASSIFIED NL

9 OF 9
AD A065304



END
DATE FILMED
4 -79
DDC


1.0
1.1
1.25
1.4
1.6
1.8
2.0
2.2
2.5
2.8
3.2
3.6
4.0
4.5
5.0
5.6
6.3
7.1
8.0
9.0
MICROCOPY RESOLUTION TEST CHART
NATIONAL BUREAU OF STANDARDS-1963-A

MASS SPECTRAL STUDIES OF $(SN)_x$ VAPORS

F. E. Saalfeld, J. J. DeCorpo, J. R. Wyatt,
P. T. Mah, and W. N. Allen*

Chemistry Division
Naval Research Laboratory
Washington, D. C. 20375

INTRODUCTION

Recent investigations[1-3] of polymeric sulfur nitride, $(SN)_x$, have created considerable interest in the scientific community. Although most emphasis has been on the conducting properties of $(SN)_x$ and the mechanism of its conduction, several physical and chemical studies have also been made. Smith *et al.*[4,5] showed from mass spectrometric data that the $(SN)_x$ vapor species formed by sublimation of the crystal is a single species, $(SN)_4$, having a "linear" structure. These studies also revealed a hydride impurity of 1–5 atom percent. No other bulk impurity was detected.

This paper reports a more detailed investigation of the hydride impurity. We show that the hydride impurity consists of a single species with a molecular weight of 215 ± 5 amu. The magnitude of the hydride impurity concentration in $(SN)_x$ is rather surprising and has been confirmed by other workers.[6] The hydride impurity or its precursor may play a role in the solid-state polymerization of S_2N_2 to $(SN)_x$. We have examined $(SN)_x$ samples prepared in this laboratory and two other laboratories,[7] and find the hydride results reported here independent of preparation.

In addition, we also report preliminary data on the vapor species observed when $(SNBr_{.35})_x$ is sublimed.[8-11] The mass spectral study of the vapors of this brominated compound provides evidence for the existence of SNBr.

EXPERIMENTAL

The apparatus used to study $(SN)_x$ samples was described previously.[5] For completeness, however, we will briefly review it here. All electron impact spectra were recorded by an Extranuclear quadrupole mass spectrometer equipped with a molecular beam, high-efficiency ionizer. The $(SN)_x$ was placed in a heated Knudsen cell from which the vapors effused, forming a molecular beam. This molecular beam was mechanically chopped. This eliminates the mass spectra of background gases and allows detection of only mass peaks due to the species in the molecular beam. All electron-impact spectra were obtained with use of identical instrument settings. The electron energy was normally set at 14 electron volts. Spectra were also obtained from an open Teflon® cell and were identical within experimental error with the spectra obtained from the Knudsen cell.

Appearance potential (A.P.) measurements were made to help identify the

*NRL-NRC Research Associate 1976–1977. Manuscript received June 14, 1977.

0077-8923/78/0313-0759 $1.75/1© 1978, NYAS

volatile species in the electron beam. The A.P.s were obtained from ionization efficiency curves (plots of ion current vs. ionizing electron voltage), which were measured by time-averaging the ion currents. Only relative appearance potentials were desired. Therefore, linear extrapolations of the straight-line portion of the ionization efficiency curves were used to determine the appearance potential. We estimate the accuracy of our reported appearance potentials as ± 0.6 of a volt, and the precision of the measurement was ± 0.3.

Phase-angle mass spectrometry[12] was used to identify the mass of the major neutral molecular precursors of the species in the ion beam. The time-of-flight of the neutral molecules from the chopper, which is located just behind the molecular beam skimmer to the ion source, is a function of the mass of the neutral species and is manifested in different flight times that correspond to different phases angles. All ions from the same neutral molecular species will be characterized by identical phase angles. Compounds with well-characterized mass spectra such as benzophenone, benzil, and salicyclic acid were used as standards to calibrate the phase angle vs. mass. This calibration curve was then used to determine the mass of the neutral species volatilized from $(SN)_x$ and $(SNBr_{.35})_x$.

A modified Varian CH7 mass spectrometer was used to measure the field ionization (FI) and field desorption (FD) mass spectra of the $(SN)_x$ vapors. The FI spectrum reported represents an average of 20 spectra and are typical of the results obtained over a temperature range 100–160°C. The FD spectrum reported is also the average of 20 spectra over a temperature range of 30–200°. The FD spectrum was temperature independent in this temperature range. As reported[5] previously, the FD field emitter was prepared by subliming various samples of $(SN)_x$ under vacuum at 180–200°C on the field emitter surface.

Of critical importance in the hydride studies was the measurement of the ion isotope abundances at each of the $(SN)_x$ ion clusters. The techniques for measuring isotope ratios are well known. Beynon[13] presents an excellent description of these measurement techniques and their potential errors.

Results and Discussion

$(SN)_x$ Vapors

The mass spectral properties of $(SN)_x$ vapors have been reported previously.[4,5] Therefore, these results will be only briefly summarized. The mass spectra, electron impact, field desorption, and field ionization of $(SN)_x$ vapors and S_4N_4 vapors are given in Figure 1, and the A.P.s are shown in Table 1. From Figure 1 and Table 1 we can make the following observations: (1) the electron impact spectra of $(SN)_x$ vapors and S_4N_4 are different; (2) the A.P. of the major ions from $(SN)_x$ vapors and S_4N_4 are different; (3) the field desorption spectra of $(SN)_x$ vapors and S_4N_4 are identical; and (4) the field ionization spectra of $(SN)_x$ vapors and S_4N_4 are considerably different. The field ionization mass spectrum of $(SN)_x$ vapors shows the major ion as $(SN)_3^+$, whereas the S_4N_4 field ionization spectrum shows only a molecular weight ion at mass 184.

The electron impact data, by phase angle detection, show, with one exception (see below), that the $(SN)_x$ vapor consists of only one species (all ions in the $(SN)_x$

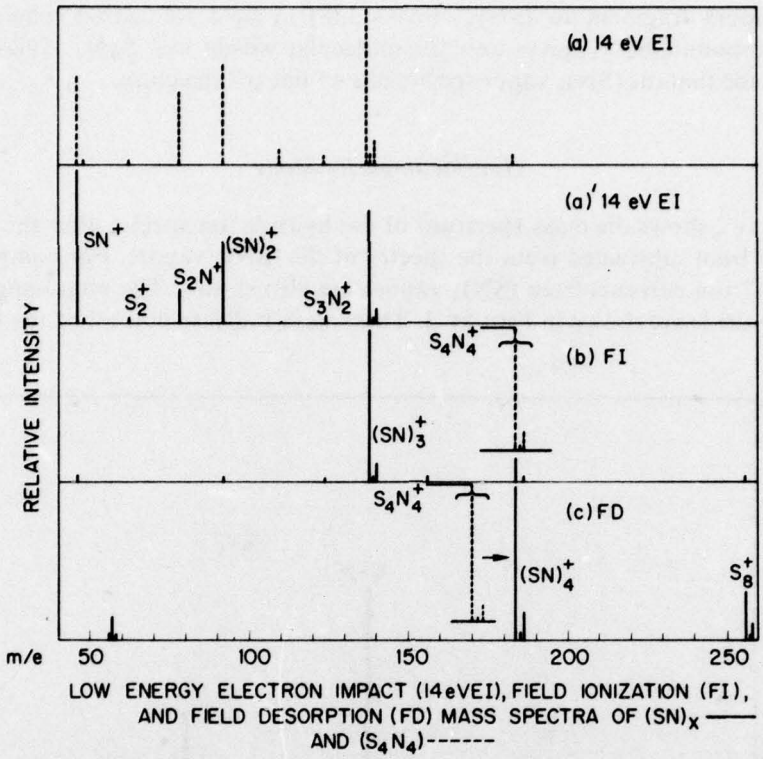


FIGURE 1. The electron impact, field ionization, and field desorption mass spectra of $(SN)_x$ and S_4N_4.

vapor spectrum have the same phase angle) with a molecular weight of 190 ± 10. The only reasonable chemical composition for this is $(SN)_4$ (mol wt 184). The fact that the FD spectra of $(SN)_x$ vapors and S_4N_4 are identical under this very gentle type of ionization confirms 184 as the molecular weight and also the chemical composition. According to Beckey and Schulten,[14] linear molecules fragment under field ionization, whereas cyclic compounds do not. Therefore, since the

TABLE 1

COMPARISON OF APPEARANCE POTENTIALS FOR VARIOUS IONS FROM S_2N_2, S_4N_4, AND $(SN)_x$ VAPORS

Ion (m/e)	S_2N_2	S_4N_4	$(SN)_x$
SN^+ (46)	13.0	14.1	13.4
S_2^+ (64)			12.9
S_2N^+ (78)	12.2		10.1
$S_2N_2^+$ (92)	11.5	13.7	11.2
$S_3N_2^+$ (124)			10.5
$S_3N_3^+$ (138)		12.3	9.5
$S_4N_4^+$ (184)		10.4	9.8

$(SN)_x$ vapors fragment to $(SN)_3^+$ (mass 138) in field ionization whereas the cyclic compound, S_4N_4, gives only the molecular weight ion, $S_4N_4^+$ (mass 184), we conclude that the $(SN)_x$ vapor species has a "linear" structure.

Hydride Impurity Study

FIGURE 2 shows the mass spectrum of the hydride ion species after the $(SN)_x^+$ ions have been subtracted from the spectra of the $(SN)_x$ vapors. For comparison, the $(SN)_3^+$ ion currents from $(SN)_x$ vapors are also shown. The phase-angle data for the hydride are shown in FIGURE 3. These data indicate that all of the hydride

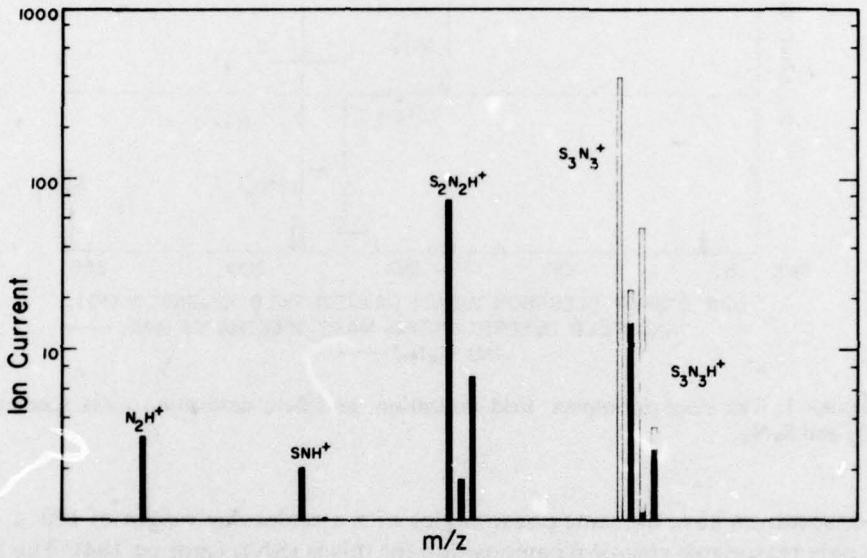


FIGURE 2. The mass spectrum of the hydride impurity observed in the $(SN)_x$ vapors. The hydride spectrum is given in the solid bars. For comparison, the $S_3N_3^+$ ions from the $(SN)_x$ vapor species are shown with open bars.

ions originate from a single neutral species having a molecular weight 215 ± 5 amu). A reasonable chemical composition for this molecular weight is HS_5N_4. The clastogram for the hydride is shown in FIGURE 4. A clastogram is the measurement of the ion intensities as a function of the ionization energy. The hydride clastogram shows the common relationships between the various hydride-containing ions and supports the conclusion of the phase-angle measurements: that the hydride is a single neutral species.

The hydride impurity is not observed in the FI or FD spectra. This observation suggests that the hydride impurity, HS_5N_4, may have a linear structure.

Solid-state, nmr studies were performed in our laboratory by Dr. Henry Resing. These nmr results are very preliminary; however, they do show a hydrogen-containing species in the solid $(SN)_x$ samples. Interpretation of the nmr spectra is not clear as to whether the hydrogen species is concentrated on the

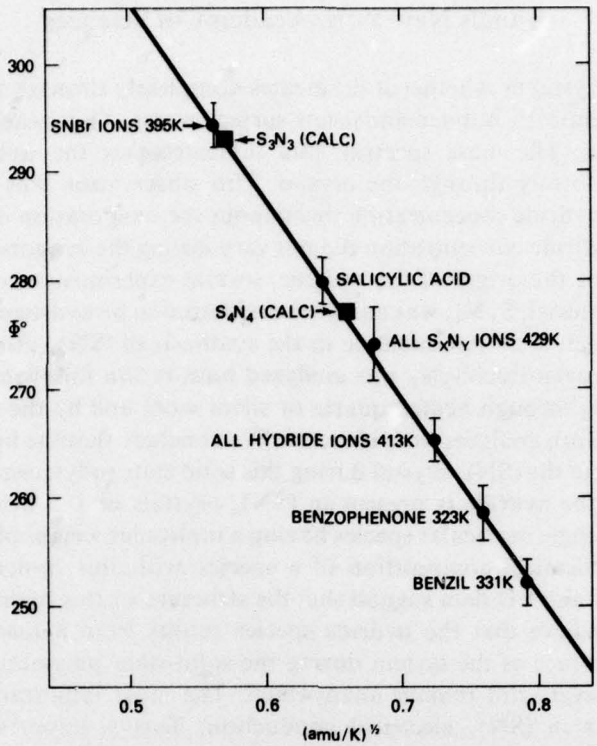


FIGURE 3. Phase-angle data for $(SN)_x$ vapor ions, hydride impurity ions, and $(SNBr_{.35})_x$ vapor ions. Also shown are the phase-angle data for the calibration compounds. Data indicate that only one species is present in $(SN)_x$ vapors, one in the hydride vapors, and one in the $(SNBr_{.35})_x$ vapors.

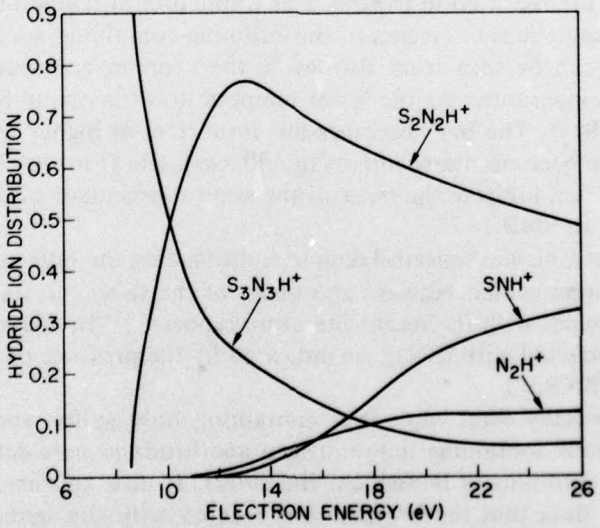


FIGURE 4. Clastogram (measurement of ion current intensity vs. ionizing energy) of hydride ions. Curves show parent-daughter relationship between ions, e.g. $S_3N_3H^+$ produces $S_2N_2H^+$ which fragments to SNH^+. This relationship suggests that all hydride ions have the same neutral precursor.

surface of the crystal or whether it permeates completely through the system. The hydrogen is chemically bonded and is not surface water. This system is now being actively studied. The mass spectral data indicates that the hydride is evenly distributed uniformly through the crystal. This observation was determined by measuring the hydride concentration throughout the evaporation of several $(SN)_x$ crystals. The hydride concentration did not vary during the evaporation.

To determine the origin of the hydride, several experiments were carried out. The starting material, S_4N_4, was analyzed and found to be hydrogen-free. In addition, S_2N_2, which is an intermediate in the synthesis of $(SN)_x$ also was analyzed and found hydrogen-free. S_2N_2 was analyzed both *in situ* following its formation by passing S_4N_4 through heated quartz or silver wool and by the evaporation of S_2N_2 crystals. Both analyses were identical. We conclude that the hydrogen species is introduced into the $(SN)_x$ crystal during this solid state polymerization.

We believe the hydride is present in $(SN)_x$ crystals at 1–5 atom percent and vaporizes as a single molecular species having a molecular weight of 215 ± 5 amu. A reasonable chemical composition of a species with this molecular weight is HS_5N_4. Our FI and FD data suggest that the structure of this hydride is probably "linear." We believe that the hydride species results from a reaction involving water on the surface of the system during the solid-state polymerization. Several questions, however, still remain unanswered. The most important is what role the hydride has in $(SN)_x$ electrical conduction. This is important because all $(SN)_x$ material that we have analyzed contains the hydride species.

$(SNBr_{.35})_x$ Studies

We have also studied the recently reported[8–11] $(SNBr_{.35})_x$ species. Mass spectra of $(SNBr_{.35})_x$ are reported in FIGURE 5 as a function of temperature. The results of the phase-angle measurements of the bromine-containing species are given in FIGURE 3. As can be seen from FIGURE 5, the bromine-containing ionic species change with temperature. At the lower temperatures the major bromine-containing species is Br_2^+. The Br_2^+ becomes less important at higher temperatures and the $SNBr^+$ ion becomes more important. Phase-angle (FIGURE 3) measurements on the $SNBr^+$ ion indicate the mass of the neutral precursor of the $SNBr^+$ to be 129 ± 8 amu, or SNBr.

We interpret the mass spectral data to indicate that the bulk of the bromine in $(SNBr_{.35})_x$ is intercalated between the fibers of the $(SN)_x$ crystal. This interpretation is consistent with the recent literature reports.[10,11] In addition, some of the bromine has reacted with $(SN)_x$, as indicated by the presence of ions at m/e 125 and m/e 127 ($SNBr^+$).

It is noteworthy that, while ions containing only sulfur and bromine were observed, no ions containing only nitrogen and bromine were detected. This suggests that the bromine is bonded to the sulfur. It also appears from our mass spectrometric data that the bromine has reacted with the hydrogen-containing species to produce HBr. Note the peaks present at m/e 80 and m/e 82 which appear at lower temperatures. These results are very interesting and raise the question, "Has one improved the conductivity by removing the hydrogen-containing species?" Our data is not sufficient to answer the question at this time.

Conclusions

In this report we have summarized previous studies on $(SN)_x$ vapors and reported a series of new results on a hydride impurity in $(SN)_x$ and the mass spectrum of the vapor from $(SNBr_{.35})_x$. The hydride impurity vaporizes as a single species with a molecular weight of 215 ± 5 amu. We believe the hydride may have a "linear" structure with chemical composition of HS_5N_4. Mass spectra of $(SNBr_{.35})_x$ vapors show two principal brominated species: Br_2 and SNBr. The Br_2 can be distilled from the crystal at lower temperatures. At higher temperatures the major brominated species is SNBr. Furthermore, no hydride was observed in the $(SNBr_{.35})_x$ material.

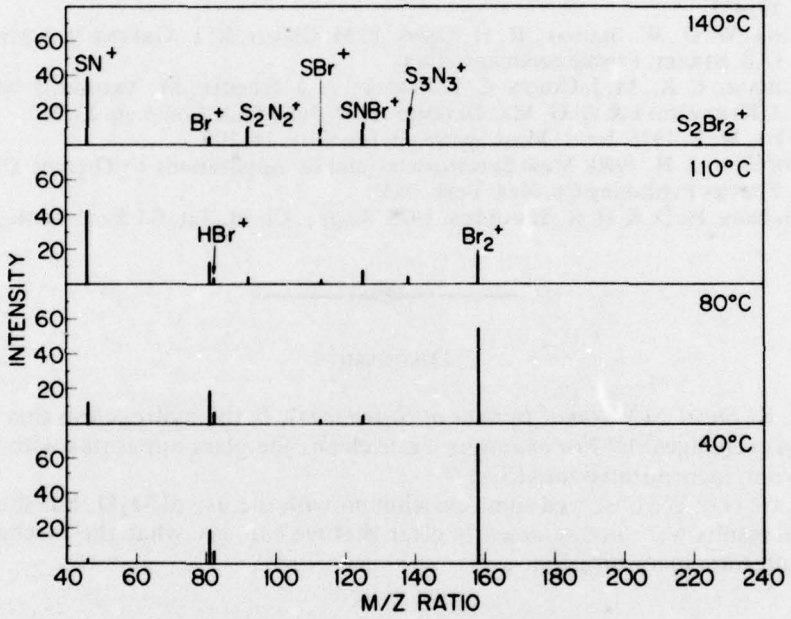


FIGURE 5. The mass spectra of $(SNBr_{.35})_x$ vapors as a function of temperature. The change of the spectra with temperature is evident. Only major monoisotopic peaks are included.

Acknowledgment

We wish to acknowledge the invaluable assistance of Dr. R. D. Smith, who was an NRC-Research Associate at NRL during much of the time this work was performed, Professor A. G. MacDiarmid and coworkers at the University of Pennsylvania, and Dr. James Sphon of the F.D.A. for the FI and FD measurements.

Notes and References

1. Walatka, V. V., Jr, M. M. Labes & J. H. Perlstein. 1973. Phys. Rev. Lett. **31**: 1139.
2. Greene, R. L., P. M. Grand & G. B. Street. 1975. Phys. Rev. Lett **34**: 89.

3. BRIGHT, A. A., M. J. COHEN, A. F. GARITO, A. J. HEEGER, C. M. MIKULSKI, P. J. RUSSO & A. G. MACDIARMID. 1975. Phys. Rev. Lett. **34:** 206.
4. SMITH, R. D., J. R. WYATT, J. J. DECORPO, F. E. SAALFELD, M. J. MORAN & A. G. MACDIARMID. 1976. Chem. Phys. Lett. **41:** 362–364.
5. SMITH, R. D., J. R. WYATT, J. J. DECORPO, F. E. SAALFELD, M. J. MORAN & A. G. MACDIARMID. 1977. J. Am. Chem. Soc. **99:** 1726–1730.
6. FRISCH, M. A. IBM Research Lab. Yorktown Heights, N. Y. Private communication.
7. In addition to $(SN)_x$ crystals prepared at the Naval Research Laboratory, samples were also supplied by Professor A. G. MacDiarmid of the University of Pennsylvania and Dr. G. Brian Street of IBM (San Jose, Calif.) The hydrogen atom concentration for these samples varied between 2 and 5 atom percent.
8. STREET, G. B., W. D. GILL, R. H. GEISS, R. L. GREENE & J. J. MAYERLE. 1977. Chem. Commun. **12:** 393.
9. AKHTAR, M., J. KLEPPINGER, A. G. MACDIARMID, J. MILLIKEN, M. J. MORAN, C. K. CHIANG, M. J. COHEN, A. J. HEEGER & D. L. PEEBLES. 1977. Chem. Commun. **13:** 473.
10. GILL, W. D., W. BLUDAU, R. H. GEISS, P. M. GRANT, R. L. GREENE, J. J. MEYERLE & G.B. STREET. Private communication.
11. CHIANG, C. K., M. J. COHEN, C. L. PEEBLES, A. J. HEEGER, M. AKHTAR, J. MILLIKEN, J. KLEPPINGER & A. G. MACDIARMID. 1977. Solid State Commun. **23:** 607.
12. FITE, W. L. 1975. Int. J. Mass Spectrom. Ion Phys. **16:** 109.
13. BEYNON, J. H. 1960. Mass Spectrometry and its Applications to Organic Chemistry. Elsevier Publishing Co. New York, N.Y.
14. BECKEY, H. D. & H. R. SCHULTEN. 1975. Angew. Chem., Int. Ed. Engl. **14:** 403.

DISCUSSION

A. R. SIEDLE (*National Bureau of Standards*): Is the hydrogen in this hydride species exchangeable? For example, if one cleans the glass apparatus with D_2O, is deuterium incorporated into $(SN)_x$?

SAALFELD: We observed some enrichment with the use of D_2O, but the experimental results were not sufficiently clear that we can say what the mechanism is for deuterium incorporation.

CHARACTERIZATION OF POLYMERIC SULFUR NITRIDE $(SN)_x$ AS AN ELECTRODE MATERIAL*

Robert Nowak, Włodzimiers Kutner,† and Harry B. Mark, Jr.

Department of Chemistry
University of Cincinnati
Cincinnati, Ohio 45221

Alan G. MacDiarmid

Department of Chemistry
University of Pennsylvania
Philadelphia, Pennsylvania 19104

Polymeric sulfur nitride, $(SN)_x$, is currently being studied as an electrode material in aqueous media[1,2] with the ultimate goal of producing chemically modified electrodes.[3] This material is of particular interest in this area, since an electrochemically active species can, in principle, be covalently bonded to it without the loss of its electrical properties.

Electrodes were prepared by exposing only one face of an $(SN)_x$ crystal to the solution at a time. *Parallel* and *perpendicular* electrodes are those which had either the sides or ends of the $(SN)_x$ fiber bundles exposed to the electrode/solution interface, respectively. Unless otherwise noted, the electrochemical behavior of these electrode surfaces was identical.

Preliminary studies using cyclic voltammetry and cyclic chronoamperometry have shown that $(SN)_x$ can be used as an electrode material in aqueous media under a variety of conditions.[1] Faradaic background currents, prior to cathodic or anodic breakdown (ca. -1.25 and $+0.7$ V vs. SCE in 0.5 M KCl, respectively), were observed which indicated that surface functional groups undergo oxidation and reduction reactions as the potential is scanned negatively and positively, respectively. Current magnitudes increased as the concentration of supporting electrolyte was increased or as the cation was changed in the order: lithium, sodium, potassium, and cesium. Higher charge-density cations such as lithium and calcium also extended the potential at which cathodic breakdown occurred. No hydrogen evolution was observed at cathodic breakdown potentials above pH = 1.

The $Fe(CN)_6^{3-}/Fe(CN)_6^{4-}$ couple was used in cyclic voltammetric and chronoamperometric experiments to compare the behavior of $(SN)_x$ electrodes with other solid electrode materials.[2] A typical cyclic voltammogram of $K_3Fe(CN)_6$ obtained with an $(SN)_x$ electrode is shown in FIGURE 1. It was found that this couple behaves nearly the same at $(SN)_x$ and platinum electrodes under the same experimental conditions.[1]

Electrochemical dependence on crystal orientation (*parallel* and *perpendicular*)

*Supported by the National Science Foundation, grant CHE76-04321. R.N. is the recipient of The Edward Weston Fellowship for 1976 from the Electrochemical Society. Manuscript received Oct. 3, 1977.

†On leave from the Institute of Fundamental Problems Chemistry, Warsaw, Poland.

0077-8923/78/0313-0767 $1.75/1© 1978, NYAS

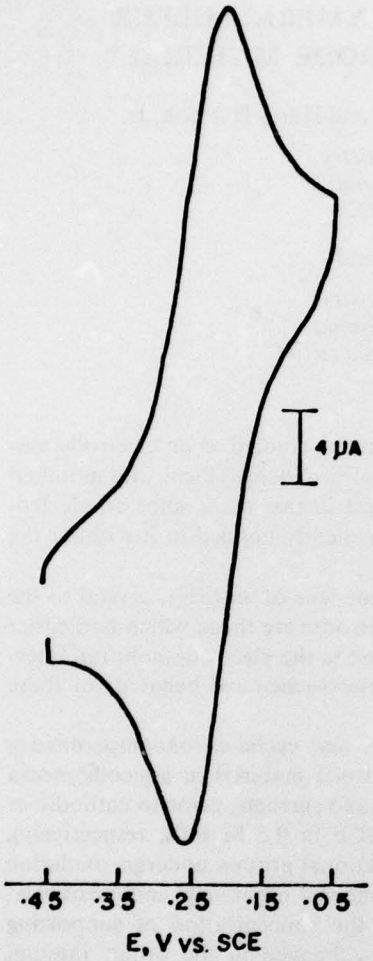


FIGURE 1. Cyclic voltammogram of 0.05 M $K_3Fe(CN)_6$ in 0.05 M KCl at $(SN)_x$ electrode. Scan rate = 0.020 V s^{-1}.

and the first example of chemical modification of an $(SN)_x$ electrode have been reported in lead deposition studies.[4]

In the present study the kinetic probe technique[5] with the soluble redox couples, IO_3^-/I^- and I_2/I^-, was used. These systems, which have been widely studied,[6] have slow electron-transfer kinetics and were found to be convenient for the characterization of the $(SN)_x$/solution interface before and after chemical modification. This modification consisted of brief immersion of $(SN)_x$ electrodes into solutions containing various M^{n+} species followed by thorough rinsing with water.

In the negative potential region the iodate system was used to study the effects of silver(I), palladium(II), or chromium(III) pretreatment on $(SN)_x$ electrodes. After pretreatment of $(SN)_x$ electrodes with these metal cations catalysis, i.e., the positive shift in the value of the iodate reduction peak potential, was observed.

For example, FIGURE 2 illustrates the influence of Pd(II) pretreatment on background currents (dashed) and iodate reduction (solid) using the same $(SN)_x$ electrode. The value of the cathodic peak potential becomes more positive ca. 0.30 V after pretreatment of this electrode with Pd(II) solution. It is also noteworthy that gas bubbles, presumably hydrogen, form on the surface of the Pd(II) pretreated electrode in the cathodic breakdown potential region. Silver and palladium are most probably present in the metallic state on the electrode surface because of the chemical reduction of these ions by $(SN)_x$ surface functional groups. Since the reduction of Cr^{3+} is not observed at $(SN)_x$ electrodes,[1] this species may be present on the electrode surface in some complexed or strongly absorbed state. The catalytic effect on iodate reduction at *parallel* electrodes is most dramatic in this instance. Catalysis with respect to the reduction of iodate was also observed on untreated $(SN)_x$ electrodes which were electrochemically oxidized and on silver ion pretreated $(SN)_x$ electrodes which were electrochemically or chemically (with periodate) oxidized.

Studies of the I_2/I^- system with modified $(SN)_x$ electrodes revealed that palladium(II), silver(I), and mercury(II) pretreatment produce a modified surface that is intermediate in its voltammetric behavior in iodide solutions between the metallic state and unmodified $(SN)_x$. This effect was only permanent with repeti-

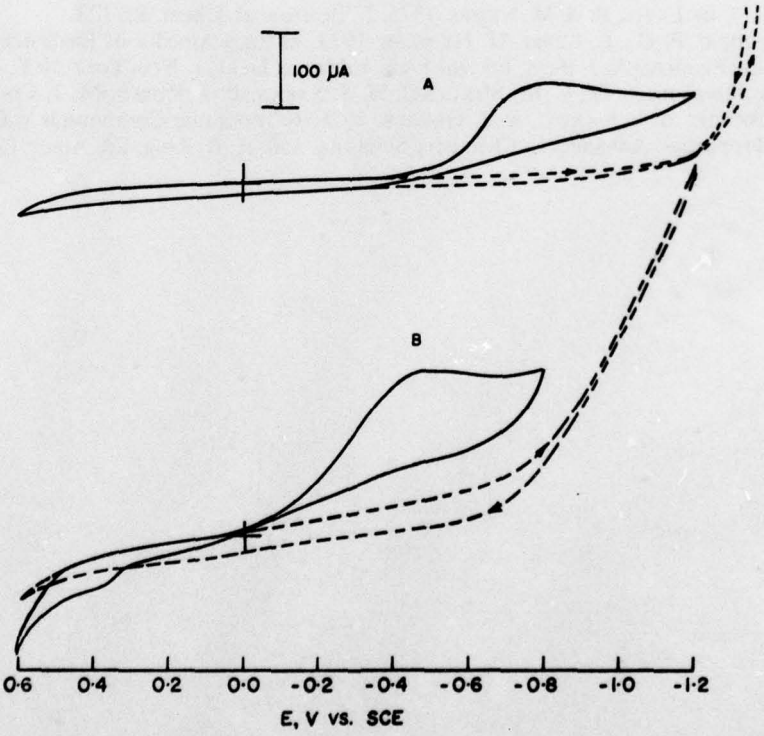


FIGURE 2. Cyclic voltammograms recorded with *perpendicular* $(SN)_x$ electrode in 0.04 M KIO_3 and 0.25 M acetate buffer solution. A: untreated $(SN)_x$ electrode; B. the same electrode as in A, but immersed in 0.02 M $PdCl_2$ solution for approximately one minute. Dash lines = curves recorded in 0.25 M acetate buffer without KIO_3 present. Starting potential = +0.6 V. Scan rate = 0.05 V s^{-1}.

tive cycling for palladium(II) pretreated electrodes. Electrodes pretreated with Cr^{3+}, Eu^{3+}, Fe^{3+}, or Fe^{2+} showed no catalytic behavior with respect to the I_2/I^- couple.

In conclusion, it should be noted that in addition to its other metallic properties,[7] $(SN)_x$ behaves much like a metal with respect to its electrochemistry, and further, it appears that it can be chemically modified quite easily under extremely mild conditions.

A more detailed study of the chemical modification of $(SN)_x$ electrodes will be presented in a future publication.[2]

Notes and References

1. Nowak, R. J., W. Kutner, H. B. Mark, Jr., & A. G. MacDiarmid. 1978. J. Electrochem. Soc. **125:** 232.
2. Nowak, R. J., W. Kutner, H. B. Mark, Jr., & A. G. MacDiarmid. 1977. Submitted to J. Electrochem. Soc.
3. See, for example, Moses, P. R. & R. W. Murray. 1977. J. Electroanal. Chem. **77:** 393, and references therein.
4. Nowak, R. J., H. B. Mark, Jr., A. G. MacDiarmid & D. Weber. 1977. J. Chem. Soc. Chem. Comm. **9.**
5. Gierst, L., E. Nicolas & L. Tytgat-Vandenberghen. 1970. Croat. Chem. Acta **42:** 117; de Levie, R. & M. Nemes. 1975. J. Electroanal. Chem. **58:** 123.
6. Desideri, P. G., L. Lepri, D. Heimler. 1973. *In* Encyclopedia of Electrochemistry of the Elements A. J. Bard, Ed. vol 1: ch. 3. Marcel Dekker. New York, N.Y.
7. MacDiarmid, A. G., C. M. Mikulski, M. S. Saran, P. J. Russo, M. J. Cohen, A. A. Bright, A. F. Garito, A. J. Heeger. 1976. *In* Inorganic Compounds with Unusual Properties. Advances in Chemistry Series no. 150. R. B. King, Ed. Amer. Chem. Soc.

LIGHT SCATTERING IN BROMINATED $(SN)_x$*

H. Temkin and D. B. Fitchen

Physics Department
Cornell University
Ithaca, New York 14853

G. B. Street and W. D. Gill

IBM Research Laboratory
San Jose, California 95193

The first successful modification of the metallic polymer $(SN)_x$ has been recently reported.[1,2] The physical properties of crystalline samples were significantly altered by the addition of bromine, up to $(SNBr_{0.5})_x$. The most pronounced change occurs in the dc conductivity in the direction of $(SN)_x$ chains. It increases by a factor of ten, up to $2 \times 10^4\ \Omega^{-1}\ cm^{-1}$ at room temperature. The superconducting transition temperature remains at 0.3°K. The appearance of the crystal changes from golden to bluish-black, reflecting the 1 eV red shift of the "longitudinal" plasma edge. Electron-microscope diffraction experiments show practically no change in the $(SN)_x$ lattice parameters upon bromination. The new feature observed is a weak superlattice of $(0, \frac{1}{2}k, 0)$ period. Based on these and other data, a model of fibrous $(SN)_x$ structure, with the bromine molecules on the outside of the fibers, has been proposed.[2]

In this note we report preliminary results of a Raman-scattering investigation of single crystals of brominated $(SN)_x$, prepared as $(SNBr_{0.4})$. We find two very strong bands at 154 and 222 cm^{-1}, a number of overtones of the 154 cm^{-1} fundamental, and weaker modes at 450, 660, and 840 cm^{-1}. All the features observed are strongly polarized and can be seen only with both incident and scattered light polarized in the direction of the polymer chains (α_{yy}).

Spectra were recorded with a Spex 1401 double monochromator with photon-counting detection and digital data storage. Various laser wavelengths, from 4579 Å to about 6100 Å were obtained from an argon ion laser and a tunable dye laser.

All the measurements were done at 300°K or 80°K with use of a back-scattering geometry. The incident power level was kept below 10 mW in a spot of about 0.5 mm dia. Higher powers result in bleaching of bromine off the sample, visible as copper-colored spots. The sample was kept in an argon atmosphere while at room temperature.

In FIGURE 1 we show the polarized Raman spectrum of a pure crystal of $(SN)_x$ before exposure to bromine. The principal features can be found at 456, 658, and 786 cm^{-1} and are in good agreement with spectra reported previously for $(SN)_x$.[3] The broad band centered at 890 cm^{-1}, better resolved in this spectrum, appears

*Work at Cornell University supported by the National Science Foundation through the Materials Science Center. Manuscript received June 6, 1977.

0077-8923/78/0313-0771 $1.75/1© 1978, NYAS

to be an overtone of the 456 cm^{-1} mode. No Raman bands can be seen in the region between 120 and 250 cm^{-1}.

FIGURE 2 shows the polarized resonant Raman spectrum of a $(SNBr_{0.4})_x$ sample at 80°K taken with 4579 Å laser excitation. The most prominent feature is a line at 154 cm^{-1}. Higher harmonics of this line (up to 5th order) can be seen at 315, 473, 628, 792, and 847 cm^{-1} (± 2 cm^{-1}), implying that this is resonance scattering. The spectrum is very anisotropic. The scattering strength of the α_{yy} polarization of the fundamental is about ten times larger than that of the α_{yy} and α_{xx} components.

When one moves to red laser excitation (out of resonance), only the second

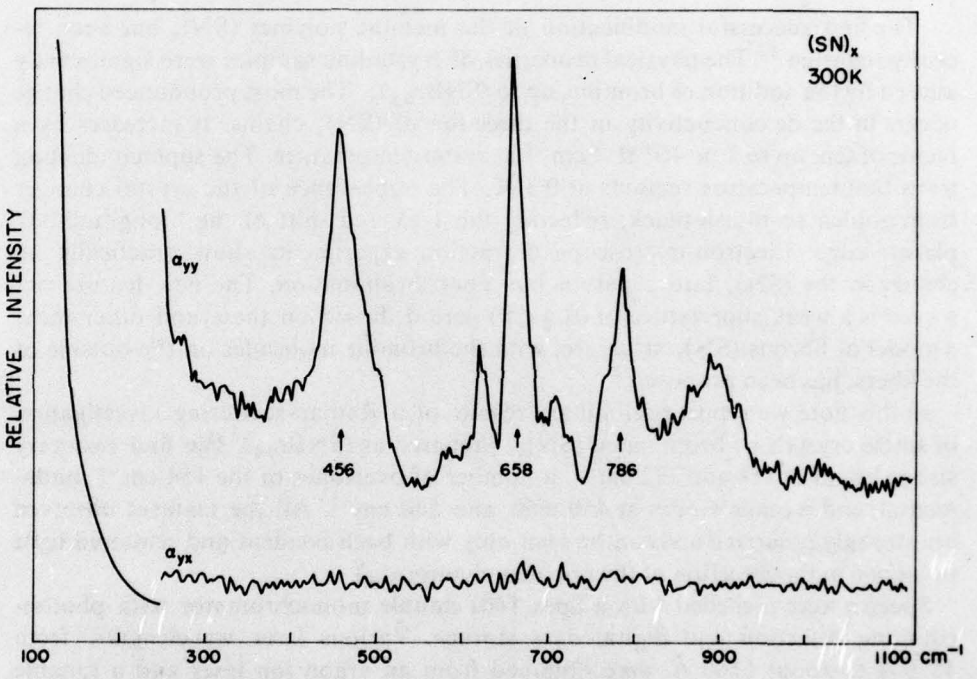


FIGURE 1. Polarized Raman spectra of pure $(SN)_x$ at 300°K taken with 6116 Å laser line.

harmonic of the 154 cm^{-1} line can be seen. Another strong feature (previously obscured) becomes clearly visible. This is the line at 222 cm^{-1}, shown in FIGURE 2. This second line shows the same polarization behavior as the 154 cm^{-1} mode. We do not observe any overtones of the 222 cm^{-1} mode. No other bands of comparable strength were seen down to 30 cm^{-1}.

The two strong bands are rather wide. At 300°K the FWHM is ~20 and ~40 cm^{-1} for the 154 and 222 cm^{-1} lines, respectively. These widths decrease by a factor of two at 80°K.

Weaker and broader features can be seen, as shown in the inset of FIGURE 2, at 450, 660, and 840 cm^{-1}. Their room-temperature widths are unusually large, on the order of 70 cm^{-1}. They are only about half as wide at 80°K. This makes it possible

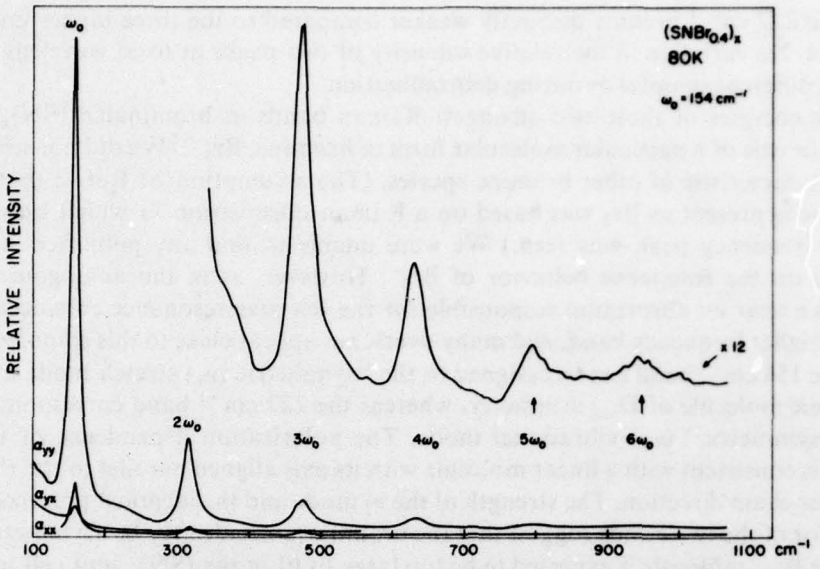


FIGURE 2. Resonant Raman spectra of brominated $(SN)_x$ at 80°K with 4579 Å laser line.

to distinguish these bands from the overtones of the two low-energy modes. These three bands can be seen only with red laser excitation. They are strongly polarized; nothing is visible in the α_{yx} or α_{xx} polarizations.

At incident powers in excess of 10 mW, partial debromination occurs, probably due to local sample heating. All the spectral features remain, but the two bands at

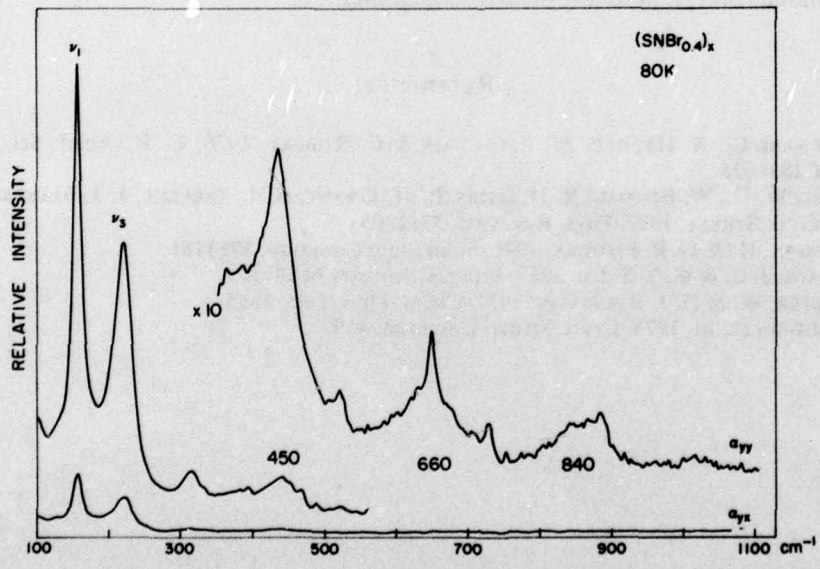


FIGURE 3. Polarized Raman spectra of brominated $(SN)_x$ at 80°K taken with 6116 Å laser line. Full-scale intensity of the expanded part is comparable to that of FIGURE 1.

154 and 222 cm^{-1} become distinctly weaker compared to the three higher energy features. No variation in the relative intensity of two peaks at fixed wavelength is seen in different samples or during debromination.

The energies of these two strongest Raman bands in brominated $(SN)_x$ are characteristic of a particular molecular form of bromine, Br_3^-.[4] We did not see any lines characteristic of other bromine species. (The assumption of Ref. 2 that the bromine is present as Br_2 was based on a Raman observation in which only the higher frequency peak was seen.) We were unable to find any published information on the resonance behavior of Br_3^-. However, as in the analogous I_3^-,[5] there is a near uv absorption responsible for the selective resonance enhancement of the higher frequency band, and many overtones appear close to this resonance.

The 154 cm^{-1} band can be assigned to the "symmetric (ν_1) stretch mode of the triatomic molecule of $D_{\infty h}$ symmetry, whereas the 222 cm^{-1} band corresponds to the "asymmetric" (ν_3) vibrational mode. The polarization dependence of these bands is consistent with a linear molecule with its axis aligned parallel to the $(SN)_x$ polymer chain direction. The strength of the ν_3 mode and the identical polarization behavior of the two bands suggest that the bromine molecule may be asymmetric.

The Br_3^- molecule is expected to be too large to fit in the $(SN)_x$ unit cell in the *b* direction ($b = 4.43$ Å[6]) and could be responsible for the superlattice formation observed in brominated samples.[2]

Of the Raman features observed at 450,660, and 840 cm^{-1}, the first two have energies very similar to bands observed in pure $(SN)_x$. The 840 cm^{-1} band might be the perturbed 786 cm^{-1} $(SN)_x$ mode. The polarization behavior of all three modes is very similar to that observed in pure $(SN)_x$.[3] The larger width of these bands is consistent with the increased disorder of the $(SN)_x$ fibers observed for the brominated samples.

Further experiments are in progress to examine the unusual Raman features of brominated $(SN)_x$ and to test the Br_3^- assignment.

References

1. Bernard C., A. Herold, M. Lelauvain & C. Robert. 1976. C. R. Acad. Sci., Ser. C283: 625
2. Gill, W. D., W. Bludau, R. H. Geiss, P. M. Grant, R. L. Greene, J. J. Mayerle & G. B. Street. 1977. Phys. Rev. Lett. 38: 1305
3. Temkin, H. & D. B. Fitchen. 1976. Solid State Commun. 19: 1181.
4. Evans, J. C. & G. Y-S. Lo. 1967. Inorg. Chemistry 6: 1483.
5. Kiefer, W. & H. J. Bernstein. 1972. Chem. Phys. Lett. 16: 5
6. Boudeulle, M. 1975. Cryst. Struct. Commun. 4: 9.

STRUCTURE OF BROMINATED $(SN)_x$: RAMAN SCATTERING AND X-RAY DIFFRACTION STUDIES*

Z. Iqbal†

Energetic Materials Division
Army Armament Research and Development Command
Dover, New Jersey 07801

R. H. Baughman

Corporate Research Center
Allied Chemical Corporation
Morristown, New Jersey 07960

and

J. Kleppinger and A. G. MacDiarmid

Department of Chemistry and
Laboratory for Research on the Structure of Matter
University of Pennsylvania
Philadelphia, Pennsylvania 19104

INTRODUCTION

Polymeric sulfur nitride, $(SN)_x$, has been intensively investigated in recent years as the first example of a metallic and superconducting linear polymer.[1] The optical and electronic properties of $(SN)_x$ correspond to those of an anisotropic three-dimensional metal.[2] Recently, halogen derivatives of $(SN)_x$ have been prepared[3-7] and characterized by optical, diffraction, and conductivity measurements[4-7] for relatively stable compositions corresponding to $(SNBr_{0.4})_x$[4-7] and $(SNBr_{0.25})_x$.[6] The optical reflectivity spectrum shows a red-shift of the plasma edge in the chain direction of ~ 1.0 eV compared with $(SN)_x$, but by contrast with normal $(SN)_x$, the reflectivity perpendicular to the chains was found by Chiang *et al.*[6] to be nonmetallic, thus suggesting that $(SNBr_{0.4})_x$ crystals are more anisotropic. The room-temperature conductivity of brominated $(SN)_x$ was found to be about an order of magnitude higher than in normal $(SN)_x$.

The density of $(SNBr_{0.4})_x$, 2.65 g/cm^3, is significantly higher than that of $(SN)_x$, 2.31 g/cm^3.[4,5] Electron diffraction data[4] indicate that despite an approximately 50% volume expansion on bromination, the *a*- and *c*-lattice parameters remain unchanged and the crystals decrease in perfection. No measurable change in the *b*-axis dimension was observed, but diffuse scattering corresponding to a chain direction spacing of about 2*b* was reported.[4] In contrast to these results Bernard *et al.*[3] have reported powder x-ray diffraction results in which only the chain axis spacing of $(SN)_x$ is unaffected by bromination.

*Manuscript received July 7, 1977.
†Present address: Konstanz University, D-7750 Konstanz, Germany.

0077-8923/78/0313-0775 $1.75/1© 1978, NYAS

A structural model of $(SNBr_{0.4})_x$ has been proposed by Street *et al.*[4] and Gill *et al.*,[7] in which bromine resides in the interfiber regions as Br_2. In this paper we present detailed single-crystal Raman and x-ray diffraction data on brominated $(SN)_x$ compositions. Using this data, a model is proposed for the structure of brominated $(SN)_x$.

Experimental

Normal monoclinic $(SN)_x$ crystals were prepared by the usual procedures.[8] When $(SN)_x$ is reacted with 60 torr of bromine at 295°K, crystals of composition $(SNBr_{0.55})_x$ are obtained, which give blue-black crystals of composition $(SNBr_{0.4})_x$ on pumping for 30 minutes. When $(SNBr_{0.4})_x$ crystals are pumped on at 295°K for 45 hours or more, the bromine content decreases and compositions of $\sim(SNBr_{0.33})_x$ or lower are obtained. Copper-colored crystals of composition $(SNBr_{0.25})_x$ and $(SNBr_{0.27})_x$ were obtained by annealing crystals of $(SNBr_{0.4})_x$ at ~ 359°K with pumping for 30 and 15 hours, respectively. The as-synthesized samples used in this study are analytically pure. All samples were analyzed for Br, S, and N, and the sum of these figures add to 100 ± 0.3%. Within this experimental uncertainty the molar ratio of S:N is unity.

Mass spectral data show that bromine- but not S- or N-containing species are given off from $(SNBr_{0.4})_x$ at 295°K. The amount of bromine observed mass spectroscopically when a sample of $(SNBr_{0.4})_x$ or $(SNBr_{0.33})_x$ is pumped at 295°K is greater than that observed from copper-colored $(SNBr_{0.27})_x$.

The Raman scattering date were obtained with a triple monochromator system and associated variable temperature and high-pressure sampling equipment described elsewhere.[9] Scans were repeated a number of times from the same spot in the crystal to check for sample damage by laser heating. Stokes to anti-Stokes intensity ratios of the Raman lines, however, did not indicate sample heating to be greater than ~ 10°K at 30 mW power.

Results and Discussion

Raman-Scattering Data and Analysis

Three Raman peaks at 154, 230, and 304 cm^{-1} are observed in different crystals of brominated $(SN)_x$ at 295°K (Figure 1). The peak at 305 cm^{-1} is extremely broad at 295°K, whereas the 230 cm^{-1} line is asymmetric. From Figure 1 it is evident that the line at 230 cm^{-1} is more intense in the freshly brominated sample and drops in intensity relative to the lines at 154 and 305 cm^{-1} with decreasing bromine content. The Raman peaks are exclusively YY-polarized (where Y is the chain direction) in all the brominated crystals examined (Figure 2). The relative intensities and peak frequencies of the Raman lines did not vary with excitation frequencies ranging from 457.9 to 514.5 nm.

With decreasing temperature, the integrated intensities of the 154 and 304 cm^{-1} lines increase appreciably below 200°K (Figures 3 and 4a), and there is a substantial narrowing of the 304 cm^{-1} line. The 304 and 154 cm^{-1} lines increase in

frequency to values of 316 and 159 cm^{-1}, respectively, at 15°K, whereas the 230 cm^{-1} line decreases in peak frequency to 219 cm^{-1} at 15°K. The line-width of the 154 cm^{-1} peak is linear with temperature above ~ 100°K (FIGURE 4b), in essential agreement with anharmonic lattice dynamics,[11] whereas the 304 cm^{-1} line shows substantial nonlinearity in line-width with temperature (FIGURE 4b). Relatively weak peaks at 473, 638, and 788 cm^{-1} are observed in the YY spectrum at

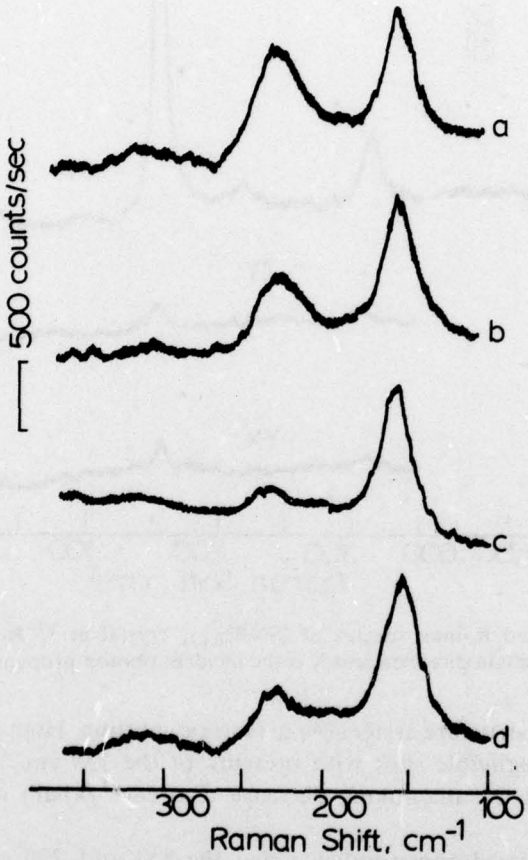


FIGURE 1. Raman spectra between 100 and 400 cm^{-1} at 295°K of: (a) freshly brominated $(SN)_x$ crystal; (b) same crystal as in (a) but after pumping on for 2 hours in a vacuum of 10^{-4} torr at 295°K; (c) blue-black $(SNBr_{0.4})_x$ crystal that had been stored in a 10^{-2}–10^{-3} torr vacuum for 1 to 2 months; and (d) copper-colored $(SNBr_{0.27})_x$ crystal.

15°K. These lines broaden out into the background level above 120°K. A Raman line corresponding to the relatively strong SN band at 658 cm^{-1} in $(SN)_x$[10] was not observed. The infrared spectra between 600 and 1200 cm^{-1} of a $(SN)_x$ film on KBr recorded in a vacuum cell with NaCl windows, after increasing levels of bromination *in situ* showed the near disappearance of the strong $(SN)_x$ infrared line at 995 cm^{-1} and appreciable reduction in intensity of the strong $(SN)_x$ absorption at 670 cm^{-1}. Also, high-resolution scans of the 154 cm^{-1} Raman peak

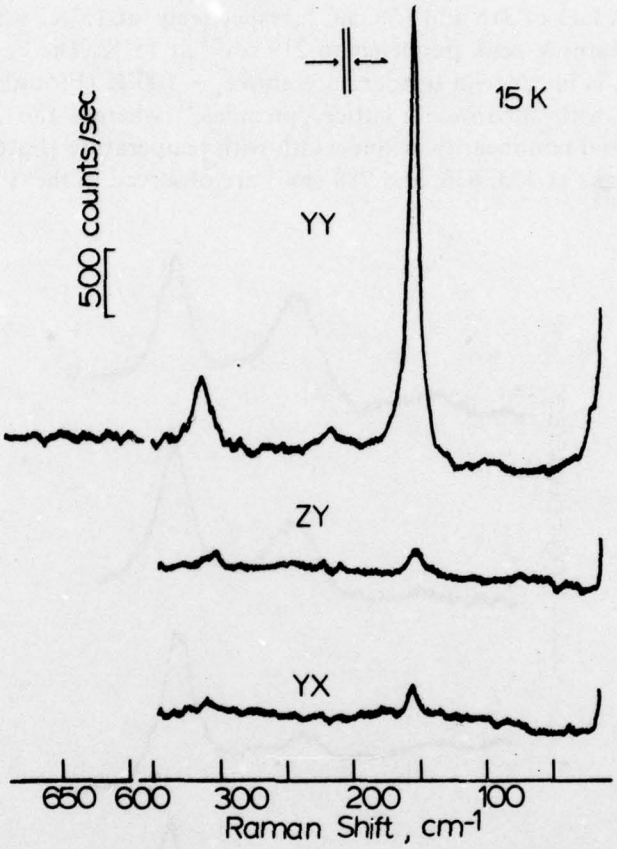


FIGURE 2. Polarized Raman spectra of $(SNBr_{0.4})_x$ crystal at 15°K. Scattering angle is about 110°. Y is the chain direction and X is the incident photon propagation direction.

did not reveal fine structure assignable to isotope splitting. High-pressure measurements indicated negligible shift with pressure of the 154 cm^{-1} line, but the 234 cm^{-1} line showed an anamolous decrease (0.8 cm^{-1}/kbar) in frequency with pressure.

The data discussed above indicate that the 154 and 230 cm^{-1} lines behave differently under varying conditions and hence are assignable to two different sites of bromine in brominated $(SN)_x$. By anology with the spectra of Br_2 in the gaseous,[12] crystalline[13] and intercalated graphite[14] phases, we assign the 230 cm^{-1} line to electronically perturbed Br_2 in $(SN)_x$. This Br_2 might in part be complexed with Br_3^- to form Br_5^-. In accordance with Temkin *et al.*[15] the 154 cm^{-1} line can be assigned to the symmetric stretching mode of Br_3^-. The observation of temperature-dependent lines at 304, 473, 638, and 788 cm^{-1}, assignable as harmonics of the 154 cm^{-1} peak, indicates that the 154 cm^{-1} line is resonance-enhanced.

X-RAY DIFFRACTION MEASUREMENTS

X-ray diffraction measurements on brominated $(SN)_x$, by powder and single-crystal techniques, indicate a series of reflections that have positions in reciprocal

space similar to those of normal $(SN)_x$. Substantially higher structural disorder is evident for the heavily brominated $(SN)_x$ compared with the unbrominated polymer. Correspondingly, only about five independent, relatively sharp reflections have been observed on *h*0*l* Weisenberg photographs. These reflections were indexed by analogy with the corresponding diffraction pattern for unbrominated $(SN)_x$. These reflections are the 100, 002, $10\bar{2}$, $20\bar{2}$, and $20\bar{4}$. Gross twinning is observed whereby the twins are related by a 180° rotation about a^*. This type of twinning is present in the parent $(SN)_x$[16] and arises because of the nonuniqueness of the synthesis of the polymer from the dimer phase.[17,18] Weak powder-diffraction lines corresponding to NH_4Br, probably resulting from surface reaction, were observed for most of the samples. These lines provided internal calibration for correcting for camera radius and film-shrinkage errors.

Important interplanar spacings and derived unit cell parameters are compared in TABLE I together with the corresponding information for unbrominated $(SN)_x$. At low bromine concentration $(SNBr_{0.049})_x$ the observed reflections are consistent

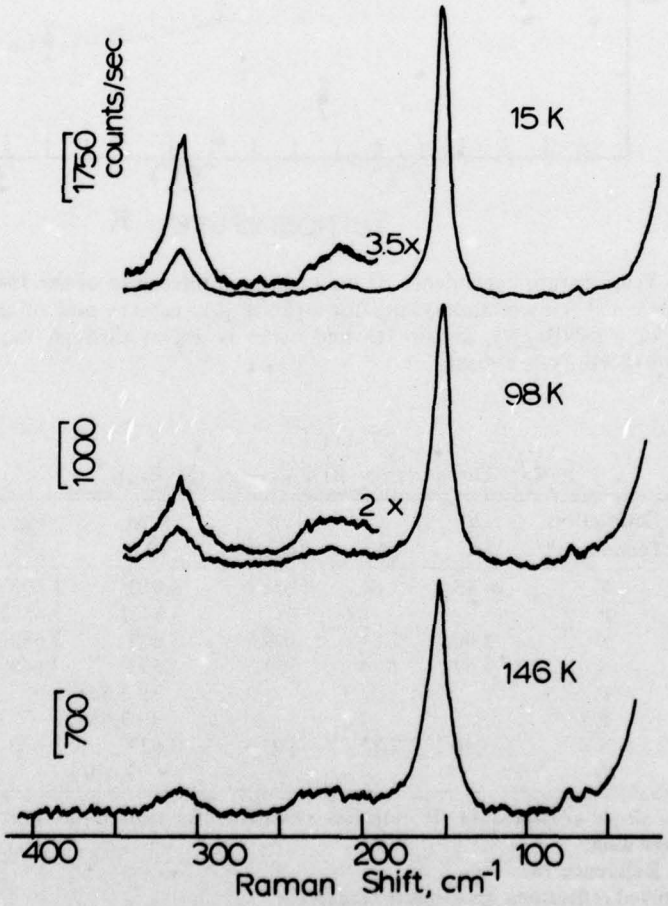


FIGURE 3. Raman spectra of $(SNBr_{0.4})_x$ crystal at various temperatures. Note that the spectra for 146, 98, and 15°K were run at factors of 1.4, 2.0, and 3.5, respectively, lower instrumental sensitivity.

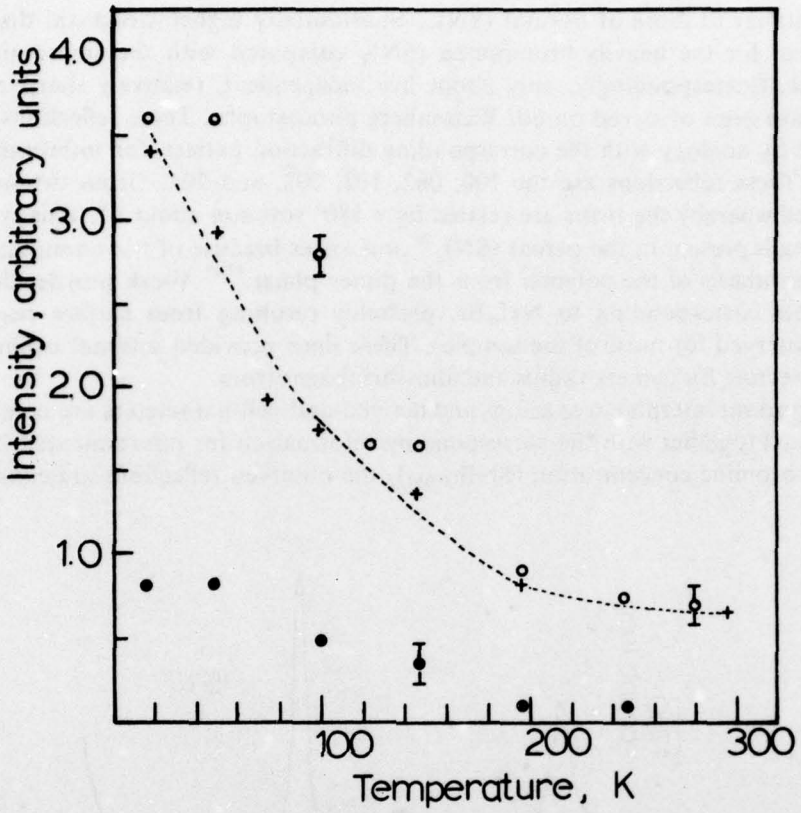


FIGURE 4a. Temperature dependence of the integrated intensities of the 154 cm^{-1} (open circles) and 304 cm^{-1} (closed circles) lines for a $(SNBr_{0.4})_x$ crystal, and of the 154 cm^{-1} line (crosses) for a $(SNBr_{0.27})_x$ crystal. Dotted curve is drawn through the data points obtained for the $(SNBr_{0.27})_x$ crystal.

TABLE I

X-RAY DIFFRACTION RESULTS ON $(SNBr_y)_x$

y	Diffraction Technique*	a [Å]	c [Å]	β degrees	d_{100} [Å]	d_{002} [Å]	$d_{10\bar{2}}$ [Å]
0†	S	4.15	7.64	109.7	3.910	3.595	3.247
0.049	P				3.873‡	3.657‡	3.231
0.25§	S	3.90	7.81	109.5	3.673	3.680	3.186
0.25¶	S	3.92	7.74	109.5	3.692	3.649	3.179
0.27§	P				← 3.633 ‖ →		3.160
0.39	P				← 3.633 ‖ →		3.155
0.40	S	3.86	7.72	110.3	3.622	3.620	3.167
0.40	G				← 3.670 ‖ →		3.153

*S indicates single crystal data, P indicates powder-diffraction data, and G indicates Gandolfi camera data.

†Data from Reference 18.

‡Poorly resolved reflections, spacings inaccurate.

§Obtained by thermally annealing $(SNBr_{0.40})_x$ while pumping at 85°C.

¶Second crystal from same bromination run as for the above data.

‖ These reflections are unresolved.

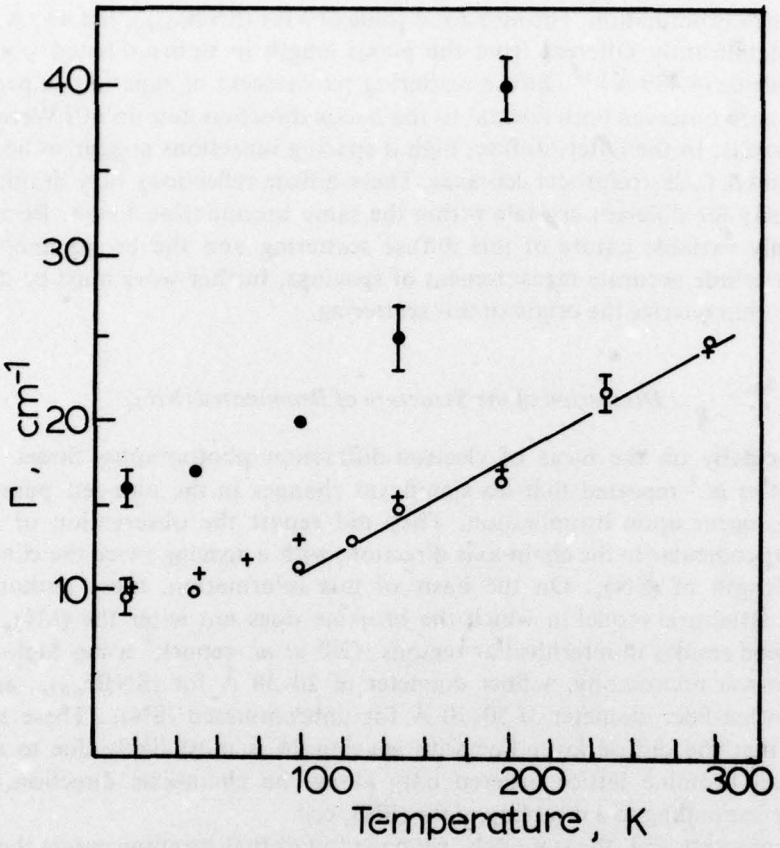


FIGURE 4b. Temperature dependence of the line-width at half maximum (Γ) for the 154 cm^{-1} (open circles) and 304 cm^{-1} (closed circles) lines for a $(SNBr_{0.4})_x$ crystal. The data for the 154 cm^{-1} line of a $(SNBr_{0.27})_x$ crystal are shown by crosses. Full line is a linear fit to the data points for the 154 cm^{-1} line above 100°K.

with a unit cell having essentially identical parameters with those of unbrominated $(SN)_x$. However, for the heavily brominated samples $(SNBr_{0.25})_x$ and above, significant changes in the unit-cell parameters were observed. The most important of these changes are: (1) a decrease in the interplanar spacing for the closest packed plane in unbrominated $(SN)_x$, the $10\bar{2}$ plane; (2) a decrease in the a-axis length; and (3) an increase in the c-axis length. Note that the changes in axial lengths upon heavy bromination result in near equality of a and $c/2$. These dimensions correspond to the interchain separations in the respective axial directions.

Although these trends are clear, there is appreciable scatter in the results obtained from different samples within the same bromination batch (see TABLE I). This might be due in part to differences in the extent of bromination of individual crystals within a batch. Note that $d_{10\bar{2}}$ is more accurately determined than are d_{100} and $d_{00\bar{2}}$, since the former can be calculated from the high angle spacing for $d_{20\bar{4}}$.

In agreement with previous results,[3,4,7] the chain-axis length seems to be in-

sensitive to bromination. The measured value of b for $(SNBr_{0.40})_x$ is 4.431 Å, which is not significantly different from the b-axis length in unbrominated polymeric sulfur nitride (4.439 Å).[18] Diffuse scattering reminescent of superlattice periodicities has been observed both normal to the b-axis direction and on $h0l$ Weisenberg photographs. In the latter, diffuse, high d-spacing reflections appear to lie on the h, 0, 0 and h, 0, $2\bar{h}$ reciprocal cell axes. These diffuse reflections vary dramatically in intensity for different crystals within the same bromination batch. Because of the highly variable nature of this diffuse scattering and the broad line-widths, which preclude accurate measurement of spacings, further work must be done in order to characterize the origin of this scattering.

Discussion of the Structure of Brominated $(SN)_x$

Principally on the basis of electron-diffraction photographs, Street *et al.*[4] and Gill *et al.*[7] reported that no significant changes in the unit-cell parameters of $(SN)_x$ occur upon bromination. They did report the observation of diffuse lines perpendicular to the chain-axis direction, with a spacing twice the chain-axis repeat length of $(SN)_x$. On the basis of this information, these authors proposed a structural model in which the bromine does not enter the $(SN)_x$ lattice but instead resides in interfibrillar regions. Gill *et al.* report,[7] using high-resolution electron microscopy, a fiber diameter of 20–30 Å for $(SNBr_{0.4})_x$, as compared with a fiber diameter of 50–70 Å for unbrominated $(SN)_x$. These authors believe that the diffuse layer line with spacing $2b$ is most likely due to a commensurate bromine lattice ordered only along the chain-axis direction, rather than corresponding to a doubling of the $(SN)_x$ cell.

By constrast with these models, we have found that bromine enters the $(SN)_x$ lattice so as to form a true lattice insertion compound. Bromine is most likely present to some degree in both interfibrillar and crystalline regions as Br_2, Br_3^-, and possibly higher polyanions, with a relative concentration dependent upon temperature and pressure. However, a more simplistic model is consistent with presently available data. According to this model Br_2 molecules enter the $(SN)_x$ lattice as an array in the chain-axis direction so that a Br_2 molecule occupies the crystal site of a S—N—S—N chain linkage. The bromine molecules are parallel within the array and lie within the $10\bar{2}$ plane, which is the closest packed plane in unbrominated $(SN)_x$.

In order to show that this model is consistent with the similar diffraction patterns of brominated and unbrominated $(SN)_x$, it is necessary to demonstrate that a linear array of Br_2 molecules can take the position of an $(SN)_x$ chain without causing major disruption of the $(SN)_x$ packing. Regarding this, it is important to mention two points. First, the packing volume of Br_2, calculated by extrapolating the unit-cell volume of solid bromine to 25°C, is 68.1 Å.[19] An essentially identical volume (66.3 $Å^3$) is calculated for the —S—N—S—N— chain linkage in polymeric sulfur nitride, using the measured unit cell parameters.[18] Second, the separations of close-packed Br_2 molecules arranged as in solid Br_2 is 4.55 Å,[20] which is close to the chain-axis repeat dimension of polymeric sulfur nitride (4.439 Å).[18] This information suggests that a linear array of Br_2 molecules can

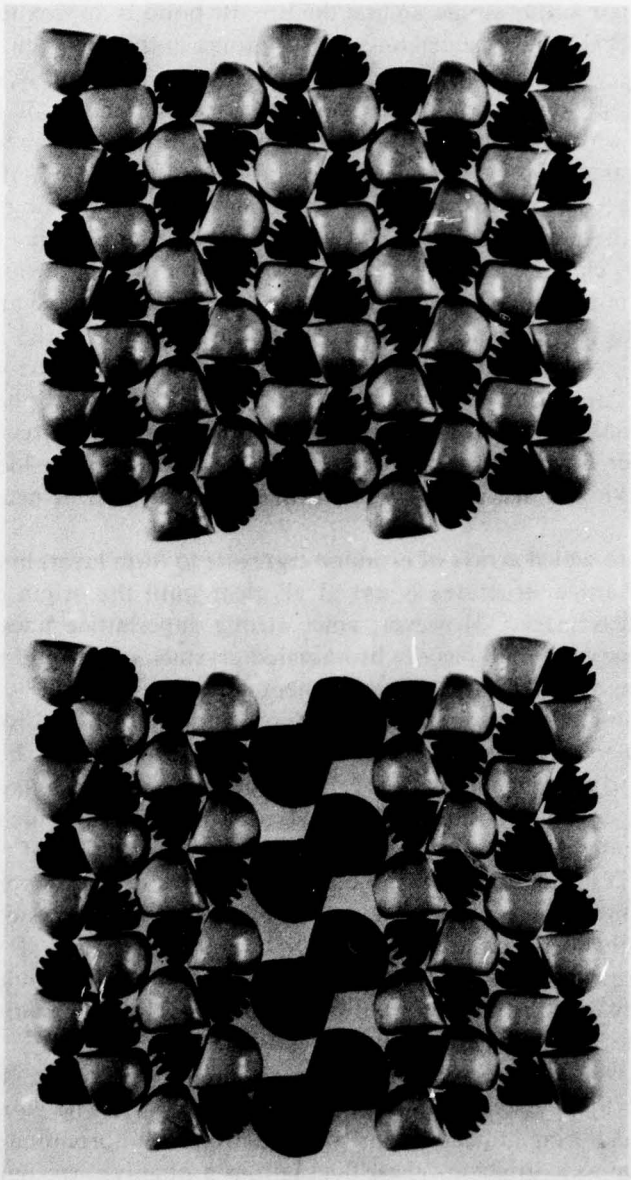


FIGURE 5. The $10\bar{2}$ plane of $(SN)_x$ before (*top*) and after (*bottom*) the lattice insertion of a chain-axis array of Br_2 molecules. In order of decreasing sizes, the balls represent the van der Waals dimensions of bromine, sulfur, and nitrogen, respectively.

replace an $(SN)_x$ chain in the crystal without profoundly affecting the crystal packing of neighboring $(SN)_x$ chains.

A model that depicts the predicted packing arrangement of an array of Br_2 molecules in an $(SN)_x$ lattice is shown in FIGURE 5. The closest packed plane in $(SN)_x$ is represented. Note that the atoms sit at positions close to those formerly

occupied by chain sulfur atoms, so that the Br—Br bond is approximately parallel to the vector between nearest neighbor sulfur atoms in the $(SN)_x$ chain. Note also that for a defect-free crystal, successive $(SN)_x$ chains alternate in direction, denoted either "up" or "down," corresponding to the direction of the sulfur-to-nitrogen bond which is roughly parallel to the chain direction. The bromine array in FIGURE 5 was placed in the crystal position of an "up" chain. If the bromine array had replaced a "down" chain, an equivalent bromine-packing array results. In either case there are two equivalent ways in which the bromine array can replace the $(SN)_x$ chain, which are related by operation of the 2_1 symmetry axis of the replaced chain in the original lattice. Note that if the bromine array separates two neighboring $(SN)_x$ chains in a periodic packing sequence in the $10\bar{2}$ plane, the "up"–"down" sequence of these chains is disrupted. From previous work[17] we know that the "up"–"down" chain sequence in the $10\bar{2}$ plane of polymeric sulfur nitride is occasionally interrupted by chains having an opposite direction from that which is proper for a periodic structure. These misfit chains, which can be arranged as stacking faults, do not result in major disruption of nearest neighbor packing.

The extent to which arrays of bromine segregate to form layers and other quasi-periodic superlattice structures is not at all clear until the origin of the diffuse scattering is determined. However, since strong superlattice lines are not reproducibly observed for all heavily brominated crystals, one would think that the substitution has a highly statistical component.

Vacancies might be present in the Br_2 arrays, and some of the bromine appears to be adsorbed on the surface of fibrils or in the interfibrillar voids. For this reason it is is difficult to use the macroscopic cell volume and observed bulk density alone to make strong conclusions about the validity of the present arguments. Using the unit cell parameters for $(SNBr_{0.4})_x$ in TABLE 1, 10% substitution of —SNSN— by Br_2 would result in a unit-cell density equal to the bulk density reported by Street *et al.* (2.65 g/cm^3).[4] This corresponds to a composition in the crystalline phase of $(SNBr_{0.11})_x$ with no bromine vacancies. On the other extreme, if 11.3% of the lattice sites are vacant, a unit-cell composition $(SNBr_{0.40})_x$ would result in a unit-cell density equal to the reported bulk density. Such a high concentration of vacancies in the Br_2 arrays seems unlikely.

Kim *et al.*[21] have observed that the small-angle x-ray scattering present for unbrominated $(SN)_x$ essentially disappears in $(SNBr_{0.40})_x$. The equatorial orientation of this scattering indicates density fluctuations in unbrominated $(SN)_x$ normal to the chain-axis direction. These fluctuations probably correspond to density-deficient, interfibrillar regions of the polymer. Since this scattering is not observed for $(SNBr_{0.40})_x$, these measurements suggest that bromination largely eliminates these density fluctuations. In the model of Street *et al.*[4] and Gill *et al.*[7], bromine enters only the regions between unmodified $(SN)_x$ fibers. So as to agree with the reported macroscopic density, this model would require an average density of 3.36 g/cm^3 for the interfibrillar regions.[22] This density is reasonably close to the density of liquid bromine (3.12 g/cm^3 at 20°C).[23] However, the corresponding electron density difference between the bromine containing interfibrillar regions and the $(SN)_x$ fibers would be 0.2 electrons/Å^3. Since for this model 38% of the electrons in the brominated polymer are in the interfibrillar regions with the higher electron

density, this density difference should result in strong small-angle scattering. This strong scattering is not observed.

The lattice-insertion model does not seem to have this apparent liability, since bromine addition to the $(SN)_x$ lattice can result in a vanishing electron-density difference between the crystal fibers and the interfibrillar regions. The observed overall density (2.65 g/cm^3) and a vanishing electron-density difference is calculated for a crystalline region composition $(SNBr_{0.04})_x$. The remaining 90% bromine in $(SNBr_{0.40})_x$ would then reside in interfibrillar regions having a density of 2.87 g/cm^3. Errors in the bulk density and unit-cell volume of $(SNBr_{0.40})_x$ could substantially affect the calculated distribution of bromine between crystalline and interfibrillar regions, but will not alter the basic conclusion of the arguments presented here. Neglecting these uncertainties, this calculated composition is a lower limit estimate, because the presence of vacancies in the Br_2 arrays would require an increased bromine concentration in the lattice. Note that this model for the structure of brominated $(SN)_x$ is consistent with the Raman results presented in the previous section.

It is surprising that the $10\bar{2}$ spacing and the unit-cell volume slightly decrease as a consequence of bromination, since the occupation volume of Br_2 in solid bromine (68.1 Å^3)[19] is slightly higher than the occupation volume of —SNSN— in normal polymeric sulfur nitride (66.3 Å^3)[18] and the van der Waals radius of bromine (1.85 Å) is usually taken to be slightly larger than that of sulfur (1.80 Å).[24] Both these effects could be due either to the presence of Br_2 vacancies or to appreciable bonding between the Br_2 arrays and the $(SN)_x$ chains. Specifically, the short interplanar spacing between the $10\bar{2}$ planes suggests the possibility of strong interaction of a bromine array with $(SN)_x$ in neighboring $10\bar{2}$ planes. This might occur along with an important weakening of the Br—Br bond. Even though the samples examined are analytically pure, we cannot completely exclude the possibility that impurity, fiber dimension, or surface effects significantly affect the unit-cell parameters.

The line-widths observed in powder diffraction scans were used to estimate the fiber dimensions in brominated $(SN)_x$ via the Scherrer equation.[25] Corrections were made for minor instrumental broadening assuming Gaussian profiles. The calculated dimensions normal to the $10\bar{2}$ plane are 150, 120, and 110 Å for, respectively, $(SNBr_{0.049})_x$, $(SNBr_{0.27})_x$, and $(SNBr_{0.39})_x$. Correction of these results for broadening of the second kind (paracrystalline distortions), by the method of Bonart *et al.*[25,26] for the $10\bar{2}$ and $20\bar{4}$ reflections, did not significantly change these results. The 100 and 002 reflections essentially coincide for the higher bromination level samples, and peak overlap precluded evaluation for these reflections in $(SNBr_{0.049})_x$. The dimensions calculated from the line-width of these superimposed reflections are 100 and 87 Å, respectively, for $(SNBr_{0.27})_x$ and $(SNBr_{0.39})_x$. The results at low bromination level are reasonably consistent with those obtained by Boudeulle[16] from line-width measurements on unbrominated $(SN)_x$. She obtained dimensions of 205 Å and 150 Å for the $10\bar{2}$ and 100 planes, respectively. These results suggest that the fiber dimensions in lateral directions decrease on bromination, as was concluded by Gill *et al.*[7] However, the fiber dimensions indicated by the line-width analysis are significantly higher than those reported by these authors[7] on the basis of high-resolution electron microscopy [50–70 Å

for $(SN)_x$ and 20–30 Å for $(SNBr_{0.4})_x$]. It is not clear whether this discrepancy arises because of sample differences, perhaps originating during the preparation of samples suitable for electron microscopy, or because of the insensitivity of the line-width of the investigated reflections to defects such as twin boundaries. From previous work we know that gross structural defects occur down to the molecular scale in $(SN)_x$.[16–18]

Temkin *et al.*[15] have recently proposed a structural model that differs from the model of Street *et al.*[4] and Gill *et al.*[7] in that the bromine enters the interfibrillar regions as Br_3^- rather than Br_2. This assignment is made based on the similar Raman spectra of brominated $(SN)_x$ and Br_3^- ions in organic salts. The x-ray diffraction results discussed above appear to be inconsistent with the original models of Street *et al.*[4] and Gill *et al.*[7], as well as the new model of Temkin *et al.*,[27] since none of these models permit the presence of bromine in the $(SN)_x$ lattice. It might well be true, however, that the interfibrillar bromine present in $(SN)_x$ is Br_3^-. Because of the fairly low concentration calculated for the lattice bromine, it is conceivable that the associated Raman lines are unobserved. More work is required to clarify this point.

Acknowledgments

We wish to thank Dr. A. J. Heeger, Mrs. J. Milliken, and Mr. M. J. Moran (University of Pennsylvania) for helpful discussions and for providing the samples used in this study. We should also like to thank Mr. H. Minor (Allied Chemical Corp.) for taking the x-ray diffraction photographs, and Dr. H. G. Kim (Allied Chemical Corp.) for discussion of his small-angle x-ray scattering data.

Notes and References

1. Recent reviews are: Geserich, H. P. & L. Pintschovius. 1976. *In* Advances in Solid State Physics. Vol. XVI. J. Treusch, Ed. Vieweg, Braunschweig, Germany; Greene, R. L. & G. B. Street. 1977. Chemistry and Physics of One-dimensional Metals. H. J. Keller. Ed. Plenum Press. New York, N.Y.; Hsu, C. & M. M. Labes. 1974. J. Chem. Phys. **61**: 4640–4645; MacDiarmid, A. G., C. M. Mikulski, M. S. Saran, P. J. Russo, M. J. Cohen, A. A. Bright, A. F. Garito & A. J. Heeger. 1976. Advances in Chemistry Series, no. 150. R. B. King, Ed.; Baughman, R. H., P. A. Apgar, R. R. Chance, A. G. MacDiarmid & A. F. Garito. 1977. J. Chem. Phys. **66**: 401–409.
2. Bright, A. A., M. J. Cohen, A. F. Garito & A. J. Heeger. 1975. Appl. Phys. Lett. **26**: 612–615.
3. Bernard, C., A. Herold, M. Lelaurain & G. Robert. 1976. C. R. Acad. Sc. Paris C **283**: 625–627.
4. Street, G. B., W. D. Gill, R. H. Geiss, R. L. Greene & J. J. Mayerle. 1977. Chem. Commun.: 407.
5. Akhtar, M., J. Kleppinger, A. G. MacDiarmid, J. Millikan, M. J. Moran, C. K. Chiang, M. J. Cohen, A. J. Heeger & D. L. Peebles. 1977. Chem. Commun.: 473–474.
6. Chiang, C. K., M. J. Cohen, D. L. Peebles, A. J. Heeger, M. Akhtar, J. Kleppinger, J. Milliken & M. J. Moran. 1977. Solid State Commun. **23**: 607–612.
7. Gill, W. D., W. Bludau, R. H. Geiss, P. M. Grant, R. L. Greene, J. J. Mayerle & G. B. Street. 1977. Phys. Rev. Lett. **38**: 1305–1308.

8. MIKULSKI, C. M., P. J. RUSSO, M. J. SARAN, A. G. MACDIARMID, A. F. GARITO & A. J. HEEGER. 1975. J. Amer. Chem. Soc. **97**: 6358–6363.
9. IQBAL, Z. & C. W. CHRISTOE. 1976. Solid St. Commun. **18**: 269–273.
10. TEMKIN, H. & D. FITCHEN. 1976. Solid St. Commun. **19**: 1181–1184.
11. See, for example, COCHRAN, W. 1973. The Dynamics of Atoms in Crystals. Chap. 18. Edward Arnold Publishers. London, England.
12. HERZBERG, G. 1950. Spectra of Diatomic Molecules. D. Van Nostrand Co., Inc. New York, N.Y.
13. CAHILL, J. E. & G. E. LEROI. 1969. J. Chem. Phys. **51**: 4514–4519.
14. SONG, J. J., D. D. L. SUNG, P. C. EKLUND & M. S. DRESSELHAUS. 1976. Solid St. Commun. **20**: 1111–1115.
15. TEMKIN, H., D. B. FITCHEN & G. B. STREET. This volume.
16. DOUILLARD, A. 1972. Ph.D. Thesis. Claude Bernard University. Lyon, France; BOUDEULLE, M. 1974. Ph.D. Thesis. Claude Bernard University. Lyon, France.
17. BAUGHMAN, R. H., R. R. CHANCE & M. J. COHEN. 1976. J. Chem. Phys. **64**: 1869–1876; BAUGHMAN, R. H. & R. R. CHANCE. 1976. J. Polym. Sci. Phys. Ed. **14**: 2019–2035.
18. COHEN, M. J., A. F. GARITO, A. J. HEEGER, A. G. MACDIARMID, C. M. MIKULSKI, M. S. SARAN & J. KLEPPINGER. 1976. J. Amer. Chem. Soc. **98**: 3844–3848.
19. HAWES, L. L. 1959. Acta Cryst. **12**: 34–35.
20. VONNEGUT, B. & B. E. WARREN. 1936. J. Amer. Chem. Soc. **58**: 2459–2461.
21. KIM, H. G. *et al.* Unpublished results.
22. STREET, G. B. Private communication.
23. CRC Handbook of Chemistry and Physics. 50th edit. 1969. The Chemical Rubber Co.
24. BONDI, A. 1968. Physical Properties of Molecular Cyrstals, Liquids and Gases. John Wiley & Sons. New York, N.Y.
25. ALEXANDER, L. E. 1969. X-Ray Diffraction Methods in Polymer Science. Chap. 7: 423–453. Wiley-Interscience. New York, N.Y.
26. BONART, R., R. HOSEMANN & R. L. MCCULLOUGH. 1963. Polymer **4**: 199.

THE LINEAR CHAIN MERCURY COMPOUNDS: $Hg_{2.86}AsF_6$ AND $Hg_{2.91}SbF_6$. ELECTRICAL CONDUCTIVITY, OPTICAL REFLECTANCE, AND THERMOELECTRIC STUDIES*

Ronald J. Gillespie,† Duane Chartier,† Brent D. Cutforth,†
W. Ross Datars,‡ and André Van Schyndel‡

† Department of Chemistry
‡ Department of Physics
McMaster University
Hamilton, Ontario, L8S 4M1, Canada

INTRODUCTION

The compounds $Hg_{2.86}AsF_6$ and $Hg_{2.91}SbF_6$ were discovered at McMaster University in 1971 during an investigation of the formation of polymercury cations Hg_x^{n+}.[1] The reactions of mercury with SbF_5 and AsF_5 in solution in SO_2 were found to lead to the formation of the linear Hg_3^{2+} and Hg_4^{2+} cations in the form of their soluble hexafluoroarsenate and hexafluoroantimonate salts, together with an insoluble crystalline material with a golden metallic appearance.[2,3] Determination of the structures of these insoluble products showed that they have the compositions $Hg_{2.86}AsF_6$ and $Hg_{2.91}SbF_6$.[4,5] A better method for making large crystals of these materials has subsequently been found to be the reaction of metallic mercury with $Hg_3(AsF_6)_2$ or $Hg_3(SbF_6)_2$ at -10 to -20°C in solution in SO_2.[6] The reaction is slow but good crystals are usually obtained after approximately one week.

The two compounds have essentially the same structure (FIGURE 1).[4,5] The AsF_6^- or SbF_6^- octahedra are situated in a tetragonal lattice with a = 7.54 Å and c = 12.32 Å for $Hg_{2.86}AsF_6$ and a = 7.67 Å and c = 12.61 Å for $Hg_{2.91}SbF_6$. There are four AsF_6^- or SbF_6^- ions per unit cell. These anions form a framework with linear, nonintersecting, mutually perpendicular channels in which infinite linear mercury chains are situated. A schematic view of the relationship of the mercury chains in four planes perpendicular to the c axis is shown in FIGURE 2. The shortest distance between two chains in consecutive planes occurs where the chains cross and is 3.09 Å in $Hg_{2.86}AsF_6$ and 3.15 Å in $Hg_{2.91}SbF_6$. The mercury atoms in the chains have a nominal formal charge of +0.35 and are separated, on average, by 2.64 Å. Since the intrachain mercury-mercury distance is incommensurate with the tetragonal lattice, each mercury atom has a different chemical environment.

ELECTRICAL CONDUCTIVITY MEASUREMENTS

Since there is a nonintegral charge on each mercury atom, the conduction band arising from the overlap of the mercury orbitals is expected to be partially filled.

*Manuscript received August 29, 1977. Correspondence to R.J.G.

0077-8923/78/0313-0788 $1.75/1© 1978, NYAS

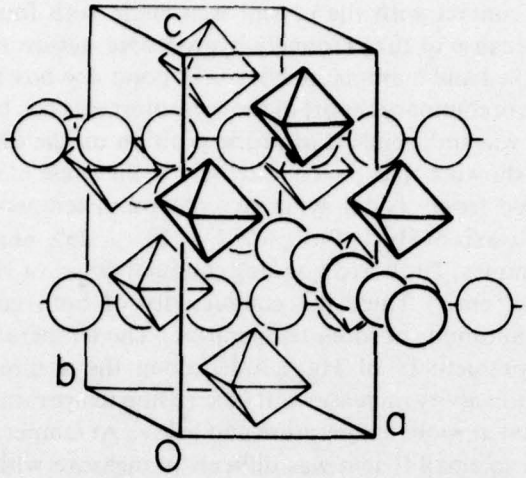


FIGURE 1. The structure of $Hg_{2.86}AsF_6$ and $Hg_{2.91}SbF_6$, showing the linear mercury chains and the octahedral anions.

It was predicted,[4] therefore, that there would be a very high conductivity along the chains and a lower conductivity in the c-direction perpendicular to the chains. A considerable conductivity along the c axis might, nevertheless, be expected, as the interchain distances of 3.09 Å in $Hg_{2.85}AsF_6$ and 3.15 Å in $Hg_{2.91}SbF_6$ are comparable to the Hg-Hg distance in the metal (3.00 Å).

Resistivity was measured by the Montgomery[7] technique with an ac (9.8 Hz)

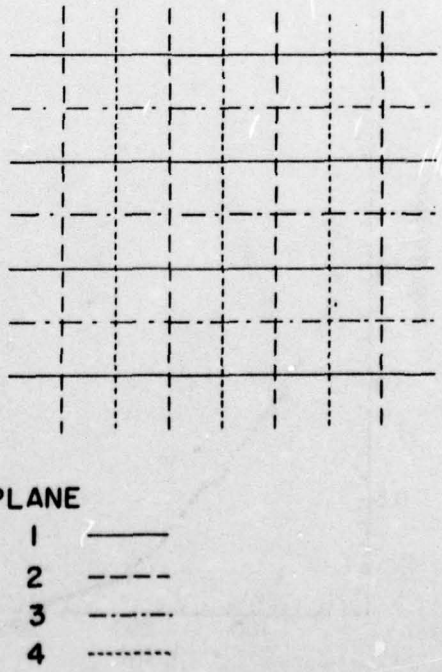


FIGURE 2. Arrangement of the mercury chains in the structures of $Hg_{2.86}AsF_6$ and $Hg_{2.91}SbF_6$.

bridge. Electrical contact with the crystal was made with four platinum spring contact probes. Because of the extremely hygroscopic nature of the compounds, samples were handled and manipulated in a very good dry box and were mounted in a sealed tube. A preliminary report of the measurements has been published.[8]

The resistivity was independent of probe position on the (001) crystal face of both compounds, showing that the conductivity is the same along the **a** and **b** directions as expected from crystal symmetry. At room temperature, the conductivity σ_a along the **a**-axis of $Hg_{2.91}SbF_6$ is $8.7 \times 10^3 \pm 25\%$ ohm^{-1} cm^{-1} as determined from six samples. The corresponding conductivity σ_a of $Hg_{2.86}AsF_6$ is of the order of 10^4 ohm^{-1}cm^{-1}. Thus, the conductivity of both compounds is comparable to that of antimony at room temperature. The temperature dependence of the normalized conductivity of $Hg_{2.86}AsF_6$ along the **a** direction is shown in FIGURE 3. The conductivity increases with decreasing temperature, showing that it behaves like a metal at room temperature and below. At temperatures below 10°K, the resistivity was so small that it was difficult to measure with the samples that were used. There seems to be little evidence of residual resistivity as found in most metals.

The electrical anisotropy was determined from measurements on a crystal face that was approximately 26° from the ac plane. Unfortunately, the ac plane does not occur as a natural growth plane. At room temperature, the conductivity ratio σ_a/σ_c determined by the Montgomery method is 100 for $Hg_{2.86}AsF_6$ and 40 for $Hg_{2.91}SbF_6$. The temperature dependence of the normalized conductivity of

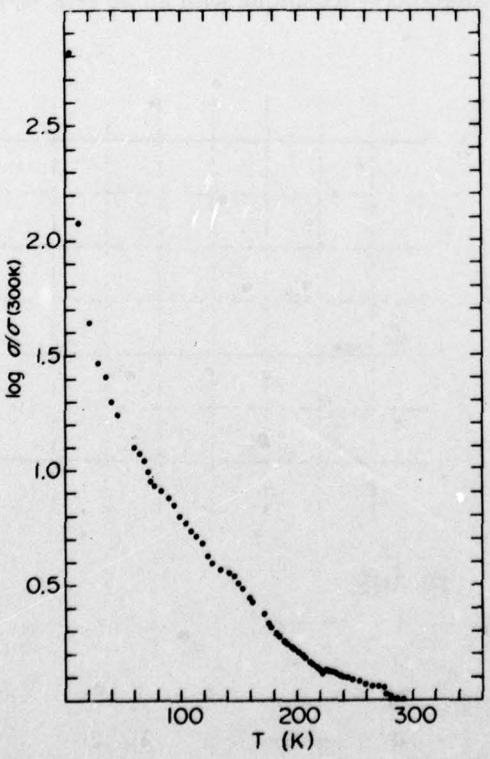


FIGURE 3. Logarithm of the normalized conductivity in the (001) plane as a function of temperature in an oriented $Hg_{2.86}AsF_6$ crystal.

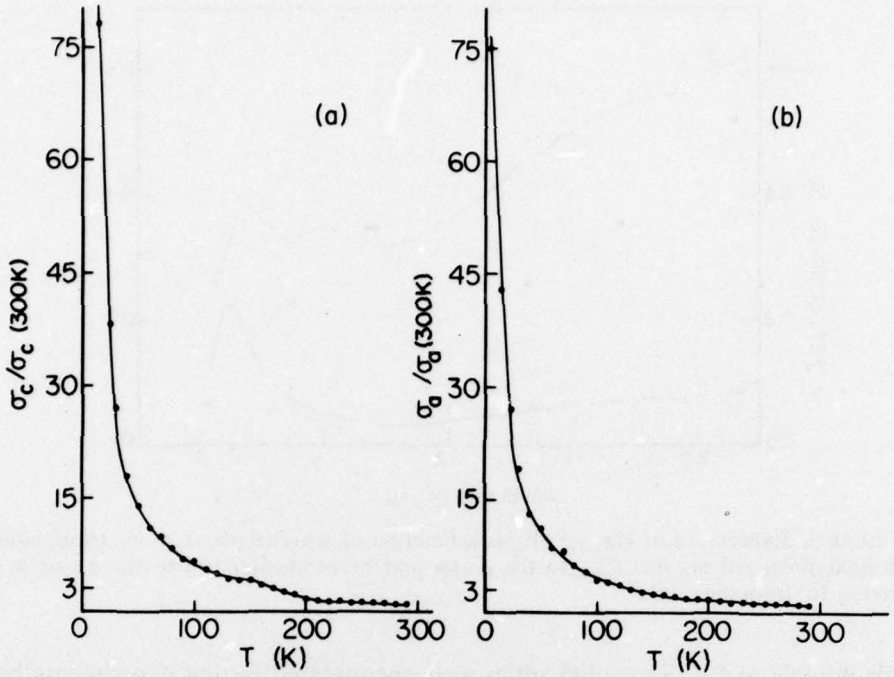


FIGURE 4. Normalized conductivity of $Hg_{2.91}SbF_6$ as a function of temperature (a) along the **c** direction, and (b) along the **a** direction.

$Hg_{2.91}SbF_6$ along the **a** and **c** directions is shown in FIGURE 4. The conductivity along both directions is metallic between room temperature and 4.2°K with a conductivity ratio $\sigma_{4.2}/\sigma_{300}$ of approximately 150. The conductivity is anisotropic over the whole temperature range with approximately the same value of σ_a/σ_c. Residual resistivity in $Hg_{2.91}SbF_6$ at 4.2°K is again very small. The temperature dependence of the conductivity along the **a** and **c** directions of $Hg_{2.86}AsF_6$ is similar, and the electrical anisotropy is approximately independent of temperature down to 4.2°K.

The relatively rapid change in conductivity between 150° and 200°K in FIGURE 4 (a) is attributed to a phase transition.

These measurements show that these compounds are highly anisotropic metallic conductors. The mercury-mercury distance along the chains is short enough to cause significantly more intrachain than interchain conductivity. However, they are not true one-dimensional materials because the interchain Hg-Hg distance is not large and is indeed only slightly greater than that in the pure metal. There is also no metal insulator transition that is believed to be characteristic of a true one-dimension material.

ANISOTROPIC OPTICAL REFLECTANCE

Crystals of $Hg_{2.91}SbF_6$ were placed in an inert atmosphere inside a sealed quartz tube for the optical measurements. The reflectance was measured at an

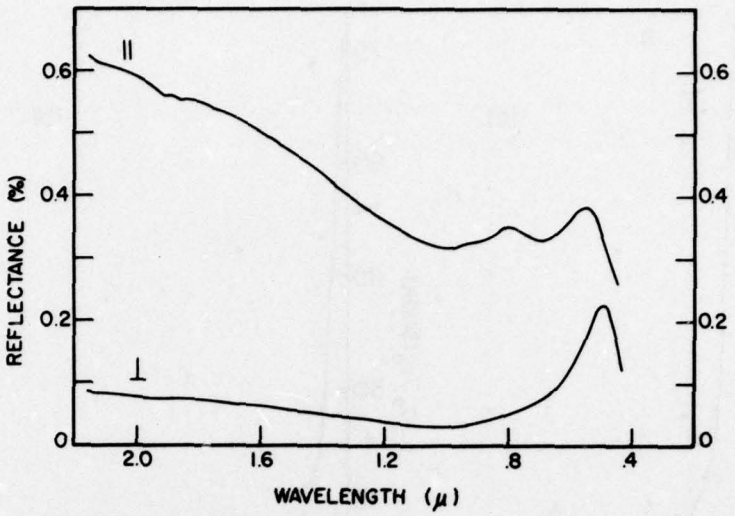


FIGURE 5. Reflectance of $Hg_{2.91}SbF_6$ as a function of wavelength at room temperature with light polarized parallel ($\perp$) to the *a*-axis and perpendicular ($\parallel$) to the *a*-axis in a direction 26° from the *c* axis.

incident angle of 19°. Some difficulties were encountered during experiments because of the deterioration of reflecting surfaces even when samples were sealed in tubes. There was, however, little apparent change of surface quality when the present results were taken. Experiments were performed on as-grown surfaces but, since the plane containing both the a and c directions is not a natural growth face, the surface that was used for the anisotropic measurements was approximately 26° from the ac plane and was probably either a (103) or a (105) plane. Positive identification of this plane was not possible because x rays could not penetrate the quartz tube. Reflectance intensity as a function of direction of polarization was used to determine the direction of high reflectance which was parallel to the a axis on the isotropic crystal face. The spectra were taken with a Spex grating spectrometer. A Polaroid HR sheet polarizer was used to extend the polarized spectral range to about 2 μm. The background was determined from the reflectance spectrum of a small aluminum mirror placed inside a section of the quartz tube. The absolute reflectance was measured at 6328 Å with a He-Ne laser and was found to be 0.35 ± 25%. A preliminary report of the measurements has been published.[9]

The reflectance spectra for light polarized parallel and perpendicular to the a direction are shown in FIGURE 5. With parallel polarization, there are two peaks in the visible at 5500 and 8000 Å and an increase in reflectance in the infrared which varied somewhat from sample to sample. The reflectance for the perpendicular polarization has a sharp peak at 4900 Å and is small in the infrared with a value of about 4% at 1 μm. These results confirm the view that $Hg_{2.91}SbF_6$ is a highly anisotropic metal. It is possible that the peak at 4900 Å is a component of the strong peak in the parallel spectrum because the perpendicular direction is about 26° from the *c* axis. The presence of peaks in the visible region for both polarizations explains the color changes observed with the eye. The anisotropic crystal surface was highly reflecting with a red color tinge with parallel polariza-

tion and duller with a greenish color when viewed with perpendicular polarized light. The isotropic *ab* plane showed no color or intensity change with change of polarization direction.

A dielectric model based on the standard Drude equation for an electron gas and two Lorentzian functions for the peaks in the visible[10] was fitted to the parallel reflectance spectra.

$$\epsilon = \epsilon^D + \epsilon^L$$

where

$$\epsilon^D = -\omega_p^2(\omega^2 - i\omega/\tau)$$

and

$$\epsilon^L = \epsilon_\infty + \sum_n \omega_{pn}^2/[(\omega_{On}^2 - \omega^2) - i\omega/\tau_n].$$

Here ϵ^D denotes the intraband term with the Drude parameters ω_p and τ. ϵ^L denotes the Lorentz term which could be due to interband transitions. The model was fitted to the experimental spectrum as shown in FIGURE 6, using the following values: for the Drude parameters, $h\omega_p = 2.86$ eV, $\tau/h = 1.75\ \text{eV}^{-1}$; for the Lorentzian parameters; $h\omega_{p1} = 1.51$ eV, $\tau_1/h = 1.39\ \text{eV}^{-1}$, $h\omega_{01} = 2.00$ eV, $h\omega_{p2} = 2.19$ eV, $\tau_2/h = 1.09\ \text{eV}^{-1}$, $h\omega_{02} = 1.45$ eV, $\epsilon_\infty = 2$.

The conductivity at zero frequency was calculated in the standard manner from the Drude parameters to be $1.3 \times 10^3\ \text{ohm}^{-1}\text{cm}^{-1}$. This compares with the value

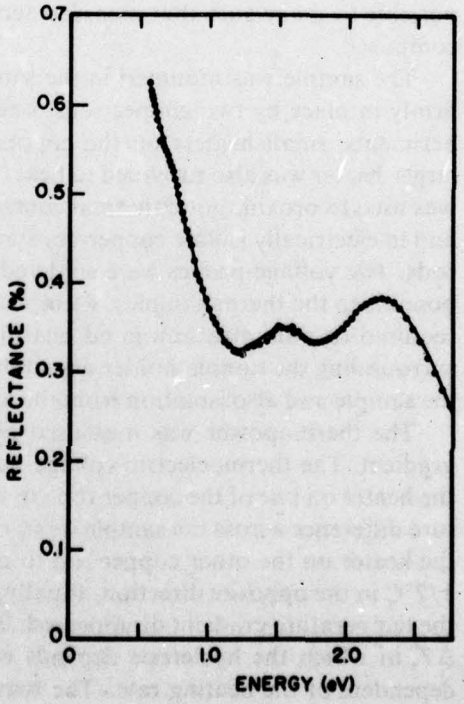


FIGURE 6. Reflectance of $Hg_{2.91}SbF_6$ as a function of photon energy. The solid curve is a fit of a dielectric model consisting of a Drude term and two Lorentzian functions.

of 8.7×10^3 ohm^{-1} cm^{-1} reported in the preceding section. It is not clear at the present time whether the discrepancy between the two values is significant.

The polarized reflectance spectra of $Hg_{2.91}SbF_6$ are similar to those of other quasione-dimensional materials such as TTF-TCNQ,[11] $(SN)_x$[12] and the platinum compounds.[13] As in $(SN)_x$ it appears that there is interchain coupling which reduces the anisotropy and causes conductivity in the c direction.

In summary, we have shown, from polarized reflectivity measurements on single-crystal $Hg_{2.91}SbF_6$ that light polarized parallel to the mercury chains exhibits a strong metallic-like plasma edge and has a large reflectivity in the infrared. The reflectance for light polarized perpendicular to this direction is an order of magnitude weaker. Thus, the anisotropic nature of the conductivity in this material has been established.

Thermoelectric Power

We have studied the thermoelectric power of $Hg_{2.86}AsF_6$ to obtain further information on the nature of the electrical conduction in this compound. The Seebeck coefficient is a direct measurement of the intrinsic properties of a metal even when anisotropy and crystal imperfections result in some irreproducibility in electrical conductivity measurements.[14] The Seebeck coefficient, which is independent of geometry, is a zero-current measurement, so that breaks in a current path, unless accompanied by large breaks in the heat-flow paths, do not produce appreciable effects. Furthermore, any decomposition resulting in the formation of elemental mercury is detected, particularly at the melting point of mercury, as an additional component in the Seebeck coefficient. Thus, with this method, it is possible to make sure that measurements are made on samples that have not decomposed.

The sample was mounted in the sample holder inside a dry box and was held firmly in place by two copper rods, one of which was spring-loaded. For the experiments, small heaters on the copper rods heated the sample directly and a larger heater was also provided to heat the whole sample holder. G.E. 7031 varnish was used to provide good thermal contact between the heater wires and the copper and to electrically isolate copper-constantan thermocouples attached to the copper rods. The voltage probes were soldered directly on to the copper rods as close as possible to the thermocouples. Electrical leads were thermally anchored wherever required to minimize unwanted heat-flow and thermal gradients. A copper can surrounding the sample holder assembly provided an isothermal environment for the sample and also isolation from the atmosphere.

The thermopower was measured by using a slowly alternating temperature gradient. The thermoelectric voltage was measured while current was supplied to the heater on one of the copper rods in contact with the sample until the temperature difference across the sample was 1/2°C, and then the current was switched to the heater on the other copper rod to produce a temperature difference of about 1/2°C in the opposite direction. Finally, the first heater was turned on again until the temperature gradient disappeared. This produced a hysteresis curve of ΔV vs. ΔT, in which the hysteresis depends on the rate of heating but the slope is independent of the heating rate. The temperature of the sample does not vary by

more than 1°C, so that, providing the thermopower does not vary rapidly with temperature, the hysteresis curve has a linear slope and forms a closed loop. The measurements thus represent an average thermopower over approximately 1°C for both signs and varying magnitude of the temperature gradient.

The accuracy of the method for small samples and with mechanical contacts was evaluated in experiments with lead and nickel pellets of the same size as the $Hg_{2.86}AsF_6$ crystals.

The absolute thermopower of copper (S_{Cu}) was evaluated from the average value of S_{CuPb} by subtracting S_{Pb} determined by Christian *et al.*[15] In the higher temperature region, the data are in excellent agreement with the accepted values of the diffusion thermopower.[16] S_{Cu} was subtracted from the thermopower of $Hg_{2.86}AsF_6$ – Cu to obtain the absolute thermopower of $Hg_{2.86}AsF_6$.

The thermopower along the **c** axis (S_c) was determined from crystal platelets that could be inserted into the holder with the **c**-axis along the temperature gradient. Suitable crystals for the measurement of the thermopower along the **a** and **b** axes ($S_{a,b}$) were not obtained. However, the net thermopower for a polycrystalline sample can be written as (**1**)[17]

$$S = \frac{\sigma_c S_c + \sigma_{a,b} S_{a,b}}{\sigma_c + \sigma_{a,b}}. \qquad (1)$$

Since $\sigma_c \ll \sigma_{a,b}$, the thermopower measured for a polycrystalline sample is approximately $S_{a,b}$. Four polycrystalline samples were used to determine $S_{a,b}$ in this way.

The temperature dependence of $S_{a,b}$ is shown in FIGURE 7 for the largest and smallest samples, their length along the temperature gradient differing by a factor

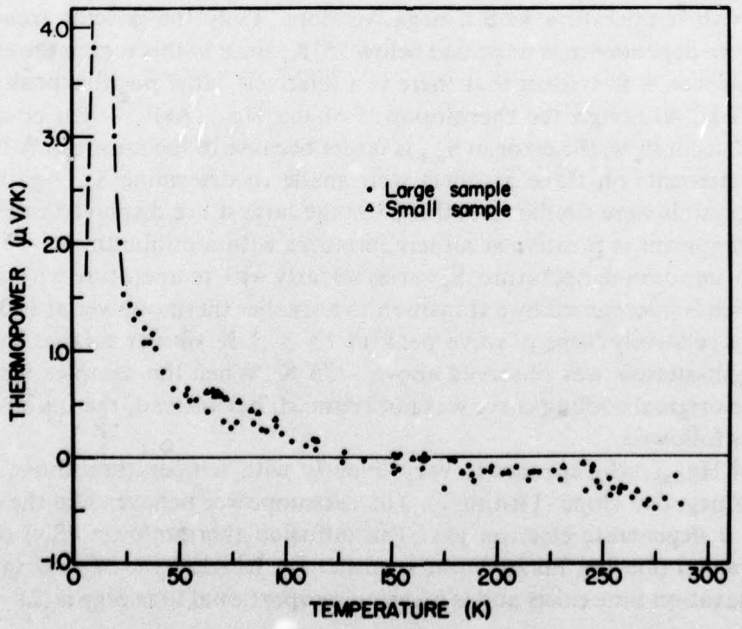


FIGURE 7. The temperature dependence of the thermopower S_{ab} of $Hg_{2.86}AsF_6$.

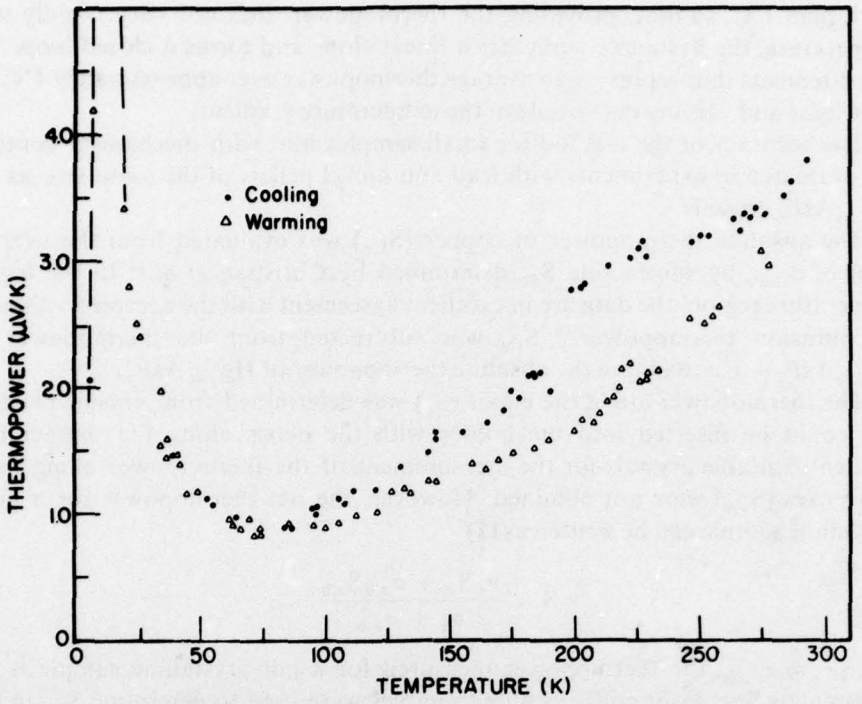


FIGURE 8. The temperature dependence of the thermopower S_e of $Hg_{2.86}AsF_6$.

of five. The identical results for both samples demonstrates the validity of the measuring technique. About 140 ± 20 K, the thermopower is negative and varies linearly with temperature with a negative slope. Only the general trend of the temperature dependence is indicated below 25°K, since in this region the errors are large. However, it is evident that there is a relatively large positive peak centered at 13 ± 3 K. Although the thermopower of the $Hg_{2.86}AsF_6$ – Cu coupled was measured accurately, the error in $S_{a,b}$ is larger because of the uncertainty in S_{Cu}.

Measurements on three platelets were made to determine S_c. Again, results from all crystals were similar, and those for the largest are displayed in FIGURE 8. The thermopower is positive at all temperatures with a minimum at ~75°K. On cooling from room temperature, S_c varies linearly with temperature with a positive slope which is interrupted by a transition to a smaller thermopower at 190 ± 10°K. There is a relatively large positive peak at 13 ± 3 K similar to that in S_{ab}. On warming, hysteresis was observed above ~75°K. When the samples were cycled again, the original cooling curve was not retraced, but instead, the initial warming curve was followed.

$S_{a,b}$ of $Hg_{2.86}AsF_6$ appears to vary linearly with temperature above ~120 K and has a negative slope (FIGURE 7). The thermopower behaves like the diffusion term for a degenerate electron gas. The diffusion thermopower (S_D) of a free-electron metal obeying Fermi-Dirac statistics for which $T_F \gg T$ and in which a single relaxation time exists and is inversely proportional to energy is (2)

$$S_D = -\frac{(\pi k)^2 T}{6|\epsilon|E_F} \qquad (2)$$

where E_F is the Fermi energy and T is the temperature.[14] A fit of the linear portion of the thermopower data of FIGURE 7 to Equation 1 yields a Fermi energy at 4.3 ± 0.5 eV, and the negative slope indicates that conduction is by electrons. The linear temperature dependence is characteristic of a metal and does not depend on its dimensionality. Thus, it cannot be used to determine the possible one-dimensional nature of the compound.

It is of interest to compare E_F determined from the thermopower results with that expected for the electron density in the channels containing the mercury atoms. We assume the AsF_6^- octahedra to be spherical with a radius of 2–3 Å, and that there are 1.65 conduction electrons per mercury atom with a formal charge of +0.35 required for charge neutrality. Then the Fermi energy is 4.1 eV. Alternatively, a one-dimensional free electron density of states may be used to estimate E_F, although the use of a one-dimensional density of states may oversimplify the problem. In this model there are, on average, 2.86 mercury atoms per unit cell distance of 7.54 Å each with a nominal valence of +1.65. This electron density corresponds to a Fermi energy of 3.7 eV. The values of E_F for both models are in reasonable agreement with the measured value of 4.3 eV and are not sufficiently different to enable one to distinguish between the two models.

The temperature dependence of S_c, shown in FIGURE 8, is linear with a positive slope above 100°K. Therefore, whereas electrons are the dominant carriers along the **a**,**b** axes, holes are the majority carriers in the **c** direction. This clearly demonstrates the anisotropic nature of the conductivity. The conduction along the **c** axis must cross the regions where the mercury chains cross. Here, the mercury atoms are separated, on average, by only ~3.1 Å compared to much larger distances anywhere else in the **c** direction. Thus, we can visualize electrical conduction in the **c** direction as occurring at chain crossings with subsequent diffusion along the chains in the **a** and **b** directions to the next set of chain crossings. Thus, the conductivity along **c** does not have a one-dimensional path.

Between 180°K and 200°K there is evidence of a transition with a ~70% decrease in the value of S_c on cooling. This is not thought to be due to elemental mercury, since it would then have to occur much closer to 234°K, the melting point of mercury. This transition is also observed in differential thermal analysis experiments[18] and in the c-axis resistivity measurements[8] where the change in the resistivity is of similar magnitude to the change in S_c. This transition may result from an ordering of mercury atoms from their somewhat random intrachain spacings so that, for example, their interchain distance is minimized wherever chains cross. This explanation seems reasonable, since no anomalies are observed for $S_{a,b}$ in this temperature range and therefore the transition must be related in some way to the interchain conduction process.

$S_{a,b}$ becomes positive below 140 ± 20°K with a maximum at 13 ± 3°K and then decreases to zero at still lower temperatures. This peak is typical of phonon drag thermopower (S_g) enhancement. Generally, it has been found that peaks in S_g occur in the temperature range $0.1\,\theta_D < T < 0.2\,\theta_D$, where θ_D is the Debye temperature; i.e., the Debye temperature is presumably in the range 65–130°K. According to Ziman,[19] S_g should be proportional to T^{-1} for $T \gtrsim \theta_D$. Subtracting the diffusion component from the total thermopower, we obtain S_g, which when plotted against T^{-1}, is indeed linear in the range 100–25°K, as shown in FIGURE 9. A plot of $S_{a,b}$ versus T^{-1} is also quite linear below 100°K, since S_D contributes very little at low temperatures.

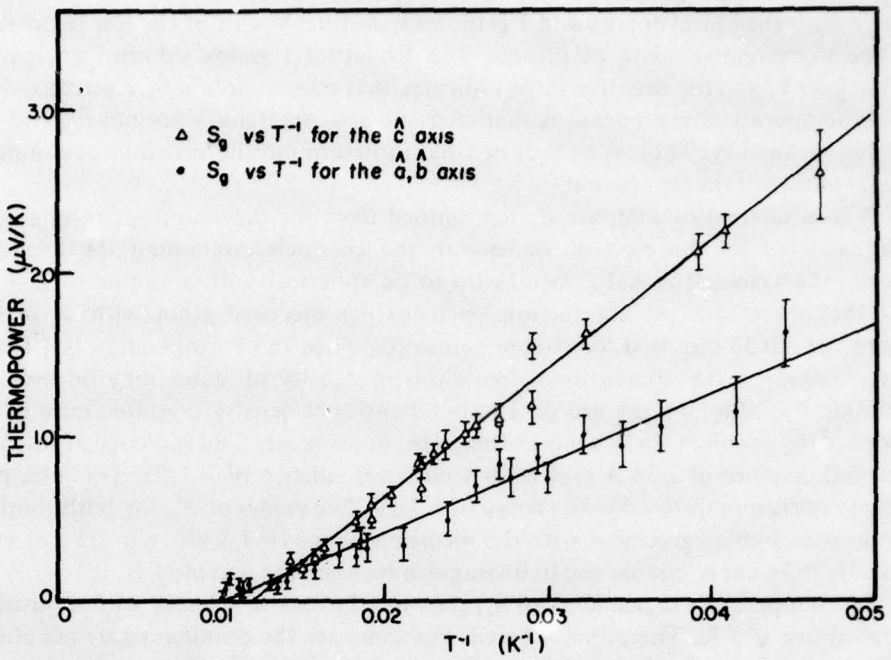


FIGURE 9. The temperature dependence of the phonon drag thermopower S_g of $Hg_{2.86}AsF_6$.

The positive nature of S_g for electron conduction in the **a,b** directions can occur when electron scattering by Umklapp U-processes is more frequent than scattering by normal N-processes.[19] However, at low temperatures U-processes will "freeze out" if the Fermi surface is not close to the Brillouin zone boundaries but can exist down to the lowest temperatures if there is a multiple-connected surface or if the Fermi surface is close to the Brillouin zone boundary. Multiple-connected surfaces along the **a,b** directions causing the positive phonon decay thermopower can be visualized by constructing a two-dimensional reciprocal lattice using the inter- and intrachain mercury distances of a particular plane for unit cell parameters. The Brillouin zones thus constructed do indeed generate connected Fermi surfaces when a free-electron Fermi sphere is used in a single orthogonalized-plane-wave construction.

Below ~ 75°K, S_c is very similar to $S_{a,b}$. N-processes can now be the cause of the positive phonon decay component, since electrical conduction is hole-like. However, since conduction in the **c** direction also involves diffusion along the chains in the **a** and **b** directions, we may also be observing U-processes occurring along the **a** and **b** directions.

The present results may help to explain the large temperature dependence of the electrical conductivity of the linear chain mercury compounds, which is comparable to that of many pure metals. The large phonon drag peak indicates that phonon scattering is important and the low Debye temperature indicates a significant density of low-energy phonons. These properties give a strong temperature dependence of the phonon resistivity and a large resistence ratio.[20] A large phonon-drag component also acts to reduce the resistivity.

We conclude from the thermoelectropower experiment that there is metallic

electron-dominated conduction along the **a** and **b** directions of $Hg_{2.86}AsF_6$. Holes are the majority carriers in the **c** direction. This amply confirms the anisotropic nature of the compound. The thermopower of $Hg_{2.86}AsF_6$ is described by $S = S_D + S_g$, where S_D is the diffusion component and S_g is the phonon drag component. The Fermi energy is evaluated to be 4.3 ± 0.5 eV from S_D. S_g is the dominant below 100°K and appears to be caused largely by Umklapp processes. The Debye temperature is estimated to be between 65° and 130°K. There is a change in the thermopower between 180°K and 200°K along the **c** axis but not along the **a,b** axes.

References

1. Gillespie, R. J. & P. K. Ummat. 1971. J. Chem. Soc. Chem. Comm. 1168.
2. Cutforth, B. D., C. G. Davies, P. A. W. Dean, R. J. Gillespie, P. R. Ireland & P. K. Ummat. 1973. Inorg. Chem. **12:** 1343.
3. Cutforth, B. D., R. J. Gillespie & P. R. Ireland. Chem. Comm.: 723.
4. Brown, I. D., D. B. Cutforth, C. G. Davies, R. J. Gillespie, P. R. Ireland & J. E. Vekris. Can. J. Chem. **52:** 791.
5. Baranyi, A., B. D. Cutforth, W. R. Datars & R. J. Gillespie. Unpublished work.
6. Cutforth, B. D. 1975. Ph.D. Thesis. McMaster University. Hamilton, Ont., Canada.
7. Montgomery, H. C. 1971. J. Appl. Phys. **42:** 2971.
8. Cutforth, B. D., W. R. Datars, A. Van Schyndel & R. J. Gillespie. 1977. Solid State Commun. **21:** 377.
9. Koteles, E. S., W. R. Datars, B. D. Cutforth & R. J. Gillespie. 1976. Solid State Commun. **20:** 1129.
10. Wooten, F. 1972. Optical Properties of Solids: 42. Academic Press. New York, N.Y.
11. Bright, A. A., A. F. Garito & A. J. Heeger. 1973. Solid State Commun. **13:** 943.
12. Bright, A. A., M. J. Cohen, A. F. Garito, A. J. Heeger, C. M. Mikulaki, P. J. Russo & A. G. MacDiarmid. 1975. Phys. Rev. Lett. **34:** 206; Grant, P. M., R. L. Greene & G. B. Street. 1975. Phys. Rev. Lett. **35:** 1743.
13. Kuse, D. & H. R. Seller. 1971. Phys. Rev. Lett. **27:** 371.
14. Barnard, R. D. 1972. Thermoelectricity in Metals and Alloys. Halsted Press. New York, N.Y.
15. Christian, J. W., J. P. Jan, W. P. Pearson & I. M. Templeton. 1958. Proc. Roy. Soc. (London) **A245:** 213.
16. Pearson, W. B. 1961. Solid State Phy. (USSR) **3:** 1411.
17. Hübner, R. P. 1972. Solid State Phys. **27:** 63.
18. van Schyndel, A., W. R. Datars, B. D. Cutforth & R. J. Gillespie. To be published.
19. Ziman, I. M. 1960. Electrons and Phonons. Claredon Press. Oxford, England.
20. Tauc, J. 1962. Photo and Thermoelectric Effects in Semiconductors. Ch. 4. Pergamon Press. New York, N.Y.

Discussion

Alan G. MacDiarmid: Have you found anything intermediate between the Hg_4 and Hg_x?

Gillespie: We have not found any evidence for any intermediates, but it is quite possible that there are other Hg_x^{y+} species.

James Burlich (*Cornell Univ., Ithaca, N.Y.*): Could you comment on the free mercury you observe?

Gillespie: My view is that the mercury comes from decomposition, perhaps catalyzed by traces of water.

$Hg_{3-\delta}AsF_6$: A NOVEL ANISOTROPIC SYNTHETIC METAL*

A. J. Heeger† and A. G. MacDiarmid‡

† Department of Physics
‡ Department of Chemistry
Laboratory for Research on the Structure of Matter
University of Pennsylvania
Philadelphia, Pennsylvania 19104

INTRODUCTION

A new class of anisotropic conductors containing metallic chains of mercury atoms has recently been reported.[1] These compounds, with nominal formula Hg_3AsF_6 and Hg_3SbF_6, consist of metallically bonded polymercury cations in a tetragonal lattice consisting of an array of $(AsF_6)^-$ or $(SbF_6)^-$ anions.[2] The mercury chains are situated in nonintersecting channels along the **a** and **b** axes of the tetragonal lattice; there are no chains along **c**. The diffuse scattering sheets observed in x-ray[2] and neutron[3] diffraction studies indicate that there is no phase coherence between the polymercury chains and that the Hg-Hg distance within a chain is 2.64 Å. Since the lattice constant is $a = b = 7.54$ Å, the empirical structural formula (assuming all anion sites are occupied) is $Hg_{2.86}AsF_6$, implying that the mercury atoms in a chain are incommensurate with the unit cell of the tetragonal lattice.

These polymercury cation compounds $Hg_{2.86}AsF_6$ (hereafter $Hg_{3-\delta}AsF_6$) and $Hg_{2.91}SbF_6$ have anisotropic electrical conductivities[4,5] and anisotropic optical properties[6,7] consistent with relatively weak interchain electronic coupling. The $Hg_{3-\delta}AsF_6$ compound remains metallic[4,5,8] to low temperatures with no indication of residual resistance and a linear term in the specific heat,[9] which is unusually large compared to that expected from the electronic density of states.[8] Below 4.1°K, $Hg_{3-\delta}AsF_6$ becomes an anisotropic superconductor in low magnetic fields[5] and exhibits an anisotropic Meissner effect.[10] In this brief review, we focus on $Hg_{3-\delta}AsF_6$, where a wide range of data on the structural and electronic properties are now available.

This brief review emphasizes the recent studies carried out in a collaborative effort at the University of Pennsylvania and with colleagues at Argonne National Laboratory and Brookhaven National Laboratory. The structural studies (see STRUCTURE) were carried out by A. J. Schultz *et al.*[3] at Argonne and by J. M. Hastings *et al.*[11] at Brookhaven. N. D. Miro and associates were primarily responsible for the synthesis, crystal growth, and density measurements[12] (see SYNTHESIS AND CRYSTAL GROWTH). The optical reflectance studies[7] were carried

*Work at the University of Pennsylvania primarily supported by the National Science Foundation MRL Program under grant DMR 76-00678. Synthesis and chemical studies were supported by the National Science Foundation under grant CHE-77-02207-A01. Manuscript received August 31, 1977.

0077-8923/78/0313-0800 $1.75/1© 1978, NYAS

out by D. L. Peebles *et al.* (OPTICAL PROPERTIES). The nmr studies[8] are the work of E. Ehrenfreund and P. R. Newman (NUCLEAR MAGNETIC RESONANCE). The studies of the electrical transport[5] (ELECTRICAL PROPERTIES) are the work of C. K. Chiang *et al.* The measurements of the Meissner effect[10] (ANISOTROPIC MEISSNER EFFECT) were carried out by R. Spal with important contributions on the *ac* susceptibility by C. K. Chiang and A. Denenstein. The reader is referred to the original papers for additional discussion of the results and more detailed experimental data (see Refs. 3, 5, 7, 8, 10–12, 12a, and 16).

STRUCTURE[2,3,11]

The crystallographic structure of the $Hg_{3-\delta}AsF_6$ compound has been determined at room temperature by Brown *et al.*[2] and confirmed by Schultz *et al.*,[3]

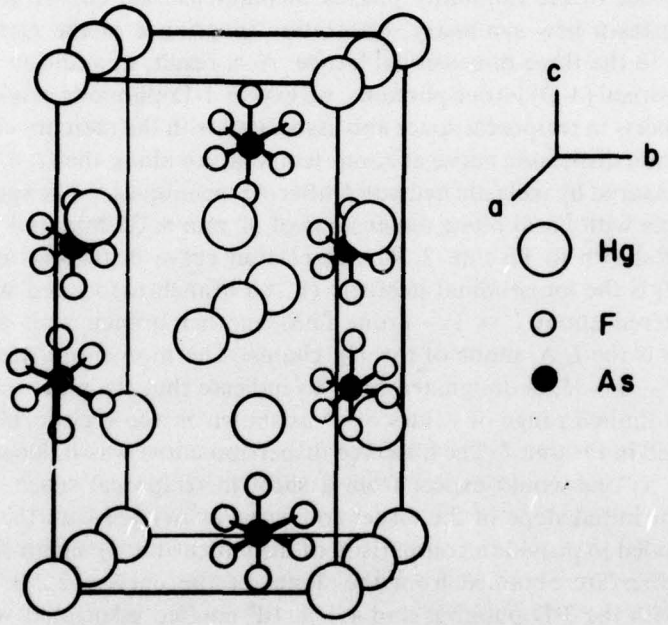


FIGURE 1. View of the crystal structure of $Hg_{2.86}AsF_6$.

using neutron diffraction. This compound has a body-centered tetragonal space group $I4_1/amd$ (D_{4h}^{19}) with four formula units of $Hg_{3-\delta}AsF_6$ per unit cell. It is convenient to separate the lattice into two parts: the host lattice (AsF_6 lattice) and the mercury chains. The host lattice is formed by a body-centered tetragonal array of well-separated AsF_6 octahedra. The mercury chains lie in nonintersecting channels in the [100] and [010] directions, equivalent by tetragonal symmetry. A sketch of the crystal structure is shown in FIGURE 1.

In addition to the Bragg reflections, Brown *et al.*[2] found two sets of equidistant sheets in reciprocal space with very strong diffuse intensity. They associated each direction of diffuse sheet with the corresponding direction of the linear channel in

real space. The diffuse intensity arises from the mercury atoms, and its distribution in a sheet implies that there is no phase coherence between the neighboring chains. These diffuse sheets can therefore be viewed as Bragg reflections from a 1-D lattice. The elastic origin of such scattering was demonstrated by the neutron study of Schultz *et al.*[3]

Important information concerning the spread of the order of the Hg atoms within individual chains can be obtained by measuring the width of the sheet.[11] Elastic neutron scattering scans along the [k00] direction, for different temperatures ranging from room temperature to 30°K, always yield a resolution-limited width of $0.018a^*$ ($a^* = 2\pi/a$ where $a = 7.55$ Å) for the first sheet. Taking this value as a lower bound for the 1-D order along the chain direction, a coherence length in excess of 400 Å or 150 Hg-Hg spacings is obtained.[11] At the scale of the experimental resolution, there is long-range order of the mercury atoms in the chain direction at all temperatures.

The existence of the randomly phased incommensurate chains at room temperature implies a new symmetry, translation invariance of the mercury chains with respect to the three-dimensional lattice. As a result, in addition to the usual three-dimensional (3-D) lattice phonons, we expect 1-D phonons originating from the diffuse sheets in reciprocal space and associated with the mercury chains.

The phonon dispersion curve at room temperature along the $(\zeta, 0, 0)$ direction has been measured by inelastic neutron scattering techniques.[11] The spectrum from a large sample with basal plane dimensions of 32 mm × 32 mm and 2 mm along the c-axis is shown in FIGURE 2. The dispersion curve beginning at the Bragg peak ($\zeta = 2$) is the longitudinal acoustic (L.A.) branch associated with the 3-D lattice. Centered about $\zeta = 3 - \delta$ one finds another branch with a very steep slope, which is the L.A. mode of the Hg chains. The momentum transfer about the point, $\zeta = 3 - \delta$, is designated by X to indicate that the measurements were made over a limited range of values of c^* as shown in the reciprocal lattice diagram included in FIGURE 2. The observed dispersion curve was independent of the value of c^*, as one would expect from a sheet in reciprocal space. The dashed lines, with the initial slope of the dispersion curve associated with the 3-D lattice, have been added to provide a comparison of the lattice and Hg-chain stiffness. The sound velocities are obtained from the slopes of the curves: 2.2×10^5 cm/sec associated with the 3-D phonons and 4.4×10^5 cm/sec associated with the 1-D phonons.

Synthetic metals with anisotropic and/or quasione-dimensional (1-D) electronic properties have been intensely studied in recent years. Examples include the well-known organic metals such as TTF-TCNQ and related derivative salts,[13] KCP and related platinum-chain compounds,[13] as well as $(SN)_x$[13] and the $(SNBr_y)_x$ deriatives.[14] However, the polymercury chain compound, $Hg_{3-\delta}AsF_6$, is a unique example of *elastic* one-dimensionality, with the 1-D phonon spectrum[11] resulting directly from the incommensurate chain structure.

Analysis of the crystal growth[12,12a] leads to the conclusion that mass transport of the mercury atoms occurs along the chain channels at room temperature. Thus the atoms are mobile, and the presence of interchain interactions can be expected to lead to phase ordering of the mercury chains at lower temperatures. On cooling, a progressive phase ordering between mercury chains has been found through elastic neutron scattering studies. Short-range order gradually builds up, with

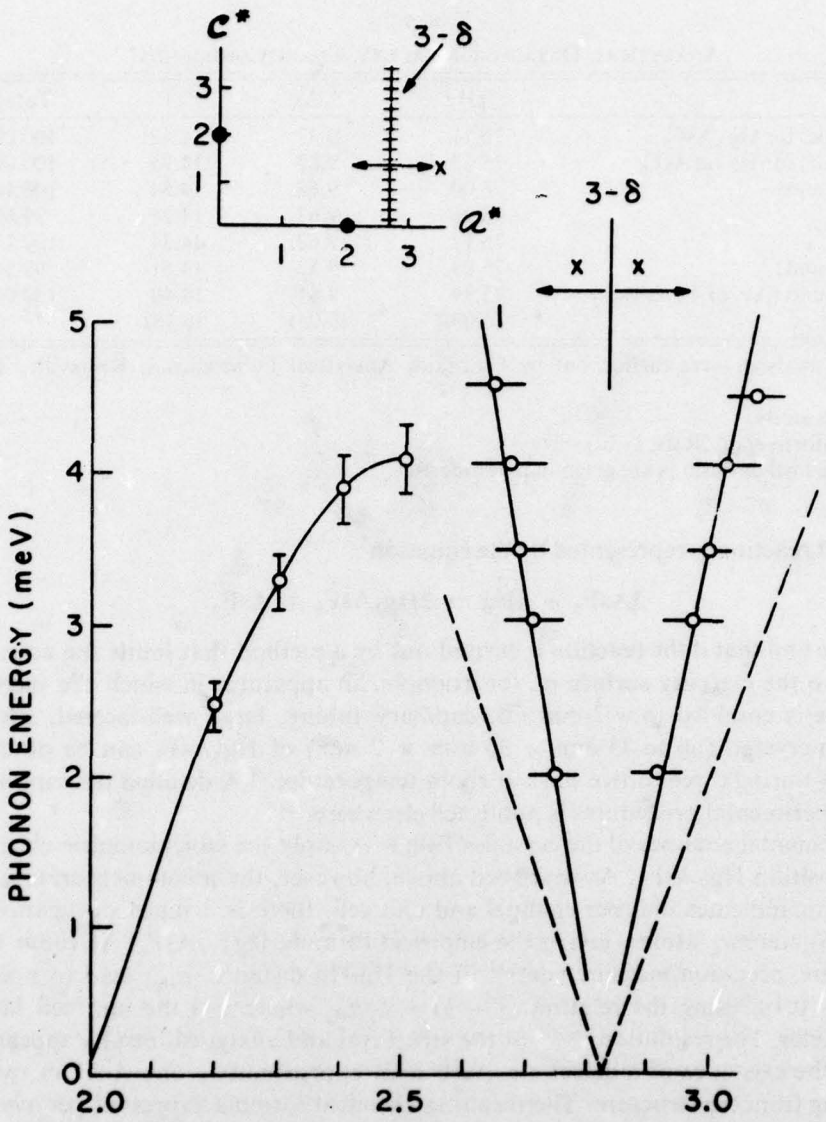


FIGURE 2. Room-temperature phonon-dispersion curve. The inset at the top is a diagram of the a^*c^* plane, showing the location of the $(3-\delta)$ sheet. The dispersion curve associated with the Hg chains centered about $\xi - 2.82$ was measured for various values of x, i.e., $(\xi, 0, x)$.

transverse coherence lengths of a few lattice constants, as a result of parallel chain-chain interactions. At 120°K, the competing orthogonal chain-chain interaction leads to three-dimensional order and a phase-ordering phase transition.

SYNTHESIS AND CRYSTAL GROWTH[1-3,12,-2a]

Cutforth,[1] Cutforth *et al.*,[1a] and Brown *et al.*[2] have described the synthesis of $Hg_{3-\delta}AsF_6$ by the reaction of mercury with a solution of AsF_5 in liquid SO_2. The

TABLE 1
ANALYTICAL DATA FOR MERCURY CHAIN COMPOUNDS*

	%Hg	%As	%F	Total
Calc. for Hg_3AsF_6	76.11	9.47	14.42	100.00
Calc. for $Hg_{2.86}AsF_6$	75.23	9.82	14.95	100.00
Found†	76.00	9.62	14.54	100.16
	75.96	9.67	14.25	99.88
	76.17	9.62	14.34	100.13
Found‡	75.83	9.52	14.61	99.96
Found (Av. of 4 analyses)	75.99	9.61	14.44	100.04
	(0.09)§	(0.05)	(0.15)	

*All analyses were carried out by Galbraith Analytical Laboratories, Knoxville, Tenn. 37921.
†This study.
‡Cutforth *et al.* (Refs. 1, 1a).
§Standard deviations are given in parenthesis.

overall reaction is represented by the equation

$$3AsF_5 + 6Hg \rightarrow 2Hg_3AsF_6 + AsF_3.$$

We find that if the reaction is carried out by a method that limits the access of AsF_5 to the mercury surface in, for example, an apparatus in which the mercury surface is confined in a 2-mm i.d. capillary tubing, large well-faceted, silvery-golden crystals (up to 35 mm × 35 mm × 2 mm) of Hg_3AsF_6 can be obtained readily during three to five days at room temperature.[14] A detailed description of the experimental procedures is published elsewhere.[12a]

Elemental analyses of the crystals (TABLE 1) imply the stoichiometric chemical composition Hg_3AsF_6. As described above, however, the incommensurate chain structure indicates that per channel and unit cell, there is a mean occupation of $(3 - \delta)$ mercury atoms, giving the empirical formula $Hg_{3-\delta}AsF_6$. At room temperature, precision measurements[11] of the Hg-Hg distance, a_{Hg}, lead to a value of $\delta = 0.18$, using the relation $(3 - \delta) = a/a_{Hg}$ where a is the unit cell lattice parameter. The resolution[3,12,12a] of the structural and analytical results appears to be in the existence of a defect structure with approximately one AsF_6 in twenty missing from the structure. The resulting chemical formula expressed per average unit cell would be $Hg_{2.82}AsF_{6_{0.94}}$. Density measurements[12,12a] have confirmed this picture. The measured density is found to be $\rho_{meas} = 7.05 \pm .01$ g/cm^3 in close agreement with the calculated value $\rho_{calc} = 7.04$ g/cm^3 based on the known structure and the above formula. An alternative suggestion of 6% excess Hg disordered in the lattice would lead to a density of 7.49 gm/cm^3. Thus, the mercury chain salt is evidently a stoichiometric compound in an incommensurate structure.

OPTICAL PROPERTIES[7]

Polarized reflectance studies from single crystal faces of anisotropic $Hg_{3-\delta}AsF_6$ were carried out. The results indicate metallic behavior for electronic excitations along the chains in the a–b plane) with free electron Drude theory giving a

satisfactory initial description of the data. The plasma frequency is found to be $\hbar\omega_p = 4.8$ eV and, combined with the electron density, yields a free electron optical conductivity in the a–b plane at room temperature is $\sigma_{opt} = (4\pi)^{-1}\omega_p{}^2\tau \simeq 10^4(\Omega\text{-cm})^{-1}$ in good agreement with the measured dc value. The results of studies of reflectance from crystal faces at an angle with the **a**–**b** plane have been analyzed in terms of normal incidence reflectance from an anisotropic medium in which $\epsilon_{ab}(\omega)$ is the Drude dielectric function characteristic of simple metallic behavior and ϵ_c is constant (ϵ_{ab} refers to light polarized in the **a**–**b** plane defined by directions of the two sets of Hg chains; ϵ_c refers to light polarized along **c** and perpendicular to both sets of chains).

$$\epsilon_{ab}(\omega) = \epsilon_\infty - \frac{\omega_p{}^2}{\omega^2 + i\omega/\tau} \tag{1a}$$

$$\epsilon_c(\omega) = \epsilon_\infty \tag{1b}$$

where ϵ_∞ is the core dielectric constant, $\omega_p{}^2 = 4\pi Ne^2/m^*$ is the square of the plasma frequency with N the number of free electrons per unit volume, m^* the effective mass, and τ the electron scattering time.

The results are summarized in FIGURES 3a and 3b. FIGURE 3a shows a fit (dashed curve) to the **a**–**b** plane reflectance (solid curve) using the Drude dielectric function (**1a**) in the Fresnel Equation for normal incidence reflectance.

$$\mathcal{R} = \frac{|\epsilon| + 1 - [2(|\epsilon| + \epsilon_1)]^{1/2}}{|\epsilon| + 1 + [2(|\epsilon| + \epsilon_1)]^{1/2}} \tag{2}$$

where $\epsilon = \epsilon_1 + i\epsilon_2$. To obtain the dashed curve a least square fit was carried out arbitrarily restricting the input to the range 1.3 eV–4.2 eV. The free parameters

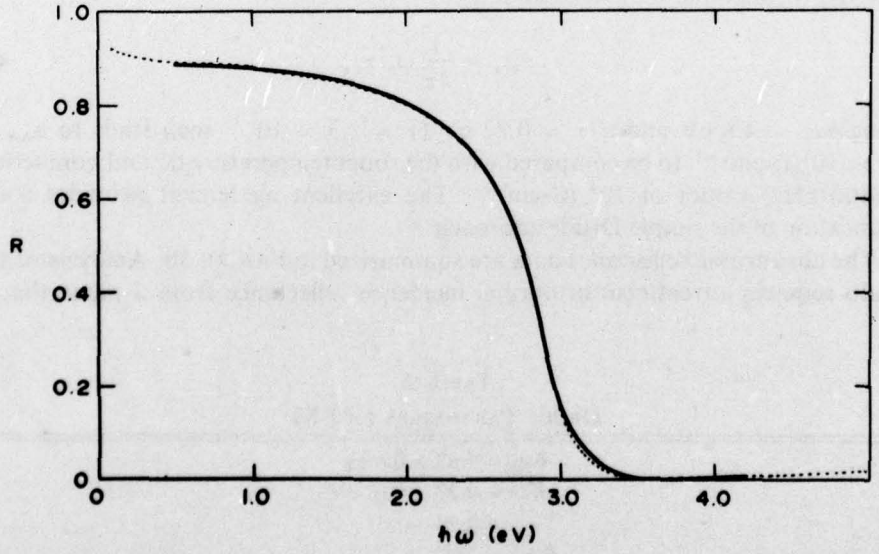


FIGURE 3a. Drude fit (dashed line) to the **a**–**b** face reflectance (solid line). The experimental curve represents the raw data with a uniform $\frac{1}{2}$% subtracted.

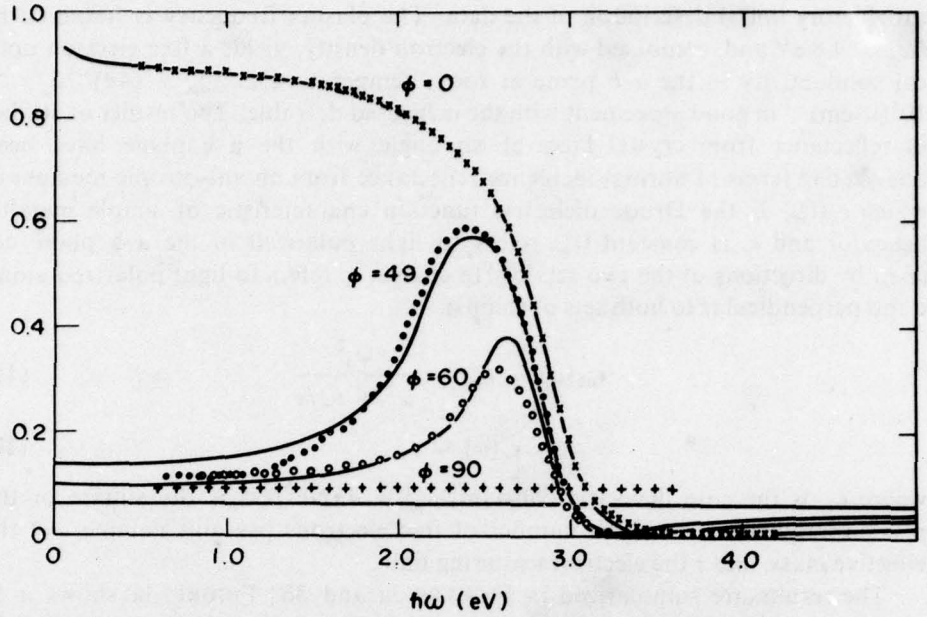


FIGURE 3b. Normal incidence reflectance of the anisotropic faces. The solid curves are calculated by the parameters in TABLE 1. There are no additional parameters.

were ω_p, ϵ_∞, and τ, since the absolute reflectance was determined by a wide-angle photovoltaic detector. Trial fits with a 1% change in reflectance gave only small changes in parameters. The results are summarized in TABLE 2.

The values for ω_p and τ can be used to obtain a measure of the optical conductivity through the standard relation

$$\sigma_{\text{opt}} = \frac{1}{4\pi}\omega_p^2\tau. \tag{3}$$

Using $\hbar\omega_p = 4.8$ eV and $\hbar/\tau = 0.27$ eV ($\tau = 2.3 \times 10^{-15}$ sec.) leads to $\sigma_{\text{opt}} = 1.2 \times 10^4(\Omega\text{-cm})^{-1}$, to be compared with the room temperature dc and contactless ac (100 kHz) values of 10^4 $(\Omega\text{-cm})^{-1}$. The excellent agreement provides some justification of the simple Drude approach.

The anisotropic reflectance data are summarized in FIGURE 3b. Analysis of the results requires a treatment of normal incidence reflectance from a plane that is

TABLE 2

DRUDE PARAMETERS (300°K)

$\hbar\omega_p = 4.82 \pm 0.6$ eV
$\hbar/\tau = 0.27 \pm 0.01$ eV
$\epsilon_\infty = 2.70 \pm .55$
$\dfrac{\hbar\omega_p}{\epsilon_\infty^{1/2}} = 2.93 \pm .03$

not coincident with the principal optical axes of the solid. For a uniaxial (tetragonal) crystal, the dielectric tensor is defined

$$\epsilon = \begin{pmatrix} \epsilon_{ab} & 0 & 0 \\ 0 & \epsilon_{ab} & 0 \\ 0 & 0 & \epsilon_c \end{pmatrix} \tag{4}$$

where $\epsilon_{ab} = \epsilon_c - \omega_p^2/(\omega^2 + i\omega/\tau)$ corresponds to the dielectric function along the chains, and $\epsilon_c = \epsilon_\infty$ corresponds to the assumed constant perpendicular value. The anisotropic reflectance can be calculated directly from the dielectric tensor in terms of ϵ_{ab} and ϵ_c. The theoretical results for $\mathcal{R}(\varphi, \omega)$ are shown in FIGURE 3b, using the parameters from TABLE 2 for ω_p, ϵ_∞, and τ. FIGURE 3b presents a direct comparison of the theoretical curves to the data with *no additional parameters*. The overall good qualitative and quantitative agreement provides additional confirmation of the validity of the simple one-dimensional Drude treatment of this anisotropic metal.

NUCLEAR MAGNETIC RESONANCE[8]

Nuclear magnetic resonance (nmr) is a measure of the local susceptibilities at the sites of the nuclei and may be used as a probe of the respective amplitudes of the conduction-electron wave function at the the various sites. The Knight shift and the spin-lattice relaxation are related to the Fermi surface parameters of the metal and can yield information about the static and dynamic properties of the conduction electrons. The experimental results of the ^{19}F and ^{199}Hg nuclear spin-lattice relaxation rates and the ^{199}Hg Knight shift are therefore of fundamental importance in the description of the electronic structure of this novel synthetic metal.

We show in FIGURE 4 the ^{199}Hg Knight shift measured at 7.0 MHz as a function of temperature. Within the experimental accuracy the ^{199}Hg Knight shift has no temperature dependence in the range 1.5–300°K. Measurements of $K(^{199}Hg)$ at 4.4 and 10 MHz showed similar temperature independence, and their values at 4.2°K are also shown in FIGURE 4. Thus the ^{199}Hg shift is +1.9% independent of magnetic field and temperature.

The nuclear spin-lattice relaxation rate $1/T_1$ is proportional to the temperature both for the ^{199}Hg line and for the ^{19}F line. However, $[T_1(^{19}F)T] = 340$ sec K, whereas $[T_1(^{199}Hg)T] = 7.5 \times 10^{-3}$ sec K; a ratio of approximately 5×10^4.

The overall features are characteristic of metals. Furthermore, since K and (T_1T) measure the local fields at the nucleus, comparison of the ^{199}Hg and ^{19}F relaxation rates would give direct information about the spatial distribution of the conduction-electron wave functions. In the metallic system $Hg_{3-\delta}AsF_6$, the ratio between the relaxation rates can be written as

$$\frac{[T_1(^{19}F)]^{-1}}{[T_1(^{199}Hg)]^{-1}} = \left[\frac{\gamma(^{19}F)\langle\psi_F^2(0)\rangle}{\gamma(^{199}Hg)\langle\psi_{Hg}^2(0)\rangle}\right]^2, \tag{5}$$

where $\langle\psi_i^2(0)\rangle$ (i = F or Hg) is the mean square (at the nucleus i) of the con-

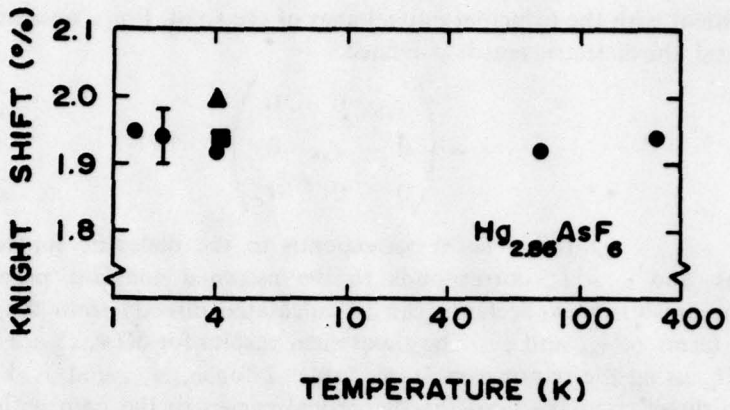


FIGURE 4. The ^{199}Hg Knight shift vs. temperature at an external field of 9.5 kOe (○). At 4.2°K, data for 5.6 kOe (△) and 12.9 kOe (□) are shown for comparison. A representative error bar is shown for the 2.1°K data point.

duction-electron wave function at the Fermi energy. Comparing the two rates at 4.2°K, we obtain $\langle\psi_F^2(0)\rangle / \langle\psi_{Hg}^2(0)\rangle \approx 10^{-3}$, indicating that the conduction electrons reside primarily on the mercury chains. Thus one may expect the metallic properties to be dominated by electronic band structure originating from the mercury electrons.

The Knight shift in metals may be written as

$$K \equiv \Delta H/H_{res} = \mu_B^{-1} H_{hfs} \chi, \tag{6}$$

where χ is the susceptibility per atom and H_{hfs} is the hyperfine field, which for s electrons is given by $H_{hfs} = (8\pi/3)\mu_B \langle\psi^2(0)\rangle$ and $\psi^2(0)$ is normalized in an atomic volume. The temperature independence of $K(^{199}\text{Hg})$ thus shows that the susceptibility is temperature independent in the range 1.5–300°K and in external magnetic fields ranging from 5.6 to 13 kOe in agreement with direct measurements of the susceptibility, using a Faraday balance.[9] The hyperfine field for the 6s electrons for the free mercury atom is estimated as $H_{hfs}^{at.} = 25.8 \times 10^8$ Oe. In the solid, the 6s wave functions have a greater spatial extent than in the atom, and thus a somewhat smaller hyperfine field (say, 20×10^6 Oe) is expected. Assuming that all of $K(^{199}\text{Hg})$ arises from the mercury 6s electrons, we obtain for the magnetic susceptibility of the conduction electrons: $\chi = 1.5 \times 10^{-5}$ cm^3 per mole of $Hg_{2.86}AsF_6$ units. Assuming no enhancement of the Pauli susceptibility $\chi = 2\mu_B^2 N(0)$, we obtain for the density of states at the Fermi energy, $N(0) \cong 8 \times 10^{-2}$ per eV per Hg atom for single-spin direction.

The nuclear relaxation rate in metals is related to the Knight shift via the Korringa relation

$$(4\pi k_B)^{-1} \hbar (\gamma_e/\gamma_N)^2 / K^2 T_1 T = \xi, \tag{7}$$

where $\xi = 1$ for a free-electron metal. When the electron-electron interaction is included, $\xi = K(\alpha) > 1$, and the relaxation rate is "enhanced." Here, α is the Stoner enhancement factor of the Pauli susceptibility. When electrons other than s electrons contribute to K and T_1 via core polarization, for instance, $\xi < 1$,

the relaxation is "reduced." For $Hg_{3-\delta}AsF_6$, we find that $\xi > 1$ and that it depends on the external magnetic field increasing from $\xi = 2.0$ at 5.6 kOe to $\xi = 3.0$ at 12.9 kOe. Thus, the relaxation rate is enhanced (over that expected from the simple Korringa relation), and it is field dependent.

For anisotropic quasione-dimensional metals, enhancement of 2–3 as observed here may perhaps arise from the Coulomb enhancement factor $K(\alpha)$ even for $\alpha \ll 1$. For instance, when two pieces of the Fermi surface are nested [as is the case in a one-dimensional (1-D) metal], $K(\alpha)$ may assume a large value at $k_BT \ll E_F$, even for $\alpha \ll 1$. However, since no magnetic transition is observed in this substance down to 1.2 K, it is likely that $K(\alpha) \approx 1$ and that the field dependence of the enhancement is not the result of a Coulomb-enhanced relaxation rate.

A field dependence of the (enhanced) nuclear relaxation rate has been observed in 1-D metallic systems like tetrathiafulvalene-tetracyanoquinodimethane (TTF-TCNQ), quinolinium $(TCNQ)_2$, and so on. However, in contrast to the present case of $Hg_{3-\delta}AsF_6$, T_1^{-1} in those systems increases as the magnetic field is decreased because of the $\omega^{-1/2}$ dependence of the 1-D diffusive spin-correlation functions at long wavelength. Thus it appears that the field dependence of $[T_1(^{199}Hg)]^{-1}$ is special for $Hg_{3-\delta}AsF_6$ and that related field-dependent quantities such as the conductivity may be playing a role.

Above ~100°K, the fluorine relaxation rate $[T_1(^{19}F)]^{-1}$ deviates from the Korringa law ($T_1^{-1} \propto T$) and increases much more rapidly as the temperature is increased (FIGURE 5), reaching a maximum at ~220°K and then decreasing as the temperature is further increased. This behavior can be understood in terms of mechanical rotation of the AsF_6^- octahedra. Assuming that this rotation is described by a single (temperature-dependent) correlation time τ_c, the dipolar coupling between the ^{19}F spins leads to the following expression for $T_1(^{19}F)$

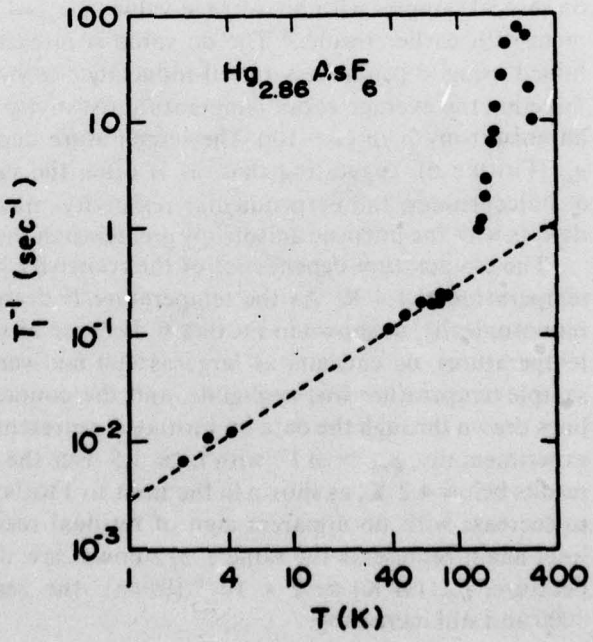


FIGURE 5. $[T_1(^{19}F)]^{-1}$ vs. temperature on a log-log scale for $Hg_{2.86}AsF_6$ at 10 MHz. The broken line represents a Korringa law $T_1^{-1} \propto T$.

$$[T_1(^{19}\mathrm{F})]^{-1} = \frac{6}{5}\frac{[\gamma(^{19}\mathrm{F})]^4\hbar^2}{b_F^6}\left[\frac{\tau_c}{1+\omega^2\tau_c^2}+\frac{4\tau_c}{1+4\omega^2\tau_c^2}\right], \qquad (8)$$

where b_F is the shortest distance between two neighboring ^{19}F nuclei. At $\omega = 2\pi \times 10^7$ sec^{-1}, the maximum of $[T_1(^{19}\mathrm{F})]^{-1}$ occurs at $T \cong 220$°K, which corresponds to $\tau_c(220°\mathrm{K}) \cong 0.6\,\omega^{-1} = 9.5 \times 10^{-9}$ sec. Below 220°K, the exponentially decreasing $[T_1(^{19}\mathrm{F})]^{-1}$ suggests that τ_c may be described by a single activation energy: $\tau_c = \tau_0 \exp(\Delta U/k_B T)$ with $^{13}\Delta U/k_B \cong 1900$°K. The value of $[T_1(^{19}\mathrm{F})]^{-1}$ at the maximum (~ 80 sec^{-1}) yields a value 2.30 Å for b_F which, when compared to the minimal F-F distance (2.35 Å), gives quantiative support for the above analysis. This relaxation process is thus ineffective at low temperatures, and therefore the relatively weak Korringa process is observable.

The nmr results thus indicate that the conduction electrons are mainly confined to the mercury chains, and their wave functions do not spread much outside these chains onto the AsF_6^- anions. A two-dimensional network of interpenetrating weakly interacting linear chains of conduction electrons is implied. A simplified band structure for this network has been modeled[8] with the conclusion that even for relatively strong interchain parameters the Fermi surface remains essentially "one-dimensional"; i.e., large pieces of the surface are flat and perpendicular to the k_x and k_y axes.

Electrical Properties[5]

The electrical resistivity in the **a–b** plane is isotropic in agreement with the structural observations of two sets of perpendicular chains in the **a–b** plane and overall tetragonal symmetry. Room-temperature values for ρ_{ab} were reproducible on several samples with an average value of $\rho_{ab} = 1 \times 10^{-4}$ Ω-cm in good agreement with earlier results.[4] The dc value is in excellent agreement with that obtained using a contactless rf self-inductance technique (100 kHz). Along the **c** direction the average room temperature resistivity is 7×10^{-3} (Ω-cm), indicating an anisotropy $\rho_c/\rho_{ab} \sim 10^2$. The temperature dependence of ρ_c follows that of ρ_{ab} (Figure 6), suggesting that, as is often the case in the anisotropic layered dichalcogenides, the perpendicular resistivity may be determined by structural defects with the intrinsic anisotropy greater than the measured value.

The temperature dependence of the resistivity has been measured from room temperature to 1.4°K. As the temperature is decreased, the resistivity decreases monotonically, as shown in Figure 6. Because of the very small resistivity at low temperatures, dc currents as large as 400 ma were required; any effect on the sample temperature was negligible, and the contacts remained ohmic. The solid lines drawn through the data on Figure 6 represent a 3/2-power law dependence; experimentally, $\rho_{ab} \simeq AT^n$ with $n \simeq 1.5$ over the entire temperature range. The results below 4.2°K, as shown in the inset to Figure 6, indicate that ρ_{ab} continues to decrease with no apparent sign of residual resistivity. The solid curve in the inset again represents the same T 3/2-power law dependence. At the lowest temperature, $\rho_{ab}(1.4°\mathrm{K}) \simeq 2 \times 10^{-8}$ (Ω-cm); the resistivity ratio is in excess of 3000 and still increasing.

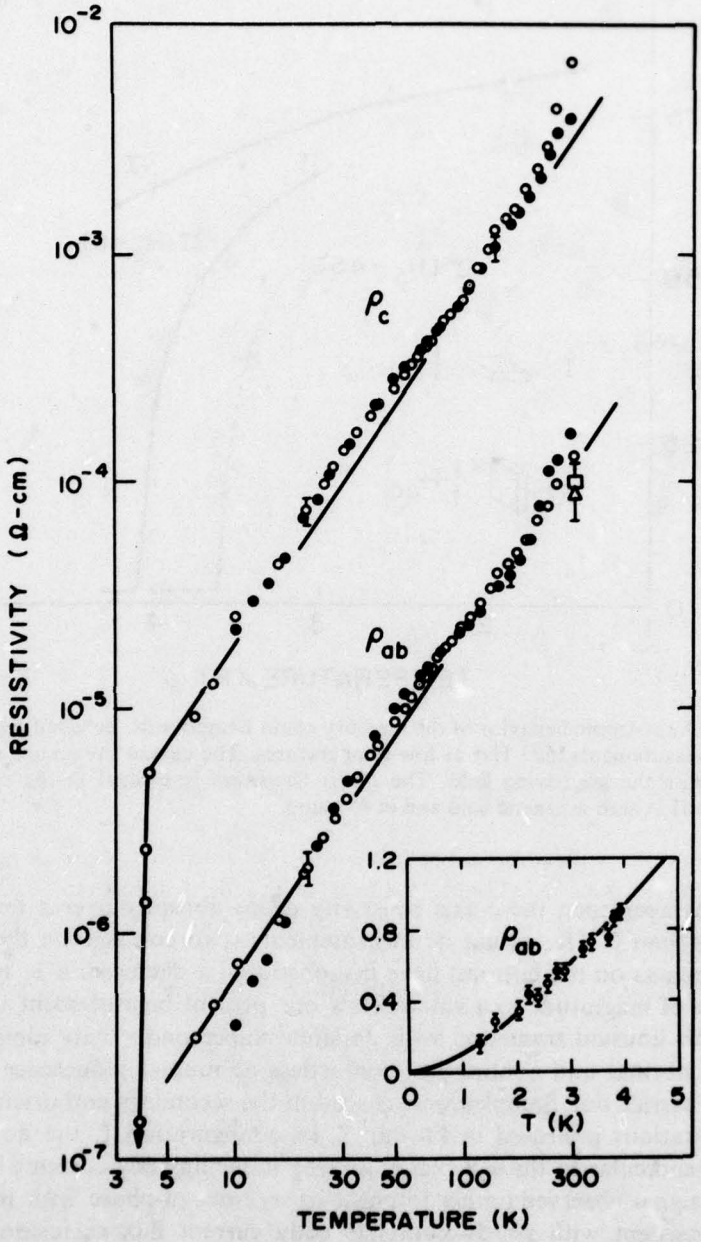


FIGURE 6. Temperature dependence of the resistivity of the mercury-chain compounds. The solid line represents a 3/2-power law dependence for comparison. Inset shows the data below 4.2°K; the solid curve is a 3/2-power temperature dependence. Open and closed circles represent two independent samples (data are normalized at 77°K to the average). Values for ρ_{ab} (300°K) obtained from optical studies (□) and contactless ac measurements (△) are also shown.

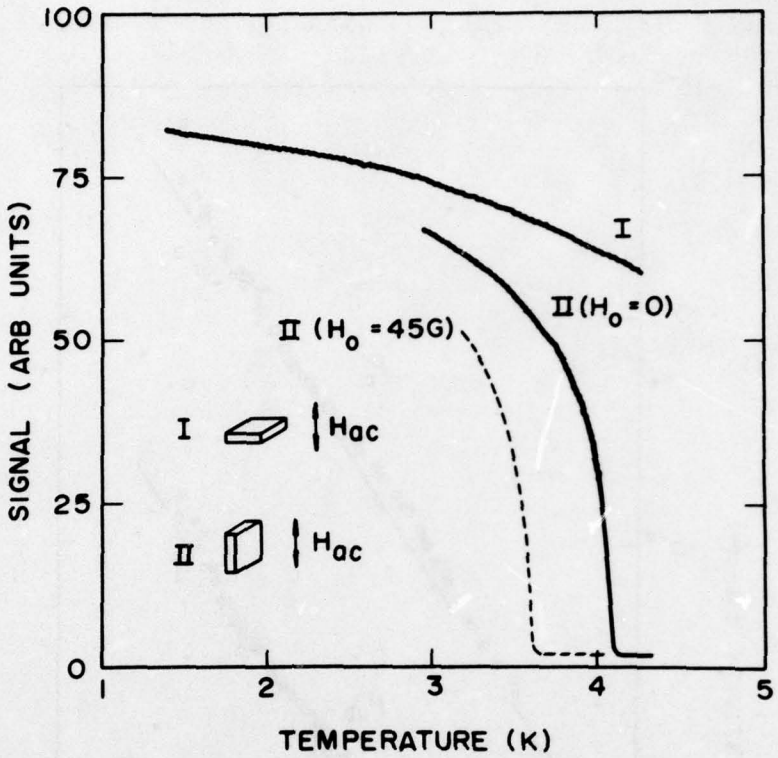


FIGURE 7. Anisotropic behavior of the mercury chain compounds, detected by ac mutual inductance measurements (523 Hz) at low temperatures. The curves shown are $\pi/2$-out-of-phase (ΔL) with the ac driving field. The *c*-axis transition is evident in the curves from configuration II in zero magnetic field and in 45 gauss.

At low temperature, the *c*-axis resistivity drops abruptly over a temperature interval less than 0.2°K; actual dc measurements (two contacts on the top face and two contacts on the bottom) have demonstrated a decrease in ρ_c by at least three orders of magnitude to a value below our present measurement capability. To verify this unusual transition with apparent superconductivity along c while ρ_{ab} remains normal and continuous, contactless ac mutual inductance measurements were carried out. Samples were placed in the secondary coil oriented in the two configurations indicated in FIGURE 7. In configuration I, the ac magnetic field is perpendicular to the a–b plane, thereby inducing eddy currents in the a–b plane. The signal observed (either in-phase or $\pi/2$-out-of-phase with the driving field) is consistent with nearly complete eddy current flux exclusion resulting from the high a–b plane conductivity. The signal is continuous as a function of temperature with temperature dependence consistent with that observed in the dc measurements. In configurationII, the ac magnetic field is in the a–b plane, thus driving current along the c-direction. Above the transition, because of the relatively large value of ρ_c, the signal is near zero. At the transition ρ_c drops abruptly, and the signal rises consistent with complete eddy current flux exclusion.

The effect of a small magnetic field on the sample is alwo shown in FIGURE 7. The resistance is suppressed to lower temperatures, indicating the existence of a

critical magnetic field. The critical field transition has been observed directly by varying the magnetic field at fixed temperature with the dc techniques. The measured critical field at 1.4°K is 380 G.

The normal state resistivities exhibit a large and unusual magnetoresistance, as shown in FIGURES 8a and 8b. Typical curves of the change in resistance as a function of magnetic-field strength are shown in the inset to FIGURE 8a for the two different configurations shown schematically. Configuration A is primarily sensitive to ρ_{ab}, configuration *B* is primarily sensitive to ρ_c; however, we plot in FIGURES 8a and 8b the actual measured resistances, and not analyzed resistivities. The temperature dependence of $\Delta R/R(0) = [R(10\text{ kG}) - R(0)]/R(0)$ as plotted in FIGURE 8a shows that a large and strongly increasing magnetoresistance effect is observed below 30°K. The strong temperature dependence shown in FIGURE 8a arises completely from the temperature dependence of ρ_{ab} and ρ_c, since the measured values of $\Delta R = [R(10\text{ kG}) - R(0)]$ are temperature independent, whereas the magnitude, for example, of ρ_{ab} decreases by more than an order of magnitude on cooling from 26°K to 4.2°K.

The angular dependence of the magnetoresistance at 1 kG is shown in FIGURE 8b, using the two different probe configurations of FIGURE 8a with correspondingly different current flow patterns. The two curves have similar magnitude and identical symmetry with $\Delta R/R$ maximum for $\mathbf{H} \| \mathbf{c}$. The magneto-

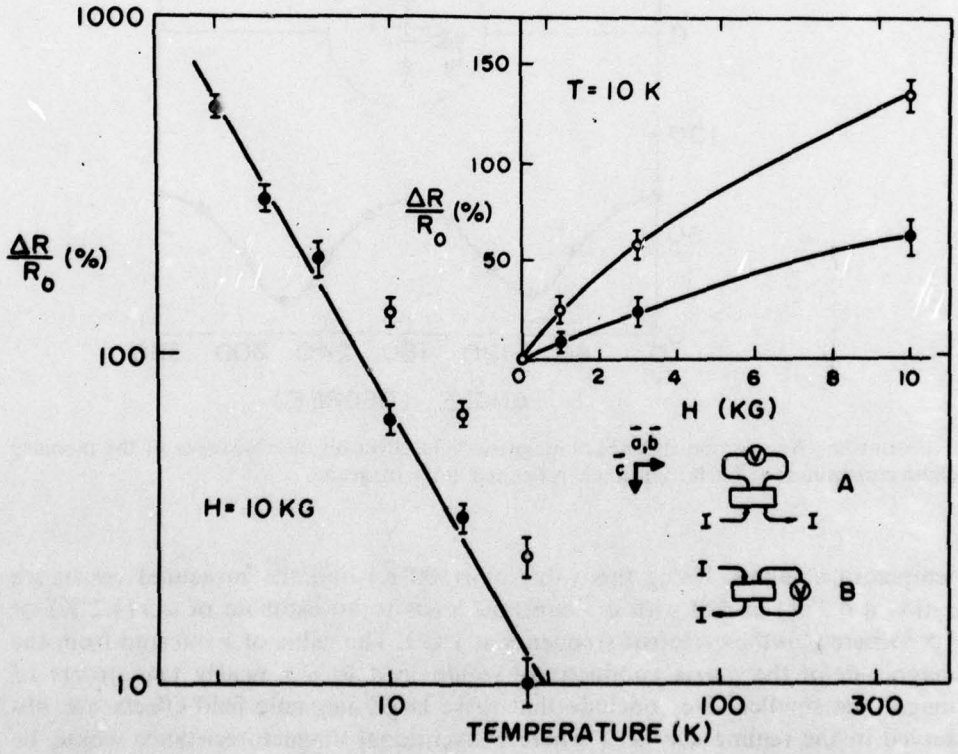


FIGURE 8a. Effects of magnetic field on the resistance of the mercury-chain compounds; $\Delta R(10\text{ kG})/R(0)$ vs. temperature for the two configurations shown in the sketch. The inset shows *R* vs. *H* at 10°K for both configurations.

resistance appears to be independent of the orientation of the field with respect to the direction of primary current flow, implying that the effect does not result directly from the Lorentz force. This is consistent with the nonquadratic dependence shown in the inset to FIGURE 6a.

As described above, the optical reflectance data have been analyzed to obtain the plasma frequency, $\hbar\omega_p = 4.8$ eV, and the mean free scattering time, $\tau = 2.3 \times 10^{-15}$, implying a room temperature optical conductivity, $\sigma_{opt} = (4\pi)^{-1}\omega_p^2\tau = 1.2 \times 10^4\ (\Omega\text{-cm})^{-1}$, in excellent agreement with the directly measured room-

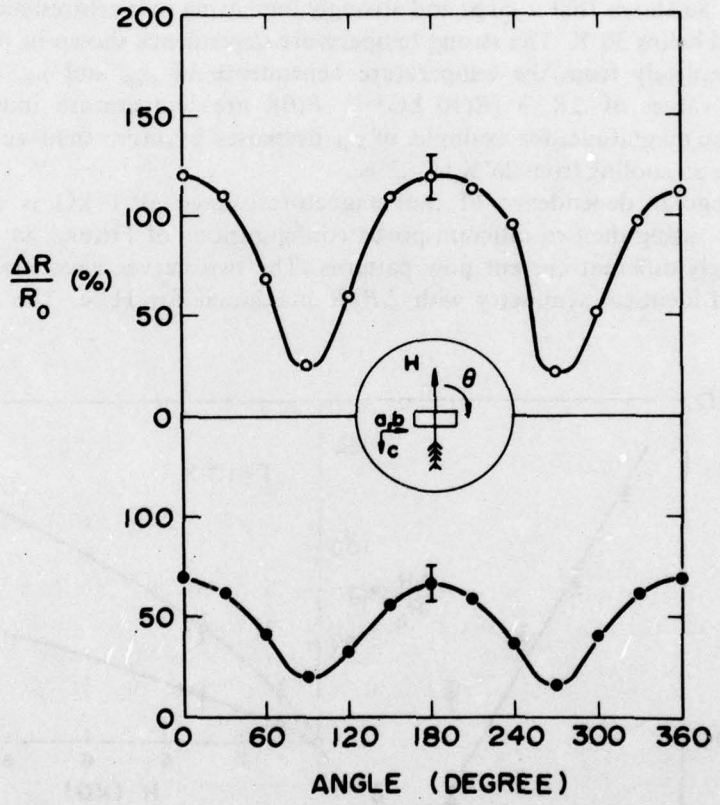


FIGURE 8b. Angular dependence of magnetic field effect on the resistance of the mercury chain compounds at 4.2°K. The angle is defined in the diagram.

temperature values. Using this value of $\tau(300°K)$ and the measured resistance ratio (at 4.2°K) of 500 with ω_p^2 constant leads to an estimate of $\omega_c\tau(4.2°K) \simeq 10^{-2}$ where ω_c is the cyclotron frequency at 1 kG. The value of τ inferred from the magnitude of the c-axis conductivity would lead to $\omega_c\tau$ nearly two orders of magnitude smaller. We conclude that these large magnetic field effects are observed in the regime $\omega_c\tau \ll 1$ where conventional magnetoresistance would be small.

The apparent absence of residual resistivity, the unusual temperature dependence, and the large magnetoresistance, may be intimately related. The approach

toward saturation of R vs H as shown in FIGURE 8a, coupled with the observation that $\Delta R(T) = [R(10\text{ kG}) - R(0)]$ is independent of temperature, can be interpreted as arising from a residual resistance that is field dependent going to smaller values, perhaps even to zero, as $H \rightarrow 0$. It is interesting to speculate on the possibility that one-dimensional fluctuation phenomena associated with the incommensurate Hg chains might be playing a role. The observation of a Meissner effect[10] (See ANISOTROPIC MEISSNER EFFECT) in the presence of finite **a**–**b** plane resistivity provides additional evidence of an extended fluctuation regime.

In approaching the question of the *c*-axis superconductivity, the possibility of metallic Hg filaments must be considered, particularly since the observed transition is close to that of free Hg (4.15°K). Superconductivity along **c** with ρ_{ab} normal and continuous would require thin filaments running straight along the *c*-axis (any change in ρ_{ab} at the transition is no greater than a few per cent). Submicron-diameter filaments would lead to a broadened transition and large (nonbulk) values for H_c. In the low-frequency ac experiments, the eddy currents sample an effective volume equal to about 80% of the total volume at the peak in ΔR, so that surface effects and small-volume filaments should not dominate. In an attempt to detect filaments, we set the external field within 30 G of H_c and applied a current of 0.5 A through a crystal (area of 0.2 cm^2) without driving the sample normal.

It is known that $Hg_{3-\delta}AsF_6$ reacts with air liberating free Hg. Accordingly, we have attempted to detect free Hg in the samples. In our initial experiments, three samples were studied: Sample 1 was sealed in a glass container for ac measurements without prior handling, Sample 3 was visibly surface-tarnished because of handling over a period of weeks in the course of performing dc measurements, and Sample 2 was intermediate. Careful examination with the ac technique, using configuration I (see FIGURE 7) and high amplification, showed a small step at 4.15°K (width less than .01°K) for samples 2 and 3 consistent with a Meissner effect from 5×10^{-4} of the sample volume and 2×10^{-3} of the sample volume, respectively. Sample 1 showed no effect, setting an upper limit of 10^{-4} volume fraction of mercury (the current limit of our detectability). However, detailed temperature scans of the *c*-axis phase transition in these samples showed that all features were unchanged and separated in temperature from the weak free Hg Meissner effect (when observed). We have observed the *c*-axis transition in many samples from different single-crystal growths, in some cases using freshly prepared beautiful silvery-golden crystals, in others, crystals more than a year old with tarnished surfaces, and in powdered samples. In every case, the transition was observed. Our preliminary conclusion, based on the above facts and related data is that the observed *c*-axis superconductivity is consistent in all respects with a bulk effect. The most convincing and direct evidence, however, comes from studies of the Meissner effect.

ANISOTROPIC MEISSNER EFFECT[10]

Magnetization measurements on single crystals and powders of $Hg_{3-\delta}AsF_6$ show flux expulsion when samples are cooled in a small magnetic field, indicating superconductivity below 4.1°K. The observation of anisotropic flux expulsion with magnitude dependent upon the orientation of the external field with respect to the

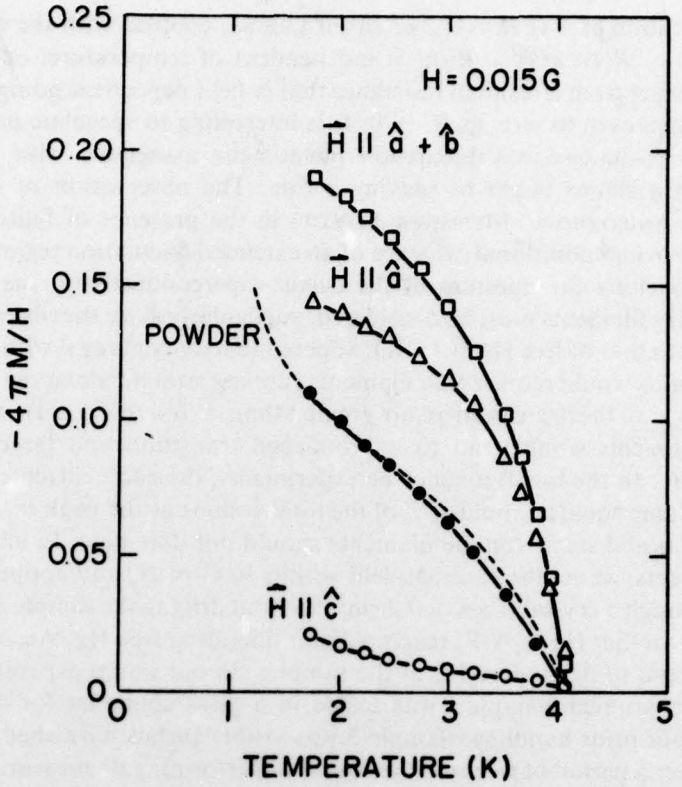


FIGURE 9. Temperature dependence of $(-4\pi M/H)$ at $H = 0.015$ G for single crystals and a powder sample. The dashed curve represents the ac susceptibility ($\nu = 500$ Hz) data for the powder sample.

crystalline axes confirms the anisotropic superconductivity discovered in conductivity measurements.

The Meissner effect was observed on single-crystal samples and on powders. In each case, the sample was cooled in a constant external field, and the induced magnetic moment was measured with a SQUID magnetometer. The magnetization results differ from the usual Meissner effect in three respects. First, the flux expulsion is anisotropic; i.e., the magnitude depends strongly on the orientation of the applied field with respect to the crystalline axes. Second, the temperature dependence of the flux expulsion is not a step function, but rather a continuously increasing function for $T < T_c$. Third, $(-4\pi M/H)$ is field dependent even at fields less than 10^{-4} of the thermodynamic bulk critical field.

The data for $(-4\pi M/H)$ are shown in FIGURE 9 for an applied magnetic field of $H_0 = 0.015$ gauss. When the external field is applied in the crystallographic **a**–**b** plane, a large temperature-dependent diamagnetism is observed, indicative of 20% flux expulsion at 1.6°K in 0.015 gauss. Even at $T/T_c < 0.5$, the magnitude is increasing toward larger values. For $\mathbf{H} \| \mathbf{c}$, the onset of flux expulsion occurs at precisely the same temperature. However, as shown in FIGURE 9, the measured

magnetic moment is more than an order of magnitude (approximately a factor of 15) smaller with $\mathbf{H} \parallel \mathbf{c}$ than with $\mathbf{H} \parallel \mathbf{a}$.

A smaller anisotropy is observed in the **a**–**b** plane. Measurements with H = 0.015 G applied along a (110) direction, $\mathbf{H} \parallel (\mathbf{a} + \mathbf{b})$, gave results approximately 25% larger than for $\mathbf{H} \parallel \mathbf{a}$. Demagnetization corrections estimated from the sample shapes and measured magnetization are less than about 5%.

In addition to single crystal studies, we have carried out measurements on fine- and coarse-powdered samples. We find that in all cases the data from powdered samples are consistent with a simple powder average, $M(\text{powder}) \simeq 1/3M(\mathbf{H} \parallel \mathbf{c}) + 2/3M(\mathbf{H} \parallel \mathbf{a})$, to within an accuracy limited by the small anisotropy observed in the **a**–**b** plane. The powder data for H = 0.015 G are shown in Figure 9.

A comparison of the dc flux expulsion and the ac susceptibility is also shown in FIGURE 9. Because of the high **a**–**b** plane conductivity, low-frequency ac measurements on single crystals inevitably lead to eddy-current effects; whereas the powder data avoid such difficulties. The ac and dc results are in agreement. The ac data extend the temperature range down to 1.2°K and show a clear indication of an upturn toward complete flux expulsion at the lowest temperatures.

The experimental results for $(-4\pi M/H)$ exhibit an unusual magnetic field dependence. The data for $\mathbf{H} \parallel (\mathbf{a} + \mathbf{b})$ are shown in FIGURE 10 for applied magnetic

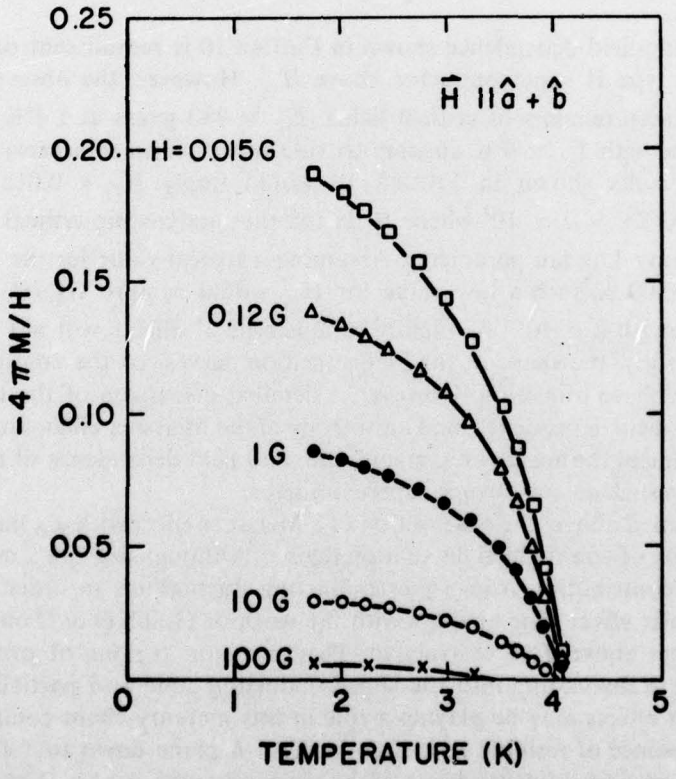


FIGURE 10. Temperature dependence of $(-4\pi M/H)$ at different magnetic fields for a single crystal sample; $\mathbf{H} \parallel \hat{a} + \hat{b}$).

fields of $H = 0.015$ G, 0.12 G, 1.0 G, and 100 G, FIGURE 10 demonstrates that the magnitude of the incomplete Meissner effect is a function of field even at $H/H_c < 4 \times 10^{-5}$ where $H_c = 380$ G is the critical field obtained from resistance measurements at 1.4°K. The uniform increase in $(-4\pi M/H)$ with decreasing field makes extrapolation to zero field impossible, but complete flux expulsion is not ruled out by the data.

The observation of flux expulsion with the magnitudes indicated in FIGURES 9 and 10 provides additional evidence of superconductivity below 4°K and implies that the superconductivity does not arise from a small volume of interconnected free Hg filaments. The latter would be expected to trap flux rather than expel it. The agreement between the static flux exclusion and ac susceptibility indicated in FIGURE 9 shows that there is no evidence of trapped flux due to multiply connected superconducting regions. Moreover, the large anisotropy and unusual temperature and field dependence appear to be inconsistent with filamentary effects. An array of superconducting Hg filaments weakly coupled by intervening metal might lead to bulk superconductivity through the proximity effect. Such a system, however, would be expected to show isotropic flux expulsion, particularly at low fields. Anisotropy can arise from internal field corrections due to the demagnetization field. However, in the extreme case of long cylinders, the maximum anisotropy would be 2:1, whereas the experimental values are an order of magnitude larger at low fields.

The strong-field dependence shown in FIGURE 10 is reminiscent of flux penetration in a type II superconductor above H_{c_1}. However, the observation from resistance measurements of critical fields ($H_c \simeq 380$ gauss at 1.4°K) consistent in magnitude with $T_c \simeq 4$°K appears to rule out such an interpretation. Moreover, the results shown in FIGURE 10 would imply $H_{c_1} < 0.015$ gauss, or $H_c/H_{c_1} = \sqrt{2}\kappa > 2 \times 10^4$ where H_c is the thermodynamic critical field and κ is the Ginsburg-Landau parameter. Assuming a typical value for the penetration depth, $\lambda \simeq 500$ Å, such a low value for H_{c_1} would require $(H_c/H_{c_1} \simeq \lambda/\xi)$ a coherence length $\xi < 10^{-2}$ A. Finally, simple type II effects will not explain the large anisotropy, the shape of the magnetization curves, or the continuity of σ_{ab} through the phase transition. However, a detailed discussion of the temperature dependence, field dependence, and anisotropy of the Meissner effect must await an understanding of the anisotropy, magnitude, and field dependence of the penetration depth in such an anisotropic superconductor.

As discussed above, the observation of a Meissner effect with σ_{ab} finite suggests the possibility of an extended fluctuation regime. Although finite, σ_{ab} might have a substantial contribution from superconducting fluctuations in order to allow a finite Meissner effect. The analogy with the work of Golub *et al.*[15] on fluctuation diamagnetism above T_c is instructive. They envision regions of order, the coherence length fluctuating into the superconducting state and partially expelling flux. Similar effects may be playing a role in this mercury-chain compound. The apparent absence of residual resistance in the *a*–*b* plane down to 1.4°K and the unusual magnetic field dependence of the resistivity with $\omega_c\tau \ll 1$ are consistent with this interesting possibility. Alternatively, taken at face value, the experimental results below 4°K can be viewed as evidence of anisotropic supercon-

ductivity. If this is indeed the case, the possibility of non-*s*-wave pairing in this anisotropic metal is worthy of speculation.

Summary and Conclusion

The interesting and unusual electronic properties of $Hg_{3-\delta}AsF_6$ result directly from the remarkable incommensurate polymercury chain structure. The quasi-one-dimensional metallic behavior of the orthogonal sets of chains, their interaction along the c-axis and the related coupling to the one-dimensional chain phonons are fundamental features to be considered in any attempts toward microscopic theoretical understanding of the transport properties, magnetic field-dependent resistivity and anisotropic superconductivity.

Some additional insight can be obtained from studies of the anisotropic thermoelectric power.[16] The results obtained from single crystals are shown in FIGURE 11a (**a**–**b** plane) and FIGURE 11b (*c*-axis). The thermopower is positive, with overall magnitude of the order of a few microvolts per degree, values typical of metallic behavior. At room temperature the results are 1.5 μV/°K and 2.2 μV/°K for the (**a**–**b**) plane and c-axis, respectively. The anisotropy in the magnitude of the thermopower is relatively small compared to the electrical resistivity where the anisotropy is of order 100 to 1.

Above 220°K, the thermopower is approximately a linear function of temperature. The electron-diffusion thermopower can be written as

$$S = \frac{\pi^2 k^2 T}{3e}\left[\frac{\partial \ln \sigma_{(\epsilon)}}{\partial \epsilon}\right]_{E_F} . \tag{9}$$

For temperatures above the Debye temperature Θ and assuming energy-independent scattering, (**9**) can be expressed as

$$S = \frac{2\pi^2}{3}\frac{k^2 T}{e} N(0) \tag{10}$$

where $N(0)$ is the density of states (one sign of spin) at the Fermi energy. The relatively weak anisotropy observed in the thermopower suggests ((**9**) and (**10**)) that the larger anisotropy in conductivity is predominantly the result of very strong scattering along the c-axis. From the slope of the data we obtain $N(0) \simeq 0.14$ states/eV/carrier or 0.05 states/eV/Hg atom, assuming one carrier for each AsF_6 anion. This value is to be compared with 0.08 states/eV/Hg atom obtained from the Knight shift.[8]

The thermopower in the low-temperature range is also anisotropic. In the **a**–**b** plane, a maximum is found with peak value at 15°K. Measurement of four samples shows that the peak size varies from sample to sample in the range from 0.8 μV/°K to 1.5 μV/°K. This variation and the overall peak structure are consistent with a phonon drag contribution which is typically sensitive to the impurity and/or defect concentration in the sample. In the c-direction, there is a smaller peak that occurs near 60°K. Since phonon drag thermopower peaks typically appear at about $\frac{1}{10}$–$\frac{1}{5}$ of Θ, the structure observed at 15°K (**a**–**b** plane) and 60°K (c-axis)

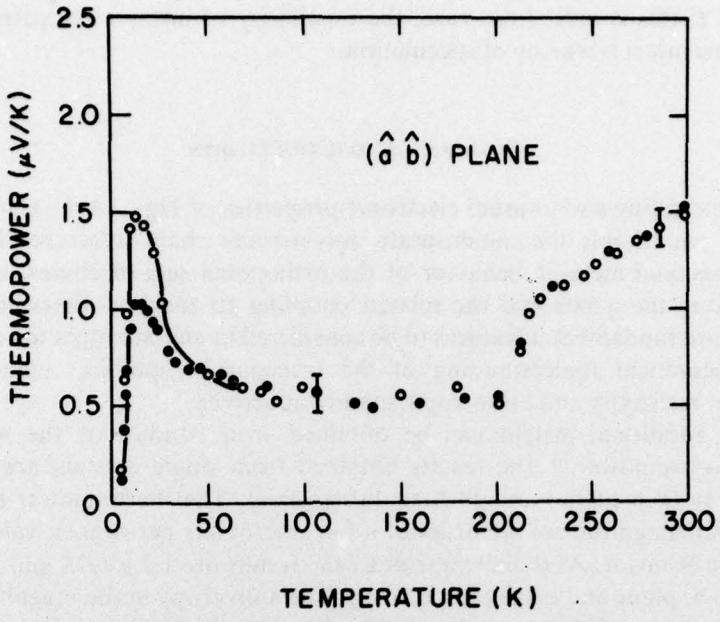


FIGURE 11a. Thermoelectric power of $Hg_{3-\delta}AsF_6$ single crystal (a–b plane).

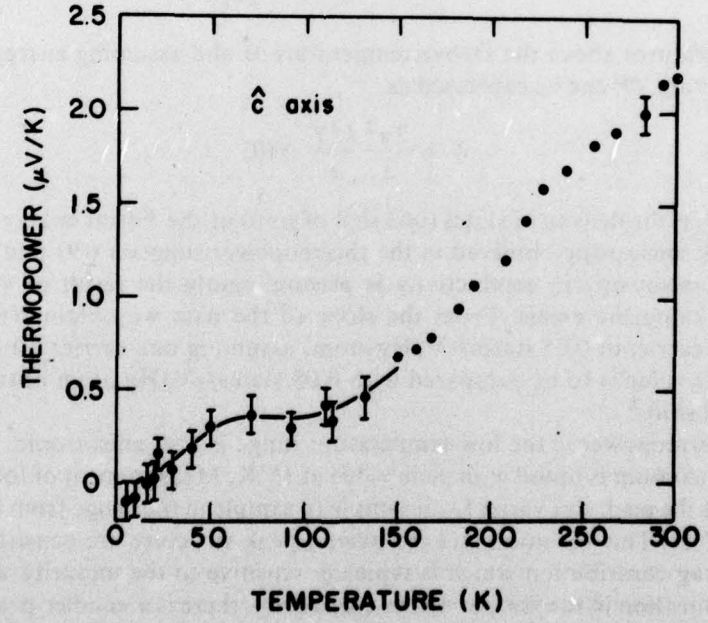


FIGURE 11b. Thermoelectric power of $Hg_{3-\delta}AsF_6$ single crystal (c-axis).

suggests an anisotropic phonon spectrum. It is particularly interesting, however, that the c-axis thermopower with peak near 60°K suggests stronger coupling to the 1-D phonos ($\Theta_{1\text{-}D} \simeq 600$°K), whereas the a–b plane results with peak near 15°K suggest stronger coupling to the 3-D phonons,($\Theta_{3\text{-}D} \simeq 80$°K).

These results suggest metallic behavior along the c-axis with relatively strong scattering leading to the observed electrical anisotropy. The apparent stronger coupling of the *c*-axis transport to the 1-D phonons may be an important clue toward understanding the anisotropic superconductivity.

Extension of the experimental results to lower temperatures and to include alloy systems with known concentrations of impurity atoms are planned in order to further characterize the low-temperature properties and provide information on the mechanisms involved.

References

1. Cutforth, B. D. 1975. Ph.D. Thesis. McMaster University. Hamilton, Ontario, Canada.

1a. Cutforth, B. D., W. R. Datars, R. J. Gillespie & A. van Schyndel. Adv. Chem. Ser. **150.**

2. Brown, I. D., B. D. Cutforth, C. G. Davies, R. J. Gillespie, P. R. Ireland & J. E. Vekris. 1974. Can. J. Chem. **52:** 791.

3. Schultz, A. J., J. M. Williams, N. D. Miro, A. G. MacDiarmid & A. J. Heeger. Inorg. Chem. In press.

4. Cutforth, B. D., W. R. Datars, A. van Schyndel & R. J. Gillespie. 1976. Solid State Commun. **21:** 377.

5. Chiang, C. K., R. Spal, A. Denenstein, A. J. Heeger, N. D. Miro & A. G. MacDiarmid. 1977. Solid State Commun. **22:** 293.

6. Koteles, E. S., W. R. Datars, B. D. Cutforth & R. J. Gillespie. 1976. Solid State Commun. **20:** 1129.

7. Peebles, D. L., C. K. Chiang, M. J. Cohen, A. J. Heeger, N. D. Miro & A. G. MacDiarmid. 1977. Phys. Rev. B **15:** 4607.

8. Ehrenfreund, E., P. R. Newman, A. J. Heeger, N. D. Miro & A. G. MacDiarmid. Phys. Rev. B. **16:** 781.

9. Wei, T., A. F. Garito, C. K. Chiang & N. D. Miro. Phys. Rev.

10. Spal, R., C. K. Chiang, A. Denenstein, A. J. Heeger, N. D. Miro & A. G. MacDiarmid. Phys. Rev. Lett. **39:** 650.

11. Hastings, J. M., J. P. Pouget, G. Shirane, A. J. Heeger, N. D. Miro & A. G. MacDiarmid. Phys. Rev. Lett. **39:** 1484.

12. Miro, N. D., A. G. MacDiarmid, A. J. Heeger, A. F. Garito, C. K. Chiang, A. J. Schultz & J. M. Williams. Inorg. Nucl. Chem. In press.

12a. Miro, N. D., A. G. MacDiarmid, A. J. Heeger, A. F. Garito, C. K. Chiang & A. R. McGhie. 1977. 5th Inter. Conf. Crystal Growth. Boston, Mass. July.

13. Keller, H. J., Ed. 1975. Low-Dimensional Cooperative Phenomena. Plenum Press. New York, N.Y.; Lecutre Notes in Physics **34,** One-Dimensional Conductors. Springer. New York, N.Y. 1975;Berlinsky, A. J. 1976. Contemp. Phys. **17:** 331; Andre, J. J., A. Bieber & F. Gautier. 1976. Ann. Phys. **1:** 145. Keller, H. J., Ed. 1977. Chemistry and Physics of One-Dimensional Metals. Plenum Press. New York, N.Y.

14. Akhtar, M., J. Kleppinger, A. G. MacDiarmid, J. Milliken, M. J. Moran, C. K. Chiang, M. J. Cohen, A. J. Heeger & D. L. Peebles. 1977. Chem. Commun. **473.** Solid State Commun. **23:** 607.

14a. Street, G. B., W. D. Gill, R. H. Geiss, R. L. Greene & J. J. Mayerle. 1977. Chem. Commun. **407.**

14b. GILL, W. D., W. BLUDAU, R. H. GEISS, P. M. GRANT, R. L. GREENE, J. J. MAYERLE & G. B. STREET. 1977. Phys. Rev. Lett. **38:** 1305.
15. GOLUB, J. P., M. R. BEASLEY, R. CALLAROTTI & M. TINKHAM. 1973. Phys. Rev. B. **7:** 3039.
16. CHIANG, C. K., R. SPAL, A. DENENSTEIN, A. J. HEEGER, N. D. MIRO & A. G. MACDIARMID. 1976. Proc. Conf. Thermoelectric Power in Metals. Michigan State Univ. East Lansing, Mich.

DISCUSSION

RICHARD FERGUSON (*Univ. of British Columbia, Vancouver, Canada*): The superconducting transition temperature of $Hg_{2.86}AsF_6$ is very close to the value for free mercury. How do you exclude the possibility for free mercury?

HEEGER: One worries about the question of free mercury when one see a transition so close. The transition temperature value as best we can measure is 4.1°K, very slightly off the free mercury. The most convincing evidence lies in the observed 20:1 anisotropy in the Meisner effect. This cannot be explained by any simple mechanism that I know about. The most one can get from internal field corrections in cylindrical filaments is 2 to 1, whereas we find 20 to 1. Also, the magnitude of the flux exclusion is of the order of 20%, even at these intermediate temperatures. Finally, we have done some detailed experiments looking at DSC traces and also looking at Meisner effect with very high sensitivity looking for superconductivity at 4.15°K from samples that we have exposed to air in an attempt to drive mercury out. One can, by crude handling of samples, see a tiny step of order 10^{-4} in the conductivity right at the mercury phase transition separated from the bulk transition. Moreover, you can make even that go away by handling the samples more carefully.

TOBIN MARKS (*Northwestern Univ., Evanston, Ill.*): My impression is that mercury compound is extremely air-sensitive. What sort of contacts did you use for the dc conductivity measurements?

HEEGER: In some cases, none; that is, we did low-frequency measurements with no contacts to verify the magnitude of the conductivity and the details of the phase transition. In other cases we did conventional four-probe measurements on the samples.

COMMON ABBREVIATIONS

A	Acceptor
A	electron affinity
Adn	acridinium
BP	4,4′-dipyridyl
BTP	bithiopyran
bqdH, $bqdH_2$	1,2-benzoquinonedioxime
CDW	charge density wave
CP	tetracyanoplatinate
D	donor
DMF	*N*,*N*-dimethylformamide
DMSO	dimethylsulfoxide
dpgH, $dpgH_2$	diphenylglyoxime
DSC	differential scanning calorimetry
DTA	differential thermal analysis
E_A	electron affinity
E_g	band gap
E_M	Madelung energy
en	ethylenediamine
esr, ESR	electron spin resonance
Et	ethyl
E_{vdw}	van de Waal's energy
FIR	far infrared
g	electron phonon coupling constant
HMTSF, HMTSeF	hexamethylenetetraselenafulvalene
I, I.P.	ionization energy
IR	infrared
J	magnetic exchange constants
KCP	$K_2Pt(CN)_4Br_{0.3} \cdot 3.2H_2O$
L	ligand
L-L	bidentate ligand
Me	methyl
MO	molecular orbital
NIR	near infrared
NMP	*N*-methylphenaznium
NMR	nuclear magnetic resonance
p	polarization energy
PcH_2	phthalocyanine
Phen	phenazine
Ph	phenyl
Qn	quinolinium
R	reflectively, organic substituent group
S	thermoelectric power
t	charge transfer integral

T	temperature
T_1	nuclear spin lattice relaxation time
T_2	spin-spin relaxation time
TCNQ	7,7,8,8-tetracyano-*p*-quinodimethane
TCP	tetracyanoplatinate
THF	tetrahydrofuran
TSF, TSeF	tetraselenafulvalene
TTF	tetrathiofulvalene
TTT	tetrathiotetracene
U	coulomb repulsion
UV	ultraviolet
V	potential
VDW	van der Waals
VIS	visible
Δ	activation energy
ϵ	dielectric constant
λ	wavelength
μ	mobility
ν	frequency
ρ	resistivity, number of electrical charges per molecule
σ	electrical conductivity
χ	magnetic susceptibility
ω	frequency ($2\pi\nu$)

CONSTANTS

Avogadro's Number, N	$= 6.023 \times 10^{23}$ molecules mole^{-1}
Bohr magneton, μ_B, μ	$= 5.789 \times 10^{-9}$ eV Gauss^{-1}
Boltzman's constant, k or k_b	$= 8.618 \times 10^{-11}$ eV °K^{-1}
electron charge, e	$= 1.602 \times 10^{-19}$ coulomb
electron mass, m_e	$= 9.11 \times 10^{-31}$ kg
1 eV	$= 3.82 \times 10^{-17}$ kcal
	$= 1.602 \times 10^{-19}$ J
	$= 1.602 \times 10^{-12}$ erg
1 eV molecule^{-1}	$= 23.06$ kcal/mole^{-1}
	$= 96.52$ kJ mole^{-1}
	$= 8{,}066$ cm^{-1} $= 1239.7$ nm
	$= 11{,}605$°K
Planck constant, h	$= 4.14 \times 10^{-21}$ eV sec^{-1}
$\hbar$	$= 6.59 \times 10^{-22}$ eV sec^{-1}

Author Index

(Italicized page numbers refer to comments in discussions)

Abkowitz, M. A., 459–466
Akhtar, M., 726–736
Allen, W. N., 759–766
Amiell, J., 467–480
Andersen, Jan R., 293–300, 343–354
Anzai, Hiroyuki, 256–268
Ashwell, G. J., 417–441

Balch, Alan L., 651–662
Barton, Jacqueline K., 686–700
Baughman, R. H., 705–725, 775–787
Bechgaard, Klaus, 293–300, 467–480
Bloch, Aaron N., *165*, *209*, *332*, 366–368, *458*
Bradley, Mark G., 588–593
Bray, J. W., 407–416
Brill, J. W., 459–466
Burlich, James, *799*

Candela, G. A., 377–381
Cape, T., 377–381
Cava, M. P., 355–360
Chaikin, Paul M., 128–144, 459–466
Chance, R. R., 705–725
Chartier, Duane, 788–799
Chen, C. H., *78*
Chiang, C. K., 726–736
Clardy, J., 382–394
Clark, R. J. H., *495*, 672–685
Cohen, M. J., 726–736
Coleman, Lawrence B., 316–332, *441*, *458*
Coler, M., *538*
Comès, Robert, 234–243, *406*
Conwell, Esther, 183–209, *458*
Coppens, P., *60*, 244–255, *538*
Cornish, T. F., 525–538
Cowan, Dwaine O., 366–368
Craven, Robert A., 343–354
Cuellar, E., 580–587
Cutforth, Brent D., 788–799

Datars, W. Ross, 788–799
Dauplaise, D., 382–394
Davis, M., *744*
Day, P., 9–24, *110*, *495*, *558*
DeCorpo, J. J., 759–766
Delhaes, P., 467–480
Duke, C. B., 166–178, *315*, *331*

Elbaum, C., 745–758
Eley, D. D., 417–441
El Sharif, Mohammed, 663–671
Endres, Helmut, 617–632, 663–671
Engler, Edward M., *60*, *78*, 293–300, 343–354
Epstein, Arthur J., *165*, 183–209, *233*, *416*, *458*, 459–466
Etemad, Shahab, 343–354, 737–744

Fabre, J. M., 467–480
Ferguson, Richard, *822*
Finnegan, T. F., 377–381
Fitchen, D. B., 771–774
Flandrois, S., 467–480
Froix, M. F., 459–466

Gamble, F. R., 86–110
Garito, A. F., 301–315
Geiss, R. H., 737–744
Geoffroy, Gregory L., 588–593
Gill, W. D., 737–744, 771–774
Gillespie, Ronald J., 788–799
Giral, L., 467–480
Glick, M., 377–381
Gliemann, Günter, 539–559
Goetz, Fred, *360*, *736*
Gordon, J. G., II, 580–587, *593*
Grant, Paul, *291*
Gray, H. B., 580–587
Green, Dennis C., 361–365
Greene, R. L., 737–744
Griffiths, C. H., 459–466
Gunning, W., 459–466

Hadek, V., 580–587
Haen, P., 701–704
Hart, H. R., Jr., 407–416
Hashmall, J. A., 377–381
Heeger, A. J., *331*, *332*, 459–466, 726–736, 800–822
Hoffman, Brian, *538*, *616*
Hsu, C.-H., 580–587

Ilsley, W., 377–381
Interrante, L. V., 407–416, *616*
Iqbal, Z., 775–787
Isett, L. C., 61–78, 395–406, *416*

Jacobsen, C. S., 467–480
Johnson, P. L., 525–538
Junker, W. R., 745–758

Kao, H. I., 745–758

Kasper, J. S., 407–416
Keeney, Mark E., 588–593
Kelber, J., 525–538
Keller Heimo J., 442–458, 617–632, *662*, 663–671
Keryer, G., 467–480
Kistenmacher, Thomas J., 333–342, *538*
Klemm, Richard A., *144*
Kleppinger, J., 726–736, 775–787
Kokoszka, G. F., 377–381
Kommandeur, J., *315*, *725*
Krug, William P., 366–368
Kruger, A. A., 79–85
Kutner, Włodzimers, 767–770
Kuyper, J., 737–744

Labes, M. M., 745–758
Lakshmikantham, M. V., 355–360
LaPlaca, S. J., 369–376
Lehmann, R., 617–632
Lippard, Stephen J., 686–700
Little, W. A., 459–466
Louis, E. J., 726–736
Love, P., 745–758

MacDiarmid, Alan G., 726–736, *757*, 767–770, 775–787, *799*, 800–822
Mah, P. T., 759–766
Mann, K., 580–587
Mark, Harry B., Jr., 767–770
Marks, Tobin J., 594–616, *822*
Martin, Reinhold, 663–671
McGhie, A. R., 301–315
Meerschaut, A., 701–704
Mègnamisi-Bélombé, Michel, 633–650
Megtert, S., 234–243
Meinwald, J., 382–394
Metzger, Robert Melville, 145–165, *255*, *292*
Meyer, Thomas J., 496–508
Miller, Joel S., 1–8, 25–60, 183–209, 459–466, *616*
Milliken, J., 726–736
Monceau, P., 701–704
Moran, M. J., 726–736
Morawitz, H., 179–182
Moroni, W., 442–458
Murakami, Mutsuaki, 269–292
Myer, G., 745–758

Nigrey, P. J., 301–315
Nöthe, D., 442–458
Novatny, M., 459–466
Nowak, Robert, 767–770

Ohno, Teruaki, 256–268
Ong, N. P., *292*

Pasquali, G., 525–538
Patel, Vishnu V., 343–354
Peebles, D. L., 726–736
Perez-Albuerne, E. A., 395–406
Perlstein, J. H., 61–78, *209*, *291*, *457*, *616*
Peterson, Selmer W., 560–579
Piacente, P. A., 407–416
Poehler, Theodore O., 366–368
Pouget, J. P., 234–243
Poveda, Arnulfo, 617–632
Putnik, C., 525–538

Reis, Arthur H., *110*, 560–579
Reynolds, G. A., 61–78
Rouxel, Jean, *110*, 701–704
Row, T. N. Guru, 244–255

Saalfeld, F. E., 759–766
Salamon, M. B., 525–538
Samson, S., 580–587
Saran, Mohan, *744*
Schaffman, M. J., 525–538
Schechtman, Barry, *725*
Schultz, A. J., 509–515, 525–538
Scott, Bruce A., 343–354, 369–376
Scott, J. C., 382–394
Shirakawa, H., 726–736
Siedle, A. R., *232*, *360*, 377–381, *766*
Silverman, B. D., *165*, 369–376
Slade, M. L., 459–466
Smith, R. D., 737–744
Somoano, R., *110*, *292*, *441*, 580–587
Soos, Z. G., *127*, 442–458, *725*
Stanley, George C., *593*
Street, G. B., 737–744, 771–774
Stucky, Galen, 525–538

Takabe, Teruhiro, 256–268
Tanaka, Chizuko, 256–268
Tanaka, Jiro, 256–268
Tanaka, Masashi, 256–268
Tanner, D. B., 459–466
Taube, Henry, 481–495
Temkin, H., 382–394, 771–774
Thomas, G. A., 79–85
Träger, Ulrich, 663–671
Tomkiewicz, Yaffa, 343–354
Toreilles, E., 467–480
Torrance, J., *24*, 210–233, 369–376, *538*, *559*

Underhill, A. E., 516–524

Van Allen, J. A., 61–78
Van de Sand, H., 617–632

Van Duyne, R. P., 377–381
Van Schyndel, André, 788–799
Vu, Dong, 617–632

Wallwork, S. C., 417–441
Washecheck, D. M., 525–538
Watkins, G. D., 407–416
Welber, B., 369–376
Willett, Roger D., 111–127
Williams, Jack M., 509–515, 525–538
Williams, R., 580–587
Willis, M. R., 417–441
Wood, D. J., 516–524
Woodward, J., 417–441
Woyciesjes, P. M., 377–381
Wudl, F., 79–85, *360*, *736*
Wyatt, J. R., 759–766

Yamagishi, F. G., 301–315
Yersin, Hartmut, 539–559
Yoshimura, Susumu, 269–292